30th International QUENCH Workshop

16-18 December 2025
Karlsruhe Institute of Technology
Karlsruhe, Germany

Editor: Martin Steinbrück

DOI: 10.5445/IR/1000189487

AGENDA

30th International QUENCH Workshop

Karlsruhe Institute of Technology, Campus North, H.-von-Helmholtz-Platz 1, 76344 Egg.-Leopoldshafen, Germany
16-18 December 2025

Meeting Location: Fortbildungszentrum für Technik und Umwelt (FTU), Auditorium (Aula)

Tuesday, 16 Dec 2025

8:30	**Registration**	
9:00	Welcome	M. Steinbrück, W. Tromm, KIT
9:10	Update of the QUENCH Program	M. Steinbrück, KIT
	JUBILEE SESSION 30 YEARS QWS (Chair: F. Gabrielli, KIT)	
9:30	History of nuclear research in Karlsruhe (working title)	M. Popp, invited
10:00	Overview of the CODEX experimental programme	Z. Hozer, HUN-REN
10:30	**Coffee break (Group Photo)**	
11:00	Materials science for nuclear safety. From unexpected findings to improved severe accident codes	M. Steinbrück, KIT
11:30	The importance of taking into account the temperature gradient on the processes occurring in the cladding tube during high-temperature oxidation, melting and mechanical deformation	J. Stuckert, KIT
12:00	Neutron imaging investigations of hydrogen in cladding tube materials	M. Grosse, KIT
12:30	From QUENCH-01 to QUENCH-ATF-2: Three Decades of AC²/ATHLET-CD Validation using QUENCH Experiments	T. Hollands, GRS
13:00	**Lunch**	
	LONG-TERM DRY STORAGE – SYSTEM ZR-H (Chair: D. Schaefer, KIT)	
14:00	The SPIZWURZ project, overview and single effect tests	M. Grosse, KIT
14:20	Experimental results of the SPIZWURZ bundle test	J. Stuckert, KIT
14:50	Hydride Morphology in Zirconium Tubes After SPIZWURZ Bundle Tests: Experimental Data and Preliminary Simulation Results	M. Kolesnik, KIT
15:10	SPIZWURZ Benchmark	A. Rezchikova, GRS
15:30	**Coffee break**	

16:00	Hydrogen in Claddings - Investigations on Hydrogen Axial Mobility, Role of Liner and Creep	J. Bertsch, PSI
16:30	Dedicated investigation of secondary hydriding: Experimental insights and modelling	M. Kpemou, ASNR

Wednesday, 17 Dec 2025

	MODELLING AND CODE APPLICATION I (Chair: M. Cazado, KIT))	
9:00	Expanding the Capability of the ASTST VER3.5 System Thermal Hydraulic and SCDAPSIM Modeling Options to Support the Fukushima Daiichi Decommissioning R&D Analysis and Assessment	R. Pericas, ISS
9:20	Analysis of the COAL Reflooding Experiments: Recent Simulations with AC²	G. Stahlberg, RUB
9:40	Validation of AC2/ATHLET using QUENCH data	L. Lovasz, GRS
10:00	Modeling of QUENCH-06 and QUENCH-20 tests with RELAP/SCDAPSIM, Focus on Bundle Asymmetry	T. Kaliatka, LEI
10:20	**Coffee break**	
	MODELLING AND CODE APPLICATION II (Chair: L. Lovasz, GRS)	
10:50	Infinite lattice depletion of accident-tolerant fuel pin-cells with OpenMC and cladding inventory analysis with FISPACT-II	P. Bochtler, BASE
11:20	Simulation of Cr-coated Zry-4 cladding tube ballooning and burst behavior using MERCURY	D. Lee, KAERI
11:40	Simulating Cr-Coating Behavior with AC²: From QUENCH Analysis towards Integral Plant Application	G. Stahlberg, RUB
	EXPERIMENTS (Chair: L. Lovasz, GRS)	
12:00	COSMOS-H first experiments at the new thermohydraulic facility	S. Gabriel, KIT
12:20	Synergistic influence of oxygen, hydrogen and microstructure on thermal shock behavior of PHWR cladding subjected to integral LOCA test	T. Sawarn, BARC
13:00	**Lunch**	
14:00	Technical tour to FR2 Nuclear Museum and KATRIN facility	
17:30	**Dinner (Restaurant Ritter, Büchenau)**	

Thursday, 18 Dec 2025

	ATF CLADDING I (Chair: M. Grosse, KIT))	
9:00	Results of the IAEA Coordinated Research Project (CRP) on 'Testing and Simulation of Advanced Technology and Accident Tolerant Fuels (ATF-TS)' (2020–2024) and Plans for the Next CRP"	A. Khaperskaia, IAEA

9:30	Separate effects tests with ATF cladding materials within the IAEA ATF-TS CRP	M. Sevecek, CTU
9:55	Development Status of Accident-Tolerant Control Rods in Light Water Reactors at CRIEPI	K. Nakamura, CRIEPI
10:15	Post-test examination of the integral air ingress experiment CODEX-ATF-AIT	R. Farkas, HUN-REN
10:30	**Coffee break**	
	ATF CLADDING II (Chair: M. Sevecek, CTU)	
11:00	Accident tolerant fuel: Cr coated cladding development at Westinghouse	K. Frederick, WEC
11:20	Oxidation and degradation of Cr-coated zirconium alloy: Effect of Cr thickness	M. Steinbrück, KIT
11:45	Effect of initial Cr-coating thickness on the high-temperature steam oxidation behavior of Cr-coated Zr-based alloys: Comparison between TGA experiments conducted at several institutes using “Equivalent Chromium Reacted” (ECrR) parameter	J.-C. Brachet, CEA
12:10	Steam Oxidation of Cr-Coated Zircaloy-4 Rods Across a Wide Range of Heating Rates	D. Bachurina, KIT
12:30	Multiscale Insights into Embrittling Mechanisms of Cr-Coated Zircaloy Cladding under Ultra-High Temperature Conditions	T. Liu, SJTU
12:50	**Lunch**	
	ATF CLADDING III (Chair: D. Bachurina, KIT)	
14:00	Behaviour of Fuel Cladding with Cr Coating during LOCA and Study of Oxygen Diffusion into Zr-alloy using Different methods	V. Boucek, UJP
14:20	High-Temperature Oxidation of Cr Coated Claddings with Interdiffusion Barrier & Solute (Al, Si) Additions	B. Nowak, Queen’s University
14:40	Experimental Observations on the CHF Performance of Cr/ CrN-Coated Zircaloy-4 in Low-Pressure Flow Boiling	N. Wefers, KIT
15:00	Update of the KIT contributions to the SCORPION project	M. Grosse, KIT
15:30	**Closure of the Workshop**	M. Steinbrück, KIT


30th International QUENCH Workshop

Martin Steinbrück
KIT

Update of the QUENCH program

The 30th International QUENCH Workshop, held at Karlsruhe Institute of Technology (KIT) from December 16–18, 2025, provided an update on the QUENCH program, which focuses on reactor safety research under severe accident (SA) and design-basis accident (DBA) conditions. Key topics included experimental investigations on Accident Tolerant Fuel (ATF) cladding concepts, long-term dry intermediate storage of spent fuel, and modeling for code validation. The talk highlighted recent advancements in bundle and separate-effects tests, including high-temperature oxidation and quench experiments on ATF materials such as Cr-coated ZIRLO, FeCrAl, and SiC composites. International collaborations under OECD-NEA, IAEA, and EC projects were emphasized, alongside progress in hydrogen behavior studies during extended storage and neutron radiography campaigns. Future directions involve Phase 2 of QUENCH-ATF, safety research for Small Modular Reactors (SMRs), and integration with fusion programs. These efforts aim to enhance accident management strategies and support the development of robust safety concepts for current and next-generation nuclear systems.

Karlsruhe Institute of Technology

Update of the QUENCH program

M. Steinbrueck, J. Stuckert, M. Grosse, D. Bachurina, D. Schaefer

30th International QUENCH Workshop

Karlsruhe Institute of Technology, 16-18 Dec 2025

Outlook

- Current topics
- Experimental facilities
- ATF activities
- Long-term dry intermediate storage activities
- Modelling / Code validation
- Reporting
- Future planning

QUENCH program

Separate-effects tests

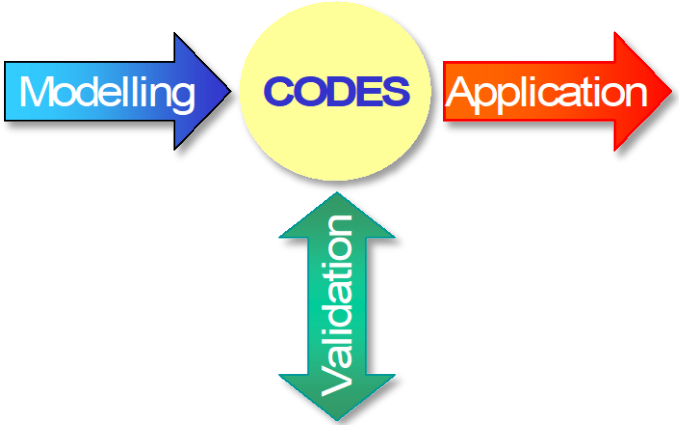

Bundle experiments

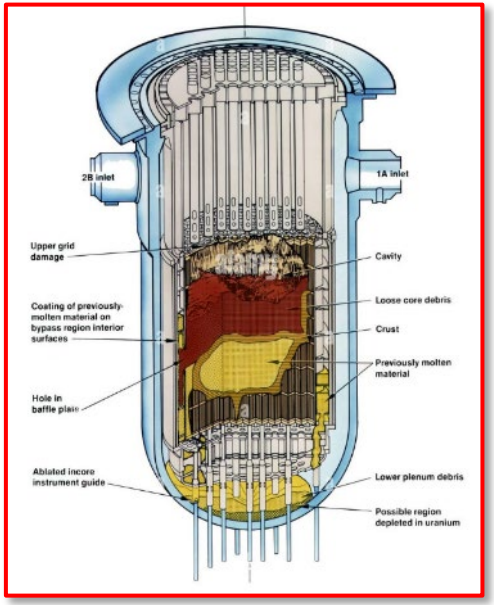

Application for simulation of nuclear accident scenarios

Current topics

- **Accident tolerant fuel (ATF) cladding**
  - ATF research after Fukushima Daiichi accidents
  - Characterization of promising ATF cladding concepts at (very) high temperatures
  - Degradation mechanisms and kinetic data
  - Max. temperature and coping time for AMMs

- **Long-term dry intermediate storage**
  - No final storage on the horizon in Germany and many other countries
  - Hydrogen/hydride behavior in Zr cladding during 50-100 years storage e.g. in CASTOR casks
  - Hydride reorientation and its effect on mechanical properties

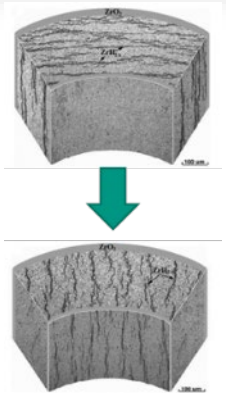

QUENCH/LICAS facility

- Unique out-of-pile bundle facility to investigate reflood of an overheated reactor core
- 21-31 electrically heated fuel rod simulators;
  T up to >2000°C
- Extensive instrumentation for T, p, flow rates, level, etc. + MS
- So far, 20+1 experiments on SA performed (1996-today)
  - Influence of pre-oxidation, initial temperature, flooding rate
  - B_4C, Ag-In-Cd control rods
  - Air ingress; debris formation
  - Advanced cladding alloys & ATF
- 7+1 DBA LOCA experiments with separately pressurized fuel rods
- Upgrade of PC's and control software

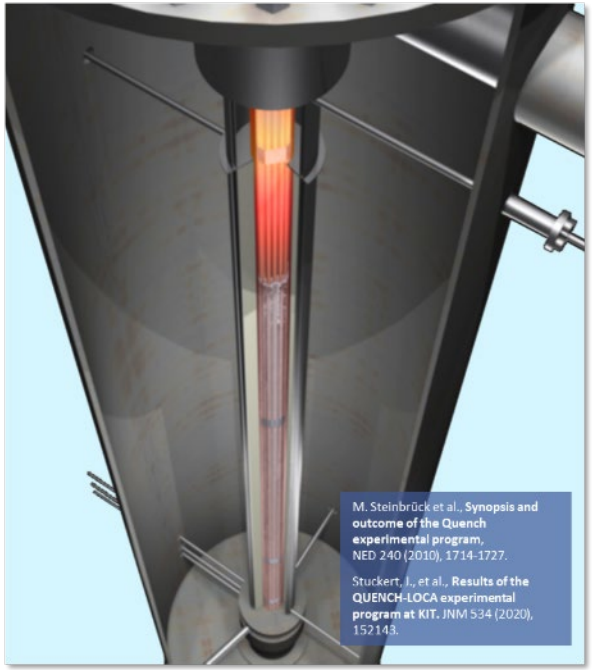

Experimental setup for ATF research (SET)

QUENCH-SR
- 10-15 cm cladding tube segments
- Fast inductive heating up to 2000°C
- Water quench

DTA-TG systems
- Max. temp. 1600°C (1250°C in steam)

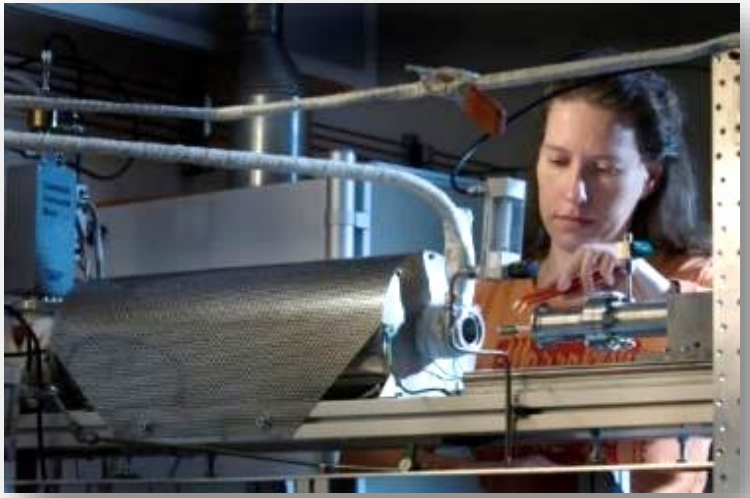

Tube furnaces
- Max. temp. 1600°C (all atmospheres)
- Sample airlock

All systems with water steam supply and mass spectrometer coupling

Test facilities for long-term storage research

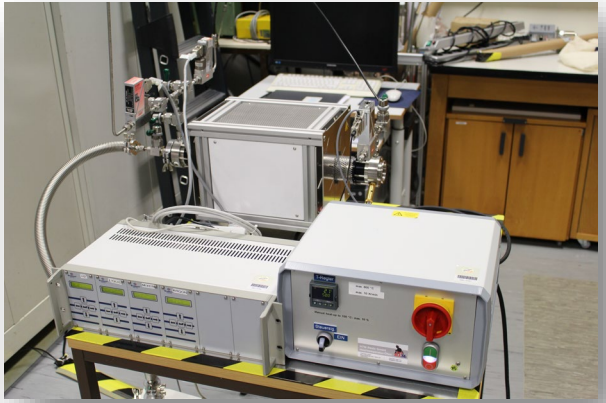

INCHAMEL
- Apparatus for in-situ neutron radiography experiments under defined mechanical load and temperature

VAKO
- Sieverts chamber for hydrogen loading of small Zry samples

HOKI
- 2.5 m long furnace for hydrogen pre-loading of cladding tubes for bundle tests

QUENCH activities on ATF cladding materials

- Bundle tests in the framework of OECD-NEA QUENCH-ATF
- Single-rod oxidation and quench tests of ATF cladding segment samples
- HT furnace tests with small samples in various atmospheres for analysis of oxidation kinetics and degradation mechanisms
- Tests on all promising ATF cladding concepts, including Cr-coated Zry, FeCrAl, SiC-based composites
- Data for model development, code validation and code application

International collaborations on ATF cladding

- OECD-NEA Joint Undertaking QUENCH-ATF
  - KIT is Operating Agent of the project
  - Three bundle experiments with Cr-coated ZIRLO provided by Westinghouse (USA)
  - Phase 2 under preparation
- IAEA Coordinated Research Project ATF-TS
  - Completed, TECDOC reports in 3 volumes to be published
  - Final international meeting co-organized
- EC Projects SCORPION and IL TROVATORE
  - KIT coordinates WPs on fuel-cladding-coolant interaction
- EC Project CONNECT-NM
  - New project CROCODOX (CEA) accepted
- OECD-NEA project SCIP-V

QUENCH-ATF3 test preparation

- ZIRLO cladding tubes at NNL for Cr coating by PVD, ready to be shipped
- Spacer grids provided by WEC
- All other materials for bundle construction are available
- Test conduct planned for 2026 (as early as possible)
- Test scenario: slightly modified QUENCH-11 with boil-off phase, max. temperatures of 1600°C and 50 g/s flooding rate

Separate-effects tests on ATF cladding

- Isothermal and transient tests with different coating types
  - Cr, Cr-Al, Cr-Si with and w/o Mo diffusion barrier
  - In the framework of an TCOFF-2/NEST internship (Brock Nowak, Queens University)
- Transient tests on Cr/Zry cladding failure
  - QUENCH-SR tests up to melt release
  - In cooperation with ASNR (Martial Kpemou)
- Experiments in different atmospheres (steam, O_2, air) above eutectic temperature
- Experiments with porous SiC in various atmospheres (SCORPION)

Activities on long-term intermediate storage

- Work was embedded in the German project SPIZWURZ (GRS, KIT) and the HGF HOVER infrastructure program
  - Completed in 2025
  - 8-month lasting bundle test
  - Post-test analyses and benchmark exercises well progressed
- Various SETs on hydrogen dissolution and precipitation in zirconium alloys
- Neutron radiography and tomography campaigns
- Follow-up project SPIZWURZ+ under preparation
  - Advice: Feasibility study showing capability of smoother cool-down phase

Modelling and code validation

- QUENCH bundle tests are part of validation matrices of most SFD code systems
- Benchmark exercise (blind & open phase) on QUENCH-ATF2 test coordinated by GRS
- Benchmark exercise (blind & open phase) on SPIZWURZ bundle test coordinated by GRS
- Pre-test calculations for SPIZWURZ+
- Separate-effects test data are available for model development

Reporting

- Several papers
- Invited lectures
  - MRS Spring Meeting, Seattle
  - Reactor Safety Commission (RSK)
  - Shanghai Jiao Tong University
  - INCT Warsaw
  - IAEA Technical Meeting
- Visit of journalists at QUENCH
- Two evaluations with outstanding results for NUSAFE program

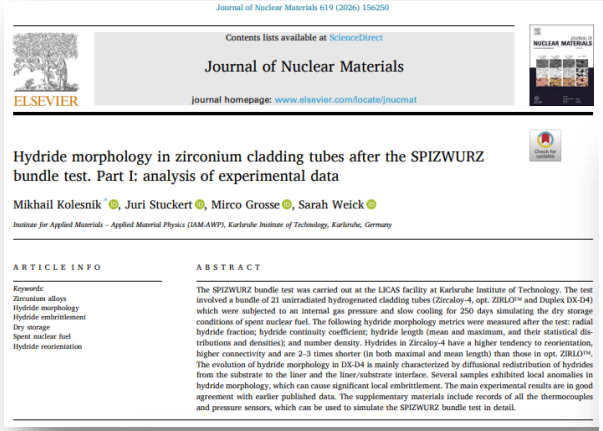
Journal of Nuclear Materials 619 (2026) 156250

Contents lists available at ScienceDirect

Journal of Nuclear Materials

journal homepage: www.elsevier.com/locate/jnucmat

Hydride morphology in zirconium cladding tubes after the SPIZWURZ bundle test. Part I: analysis of experimental data

Mikhail Kolesnik, Juri Stuckert, Mirco Grosse, Sarah Weick

Institute for Applied Materials – Applied Material Physics (IAM-AWP), Karlsruhe Institute of Technology, Karlsruhe, Germany

ARTICLE INFO

Keywords:
Zirconium alloys
Hydride morphology
Hydride embrittlement
Dry storage
Spent nuclear fuel
Hydride reorientation

ABSTRACT

The SPIZWURZ bundle test was carried out at the LICAS facility at Karlsruhe Institute of Technology. The test involved a bundle of 21 unirradiated hydrogenated cladding tubes (Zircaloy-4, opt. ZIRLO™ and Duplex DX-D4) which were subjected to an internal gas pressure and slow cooling for 250 days simulating the dry storage conditions of spent nuclear fuel. The following hydride morphology metrics were measured after the test: radial hydride fraction; hydride continuity coefficient; hydride length (mean and maximum, and their statistical distributions and densities); and number density. Hydrides in Zircaloy-4 have a higher tendency to reorientation, higher connectivity and are 2–3 times shorter (in both maximal and mean length) than those in opt. ZIRLO™. The evolution of hydride morphology in DX-D4 is mainly characterized by diffusional redistribution of hydrides from the substrate to the liner and the liner/substrate interface. Several samples exhibited local anomalies in hydride morphology, which can cause significant local embrittlement. The main experimental results are in good agreement with earlier published data. The supplementary materials include records of all the thermocouples and pressure sensors, which can be used to simulate the SPIZWURZ bundle test in detail.

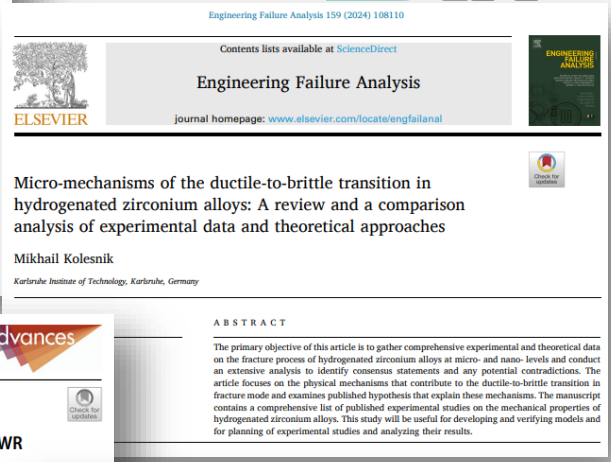
Engineering Failure Analysis 159 (2024) 108110

Contents lists available at ScienceDirect

Engineering Failure Analysis

journal homepage: www.elsevier.com/locate/engfailanal

Micro-mechanisms of the ductile-to-brittle transition in hydrogenated zirconium alloys: A review and a comparison analysis of experimental data and theoretical approaches

Mikhail Kolesnik

Karlsruhe Institute of Technology, Karlsruhe, Germany

ABSTRACT

The primary objective of this article is to gather comprehensive experimental and theoretical data on the fracture process of hydrogenated zirconium alloys at micro- and nano- levels and conduct an extensive analysis to identify consensus statements and any potential contradictions. The article focuses on the physical mechanisms that contribute to the ductile-to-brittle transition in fracture mode and examines published hypothesis that explain these mechanisms. The manuscript contains a comprehensive list of published experimental studies on the mechanical properties of hydrogenated zirconium alloys. This study will be useful for developing and verifying models and for planning of experimental studies and analyzing their results.

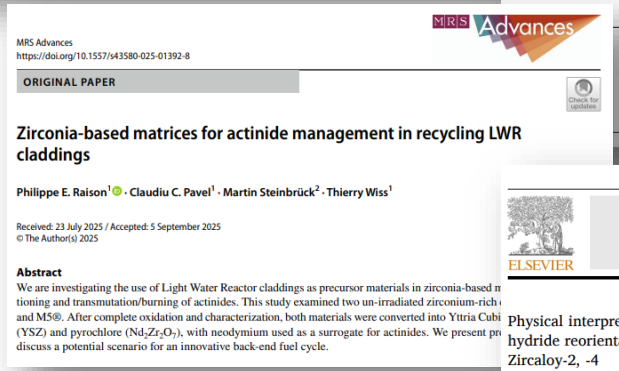
MRS Advances

https://doi.org/10.1557/s43580-025-01392-8

ORIGINAL PAPER

Zirconia-based matrices for actinide management in recycling LWR claddings

Philippe E. Raison[1] · Claudiu C. Pavel[1] · Martin Steinbrück[2] · Thierry Wiss[1]

Received: 23 July 2025 / Accepted: 5 September 2025
© The Author(s) 2025

Abstract

We are investigating the use of Light Water Reactor claddings as precursor materials in zirconia-based m
tioning and transmutation/burning of actinides. This study examined two un-irradiated zirconium-rich
and M5®. After complete oxidation and characterization, both materials were converted into Yttria Cubi
(YSZ) and pyrochlore ($Nd_2Zr_2O_7$), with neodymium used as a surrogate for actinides. We present pr
discuss a potential scenario for an innovative back-end fuel cycle.

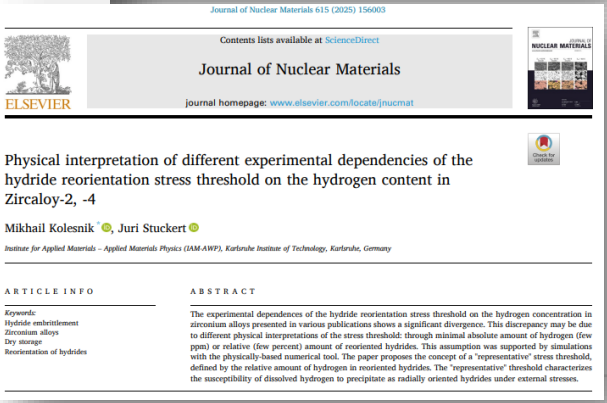
Journal of Nuclear Materials 615 (2025) 156003

Contents lists available at ScienceDirect

Journal of Nuclear Materials

journal homepage: www.elsevier.com/locate/jnucmat

Physical interpretation of different experimental dependencies of the hydride reorientation stress threshold on the hydrogen content in Zircaloy-2, -4

Mikhail Kolesnik, Juri Stuckert

Institute for Applied Materials – Applied Materials Physics (IAM-AWP), Karlsruhe Institute of Technology, Karlsruhe, Germany

ARTICLE INFO

Keywords:
Hydride embrittlement
Zirconium alloys
Dry storages
Reorientation of hydrides

ABSTRACT

The experimental dependences of the hydride reorientation stress threshold on the hydrogen concentration in zirconium alloys presented in various publications shows a significant divergence. This discrepancy may be due to different physical interpretations of the stress threshold: through minimal absolute amount of hydrogen (few ppm) or relative (few percent) amount of reoriented hydrides. This assumption was supported by simulations with the physically-based numerical tool. The paper proposes the concept of a "representative" stress threshold, defined by the relative amount of hydrogen in reoriented hydrides. The "representative" threshold characterizes the susceptibility of dissolved hydrogen to precipitate as radially oriented hydrides under external stresses.

Perspectives

- Reactor safety research confirmed for the current and next HGF funding periods until 2035
- Three new positions for the QUENCH team to fill retirement gaps
- Future topics
  - Behavior of ATF materials under DBA and SA conditions (QUENCH-ATF Phase 2)
  - Safety research for long-term intermediate storage (Zr-H, SPIZWURZ+)
  - Safety research for SMRs (LWR- and GFR-type)
  - Joint projects with FUSION program

Acknowledgement

- Helmholtz Association for funding program NUSAFE at KIT
- Program NUSAFE and IAM institute's management for broad support of our activities
- EC for funding the projects SEAKNOT, IL TROVATORE and SCORPION
- OECD-NEA and partners for support of QUENCH-ATF

- And last but not least the QUENCH team:
  M. Kolesnik, ~~J. Laier~~, J. Moch, U. Peters, C. Roessger, U. Stegmaier, ~~S. Weick~~

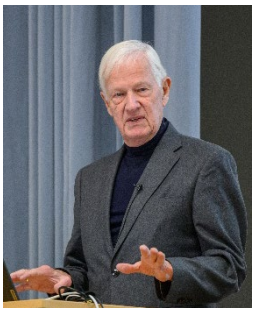

Manfred Popp

The history of nuclear research in Karlsruhe

The presentation provides a comprehensive historical overview of nuclear research in Karlsruhe, tracing its development from the discovery of nuclear fission in 1938 to the establishment and current role of the Karlsruhe Institute of Technology (KIT). It begins with the German Uranium Project (1939–1945), which, unlike the highly industrialized Manhattan Project, was primarily a scientific exploration. Although extensive work was carried out on reactor physics, isotope separation, and nuclear data, Germany did not develop an atomic bomb. Evidence from the Farm Hall transcripts and later assessments by international physicists indicates that key technical knowledge and a focused weapons program were lacking.

After 1945, nuclear activities in Germany gradually resumed with an emphasis on theoretical studies and peaceful applications. The founding of the Gesellschaft für Kernforschung (KfK) in 1956 marked the start of large-scale nuclear research in Karlsruhe. Over the following decades, KfK built major experimental facilities, including research reactors, reprocessing plants, and extensive reactor safety programs. During the 1960s and 1970s, Karlsruhe became a central hub of German and European nuclear technology, with research covering reactor technology, fast breeder reactors, the nuclear fuel cycle, materials under irradiation, safeguards, and later fusion reactor technology.

From the late 1970s onward, energy policy shifts, major nuclear accidents (Three Mile Island and Chernobyl), and declining public acceptance led to the termination of key projects such as the Wackersdorf reprocessing plant and the fast breeder reactor SNR-300. This triggered a profound restructuring of the research center. Nuclear activities were reduced and refocused, while new programs emerged in environmental research, nanotechnology, astroparticle physics, medical technology, and synchrotron-based methods.

The merger of the Karlsruhe Research Center with the University of Karlsruhe to form KIT represents the culmination of this transformation. Today, KIT integrates strong basic research with large-scale applied science. Core nuclear competencies remain, particularly in reactor safety, radioactive waste management, and fusion research, and continue to shape KIT's guiding principle: new technologies must be thoroughly understood and rigorously tested before being deployed.

KfK

Forschungszentrum Karlsruhe
in der Helmholtz-Gemeinschaft

KIT
Karlsruher Institut für Technologie

Discovery of Fission on 16./17.Dezember 1938

Energiequellen

1. Gravitation
   Wasserkraft

2. Elektromagnetismus
   Sonne, Wind, Holz
   Kohle, Öl, Erdgas

3. Kernkraft

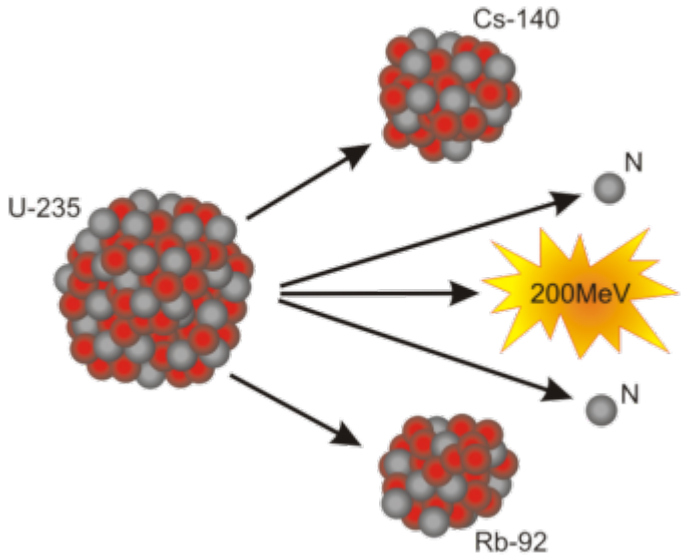

The Pre-History

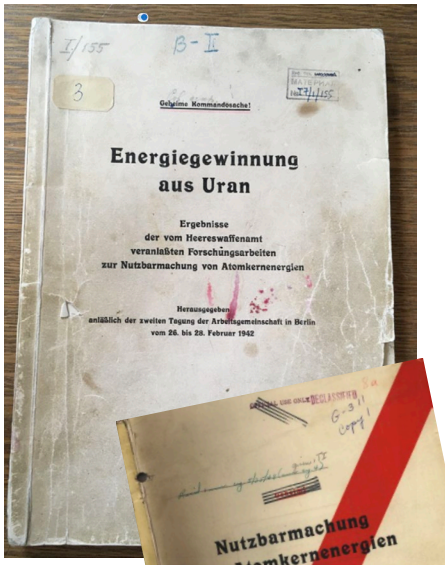

The German Uranium Project
1939-1945

400 Secret Reports
Report of Army Ordnance 2/1942
FIAT-Reports 1948
500 publications in Nuclear Physics
Farm Hall transcripts

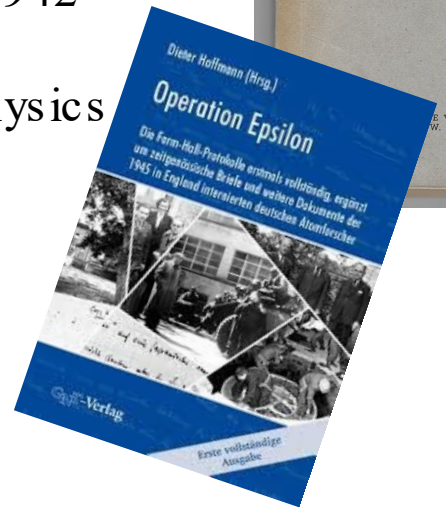

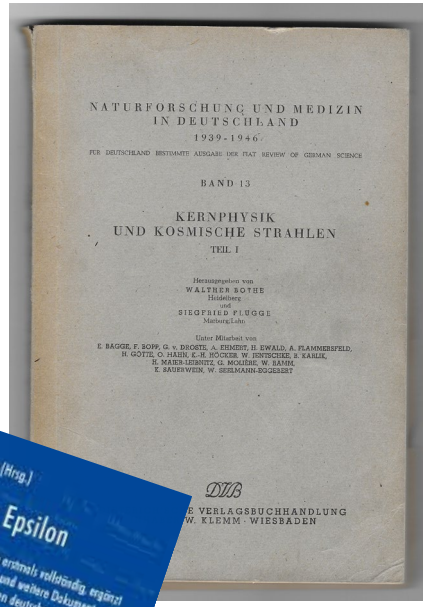

Pre-History 2

Manhattan Project	versus	Uranium Project
1942-1945		1939-1945
2 billion $	1 $ = 5 RM	10 Mio RM = 2 million $
140 000	Personal	100
	1000 : 1	
Huge industrial project		Scientific exploration

Results of the Uranium Project

400 Reports on

- Reactor physics (Heisenberg, Wirtz, Höcker, Döpel, Diebner)
- Isotope separation (Harteck, Groth, Clusius, Bagge)
- Nuclear Data (Bothe, Gentner, Kopfermann, Stetter, Jentschke, Maier-Leibnitz, Otto Haxel)l

No reports after may 1940:

- Explosive (Heisenberg)
- Plutonium (v. Weizsäcker)
  -)

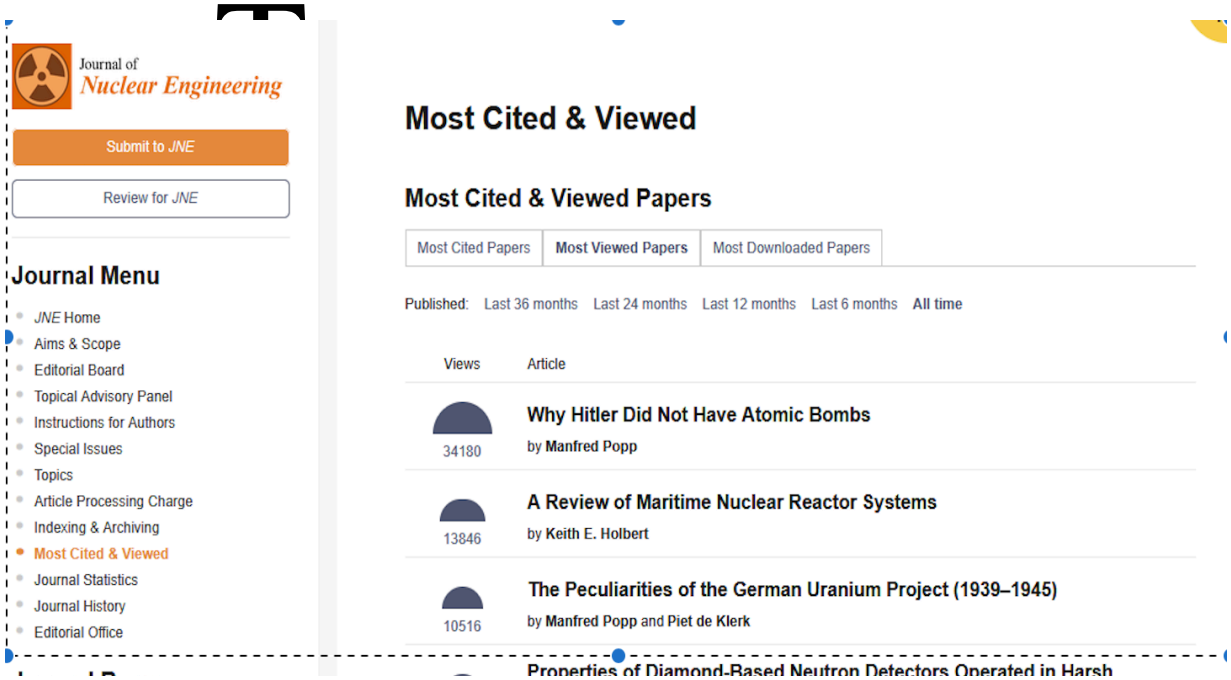

Pre-History 2

Manhattan Project	versus	Uranium Project
1942-1945		1939-1945
2 billion $	1 $ = 5 RM	10 Mio RM = 2 million $
140 000	Personal	100
	1000 : 1	
Huge industrial project		Scientific exploration

Uranium Project: Reactor Physics

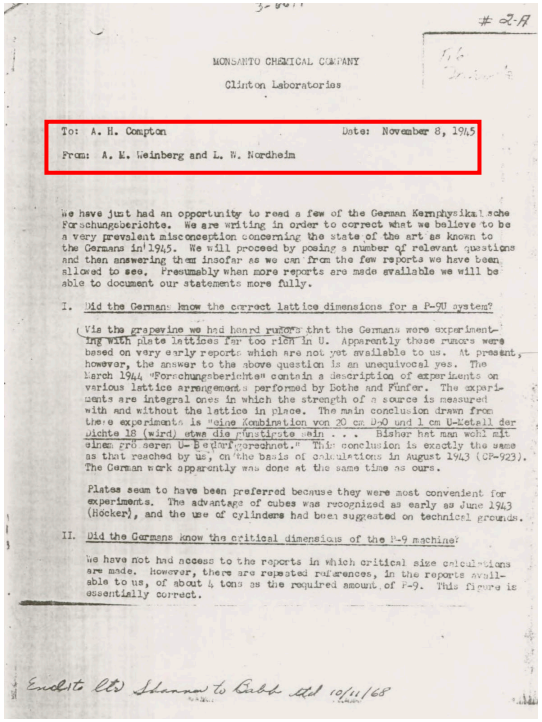

MONSANTO CHEMICAL COMPANY

Clinton Laboratories

To: A. H. Compton Date: November 8, 1945

From: A. M. Weinberg and L. W. Nordheim

We have just had an opportunity to read a few of the German Kernphysikalische Forschungsberichte. We are writing in order to correct what we believe to be a very prevalent misconception concerning the state of the art as known to the Germans in 1945. We will proceed by posing a number of relevant questions and then answering them insofar as we can from the few reports we have been allowed to see. Presumably when more reports are made available we will be able to document our statements more fully.

I. Did the Germans know the correct lattice dimensions for a P-9U system?

Via the grapevine we had heard rumors that the Germans were experimenting with plate lattices for too rich U. Apparently these rumors were based on very early reports which are not yet available to us. At present, however, the answer to the above question is an unequivocal yes. The March 1944 "Forschungsberichte" contain a description of experiments on various lattice arrangements performed by Dobbe and Fünfer. The experiments are integral ones in which the strength of a source is measured with and without the lattice in place. The main conclusion drawn from these experiments is "eine Kombination von 20 cm D2O und 1 cm U-Metall der Dichte 18 (wird) etwa die günstigste sein . . . Bisher hat man wohl mit einem pro seren U- Bedarf gerechnet." This conclusion is exactly the same as that reached by us, on the basis of calculations in August 1943 (CP-923). The German work apparently was done at the same time as ours.

Plates seem to have been preferred because they were most convenient for experiments. The advantage of cubes was recognized as early as June 1943 (Höcker), and the use of cylinders had been suggested on technical grounds.

II. Did the Germans know the critical dimensions of the P-9 machine?

We have not had access to the reports in which critical size calculations are made. However, there are repeated references, in the reports available to us, of about 4 tons as the required amount of P-9. This figure is essentially correct.

Enclosure ltr Shannon to Gibbs dtd 10/11/48

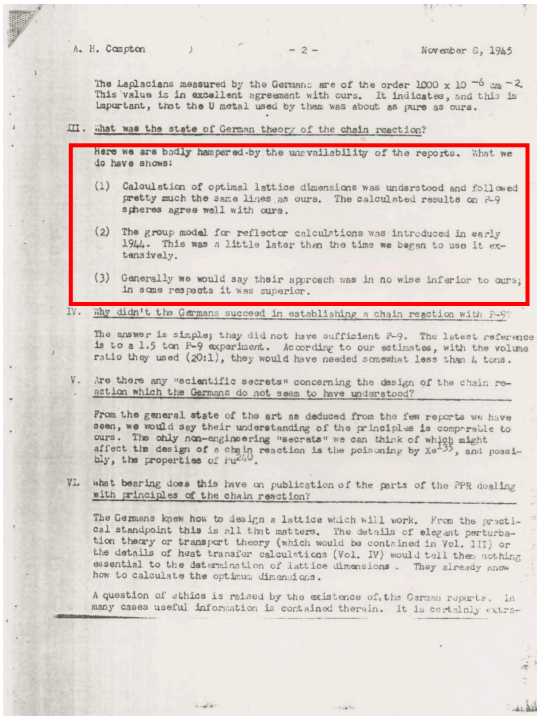

A. H. Compton - 2 - November 8, 1945

The Laplacians measured by the Germans are of the order 1000 x 10^{-6} cm^{-2}. This value is in excellent agreement with ours. It indicates, and this is important, that the U metal used by them was about as pure as ours.

III. What was the state of German theory of the chain reaction?

Here we are badly hampered by the unavailability of the reports. What we do have shows:

(1) Calculation of optimal lattice dimensions was understood and followed pretty much the same lines as ours. The calculated results on P-9 spheres agree well with ours.

(2) The group model for reflector calculations was introduced in early 1944. This was a little later than the time we began to use it extensively.

(3) Generally we would say their approach was in no wise inferior to ours; in some respects it was superior.

IV. Why didn't the Germans succeed in establishing a chain reaction with P-9?

The answer is simple; they did not have sufficient P-9. The latest reference is to a 1.5 ton P-9 experiment. According to our estimates, with the volume ratio they used (20:1), they would have needed somewhat less than 4 tons.

V. Are there any "scientific secrets" concerning the design of the chain reaction which the Germans do not seem to have understood?

From the general state of the art as deduced from the few reports we have seen, we would say their understanding of the principles is comparable to ours. The only non-engineering "secrets" we can think of which might affect the design of a chain reaction is the poisoning by Xe^{135}, and possibly, the properties of Pu^{240}.

VI. What bearing does this have on publication of the parts of the PPR dealing with principles of the chain reaction?

The Germans knew how to design a lattice which will work. From the practical standpoint this is all that matters. The details of elegant perturbation theory or transport theory (which would be contained in Vol. III) or the details of heat transfer calculations (Vol. IV) would tell them nothing essential to the determination of lattice dimensions. They already know how to calculate the optimum dimensions.

A question of ethics is raised by the existence of the German reports. In many cases useful information is contained therein. It is certainly extra-

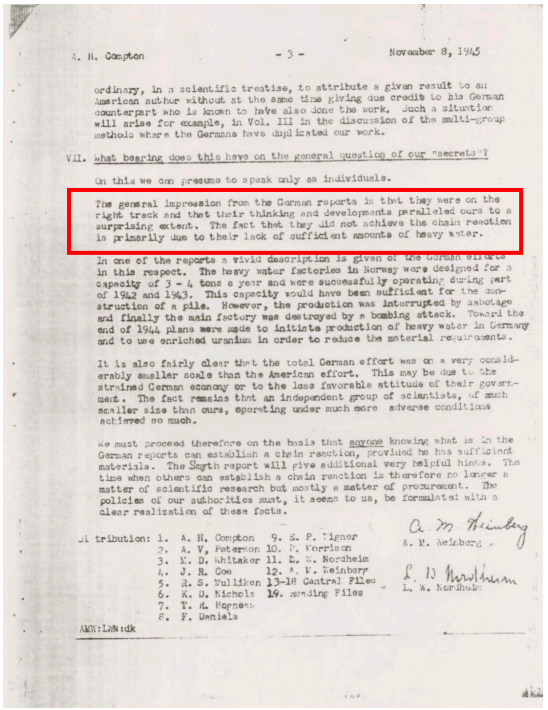

A. H. Compton - 3 - November 8, 1945

ordinary, in a scientific treatise, to attribute a given result to an American author without at the same time giving due credit to his German counterpart who is known to have also done the work. Such a situation will arise for example, in Vol. III in the discussion of the multi-group methods where the Germans have duplicated our work.

VII. What bearing does this have on the general question of our "secrets"?

On this we can presume to speak only as individuals.

The general impression from the German reports is that they were on the right track and that their thinking and developments paralleled ours to a surprising extent. The fact that they did not achieve the chain reaction is primarily due to their lack of sufficient amounts of heavy water.

In one of the reports a vivid description is given of the German efforts in this respect. The heavy water factories in Norway were designed for a capacity of 3 - 4 tons a year and were successfully operating during part of 1942 and 1943. This capacity would have been sufficient for the construction of a pile. However, the production was interrupted by sabotage and finally the main factory was destroyed by a bombing attack. Toward the end of 1944 plans were made to initiate production of heavy water in Germany and to use enriched uranium in order to reduce the material requirements.

It is also fairly clear that the total German effort was on a very considerably smaller scale than the American effort. This may be due to the strained German economy or to the less favorable attitude of their government. The fact remains that an independent group of scientists, of much smaller size than ours, operating under much more adverse conditions achieved so much.

We must proceed therefore on the basis that anyone knowing what is in the German reports can establish a chain reaction, provided he has sufficient materials. The Smyth report will give additional very helpful hints. The time when others can establish a chain reaction is therefore no longer a matter of scientific research but mostly a matter of procurement. The policies of our authorities must, it seems to us, be formulated with a clear realization of these facts.

A. M. Weinberg

L. W. Nordheim

Distribution: 1. A. H. Compton 9. S. P. Tigner
2. A. V. Peterson 10. P. Morrison
3. M. D. Whitaker 11. L. W. Nordheim
4. J. R. Cox 12. A. M. Weinberg
5. R. S. Mulliken 13-18 Central Files
6. K. D. Nichols 19. Reading Files
7. T. M. Hogness
8. F. Daniels

AMW:LWN:dk

The reactor experiments

Year			
1940	Hamburg (Harteck)		
	185 kg U/ 15 t CO_2 ice		
	Berlin/Haigerloch	Leipzig	HWA (Gottow/Stadtilm)
	Heisenberg/Wirtz	Heisenberg/Döpel	Diebner
1940	B1 uranium oxide/paraffin	L1 uranium oxide/paraffin	G1 uranium oxide/Paraffin194119419
	B2 uranium oxide/paraffin	L2 142 kg U/ 164 kg D_2O	G2a 200 kg U, 220l D_2O-
1942	B3 551 kg U/ 44 kg paraffin	L3 uranium metal/150 l D_2O	G2b 200 kg U, 220l D_2O-ice
	B4 740 kg U/ 37 kg paraffin	L4 755 kg U/164 kg D_2O	
	B5 864 kg U/ 8 kg paraffin		
1943	B6a-d 0,9 -2,2 t U/1,5 t D_2O		G3a 540 kg U/525 l D_2O
1944	B7 2,2 t U/1,5 t D_2O		G3b 540 kg U/525 l D_2O
1945	B8 1,5 t U/1,5 t D_2O/ 10 t graphite		G4 ?

Uranium Project: Reactor Physics

The German Reactor Experiments 1940-1945
in the Light of Modern Reactor Physics

Ron Dagan, Manfred Popp
Karlsruhe Institute of Technology, Hermann von Helmholtz-Platz 1, 76344 Eggenstein-Leopoldshafen
ron.dagan@kit.edu; popp@kit.edu,

Farm Hall (07/45 – 01/46)

Heisenberg v. Weizsäcker Hahn Diebner Gerlach Harteck von Laue Wirtz Bagge und Korsching

3.9 Heisenberg on the atomic bomb at Farm Hall

August 6 Heisenberg tries to calculate the critical mass of a bomb with 20 kt power. He got 1 t, but only by mistake. His result should have been 12,5 t.
August 14, Heisenberg gives a lecture on the physics of the bomb,

Hans Bethe:
„ These two lectures prove to me that Heisenberg, the scientific leader of the German effort, did not work on a bomb. They show that he did not know critical information, and that he could have derived the information if he had tried.“
Bethe, Hans: The German Uranium Project, Physics Today (2000) 34-36

Edward Teller:

Theoretical Nuclear Technology 1946-1955 Göttingen

1946 No nuclear physicist invited to the USA

1948 Max-Planck-Institut für Physik in Göttingen

Physikalische Studien-Gesellschaft

1955 Geneva Conference: Atoms for Peace

Karl Wirtz and Otto Hahn

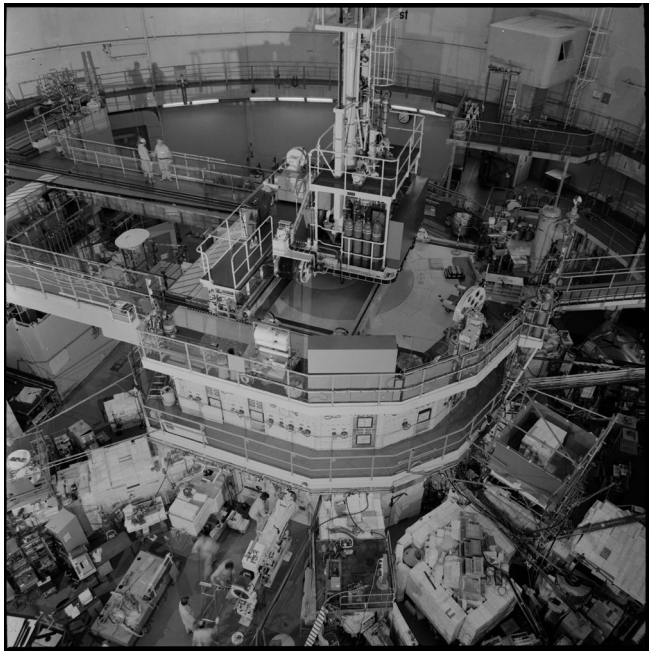

Juli 1956 Company for Reactor-Construction and -Operation

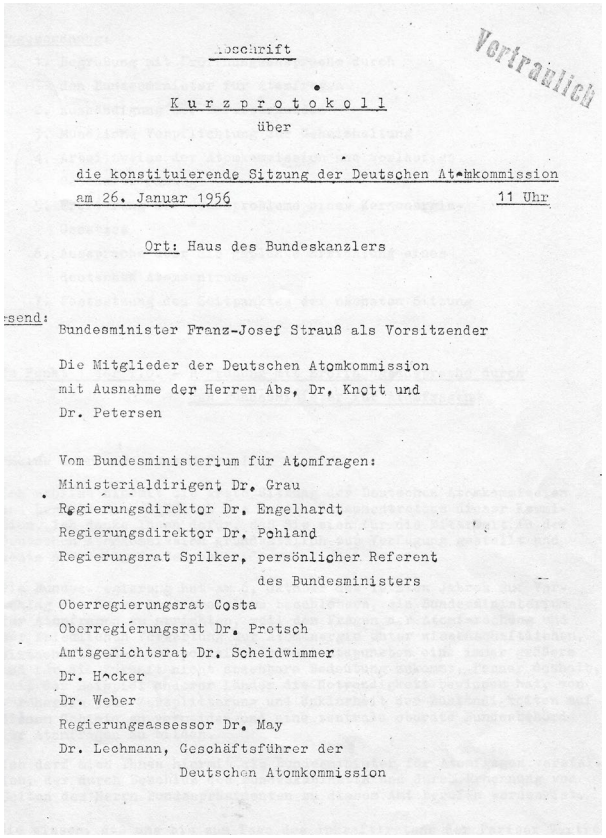

Abschrift

Vertraulich

Kurzprotokoll

über

die konstituierende Sitzung der Deutschen Atomkommission
am 26. Januar 1956 11 Uhr

Ort: Haus des Bundeskanzlers

ssend:

Bundesminister Franz-Josef Strauß als Vorsitzender

Die Mitglieder der Deutschen Atomkommission
mit Ausnahme der Herren Abs, Dr. Knott und
Dr. Petersen

Vom Bundesministerium für Atomfragen:
Ministerialdirigent Dr. Grau
Regierungsdirektor Dr. Engelhardt
Regierungsdirektor Dr. Pohland
Regierungsrat Spilker, persönlicher Referent
des Bundesministers
Oberregierungsrat Costa
Oberregierungsrat Dr. Protsch
Amtsgerichtsrat Dr. Scheidwimmer
Dr. Hacker
Dr. Weber
Regierungsassessor Dr. May
Dr. Lechmann, Geschäftsführer der
Deutschen Atomkommission

Birth of the Karlsruhe Research Center.

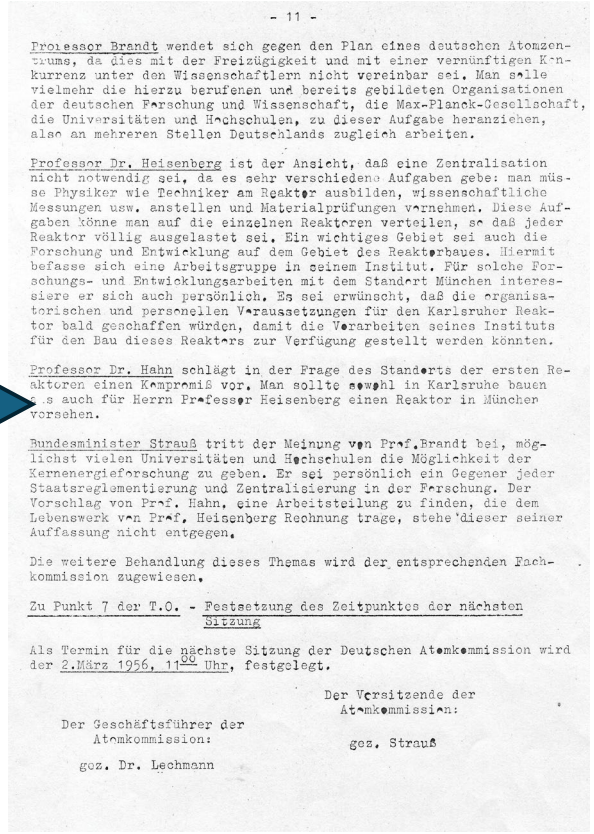

- 11 -

Professor Brandt wendet sich gegen den Plan eines deutschen Atomzentrums, da dies mit der Freizügigkeit und mit einer vernünftigen Konkurrenz unter den Wissenschaftlern nicht vereinbar sei. Man solle vielmehr die hierzu berufenen und bereits gebildeten Organisationen der deutschen Forschung und Wissenschaft, die Max-Planck-Gesellschaft, die Universitäten und Hochschulen, zu dieser Aufgabe heranziehen, also an mehreren Stellen Deutschlands zugleich arbeiten.

Professor Dr. Heisenberg ist der Ansicht, daß eine Zentralisation nicht notwendig sei, da es sehr verschiedene Aufgaben gebe: man müsse Physiker wie Techniker am Reaktor ausbilden, wissenschaftliche Messungen usw. anstellen und Materialprüfungen vornehmen. Diese Aufgaben könne man auf die einzelnen Reaktoren verteilen, so daß jeder Reaktor völlig ausgelastet sei. Ein wichtiges Gebiet sei auch die Forschung und Entwicklung auf dem Gebiet des Reaktorbaues. Hiermit befasse sich eine Arbeitsgruppe in seinem Institut. Für solche Forschungs- und Entwicklungsarbeiten mit dem Standort München interessiere er sich auch persönlich. Es sei erwünscht, daß die organisatorischen und personellen Voraussetzungen für den Karlsruher Reaktor bald geschaffen würden, damit die Vorarbeiten seines Instituts für den Bau dieses Reaktors zur Verfügung gestellt werden könnten.

Professor Dr. Hahn schlägt in der Frage des Standorts der ersten Reaktoren einen Kompromiß vor. Man sollte sowohl in Karlsruhe bauen als auch für Herrn Professor Heisenberg einen Reaktor in München vorsehen.

Bundesminister Strauß tritt der Meinung von Prof. Brandt bei, möglichst vielen Universitäten und Hochschulen die Möglichkeit der Kernenergieforschung zu geben. Er sei persönlich ein Gegner jeder Staatsreglementierung und Zentralisierung in der Forschung. Der Vorschlag von Prof. Hahn, eine Arbeitsteilung zu finden, die dem Lebenswerk von Prof. Heisenberg Rechnung trage, stehe dieser seiner Auffassung nicht entgegen.

Die weitere Behandlung dieses Themas wird der entsprechenden Fachkommission zugewiesen.

Zu Punkt 7 der T.O. - Festsetzung des Zeitpunktes der nächsten Sitzung

Als Termin für die nächste Sitzung der Deutschen Atomkommission wird der 2.März 1956, 11[30] Uhr, festgelegt.

Der Vorsitzende der
Atomkommission:

gez. Strauß

Der Geschäftsführer der
Atomkommission:

gez. Dr. Lechmann

Karlsruhe Nuclide Chart

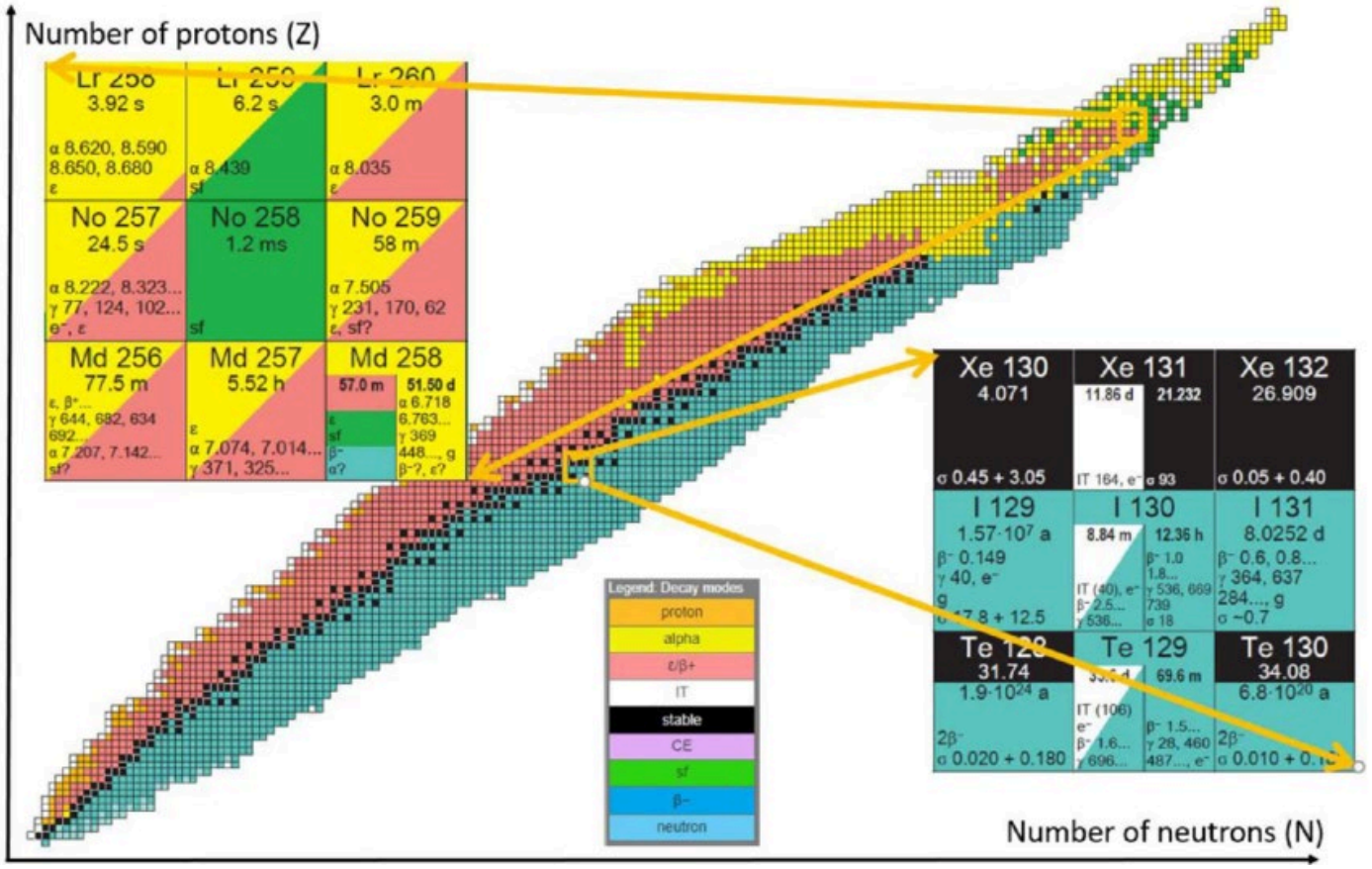

1958: 1517 – 2022:4017. W. Seelmann-Eggebert (1915-1988) until 1981
Gerda Pfennig (+2017) until 2015
Since 2006 JRC Karlsruhe, sinde 2012 Nucleonica

The reactor station grew…..

…..until end of 1958 in 5 steps:

A – C (70 Mio DM) Kernreaktor GmbH. - K1
D – E (70 Mio DM) Bund und Land - K2

Main Project: FR-2

15 Institutes
Administration Building
Central Workshop
Computer center
Canteen

Architect: Erich Schelling

1961: Large experimental facilities

Multi-purpose research reactor MZFR
- Hot-Steam-Reactor Großwelzheim /Main

Compact Ba-cooled nuclear reactor
- Nuclear Power Station
- Niederaichbach/Isar ($D_2O - CO_2$)

Pilot-Reprocessing plant Karlsruhe

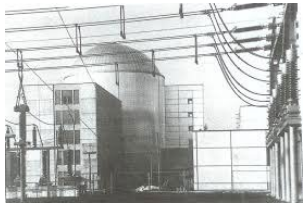



The project-structure of KfK

- Institutes: Expert
- Projects: Finances
- Directors of institutes and projects on equal footing
- R&D-Commissions decide
- Internal reporting system

KfK- Program in the 1970s.

- Reactortechnology
- Material research (radiation damage)
- Fast Breeder
- Instrumental fissile material flow control (Safguards)
- Actinides
- Nuclear fuel cycle (reprocessinf, waste management and final storage)
- First steps into environmental research

Nuclear - and Computer-technology grow in parallel

counter

1957 Computing center

Reason: digital measurements in nuclear physics :

„Otto Hahn‘s table“

1960s: First joint ventures with the university

Institut für Kernverfahrenstechnik (separartion nozzle)

- 1958 TH Karlsruhe: Professorship for Erwin Willy Becker
- 196? Institute built by BMAt
- 196? Extension and technolpgy center by KfK

1964 Rektor as guest in supervisory committeee

Institute for nuclear physics

- 1964 new building, also for University
- University propvides workshop (until 2009)
- No joint program

1967 University may use the KfK Computing center
1964 -1970 joint calls of professors with difficulties

End of 1960s Jahre: 1 st ideas of phasing out nuclear research

1969 Begin of Biblis A (1300 MWe)

1968 Landing on the Moon

1969 KfK-Kommission "Future tasks of kfK
1971 Presentation by Prof. Horst Böhm

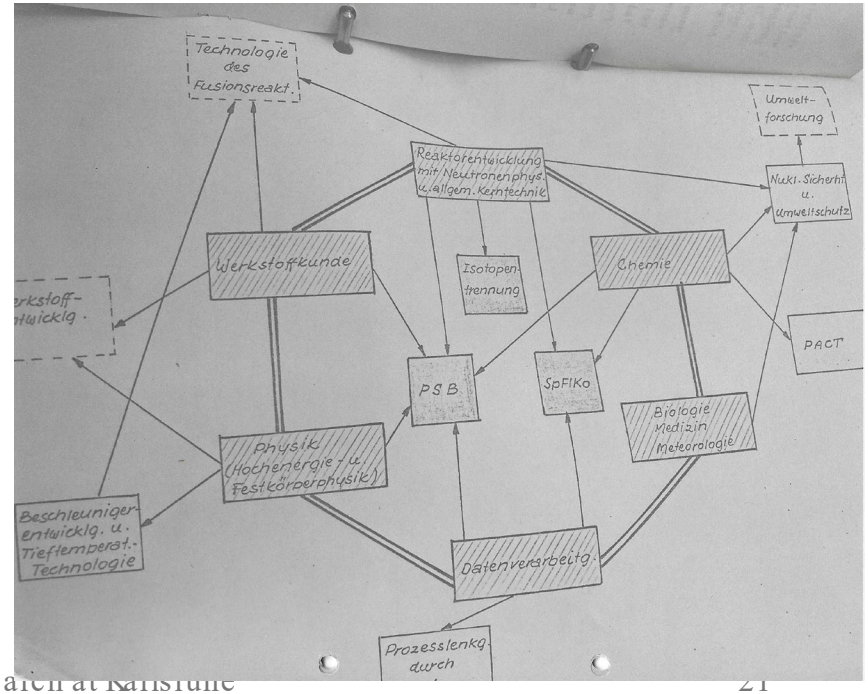

Early 1970s: The planned progress by big science

ICE und TRANSRAPID

AIRBUS und ARIANE

THTR 300 und SNR 300

1972 : Diversification of nuclear research centers

1. März 1972: Quickborner Team:
   „Mobility and Diversification of nuclear research centers

New structure:
   Federal Government 90 %, Land 10%
   Industrial Organization

New activities:
Environmental research and technology
Biology and Medicine

1974 : New Energy Policy

1973	4th „Atomprogramm“ 1973-1976
1973	1st Energy crises
1974	1.Energy-Program “Away from oil!"
	45 GWe Kernenergie
	Stabilisation of domestic coal production
1974	1st non-nuclear energy eseach Energieforschung
	1st Energy research program

New tasks for KfK: back to nuclear
Nuclear Safety, Reprocessing, Waste Managemant and Storage, Fast Breeder.

The international sodium fast breeder cooperation

International consensus: Breeders necessary because of Limitations of the world's unranium reserves

Breeder development
in Europe: F, NL, B, F, D
World: USA, UdSSR, Japan, Indien

All (!) for Na-cooled breeder
Int. Exchange of know how

1970 Phenix, SNR 300, Phenix (F), BN350(UdSSR), Monju (J), Kalpakkam,
1980 Superphenix (F) , planning SNR2 (D, B, NL) by utilities
.
44. MeetingKfK-AR in May1986 in Creys-Malville

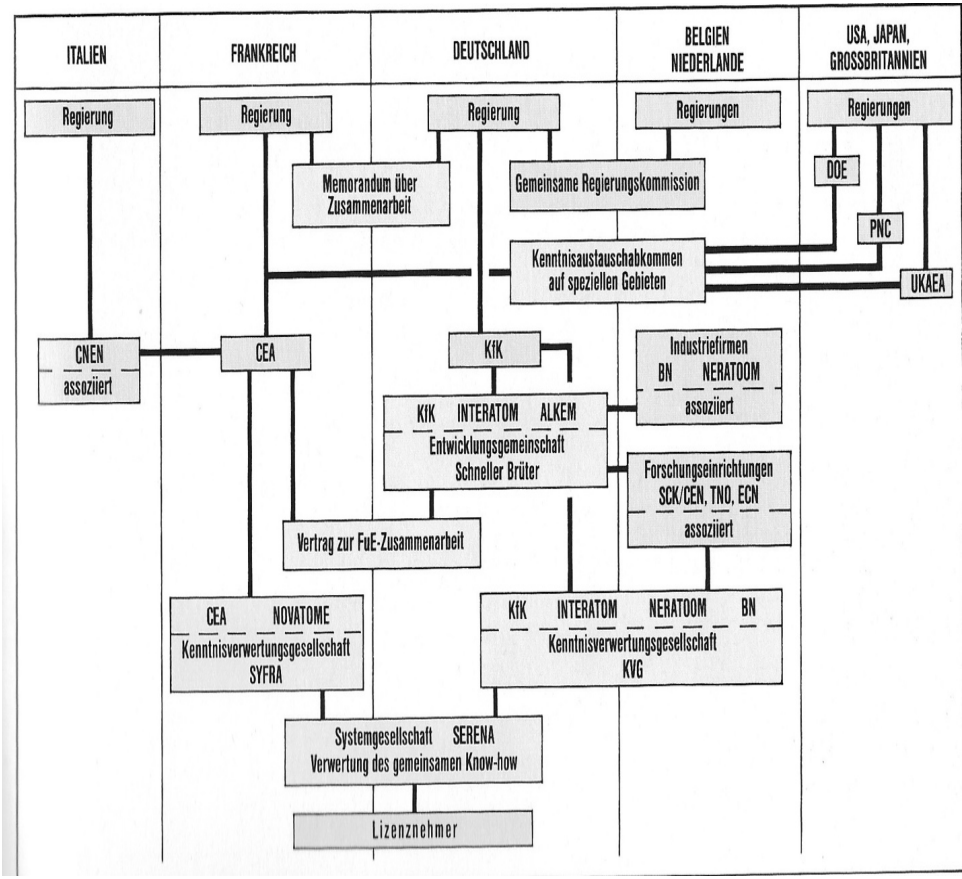

Project Reprocessing (1st civil plant)

1974 DWK founded

1978. Test facility MILLI (35 kg Pu)

1979 KfK as industrial partner for DWK
for the construction of Wackersdorf plant

1979 TEKO (Test facility for components)

Annually 12,5 Mio DM Licences fromr DWK.

Development of MOX-fuel

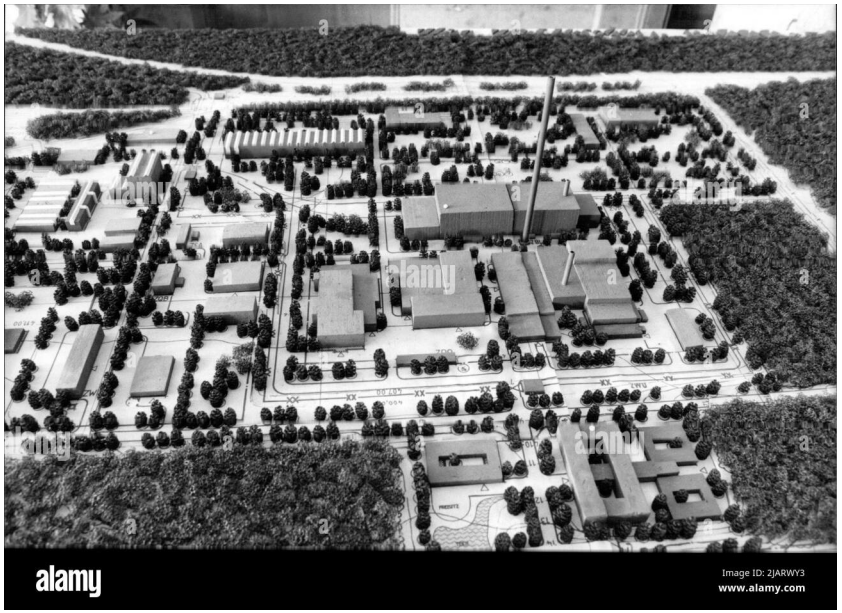

Project Nuclear Safety

1972 Project Nuclear Safety

1975-1991 HDR-Safety research proram

1979 Three mile Island

Conrributions th German risk study for NPPs

198?-1992 BETA fro core melt-concrete interctio

1986 Cernobyl

1987 Begin of „hypotheticak accidents

1991 Begin of design work for EPR

1991 Begin of cooperation with Russia, later in EU-Japan-USA-program

Fusion reactor technology

:

- Superconducting magnets
- 1976 Tokamak coil
  for international competetion at Oak Ridge (USA),
  1987: highest ranking
- Blanket (more dpa than breeder
- Tritium-Laboratory

Kernphysik

Keine Gemeinsamkeit mit Uni-Kernphysik, da BMFT eine weitere Verstärkung der Elementarteilchenpjysik ablehnte.

GALLEX–Experiment im Gran Sasso

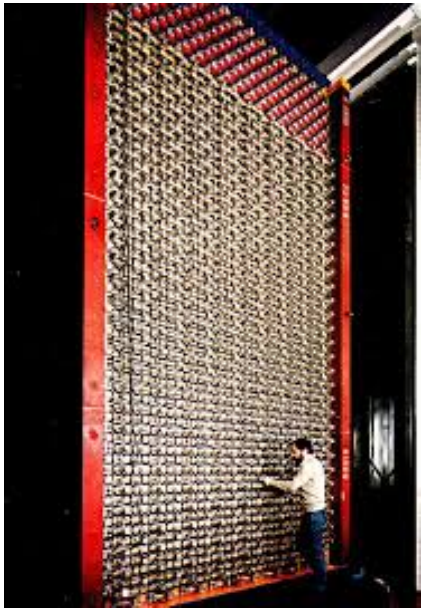

KARMEN: Neutrino-Experiment at SNS Rutherford (GB)

KASKADE: Cosmicde

1986 Decline of public and political acceptance of nuclear power and big science

Large accidents:

- Challenger
- Cernobyl

Depression in industry in general

1989/1991 two abrupt project terminations

KfK-planning for reduction of nuclear power program

May1989 Stop of the almost completet reprocessing facility at Wackersdorf by the utilities because of dumping offers from France.

March 1991, decision not to start hot operation of SNR 300.

My turn as CEO started exactly on that day

Kfk-planning for faster reduction of nuclear program

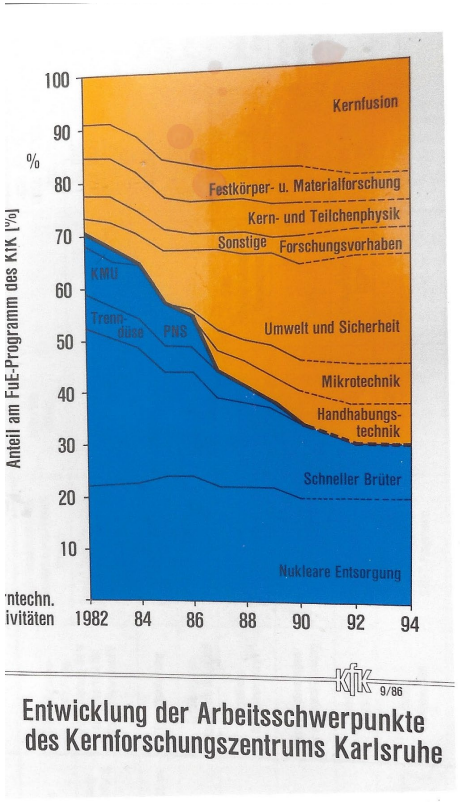

Entwicklung der Arbeitsschwerpunkte des Kernforschungszentrums Karlsruhe

Framework for programatic change

- Budgetary strains because of re-unification
- Poor proposals by external advisrory committee
- Loss of 750 positions

+. High Quality and Motivation of staff

+ More publications by stopping internal reporting sxstem

+ eserves in personnell and finance in the oversized infrastructure

Priciples for changing more than 50% of the program

- No cancellation of contracts, only early retirements
- No termination of institutes except when staff had left to new jobs.
- Convincing staff memebrs for new challenges
- New program based on special competences from nuclear
- Closure of old and openeing of new instituts (25)
- Less infratsructure more science

Der Wandel zum FZK

Umwandlung und Neuschaffung von Instituten

Aufgelöst

Institute:

- IK II (Inst. f. Kernphysik II)
- Labor f. Isotopentechnik II
- PKÜ (Kernmaterialüberwachung)

Projekte:

- PKÜ (Kernmaterialüberwachung)
- PSB (Schneller Brüter)
- HDR (Sicherheit/Handhabungstechnik)
- MZFR, KKN
- PWA (Wiederaufarbeitung/Abfallbehandlung)
- LWR-Sicherheit

Neugegründet

Institute:

- IMK 1
- IMK 2
- ITC-WGT
- INT

Projekte:

- PSA
- PKF
- PMT
- PEA
- KEF

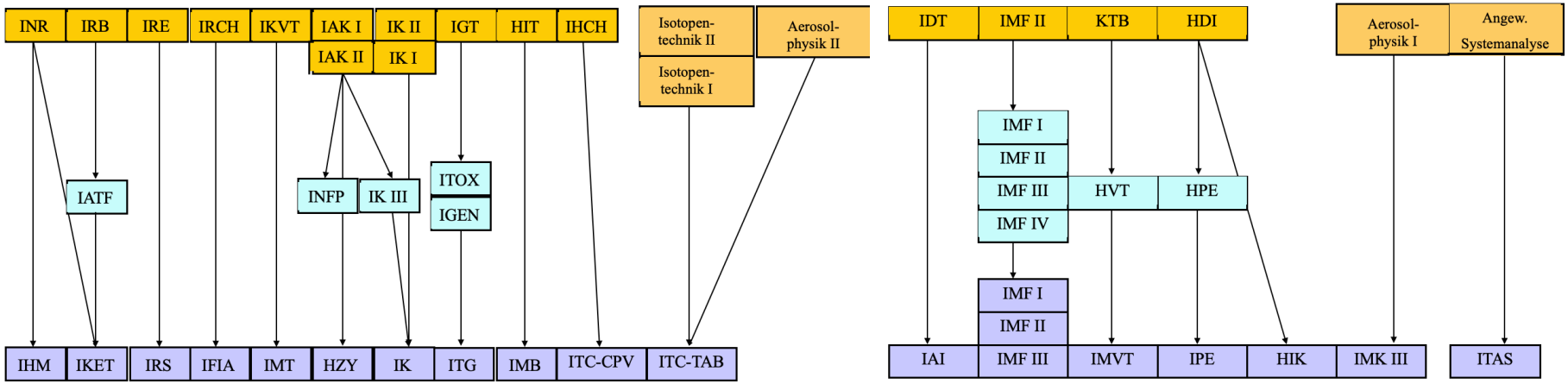

After 40 years: „Research center Karlsruhe“

Karlsruher Institut für Technologie

New program based on excellent nuclear know how:

- Use of synchrotron radiation in manufacture of micro-structures
- Nanotechnology: single atoms identification by decay, cloud chamber, radiochemistry (Gallex: few Ge atoms out of 101 t Ga Cl)
- Minimal invasive surgery (remote handling)
- Astroparticle physics

Continud nuclear R&D:

- Experiments for EPR
- Waste management and final stoprage
- Fusion reactor technology

2000: New large projects in Nuclear Physics

KATRIN-Neutrinoexperiment

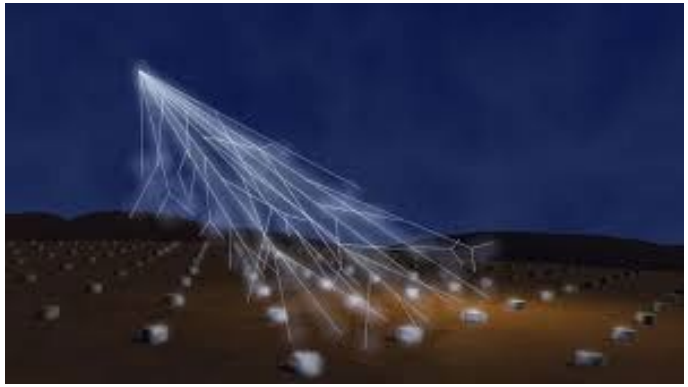

Pierre Auger Observatory

1996 -2006 from FZK to KIT

Change in research policy: less applied more excellent basic science

Program-oriented funding: less administrative steering, more evaluations

Change in FZK: less problem-oriented, more opportunity oriented program

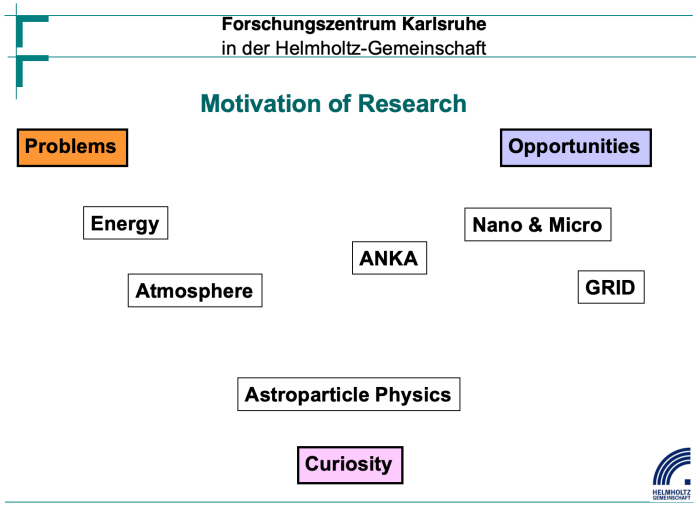

KIT represents a unique opportunity

Forschungszentrum Karlsruhe GmbH

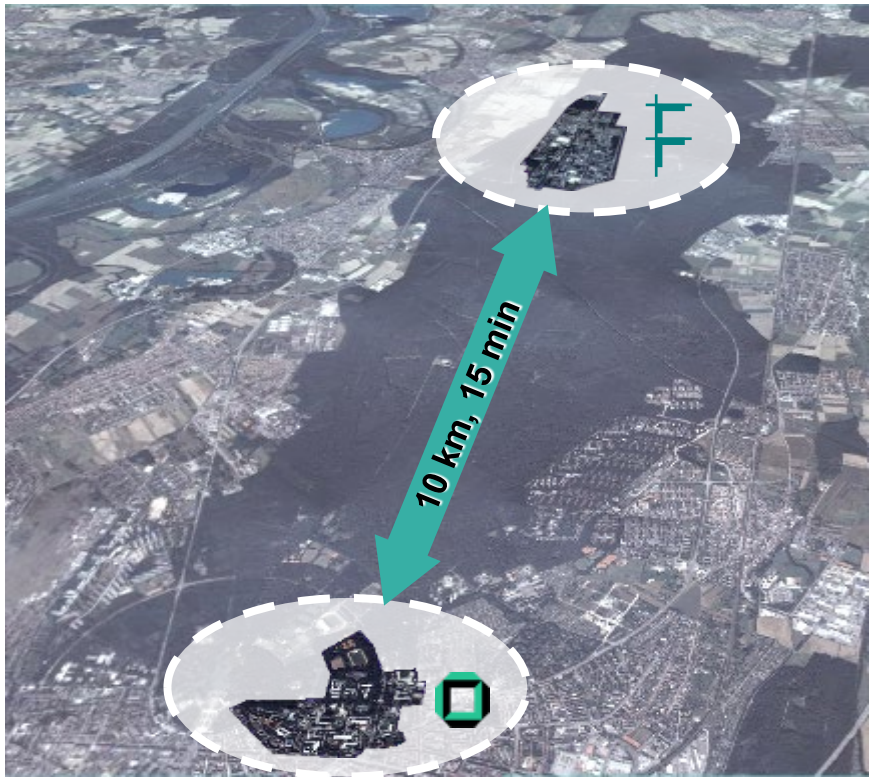

Universität Karlsruhe

KIT

Forschungszentrum Karlsruhe GmbH		Universität Karlsruhe (TH)	
10	programs	11	faculties
27	institutes	118	institutes
3,800	employees	4,000	employees
€305M	budget	€250M	budget
		18,500	students

Natural sciences and technical engineering

excellent overlap and complement
great synergies

Karlsruher Institut für Technologie

Synergies by KIT

Research center	University
Strong basic funding	poor basic funding
Demand for young scientists	Education of young scientists

Students participation in research – expert participation in lecturing

Better chances for third party financing

Broader basis for participation in Helmholtz-programs

Phases of reactor safety research

1956 : Industry can take over in 1960
1958: Begin of materials research
1965-75: HDR Safety Program (Components, pressure Vessel
1970s. German Risk study
1979: Three Miles Island.
1980s: Mitigation of accidents: BETA, CORA
1986: Cernobyl
1990s: Control of accidents: Basics for EPR, Hydrogen control
1990s: Cooperation with Russia: Hydrogen, Synchrotron,
Conversion of Russian war heads to MOX fuel

What lives on from nuclear power research in KIT?

- Directly:
  - a base load in nuclear safety research
  - Participation in European programs
  - Research for safe disposal of radioactive waste
  - Fusion reactor technology
  - Application of nuclear safety know how in other aereas.

- Indirectly:
  - The principle: What we do, we do thoroughly.
  - For us nothing is impossible.
  - New technologies need to be thoroughly investigated before used.

2006: Die KIT-Idee siegt

Zoltan Hozer
HUN-REN EK

Overview of the CODEX Experimental Programme

At the CODEX (COre Degradation EXperiment) facility, a total of 20 experiments were conducted between 1995 and 2024 to simulate fuel behavior during the early phase of core degradation. The first experiments focused on comparing VVER and PWR cladding materials. These were followed by investigations of the consequences of air ingress and control rod degradation processes. The fuel degradation event that occurred in a cleaning tank at the Paks Nuclear Power Plant (NPP) was also simulated in two dedicated experiments. Detailed analyses of loss-of-coolant accident (LOCA) scenarios in both the reactor and the spent fuel pool were performed. Specific design extension condition (DEC) scenarios were also investigated, based on NPP reference cases such as station blackout (SBO) and nitrogen injection from hydroaccumulators. The two most recent experiments were dedicated to the testing of Accident Tolerant Fuel (ATF) designs.

The experimental program included both seven-rod hexagonal (VVER-type) and 3×3 rod square-lattice (PWR-type) bundles, with heated lengths ranging from 600 mm to 1000 mm. In the early tests, UO_2 pellets were used as fuel simulants; these were later replaced with Al2O3 and ZrO_2 ceramics. A wide variety of cladding materials were employed, including traditional E110, sponge-based E110, thin-walled E110, Zircaloy-4, optZIRLO™ and Cr-coated optZIRLO™. The heating methods applied to the fuel rods were gradually refined over the years. By enabling internal pressurization of the rods, additional phenomena such as ballooning, burst, and secondary hydriding could be investigated. Temperature measurements were supported by a large number of thermocouples, which formed the core of the data acquisition system. Pressures and flow rates were also measured at several positions in the facility. The composition of the outlet gas was analyzed using thermal conductivity detectors, and later by mass spectrometry. In several specific experiments, the main parameters of the released aerosols were characterized, while in another test, on-line X-ray imaging was performed.

The maximum cladding temperatures ranged from 874 °C to 2300 °C, and the total hydrogen production reached up to 33 g. Depending on the simulated scenario, the tests were terminated either by water quenching or by slow cool-down in an argon atmosphere. Following each test, various post-test examinations were conducted to characterize the condition of the bundle. In most cases, the bundles were fixed in epoxy, and cross-sections were prepared for analysis using light optical microscopy and scanning electron microscopy. In cases where the fuel rods were not embedded, additional mechanical tests (four-point bending, ring compression), computed tomography, or prompt-gamma activation imaging were performed. Selected bundle fragments were also examined in hot vacuum extraction facilities to determine the amount of absorbed hydrogen.

Over the three decades of operation, a close collaboration developed between the CODEX and QUENCH teams. Several parallel and complementary experiments were conducted, and the CODEX program received very valuable technical support from KIT experts. Some memorable moments of this long-standing collaboration will be highlighted in the presentation.

HUN REN Centre for Energy Research

MTA Centre of Excellence

HUN-REN Hungarian Research Network

HUN-REN Centre for Energy Research

Overview of the CODEX Experimental Programme

Zoltán Hózer, Róbert Farkas, Nóra Vér

30th International QUENCH Workshop
Karlsruhe, 16-18 December 2025

Research. Innovation. Impact.

Content

CODEX experiments 1995-2025

- Core degradation experiments: scenarios, fuel design, post-test examinations
- Coolability experiments

Necessary conditions for successful execution of tests

- Materials, team, projects and financing

How was CODEX created?

- Some history, NIELS

Examples of QUENCH-CODEX co-operation

- Air ingress phenomena
- Control rod degradation

Conclusions

CODEX experiments 1995-2025

CODEX core degradation tests 1995-2025

Test	Bundle type	Pellet	Cladding material	Max. temp.	Hydrogen production	Cool-down	Test type	Year
CODEX-1	7-rod VVER	Al_2O_3	E110	>2000 °C	n.m.	slow	Scoping test	1995
CODEX-2	7-rod VVER	UO_2	E110	2400 °C	26.6 g	slow	Escalation and slow cooling down	1995
CODEX-3/1	7-rod VVER	UO_2	E110	1158 °C	0.05 g	bottom quench	Water quench at 1150 °C	1996
CODEX-3/2	7-rod VVER	UO_2	E110	1643 °C	1 g	bottom quench	Water quench at 1500 °C	1997
CODEX-AIT-1	9-rod PWR	UO_2	Zircaloy-4	2000 °C	0 g	slow	Air ingress	1998
CODEX-AIT-2	9-rod PWR	UO_2	Zircaloy-4	1880 °C	n.m.	slow	Steam oxidation and air ingress	1999
CODEX-B4C	7-rod VVER	UO_2,B_4C	E110, stainless steel	2300 °C	25 g	slow	Control rod degradation	2001
CODEX-CT-1	7-rod VVER	Al_2O_3	E110	1245 °C	33 g	bottom quench	Long term oxidation and quench	2006
CODEX-CT-2	7-rod VVER	Al_2O_3	E110	1384 °C	13 g	bottom quench	Treatment in hydrogen and quench	2006
CODEX-LOCA-200	7-rod VVER	Al_2O_3	E110, E110G	908 °C	n.a.	bottom quench	Large break LOCA	2015
CODEX-LOCA-E4	7-rod VVER	Al_2O_3	E110, E110G	874 °C	n.a.	bottom quench	Shutdown LOCA	2016
CODEX-LOCA-200B	7-rod VVER	Al_2O_3	E110, E110G	1089 °C	n.a.	bottom quench	Large break LOCA	2016
CODEX-LOCA-SFP1	7-rod VVER	Al_2O_3	E110, E110G	924 °C	n.a.	bottom quench	Spent fuel pool LOCA	2017
CODEX-LOCA-SFP2	7-rod VVER	Al_2O_3	E110, E110G	896 °C	n.a.	bottom quench	Spent fuel pool LOCA	2017
CODEX-AIT-3	7-rod VVER	ZrO_2	E110G	1625 °C	5.2 g	slow	Air ingress with oxygen and steam starvation	2018
CODEX-NITRO	7-rod VVER	ZrO_2	E110, E110G	1748 °C	11 g	slow	Nitrogen injection from hyroaccumulators	2018
CODEX-SBO	7-rod VVER	ZrO_2, Al_2O_3	E110, E110G	1900 °C	32 g	bottom quench	Station blackout	2019
CODEX-SLIM	7-rod VVER	Al_2O_3	E110G	900 °C	0.69 g	bottom quench	LOCA with thin-walled cladding	2021
CODEX-ATF	7-rod VVER	ZrO_2, Al_2O_3	optZIRLO™, Cr coated optZIRLO™	1655 °C	3 g	bottom quench	severe accident with ATF	2023
CODEX-ATF-AIT	7-rod VVER	ZrO_2, Al_2O_3	Cr coated optZIRLO™	1544 °C	4.7 g	slow	Air ingress test with ATF	2024

CODEX scenarios

Test
CODEX-1
CODEX-2
CODEX-3/1
CODEX-3/2
CODEX-AIT-1
CODEX-AIT-2
CODEX-B4C
CODEX-CT-1
CODEX-CT-2
CODEX-LOCA-200
CODEX-LOCA-E4
CODEX-LOCA-200B
CODEX-LOCA-SFP1
CODEX-LOCA-SFP2
CODEX-AIT-3
CODEX-NITRO
CODEX-SBO
CODEX-SLIM
CODEX-ATF
CODEX-ATF-AIT

Reactor accidents

- LBLOCA
- Shut-down LOCA
- LOCA in spent fuel pool
- Station blackout
- Lower head failure
- Nitrogen from hydroaccumulators
- Cleaning tank incident

Phenomena

- Escalation due to oxidation in steam and air
- Control rod degradation
- Steam starvation
- Oxygen starvation (air)
- ATF behavior in steam
- ATF behavior in steam+air

Test type	Year
Scoping test	1995
Escalation and slow cooling down	1995
Water quench at 1150 °C	1996
Water quench at 1500 °C	1997
Air ingress	1998
Steam oxidation and air ingress	1999
Control rod degradation	2001
Long term oxidation and quench	2006
Treatment in hydrogen and quench	2006
Large break LOCA	2015
Shutdown LOCA	2016
Large break LOCA	2016
Spent fuel pool LOCA	2017
Spent fuel pool LOCA	2017
Air ingress with oxygen and steam starvation	2018
Nitrogen injection from hyroaccumulators	2018
Station blackout	2019
LOCA with thin-walled cladding	2021
severe accident with ATF	2023
Air ingress test with ATF	2024

CODEX bundle designs

Test	Bundle type
CODEX-1	7-rod VVER
CODEX-2	7-rod VVER
CODEX-3/1	7-rod VVER
CODEX-3/2	7-rod VVER
CODEX-AIT-1	9-rod PWR
CODEX-AIT-2	9-rod PWR
CODEX-B4C	7-rod VVER
CODEX-CT-1	7-rod VVER
CODEX-CT-2	7-rod VVER
CODEX-LOCA-200	7-rod VVER
CODEX-LOCA-E4	7-rod VVER
CODEX-LOCA-200B	7-rod VVER
CODEX-LOCA-SFP1	7-rod VVER
CODEX-LOCA-SFP2	7-rod VVER
CODEX-AIT-3	7-rod VVER
CODEX-NITRO	7-rod VVER
CODEX-SBO	7-rod VVER
CODEX-SLIM	7-rod VVER
CODEX-ATF	7-rod VVER
CODEX-ATF-AIT	7-rod VVER

PWR and VVER bundles

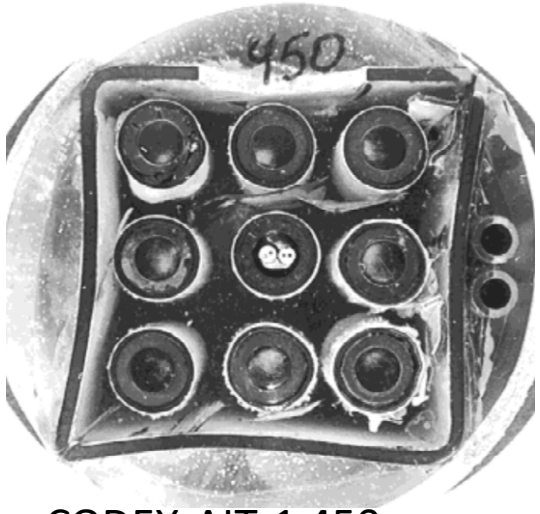

CODEX-AIT-1 450 mm

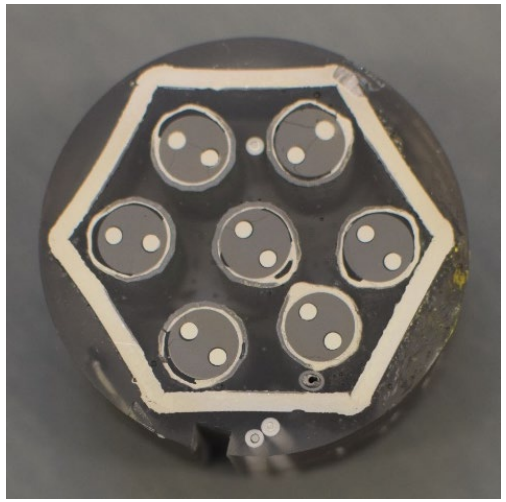

CODEX-ATF 200 mm

1 tungsten heater

2 tungsten heaters

- Closed top
- Internal pressurisation

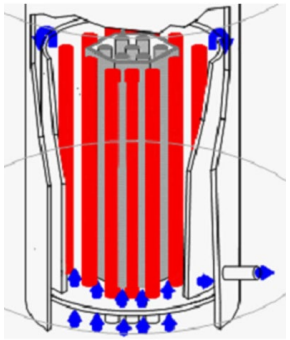

No internal heaters

- Free movement of damaged fuel segments

Post-test examinations

- Metallography
- SEM, EDX
- Endoscopy
- X-ray
- H content
- Mechanical tests
- CT
- PGAI-NR

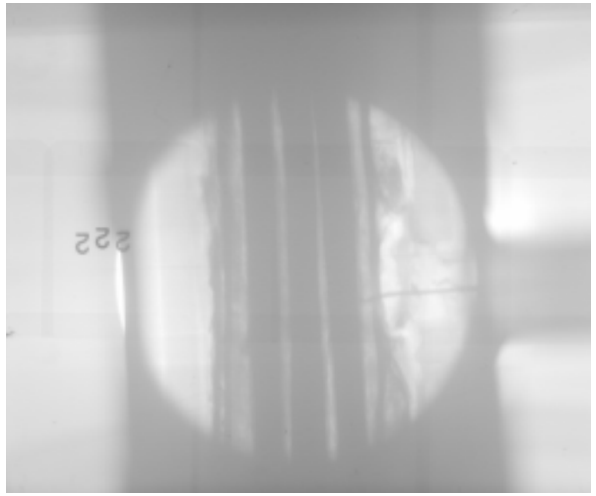

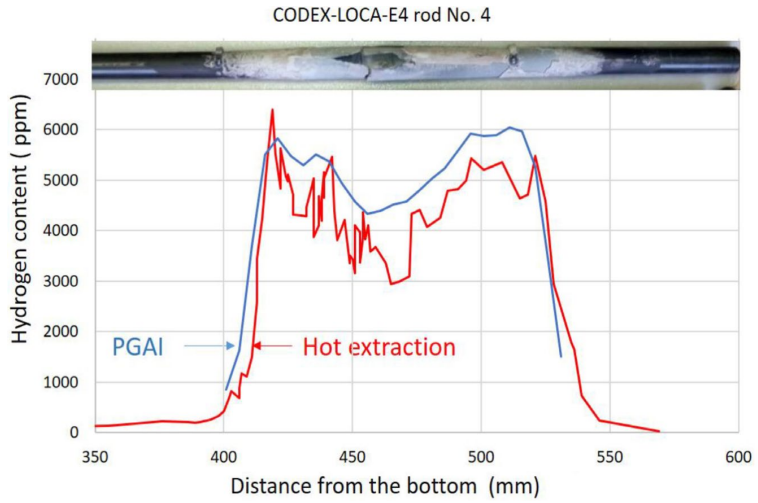

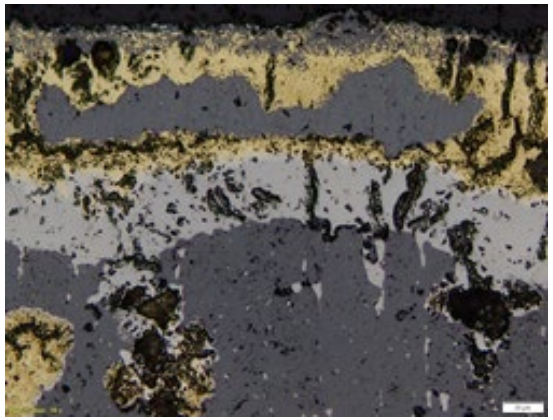

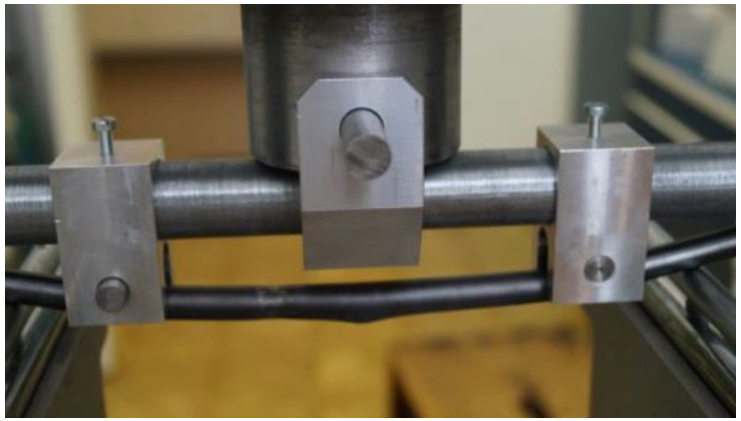

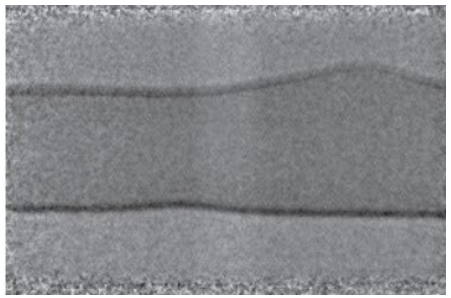

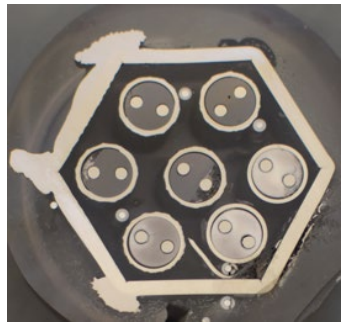

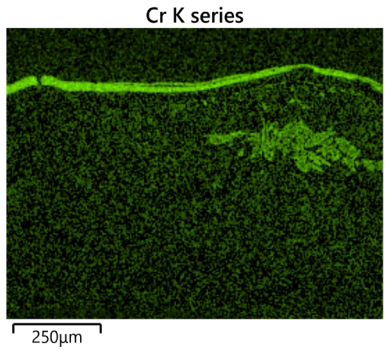

CODEX coolability tests 2008-2015

Test	Number of rods with ballooning simulator sleeves	Power peak simulation	Bypass line
CODEX-COOL-1	0	No	No
CODEX-COOL-2	0	No	No
CODEX-COOL-3	0	No	No
CODEX-COOL-4	19	No	No
CODEX-COOL-5	19	No	No
CODEX-COOL-6	19	No	No
CODEX-COOL-7	19	Yes	No
CODEX-COOL-8	19	Yes	No
CODEX-COOL-9	19	Yes	No
CODEX-COOL-10	14	No	No
CODEX-COOL-11	14	No	No
CODEX-COOL-12	14	No	No
CODEX-COOL-13	14	No	No
CODEX-COOL-14	14	No	No
CODEX-COOL-15	14	No	No
CODEX-COOL-16	14	No	No
CODEX-COOL-17	14	Yes	No
CODEX-COOL-18	14	Yes	No
CODEX-COOL-19	14	Yes	No
CODEX-COOL-20	14	Yes	No
CODEX-COOL-21	14	Yes	No
CODEX-COOL-22	14	Yes	No
CODEX-COOL-23	14	Yes	No
CODEX-COOL-24	14	Yes	Fully open
CODEX-COOL-25	14	Yes	2 mm
CODEX-COOL-26	14	Yes	2 mm
CODEX-COOL-27	19	Yes	2 mm
CODEX-COOL-28	19	Yes	Closed
CODEX-COOL-29	19	Yes	Closed
CODEX-COOL-30	19	Yes	3 mm
CODEX-COOL-31	19	No	Fully open
CODEX-COOL-32	19	No	2 mm
CODEX-COOL-33	19	No	Closed
CODEX-COOL-34	19	No	Fully open

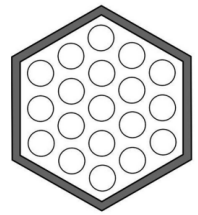

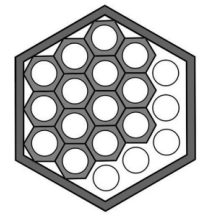

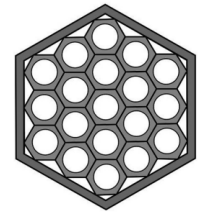

- 19 rod VVER bundles
- Simulation of ballooned section by artifical sleeves
- Thermal-hydraulic experiments
- Power peak (fuel relocation) and bypass line simulation

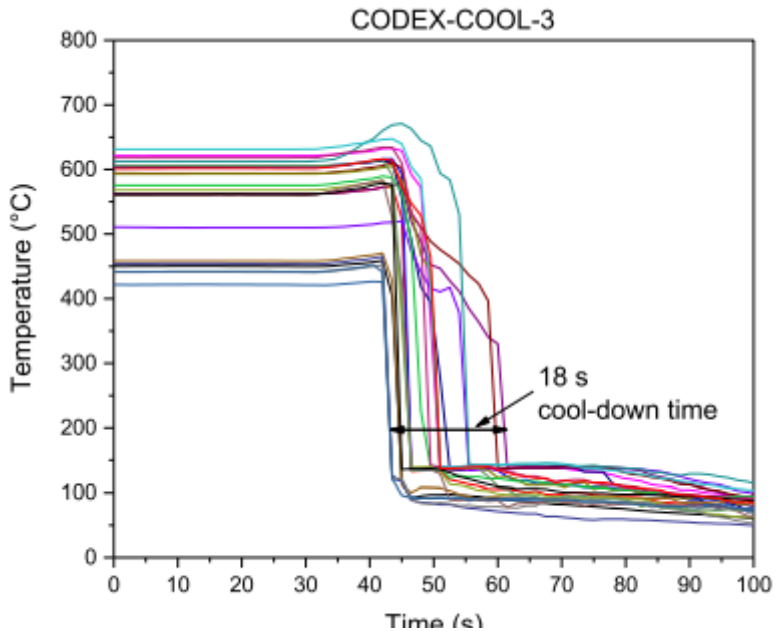

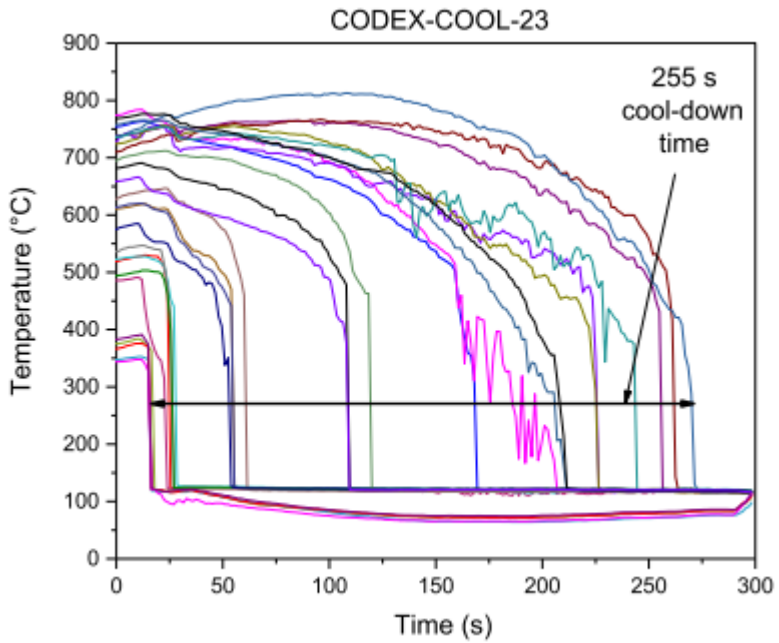

Necessary conditions for success

CODEX materials

Test	Bundle type	Pellet	Cladding material
CODEX-1	7-rod VVER	Al_2O_3	E110
CODEX-2	7-rod VVER	UO_2	E110
CODEX-3/1	7-rod VVER	UO_2	E110
CODEX-3/2	7-rod VVER	UO_2	E110
CODEX-AIT-1	9-rod PWR	UO_2	Zircaloy-4
CODEX-AIT-2	9-rod PWR	UO_2	Zircaloy-4
CODEX-B4C	7-rod VVER	UO_2,B_4C	E110, stainless steel
CODEX-CT-1	7-rod VVER	Al_2O_3	E110
CODEX-CT-2	7-rod VVER	Al_2O_3	E110
CODEX-LOCA-200	7-rod VVER	Al_2O_3	E110, E110G
CODEX-LOCA-E4	7-rod VVER	Al_2O_3	E110, E110G
CODEX-LOCA-200B	7-rod VVER	Al_2O_3	E110, E110G
CODEX-LOCA-SFP1	7-rod VVER	Al_2O_3	E110, E110G
CODEX-LOCA-SFP2	7-rod VVER	Al_2O_3	E110, E110G
CODEX-AIT-3	7-rod VVER	ZrO_2	E110G
CODEX-NITRO	7-rod VVER	ZrO_2	E110, E110G
CODEX-SBO	7-rod VVER	ZrO_2, Al_2O_3	E110, E110G
CODEX-SLIM	7-rod VVER	Al_2O_3	E110G
CODEX-ATF	7-rod VVER	ZrO_2, Al_2O_3	optZIRLO™, Cr coated optZIRLO™
CODEX-ATF-AIT	7-rod VVER	ZrO_2, Al_2O_3	Cr coated optZIRLO™

Pellets

- UO_2
- B_4C
- Al_2O_3
- ZrO_2

Claddings

- E110 (ZR-6)
- Zircaloy-4 (Karlsruhe)
- Stainless steel (ZR-6)
- E110, E110G (fuel factory)
- optZIRLO™ (CTU)
- Cr-coated optZIRLO™ (CTU)

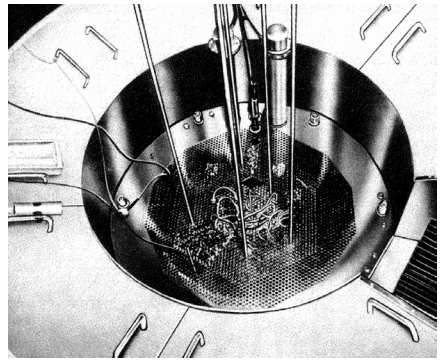

Spacer grids

- Stainless steel (manufactured)
- E110 (manufactured)
- PWR (Karlsruhe)
- VVER (fuel factory)
- Cr-coated (CTU)

Shroud

- E125 (Zr2.5Nb)
- Cr coated E125

CODEX team

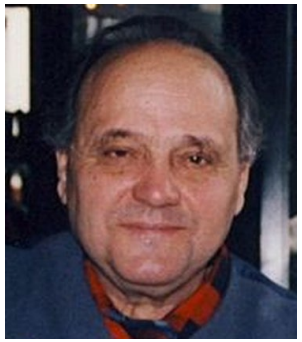

Péter Windberg

Imre Nagy

Róbert Farkas

Projects and financing

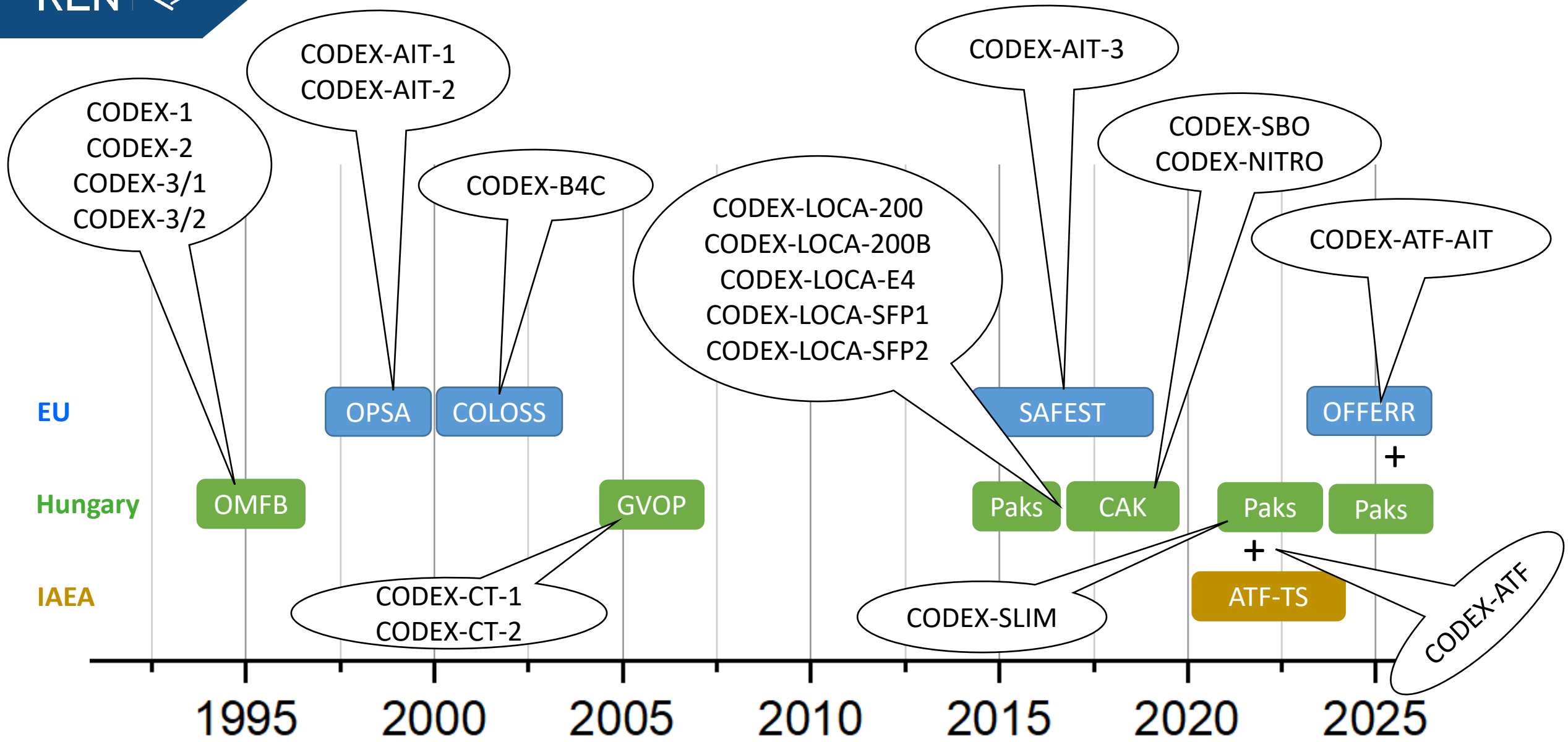

How was CODEX created?

Some history

Early 1990s: beginning of fuel research in Hungary

Visits to Karlsruhe

- László Maróti
- Lajos Matus
- Péter Windberg
- Peter Hofmann
- Gerhard Schanz
- Siegfried Hagen

- Review of severe accident experiments with Western fuel in Germany
- Potential for similar tests with VVER fuel in Hungary
  - Separate effect tests (oxidation, eutectic formation, burst, UO_2/E110 interaction, B_4C/E110 interaction, H uptake by E110)
  - Integral tests (CORA, NIELS) => CODEX

NIELS facility

CODEX – many similarities with NIELS

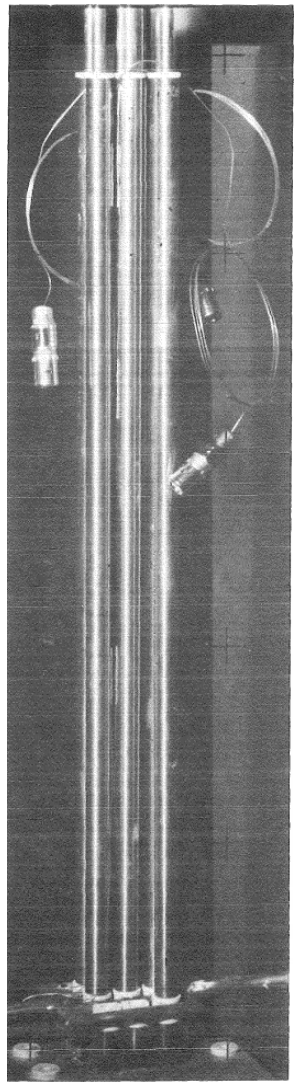

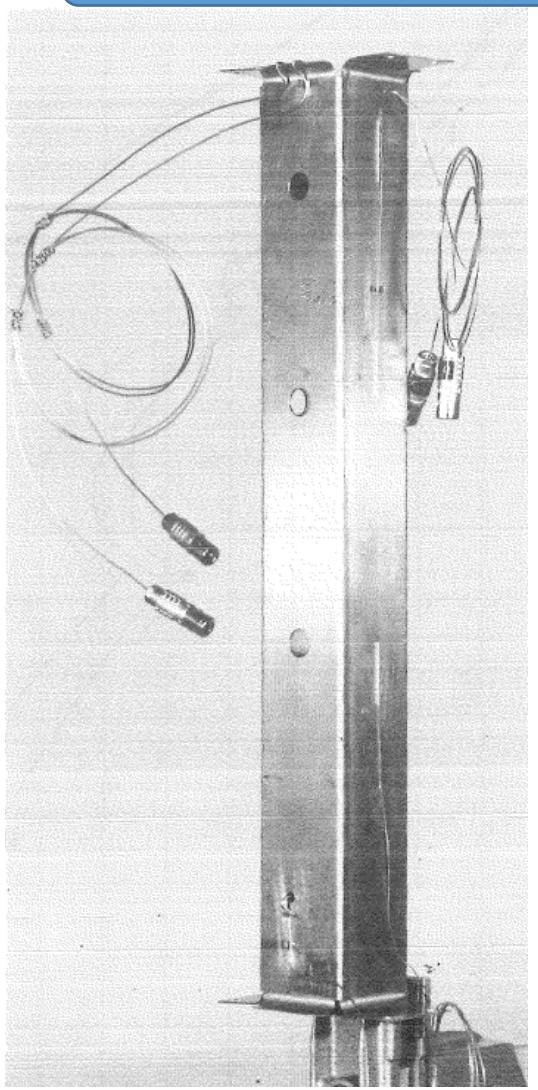

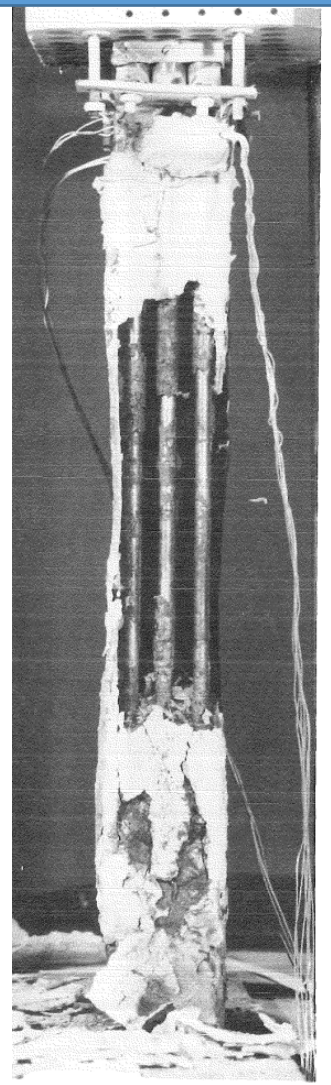

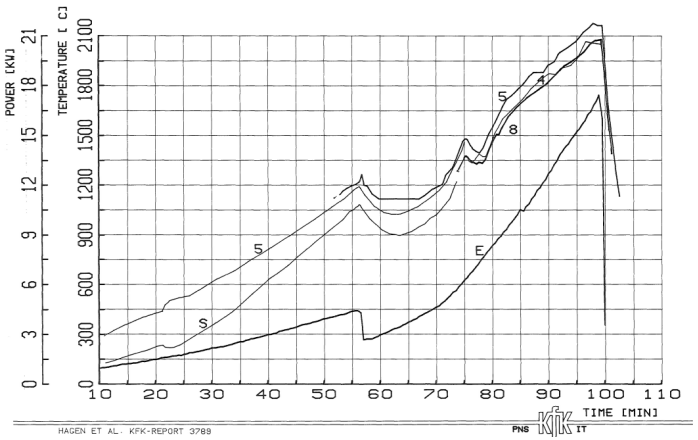

- 3x3 bundles
- 40 cm length
- Fuel rods with UO_2 and control rods
- Electrical heating
- Up to 2250 °C (melting, UO_2 dissolution by Zr)
- Experiments in 1982-1986
- Precursor of CORA (1987-1993)

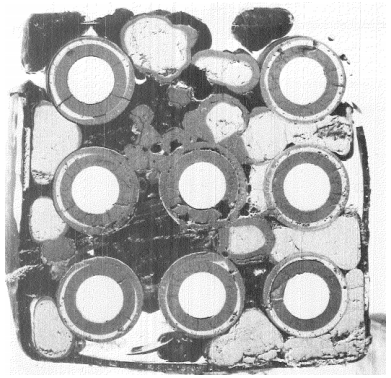

KfK 3789

Examples of QUENCH-CODEX co-operation

Air ingress experiments / OPSA project

- EU OPSA project
  (*Oxidation Phenomena in Severe Accidents*)
- Oxidation of Zr alloys in air
- Oxidation of UO_2 to higher oxides
- Proposal by Peter Hofmann:

  Air ingress CODEX tests with UO_2 using remaining materials from CORA tests
  - depleted uranium-dioxide pellets,
  - Zircaloy-4 cladding tubes,
  - PWR type spacer grid

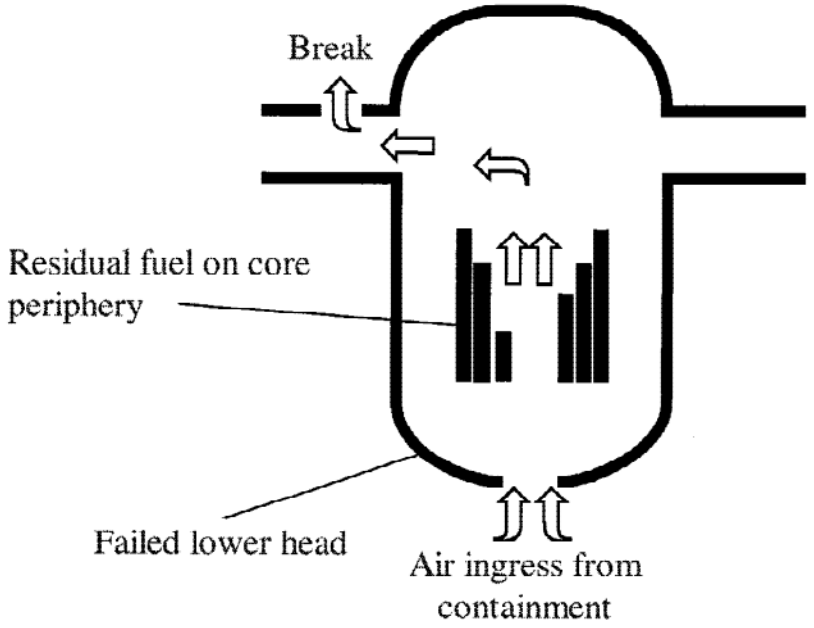

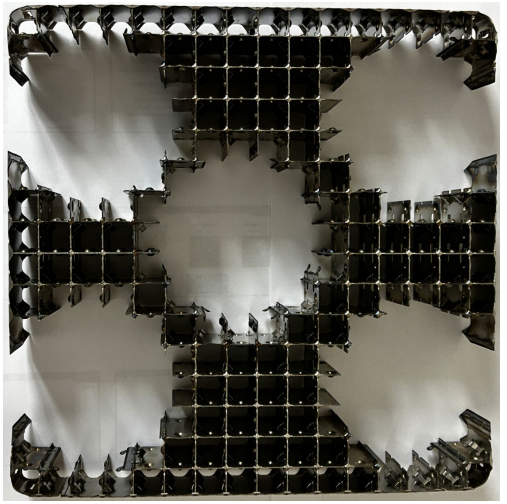

CODEX-AIT-1 (1998) and CODEX-AIT-2 (1999)

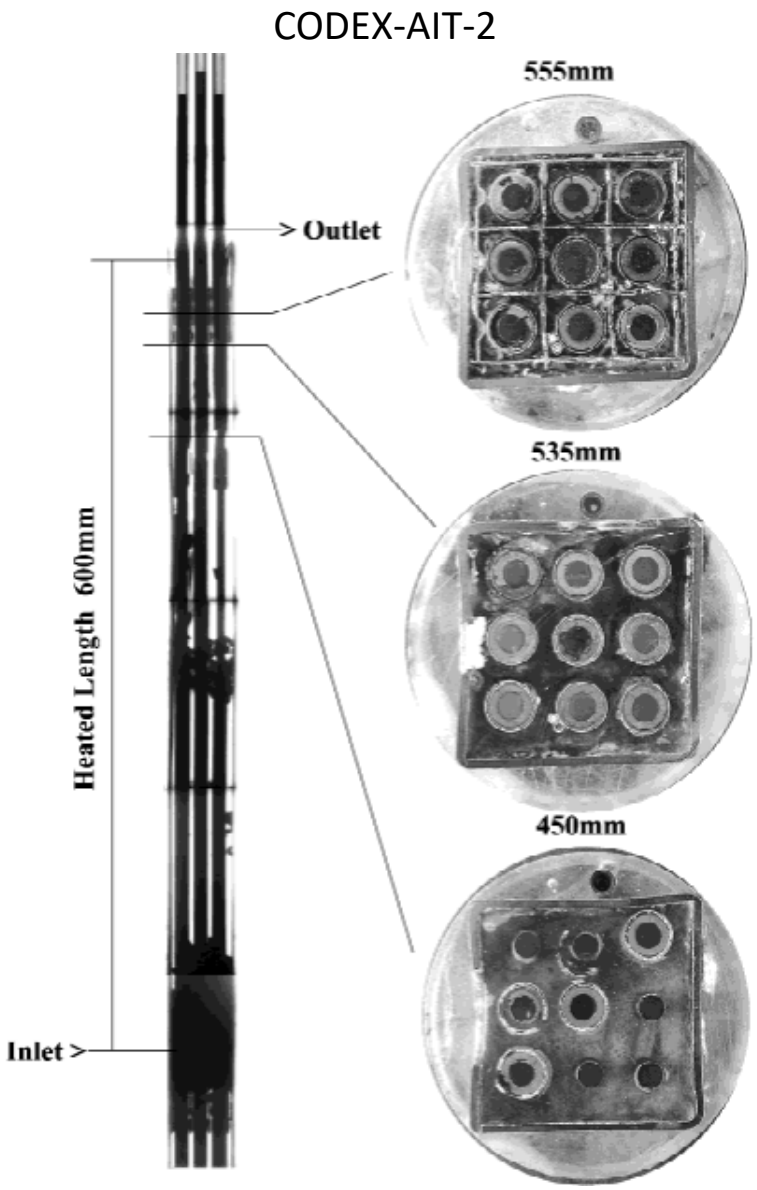

- Acceleration of oxidation and core degradation in air compared to steam
- Heavy oxidation and nitride formation on Zr surfaces
- Release of a large number of aerosol particles
- No signs of UO_2 oxidation
- Slow cool-down

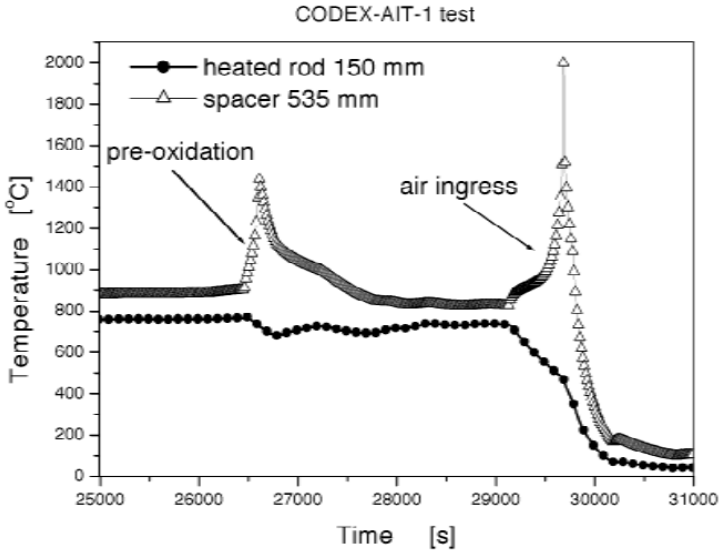

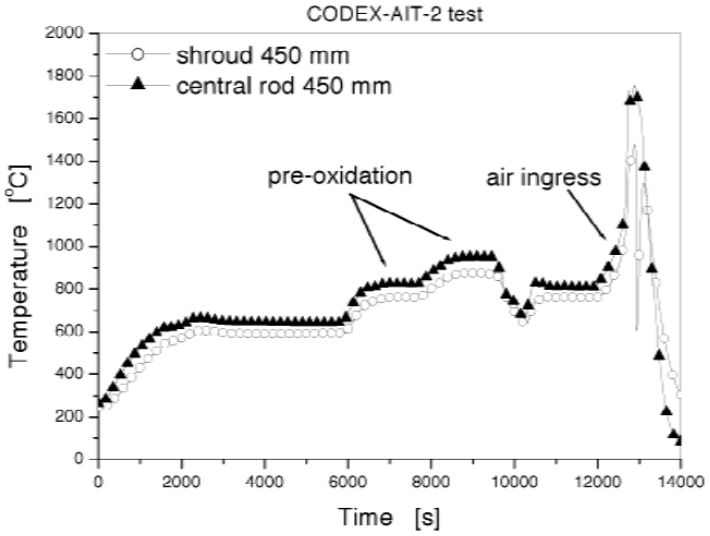

Air ingress experiments / QUENCH-10 (2004)

- EU LACOMERA project
- Test proposed by AEKI, Budapest:
  - Long pre-oxidation before air ingress
  - Final quench
- AEKI aerosol collection system
  - 10 impactors actuated at various times

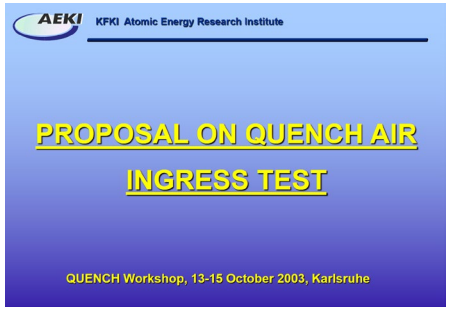

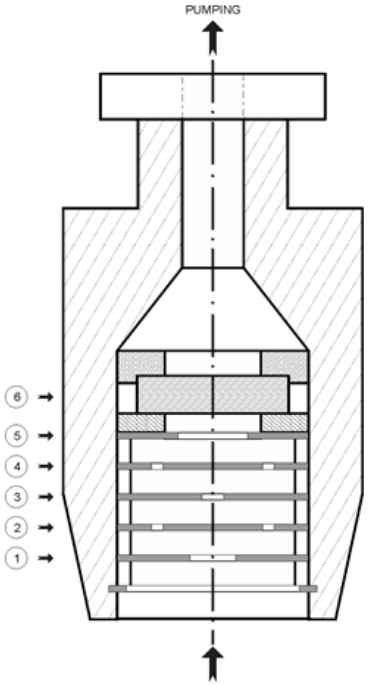

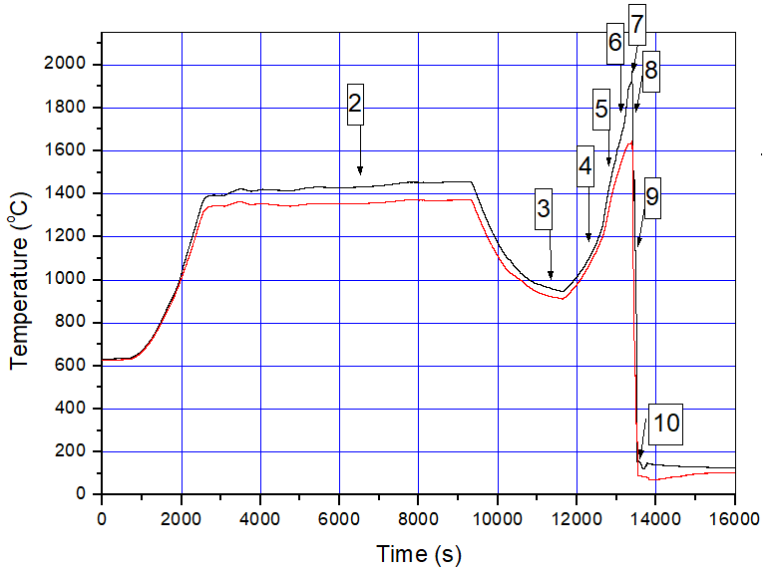

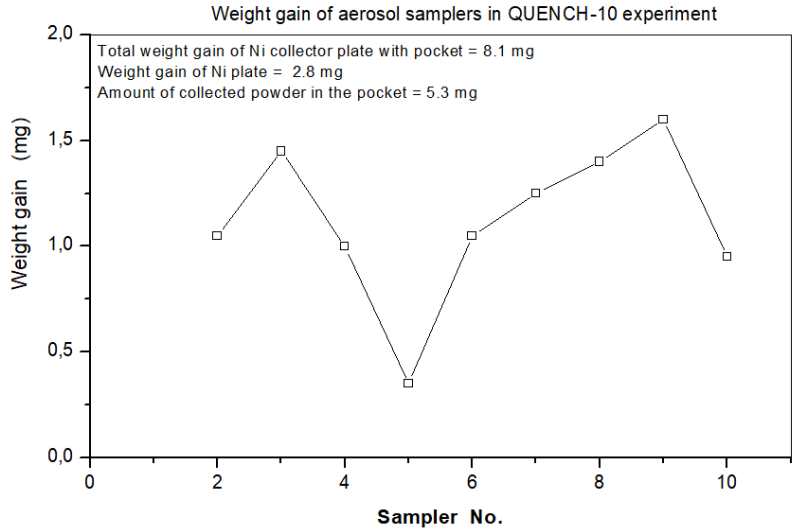

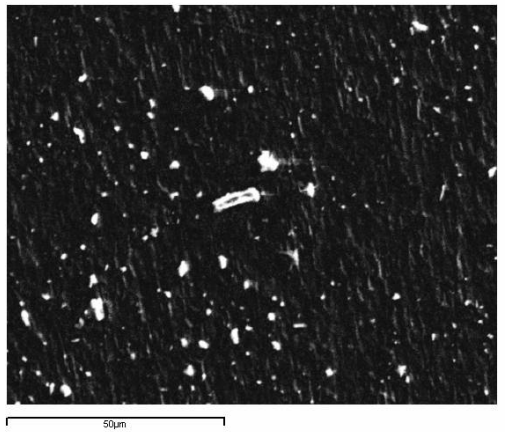

Air ingress experiments / QUENCH-16 (2011)

- EU LACOMECO project
- AEKI proposal
  - Slow oxidation and nitriding of Zr in air
  - Final quench close to melting point
- Participation of Hungarian experts at the test

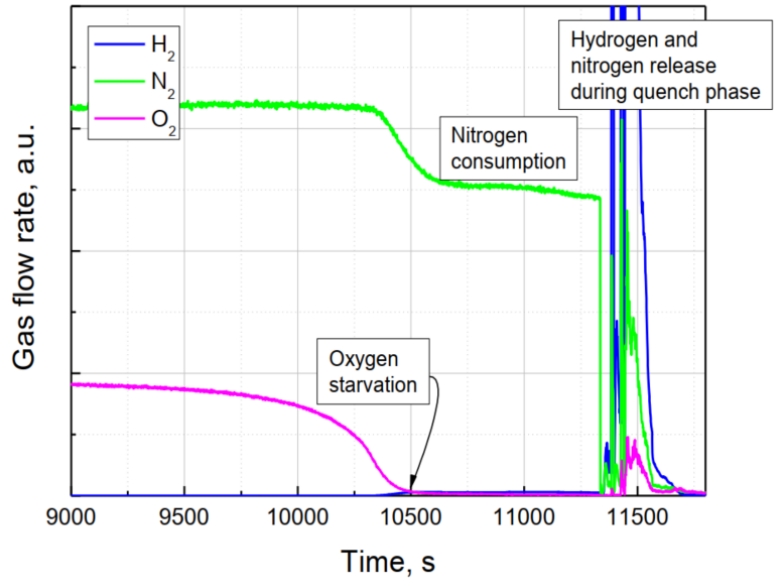

LACOMECO Final Report, 2013

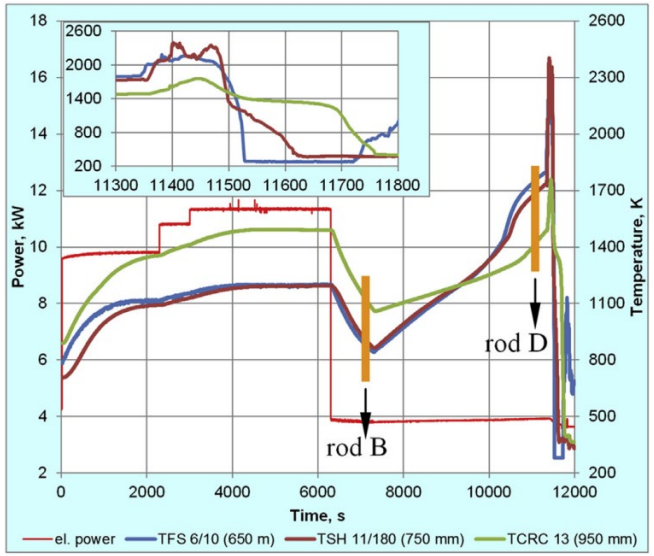

elevation: 430 mm

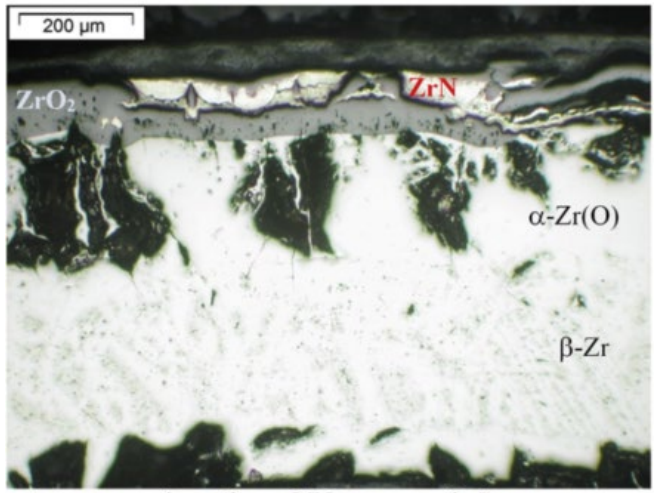

elevation: 350 mm; rod: 5

J.Stuckert and M. Steinbrück, Prog.Nucl.Energy 71 (2014) 134-141

Air ingress experiments / CODEX-AIT-3 (2018)

- EU SAFEST project
- Strong support from KIT
- Steam and oxygen starvation
- Shift of maximum temperature
- Slow cool-down – before quench conditions

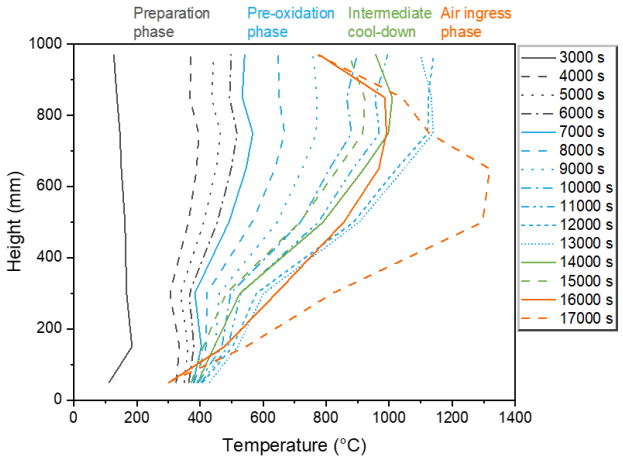

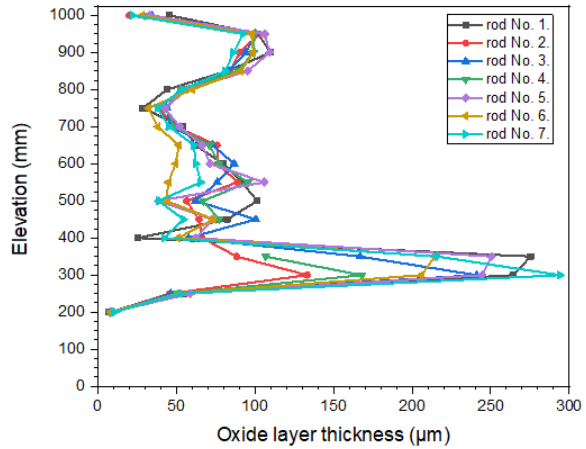

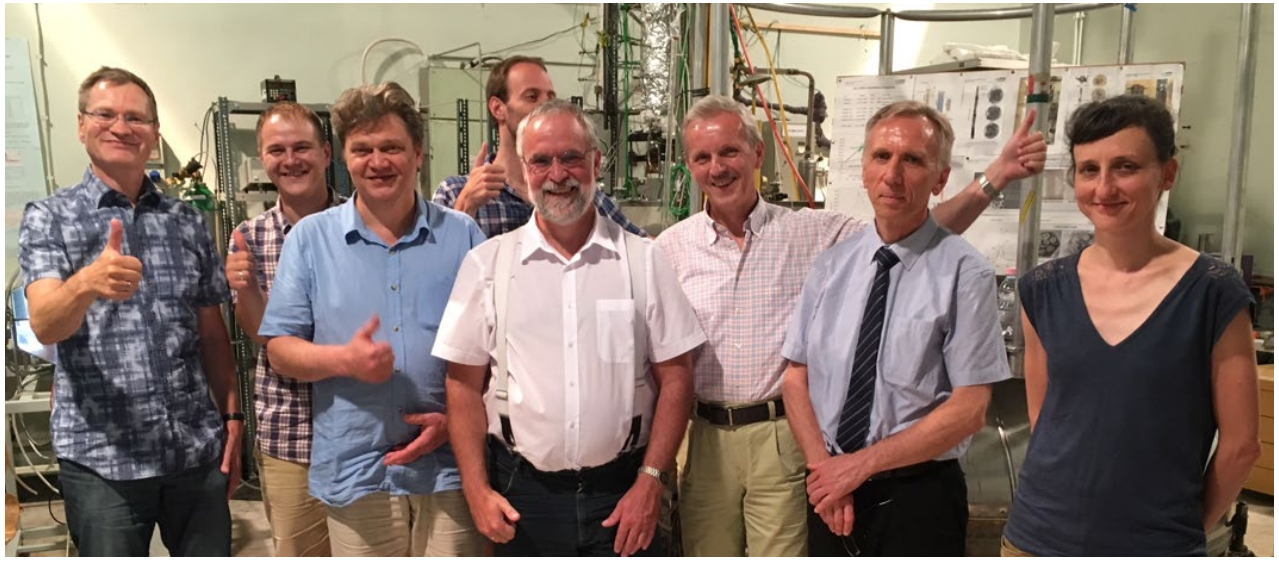

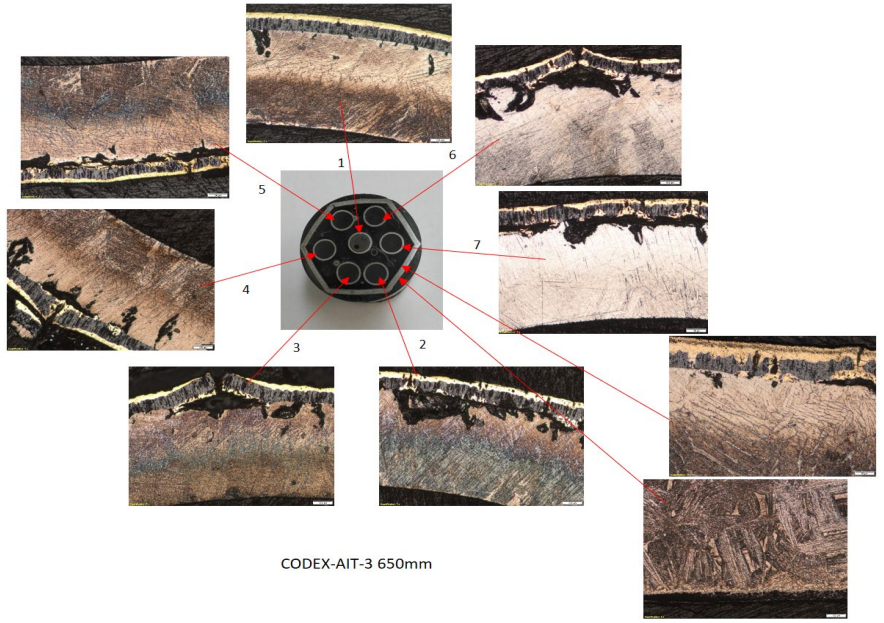

Air ingress experiments / CODEX-AIT-3 (2018)

- Transition layer between oxide and nitride
- SEM/EDS analyses by Ulrike Stegmaier

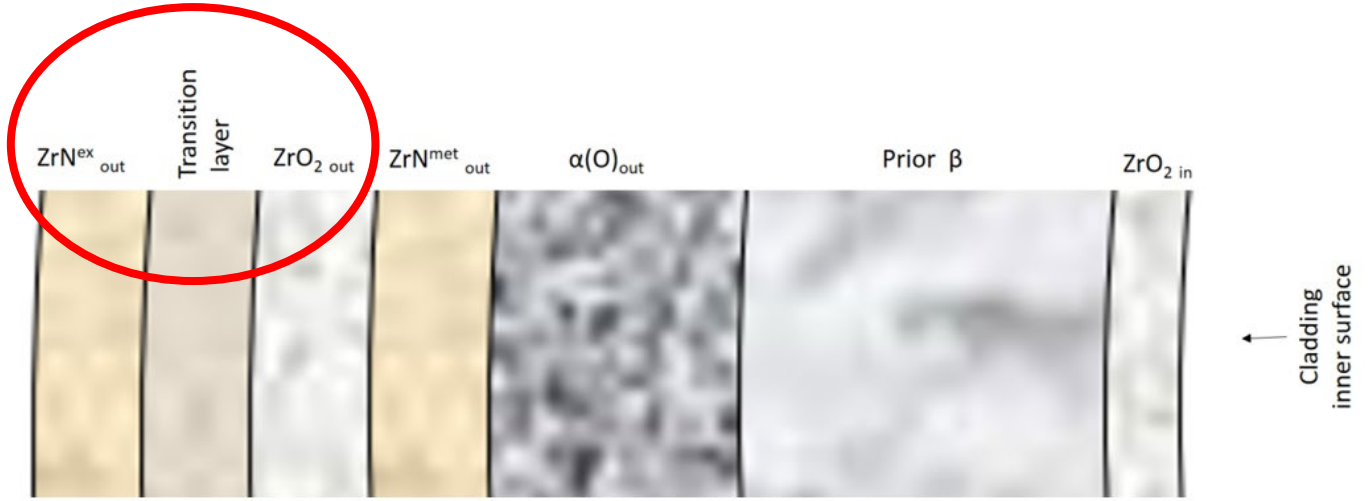

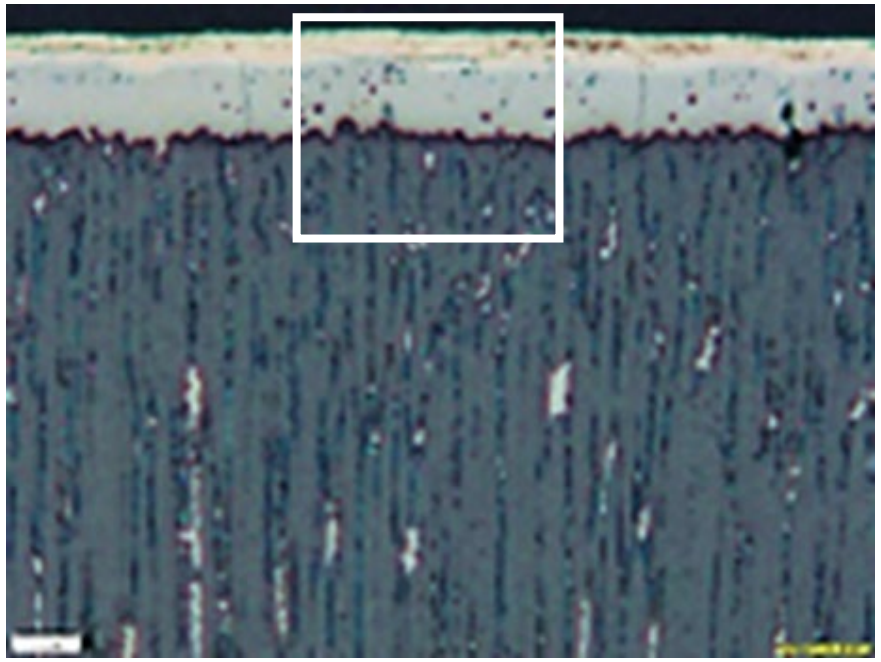

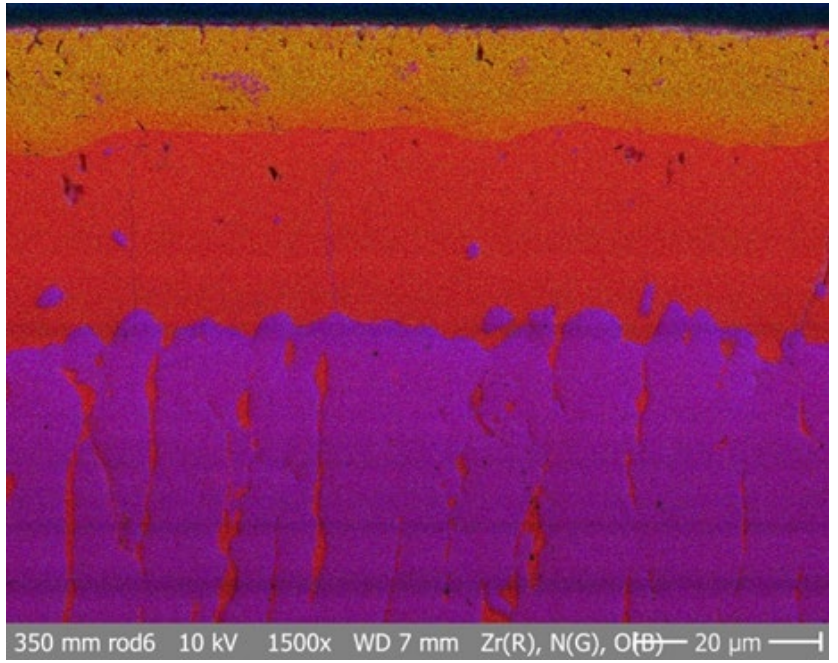

ZrN

Transition layer with Zr, O and N

ZrO_2

Air ingress experiments / CODEX-ATF-AIT (2024)

- EU OFFERR Project
- Principal researcher: Martin Steinbrück
- Visiting researchers: Juri Stuckert, Mirco Grosse
- Air ingress with Cr-coated bundle
- Thermogravimetric test at KIT with MS

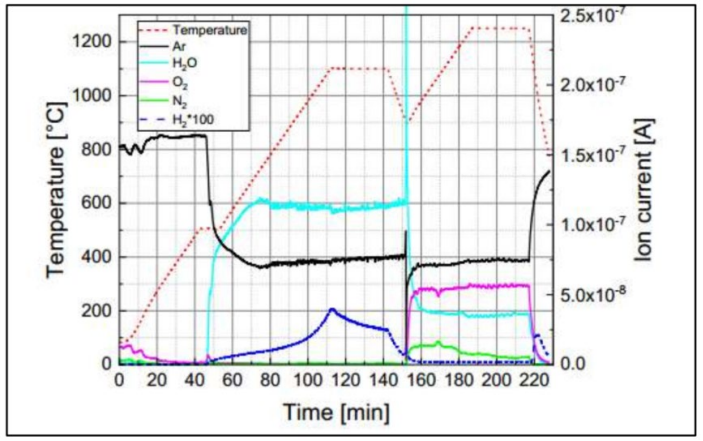

Control rod degradation/ COLOSS project

- B_4C oxidation in steam – CH_4 production ?
- Integral tests with B_4C control rods
- Very low methane production
- Confirmed by QUENCH-09, too

QUENCH-07 (2001) – reflood

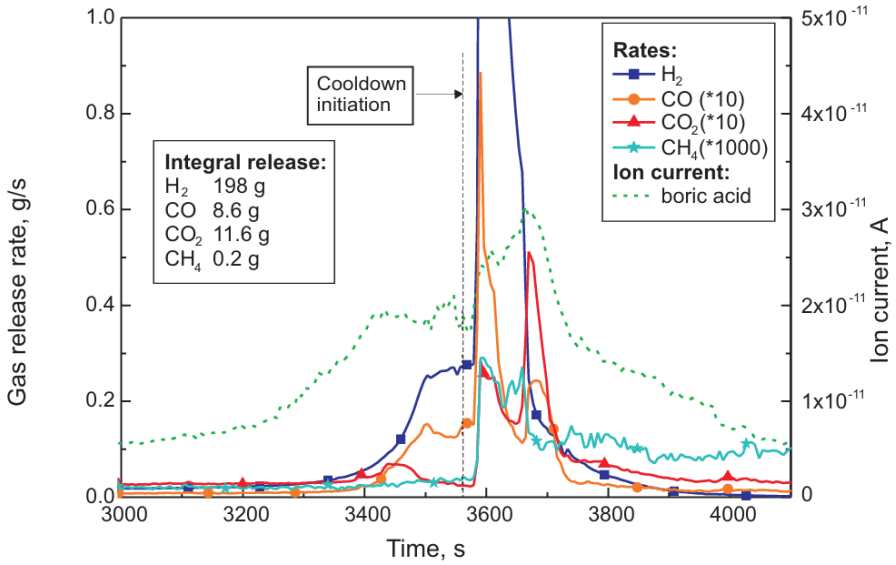

FZKA 6746

CODEX-B4C (2001) – slow cool-down

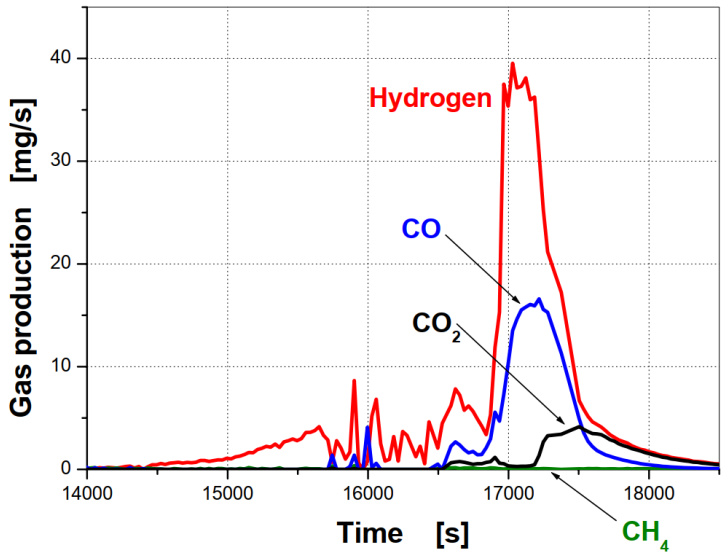

KFKI-2003-01/G

Control rod degradation/ AIC

- QUENCH-13
- Silver-indium-cadmium control rod
- Aerosol measurements by AEKI
- Large burst of aerosols (Ag-In-Cd components)

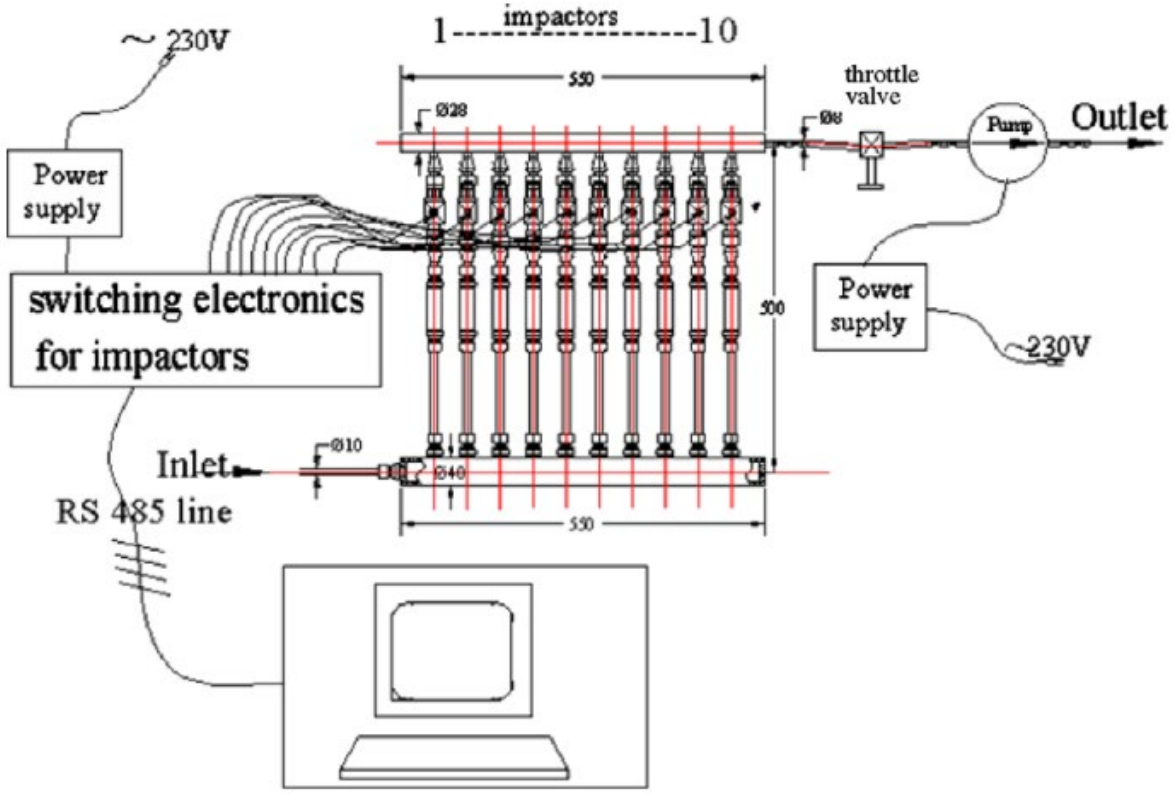

Average composition of individual aerosol particles analyzed in samples collected with AEKI impactors, wt.%.

Sample	Time (s)	O	Cd	In	Ag	W	Fe
AEKI3	11,156	38	62	–	–	–	–
AEKI4	12,129	28	19	38	0	15	–
AEKI5	13,215	25	9	17	4	39	0.3
AEKI6	13,679	15	0	4	58	14	3
AEKI7	13,742	30	0	6	2	0	52

T. Lind et al. J. Nucl. Mat. 397 (2010) 92–100

Conclusions

Conclusions

- 30 years: 20 CODEX core degradation experiments
- VVER/PWR comparison
- VVER specific reactor scenarios
- Investigation of general severe accident phenomena
- Three decades of QUENCH-CODEX co-operation
  - Parallel tests
  - Supplementary tests
  - Outstanding results in air ingress phenomena

Thank you very much!

Thank you for your attention!

Martin Steinbrück
KIT

Materials science for nuclear safety. From unexpected findings to improved severe accident codes

This presentation, delivered at the 30th International QUENCH Workshop, reviews three decades of materials science research for nuclear safety within the QUENCH program. Initially launched to quantify hydrogen generation during reflood of overheated reactor cores, the program has evolved from investigating the so-called “quench effect” to addressing complex phenomena influencing severe accident progression. Key findings include the role of water injection in triggering renewed oxidation of Zircaloy cladding, the impact of nitrogen ingress on cladding degradation and hydrogen release, and the critical influence of eutectic interactions between boron carbide and stainless steel on core melt behavior. Experimental campaigns combining large-scale bundle tests, separate-effects studies, and advanced imaging techniques have provided essential data for improving severe accident codes worldwide. The results underscore the importance of thermodynamic and kinetic considerations, as well as prototypical experimental design, in predicting accident scenarios. These insights have significantly enhanced accident management strategies and informed international safety standards for current and future reactor systems.

Materials science for nuclear safety

From unexpected findings to improved severe accident codes

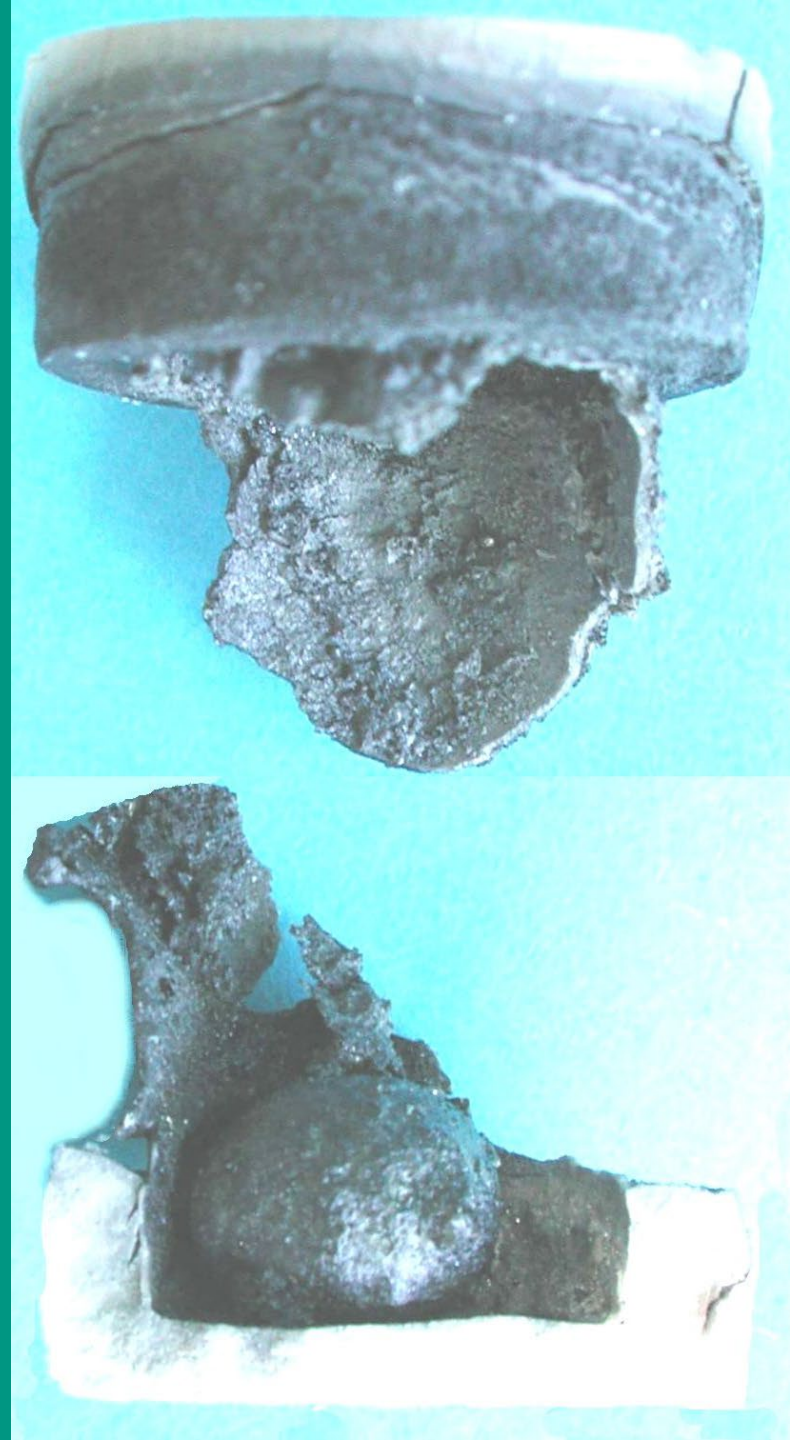

Martin Steinbrück, Mirco Große, Juri Stuckert

30th International QUENCH Workshop
16-18 December 2025, Karlsruhe, Germany

IAM-AWP

Background

- QUENCH program initiated by Peter Hofmann after completion of the CORA program
  - Determination of the hydrogen source term during reflood of an overheated reactor core
- Overviews on separate-effects tests and bundle tests during 25th QWS
  (6 years ago, https://publikationen.bibliothek.kit.edu/1000100298)

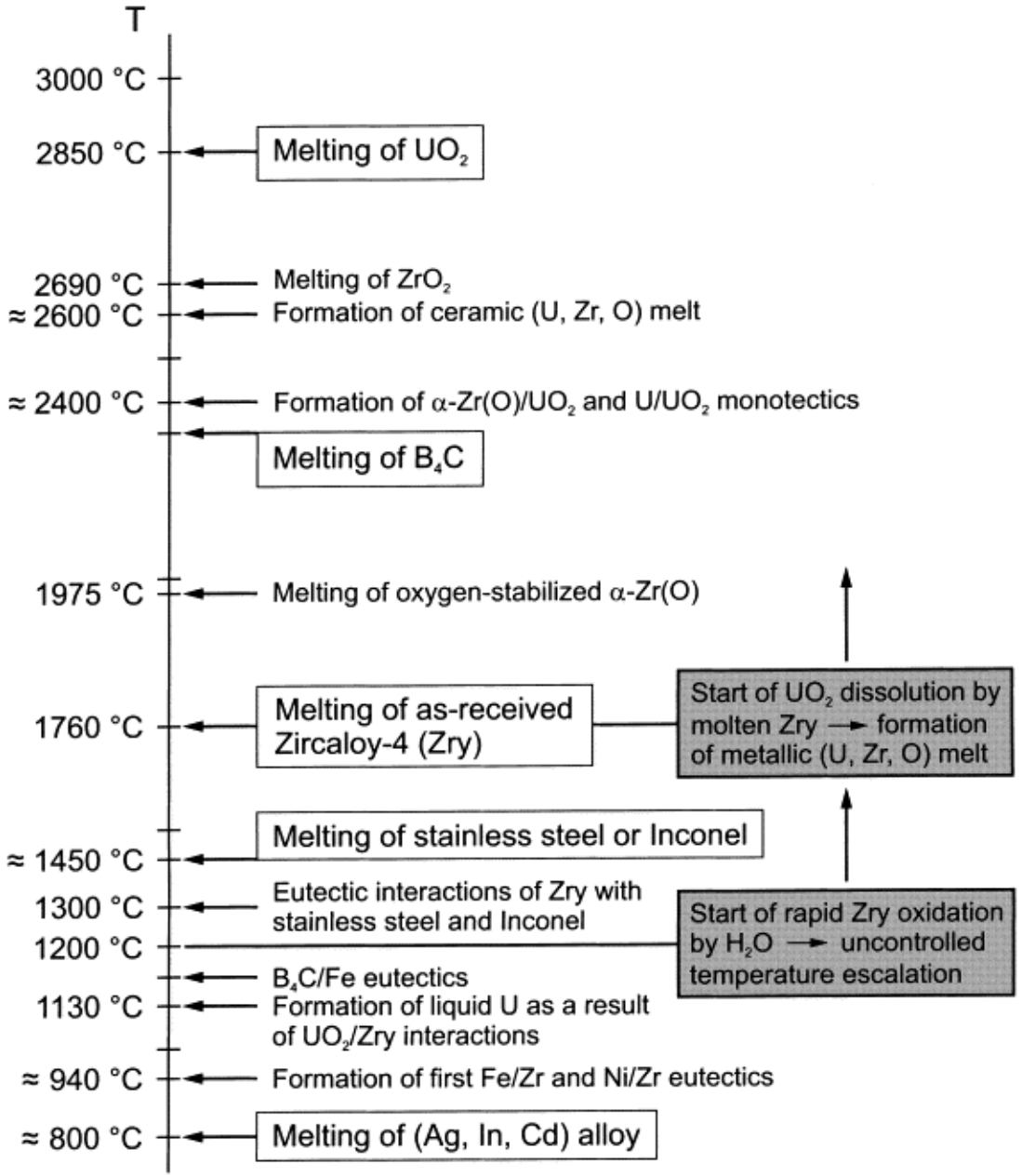

P. Hofmann, JNM 270 (1999) 194

Content

1. Background
2. The “quench effect” on hydrogen source term
3. The effect of nitrogen on cladding oxidation and degradation
4. The effect of B_4C-SS eutectic interactions on accident progression
5. Takeaways

The “quench effect” on hydrogen source term

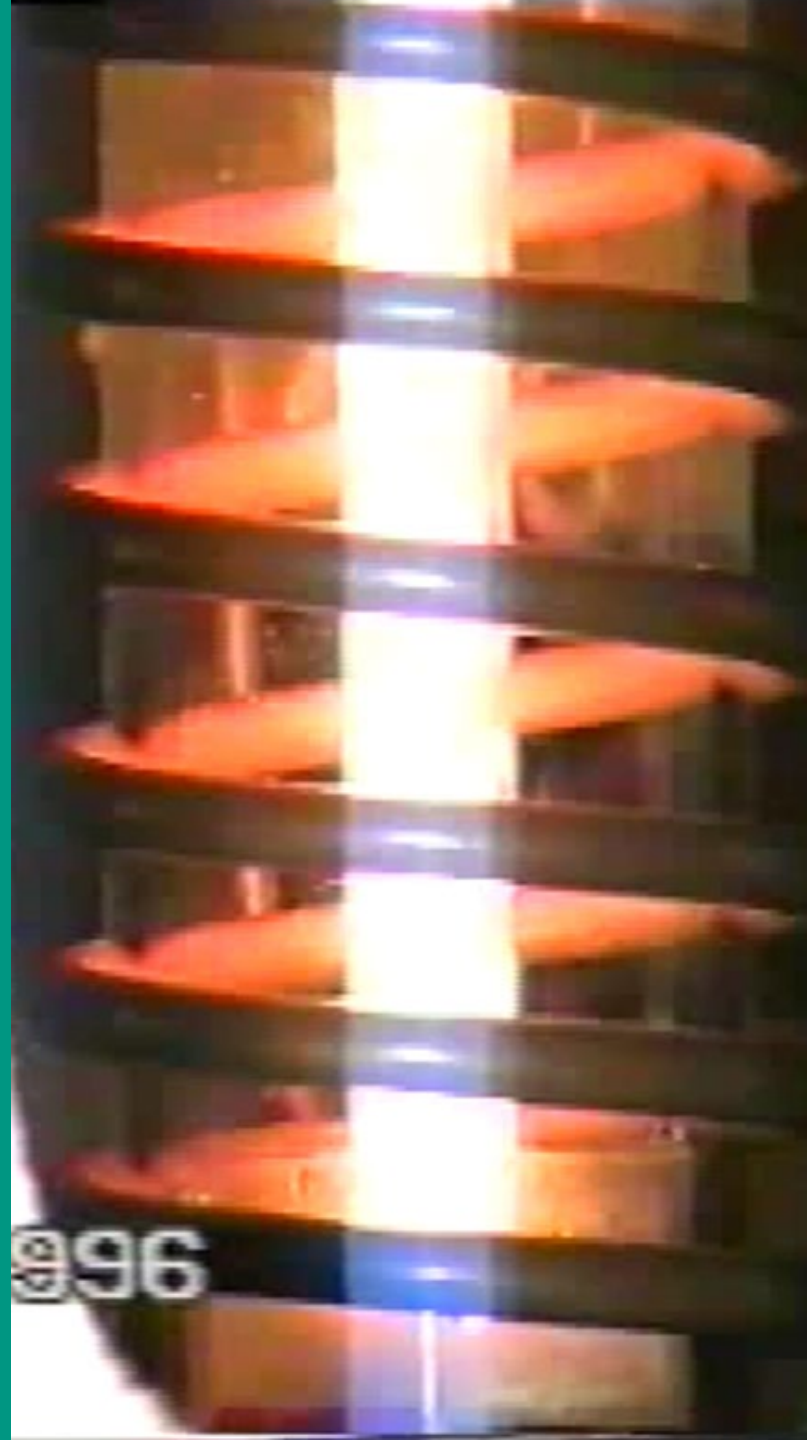

In search of the "quench effect"

- Water injection is the primary AMM for cooling an uncovered core during a severe accident scenario
- Analysis of the TMI-2 accident as well as subsequent integral in-pile and out-of-pile experiments (PBF, LOFT, PHEBUS, CORA) has shown that water injection can result in temperature runaway, which is connected with intense hydrogen release
- The QUENCH program was designed to understand this phenomenon and to provide quantitative data on the hydrogen source term
- Initially we looked for a single “quench effect”

Sepold et al., NED204 (2001) 205–220:

However, before the water succeeds in cooling the fuel elements, water injection can trigger a renewed enhanced oxidation of the Zircaloy cladding and, at the same time, cause a rapid increase in temperature and hydrogen generation.
This phenomenon was demonstrated by analyses of the TMI-2 accident and in results of out-of-pile (CORA) and in-pile LWR bundle experiments (LOFT, Phebus). It was explained as being due to the generation of new metal surfaces by cracking and fragmentation of the oxygen-embrittled cladding tubes during flooding, and to enhanced exothermal oxidation of the newly formed metal surfaces *(Hofmann et al., Report FZKA 5846, 1997)*.

Single-rod QUENCH tests – Main results

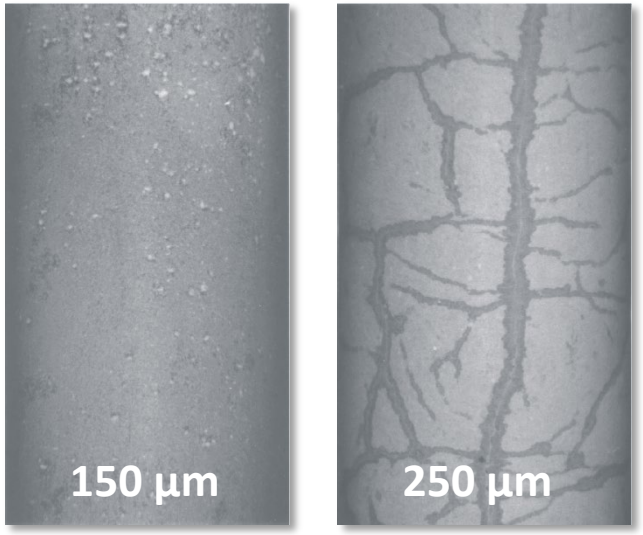

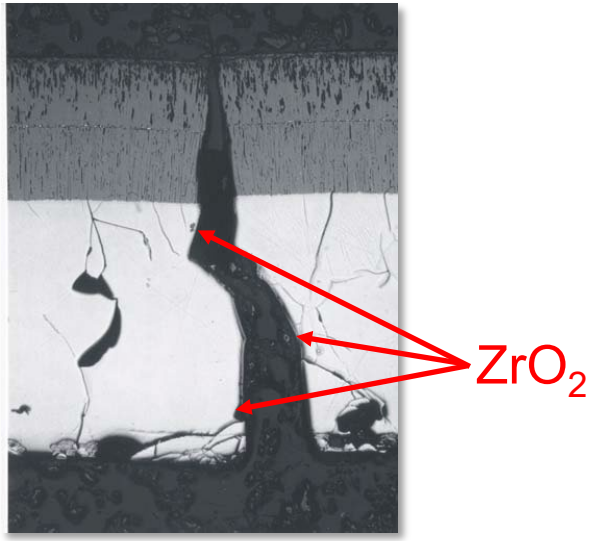

- Through-wall crack for pre-oxidation >200 µm with a density of 0.5 mm/mm^2
- Oxidation of crack surfaces connected with hydrogen generation and partly absorption by the metal

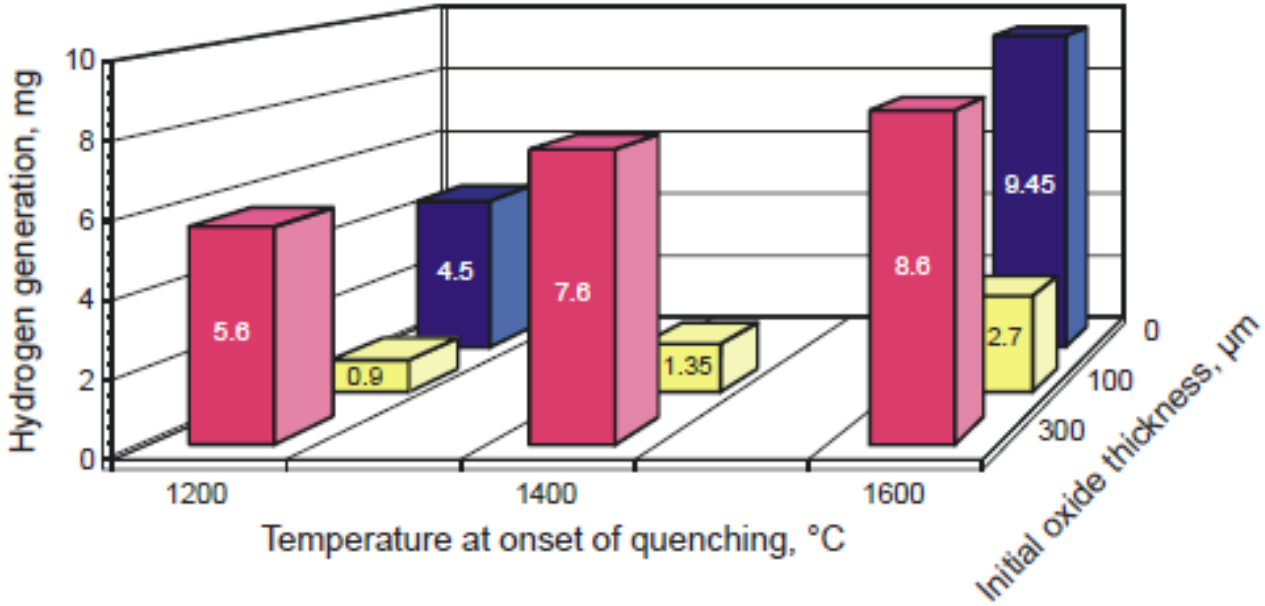

Hydrogen generation vs. oxide thickness

Crack formation in QUENCH-01 bundle test

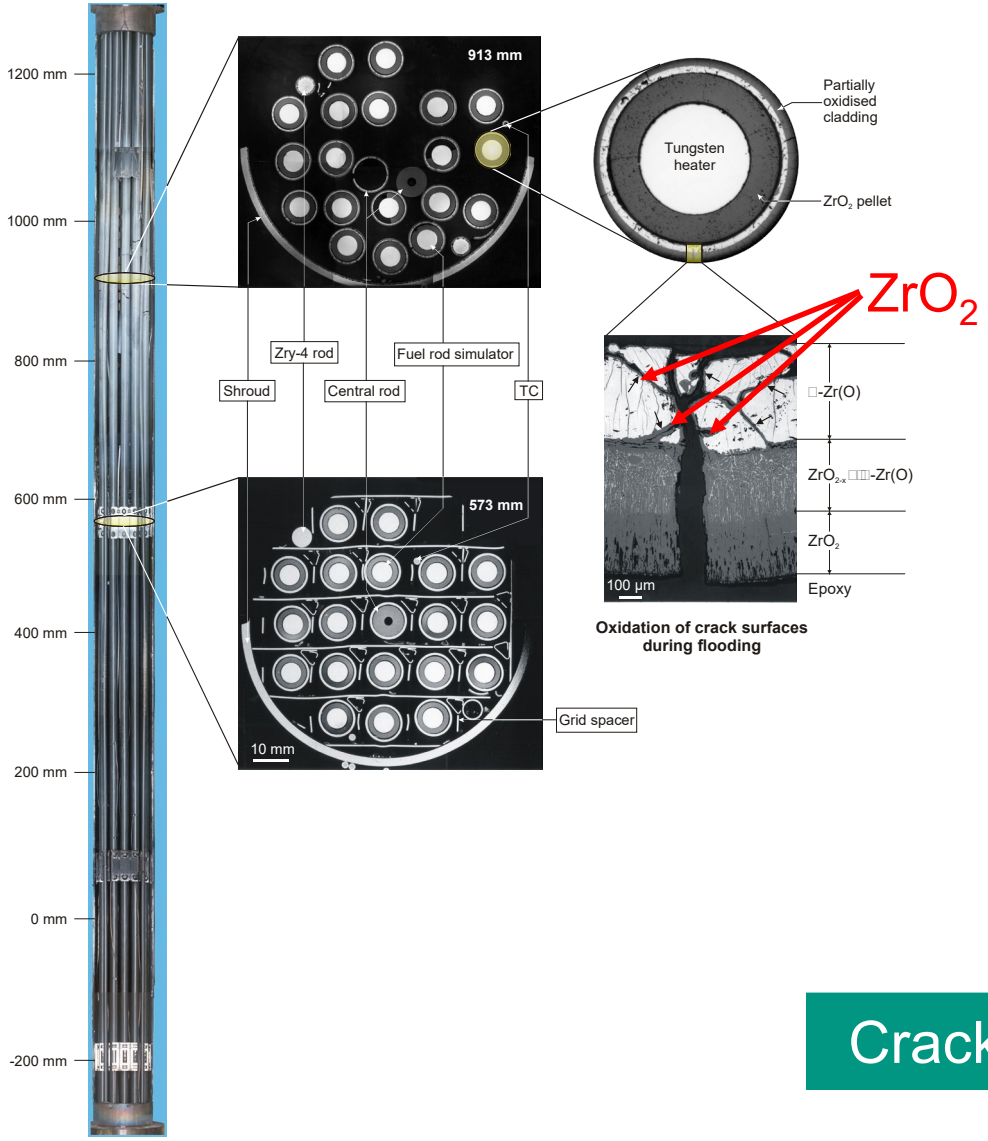

- Estimation of hydrogen production by crack oxidation gives only ca. 1-2 g for the whole bundle
- This could not explain temperature runaway during reflood

However:

- *Solution enthalpy of 1 g H_2 in 1 kg Zr increases temperature by 200 K*

Crack formation and oxidation are only minor effects

Successful reflood depends on many parameters

Reflood
Water injection → steam production

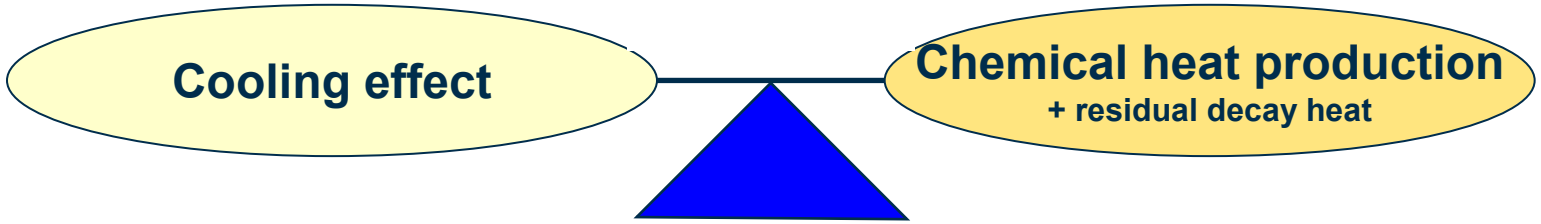

$Q_c \sim h\,(T_{Zr} - T_c)$

$Q_R \sim \Delta_R H\,(K(T)/t)^{0.5}$

$Zr + 2\,H_2O \rightarrow ZrO_2 + 2\,H_2 + 580\ kJ$

Influenced by

- **ΔT**
- Flooding rate
- Cooling medium
- Pressure
- Hydraulic diameter
- …

- **Oxidation kinetics**
- Temperature (Arrhenius type)
- Degree of pre-oxidation
- Surface available for oxidation
- Material composition
- **Steam availability**

Summary of QUENCH bundle tests

- Depending on the energy balance after reflood initiation, there will be a cooldown or temperature escalation
- Successful reflood if
  - Less chemical (and residual decay) energy is produced than can be eliminated by cooling
  - Cooling water rate is > 1 g/s rod
  - No oxidizable melt in contact with steam
- Ultimately, we discovered that a variety of factors must be considered

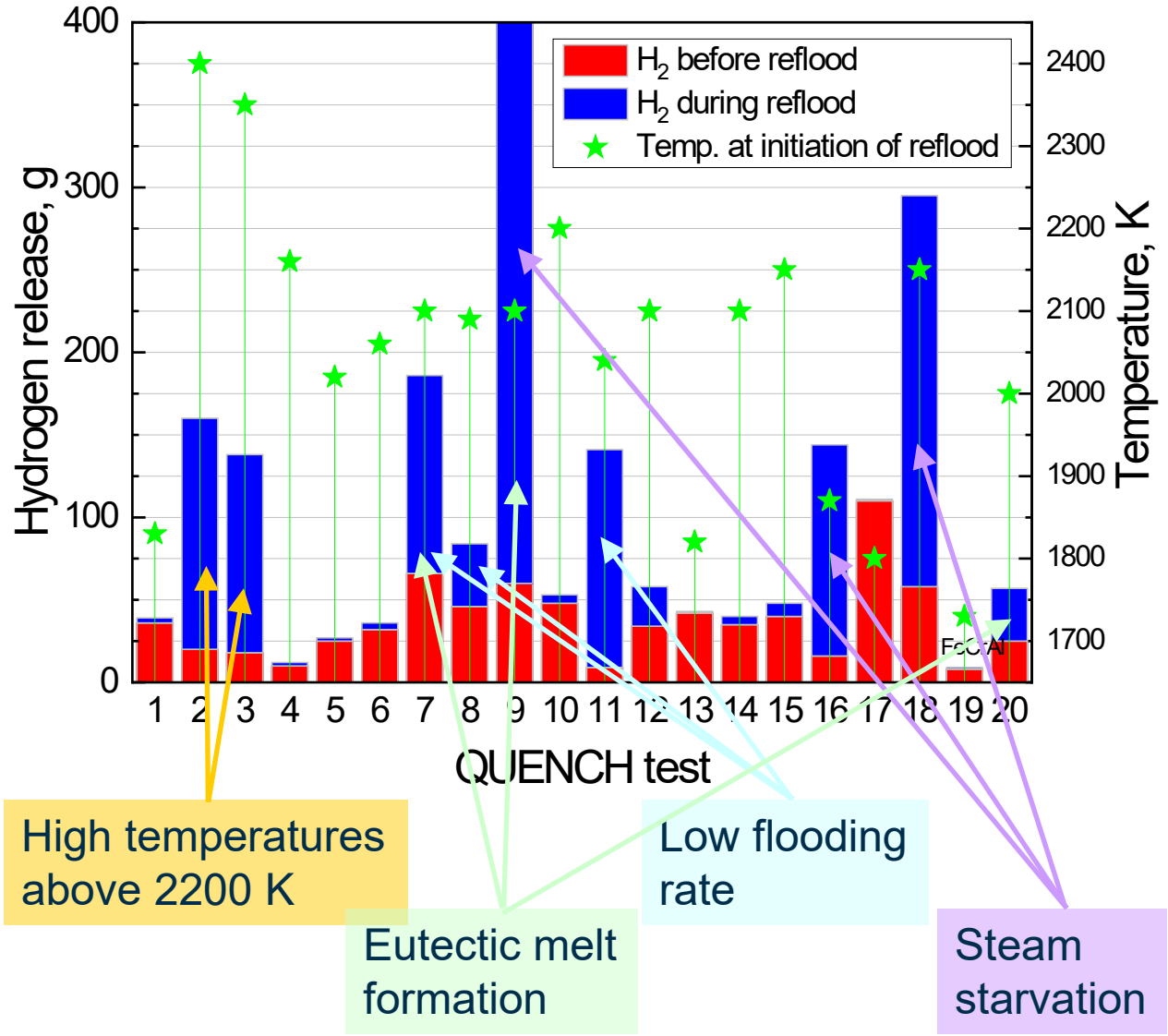

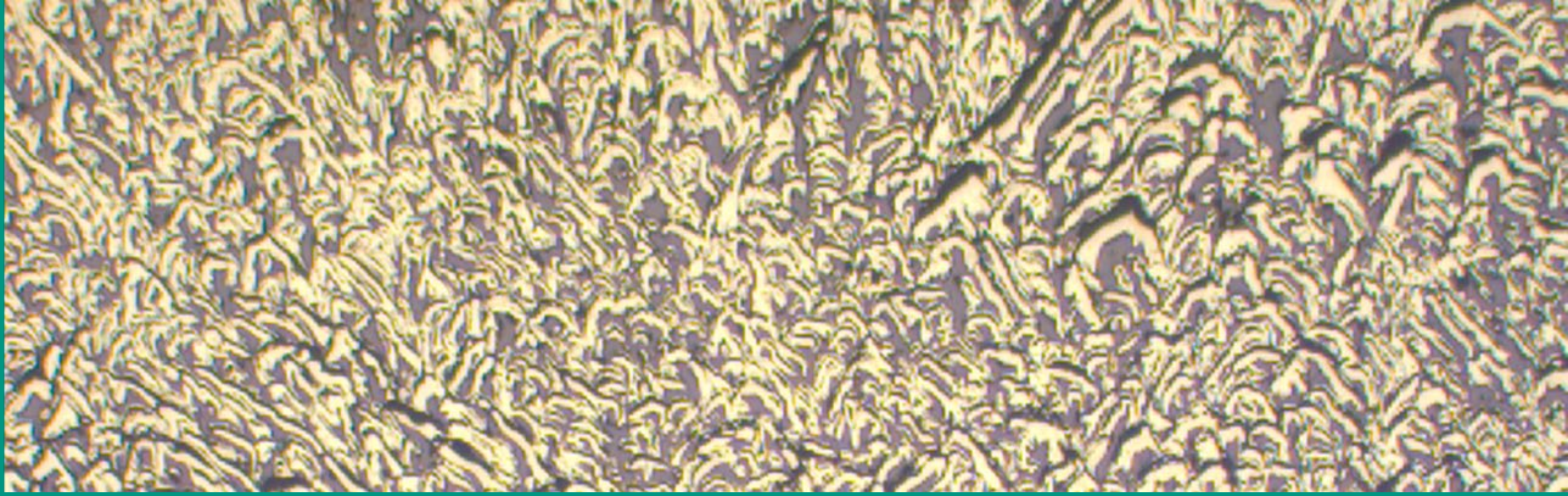

The effect of nitrogen on cladding oxidation and degradation

Nitrogen in LWRs

- The “inert” gas nitrogen is used to inertize BWR containments and in ECCS pressurizers
- Air contains nitrogen and ingress may occur into reactor core, spent fuel pond, or transportation cask
- Typically, nitrogen comes into contact with the cladding after steam oxidation, mixing with the steam

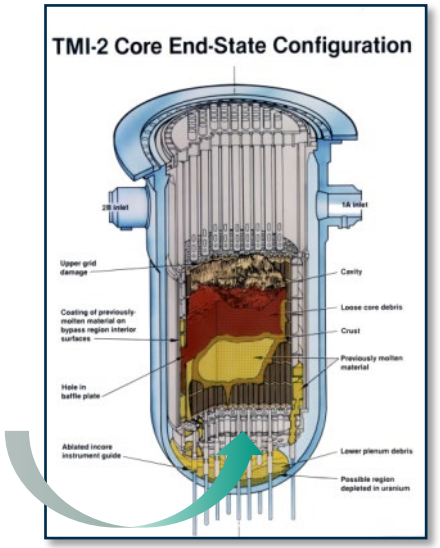

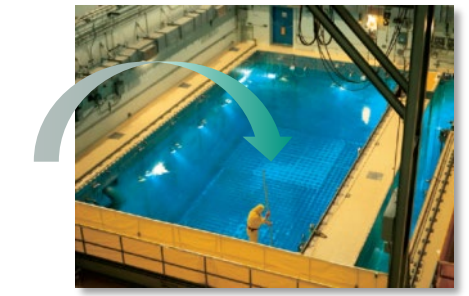

What are the consequences on hydrogen source term and cladding degradation?

The effect of nitrogen on the oxidation and degradation of Zr alloys

6 hours at 800°C

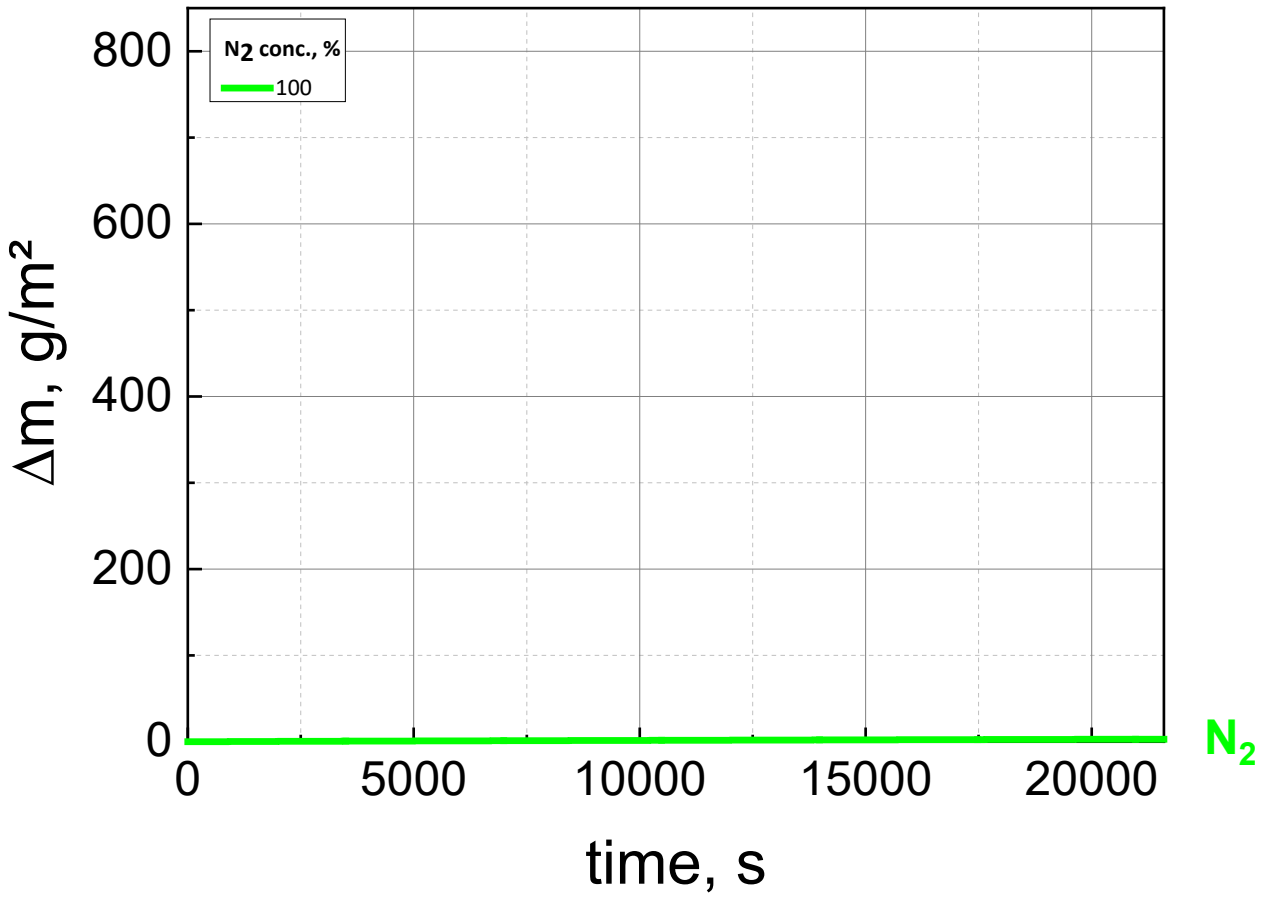

The effect of nitrogen on the oxidation and degradation of Zr alloys

6 hours at 800°C

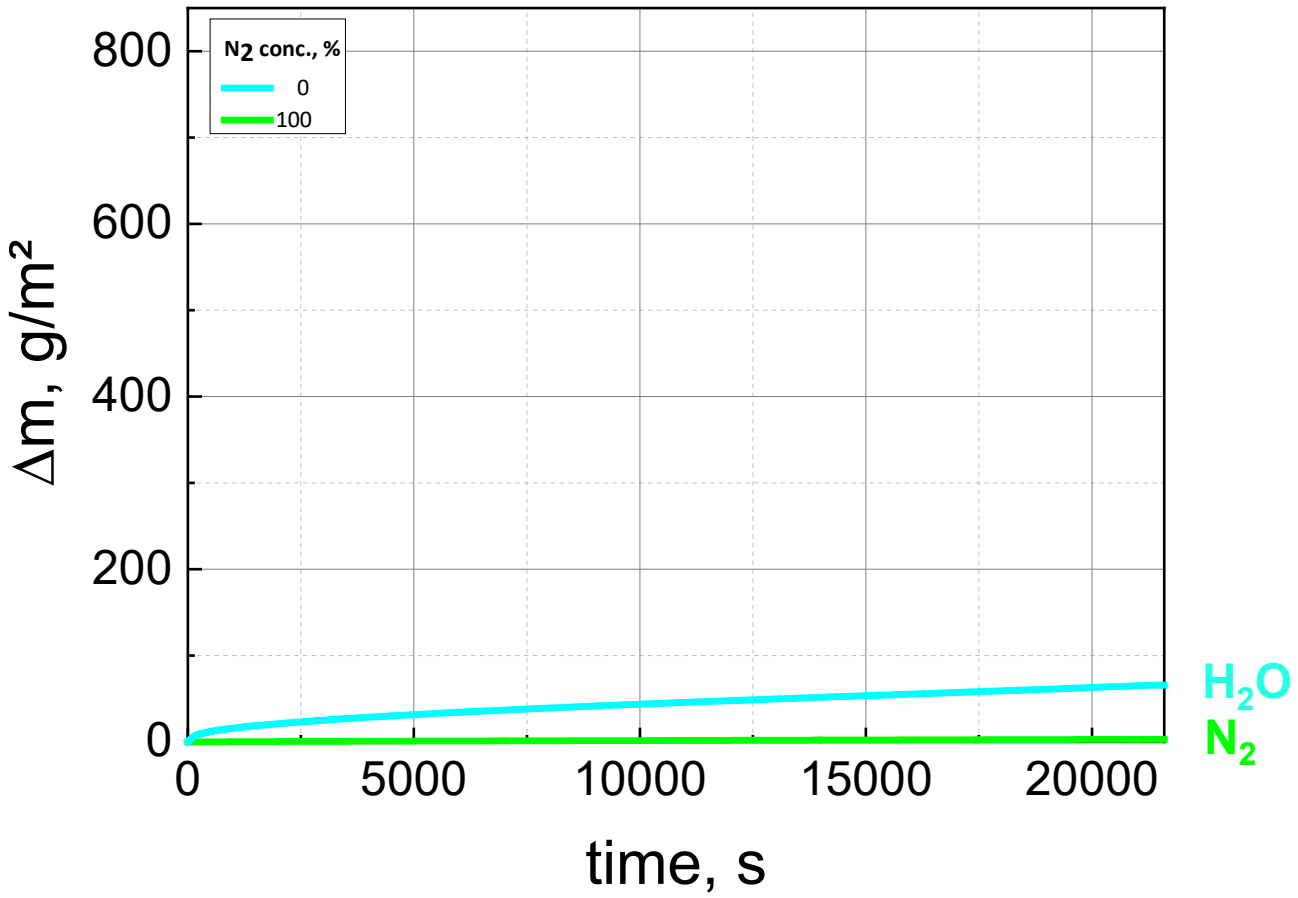

The effect of nitrogen on the oxidation and degradation of Zr alloys

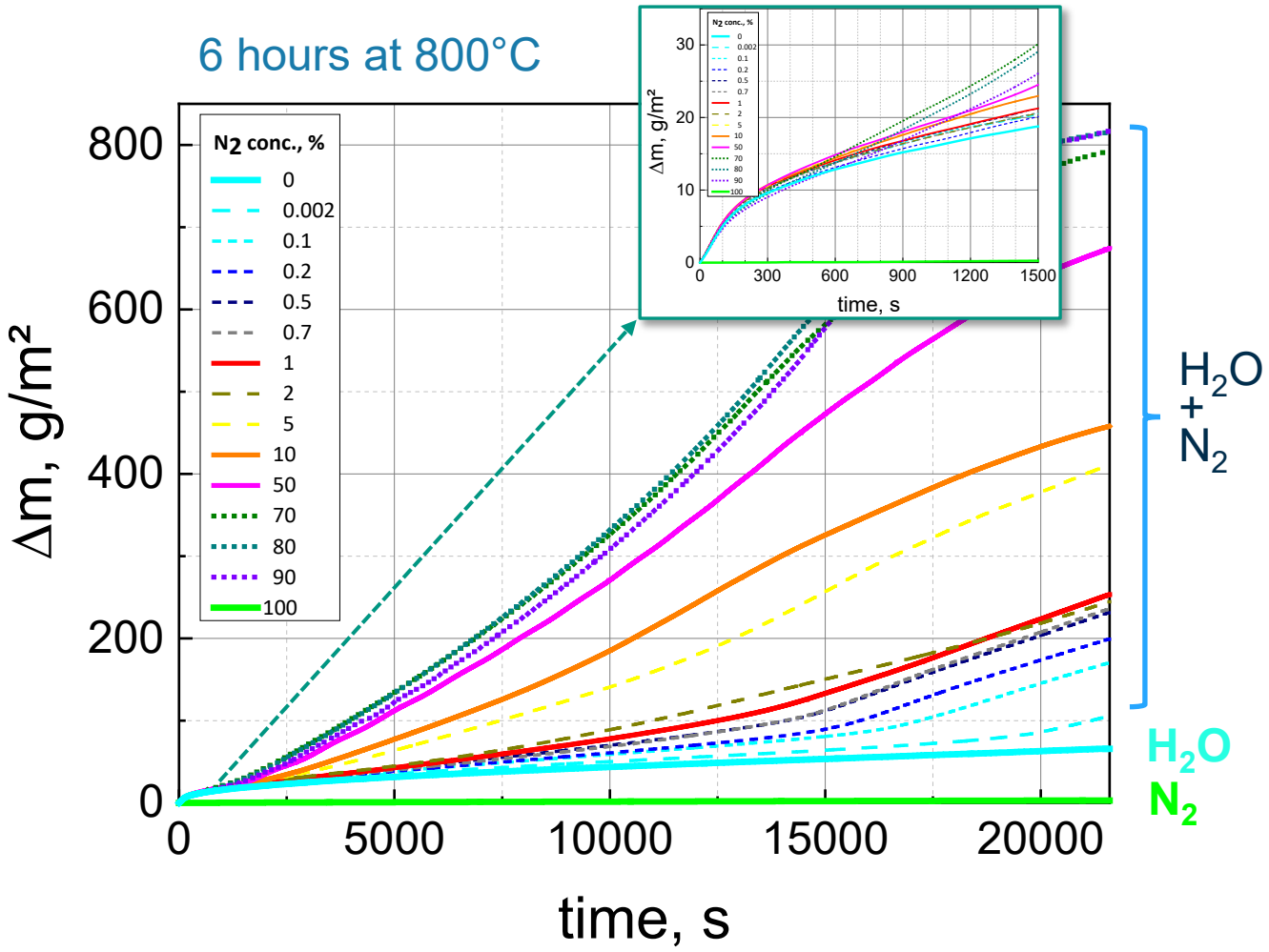

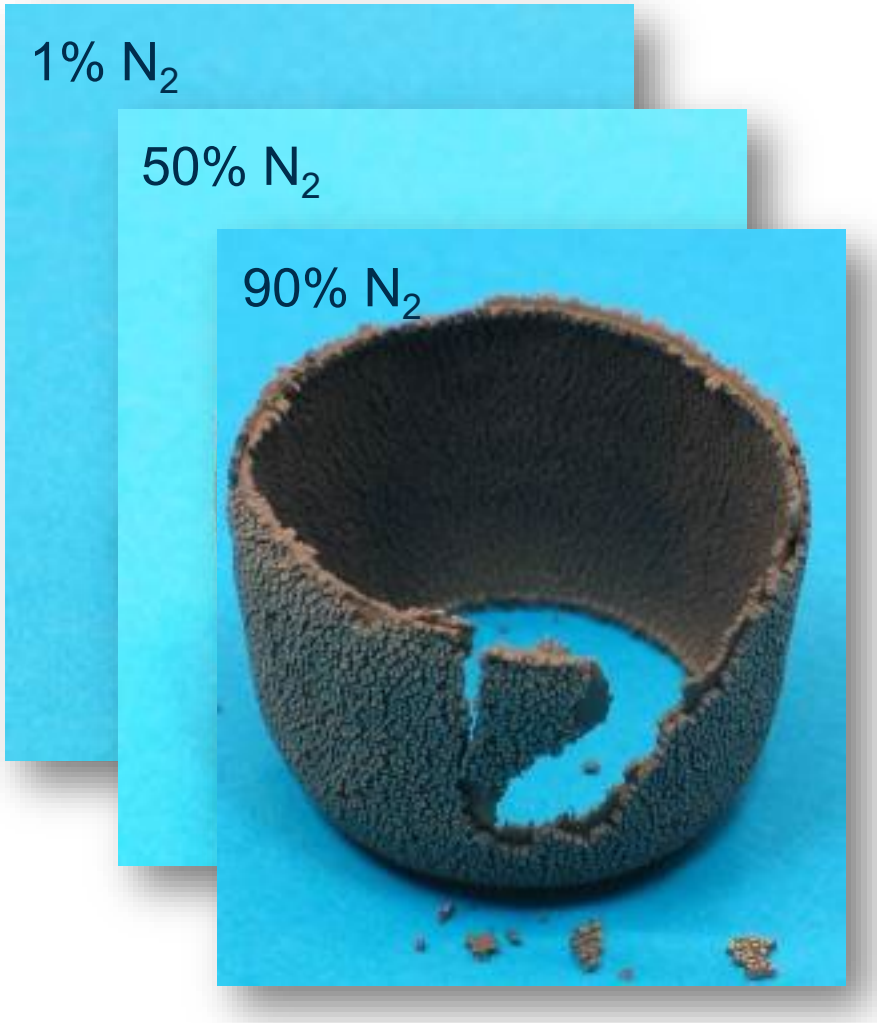

In-situ Neutron imaging

Example: 2h oxidation of Zry-4 at 900 °C in steam and steam/N_2

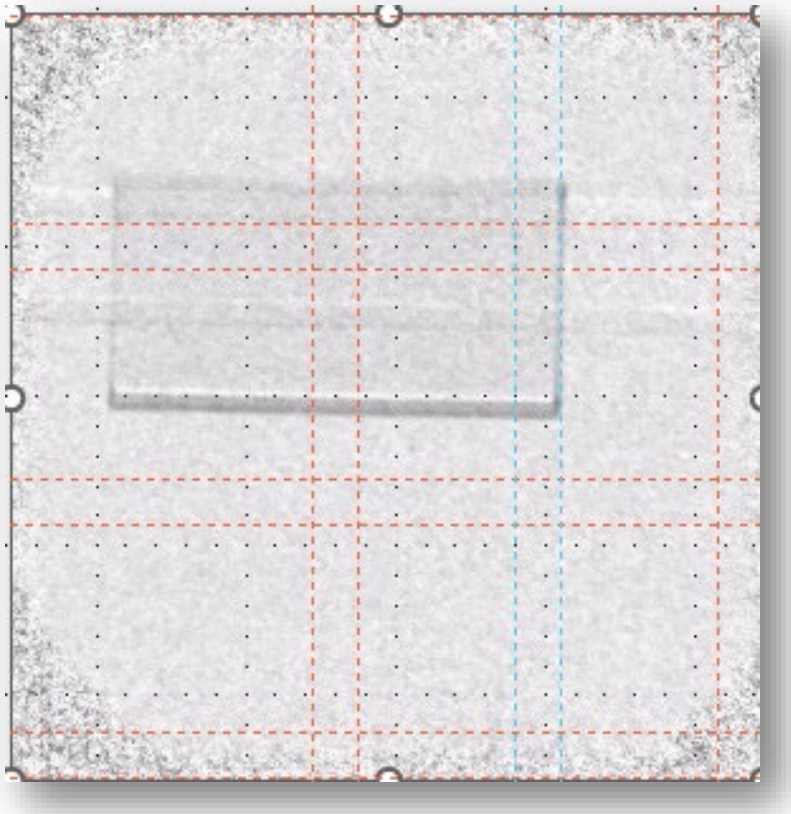

Steam

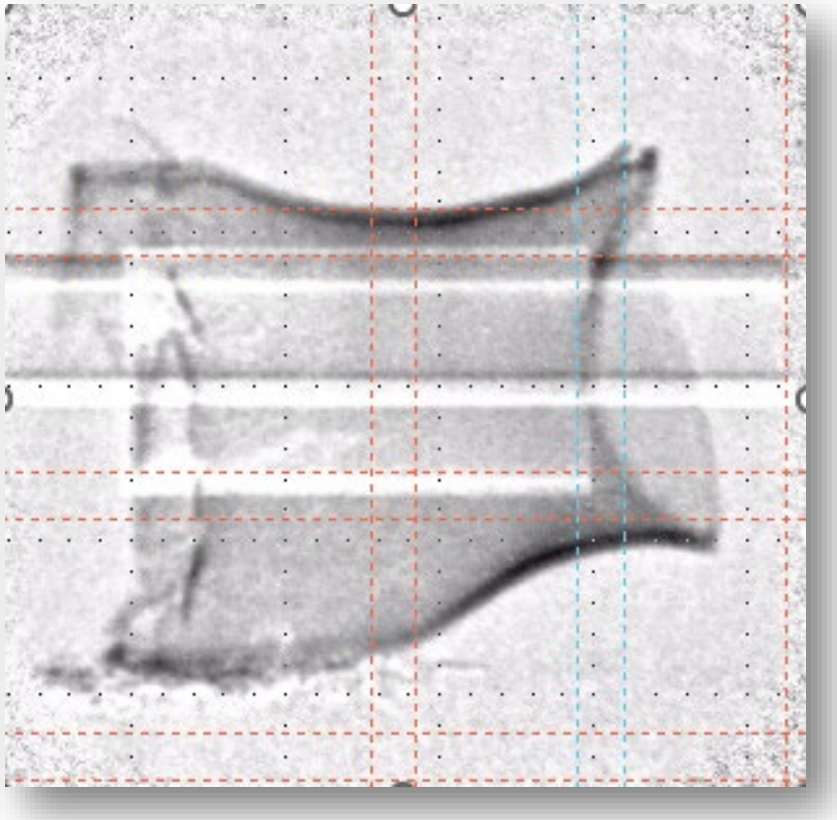

Steam + nitrogen

Grosse (2018): https://doi.org/10.1016/j.physb.2018.03.030

Mechanism of air oxidation

- Diffusion of the gas mixture through imperfections in the oxide scale to the metal/oxide interface
- Consumption of oxygen/steam
- Remaining nitrogen reacts with zirconium and forms ZrN
- ZrN is re-oxidized by fresh air with continuing reaction associated with a volume increase by 48%

➢ Formation of porous and non-protective oxide scales

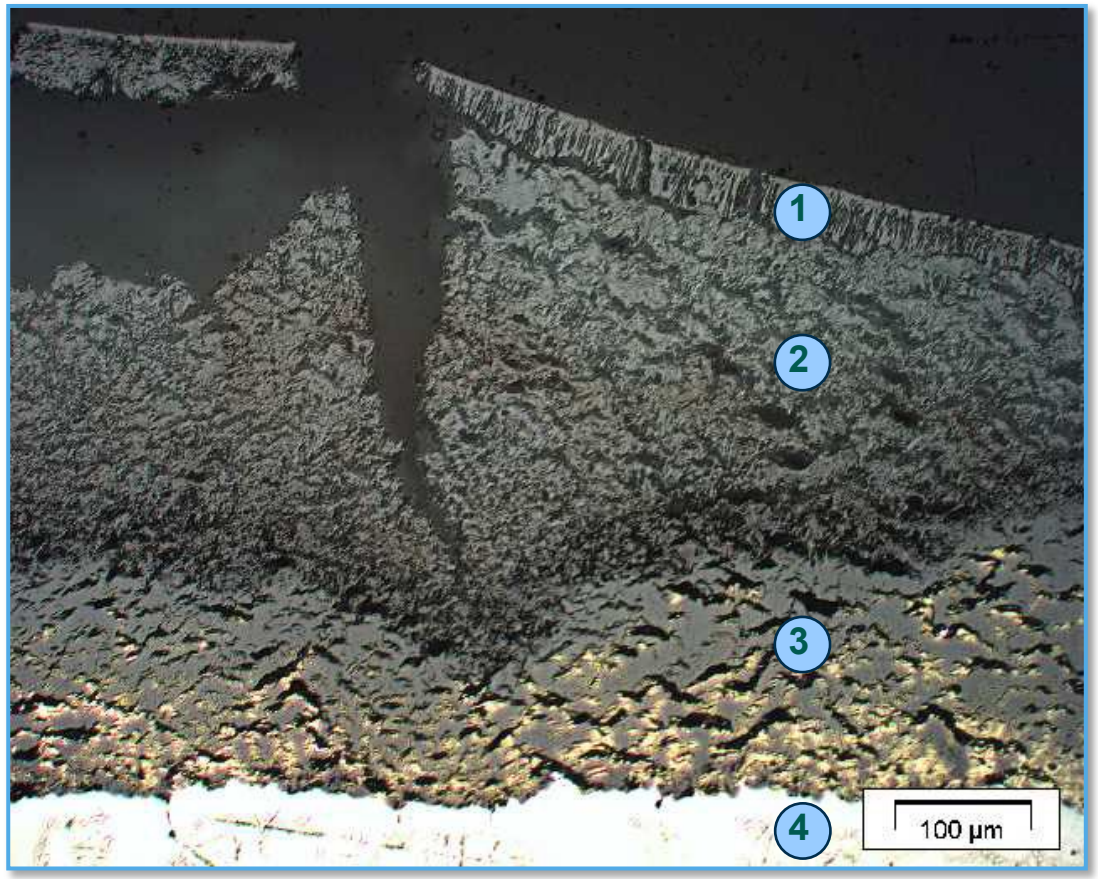

1 – initially formed dense oxide ZrO_2

2 – porous oxide after oxidation of ZrN

3 – ZrO_2 / ZrN mixture

4 – α-Zr(O)

Mechanism of air oxidation

Thermodynamic view

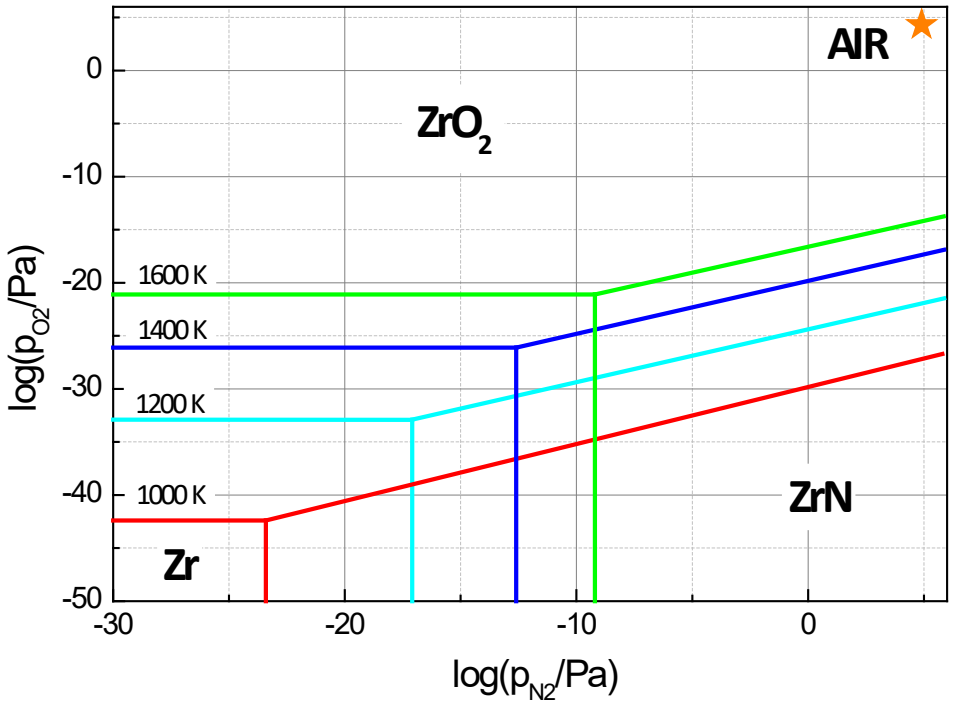

Stability diagram Zr-O-N

- ZrN only stable at very low oxygen partial pressure

Kinetic view

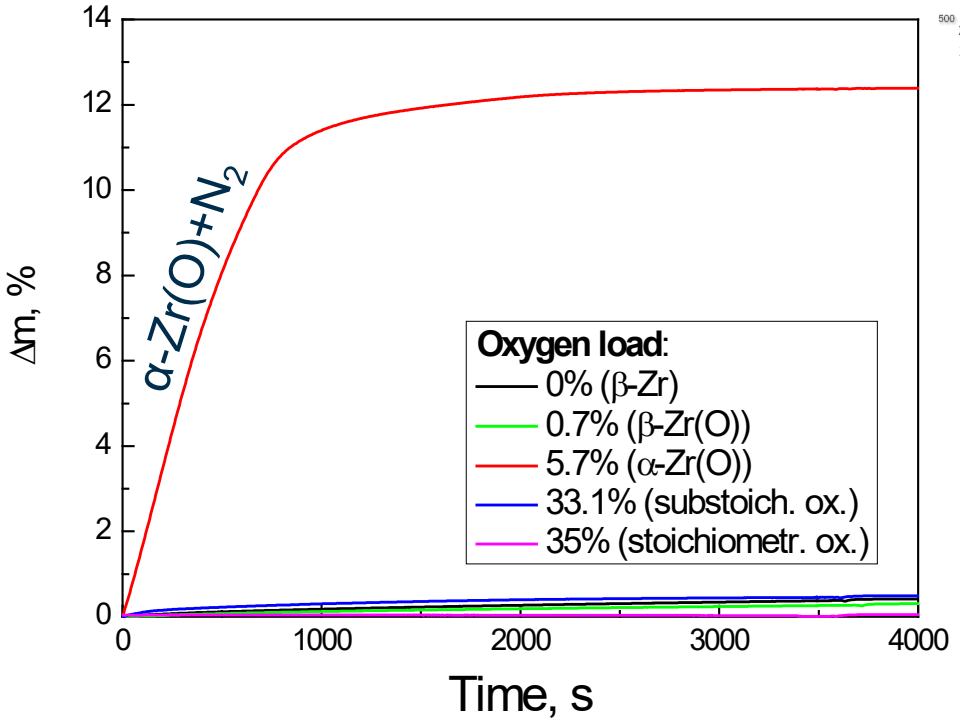

Reaction of ZrO_x with nitrogen (1200°C)

- Fast reaction of oxygen-stabilized Zr with nitrogen

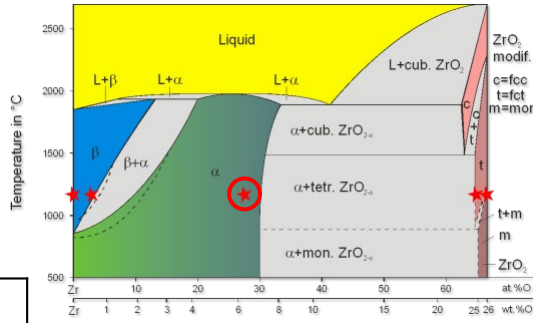

Both conditions are present locally at the metal-oxide interface

More information, see paper from Steinbrück
https://doi.org/10.1016/j.jnucmat.2009.04.018
http://dx.doi.org/10.1016/j.jnucmat.2013.12.024

Summary of oxidation in N_2 containing atmosphere

- Oxidation of zirconium alloys in atmospheres containing air or nitrogen is a very complex process, strongly dependent on experimental boundary conditions
- Nitrogen causes early loss of barrier effect against FP release and contributes to enhanced hydrogen source term
- The effect of nitrogen (“air ingress”) has been considered in the severe accident codes, using experimental data from KIT and other laboratories

Nitrogen is not an inert gas under the conditions of a nuclear accident!

The effect of B_4C-Fe eutectic interaction on accident progression

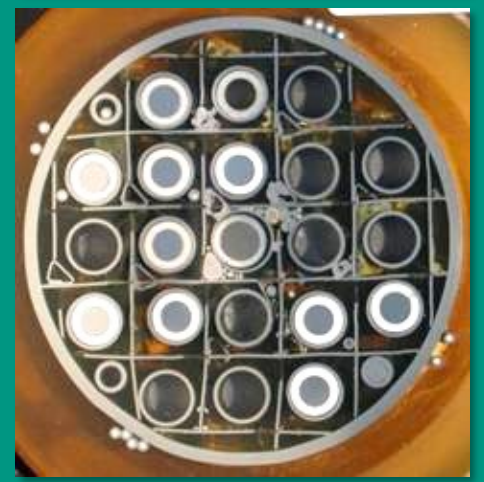

B_4C control rods in LWRs

- Boron carbide is used in boiling water reactors (BWR), VVERs, some pressurized water reactors (PWR)
- Oxidation of B_4C (containing melts) in steam produces large amounts of hydrogen, C+B containing gases, and heat
- Surrounded by stainless steel (cladding, blades) and Zry (guide tubes, canisters)

T_{eut} < 1200°C

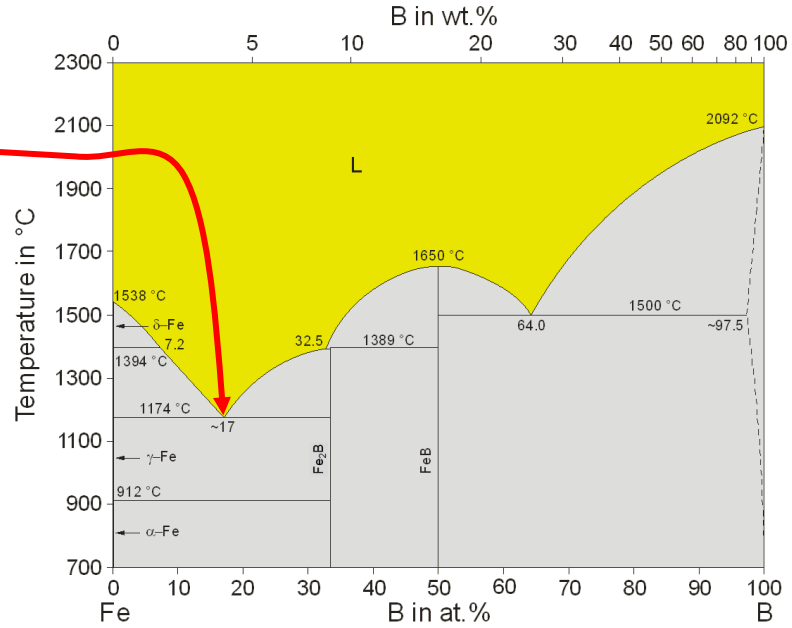

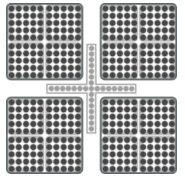

BWR control blade

B_4C pellet

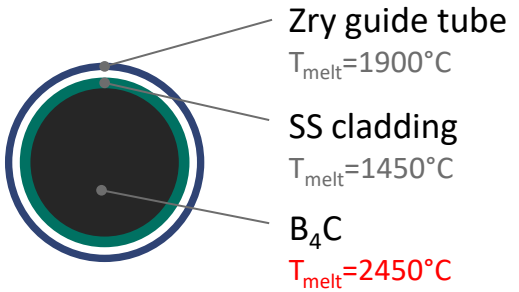

BWR control rod

Eutectic interaction of stainless steel with B_4C

1 h at approx. 1250 °C

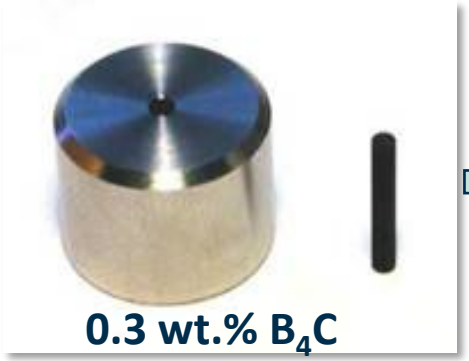

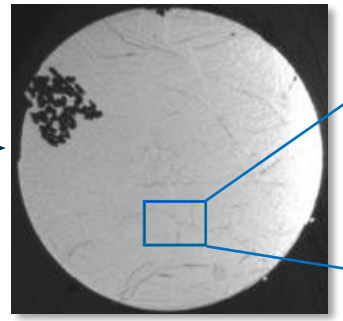

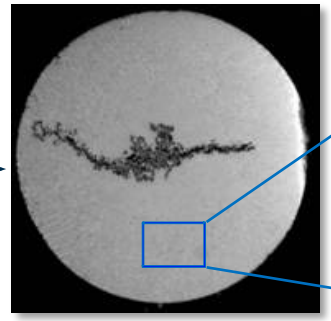

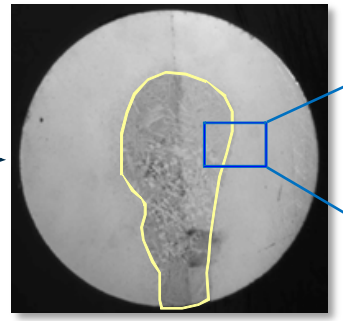

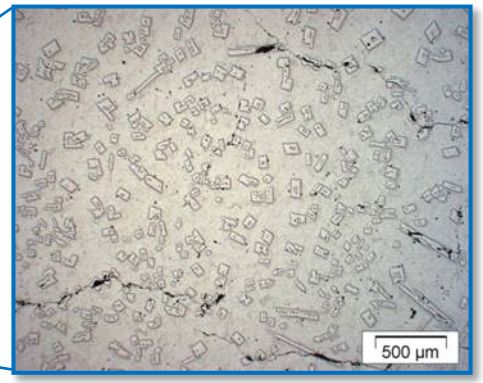

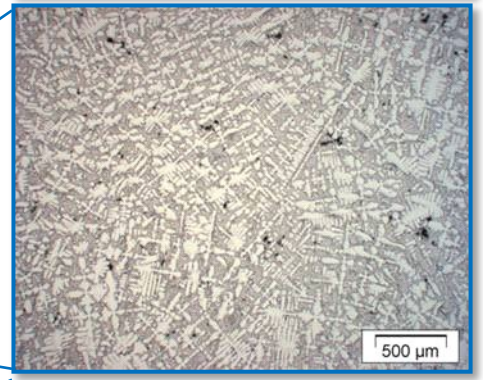

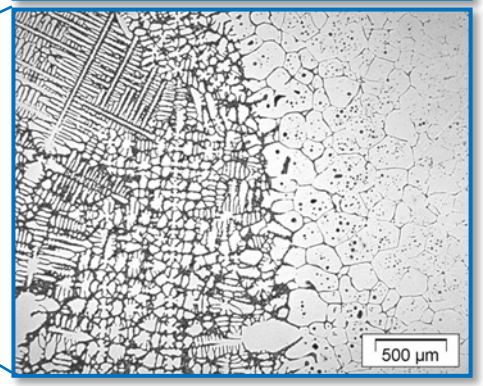

Complete liquefaction of stainless steel

1/3 of SS liquefied

Eutectic interaction of stainless steel with B_4C (kinetics)

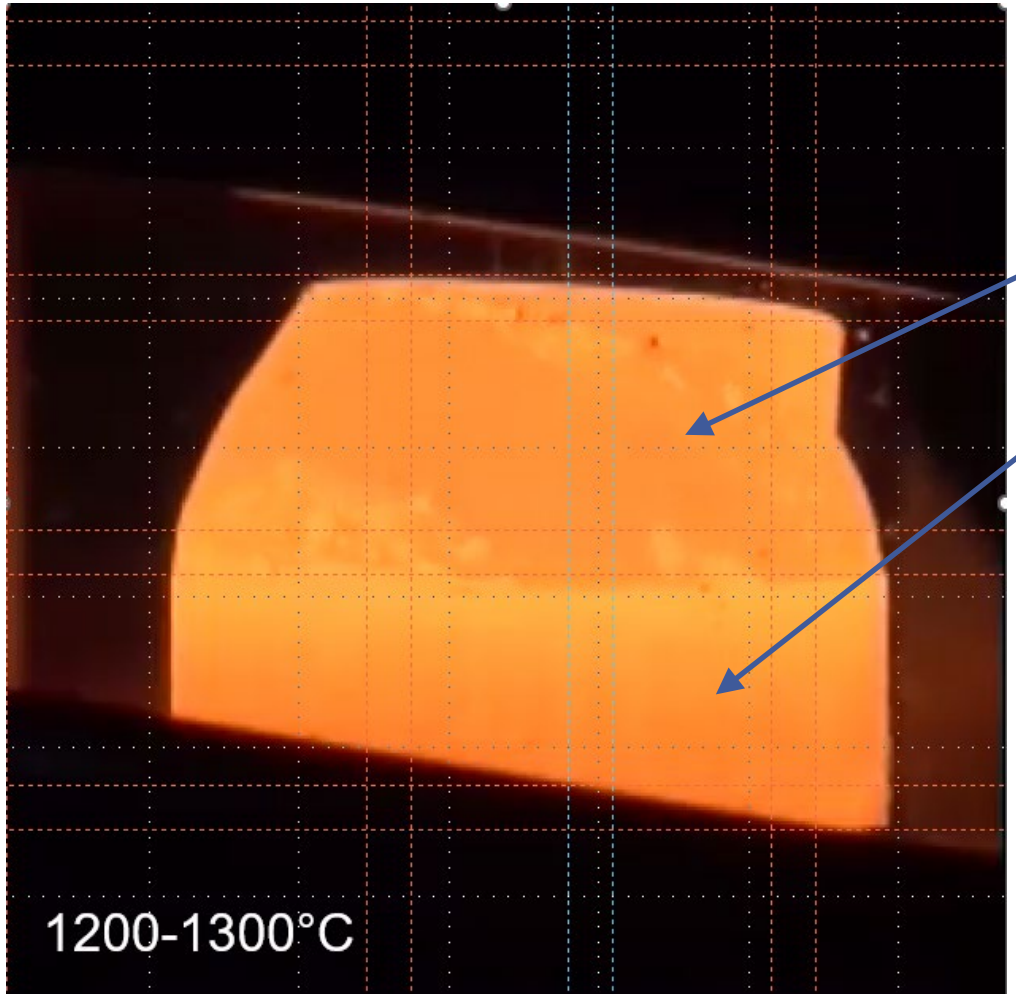

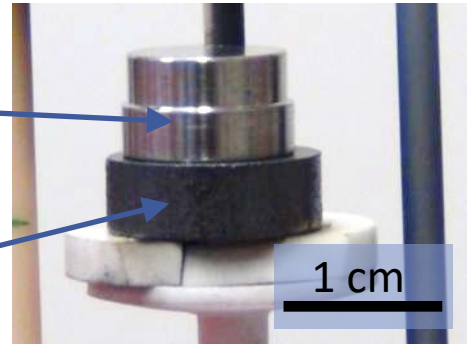

Rapid and complete melting of SS at 1250°C starting at B_4C/SS interface

Degradation of boron carbide control rods (pellet size)

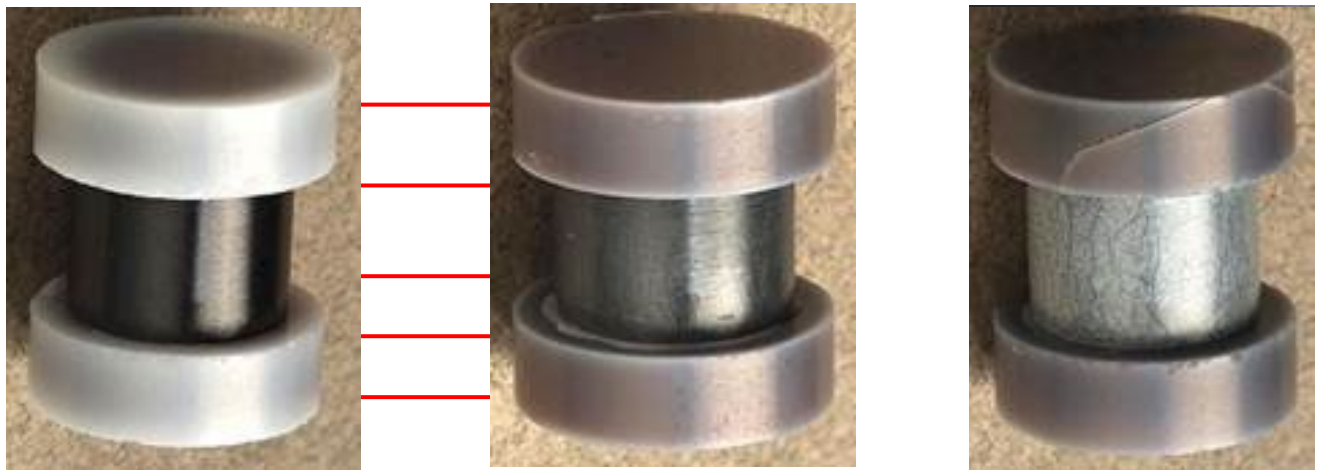

1000 °C 1200 °C 1300 °C

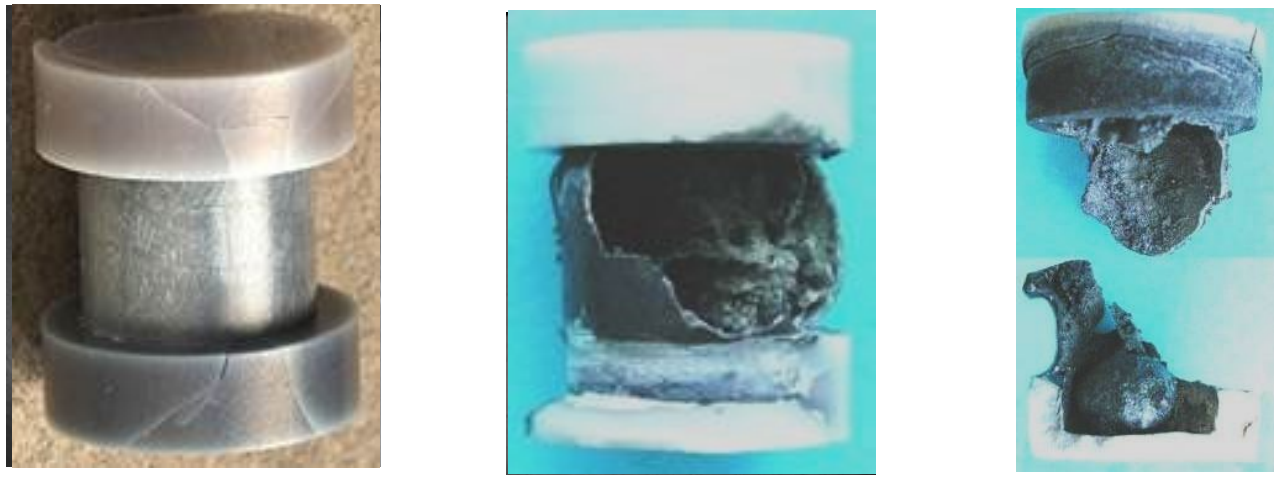

1400 °C 1500 °C 1600 °C

- Apparently intact samples up to 1400°C, but…

T ≤ 1200 °C:

- Intact specimen with B_4C/SS/Zry-4

T ≤ 1400 °C:

- Intact specimen due to “crucible effect” (melt kept by the external ZrO_2 scale)

T ≥ 1500 °C:

- Failure of the oxide shell and rapid oxidation of absorber melt and B_4C pellet

Degradation of B_4C control rods (single rod)

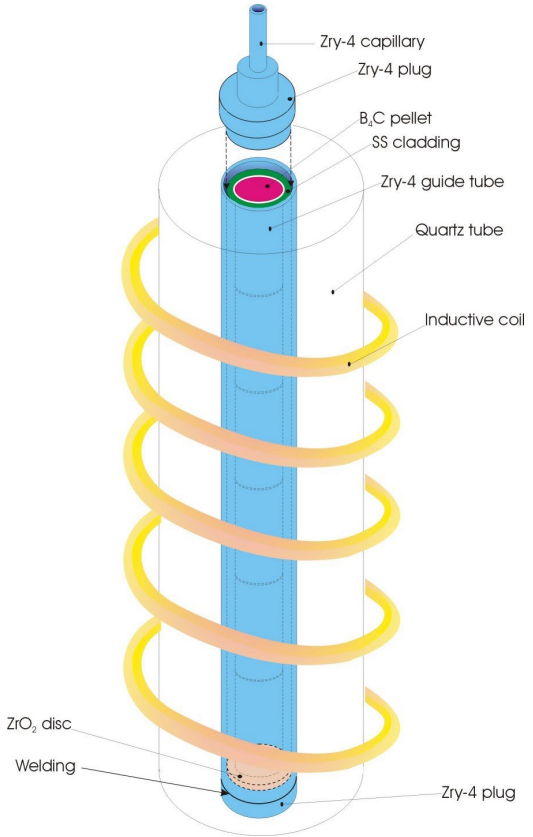

Inductive heating of the specimen in the QUENCH rig

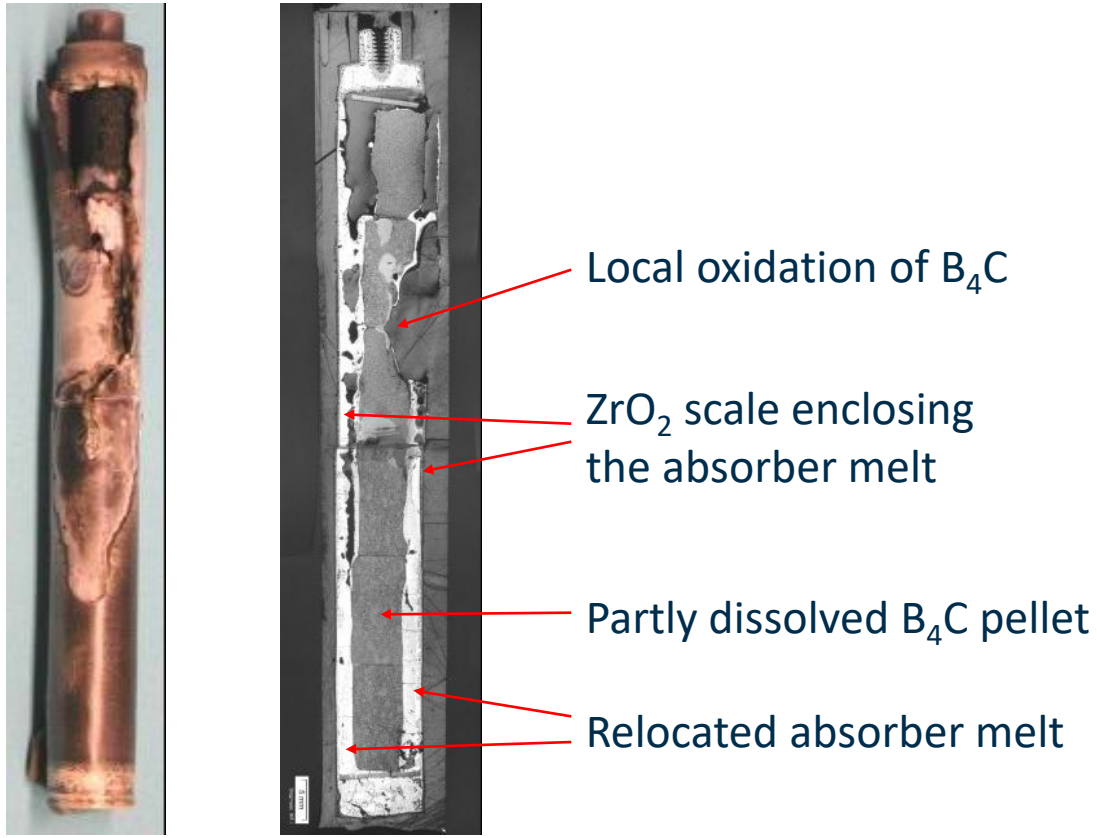

Post-test appearance and axial cross-section of a specimen after 30 min isothermal test at 1470 °C

Degradation of B_4C control blade (BWR bundle test CORA-16)

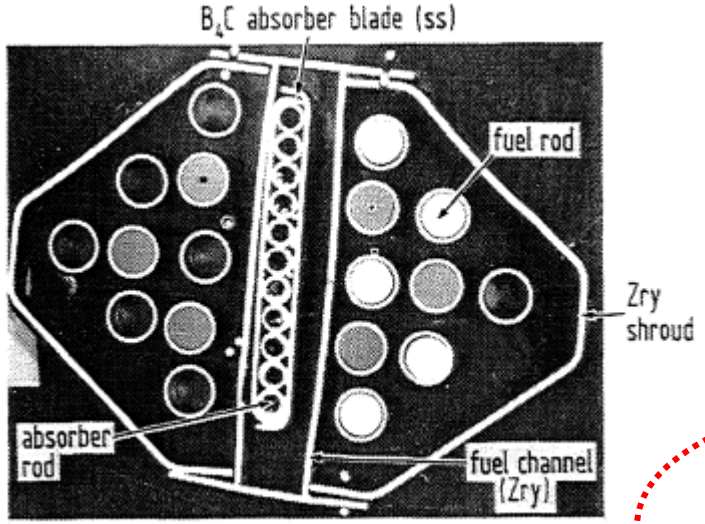

16-08 (1145mm), bottom view

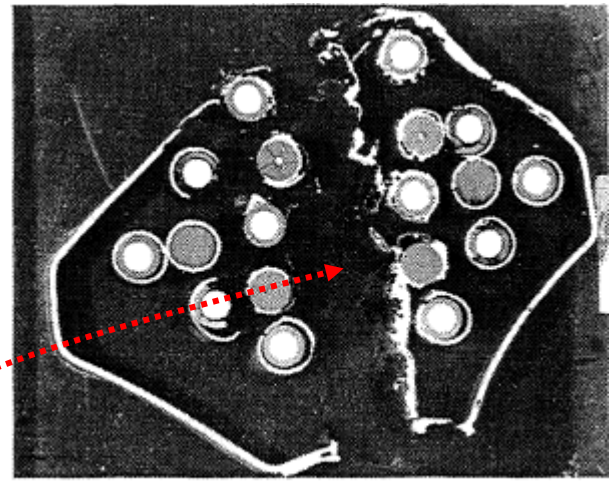
16-07 (963mm), top view

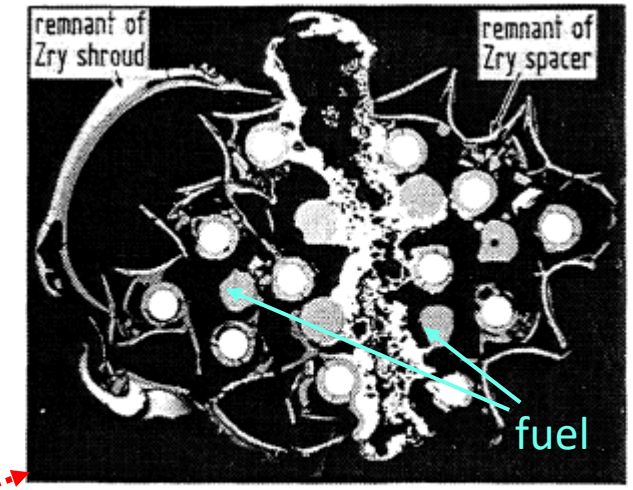

16-09 (525mm), top view
center grid spacer elevation

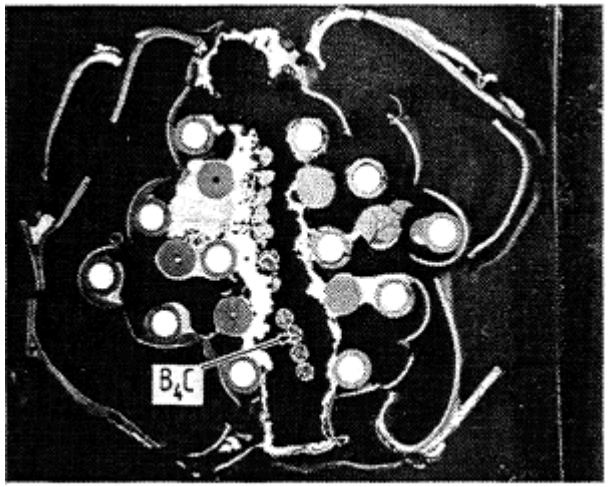

16-03 (310mm), top view

- Complete loss of absorber blade
- Dissolution of cladding and fuel
- Massive melt relocation (SS, Zry, UO_2)

16-01 (110mm), top view

Oxidation of eutectic melts

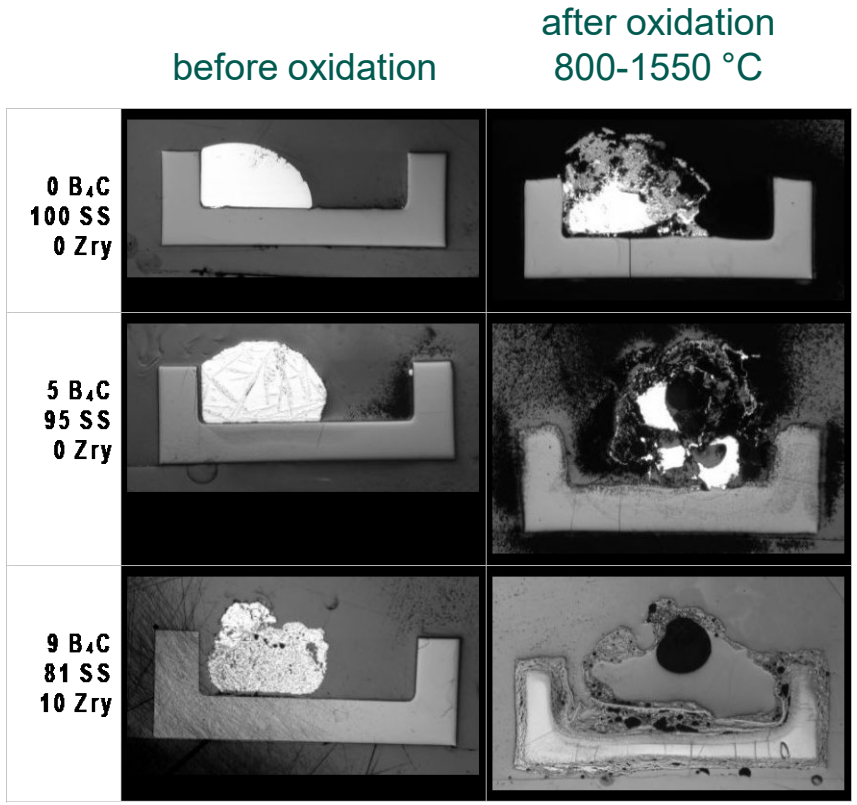

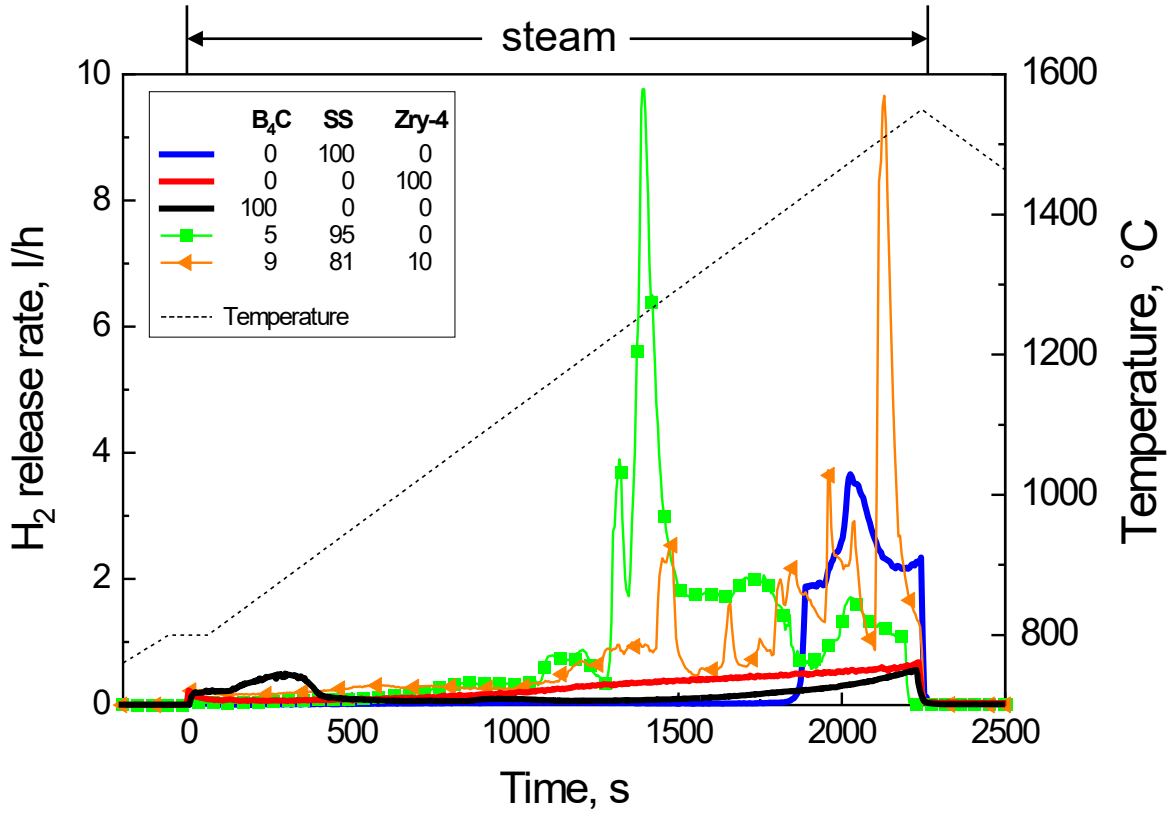

Strong interaction of oxidized melt with ZrO_2 crucible

High oxidation rates beyond melting temperature

Summary of B_4C effects in severe accidents

- Low-temperature eutectic melts form at temperatures several hundred Kelvin below the melting temperatures of the materials involved
- These chemically aggressive melts may attack surrounding core structures including fuel, thus influencing corium behavior and the FP source term
- Oxidation of B_4C and B_4C-containing melts results in the release of large amounts of hydrogen and heat
- Further reaction products (CO, CO_2, boric acids) have to be taken into account for accident analyses as well
- No methane (relevant for FP chemistry) is produced during high-temperature oxidation of B_4C

Takeaways

- Not everything is as it seems at first glance
- Experiments must be designed to be as prototypical as possible
- Equilibrium thermodynamics (also locally!) and kinetics must be considered
- The key to the success of the QUENCH program lies in the interlocking of large-scale bundle experiments, separate-effects tests, modelling, and code validation and application

Acknowledgement

- Helmholtz Association for funding program NUSAFE at KIT
- Program NUSAFE and IAM institute's management for broad support of our activities
- Funding and supporting organizations as German ministries, EURATOM program, OECD-NEA, etc.

- And last but not least the QUENCH team

Juri Stuckert
KIT

The importance of the temperature gradient for the processes occurring during high-temperature oxidation of the cladding, its mechanical deformation and oxidation of the melt

Unlike isothermal conditions in some single effect tests, prototypical reactor conditions and the bundle tests simulating them always exhibit both axial and radial temperature gradients. Such gradients are crucial for a number of effects observed in accident conditions at high temperatures. This presentation describes three such effects: (1) Redistribution of oxygen in cladding under steam starvation conditions; (2) Growth of ceramic precipitates in a metal melt during its oxidation; (3) Dependence of cladding deformation on radial temperature gradient.

In the first case, the heat flow from the pellet to the outer surface of the cladding creates a temperature gradient across the outer cladding oxide layer. In areas of steam starvation, this leads to the formation of metal precipitates in the oxide layer already at temperature (at $T \gtrsim 1200$ °C), and not only during the cooling stage.

The second case involves the release of molten cladding metal (through the degrading oxide cladding layer) into the interrod space and its oxidation in the steam. Due to the pronounced exothermic oxidation reaction, the temperature at the surface of the resulting molten pool is higher than in its bulk. This drives the formation of ceramic precipitates within the melt already at temperature, leading to its complete transition to the ceramic phase.

The third case concerns the formation of asymmetric cladding ballooning during a design basis accident. Fuel pellets can maintain their geometric shape up to burnups of 30 MWd/kgU, and a gap remains between the pellet and the cladding. Several pellets are displaced from their axisymmetrical arrangement and touch the cladding at a specific point, forming a hot spot there. As a result, the cladding begins to plastically deform at $T>600$ °C, primarily near this hot spot. As a result, the circumferential strain of the cladding can remain below 40%, significantly lower than in single rod tests with direct current heating of the cladding.

Karlsruhe Institute of Technology

Institute for Applied Materials

The importance of the temperature gradient for the processes occurring during high-temperature oxidation of the cladding, its mechanical deformation and oxidation of the melt

J. Stuckert

Institute for Applied Materials; Program NUSAFE

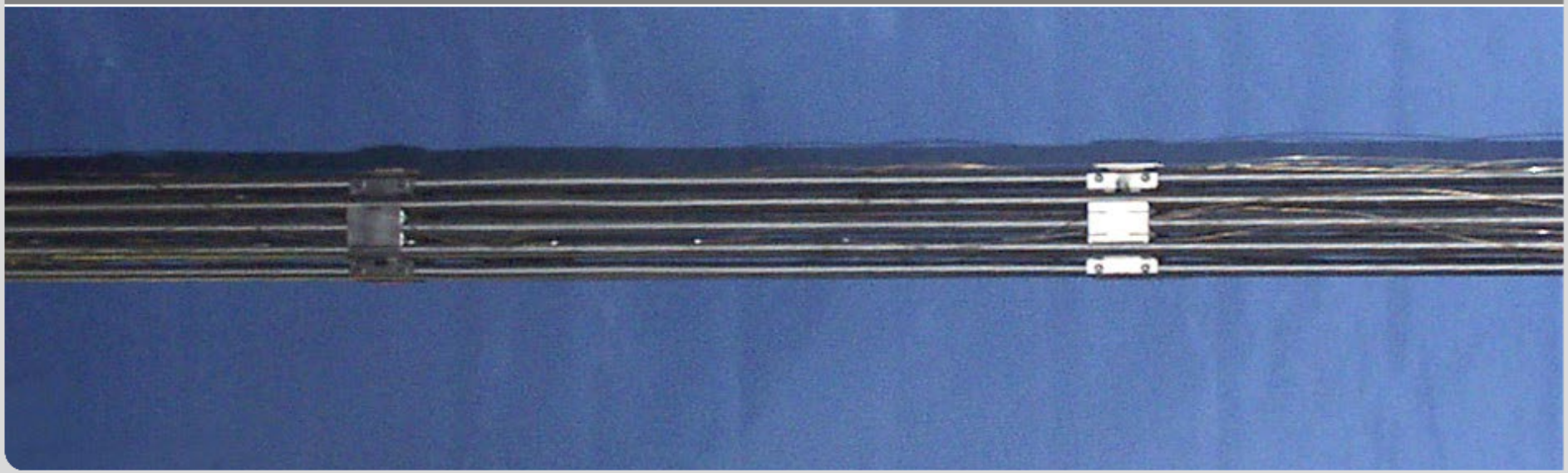

Outline

(1) Redistribution of oxygen in cladding under steam starvation conditions.

(2) Growth of ceramic precipitates in a metal melt during its oxidation.

(3) Dependence of cladding deformation on radial temperature gradient.

Evolution of outer oxide layer annealed in Ar at T≈1150 °C without radial temperature gradient: gradual diffusion of oxygen into the metal layers with decrease of ZrO_2 and increase of α-Zr(O)

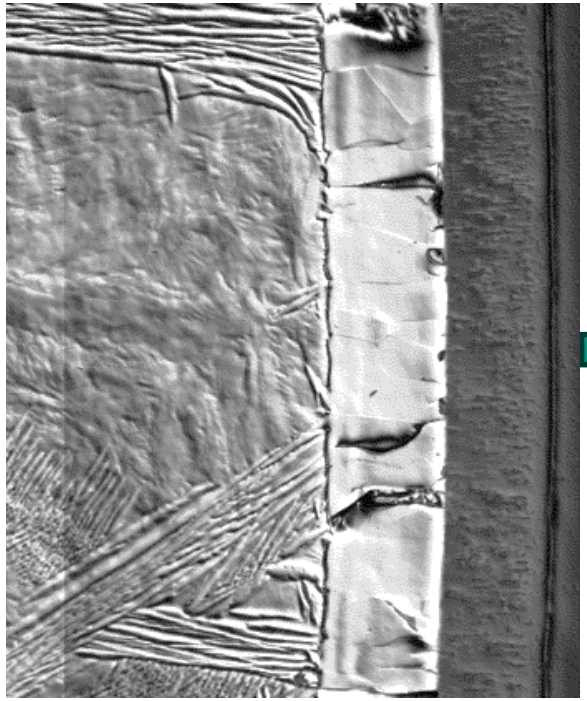

prior β-Zr α-Zr(O) ZrO_2

after oxidation in steam:
ZrO_2 73 µm, α-Zr(O) 83 µm,
β-Zr residual

α-Zr(O) ZrO_2

after **annealing** in Ar during 900 s:
ZrO_2 52 µm, α-Zr(O) 165 µm,
β-Zr residual

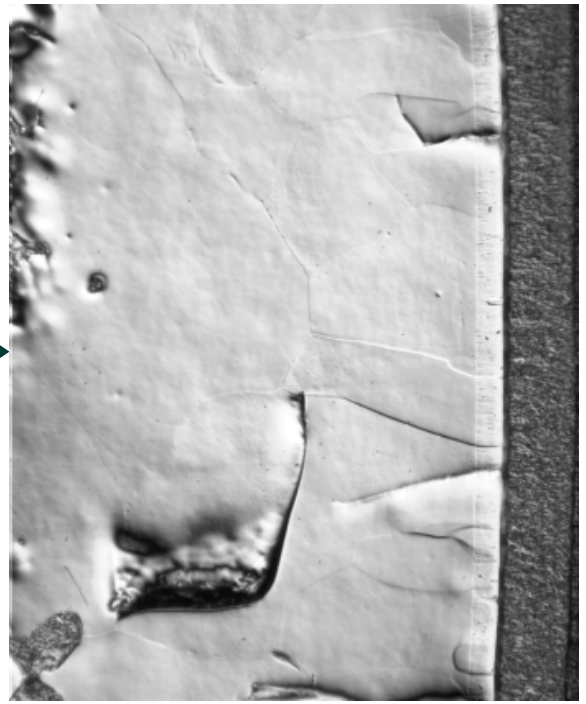

α-Zr(O) ZrO_2

after **annealing** in Ar during 1800 s:
ZrO_2 43 µm, α-Zr(O) 329 µm,
β-Zr residual

J. Stuckert et al.,
Kinetics of dissolution of oxide layer on cladding surface under oxygen starvation conditions at temperatures between 900°C and 1200°C,
QUENCH-Workshop 20 (2014),
https://www.doi.org/10.13140/RG.2.2.25819.05925

decrease of ZrO_2: $\Delta d_{ox} / t^{1/2} = 287*exp(-8473/T) = 287*exp(-70326/RT)$,

increase of α-Zr(O): $\Delta d_{\alpha} / t^{1/2} = 5*10^6*exp(-19679/T) = 5*10^6*exp(-163611/RT)$,

with $R = 8.314\ J/(mol*K)$

Radial temperature gradient across the cladding oxide layer in single rod and bundle tests (T>1100°C) with flowing steam

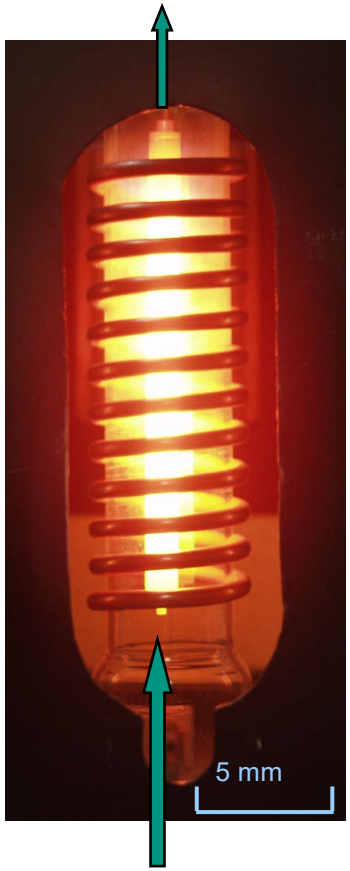

steam, 100 g/h
Ar, 90 l/h

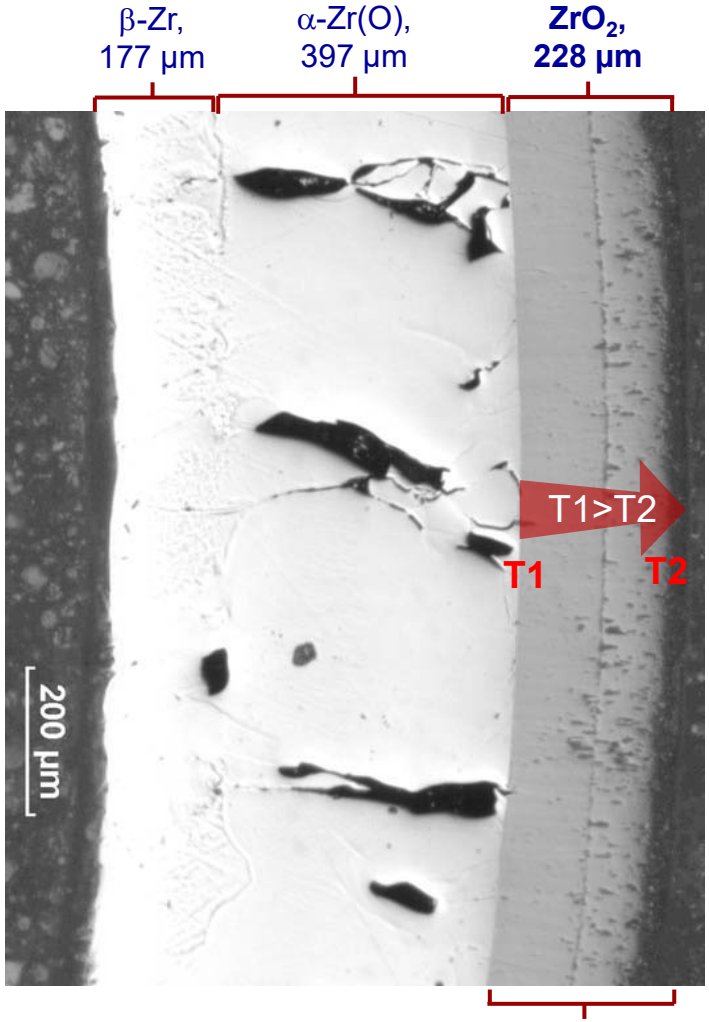

$$|\nabla T| \approx -0.2\ K/\mu m$$

QUENCH-07 bundle:
thick oxide layers
after oxidation in steam

Evolution of outer oxide layer annealed in Ar at T≈1430 °C during 1 h with radial temperature gradient: gradual diffusion of oxygen into the metal layers

reference sample after oxidation in steam during 750 s

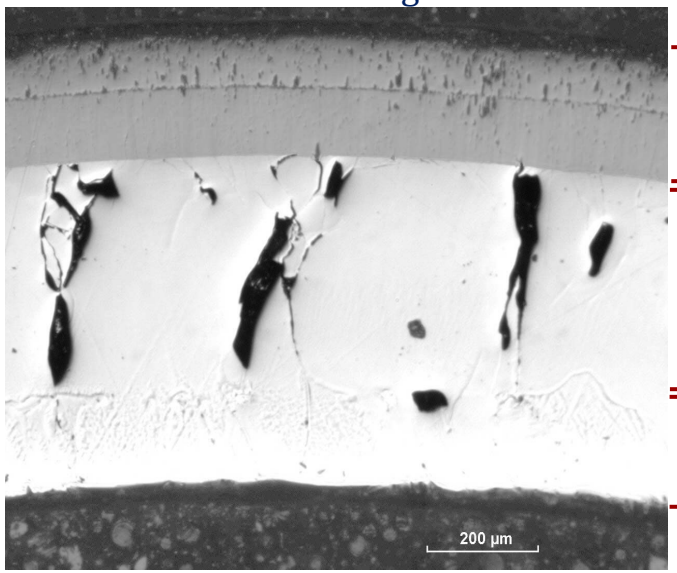

duplex layer ZrO_2, 228 µm

α-Zr(O), 397 µm

β-Zr, 177 µm

test sample after following annealing in Ar during 3 h

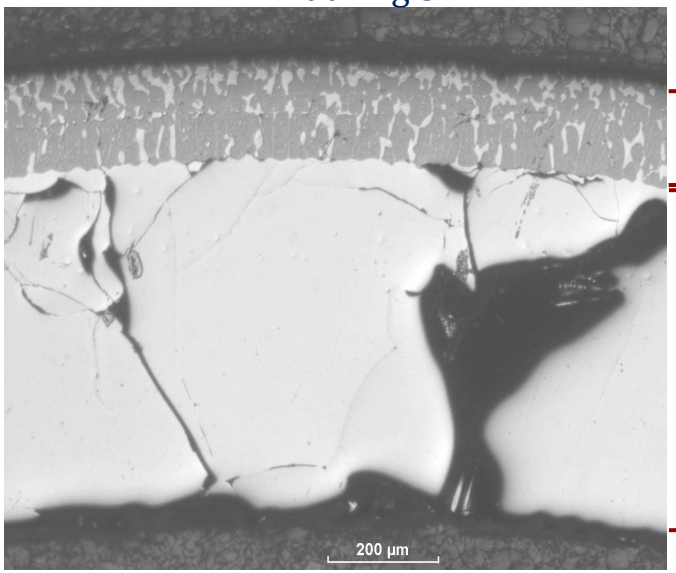

ZrO_2, 186 µm

α-Zr(O), 646 µm

J. Stuckert and M. Veshchunov, **Behaviour of Oxide Layer of Zirconium-Based Fuel Rod Cladding under Steam Starvation Conditions**, FZKA-7373 (2008), https://www.doi.org/10.5445/IR/270071587

moderate decrease of the ZrO_2 layer thickness;

disappearance of β-Zr layer;

formation of **α-Zr(O) precipitates inside ZrO_2 at temperature** */it is **not the eutectoid** phase, which can be formed due to decomposition of the sub-stoichiometric ZrO_{2-x} during the cooldown/ ;*

relative large area of precipitates: 24%

A probable explanation for the observed phenomenon is the peculiarity of the phase diagram at the sub-stoichiometric boundary of tetragonal ZrO_2

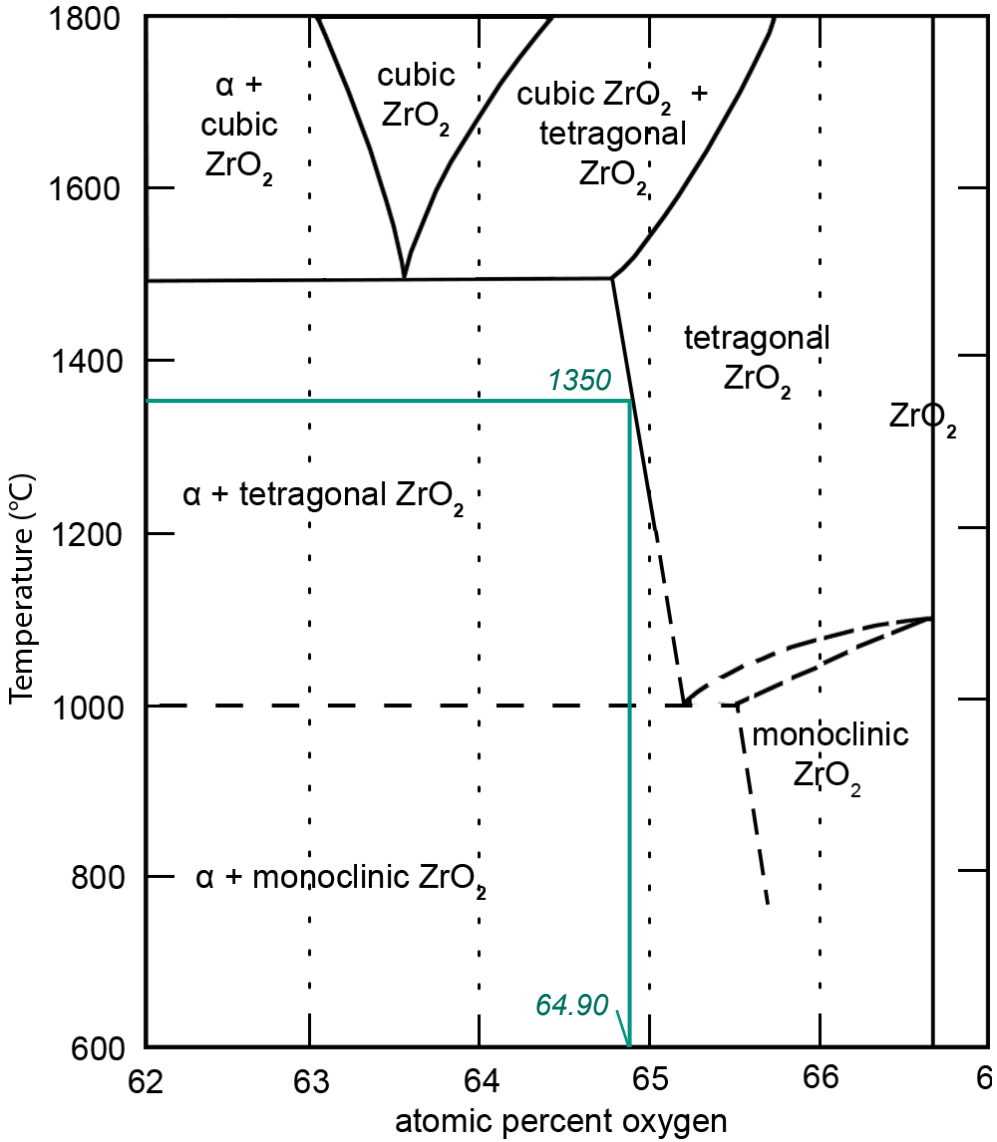

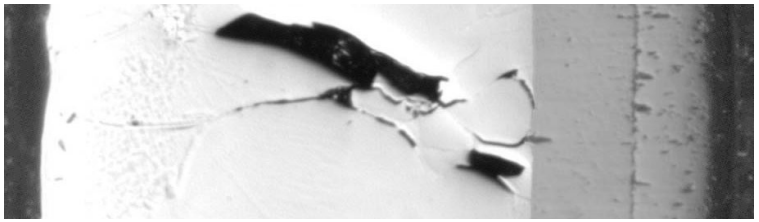

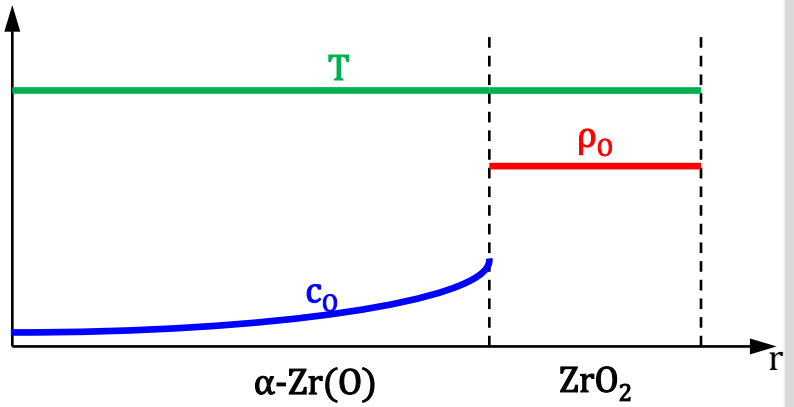

Isothermal conditions

part of Zr-O phase diagram acc. to Domagala and McPherson, Ruh and Garrett

A probable explanation for the observed phenomenon is the peculiarity of the phase diagram at the sub-stoichiometric boundary of tetragonal ZrO_2

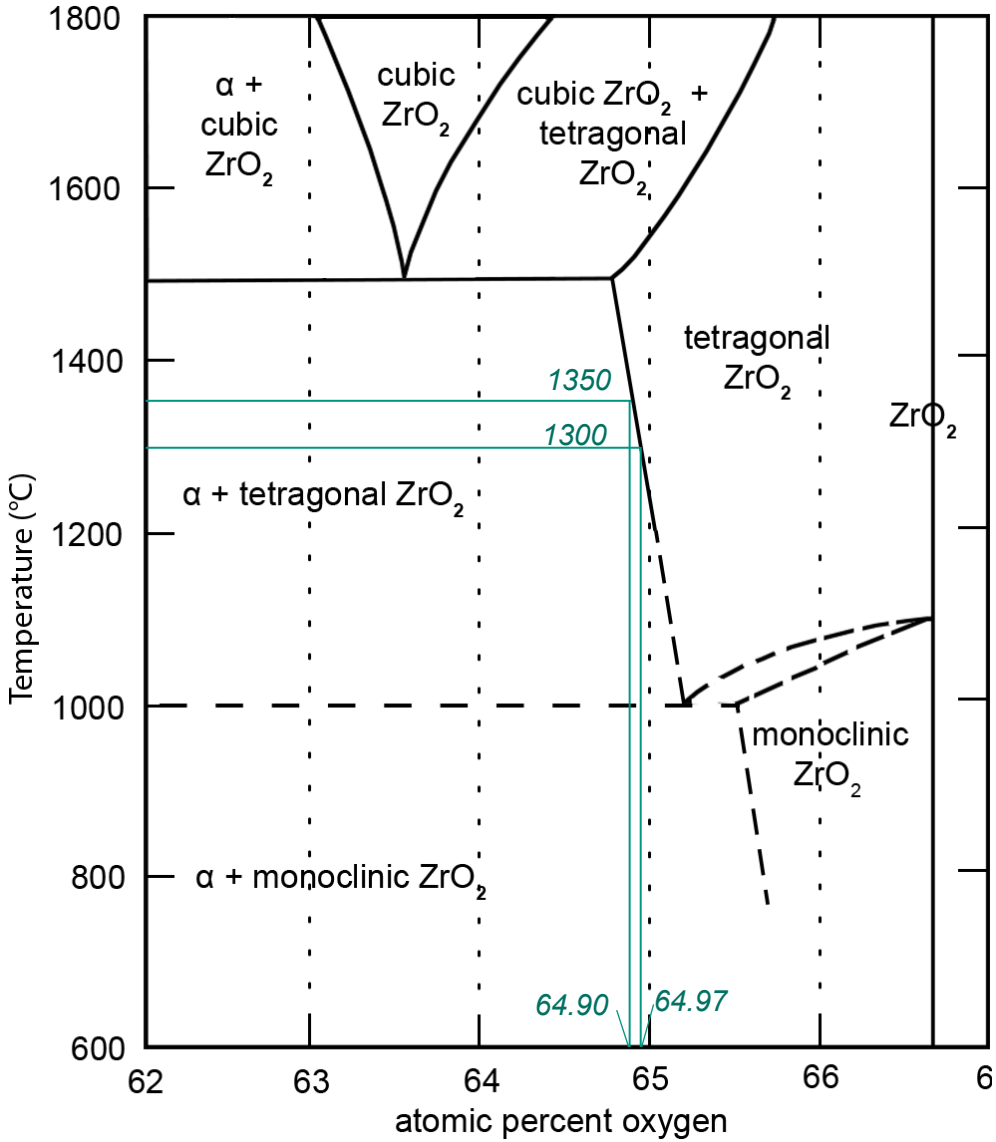

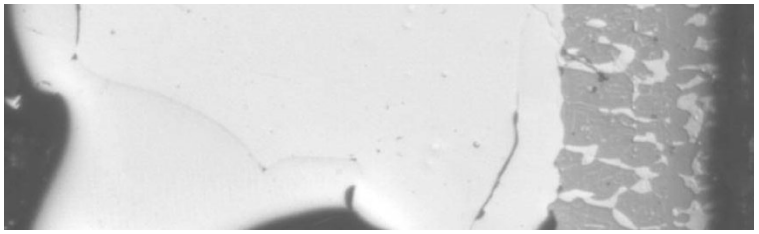

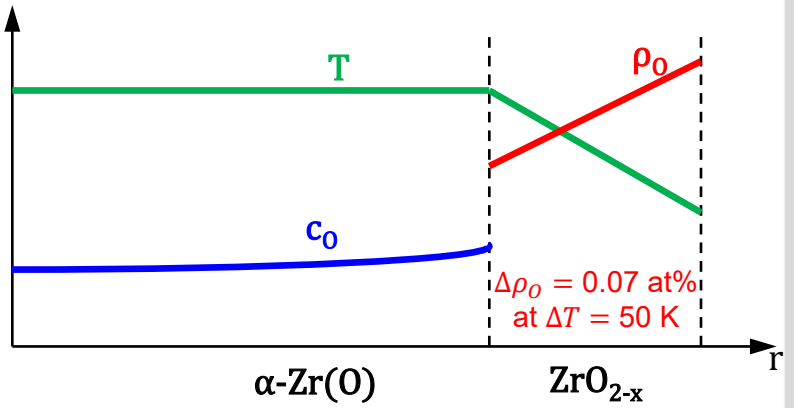

Temperature gradient

↓

Gradient of oxygen concentration

↓

Diffusion of oxygen across the oxide

part of Zr-O phase diagram acc. to Domagala and McPherson, Ruh and Garrett

Experiments at 1300 °C: formation of the outer α-Zr(O) layer after formation of α-Zr(O) precipitates

change of oxide layer after 720 s oxidation during annealing:

- monotonous decrease of the layer thickness
- formation of bulk α-Zr(O) precipitates
- formation of **α-Zr(O) layer** on outer surface of oxide

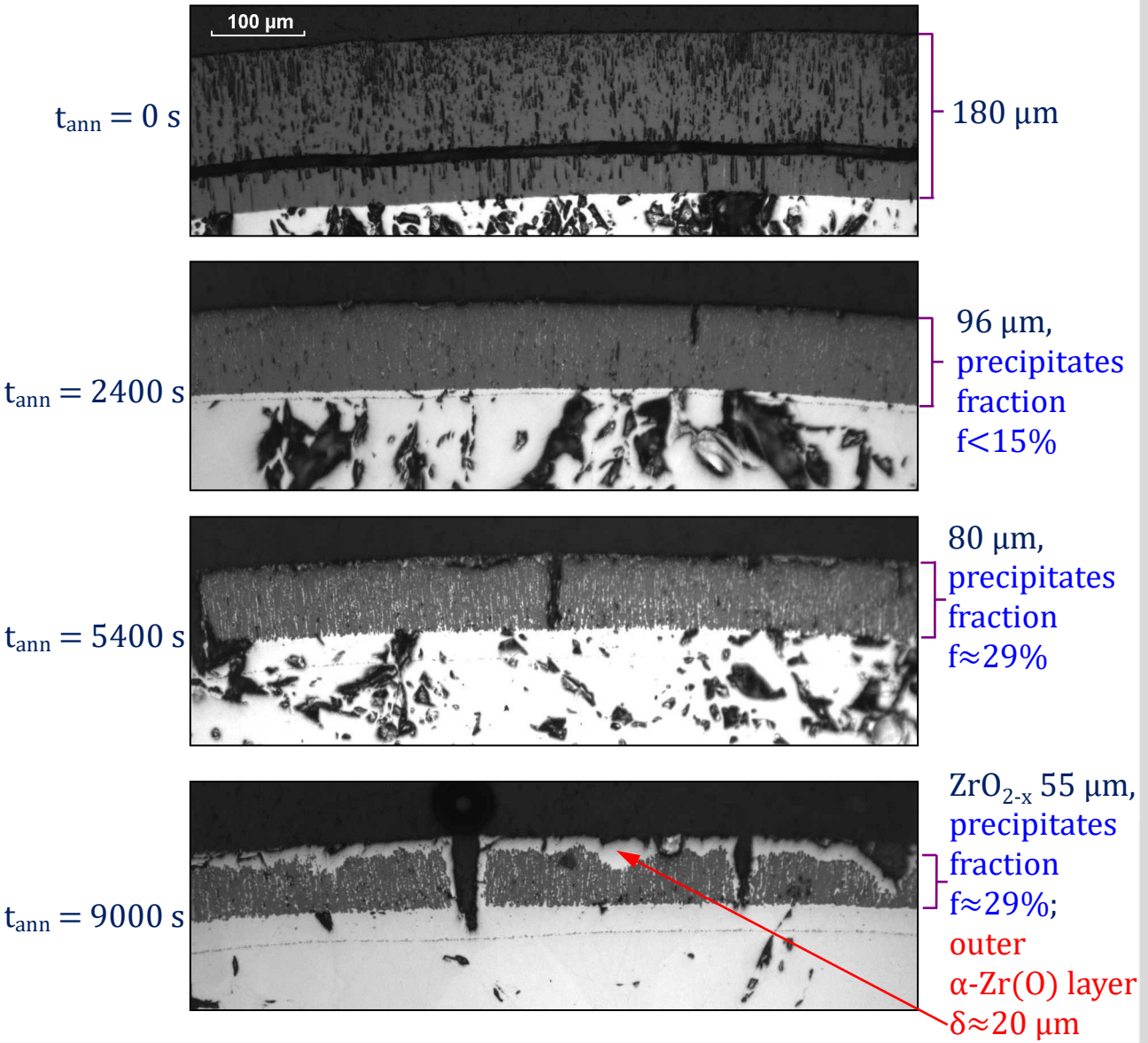

Formulas for evaluating numerical quantities

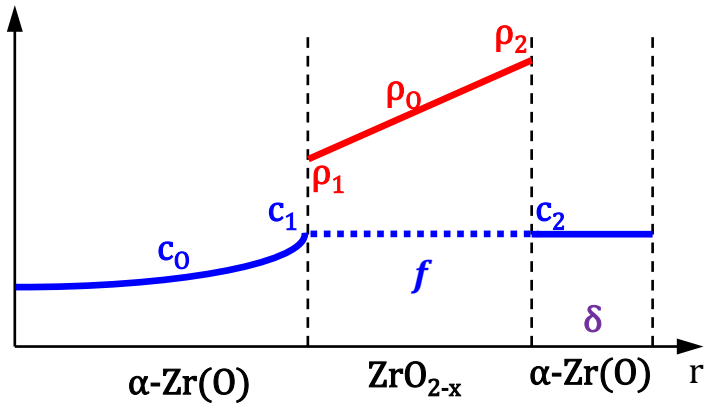

Oxygen concentration profiles in layers of the oxidized cladding after equilibration of ZrO_{2-x} phase under a temperature gradient

According to the Veshchunov's approach:

fraction of α-Zr(O) precipitates in ZrO_2:

$$f \approx \frac{D_O^{ox}}{L_{final}} \cdot \frac{\Delta\rho_O(t)}{L(t)} \cdot \frac{\rho_{Zr}}{c_{Zr}\rho_2 - c_2\rho_{Zr}} \cdot t$$

*thickness of outer α-Zr(O) layer formed after cessation of **f** increase (due to relaxation of compressive stresses):*

$$\delta_\alpha^{out} \approx D_O^{ox} \cdot \frac{\Delta\rho_O(t)}{L(t)} \cdot \frac{\rho_{Zr}}{c_{Zr}\rho_2 - c_2\rho_{Zr}} \cdot t$$

where ρ_{Zr}=35, c_{Zr} = 70, ρ_2=65, c_2=30;

for tetr. ZrO_2: $D_O^{ox}[\frac{cm^2}{s}] = 8.67 \cdot \exp(-\frac{20380}{T})$,

$D_O^{ox} = 2.05 \cdot 10^3 \mu m^2/s$ @ 1300 °C;

$\frac{\Delta\rho_O(t)}{L(t)} = const = \frac{0.07}{250} = 2.8 \cdot 10^{-3} \frac{\%}{\mu m}$ (due to $|\nabla T| \approx 0.2 \frac{K}{\mu m}$)

- The corresponding calculations give values of *f=31%* (after t=5400 s, i.e. L_{final}=80 μm) and δ=*21 μm* (after following t=3600 s), which agrees with the experiment performed at T_{pct}=1300 °C (previous slide)

Influence on air ingress after steam starvation

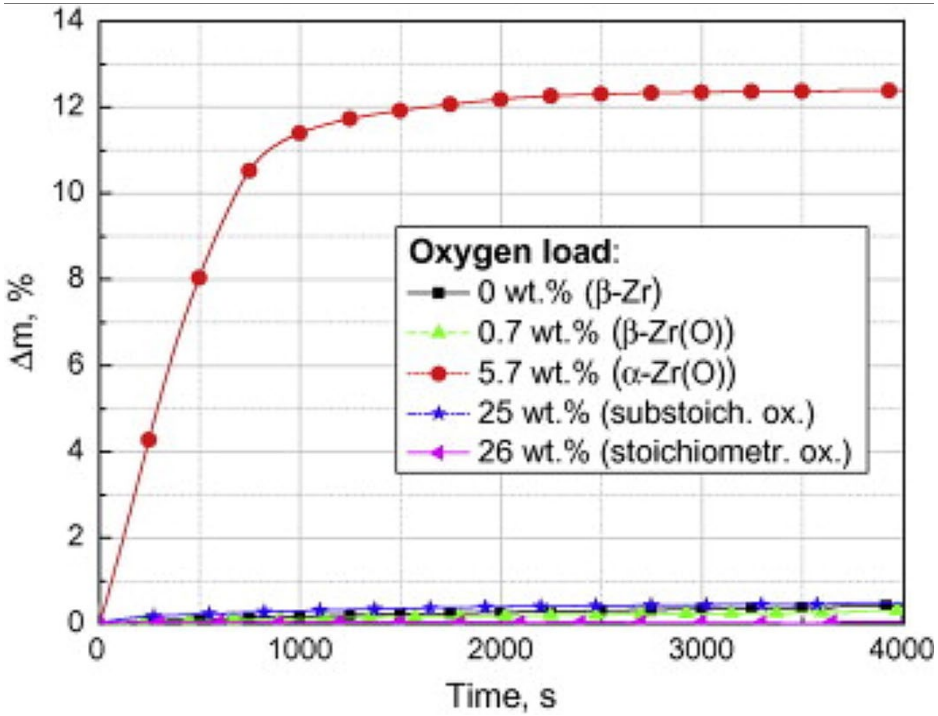

N_2 interaction only with α-Zr(O)

Martin Steinbrück,
High-temperature reaction of oxygen-stabilized α-Zr(O) with nitrogen, JNM 447 (2014), 46-55, https://doi.org/10.1016/j.jnucmat.2013.12.024

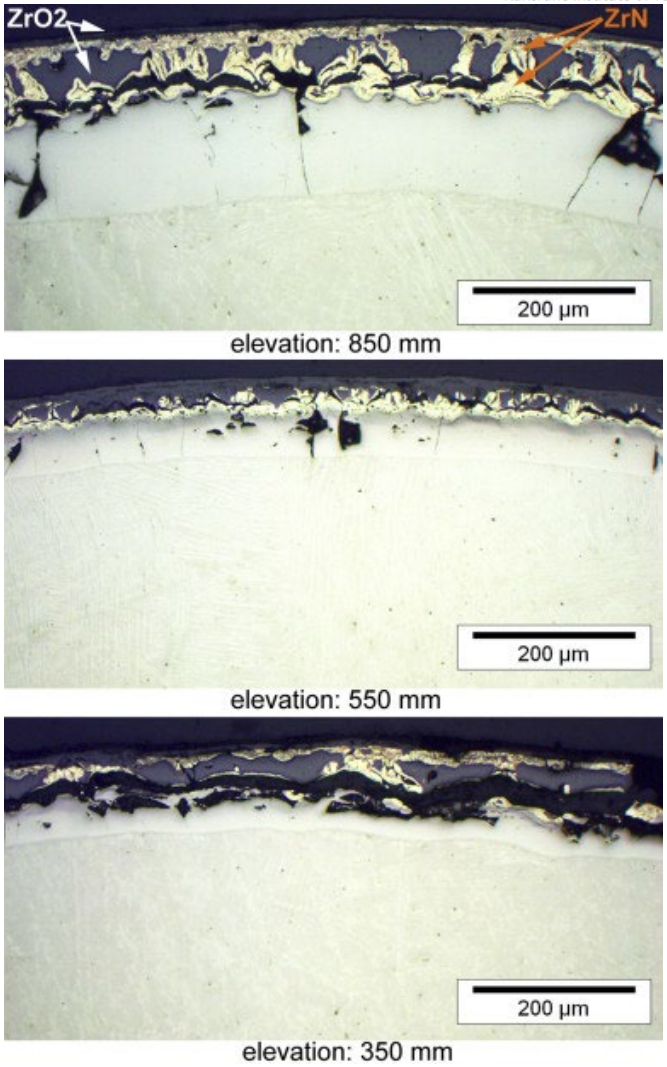

N_2 interaction with α-Zr(O) formed during the steam starvation stage of the QUENCH-16 test

J. Stuckert, M. Steinbrück,
Experimental results of the QUENCH-16 bundle test on air ingress, PNE 71 (2014), 134-141, https://doi.org/10.1016/j.pnucene.2013.12.001

Sequence of phenomena in the ZrO_2 layer due to oxygen diffusion into the inner metallic layers during steam starvation

- For T ≳ 1400 °C
  - Equilibration of ZrO_{2-x} phase (transition from stoichiometric ZrO_2 to substoichiometric ZrO_{2-x}).
  - Movement of the boundary between ZrO_{2-x} and α-Zr(O) layers, growth of α-Zr(O) precipitates inside the ZrO_{2-x} layer until the internal α-Zr(O) layer is saturated with oxygen.

- For T ≲ 1400 °C
  - Equilibration of ZrO_{2-x} phase.
  - Thickness decrease of the ZrO_{2-x} layer, growth of α-Zr(O) precipitates inside the ZrO_{2-x} layer.
  - Cessation of α-Zr(O) precipitates growth due to relaxation of compressive stresses inside the oxide layer.
  - Growth of the outer α-Zr(O) layer until the internal α-Zr(O) layer is saturated with oxygen.

(2)

Cladding melt release and relocation

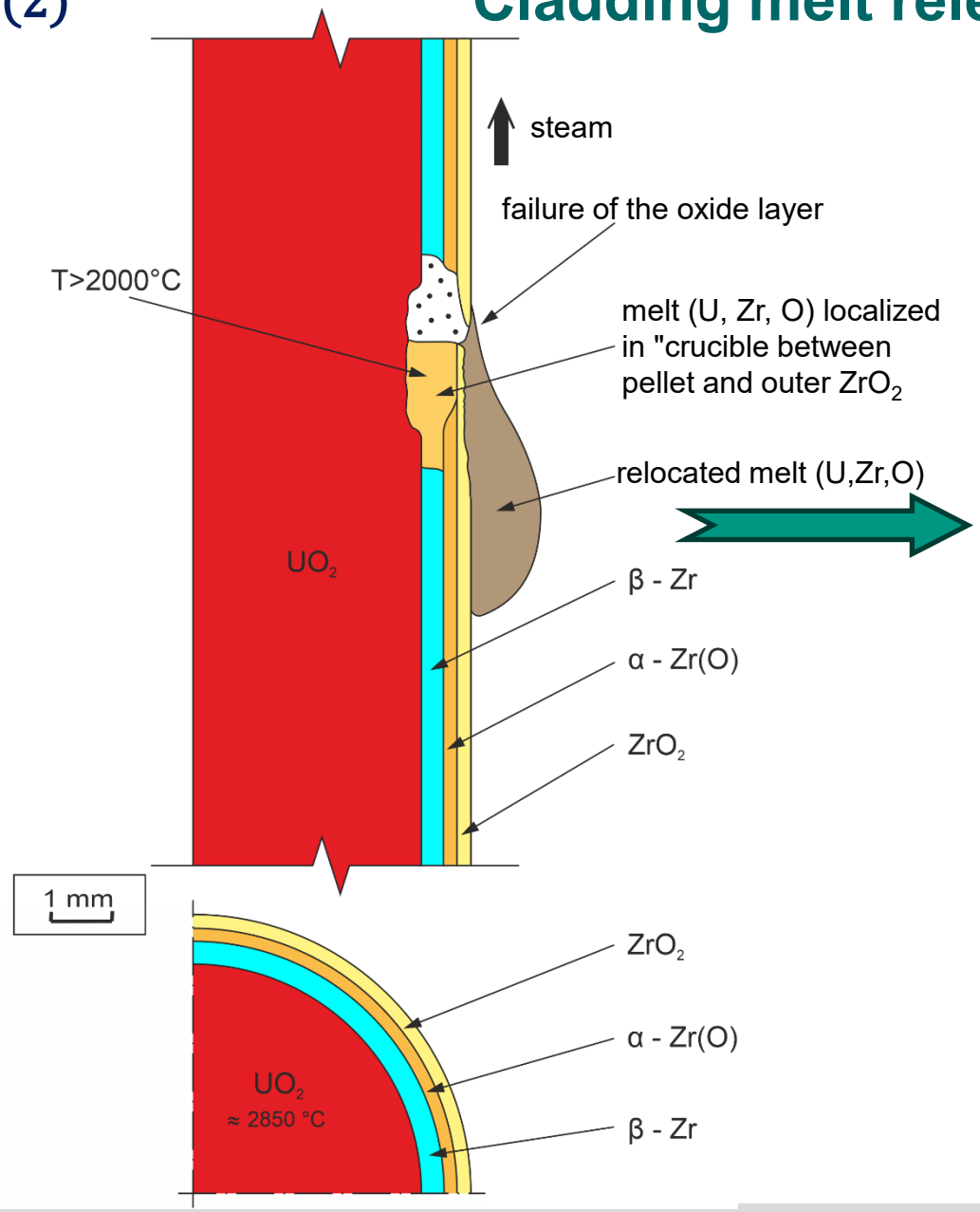

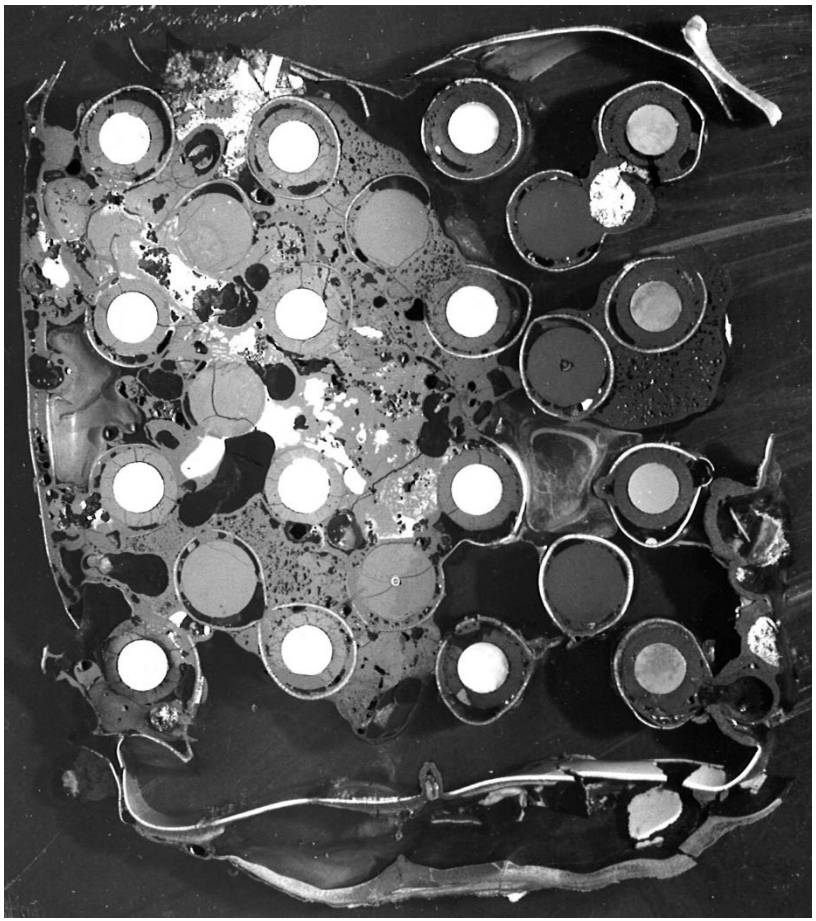

partial blockage of the CORA-05 bundle at the bundle elevation 408 mm with the melt relocated from upper elevations

Structure of frozen melt in molten pools and inside pellet/cladding gap in the QUENCH-02 bundle

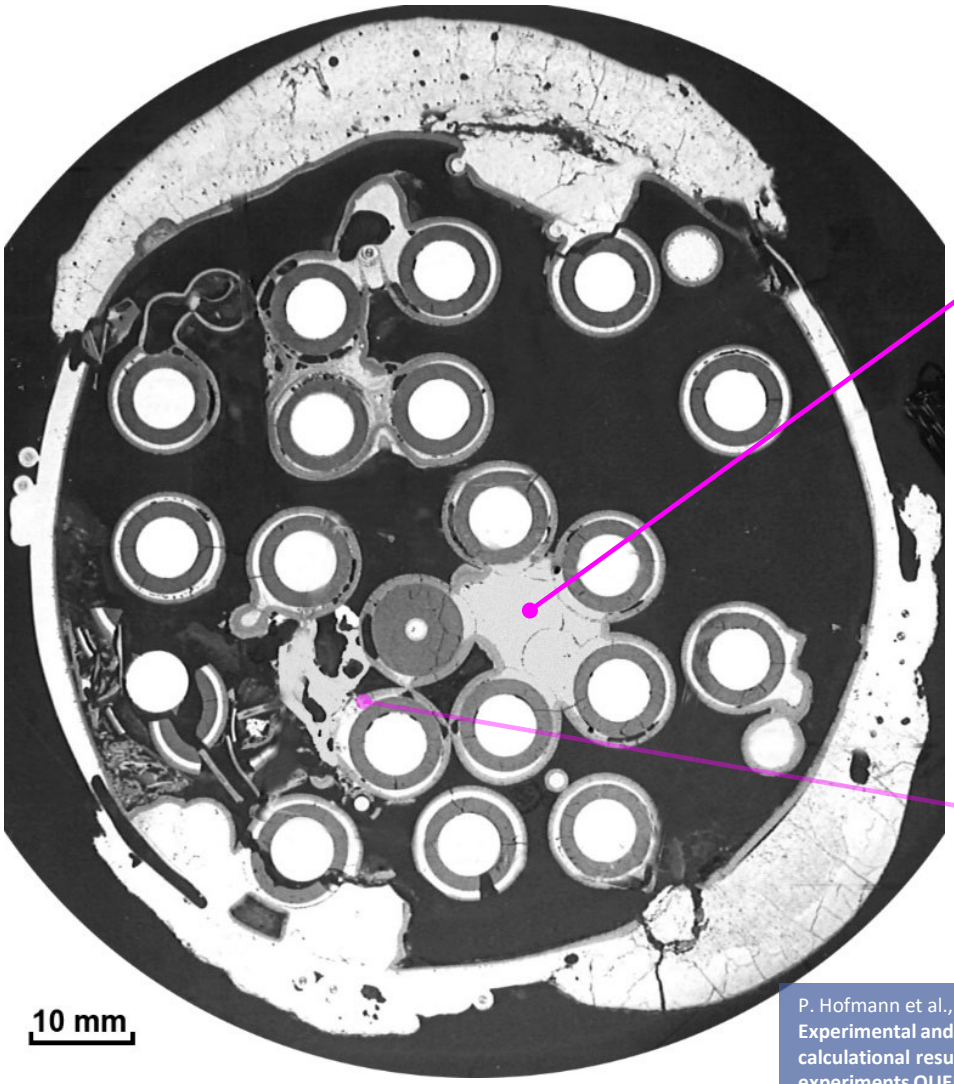

QUENCH-02 bundle, elevation 850 mm

P. Hofmann et al., **Experimental and calculational results of the experiments QUENCH-02 and QUENCH-03**, FZKA-6295 (2000)

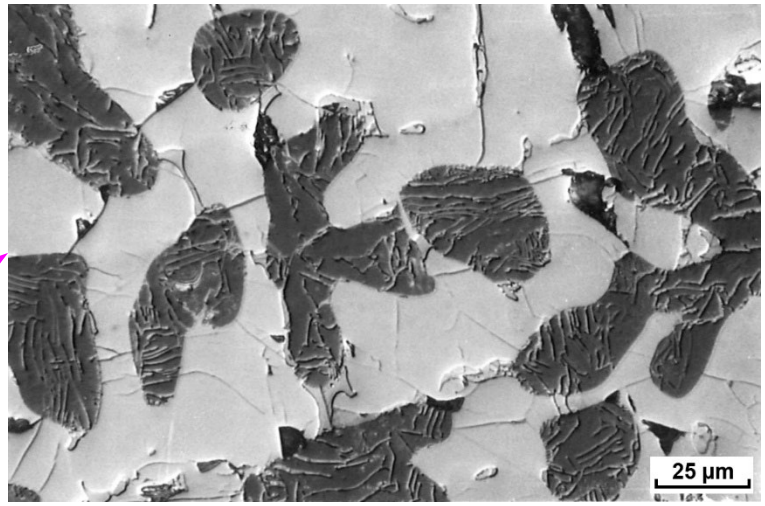

ceramic precipitates in molten pool:
43% area acc. to image analysis

ceramic precipitates in the cladding-pellet gap:
35% area acc. to image analysis

Determination of oxygen content in oxidized Zr melt

Simplified equilibrium Zr-O phase diagram

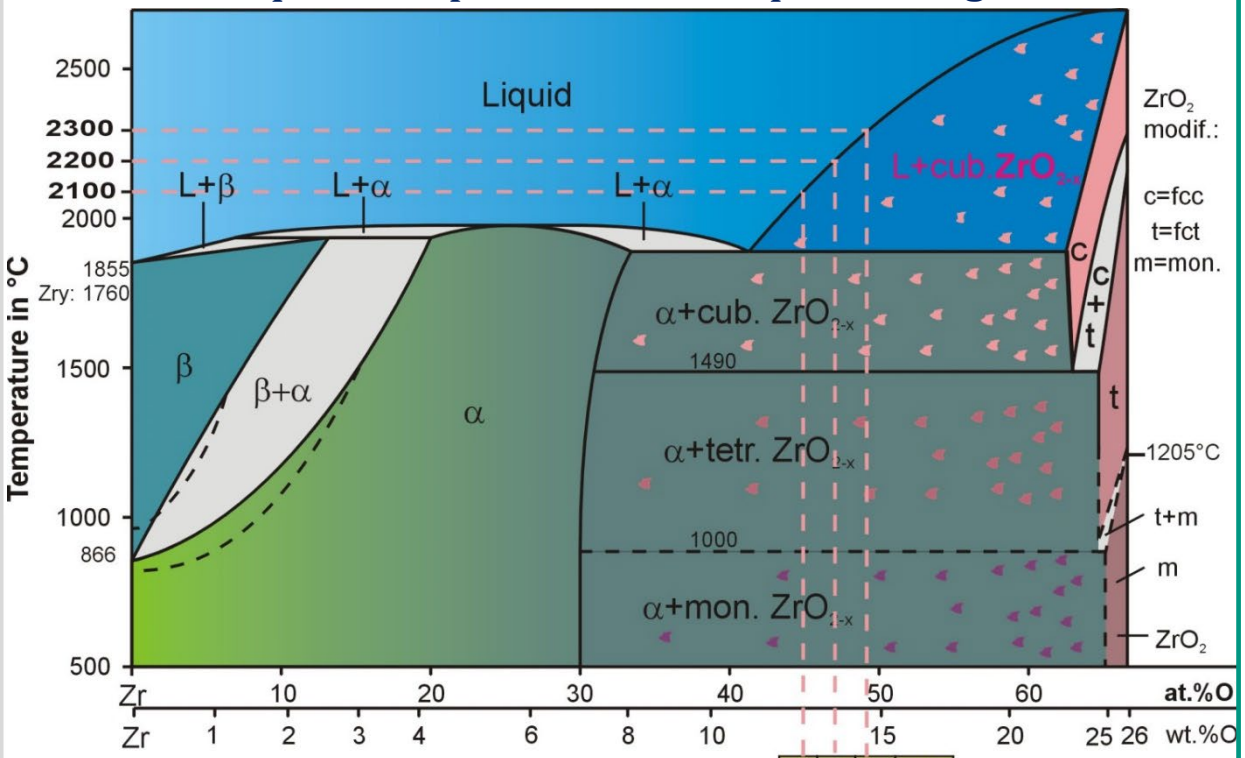

Solubility of oxygen in Zr liquid at 2100, 2200, 2300 °C:

45.3	47	49.5	at.%O
12.7	13.5	14.7	wt.%O

P. Hofmann, J. Stuckert, A. Miassoedov, M. Veshchunov, A. Berdyshev, A. Boldyrev, ZrO_2 dissolution by molten zircaloy and cladding oxide shell failure. New experimental results and modelling, FZKA-6383 (1999), https://doi.org/10.5445/IR/270046616

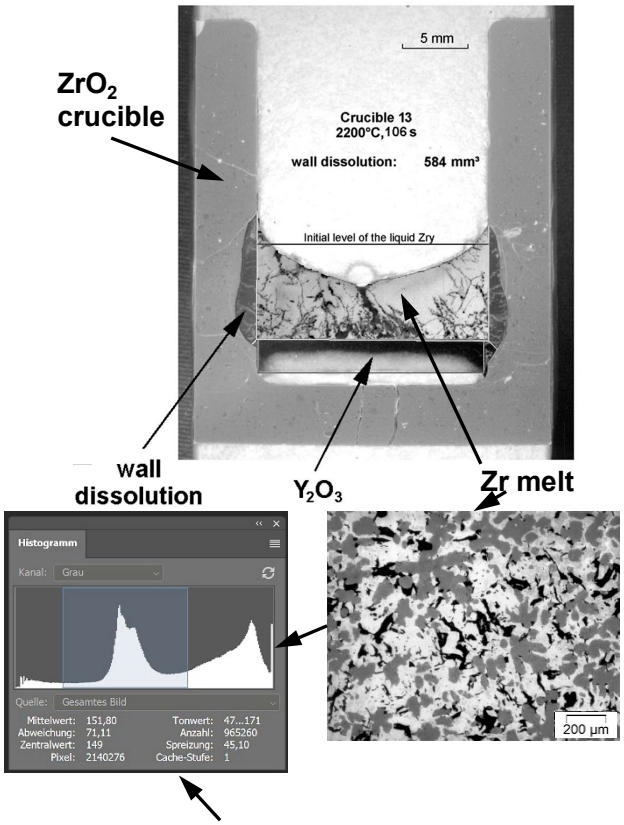

From the image analysis of the ceramic phase content in crucible tests with known relationship between dissolved ZrO_2 and the resulting amount of ceramic precipitated in the solidified melt, the following formula was derived:

$$O = 0.186 \cdot (A+34)$$

where O is in weight %, A – in area %.

Structure of frozen melt formed as molten pool in the QUENCH-16 bundle

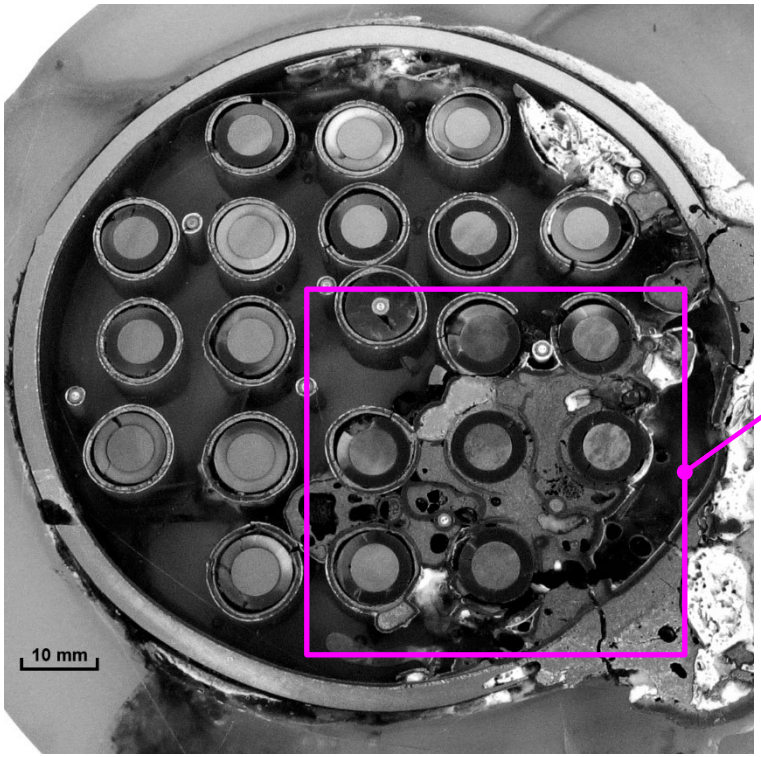

QUENCH-16, elevation 450 mm

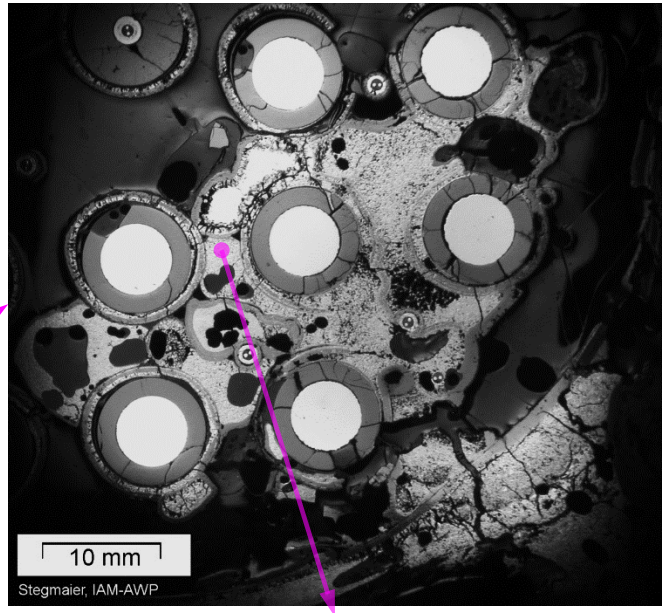

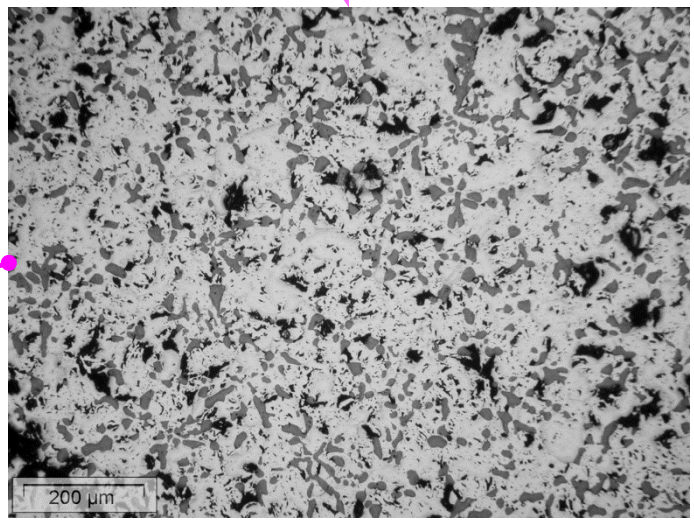

J. Stuckert, M. Steinbrück, **Experimental results of the QUENCH-16 bundle test on air ingress**, PNE 71 (2014), 134-141

area of ceramic precipitates 23% ⇨ 10.6 wt% of O,

this is <u>below</u> the solubility limit (12.7 wt% at 2100 °C)

Structure of frozen melt formed as molten pool in the QUENCH-11 bundle

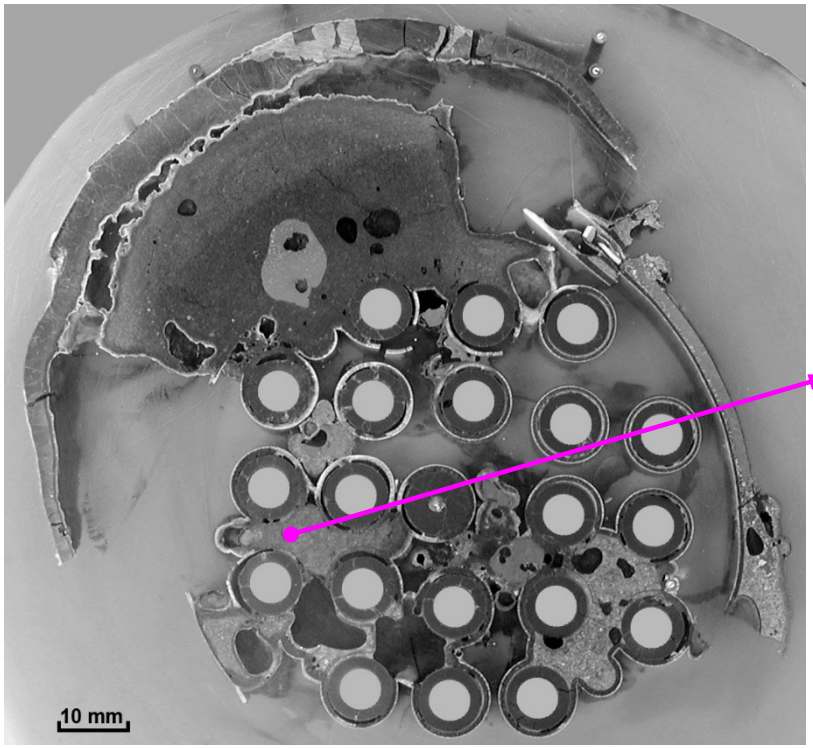

QUENCH-11 bundle test, elevation 850 mm

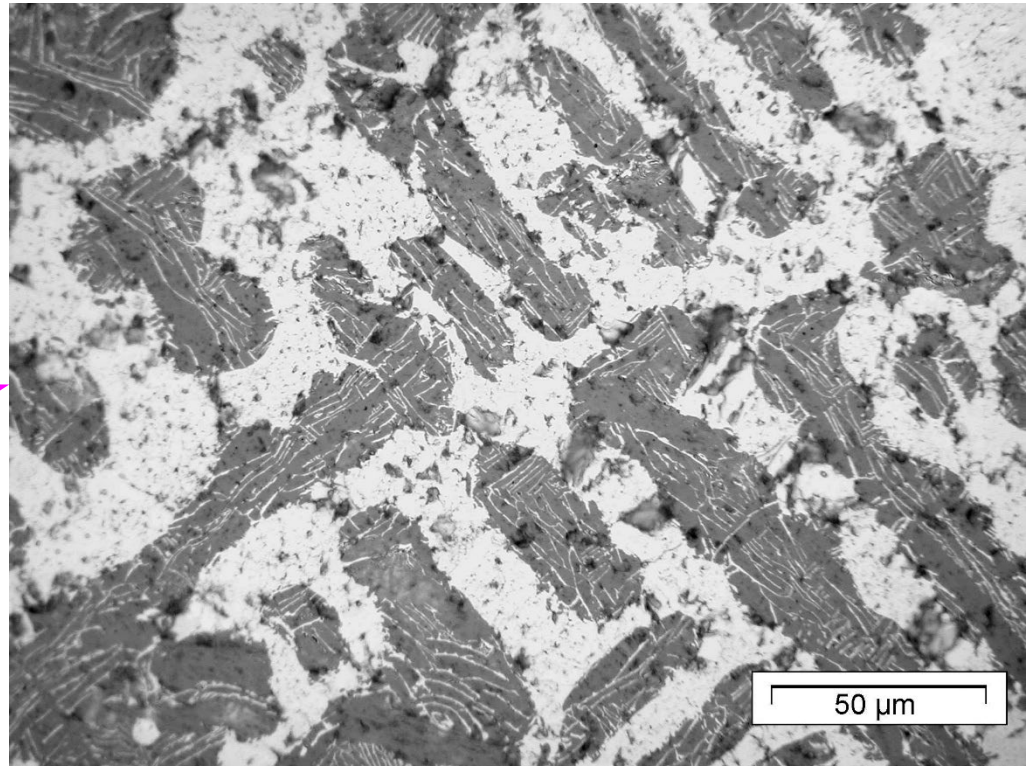

area of ceramic precipitates 56% ⇨ 16.7 wt% of O,

this is above the oxygen solubility limit

(14.7 wt% at 2100 °C)

Oxygen diffusion to the saturated melt due to T gradient

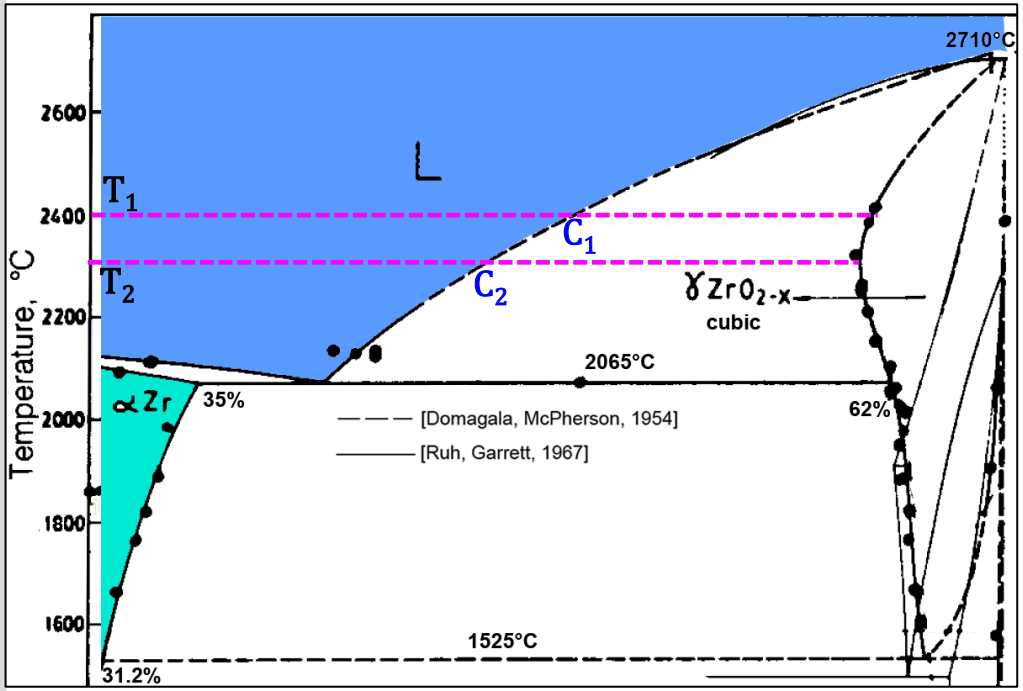

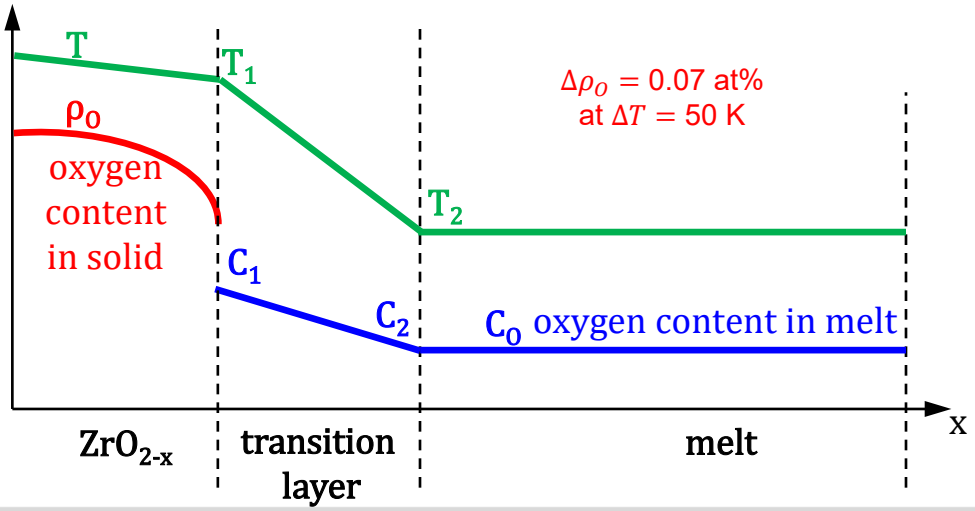

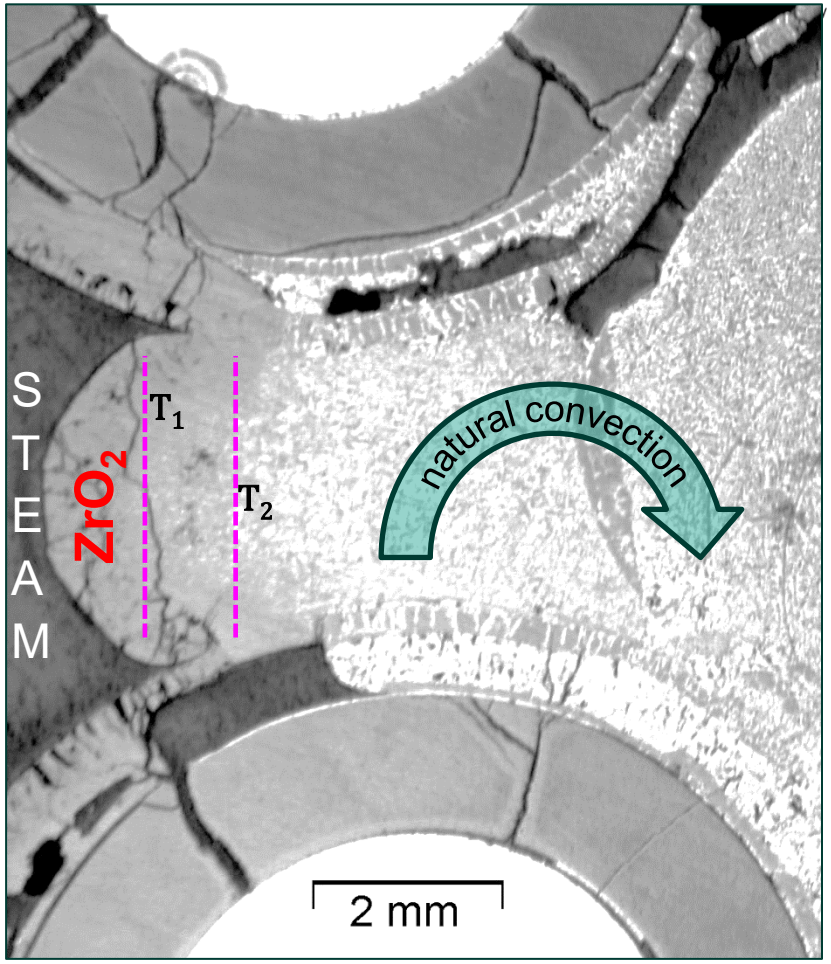

$T_1 > T_2$ due to exothermic reaction of steam with molten Zr

M. Veshchunov, J. Stuckert, A. Berdyshev, Modelling of Zr-O and U-Zr-O melts oxidation and new crucible tests, FZKA-6792 (2002), https://doi.org/10.5445/IR/270046616

Structure of frozen melt formed in the CORA-W2 bundle at temperature and during cooldown

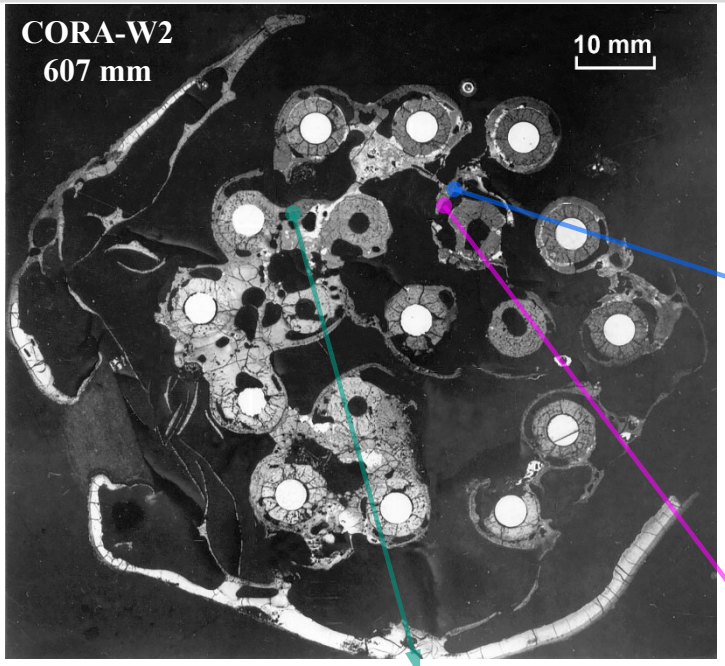

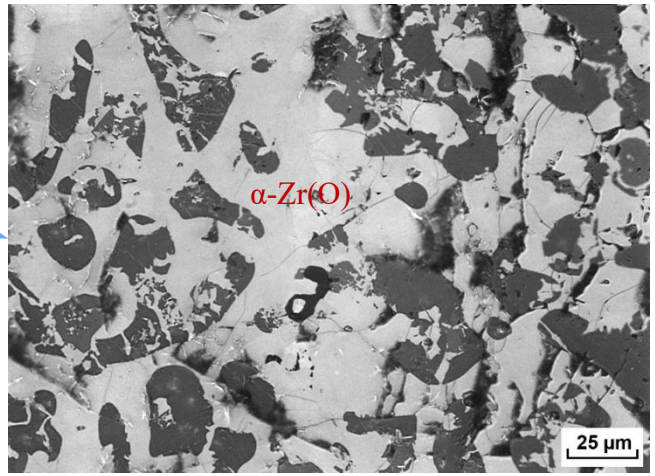

ceramic precipitates 34% → melt <u>saturated</u> with oxygen

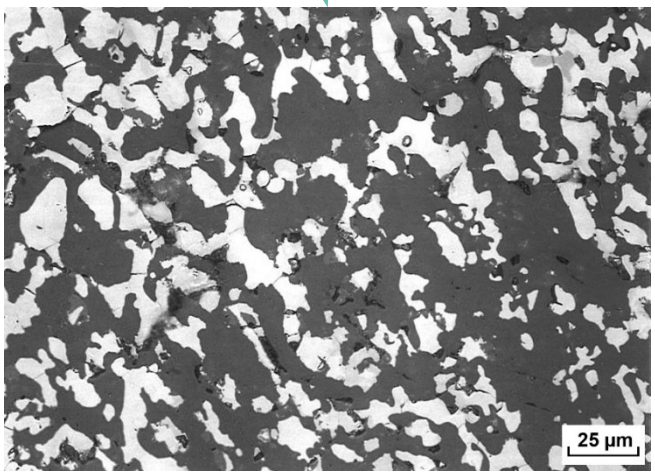

ceramic precipitates 56% → <u>oversaturated</u> melt

ceramic precipitates 68% → <u>oversaturated</u> melt

According to the EDX analysis of the oxidized melt, the zirconium content in it (in at%) is 4-8 times higher than the uranium (which entered the melt due to the dissolution of the pellets). Therefore, the presence of zirconium is the determining factor.

Oxygen uptake by molten pools at 2200 °C: comparison of two models (SVECHA mechanistical model vs. engineering approach)

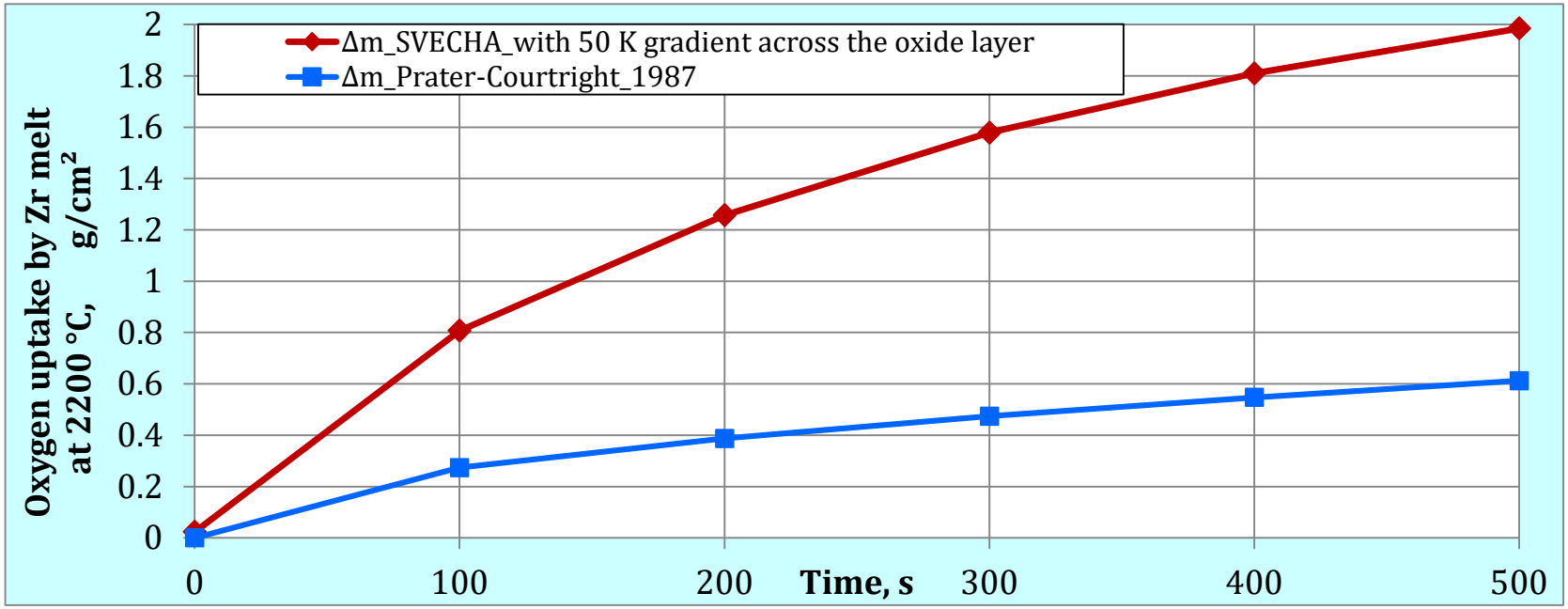

t, s	mass gain by ZrO_2 layer $\Delta m_{R\text{-}r}$, g/cm²	mass gain by ZrO_2 precipitates in melt m_f, g/cm²	total mass gain Δm_{SVECHA}, g/cm²	*Prater-Courtright mass gain Δm_{PC}, g/cm²*	$\Delta m_{SVECHA}/\Delta m_{PC}$
0	0.023	0	**0.023**	0	
100	0.057	0.751	**0.807**	0.274	3.0
200	0.088	1.169	**1.257**	0.387	3.2
300	0.120	1.458	**1.578**	0.474	3.3
400	0.153	1.657	**1.809**	0.547	3.3
500	0.182	1.803	**1.984**	0.612	3.2

- **accelerated melt oxidation due to formation of ceramic precipitates: factor 3 in comparison to the Prater-Courtright**
- **suggested kinetics:** $K_{mod}=5.74*\exp(-85900/RT)$, $g/cm^2/s^{0.5}$ *(instead $K_{PC}=5.74*\exp(-109911/RT)$, $g/cm^2/s^{0.5}$)*

Phenomena occurring in an oxidizing melt

- The analysis of the viscous melt behavior in bundles and the image analysis of the frozen melt show the formation of ceramic precipitates in the melt even in the molten state (not only during the cooldown).
- The driving mechanism for the formation of melt oversaturated with oxygen and precipitation of ceramic phase is the temperature gradient at the oxide-melt interface of the molten pool.
- According to the Zr-O phase diagram, this ensures a decreasing oxygen concentration in the transition layer and therefore diffusion of oxygen from the oxide to the saturated melt , which is then mixed as a result of natural convection.
- A numerical calculation carried out for the case with an operating temperature of 2200 °C and a temperature gradient at the melt boundary of 50 K showed that the oxidation process occurs parabolically and *three times faster* than predicted by the Prater-Courtright oxidation correlation used usually in computer codes at $T \gtrsim 1800$ °C.

Dependence of the circumferential temperature difference on the position of contact between the pellet and the cladding

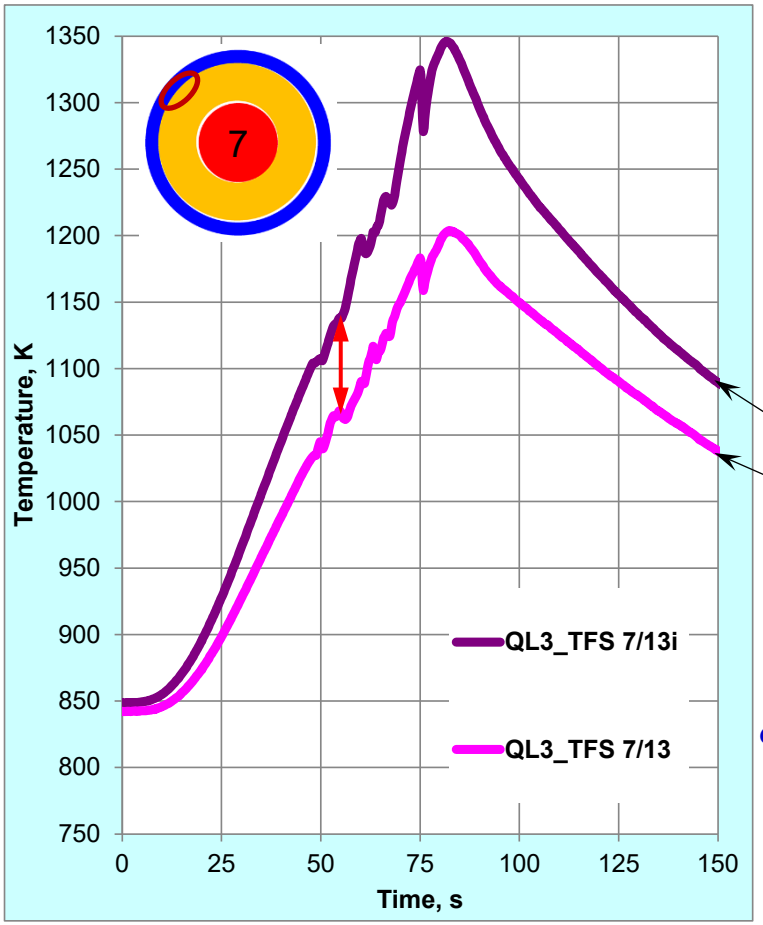

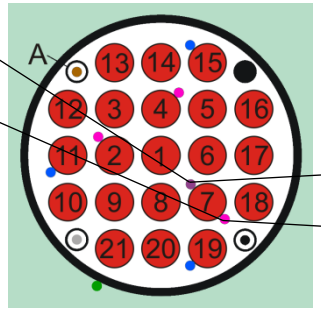

positions of two diametrically opposite TCs on the surface of the rod 7

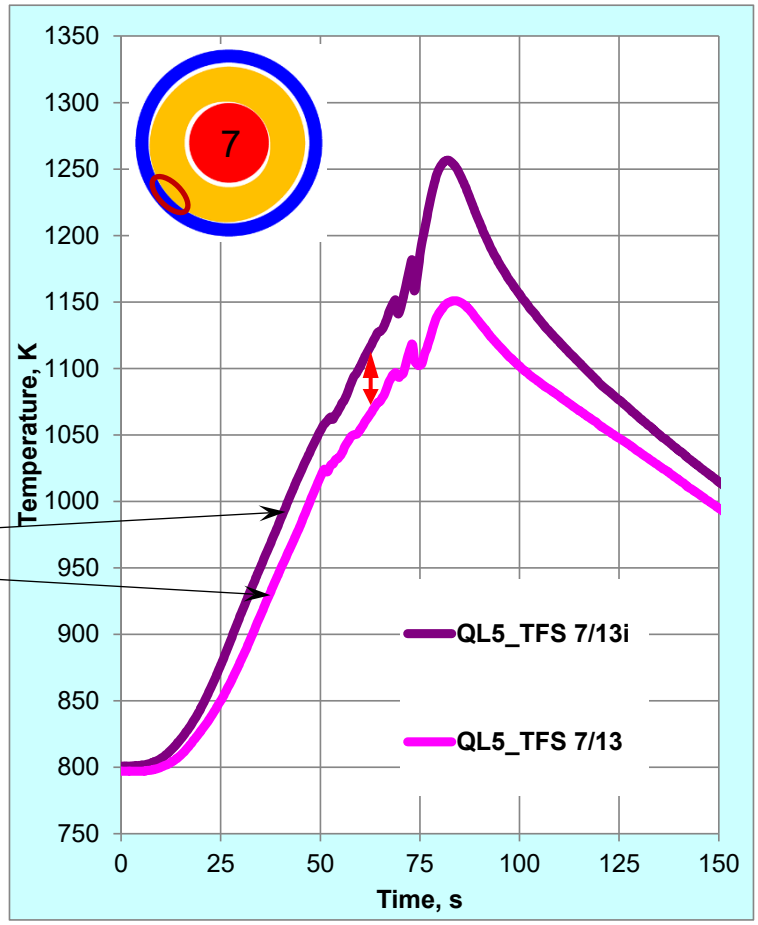

QL-3 bundle:
large circumferential difference ΔT=70 K

QL-5 bundle:
moderate circumferential gradient ΔT=50 K

Not symmetrical cladding ballooning due to point contact between pellet and cladding (QL4 bundle, rod 1, tomography of rod between 903 and 920 mm)

optical view of clad inner surface below the burst opening at 920 mm

hot spot: pellet-cladding contact

the gap is present until burnouts of 30 MWd/kgU

max gap 150 µm

not changed during ballooning

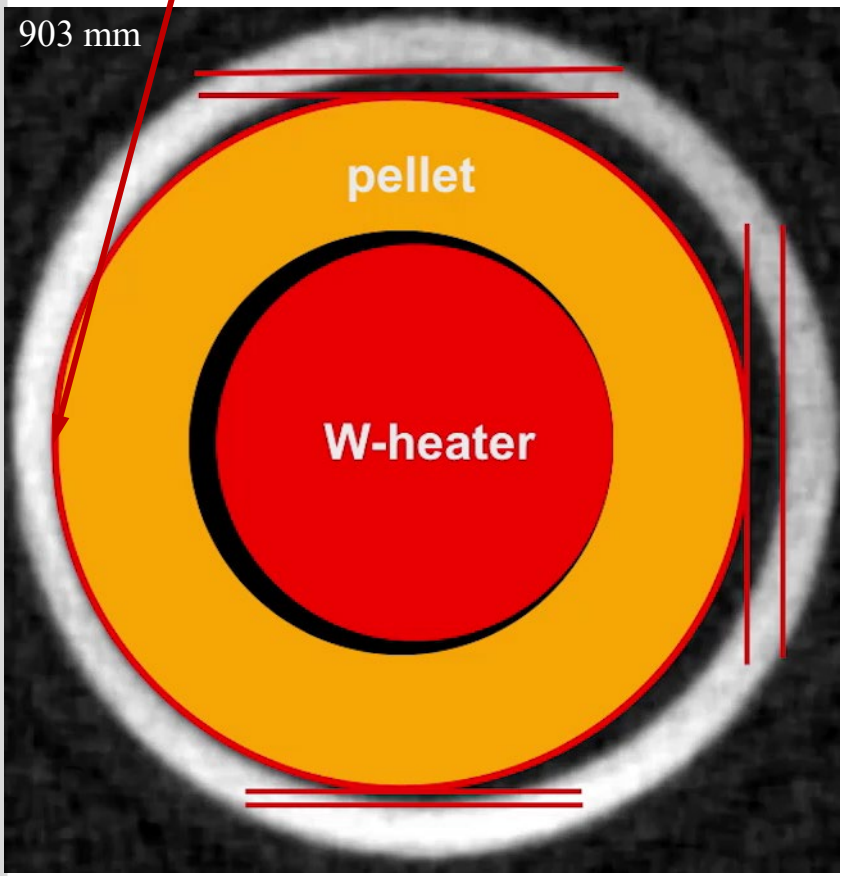

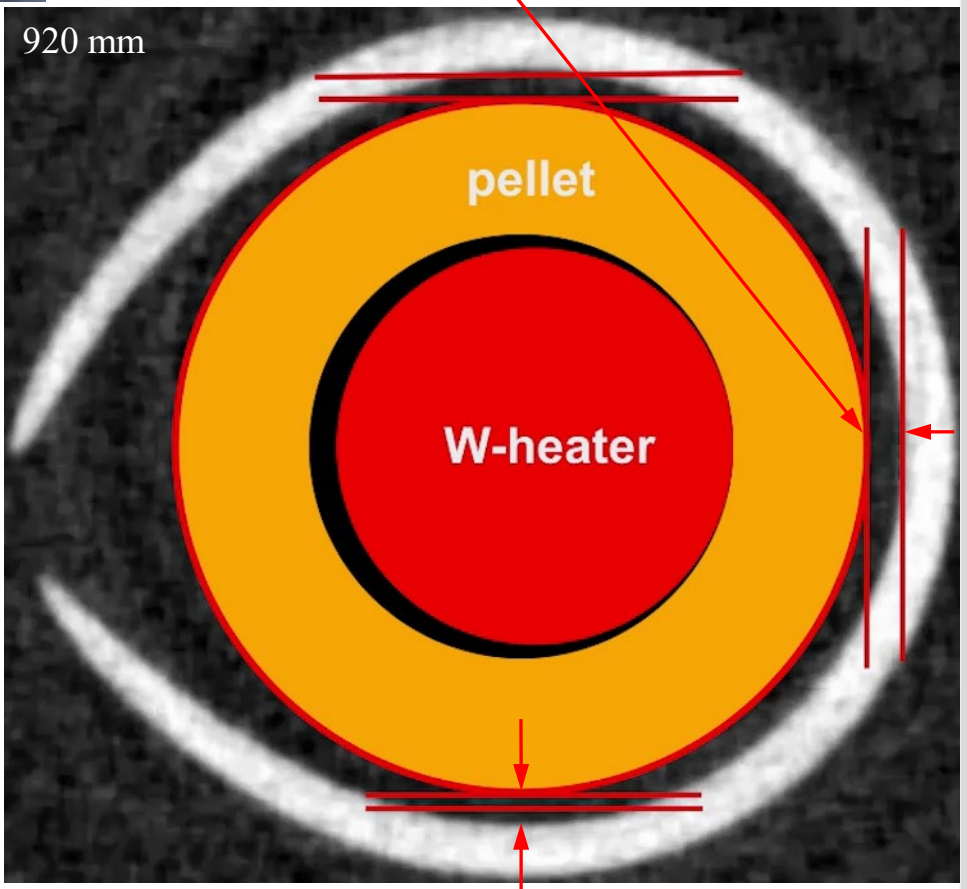

Link to movie: http://www.doi.org/10.5445/IR/1000189456

gap increased during ballooning

REBEKA burst criterion (*burst strain* vs. *circumferential ΔT*) and FR2 in-pile test data

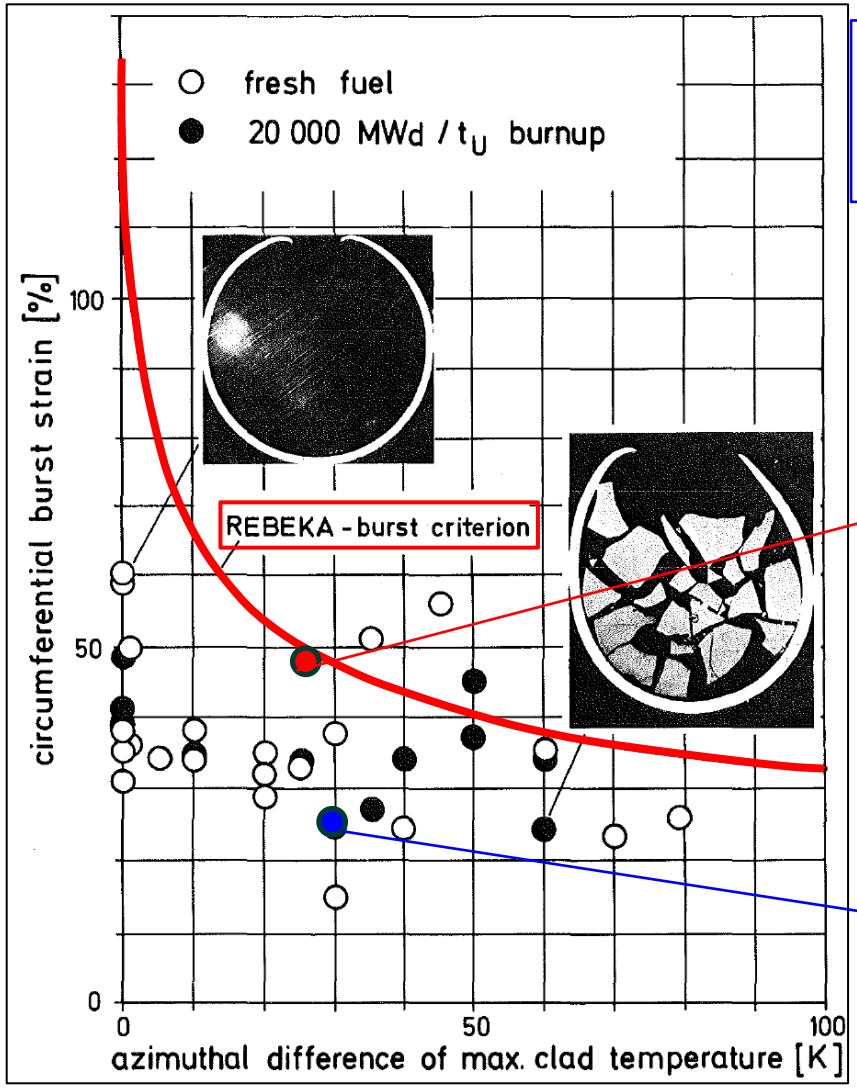

comparison of FR2 data with REBEKA burst criterium

The circumferential burst strains of cladding tubes are kept relatively small due to *temperature differences* on the cladding circumference and the anisotropic strain behavior of Zr alloys.

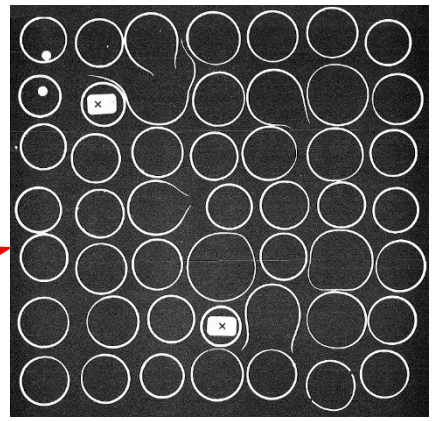

REBEKA-5 bundle at 2000 mm with maximum bundle blockage of 52%: maximum clad strain **49%**

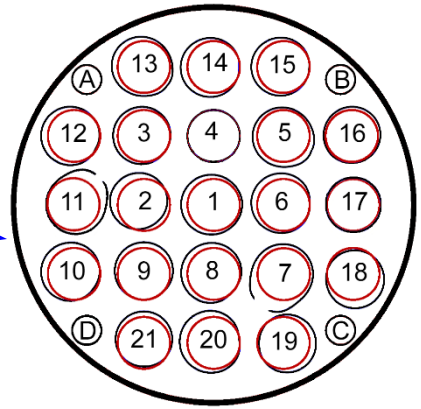

original clad
ballooned clad

QUENCH-LOCA-4 bundle at 924 mm with maximum bundle blockage of 19%: maximum clad strain **23%**

Cladding deformation under circumferential temperature gradient

- Up to burnups of 30 MWd/kgU, fuel pellets can only have point contact with the cladding (and not along their entire perimeter), which leads to a hot spot in this place.

- The cladding begins to unsymmetrical stretch in directions perpendicular to the tangent line of contact between the pellet and the cladding, and then ruptures near the contact point with additional outward deformation of the burst opening edges.

- The circumferential strains of the claddings are generally no more than 40%, which leads to maximum blockades of the bundle cross-section of about 60%, which in turn ensures full coolability of the bundle during reflood.

Acknowledgment

The author would like to thank the entire QUENCH team for their intensive work during the test preparations and post-test investigations.

Thank you for your attention

https://www.iam.kit.edu/awp/english/163.php

http://quench.forschung.kit.edu/

Mirco Große
KIT

Neutron Imaging Investigations of Hydrogen in Cladding Tube Materials

The paper gives an overview about 20 years of neutron imaging investigations by the QUENCH team of KIT. After an introduction into neutron radiography and tomography, examples of the results concerning:

- The hydrogen uptake during oxidation of cladding materials by steam, particularly the effect of breakaway on the hydrogen concentration.
- The hydrogen diffusion at temperatures between 900 and 1300°C.
- The hydrogen distribution around a crack tip at 350°C.
- The effect of the total gas flow rate on the oxidation of Zircaloy-4 in steam-nitrogen mixtures.
- The hydrogen enrichments in cladding tubes after LOCA simulation tests.
- The effect of elastic strain on the hydrogen distribution in pure zirconium.

were given. Hydrogen concentrations were determined quantitatively. Results of in-situ investigations are shown as movies in the paper.

The examples demonstrate the power of neutron imaging not only to investigate the behaviour and distribution of hydrogen in zirconium, but also to obtain new insights into the kinetic of processes occurring in cladding tubes under operational accidental conditions.

Neutron Imaging Investigations of Hydrogen in Cladding Tube Materials

Mirco Grosse, et al.,

30. Intern. QUENCH Workshop,
KIT Campus North, 2025/12/16

Basis Neutron Imaging

X-ray radiography

1895/12/22

neutron radiography

GKSS Geesthacht 1991

M. Grosse et al., Neutron Imaging Investigations of Hydrogen in Cladding Tube Materials,
30. Inter. QUENCH Workshop, KIT Campus North, 2925/12/16

Basis Neutron Imaging

$$\Sigma_{total} = \frac{-\ln\left(\frac{I - I_B}{I_0 - I_B}\right)}{s}$$

$$= \sum_i N_i \sigma_i$$

$$= \underbrace{N_{Zr}\sigma_{Zr} + \ldots}_{\Sigma_{Zry}} + N_H \sigma_H + N_O \sigma_O$$

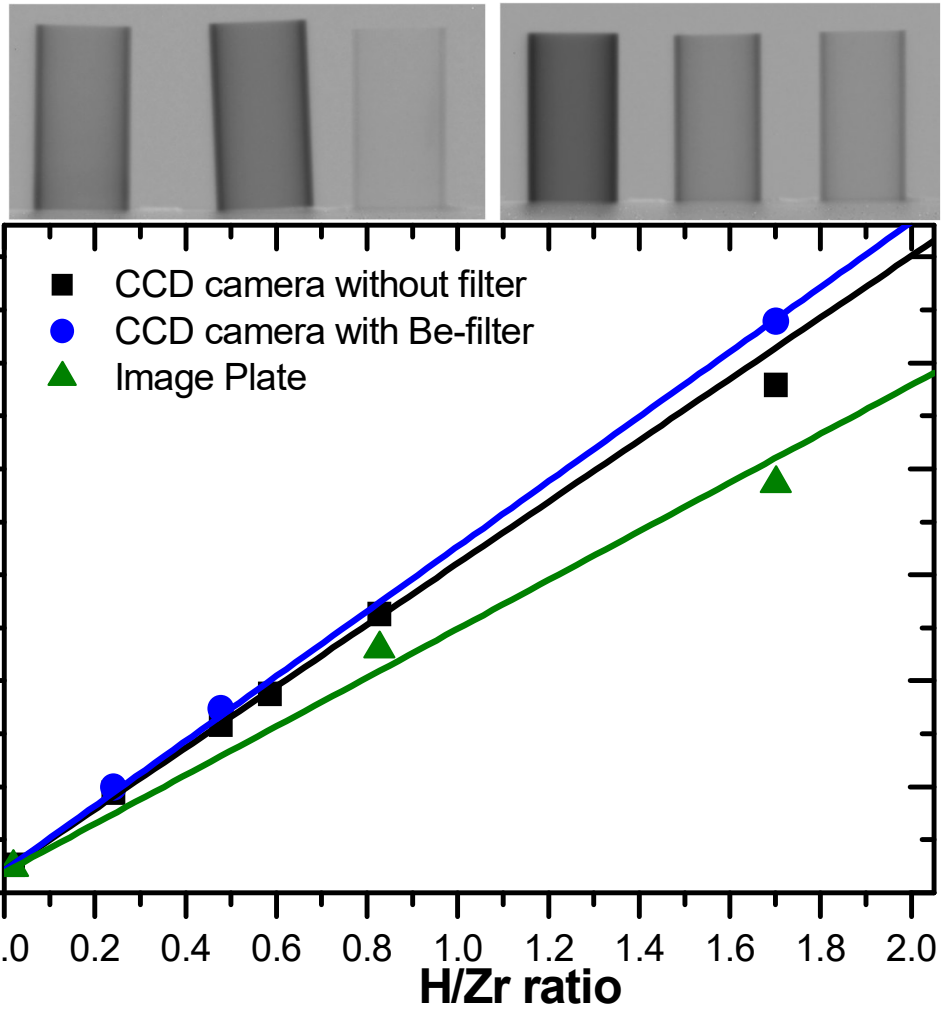

Basis Neutron Imaging

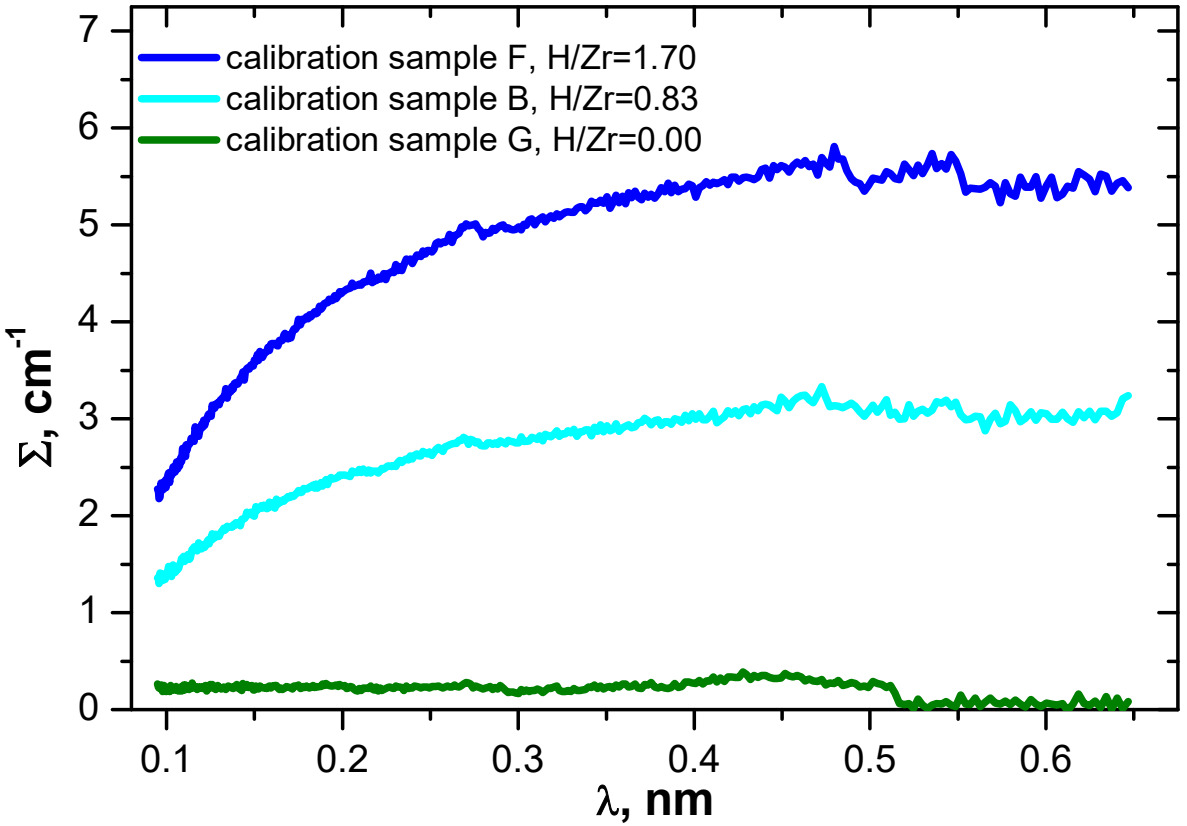

Generally:

$$\sigma_{total} \sim \lambda^4$$

$$\sigma_{total} = \sigma_{ab.} + \sigma_{coh.sc.} + \sigma_{inc.sc.}$$

$$\sin(\theta) = \frac{\lambda}{2d}$$

Neutron energy/wavelength dependence of total neutron cross section

Hydrogen uptake during oxidation by steam

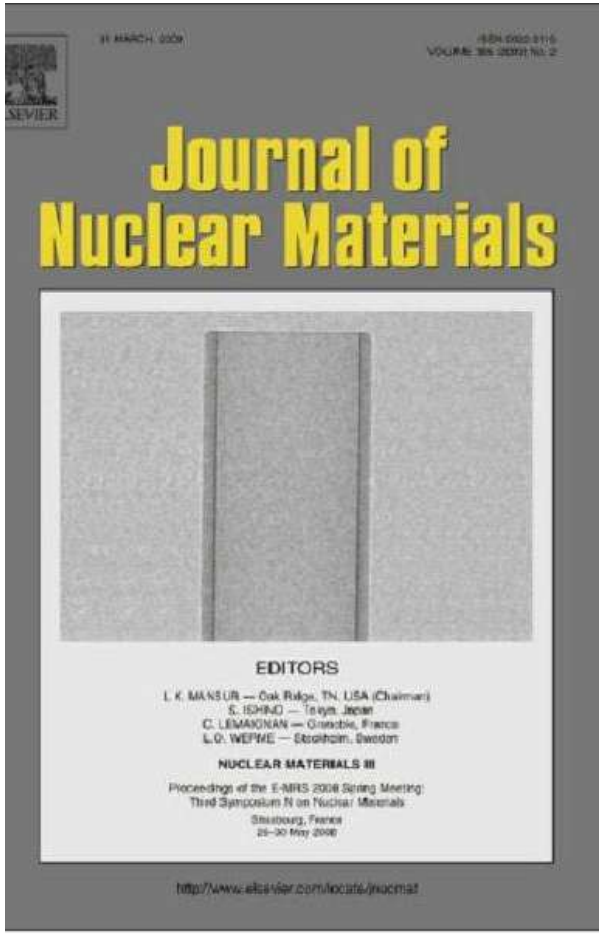

- Various ex-situ investigations of the hydrogen uptake during the oxidation in steam
- The zirconium community was sceptical about this method and our results
- Discussions about the possibilty to apply this method to investigate DHC with the colleagues from PSI at the ASTM Symposia in Chengdu 2010
- Since this time groups from France, Switzerland, Czech Republic, Hungary, USA, Canada, China, South Africa, Australia and Argentina has applied neutron imaging methods to investigate hydrogen in Zirconium

Hydrogen uptake during oxidation by steam

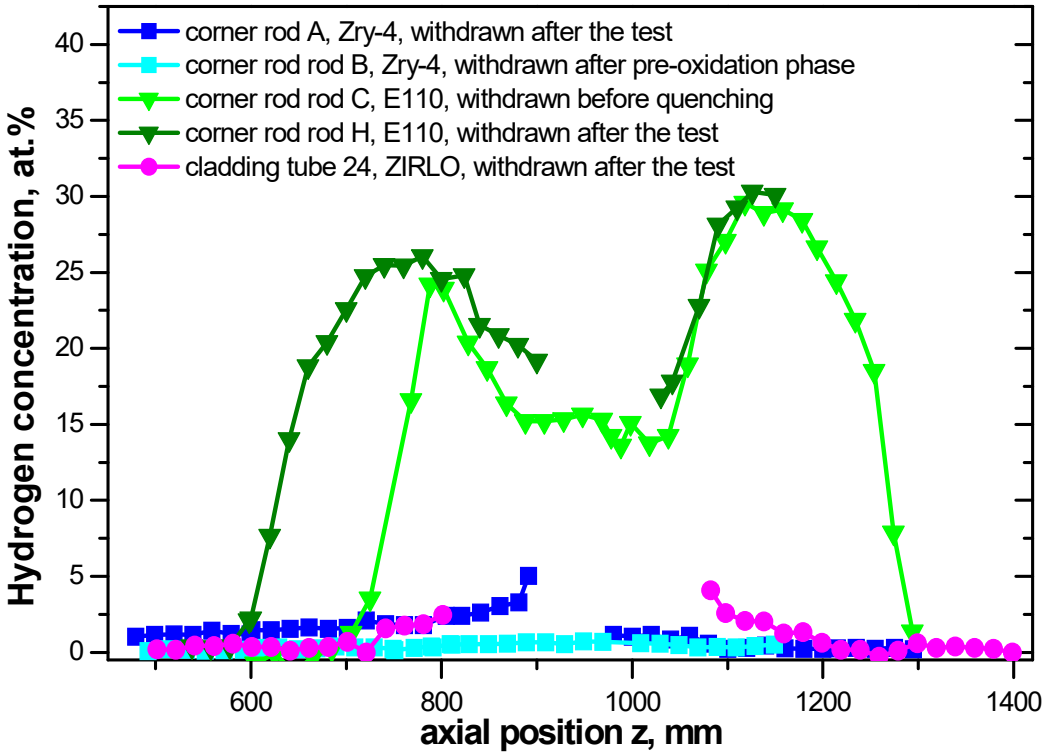

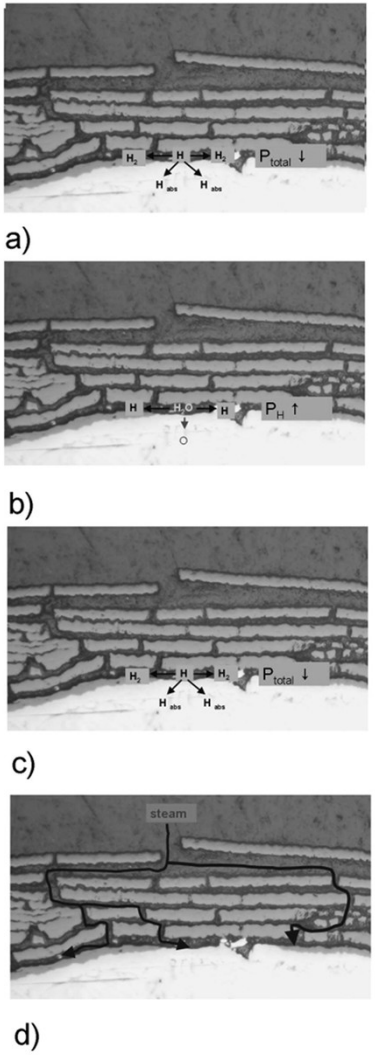

Hydrogen pump effect occurring at breakaway oxides

Neutron radiography investigations of the hydrogen uptake of cladding tubes tested in the QUENCH-ACM sub-programme

Calibration at high temperatures

Sieverts´ law:

$$C_H^{(m)} = K_S \cdot \sqrt{p_{H_2}}$$

$$K_S = \exp\left(\frac{\Delta_S S}{R} - \frac{\Delta_S H}{R \cdot T}\right)$$

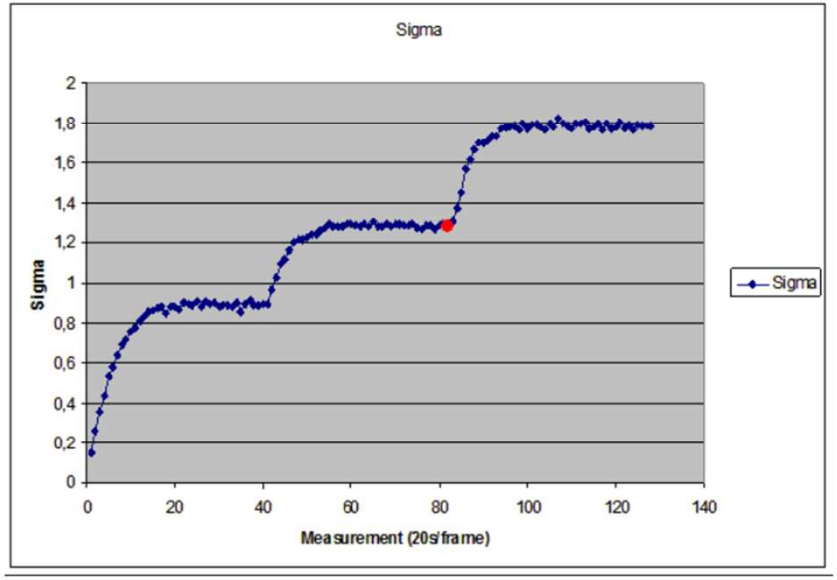

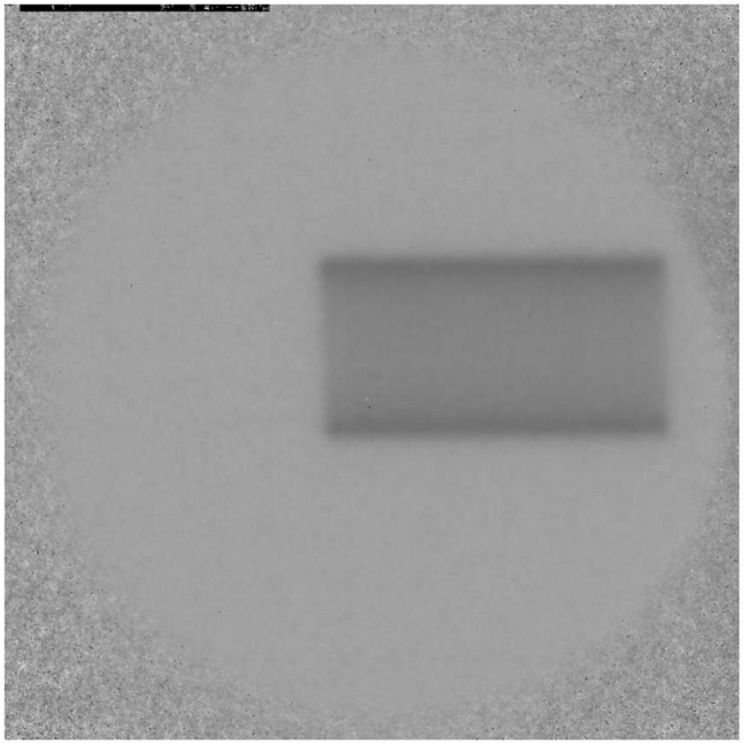

2 l/h 4 l/h 8 l/h H_2, 50 l/h Ar 1000°C

Hydrogen diffusion at high temperatures

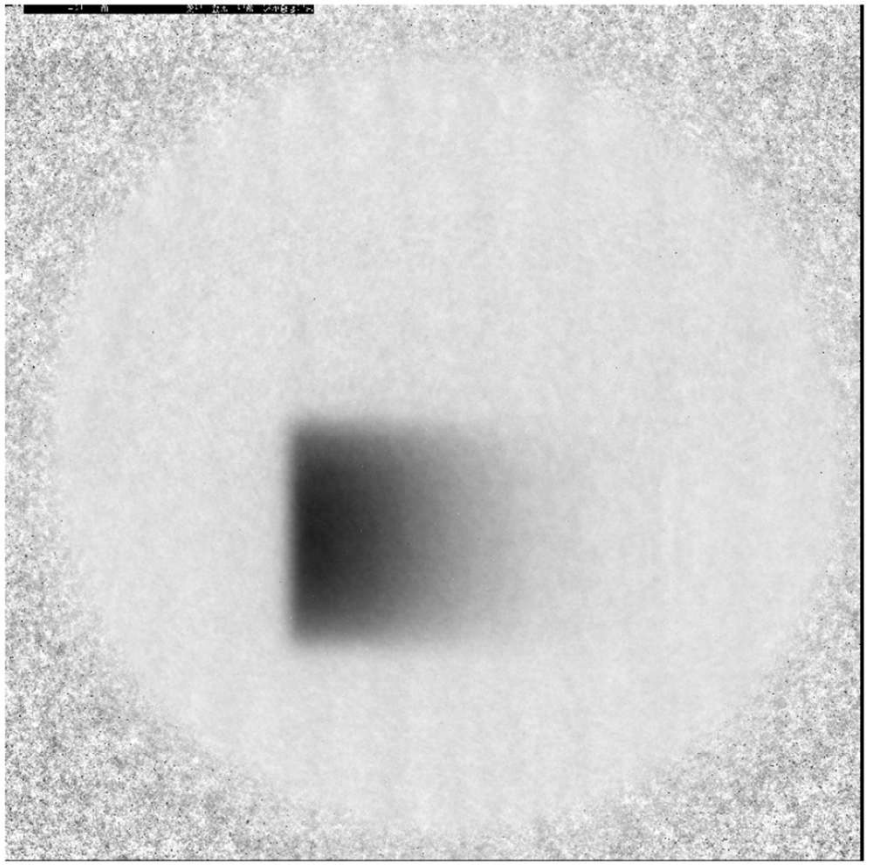

- Sample: solid cylinder pre-oxidized in Ar/O2, at one base plane the oxide layer was removed by grinding and polishing allowing hydrogen uptake through this face
- In-situ annealing's in Ar/H2 atmosphere at 900, 1000, 1100, 1200 and 1300°C
- Frame repetition time was 10 s.

Hydrogen diffusion at high temperatures

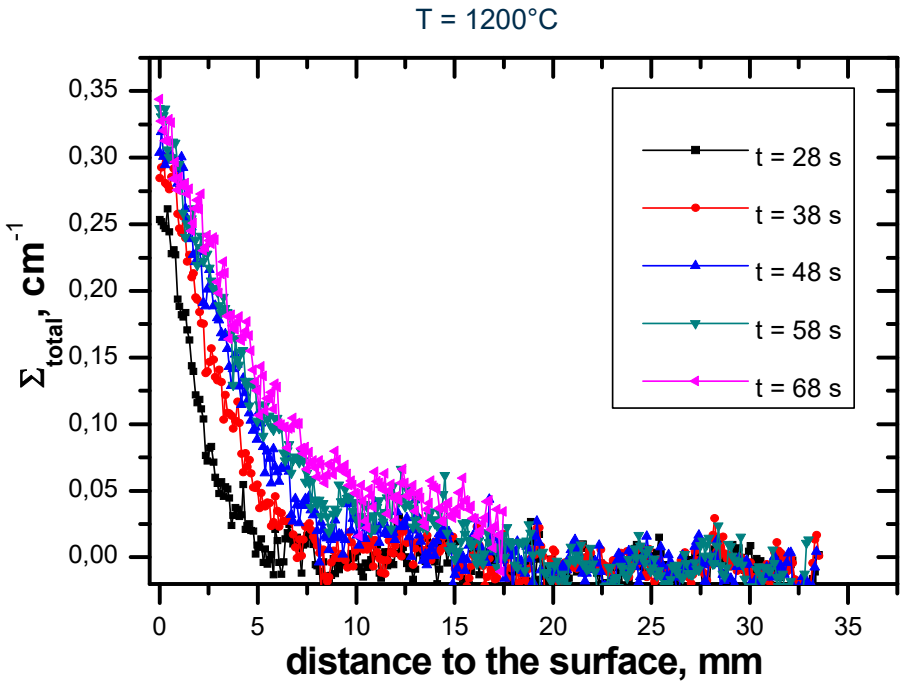

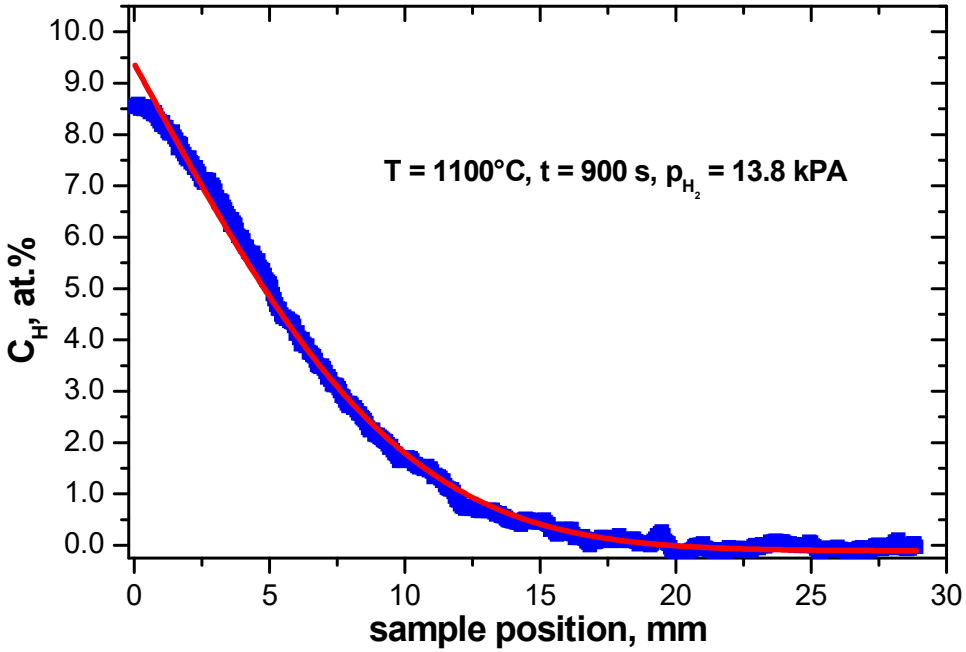

Axial distributions of the total macroscopic neutron cross section and of the hydrogen concentration

Hydrogen diffusion at high temperatures

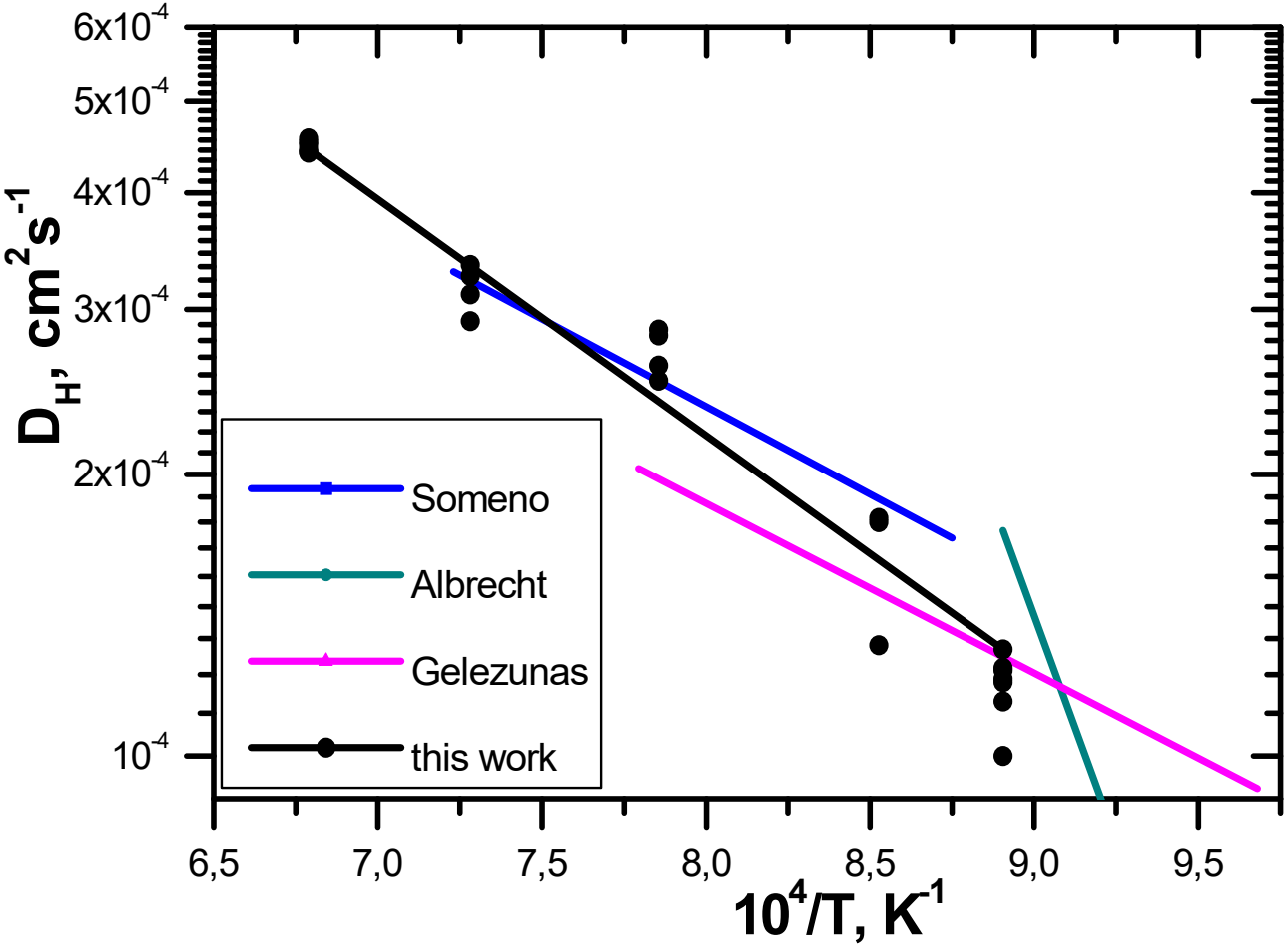

Hydrogen uptake during oxidation by steam

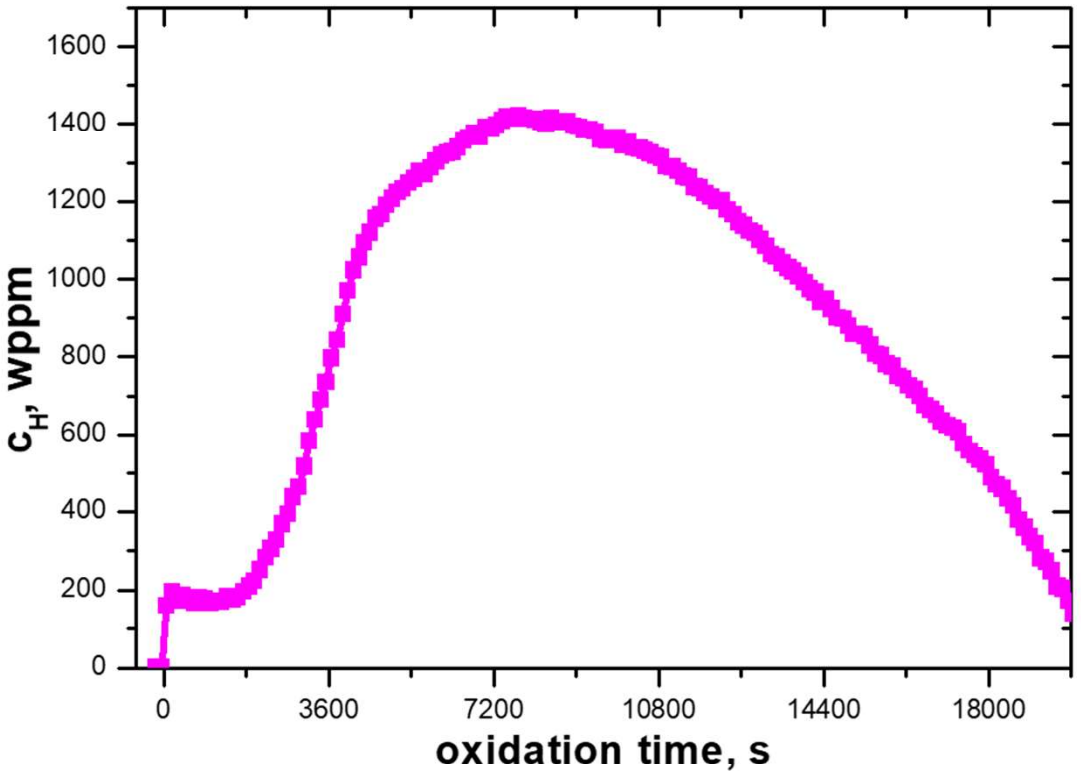

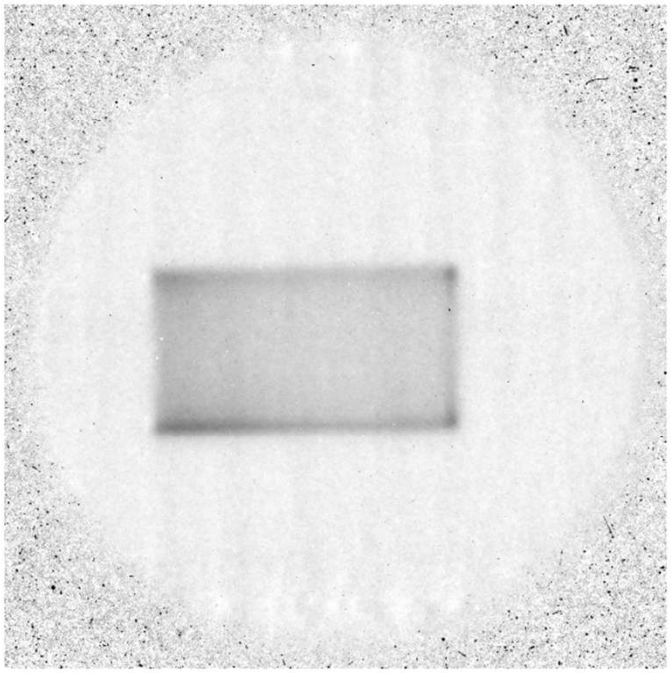

Breakaway oxidation at 1000°C

Hydrogen in zirconium

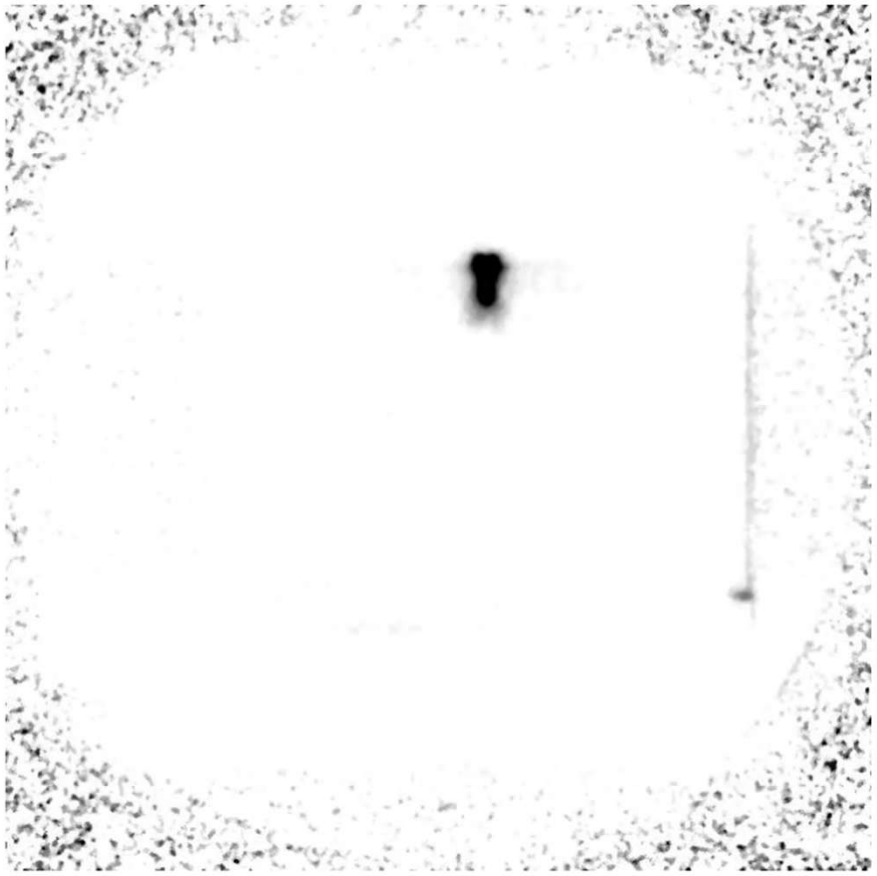

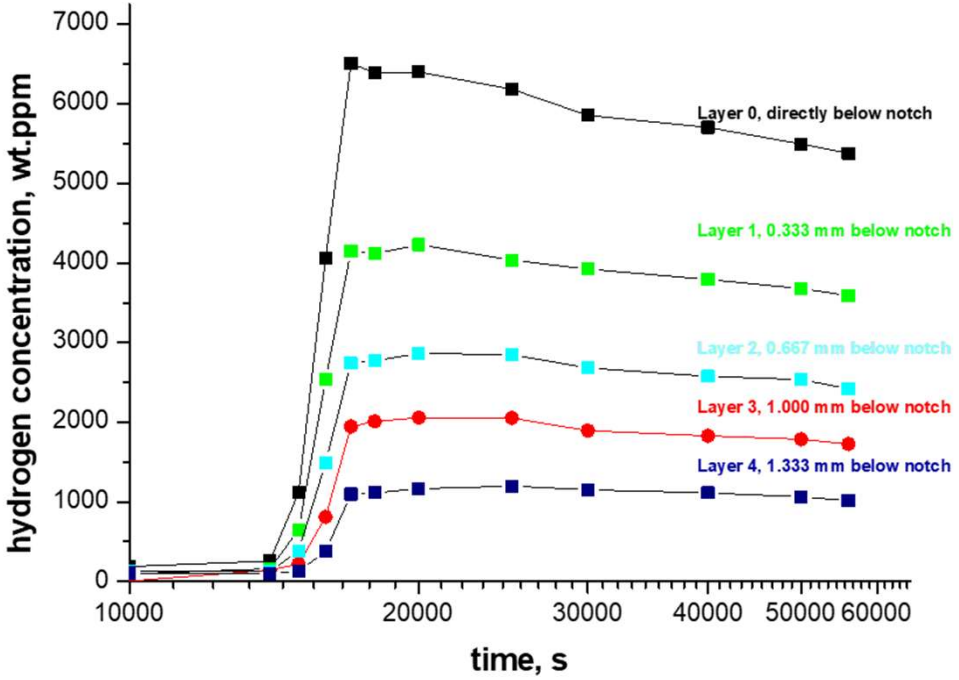

Attempts to investigate DHC by means of in-situ neutron radiography investigations

Effects of nitrogen

Flow rate model

[M. Grosse et al. ICAPP 2016]

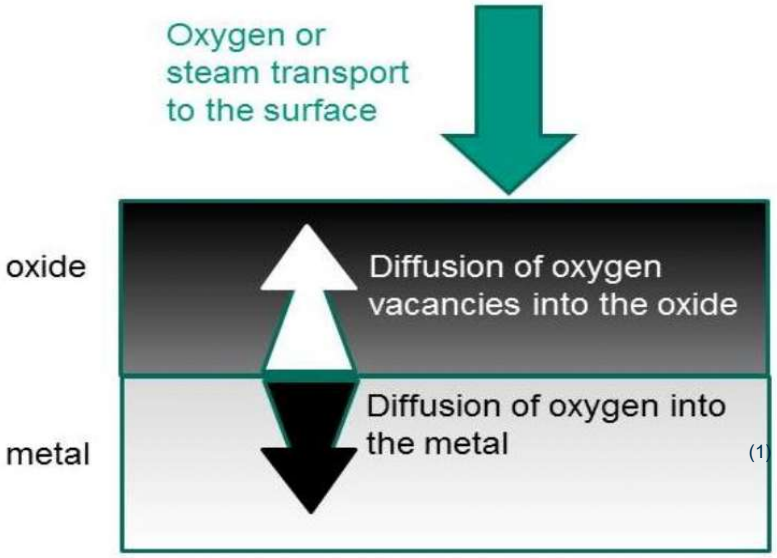

- Basic reaction with steam if an oxide layer is already formed

$$ZrO + V_o^{2+} + 2e^- + H_2O \rightarrow 2\,ZrO_2 + 2H$$

- $\dot{n}_{V_O^{2+}} = \dot{n}_{oxygen,react} = \frac{K_{n_{ox}}}{2\sqrt{t}}$ for saturation
- In the case of steam + oxygen starvation

$$\rightarrow \frac{K_{n_{ox}}}{2\sqrt{t}} - \frac{\dot{n}_{O_2}}{2} - \dot{n}_{H_2O} = \frac{\dot{n}_{N_2}}{4}$$

- If $c_N > c_{N,critical}$ -> ZrN precipitation and formation of cracks

- $\dot{x}_{res} = IF_{cracks} * \dot{x}_{linear} + (1 - IF_{cracks}) * \dot{x}_{parabolic}$
- cracks results in higher reaction rate

Effects of nitrogen

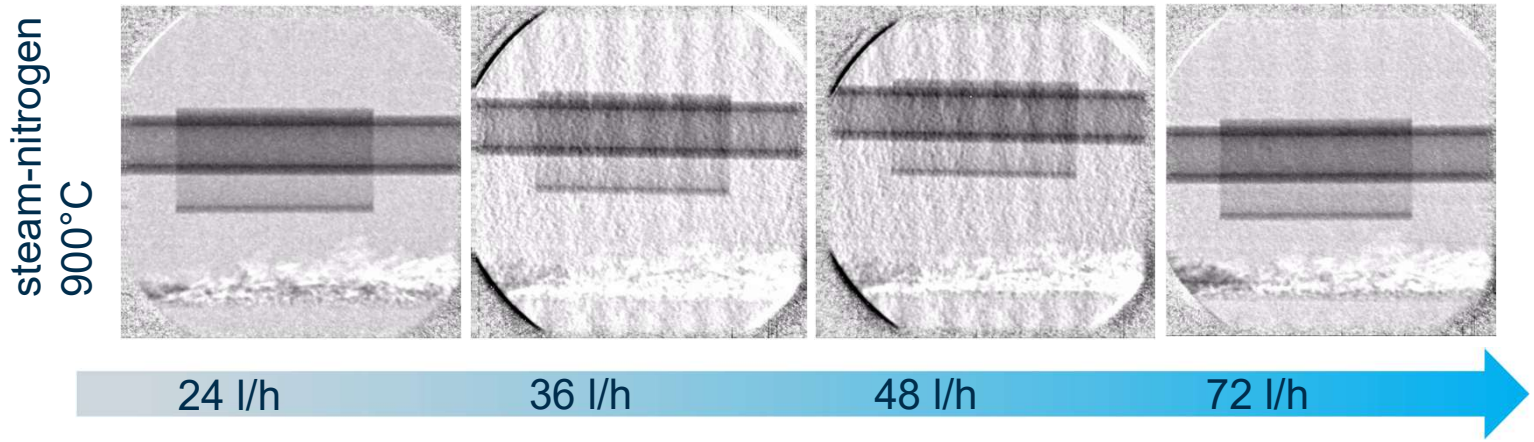

Effect of the total gas flow rate on the reaction of Zry-4 in steam nitrogen atmosphere

Post-test examinations of claddings from our LOCA tests

inner rods

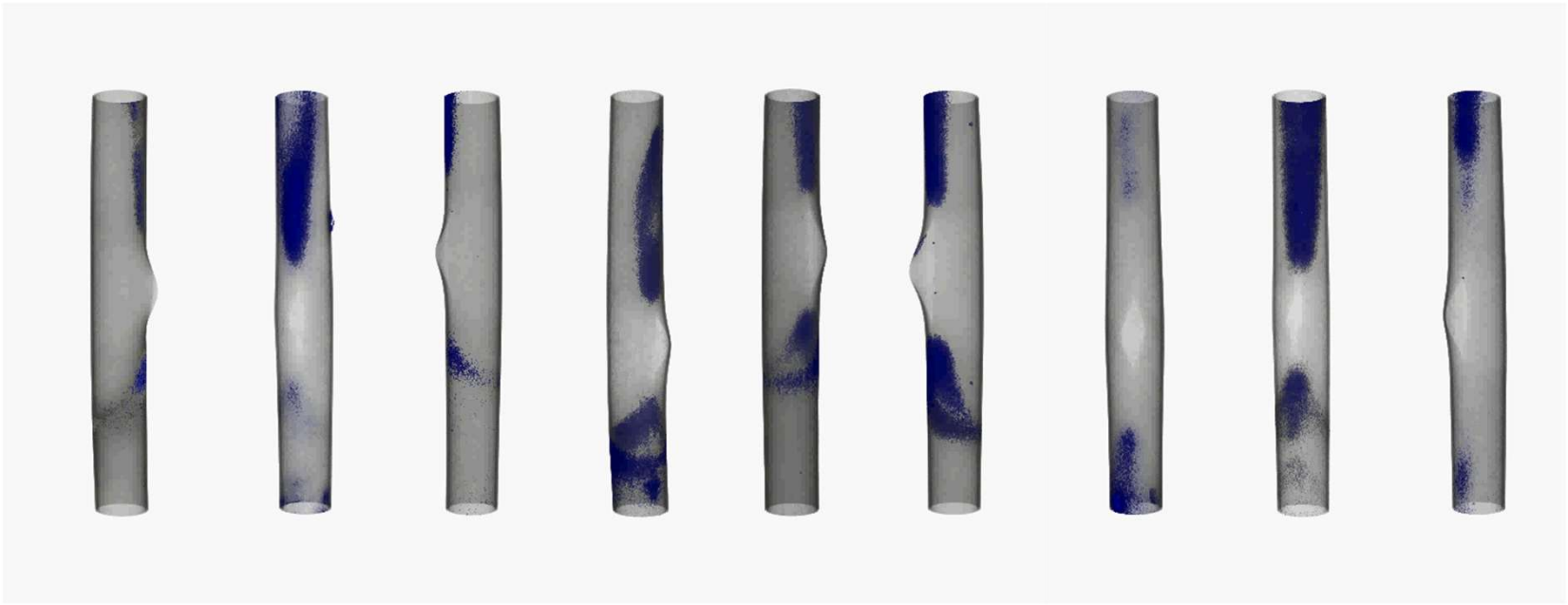

01 02 03 04 05 06 07 08 09

Samples from the inner part of the QUENCH-LOCA-3 test

Post-test examinations of claddings from our LOCA tests

- Band shaped hydrogen enrichments are formed around the berst opening non-perpendicular to the tube axis.
- Enrichments occur where the inner oxide layer ends.
- Compared to the determinations before by hot extraction, the hydrogen enrichments are lateral smaller but with higher hydrogen concentrations
- Hydrogen enrichments occur at temperatures above 1000°C (tetragonal ZrO_2)

Modeling of the hydrogen distribution

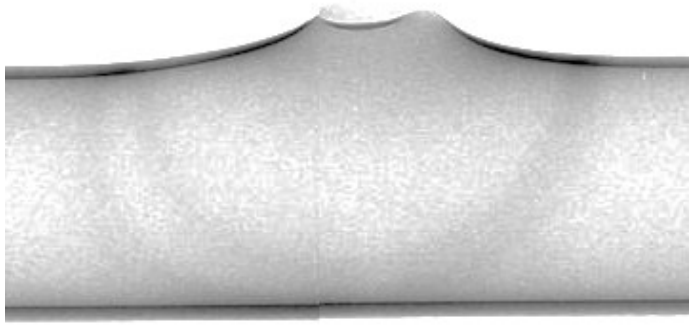

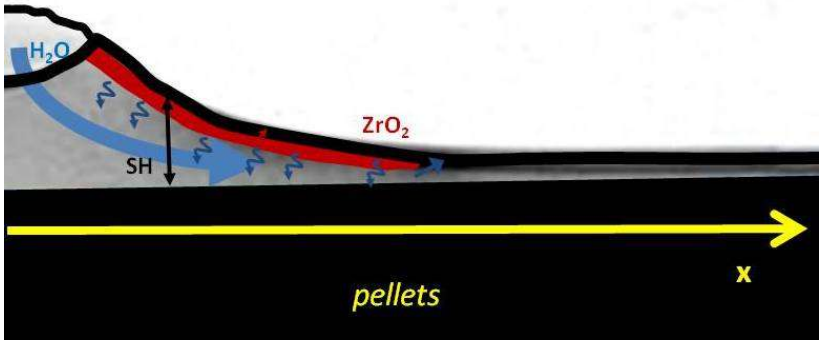

$$dc_{H_{2=}O}(x) = Max\left(\begin{pmatrix} D\frac{\delta^2 c_{H_2O}}{\delta x^2} - \frac{K_{ox}}{2\sqrt{t}} \end{pmatrix} dt \\ 0\end{pmatrix}$$

Steam transport and consumption in the gap

$$dc_{H_2}(x) = \left(\frac{K_{ox}}{2\sqrt{t}} + D\frac{\delta^2 c_{H_2}(x)}{\delta x^2}\right) dt$$

Free hydrogen production and transport

$$c_H^m(x, r=0) = K_S\sqrt{p_{total} * c_{H_2}(x)}$$

Hydrogen uptake (amount of hydrogen in the gap has to be taken into account)

$$dc_H^m(x,r) = D\frac{\delta^2 c_H^m(x,r)}{\delta x^2}$$

Hydrogen diffusion in the tube wall

Actual applications

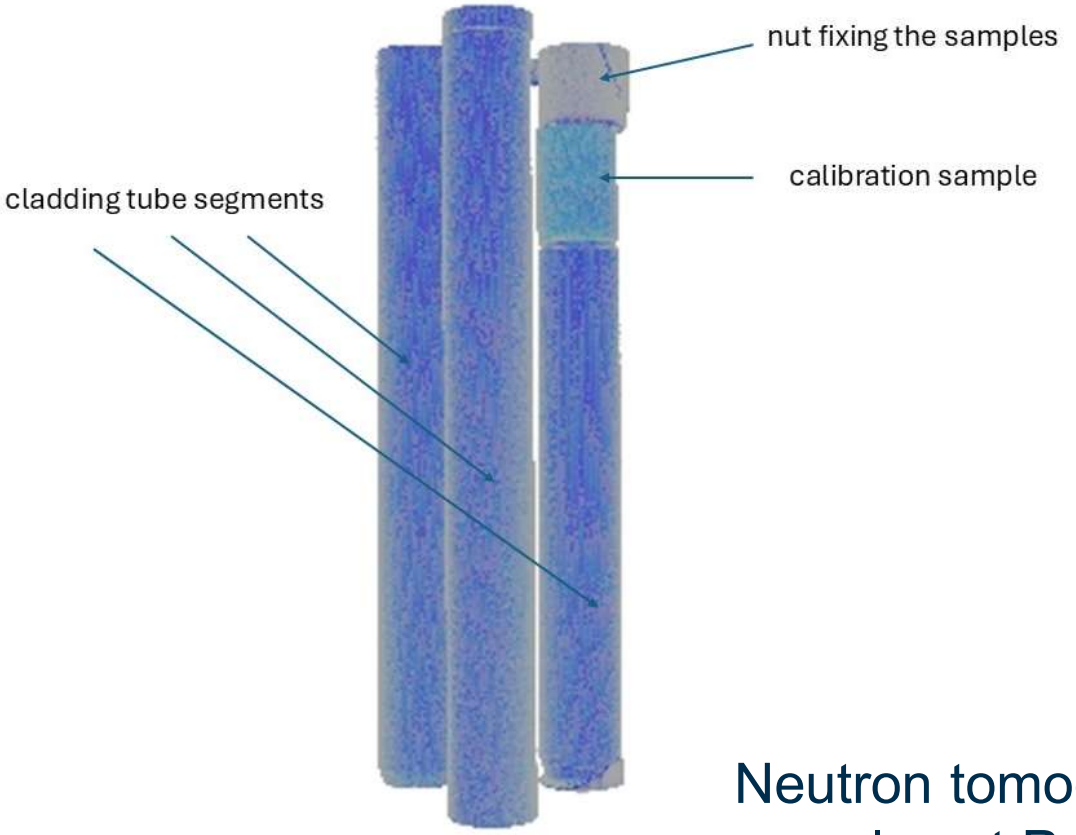

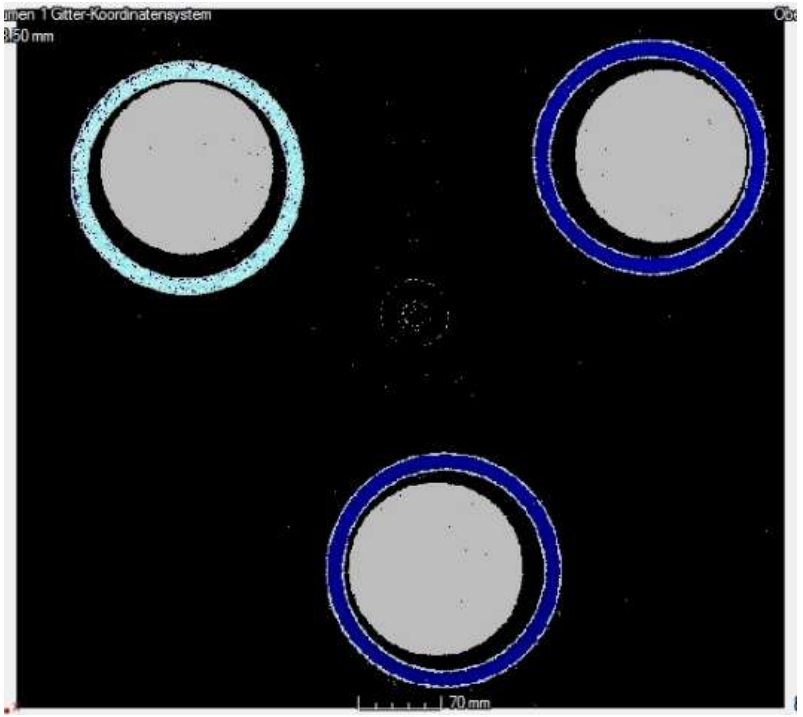

Neutron tomography measurements at SPIZWURZ samples at PorTO (ILL, France, September 2025)

Actual applications

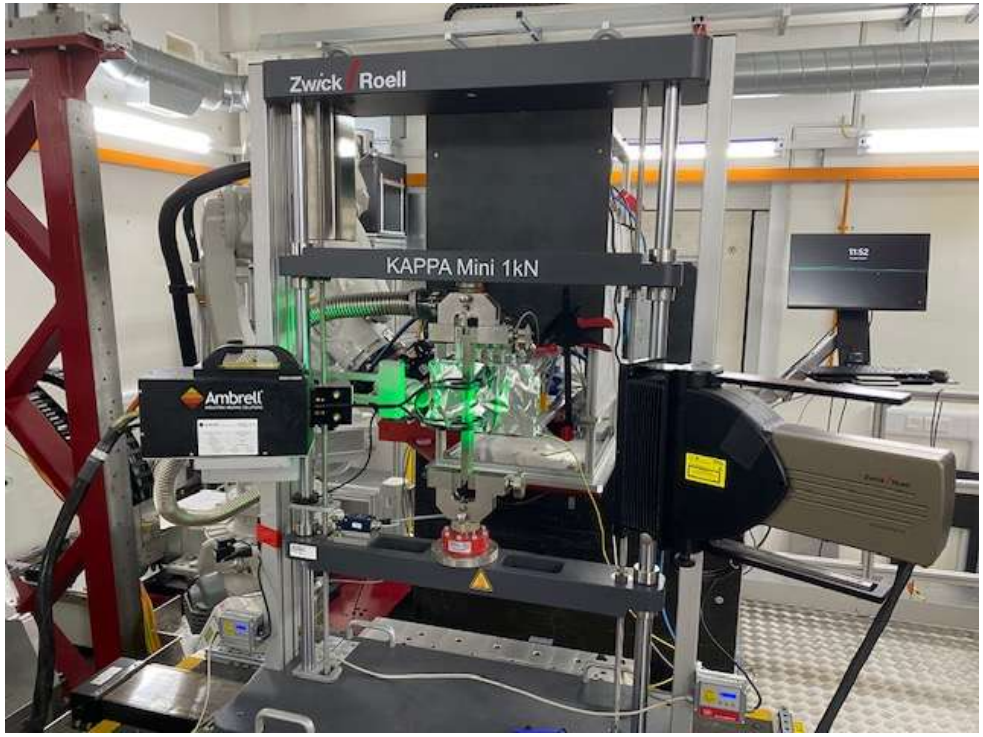

In-situ radiography measurements at the IMAT facility (ISIS, RAL, Harwell, UK, October 2025) with our INCHAMEL tensile machine

Actual applications

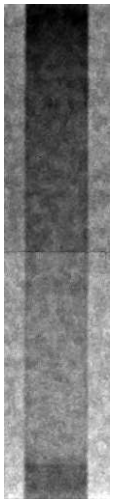

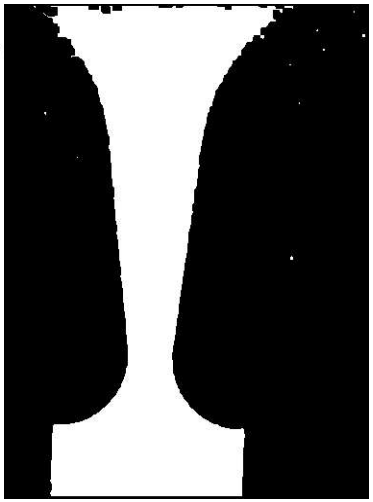

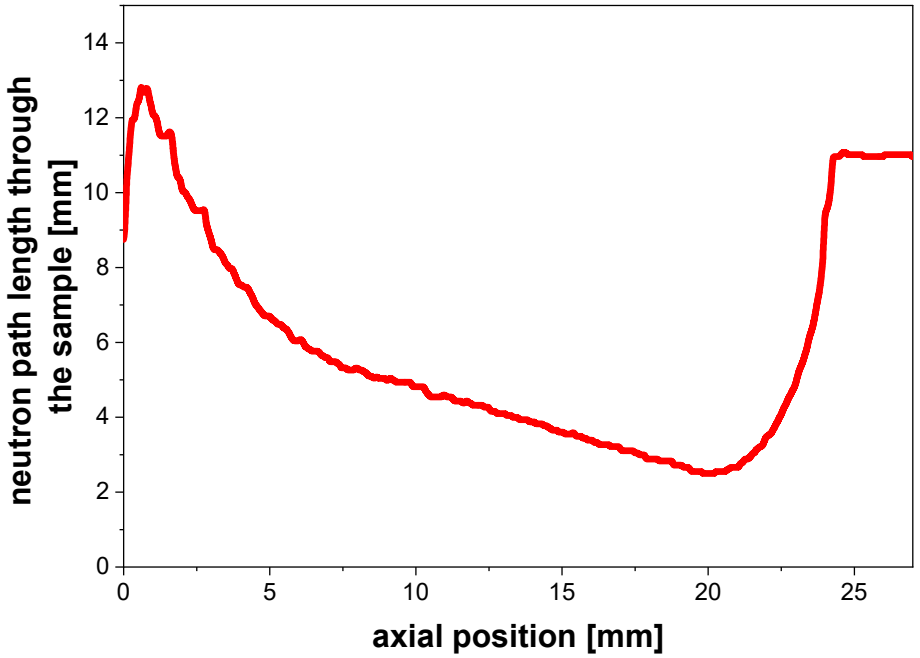

Tensile samples with stress/strain gradient

Actual applications

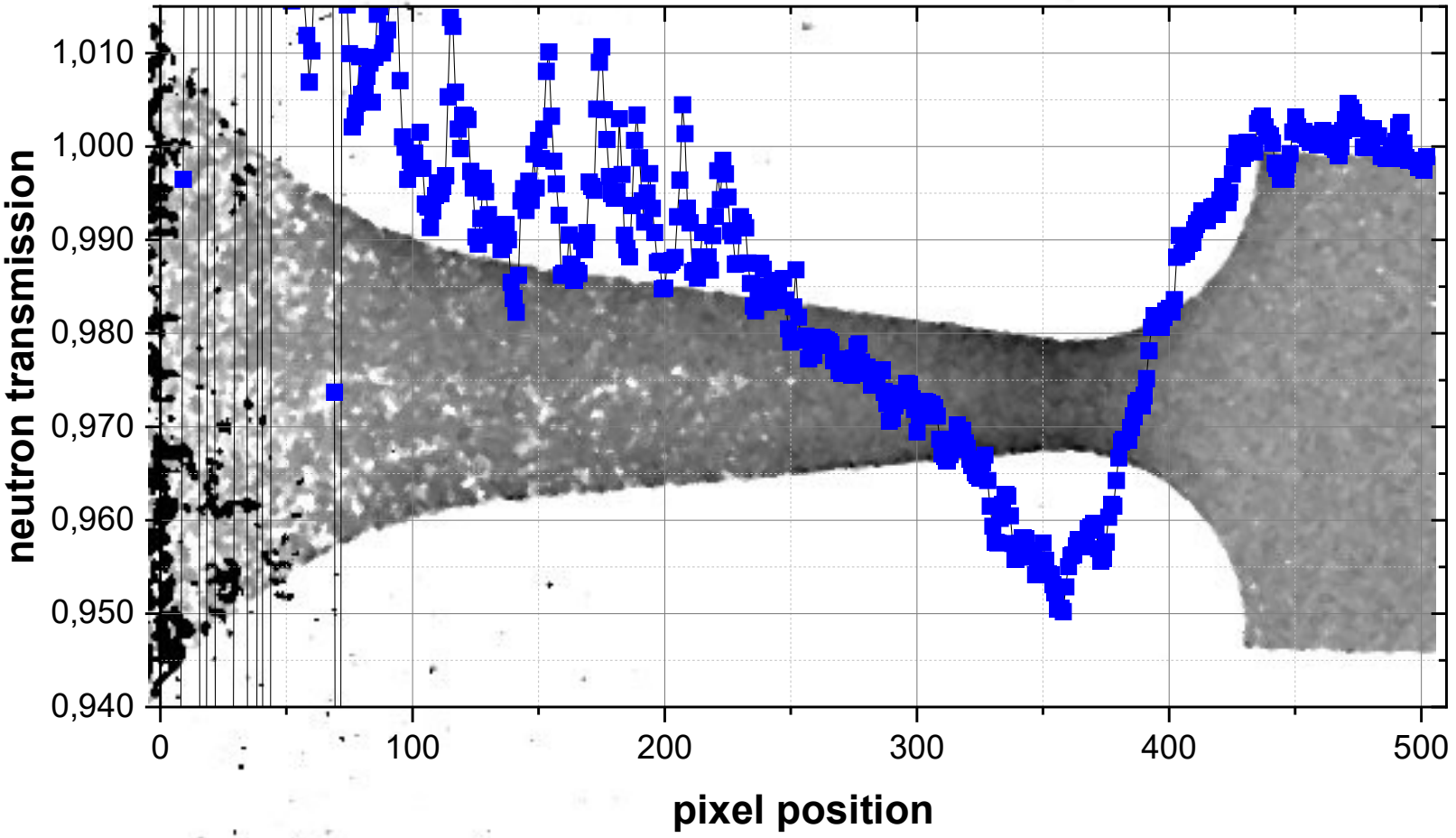

Distribution of the neutron transmission of the sample

Actual applications

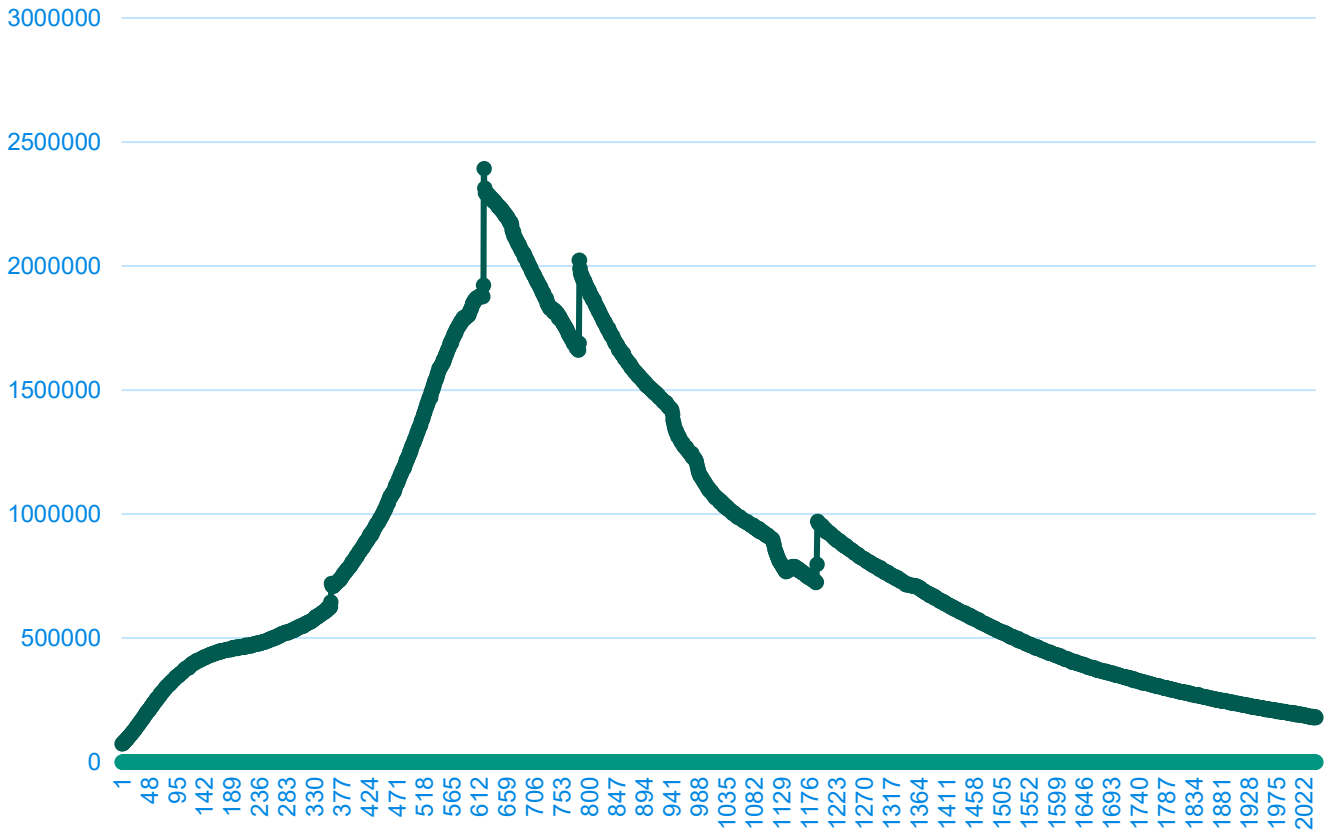

Bragg edges measured at the sample allowing to measure the strain, the temperature distribution and may be give hints on the hydrogen in solution

Actual applications

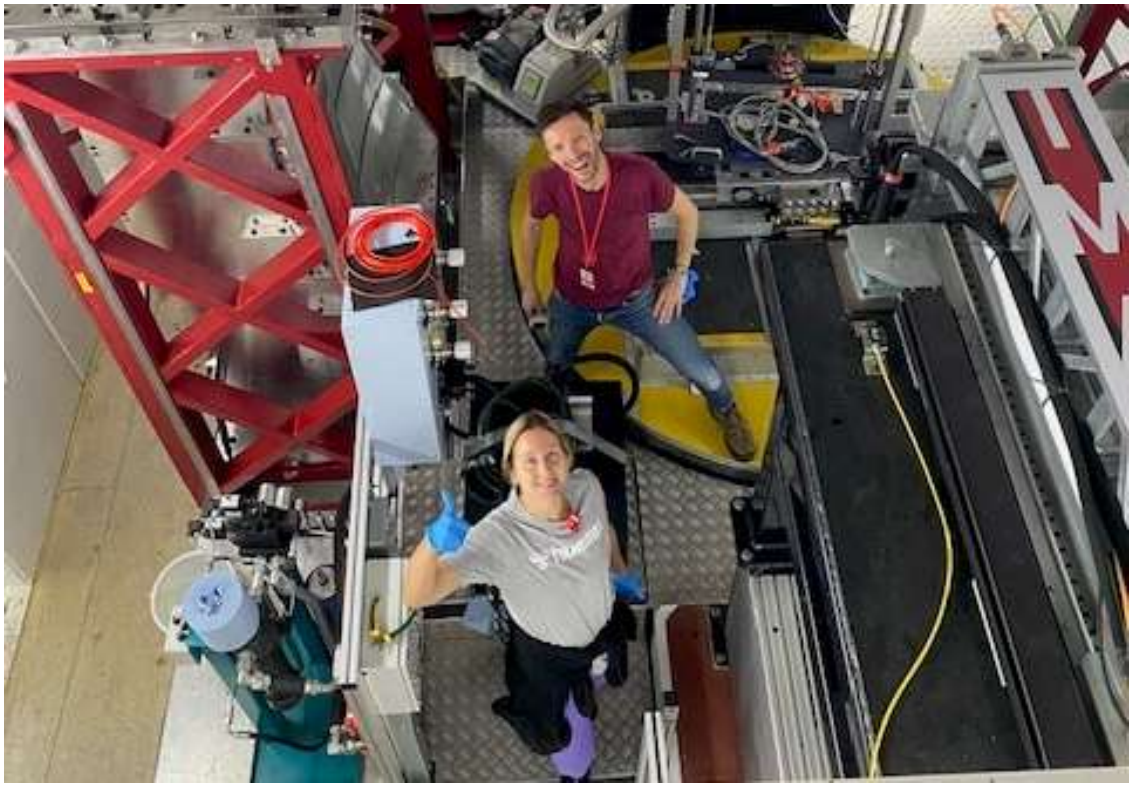

We are happy about this results even the experimental setup has to be improved.

People involved

- **Colleagues from KIT**
  - Sarah Weick
  - Conrado Roessger
  - Martin Steinbrueck
  - Ulrike Stegmaier
  - Chongchong Tang
  - Diana Bachurina
- **Placement or internchip students**
  - Marius van den Berg
  - Leaticia Ott
  - Camille Goulet
  - Enzo Muttini
  - Samuel Pulvermacher
  - Stefan Prestel

Neutron Imaging Facilities

- ConRad @ HMI
  - Nikolai Kartschilov
- ANTARES @ TUM
  - Burkhard Schillinger, Michael Schulz
- ICON, NEUTRA and BOA @ PSI
  - Anders Kaetner, Pawel Trtik, David Mannes, Jan Hovid
- ENGINE-X and IMAT @ RAL
  - Javier Santisteban
  - Winfried Kockelmann, Sylvia Britto
- PorTo and NEXT @ ILL
  - Alessandro Tengattini, Anna Fredrigo,
  - Bratislav Lukic, Lukas Helfen

Cooperations

- CNEA (Argentina)
  - Javier Santisteban
  - Pablo Vizcaino, Adrian Gomez, Sergio Soria, …
- NECSA (South Africa)
  - Robert Nshirimana
- ASNR (France)
  - Martial Kpemou
  - Severine Guilbert
- CEA (France)
  - Frederic Ott
- PSI (Switzerland)
  - Johannes Bertsch, Stefan Valence, Weija Gong, Aaron Coldeweih, Okan Yetik, Liliana Duarte

Acknowledgements

We are grateful to PSI, ILL, HMI, TU Munich and RAL for providing beamtime and support during the experiments.

We thank all colleagues from the QUENCH team supported the neutron imaging measurements, particularly Juri Stuckert and Jürgen Moch.

Thank you for your attention

Thorsten Hollands
GRS

From QUENCH-01 to QUENCH-ATF-2: Three Decades of AC²/ATHLET-CD Validation using QUENCH Experiments

For the development of software tools applied in the field of nuclear safety requirements and procedures are defined for quality assurance purposes. For example, the IAEA published a general document concerning requirements, that need to be fulfilled during code development, including verification and validation (IAEA SAFETY STANDARDS SERIES No. SSG-2). In general development, verification and validation should be separated, while the validation process should cover a phenomena orientated validation matrix, SET), and integral tests.

The QUENCH test matrix shows that several topics are covered in the history of the test series to investigate the material behaviour of fuel rod simulators during flooding of superheated cores. First, classical PWR tests were performed, followed by three tests focusing on B_4C oxidation. Additionally, the scope was on the investigation of different cladding materials like E110, Zirlo™ or M5®. Furthermore, three air-ingress tests were conducted as well as one debris test. Beside one BWR test ATF claddings become focus of the latest test campaign. Starting with one test using FeCrAl cladding two tests were already performed and one severe accident experiment is pending on Cr-coated claddings in the frame of the OECD/NSC QUENCH-ATF project. Finally, LOCA tests were carried out using different claddings for scenarios up to extended DBA. Several tests were used as benchmarks or even one ISP.

Based on the performed test matrix at KIT a validation matrix was derived for AC²/ATHLET-CD which covers most of the conducted experiments leading to several simulations using different code versions from the very beginning of the QUENCH programme and code development up to latest developments – e. g. for Cr-coated claddings – by GRS as well as national partners like RUB and KIT since the late 1990s.

Current simulations using the last code version (ATHLET-CD 3.5) compared to one released in 2012 (ATHLET-CD 2.2C) show that for QUENCHN-06 (ISP-45) with nearly no severe core damage the code version does not differ which approves an already good model basis at that time. For experiments with stronger core degradation like QUENCH-03 and -11 the current code version predicts e. g. less hydrogen compared to the older test. This might look strange, because newer code version should be better. And exactly this is the case, because an error during oxidation was fixed, but leads to less hydrogen. These results show that a permanent code validation on as much as possible experiments dealing with a wide range of phenomena and validity ranges of properties is necessary to ensure a good code performance.

From QUENCH-01 to QUENCH-ATF-2: Three Decades of AC²/ATHLET-CD Validation using QUENCH Experiments

Thorsten Hollands

30th International QUENCH Workshop

Karlsruhe Institute of Technology, Campus North

16-18 December 2025

Outline

- Impact of QUENCH Experiments for ISP, Benchmarks and Code Validation
  - Validation of Computer Codes
  - QUENCH Matrix and Application
- Progress of AC²/ATHLET-CD Validation
  - Test Matrix
  - QUENCH-03
  - QUENCH-06
  - QUENCH-11
- Conclusions and Outlook

General Guidelines for Computer Codes (IAEA SSG-2)

- QM Guidelines for computer programs.
- Separation of **Development and Verification vs. Validation**.
  - **Verification:** check, whether models are implemented correctly,
  - **Validation:** check, whether physical phenomena are described by the appropriate models (in terms of correctness),
    - Phenomena orientated validation matrix,
    - Single effect tests (SET): selected effects, clearly defined initial and boundary conditions, high instrumentation density and quality,
    - Integral tests: interaction of different effects, normally scaled test facilities, common special instrumentation.

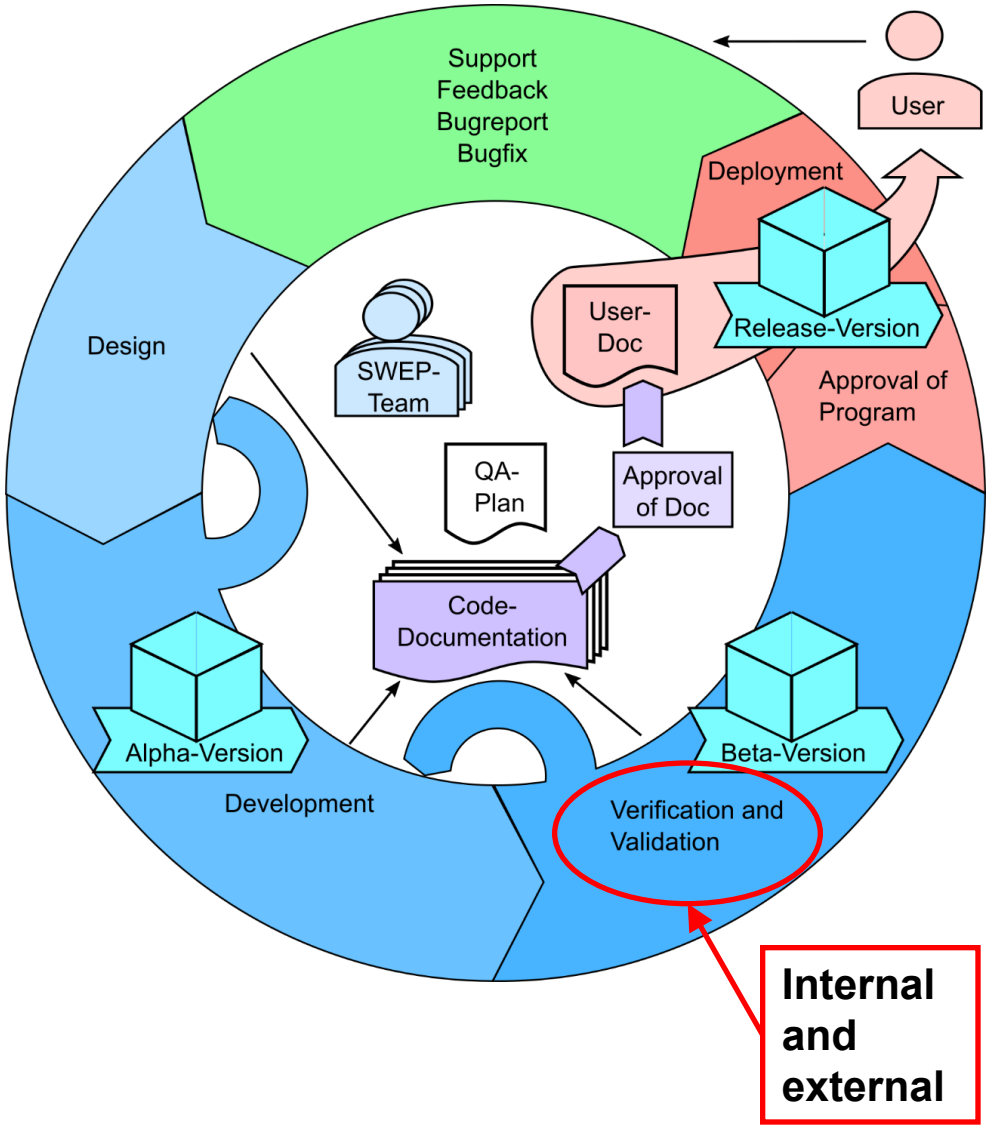

Validation of Computer Codes - Requirements for Code Validation

- IAEA SAFETY STANDARDS SERIES No. SSG-2
- OECD/CSNI In-Vessel Core Degradation Code Validation Matrix (NEA/CSNI/R(2000)21)
  - **Category 1** experiments are amongst the best qualified for code validation in their field. ISPs normally fall into this category. Data are well documented and boundary conditions are well defined (these conditions may be relaxed if there are specific unique features). Category 1 tests are strongly recommended for the validation of system codes (depending on their specific objectives)
  - **Category 2** experiments are well qualified for code validation, and could be used to increase the degree of confidence in a code's suitability for a given application. The experiment may not be unique, but valuable in the sense of parameter range.
  - **Category 3** and **4** were not considered due to the database and quality of the evaluated experiments.
  - **Cross References Matrices** were generated to evaluate the investigated experiments

QUENCH Matrix and Application (I)

Experiment	Topic	Used for
QUENCH-01	partial fragmentation of pre-oxidized cladding	Validation
QUENCH-02	no additional pre-oxidation; quenching from high temperatures	Validation
QUENCH-03	delayed flooding; 240 s after temperature escalation has started	Validation
QUENCH-04	cool-down behavior of slightly pre-oxidized cladding by injected cold steam	Validation
QUENCH-05	cool-down behavior of pre-oxidized cladding by injected cold steam	Validation
QUENCH-06	prediction of H2 source term by different code systems	**ISP-45**
QUENCH-07	impact of B4C absorber rod failure on H2, CO, CO2 and CH4 generation	Validation
QUENCH-08	Reference test to QU-07 without absorber rod	Validation
QUENCH-09	impact of B4C absorber rod failure on H2, CO, CO2 and CH4 generation in steam-starved conditions	Validation
QUENCH-10	air ingress during spent fuel storage container accident	**SARNET Benchmark**

QUENCH Matrix and Application (II)

Experiment	Topic	Used for
QUENCH-11	boil-off test with subsequent flooding	**SARNET Benchmark**
QUENCH-12	physico-chemical behavior of VVER type cladding (Zr1%Nb) during flooding	Validation
QUENCH-13	AgInCd absorber rod, aerosol	Validation
QUENCH-14	ACM series, M5® cladding	Validation
QUENCH-15	ACM series, ZIRLO™ cladding	Validation
QUENCH-16	air ingress	**SARNET Benchmark**
QUENCH-17	debris formation and coolability	Validation
QUENCH-18	air ingress, AgInCd absorber rods	**NUGENIA QUESA Benchmark**
QUENCH-19	ATF, FeCrAl cladding	**IAEA Benchmark**
QUENCH-20	BWR configuration	Validation

QUENCH Matrix and Application – Special Test Series

Experiment	Topic	Used for
QUENCH-L0	LOCA bundle commissioning test with Zircaloy-4 claddings	Validation
QUENCH-L1	LOCA bundle reference test with Zircaloy-4 claddings	**IAEA FUMAC Benchmark**
QUENCH-L2	LOCA bundle test QUENCH-L2 with M5® claddings	Validation
QUENCH-L3	LOCA bundle test with otimised ZIRLO™ cladding	Validation
QUENCH-L3HT	Extended LOCA bundle test with otimised ZIRLO™ cladding	Validation
QUENCH-L4	LOCA bundle test with pre-hydrogenated M5® claddings	Validation
QUENCH-L5	LOCA bundle test with pre-hydrogenated optimised ZIRLO™ claddings	Validation
QUENCH-ATF-1	Cr-coated, Extended DBA	**OECD QUENCH-ATF Benchmark**
QUENCH-ATF-2	Cr-coated, QUENCH-15 like scenario	**OECD QUENCH-ATF Benchmark**
QUENCH-ATF-3	Cr-coated, boil-off sceanrio with subsequent flooding	

GRS Code Package AC²

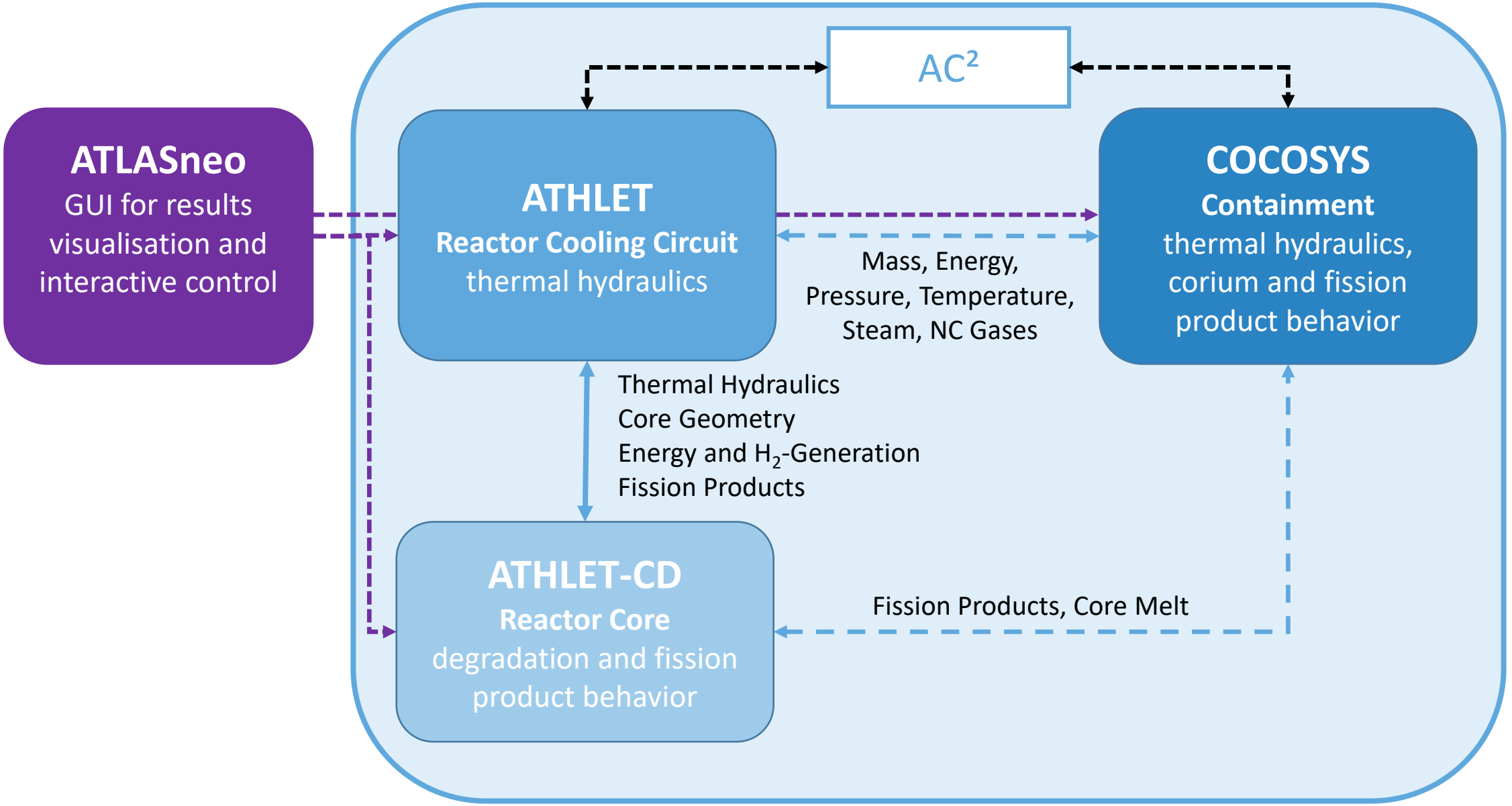

History of AC²/ATHLET-CD

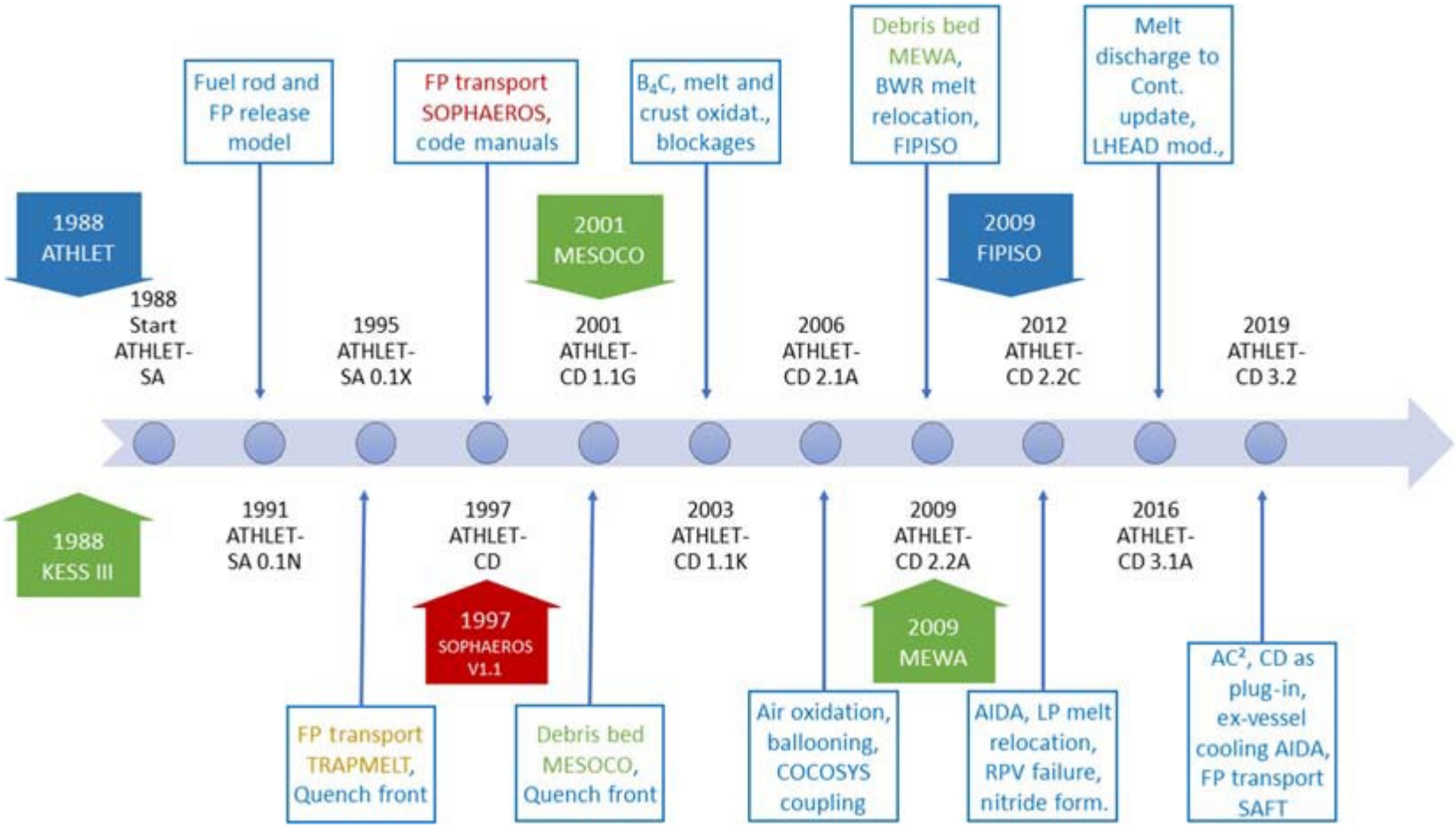

AC²/ATHLET-CD – QUENCH Validation Matrix (I)

Experiment	Calculations done by	Code Version	First Documented
QUENCH-01	GRS	1.2G	2001
QUENCH-03	RUB	1.1F, 1.2C	2001
QUENCH-04	RUB	3.1A	2002
QUENCH-05	RUB	1.1G	2002
QUENCH-06	GRS, RUB	1.1H, 3.2, 3.3	2002
QUENCH-07	GRS, RUB	1.1J, 2.0, 3.2	2006
QUENCH-08	GRS, RUB	1.1L, 2.1	2006
QUENCH-09	GRS	1.1K	2006
QUENCH-10	GRS	2.0B, 3.2	2006

AC²/ATHLET-CD – QUENCH Validation Matrix (II)

Experiment	Calculations done by	Code Version	First Documented
QUENCH-11	GRS, RUB	2.1A, 2.1B, 3.2	2006
QUENCH-12	RUB, KIT		2012
QUENCH-13	RUB	2.2A	2010
QUENCH-15	GRS	3.1A, 3.2	
QUENCH-16	GRS, RUB	2.2C, 3.2, 3.3	2012
QUENCH-17	GRS, RUB	2.2C	2016
QUENCH-18	GRS, RUB	3.1A, 3.2, 3.3	2018
QUENCH-19	GRS	3.2, 3.3.0, 3.3.1	2019
QUENCH-20	GRS	3.3.1	2022

AC²/ATHLET-CD – QUENCH Validation Matrix: Special Test Series

Experiment	Calculations done by	Code Version	First Documented
QUENCH-L0	GRS	3.1A	2016
QUENCH-L1	GRS	3.1A	2016
QUENCH-L2	GRS	3.1A	2015
QUENCH-L3	RUB	3.3	2022
QUENCH-L3HT	RUB	3.2.1, 3.3.0, 3.3.1	2022
QUENCH-ATF-1	GRS, RUB	3.3.0, 3.3.1	2024
QUENCH-ATF-2	GRS, RUB	3.3.1	2025

QUENCH-03 – Temperatures at 950 mm

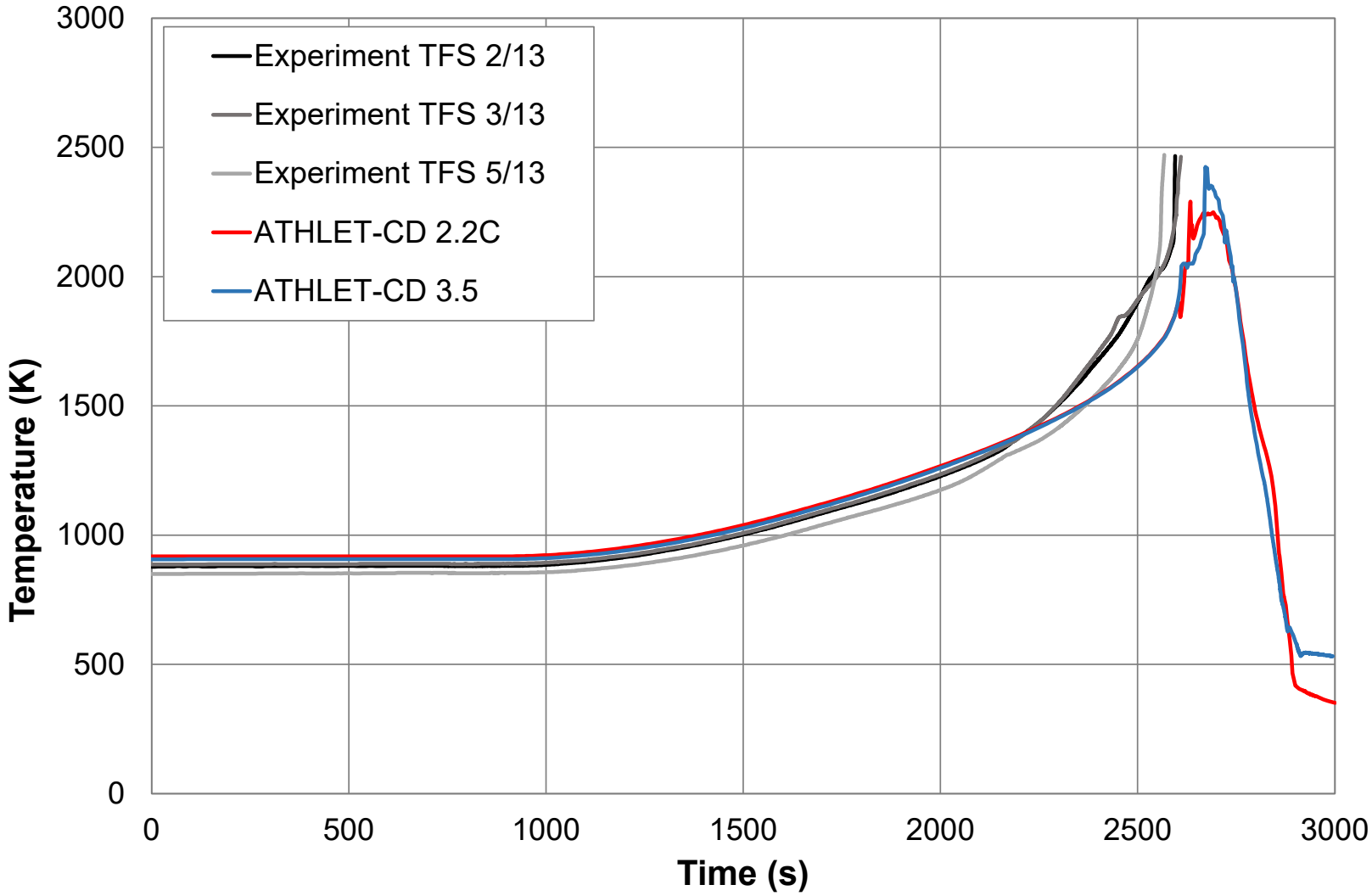

QUENCH-03 – Hydrogen Generation

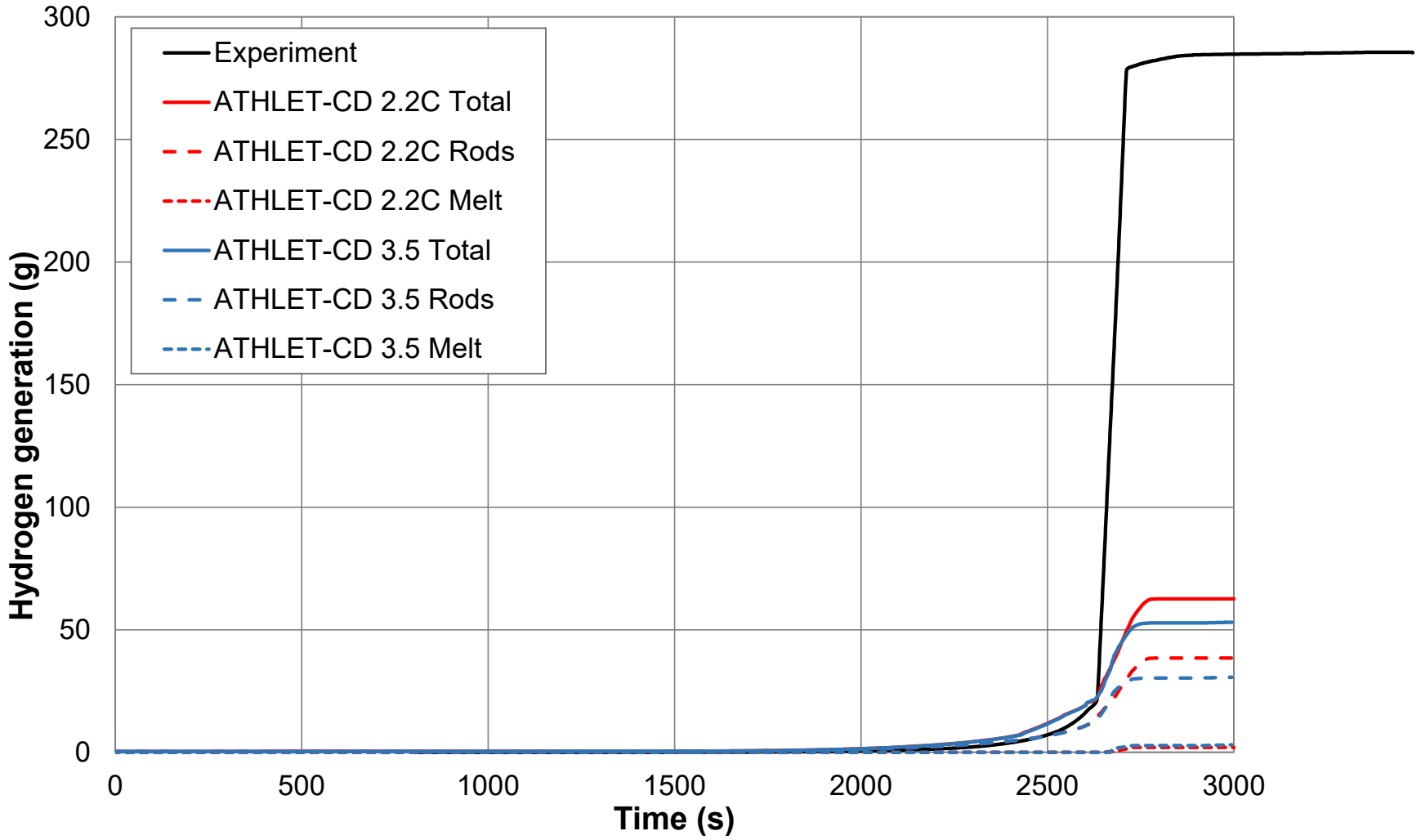

QUENCH-06 – Temperatures at 950 mm

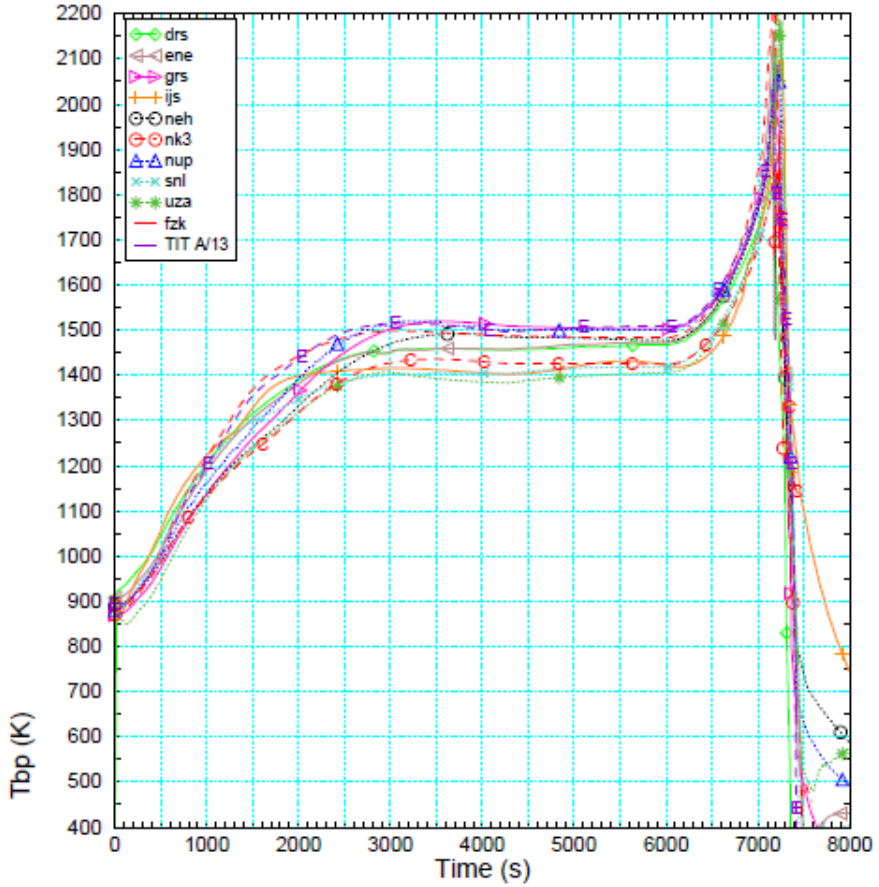

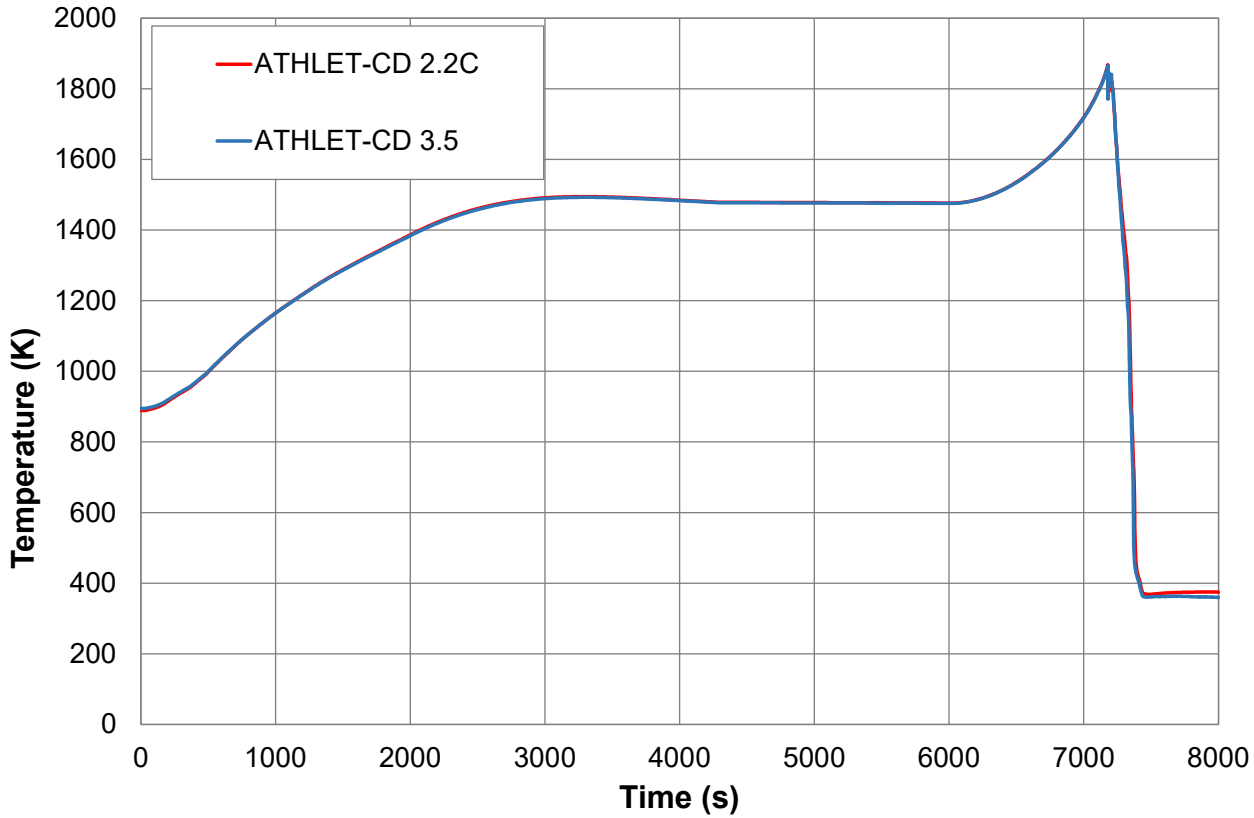

QUENCH-06 – Hydrogen Generation

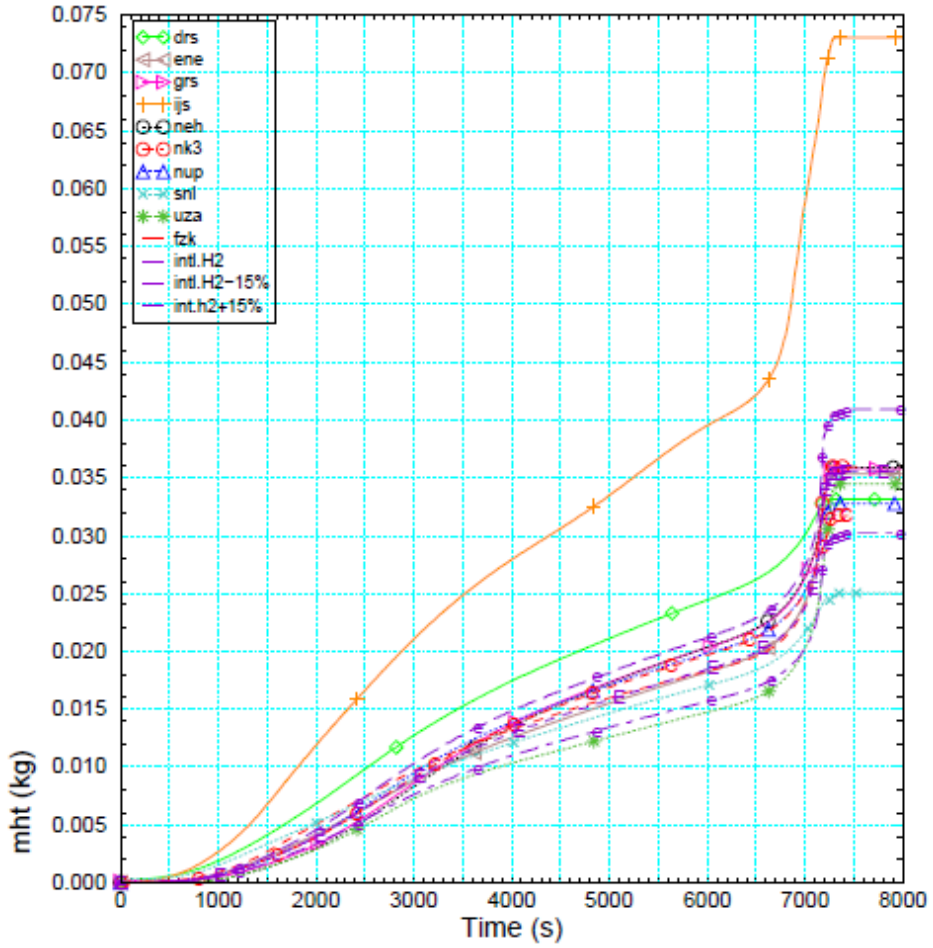

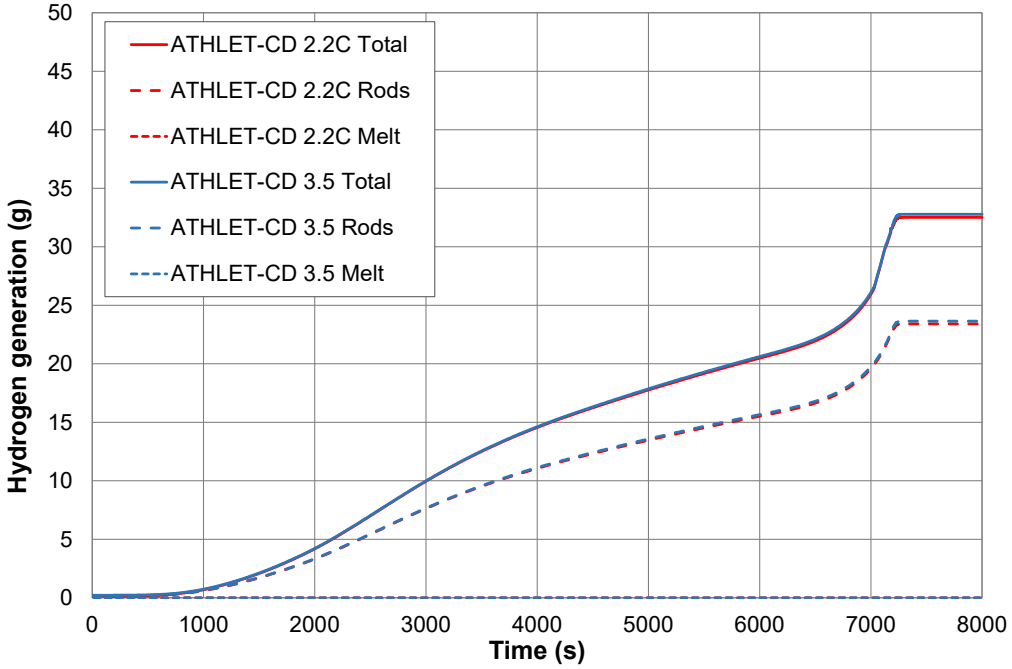

QUENCH-11 – Water Level

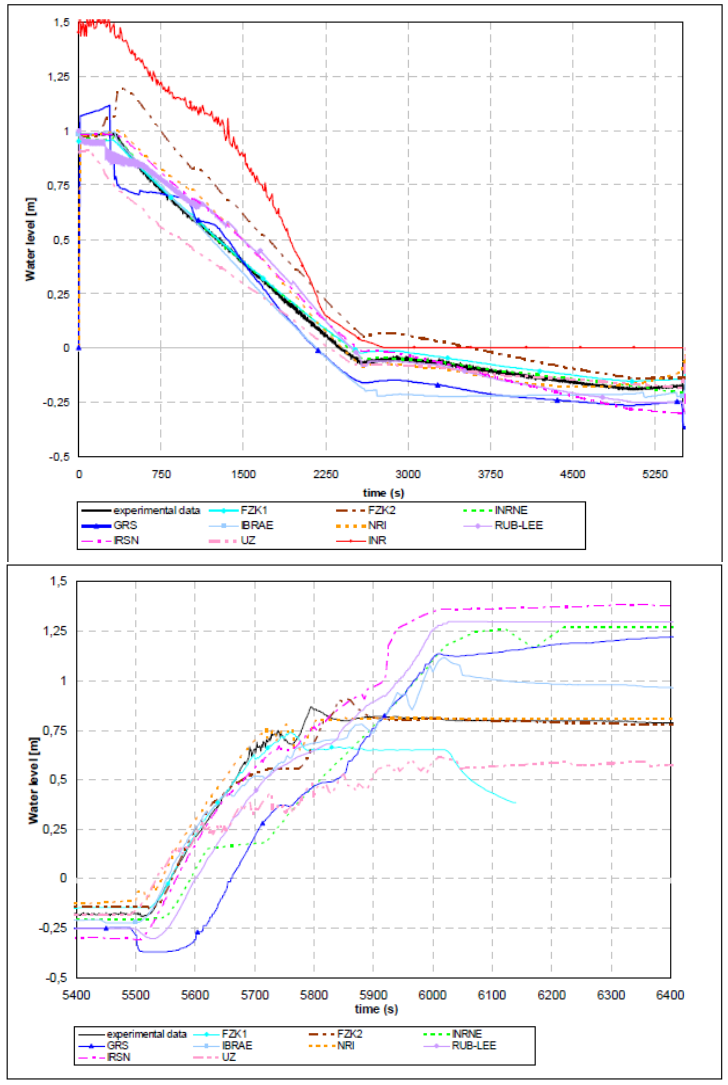

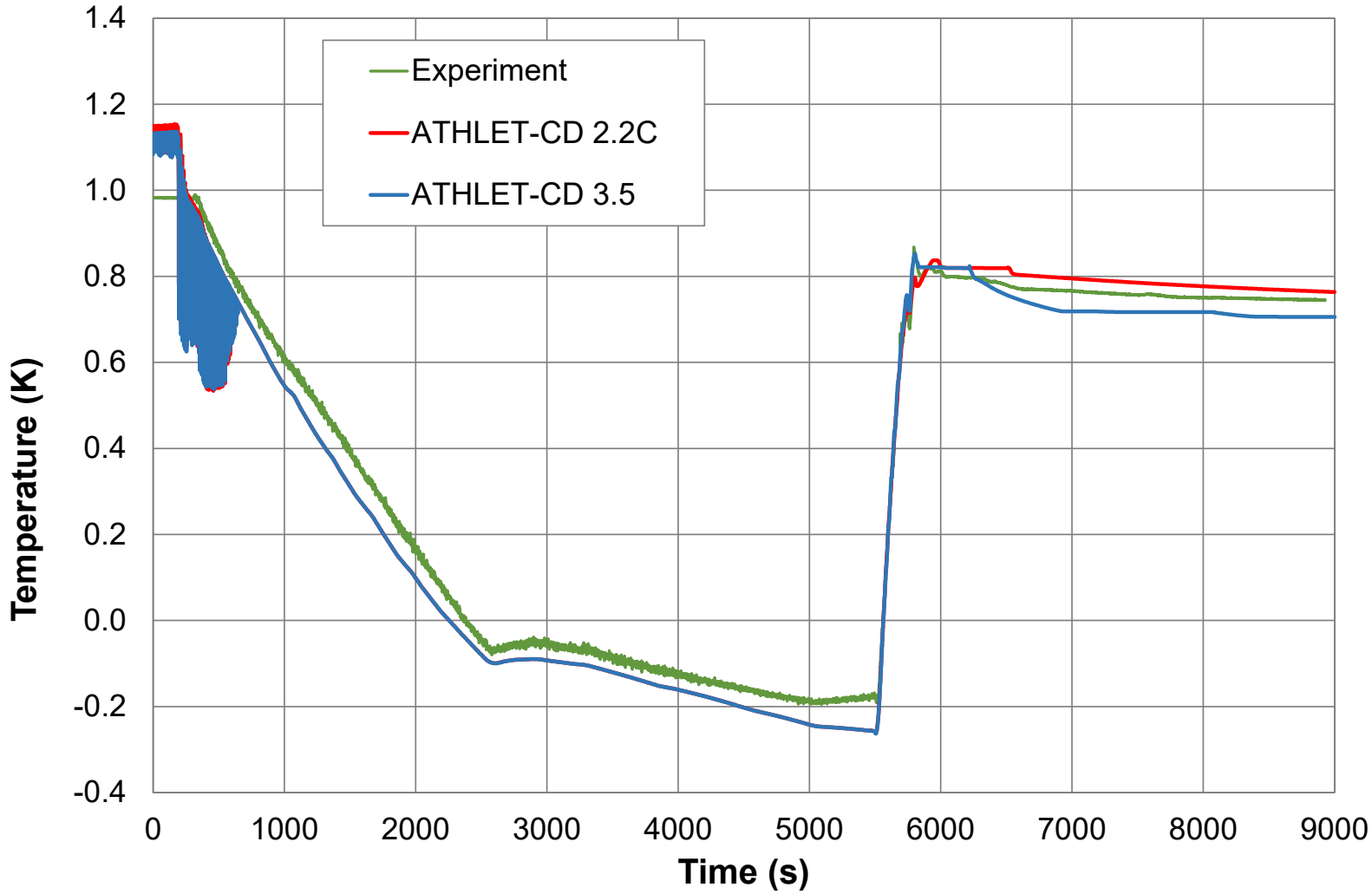

QUENCH-11 – Temperatures at 950 mm

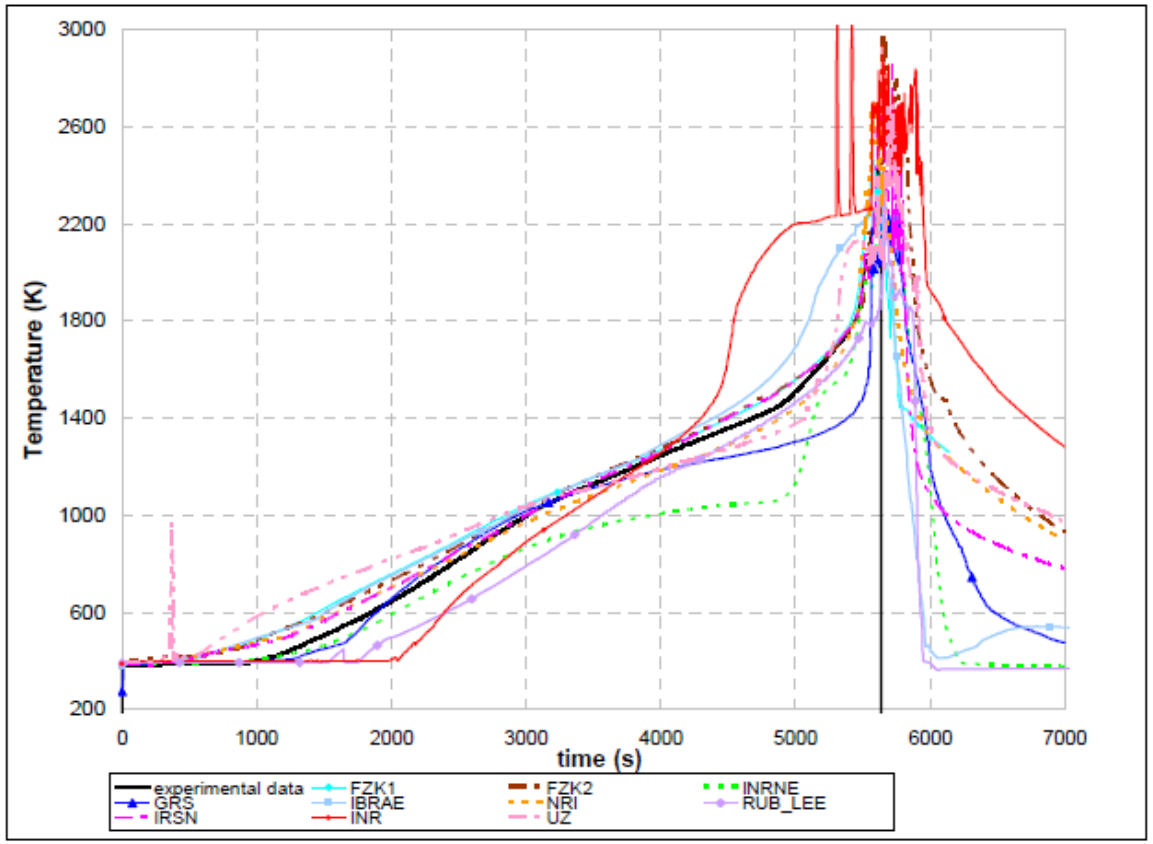

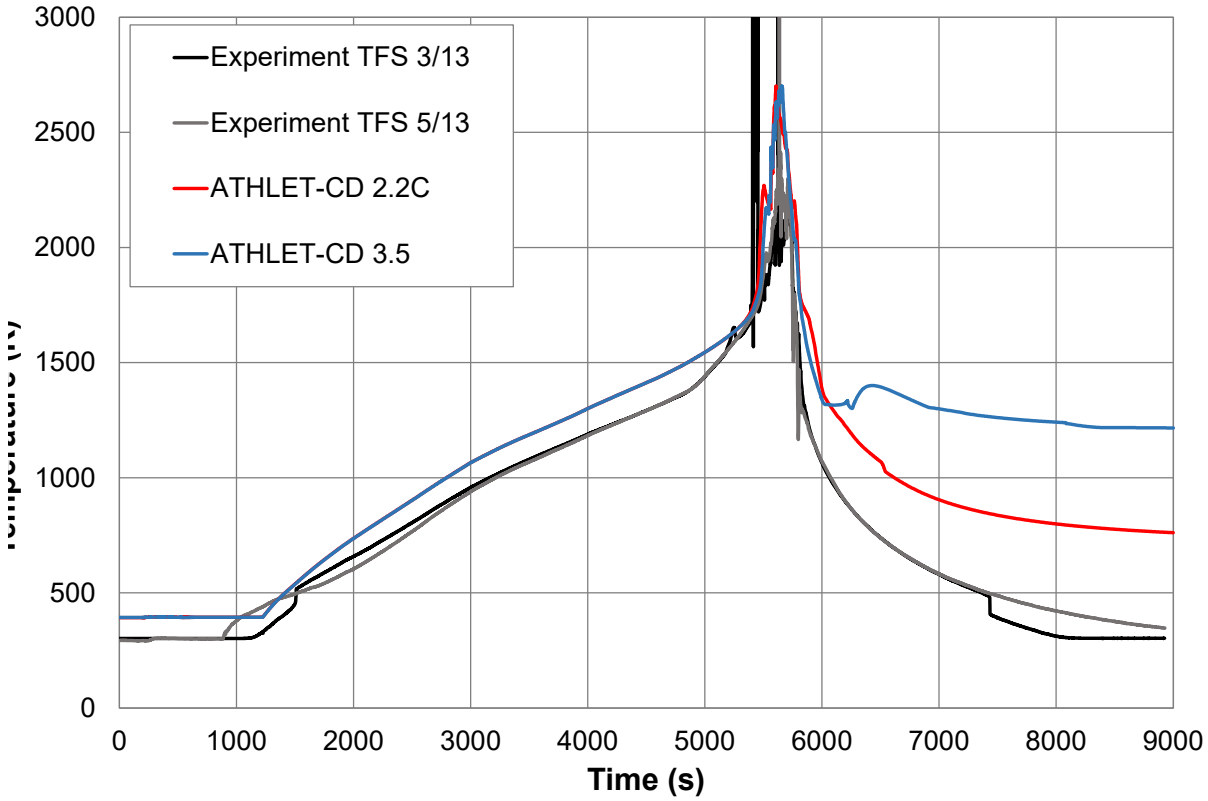

QUENCH-11 – Hydrogen Generation

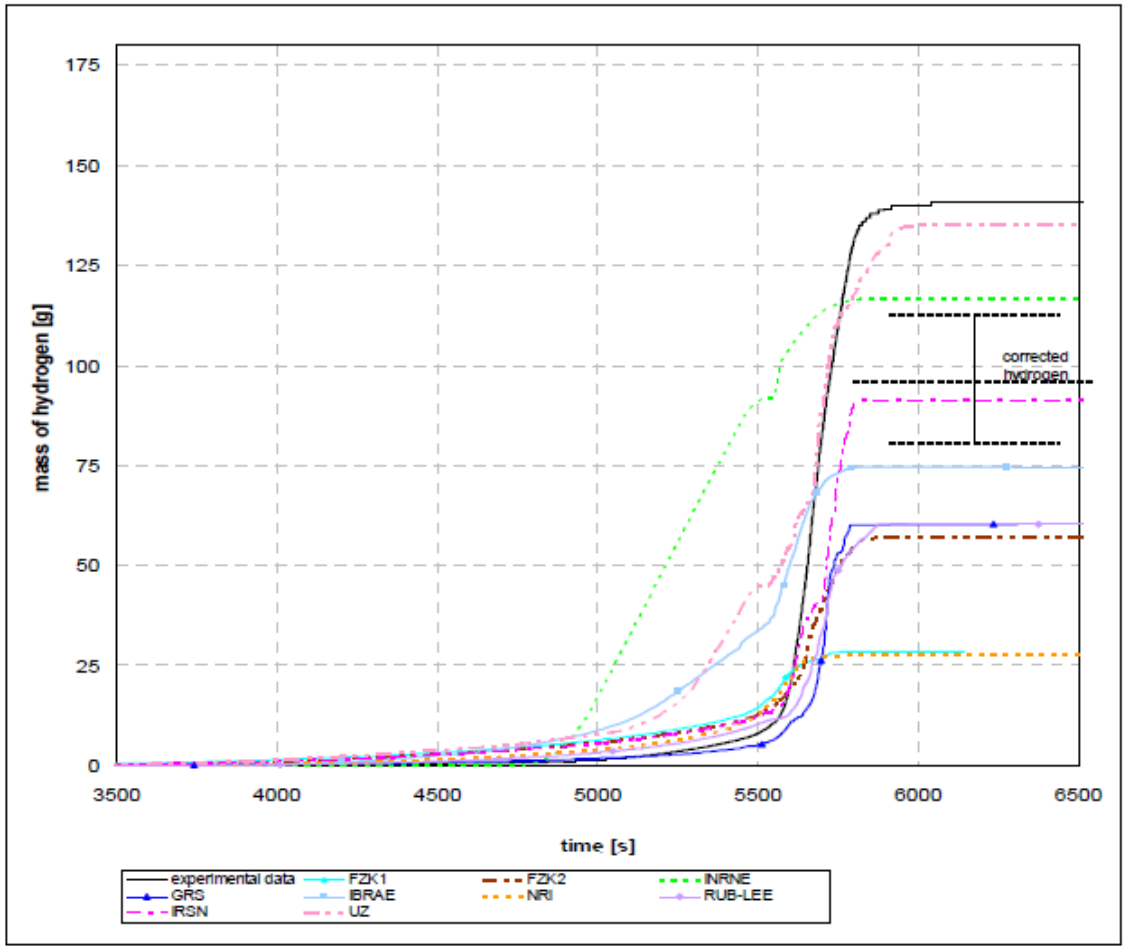

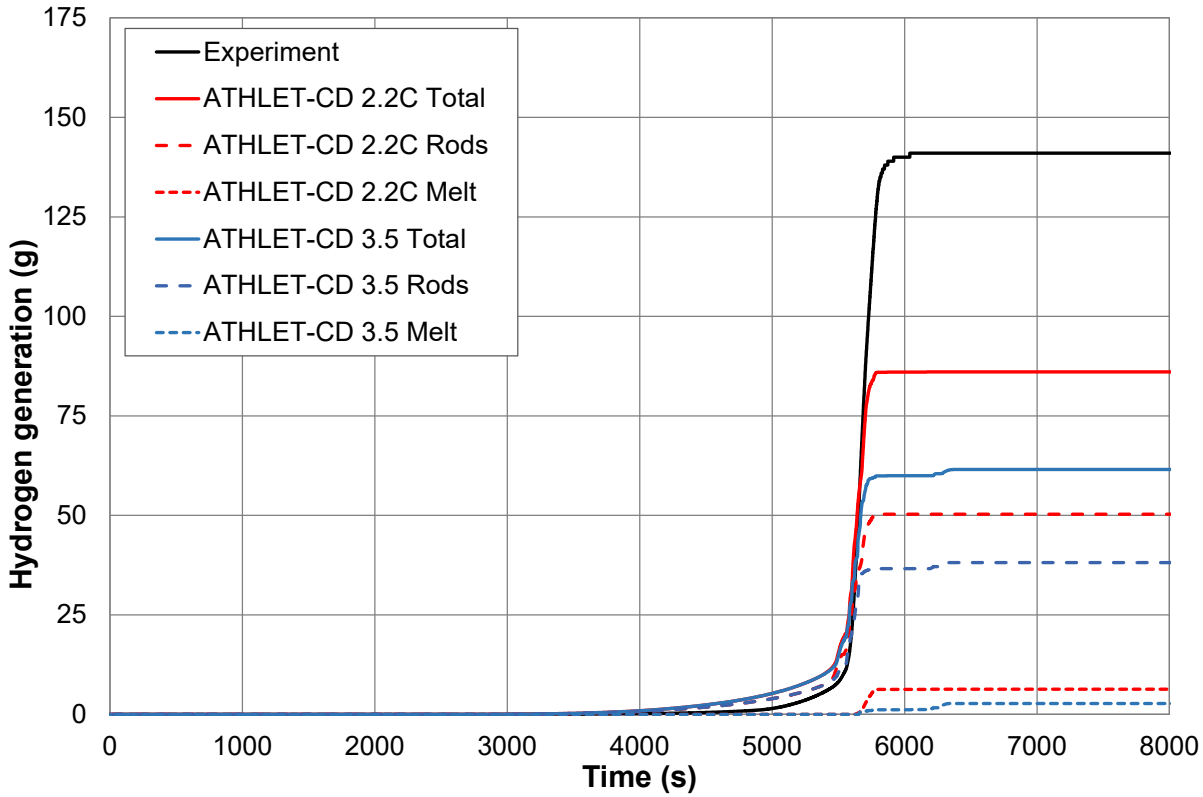

Conclusion and Outlook

- QUENCH tests are widely used for code validation
- One ISP and several Benchmarks on QUENCH tests were conducted
- Several topics are covered which led also to code improvements to be able to perform calculations
- This wide field of topics provides many data for code validation
- Beside the QUENCH tests for severe accident conditions also a series of LOCA tests was performed which was also used for code validation
- The new topics of QUENCH tests considering ATF rods are challenging for the codes, but this will again force model development and validation efforts

- **Nearly all QUENCH tests are used for AC^2/ATHLET-CD code validation for app. 30 years and documented since 25 years**
- **The validation against QUENCH tests leads to a significant code improvement and robustness**

- **Hopefully, the data base for code validation will be further enlarged by performing several new QUENCH tests**

Personal Remark

- First QWS participation in 2005
  Hidden somewhere in the back surrounded by a huge number of famous experts

- Fruitful discussions and collaborations for two decades with Martin, Juri, Mirko and the whole QUENCH team
- My Doctoral Thesis was based on KIT experiments
- Participation in some test conducts with some surprises
- **THANK YOU ALL FOR THE INTERSTING TIME AND GOOD LUCK FOR A SUCCESSFUL FUTURE OF QUENCH (or how it will be called)**
  and a healthy retirement

Acknowledgements

The development, validation, qualification and application of AC² is funded by

Federal Ministry
for the Environment, Climate Action,
Nature Conservation and Nuclear Safety

Mirco Große
KIT

The SPIZWURZ project - overview and single effect tests

The SPIZWURZ project is a cooperation between GRS, KIT-INE and KIT-IAM/AWP to investigate the hydrogen re-distribution and hydride re-orientation in cladding tubes under long-term dry storage conditions.

The paper gives first an overview about the project. Later, the measurements of the stress/strain induced by the pellets on the cladding tube of a spent fuel rod stored for more than 35 years as well as of separate effect tests of the parameters influencing hydrogen diffusion and solubility were presented.

The investigations of the spent fuel rod segment show that no significant stress is induced by the fuel on the cladding.

In preparation of the bundle test, the influence of annealing on the tensile properties of the cladding tubes was studied. Annealing at 450°C up to 14 h has only a small influence on the stress – strain curves measured. Annealing at 500°C for one hour reduces the yield stress by more than 25%. It can be concluded that the maximal temperature of the hydrogen loading is 450°C.

Results of the investigations of the hydrogen diffusion in zirconium single crystal depending on their orientation as well as the effect of elastic stress on the hydrogen solubility were presented too. Significant differences in the diffusion rate between the a and the c direction of the hexagonal lattice were found in the measurements at the single crystals. A hydrogen enrichment at the highest elastic stress were detected in a sample with stress gradient. The experimental setup of both studies should be improved to get more reliable results.

An outlook on future investigations and the SPIZWURZ+ project proposal submitted is given at the end of the presentation.

The SPIZWURZ project - overview and single effect tests

Mirco Grosse, Sarah Weick, Michel Herm

30. Intern. QUENCH Workshop,
KIT Campus North, 2025/12/18

Overview

- **SPIZWURZ** = **Sp**annungs**i**nduzierte **W**asserstoffumlagerung wäh**r**end Langzeit-**Z**wischenlagerung” (stress induced hydrogen re-distribution during long-term intermediate storage).
- Cooperation between GRS, KIT INE and KIT IAM-AWP
- Duration 06/2020 – 04/2025


Credit: Audrius Meskauskas

Purpurner Enzian (Spitzwurz)

Purple gentian

Supported by:

Federal Ministry
for the Environment, Nature Conservation,
Nuclear Safety and Consumer Protection

FKZ RS1586A/1501609B

based on a decision of
the German Bundestag

Overview

Hydrogen behaviour in cladding tubes

KIT IAM-AWP

Combination and evaluation

GRS

Stress states between fuel and cladding tube of irradiated fuel rods

KIT-INE

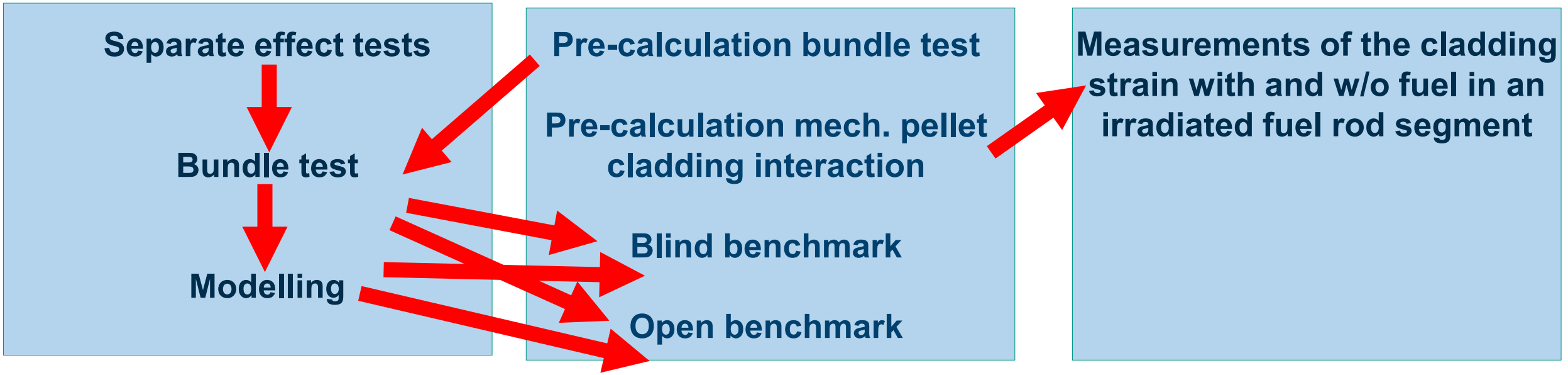

Stress states between fuel and cladding tube of irradiated fuel rods

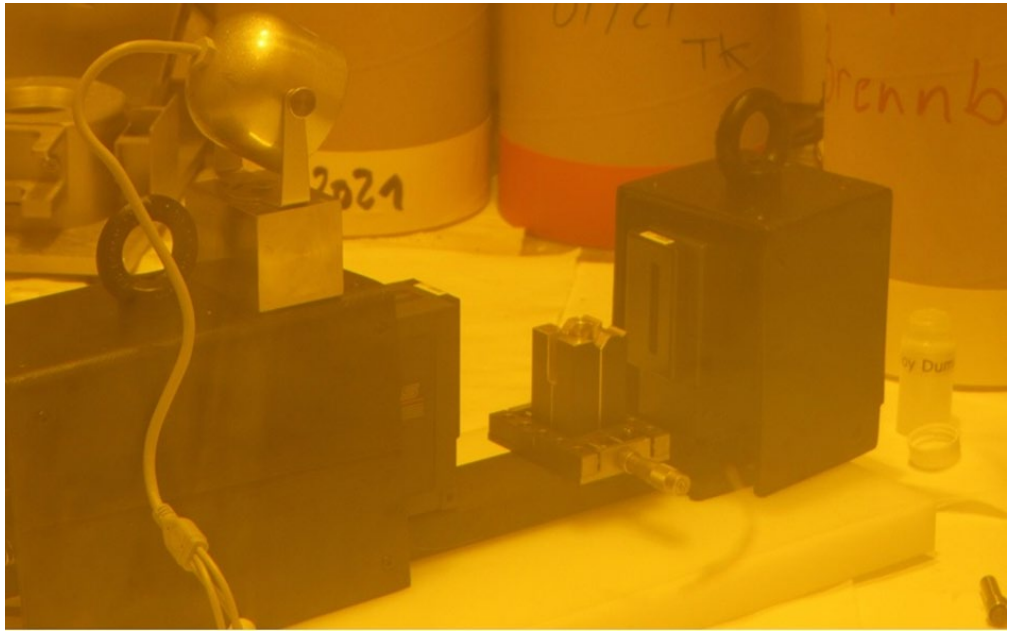

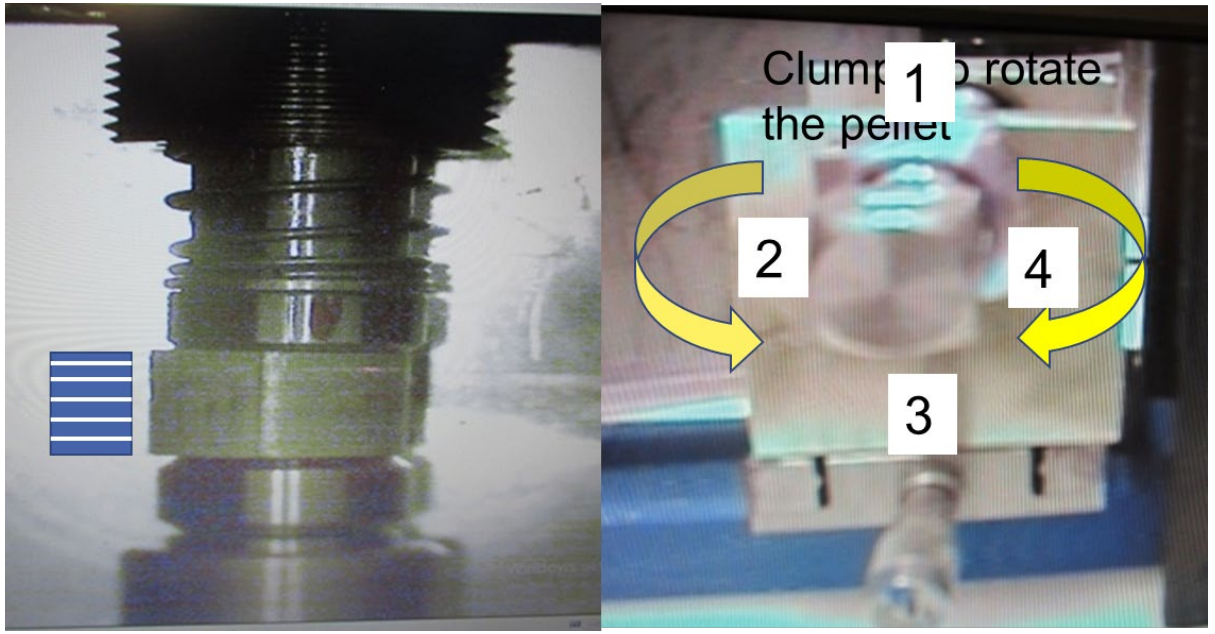

- Diameter measurements at 5 axial positions, 8 circumferential positions, 6 measurements per positions
- Chemical removing of the fuel by 50% HNO_3
- Repeating the diamter measurements

Stress states between fuel and cladding tube of irradiated fuel rods

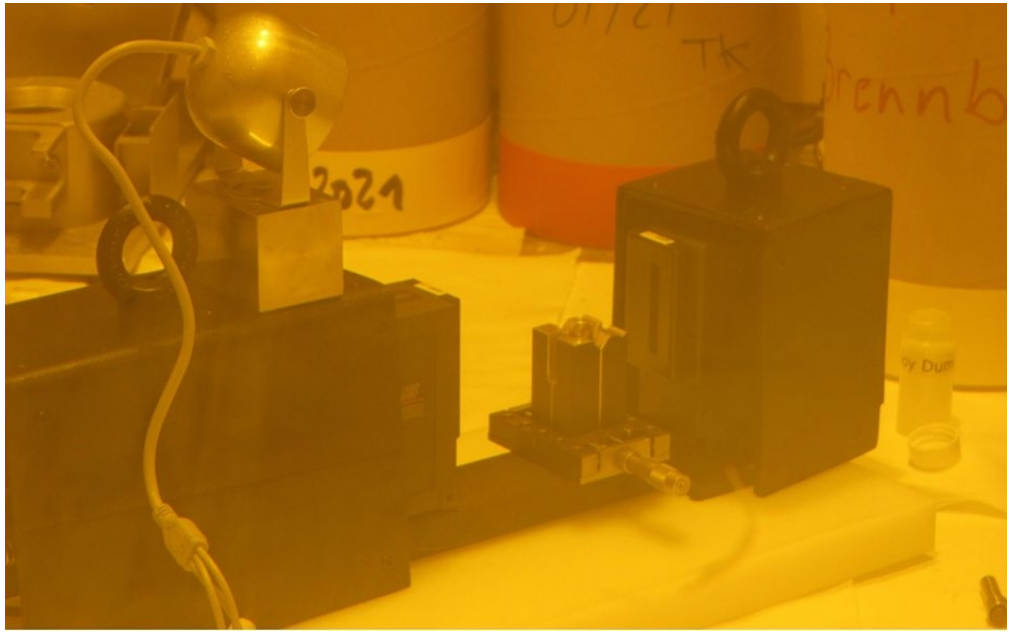

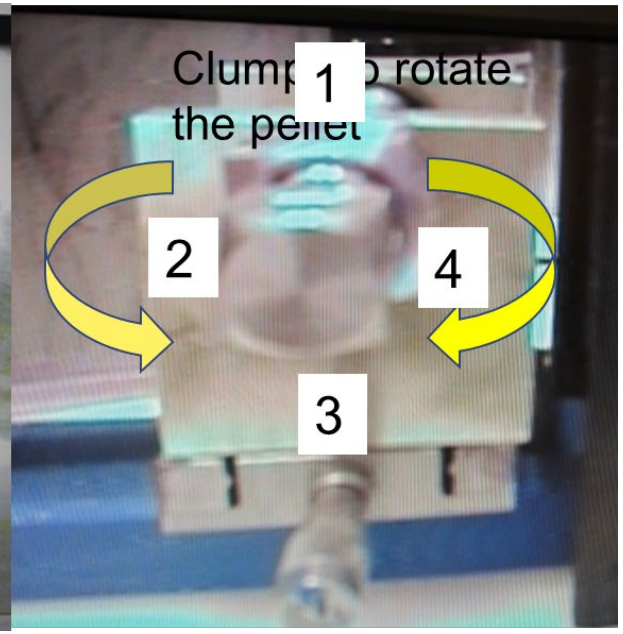

Nominal diameter:	10.750 ± 0.050 mm
Diameter with pellets:	10.700 ± 0.003 mm (slightly oval (30 .. 50 µm))
Strain after removing the pellets:	3.3 ± 3.1 µm

The pellets do not induce significant elastic stress/strain to the cladding.

Separate effect tests

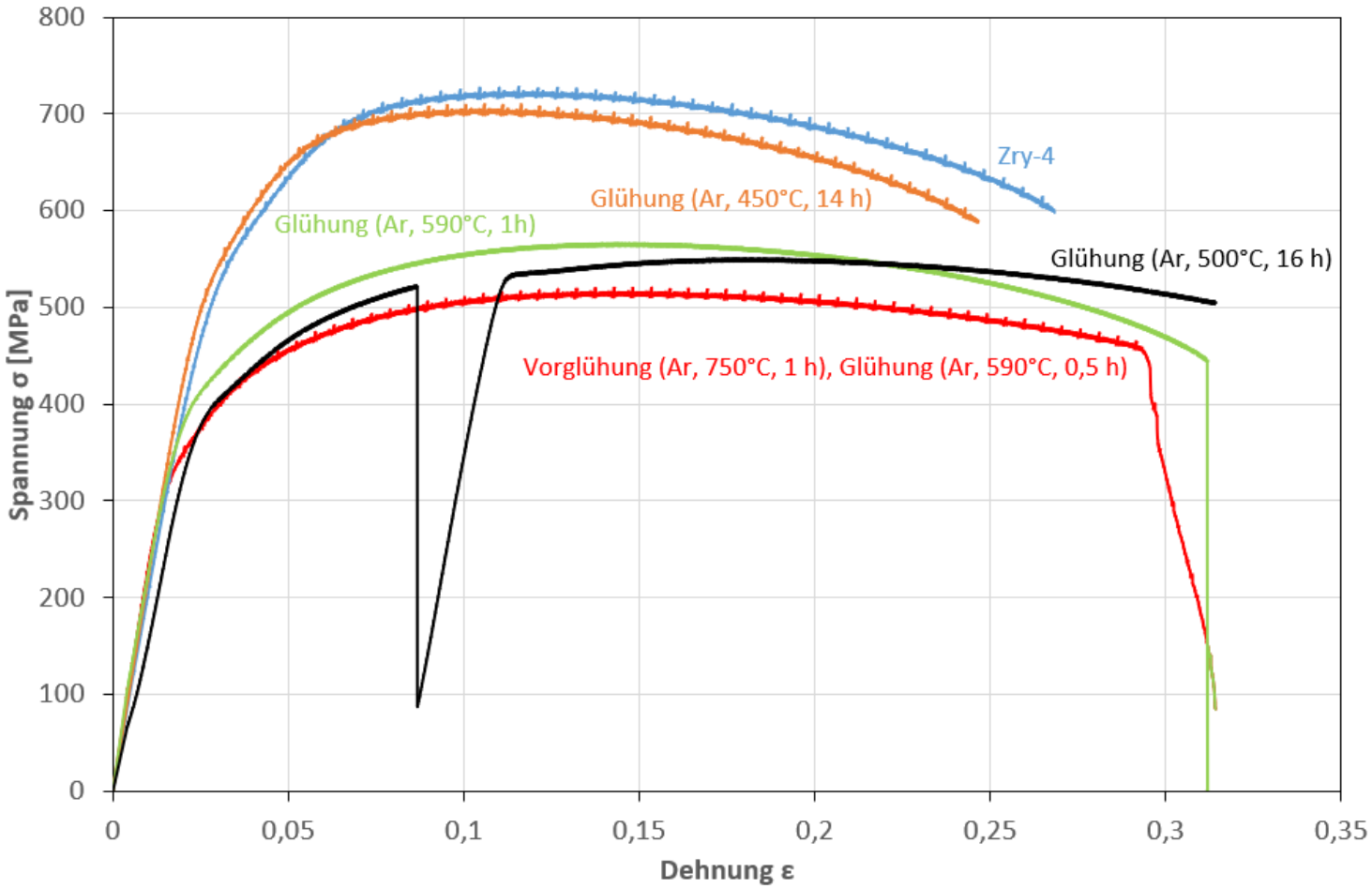

Maximal loading temperature: 450°C

- Stress/strain curves measured at tensile tests at RT to prepare the hydrogen loading of the tubes for the bundle test

Separate effect tests – Diffusion in Zr single crystals

- Zr single crystals, 6 mm diameter, 1 mm thickness with defined orientation ((0 0 0 1) and (1 0 -1 0) normal to the disc plane
- Measurements of the circumferential orientation by means of XRD
- Grinding to a more rectangular shape
- Oxidation in Ar/O_2
- Removing of the oxide layer at one side
- Annealing in H_2
- Neutron radiography measurements at IMAT (ISIS, RAL, UK)

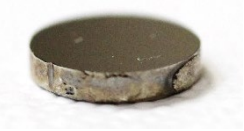

6 mm

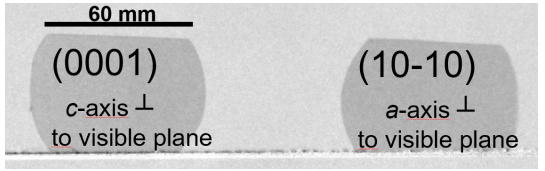

Separate effect tests – Diffusion in Zr single crystals

- Faster diffusion in the c direction (0 0 0 1) than in the a direction (1 0 -1 0)
- Uncertainties when the hydrogen uptake starts
- In-situ investigations are needed

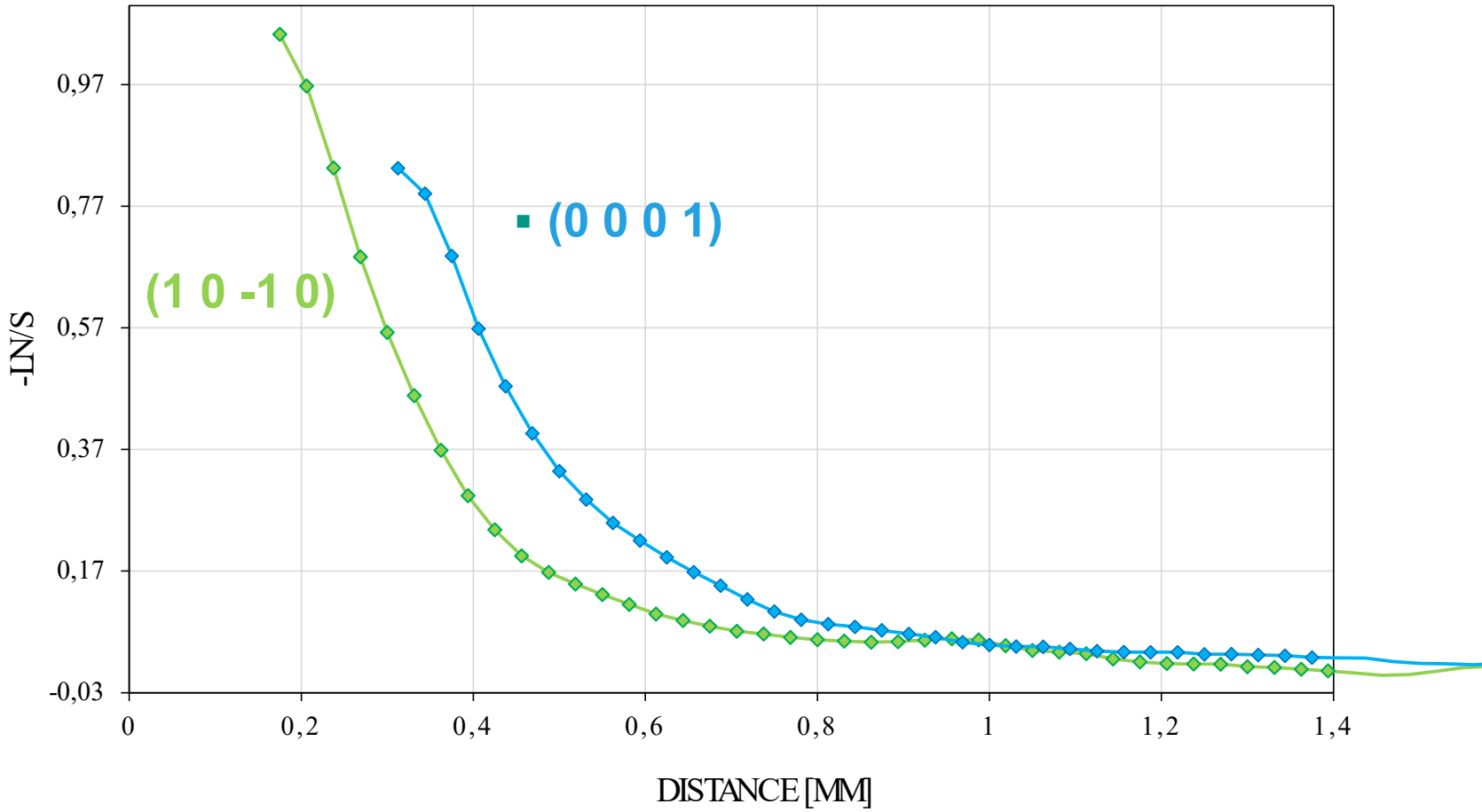

Seperate effect tests – Influence of elastic stress on the hydrogen solubility

In-situ investigations at ICON (SINQ, PSI) and IMAT (ISIS, RAL) using the ICHAMEL facilit

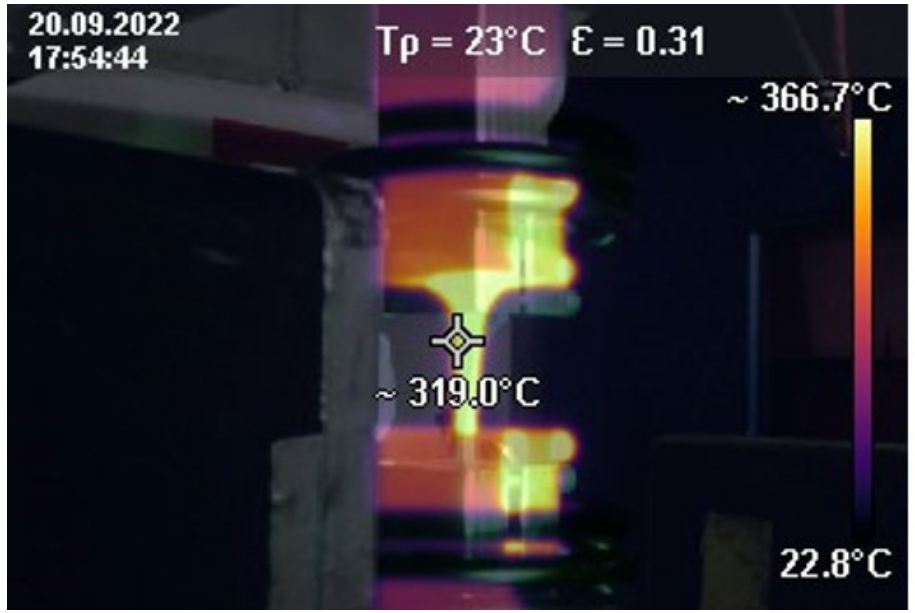

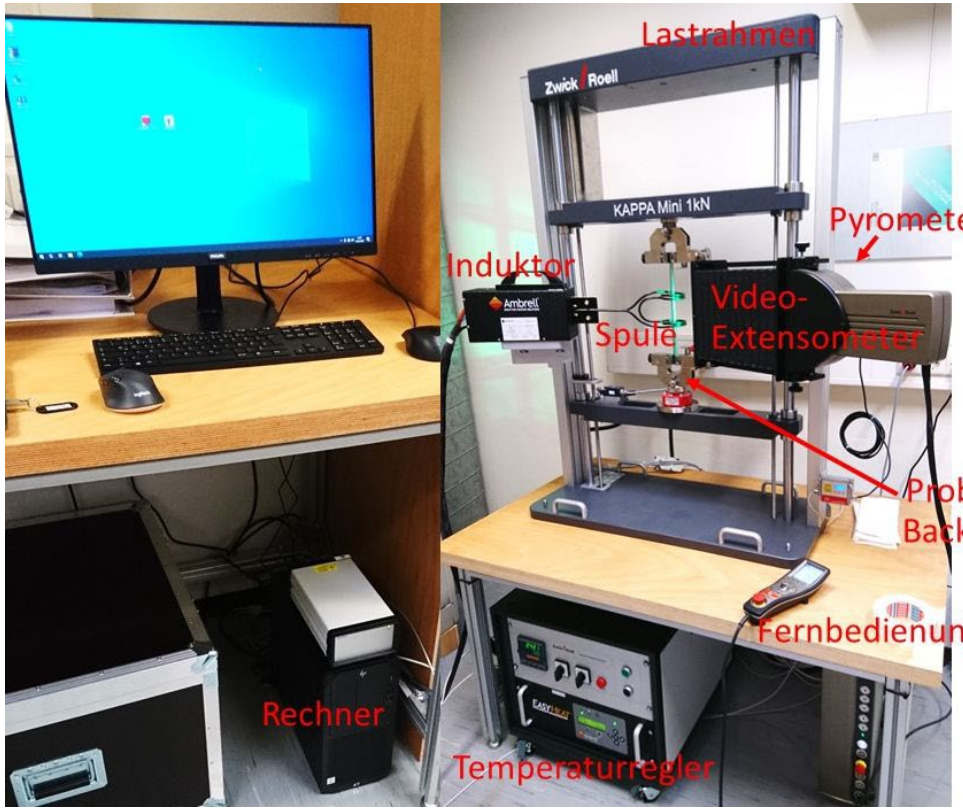

Separate effect tests – Influence of elastic stress on the hydrogen solubility

Strain distribution along the gauge

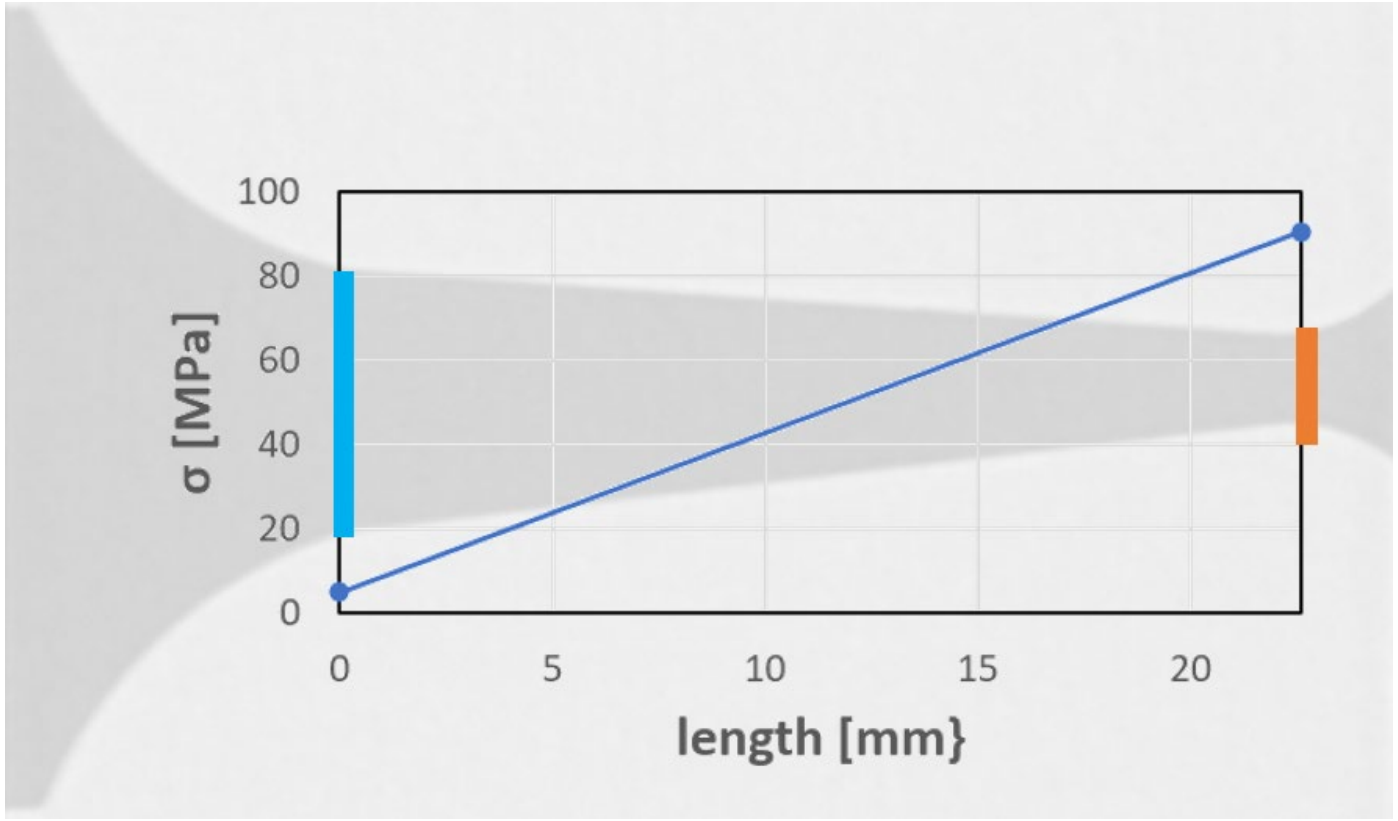

Seperate effect tests – Influence of elastic stress on the hydrogen solubility

- Commissioning experiments at ICON:
  - Problems with the pyrolytic temperature measurements
  - Outgassing by breaking the oxide layer
  - At 500°C strong creeping until fracture, hydrogen enrichments in the plastic deformed range
- Improvements in the temperature measurements and controlling were needed and performed

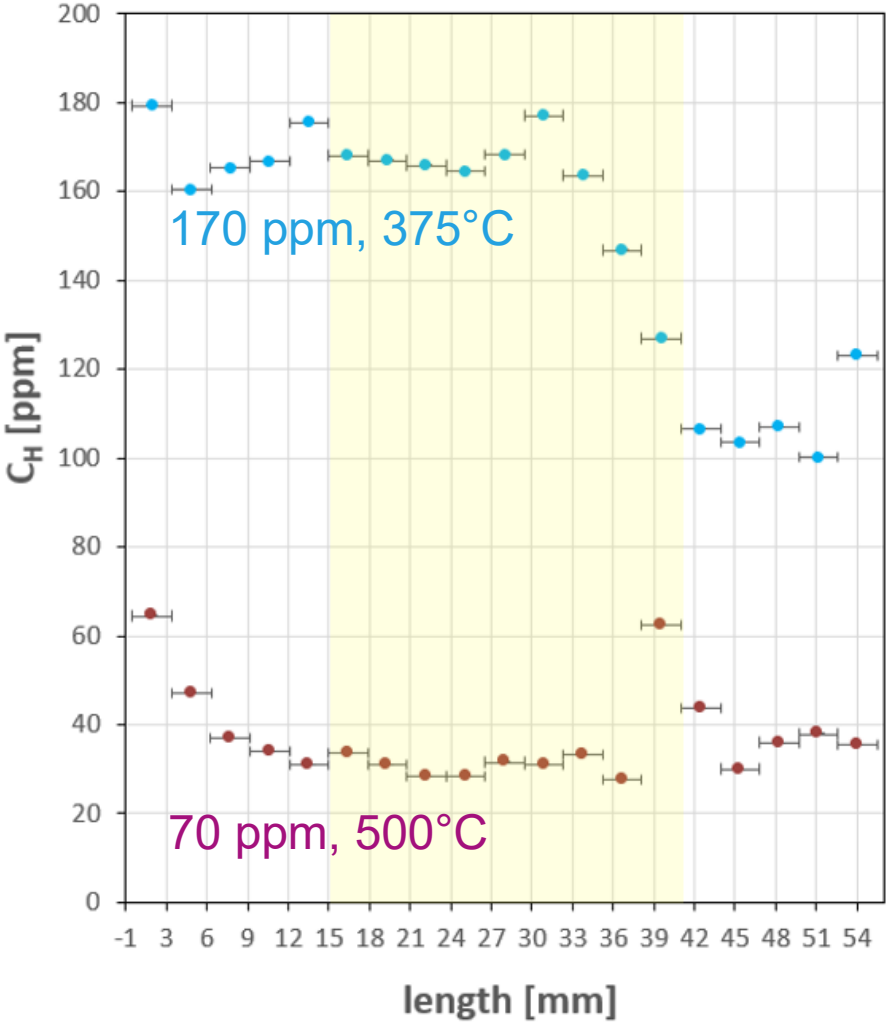

Separate effect tests – Influence of elastic stress on the hydrogen solubility

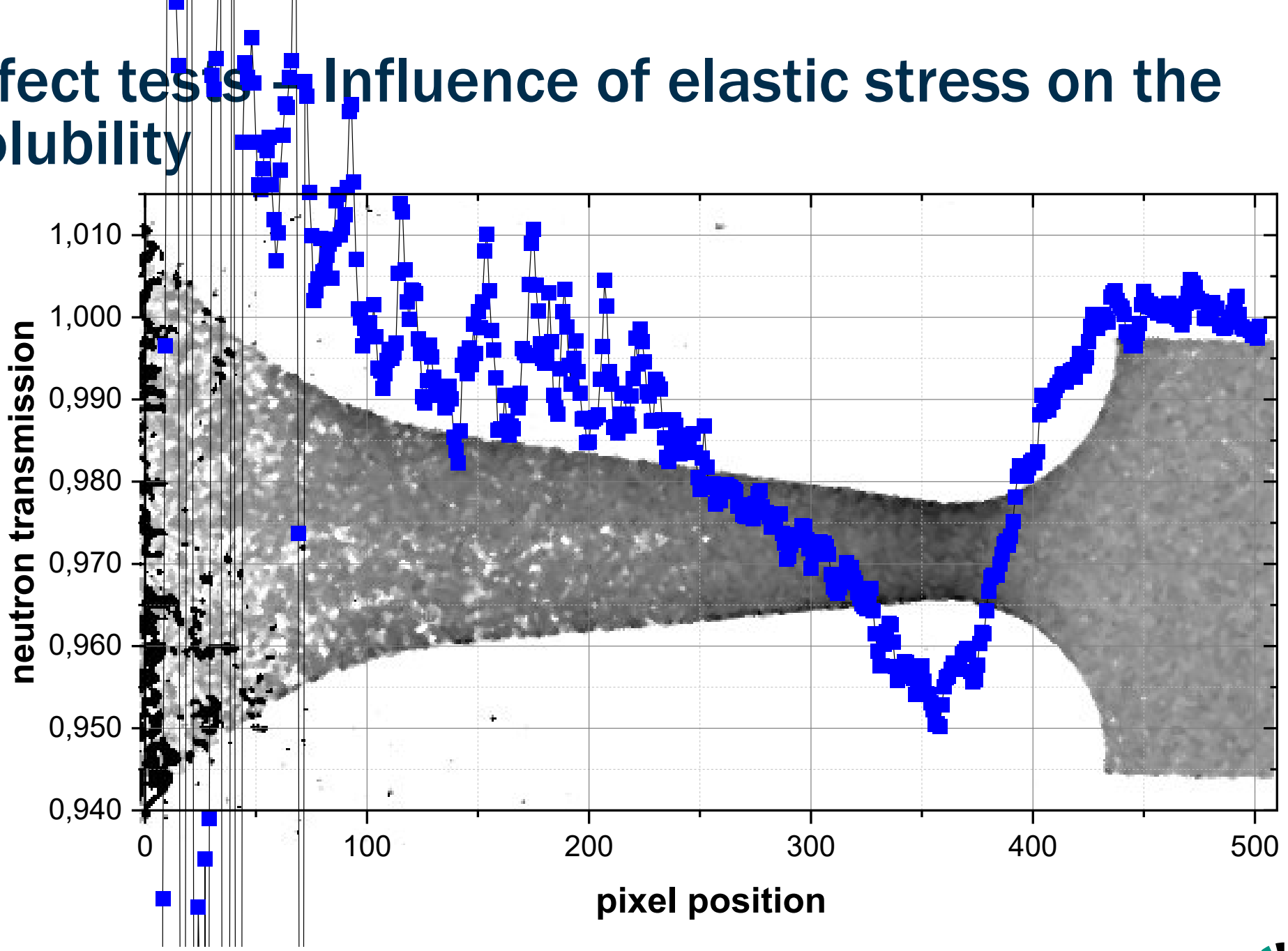

Bundle test

From May 2023 until January 2024 (250 days)

Maximal starting temperature: 405°C

Results are already published. They are used as reference in benchmark calculations

Potentials for improvements

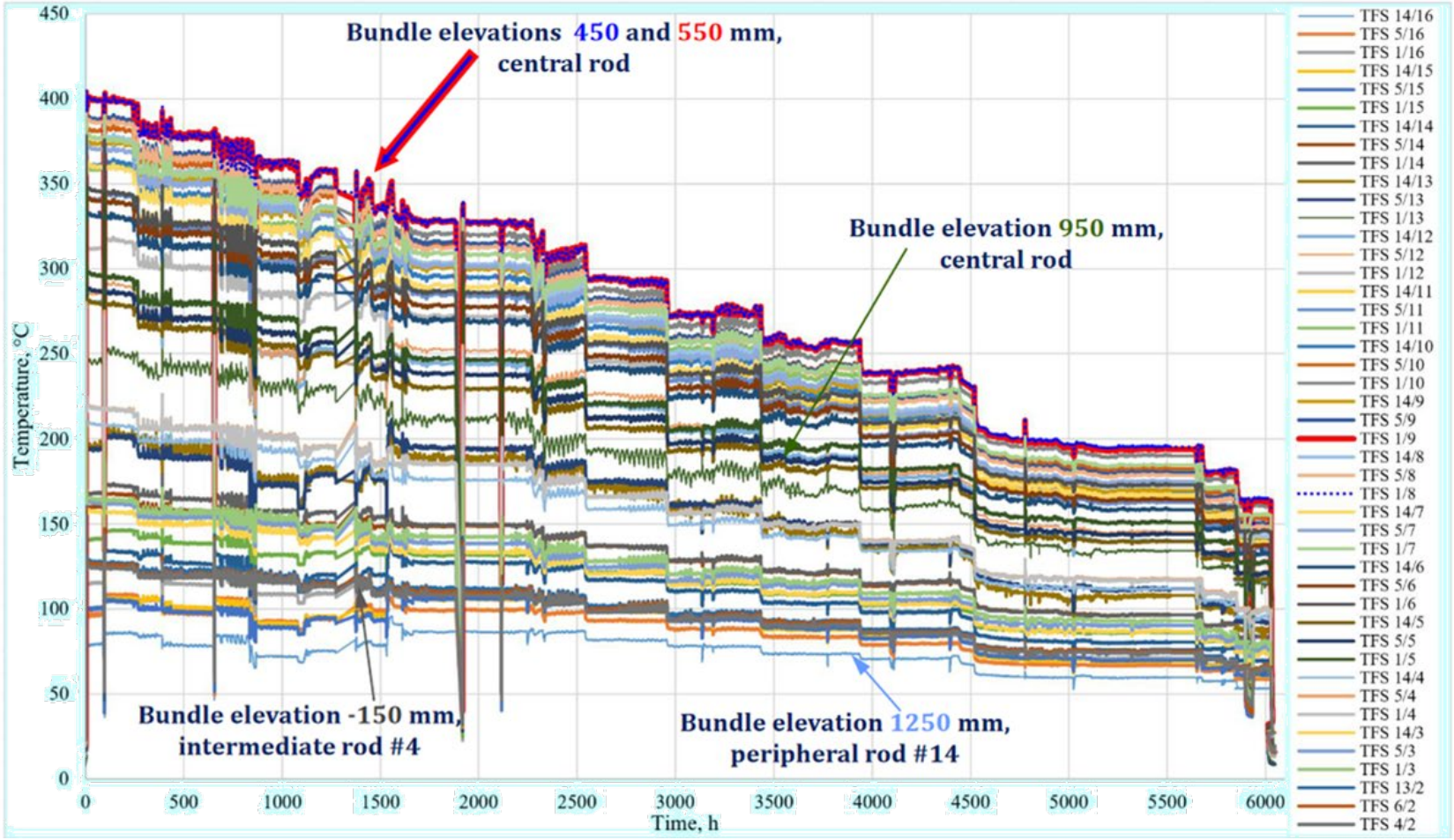

Bundle test

Main results:

Strong differences in the material behaviour between opt. ZIRLO, Zry-4 and Dx D4 (creep and hydride reorientation)

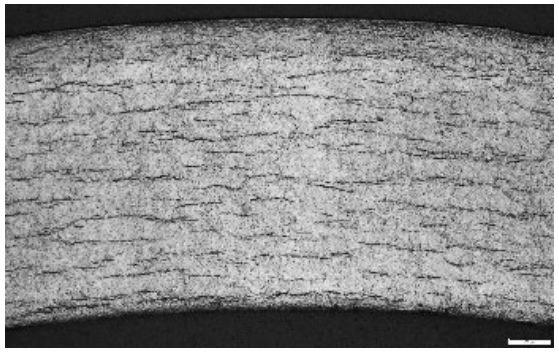

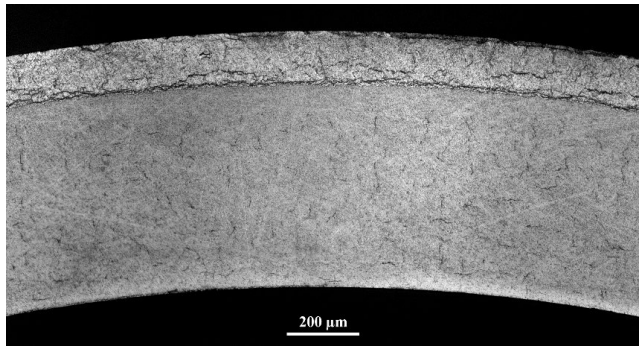

Opt. ZIRLO: strong creeping (4x stronger than Zry-4 and Dx D4) but nearly no hydride reorientation

Zry-4: radial and circumferential hydrides in the same order of magnitude

Dx D4: mostly radial hydrides

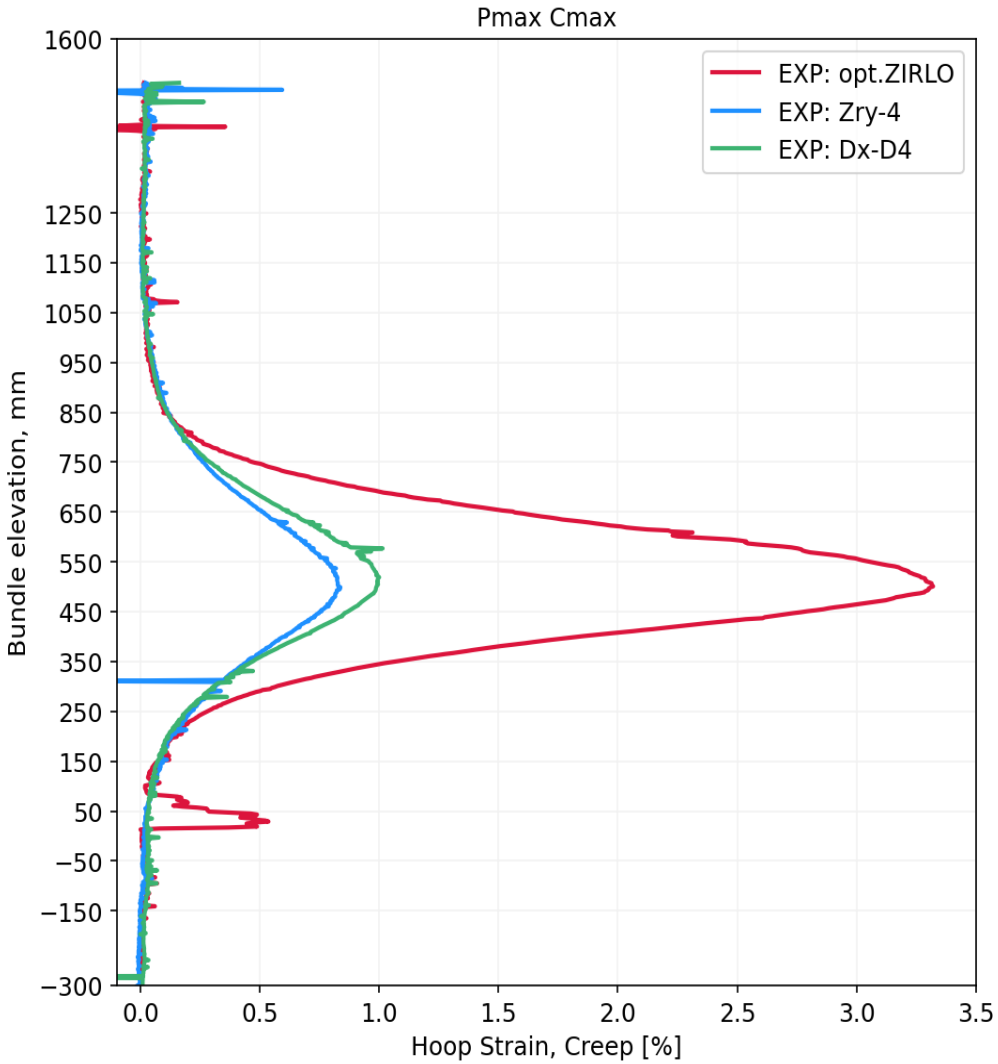

Benchmark calculations

- Good agreement between the modelling and the measured creep for Zry-4 and Dx D4
- Not satisfying agreement for opt. ZIRLO
- The codes use models derived from data mostly measured for Zry-4
- Material specific models has to be implemented into the codes

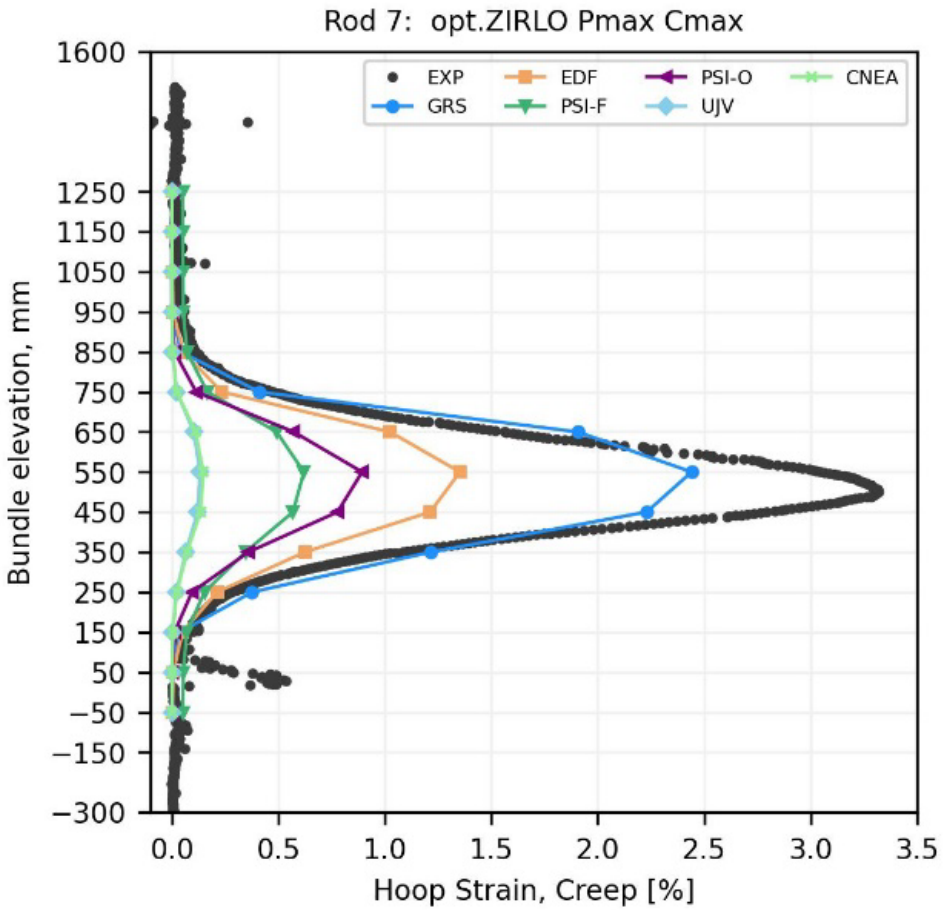

Outlook

- Proposal for SPIZWURZ+ is submitted. No final decision was made. A feasibility study required is in progress.
- Including other cladding material relevant for Germany (M5, Zry-2, E110) is proposed. Separate effect tests shall be focused on the different behaviour of the materials (creep and hydride reorientation).
- Continuing of the analysis of the SPIZWURZ test.
- Neutron microscopy shall be applied for the determination of the radial hydride fractions.

Acknowledgement

Thanks

- to all the KIT colleagues involved in the project: Juri Stuckert, Conrado Rössger, Jürgen Moch, Ursula Peters, Ulrike Stegmaier, Mikhail Kolesnik, …,
- to the colleagues from GRS and KIT-INE
- to colleagues from BGZ initiating the project

Thank you for your attention

The SPIZWURZ project - overview and single effect tests

Mirco Grosse, Sarah Weick, Michel Herm

30. Intern. QUENCH Workshop,
KIT Campus North, 2025/12/18

Juri Stuckert
KIT

Results of the SPIZWURZ bundle test

The 21-rod SPIZWURZ test bundle with three types of unirradiated claddings (opt. ZIRLO, Zry-4, DX-D4) was used to conduct a long-term integral experiment, approximately simulating dry storage conditions. A variety of parameters typical of an integrated test allowed for the acquisition of a large amount of experimental data necessary for verifying the corresponding computer codes. The claddings were preliminarily hydrogenated to concentrations of 100 and 300 wppm in a specially designed HOKI tubular furnace, distributed as uniformly as possible over a 1.3 m length. Hydrogenation was carried out at 450 °C by sequentially feeding fixed masses of hydrogen through a specially treated inner surface of the claddings. It was noted that the rate of hydrogenation of the opt. ZIRLO claddings is 1.5 times lower than for the Zry-4 claddings. After the hydrogen loading of the cladding tubes, the axial distribution of hydrogen was determined by laser scanning profilometry calibrated by hot gas extraction.

During the experiment, two values of internal rod pressure were used: 106 and 146 bar, which were maintained constant throughout the experiment (250 days). The peak cladding temperature decreased in steps of ≈15 K from 400 to 165 °C (average cooling rate ≈0.9 K/day). The maximal cooling rate during each temperature step was 6 K/h, step duration was about 10 h.

The post-test laser scanner measurements of the outer cladding diameter showed significant creep: radial deformation values are between 0.2 and 3.3% (diameter increase and the corresponding wall thinning). The largest creep of 3.3% was measured for opt. ZIRLO claddings hydrogenated to 300 wppm. The corresponding maximum creep value was 0.93% for Zry-4 and 1% for DX-D4. A clearly visible dependence of the degree of creep on the hydrogen concentration is observed for the opt. ZIRLO claddings: the creep of claddings hydrogenated to 300 wppm is 1.2-1.5 times higher than that of claddings hydrogenated to 100 wppm. A number of claddings show radially asymmetric wall thinning, which can be associated with the radial shift of the pellets from the central axis of the rod and the corresponding asymmetric heat supply along the circumference of the cladding.

The metallographic investigations revealed a uniform distribution of hydrides throughout the entire cladding circumference for all three cladding types used. In the DX-D4 claddings, hydrogen primarily diffused toward the outer liner. The degree of hydride reorientation was significantly higher in the Zry-4 claddings compared to the opt. ZIRLO claddings.

The difference in the behavior of the Zry-4 and opt. ZIRLO may be due, in part, to their different grain microstructures. Opt. ZIRLO claddings have a finer grain size than Zry-4. Moreover, although the temperatures during hydrogenation (450 °C) and the experiment itself (max. 400 °C) were relatively low, EBSD measurements showed grain growth from approx. 6 µm for the initial state to post-test 16 µm for Zry-4 (12 µm after hydrogenation), and from initial 3 µm to post-test 4.3 µm for opt. ZIRLO.

Karlsruhe Institute of Technology

Institute for Applied Materials

Results of the SPIZWURZ bundle test

J. Stuckert, M. Große, J. Moch, C. Rössger, U. Peters, T. Y. Lin, S. Weick

Institute for Applied Materials; Program NUSAFE

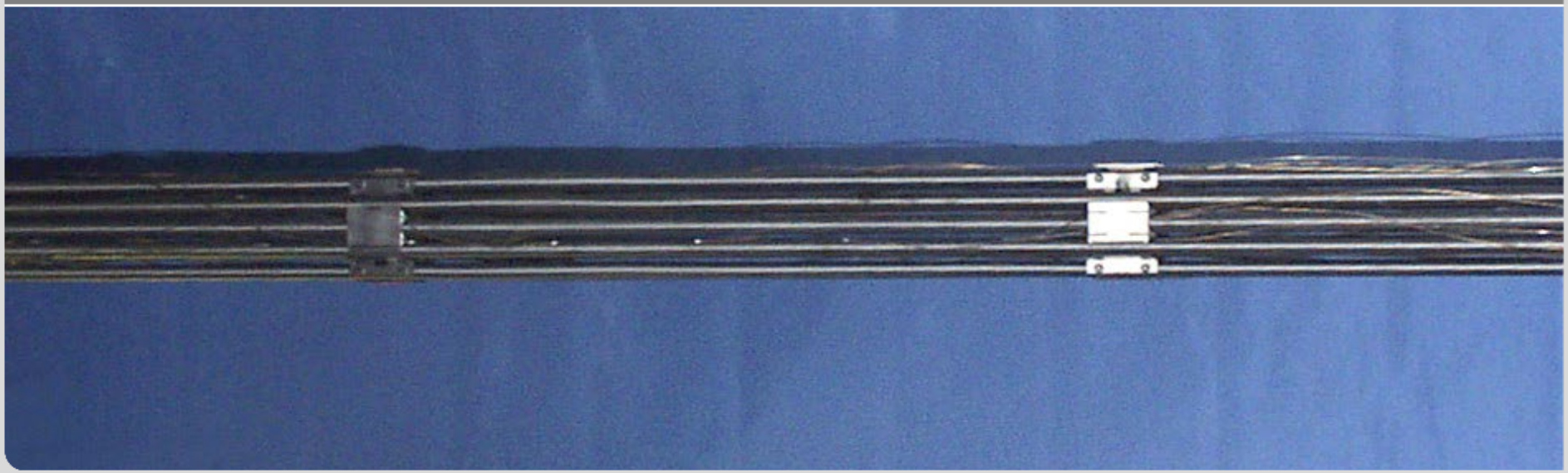

Goal of bundle test:

investigation of behavior of hydrides during the long-time dry storage of spent fuel with

- ***different cladding materials (Zry-4, opt. ZIRLO, DUPLEX)***
- ***different cladding inner pressures (140, 100 bar)***
- ***different hydrogen contents (100, 300 wppm)***
- ***different temperature histories (due to axial T profile in the bundle)***

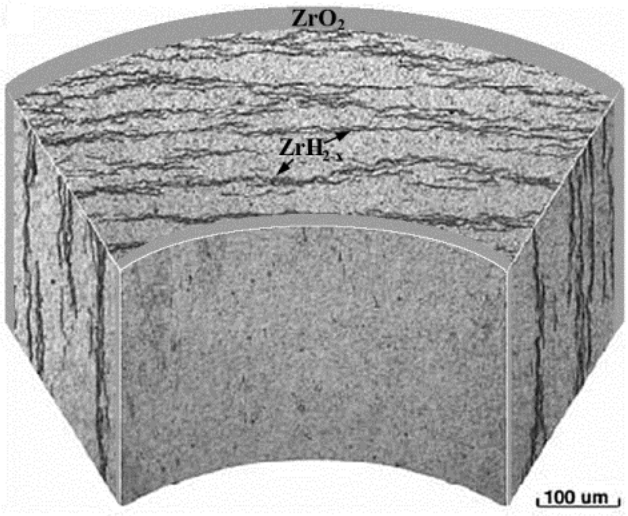

long time cool-down:
reorientation of hydrides

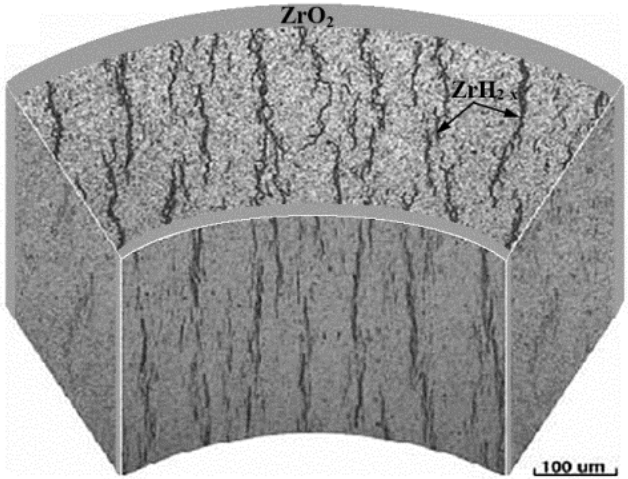

Hydrogenation of each cladding in extended pulse mode to prevent rapid formation of hydrides near to the inner cladding surface

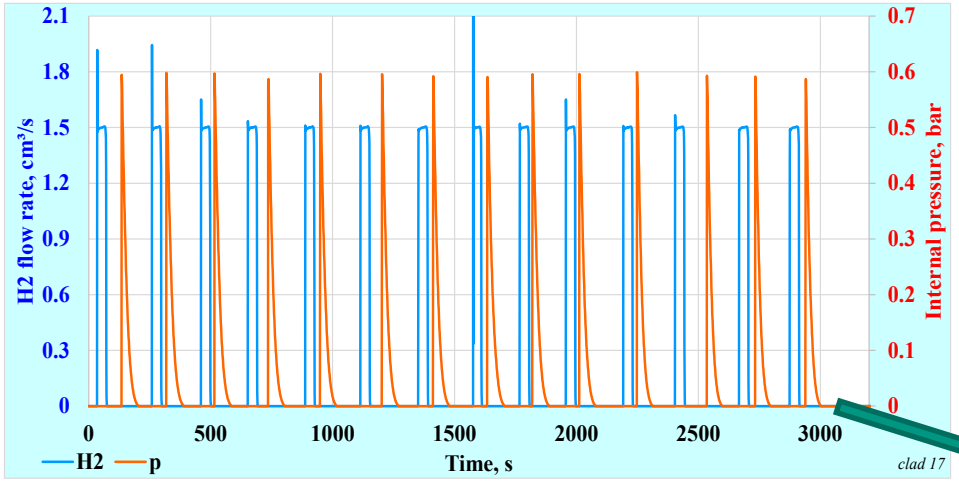

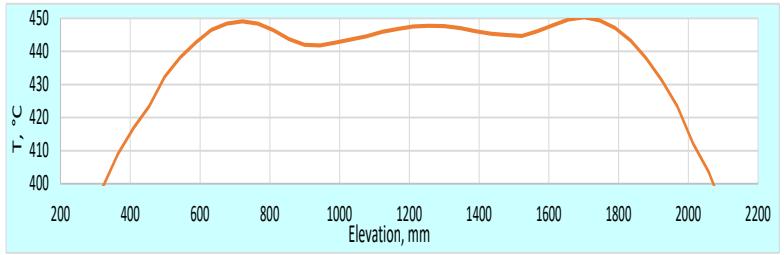

pulse filling of the internal cladding volume after special treatment of the inner cladding surface and evacuation of the cladding tube: repeated depressurization of inner cladding volume due to H_2 absorption

1) stepwise hydriding of cladding to 300 wppm H
***14 injections** with p_{max}=0.6 bar →*

$$\text{total } m_{H2} = 14 \times \left(\frac{\mu p_{max} V_{hot}}{RT_{hot}} + \frac{\mu p_{max} V_{cold}}{RT_{cold}}\right) = 0.05\ g$$

$M_{clad\ 125\ cm}$ = 170 g C_H = 0.05/170 ≈ ***300 wppm***

2) stepwise hydriding of cladding to 100 wppm H
***5 injections** with p_{max}=0.6 bar →*

$$\text{total } m_{H2} = 5 \times \left(\frac{\mu p_{max} V_{hot}}{RT_{hot}} + \frac{\mu p_{max} V_{cold}}{RT_{cold}}\right) = 0.0179\ g$$

$M_{clad\ 125\ cm}$ = 170 g C_H = 0.0179/170 ≈ ***100 wppm***

HOKI oven with axial temperature profile:
T ≈ 450 °C along the length of ≈ 1250 mm

*after pulse filling followed **homogenization** stage at 450 °C during 4 h and then almost linear cooldown to 50 °C during 12 h*

Hydrogenation duration (1 cycle) for different claddings materials

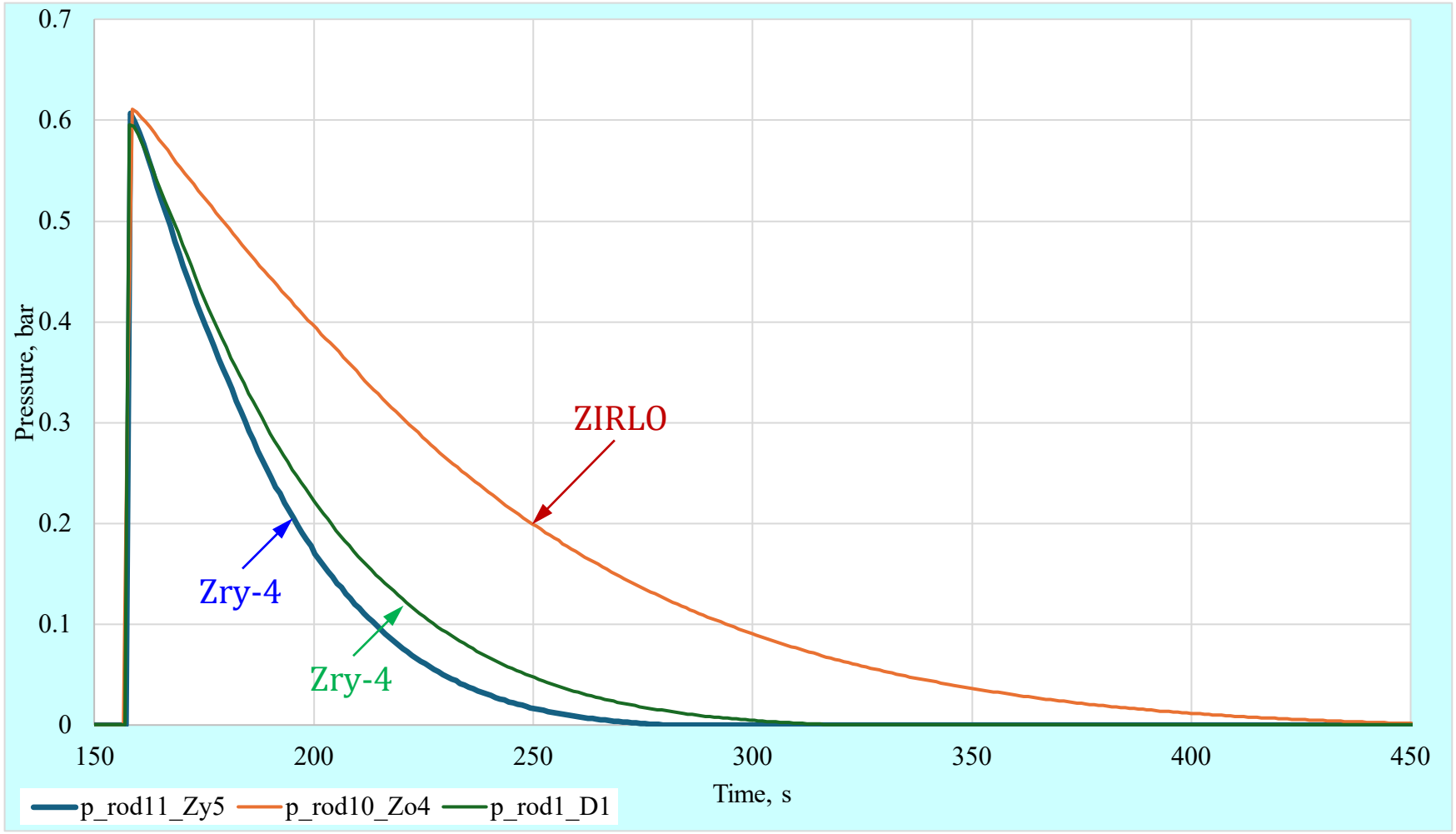

Slower charging of ZIRLO in comparison to Zry-4 (difference in diffusion coefficients?)

Determination of axial distribution of hydrogen concentration by increase of circumferential strain at each elevation

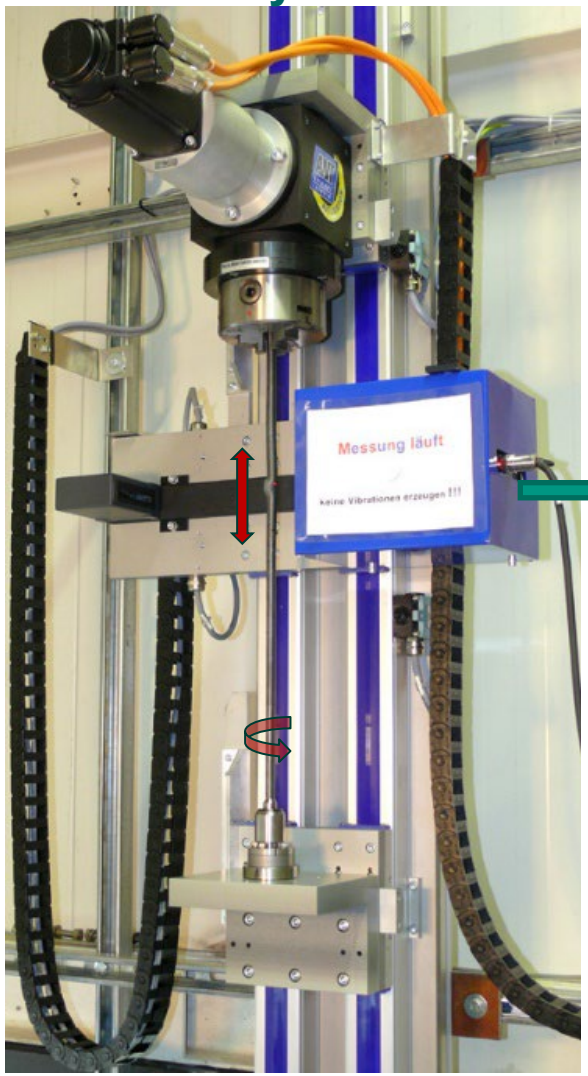

profilometry of clads with laser scanner
steps: 3° tangential, 2 mm axial
(thermal expansion ±0.3 µm for ±5 °C)

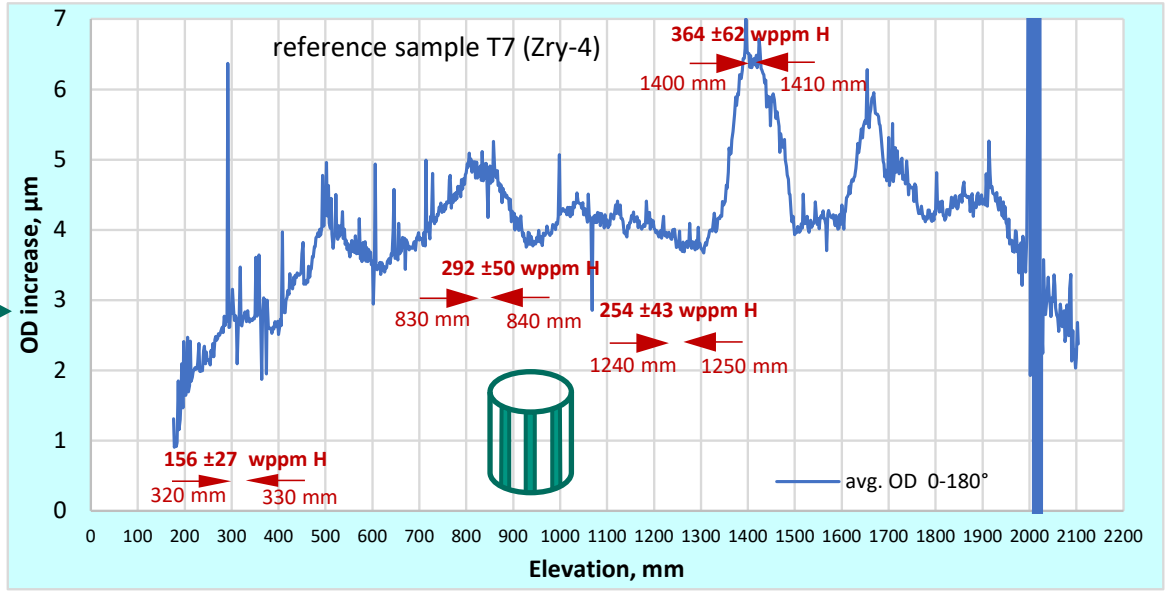

axial profile of cladding diameter increase (laser scanner)

and corresponded hydrogen concentrations
(hot extraction from 3 lamellas 10x1 mm)

Correlation between hydrogen content and increase of averaged cladding diameter

sample	ref. T4			ref. T5			ref. T6				ref. T7			
axial position, mm	750	1250	1650	750	1250	1650	405	755	1155	1455	325	835	1245	1405
OD increase, µm (laser scanner)	**7.6**	**4**	**5.5**	**8.2**	**5.5**	**4.5**	**1**	**2.5**	**2.7**	**1.5**	**2.7**	**4.8**	**3.8**	**6.5**
hot extraction, wppm	**318**	**301**	**329**	**421**	**353**	**296**	**66**	**132**	**135**	**115**	**156**	**292**	**254**	**364**
± wppm	48	45	49	105	88	74	17	33	34	29	27	50	43	62
SD				25	3	2	27	2	1	5	4	13	6	3

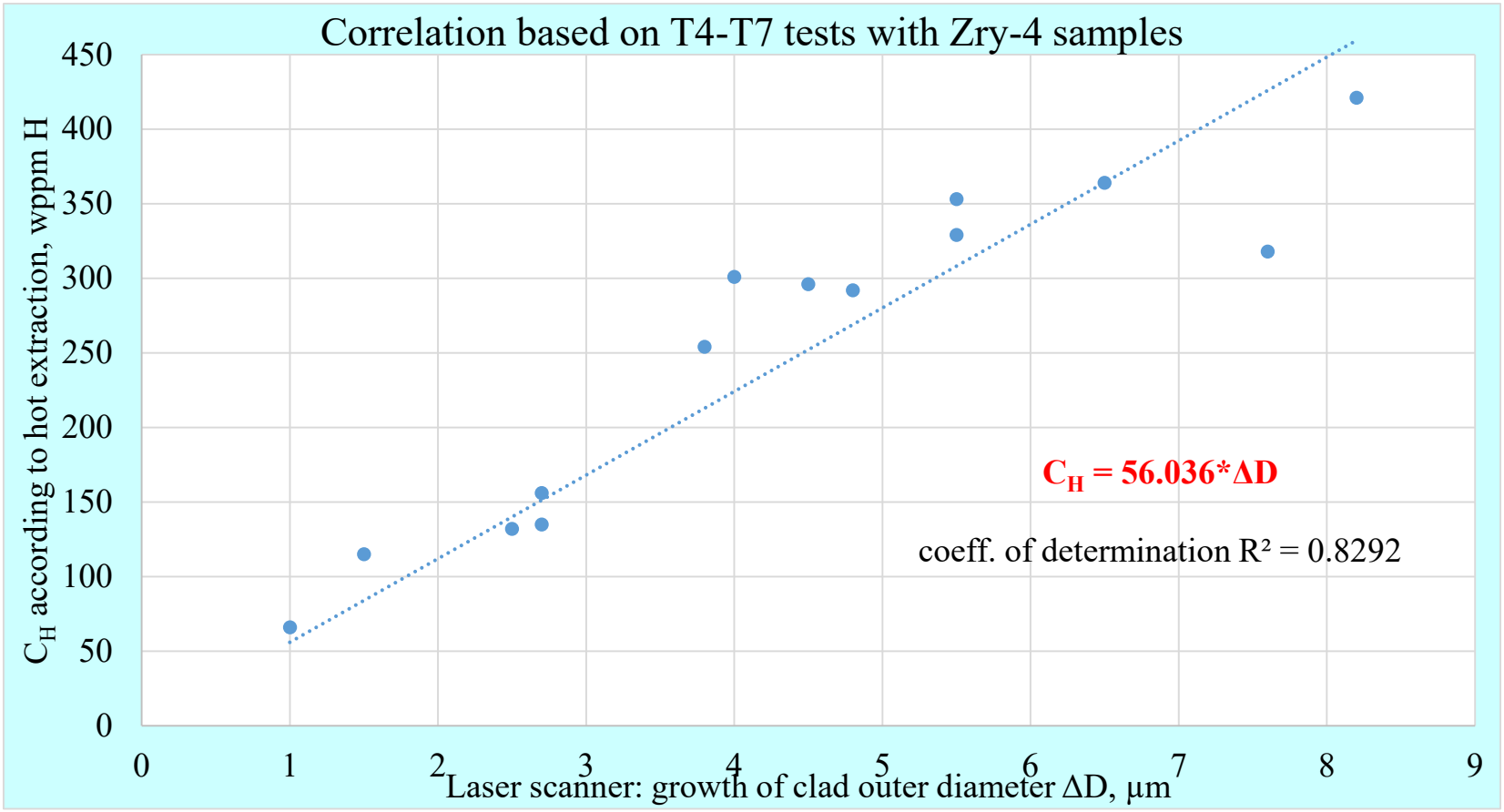

Axial hydrogen distribution for claddings: comparison of laser scanner data and post-test hot extraction

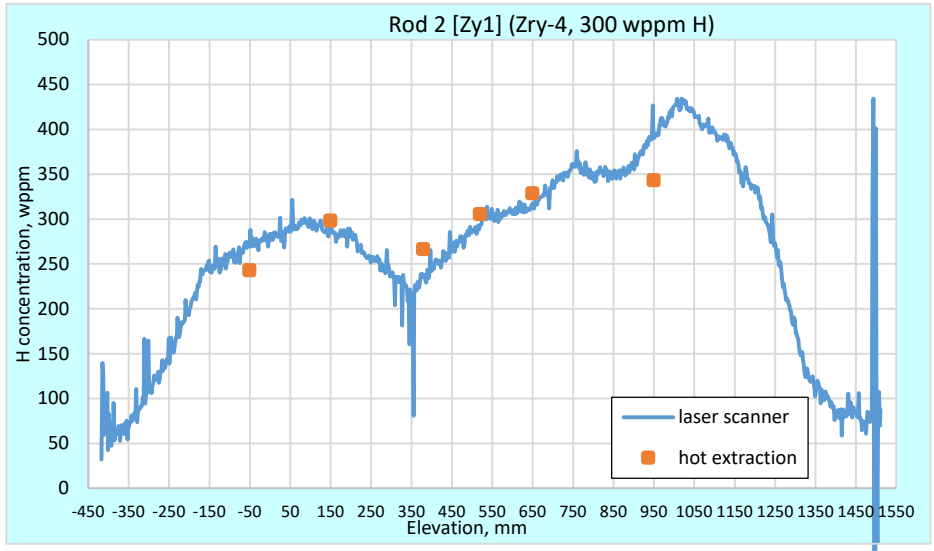

Zry-4, 300 wppm

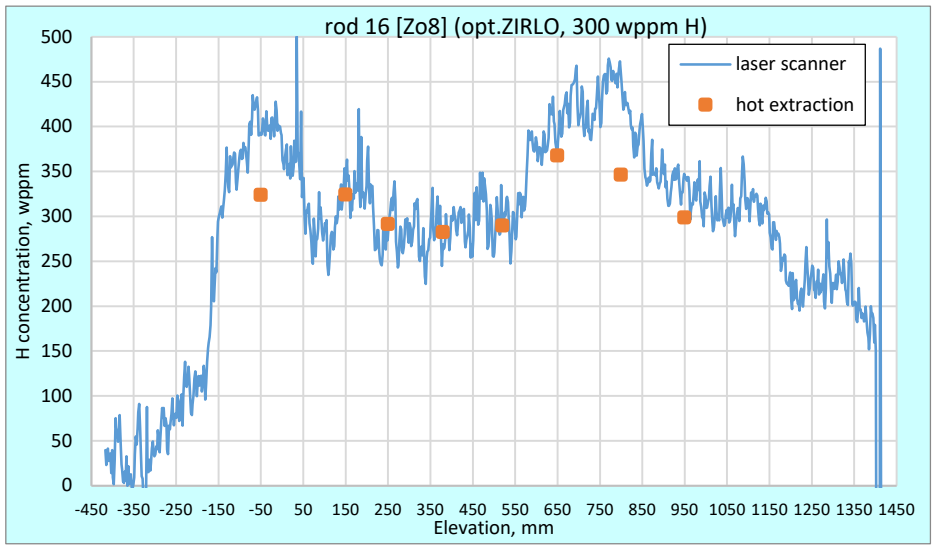

opt. ZIRLO, 300 wppm

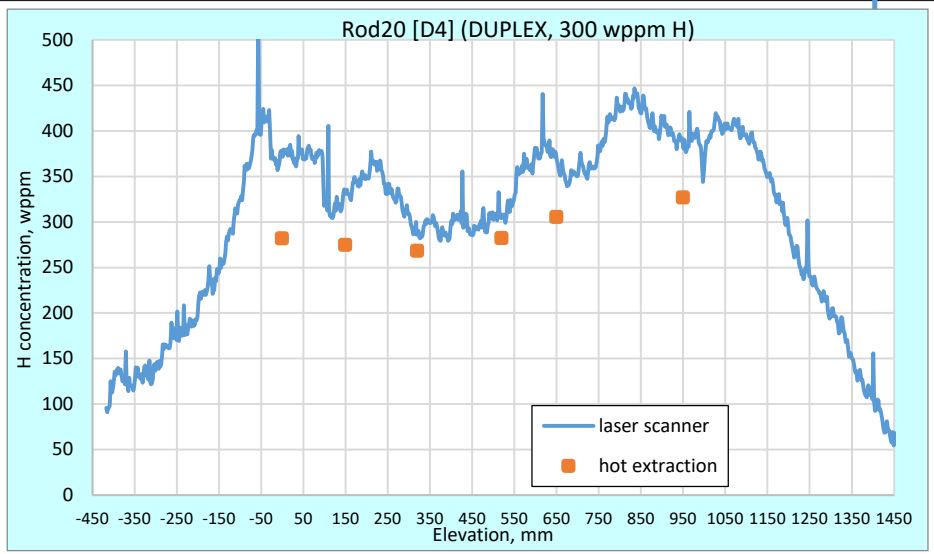

DX-D4, 300 wppm

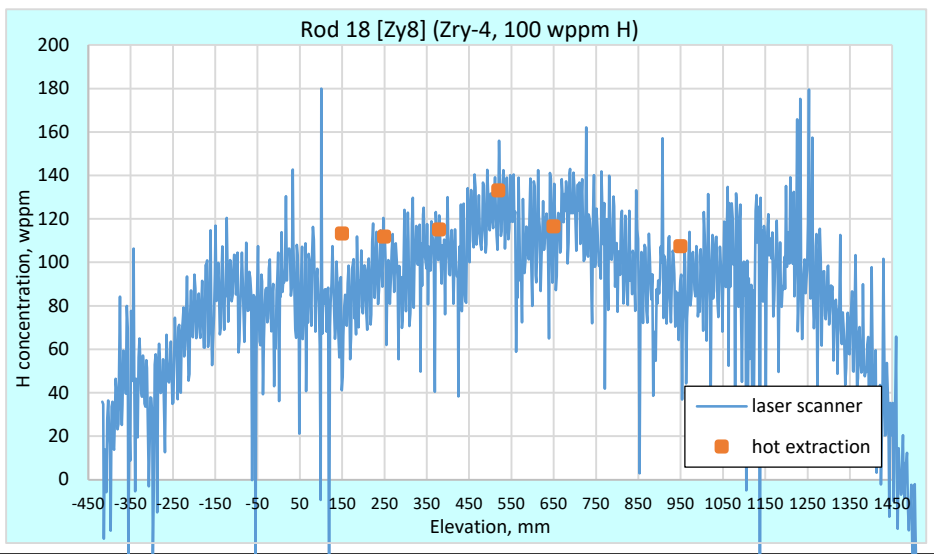

Zry-4, 100 wppm

Microstructure of as-received claddings: EBSD analysis

Euler Color 1	Euler Color 2
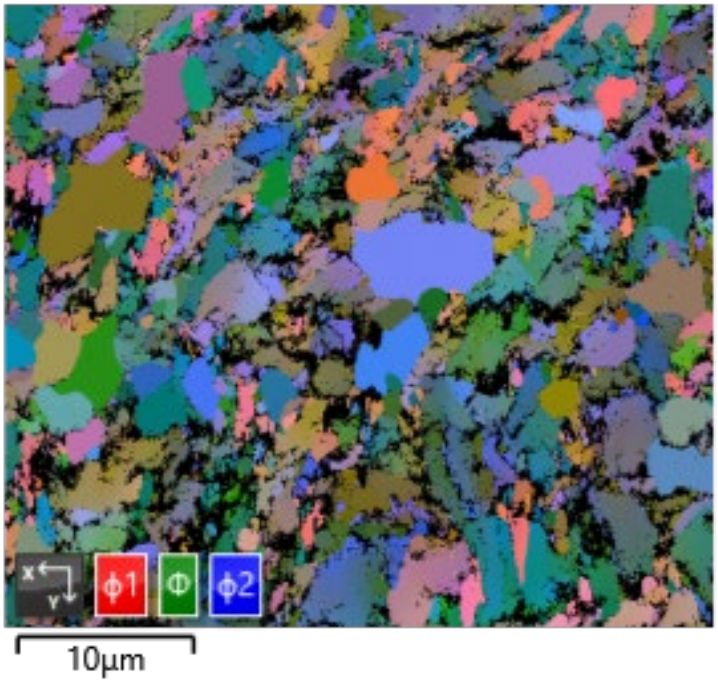	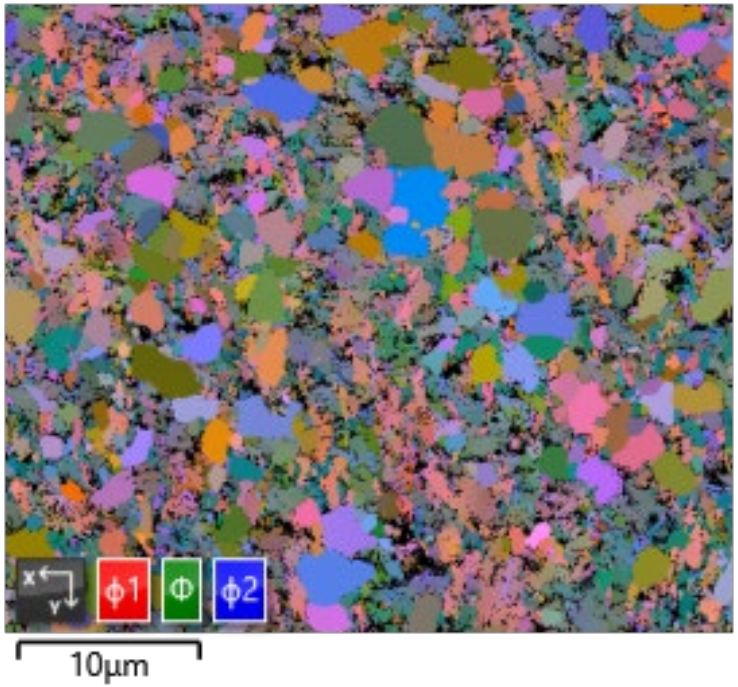
cold-worked and stress-relieved (CWSR) **Zry-4**: avg. grain area: weight mean **5.74 µm²** (biaxial grains $\overline{D} \approx 3.6$ µm, $\bar{d} \approx 2.0$ µm)	partially recrystallized (PRXA) **opt. ZIRLO**: avg. grain area: weight mean **2.92 µm²** ($\overline{D} \approx 2$ µm)

Microstructure of hydrogenated claddings: EBSD analysis

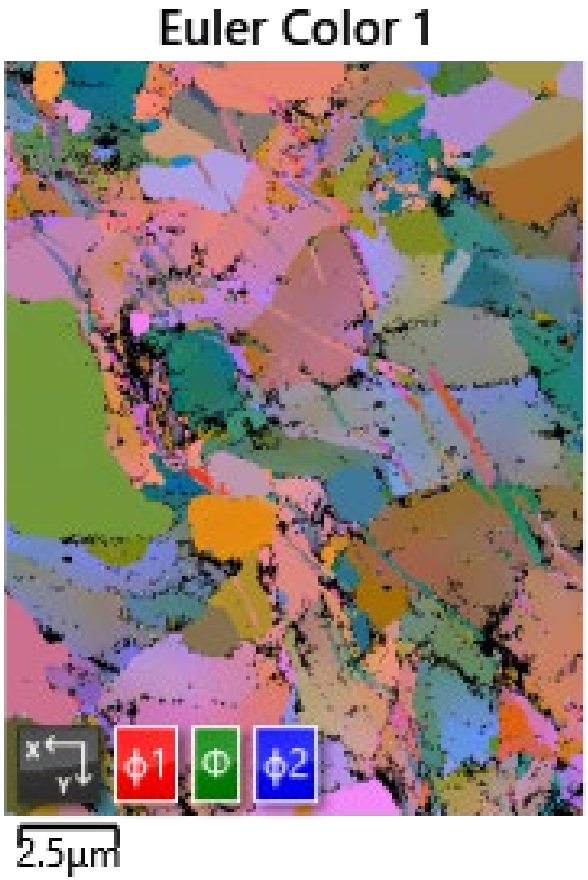

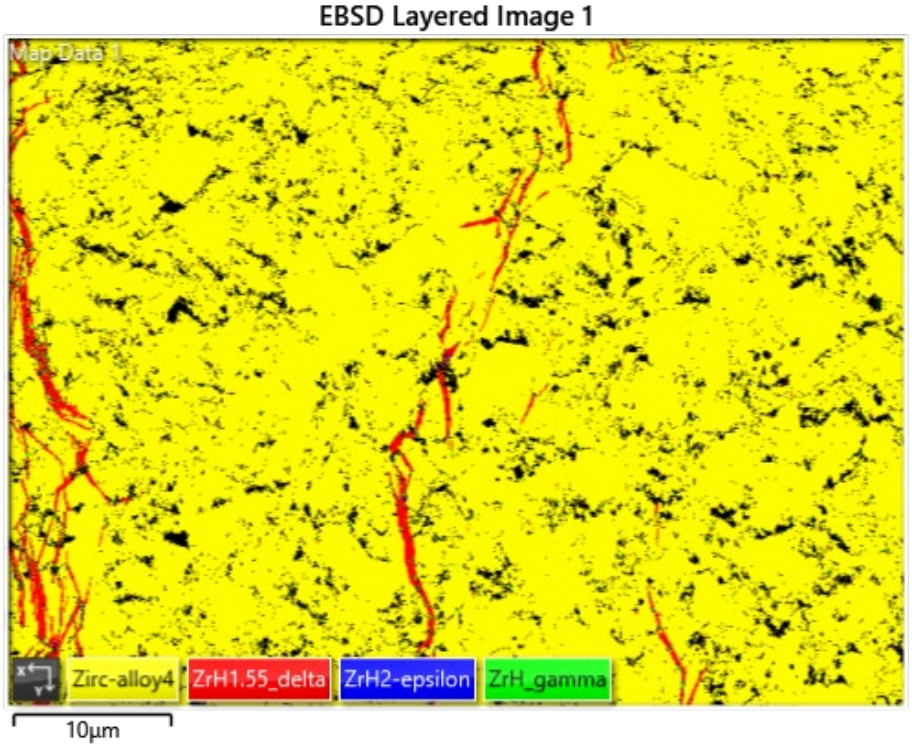

CWSR **Zry-4** hydrogenated at 450 °C (total heat treatment ≈ 1 day):
avg. grain area weight mean **12.79 µm²**
(biaxial grains $\bar{D}$ ≈ 4.9 µm, $\bar{d}$ ≈ 3.3 µm)

Zry-4:
inter- and intra-granular δ-hydrides with avg. length of ≈10 µm and width ≈0.3…0.6 µm; radial distance between hydrides ≈20 µm

doubling of the grain area in comparison to as-received cladding

SPIZWURZ bundle

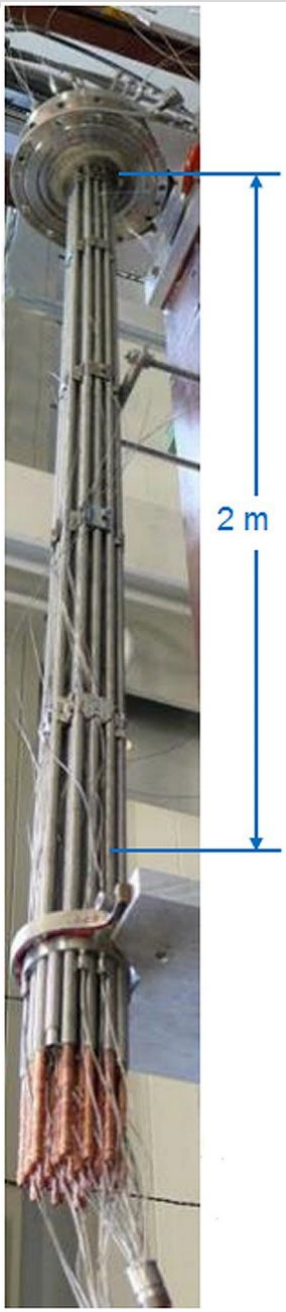

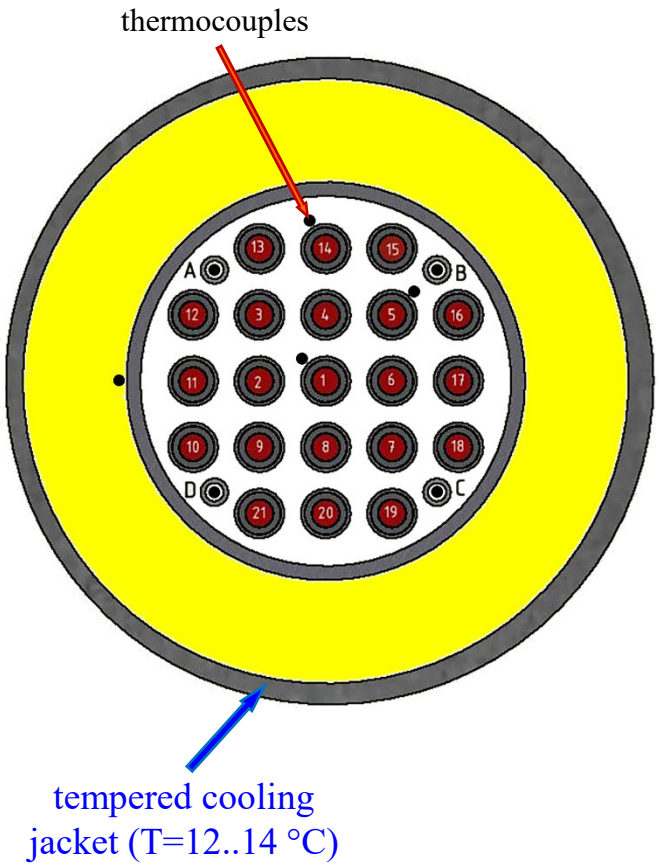

Bundle size		21 heated rods
Pitch		14.3 mm
Corner rod (4)	material	Zircaloy-4
	instrumented (A, B, C, D)	tube ∅ 6x0.5 (bottom: -1140 mm)
Grid spacer	material	Zircaloy-4
	length	42 mm
	sheet thickness	0.5 mm
	elevation of lower edge	Zry: -100, 150, 550, 1050, 1410 mm
Shroud	material	Zirconium 702 (flange: Zry-4)
	wall thickness	3.17 mm
	outside diameter	86.0 mm
	length (extension)	1600 mm (-300 mm to 1300 mm)
Shroud insulation	material	ZrO_2 fiber
	insulation thickness	~ 36 mm
	elevation	-300 to ~1000 mm
Cooling jacket	Material: inner/outer	Inconel 600 (2.4816) / SS (1.4571)
	inner tube	∅ 158.3 / 168.3 mm
	outer tube	∅ 181.7 / 193.7 mm
Thermocouples	at cladding surfaces	rods 1, 5, 9; totally 3x15=45
	inside corner rods	one at each elevation 2-16, totally 15
	at shroud outer surface	one at each elevation 3-15, totally 13

Heated rod

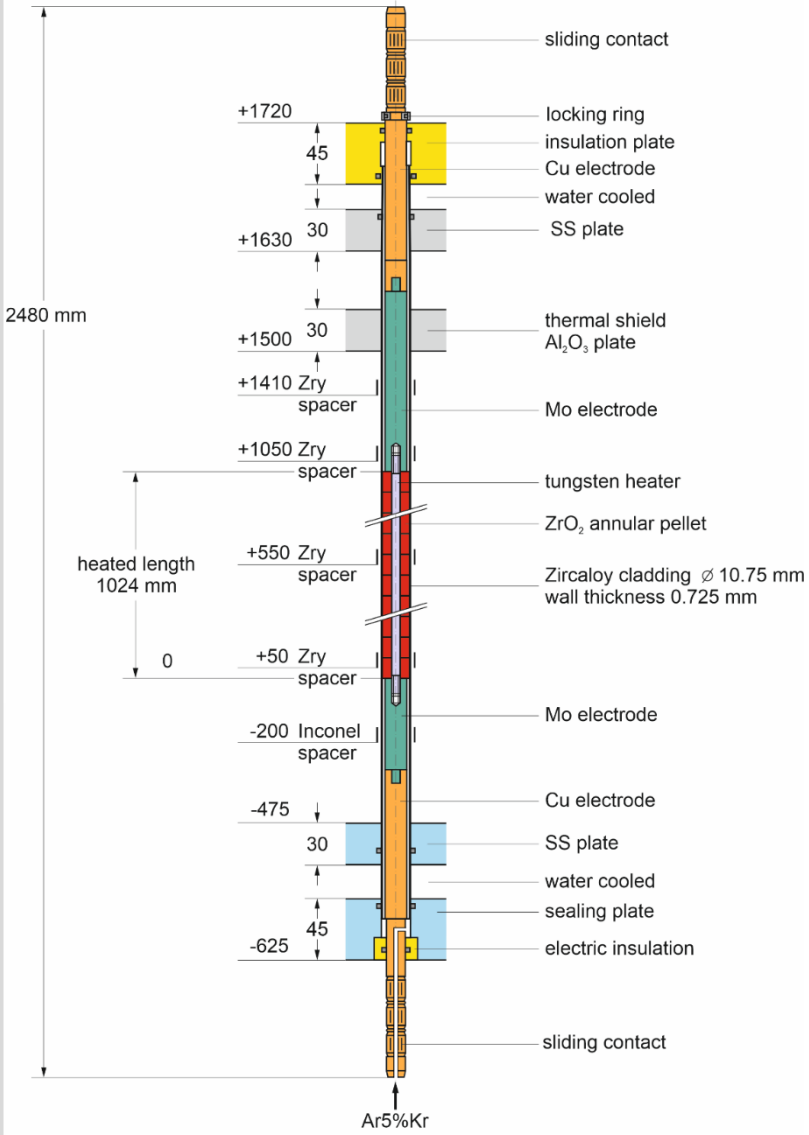

Cladding OD / ID		**10.75 / 9.3 mm**
Cladding thickness		**0.725 mm**
Cladding length	**(position in the bundle)**	**2278 mm (between -593 and 1685 mm)**
Rod length	(elevations)	2480 mm (-690 to 1790 mm)
Internal rod pressure; gas		5.5 MPa abs.; Kr
Material of middle heater		Tungsten (W)
	surface roughness	Ra=1.6 µm
Tungsten heater length		1024 mm (between 0 and 1024 mm)
Tungsten heater diameter		4.6 mm
Annular pellet	material	ZrO_2;Y_2O_3-stabilized
	dimensions	∅ 9.15/4.75 mm; L=11 mm
	surface roughness	Ra=0.3 µm
Pellet stack		0 mm to ~1020 mm
Molybdenum heaters and copper electrodes	length of upper part	766 mm (576 Mo, 190 mm Cu)
	length of lower part	690 mm (300 Mo, 390 mm Cu)
	outer diameter:	
	prior to coating	8.6 mm
	after coating with ZrO_2	9.0 mm
	coat. surface roughness	Ra=6-12 µm
	borehole of Cu-electrodes	diameter 2 mm, length 96 mm
Gas volume inside the rod	**heated**	**15 cm³**
Gas volume outside the rod	**not heated (room T)**	**20 cm³**

Bundle composition

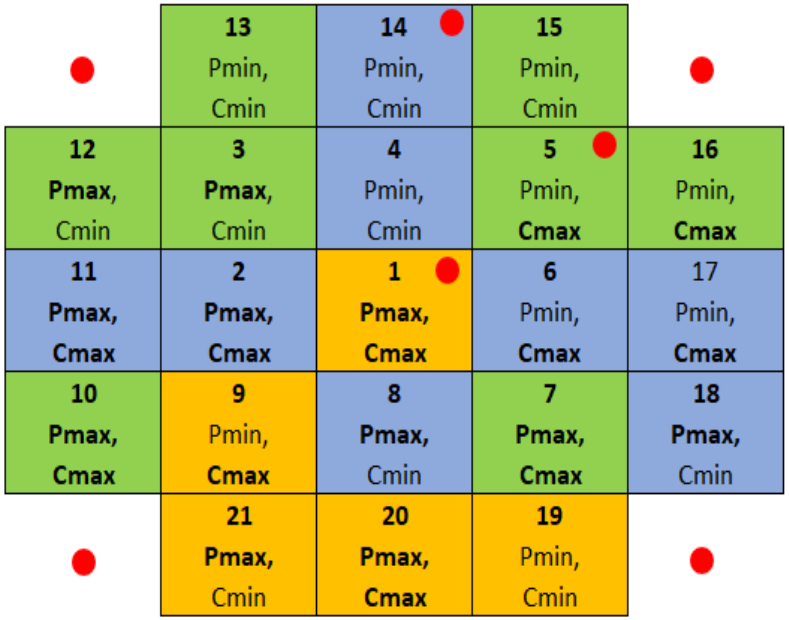

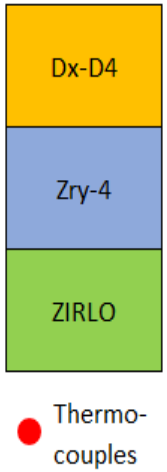

number	rod	alloy	H conc., wppm	mark
D1	1	DUPLEX	300	D1
Zry0212	2	Zry-4	300	Zy1
Zo049	3	ZIRLO	100	Zo1
Zy31	4	Zry-4	100	Zy2
Zo087	5	ZIRLO	300	Zo2
Zy85	6	Zry-4	300	Zy3
Zo156	7	ZIRLO	300	Zo3
Zry197	8	Zry-4	100	Zy4
D2	9	DUPLEX	300	D2
Zo165	10	ZIRLO	300	Zo4
Zry199	11	Zry-4	300	Zy5
Zo220	12	ZIRLO	100	Zo5
Zo221	13	ZIRLO	100	Zo6
Zy914	14	Zry-4	100	Zy6
Zo332	15	ZIRLO	100	Zo7
Zo351	16	ZIRLO	300	Zo8
Zry1021	17	Zry-4	300	Zy7
	18	Zry-4	100	Zy8
D3	19	DUPLEX	100	D3
D4	20	DUPLEX	300	D4
D5	21	DUPLEX	100	D5

hydrogen content in cladding
Cmax = 300 wppm H
Cmin = 100 wppm H

pressure inside the rod
Pmax = 146 bar
Pmin = 106 bar

Pressures inside the rods between 12.05.2023 and 18.01.2024

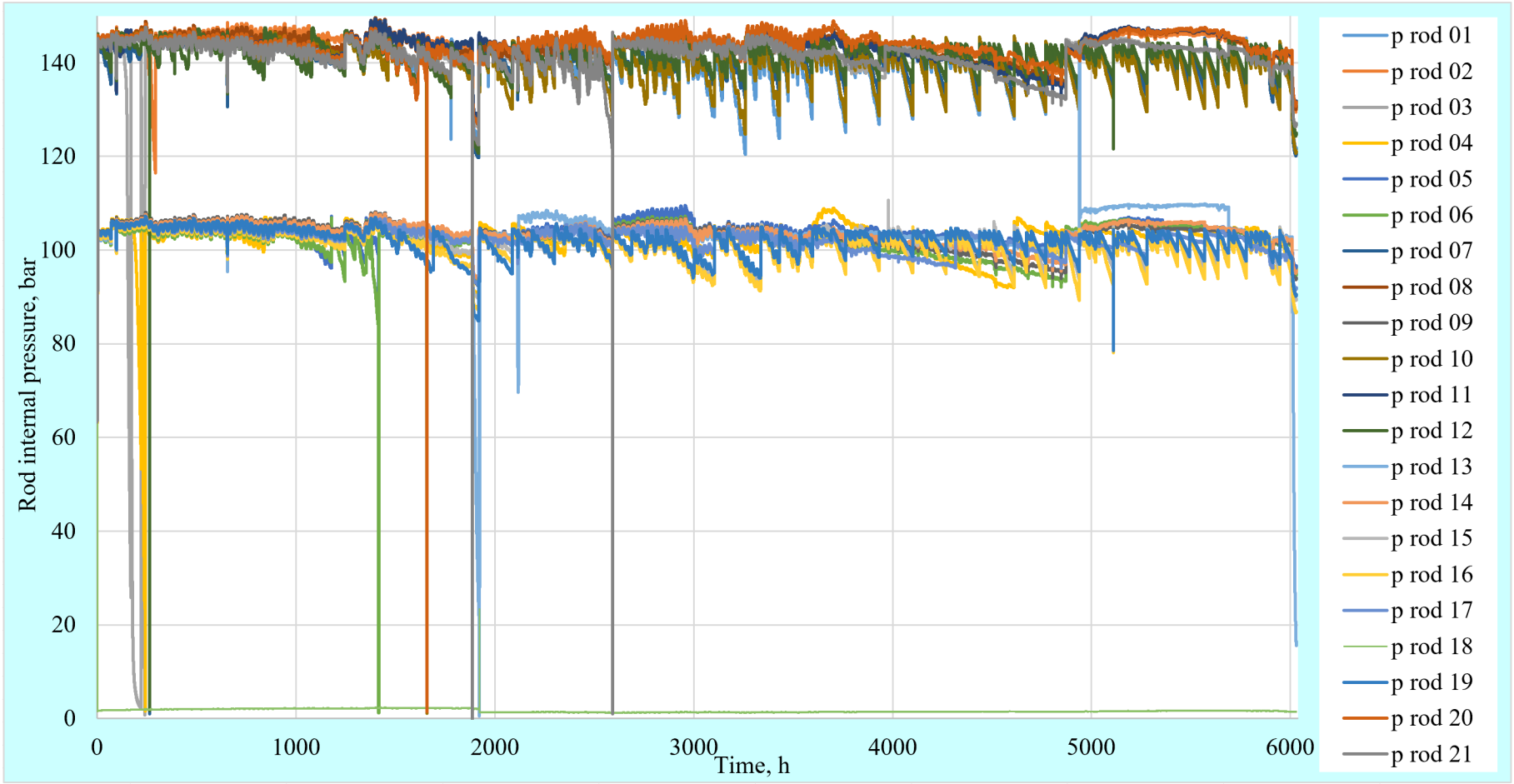

- two pressurization levels of **106 and 146 bar**
- daily refill of 7 rods with Ar+O_2 due to small leakages
- short depressurizations of 6 rods due to change of sealing rings

Reading of cladding surface thermocouples (TFS) between 12.05.23 and 18.01.24

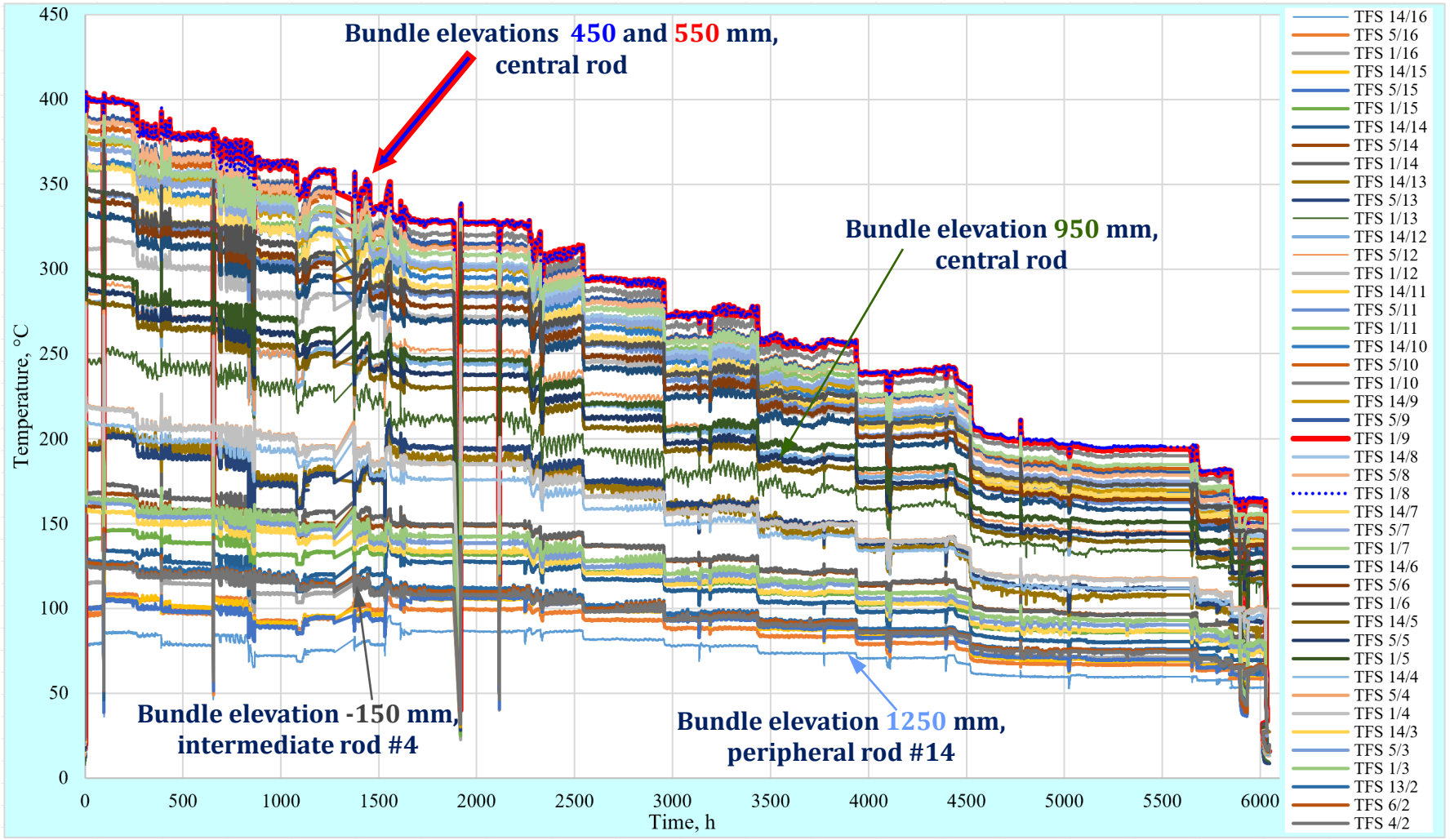

- peak cladding temperature decreased in steps with 15 K decrement and average duration of 400 h, average cooling rate 0.9 K/day
- periodic daily temperature fluctuations ≈±1.5 K for each thermocouple
- 4 el. power breakdowns

Smooth temperature decrease on the time of the power step reduction

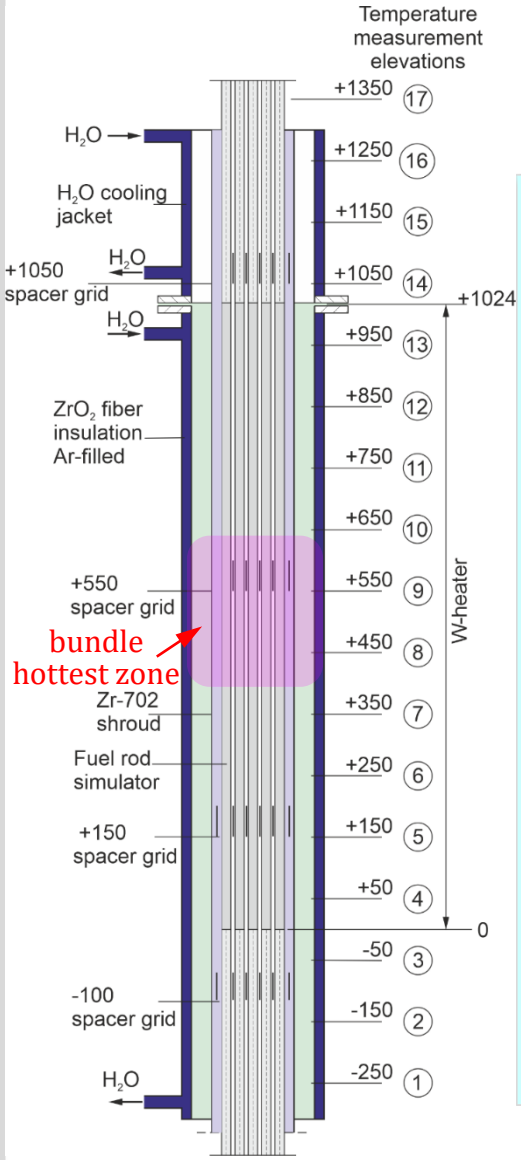

cooling rate decreased from 6 K/h ($1.7*10^{-3}$ K/s) to 0 K/s during 10 h

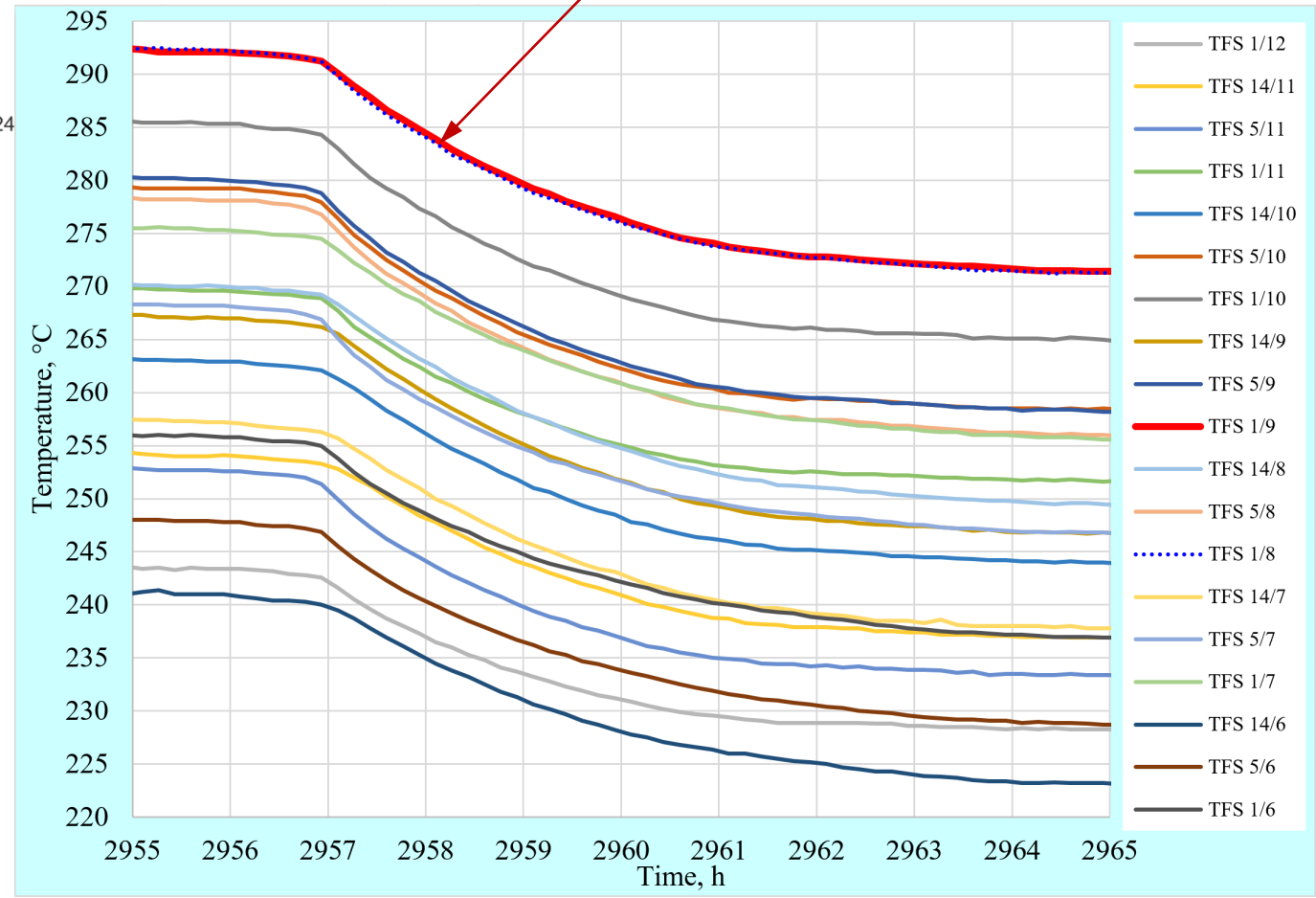

Axial temperature distribution for three rod groups

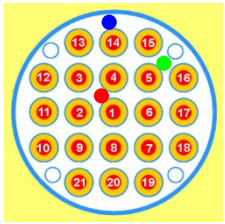

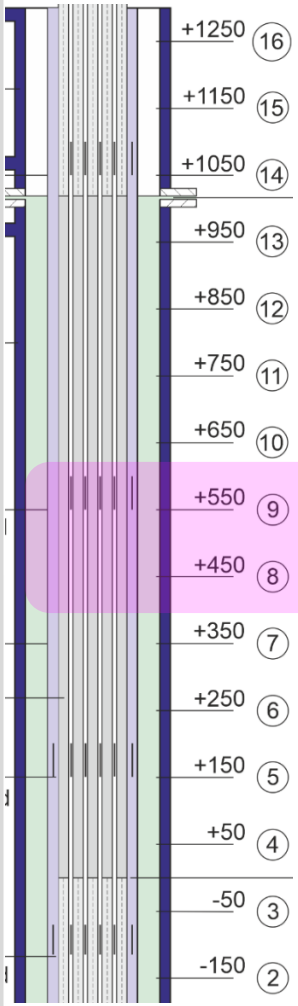

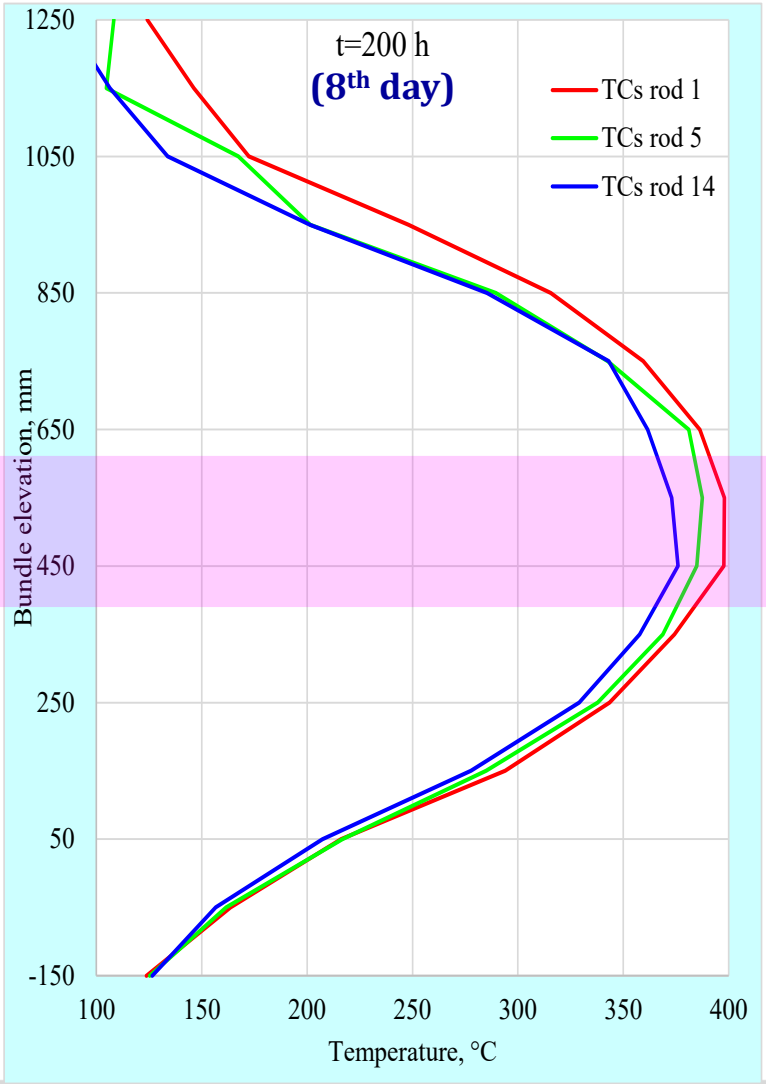

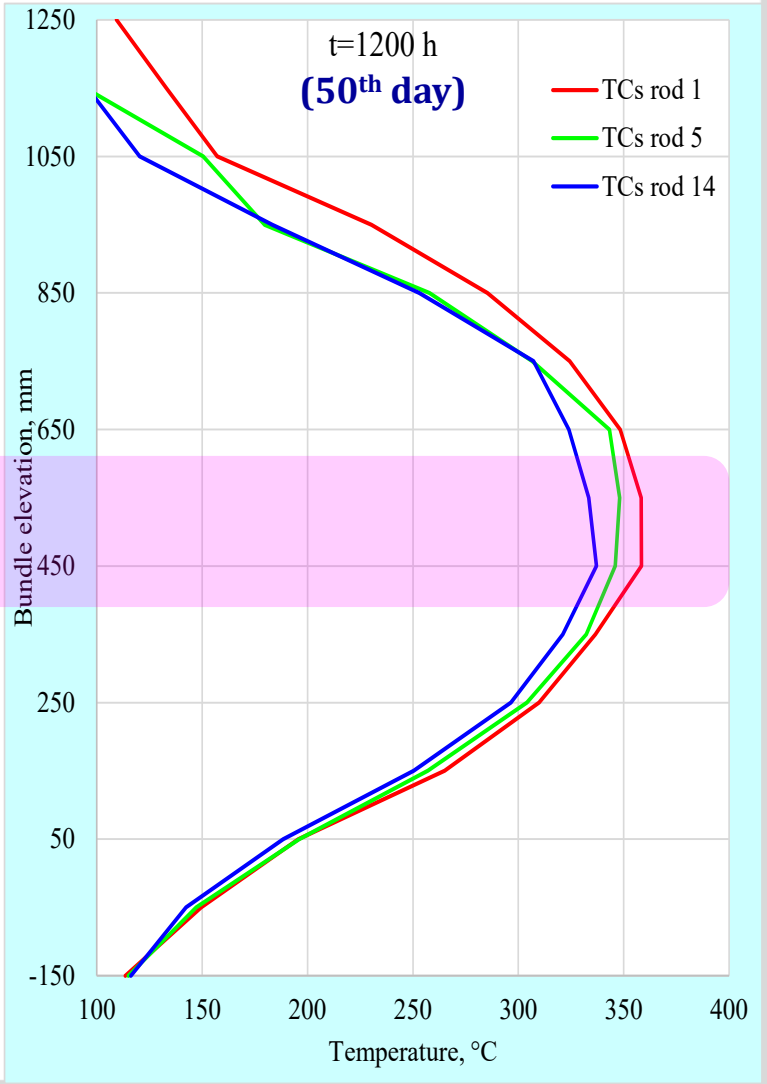

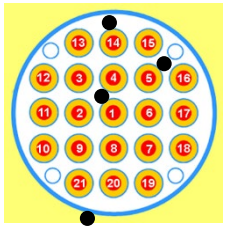

Radial temperature distribution

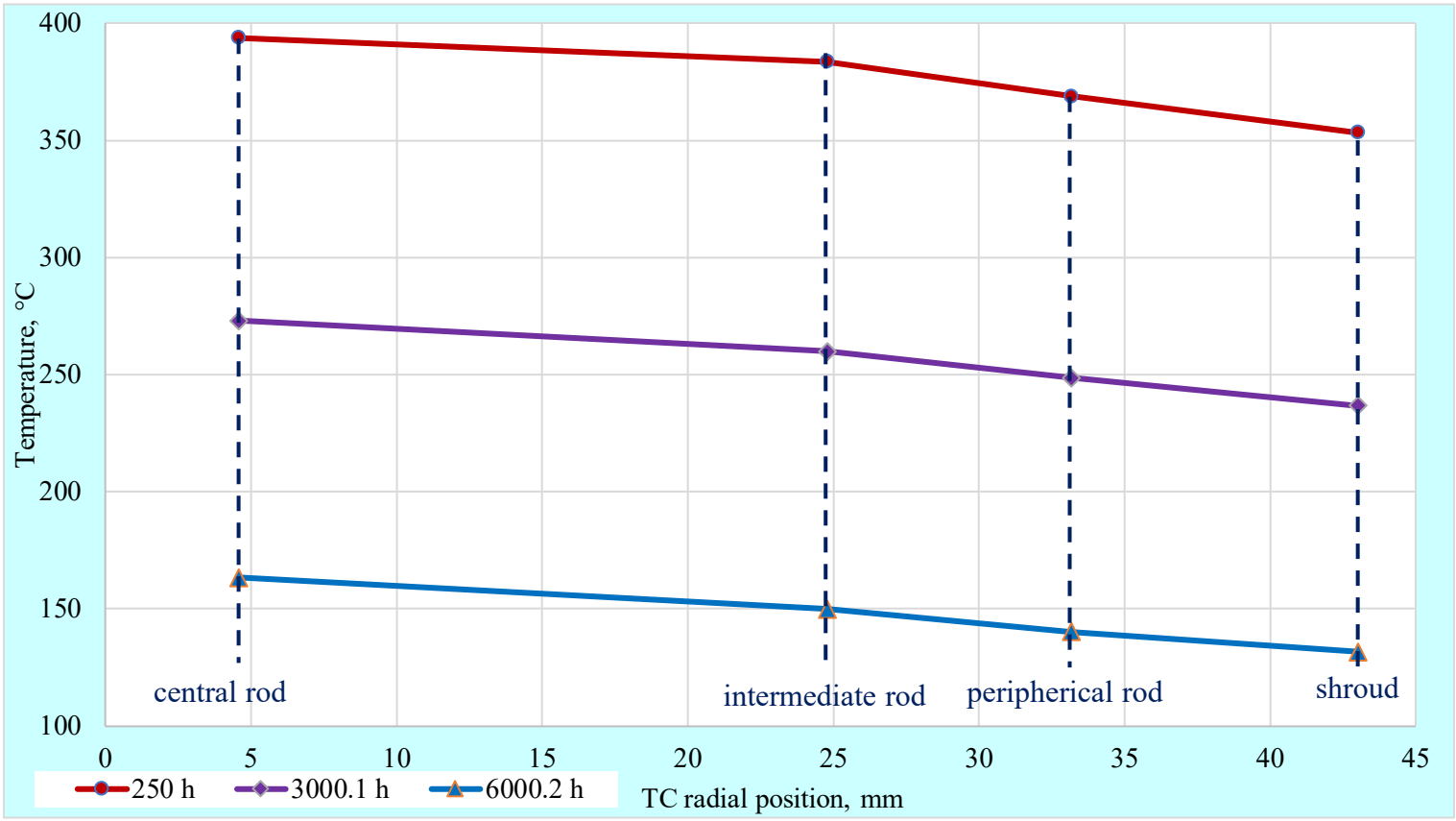

The radial temperature gradient: 40 K (test start), 30 K (test end)

Indirect estimation of radial symmetry in bundle: comparison of corner rods and shroud temperatures

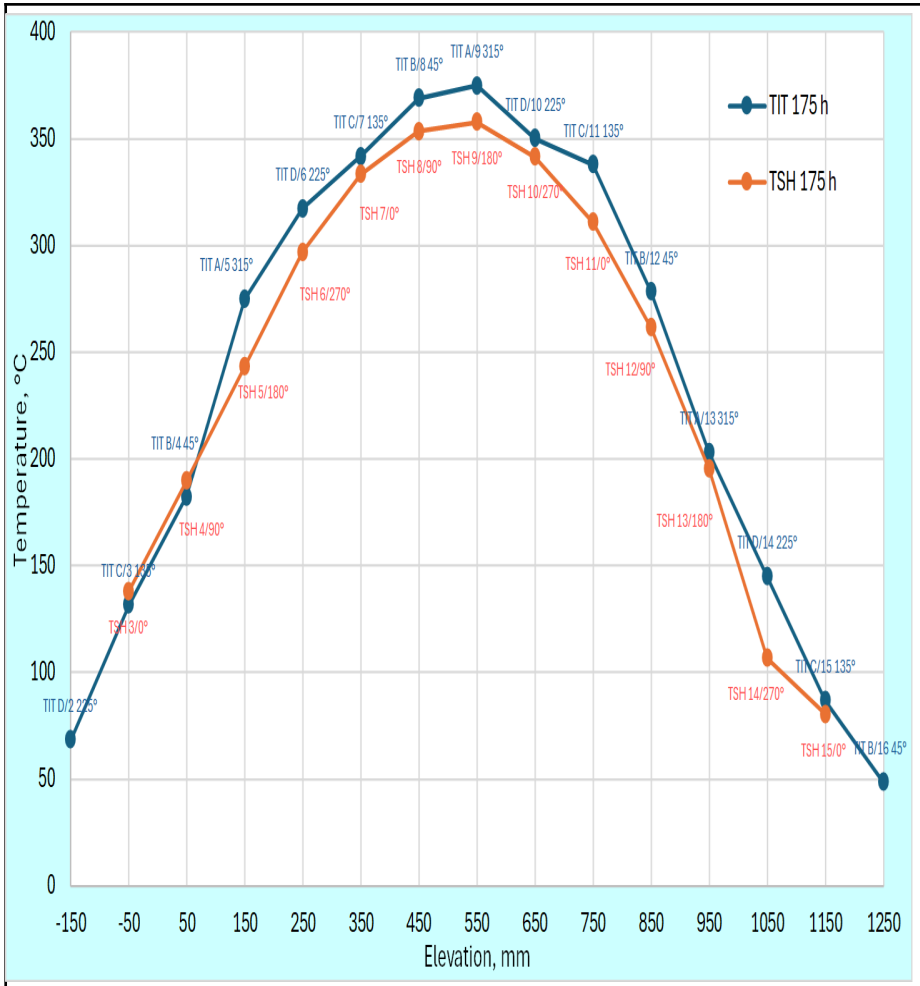

t = 175 h

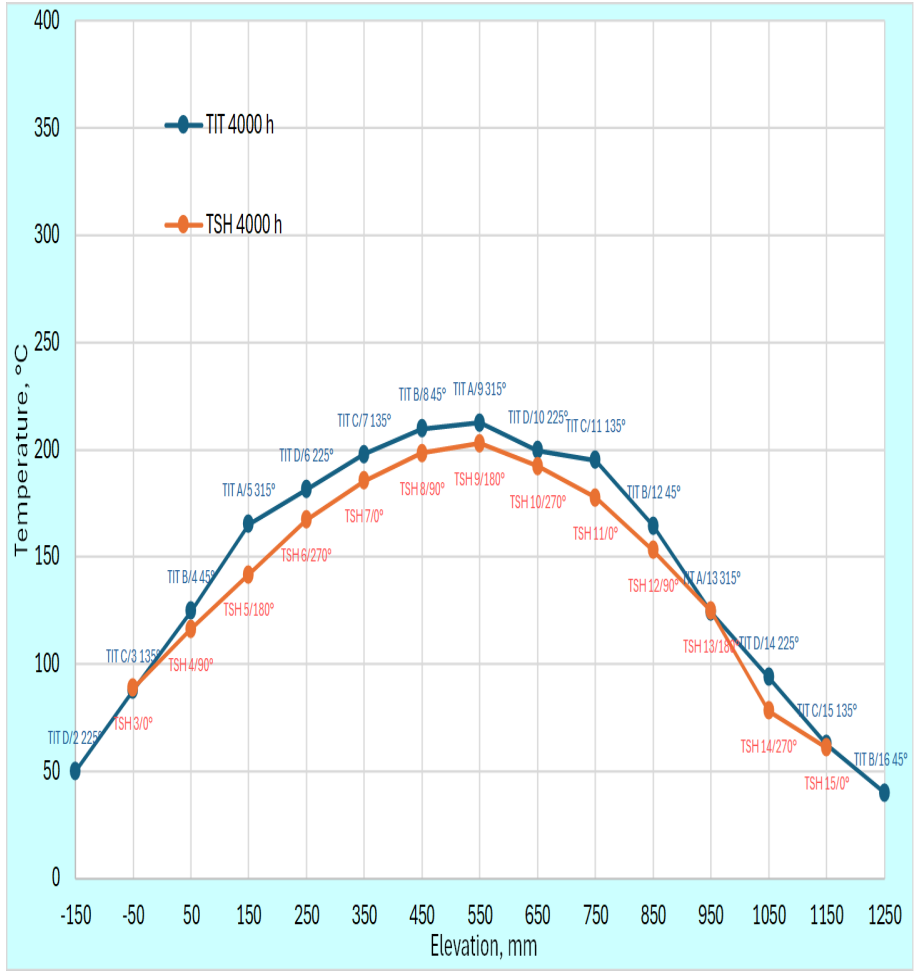

t = 4000 h

The circumferential temperature scatter is ±8 °C at the beginning of the test and ±5 °C before the end of the test

SPIZWURZ bundle: post-test view between two middle grid spacers

0°	90°	180°	270°

Results of creep measurements with the laser scanner: 1) small ovality of cladding (comparison of scanning at 4 angles); 2) influence of grid spacer springs (creep limitation)

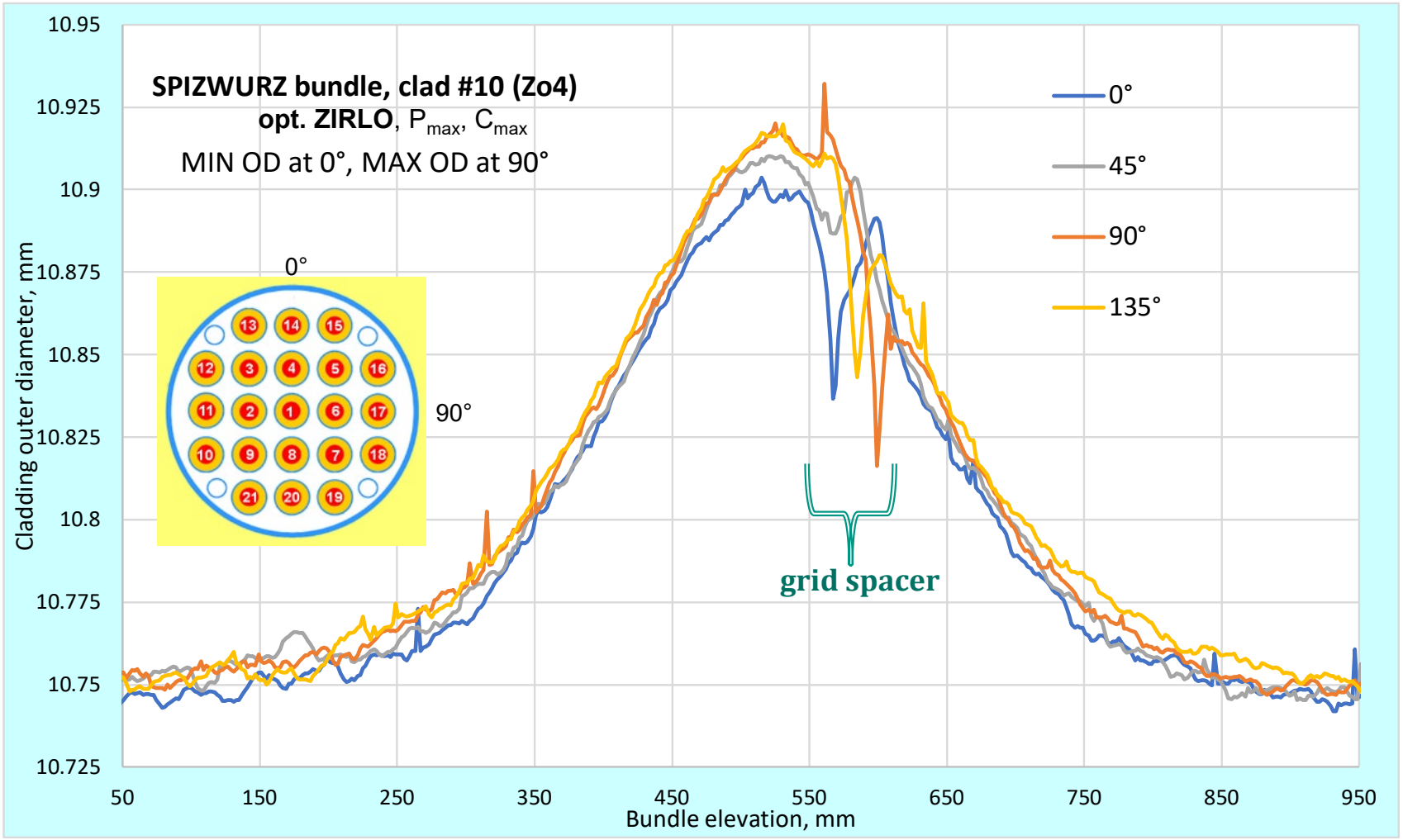

Max cladding ovality OD_{max}- OD_{min} = 20 µm at 520 mm (hottest bundle elevation);

average ovality along the cladding is 8 µm, what is comparable with delivered ovality of 5 µm

Ultrasound measurements of wall thickness along four cladding sides: not symmetrical wall thinning at each bundle elevation

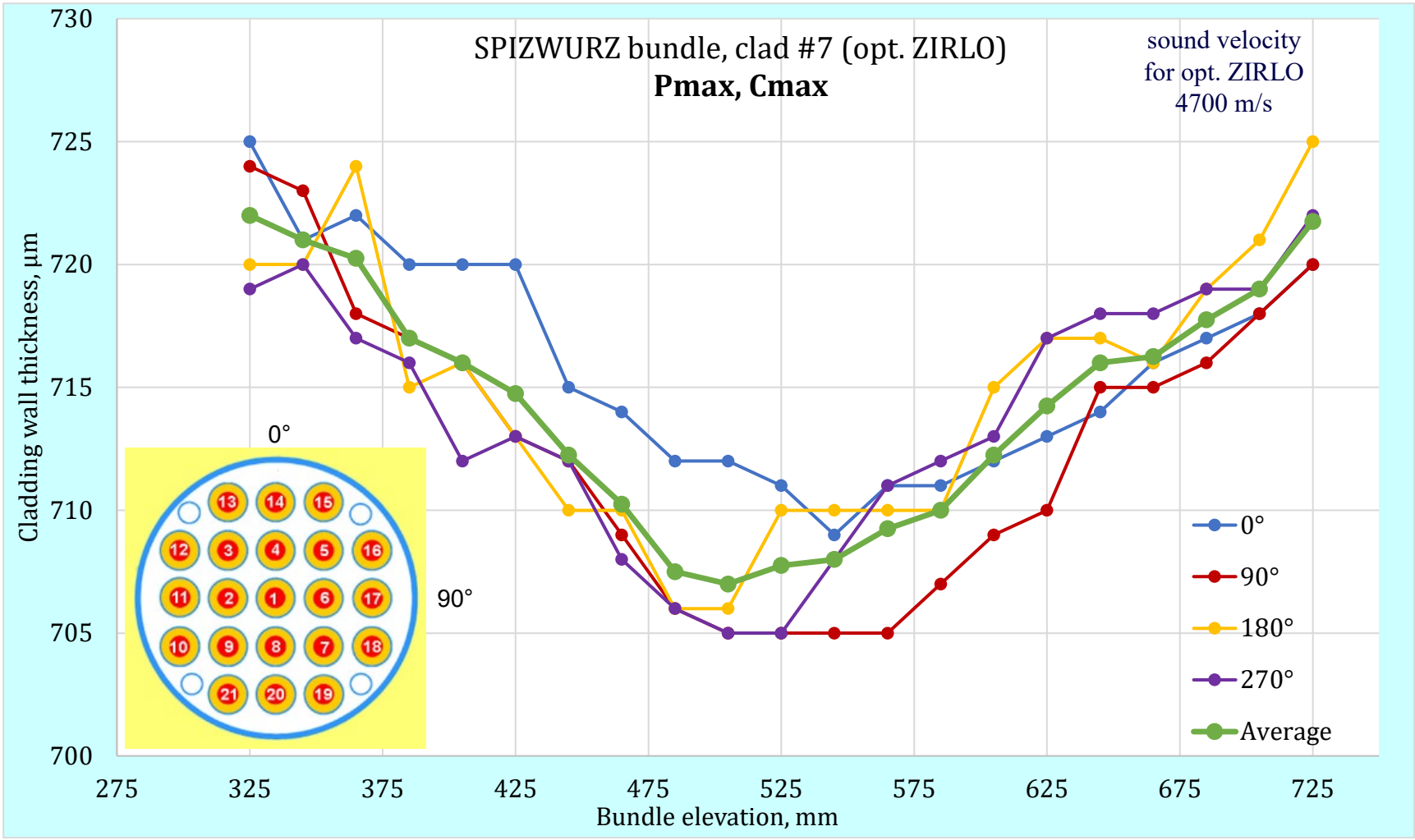

The probable reason of the asymmetrical thinning could be a shift of the pellets from the midline

2D wall thinning during cladding creep (cross-section area change): calculated dependence of thinning on the increase in outer diameter

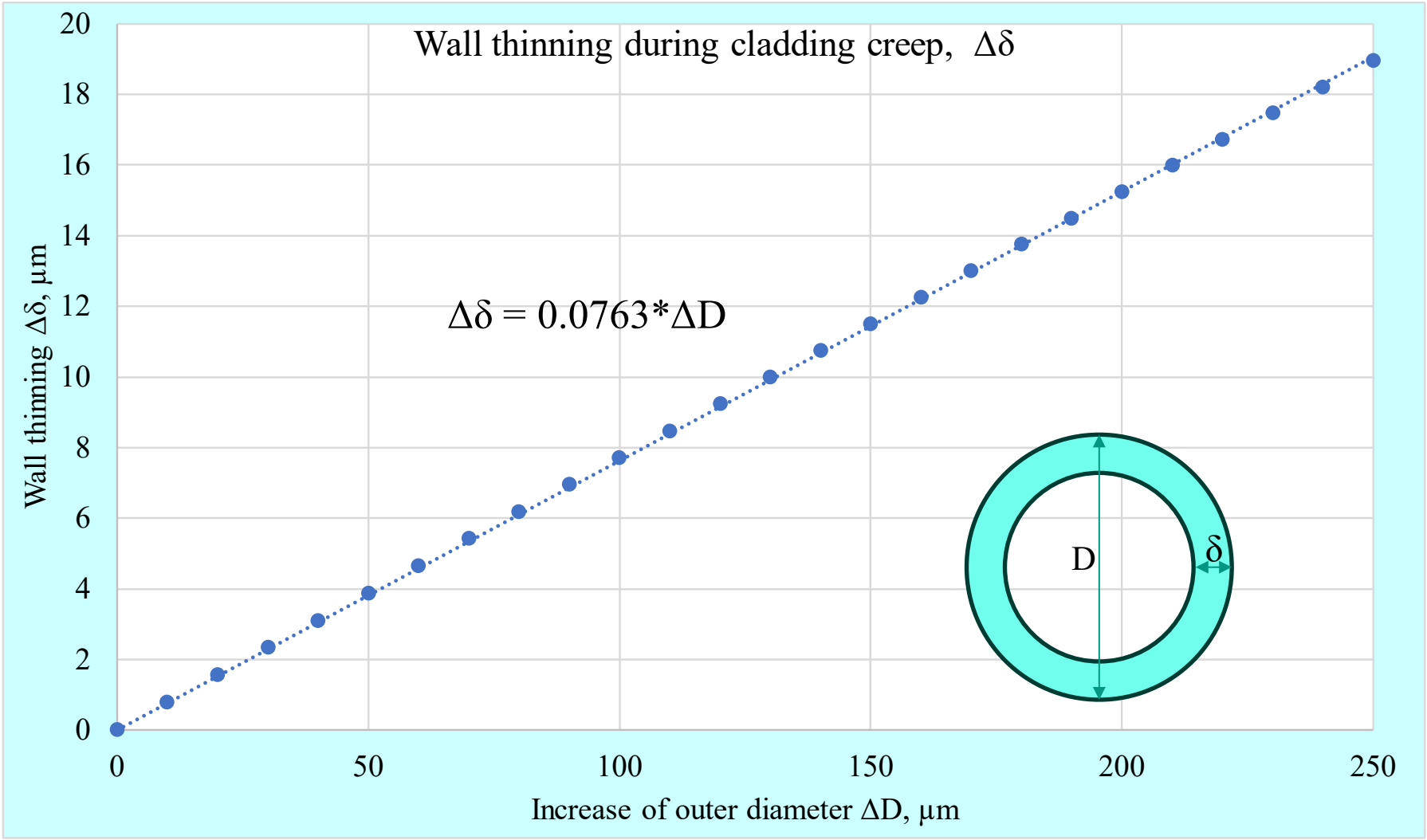

opt. ZIRLO: cladding creep, wall thinning

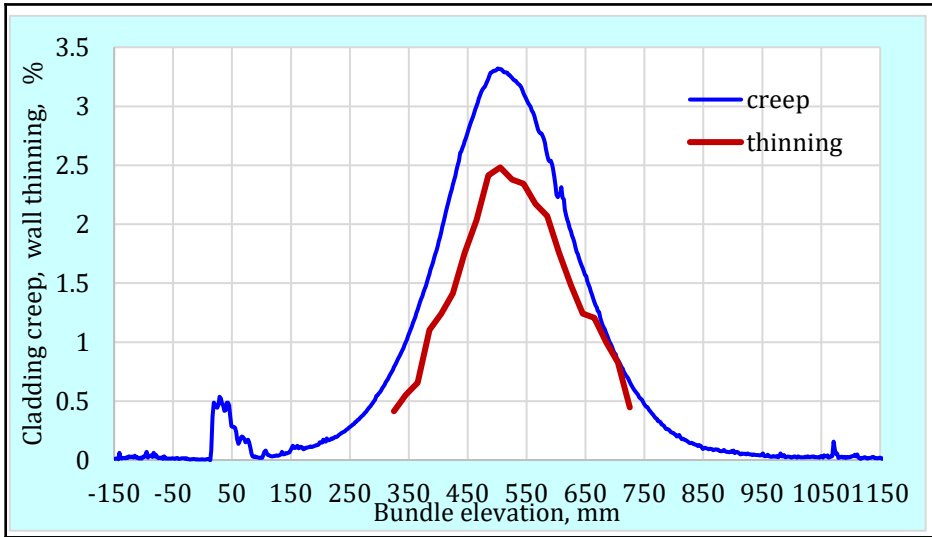

cladding 7: opt. ZIRLO, Pmax, Cmax

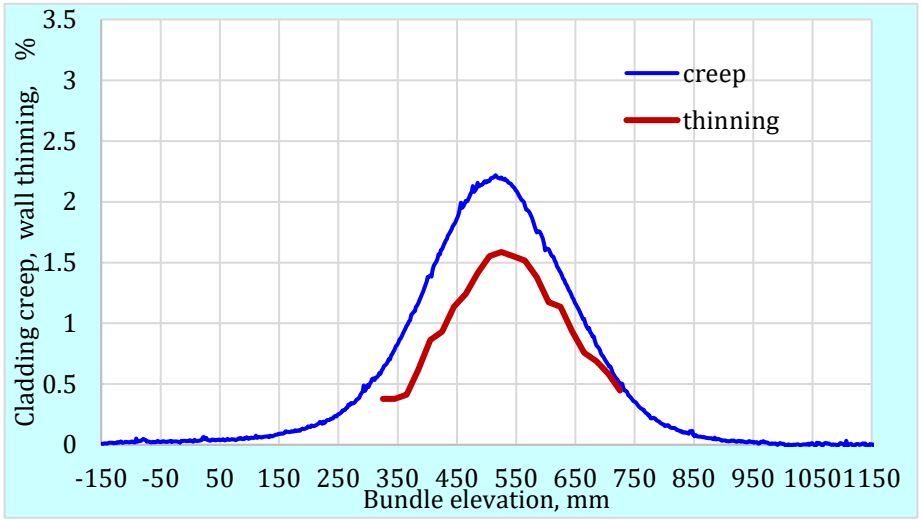

cladding 3: opt. ZIRLO, Pmax, Cmin

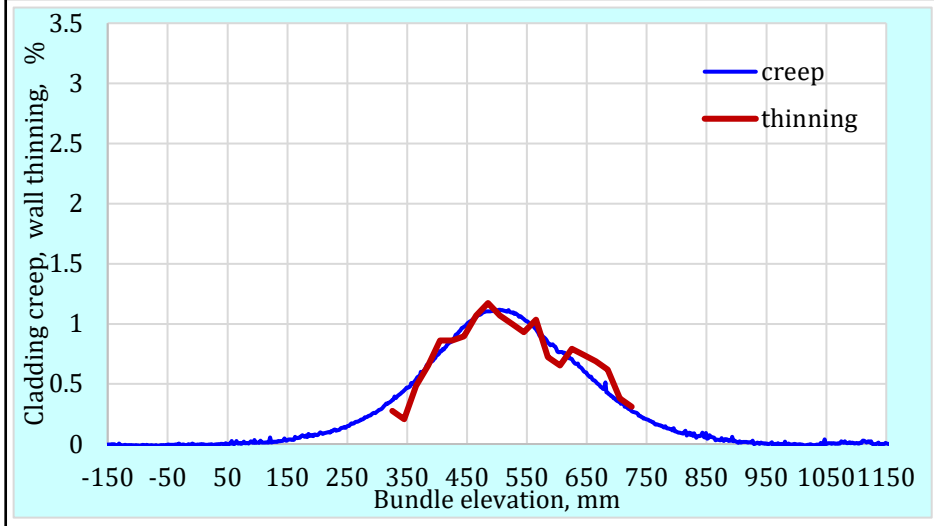

cladding 5: opt. ZIRLO, Pmin, Cmax

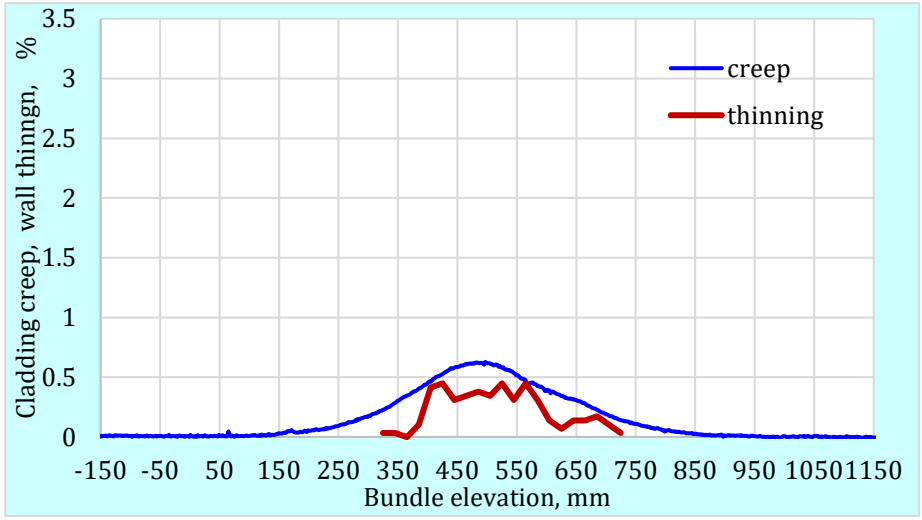

cladding 13: opt. ZIRLO, Pmin, Cmin

Zry-4: cladding creep, wall thinning

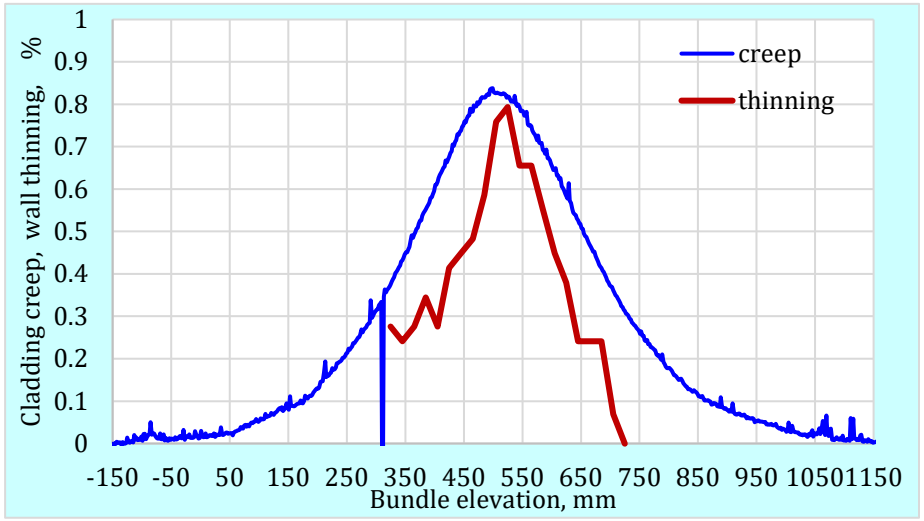

cladding 2: Zry-4, Pmax, Cmax

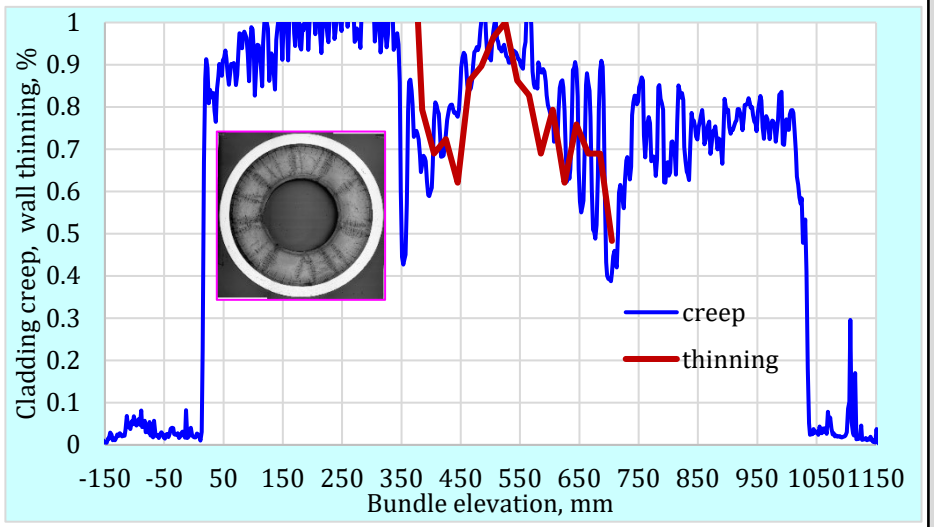

cladding 8: Zry-4, Pmax, Cmin;
contact of the cladding with the extended pellet

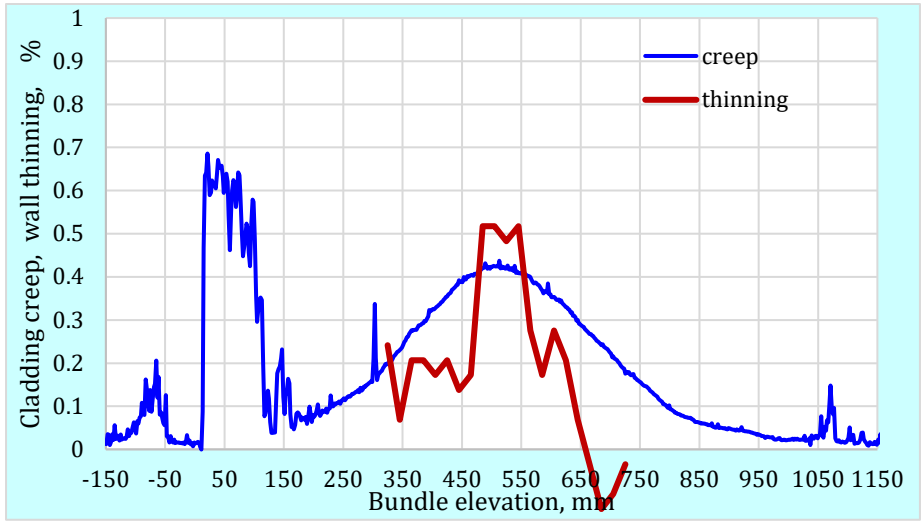

cladding 6: Zry-4, Pmin, Cmax

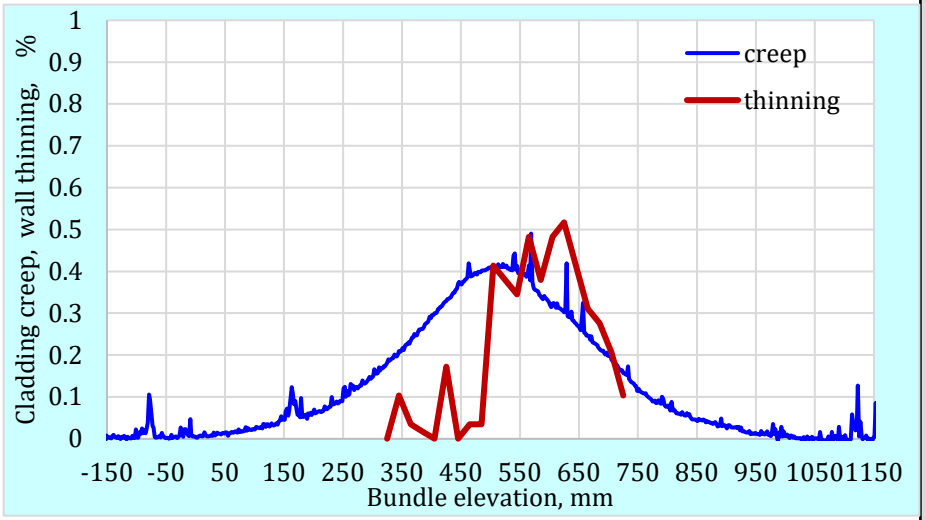

cladding 4: Zry-4, Pmin, Cmin

DX-D4 claddings: cladding creep, wall thinning

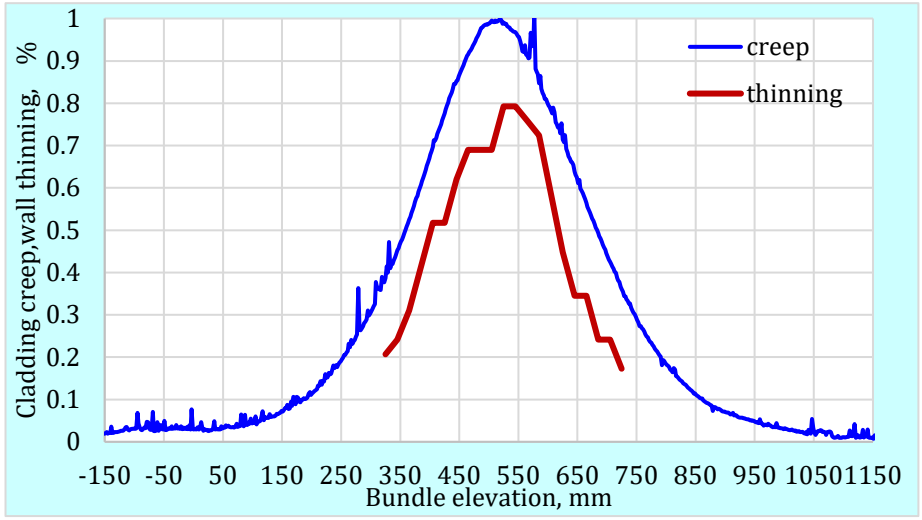

cladding 1: DX-D4, Pmax, Cmax

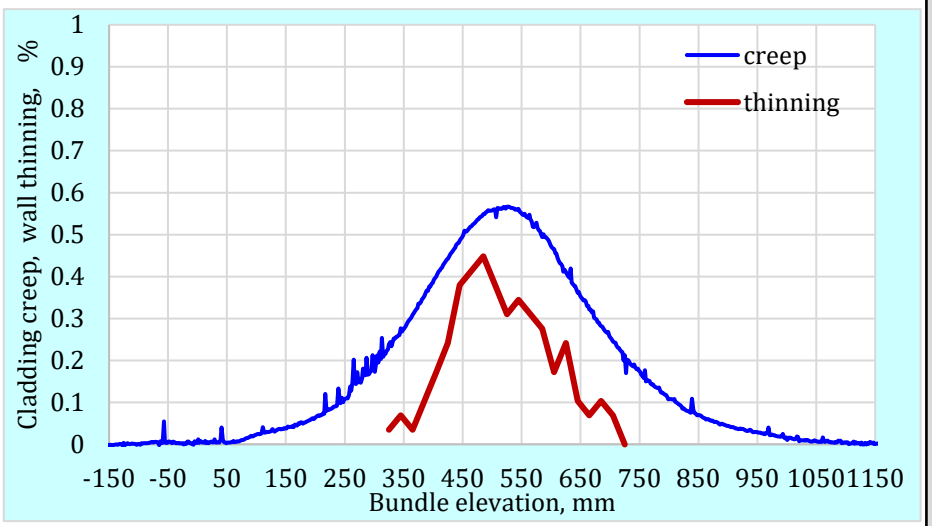

cladding 21: DX-D4, Pmax, Cmin

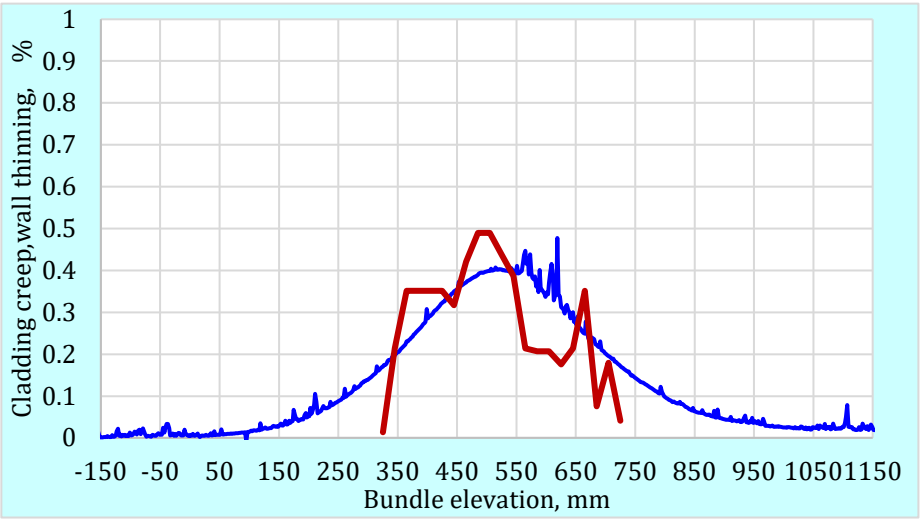

cladding 9: DX-D4, Pmin, Cmax

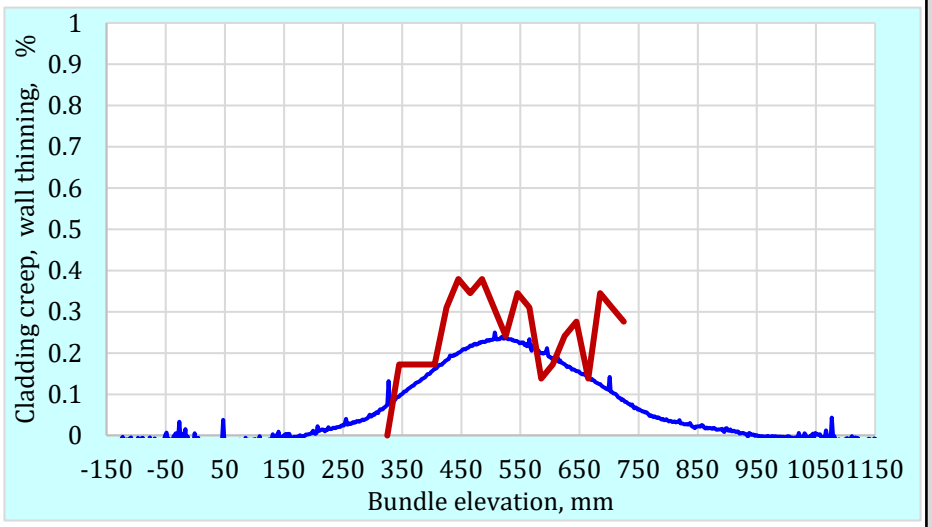

cladding 13: opt. ZIRLO, Pmin, Cmin

Post-test clad #11 (Zry-4, 146 bar, 300 wppm H), elevation 520 mm: metallographic observation of hydrides and cladding thinning

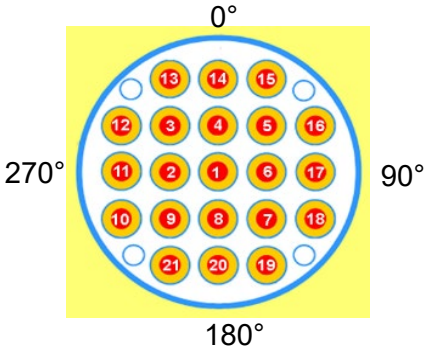

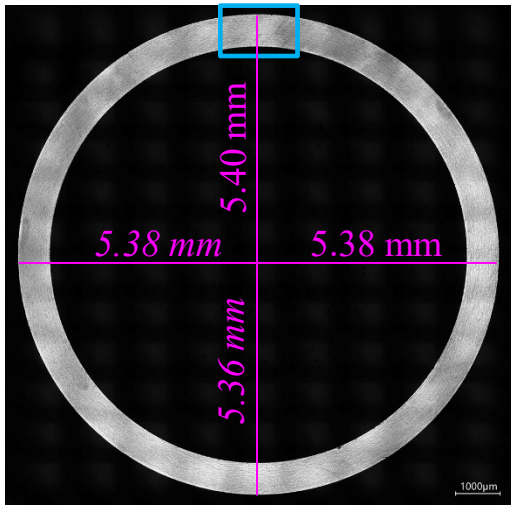

Link to movie: https://www.doi.org/10.5445/IR/1000189500

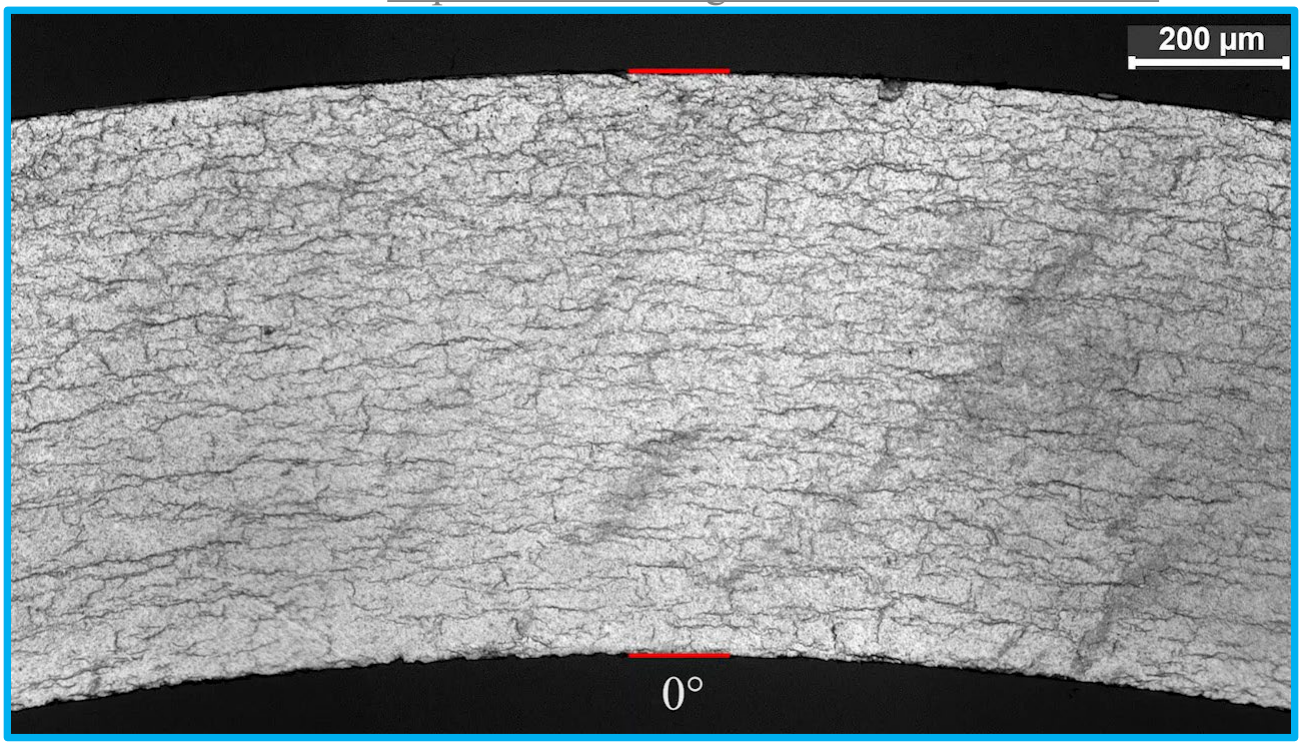

- **Circumferential homogeneity of hydrides appearance;**
- **Not very radial symmetry for the wall thinning:**

angle	wall thickness, µm
0°	**721**
90°	718
180°	711
225°	708
270°	710

Post-test clad #10 (opt. ZIRLO, 146 bar, 300 wppm H), elevation 320 mm: metallographic observation of hydrides and cladding thinning

Link to movie: https://www.doi.org/10.5445/IR/1000189571

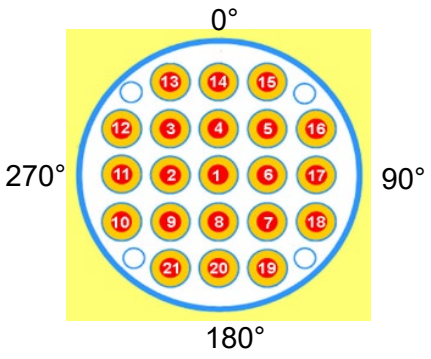

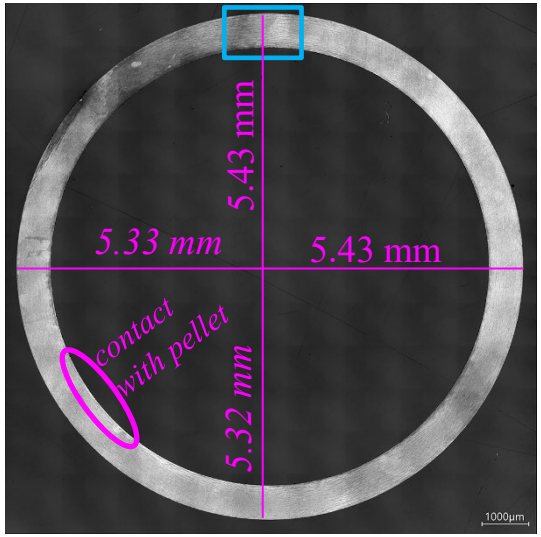

Eccentricity

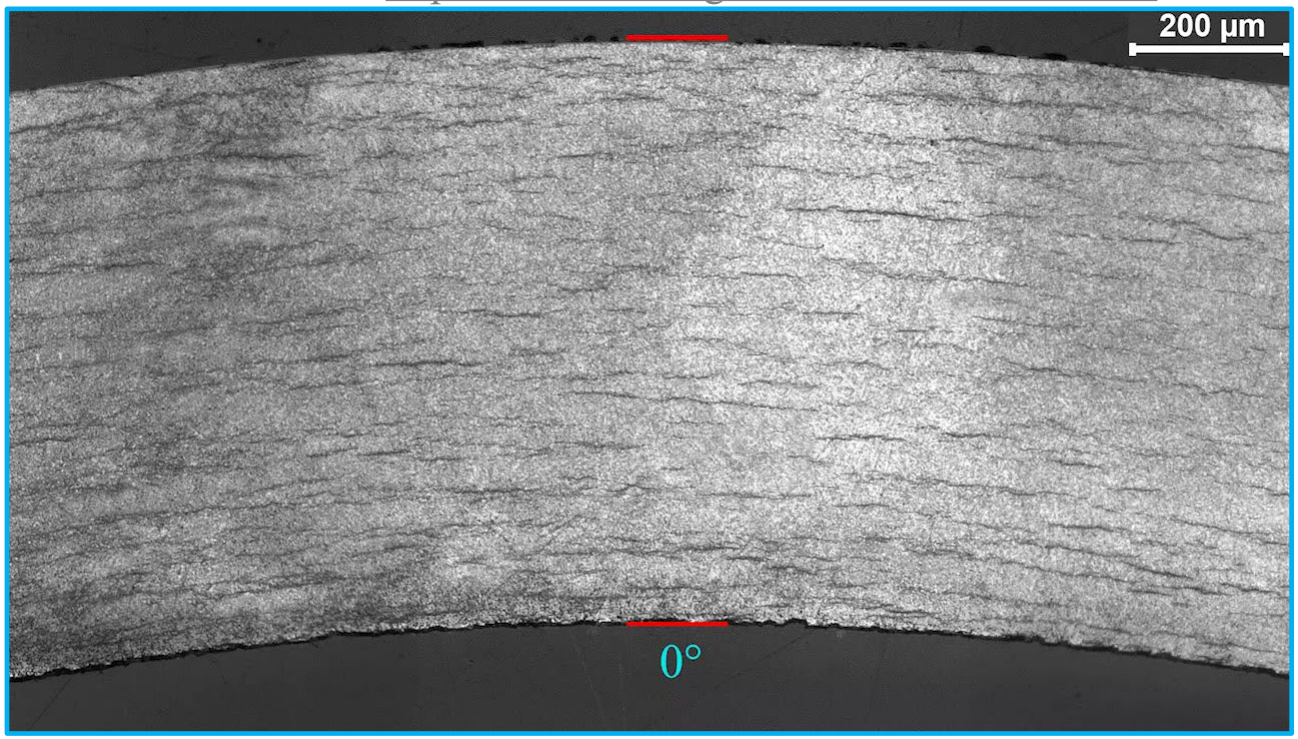

- **Circumferential homogeneity of hydrides appearance;**
- **Not very radial symmetry for the wall thinning:**

angle	wall thickness, µm
0°	721
90°	724
180°	719
225°	*716*
270°	*716*

Post-test clad #1 (DX-D4, 146 bar, 300 wppm H), elevation 520 mm: metallographic observation of hydrides and cladding thinning

Link to movie: https://www.doi.org/10.5445/IR/1000189574

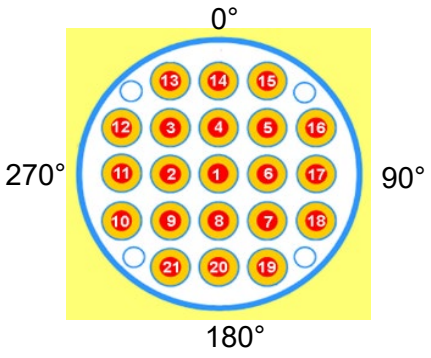

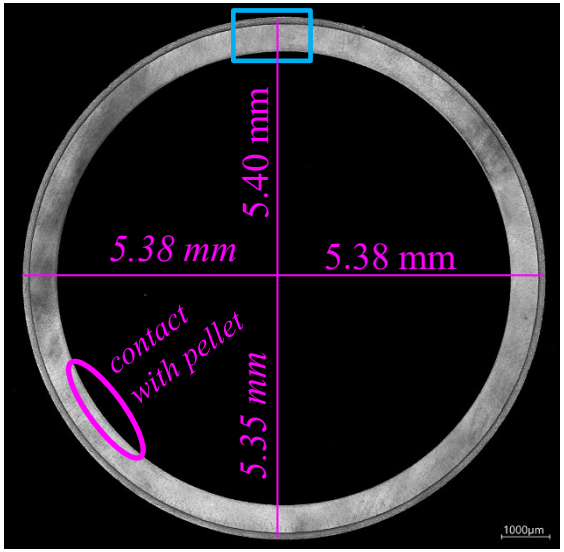

Eccentricity

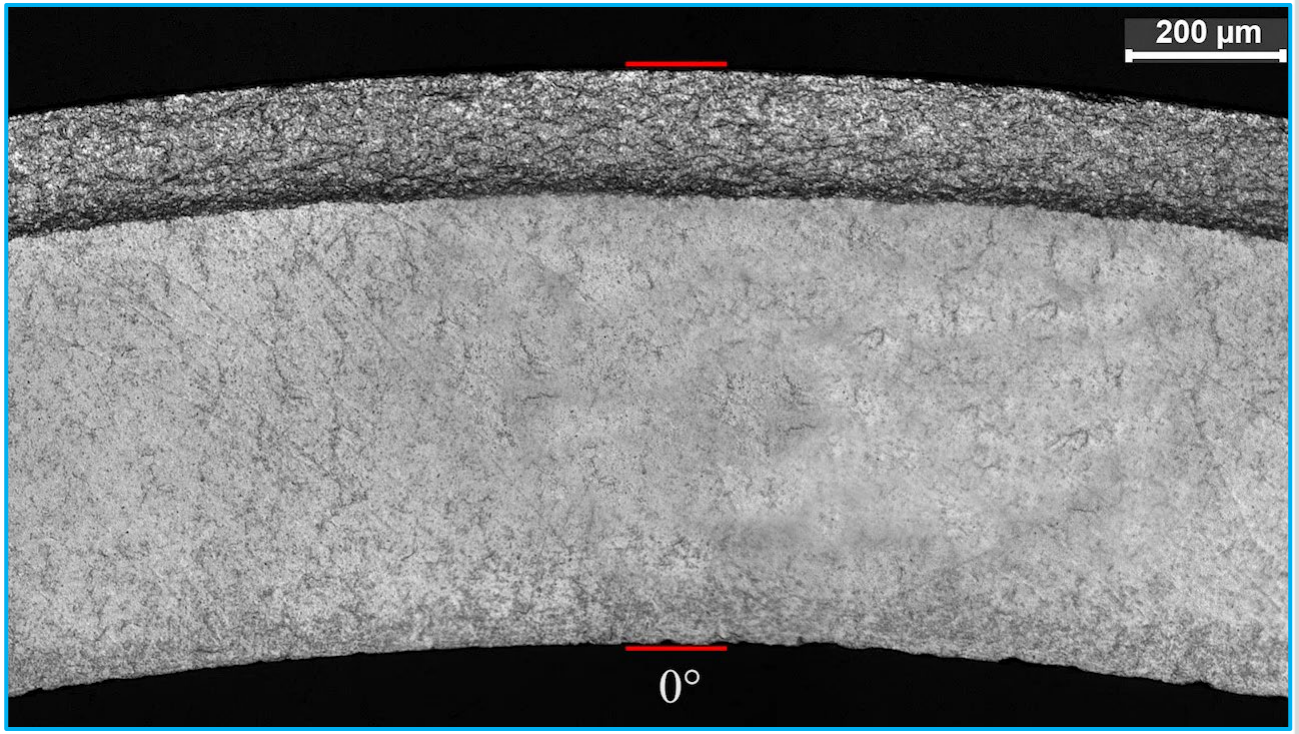

- **Circumferential homogeneity of hydrides appearance;**
- **Not very radial symmetry for the wall thinning:**

angle	wall thickness, µm
0°	716
90°	724
180°	720
225°	*712*
270°	*713*

Grain growth during hydrogenation and following bundle test for Zry-4: fresh, hydrogenated, post-test samples

Karlsruhe Institute of Technology

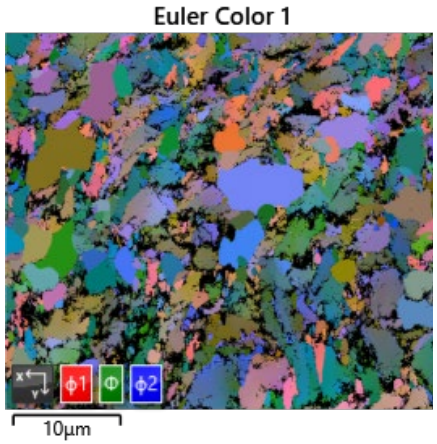

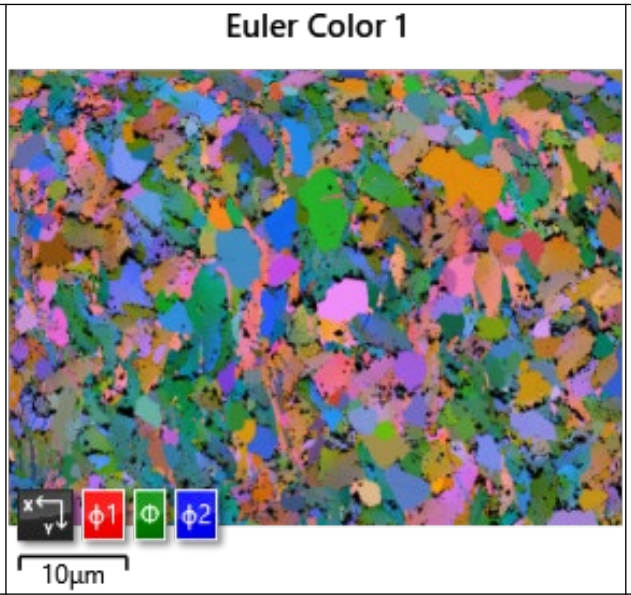

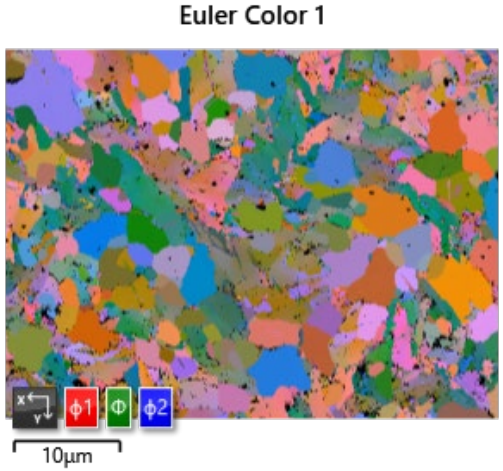

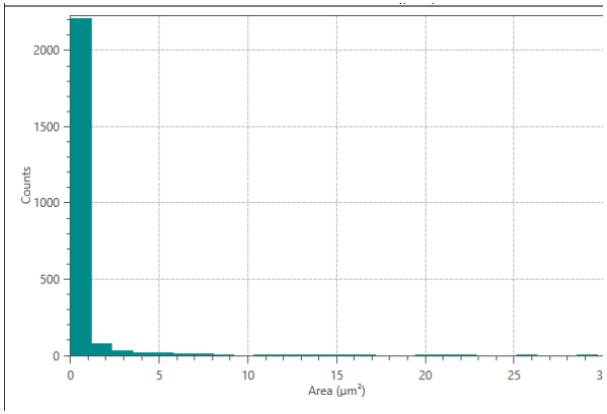

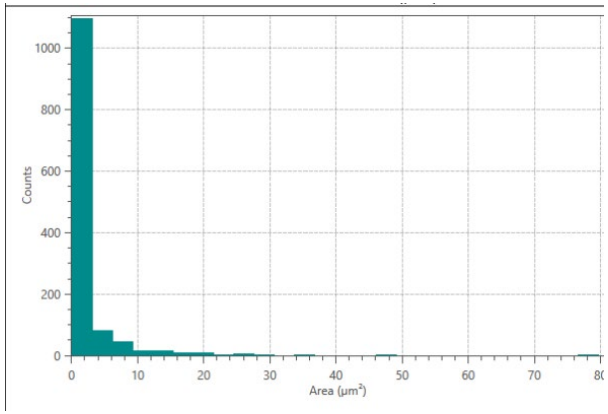

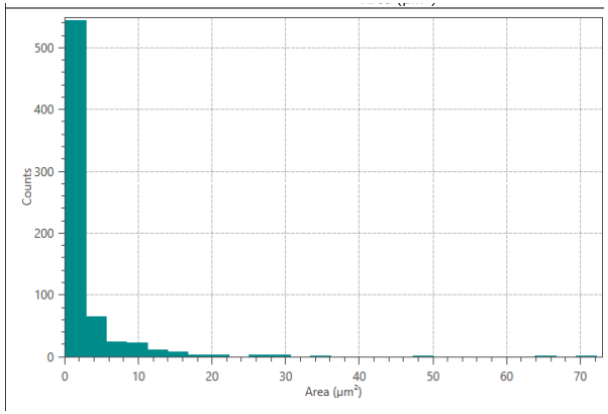

as-received: weight mean **5.74 ±1.67 µm²**, max 28.58 µm², grains 2387	300 wppm H: weight mean **12.79±4.54 µm²**, max 76.68 µm², grains 1282	bundle, 300 wppm H: weight mean **16.02±5.66 µm²**, max 69.46 µm², grains 685

IAM Institute for Applied Materials

Grain growth during hydrogenation and following bundle test for opt. ZIRLO: fresh, hydrogenated, post-test samples

Karlsruhe Institute of Technology

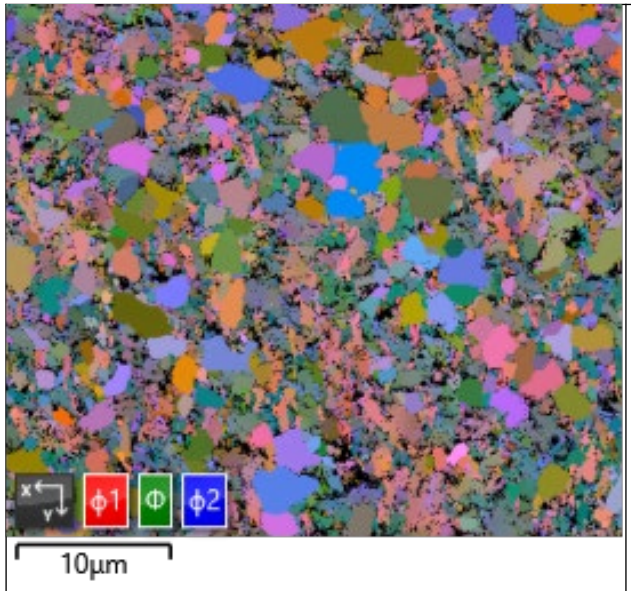	not available	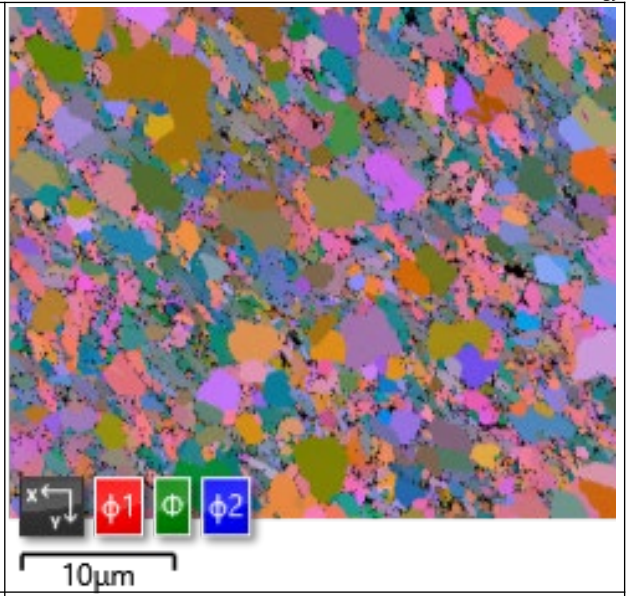
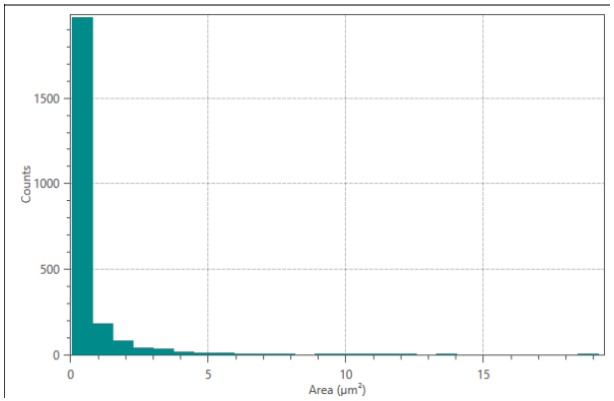	not available	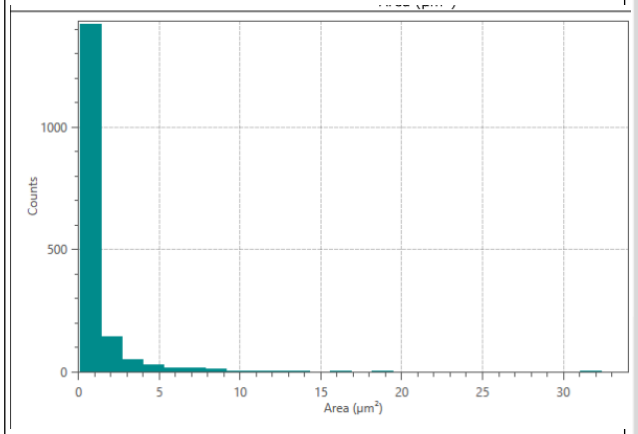
as-received: weight mean **2.92±1.16 µm²,** max 18.46 µm², grains 2363	300 wppm H	bundle, 300 wppm H: weight mean **4.33±1.72 µm²**, max 32.37 µm², grains 1696

IAM Institute for Applied Materials

Summary

- For the long-term SPIZWURZ bundle experiment, zirconium alloy tubes (opt. ZIRLO, Zry-4, DX-D4) were charged with hydrogen to 100 and 300 wppm in the special developed HOKI tube oven as homogeneously as possible along a length of 1.3 m.
- The hydrogenation was carried out at 450 °C by successively supplying fixed masses of hydrogen through the specially treated **inner** surface of claddings.
- After the hydrogen loading of the samples, the axial distribution of hydrogen was determined by laser scanning profilometry (calibrated by hot gas extraction).
- A long-term bundle test with 21 hydrogenated and pressurized cladding tubes began on 12.05.2023 and terminated on 17th January 2024. Two pressure set values were used: 106 and 146 bar. Due to small leaks in some of the rods, it was decided to maintain the pressure constant in all rods throughout the experiment (lasted 250 days) by periodically injecting the Ar+O_2 gas mixture refilled; oxygen was used for oxidation of the inner cladding surface to avoid hydrogen release from the cladding. The rod #18 was not pressurized and could be used as reference rod.
- The peak cladding temperature decreased in steps of ≈15 K from 400 to 165 °C (average cooling rate ≈0.9K/day). The maximal cooling rate during each temperature step was 6 K/h, step duration was about 10 h.

Summary (cont.)

- The post-test laser scanner measurements of the outer cladding diameter showed significant creep: radial deformation values are between 0.2 and 3.3% (diameter increase and the corresponding wall thinning).
- The largest creep of 3.3% was measured for opt. ZIRLO claddings hydrogenated to 300 wppm. The corresponding maximum creep value was 0.93% for Zry-4 and 1% for DX-D4.
- A clearly visible dependence of the degree of creep on the hydrogen concentration is observed for the opt. ZIRLO claddings: the creep of claddings hydrogenated to 300 ppm is 1.2-1.5 times higher than that of claddings hydrogenated to 100 ppm.
- A number of claddings show radially asymmetric wall thinning, which can be associated with the radial shift of the pellets from the central axis of the rod and the corresponding asymmetric heat supply along the circumference of the cladding.
- The metallographic investigations revealed a uniform distribution of hydrides throughout the entire cladding circumference for all three cladding types used. In the DX-D4 claddings, hydrogen primarily diffused toward the outer liner.
- The degree of hydride reorientation was significantly higher in the Zry-4 claddings compared to the opt. ZIRLO claddings.
- The difference in the behavior of the Zry-4 and opt. ZIRLO may be due, in part, to their different grain microstructures. Opt. ZIRLO claddings have a finer grain size than Zry-4. Moreover, although the temperatures during hydrogenation (450 °C) and the experiment itself (max. 400 °C) were relatively low, EBSD measurements showed grain growth from approx. 6 µm for the initial state to post-test 16 µm for Zry-4 (12 µm after hydrogenation), and from initial 3 µm to post-test 4.3 µm for opt. ZIRLO.

Thank you for your attention

https://www.iam.kit.edu/awp/english/163.php

http://quench.forschung.kit.edu/

Mikhail Kolesnik
KIT

Hydride Morphology in Zirconium Tubes After SPIZWURZ Bundle Tests: Experimental Data and Preliminary Simulation Results

Hydride embrittlement of zirconium cladding is a major safety concern when handling and long-term dry storage of spent nuclear fuel. The degree of embrittlement is strongly influenced by the morphology of hydrides, which includes their orientation, size, spacing, and connectivity. Under dry storage conditions, a thermomechanical cycle involving heating and subsequent slow cooling of fuel rods under internal excessive gas pressure can promote hydride reorientation in the cladding. This scenario can result in the formation of radially oriented hydrides, making the material more brittle than in its pre-storage state.

This study presents new detailed experimental data on hydride morphology in Zircaloy-4 tubes obtained from the SPIZWURZ bundle test conducted at the Karlsruhe Institute of Technology (KIT) at the LICAS facility. The test involved a 21-rod bundle that was subjected to a 250-day, stepwise cooling sequence under different internal gas pressures to simulate the thermo-mechanical conditions of dry storage. Measured parameters include the radial hydride fraction, hydride length and density, and continuity metrics such as the Hydride Continuity Coefficient (HCC) and Radial Hydride Continuity Path (RHCP).

The experimental results were compared with simulations obtained using two modeling approaches. The first approach is a kinetic ordinary differential equation (ODE)-based model capable of reproducing the average morphological parameters as functions of stress, temperature, and hydrogen content. The second approach is MORPHYD, a 3D numerical tool that simulates the nucleation and diffusion-controlled growth of disc-shaped hydrides on a virtual domain. This enables the evaluation of network connectivity and statistics of morphology parameters.

While not all samples have been fully analyzed, initial benchmarking results demonstrate consistent trends between experiments and the two modeling tools. These findings confirm the approaches' suitability for predicting hydride morphology evolution and provide a solid basis for validating them on the complete SPIZWURZ dataset.

Karlsruhe Institute of Technology

Institute for Applied Materials

Hydride Morphology in Zirconium Tubes After SPIZWURZ Bundle Tests: Experimental Data and Preliminary Simulation Results

M. Kolesnik, J. Stuckert, M. Grosse, S. Weick

30th International QUENCH –Workshop, Karlsruhe, Germany

Institute for Applied Materials; Program NUSAFE

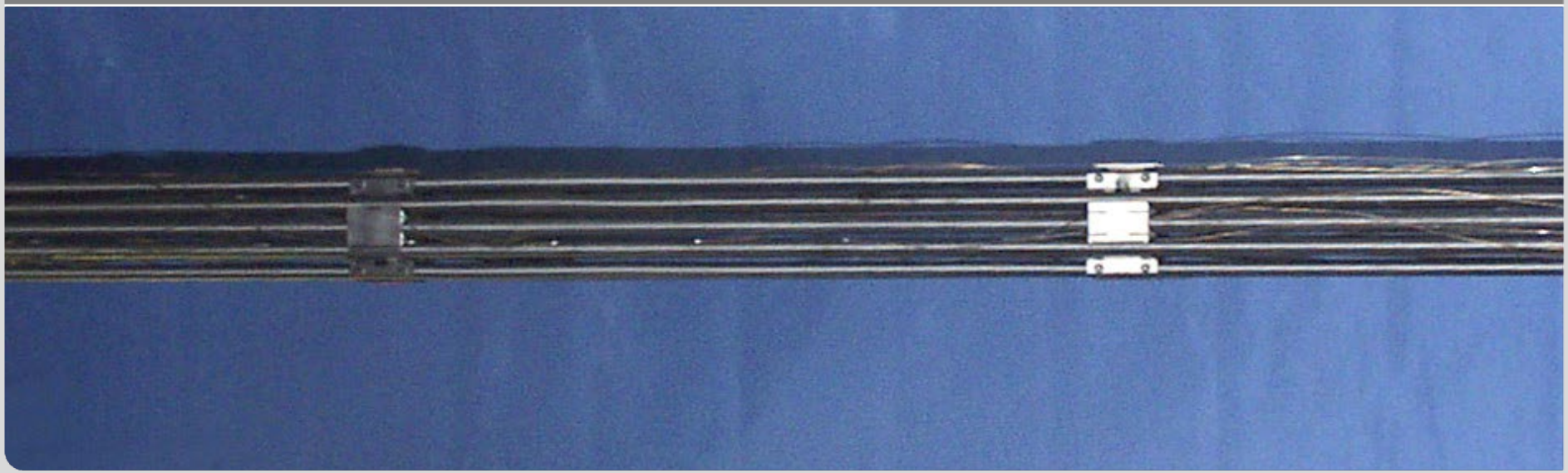

SPIZWURZ bundle test
experimental conditions

SPIZWURZ bundle:

- 21 cladding tubes
- Zircaloy-4, opt. ZIRLO, duplex DX-D4
- internal gas loading
- stepwise cooling over 250 days

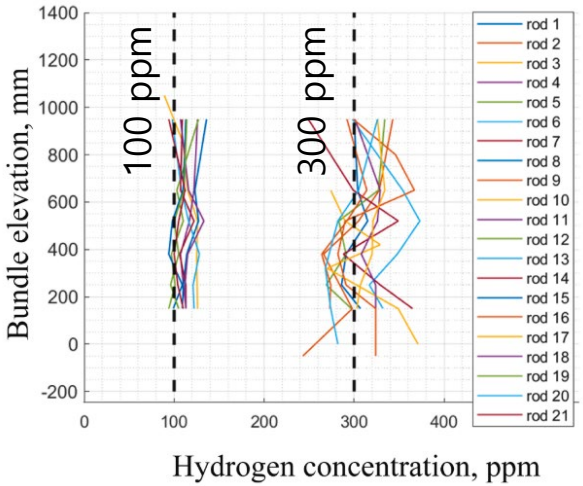

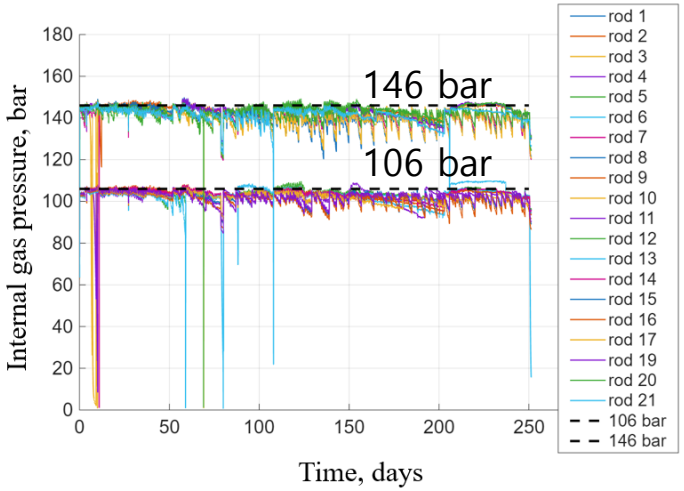

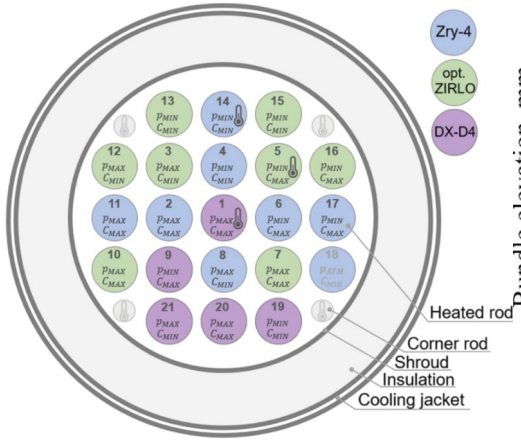

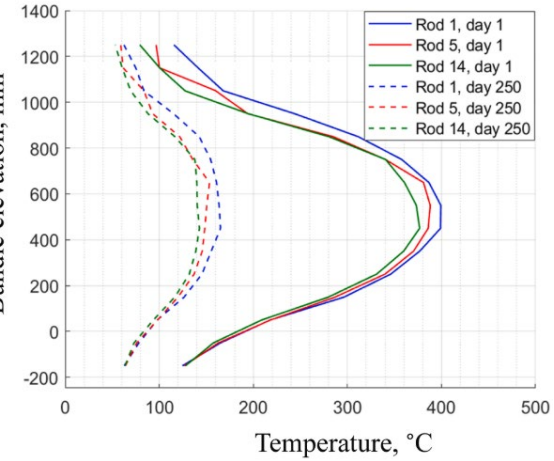

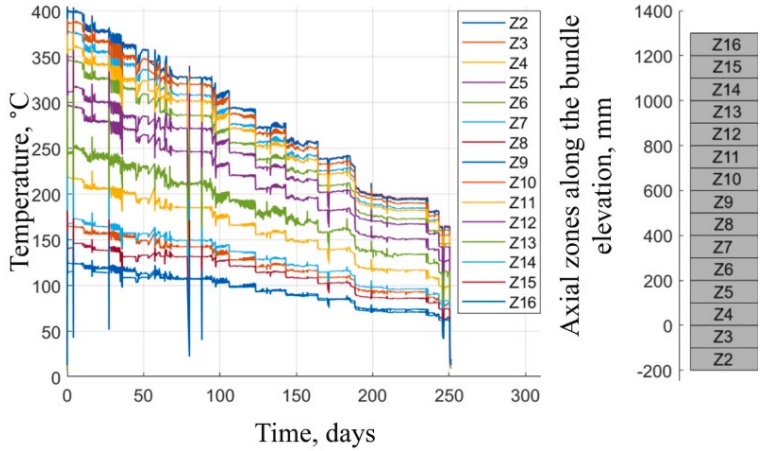

SPIZWURZ bundle test
hydride morphology measurement

Two-step micrograph processing

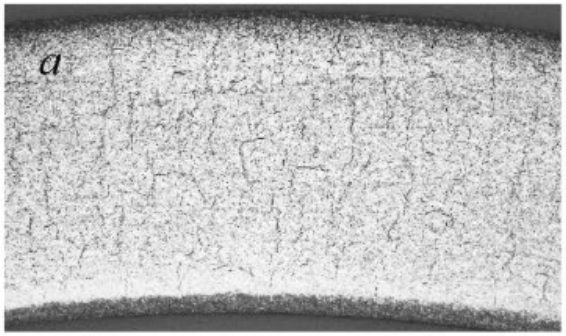

Initial micrograph

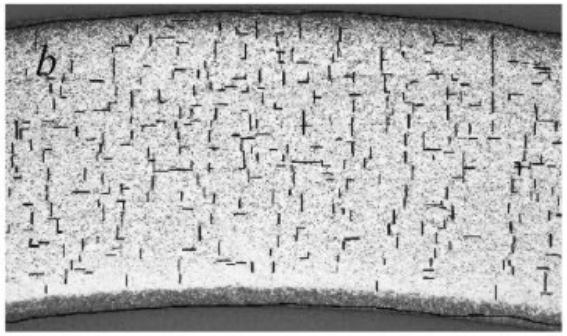

Manual phase

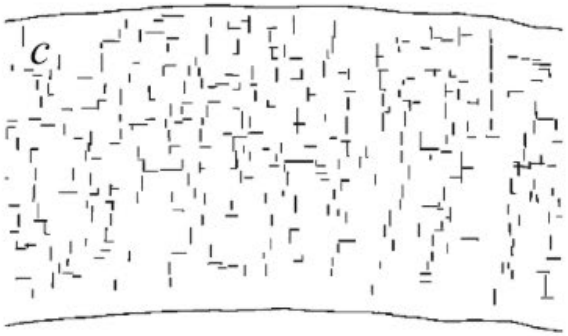

Numerical processing

Measured parameters:

- Radial hydride fraction (RHF)
- Hydride Continuity Coefficient (HCC)*
- Radial Hydride Continuity Path (RHCP)**
- Length of hydrides (with statistical distribution)
- Surface density of hydrides
- Hydride length density

*HCC – the total projection length of hydrides within 110 μm in the radial direction, normalized by thickness
**RHCP – fracture energy estimated from varying crack paths, normalized to the unhydrided sample

SPIZWURZ bundle test results
radial hydride fraction (RHF)

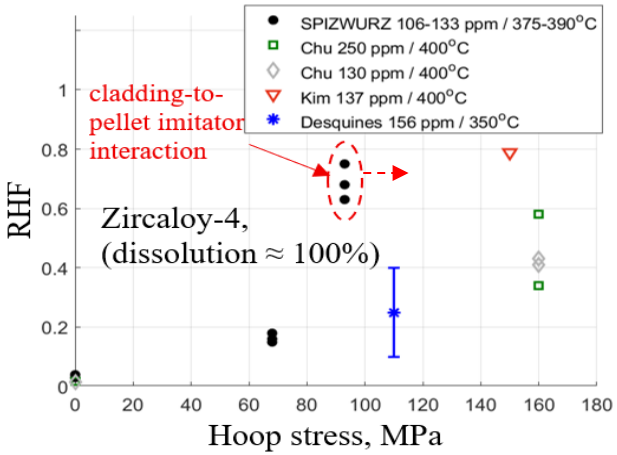

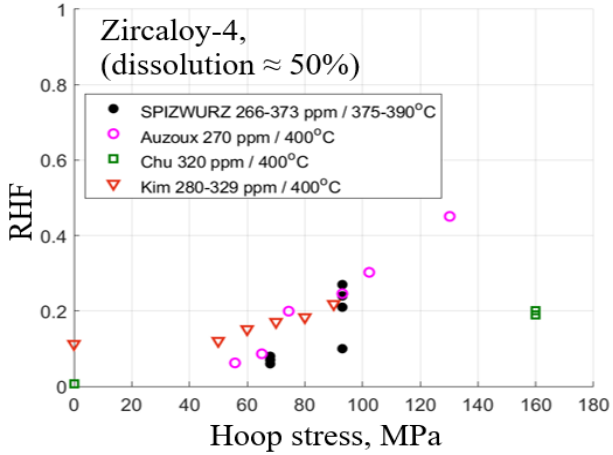

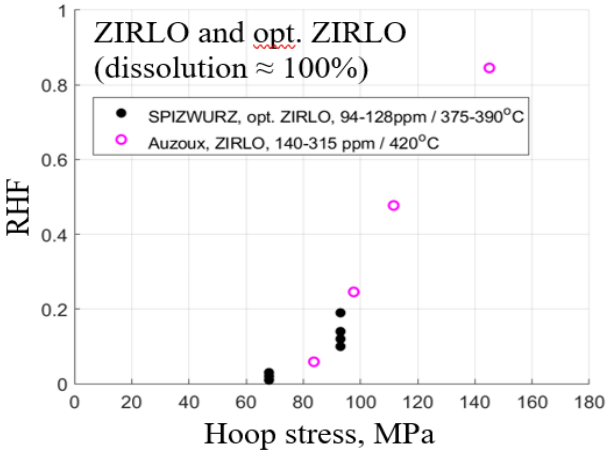

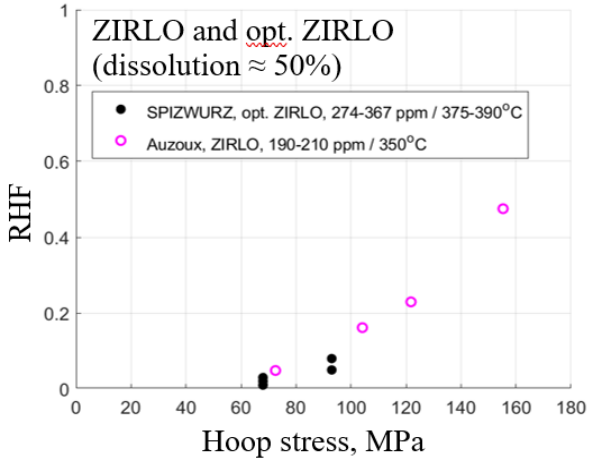

RHF increases with hoop stress, in agreement with previously published data

[1] Q. Auzoux et al., J. Nucl. Mat. 494 (2022) 153893, DOI: 10.1016/j. jnucmat.2022.153893
[2] J. Desquines et al., WRFPM (2023), 80-86, DOI: 10.1007/978-981-99-7157-2_8
[3] H.C. Chu, S.K. Wu and R.C. Kuo, J. Nucl. Mat. 373 (2008) 319-327, DOI: 10.1016/j. jnucmat.2007.06.012
[4] Y.J. Kim et al. J. Nucl. Sci. Technol. 52 (2014) 717-727, DOI: 10.1080/ 00223131.2014.978829

SPIZWURZ bundle test results

hydride reorientation: Zircaloy-4 vs. opt. ZIRLO

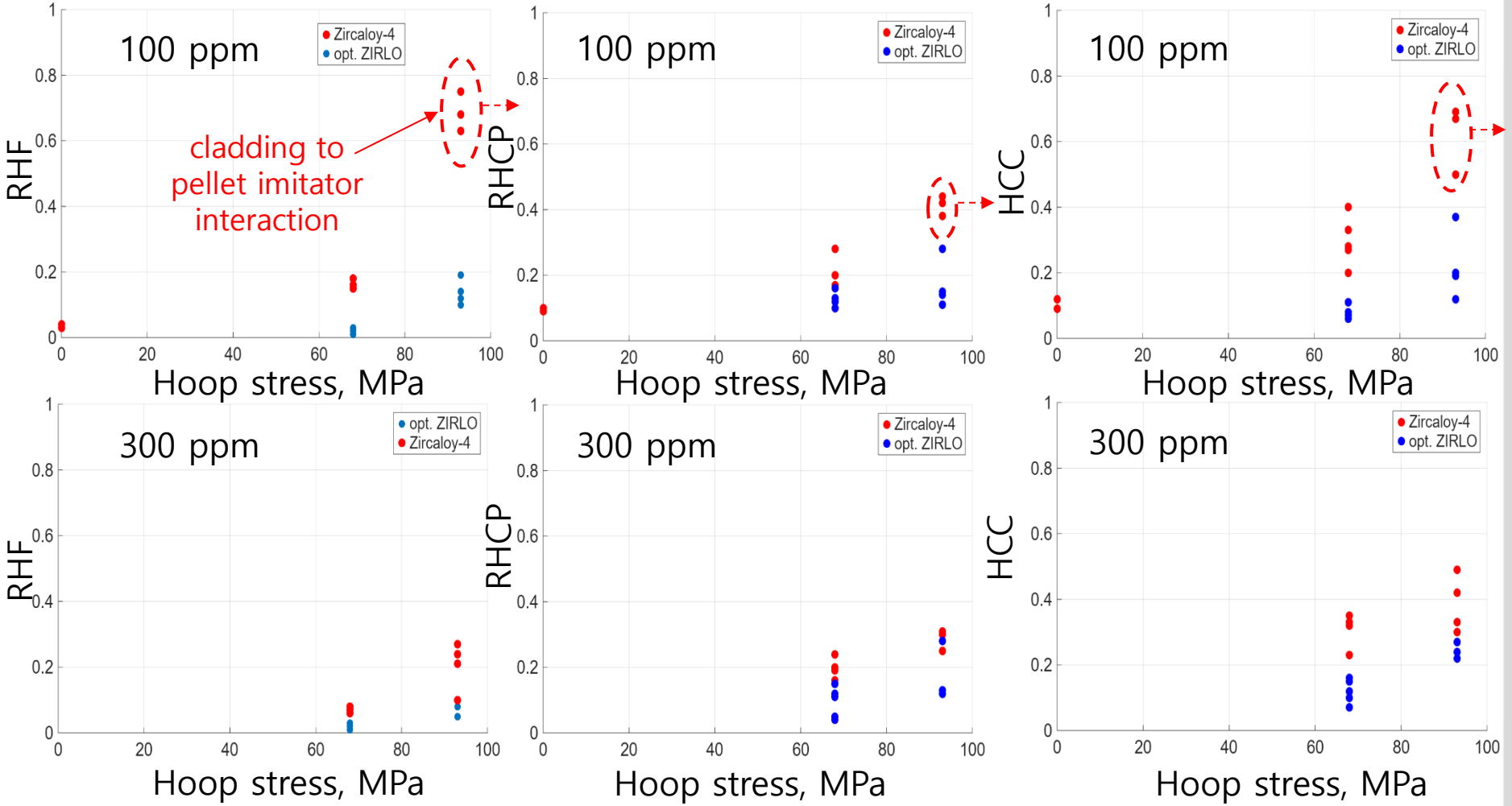

Hydride reorientation is more pronounced in Zircaloy-4 than in the opt. ZIRLO

SPIZWURZ bundle test results
length of hydrides

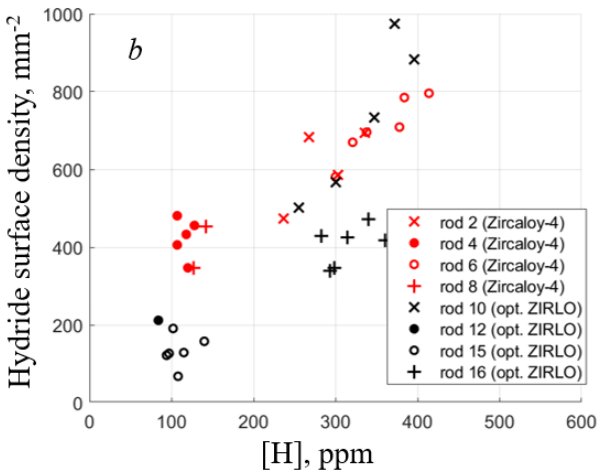

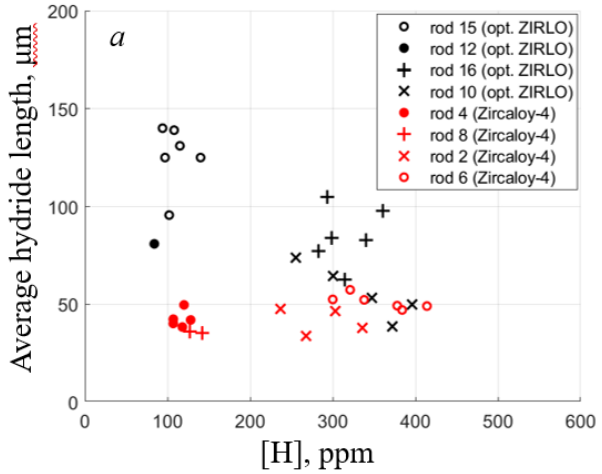

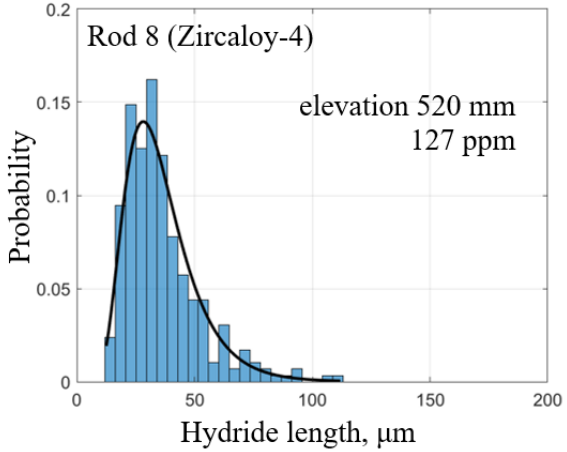

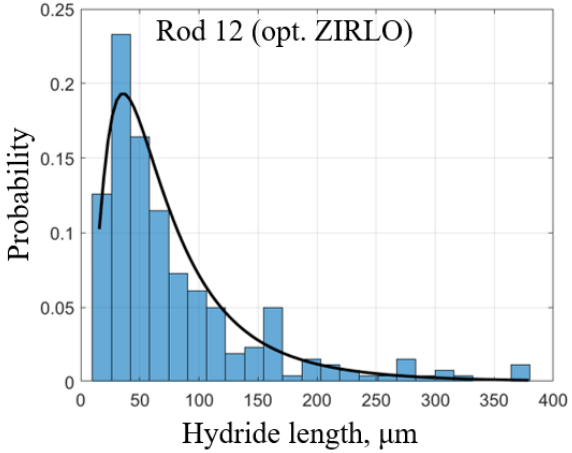

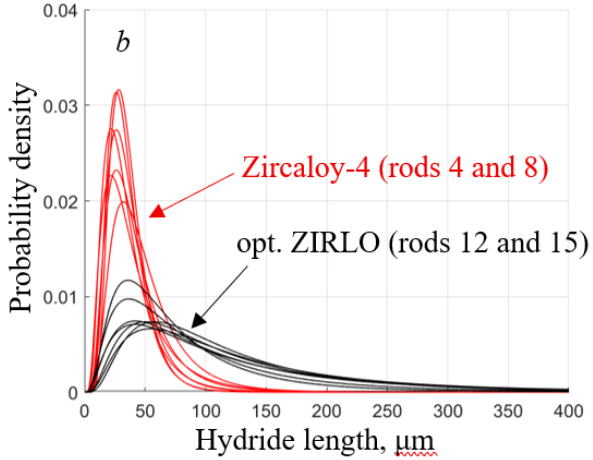

The average and maximum hydride lengths in the opt. ZIRLO are two to three times longer than those in Zircaloy-4

SPIZWURZ bundle test results
hydride length density

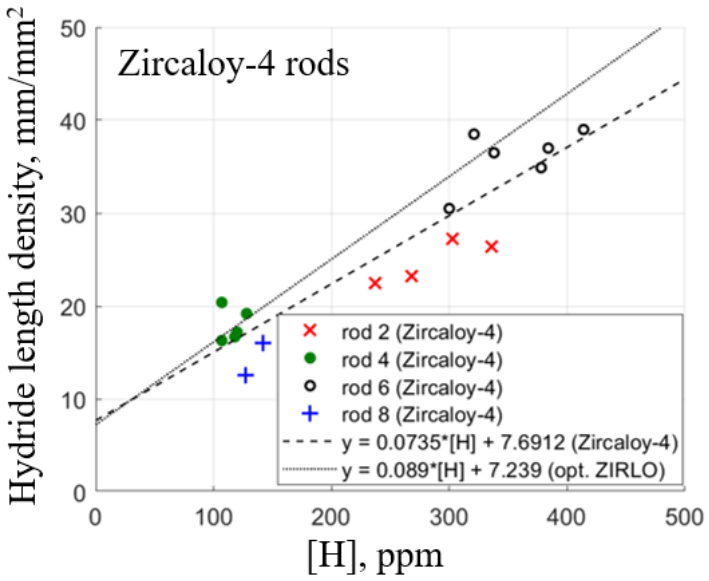

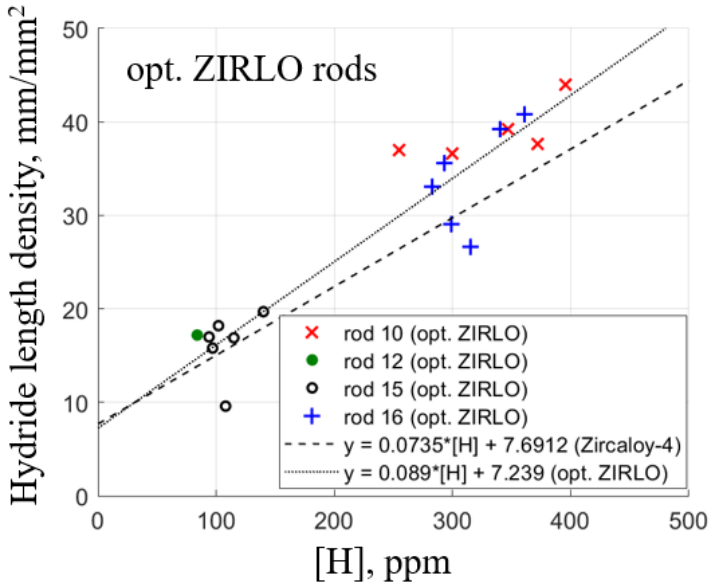

The hydride length density is almost proportional to the hydrogen content and is independent of the alloy type

SPIZWURZ bundle test results
hydride morphology in duplex alloy DX-D4

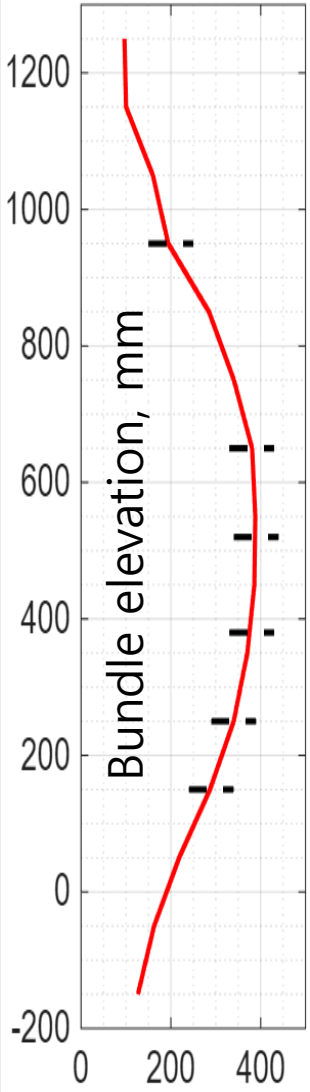

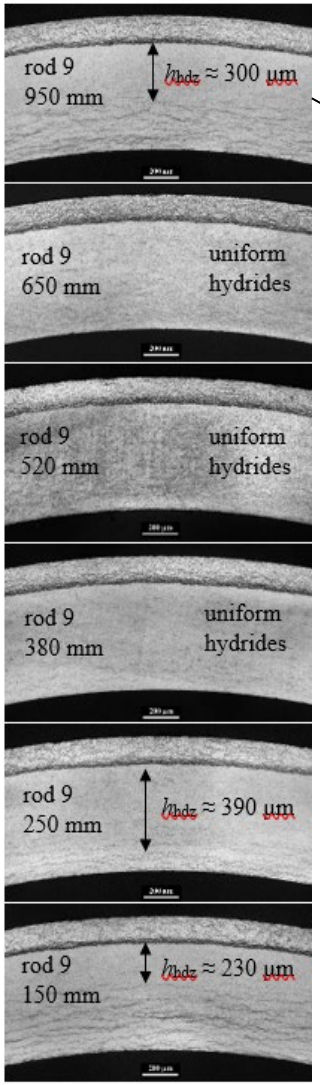

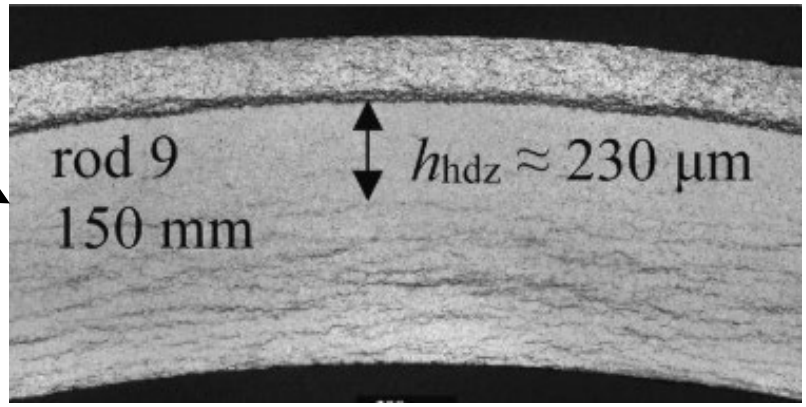

Dominant trend: redistribution of hydrogen between the substrate and the liner

The width of the HDZ at the end of the thermocycle can be estimated as:

$$h_{hdz} = 2\lambda \cdot \sqrt{\int_0^t D_H\left(T(\tau)\right) \cdot \mathrm{d}\tau}$$

$$\lambda e^{\lambda^2} \cdot \mathrm{erfc}(\lambda) = \frac{C_{ss} - C_{interface}}{C_{sub,tot} - C_{interface}} \cdot \frac{1}{\sqrt{\pi}}$$

$$\downarrow$$

$$\lambda \approx 0.01 \quad (\text{for } 300 \text{ ppm})$$

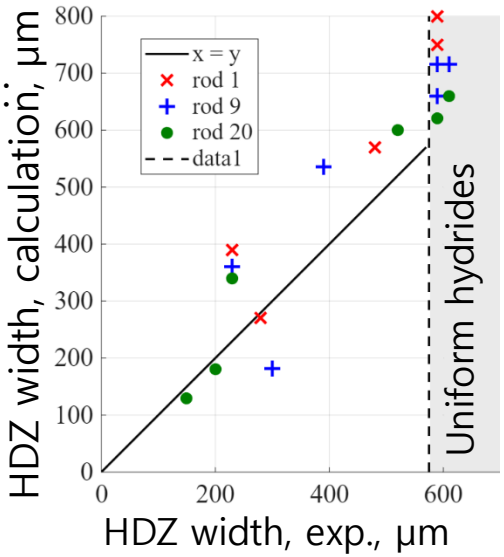

SPIZWURZ bundle test results
hydride morphology "anomalies"

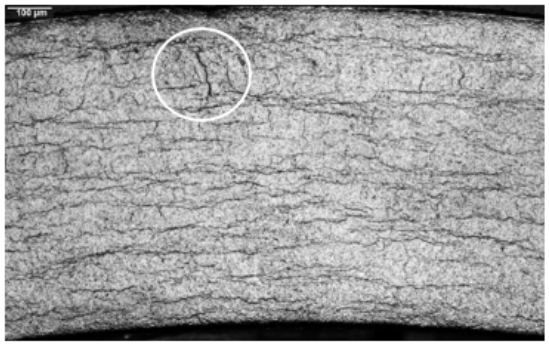

rod 2 (150 mm), RHF = 0.19 (mean)

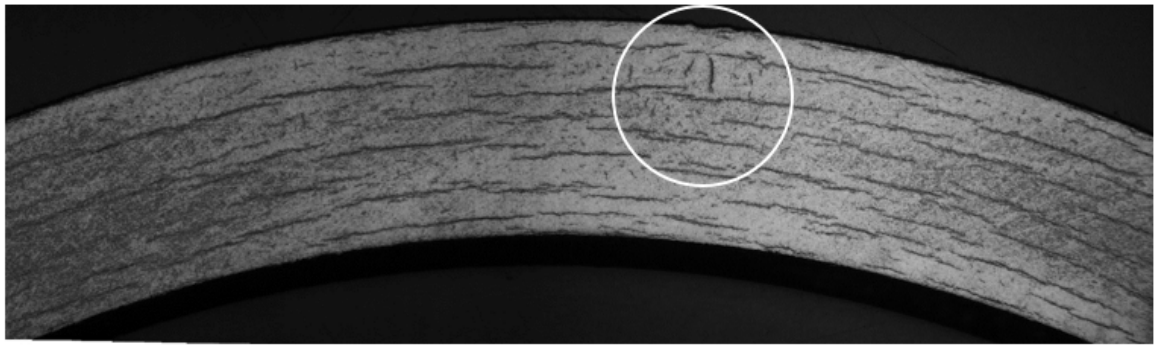

rod 13 (950 mm), RHF = 0.03 (mean)

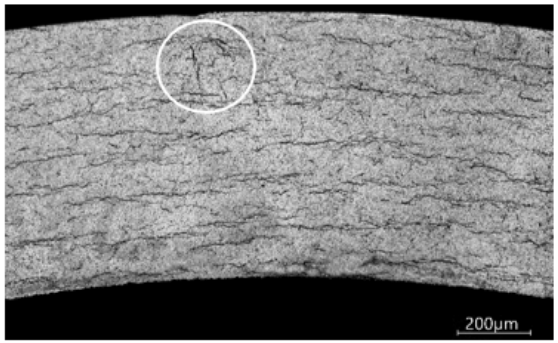

rod 4 (950 mm), RHF = 0.15 (mean)

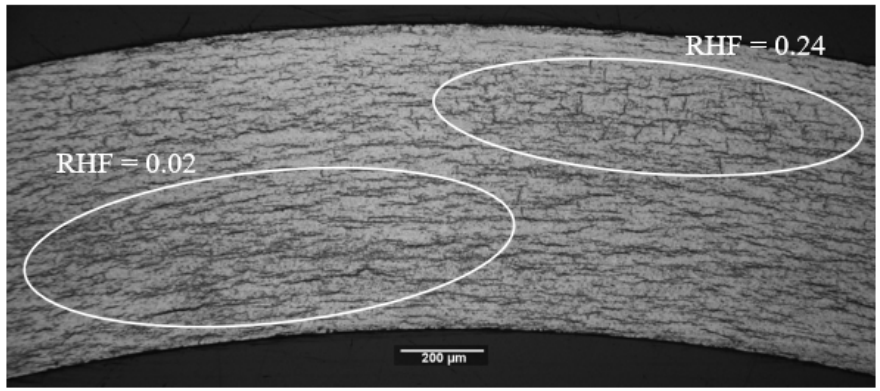

rod 7 (150 mm), RHF = 0.07 (mean)

The total number of tube cross-sections analyzed is of the order of 100

SPIZWURZ bundle simulation
Model 1 description (ODE-based)

Karlsruhe Institute of Technology

Ordinary differential equation (ODE) system for precipitation:

Cumulative radial hydride fraction

Nucleation of hydrides is according to the classical heterogeneous nucleation approximation

$$\begin{cases} \dfrac{\mathrm{d}C_s}{\mathrm{d}t} = \dfrac{C_s - C_e}{\tau_0}, \qquad \tau_0 = \dfrac{\Delta^2}{\alpha^2 D_{\mathrm{H}}} \\ \dfrac{\mathrm{d}\theta}{\mathrm{d}t} = \dfrac{F_r - \theta}{C_h} \cdot \dfrac{\mathrm{d}C_h}{\mathrm{d}t}, \quad C_h = C_{tot} - C_s \\ \dfrac{\mathrm{d}n_r}{\mathrm{d}t} = \displaystyle\int_{E_{d,\min}}^{E_{d,\max}} n \cdot g(E_d) \cdot Z(E_d) \cdot j_n \cdot F_r \cdot \exp\left(-\Delta G(E_d)/kT\right) \cdot \mathrm{d}E_d \\ \dfrac{\mathrm{d}n_t}{\mathrm{d}t} = \displaystyle\int_{E_{d,\min}}^{E_{d,\max}} n \cdot g(E_d) \cdot Z(E_d) \cdot j_n \cdot (1 - F_r) \cdot \exp\left(-\Delta G(E_d)/kT\right) \cdot \mathrm{d}E_d \end{cases}$$

Instantaneous radial hydride fraction

$$F_r = \frac{1 - f_{\mathrm{tex}}}{1 + f_0 \cdot \exp\left(-\sigma \cdot \Omega_0 / kT\right)} + f_{\mathrm{tex}}$$

Gibbs energy change

$$\Delta G(E_d) = \Omega_n \left(g_m - \Delta\mu / v_{\mathrm{H}}\right) + S_n \gamma - E_d$$

Ordinary differential equation (ODE) system for dissolution:

$$\begin{cases} \dfrac{\mathrm{d}C_s}{\mathrm{d}t} = \dfrac{C_s - C_e}{\tau_0} \\ \dfrac{\mathrm{d}\theta}{\mathrm{d}t} = 0 \\ \dfrac{\mathrm{d}n_{r,t}}{\mathrm{d}t} = 0 \end{cases}$$

[1] M. Kolesnik *et al., Comp. Mater. Sci.* 189 (2021) 110260, DOI: 10.1016/j.commatsci.2020.110260

SPIZWURZ bundle simulation
Model 1, simulation results

Rods 2, 4, 6 and 8 (Zircaloy-4):
located symmetrically within the bundle and have all possible combinations of hydrogen content (100 and 300 ppm) and internal pressure (106 and 146 bar)

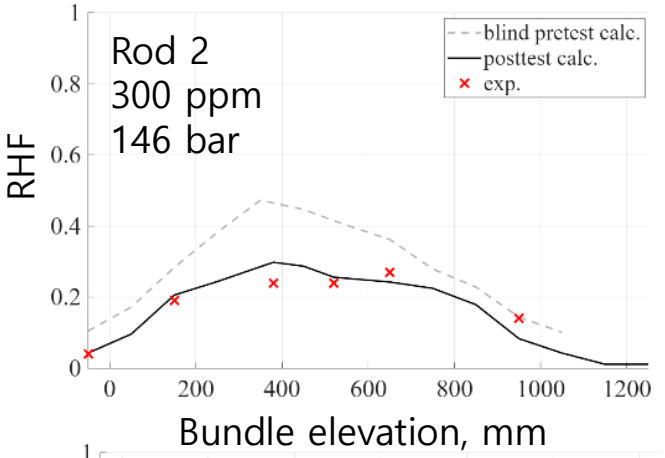

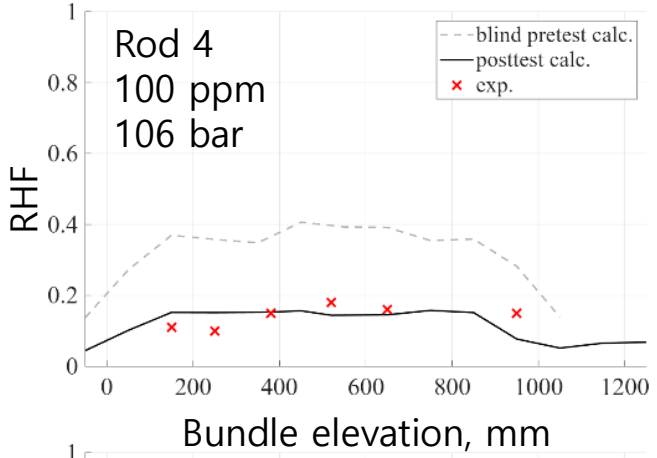

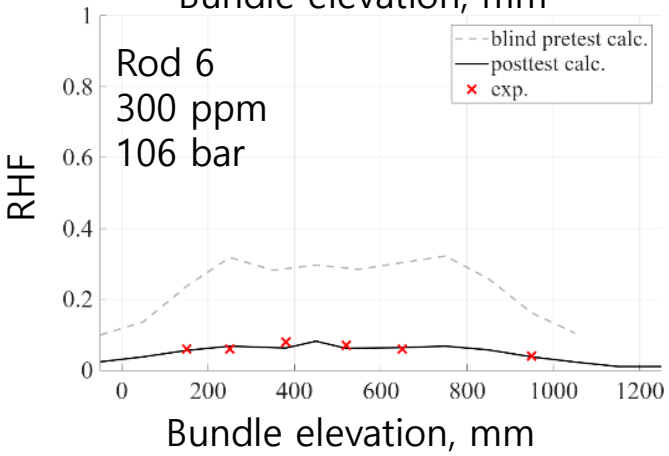

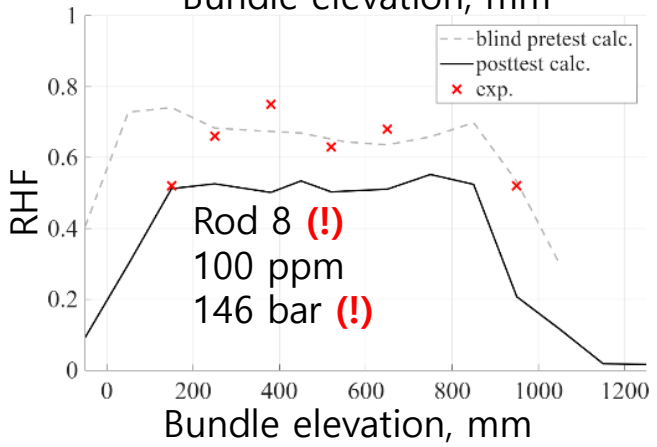

The difference in pre- and post-simulations originates from:
(i) the actual hydrogen concentration and (ii) the datasets used to fit the model parameters.

SPIZWURZ bundle simulation
Model 1, simulation results

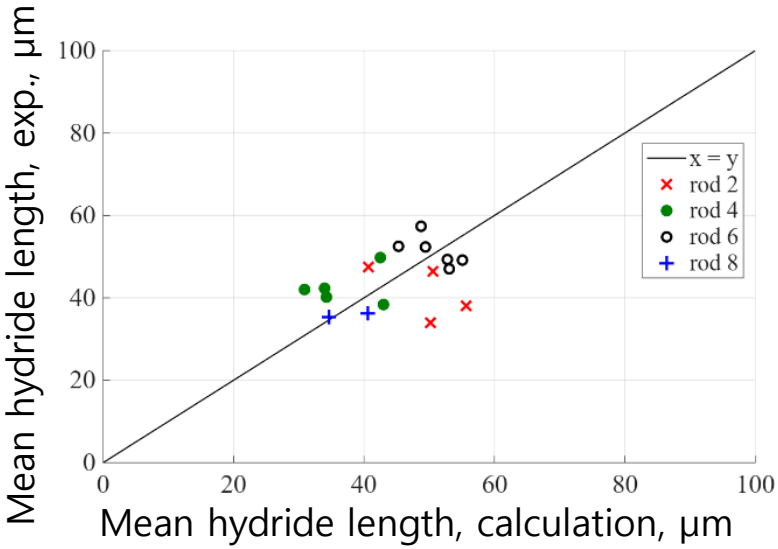

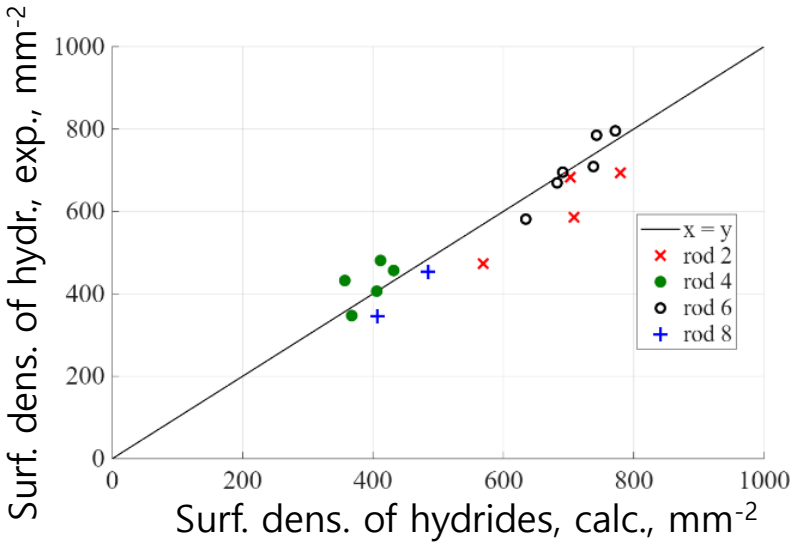

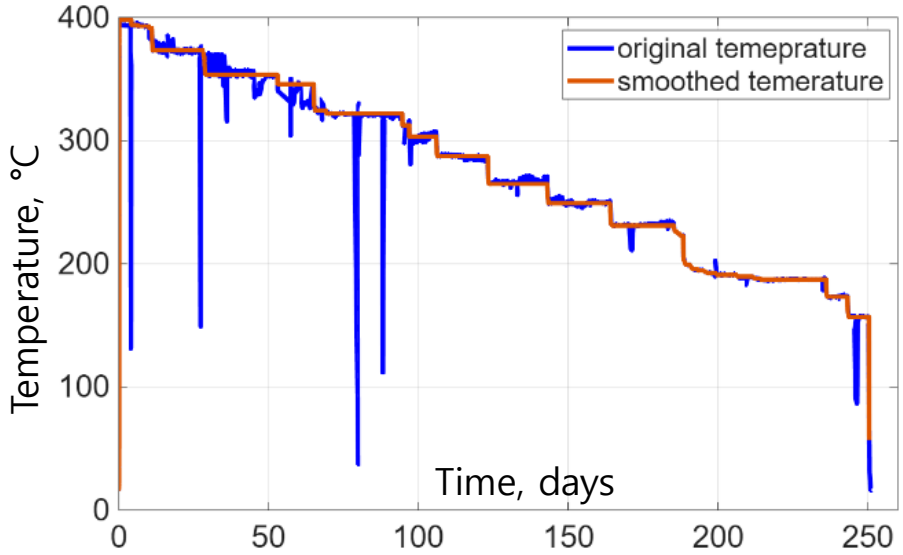

SPIZWURZ bundle simulation
Model 2 description (MORPHYD module)

Nucleation and growth of hydrides

- disk-shaped hydrides
- pre-defined nucleation sites
- classical nucleation theory
- diffusional growth
- competition of neighboring hydrides for the hydrogen in solid solution

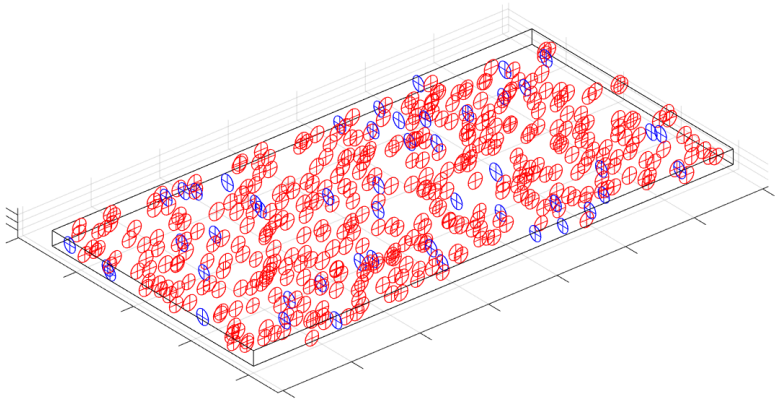

Cross-section analysis

- morphology analysis as with experimental cross-sections
- any hydride morphology metric
- statistical analysis of metrics

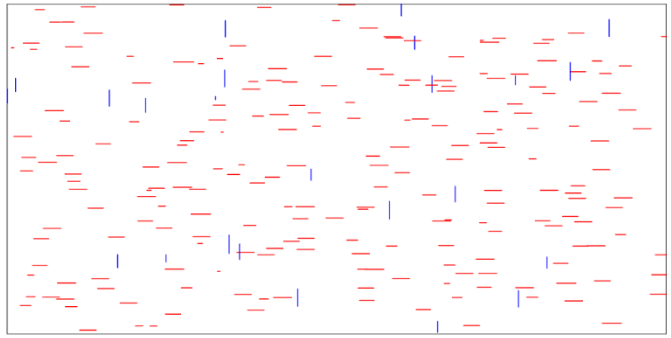

Current limitations of the MORPHYD module:

(i) precipitation only (no dissolution), (ii) valid for small hydrides

[1] M. Kolesnik and T. Aliev, *Phys. of Met. and Metal.* 104 (2023) 1414-1425, DOI: 10.1134/S0031918X22602074
[2] T. Aliev and M. Kolesnik, *Let. on Mater.* 13 (2023) 143-148, DOI: 10.22226/2410-3535-2023-2-143-148

SPIZWURZ bundle simulation
Model 2 (MORPHYD), simulation results

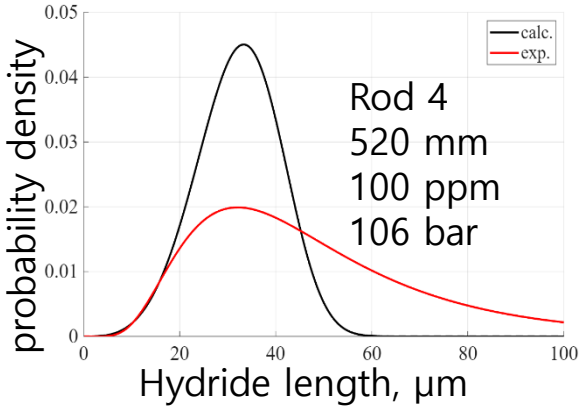

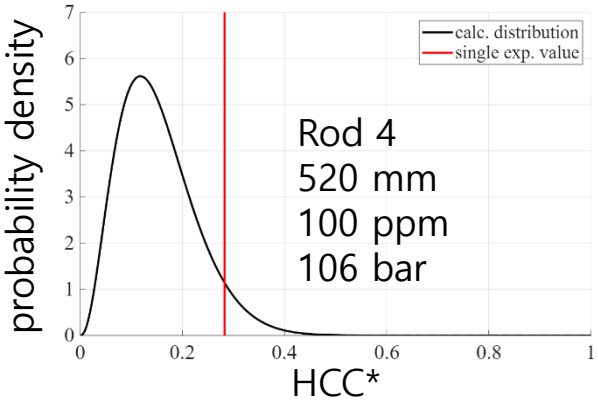

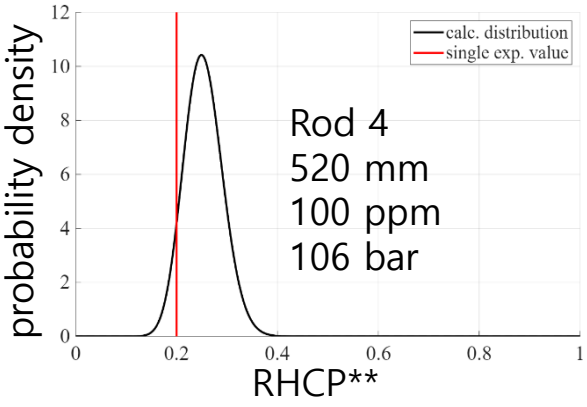

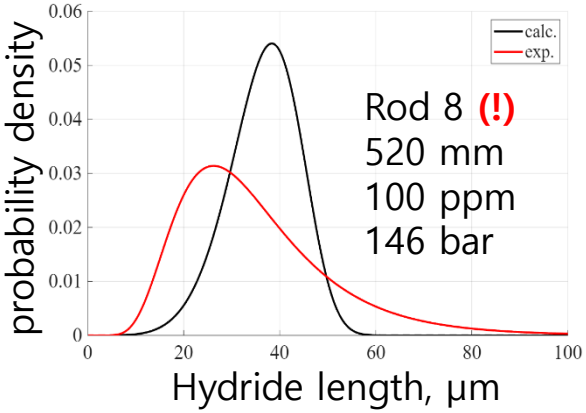

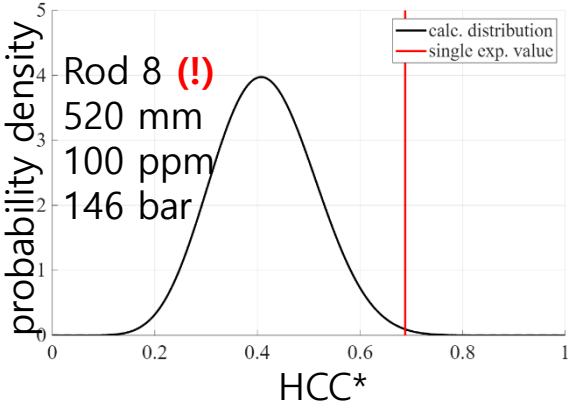

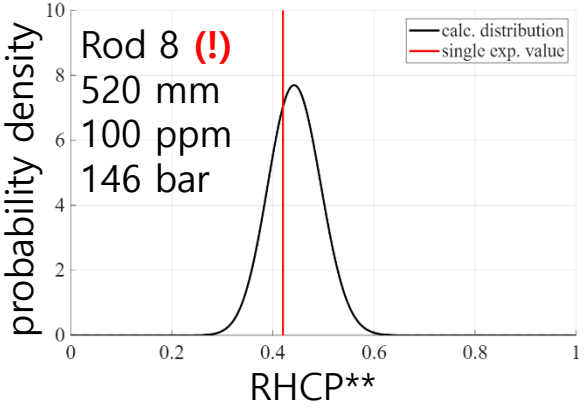

*HCC – the total projection length of hydrides within 110 μm in the radial direction, normalized by thickness
**RHCP – fracture energy estimated from varying crack paths, normalized to the unhydrided sample

Conclusion

- The measured RHF for Zircaloy-4 and opt. ZIRLO is consistent with the published data. Zircaloy-4 samples have a higher stress-induced reorientation than opt. ZIRLO under SPIZWURZ conditions;
- Both the mean and maximum hydride lengths in the opt. ZIRLO are two to three times longer than those in Zircaloy-4. Accordingly, the hydride density in opt. ZIRLO is lower than that in Zircaloy-4;
- The hydride length density is proportional to the total hydrogen concentration and is almost independent on the alloy type;
- In the duplex alloy DX-D4, after heating and slow cooling, hydrogen moves from the substrate to the liner;
- Several samples exhibited local anomalies in hydride morphology. These anomalies could significantly increase the degree of local hydride embrittlement;
- Simulations of various morphological parameters (RHF, HCC, RHCP and hydride length) showed acceptable agreement with the experiment.

Thank you for your attention

https://www.iam.kit.edu/awp/english/163.php

http://quench.forschung.kit.edu/

Aleksandra Rezchikova

GRS

SPIZWURZ Blind Benchmark

Ensuring the integrity of fuel rods during extended interim storage is critical for the safe management of spent nuclear fuel. Due to the challenges associated with conducting experiments under real conditions, associated with the use of irradiated materials and the involved long time-scales, assessing the state of spent fuel relies heavily on simulations. As a result, the development of reliable numerical tools becomes of paramount importance for predicting the behavior of spent fuel during the entire storage period.

Creep and embrittlement due to hydrogen hydride formation are significant degradation mechanisms for the cladding tubes during extended interim storage of spent nuclear fuel. To better understand these phenomena, the joint project SPIZWURZ between KIT and GRS was initiated to investigate the behavior of cladding tubes under storage conditions. The core of this research was the SPIZWURZ bundle experiment, carried out at the LICAS facility by KIT, and specifically designed to examine how slow cooling influences the properties of fuel cladding. The experiment involved a bundle of 21 fuel rod simulators, which were cooled over a period of 250 days with the maximum averaged cooling rate being 0.94°C per day. The maximum temperature reached within the bundle was 405°C at the start of the cooling transient. While the cladding tubes used were non-irradiated, they were pre-loaded with hydrogen to the levels of 100 ppm and 300 ppm to simulate hydrogen concentrations both below and above the solubility limit. Additionally, the experimental setup included three different cladding materials (Zircaloy-4, opt.ZIRLO, Duplex DX D4) and two pressurization levels of 103 and 142 bar, making the experimental matrix highly complex.

This SPIZWURZ bundle experiment also served as the foundation for an international blind benchmark coordinated by GRS, with contributions from 11 participants representing 10 different organizations. Using the temperature and pressure histories from the experiment, along with the estimated initial hydrogen content, participants were asked to calculate the creep strains and the hydrogen behavior. These calculated results were compared against experimentally measured creep and the radial hydride fractions derived from metallographic image analysis.

This blind benchmark provided a valuable opportunity to evaluate the accuracy of different models and computational approaches in predicting the state of the cladding tubes after a slow cooling transient, conditions that are highly relevant to interim storage. The presentation will summarize the results obtained from this evaluation.

SPIZWURZ
Blind Benchmark Results
30th International QUENCH Workshop

Aleksandra Rezchikova, 16th December 2025

SPIZWURZ Blind Benchmark

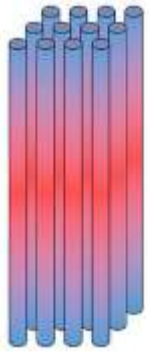

SPIZWURZ
Bundle test

Blind Benchmark

- ✓ Calculations
- ✓ Creep Behavior
- ✓ Hydrogen Behavior
- ▶ Reporting

Open Benchmark

Anticipated start - 2026

SPIZWURZ Blind Benchmark: Participation

11 Participants from
10 Organisations

Gesellschaft für Anlagen- und Reaktorsicherheit (GRS)

Karlsruhe Institute of Technology (KIT)

Axpo Switzerland

Framatome Germany

Paul Scherrer Institute (PSI)

Centro de Investigaciones Energéticas, Medioambientales y Tecnológicas (CIEMAT)

EDF France

ÚJV Řež

Seoul National University (SNU)

Comisión Nacional de Energía Atómica (CNEA)

SPIZWURZ Blind Benchmark

Key factors to consider <u>when comparing rods</u>:

- Rod position inside the bundle
- Variations in hydrogen content
- Pressure evolution throughout the test

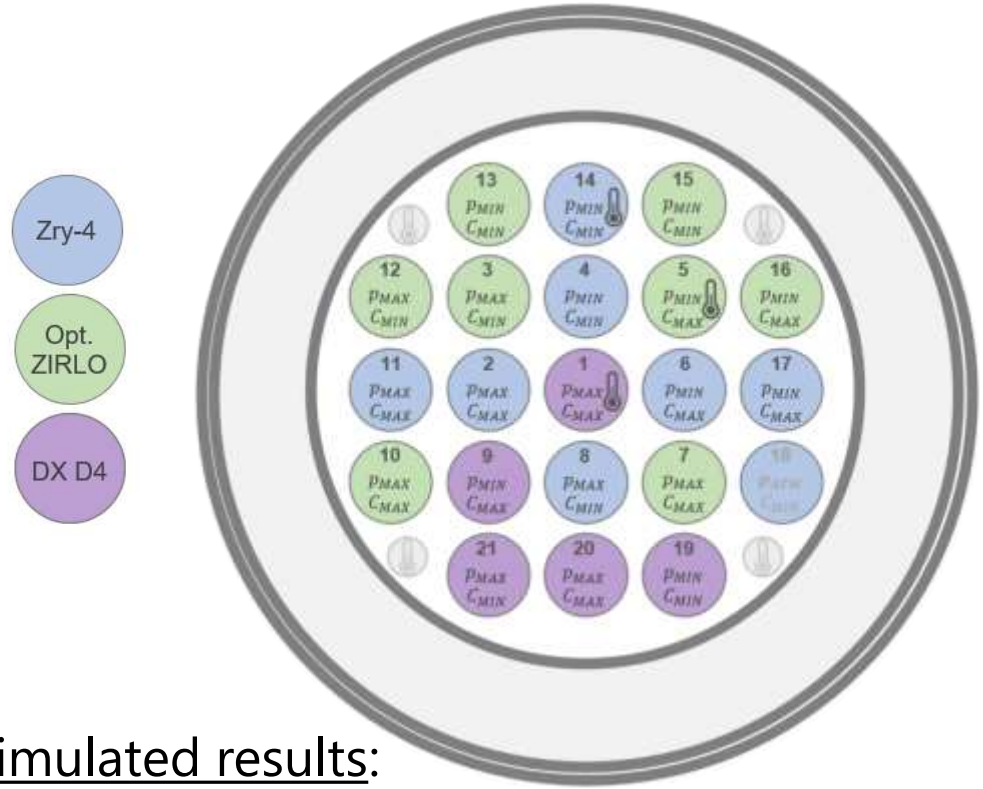

Key considerations <u>when comparing experimental and simulated results</u>:

- Differences in initial hydrogen content
- Influence of pellet–cladding interaction (PCI) — notable in Rods 6, 8, and 12

Zircaloy-4 Creep

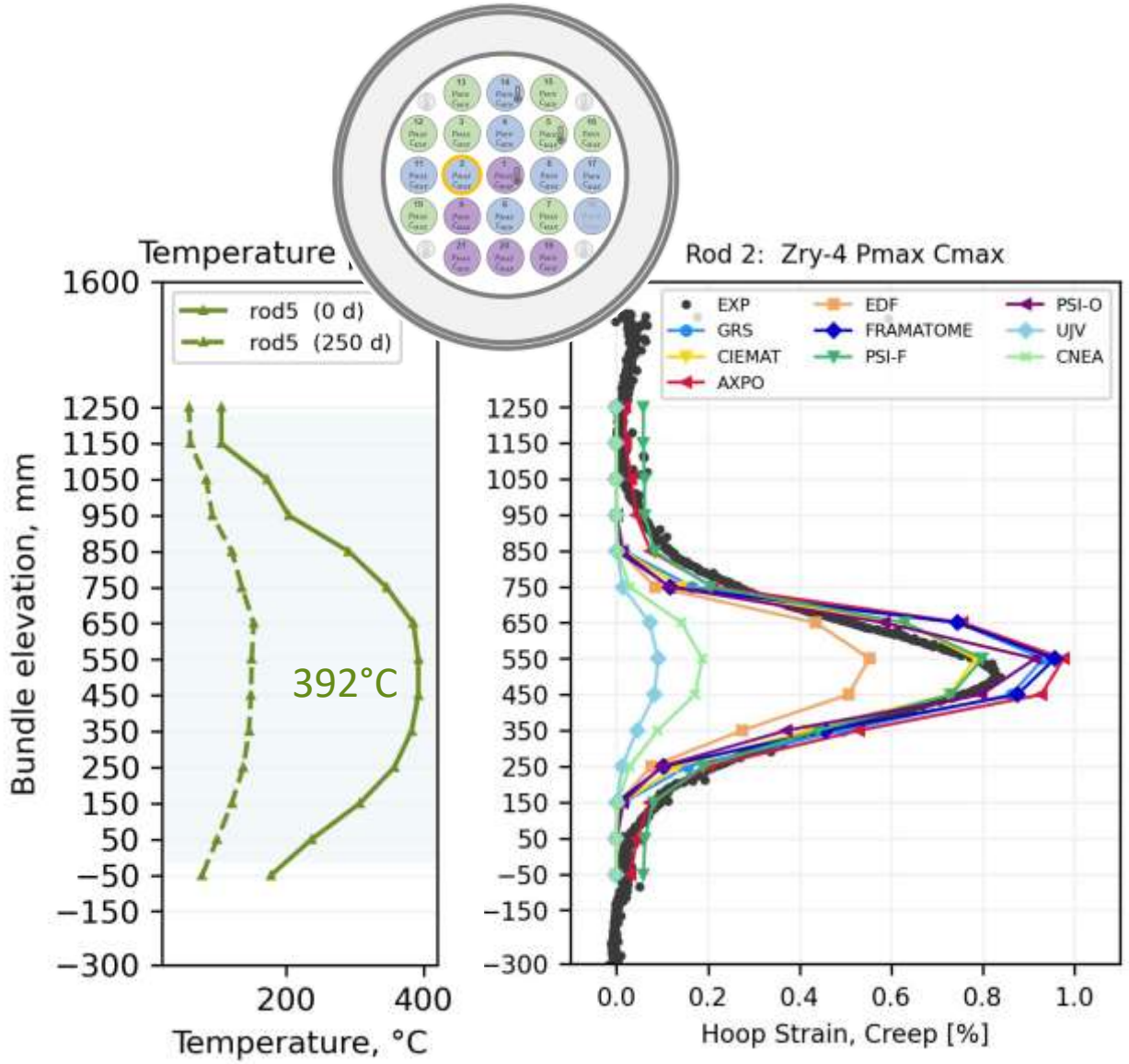

Zircaloy-4 Creep: Effect of Rod Position

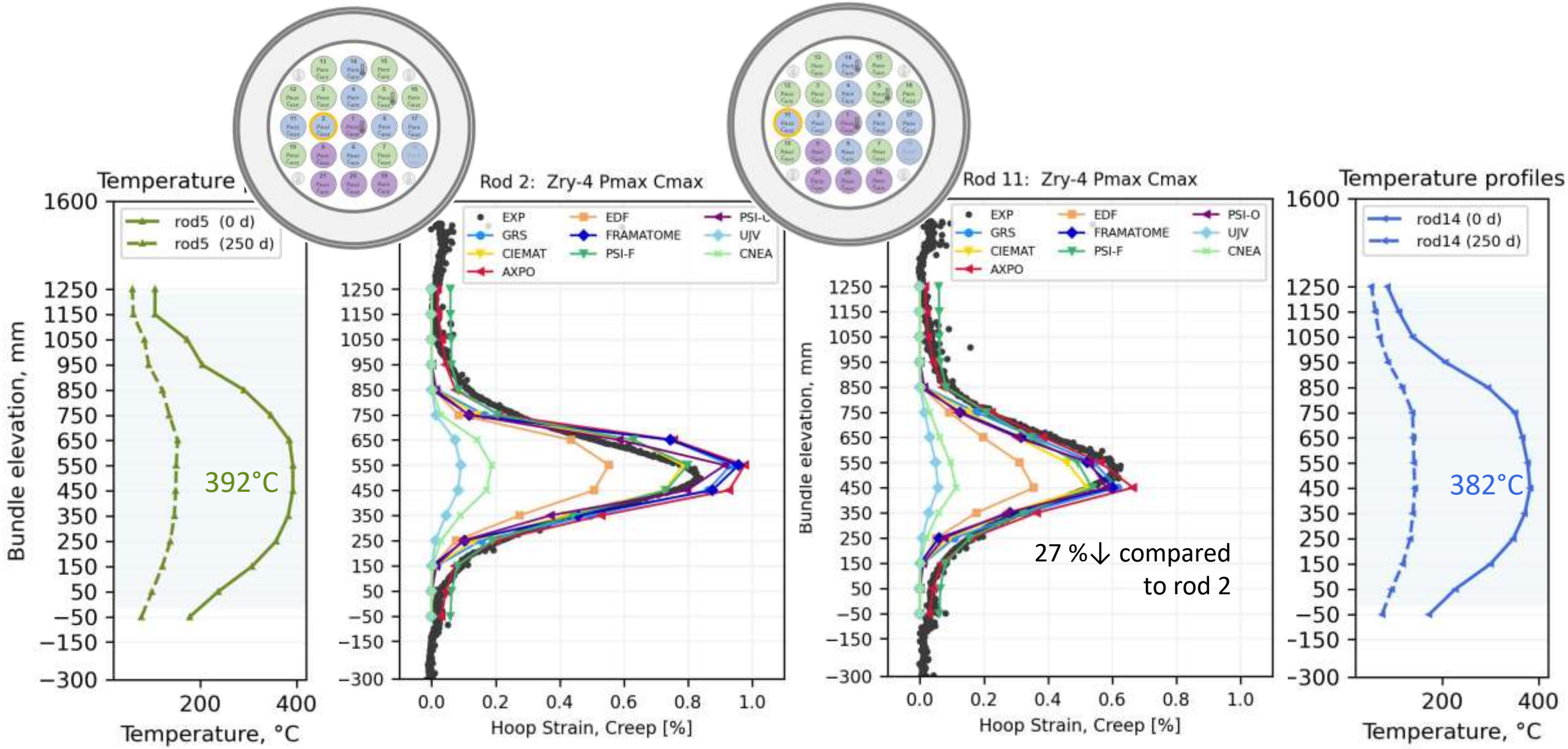

Zircaloy-4 Creep: Pressure Effect

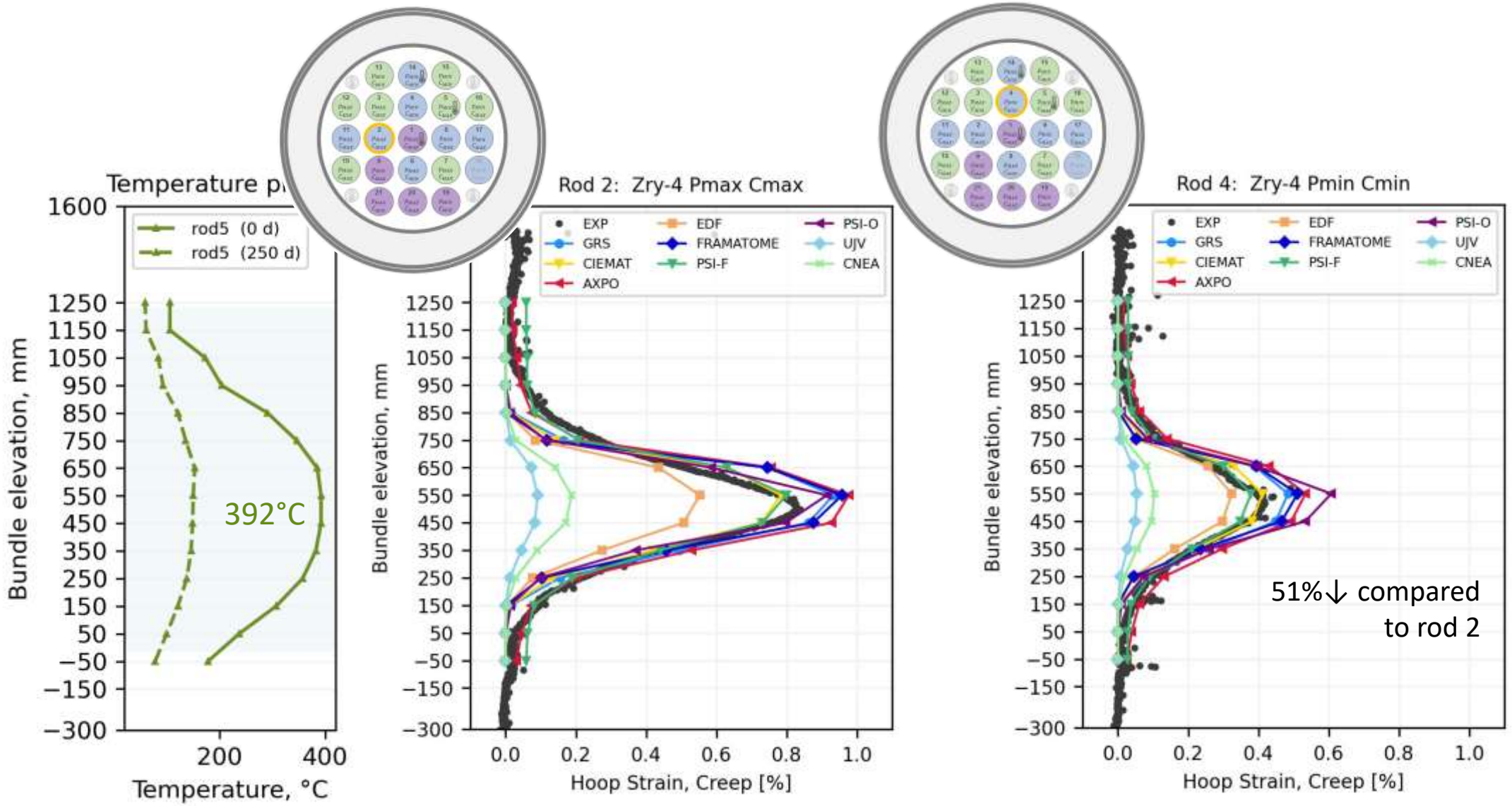

Zircaloy-4 Creep: Pressure Effect

- Most modeling approaches reasonably capture experimentally measured creep strains and their dependency on temperature and pressure
- Creep underprediction in 'colder' zones due to limited experimental data for model input

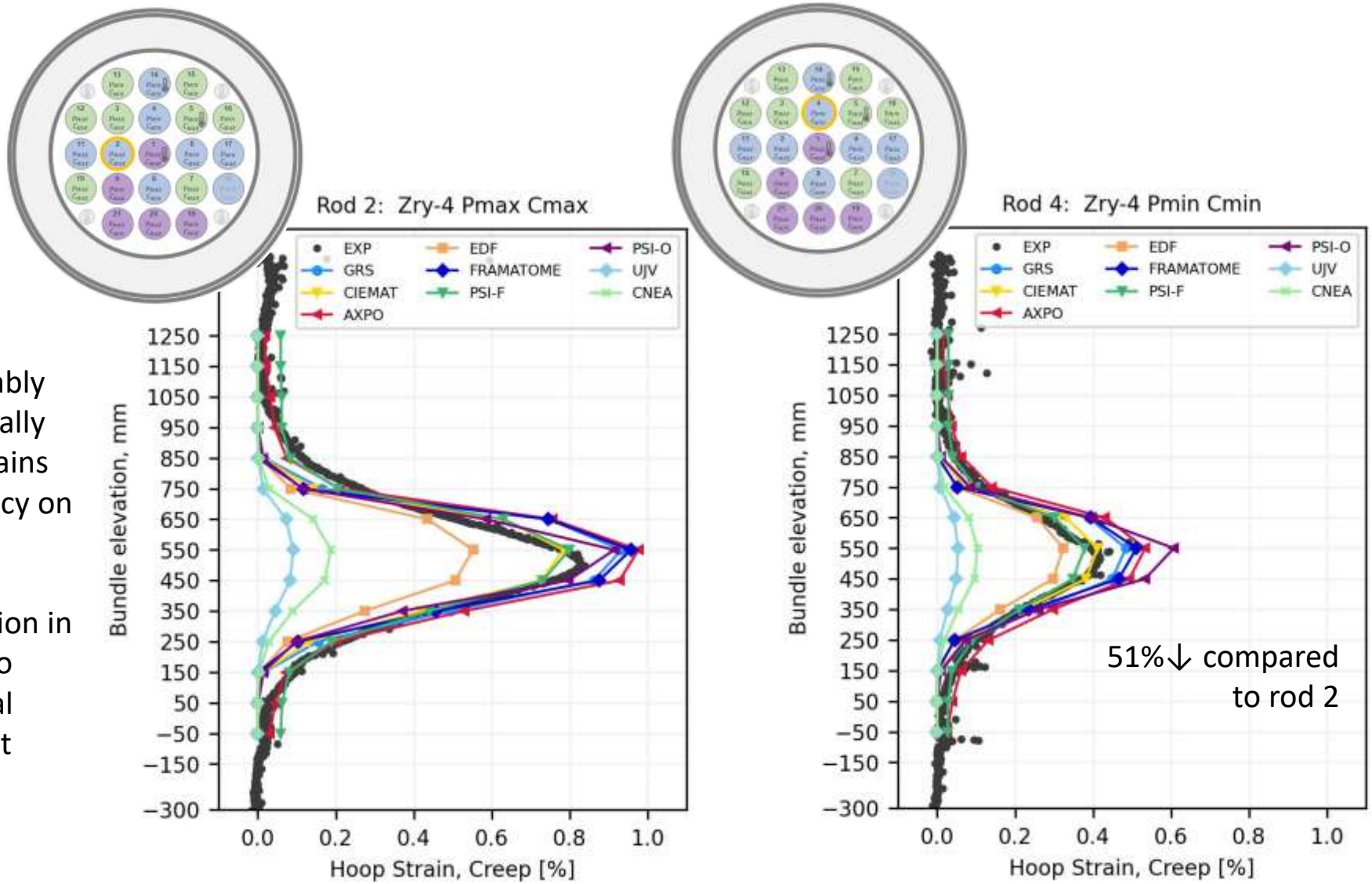

Opt.ZIRLO Creep: Effect of Rod Position

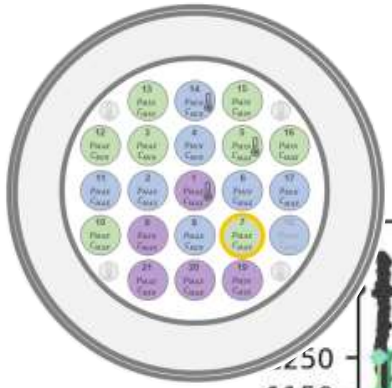

4.15x ↑ compared
to Zry-4 rod 2

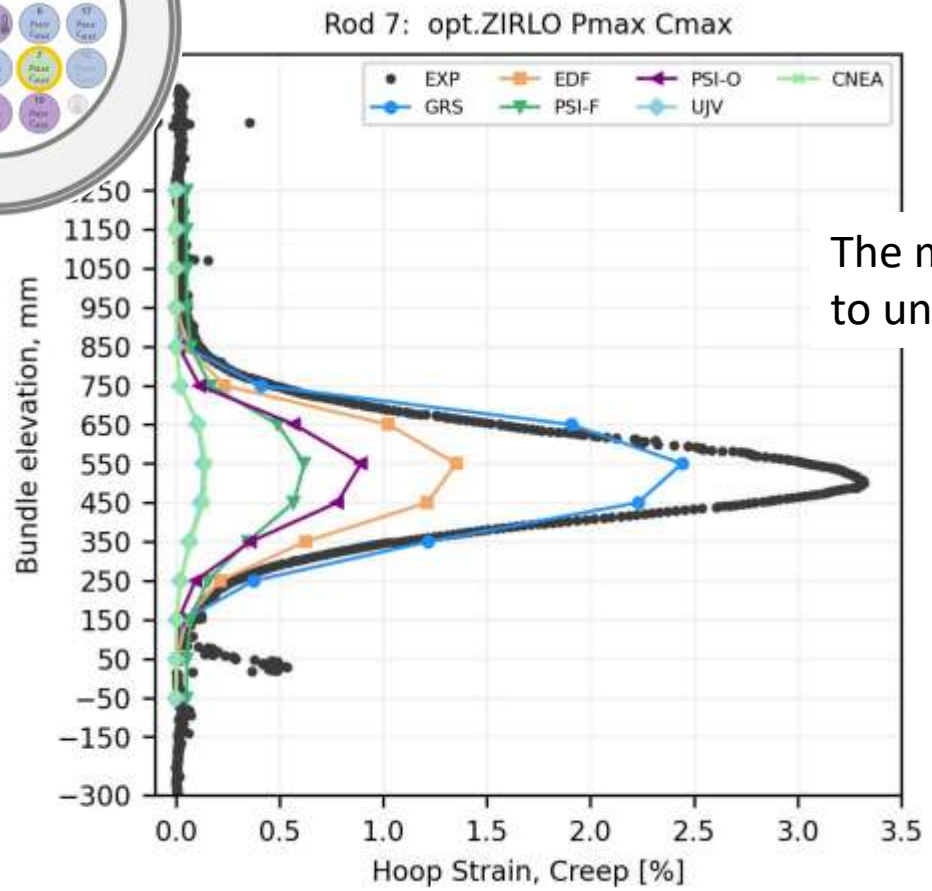

The models based on Zry-4 data tend
to underpredict the creep of Zirlo rods

Opt.ZIRLO Creep: Effect of Rod Position

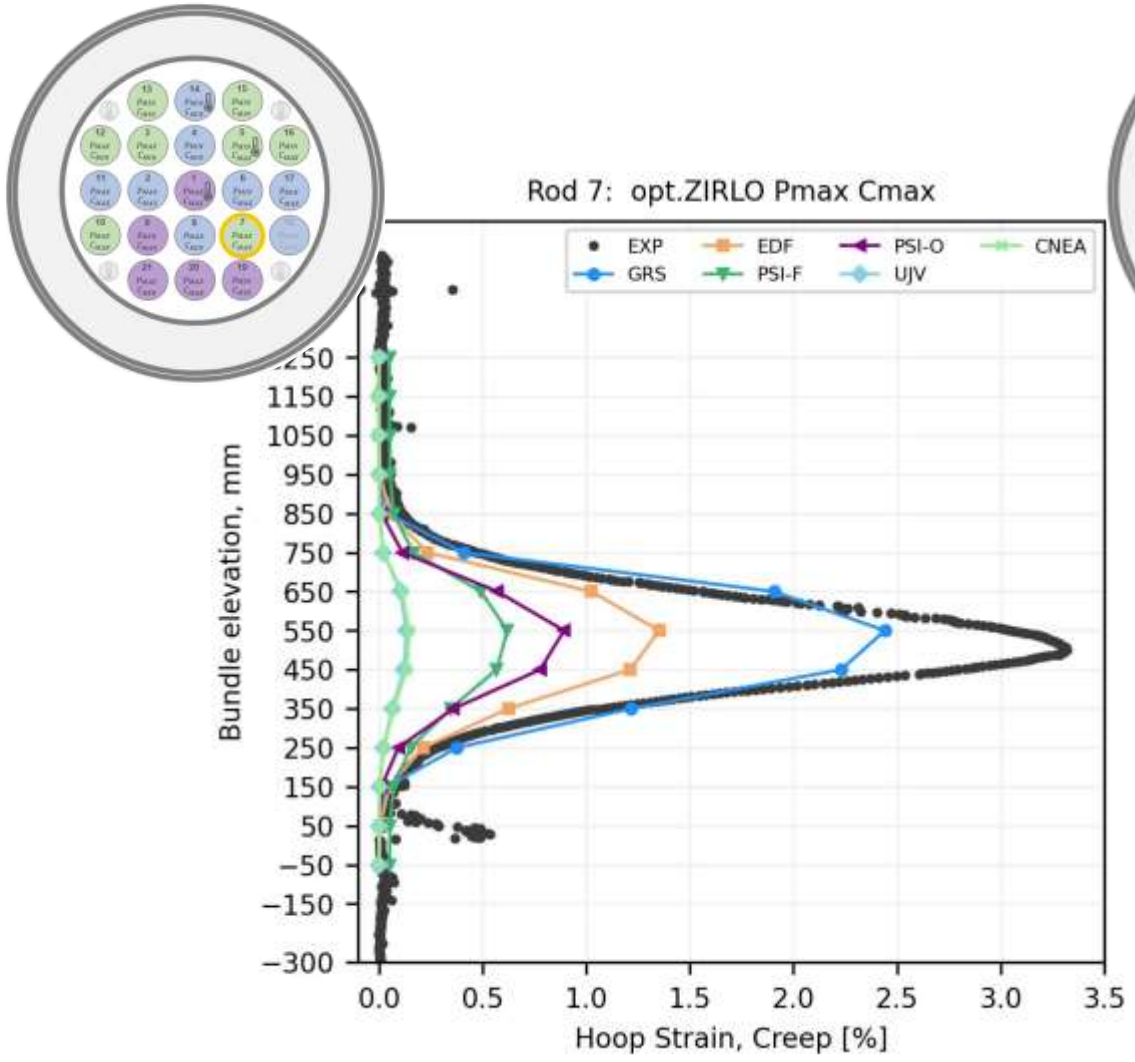

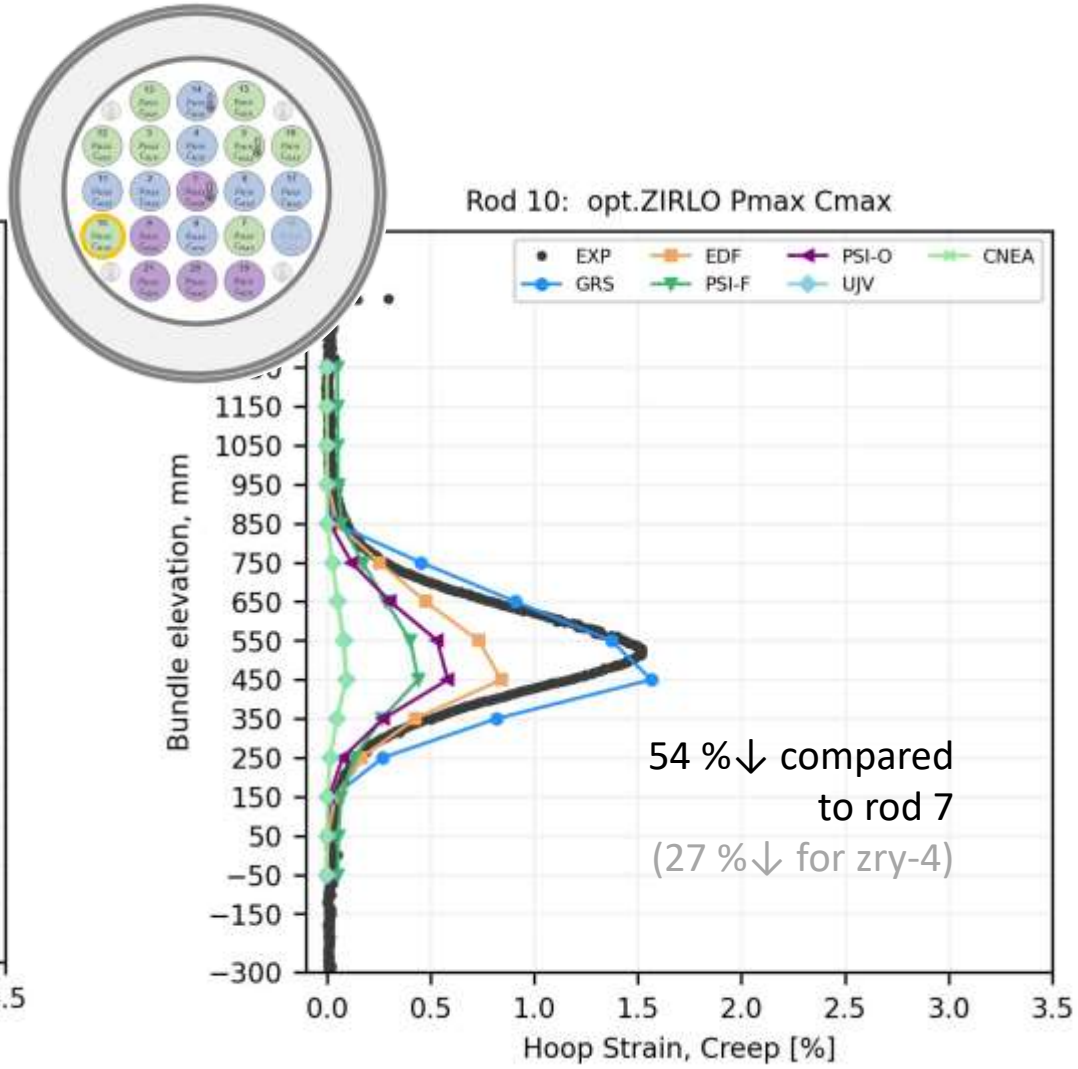

Opt.ZIRLO Creep: Pressure Effect

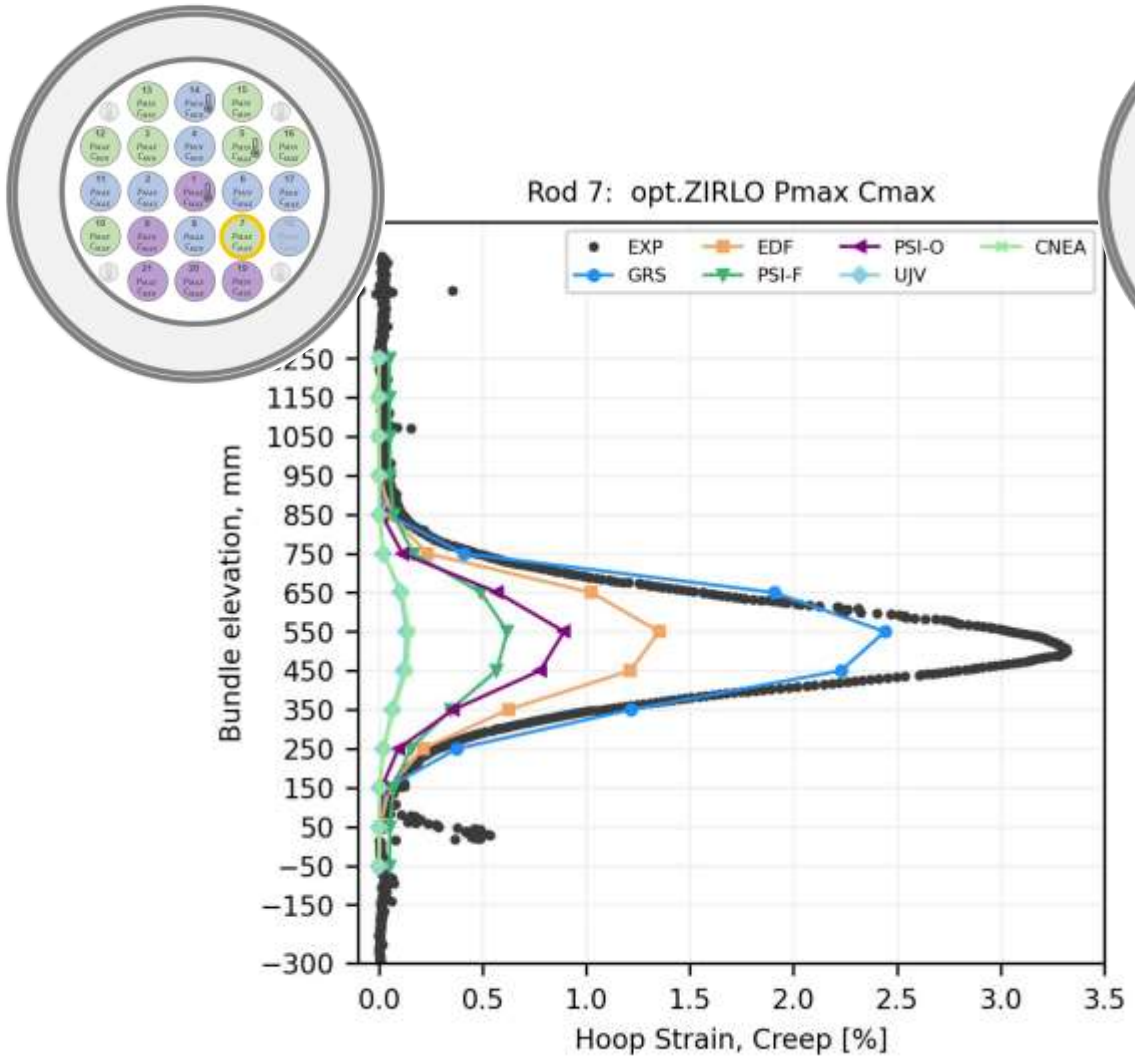

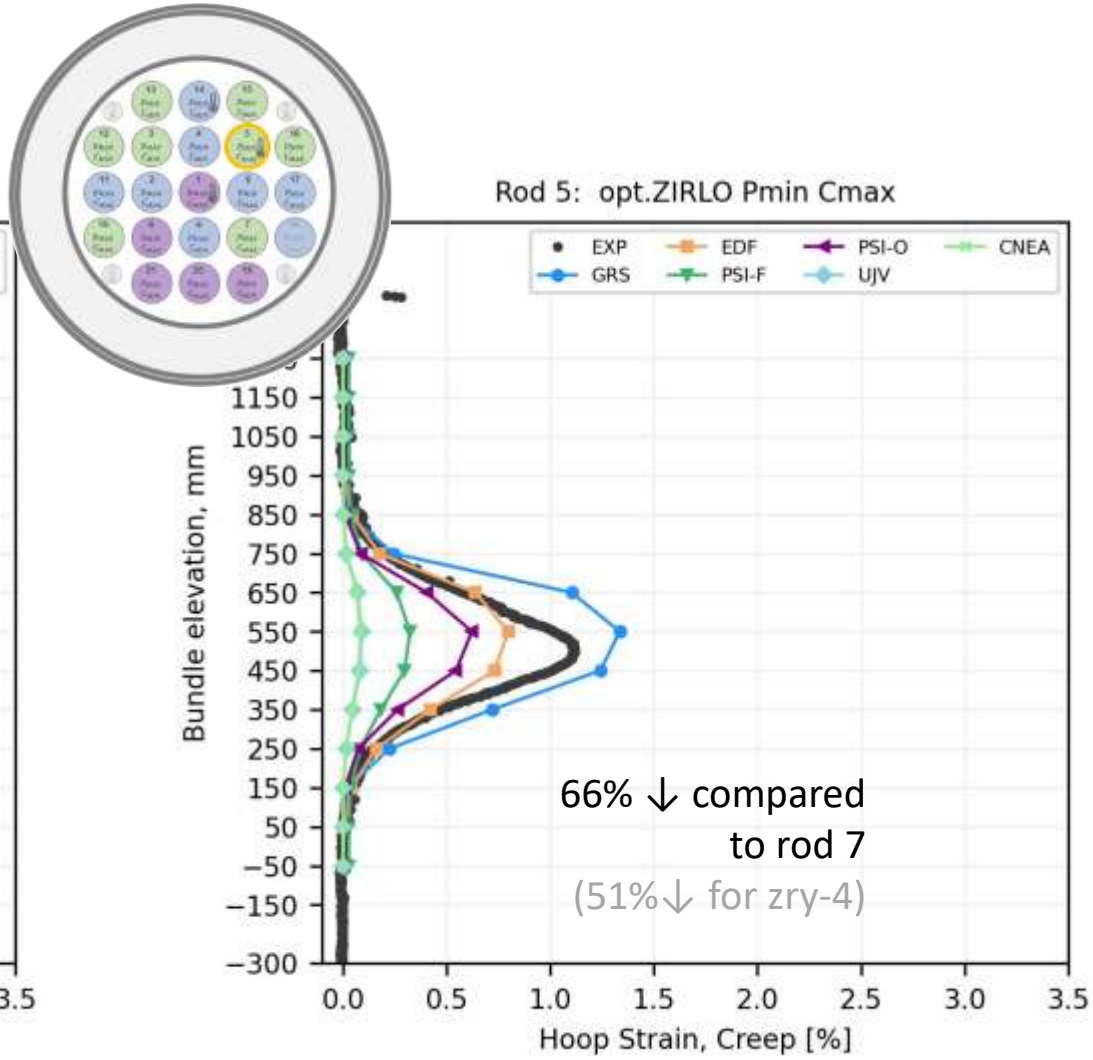

SPIZWURZ Blind Benchmark: Creep

- Existing numerical models capture well Zry-4 and DX D4 creep strains at the considered conditions, but generally underpredict creep strains for optimized ZIRLO.
- Different creep models are required for different cladding materials:
  - Duplex and Zry-4 rods show similar creep behavior, allowing them to be modeled with comparable formulations.
  - Optimized ZIRLO exhibits significantly different creep behavior, with a much stronger sensitivity to pressure and temperature changes.
  - Negligible impact of hydrogen on creep of Zry-4 and DX D4 content. Hydrogen likely promotes creep of opt.ZIRLO at high pressure, but this effect is uncertain due to experimental variability.

Zircaloy-4: Rod 2

91MPa 300wppm Inner

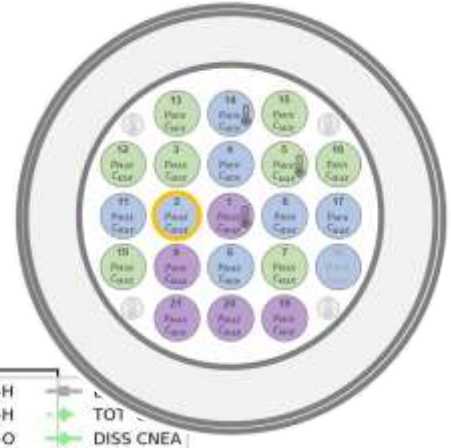

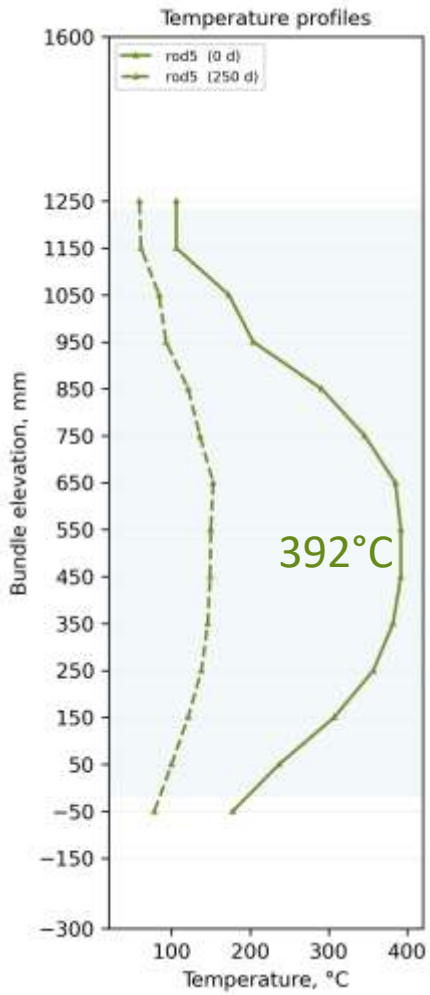

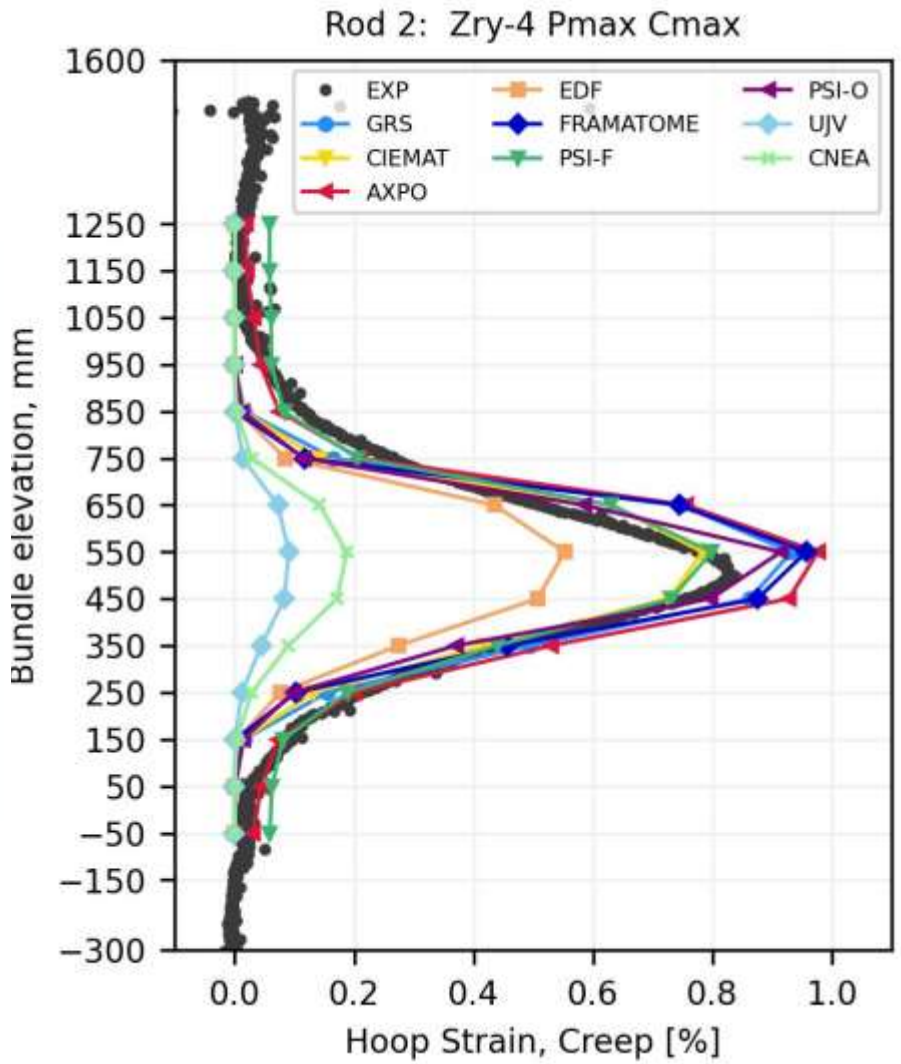

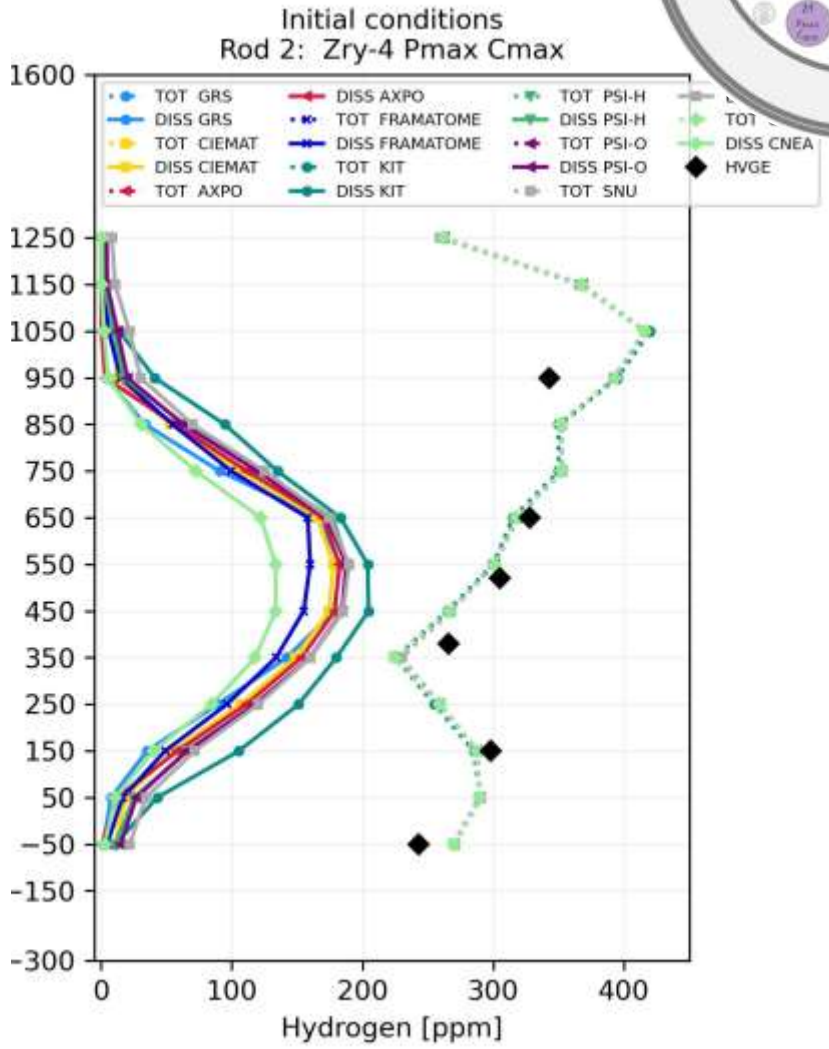

Zircaloy-4: Rod 2

91MPa 300wppm Inner

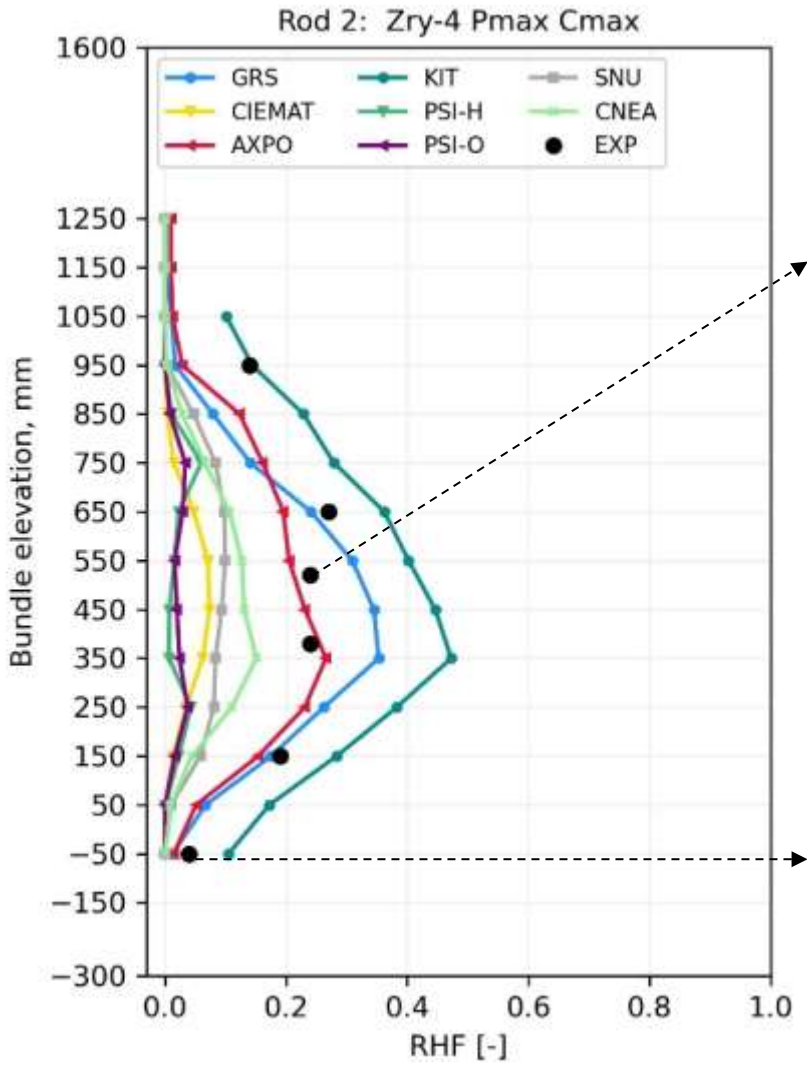

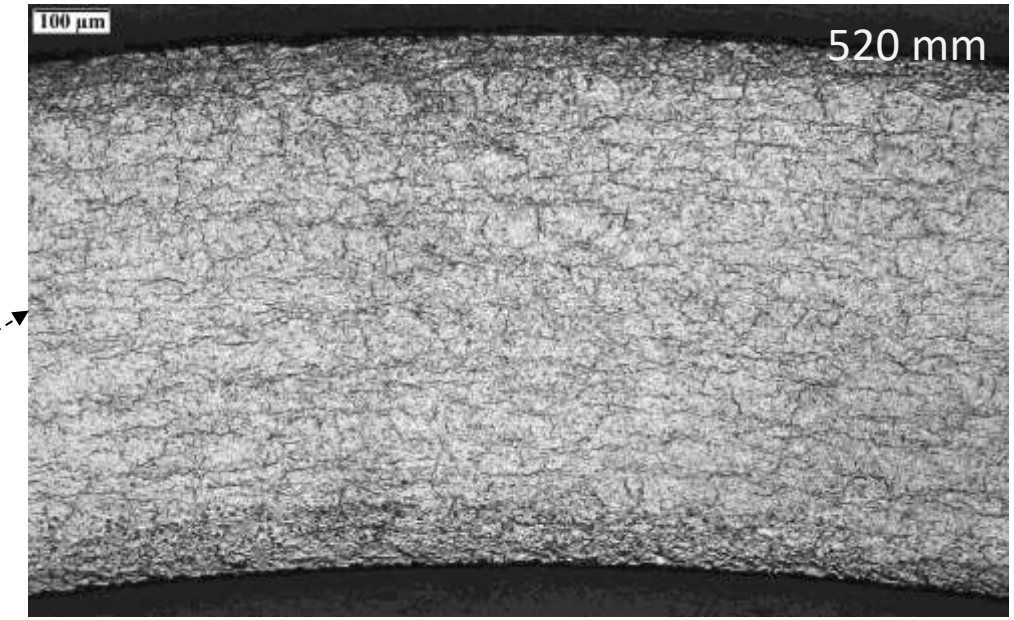

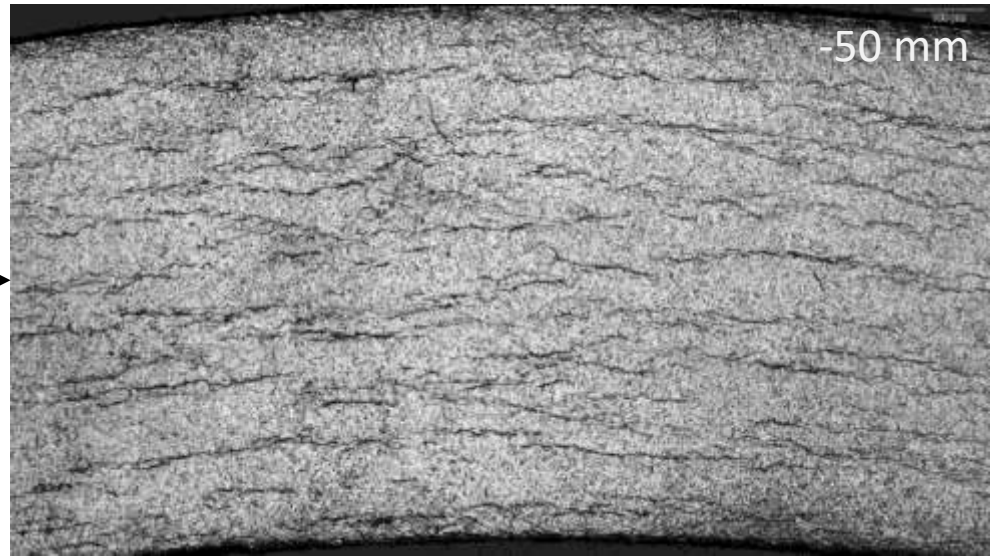

Extracted RHF shows a maximum of 27% at 650 mm

RHF predictions vary broadly from 0 to 50%

350 mm peak linked to lower initial H content

Zircaloy-4: Rod 6

66MPa 300wppm Inner

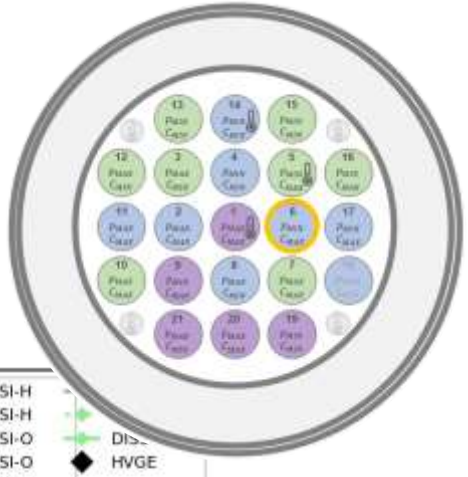

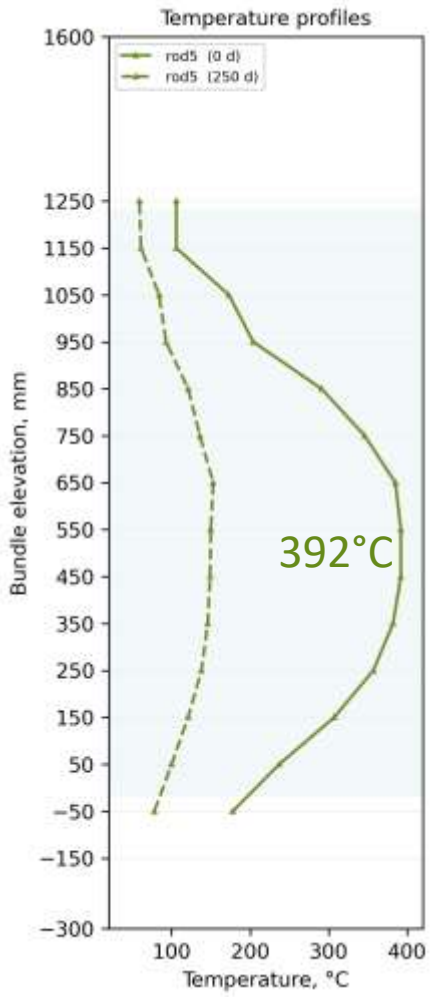

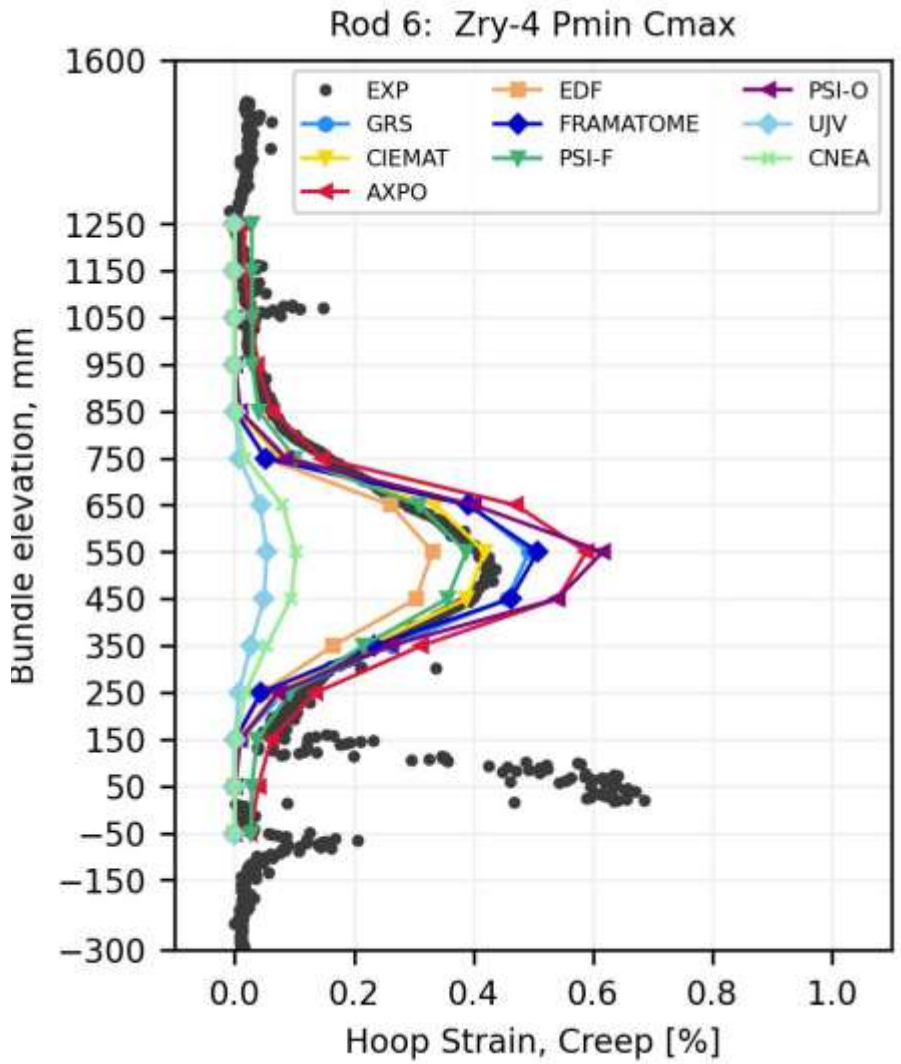

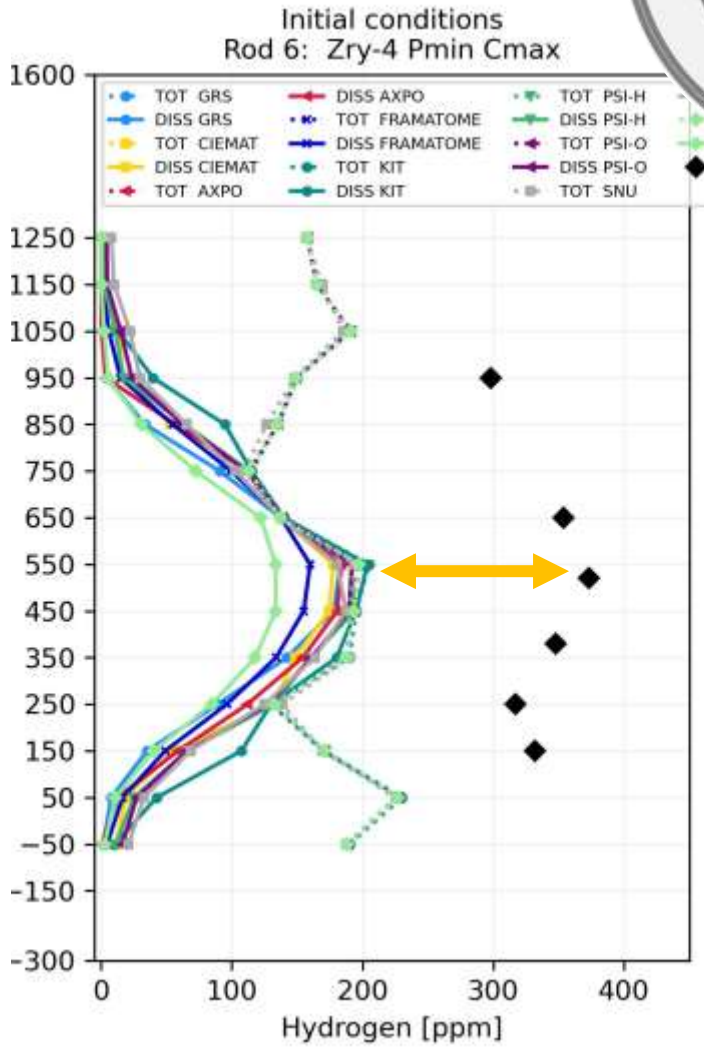

large discrepancy between HVGE and estimated hydrogen concentrations

Zry-4: Initial Hydrogen Concentration VS RHF

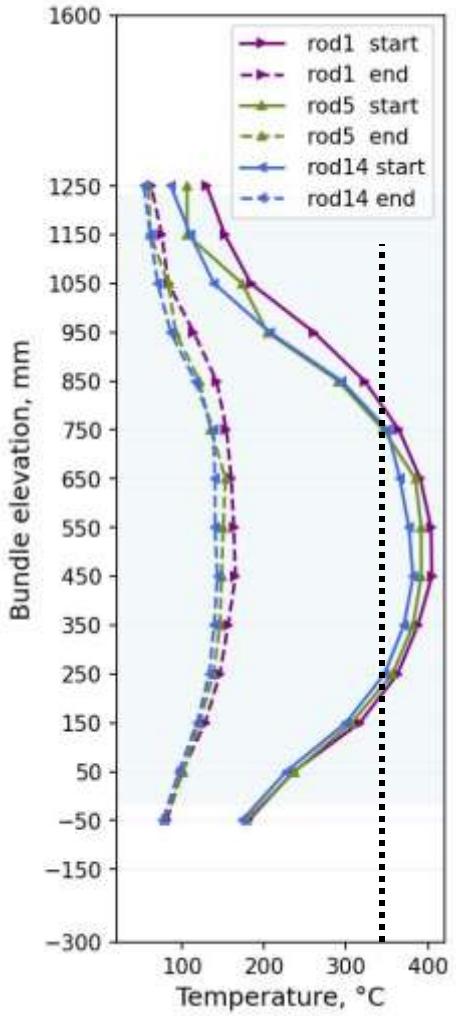

Zones 4-9
Temperatures
above 350°C

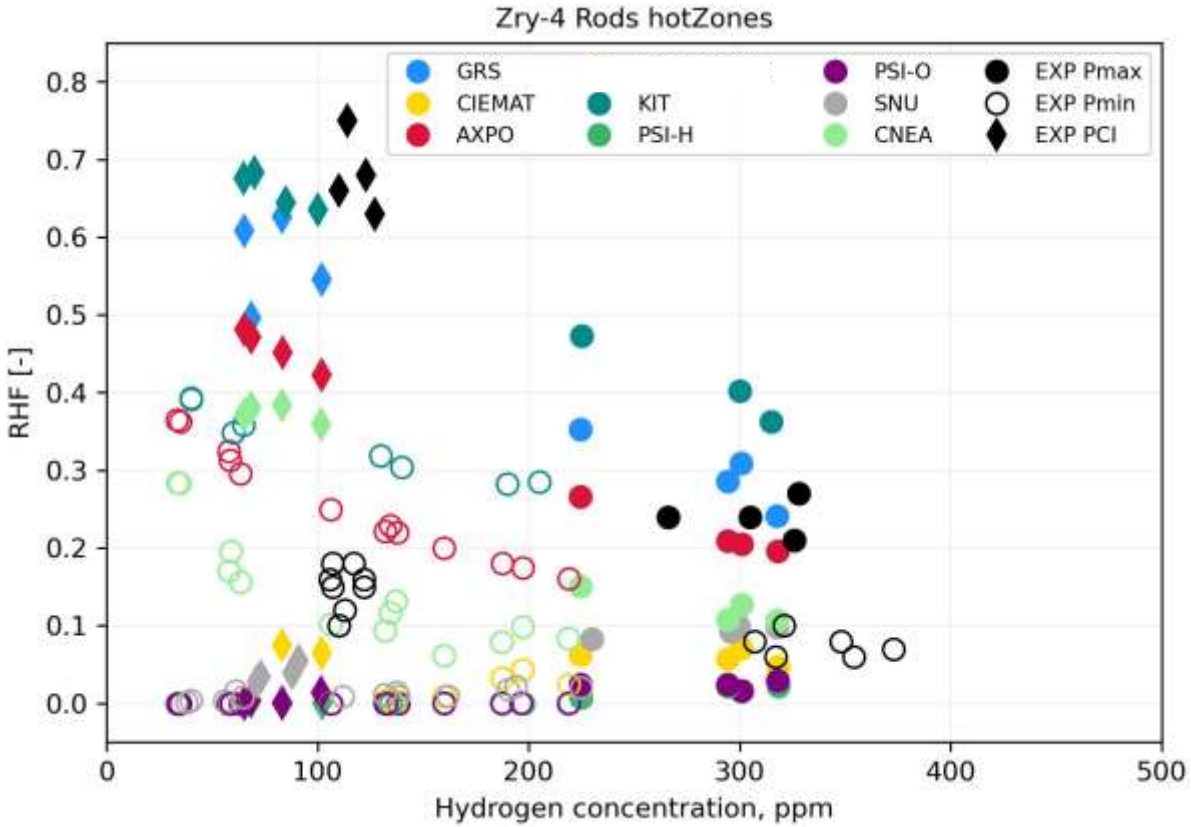

Simulations show a negative correlation between RHF and increasing initial hydrogen concentration, which is supported by experimental results

Zry-4: Initial Hydrogen Concentration VS RHF

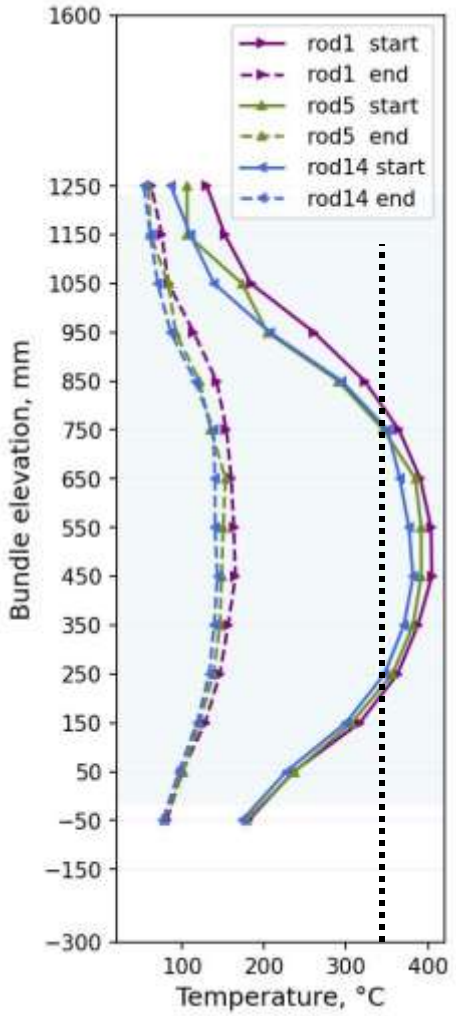

Zones 4-9
Temperatures
above 350°C

$$\left|C_{H,HVGE} - C_{H,ini}\right| < 25\%\ of C_{H,target}$$

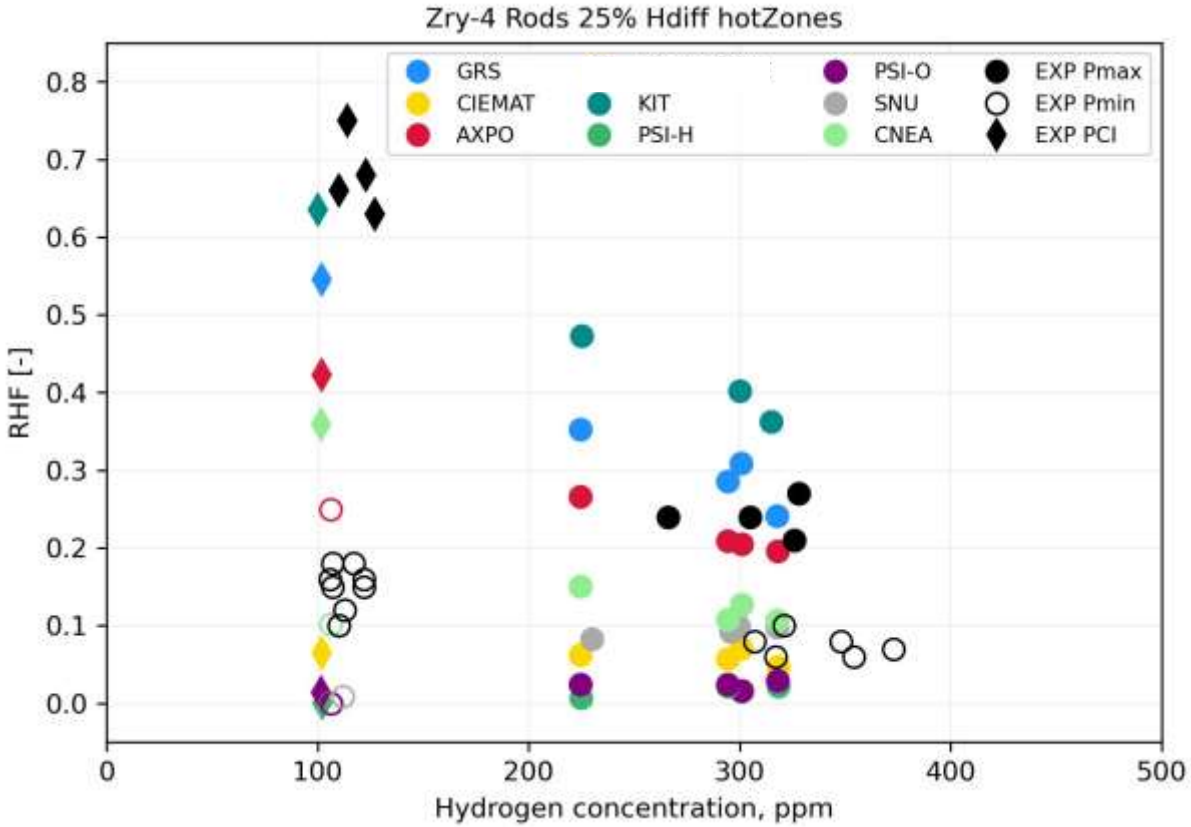

Simulations show a negative correlation between RHF and increasing initial hydrogen concentration, which is supported by experimental results

Zry-4: Starting Temperature VS RHF

$$|C_{H,HVGE} - C_{H,ini}| < 25\% \; of \; C_{H,target}$$

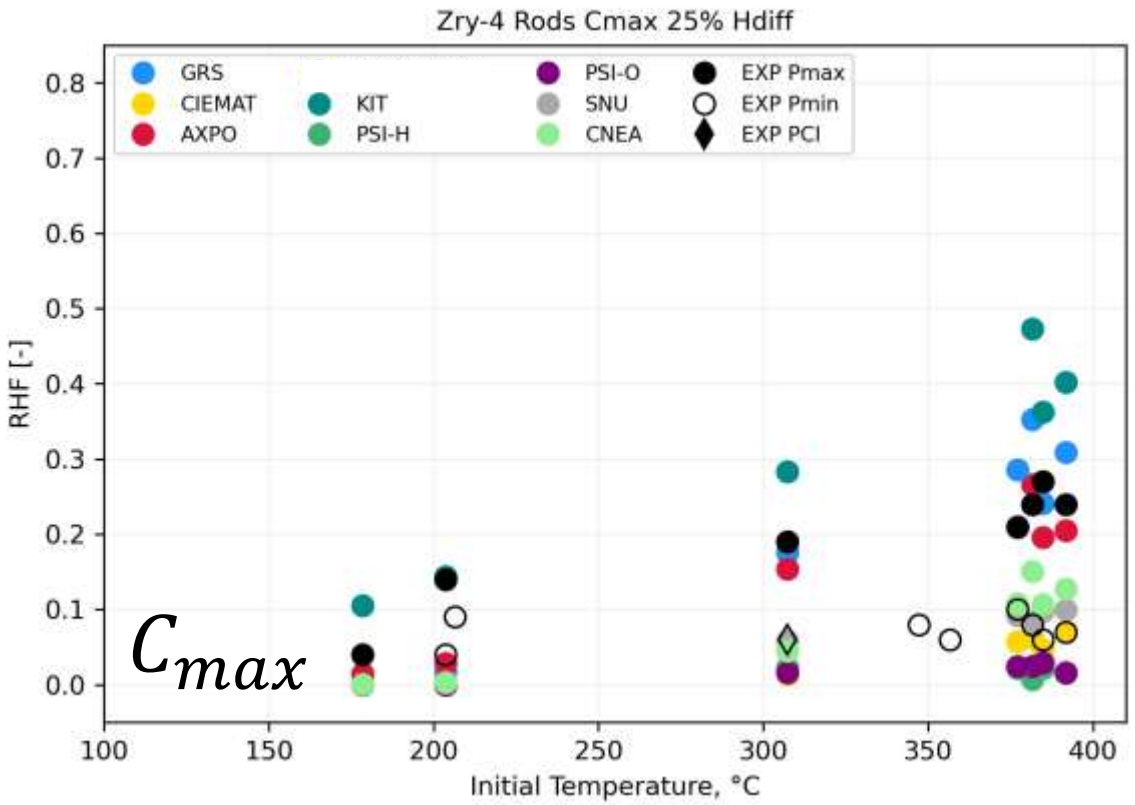

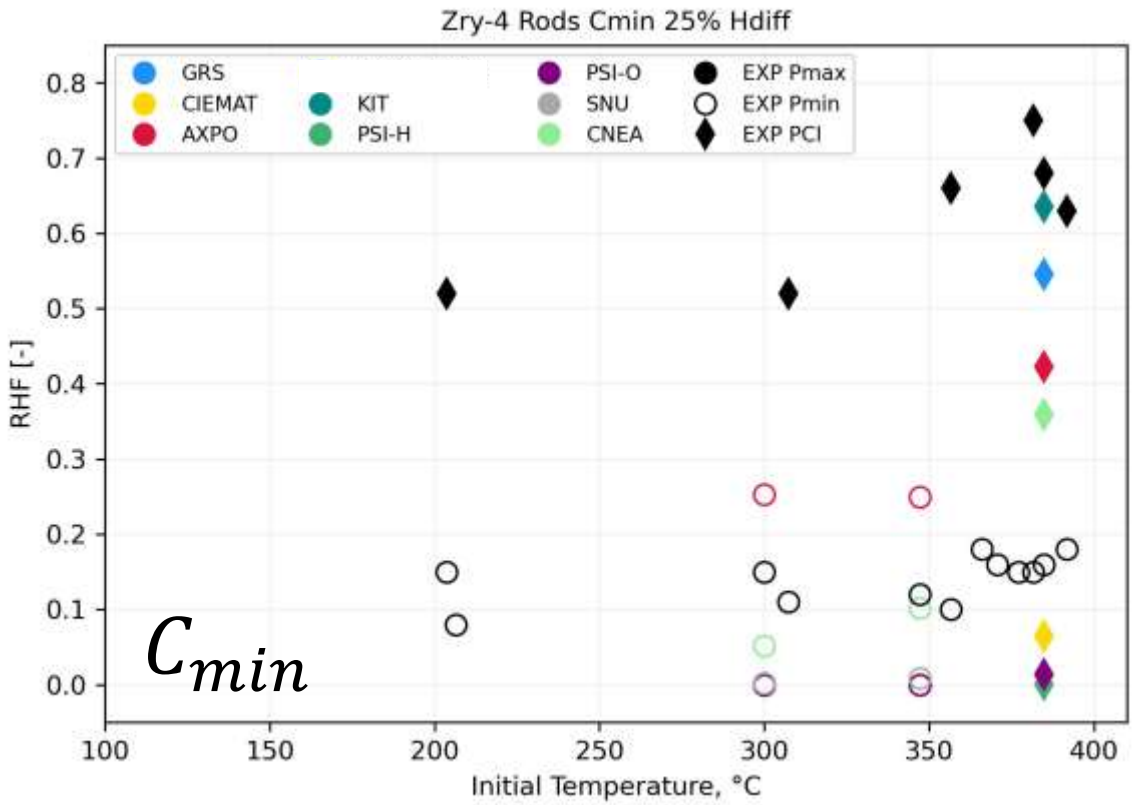

- Experiments demonstrate higher RHF at lower hydrogen concentrations, a trend partially captured by some calculations.
- Some calculations correctly capture the increase in RHF with rising initial temperatures in the zones
- Limited comparison for Cmin due to large discrepancy between initial and measured hydrogen concentrations

Opt.ZIRLO: Rod 7

91MPa 300wppm Inner

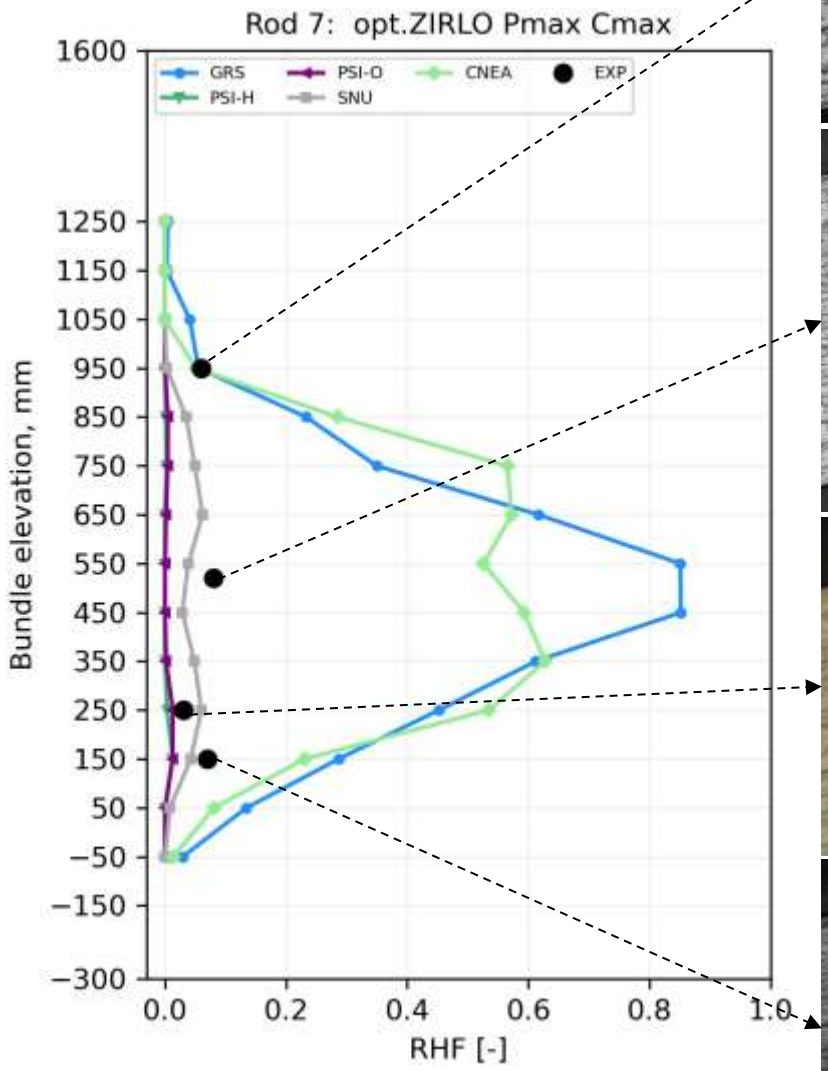

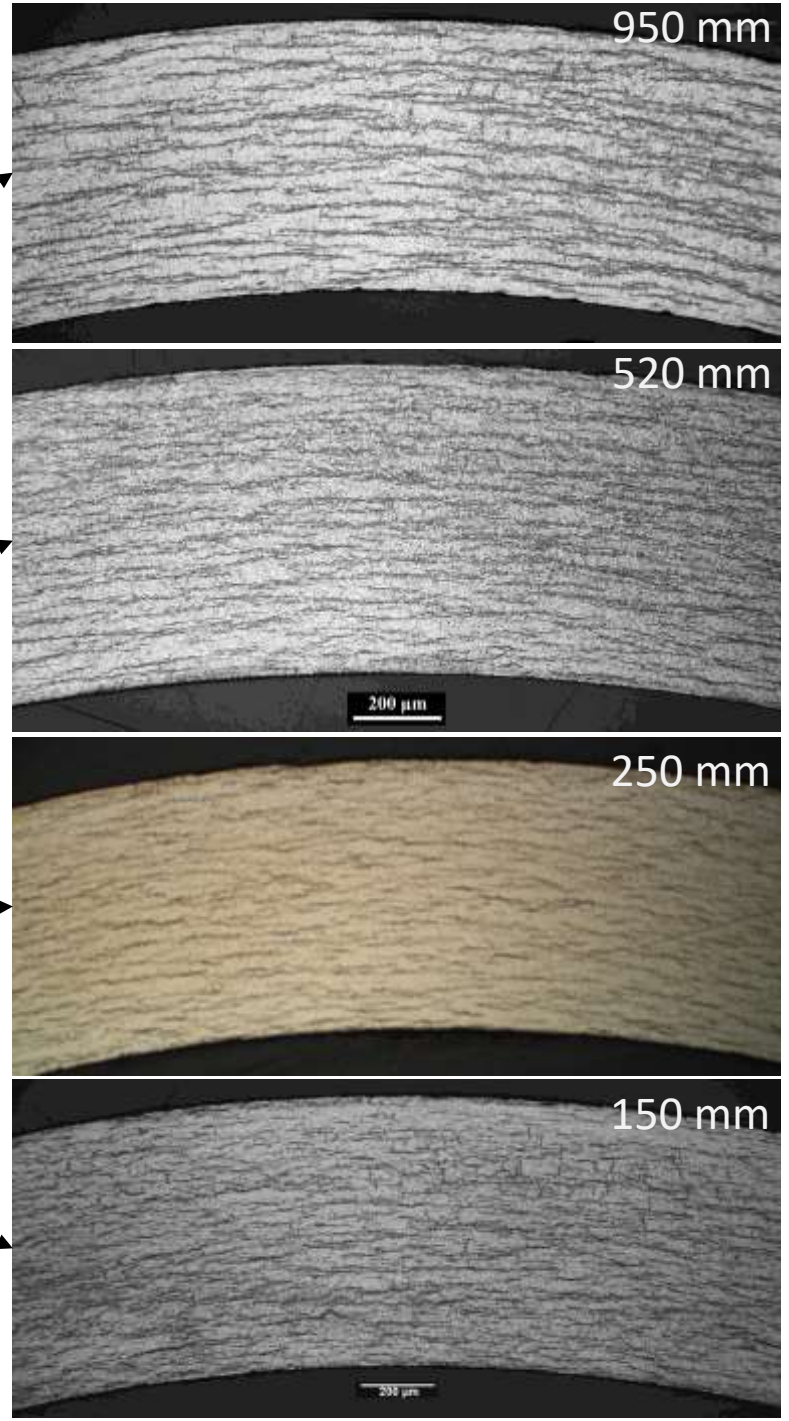

Fewer radial hydrides than in Zry-4 observed under similar conditions in opt.ZIRLO.

A threefold difference between the initial hydrogen concentrations used and the measured hydrogen limits the comparison.

Opt.ZIRLO: Initial Hydrogen Concentration VS RHF

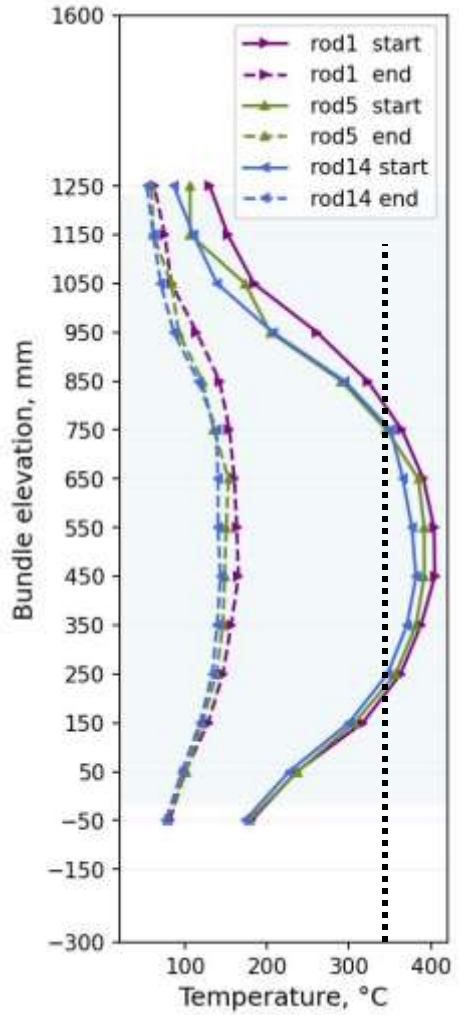

Zones 4-9
Temperatures
above 350°C

$$\left|C_{H,HVGE} - C_{H,ini}\right| < 30\%\ of C_{H,target}$$

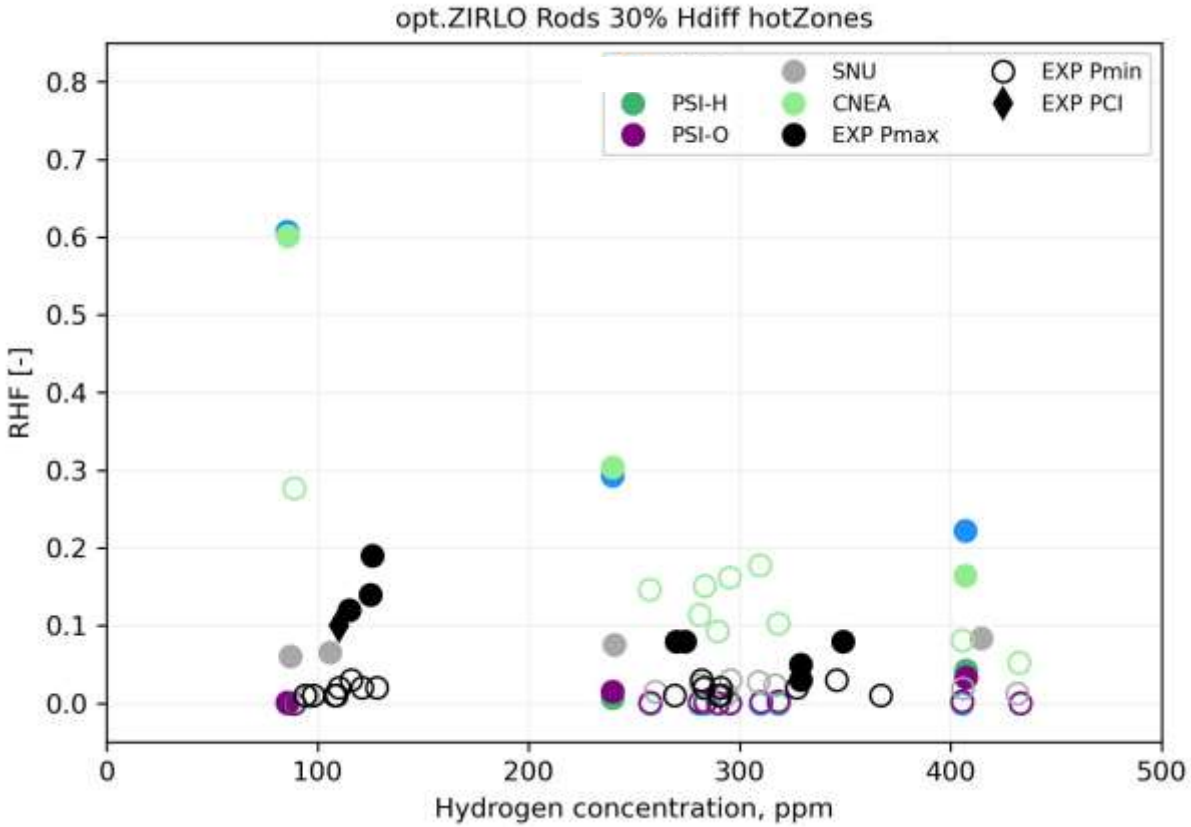

Modeling approaches that underestimated RHF for Zry-4 align better with experiments for opt. ZIRLO.

Opt.ZIRLO: Starting Temperature VS RHF

$$|C_{H,HVGE} - C_{H,ini}| < 30\% \; of \; C_{H,target}$$

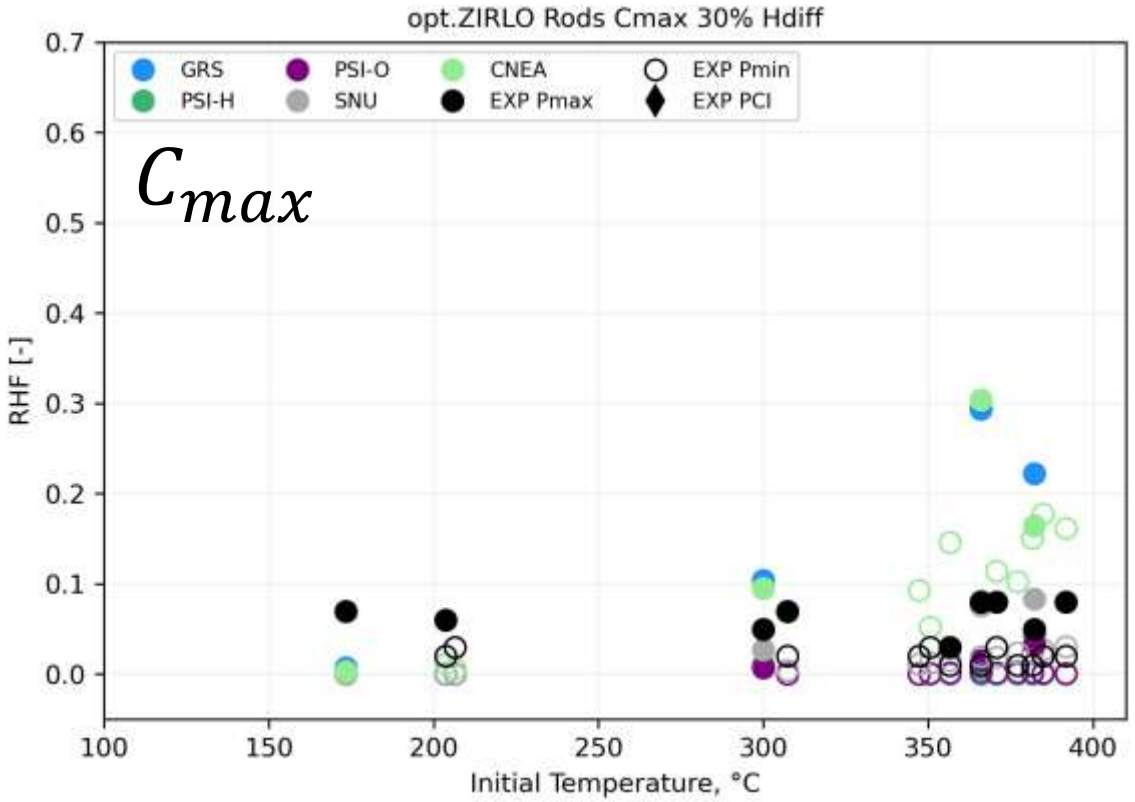

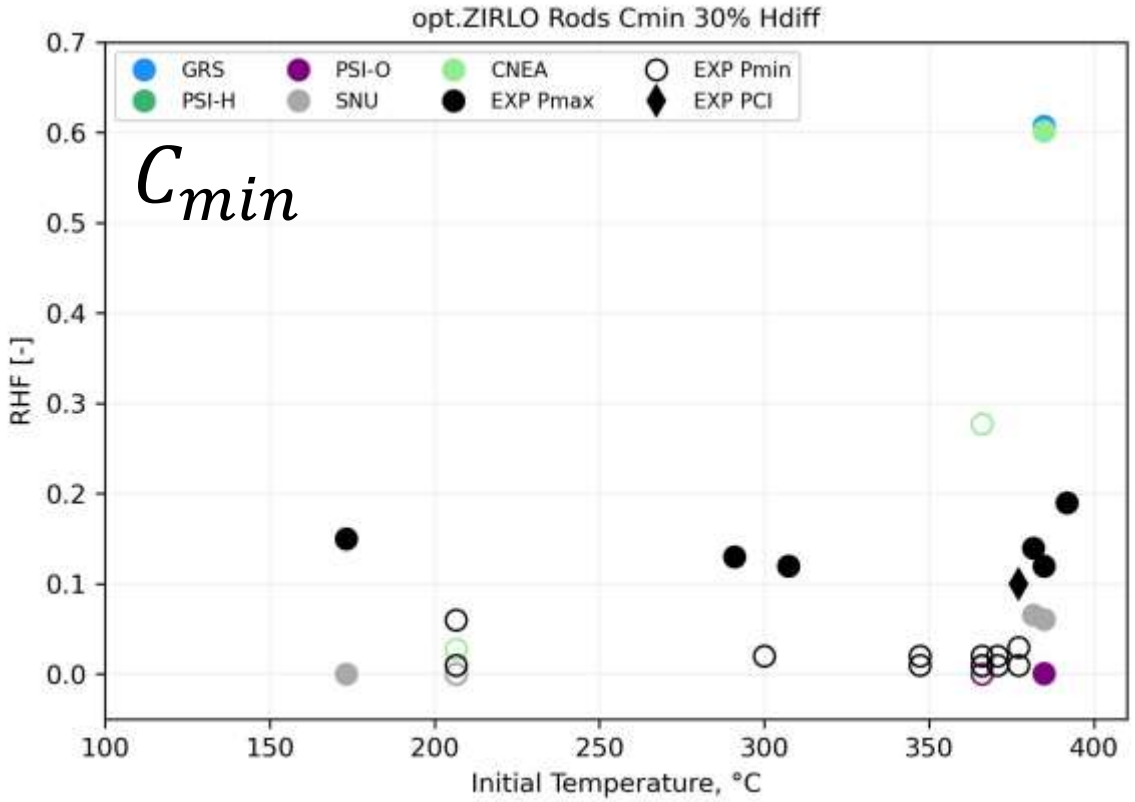

- Limited comparison due to large discrepancy between initial and measured hydrogen concentrations
- Experiments show slightly higher RHF at lower hydrogen concentrations, a trend not well captured by the simulations.
- Experiments show similar RHFs for different starting temperatures, whereas simulations indicate an increasing RHF with higher temperatures.

DX D4: Rod 1

91MPa 300wppm Central

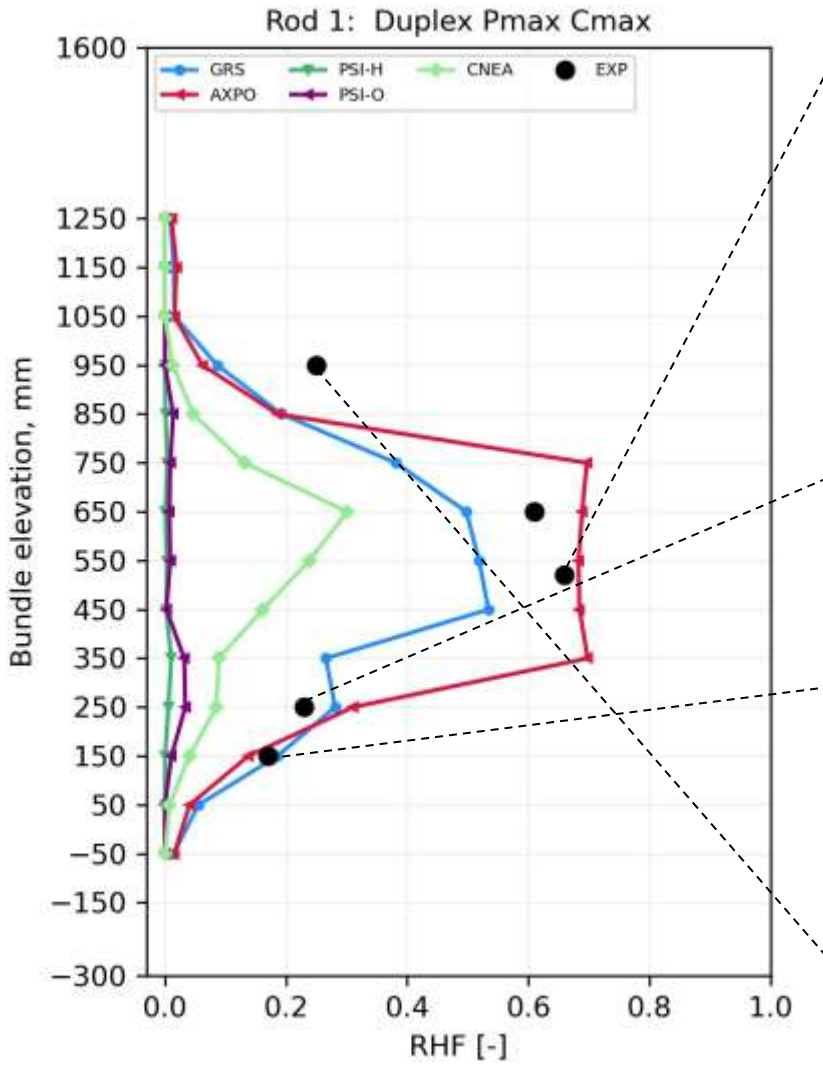

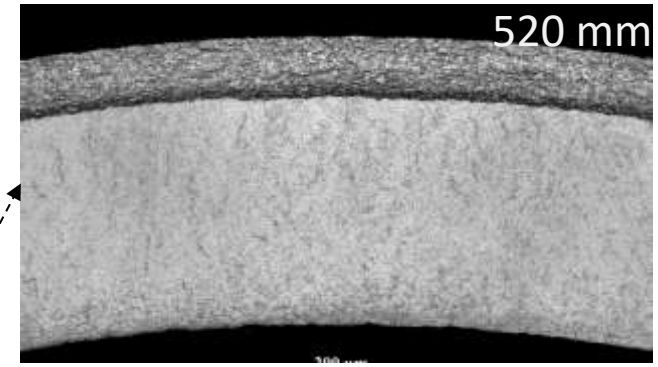

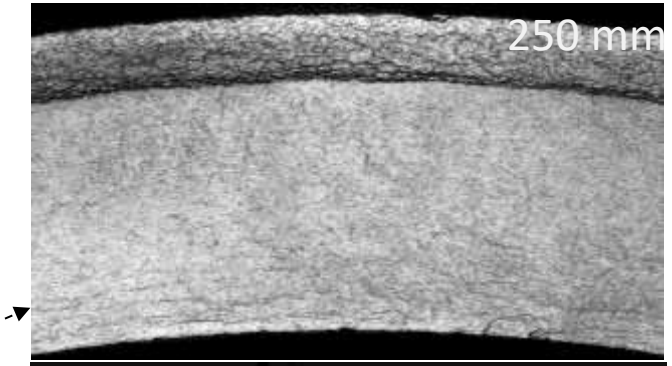

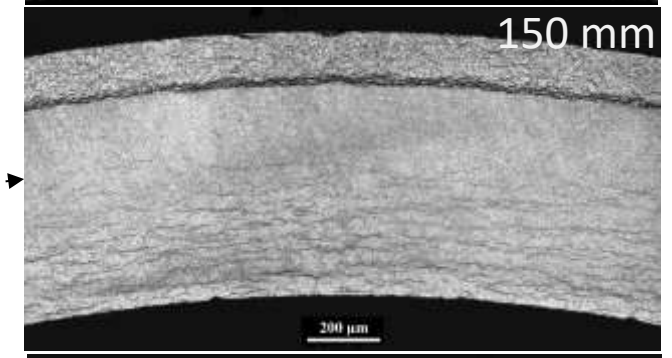

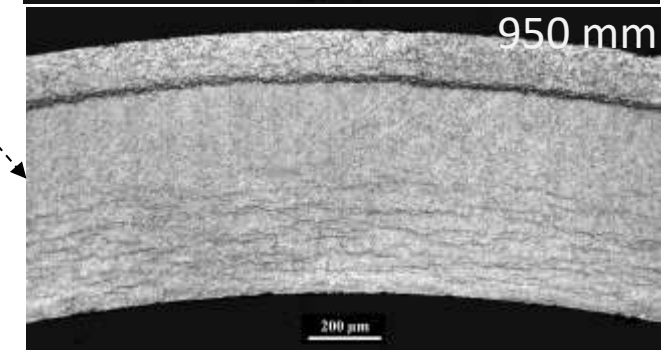

Hydride reorientation is stronger compared to Zry-4.

The extent of the depleted zone is temperature-dependent

Radial hydride orientation increases toward the liner

Most participants modeled only the bulk region of the duplex rods

DX D4: Initial Hydrogen Concentration VS RHF

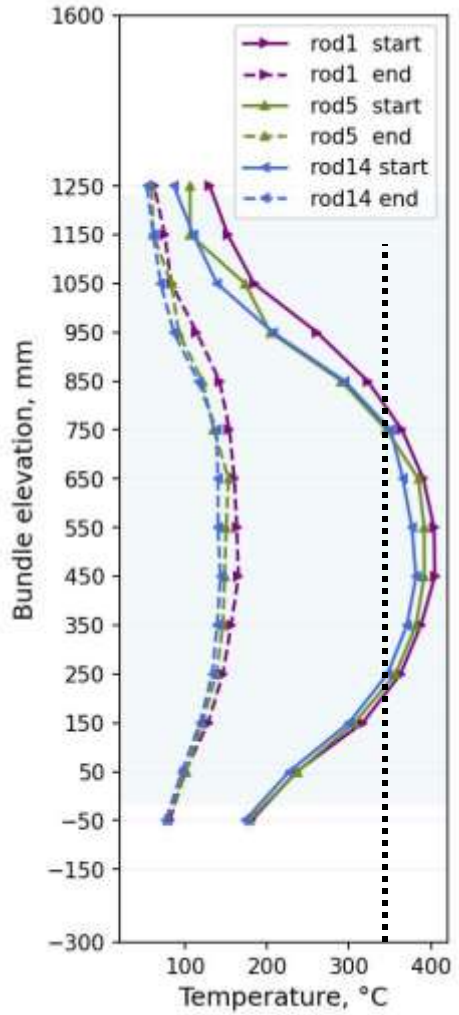

Zones 4-9
Temperatures
above 350°C

$$\left|C_{H,HVGE} - C_{H,ini}\right| < 25\%\ of C_{H,target}$$

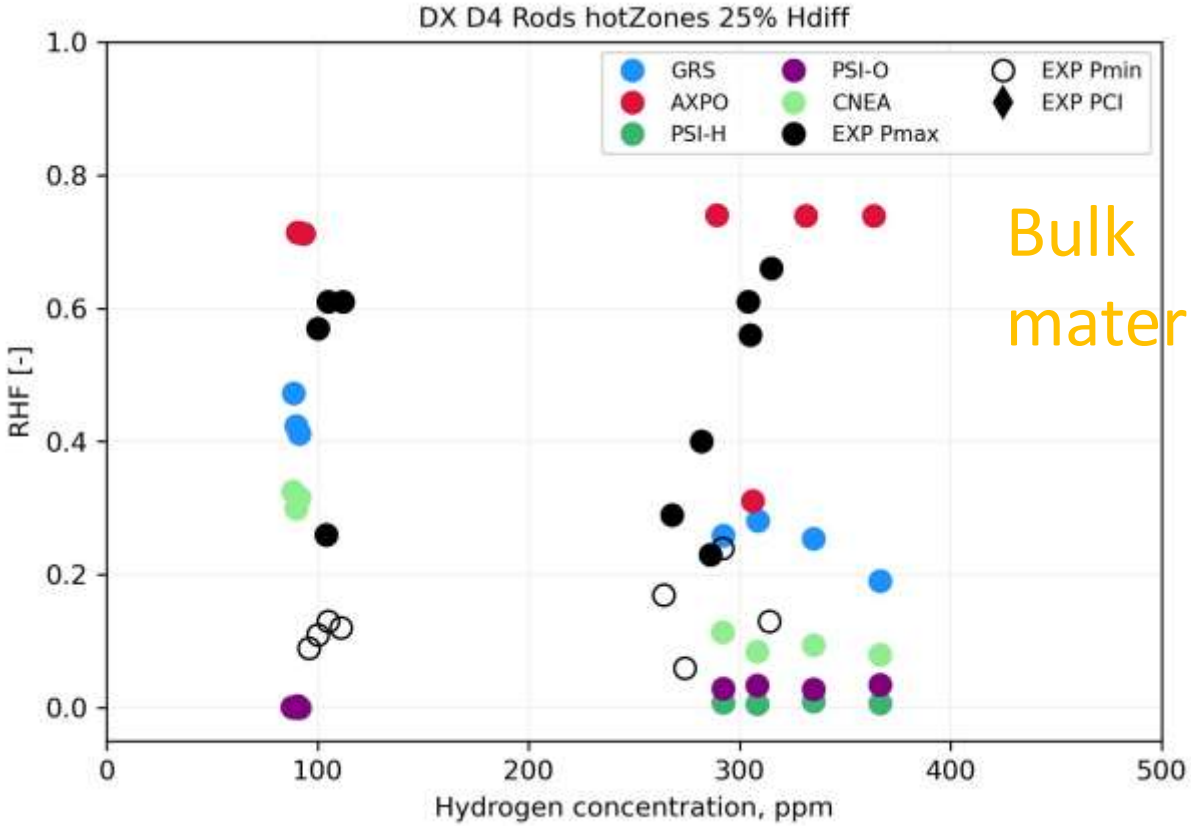

Bulk material

The modeling approach, which considers both liner and bulk, better captures the higher than in Zry-4 RHFs.

DX D4: Starting Temperature VS RHF

$$|C_{H,HVGE} - C_{H,ini}| < 25\% \; of C_{H,target}$$

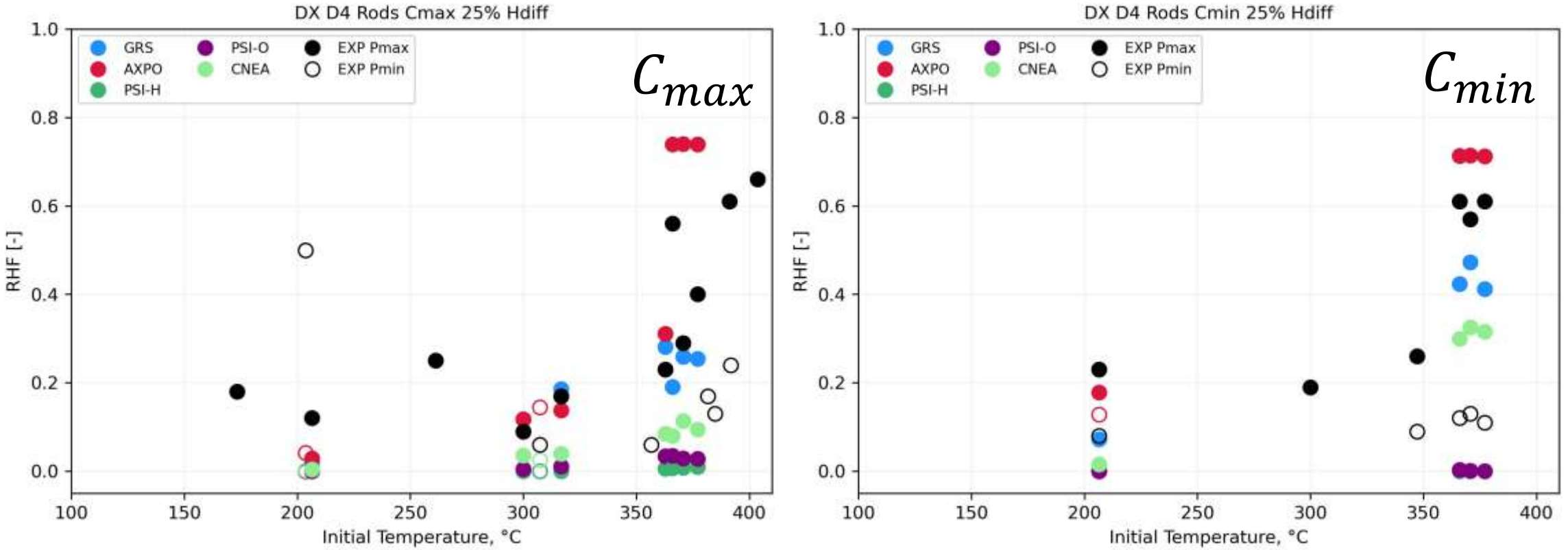

- Experiments show little difference in RHF between low and high hydrogen concentrations, while most simulations show an increasing trend for Cmin.
- Especially at high pressure, RHF increases significantly with rising starting temperature, captured partially.
- Limited comparison due to differing boundary conditions

Next steps

The preparation of the final report is underway.

Further Benchmark Activities:

- Use HVGE values to define initial hydrogen content.
- Focus on rods suitable for comparison that are unaffected by PCI.
- Model duplex rods with emphasis on radial behavior.

Gesellschaft für Anlagen- und
Reaktorsicherheit (GRS) gGmbH
Schwertnergasse 1
50667 Köln

www.grs.de

FOLLOW US

Pellet-Cladding Interaction

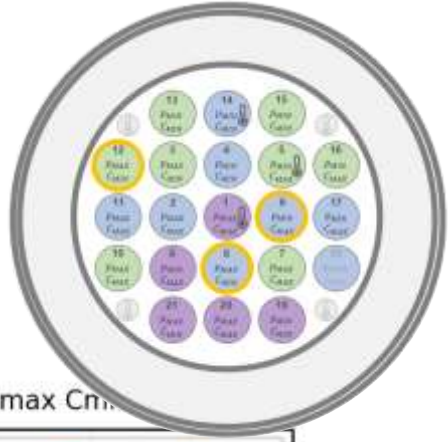

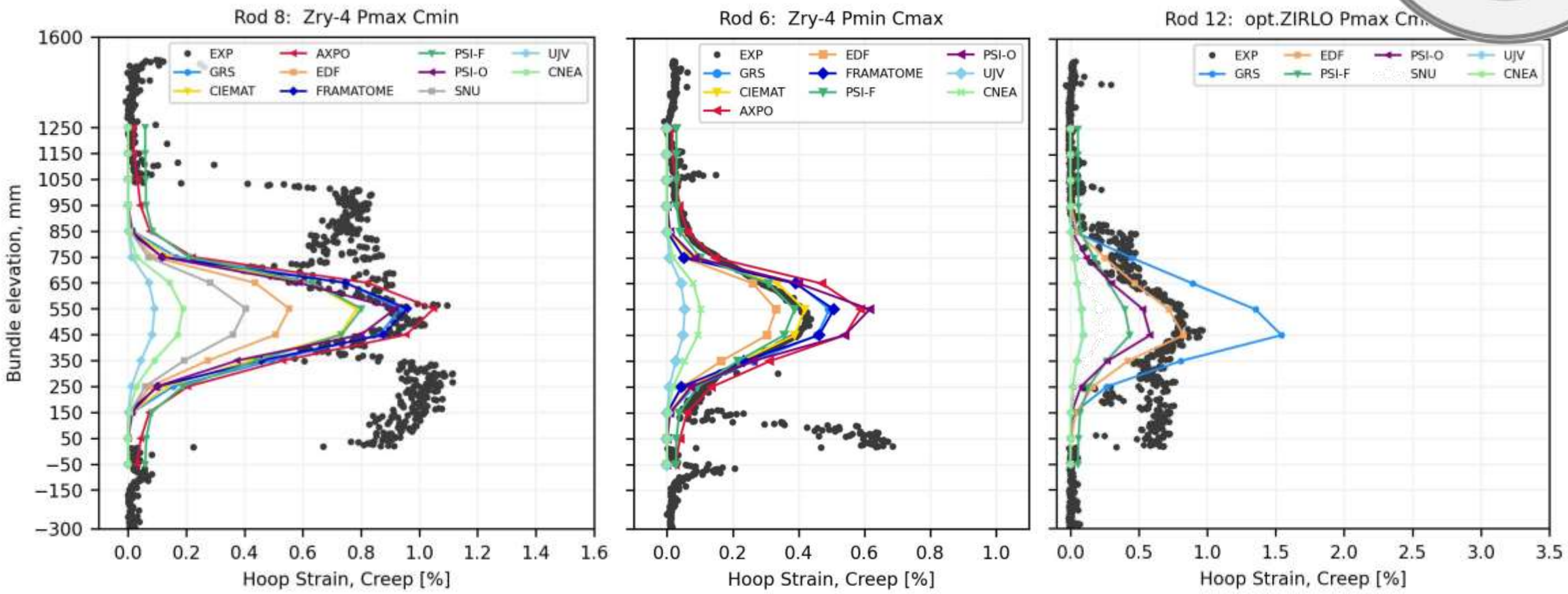

Pellet-Cladding Interaction

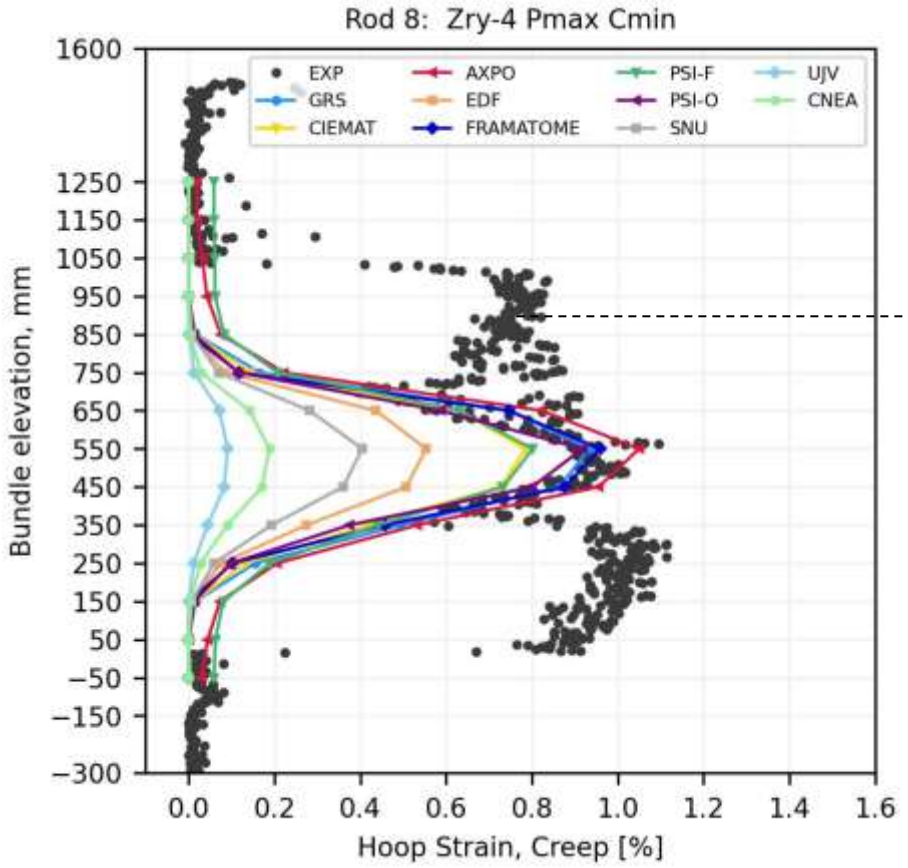

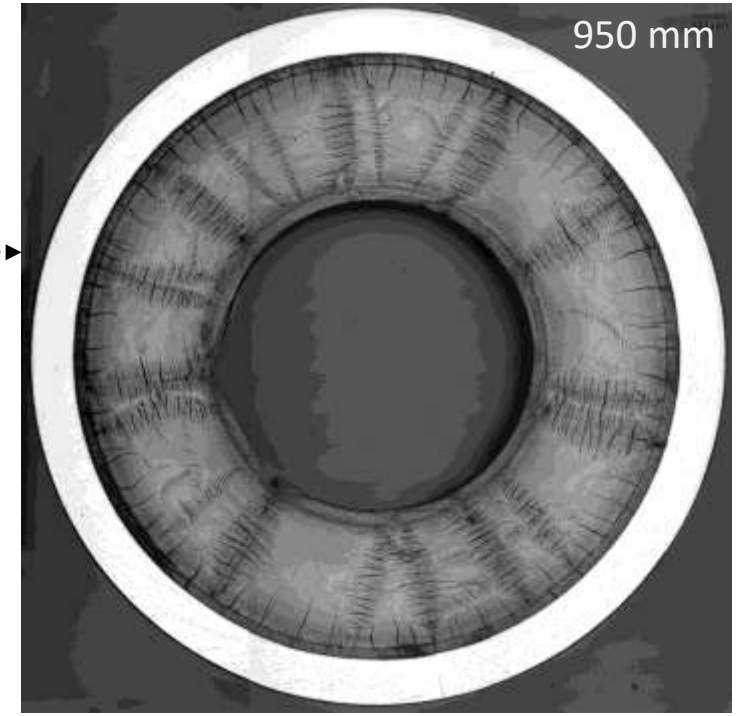

Zircaloy-4: Rod 8

91MPa 100wppm Inner

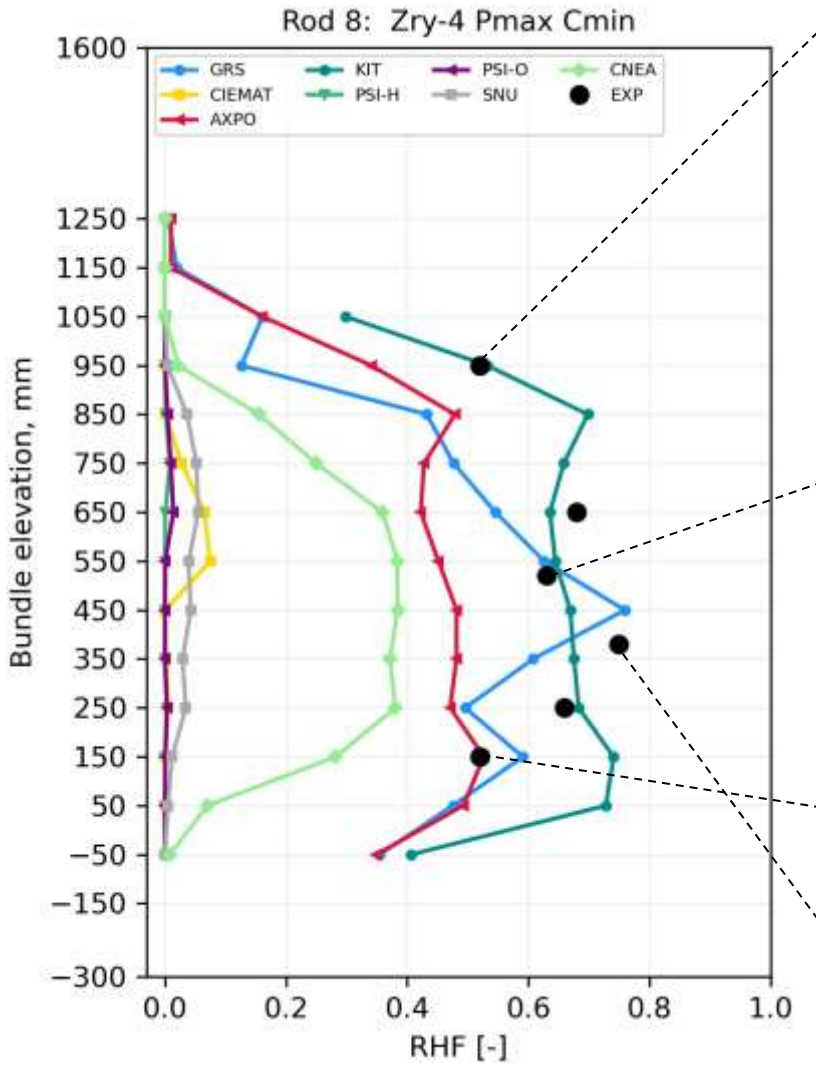

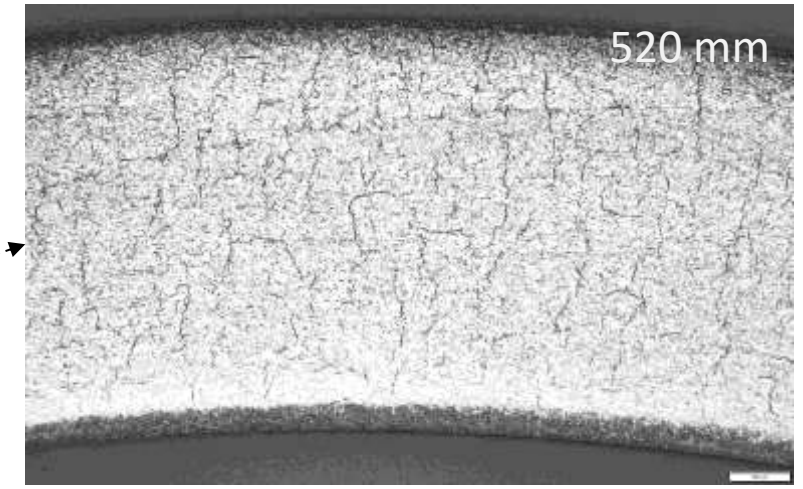

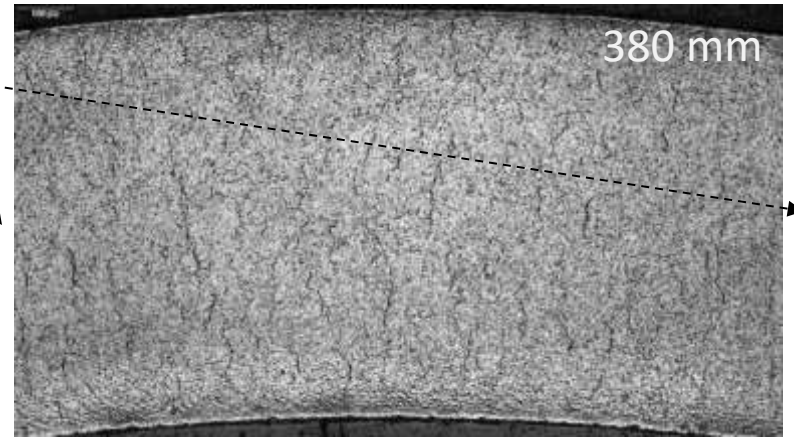

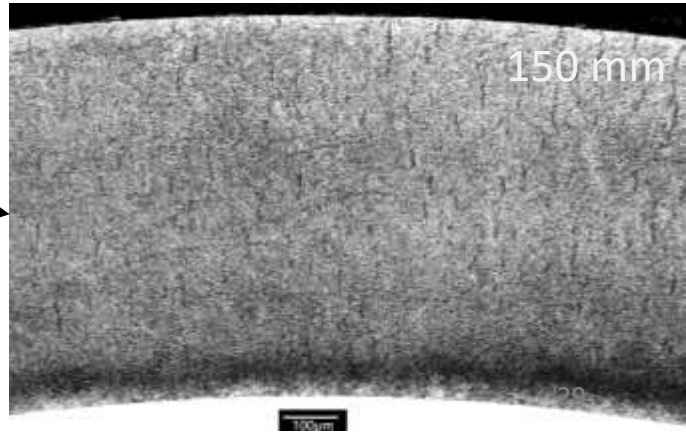

Radial hydrides present across all examined axial planes, including cold zones
Pressure-induced higher hydrogen dissolution?

H.E. Weekes, D. Dye, J.E. Proctor, D. Smith, C. Simionescu, T.J. Prior, M.R. Wenman, The effect of pressure on hydrogen solubility in Zircaloy-4, Journal of Nuclear Materials, Volume 524, 2019, Pages 256-262, ISSN 0022-3115, https://doi.org/10.1016/j.jnucmat.2019.07.012.

DX D4: Starting Temperature VS RHF

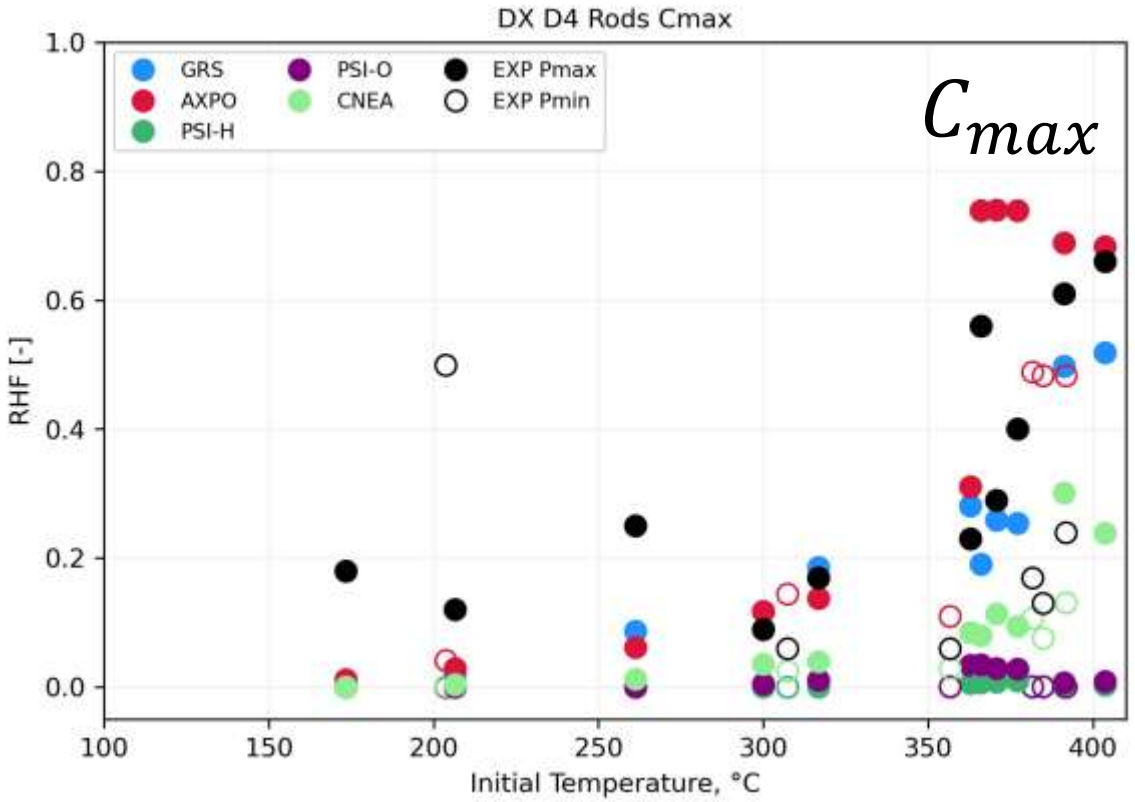

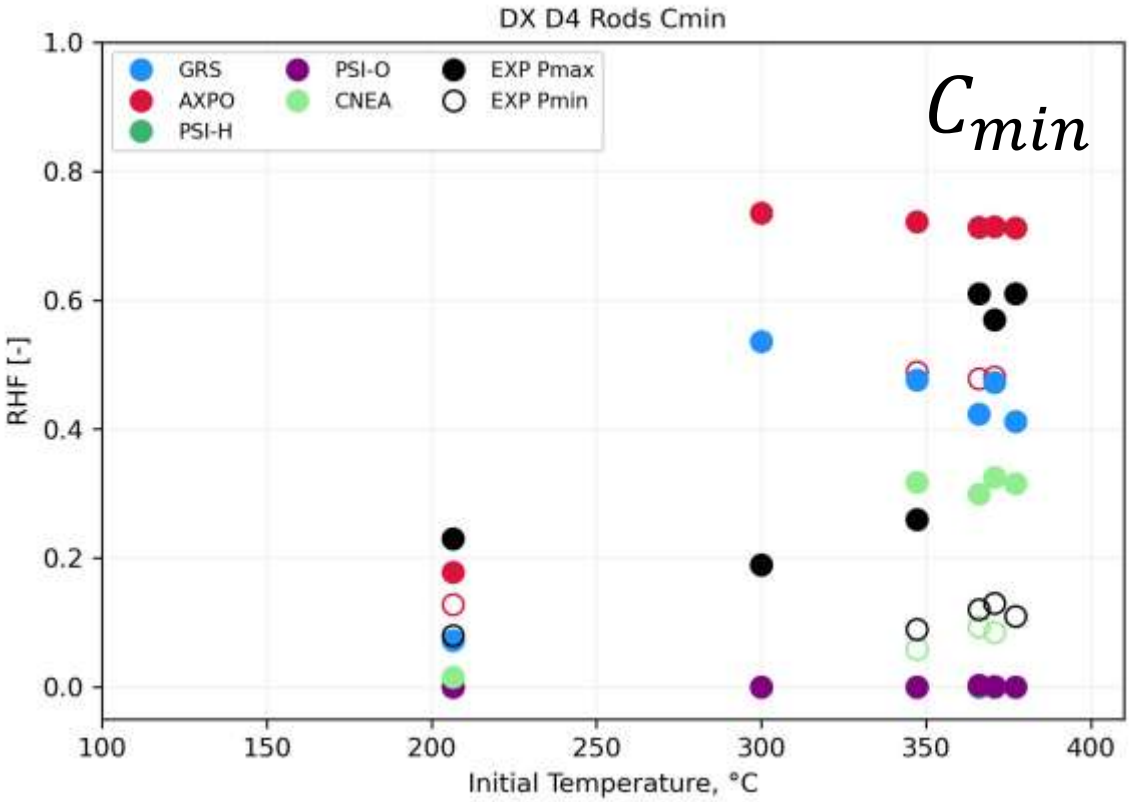

- Experiments show little difference in RHF between low and high hydrogen concentrations, while most simulations show an increasing trend for Cmin.
- Especially at high pressure, RHF increases significantly with rising starting temperature, captured partially.

Johannes Bertsch

PSI

Hydrogen in Claddings – Investigations on Hydrogen Axial Mobility, Role of Liner and Creep

Under reactor operation, corrosion takes place at the hot surface of nuclear fuel rods in the cooling water. The H2O is split up; while the oxygen leads to the formation of an oxide layer on the fuel cladding surface, a part of the hydrogen diffuses into the cladding. In water cooled reactors, the cladding typically consists of a zirconium alloy. At higher temperatures hydrogen remains in solid solution, but precipitates into a zirconium-hydrogen compound, hydrides, with decreasing temperature. These hydrides are brittle and can affect the mechanical properties of the cladding. However, the cladding being the first barrier against the release of highly radioactive fission products must keep its integrity during and after reactor service.

After reactor service and under intermediate dry storage conditions, the fuel rods remain at a certain temperature because of decay heat and keep internal pressure because of fission gas. This leads to creep of the cladding. Hydrogen in solid solution accelerates creep, hydrides slow it down. In addition, several factors make hydrogen diffuse, i.e., gradients in hydrogen concentration, in temperature, in chemical composition or in mechanical stress. Existing hydrides attract further hydrogen and grow. These effects can lead to hydrogen/hydrides accumulations and thus to weak spots in the material.

Claddings can have a compound design, namely a thin liner on the cladding substrate. The liner – for the use in pressurized water reactors at the outer cladding surface to improve corrosion resistance, and for boiling water reactors at the inner side to mitigate pellet-cladding interaction – is a purer zirconium alloy. Due to its different terminal solid solubility for hydrogen compared to the substrate, the liner accumulates hydrides during cooling down. Therefore, a liner influences the creep behavior and hydrogen mobility in the cladding. While the diffusion of hydrogen towards a liner has been well examined, the overlaying of cladding tube axial hydrogen diffusion and attraction by a liner is unknown.

To explore the role of a liner for creep and axial hydrogen diffusion, two PhD projects have been launched at PSI. Both projects use claddings with and without a liner. In the case of axial diffusion, a hydrogen concentration gradient is created by electrochemical hydrogenation; the creep test samples are homogeneously hydrogenated in a gaseous environment. Besides microstructural characterizations, the sample are investigated with high resolution neutron imaging to explore the hydrogen/hydrides distribution before and after diffusion and creep testing. The work is accompanied by model calculations, in case of creep focusing on the stress distribution using FEM, in case of axial diffusion on the mobility and precipitation of hydrides. First results and the development of the projects are described.

PSI Center for Nuclear Engineering and Sciences

Hydrogen in Claddings – Investigations on Hydrogen Axial Mobility, Role of Liner and Creep

Current PhD projects

Johannes Bertsch, Benedetta Buzzatti, Liliana Duarte,
Sebastian Niedermeyer, Robert Zubler

30th International QUENCH Workshop, 2025, Dec 16-18, KIT

- Intro
- Axiality
- Creep
- Outlook

Introduction

Hydrogen Uptake, Diffusion and Precipitation

During fuel service in the reactor hydrogen is created and diffuses into the cladding

- Embrittlement (**fracture toughness**)
- Precipitation of hydrides (**solubility!**)
- Change of **creep properties**
- **Reorientation** of hydrides
- **DHC** – Delayed Hydride Cracking

$$Zr + 2\,H_2O \rightarrow ZrO_2 + 2\,H_2$$

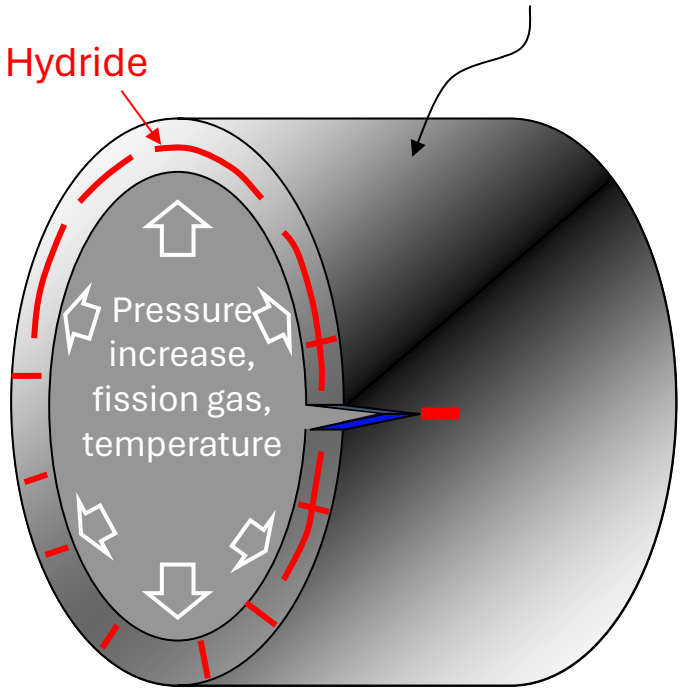

Those effects are aggravated with burn-up and deteriorate the mechanical stability of the fuel cladding.

Reduction of safety (cladding integrity) is not acceptable!

Introduction

Cladding Thermomechanics – Transportation, Handling and Dry Storage

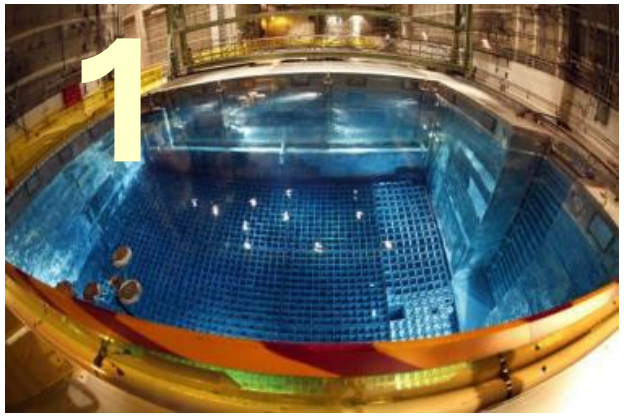

After operation: cladding embrittlement due to hydrogen redistribution and precipitation

2

- Unloading from pool
- Vacuum drying
- Packaging into transport/storage cask

→ Temperature ↑ (decay)
→ Pressure ↑ (fission gas)
→ Hydrogen in solution

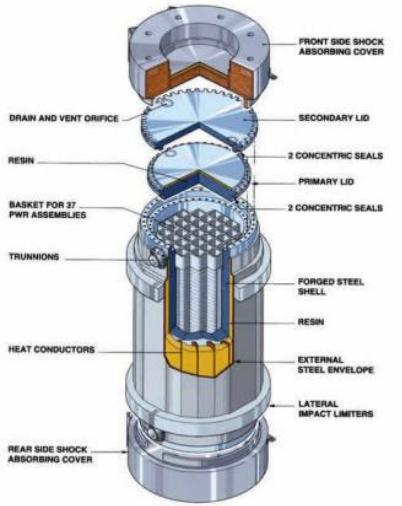

TN24 cask produced by Orano TN

- Dry storage
- Temperature going down ↓
- Hydrides precipitation, embrittlement
- Liner cladding

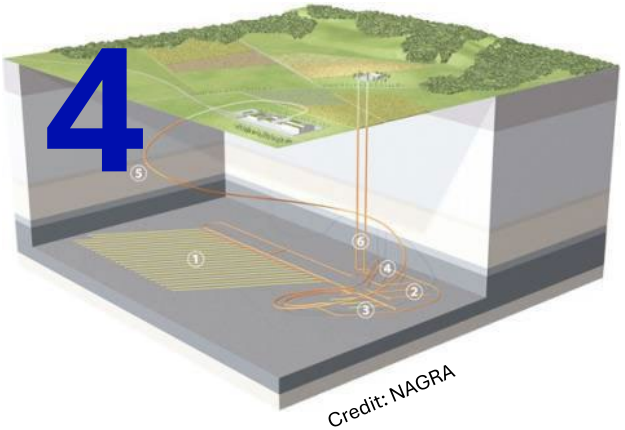

- Final handling
- Repacking

Introduction

Hydrogen Diffusion

$$J_{Diffusion} = J_{Fick} + J_{Soret} + J_{Stress} + J_{Material\ Gradient}$$

HNGD* model

1. Fickian Diffusion: net flux to regions of **lower hydrogen concentration**
2. Soret Effect: hydrogen migrates towards **cooler regions**
3. Stress-induced diffusion: towards zones of **hydrostatic tensile stress**
4. Material-driven diffusion: flux influenced by **microstructural features, irradiation damage,** or **liner presence**

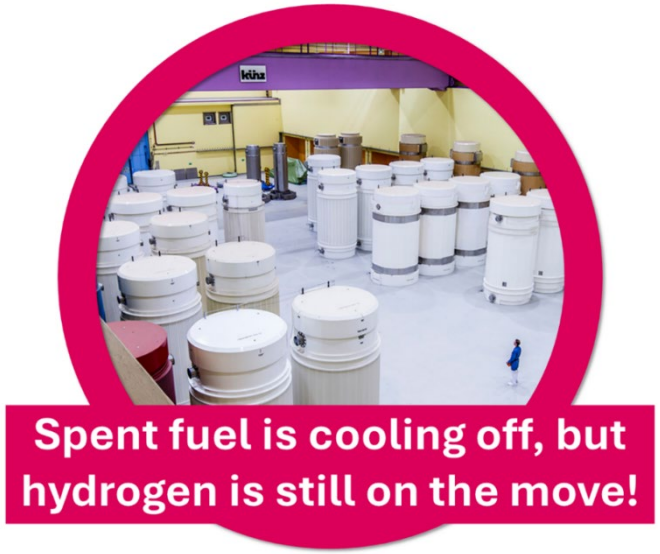

Sebastian Niedermeyer, Investigation of Hydrogen and Hydrides Distribution in Axial Cladding Direction at PSI, BGZ Workshop, 2025, Nov 25-26, Berlin

* **H**ydrides **N**ucleation, **G**rowth and **D**issolution model

Introduction

Hydrogen Diffusion and Precipitation, Influence of Liner and Stress

S. Valance, J. Bertsch, Hydrides reorientation investigation of high burn-up PWR fuel cladding, Journal of Nuclear Materials 464 (2015) 371–381, http://dx.doi.org/10.1016/j.jnucmat.2015.05.003

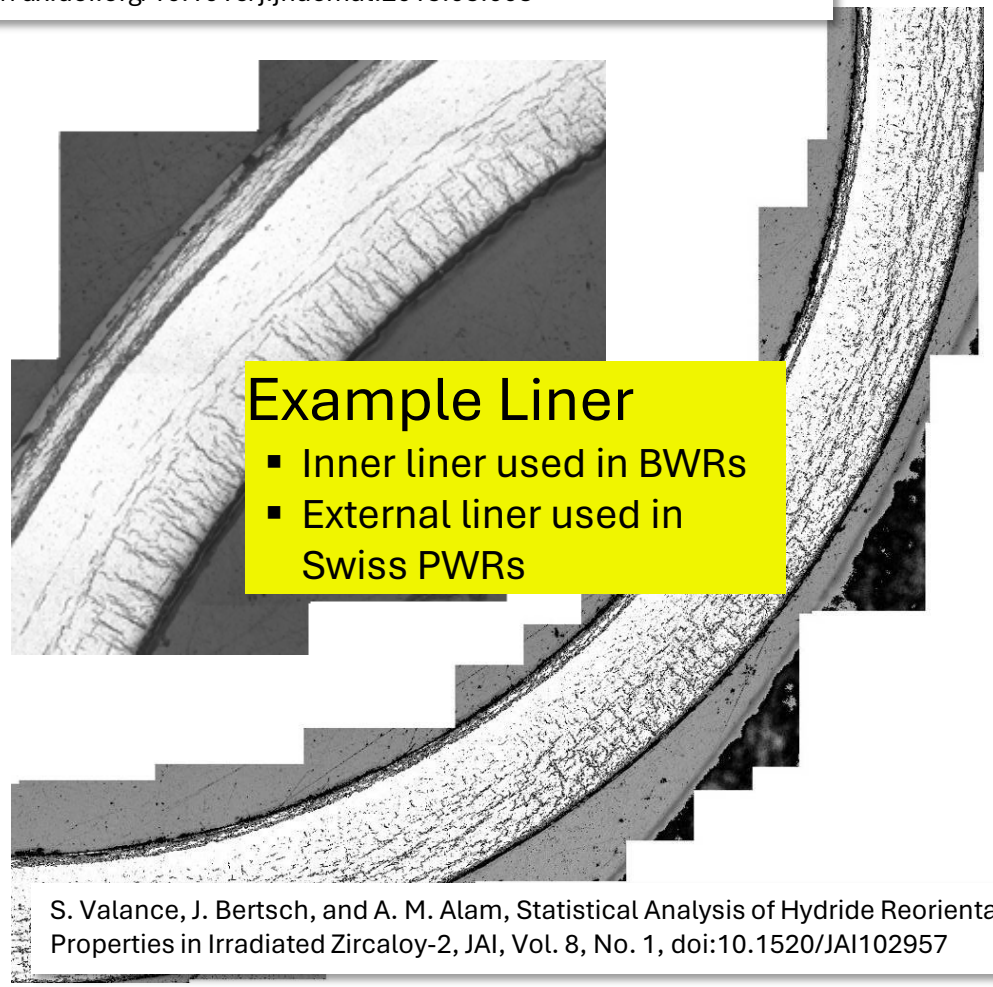

Example Liner

- Inner liner used in BWRs
- External liner used in Swiss PWRs

S. Valance, J. Bertsch, and A. M. Alam, Statistical Analysis of Hydride Reorientation Properties in Irradiated Zircaloy-2, JAI, Vol. 8, No. 1, doi:10.1520/JAI102957

Example Stress

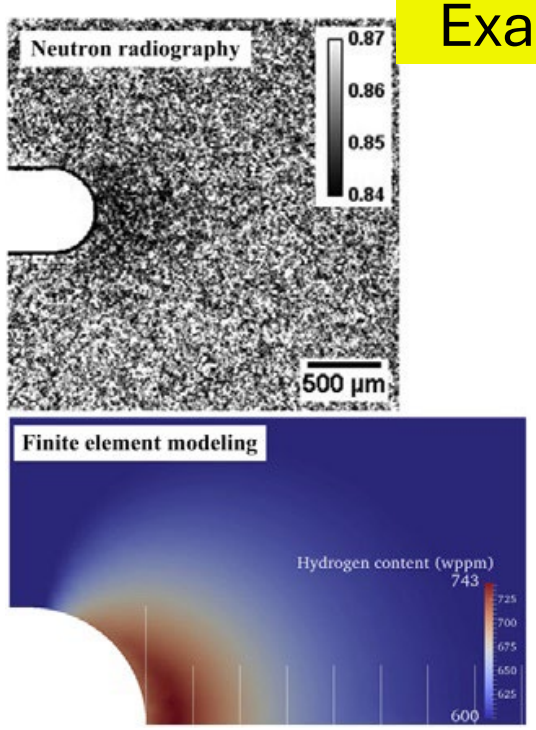

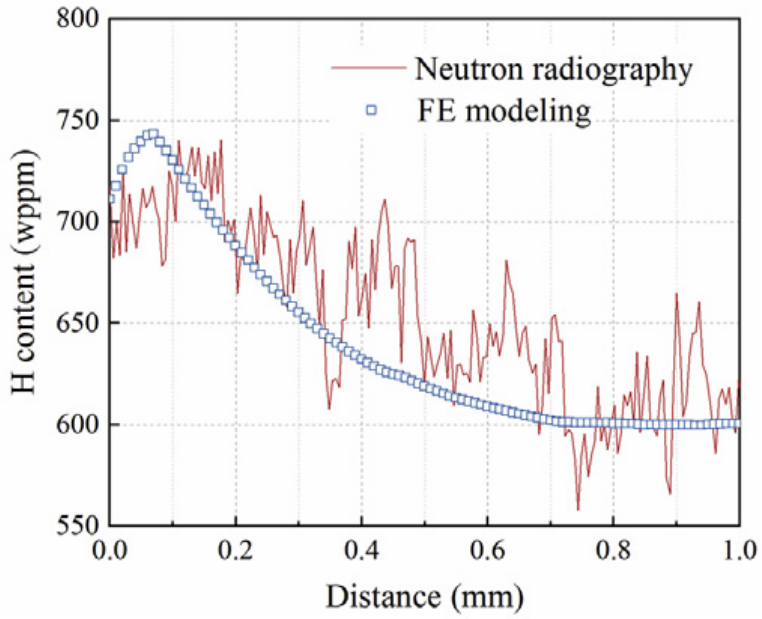

W. Gong, P. Trtik, S. Valance, J. Bertsch, Hydrogen diffusion under stress in Zircaloy: High-resolution neutron radiography and finite element modeling, Journal of Nuclear Materials 508 (2018) 459e464, https://doi.org/10.1016/j.jnucmat.2018.05.079

Introduction

Hydrogen Diffusion and Precipitation

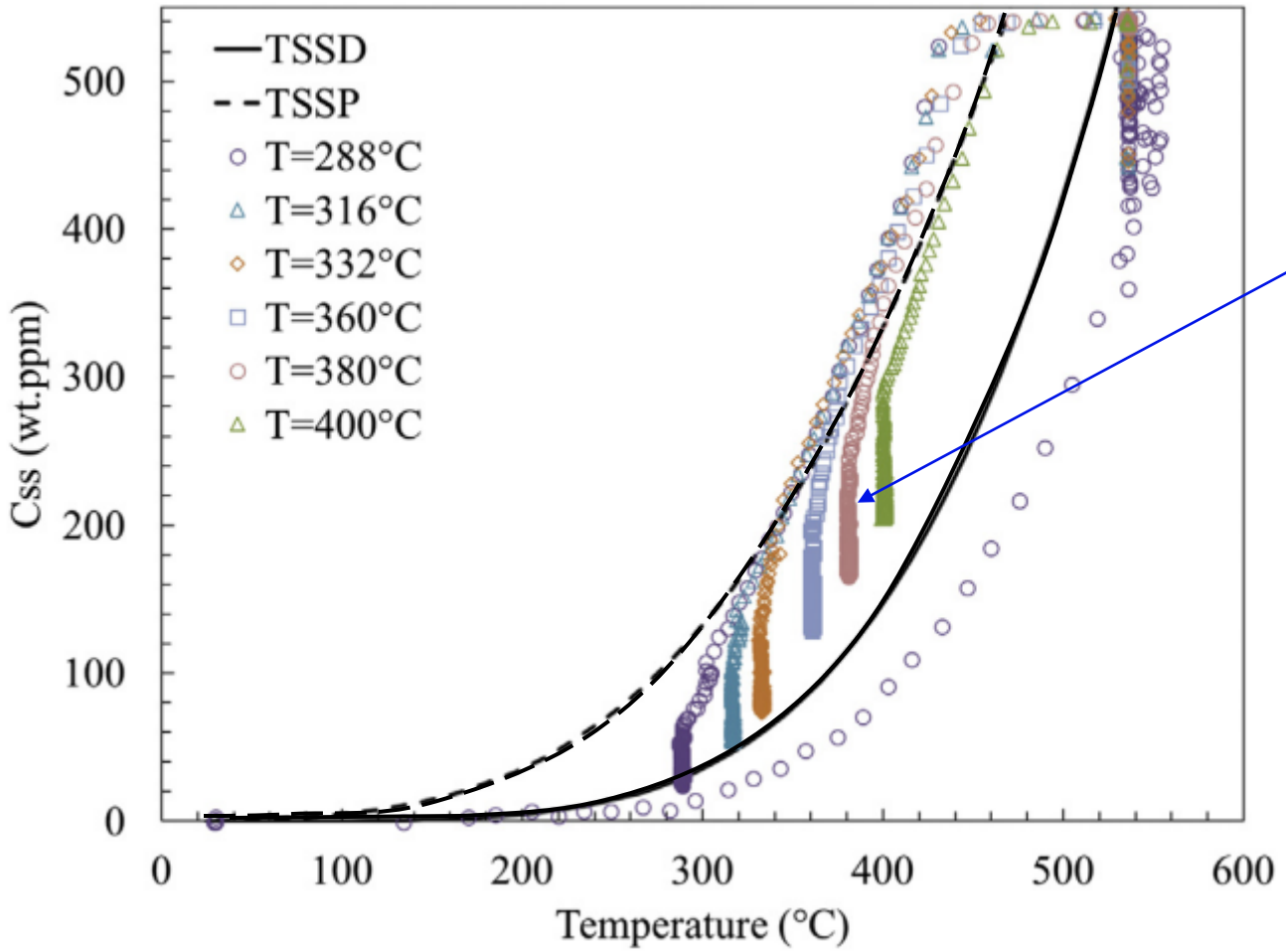

- Hysteresis (TSSP ≠ TSSD)
- Different curves for liner and substrate
- Growing hydrides attract hydrogen
- More hydrides in liner

E. Lacroix, A.T. Motta, J.D. Almer, Experimental determination of zirconium hydride precipitation and dissolution in zirconium alloy, Journal of Nuclear Materials 509 (2018) 162e167, https://doi.org/10.1016/j.jnucmat.2018.06.038

Introduction

Hydrogen, Hydrides and Creep

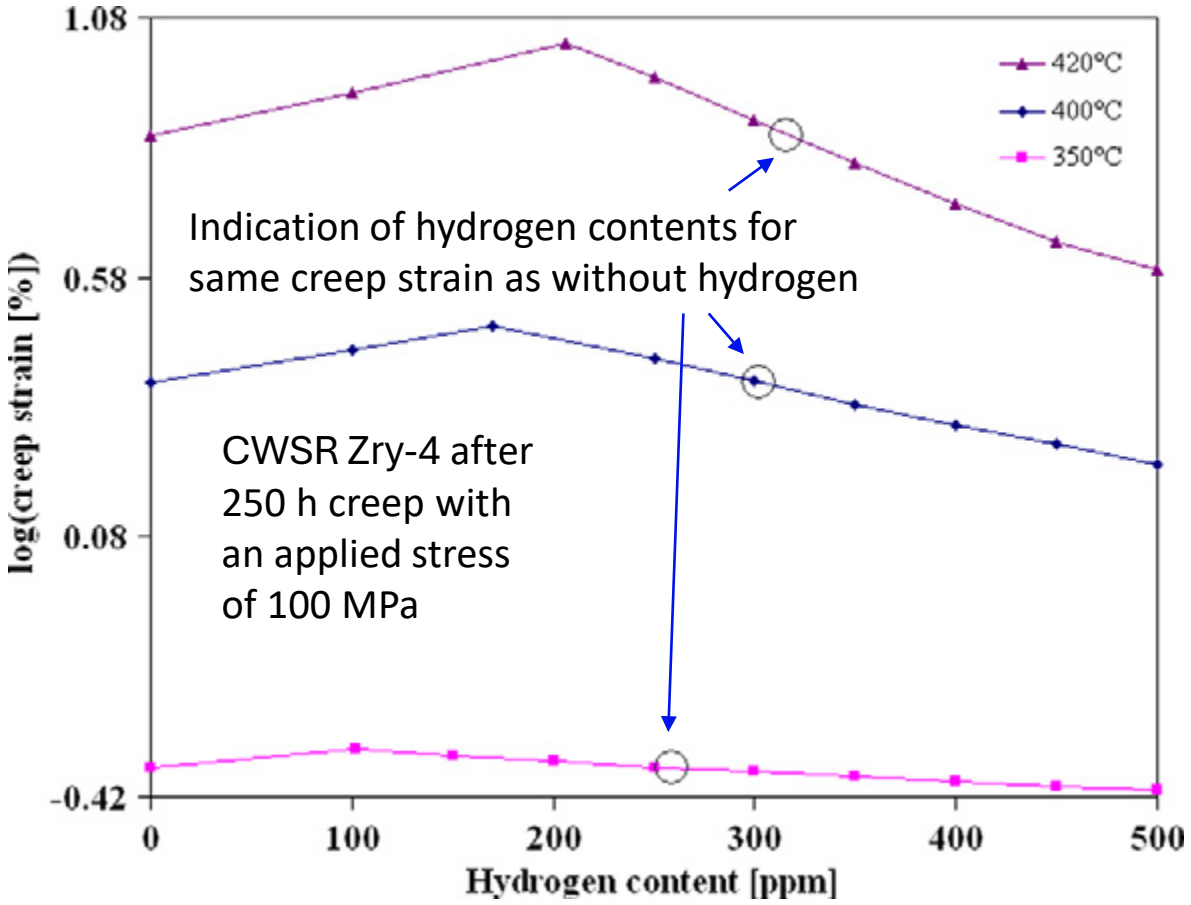

V. Mallipudi, S. Valance, J. Bertsch, Meso-scale analysis of the creep behavior of hydrogenated Zircaloy-4, Mechanics of Materials 51 (2012) 15–28, http://dx.doi.org/10.1016/j.mechmat.2012.03.003

Primary factors:

- Temperature
- Stress
- Hydrogen concentration

Secondary factors:

- Hydrogen in solid solution versus hydrides
- Hydrides orientation

} Stress dependent

Additional factors:

- Liner
  - different hydrogen terminal solubility
  - different mechanical properties

Introduction

Hydrogen, Temperature, Stress – 2 Cases for **Liner Cladding**

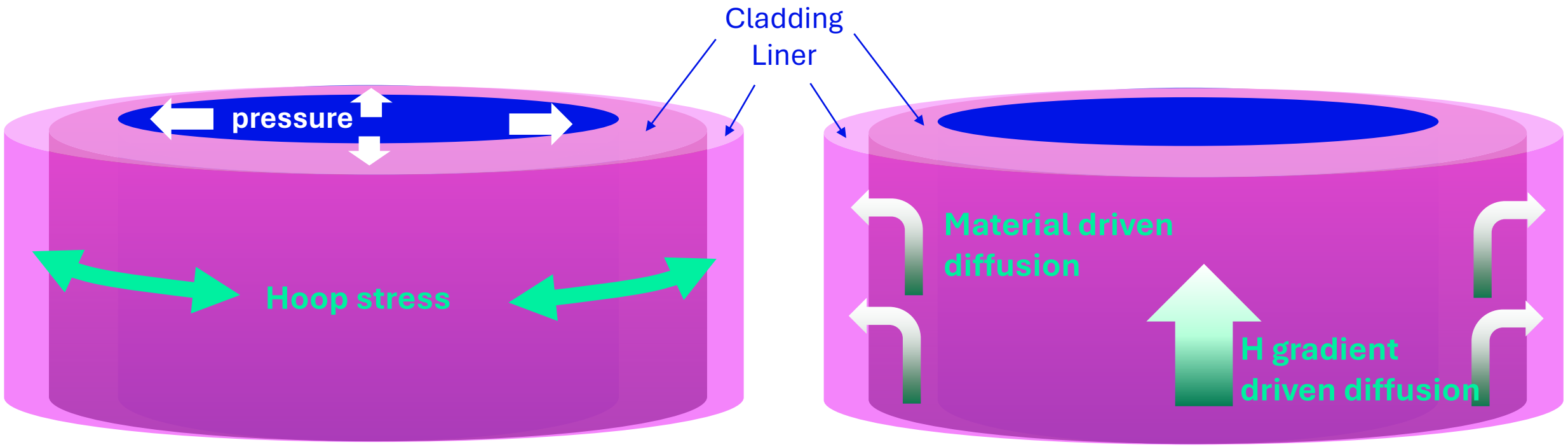

Introduction

Hydrogen, Temperature, Stress, Liner – 2 cases

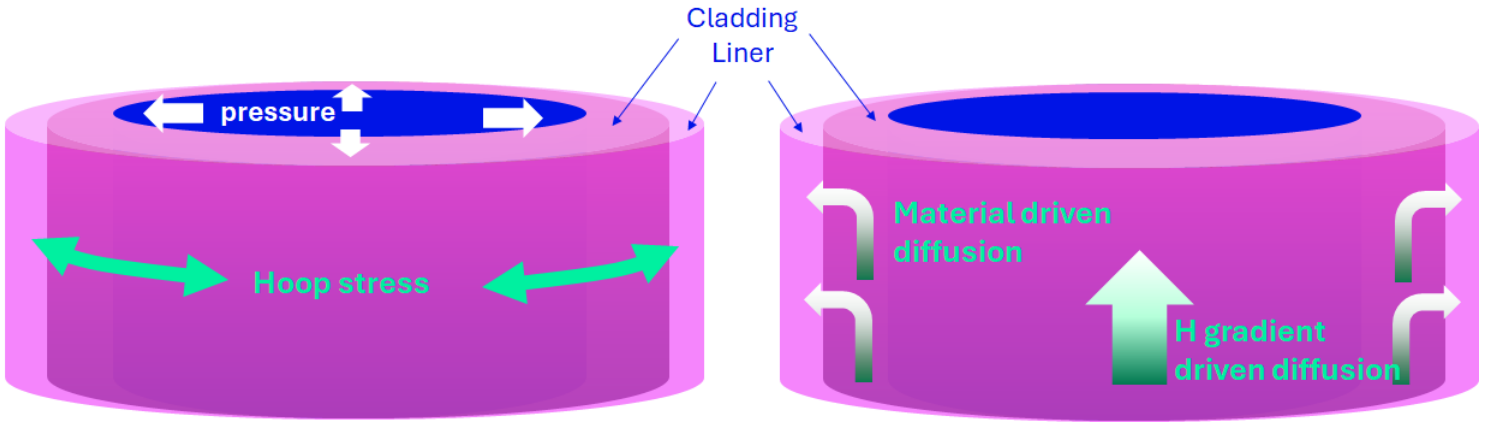

PhD project on creep

- Role of stress and liner, stress driven hydrogen diffusion and resulting creep properties
- Benedetta Buzzatti
- ETH – Zürich

PhD project on axial hydrogen mobility

- Role of liner on axial diffusion and precipitation
- HNGD model
- Sebastian Niedermeyer
- EPFL – Lausanne

Both PhD projects – High Resolution Neutron Imaging (HR-NI)

PSI

1 Neutron Imaging, ICON SINQ

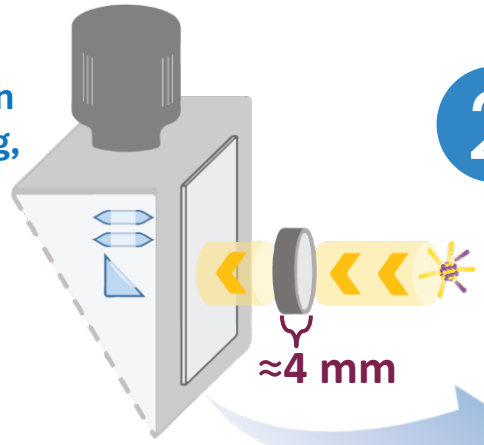

2 Image

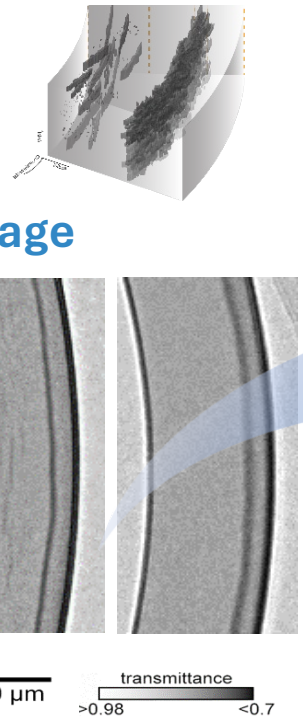

3 Quantification

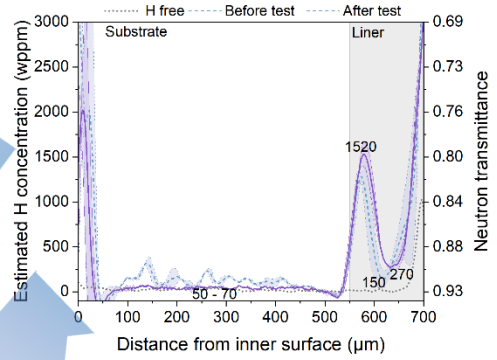

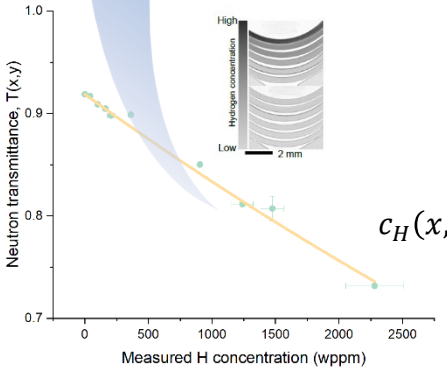

$$c_H(x,y) = \frac{\ln(\frac{T(x,y)}{0.9227})}{-9.73E-05}$$

- Spatial resolution < 10 µm
- Hydrogen from ~10 to several 1000 wppm, concentration resolution a few tens of wppm

Attenuation coefficient for neutrons

H	Zr
3.44	0.29

O. Yetik et al, 29th International QUENCH Workshop, 2024, Nov 21, KIT

Both PhD projects – HR-NI at SINQ

- Intro
- Axiality
- Creep
- Outlook

Axial Hydrogen Mobility

Comprehensive understanding of axial hydrogen diffusion is essential for **predictive modeling** and **safety assessment** of nuclear fuel rods.

- Texture
- Liner

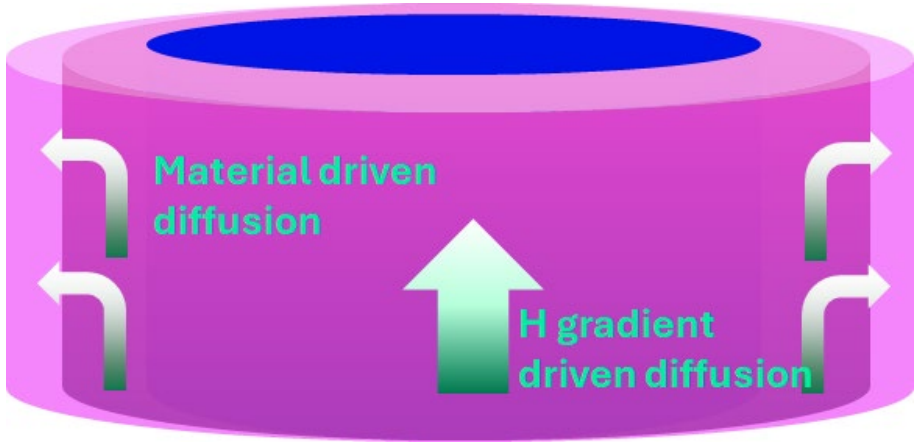

Experimental Approach – Electrochemical Hydrogenation

Approach
Concentration Gradient

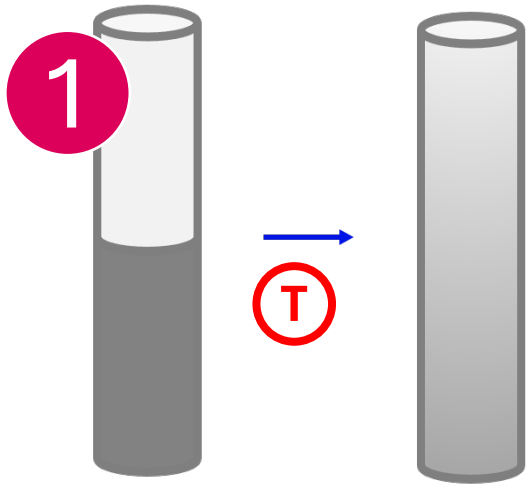

«Charged End» via electrochemical means (hydride layer) ⇨
(semi-)infinite hydrogen source upon subsequent thermal treatment

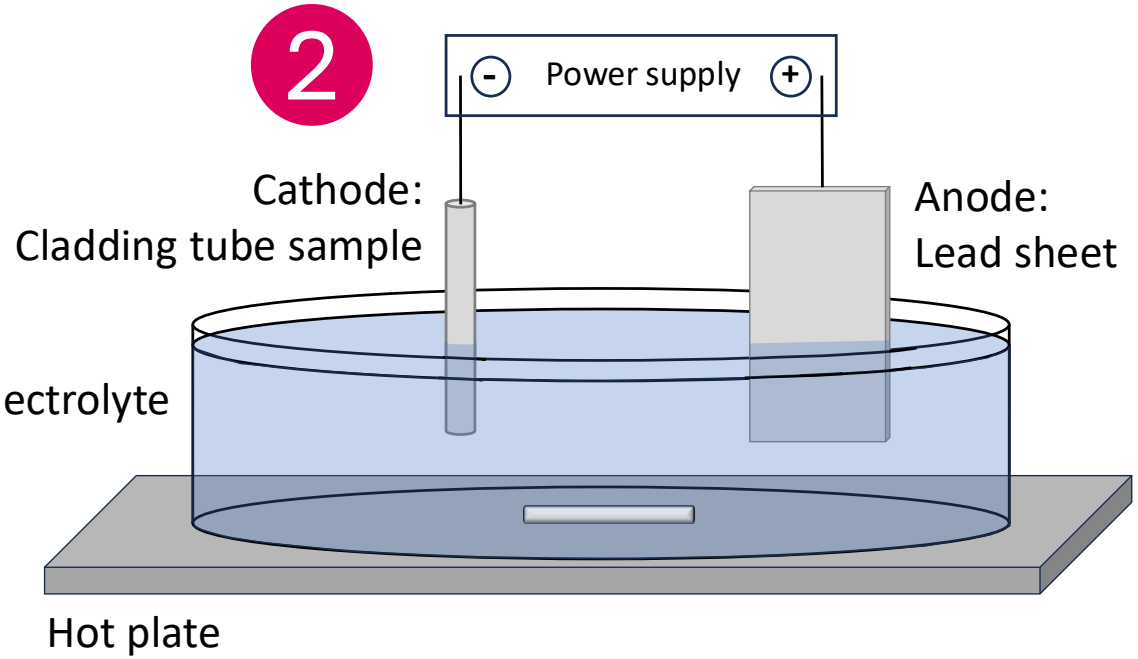

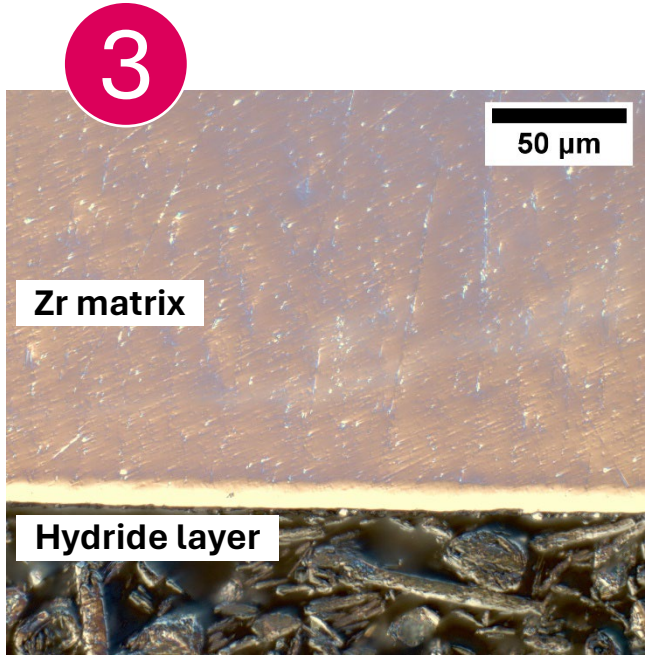

S. Niedermeyer et al, Analysis of Axial Hydrogen Diffusion and Hydride Precipitation in Zirconium Alloy Nuclear Fuel Claddings, TopFuel, 2025, Oct 5-9, Nashville, TN

Experimental Approach

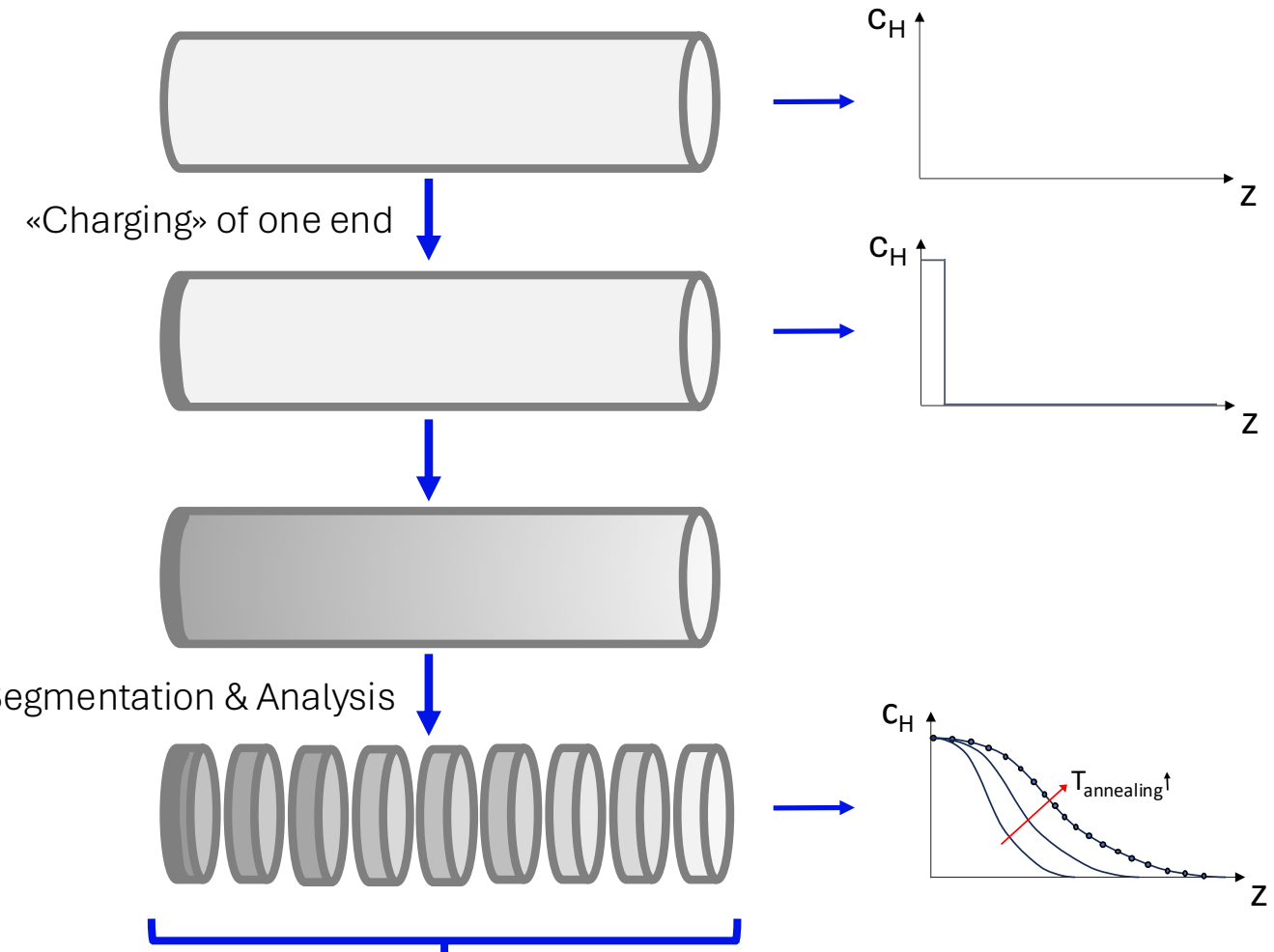

Hydrogen distribution:

- **Metallography**:
  Hydride morphology & distribution
- **Hot Gas Extraction (HGE):**
  Total hydrogen content
- **Neutron Imaging:**
  2D/3D visualization of hydrogen gradients

Preliminary Results – Diffusion Experiments

Good agreement with literature: Zircaloy 2-based alloys at comparable temperatures.

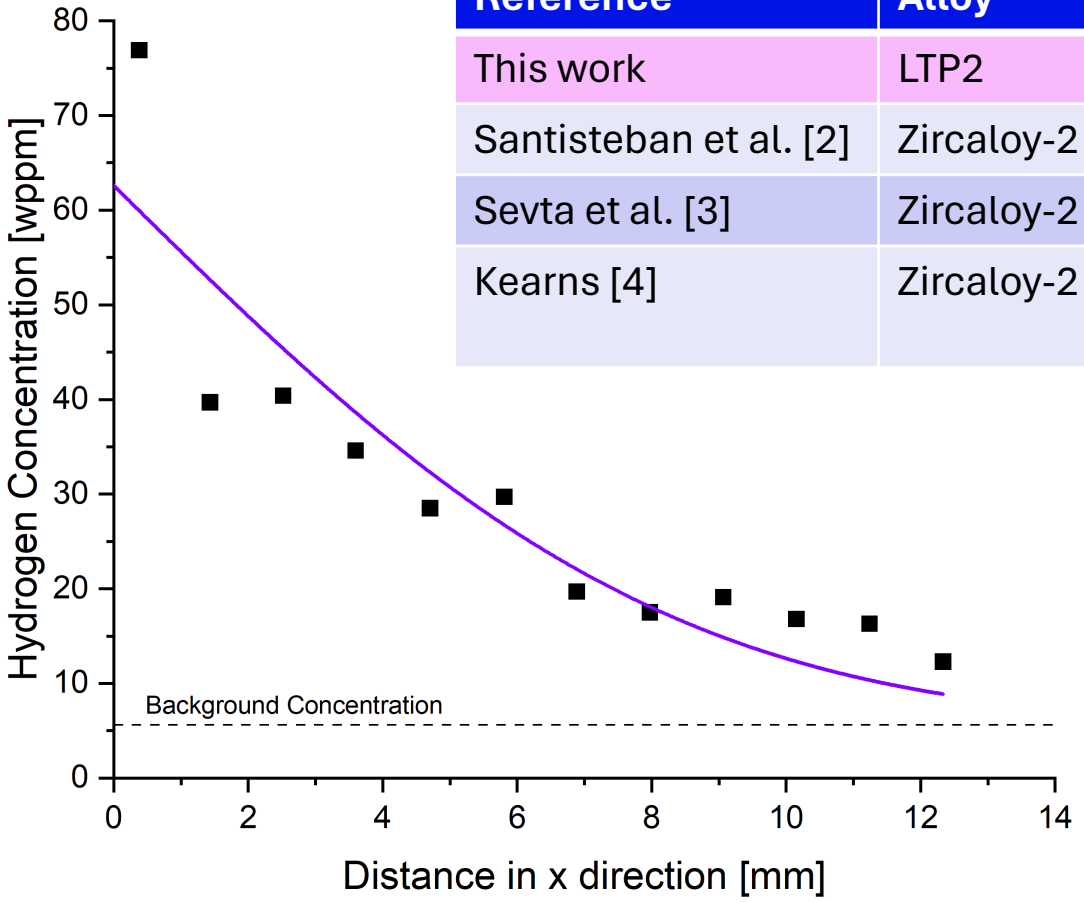

Reference	Alloy	Temperature	Diffusion Coefficient DH
This work	LTP2	300 °C	8.13×10^{-11} m²/s
Santisteban et al. [2]	Zircaloy-2 (various)	300 °C	$6 – 7 \times 10^{-11}$ m²/s
Sevta et al. [3]	Zircaloy-2	300 °C	4.25×10^{-11} m²/s
Kearns [4]	Zircaloy-2 (various)	335°C	$7.3 \times 10^{-11} – 11.8 \times 10^{-11}$ m²/s (avg. 9.84×10^{-11} m²/s)

- Diffusion experiments performed at different temperatures ⇨ enables determination of activation energy and pre-exponential factor via Arrhenius-type analysis according to

$$D_H = D_0 \times exp\left(\frac{-E_a}{RT}\right)$$

- Diffusion experiments on liner cladding are completed and await analysis.

Preliminary Results – HR-NI

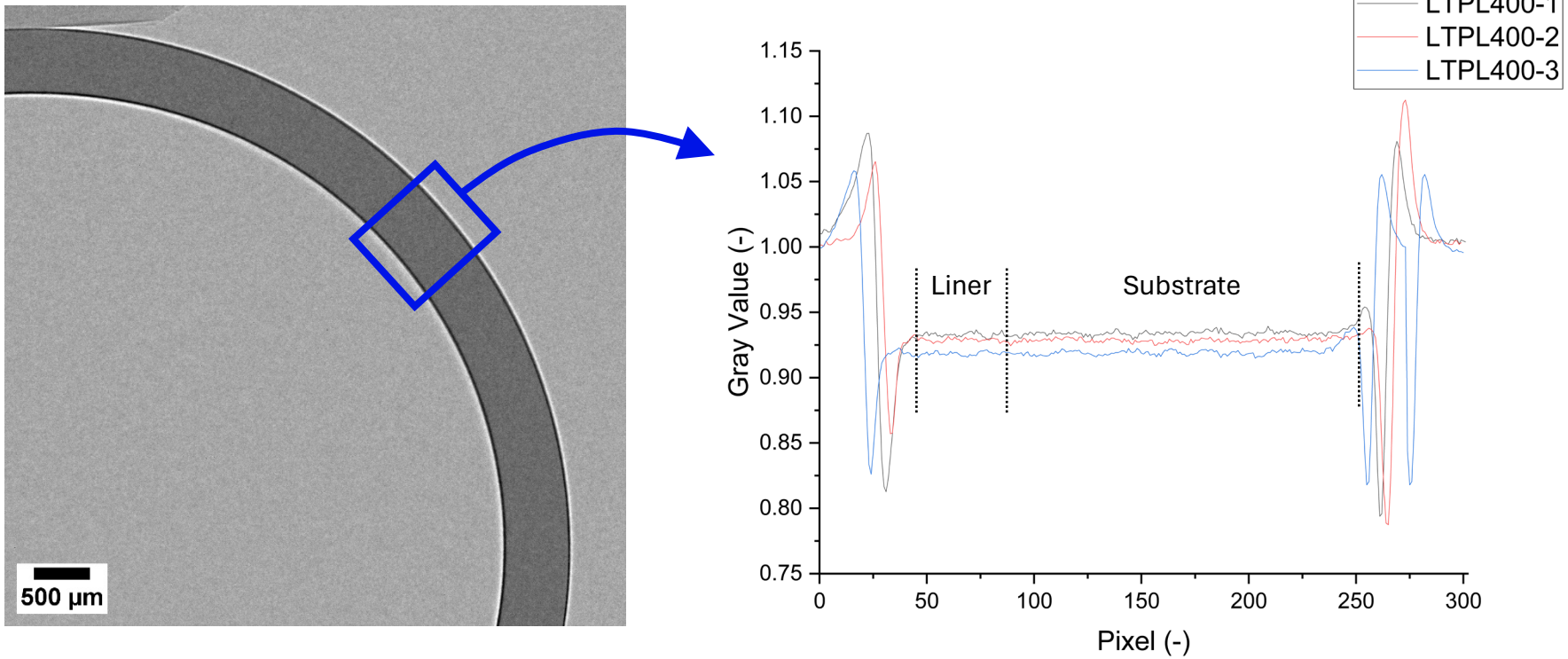

- No heterogeneity in radial direction in (inner) liner cladding validates use of 1D diffusion equations.
- Quenched!
- Differences expected for slowly cooled sections.

Preliminary Results – Model Comparison

Hydride Nucleation-Growth-Dissolution (HNGD)

- Hydride evolution by separating nucleation, growth, and dissolution
- Good agreement between experimental results and HNGD model

Simulation Parameter	Value
Hydride Layer Thickness	20 µm
Hydride Layer Concentration	17.600 wppm
Annealing Parameters	72 h @ 300 °C
Cooling Rate	quench
Node Width	20 µm

F. Passelaigue, E. Lacroix, G. Pastore, A.T. Motta, Implementation and Validation of the Hydride Nucleation-Growth-Dissolution (HNGD) model in BISON, Journal of Nuclear Materials 544 (2021) 152683, https://doi.org/10.1016/j.jnucmat.2020.152683

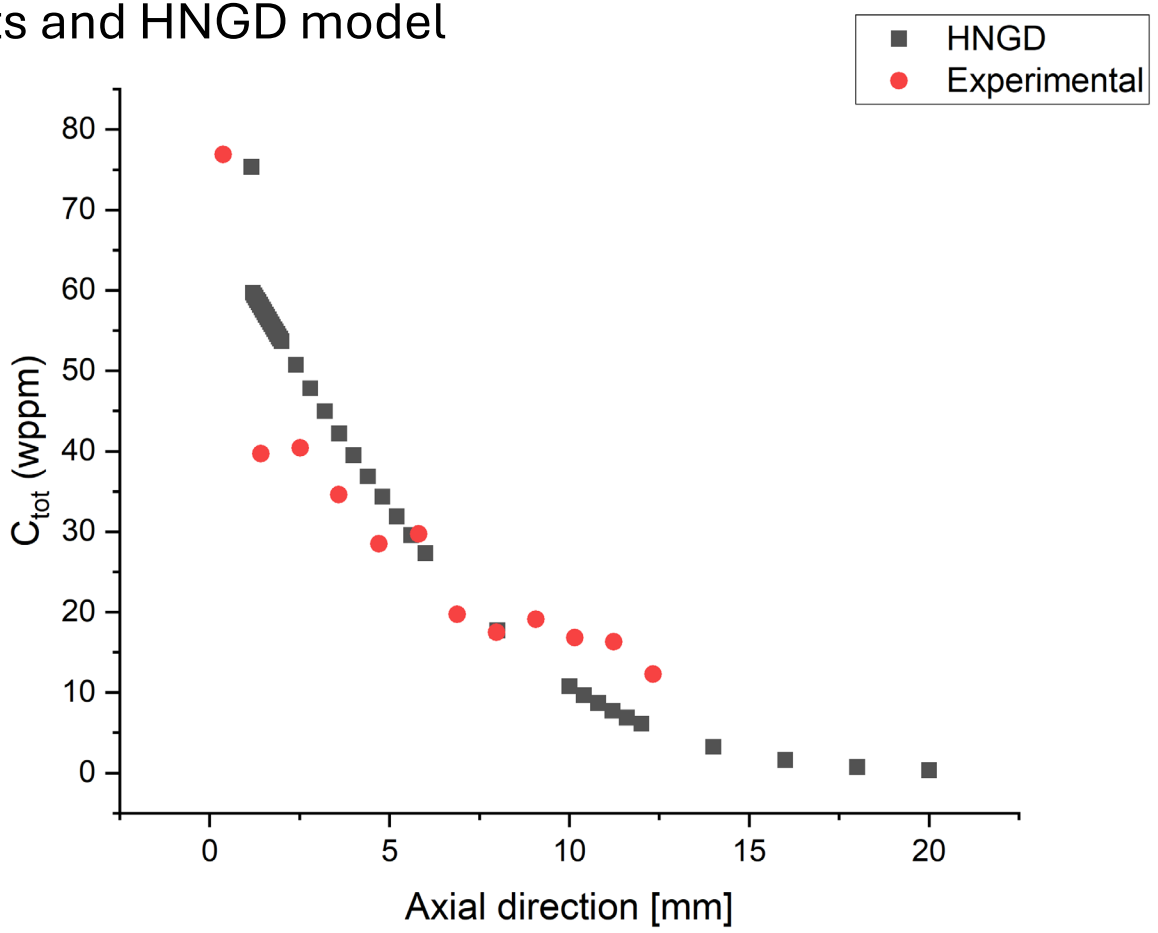

- Intro
- Axiality
- Creep
- Outlook

Creep Liner Cladding

Understanding of cladding creep in respect to intermediate dry storage

- Liner
  - Mechanical and chemical properties
  - Terminal solid solubility (TSS) for hydrogen
  - Texture/Microstructure
- Component properties

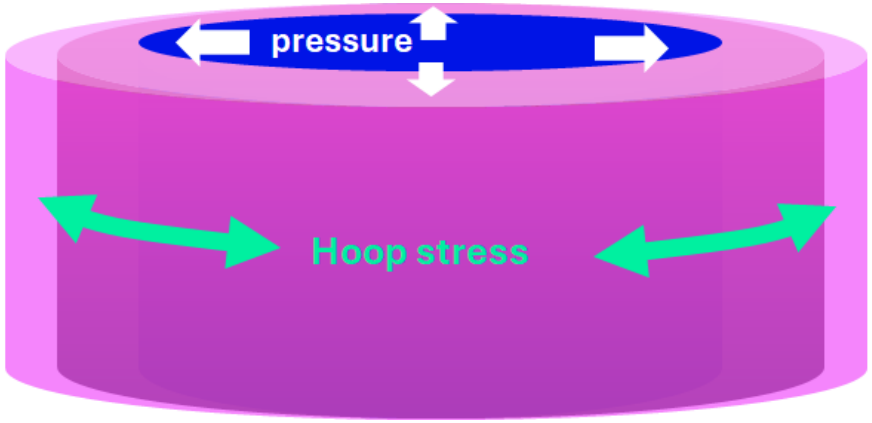

Approach – use of pre-product TREX

Obtain, as far as, possible material data of individual parts of duplex cladding

- Final product DX D4 too small wall thickness to separate materials ⇨ use pre-product TREX

Wall thickness ~ 0.75 mm
Liner thickness ~ 0.10 mm

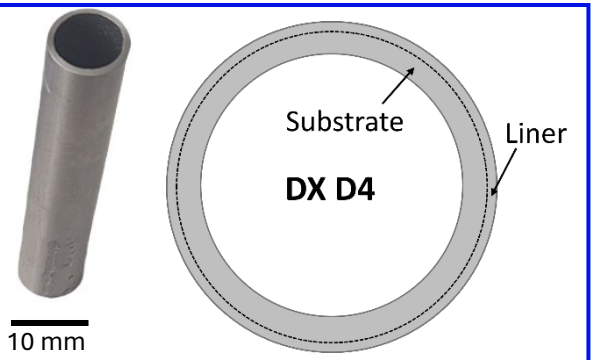

Wall thickness ~ 11 mm
Liner thickness ~ 2.5 mm

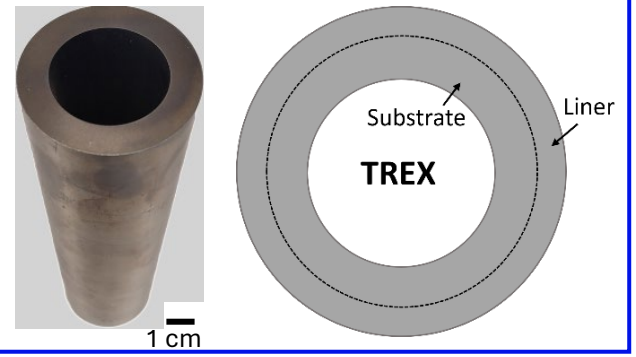

- Small samples can be machined out of the tube

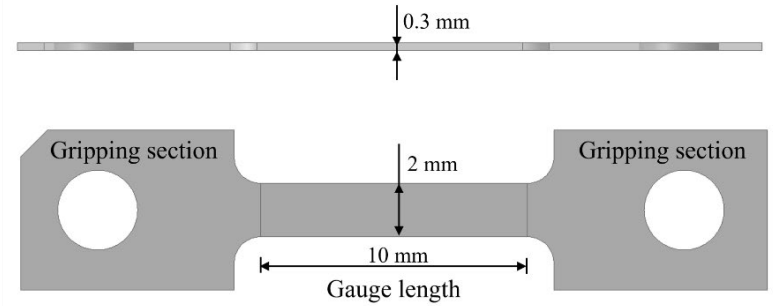

Liner and substrate dog-bone samples from TREX material

B. Buzzatti, Dry-Storage: Hydrogen Impact on Duplex Cladding, preliminary tests on mechanical properties, TopFuel, 2025, Oct 5-9, Nashville, TN

- TREX = DX D4 chemical composition of liner and substrate
  TREX ≠ DX D4 thermomechanical treatment, mechanical properties, microstructure

Approach – C-shape creep tests

Perform creep tests on C-shape samples

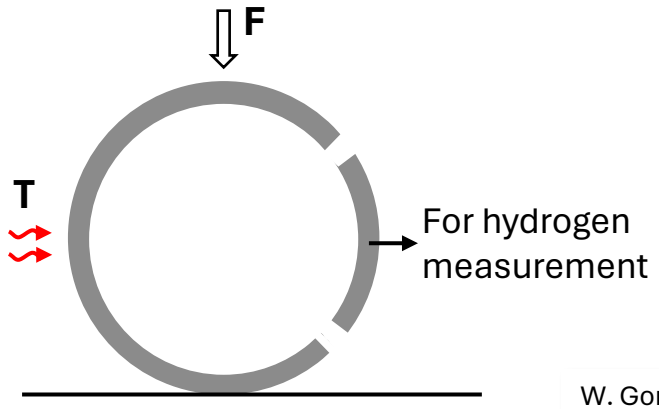

C-shaped creep compression test (3CT)

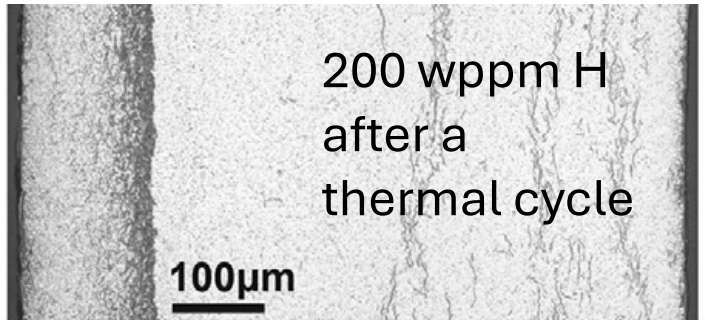

W. Gong, P. Trtik, F. Ma, Y. Jia, J. Li, J. Bertsch, Hydrogen diffusion and precipitation under non-uniform stress in duplex zirconium nuclear fuel cladding investigated by high-resolution neutron imaging, Journal of Nuclear Materials 570 (2022) 153971, https://doi.org/10.1016/j.jnucmat.2022.153971

P. Konarski, C. Cozzo, G. Khvostov, H. Ferroukhi, Modeling of hydrogen behavior in liner claddings, Journal of Nuclear Materials 573 (2023) 154125, https://doi.org/10.1016/j.jnucmat.2022.154125

Confirmed by DSC tests

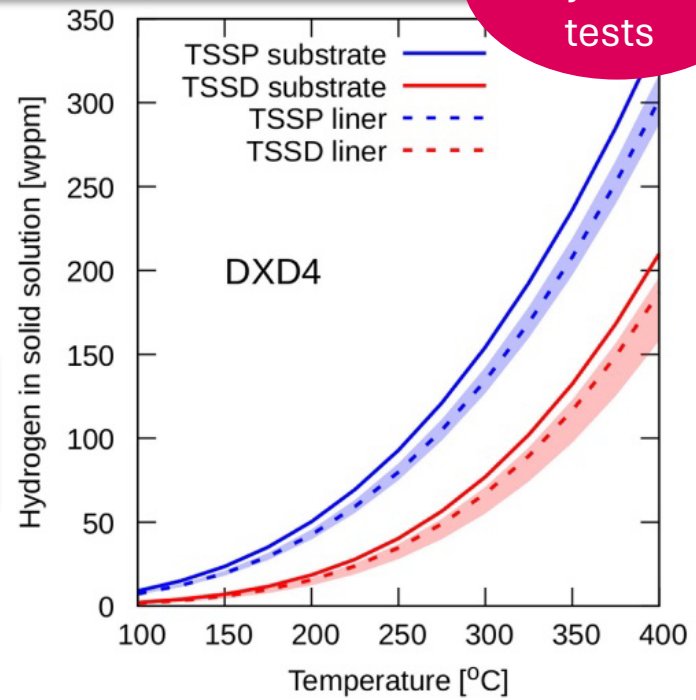

- Zry-4 and DX D4
- Hydrogenated or not, un-/irradiated, various temperatures
- Hydrogenation by gaseous process (in-house)
- Investigate hydrogen (re-)distribution with HR-NI
- Use FEM to link creep deformation and stresses, calculational feedback loop

- Hydrogen in solid solution accelerates creep, hydrides slow down creep
- Irradiation-induced hardening tends to reduce creep rate

First Results – TREX

Dogbone tests:

- Hydrogen (< 100 wppm) in TREX reduces both, $Rp_{0.2}$ and UTS
- At room temperature, crack initiation visible at $Zr(Fe, Cr)_2$ precipitates – confirmed by EDS analyses

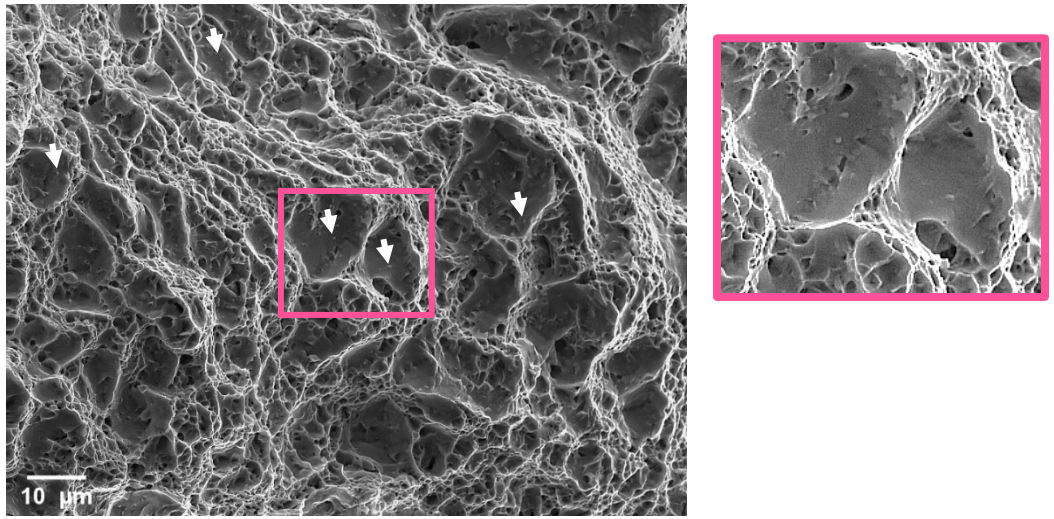

Substrate

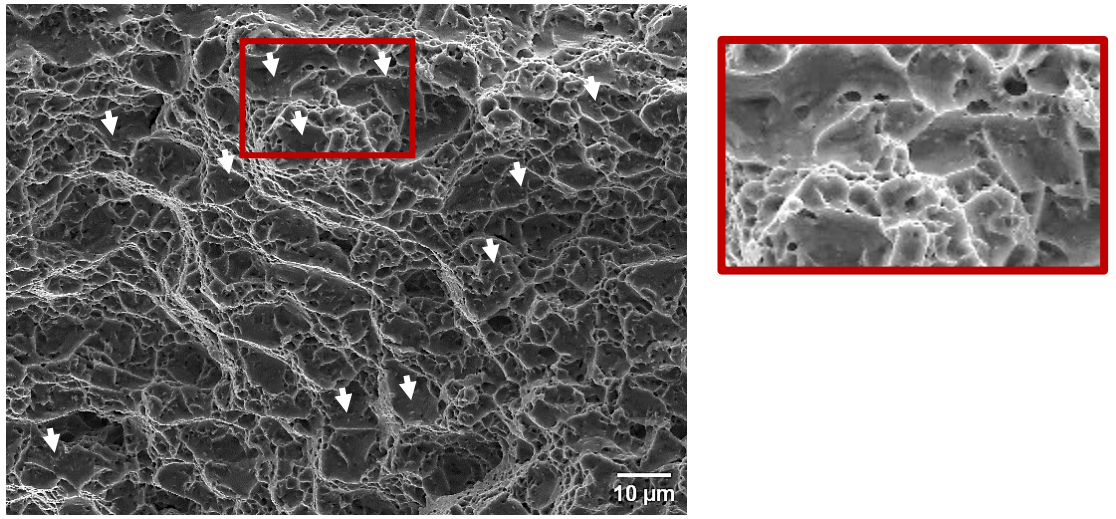

Liner

First Results – 3CT Tests

HR-NI C-shaped samples

- Imaging of DX D4 and Zr-4 as-received
- with 100 - 300 wppm of hydrogen

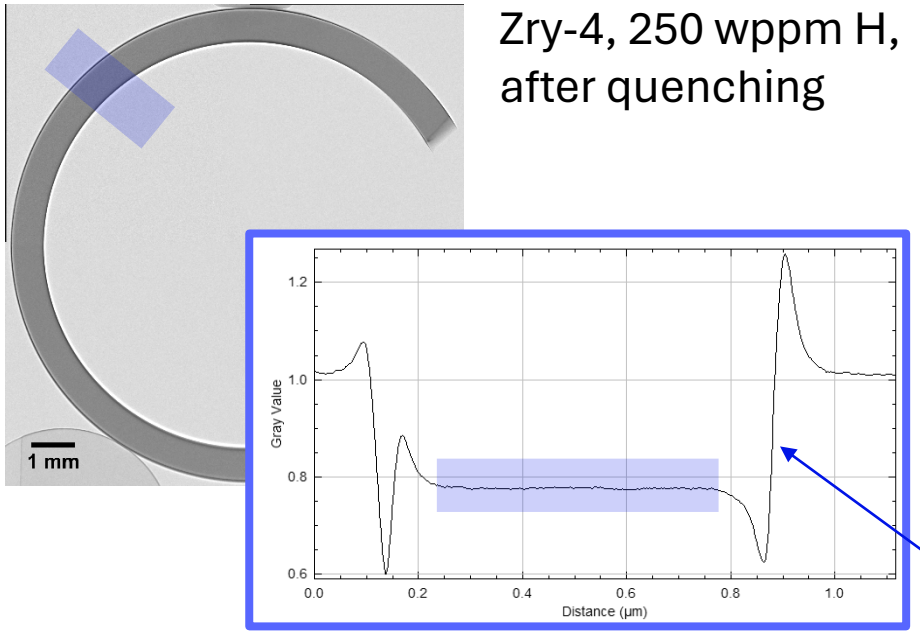

Zry-4, 250 wppm H, after quenching

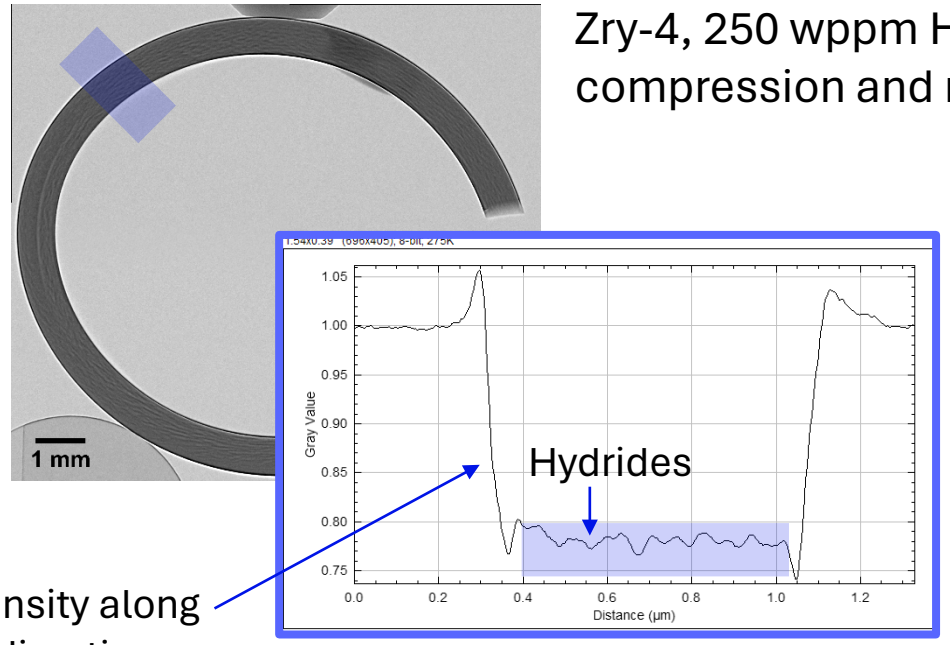

Zry-4, 250 wppm H, after full compression and natural cooling

Gray intensity along radial direction

- Intro
- Axiality
- Creep
- Outlook

Next Steps

Creep

- Continuation creep testing
- Implement FEM
- Irradiated Cladding

Axial diffusion

- Different cladding materials
- Slow cooling analyses
- Irradiated cladding

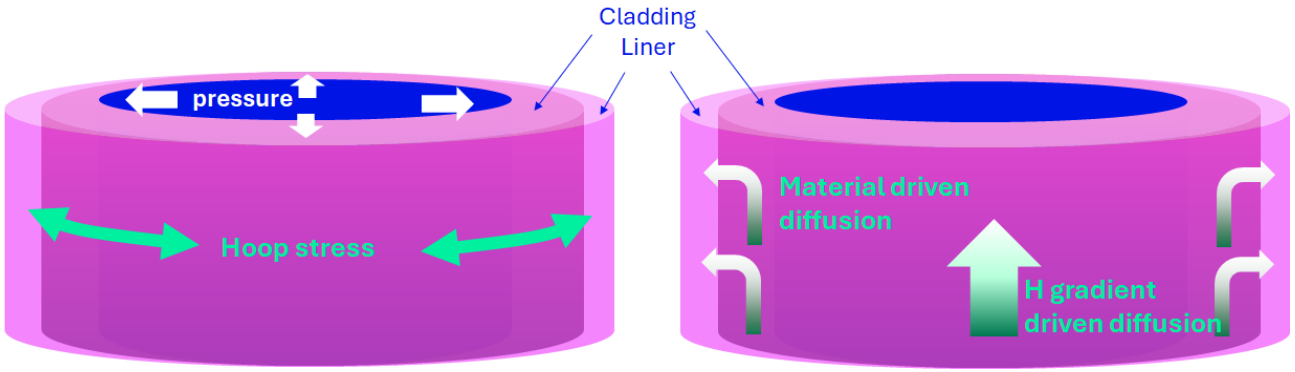

Take away messages …

… liner cladding is specific for intermediate dry storage

… liner accumulates hydrides, influencing creep and axial H diffusion

… 2 PhD projects: axial hydrogen diffusion and creep of liner cladding

My thanks go to

- BGZ for funding the axial diffusion PhD project
- swissnuclear for co-funding the creep PhD project
- Framatome for supplying test materials
- SINQ/Applied Materials Group

Thank you for your attention

Apou Martial Kpemou

ASNR

Dedicated investigation of secondary hydriding: experimental insights and modelling

Secondary hydriding, which refers to the absorption of hydrogen by the cladding inner surface following high temperature oxidation, can occur during a LOCA (Lost of Coolant Accident) transient in case of cladding burst which allows steam ingress inside the fuel rod. This hydriding phenomenon results in high hydrogen, potentially leading to cladding material embrittlement. Many research institutes conduct semi–integral tests to study the cladding behaviour during a LOCA transient. These tests combine several coupled phenomena, making it challenging to perform a detailed analysis of the secondary hydriding phenomenon.

This paper aims at presenting the new and dedicated experimental protocol developed to finely characterize the secondary hydriding phenomenon under LOCA conditions.

Separate-effects tests were conducted with controlled geometries to better characterize the secondary hydriding phenomenon on fuel claddings. These tests allow investigating oxidation duration and temperature, gap size, pellet positioning inside the cladding, steam proportion, and cladding opening size and shape influence.

The developed protocol also encompasses a series of post-test examinations to evaluate the metallurgical transformations induced by oxidation, as well as hydrogen diffusion within the cladding. The protocol was specifically designed to provide data for code validation. Based on these tests, a modelling study was conducted, under axisymmetric conditions, enabling the simulation of the secondary hydriding phenomenon using the SHOWBIZ code.

The results obtained from both the experimental and modelling work conducted in this study provide valuable insight into the phenomenology of the phenomenon and help to better understand the observations reported on deformed cladding geometries from semi-integral tests.

ASNR Autorité de sûreté nucléaire et de radioprotection

[Stuckert et al., 2020, Grosse et al., 2006]

30TH INTERNATIONAL QUENCH WORKSHOP (16 – 18 DECEMBER 2025)

DEDICATED INVESTIGATION OF SECONDARY HYDRIDING: EXPERIMENTAL INSIGHT AND MODELLING

A. M. KPEMOU, S. GUILBERT, T. TAURINES, J. DESQUINES

Context – LOCA transient

Steam High Temperature (HT) oxidation

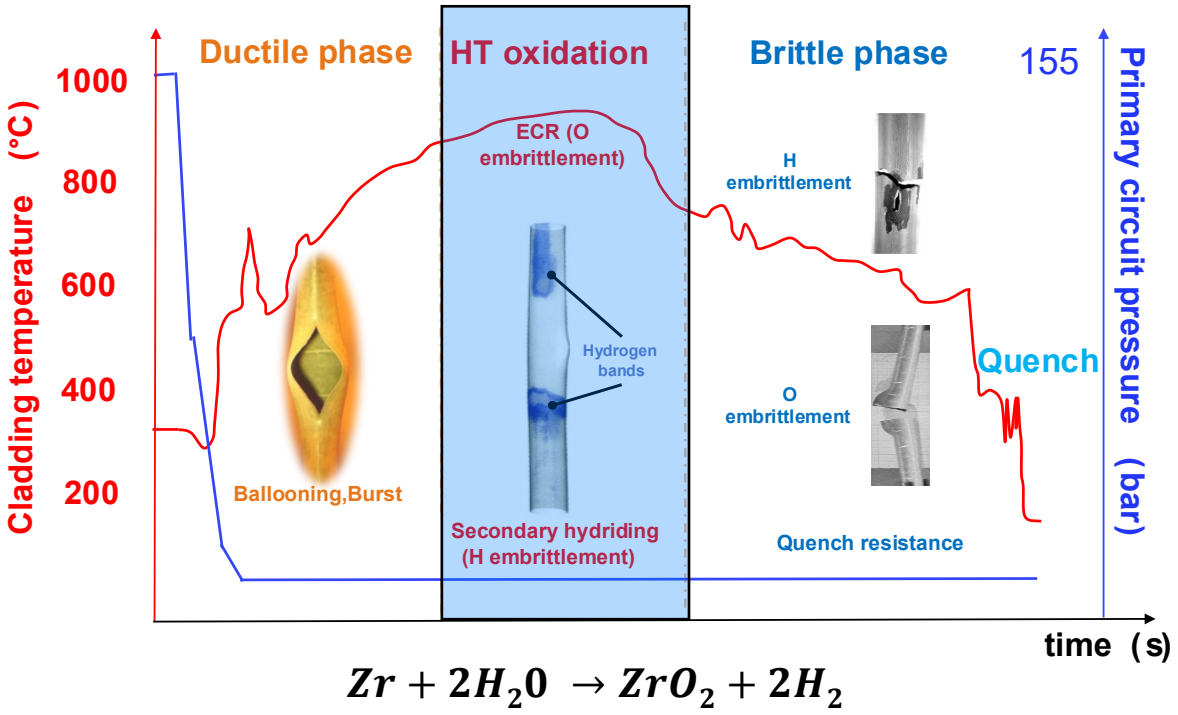

$$Zr + 2H_20 \rightarrow ZrO_2 + 2H_2$$

→ Cladding is oxidised at high temperatures

→ Hydrogen absorption at the inner cladding surface if burst (secondary hydriding phenomenon)

[Stuckert et al., 2020, Grosse et al., 2006]

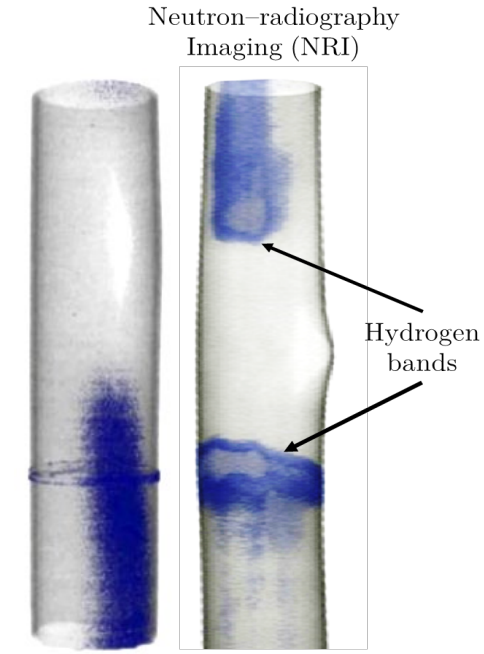

[Billone et al., 2008]

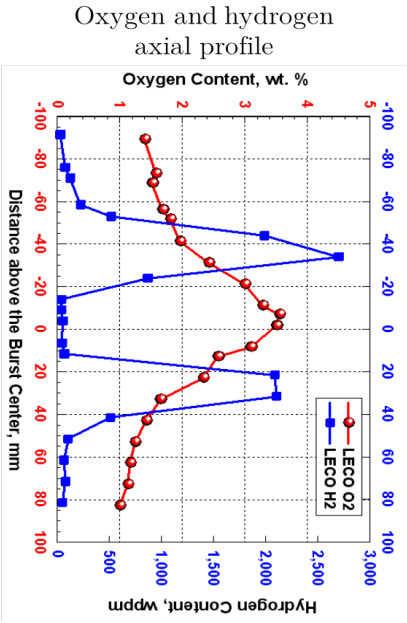

→ Two hydrogen peaks located on both sides from the opening

→ Heterogeneous hydrogen spatial distribution within the cladding

Context – problematics

Cladding 3D geometries

High Temperature (HT) oxidation

[Stuckert et al., 2020, Grosse et al., 2006]

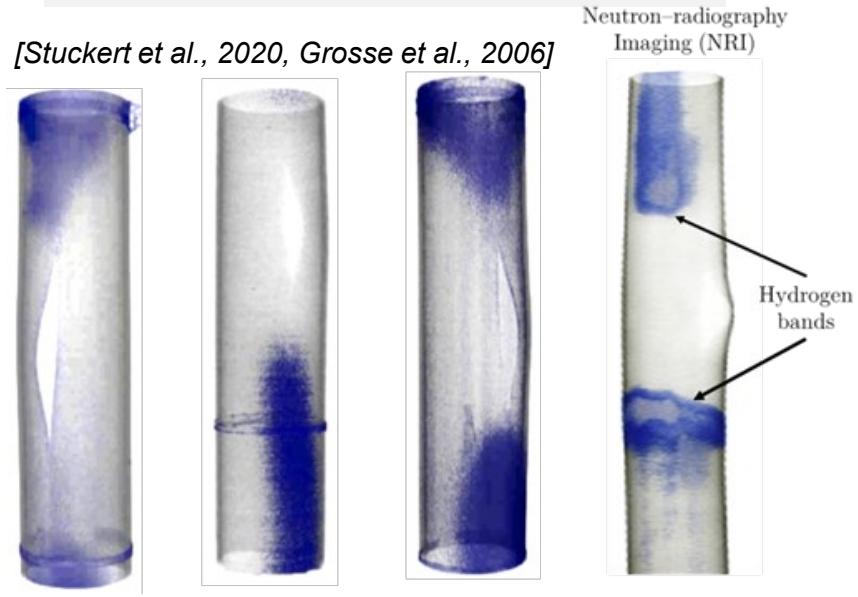

The **deformed geometry** influences **the secondary hydriding**

Brittle phase (quench)

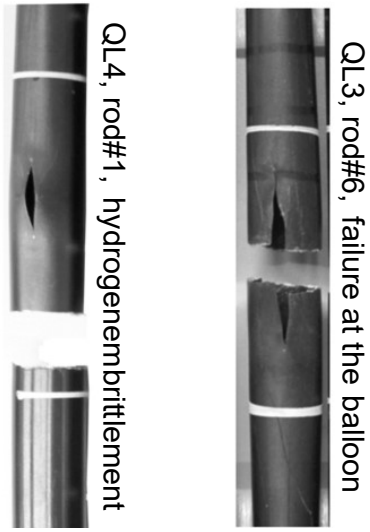

Cladding **embrittlement**

→ The secondary hydriding is studied on deformed cladding geometry

→ Studying key parameters influencing phenomenon in this configuration is complex

New approach to allow characterising the secondary hydriding phenomenon with controlled geometries

Context – Objective and approach

characterise the secondary hydriding phenomenon and its induced embrittlement on fuel claddings with controlled geometries

Experimental characterisation of secondary hydriding

→ New dedicated experimental protocol development

→ Separate effects study of the phenomenon

→ Data for code validation

Modelling of the secondary hydriding phenomenon

→ Modelling with SHOWBIZ* code

→ 1D axisymmetric modelling

→ Parametric study of the phenomenon

*SHOWBIZ: Studying Hydrogen and Oxygen Weakening Behaviour in Zirconium

Experimental methods – Applied thermal transient

The applied thermal transient

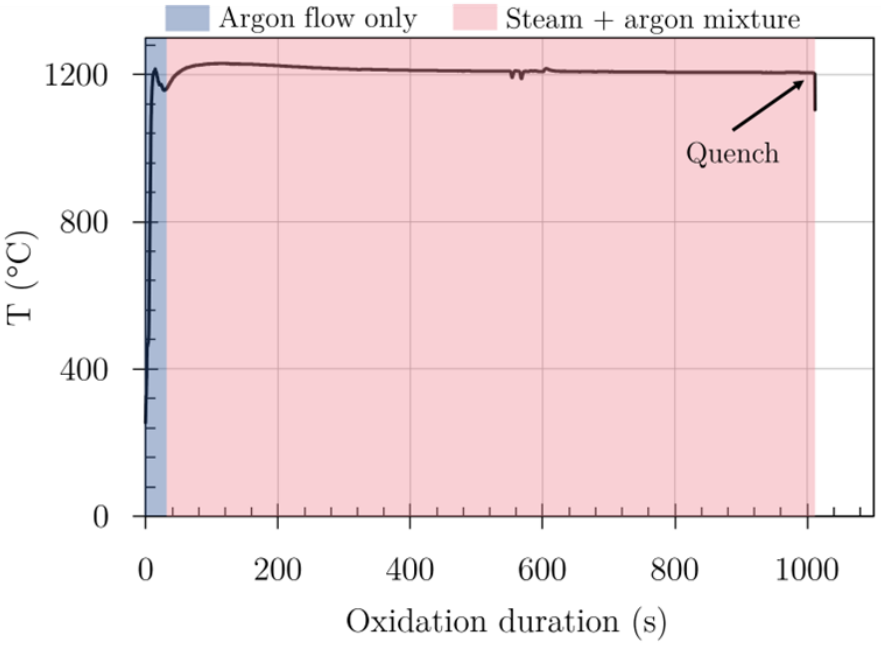

→ **Phase 1 in argon flow** to fill the sample with Ar and simulate rod gas filling before burst (T_{rate} > 50 °C/s)

→ **Phase 2 in argon (50%) + steam (50%) flow**, to allow steam ingress in the cladding for the oxidation process

Vertical furnace

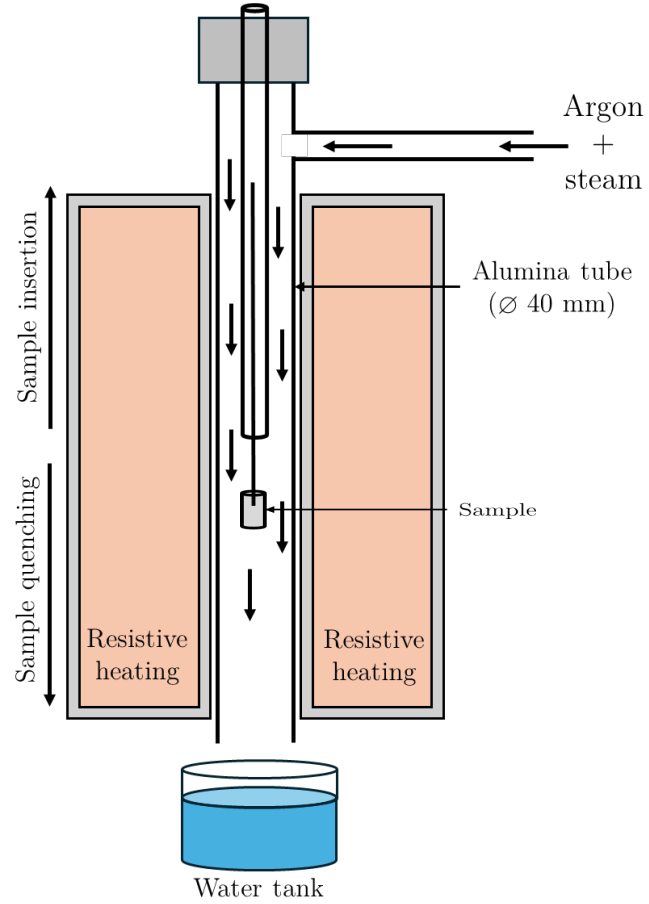

→ The cladding **ballooning** is not reproduced (non deformed cladding geometry)

→ Tests are performed under **LOCA conditions** reproducing the **HT oxidation phase**

Experimental methods – Tested samples

SETs' sample geometry

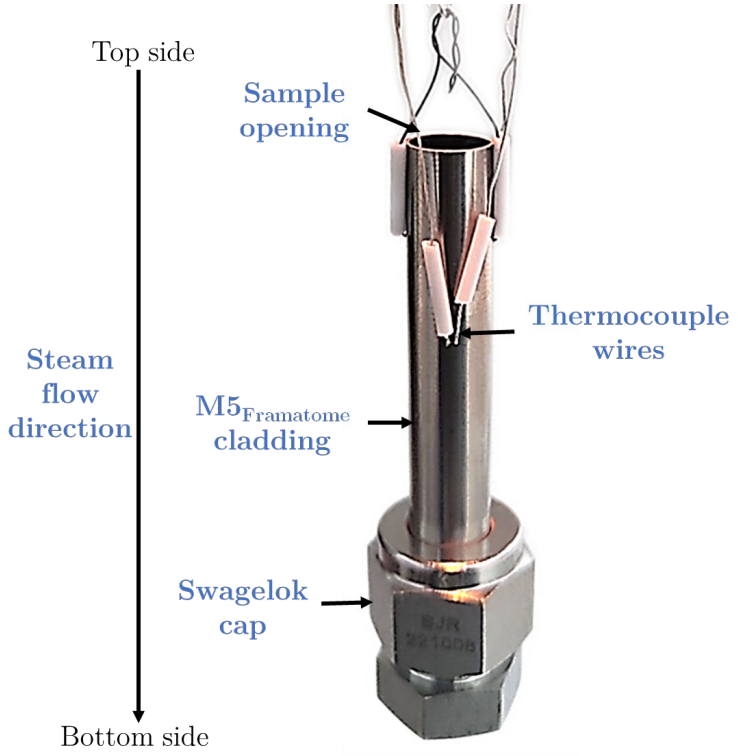

Non deformed cladding with opening at the top

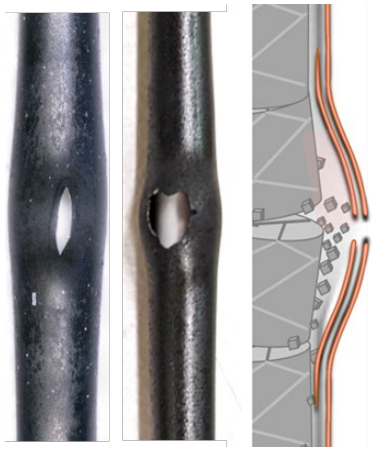

Conventional deformed cladding geometry

SOTs' sample geometry

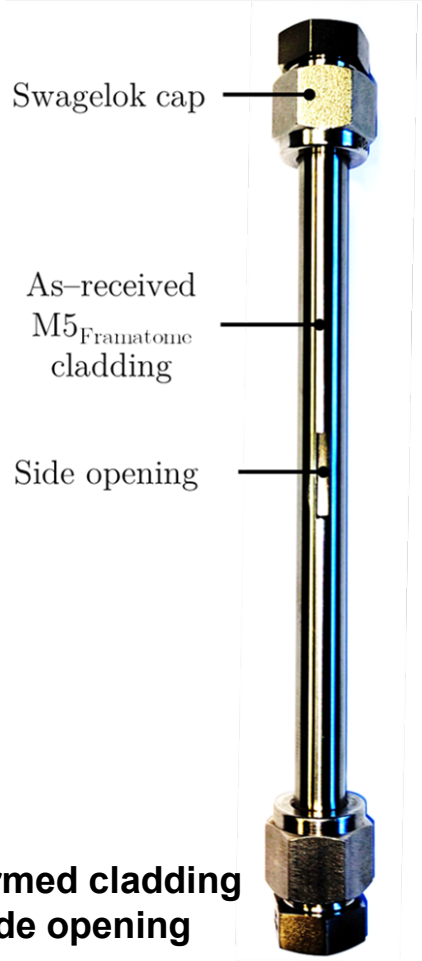

Non deformed cladding with side opening

Non-deformed cladding geometry for a better control of tests parameters

Experimental methods – Post–test characterisations

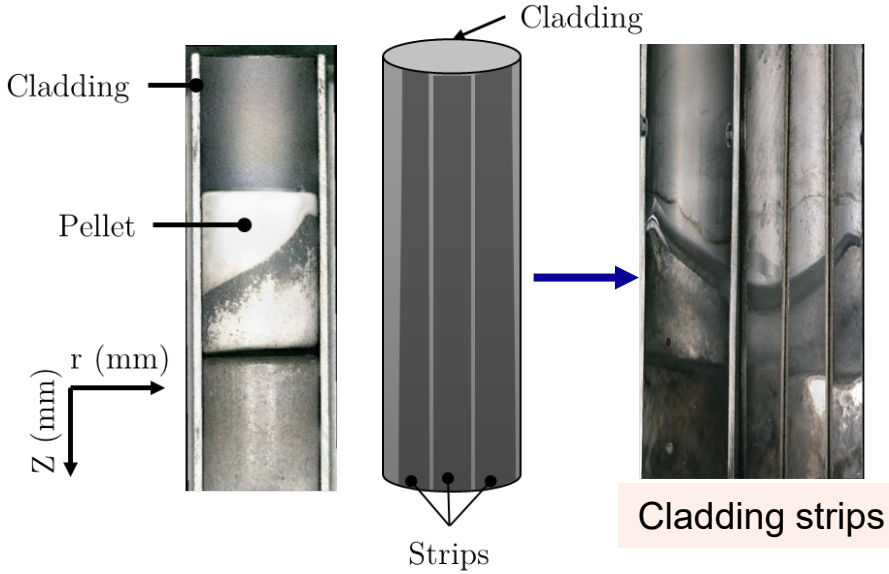

Cladding strips

Complementary H measurement techniques

→ Hot Vacuum Extraction (HVE)

→ Neutron Radiography Imaging (NRI)

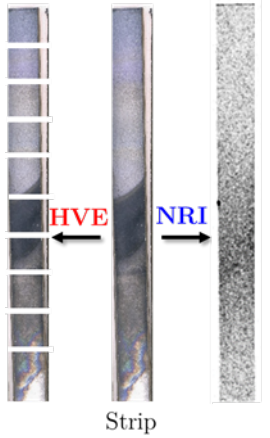

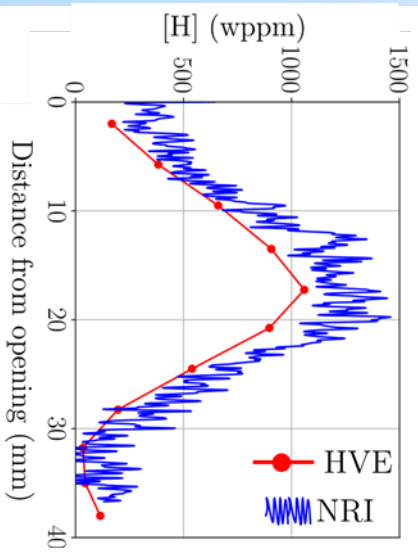

Embedded cladding strip (destructive)

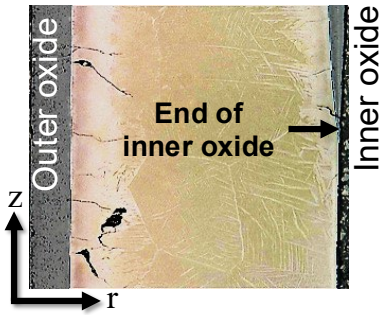

Metallographic analyses

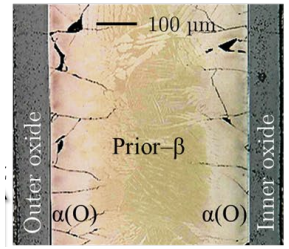

EPMA

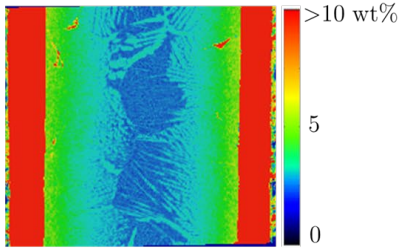

µ-LIBS

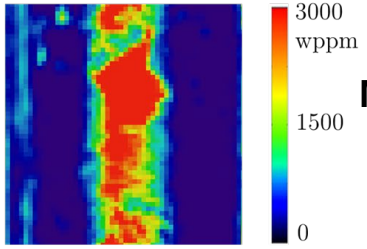

Micro–analyses

01 SEPARATE EFFECTS STUDY OF SECONDARY HYDRIDING (SETs)

Study of key parameters effects on secondary hydriding using a non-deformed cladding geometry with an opening at the top

i. Experimental methods – SETs samples geometry

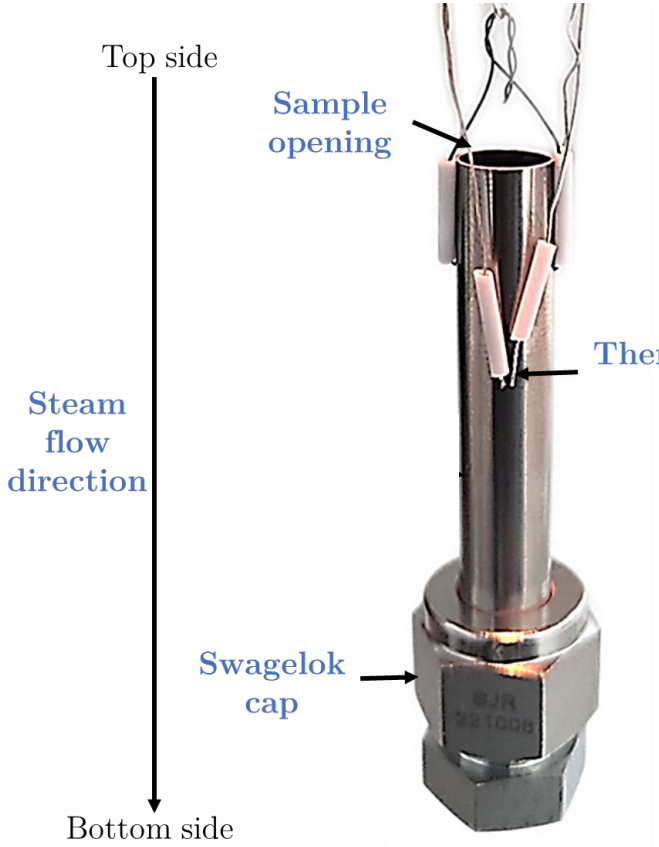

2D schematic view

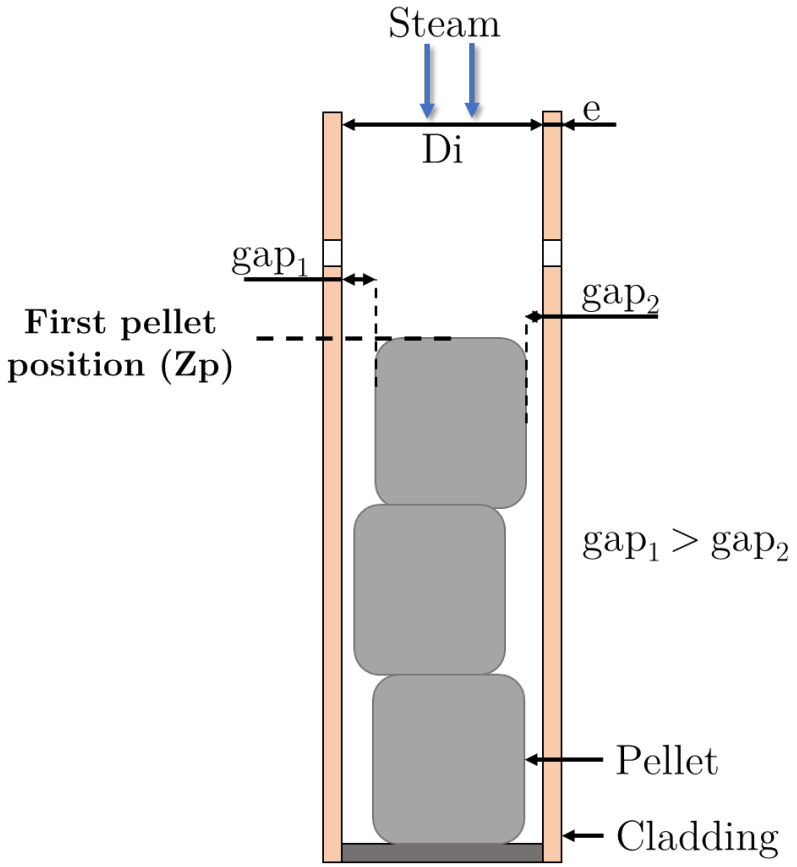

→ **Opening at the top side** of the sample (to allow axisymmetric steam ingress)

→ **Free positioning** of stacked pellets inside the cladding

→ **1D axisymmetric** modelling with well-defined boundary conditions

Experimental methods – Parametric study

Influence of **several parameters**:

→ Pellets positioning inside the cladding

→ Oxidation temperature [1100°C – 1200°C] and duration [100s – 1400s] (**)

→ Average gap size [80 µm, 130 µm, 230 µm] (**)

→ Opening size [2 mm, 4 mm] (**)

→ pre–oxide layer [6 µm, 8 µm, 12 µm] (**)

→ Steam partial pressure

(**) Modelling sensitivity study performed

Results published in [A.M. KPEMOU et al., 2025]

Pellet positioning

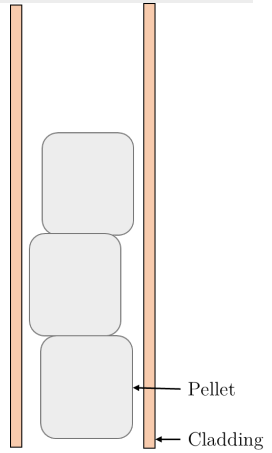

Average Gap size

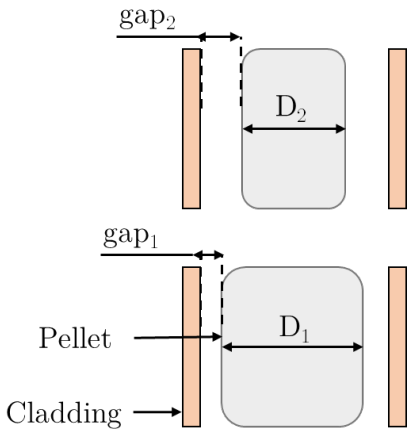

Oxidation duration and temperature

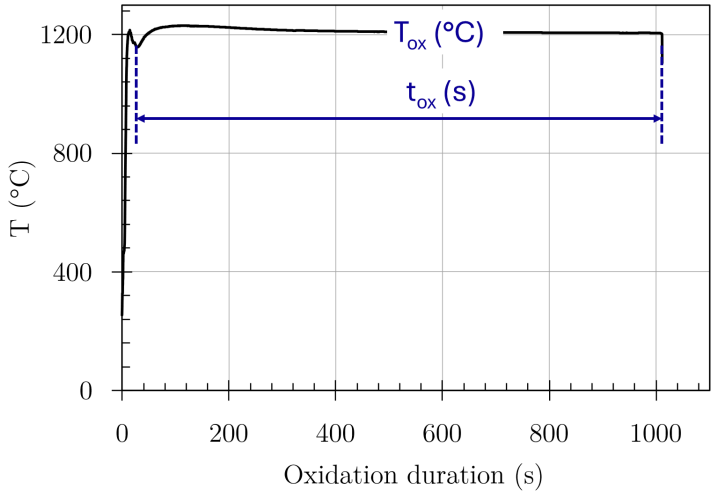

A.M. Kpemou, S. Guilbert, J. Desquines, T. Taurines, M.C. Baietto, B. Normand, J. Soulacroix, A. Ambard, F. Bourlier, A new approach to investigate secondary hydriding phenomenon on M5Framatome clads under high–temperature LOCA conditions, J. Nucl. Mater. 603 (2025) 155462. https://doi.org/10.1016/j.jnucmat.2024.155462.

Results – Influence of pellets positioning / gap variation

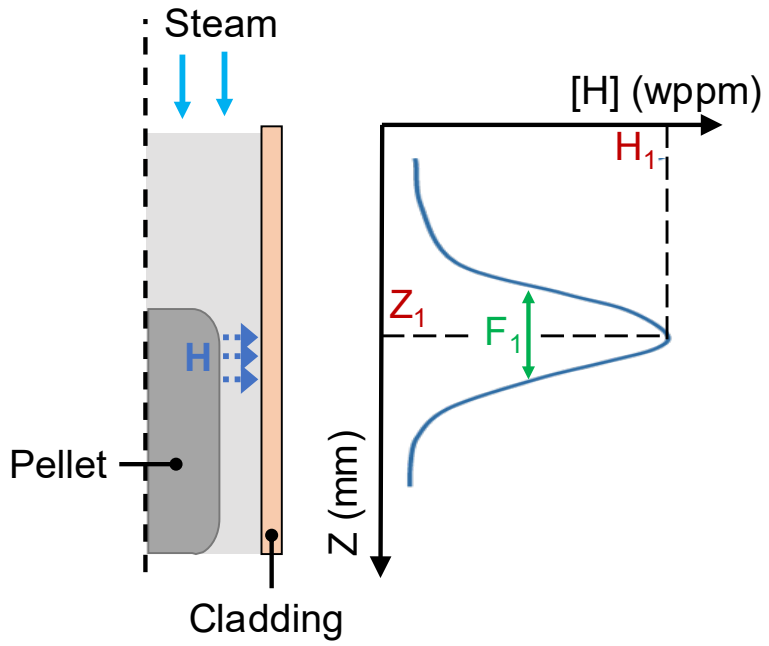

When the local gap increases (few µm)

$Z_1 < Z_2$ and $H_2 < H_1$

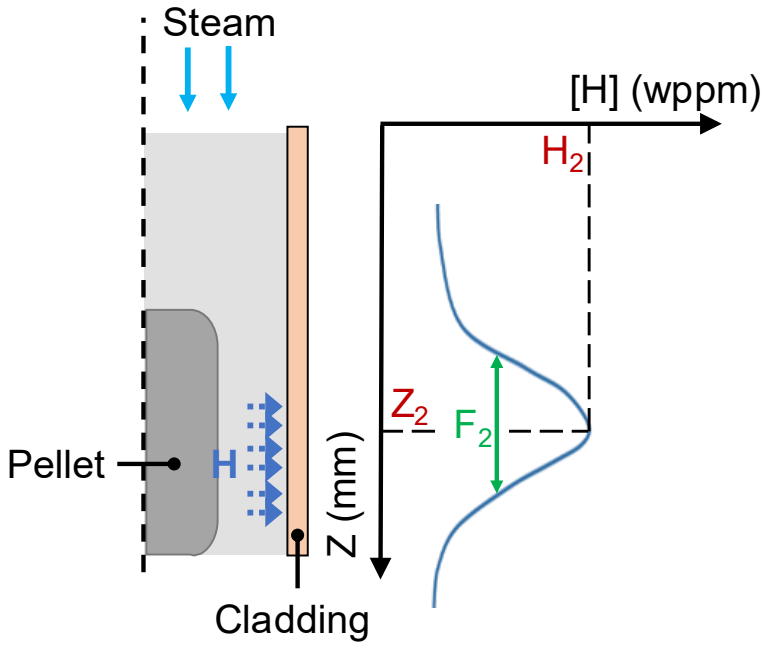

→ **Gases transport** in the gap **is reduced**

→ **H-peak** is **near the first pellet** position

→ H-profile exhibits a **narrow profile**

→ **Gases transport** in the gap is **facilitated**

→ **H-peak** shifts about **few mm** along the pellet

→ H-profile exhibits a **wider profile**

Local gap closure induce closeness of hydrogen peaks on irradiated fuel rods compare to unirradiated

[Nagase and Fuketa, 2006]

Results – Influence of oxidation temperature and duration

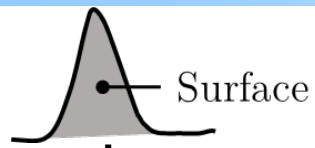

Evolution of the **overall** H content

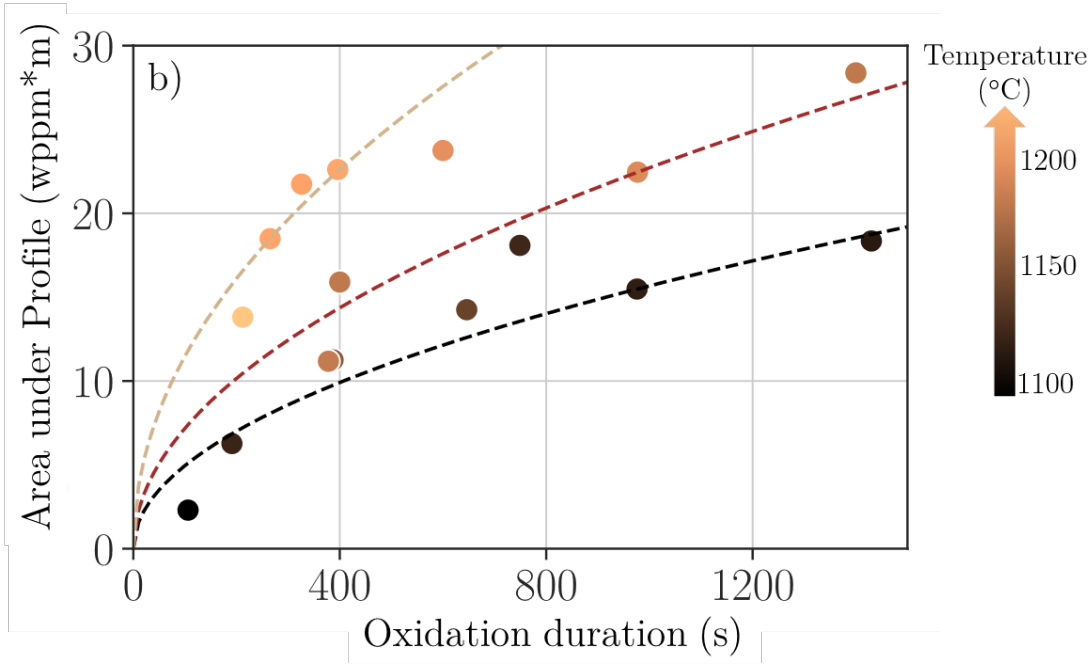

Corresponding ECR

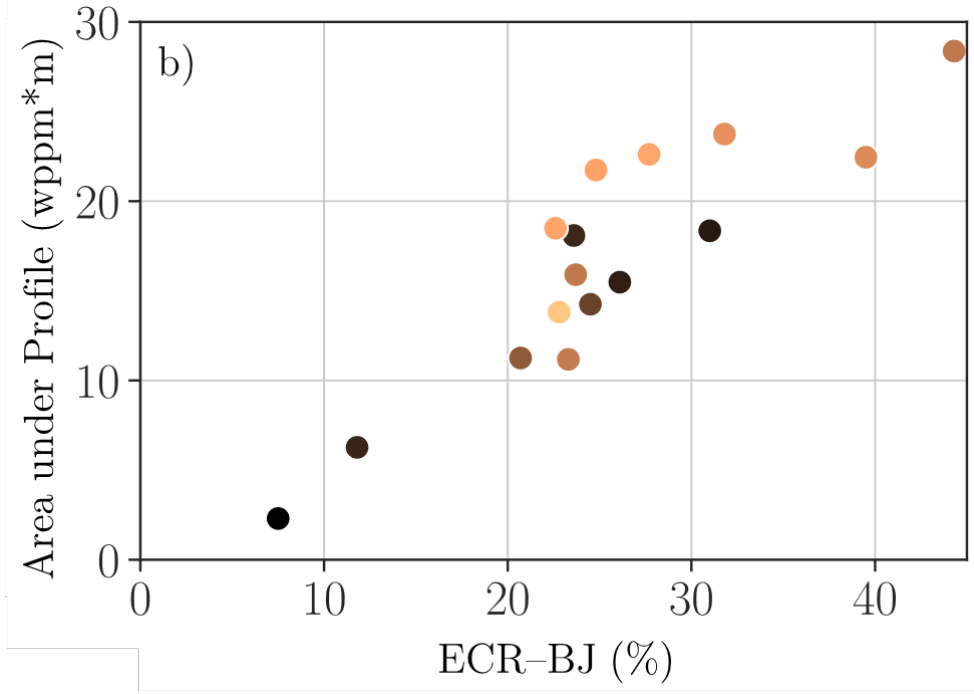

→ The total H content increases with respect to the duration (parabolic trend) and the temperature

→ The total hydrogen content increases linearly with the cladding ECR degree

Results – Secondary hydriding process

Secondary hydriding based on SETs' results

Sample schematic view

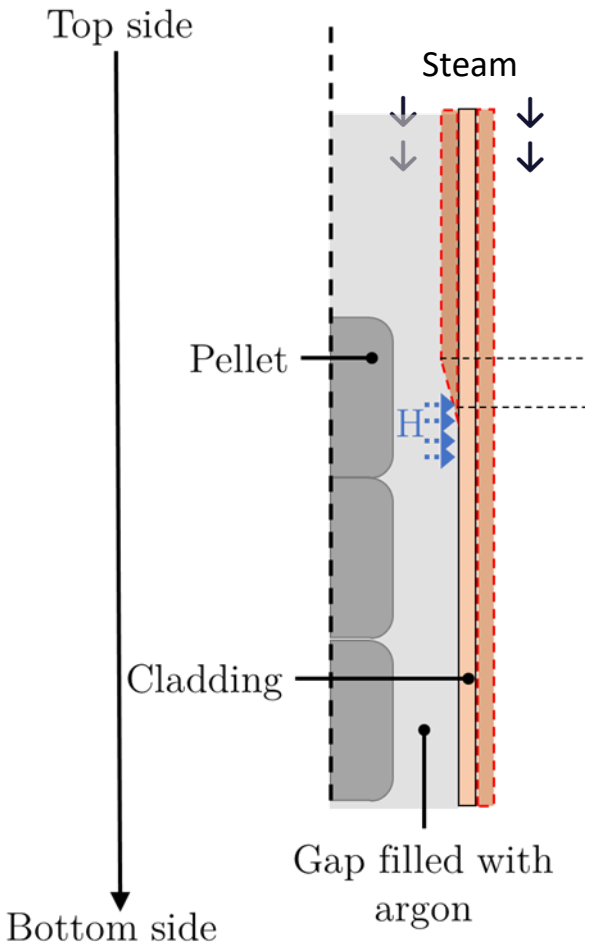

Inner oxide axial profile

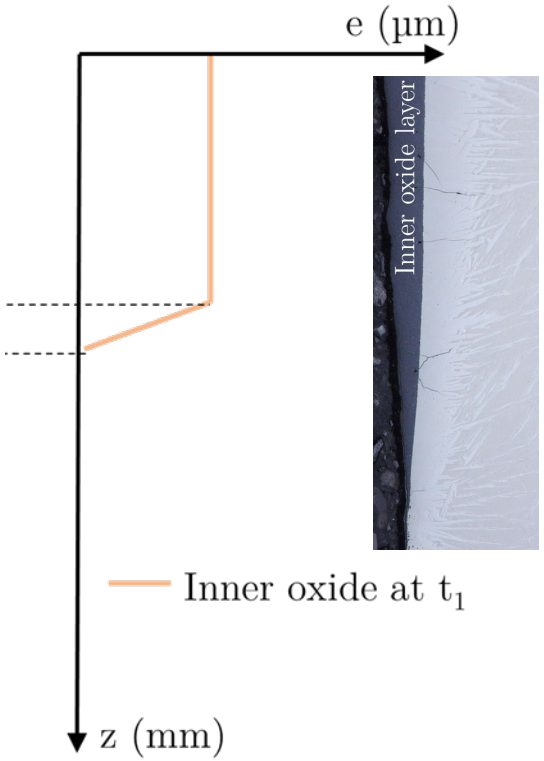

Hydrogen axial profile

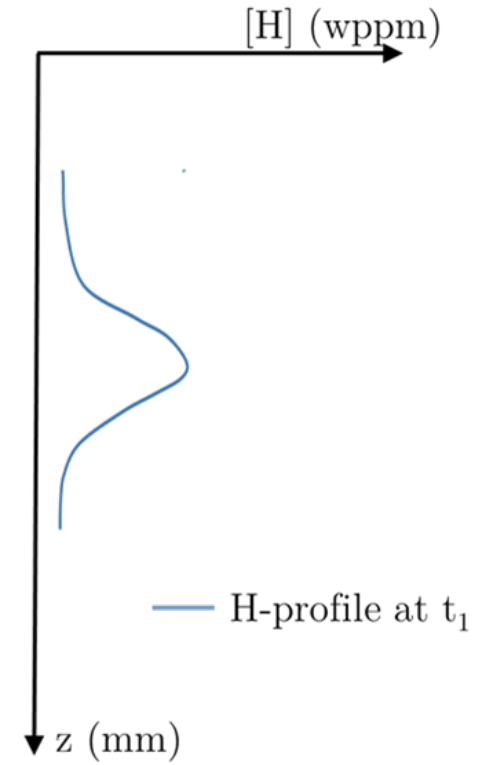

Results – Secondary hydriding process

Secondary hydriding based on SETs' results

Sample schematic view

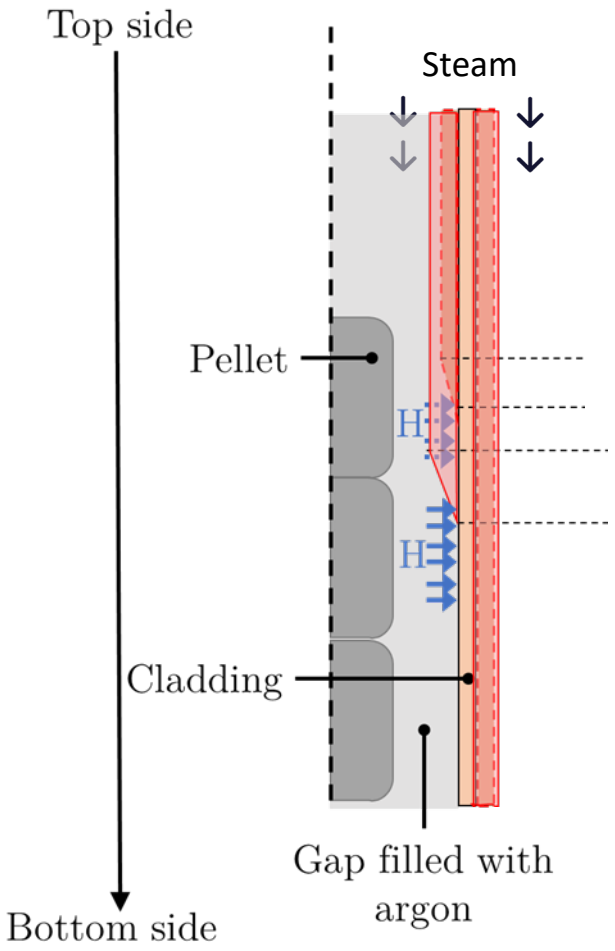

Inner oxide axial profile

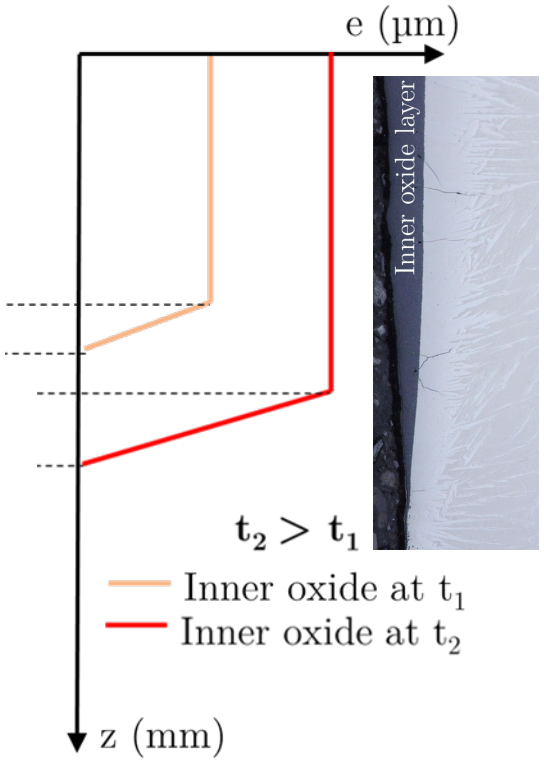

Hydrogen axial profile

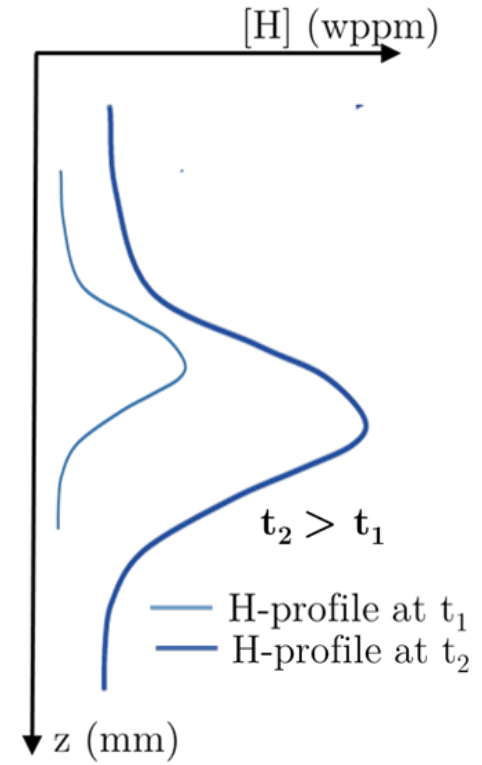

The current **understanding of the phenomenon** was used to **support** the **modelling** work

Modelling – Approach

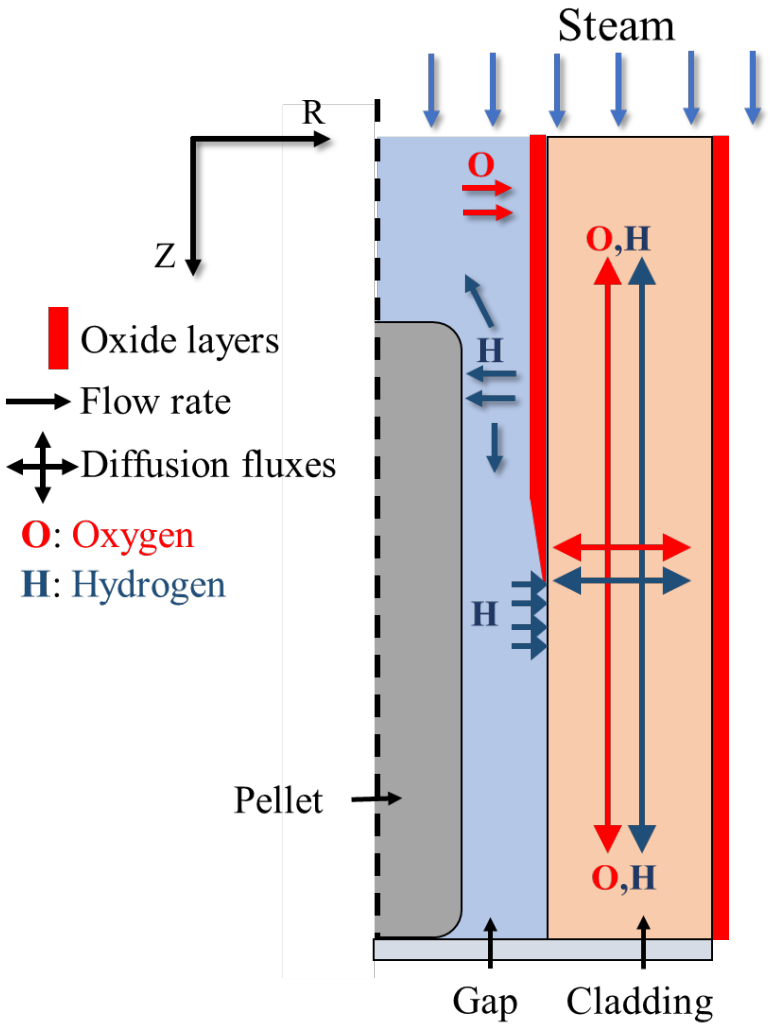

1D axisymmetric modelling with the **SHOWBIZ*** software

Gases transport (steam, filling gas, hydrogen…)

→ 1D axisymmetric modelling of the pellet and the gap

→ Steam, hydrogen and argon transport in the gap

→ Advective (Darcy + Poiseuille) and diffusive laws

Chemical reactions

→ Cladding inner and outer oxidation reaction

→ Hydrogen absorption (Sievert law where the oxide layer is thinner than 0.5 µm)

2D diffusion in the cladding

→ Oxygen and hydrogen diffusion within the material

→ Cladding metallurgical transformation due to the oxidation (ZrO_2 and α(O))

→ Simulated results' trends were found consistent with experimental results

→ Refinements of the modelling “boundary conditions are needed (Overestimation of the H uptake)

*SHOWBIZ: Studying Hydrogen and Oxygen Weakening Behaviour in Zirconium

02 SECONDARY HYDRIDING ON SAMPLE WITH A SIDE OPENING (SOTs)

Study of different opening shape and size effects on the secondary hydriding phenomenon using non-deformed sample with a side opening

Experimental methods – Sample geometry and opening shapes

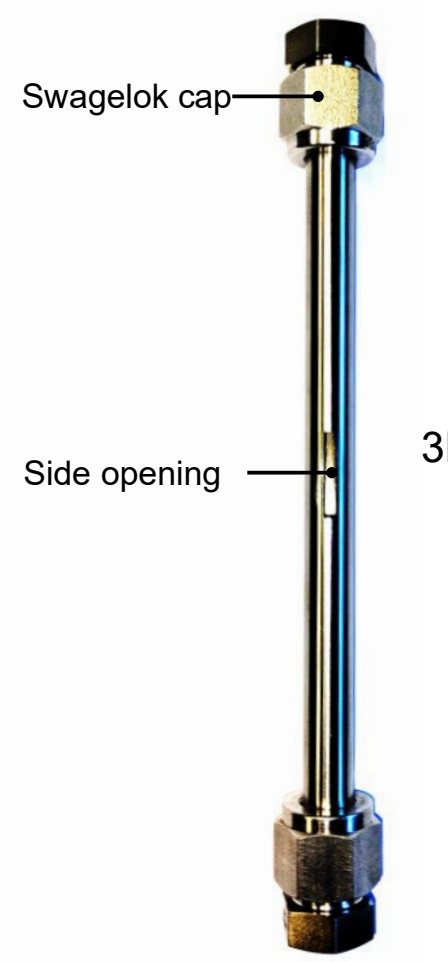

3D schematic view →

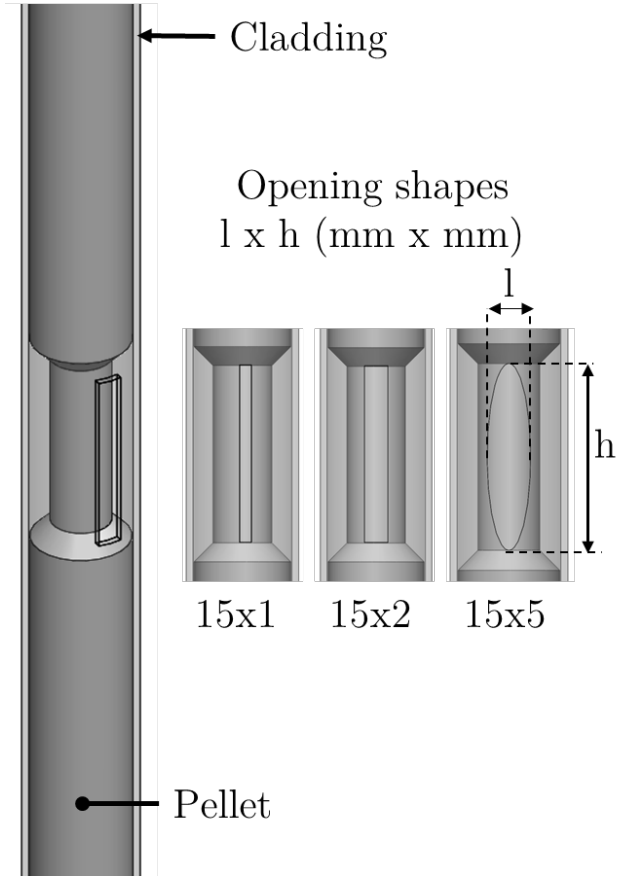

Oxidation tests on non-deformed claddings with different burst opening geometry and size

Tox : 1160 °C

tox : 300 s

ECR-BJ : 18.5 – 19.5 %

→ Non-deformed cladding with side-opening

→ Single centred alumina pellet inside the cladding

Results – Hydrogen measurements

Axial hydrogen profiles following the oxidation tests

Sample ID : **Rec_1**
Shape: Rectangular
Dimensions: 15x1 (Hxl)
Curve:

Sample ID : **Rec_2**
Shape: Rectangular
Dimensions: 15x2 (Hxl)
Curve:

Sample ID : **Ova_1**
Shape: Oval
Dimensions: 15x5 (Hxl)
Curve:

Sample ID : **Ova_2**
Shape: Oval
Dimensions: 15x5 (Hxl)
Curve:

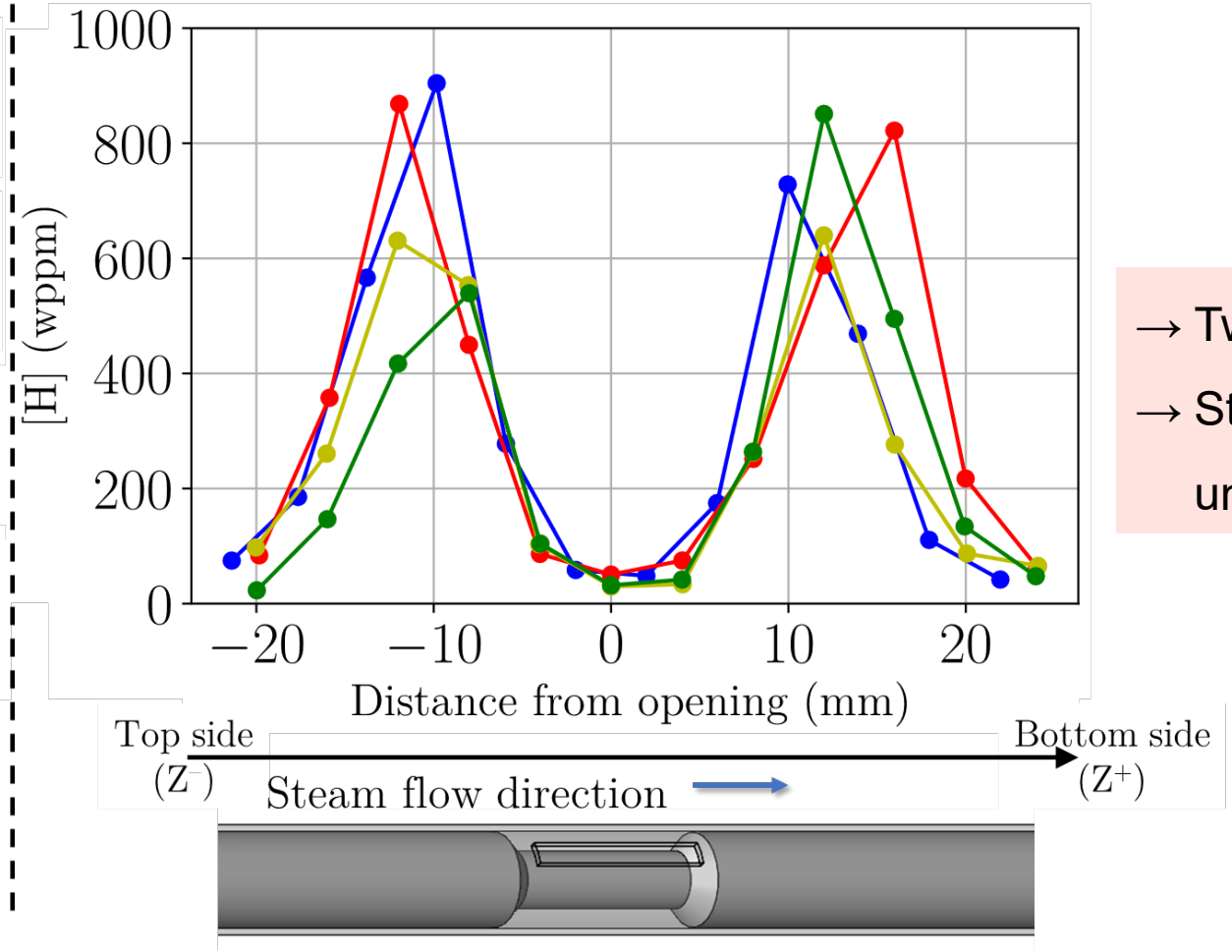

→ Two symmetrical hydrogen peaks

→ Steam transport inside the cladding uniform on either side of the opening

Results confirmed the so called “M-shape” profile following hydrogen absorption related to the secondary hydriding

Results – Effects of opening shape

Rectangular opening

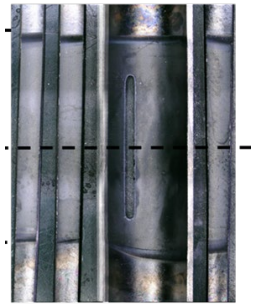

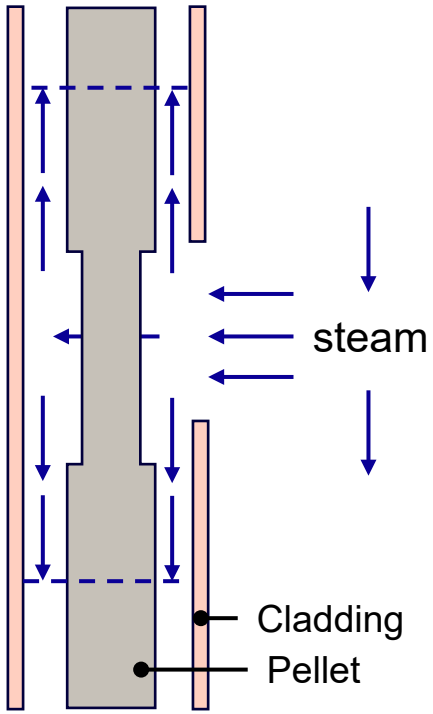

Homogeneous steam transport inside the cladding

Oval opening

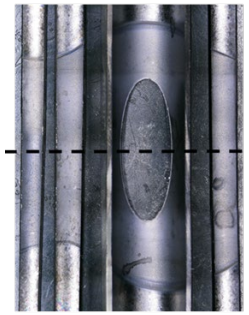

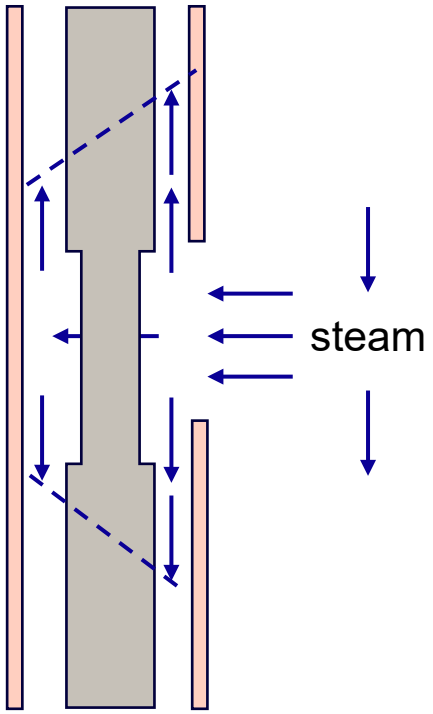

Heterogeneous steam transport inside the cladding

Could explain why

Reported NRI data

[Stuckert et al., 2020, Grosse et al., 2006]

→ Steam transport is enhanced near the opening depending on the burst geometry

Results – Effects of opening size

Average integrated area under H profile

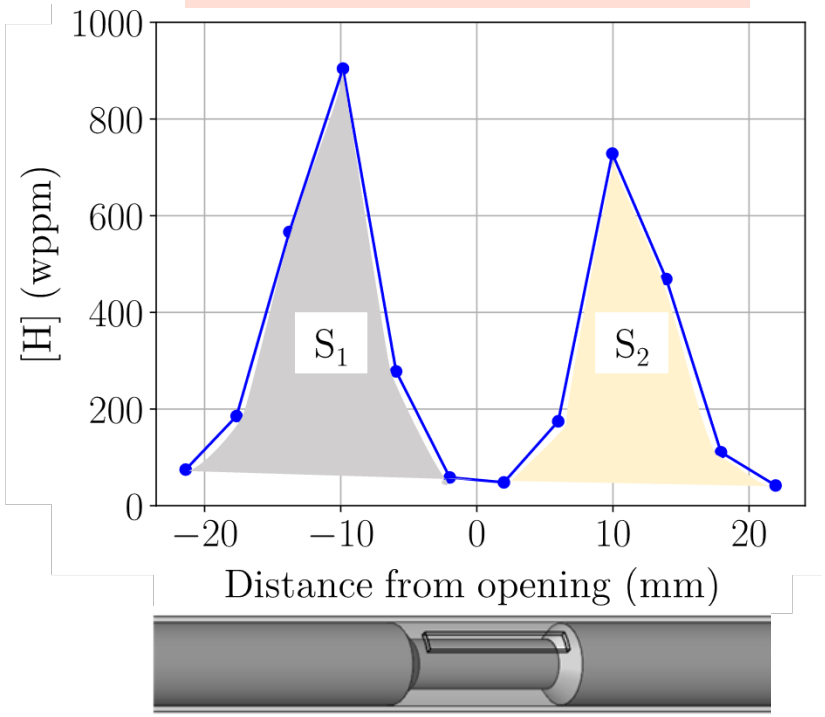

SET results with same gap size (80 µm)

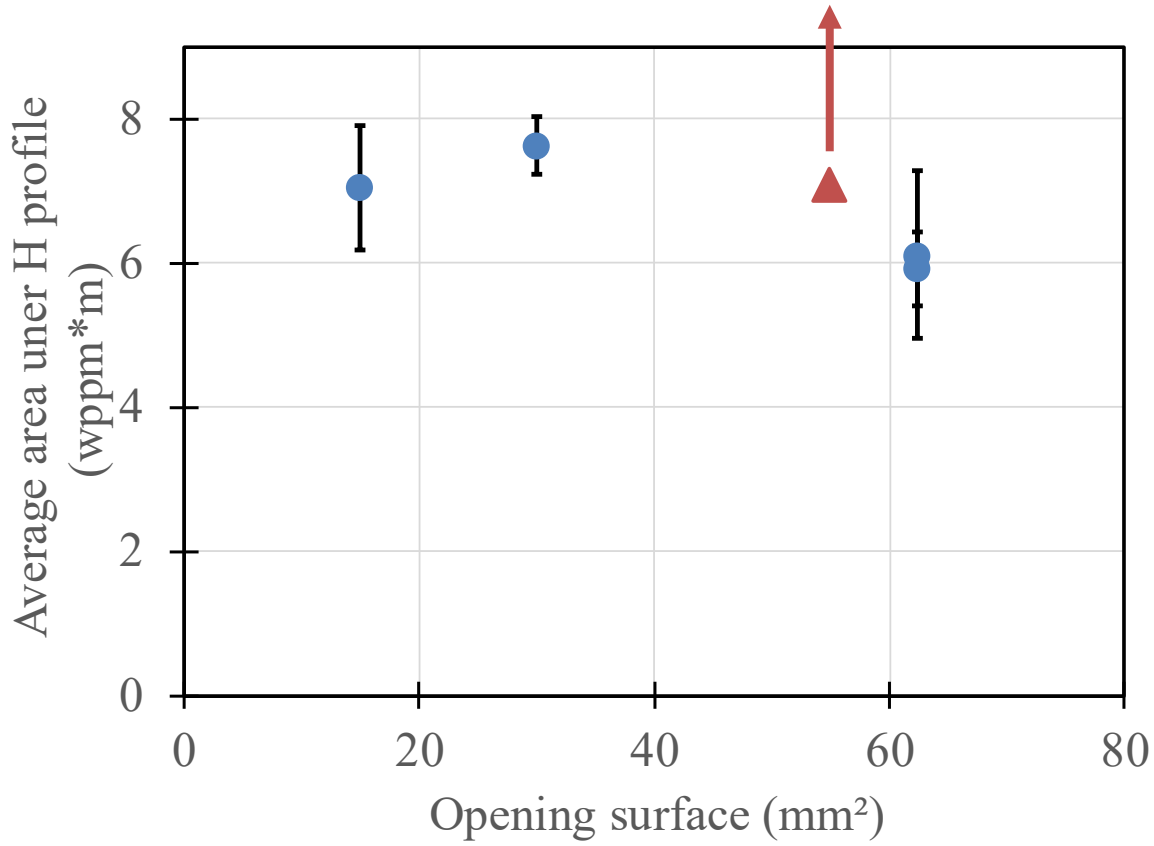

→ No significant influence of opening size on the total H content (too large opening size ?)

→ The obtained H content with SOTs is coherent with the SETs results

Conclusions

Experimental and modelling characterisation of secondary hydriding

→ The **novel** and **dedicated experimental protocol on undeformed claddings** allowed to **reproduce secondary hydriding**

→ The **effects of several parameters** were evidenced

→ The phenomenon was **finely characterised**, and the obtained results were used for **modelling work**

→ A **1D axisymmetric modelling** of the phenomenon and **sensitivity studies** were carried out

→ The obtained data help understand the reported data on semi-integral tests (irradiated and unirradiated materials)

→ The obtained data served as basis for modelling purposes and for code validation

Thank you for your attention!

Raimon Pericas

ISS

Expanding the Capability of the ASTST VER3.5 System Thermal Hydraulic and SCDAPSIM Modeling Options to Support the Fukushima Daiichi Decommissioning R&D Analysis and Assessment

Immediately after the accident at Fukushima Daiichi, Innovative Systems Software, and other members of the international SCDAP Development and Training Program (SDTP) started an assessment of the possible core/vessel damage states of the Fukushima Daiichi Units 1-3. The assessment included a brief review of relevant severe accident experiments and a series of detailed calculations using RELAP/SCDAPSIM. The calculations used a detailed RELAP/SCDAPSIM model of a representative BWR plant provided by the Comision Nacional de Seguridad Nuclear y Salvaguardias, the Mexican Nuclear Regulatory Authority. The initial assessment was originally presented to the International Atomic Energy Agency on March 21st, 2011 to support their emergency response team and later to our Japanese colleagues to support their Fukushima Daiichi specific analysis and model development activities. Additional calculations were performed using RELAP/SCDAPSIM to help refine the certainties in the thermal hydraulic boundary conditions including potential failures in the reactor coolant system leading to the depressurization of Units 1 and 3. However, those calculations were limited to the in-vessel phase of the accidents, since at that time very little was known about the conditions of vessel failure and relocation of material into the reactor cavity.

Starting in 2020, with the help of our colleagues in Japan and Europe, a new integrated BEPU code, ASYST, was created as part of a new ASYST Development and Training Program (ADTP). It was intended as a framework for our program members to extend the capabilities of RELAP/SCDAPSIM to include more advanced system thermal hydraulics modeling options including the ability to model the RCS and containment during severe accident conditions. Two main versions of ASYST are being developed. ASYST VER4.x focuses on advanced fluid and reactor systems. VER3.x focuses on the improvement of SCDAPSIM modeling options for LWRs and PHWRs. For our activities related to Fukushima Daiichi decommissioning R&D, ASYST VER3.5 is being extended to enable end-to-end BWR severe-accident analysis from in-vessel degradation through ex-vessel behavior. As described in more detail in the presentation, the modeling extensions (a) enable multiple COUPLE meshes so the reactor lower head and reactor cavity are modeled simultaneously; (b) implement a vessel creep-rupture failure trigger that opens a break coupling the lower plenum and reactor cavity thermal hydraulic volumes and initiates the slumping of the in-vessel debris into the cavity; (c) add configurable debris–water interaction/breakup options in the cavity; (d) incorporate the RELAP/SCDAPSIM/MOD4 FPTRAN.

SDTP ADTP

Development of best estimate methods for reactor and advanced fluid systems safety analysis and training

Expanding the Capability of the ASYST VER3.5 System Thermal Hydraulic and SCDAPSIM Modeling Options to Support the Fukushima Daiichi Decommissioning R&D Analysis and Assessment

Dr. Raimon Pericas and Dr. Chris Allison
Innovative Systems Software (ISS)
30th Int. QUENCH Workshop
16-18 Dec. 2025 Karlsrhue, Germany

Outline I

* Background
  * Benchmarking of BWR modeling options using CORA BWR electrically heated experiments, PBF-SFD and LOFT in-pile experiments and TMI-2.
  * Early assessment of influence of uncertainties in over TH boundary conditions on fuel melting and relocation.
  * Long time collaboration with Mexican Laguna Verde NPP (BWR type) and Fukushima Daiichi post accident activities.
* Extension of ASYST VER3.5 SCDAPSIM modeling options (improvements to de code).
  * Latest improvements on ASYST VER3.5.

Outline II

* Expansion of BWR input models for model assessment and sensitivity analysis (improvements of the BWR existing models)
  * Improving plant and facility representations with the existing capabilities of the code.

* Expansion of advanced GUI and IUA (integrated uncertainty analysis) to support model verification, analysis of results, and integrated sensitivity studies (adds on to the code)
  * Adding new capabilities to the code
  * Different analysis approach (Integrated Uncertainty Analysis)

Extension of ASYST VER3.5 SCDAPSIM modeling options

* Enable use of **multiple detailed 2D Finite Element mesh (FE)** porous media regions
* Implement **vessel creep rupture** failure of lower head and initiation of lower head debris into reactor cavity
* Add **debris-water interaction**/breakup in cavity options
* Incorporate FPTRAN detailed **fission product transport** and deposition models for TH volumes in RCS and containment
* Develop **standardized interfaces** to couple to external modules or codes for containment and source term analysis

Detailed 2D FE porous media models to describe behavior of lower plenum debris/vessel – reactor cavity

- Heat conduction
  - 2D finite element
  - gap resistance (solid/melt)
  - 1D model at crust boundary perimeter
- Molten pool behavior
  - Transient natural circulation
  - Interactions with vessel wall
  - MCCI Melt Coolability and Concrete Interaction (TBD)

* Creep rupture failure of vessel wall
* Material relocation
  * Relocation of upper plenum structures
  * Relocation of core component materials
  * Molten pool slumping
* Ex-vessel flooding - Flooding

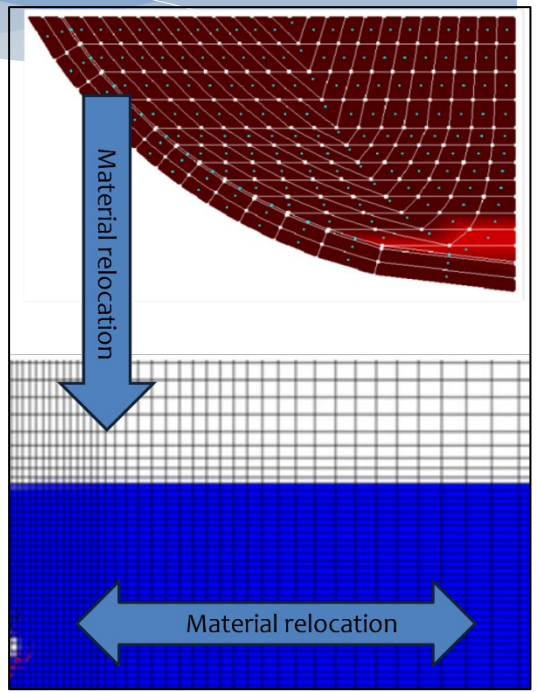

Expansion of BWR input models for model assessment and sensitivity analysis

* **Extension of original BWR full plant model** to include representative passive cooling systems for Units 1-3, containment thermal hydraulics system to perform sensitivity studies on water addition to vessel and containment and FP transport and deposition
* **Adjusting the model** from Laguna Verde to Fukushima Daiichi like type reactor.
* **Development of representative BWR core/LP/vessel/reactor cavity models** for comparisons to TMI-2 results and sensitivity studies on core TH modeling and late phase fuel relocation into lower plenum and reactor cavity
* **Development of representative BWR fuel and CBCB assembly input model** for benchmarking against CORA BWR and PBF-SFD in-pile experiment results and assembly-specific sensitivity studies

Extensions of original BWR plant model to evaluate passive cooling system influence, initial PCS failure, and containment response

RHYS – ASYST Display

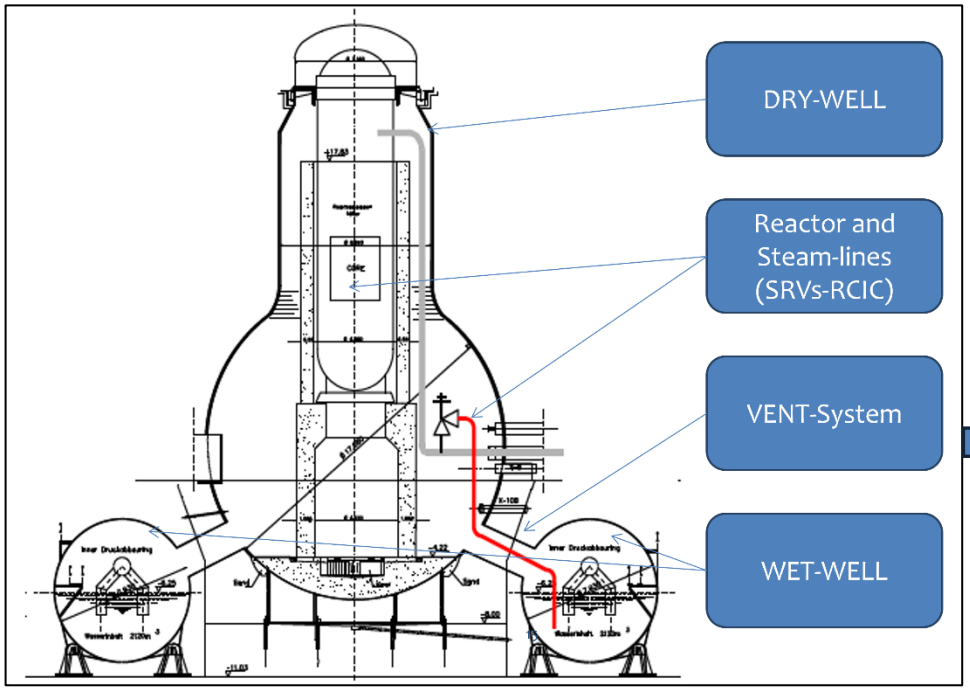

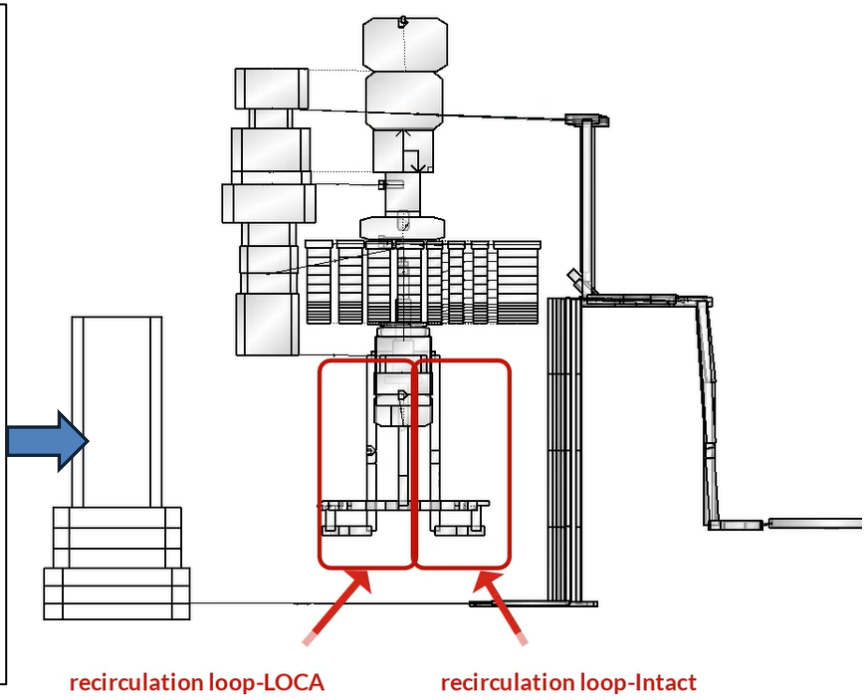

Develop improved core input model with more realistic channel box/control blade (CBCB) thermal boundary conditions

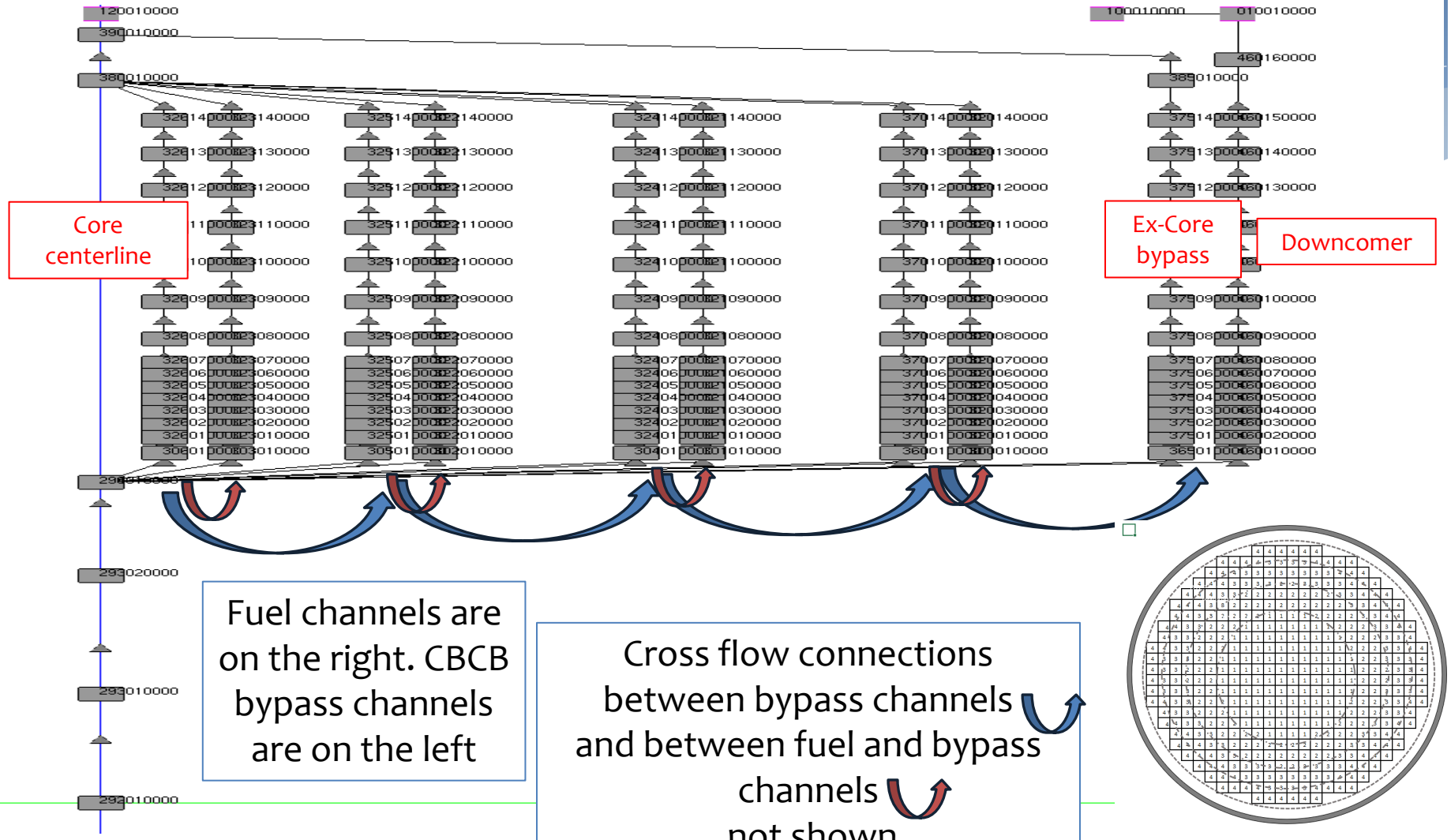

Fuel channels are on the right. CBCB bypass channels are on the left

Cross flow connections between bypass channels and between fuel and bypass channels not shown

Example- Results from improved BWR core input model – Impact of 1700 K channel box failure

[U-Zr]-O2 molten pool formation

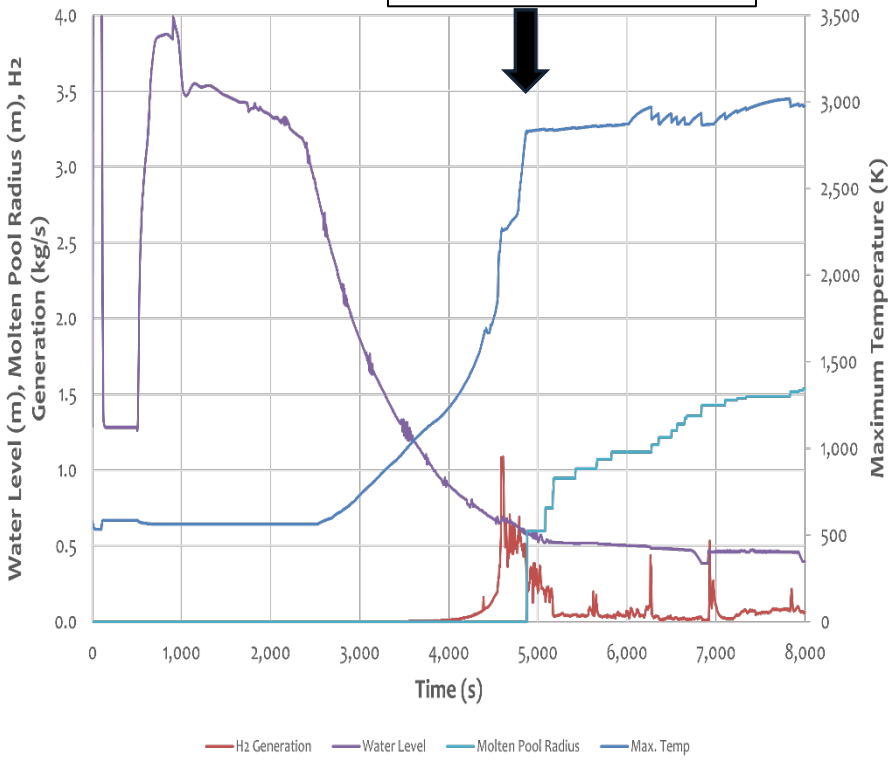

Hi Power ← Lo Power

Spreading of [U-Zr]-O2 melt to low power assemblies

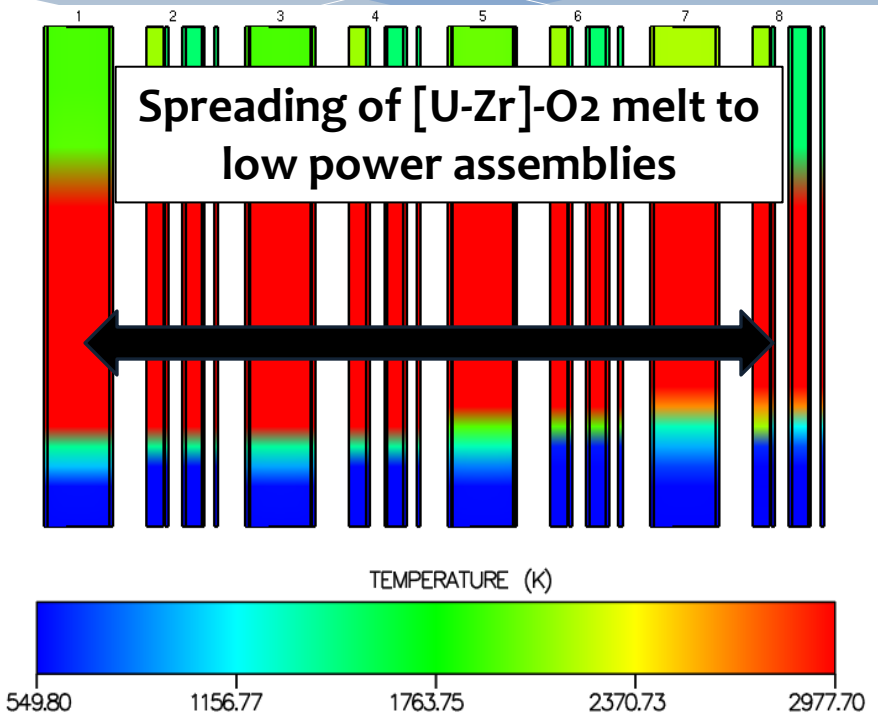

Representative core temperatures at 8000s

Extension of input model for vessel failure and melt relocation into reactor cavity

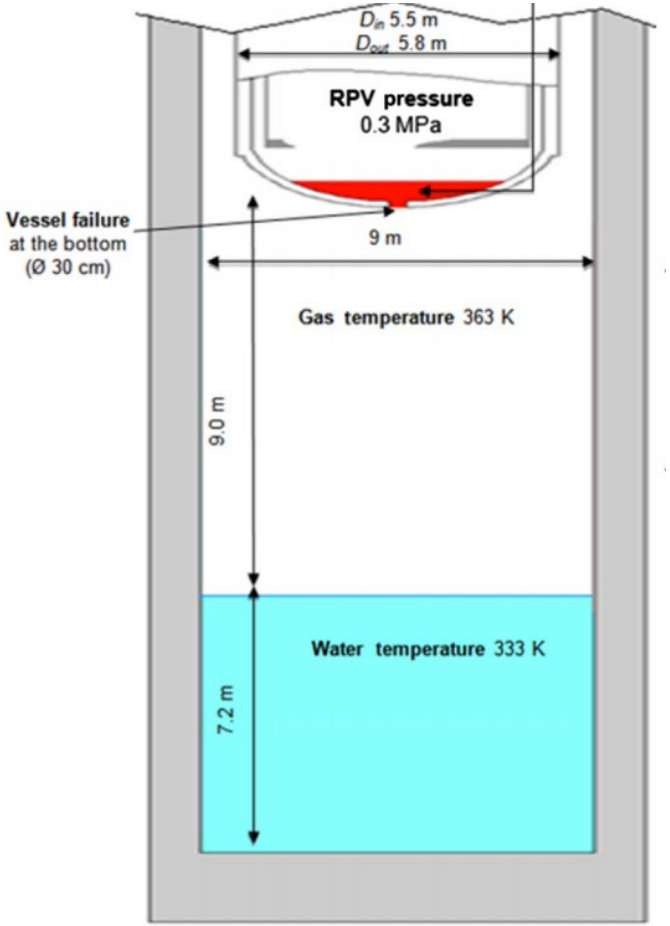

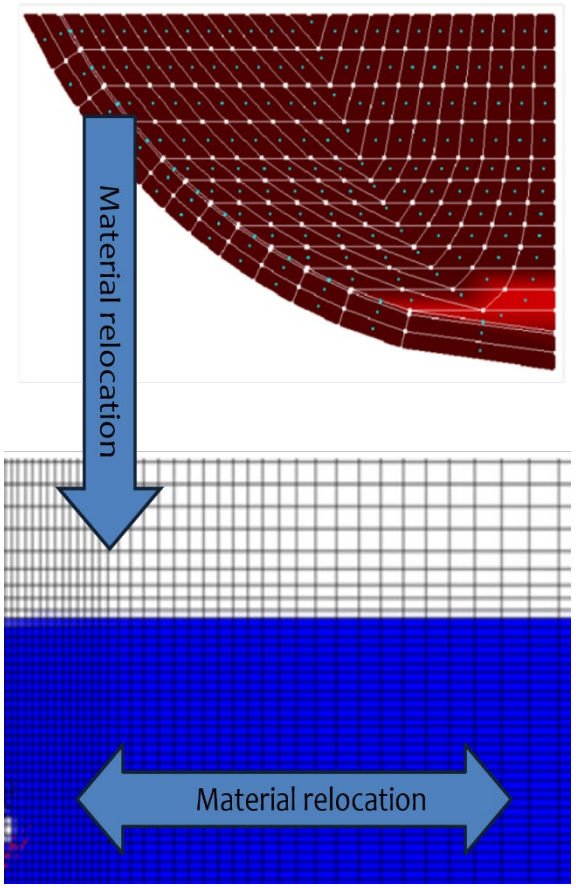

Expansion of advanced GUI Results from BWR core with 2D lower plenum porous media model – Hi Pressure scenario

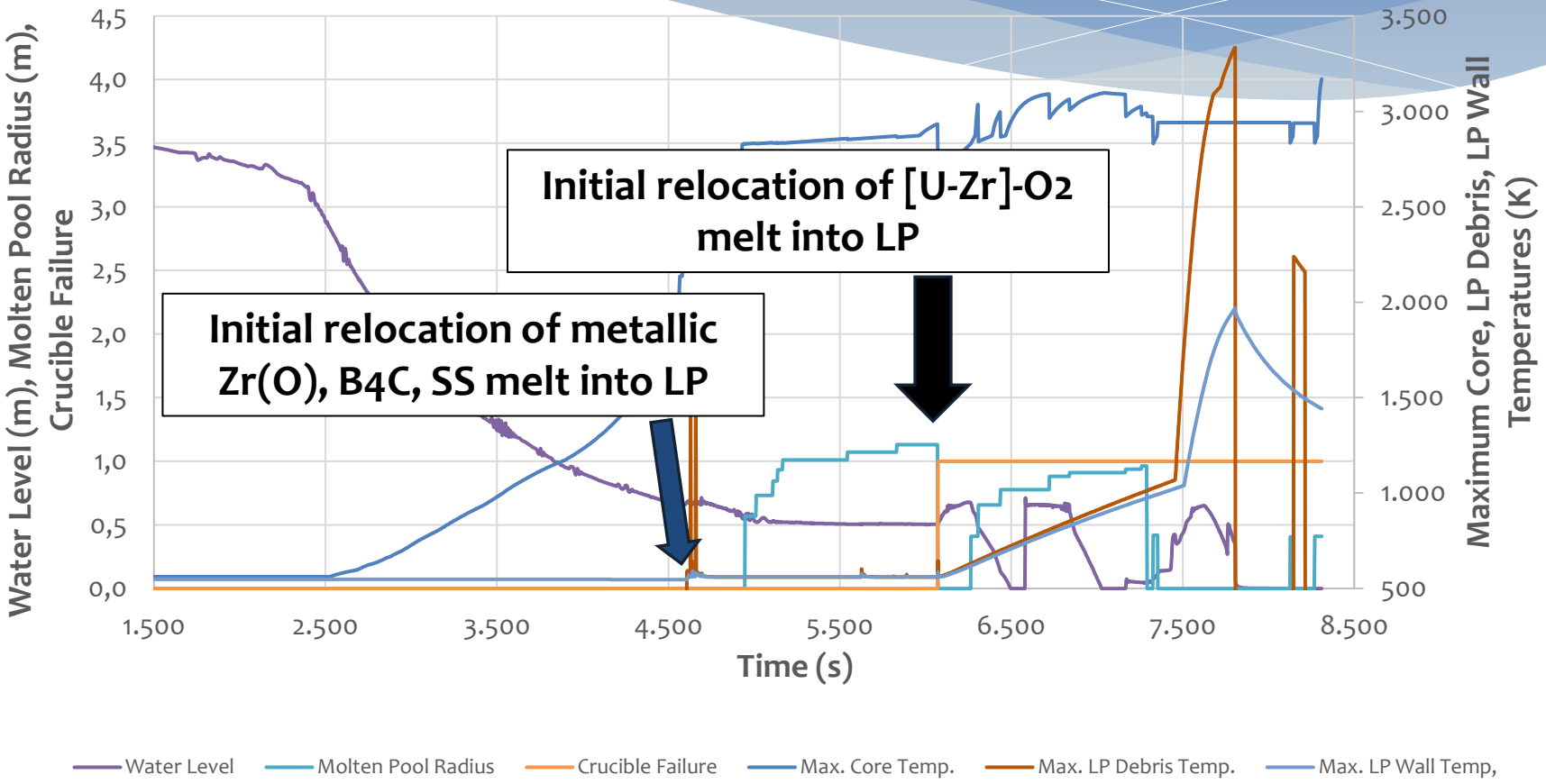

Interactive Adv3Dgui SCDAP display for hi pressure scenario

4600s

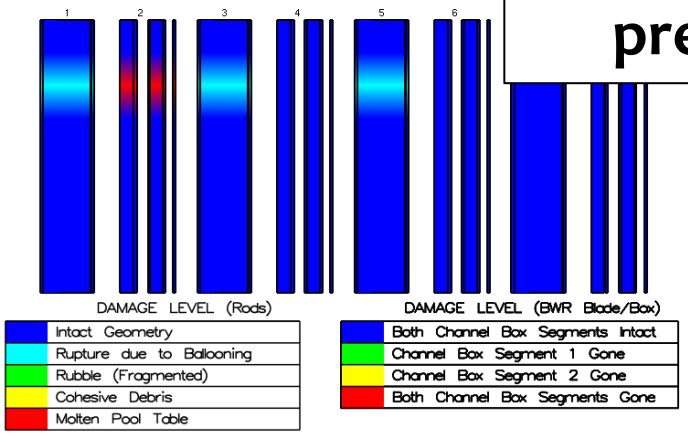

6000s

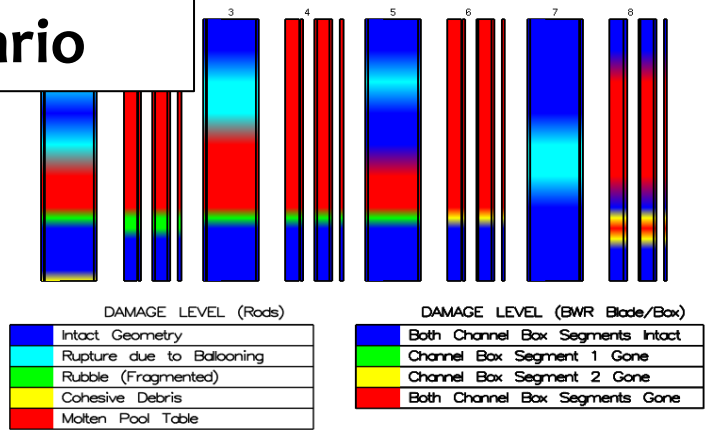

Initial melting and relocation of channel box and control blade

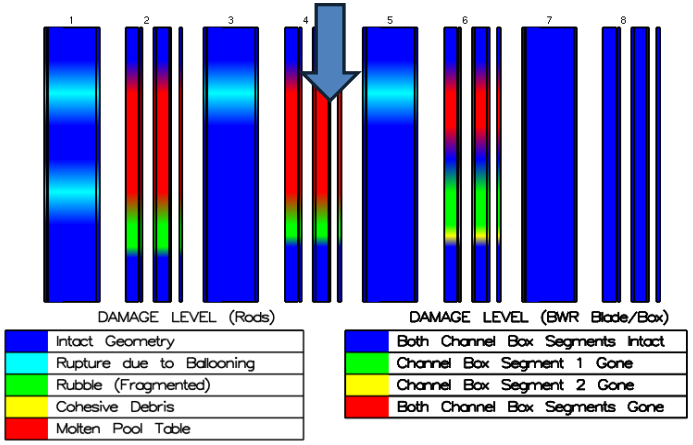

4800s

Initial relocation of [U-Zr]-O2 melt into LP

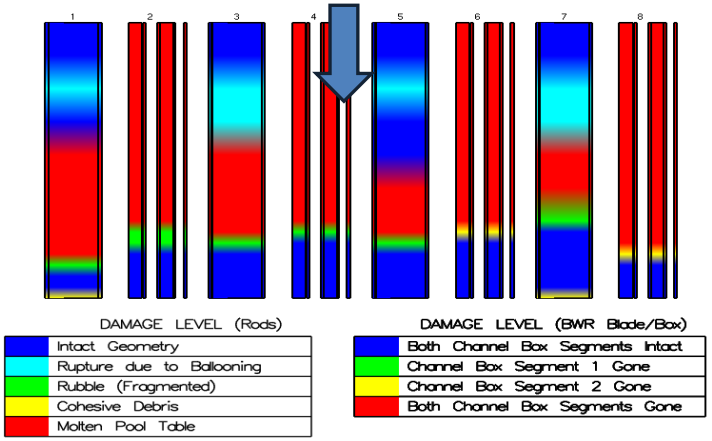

7300 s

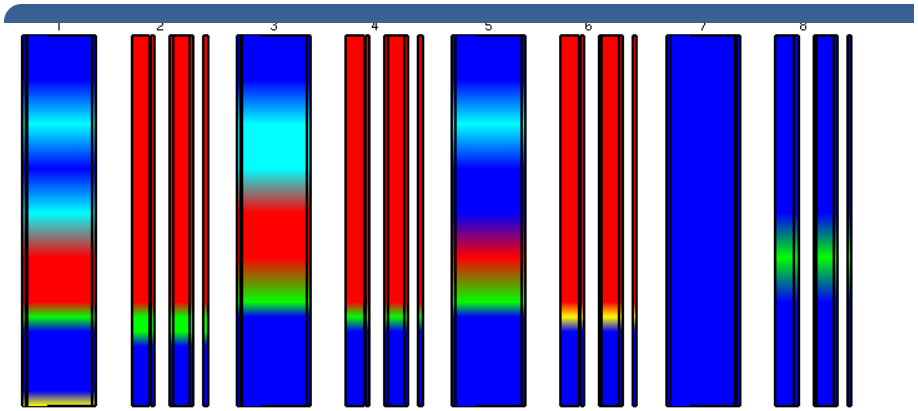

DAMAGE LEVEL (Rods)

Intact Geometry
Rupture due to Ballooning
Rubble (Fragmented)
Cohesive Debris
Molten Pool Table

DAMAGE LEVEL (BWR Blade/Box)

Both Channel Box Segments Intact
Channel Box Segment 1 Gone
Channel Box Segment 2 Gone
Both Channel Box Segments Gone

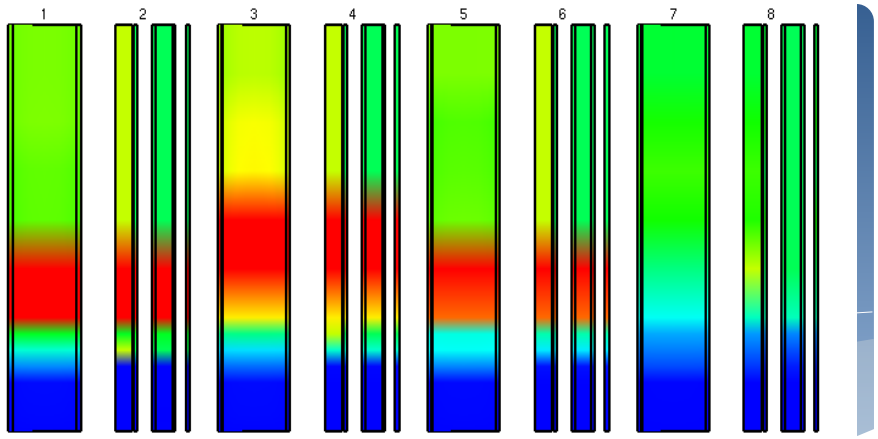

TEMPERATURE (K)

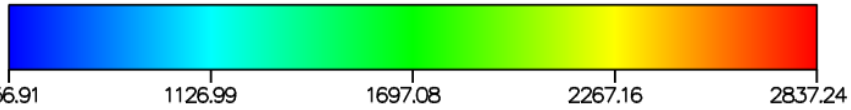

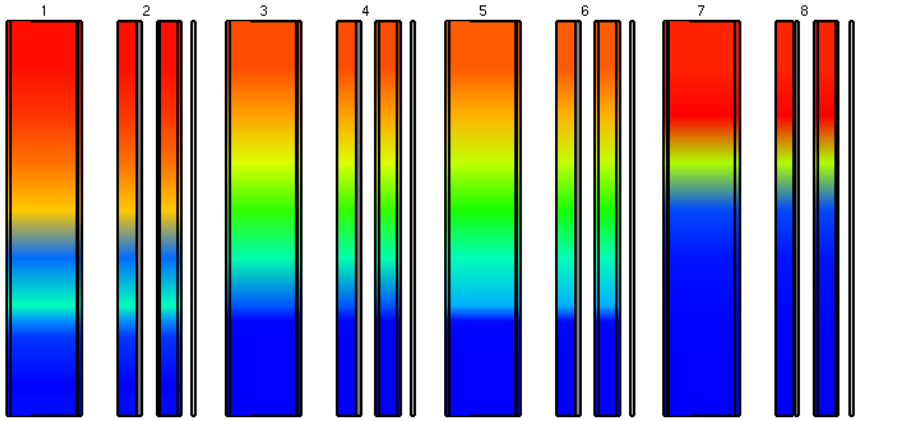

NONCONDENSABLE MASS FRACTION

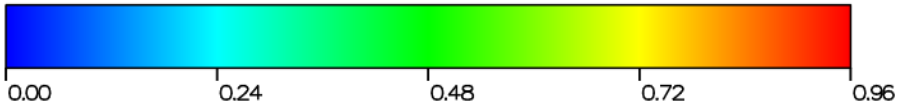

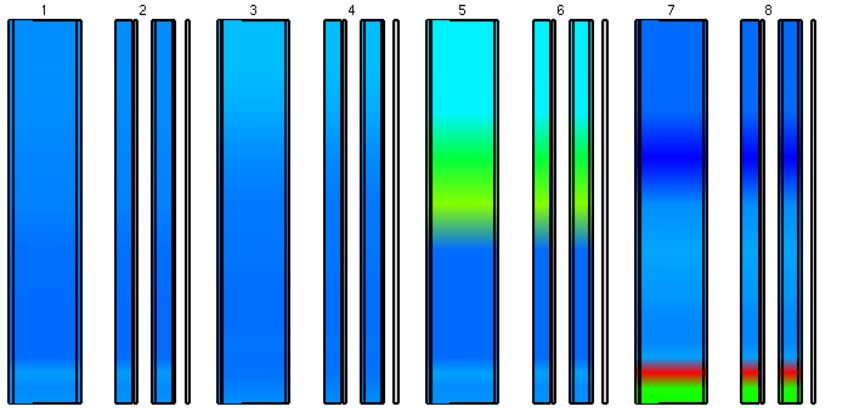

VAPOR VELOCITY (m/sec)

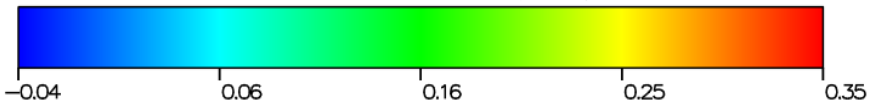

5000s

Influence of horizontal crossflows with fuel channel failure at 1700K

- Reduction in horizontal crossflows have minimal impact on overall global parameters but can impact axial and radial distributions with core and relocation of melts into lower plenum
  - Bounding case with crossflows set to zero
    - Increases peak temperatures in higher power channels
      - Decreases the time for the initial relocation of molten metallics (Zr, SS, B4C) into the lower plenum
      - May increase the amount of molten metallics in lower plenum prior to molten fuel relocation
    - Decreases the rate of radial spreading of the molten pool to the outer lower power fuel assemblies
    - May significantly delay the relocation of the molten fuel into the LP

Influence of horizontal crossflows with fuel channel failure at 750K – Core damage level at 6660 s – Peak temperatures ~ 2970 K

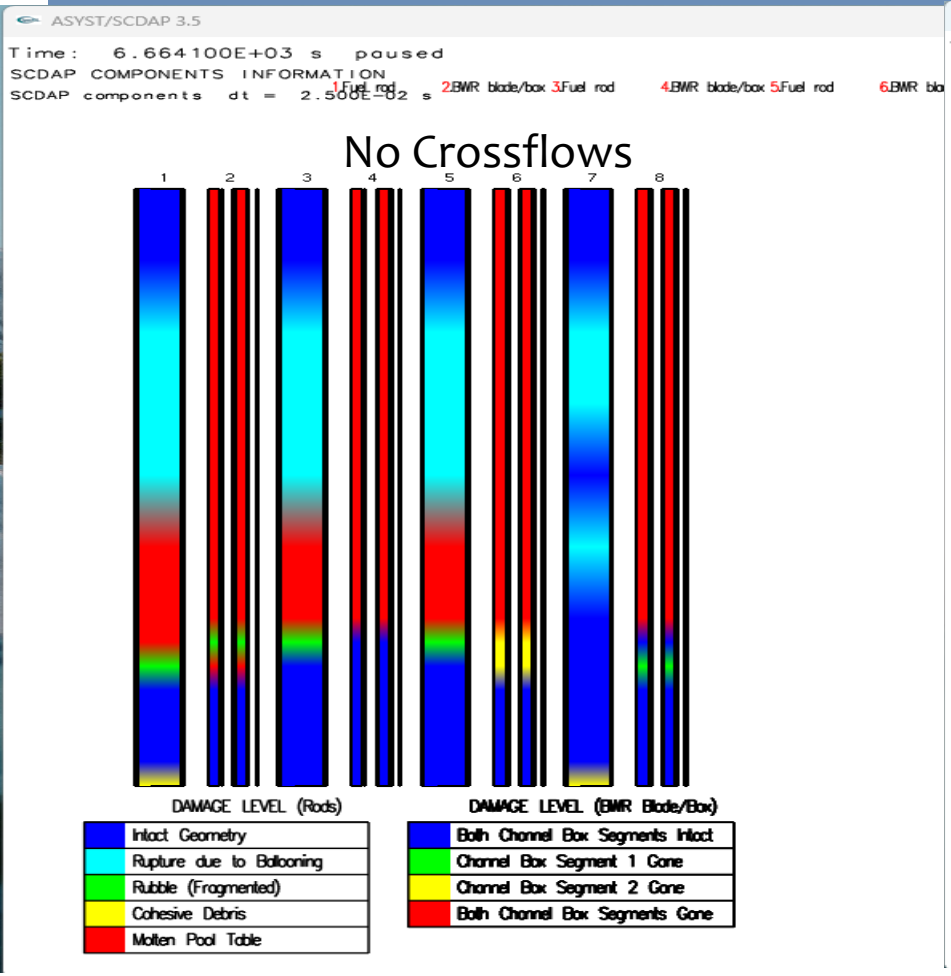

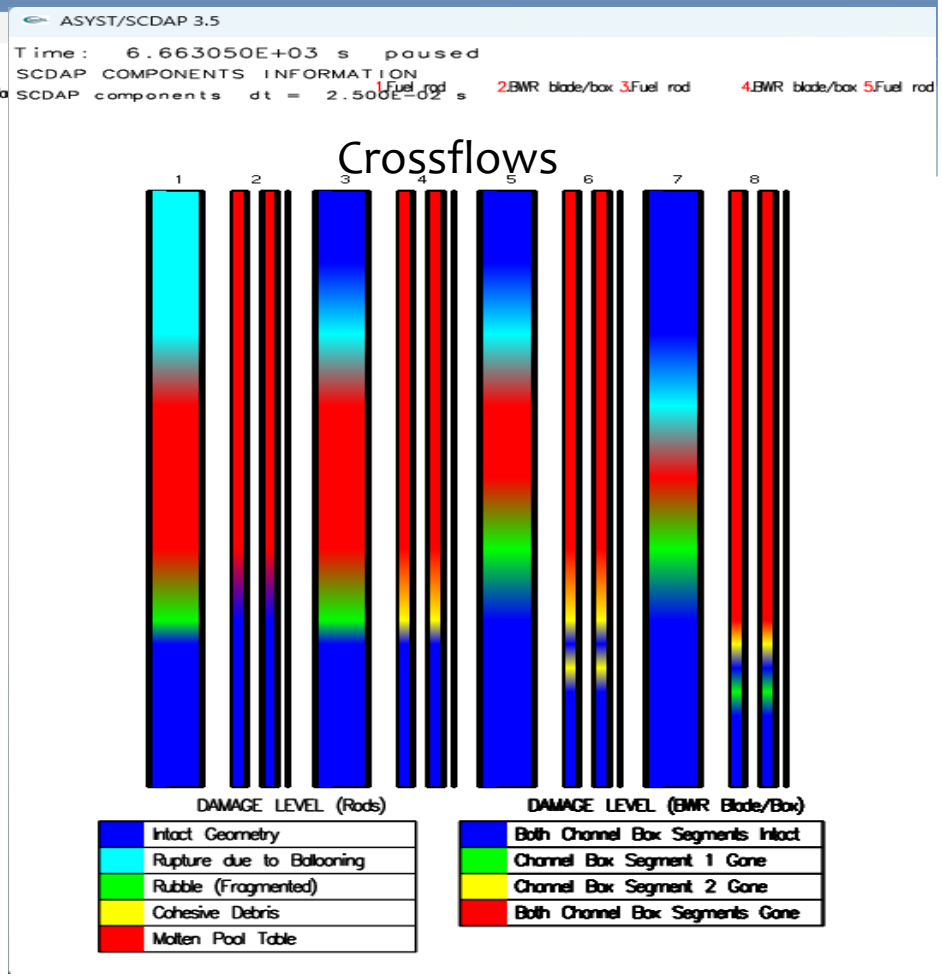

Influence of horizontal crossflows with fuel channel failure at 750K – Core temperatures at 6660 s – Peak temperatures ~ 2970 K

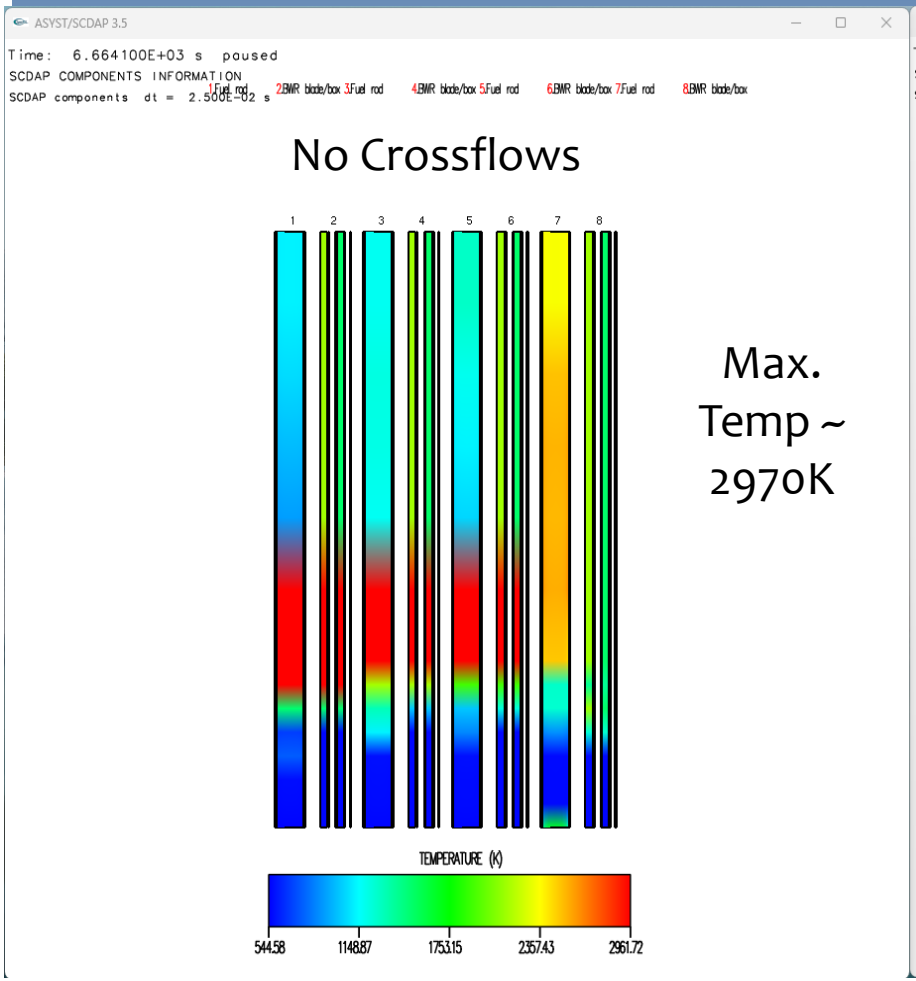

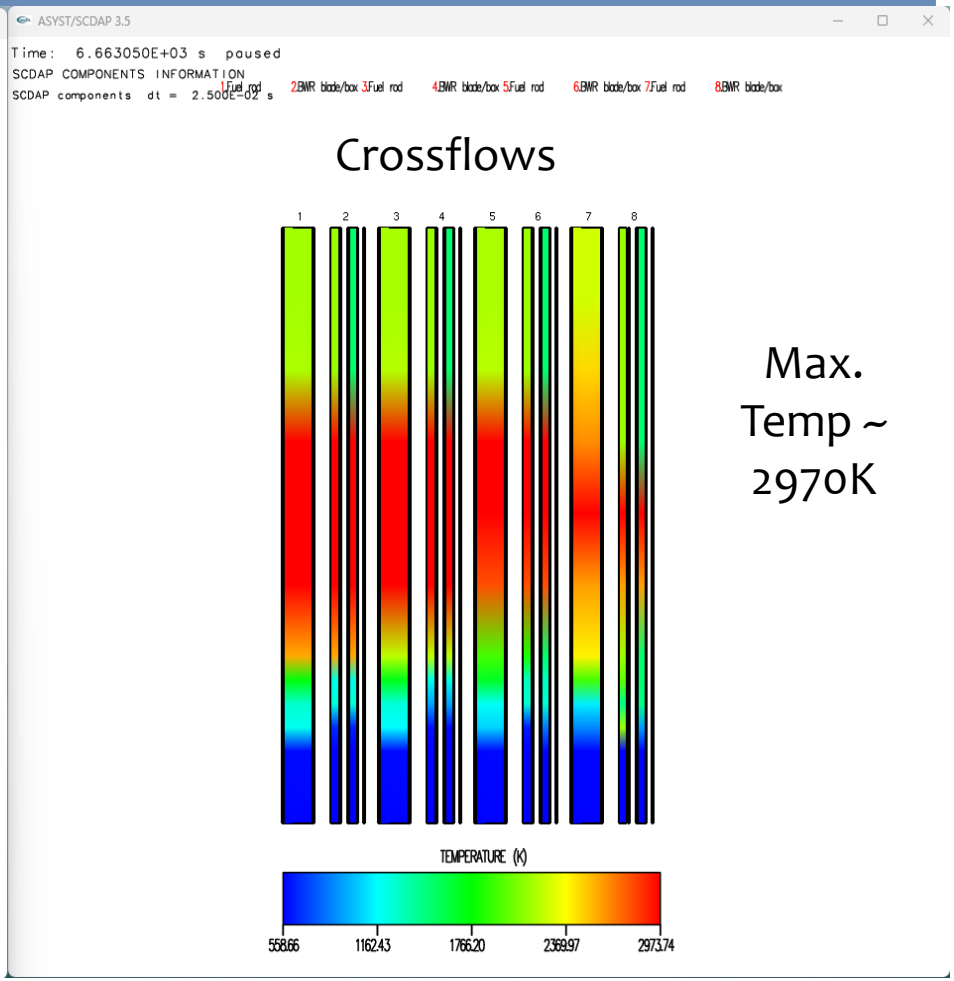

Influence of changes in horizontal crossflow – 1700 K channel failure

Crossflow

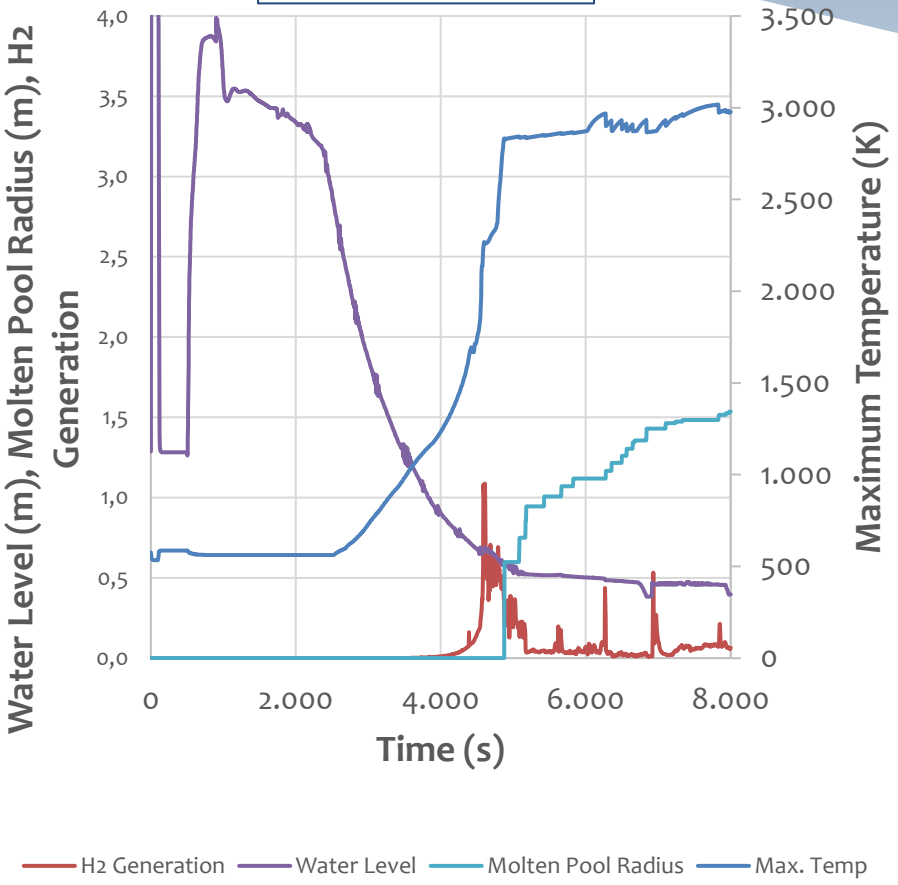

No Crossflow

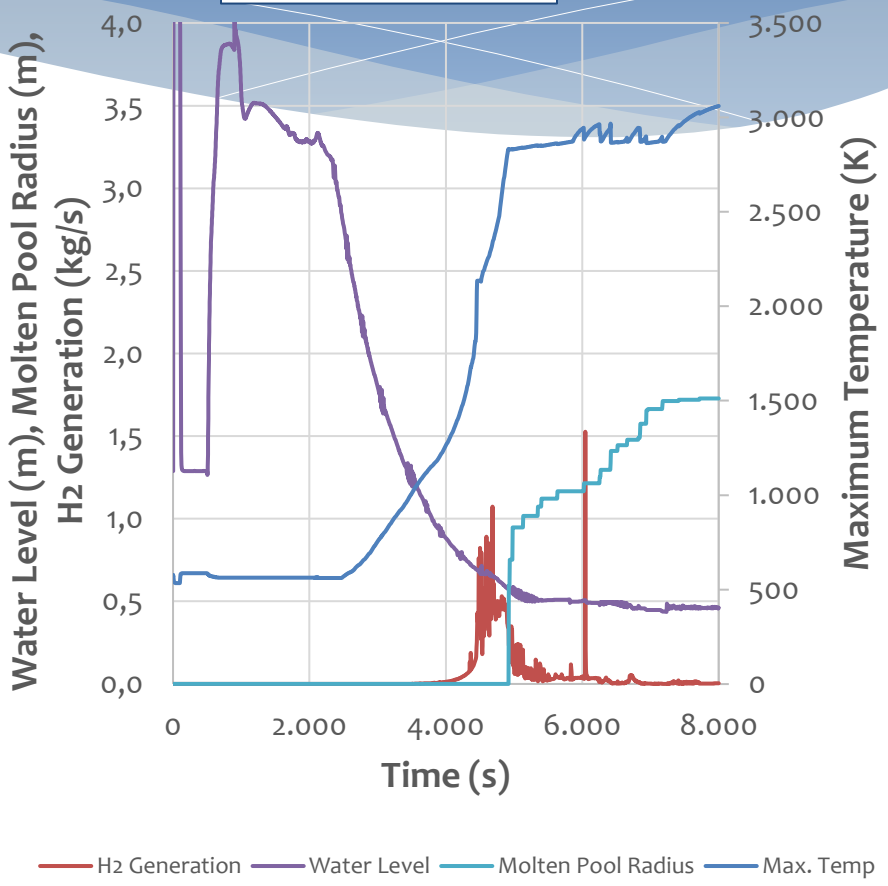

BWR core with 2D lower plenum and reactor cavity porous media model

Interactive RHYS desktop GUI

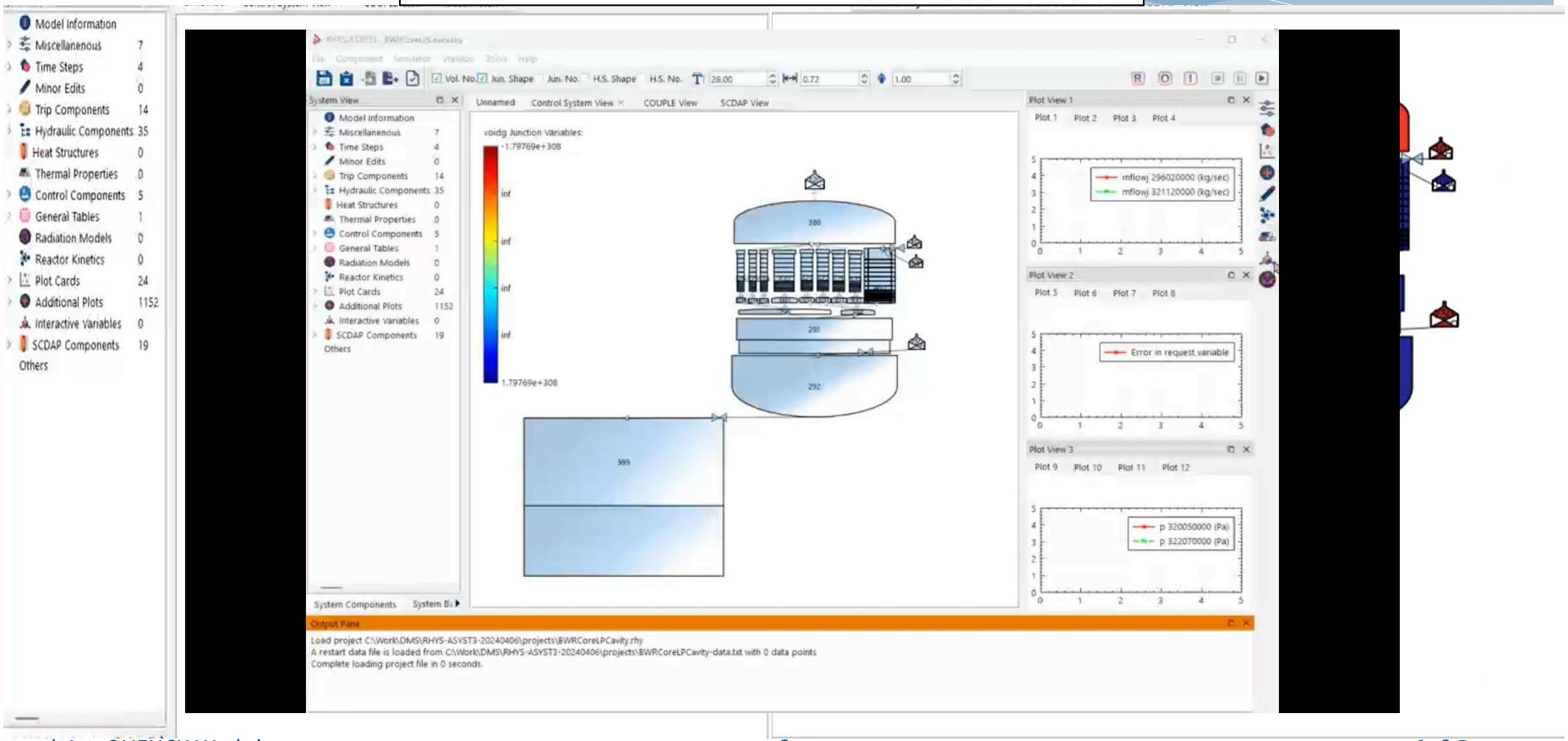

BWR core with 2D lower plenum and reactor cavity porous media model

Interactive RHYS desktop GUI running depressurization scenario

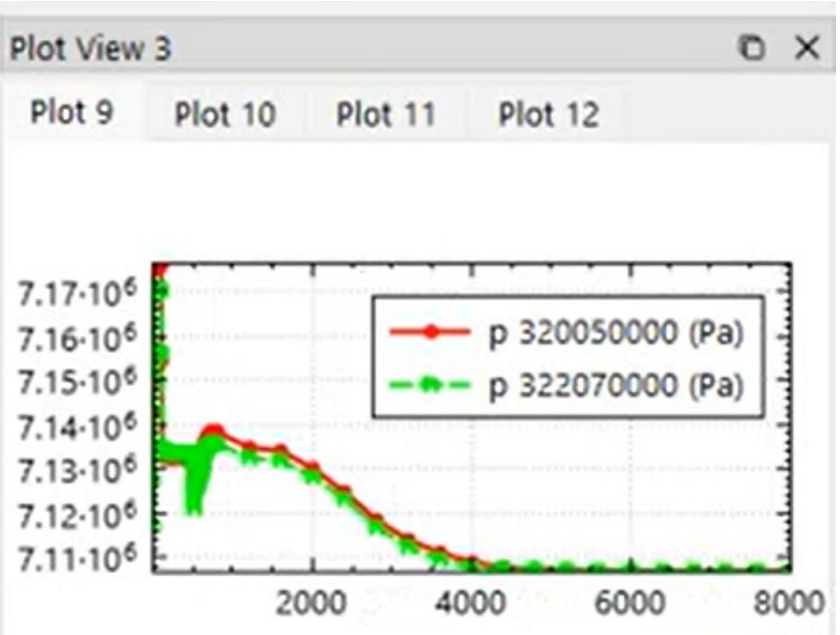

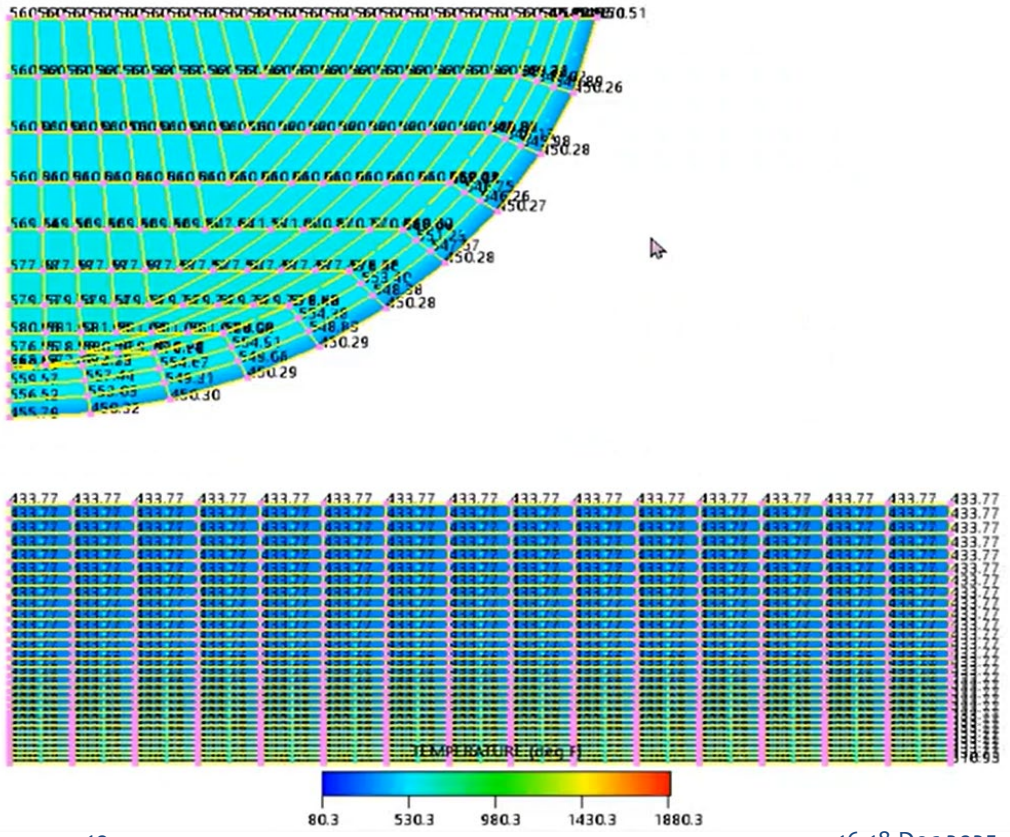

BWR core with 2D lower plenum and reactor cavity porous media model

Interactive RHYS desktop GUI running depressurization scenario

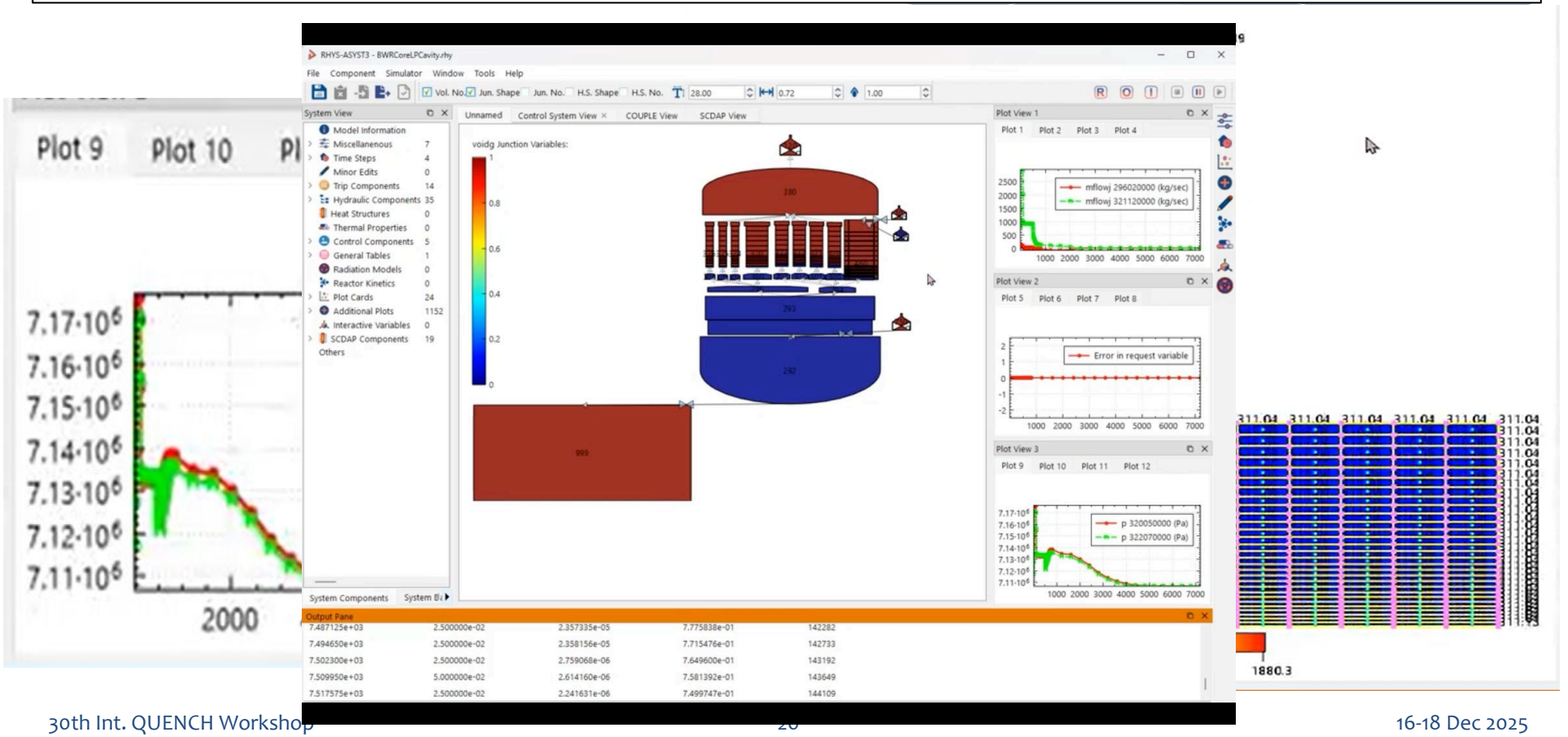

Conclusions

- Adding capabilities ex-vessel for the ASYST platform allows as to perform a broader analysis of the severe accident scenarios.
  - Ex-vessel phenomena and Fission Product transport…
- New visualization tools allow to have a better comprehension of the overall behavior of the modeled system.
  - Combination of the accurate modelling and the visualization tools allow us to see for example the influence horizontal crossflows.
  - RHYS platform allows and overall and Realtime viewing of the calculations
- Alive project on nuclear modelling
  - Continuously improving platform. Large community worldwide members using and improving the platform in many areas of expertise.
    - Adding the Integrated Uncertainty Analysis package possibility as and example.

Thank you for your attention

Dr. Raimon Pericas and Dr. Chris Allison
Innovative Systems Software (ISS)
30th Int. QUENCH Workshop
16-18 Dec. 2025 Karlsrhue, Germany

Gregor T. Stahlberg

RUB

Analysis of the COAL Reflooding Experiments: Recent Simulations with AC²

The validation of system codes for Loss-of-Coolant Accident (LOCA) scenarios, particularly those involving fuel rod deformation, requires rigorous benchmarking against experimental data to ensure reliable safety assessments. The primary objective of this work is to present the simulation results of selected COAL experiments using the AC²-ATHLET code, developed by GRS gGmbH, within the framework of the OECD-NEA ISP-53 benchmark.

The numerical analysis was performed at the Plant Simulation and Safety Group (PSS) at Ruhr-Universitaet Bochum (RUB). The modeling strategy employs a 1D lumped parameter approach to represent the thermal-hydraulic behavior of the test facility. The nodalization approach was maintained identical between the post-test analysis of the intact bundle (B0) and predictions of the deformed bundle (B2). This approach establishes a consistent basis for future investigations of B2 – beyond the scope of the current work – to directly assess the code's capability to predict the impact of flow blockage and ballooned rods without prior case-specific tuning.

The assessment strategy presented here focuses on the transient reflooding phase of the intact bundle under varying system pressures. While the simulation captures the key physical phenomena and demonstrates plausible system behavior, the results highlight specific sensitivities. In the high-pressure scenarios (20 bar), the code shows satisfactory agreement with experimental data. However, at lower pressures (3 bar), deviations regarding the quench front progression and peak cladding temperatures are observed.

Although the efficient single-channel approximation achieved satisfying agreement with the experimental data, the potential of a parallel channel model to resolve radial temperature gradients could be investigated. This extension would possibly capture flow deviations induced by the ballooned regions and complement the successful validation already achieved.

Acknowledgement

This work was carried out within the framework of the WGAMA WGFS ISP-53, whose support and collaboration have been instrumental in the successful completion of this research.

Responsibility for the content lies with the authors.

The results were obtained using the GRS software package AC² 2023.

RUB

RUHR-UNIVERSITÄT BOCHUM

Analysis of the COAL Reflooding Experiments: Recent Simulations with AC²

Gregor T. Stahlberg, Marco K. Koch

30th International QUENCH Workshop | RUB PSS | 2025 | KIT, Karlsruhe

PSS Plant Simulation and Safety
Prof. Dr.-Ing. Marco K. Koch

Agenda

- Introduction
- Modeling
- Results
- Summary

INTRODUCTION

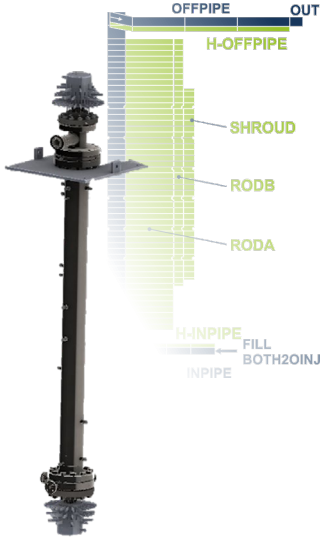

- **Framework:** OECD-NEA ISP-53 led by ASNR, France
  - International Standard Problem (ISP) to benchmark safety codes
  - Increase confidence in code validity for safety assessments
  - International cooperation (more than 12 countries)
- **Experimental Setup:** COAL test facility
  - Focus on reflooding experiments under LOCA conditions
  - Geometry: 7x7 electrically heated rod bundles (simulating PWR 17x17 design)
- **Project Phases**
  - Open Phase B0: Simulation of undeformed rods for „calibration“ of input deck
  - Blind Phase B2: Simulation of deformed ("ballooned") rods **without** prior knowledge of exp. results
  - Open Phase B2: Simulation of deformed ("ballooned") rods **with** all exp. data

INTRODUCTION
Test facility

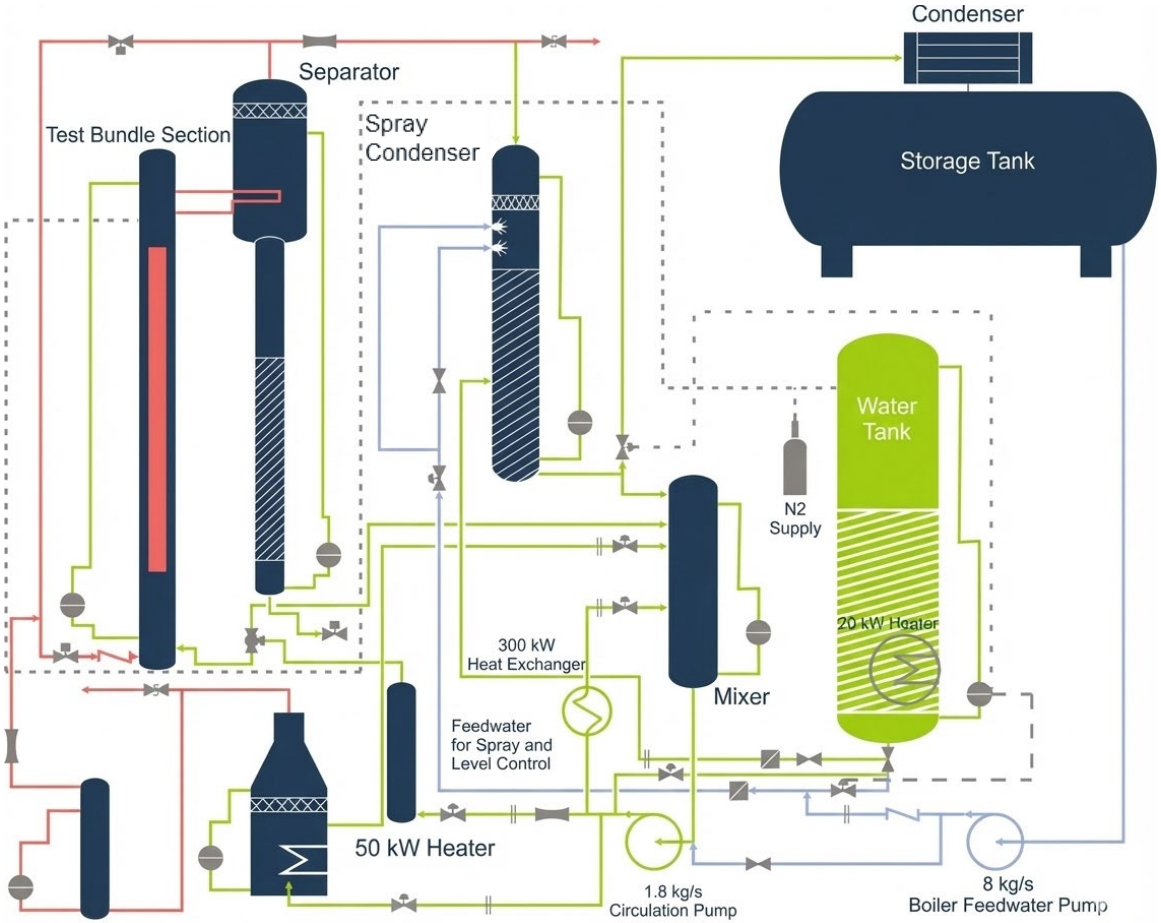

PSS Plant Simulation and Safety
Prof. Dr.-Ing. Marco K. Koch
RUHR UNIVERSITÄT BOCHUM
RUB

INTRODUCTION
Test facility

- **Facility & Conditioning**
  - Pressure Vessel: Simulates PWR Reactor Pressure Vessel up to 30 bar
  - Test Conditions: Simulation of scenarios within steam atmosphere & reflood
  - Initialization: Electrical pre-heating of rods to 300 °C
- **Test Bundle Geometry**
  - Configuration: 7x7 array (46 heater rods, 3 guide tubes)
  - Representation: Corresponds to a section of a standard 17x17 PWR core
  - Heating Profile: 3.0 m active heated length with an axial power profile
- **Components & Boundary Conditions**
  - Shroud: Actively heated flow channel (simulates adiabatic conditions)
  - Grids: Includes 2 spacer grids and 4 mixing grids for flow guidance
  - Instrumentation: Extensive thermocouple coverage (rods, guide tubes, and fluid)

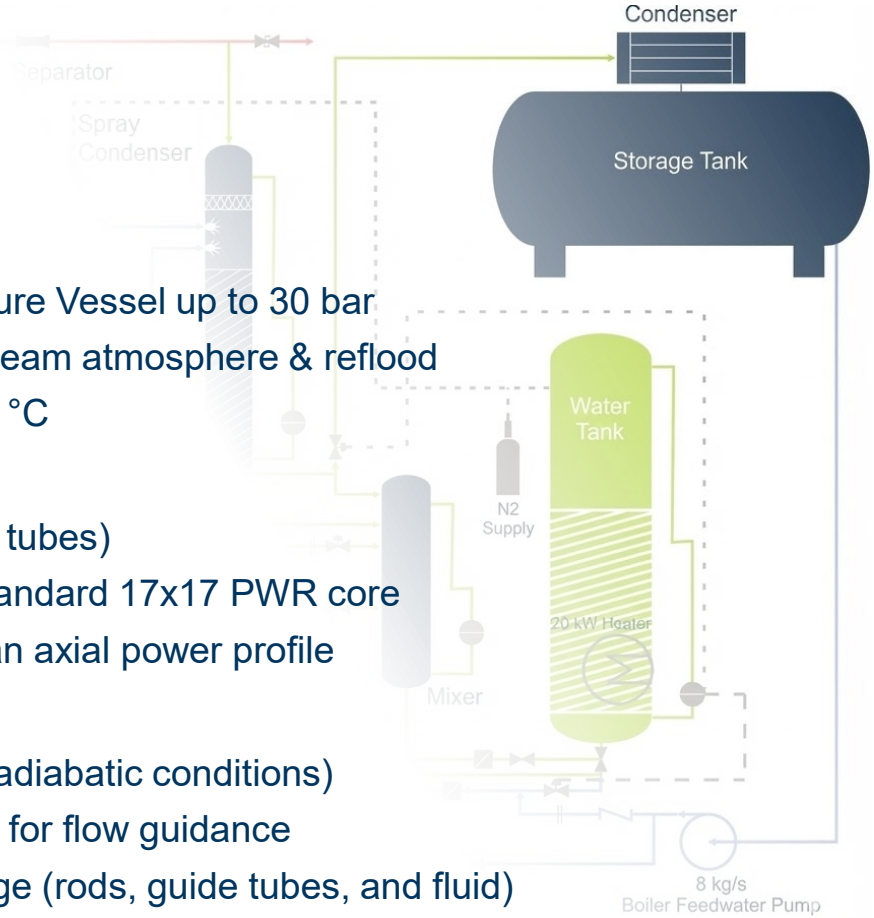

INTRODUCTION
Schematic overview of the sequence

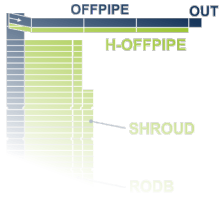

- Experimental Sequence:
  - **Step 1**: System preheating (~300°C) with steam injection, initial LOCA conditions
  - **Step 2**: Shroud is electrically heated (20 kW) to increase boundary temperatures
  - **Step 3**: Rod Heating Power is applied to the fuel rod simulators, causing a rapid temperature rise
  - **Step 4**: Water injection begins; rod temperatures peak and subsequently drop as quenching occurs
  - End of Sequence
- Simulations include all above mentioned phases

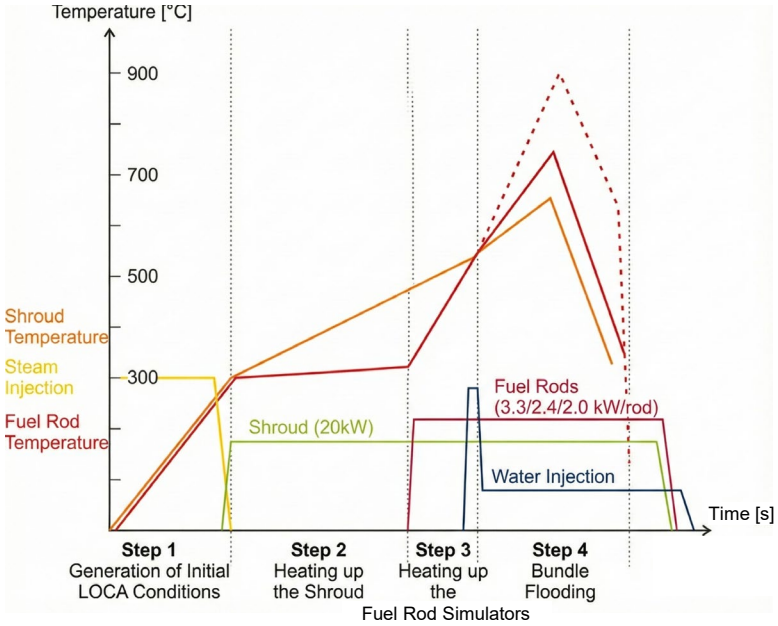

PSS Plant Simulation and Safety
Prof. Dr.-Ing. Marco K. Koch
RUHR UNIVERSITÄT BOCHUM
RUB

INTRODUCTION
Status Quo

- Experiments on flow blockage, local power increase through blockages
- Reflooding of a fuel rod bundle in the event of a loss-of-coolant accident
- Data set with AC²-ATHLET completed, tested and prospectively further developed
  - Intact Bundle, B0
  - Deformed Bundle, B2

Intact Bundle

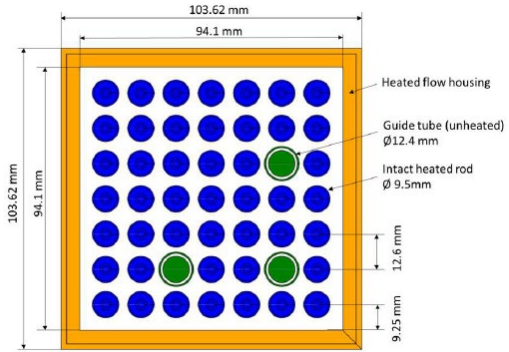

Deformed Bundle

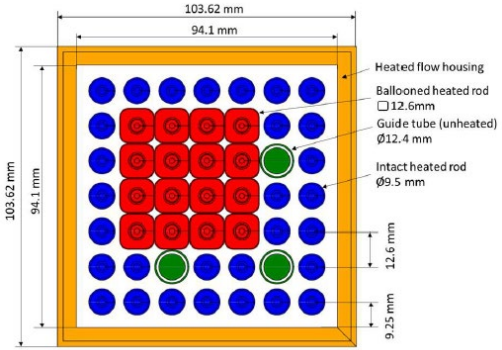

MODELING
Strategies: Balancing Precision and CPU Cost

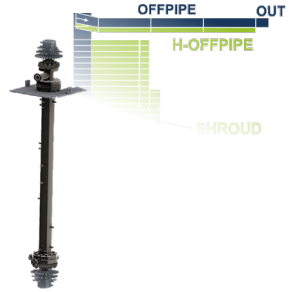

- **Simulation Objectives**
  - Capture main reflooding phenomena
  - If possible, reproduce “3D” effects (e.g., radial temperature gradients, flow deviation around ballooned regions)
- **Possible Modelling Approaches**
  - Sub-channel 3D Modelling
  - Coarse 3D Modelling (Clustered)
  - 1D Modelling (Lumped)

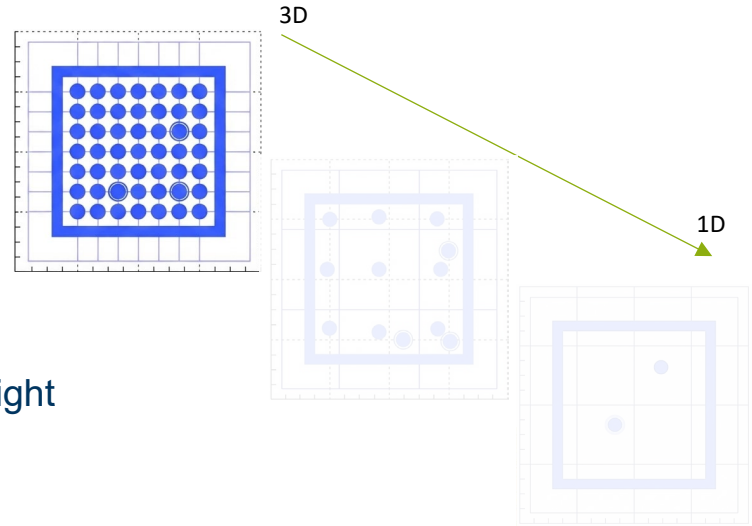

  - ➢ Detailed resolution of the geometry
  - ➢ Con: High CPU cost (up to days) vs. detailed flow insight

MODELING
Strategies: Balancing Precision and CPU Cost

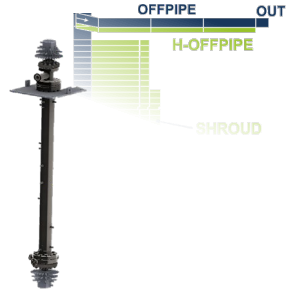

- **Simulation Objectives**
  - Capture main reflooding phenomena
  - If possible, reproduce “3D” effects (e.g., radial temperature gradients, flow deviation around ballooned regions)
- **Possible Modelling Approaches**
  - Sub-channel 3D Modelling
  - Coarse 3D Modelling (Clustered)
  - 1D Modelling (Lumped)
    - Grouping several sub-channels/rods into clusters
    - Pro: Captures radial trends with reasonable effort (up to 1 hour)
    - Relevance: Often used to balance accuracy

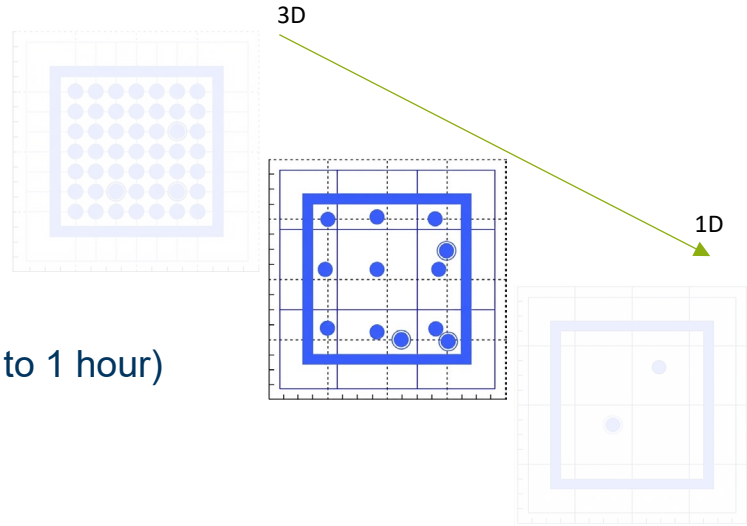

MODELING
Strategies: Balancing Precision and CPU Cost

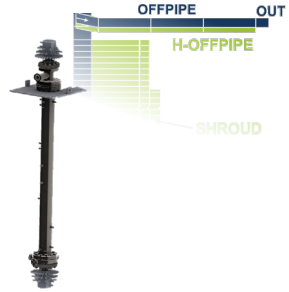

- **Simulation Objectives**
  - Capture main reflooding phenomena
  - If possible, reproduce “3D” effects (e.g., radial temperature gradients, flow deviation around ballooned regions)
- **Possible Modelling Approaches**
  - Sub-channel 3D Modelling
  - Coarse 3D Modelling (Clustered)
  - 1D Modelling (Lumped) ← **used for this work!**
    - Averaging relevant components each into one object
    - Pro: Very fast calculations (minutes)
    - Con: Underestimates radial profiles + local flow deviations

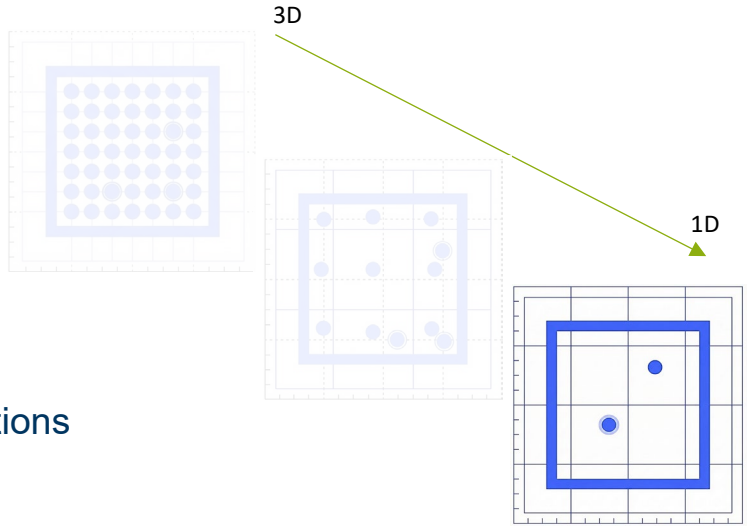

MODELING
AC² Data Set Development

- 1D-Module of ATHLET representing flow path
- Relevant components:
  - Shroud, spacer grids
  - Weighted fuel rod (RODA) and guide tube objects (RODB)
  - For experiments with deformed rods additional objects are implemented
- Components are modeled as multilayer structures (e.g. Shroud, RODs)

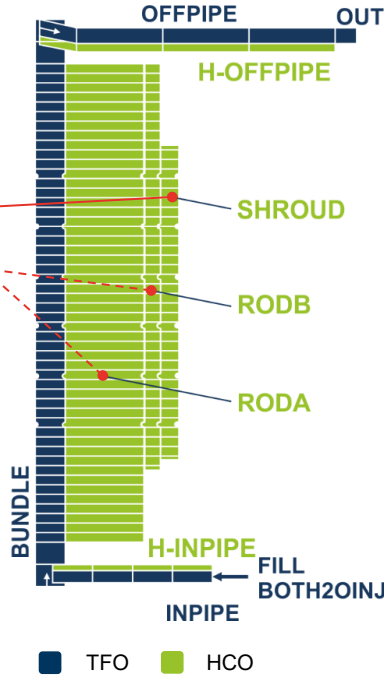

- Boundary Conditions & Power Profile
  - Pressure, Temperature
  - Axial Power Profile
  - Electric Power

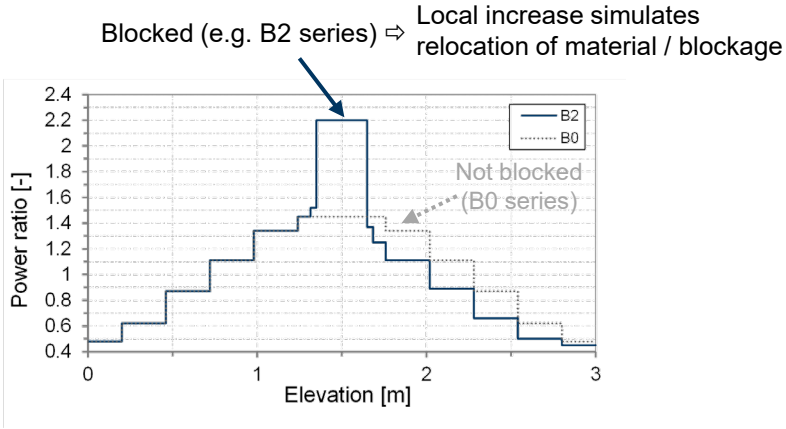

MODELING
Selected COAL-B0 Boundary Conditions

Parameter	B0-03-50	B0-20-17
Pressure	3 bar	20 bar
Inflow	50 kg/m^2/s (0,269kg/s)	17 kg/m^2/s (0,089kg/s)
Temperature of Quenchwater	74 °C	192 °C
Power per rod	3,3 kW	2,0 kW
Shroud power	20 kW	20 kW

RESULTS
B0-03-50: Selected Results

- Scenario at low pressure (3 bar) with 0,269 kg/s reflooding rate
  - Rod power at 3.3 kW
  - › Shroud temperature is qualitatively calculated but overestimated (~610°C)
  - › Timing is captured closely

Bundle Configuration

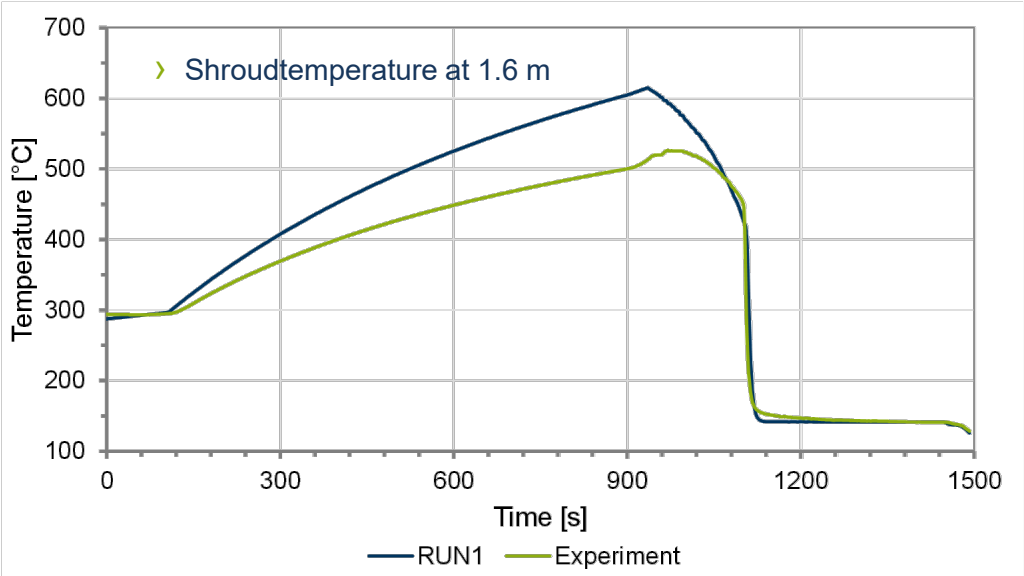

RESULTS
B0-03-50: Selected Results

- Scenario at low pressure (3 bar) with 0,269 kg/s reflooding rate
  - Rod power at 3.3 kW
  - › Calculated rod temperatures reach max. 810°C at 1.7 m and 700°C at 1.5 m
  - › Simulation shows axial shift: simulation data at 1.7 m match experimental data at 1.5 m, possibly due to delayed quenching

Bundle Configuration

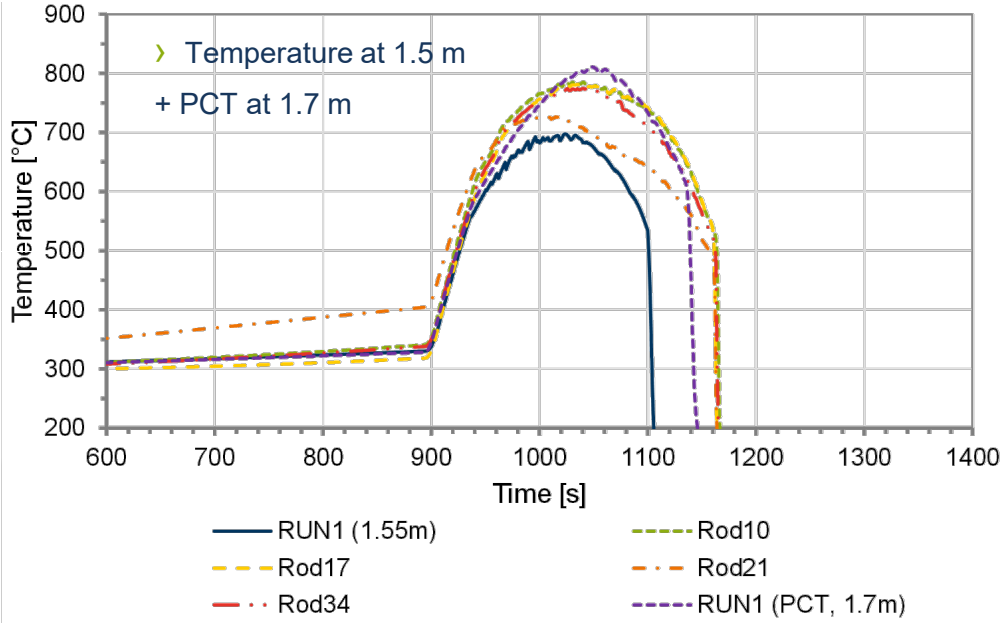

RESULTS
B0-03-50: Selected Results

- Scenario at low pressure (3 bar) with 0,269 kg/s reflooding rate
  - Rod power at 3.3 kW
  - › After reaching local plateau, the bundle is eventually fully quenched
  - › Simulation captures initial rise but overpredicts subsequent water column rise

Bundle Configuration

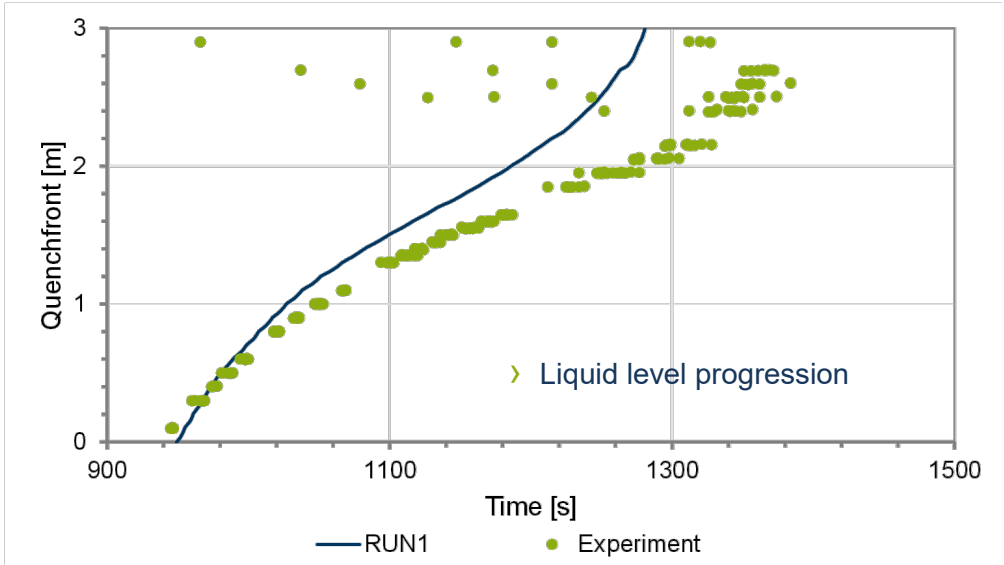

PSS Plant Simulation and Safety
Prof. Dr.-Ing. Marco K. Koch
RUHR UNIVERSITÄT BOCHUM
RUB

RESULTS
B0-03-50: Selected Results

- Scenario at low pressure (3 bar) with 0,269 kg/s reflooding rate
  - Rod power at 3.3 kW
  - › After reaching local plateau, the bundle is eventually fully quenched
  - › Simulation captures initial rise but overpredicts subsequent water column rise

Bundle Configuration

B0-03-50 key events visualized

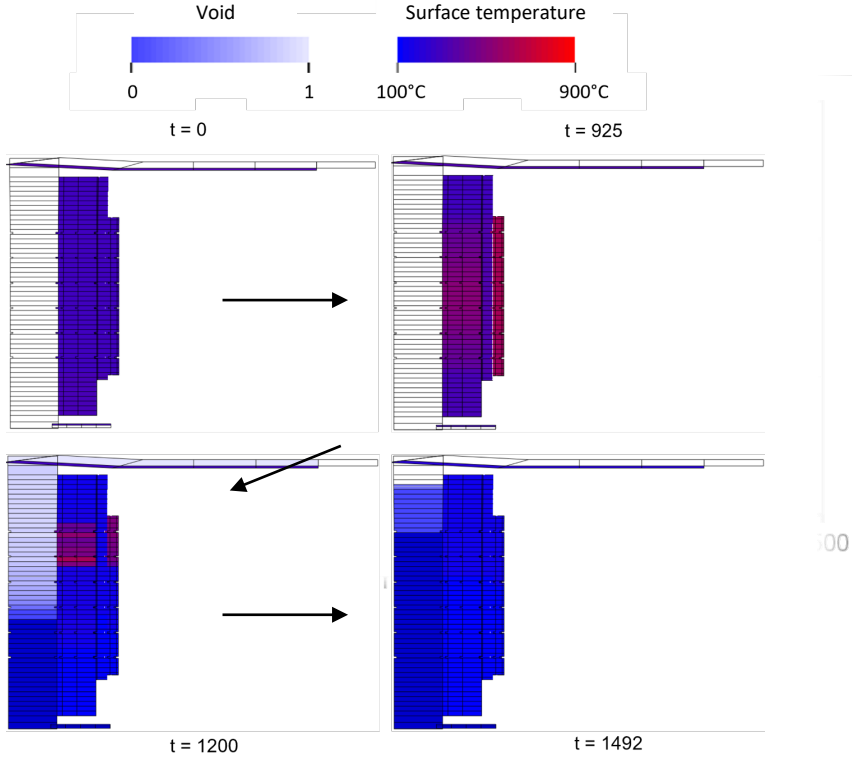

PSS Plant Simulation and Safety
Prof. Dr.-Ing. Marco K. Koch
RUHR UNIVERSITÄT BOCHUM
RUB

RESULTS
B0-20-17: Selected Results

- Scenario at higher pressure (20 bar) and lower reflooding rate (0,089 kg/s)
  - Lower rod power at 2 kW
  - › Bundle is fully quenched
  - › Rod temperatures reach max. 820°C

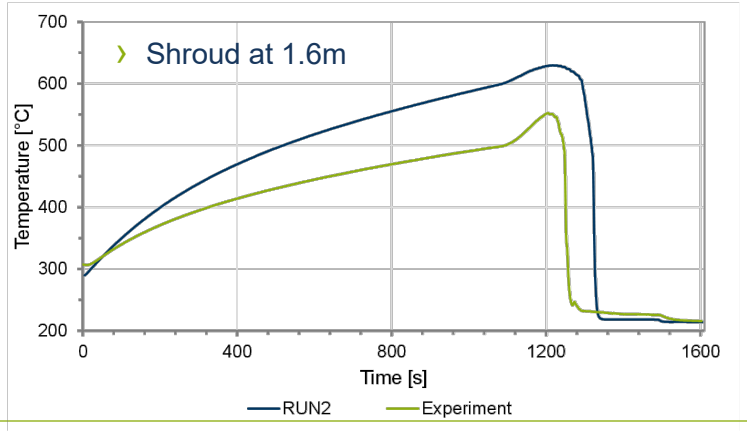

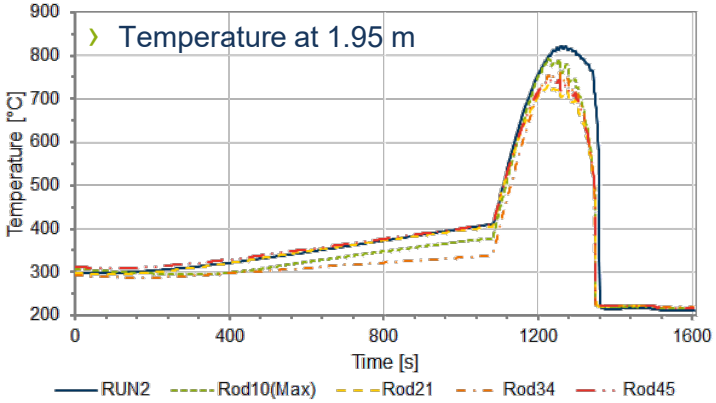

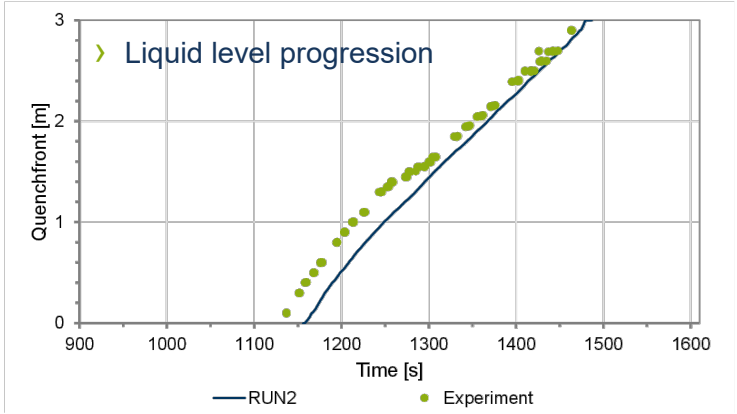

PSS Plant Simulation and Safety
Prof. Dr.-Ing. Marco K. Koch
RUHR UNIVERSITÄT BOCHUM
RUB

RESULTS
B0-20-17: Selected Results

- Scenario at higher pressure (20 bar) and lower reflooding rate (0,089 kg/s)
  - Lower rod power at 2 kW
  - › Bundle is fully quenched
  - › Rod temperatures reach max. 930°C

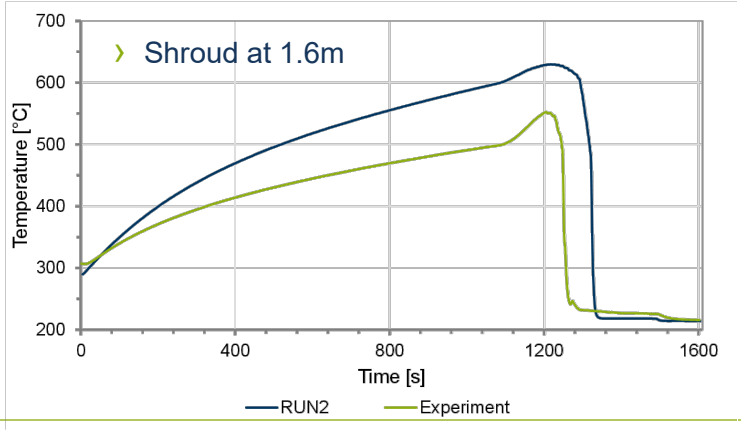

B0-20-17 key events visualized

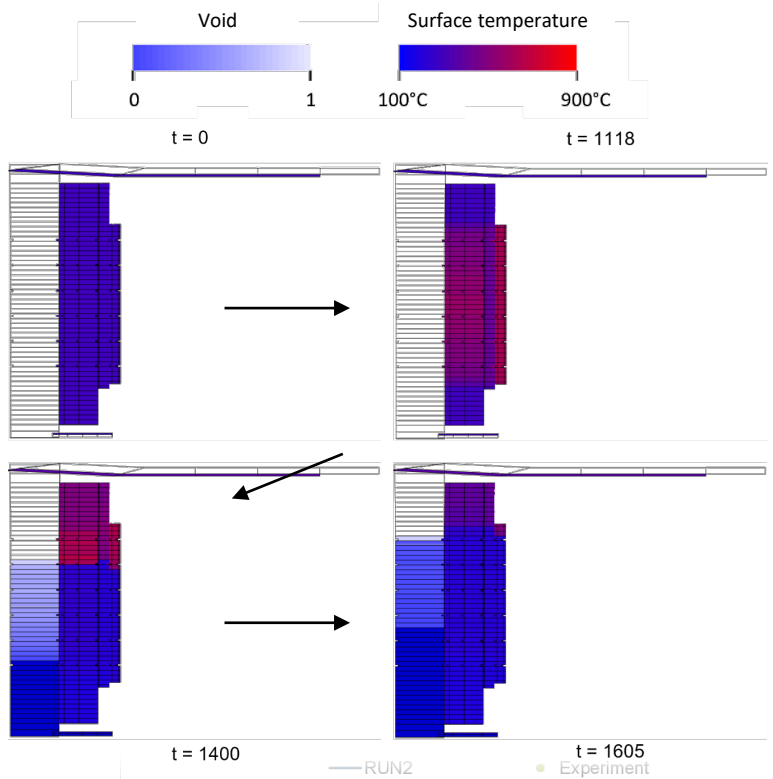

PSS Plant Simulation and Safety
Prof. Dr.-Ing. Marco K. Koch
RUHR UNIVERSITÄT BOCHUM
RUB

SUMMARY

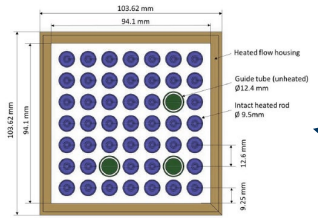

a) Bundle B0

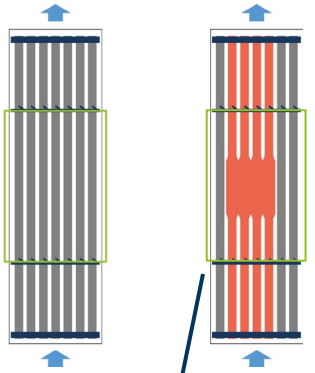

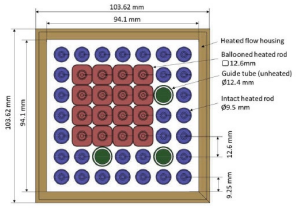

b) Bundle B2

- **Simulation Results**
  - Transient Response: ATHLET captures key physical phenomena yielding plausible behaviour throughout the reflooding phase
  - Steady-State Agreement: Satisfactory agreement prior to rod peak while deviations are observed during the heating phase
  - Like Quench-Experiments, these experiments serve as a validation of AC² capabilities to predict cladding temperatures accurately – a prerequisite for works on oxidation kinetics
- **Modelling Strategy & Outlook**
  - The current nodalization is maintained to ensure comparability between B0 and B2
  - Model Refinement: The observed discrepancies in the heating phase are identified as limitations of the 1D-approach and BC definitions
  - Investigating a multi-channel model (parallel channels) is recommended to investigate to possibly improve the radial temperature profile; additionally, sensitivity studies regarding shroud heater positioning and initial BC are advised to further enhance accuracy

REFERENCES

[NEA24] Nuclear Energy Agency: *WGAMA ISP-53*, 2025, Available at: https://www.oecdnea.org/jcms/pl_92672/wgama-isp-53

[REP15] Repetto, G., et al.: *The R&D PERFROI project on Thermal mechanical and thermal hydraulics behaviors of a fuel rod assembly during a Loss Of Coolant Accident*, NURETH-16, American Nuclear Society, Chicago (IL), 2015.

[REP17] Repetto, G., et al.: *Core Coolabilty in loss of coolant accident: the coal experiments investigating the thermal hydraulics of a rod bundle with blocked area during the reflooding*, NURETH-17, American Nuclear Society, Xi'an, China, 2017.

[REP22] Repetto, G., et al.: *COAL Experiments investigating the reflooding of a 7 x 7 rods bundle during a loss of coolant accident thermalhydraulics results*, NURETH-19, Brüssel, Belgien, 2022.

[REP23] Repetto, G., et al.: *COAL Experiments investigating the reflooding of a 7 x 7 rods bundle during a loss of coolant accident: effect of a partially blocked area with ballooned rods*, NURETH-20, Washington, USA, 2023.

[REP24] Repetto, G., et al.: *COAL reflooding experiments during a loss of coolant accident: Effect of the water flow rate, the pressure and the rod power with ballooned rods*. Nuclear Engineering and Design, Volume 429, 2024.

ACKNOWLEDGEMENT

This work was carried out within the framework of the WGAMA WGFS ISP-53, whose support and collaboration have been instrumental in the successful completion of this research.

Responsibility for the content lies with the authors.

The results were obtained using the GRS software package AC² 2023.

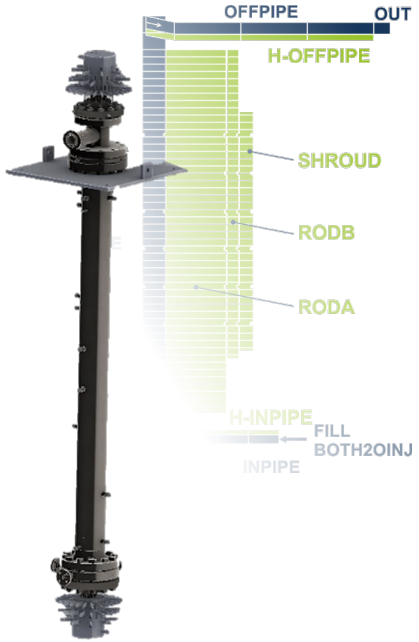

Thank you for your attention!

Gregor Stahlberg

Gregor.Stahlberg@pss.rub.de

Marco K. Koch

Marco.Koch@pss.rub.de

RUHR-UNIVERSITÄT BOCHUM

PSS Plant Simulation and Safety

Prof. Dr.-Ing. Marco K. Koch

Building: IC | Floor 2

Universitätsstr. 150

D-44801 Bochum

pss.rub.de

Liviusz Lovasz

GRS

Validation of AC2/ATHLET using QUENCH data

The QUENCH experimental series has been used to validate the severe accident code AC2/ATHLET-CD, which is developed by GRS, for multiple decades. Due to recent strategic decisions, the AC2 subprograms (ATHLET, ATHLET-CD and COCOSYS) have been further unified, particularly the ATHLET thermohydraulic subprogram and the ATHLET-CD severe accident phenomena subprogram. This unified code version of ATHLET and ATHLET-CD offers benefits to users and developers alike. However, to ensure that the refactoring and recent new developments comply with AC2's quality assurance policies, the new unified code version must be extensively validated. The first step towards fully validating the unified code version was to simulate and analyze the QUENCH-L0 experiment in detail, and the results are presented at the 30th QUENCH Workshop. Model specifications and potential future development needs are also discussed.

Validation of AC2/ATHLET using QUENCH data

Liviusz Lovasz, GRS

30th International QUENCH Workshop, Karlsruhe, 16-18.12.2025

What is AC²?

- AC²:
  - ATHLET
  - ATHLET-CD
  - COCOSYS
- Deterministic system code system for accident analysis
- Covers a wide spectrum of phenomena

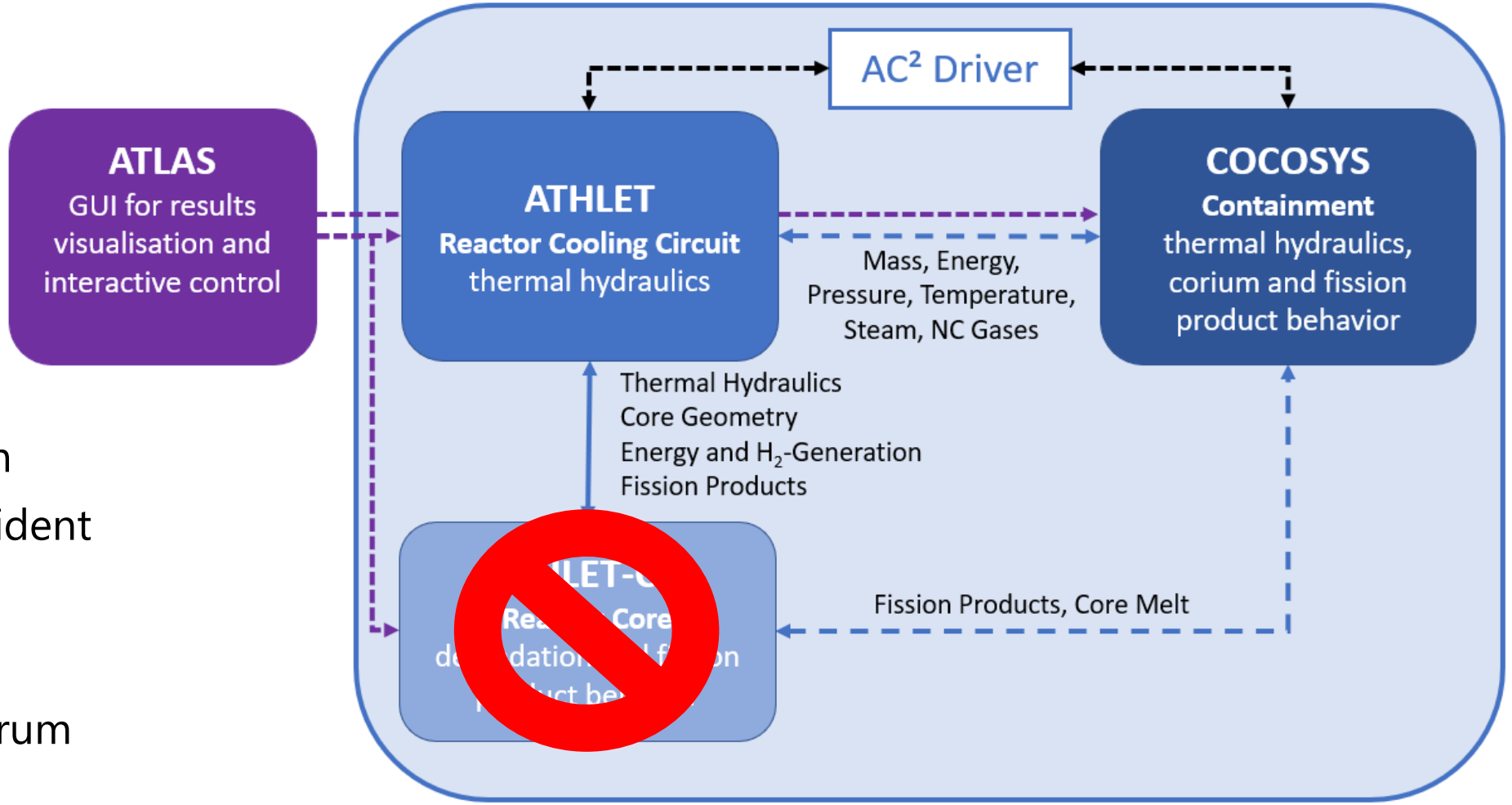

Using ATHLET-CD (up until now)

- Creating an input deck from scratch for **ATHLET-CD**
- Changing an existing **ATHLET** input deck and adapting it to **ATHLET-CD**

Simulation of the **Core**

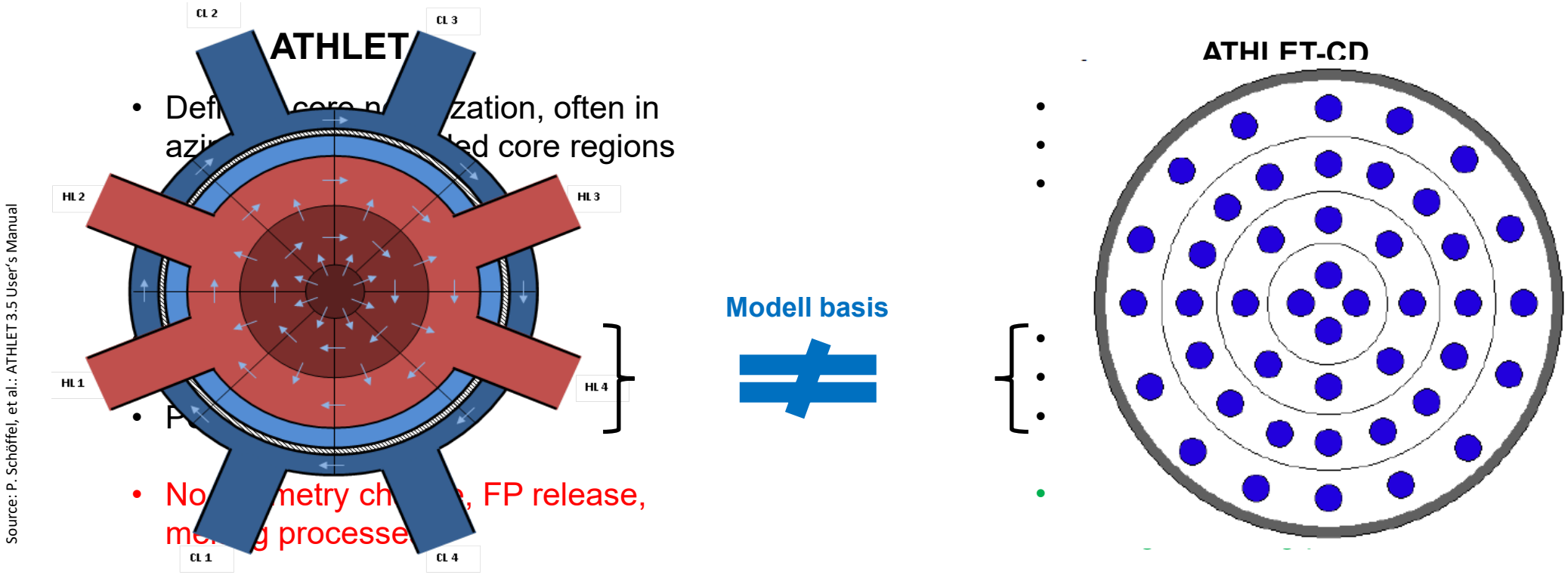

Recent development goals

- Review, refactor and transfer or newly develop ATHLET-CD models to ATHLET to cover:
  - Heat generation ✓
  - Heat radiation static ✓ + dynamic ✗
  - Oxidation ✓
  - Fuel deformation ✓
  - Fission product release and transport ✓
  - Structure melting ✓ and relocation ✗

Overall goals

- Create flexibly usable simulation tool for severe accidents
  - Simple to use for the user
  - Simple to maintain and extend for the developer

- Focus is still on conventional nuclear applications
  - Gen III+ reactors
  - SMR-s
  - Research reactors
  - Spent fuel pools, interim storage

Validation

- Significantly changed code
  - New models
  - New nodalization

- Validation required
  - QUENCH experiment series (among others) plays a big role
  - Step by step validation
    - DBA phenomena
    - BDBA phenomena

Validation – QUENCH-L0

- Goal of the experiment
  - Investigate ballooning / bursting and hydriding

- Goal of modelling / validation:
  - Nodalization
  - Basic heat transfer
  - Oxidation
  - Ballooning and bursting

QUENCH-L0 Experiment

- 21 differently pressurized rod simulators with Zr-4 cladding
- Electrically heated
  - Rapid heating to 1070 °C
  - Bottom quenching

Map of bundle filling

Pressure, bar	Number of rods
3 (system p)	1
35	2
40	4
45	3
50	9
55	2

Source: J. Stuckert, M. Große, C. Rössger, M. Steinbrück, M. Walter, QUENCH - LOCA - REPORTS Nr. 1, Results of the commissioning bundle test QUENCH-L0 performed under LOCA conditions (SR-7571), KIT, 2015

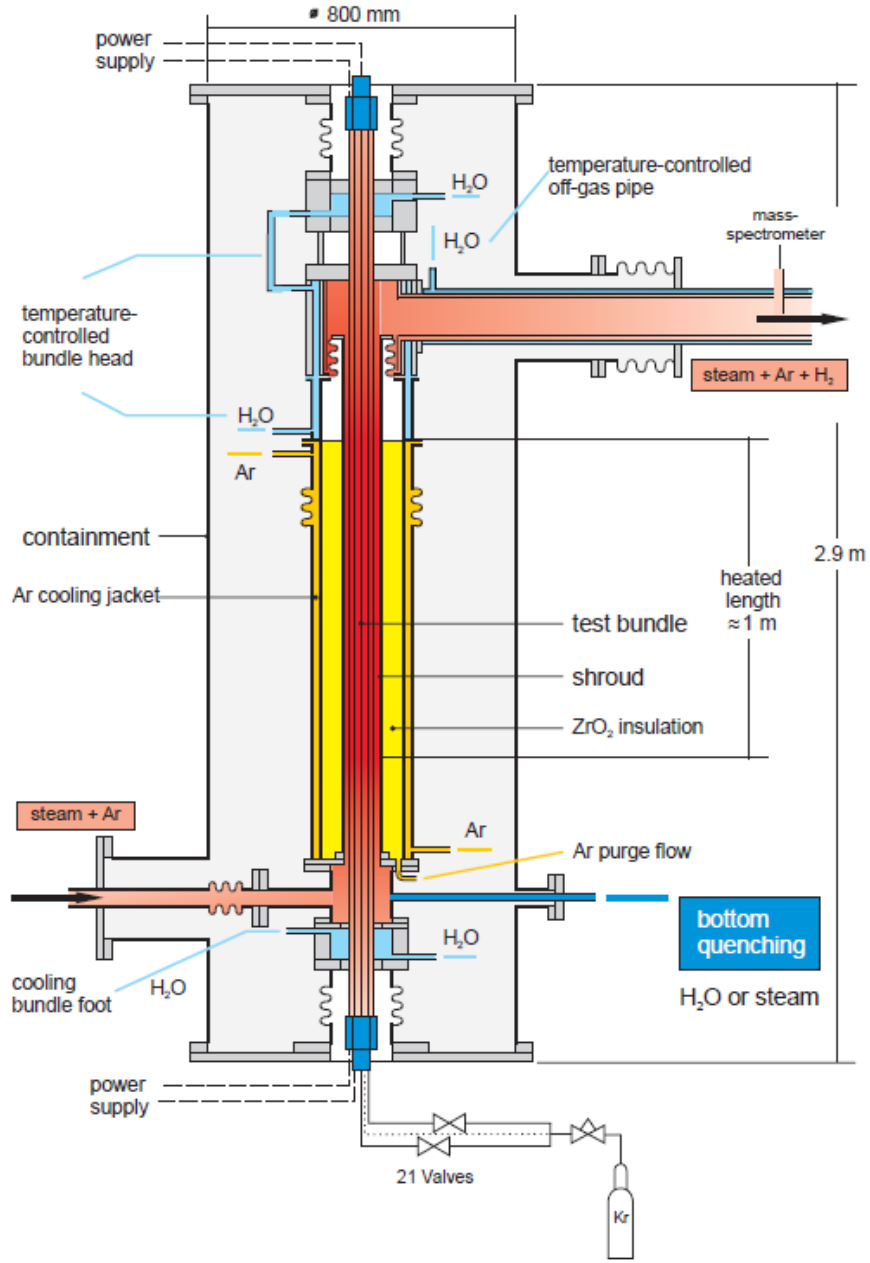

Source: J. Stuckert, M. Große, C. Rössger, M. Steinbrück, M. Walter, QUENCH - LOCA - REPORTS Nr. 1, Results of the commissioning bundle test QUENCH-L0 performed under LOCA conditions (SR-7571), KIT, 2015

QUENCH-L0 Simulation – old (ATHLET-CD)

- Two thermohydraulic objects horizontally
  - 20 axial subdivision, cross connection
- Rods grouped in 9 segments
  - Based on their initial pressure
  - Pressure evolution not calculated
    - Via user signal implemented
  - Heat radiation incorrect
    - Heat radiation only from I to I-1 / I+1 Object
- Delivers acceptable results
  - Known flaws
  - Limitations

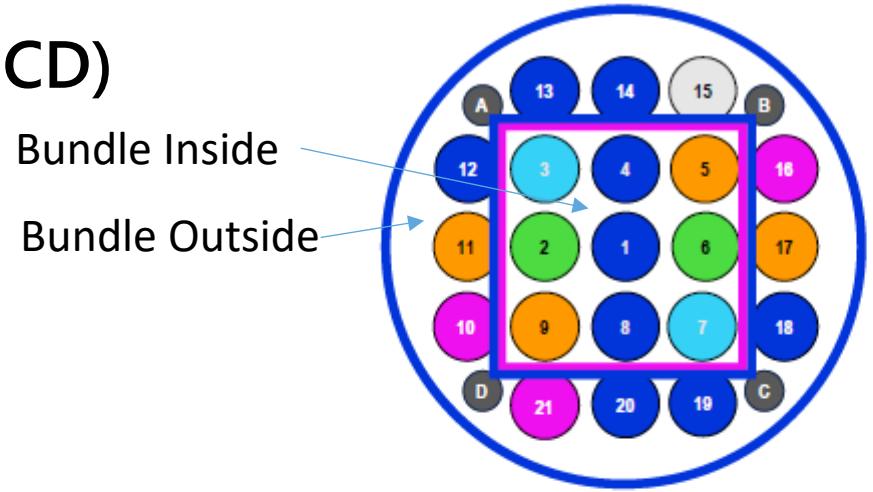

Table 5. Rod model numbering

Radial Position	Rod #, model	Rod Press., bar	Rod #, Experiment
Inner Bundle	1	50	1
	2	35	2, 6
	3	40	5, 9
	4	50	4, 8
	5	55	3, 7
Outer Bundle	6	3	15
	7	40	11, 17
	8	45	10, 16, 21
	9	50	12, 13, 14, 18, 19, 20

Source:
Di Nora, V. A.; Wielenberg, A.; Lovasz, L; Schöffel, P. J., Integration and Validation of Models for Thermal-Mechanical Behaviour of Nuclear Fuel Rods in ATHLET, Annals of Nuclear Energy Volume 227, Part A, February 2026, 111915

QUENCH-L0 Simulation – new (ATHLET+)

- Two thermohydraulic objects horizontally
  - 20 axial subdivision, cross connection
- Each rod modelled individually (21+4)
  - Pressure evolution **IS** calculated
    - Rod deformation, inclusive feedback to TH
    - Gap heat conductance
  - Heat radiation between all objects calculated
    - Static, inclusive shroud

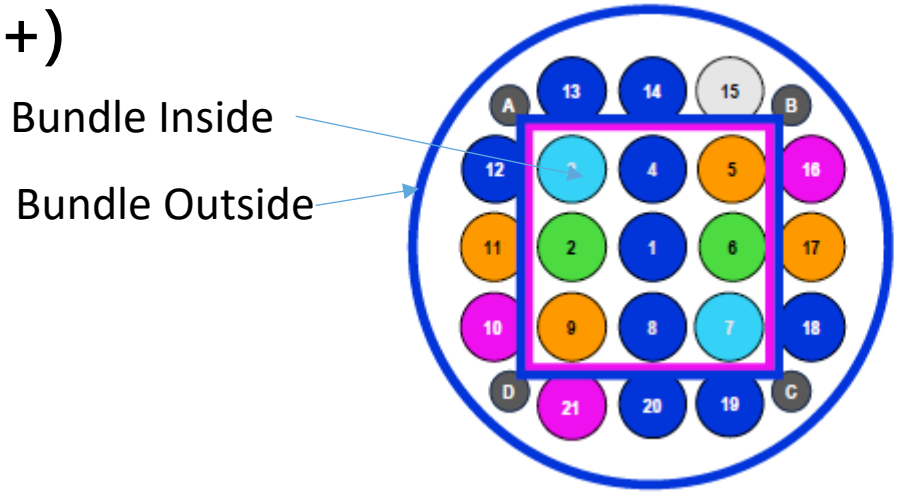

Source:
Di Nora, V. A.; Wielenberg, A.; Lovasz, L; Schöffel, P. J., Integration and Validation of Models for Thermal-Mechanical Behaviour of Nuclear Fuel Rods in ATHLET, Annals of Nuclear Energy Volume 227, Part A, February 2026, 111915

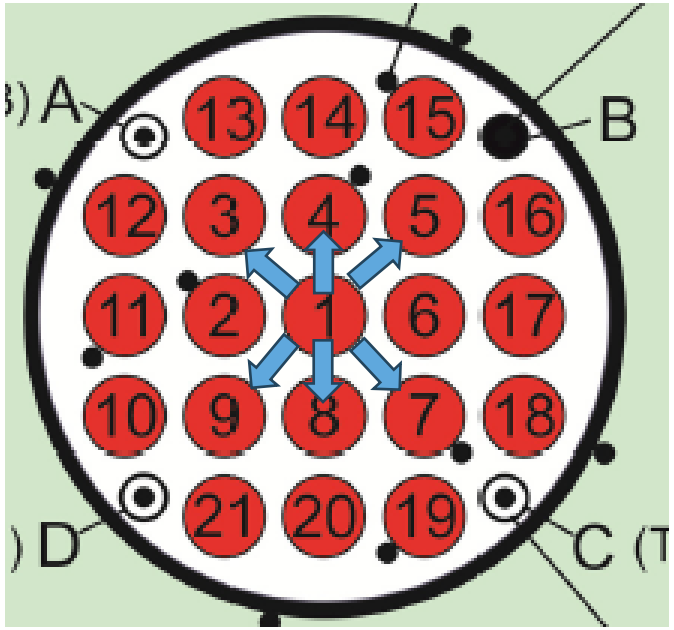

Source: J. Stuckert, M. Große, C. Rössger, M. Steinbrück, M. Walter, QUENCH - LOCA - REPORTS Nr. 1, Results of the commissioning bundle test QUENCH-L0 performed under LOCA conditions (SR-7571), KIT, 2015

QUENCH-L0 Simulation – new (ATHLET+)

- Detailed nodalisation too much?
- Standard DBA nodalization for LWR:
  - 2-3 “rings”, azimuthal subdivision 4-8 ~ 25

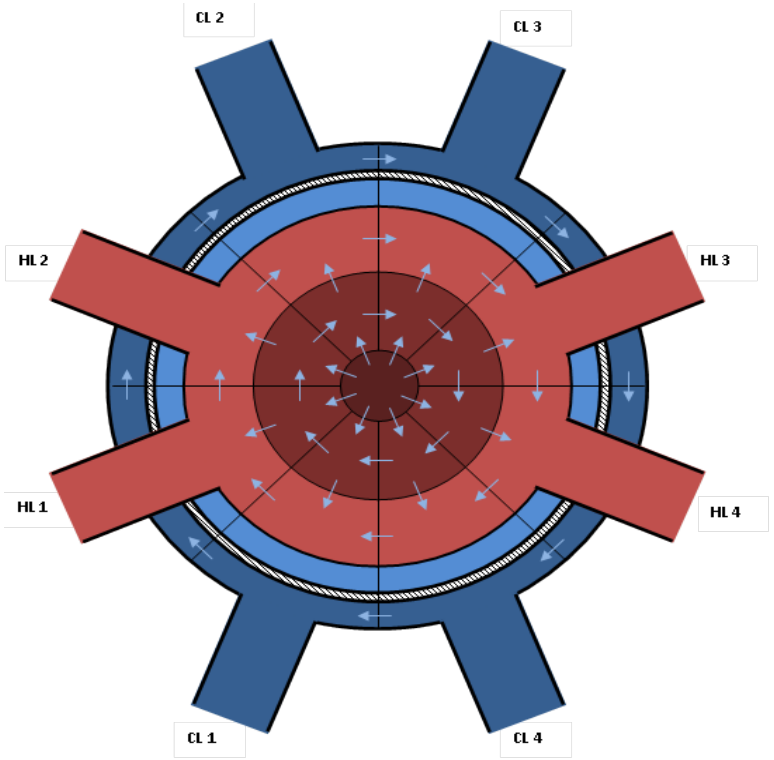

Source: P. Schöffel, et al.: ATHLET 3.5 User’s Manual

- QUENCH L0 nodalization
- 21+4+1 objects = 26

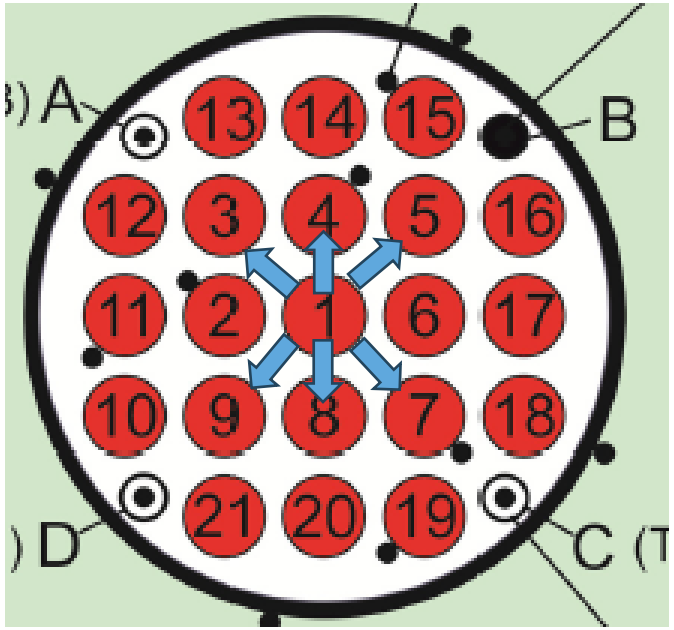

Source: J. Stuckert, M. Große, C. Rössger, M. Steinbrück, M. Walter, QUENCH - LOCA - REPORTS Nr. 1, Results of the commissioning bundle test QUENCH-L0 performed under LOCA conditions (SR-7571), KIT, 2015

QUENCH-L0 Simulation – new (ATHLET+)

- Analysed at:
  - Elevation 950 mm for Rod 2, 19 + Shroud
  - Elevation 450 mm for Rod 7
  - Pressure of Rod 2, 19
  - Burst times
  - Strain

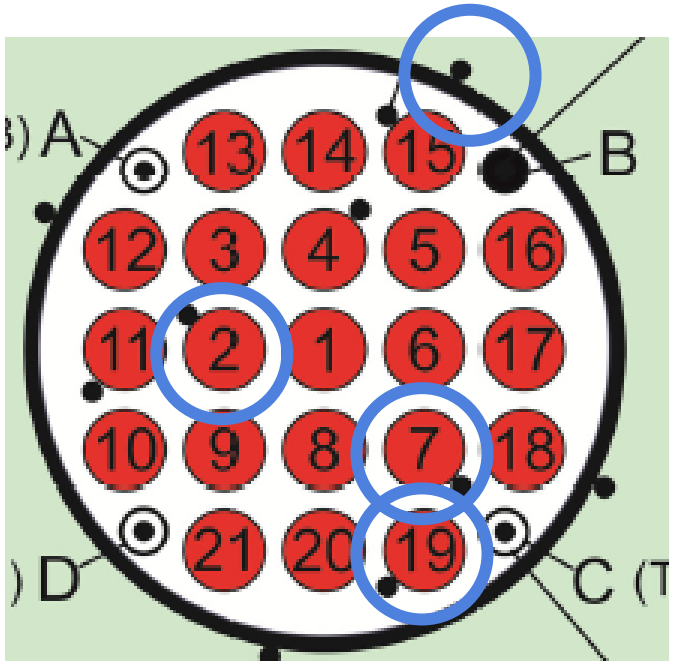

Source: J. Stuckert, M. Große, C. Rössger, M. Steinbrück, M. Walter, QUENCH - LOCA - REPORTS Nr. 1, Results of the commissioning bundle test QUENCH-L0 performed under LOCA conditions (SR-7571), KIT, 2015

QUENCH-L0 Simulation – new (ATHLET+)

- Rod 2 elevation (950 mm):
  - Good agreement with measurement
  - Slight underestimation before quench
  - Qualitative similarity after quench
    - Faster dryout after quench

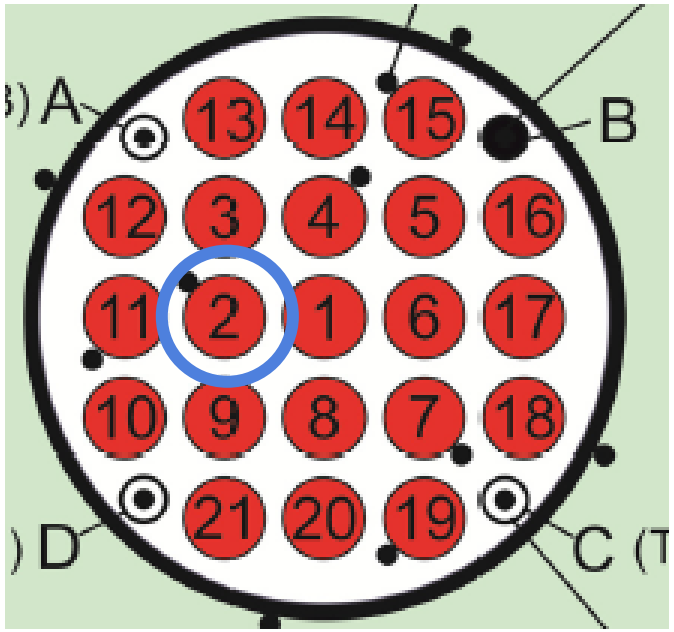

Source: J. Stuckert, M. Große, C. Rössger, M. Steinbrück, M. Walter, QUENCH - LOCA - REPORTS Nr. 1, Results of the commissioning bundle test QUENCH-L0 performed under LOCA conditions (SR-7571), KIT, 2015

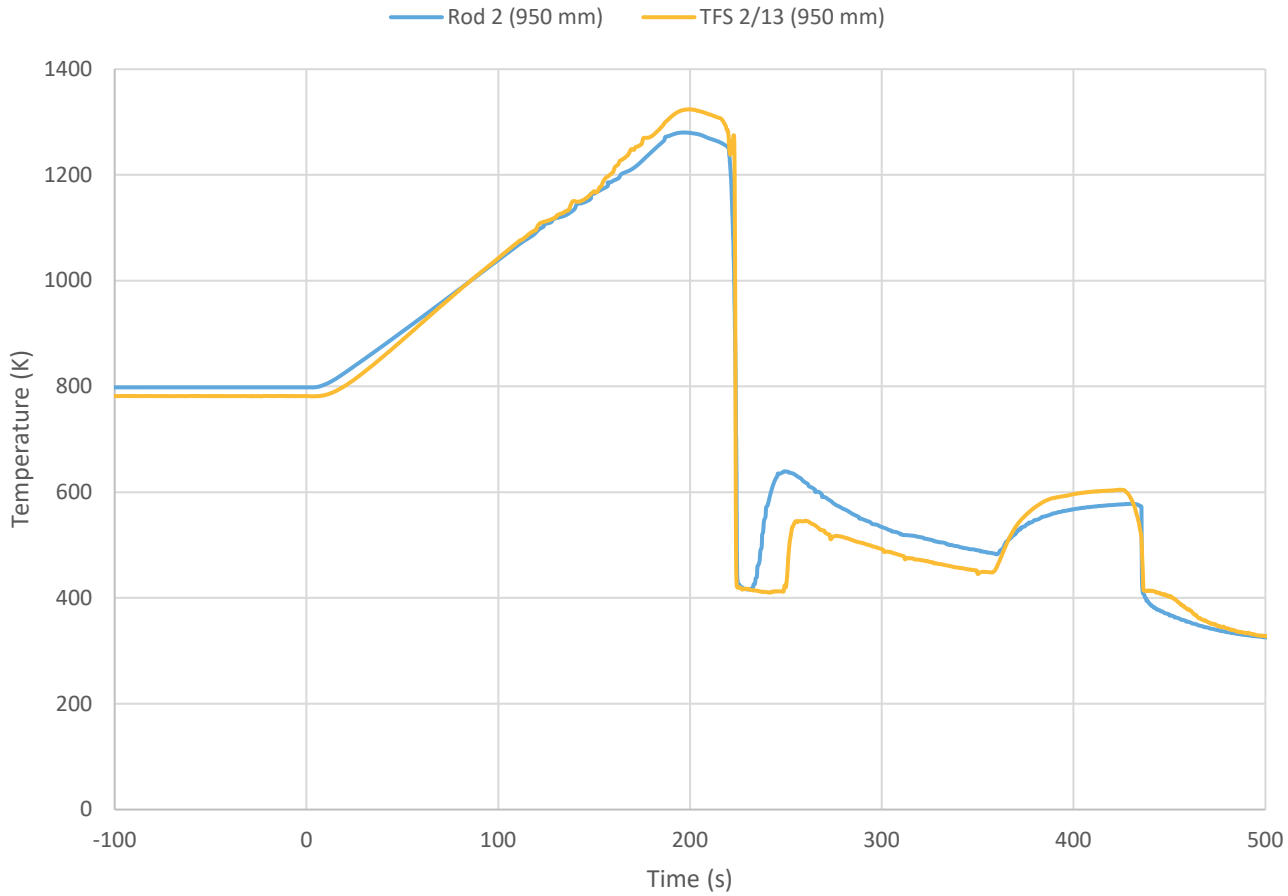

QUENCH-L0 Simulation – new (ATHLET+)

- Rod 19 elevation (950 mm):
  - Similar qualitatively to Rod 2
  - Overestimation of temperatures
    - Location of TC

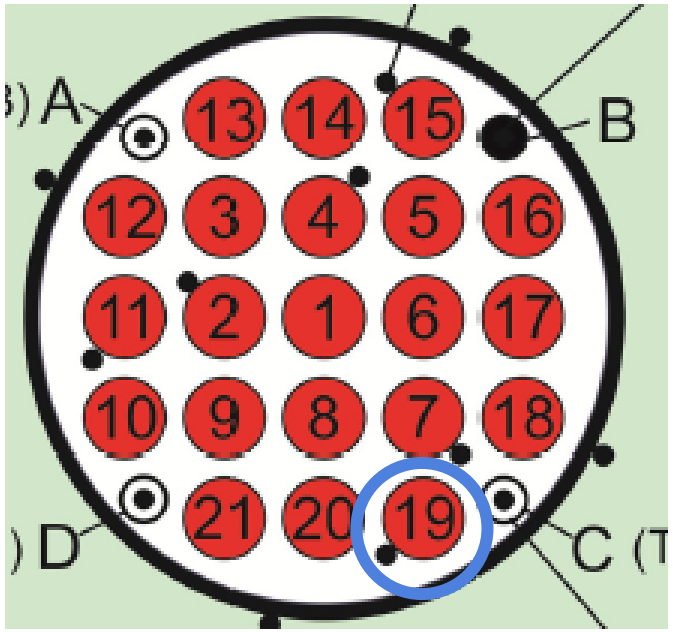

Source: J. Stuckert, M. Große, C. Rössger, M. Steinbrück, M. Walter, QUENCH - LOCA - REPORTS Nr. 1, Results of the commissioning bundle test QUENCH-L0 performed under LOCA conditions (SR-7571), KIT, 2015

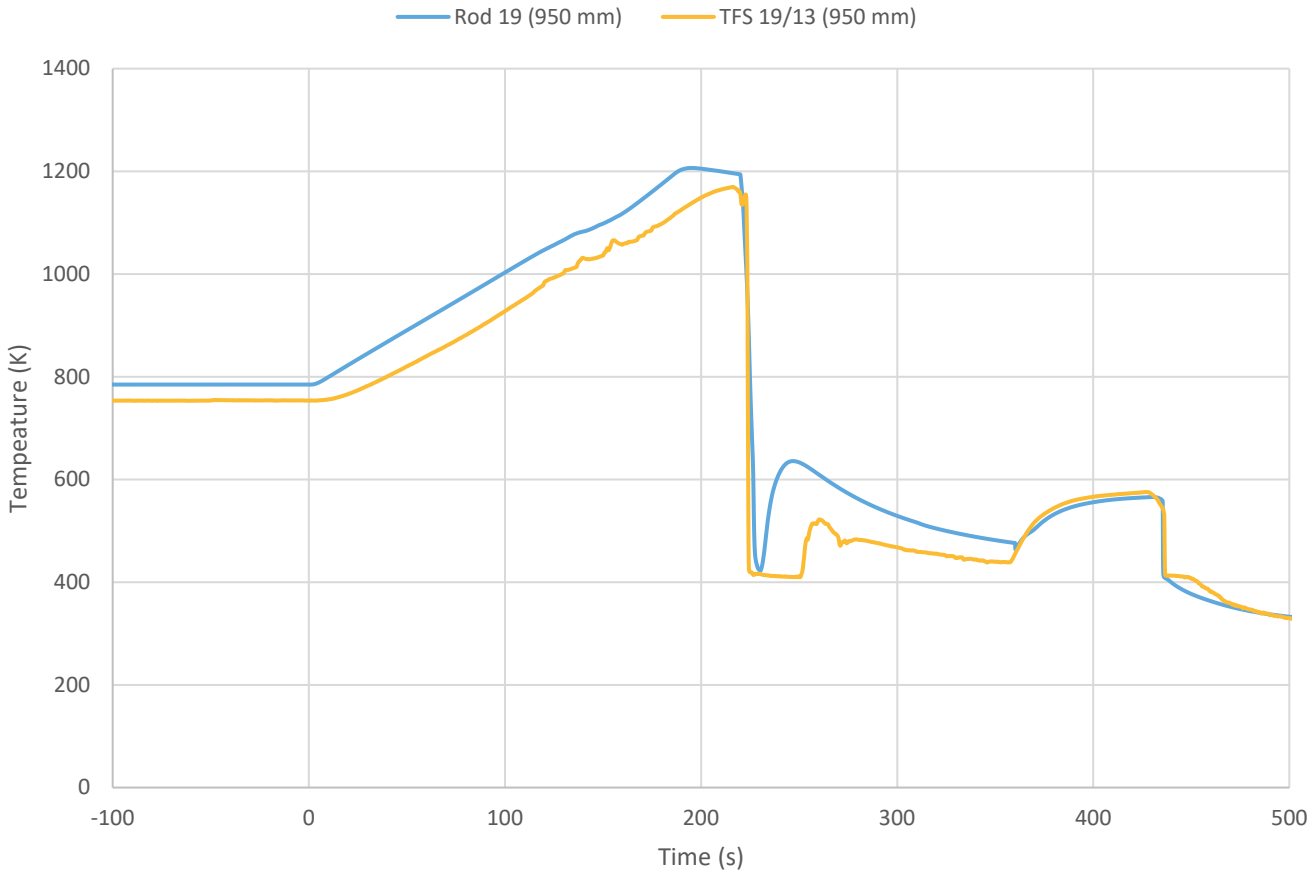

QUENCH-L0 Simulation – new (ATHLET+)

- Shroud elevation (950 mm):
  - Temperature overestimation
  - Cooling process well replicated

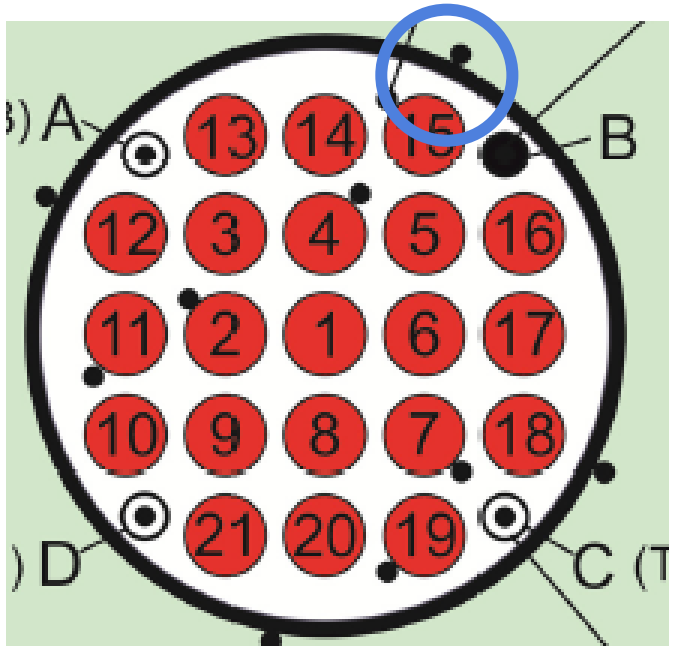

Source: J. Stuckert, M. Große, C. Rössger, M. Steinbrück, M. Walter, QUENCH - LOCA - REPORTS Nr. 1, Results of the commissioning bundle test QUENCH-L0 performed under LOCA conditions (SR-7571), KIT, 2015

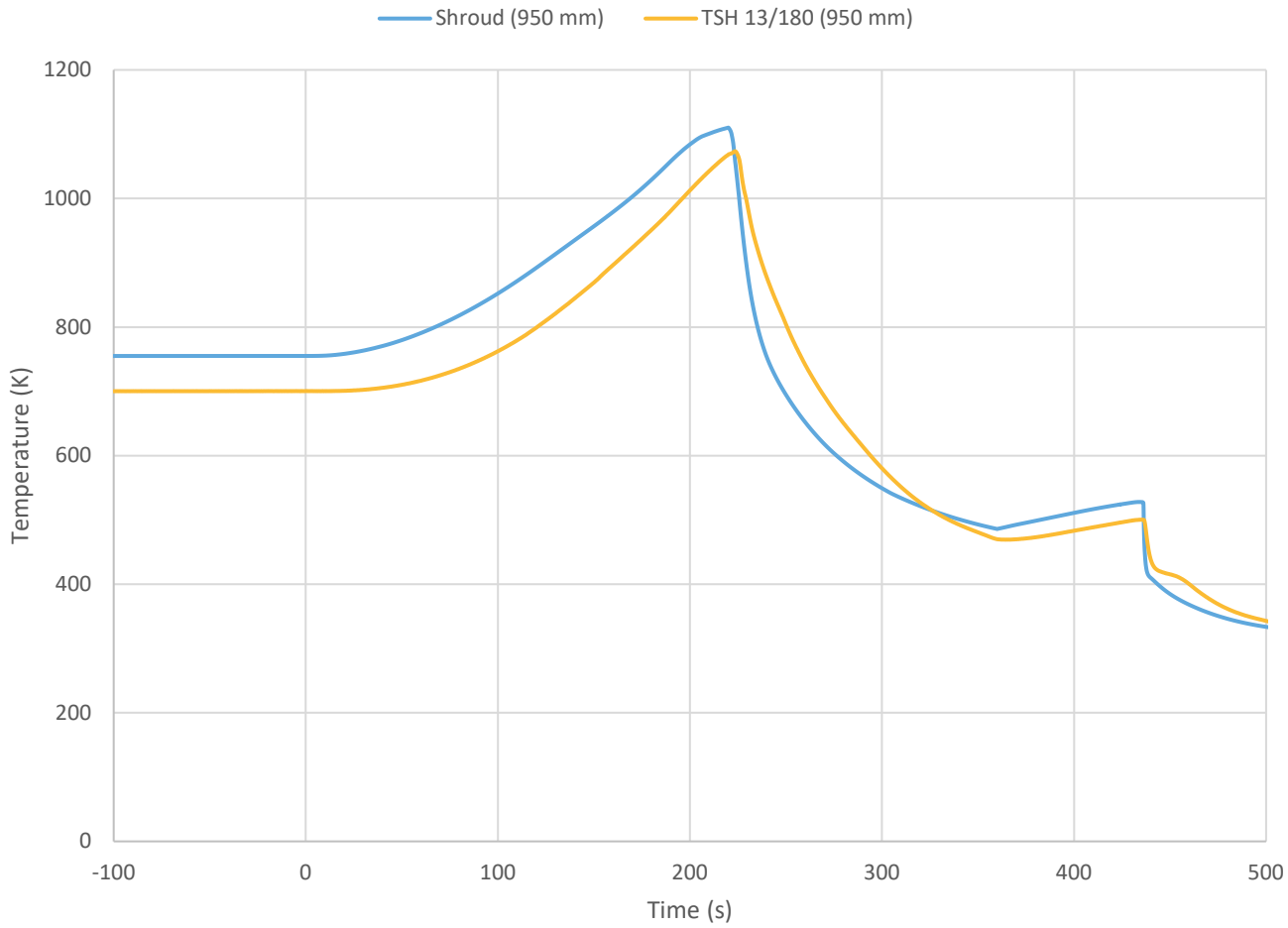

QUENCH-L0 Simulation – new (ATHLET+)

- Rod 7 elevation 450 mm:
  - Overestimation until quenching

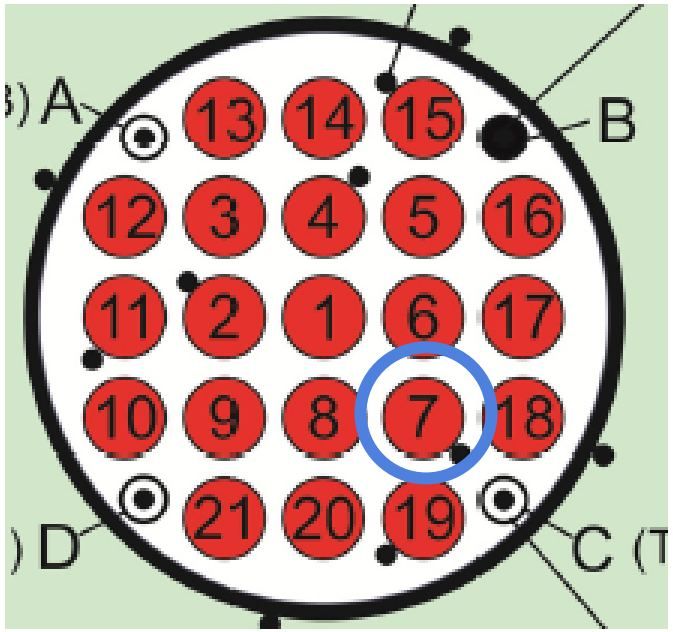

Source: J. Stuckert, M. Große, C. Rössger, M. Steinbrück, M. Walter, QUENCH - LOCA - REPORTS Nr. 1, Results of the commissioning bundle test QUENCH-L0 performed under LOCA conditions (SR-7571), KIT, 2015

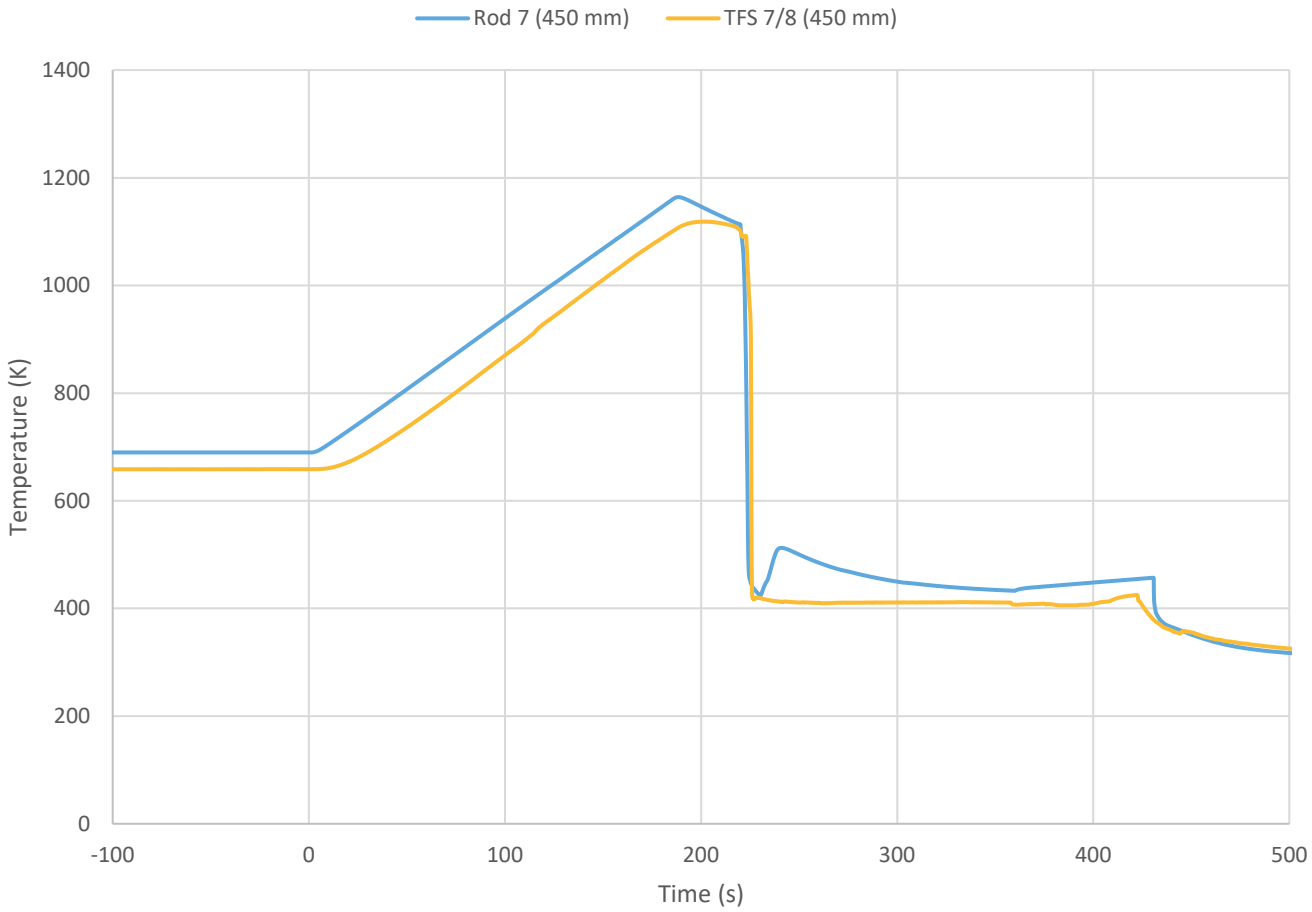

QUENCH-L0 Simulation – new (ATHLET+)

- Rod 2 pressure:
  - Smaller increase of internal pressure
  - Burst time well predicted
  - Increase of rod diameter

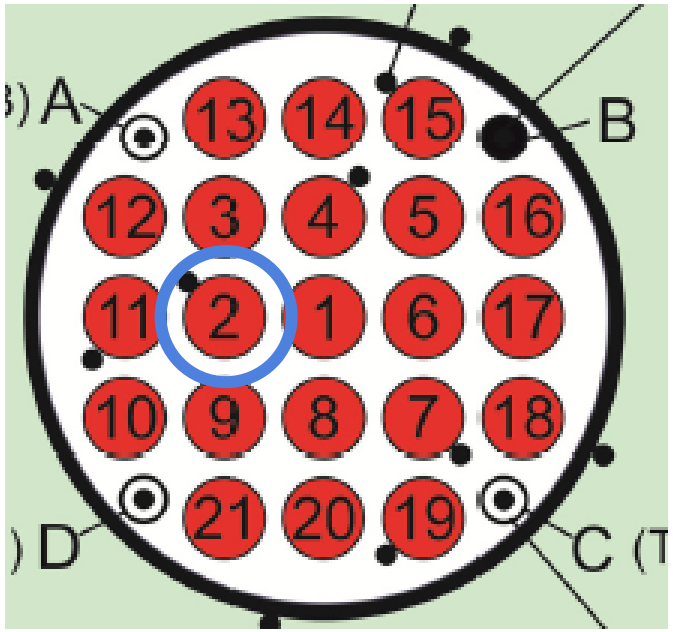

Source: J. Stuckert, M. Große, C. Rössger, M. Steinbrück, M. Walter, QUENCH - LOCA - REPORTS Nr. 1, Results of the commissioning bundle test QUENCH-L0 performed under LOCA conditions (SR-7571), KIT, 2015

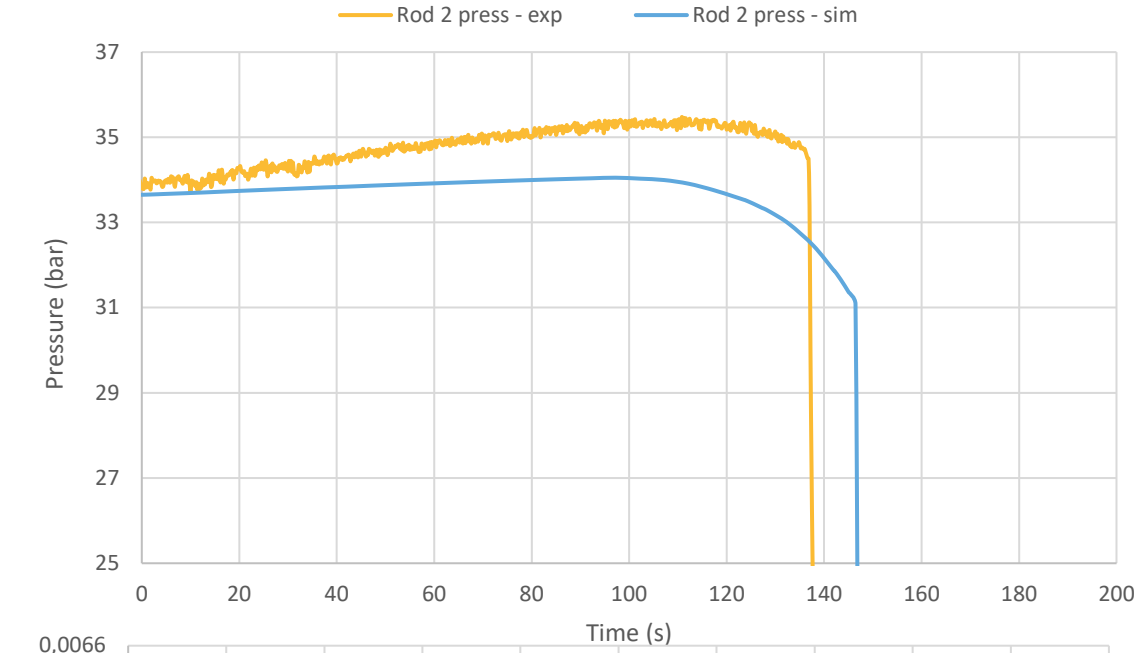

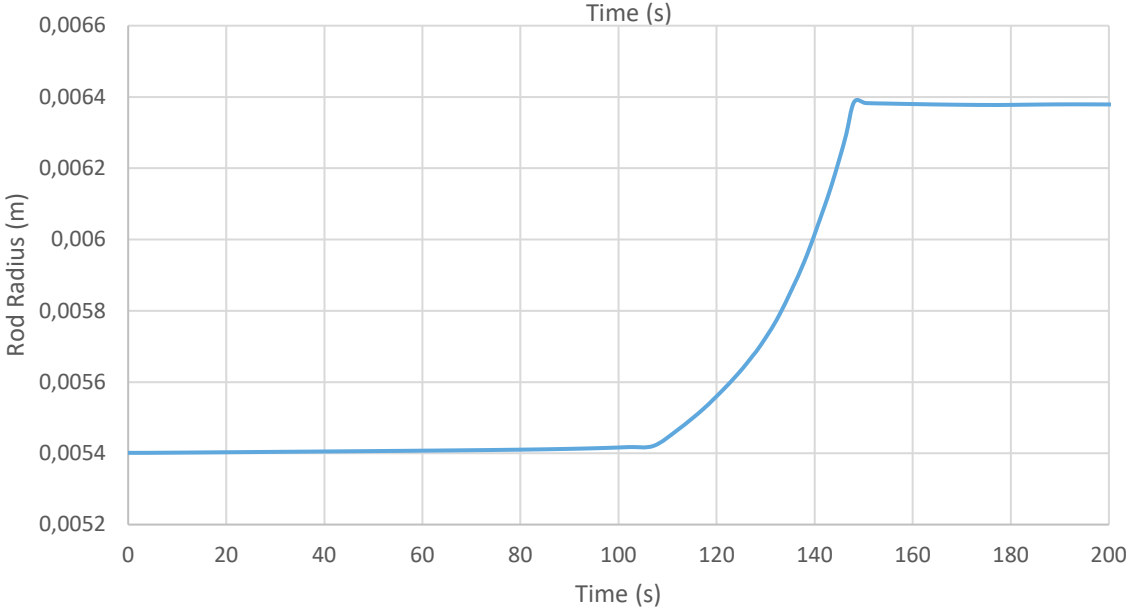

QUENCH-L0 Simulation – new (ATHLET+)

Feedback on the thermohydraulics

- Overall blockage of the channel: 53% (sim.)
- All balloonings at the same elevation (nodalization dependent)
- Experimental data if all ballooning happened at the same elevation: 46% (exp.)

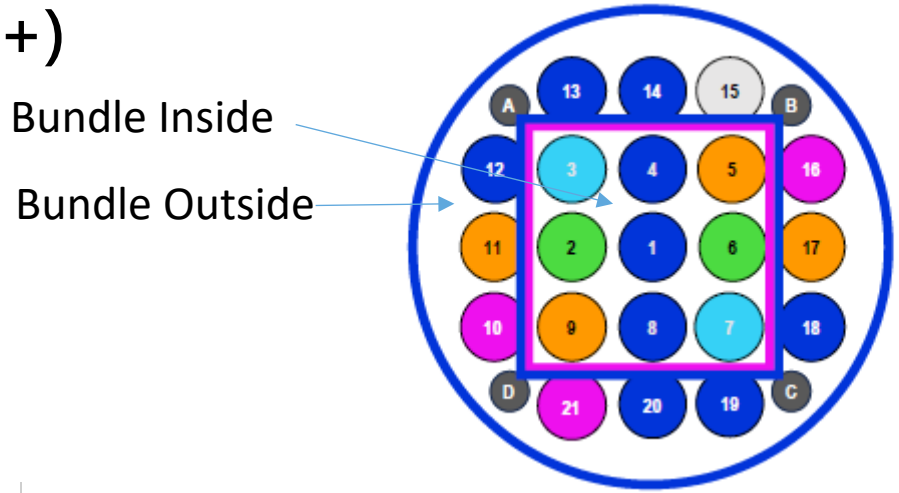

Source:
Di Nora, V. A.; Wielenberg, A.; Lovasz, L; Schöffel, P. J., Integration and Validation of Models for Thermal-Mechanical Behaviour of Nuclear Fuel Rods in ATHLET, Annals of Nuclear Energy Volume 227, Part A, February 2026, 111915

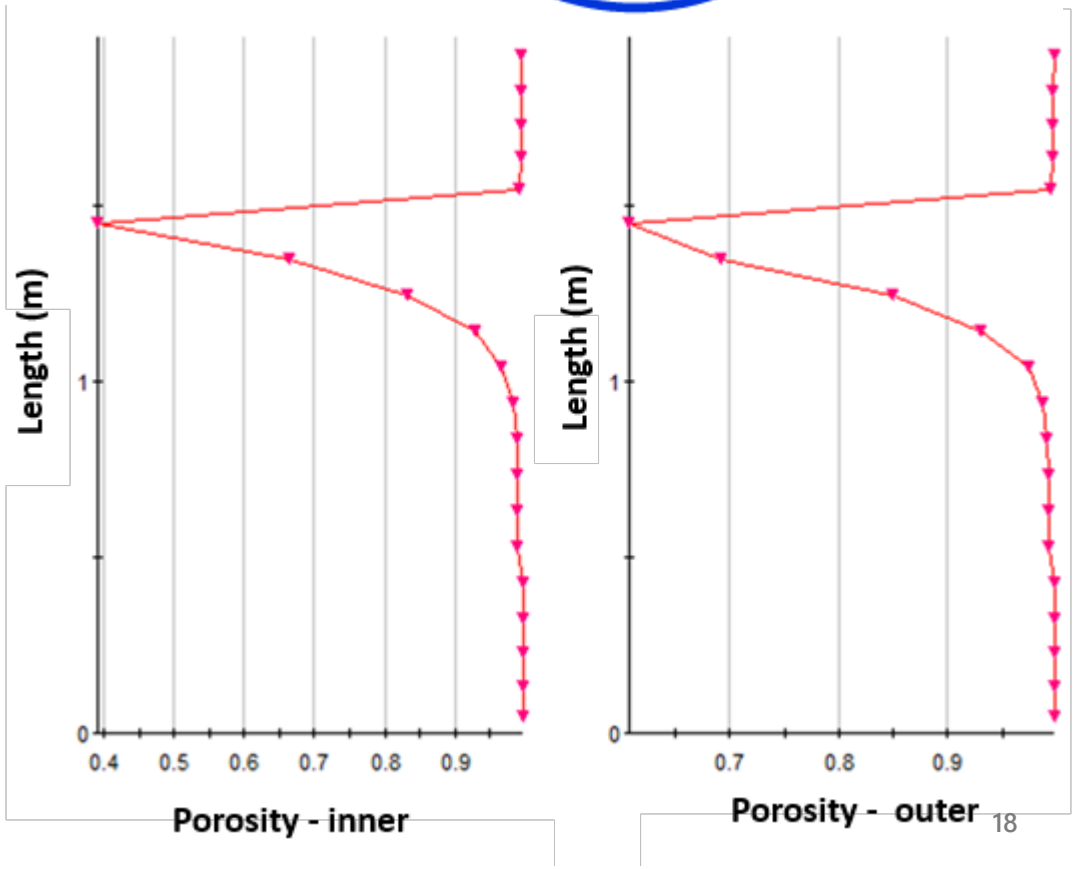

QUENCH-L0 Simulation – new (ATHLET+)

Cause of burst is strain limit: 38%

- Relative good agreement
- Burst times good agreement
- Overall H_2 production underestimated
  - No burst oxidation
  - Temperature at lower elevation underestimated

	Exp. Strain (%)	Sim. Strain (%)
Rod 2	33.8	~38
Rod 19	27.2	~38
Rod 7	40.0	~38

	Exp. Burst Time (s)	Sim. Burst Time (s)
Rod 2	136.8	146
Rod 19	159.6	157
Rod 7	114.2	123

	Exp. Hydrogen gen (g)	Sim. Hydrogen gen (g)
Rod 2	1	0.7

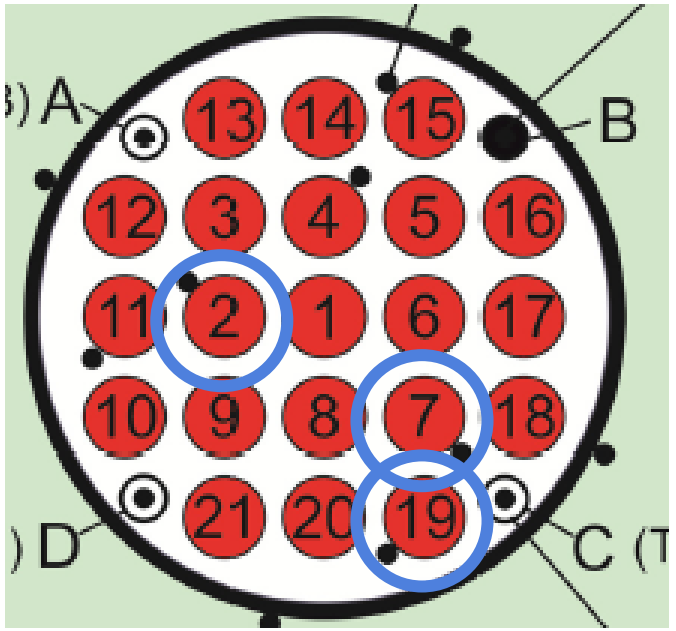

Source: J. Stuckert, M. Große, C. Rössger, M. Steinbrück, M. Walter, QUENCH - LOCA - REPORTS Nr. 1, Results of the commissioning bundle test QUENCH-L0 performed under LOCA conditions (SR-7571), KIT, 2015

ATHLET+ Validation - Conclusions

- ATHLET+ incorporates and extends ATHLET-CD models
  - Focus of current development
    - DBA phenomena (qualitatively) covered
    - BDBA phenomena under development
- Due to significant modelling changes → Validation needed
- QUENCH LOCA L0 analysed
  - ATHLET input deck created
    - Eliminated old simplifications
  - Phenomena qualitatively covered
- More knowledge with ATHLET+ needed
- Further validation of DBA and BDBA phenomena

Thank you for your attention!

The development and validation of AC²/ATHLET-CD are supported by the German Federal Ministry for the Environment, Climate Action, Nature Conservation and Nuclear Safety.

Supported by:

Federal Ministry
for the Environment, Climate Action,
Nature Conservation and Nuclear Safety

based on a decision of
the German Bundestag

Tadas Kaliatka

LEI

Modeling of QUENCH-06 and QUENCH-20 tests with RELAP/SCDAPSIM, Focus on Bundle Asymmetry

Reflooding of an overheated reactor core is a critical severe-accident management strategy, but it can intensify zirconium oxidation and hydrogen production, requiring detailed investigation of the reflood phase. The QUENCH integral tests, performed in Forschungszentrum Karlsruhe, provide valuable experimental data for studying these phenomena. In this work, the QUENCH-06 and QUENCH-20 experiments are simulated using the severe accident code RELAP/SCDAPSIM to evaluate key modeling approaches and benchmark code predictions against measured data.

Although both tests follow similar thermal–hydraulic transient and experimental phases, they differ significantly in bundle configuration. QUENCH-06 employs a symmetric, electrically heated fuel rod bundle, while QUENCH-20 features a strongly asymmetric configuration due to two absorber control blades positioned at two sides of a rectangular bundle. These differences significantly influence phenomenology and physical processes during these experiments. Also, it significantly influences modeling of physical processes. An additional difficulty for the numerical investigation is the fact that all severe accident codes are considering symmetricity (bundle or core are modeled from the cylindric coordination aspects).

To address this, three distinct component-level modeling strategies were developed to approximate the asymmetric QUENCH-20 geometry. The simulations are evaluated against key experimental parameters including bundle temperature evolution (claddings and shroud), oxidation behavior and hydrogen release. The results demonstrate notable differences in local thermal response and oxidation rates depending on the selected modeling approach, with no single method fully reproducing all measured phenomena. However, specific approaches show improved prediction of radial temperature gradients and hydrogen generation trends.

Based on the findings, practical recommendations are proposed for modeling asymmetry in severe accident codes, emphasizing best practices for nodalization, power distribution, and representation of absorber blade regions. The study highlights both the capabilities and limitations of RELAP/SCDAPSIM for asymmetric reflood scenarios and provides guidance for future modeling of complex core geometries.

LITHUANIAN ENERGY INSTITUTE

Modeling of QUENCH-06 and QUENCH-20 tests with RELAP/SCDAPSIM, Focus on Bundle Asymmetry

Dr. Tadas Kaliatka, Dr. Noura Elsalamouny
Lithuanian Energy Institute

30th International QUENCH Workshop
2025–12–17

Uncertainty and Sensitivity Analysis of QUENCH-03 and QUENCH-06 Experiments

T. Kaliatka, A. Kaliatka, V. Vileiniskis

20th International QUENCH Workshop

Modeling of QUENCH 10 and 16 Experiments on Air Ingress Using RELAP/SCDAPSIM mod 3.5

2016

Tadas Kaliatka

Implementation of QUENCH-10 experiment modelling experience for the modelling of severe accidents in spent fuel pools

2017

Tadas Kaliatka

Post-test calculation results of QUENCH experiments using different RELAP/SCDAPSIM Mod3.5 code versions

2018

Tadas Kaliatka

Evaluation of the processes in the BWR and VVER spent fuel pools during severe accident conditions

2019

T. Kaliatka, A. Kaliatka, V. Vileiniskis

Implementation of LEI experience on modeling and uncertainty quantification of QUENCH tests for the development of QUENCH-20 numerical model

Noura Elsalamouny, Tadas Kaliatka

2021

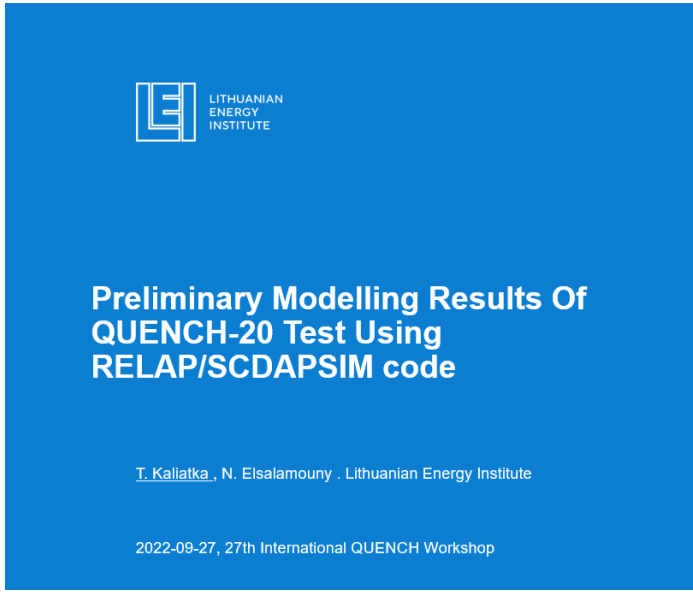

2022

QUENCH test

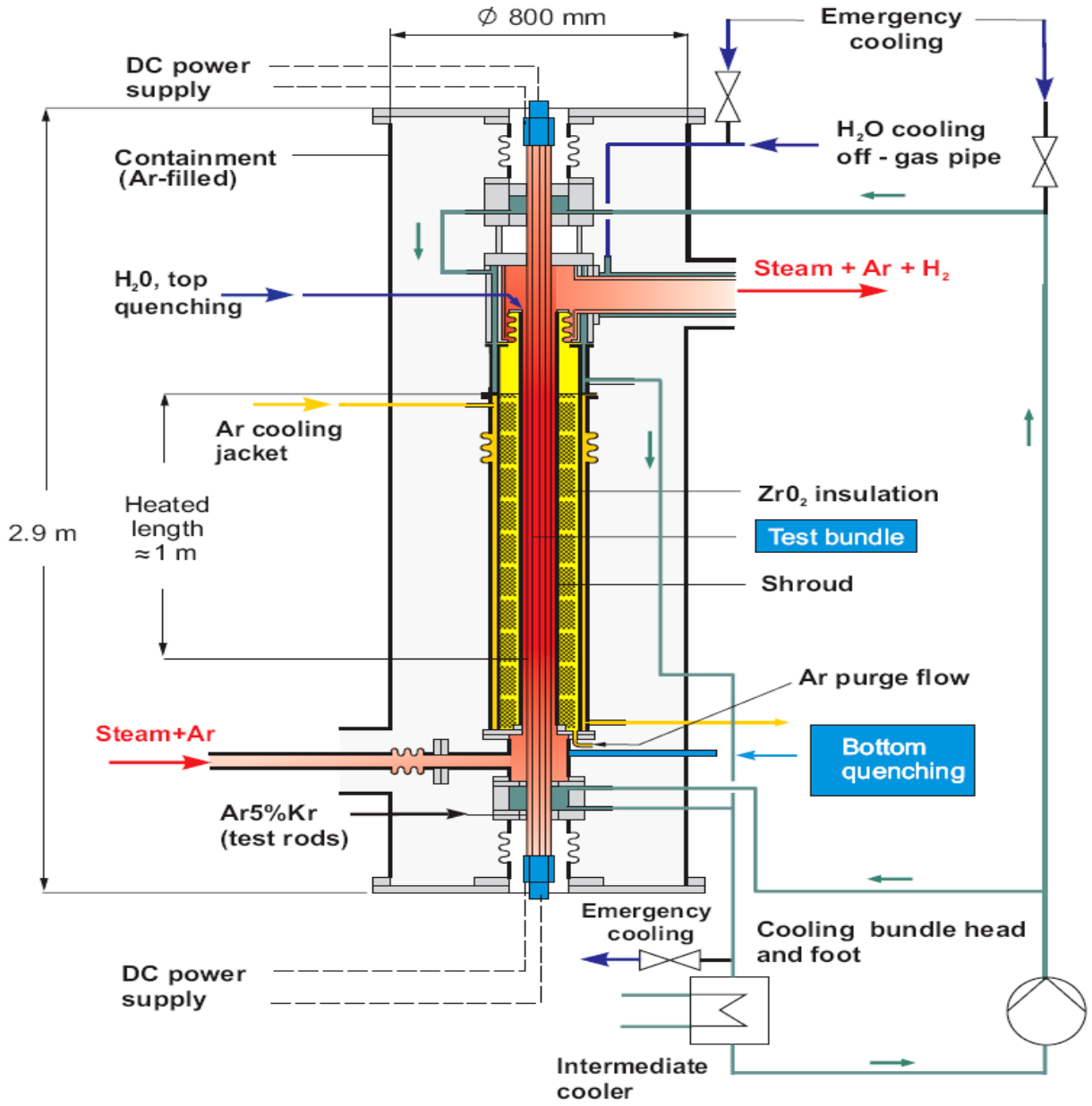

QUENCH/LICAS facility

- Unique out-of-pile bundle facility to investigate reflood of an overheated reactor core
- 21-31 electrically heated fuel rod simulators; T up to >2000°C
- Extensive instrumentation for T, p, flow rates, level, etc. + MS
- So far, 20+1 experiments on SA performed (1996-today)
  - Influence of pre-oxidation, initial temperature, flooding rate
  - B_4C, Ag-In-Cd control rods
  - Air ingress; debris formation
  - Advanced cladding alloys & ATF
- 7+1 DBA LOCA experiments with separately pressurized fuel rods

Focus on QUENCH-06 and especially on QUENCH-20

Similarities and differences between QUENCH-06 and QUENCH-20

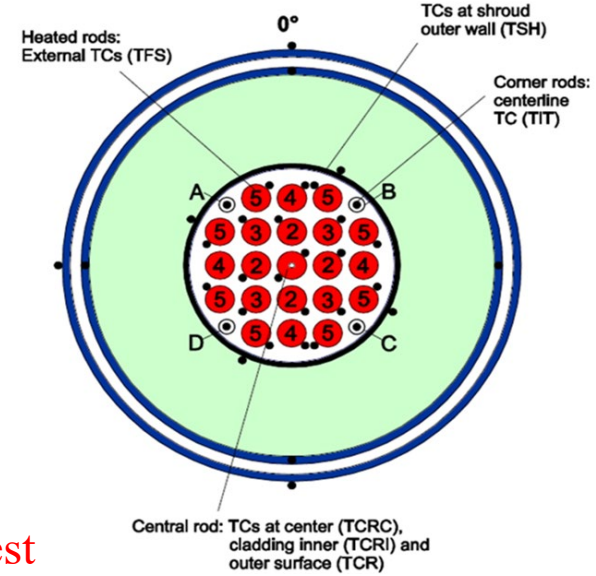

QUENCH-06 test

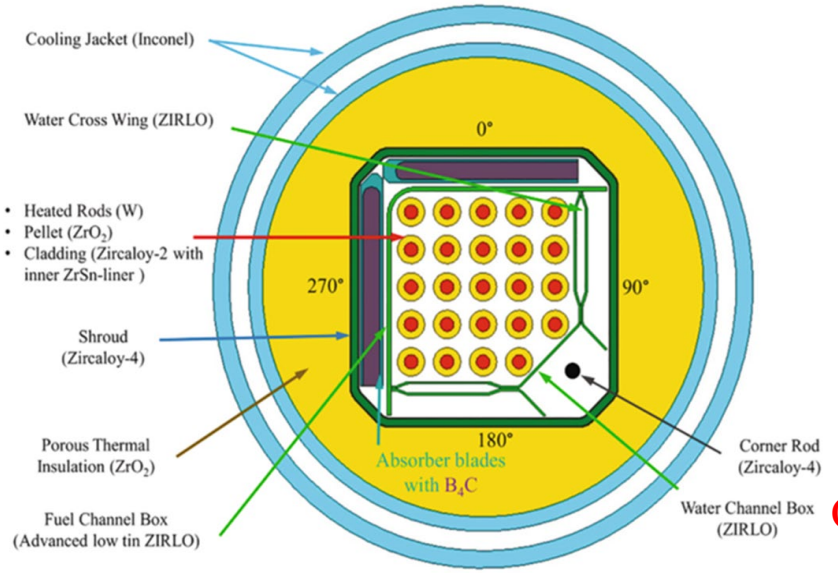

QUENCH-20 test

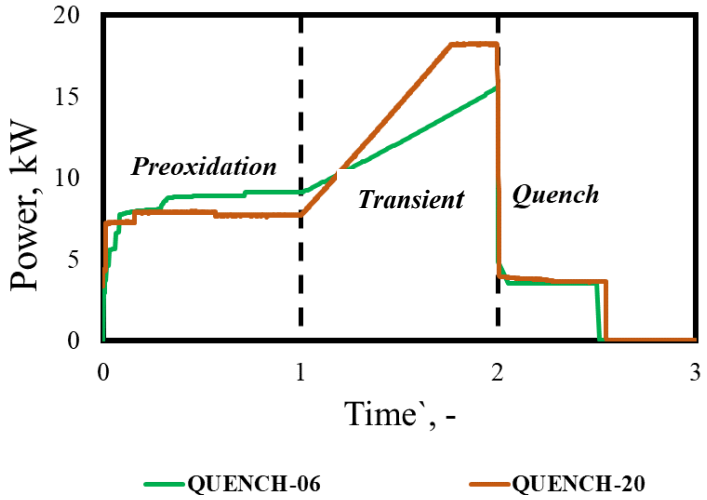

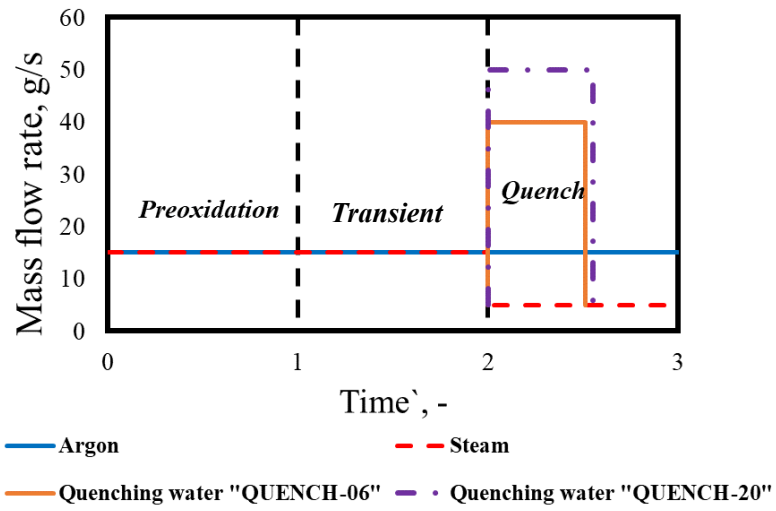

Model development and Reference calculation QUENCH-06

The Figures Of Merit (FOM's) for QUENCH-06

- Total hydrogen generation
- Cladding temperature

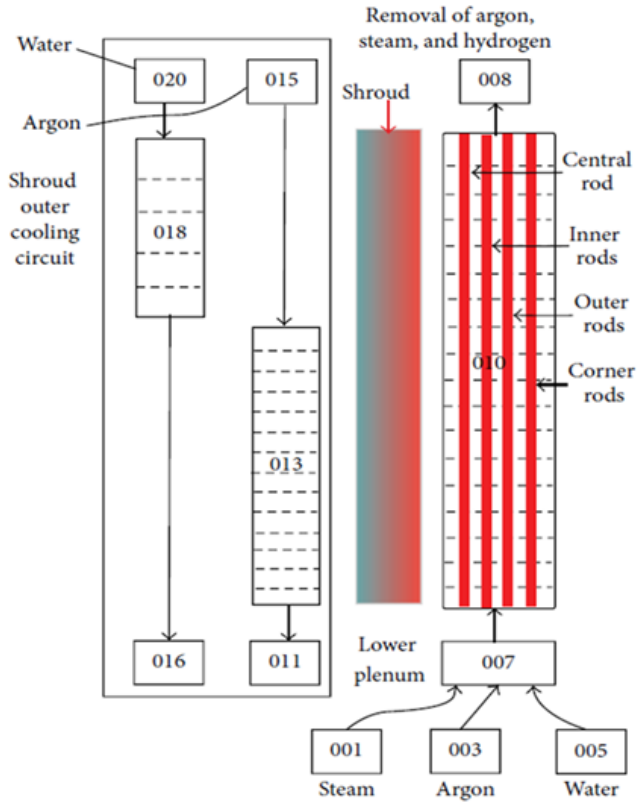

RELAP part

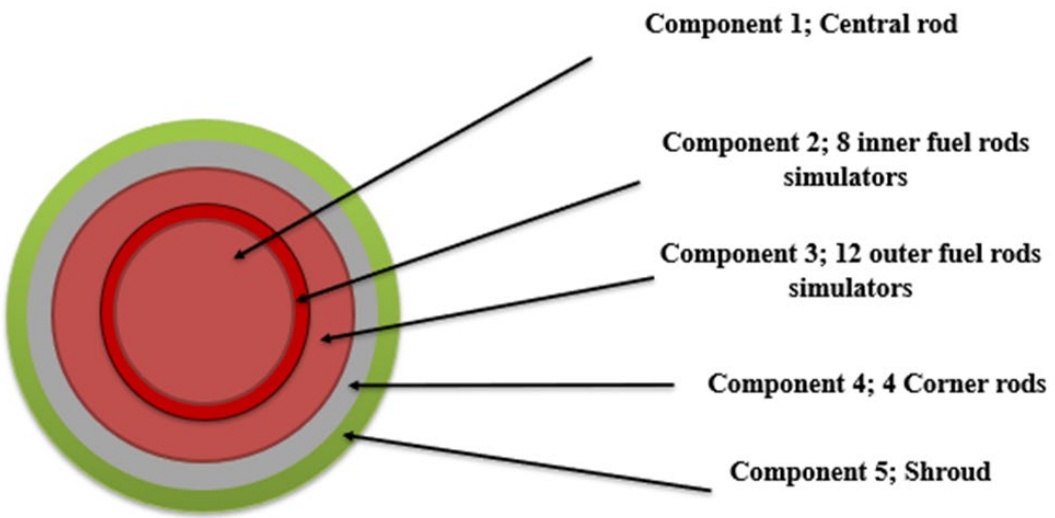

SCDAP part

Reference calculation

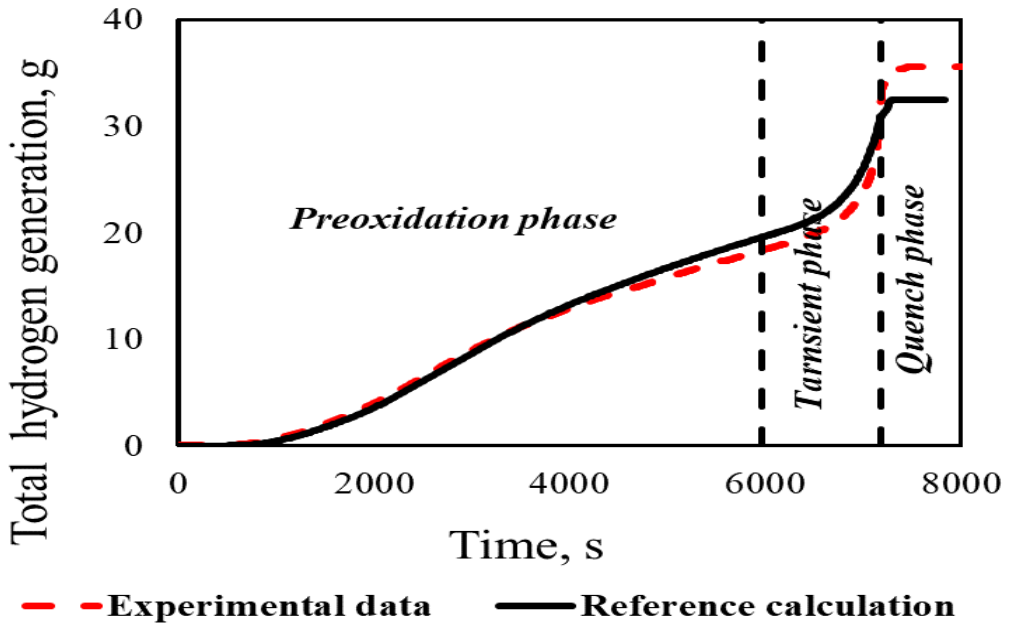

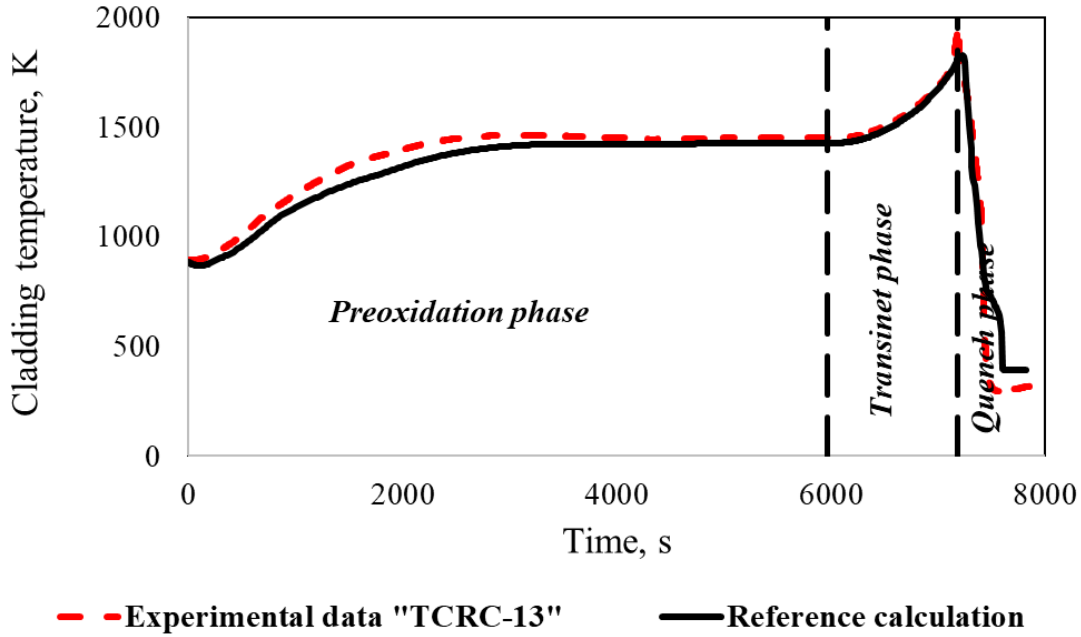

950 mm form the bottom

Application of BEPU approach

Approaches

- GRS
- IPSN
- CSAU
- ENUSA
- GSUAM
- BEAU

GRS

Gesellschaft für Anlagen- und Reaktorsicherheit (German Nuclear Safety Organisation)

Tools

- SUSA
- SUNSET
- DAKOTA
- RAVEN

SUSA

(Gesellschaft für Anlagen- und Reaktorsicherheit)

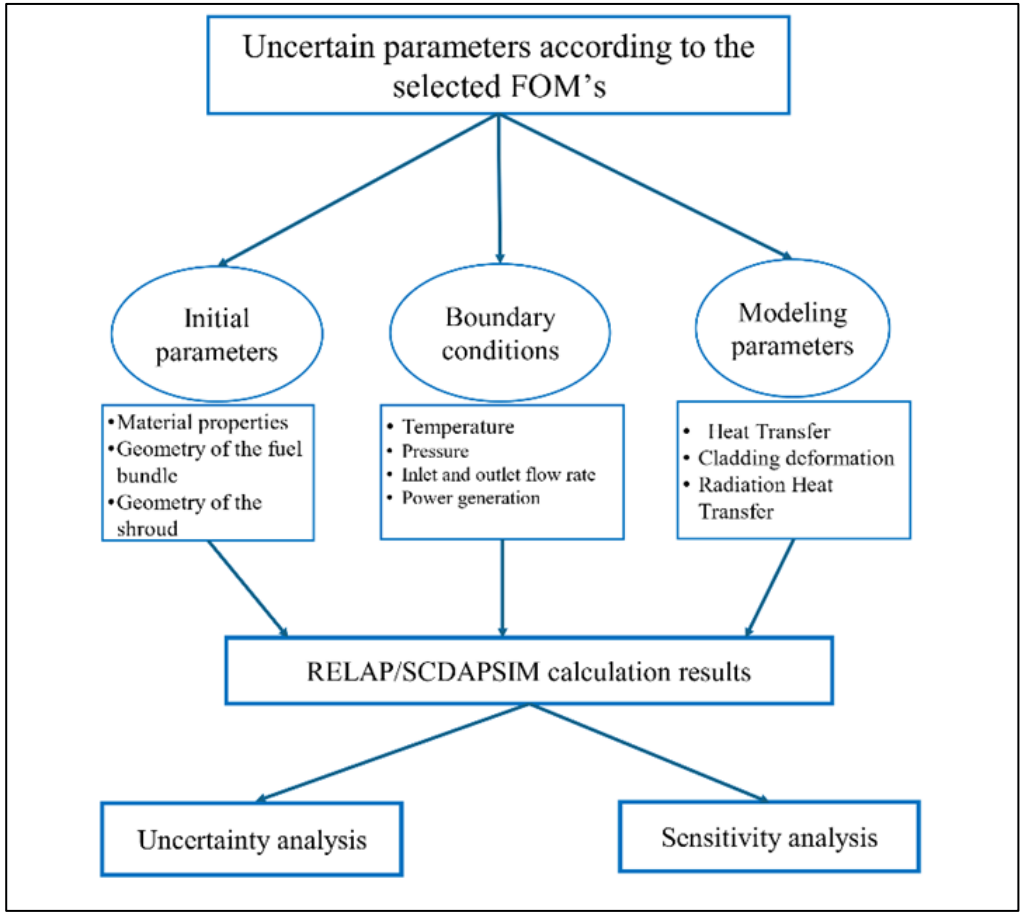

Schematic view of the application of the best estimate approach

Uncertainty analysis of QUENCH-06 test

Uncertain parameters:

- Boundary conditions
- Shroud material thermal properties
- Geometry parameters
- Modeling parameters

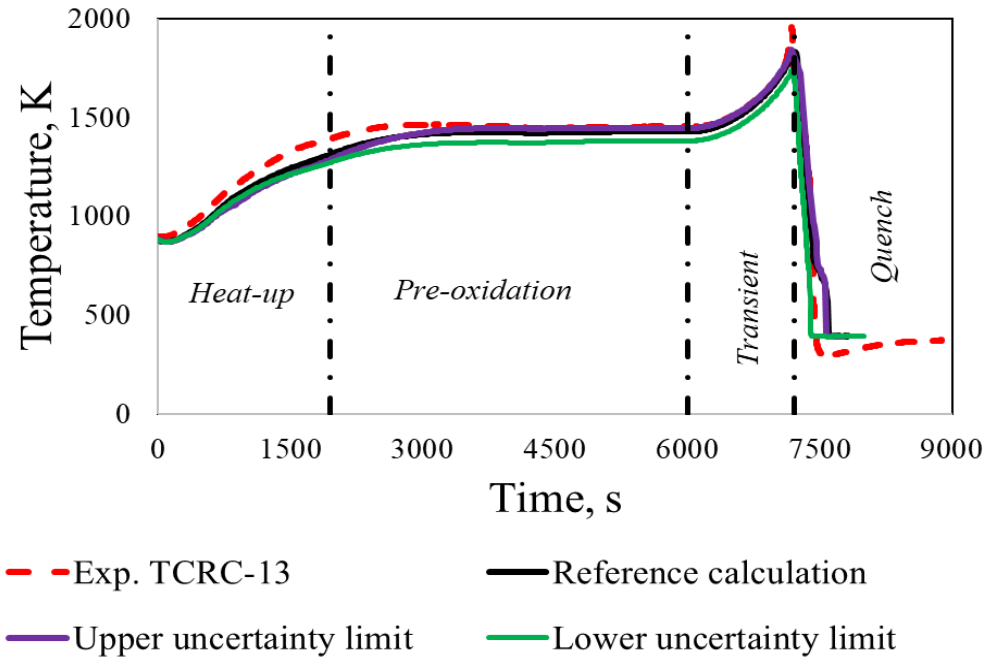

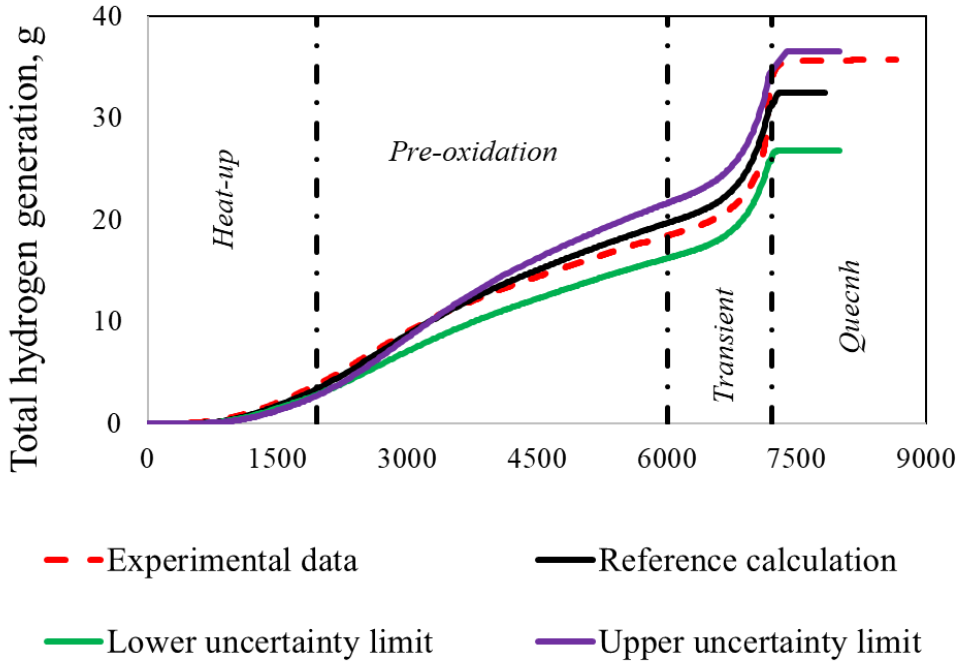

The uncertainty analysis within BEPU approach allows to evaluate appropriateness of modeling results.

Results of sensitivity analysis of QUENCH-06 test

Influence of uncertain parameters	Phase			
	Heat up (the 1500s)	Pre-oxidation (5000s)	Transient (6500s)	Quench (7350s)
Total hydrogen generation	Cladding thickness (influence +0.85), Electrical power (influence +0.55), Thickness of the Insulator (influence -0.27).	Electrical power (influence +0.82), Cladding thickness (influence +0.43), Steam mass flow rate at the bundle inlet (influence -0.35).	Electrical power (influence +0.85), Steam mass flow rate at the bundle inlet (influence -0.36), Cladding thickness (influence +0.32).	Electrical power (influence +0.81), Steam mass flow rate at the bundle inlet (influence -0.35), Thickness of the Insulator (influence -0.29).
Temperature of the central rod at 950 mm	Cladding thickness (influence +0.8), Electrical power (influence +0.58).	Electrical power (influence +0.78), Steam mass flow rate at the bundle inlet (influence -0.43).	Electrical power (influence +0.81), Steam mass flow rate at the bundle inlet (influence -0.39).	Quench water injection to the experiment section (influence +0.97).
Oxide layer thickness			Electrical power (influence +0.8), Steam mass flow rate at the bundle inlet (influence -0.4), Cladding thickness (influence +0.35).	Electrical power (influence +0.8), Steam mass flow rate at the bundle inlet (influence -0.4).

Results of sensitivity analysis of QUENCH-06 test

Material properties and **thickness of the surrounding structures** for the test facilities as well as **boundary conditions** that describe the heat transfer from the fuel bundle to the surrounding structures have a high impact on calculation results.
For the late bundle degradation phase the influence of **SCDAP parameters and models related to the fuel cladding rupture, oxidation, and bundle degradation plays a significant role.**

QUENCH-20, asymmetric geometry

The QUENCH-20 test developed models: *Pseudo symmetrical model*

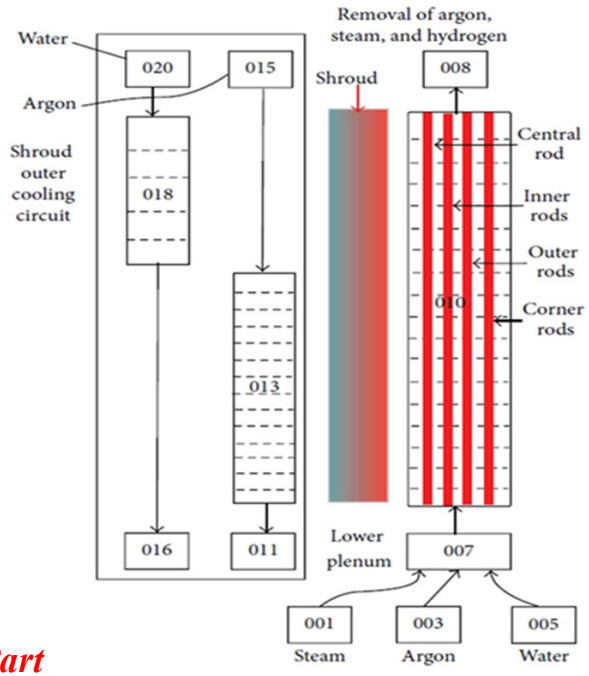

RELAP Part

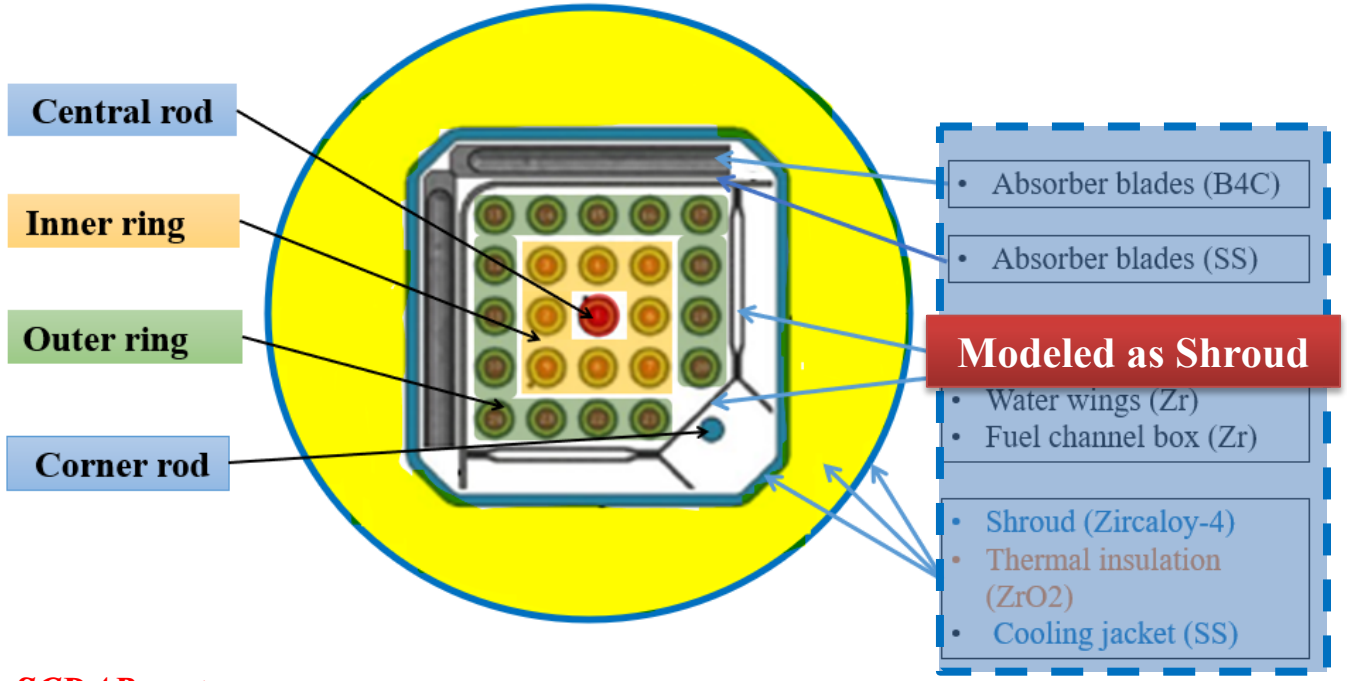

SCDAP part

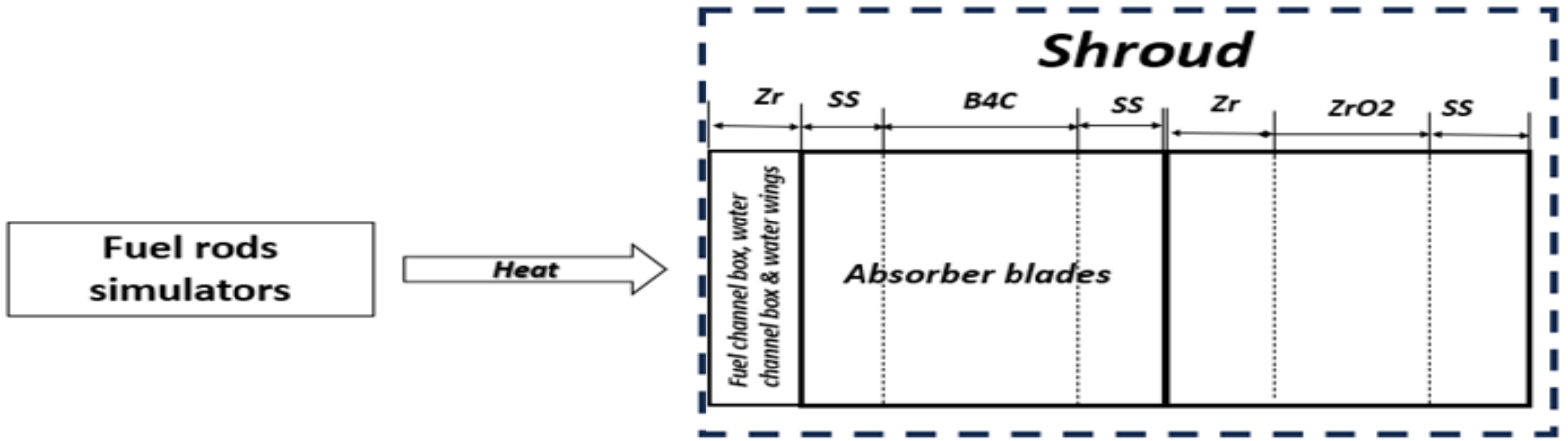

The QUENCH-20 test developed models: *Pseudo symmetrical model*

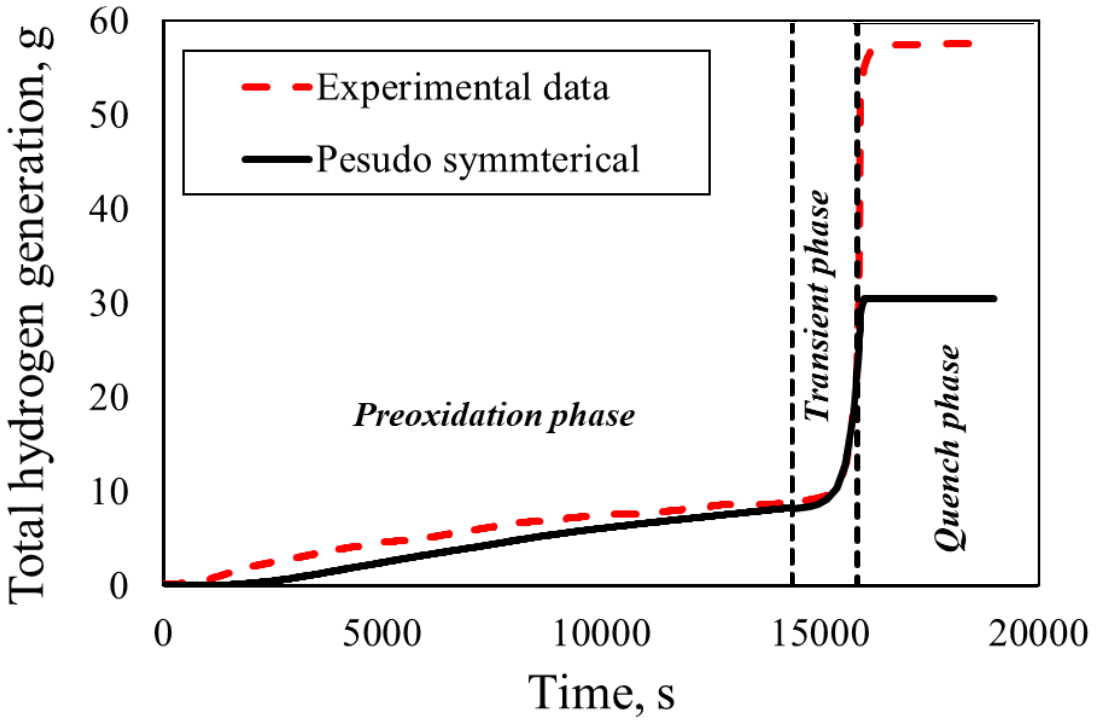

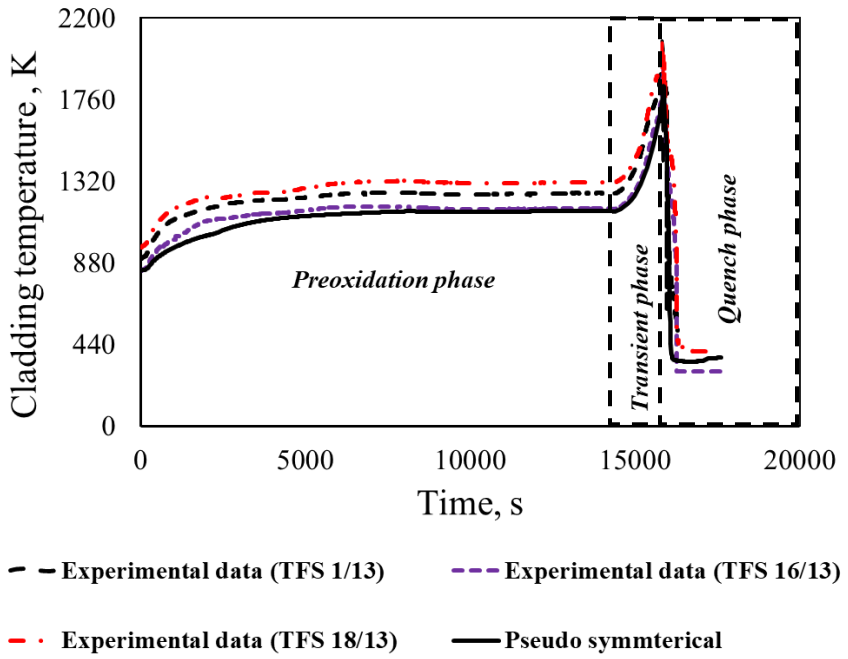

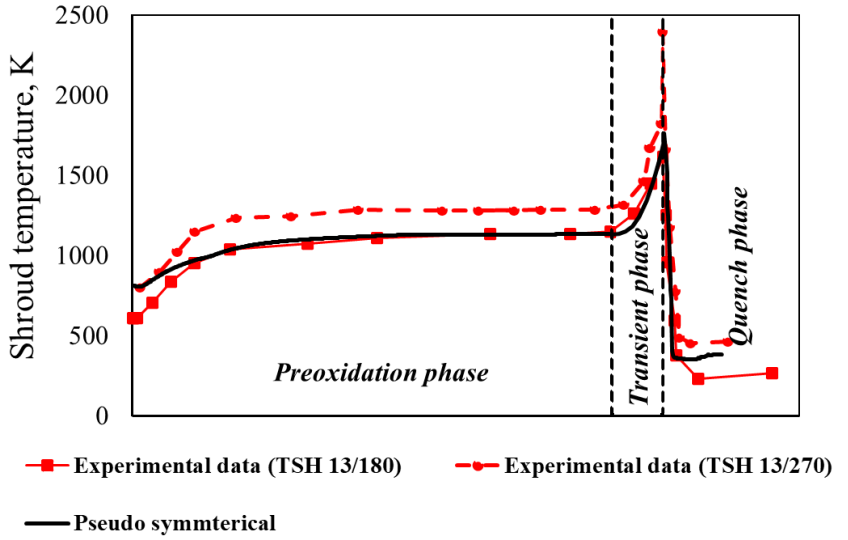

The QUENCH-20 test developed models: *Component level model*

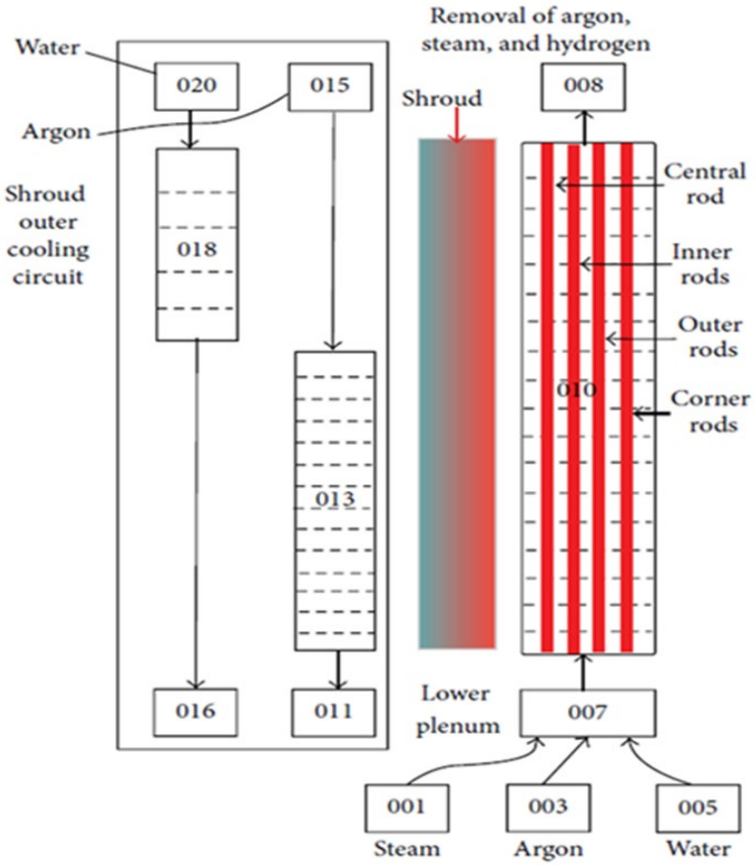

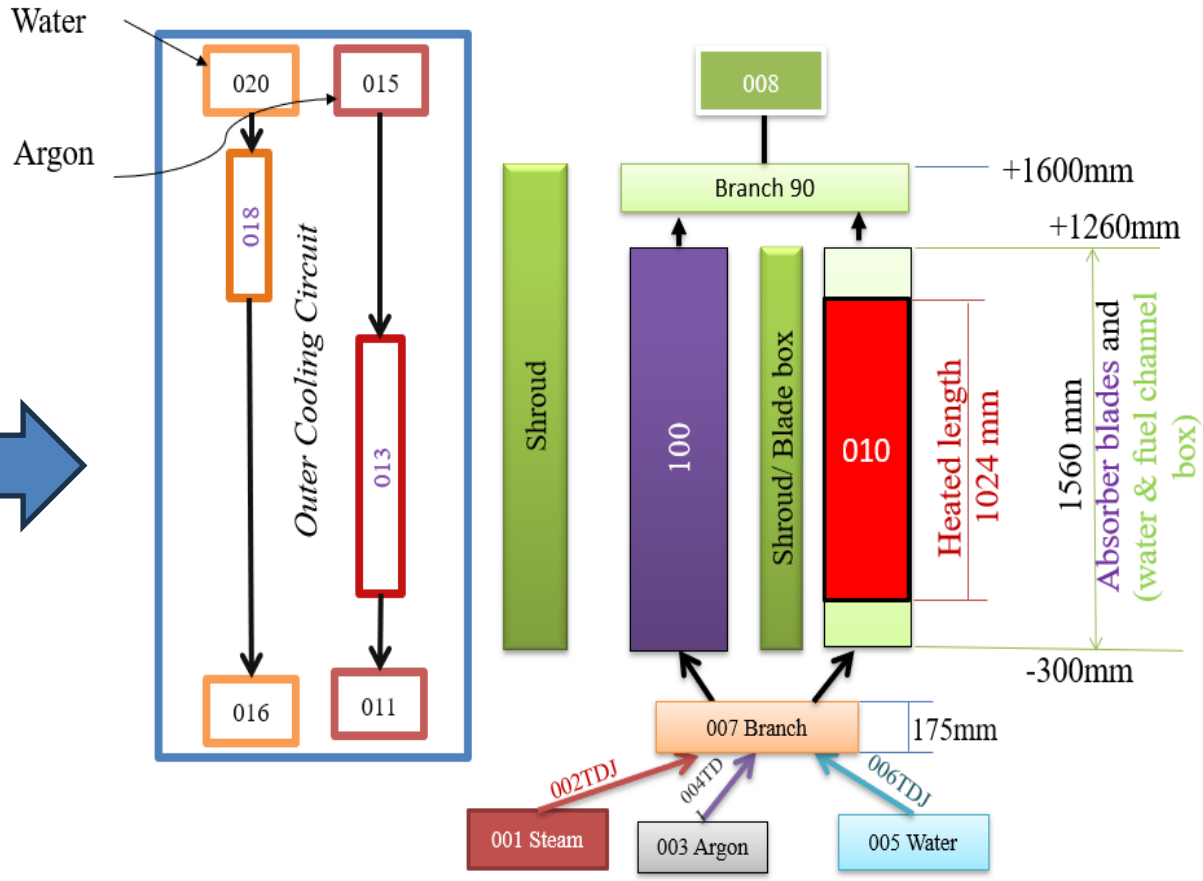

RELAP Part

The QUENCH-20 test developed models: *Component level model*

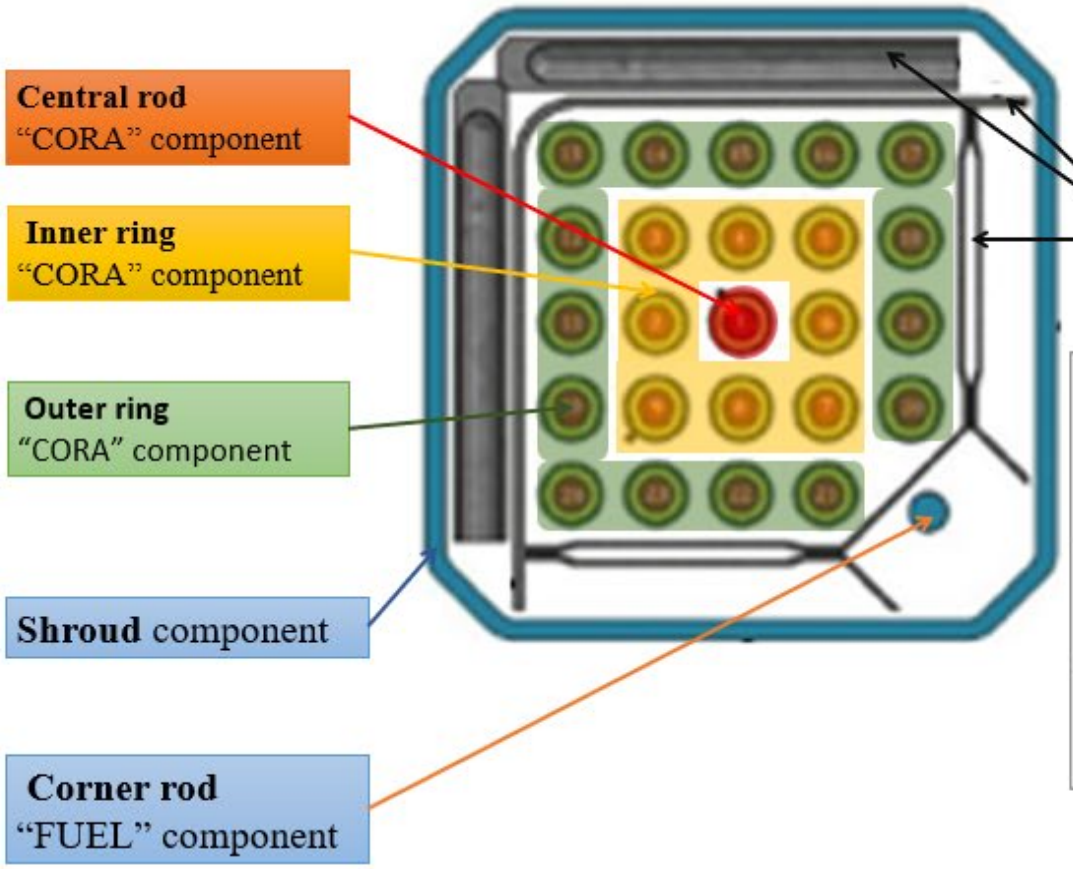

Approach 1:
Absorber blades, fuel channel box, water channel box, and water wings as a "Shroud" component.

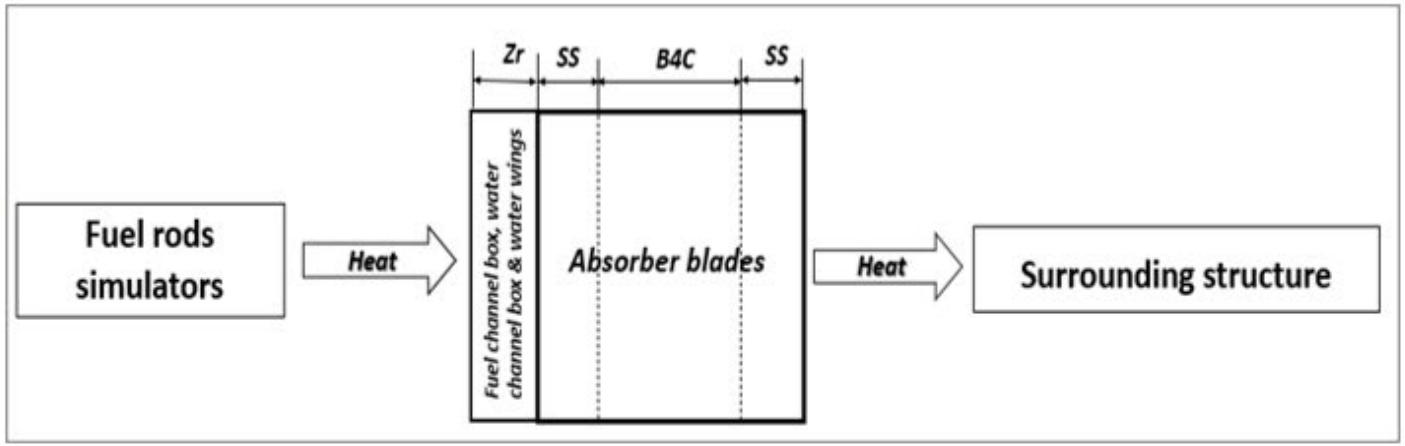

No B_4C oxidation !

SCDAP part

The QUENCH-20 test developed models: *Component level model*

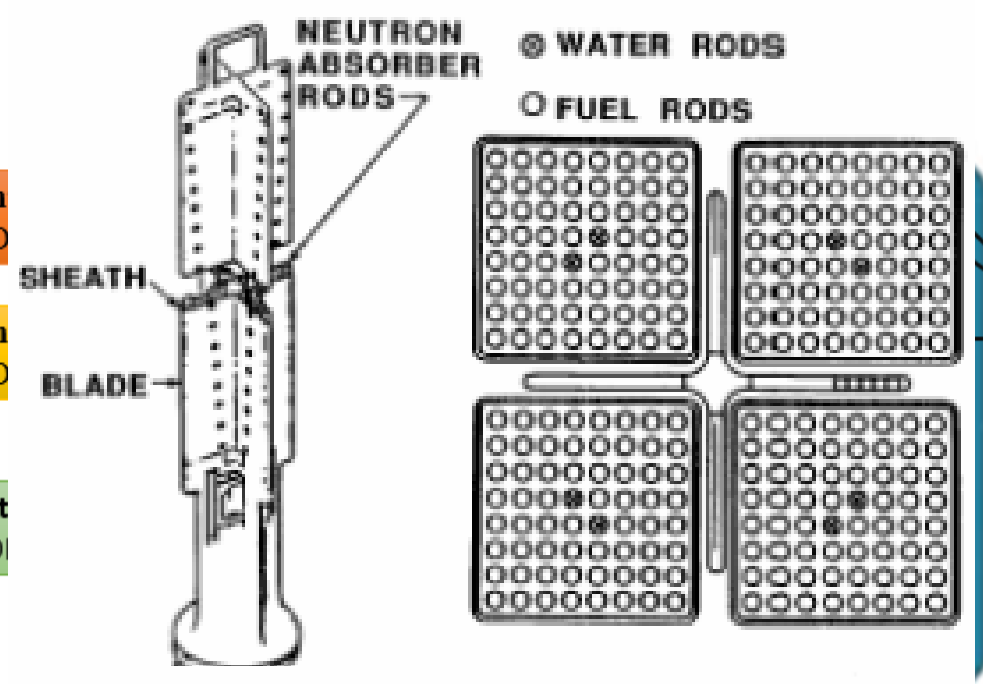

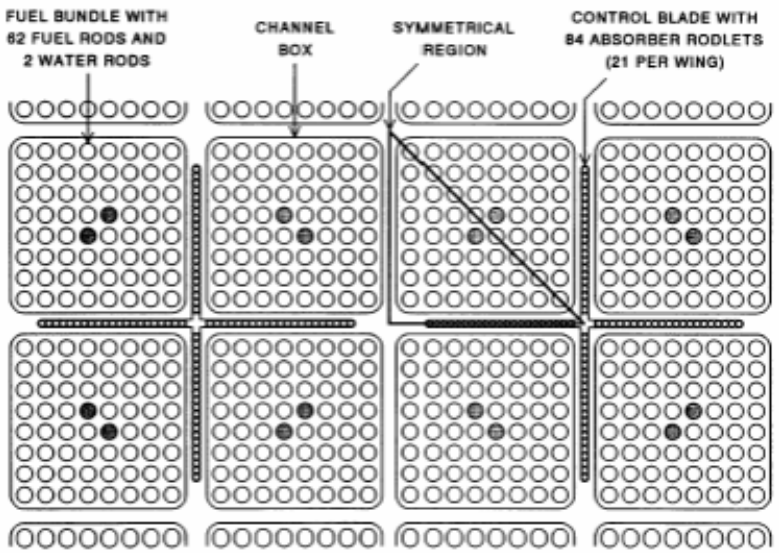

Cen "CO

Inn "CO

Out "CO

Shr

Corne "FUEL

Approach 2:
Absorber blades, fuel channel box, water channel box, and water wings box as "Blade box" component

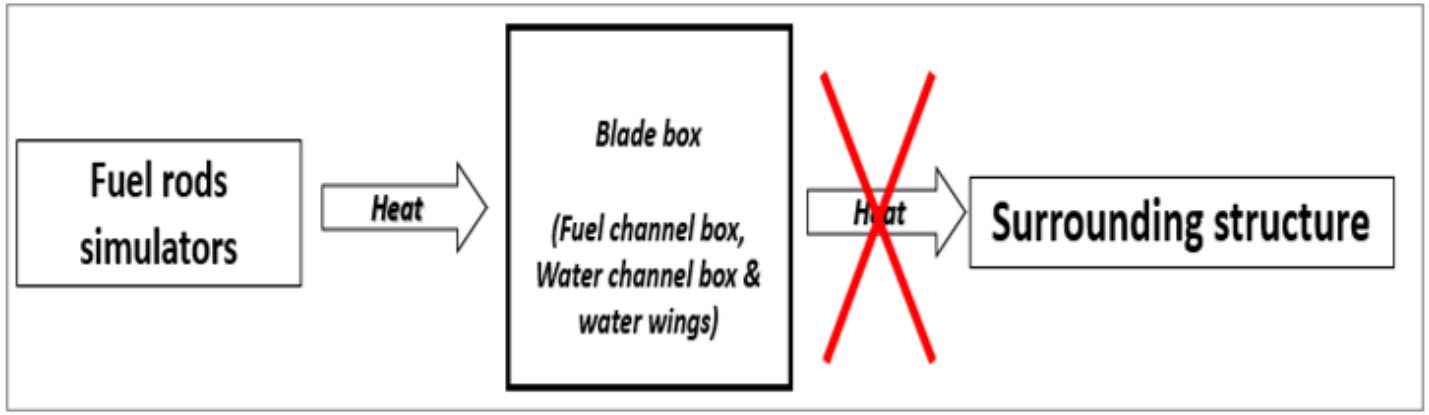

B_4C oxidation was not achieved due to low temp. !

The QUENCH-20 test developed models: *Component level model*

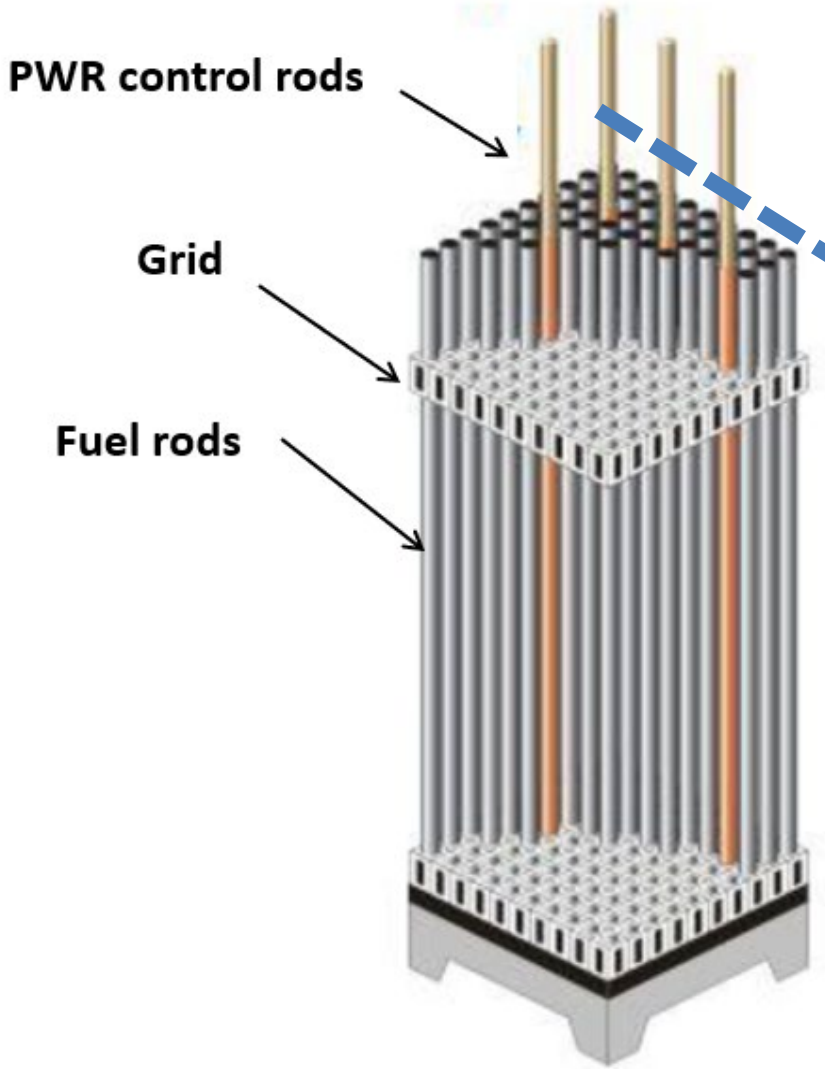

Approach 3:
Absorber blades as PWR CR component; fuel channel box, water channel box, and water wings as "Shroud" component

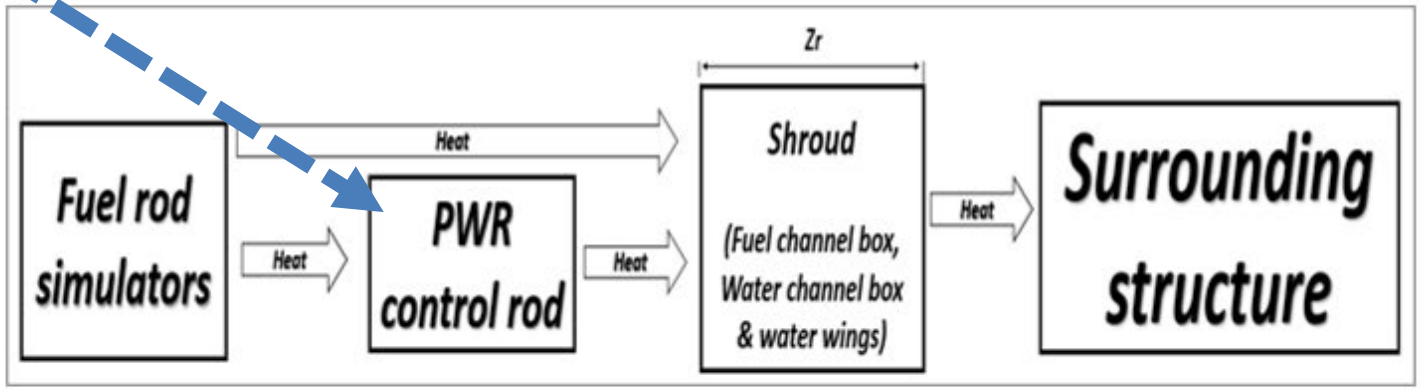

B_4C oxidation achieved !

Results for QUENCH-20 modeling

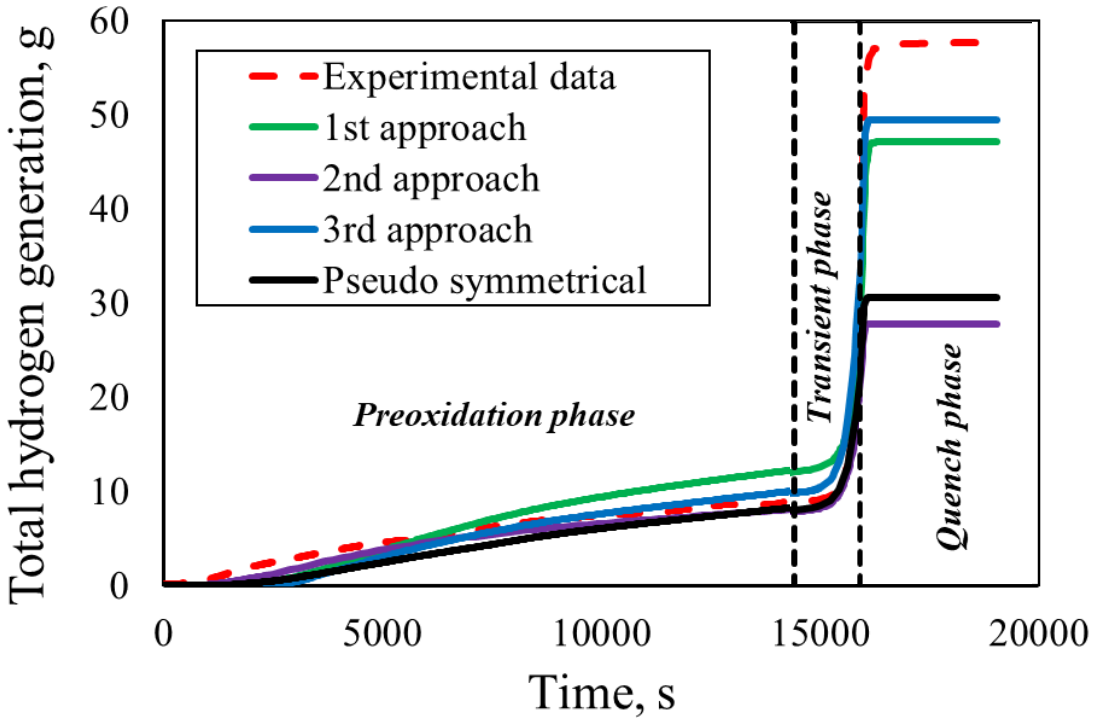

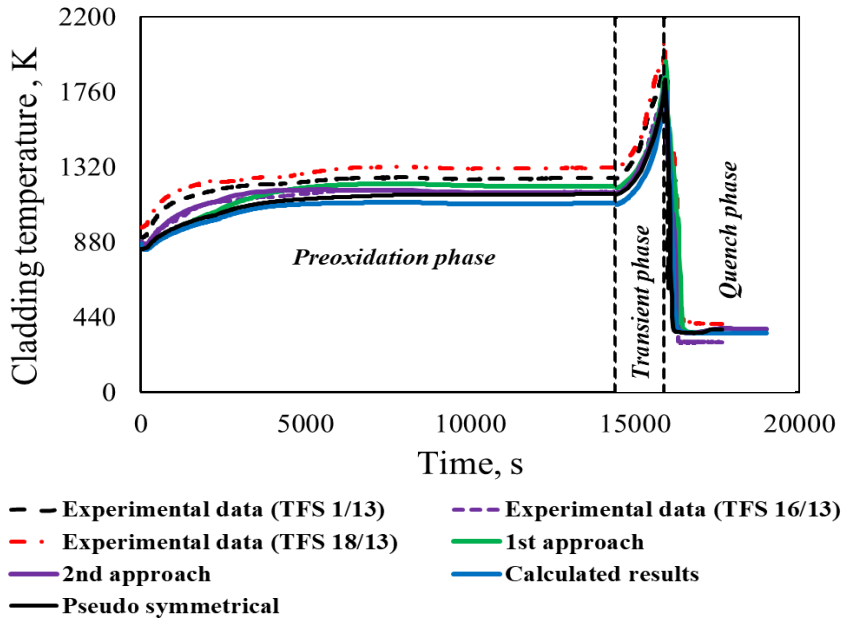

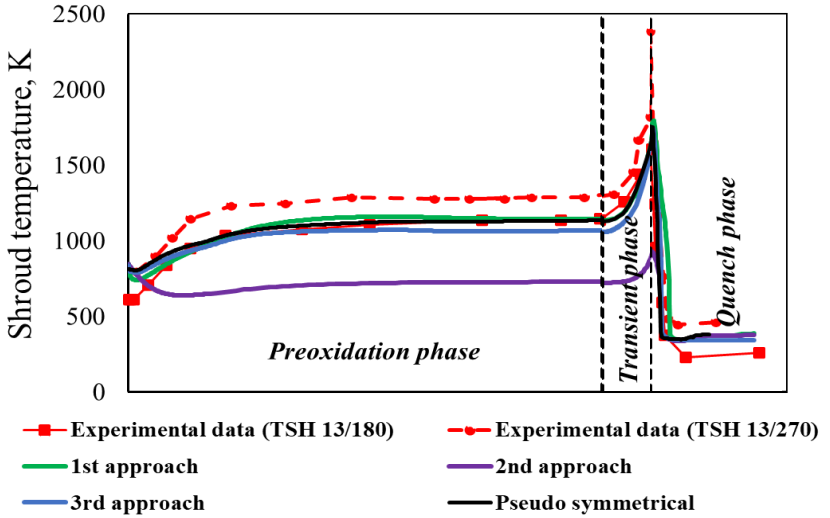

Approach 3, gas release from the B_4C oxidation processes

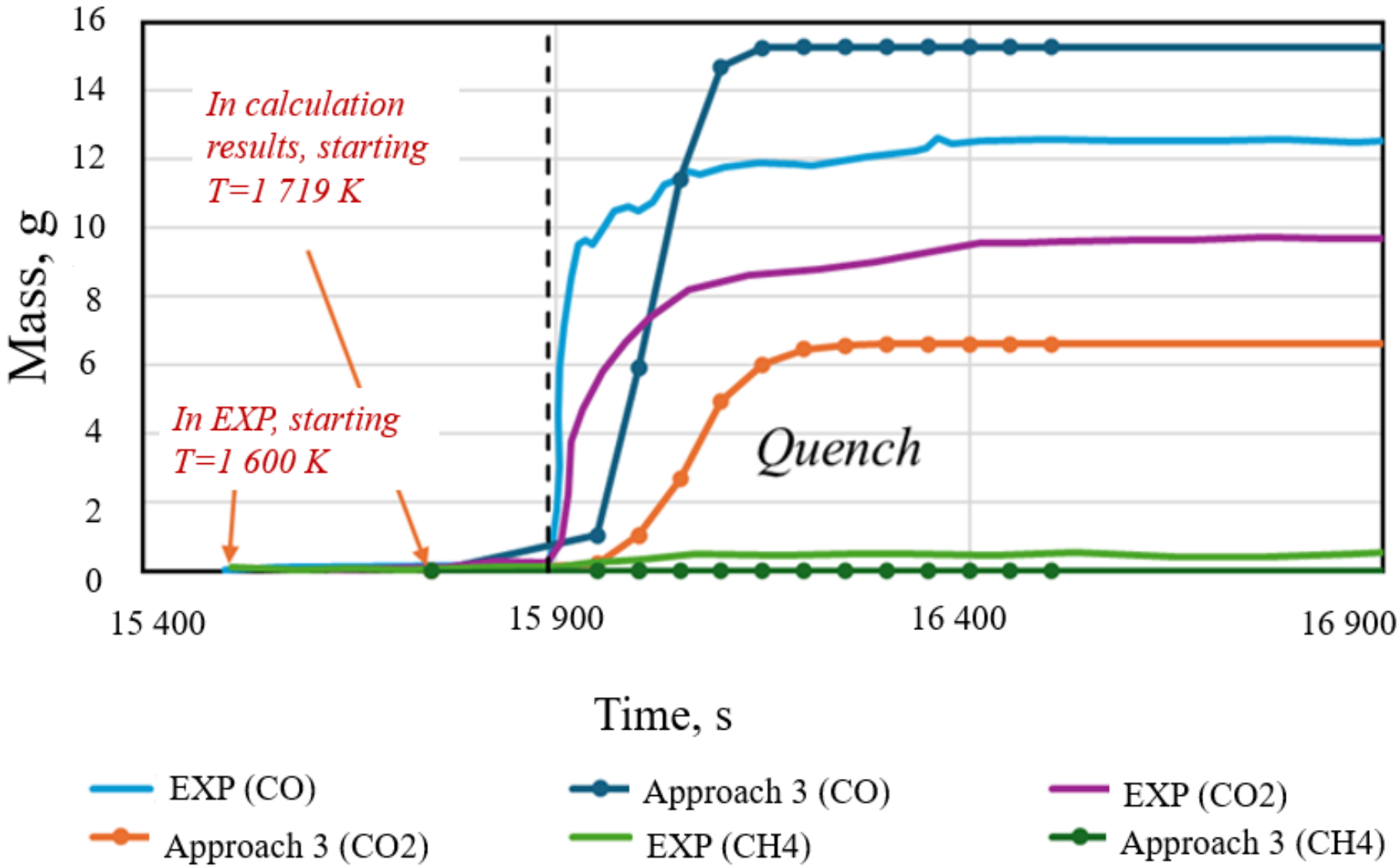

CONCLUSIONS AND RECOMMENDATIONS

To develop a methodology for investigating physical processes in nuclear facilities with both symmetric and asymmetric geometries, numerical investigations of severe accident experiments that resulted in partial core melting were conducted. The investigations, performed applying the BEPU approach and severe accident code RELAP/SCDAPSIM together with the SUSA statistical tool, allowed us to summarise the following conclusions:

The BEPU-based uncertainty analysis confirms the reliability of simulation results for the facilities with symmetric geometry; in most analysed cases, the calculated ranges bound experimental data.

Sensitivity analysis highlights:

- Material properties and boundary conditions strongly affect results (Spearman rank correlation coefficient >0.78).
- SCDAP parameters related to cladding rupture and oxidation significantly influence late-phase degradation (Spearman rank correlation coefficient >0.4).

CONCLUSIONS AND RECOMMENDATIONS

Building on insights from symmetric geometry experiments, a methodology for the asymmetric geometry was developed and applied. Pseudo-symmetrical and 3 component-level modelling approaches were developed and evaluated for QUENCH-20 experiment:

- Pseudo-symmetrical: this approach allows obtaining accurate pre-quenching results but underestimates hydrogen generation during quenching by ~30%.
- SCDAP Shroud component: using this approach, the obtained results match temperature data well; underestimates hydrogen (~18% or 10g) due to missing B_4C oxidation modelling.
- SCDAP Blade box component: this approach allows obtaining a good temperature match for cladding; it lacks heat transfer modelling, causing underestimation of oxidation and hydrogen (~50% lower).
- SCDAP PWR control rod + Shroud components: this approach allows the best match with experimental data, calculated hydrogen generation (~12% less); includes B_4C oxidation effects.

Dr. Tadas Kaliatka, Lithuanian Energy Institute

Tadas.Kaliatka@lei.lt

Peter Ulrich Bochtler

BASE

Infinite lattice depletion of accident-tolerant fuel pin-cells with OpenMC and cladding inventory analysis with FISPACT-II

The operation of nuclear power plants with accident-tolerant fuels is foreseeable in the EU. To assess these developments, the BASE in-house research project “ReUnFis” is seeking to assess how such a use would be impacting waste streams and safety aspects than can be derived from the isotopic inventories.

Neutronic impacts due to necessary enrichment offsets reported in (Hall et al. 2021) for FeCrAlC26m and a M5-like alloy with 20 µm Cr (Hall et al. 2021; Reaktor-Sicherheitskommission 2020; Kecek et al. 2016) and changing moderator to fuel ratio are studied through some observables derived from OpenMC (Romano et al. 2015; Romano et al. 2021) infinite lattice depletion simulations of accident-tolerant fuel pin-cells up to 75 MWd/kgHM.

The comparison of the cladding inventory for JEFF-3.3 nuclear data library (Plompen et al. 2020) with FISPACT-II (Sublet et al. 2017) demonstrates how for material activation and transmutation problems both codes can be used in a complementary way.

Various cladding metrics (activity, contact dose rate and elemental build-up) of doped fuel (Arborelius et al. 2006; Hall et al. 2021) with M5-like alloy +20 µm Cr, FeCrAlC26m and SiC filament-wound duplex tube (Koyanagi et al. 2024; Noda et al. 2002) + 10 µm Cr (Quillin et al. 2022; Mouche et al. 2021) are compared in decay space up to 100 y at decay times that may also be relevant to QUENCH experiments. Finally, the presentation highlights the impact of impurity levels (Parga 2018; Yeom et al. 2019; Atlantic Equipment Engineers 2025) and the impact of nuclear data JEFF-4 (NEA 2025) for the case of a M5-like alloy +20 µm Cr.

References

Arborelius et al. (2006) Arborelius, J., Backman, K., Hallstadius, L., Limbäck, M., Nilsson, J., Rebensdorff, B., Zhou, G., Kitano, K., Löfström, R. & Rönnberg, G.: Advanced Doped UO2 Pellets in LWR Applications. Journal of Nuclear Science and Technology 43(9), 967–976, DOI 10.1080/18811248.2006.9711184, 2006.

Atlantic Equipment Engineers (2025) Atlantic Equipment Engineers: Datasheet CR-102-105, Chromium Powder, Electrolytic, https://docs.google.com/document/d/1nOtHzZLs93N8a96WYtCCJGTKnPxhrXcD/edit, abgerufen am 17. Januar 2025

Hall et al. (2021) Hall, R., Sweet, R., Belles, R. & Wieselquist, W. A.: Extended Enrichment Accident Tolerant LWR Fuel Isotopic and Lattice Parameter Trends, Oak Ridge National Laboratory (ORNL), ORNL/TM-2021/1961, 2021.

Kecek et al. (2016) Kecek, A., Tuček, K., Holmström, S. & van Uffelen, P.: Development of M5 Cladding Material Correlations in the TRANSURANUS Code, ISBN 9279646559, Publications Office of the European Union, 2016.

Koyanagi et al. (2024) Koyanagi, T., Hu, X., Petrie, C. M., Singh, G., Ang, C., Deck, C. P., Kim, W.-J., Kim, D., Sauder, C. & Braun, J.: Hermeticity of SiC/SiC composite and monolithic SiC tubes irradiated under radial high-heat flux. Journal of Nuclear Materials 588, 154784, 2024.

Mouche et al. (2021) Mouche, P. A., Koyanagi, T., Patel, D. & Katoh, Y.: Adhesion, structure, and mechanical properties of Cr HiPIMS and cathodic arc deposited coatings on SiC. Surface and Coatings Technology 410, 126939, 2021.

Noda et al. (2002) Noda, T., Fujita, M., Araki, H. & Kohyama, A.: Effect of nuclear data and impurities on the evaluation of induced activity of CVI SiCf/SiC composites. Fusion Engineering and Design 61, 711–716, 2002.

NEA (2025) Nuclear Energy Agency (NEA): JEFF-4.0 nuclear data library is now available, https://www.oecd-nea.org/jcms/pl_107619/jeff-4-0-nuclear-data-library-is-now-available, abgerufen am 27. Oktober 2025, Stand vom 2. Juli 2025.

Parga (2018) Parga, C. J.: M5 Alloy Specification for TREAT Conceptual Fuel Cladding Selection, Idaho National Lab.(INL), Idaho Falls, ID (United States), 2018.

Plompen et al. (2020) Plompen, A. J. M., Cabellos, O., Saint Jean, C. de, Fleming, M., Algora, A., Abstract for 30th International QUENCH Workshop 10.11.2025

Angelone, M., Archier, P., Bauge, E., Bersillon, O. & Blokhin, A.: The joint evaluated fission and fusion nuclear data library, JEFF-3.3. The European Physical Journal A 56(7), 181, 2020.

Quillin et al. (2022) Quillin, K., Yeom, H., Dabney, T., Willing, E. & Sridharan, K.: Microstructural and nanomechanical studies of PVD Cr coatings on SiC for LWR fuel cladding applications. Surface and Coatings Technology 441, 128577, 2022.

Reaktor-Sicherheitskommission (2020) Reaktor-Sicherheitskommission: Ergebnisse und Empfehlungen der 514. Sitzung, http://www.rskonline.de/sites/default/files/reports/epanlagersk514hp_0.pdf, abgerufen am 5. Januar 2024

Romano et al. (2015) Romano, P. K., Horelik, N. E., Herman, B. R., Nelson, A. G., Forget, B. & Smith, K.: OpenMC: A state-of-the-art Monte Carlo code for research and development. Annals of Nuclear Energy 82, 90–97, 2015.

Romano et al. (2021) Romano, P. K., Josey, C. J., Johnson, A. E. & Liang, J.: Depletion capabilities in the OpenMC Monte Carlo particle transport code. Annals of Nuclear Energy 152, 107989, 2021.

Sublet et al. (2017) Sublet, J.-C., Eastwood, J. W., Morgan, J. G., Gilbert, Fleming, M. & Arter, W.: FISPACT-II: an advanced simulation system for activation, transmutation and material modelling. Nuclear Data Sheets 139, 77–137, 2017.

Yeom et al. (2019) Yeom, H., Dabney, T., Johnson, G., Maier, B., Lenling, M. & Sridharan, K.: Improving deposition efficiency in cold spraying chromium coatings by powder annealing. The International Journal of Advanced Manufacturing Technology 100, 1373–1382, 2019.

Federal Office
for the Safety of
Nuclear Waste Management

Infinite lattice depletion of accident-tolerant fuel pin-cells with OpenMC and cladding inventory analysis with FISPACT-II

Intermediate results of project 4724B50001

Peter Bochtler

Quench Workshop, Karlsruhe, Germany

16-18.12.2025

Agenda

1. OpenMC burn-up simulations of ATF pin-cells
2. Code-to-code comparison of clad inventory: FISPACT-II vs. OpenMC
3. ATF cladding metrics from FP-II

Motivation for in-house simulations

It is foreseeable that power reactors in Europe will run with accident-tolerant fuels.

In-house research project “ReUnFis” is seeking to answer how the use of such fuels could be impacting waste streams and safety aspects (that can be derived from the isotopic inventories).

BASE advises and supports the Federal Ministry for the Environment, Climate Action, Nature Conservation and Nuclear regarding issues of disposal of radioactive waste and nuclear safety.

BMUKN

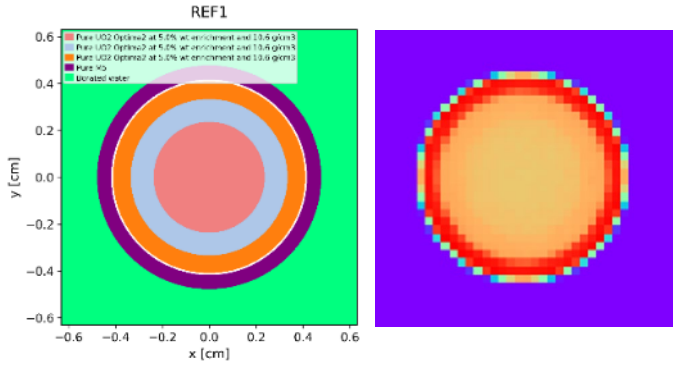

- Period: July 24 to December 26
- Burn-up simulation of pin-cells with M5+20µmCr, FeCrAlC26M, SiC/SiC+10µmCr in OpenMC
- ATF cladding metrics (opt. impurities) with FP-II

Codes, methods, tools and data

Codes & Methods

OpenMC[18][19] originally developed by MIT CRPG (Paul Romano),
now community-developed Monte Carlo neutron and photon transport simulation code:
https://github.com/openmc-dev/openmc

Methods

Continuous energy neutron transport “collapse” with track length tallies into reaction rate average determination through many samples (k-eigenvalue method, method of successive generations[30], see docs.openmc.org and e.g. [23]).

→ Solving neutron transport coupled inventory equations with matrix exponentials + IPF CRAM48[30,31,32] + CE/LI integrator[34]

→ Providing tallied neutron spectra for FISPACT-II

Codes & Methods

FISPACT-II[20] code developed by UKAEA, available through OECD-NEA:
https://www.oecd-nea.org/tools/abstract/detail/nea-1890/

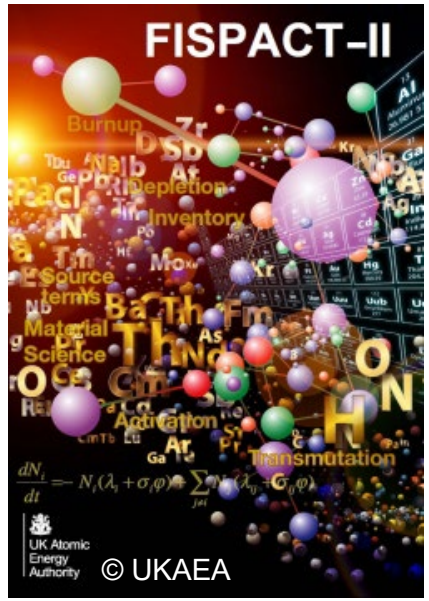

Methods

Point depletion of entire material (here ATF cladding) „lump" with OpenMC tallied neutron spectra in CCFE-709 or UKAEA-1102 group structure[14] and flux level (at each BU step).

→ Solving (only) inventory equations with Livermore Solver for Ordinary Differential Equations (LSODE)[24] with adaptive time stepping

Additional methods for inventory uncertainty estimation (pathway analysis) and self-shielding correction.

Tools and Data

Computing on R&D-server with jupyter-notebooks[25] (python virtual environments) + complementary calculations on ZUSE HPC-system „Lise“ (test account)

OpenMC python API (OpenMP, OpenMPI)
FISPACT python pseudo API pypact by Thomas Stainer: *https://github.com/fispact/pypact*

Neutronics material maker originally created by Jonathan Shimwell:
https://github.com/fusion-energy/neutronics_material_maker

Nuclear data sources

- *https://git.oecd-nea.org/fispact/nuclear_data*
- *https://databank.io.oecd-nea.org/data/jeff*
- *https://openmc.org/data-libraries/*

.JSON material database for (ATF) materials

Literature research on

- Composition of 5.0, 5.1 and 5.6 wt% UO_2, Zr-alloys, FeCrAl and SiC as well as Al_2O_3, Cr_2O_3 and Cr
- Impurity levels in materials see e.g. [16]

Creation of .JSON material database (neutronics materials maker) for OpenMC and FISPACT-II

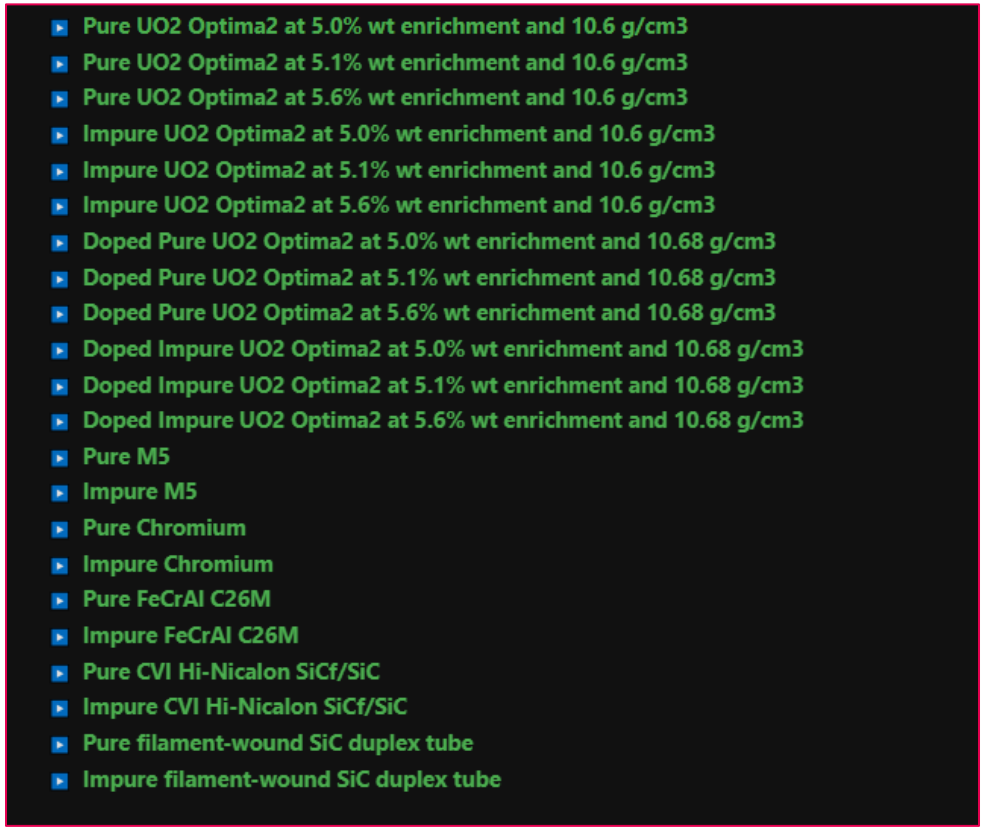

Note: Please note that „M5“ is a „M5-like“ Zr-alloy according to the reported references.

Modelling accident-tolerant fuel pin-cells in OpenMC (jeff-3.3)

Pin-cell cases overview for „PWR“

	REF1	REF3a	ATF1a	ATF2a	ATF3a
Density [g/cm^3]	10.6[1]	10.68[1] *A)*	10.68[1] *A)*	10.68[1] *A)*	10.68[1] *A)*
Enrichment [wt%]	5.0	5.0	5.1[2]	5.6[2]	5.0
Cladding	M5[3]	M5[3]	M5[3] +20 µm Cr[2]	FeCrAl C26m[2]	Filament-wound SiC duplex tube[6] +10 µm Cr[7],[8]
Thickness [mm]	0.601[4]	0.601[4]	0.621	0.385[2]	0.81[5]
HM per model [g/cm]	4.9225	+0.65%	+0.65%	+0.65%	+0.65%

A) doped with 200 ppm Al_2O_3 +800 ppm Cr_2O_3[2]

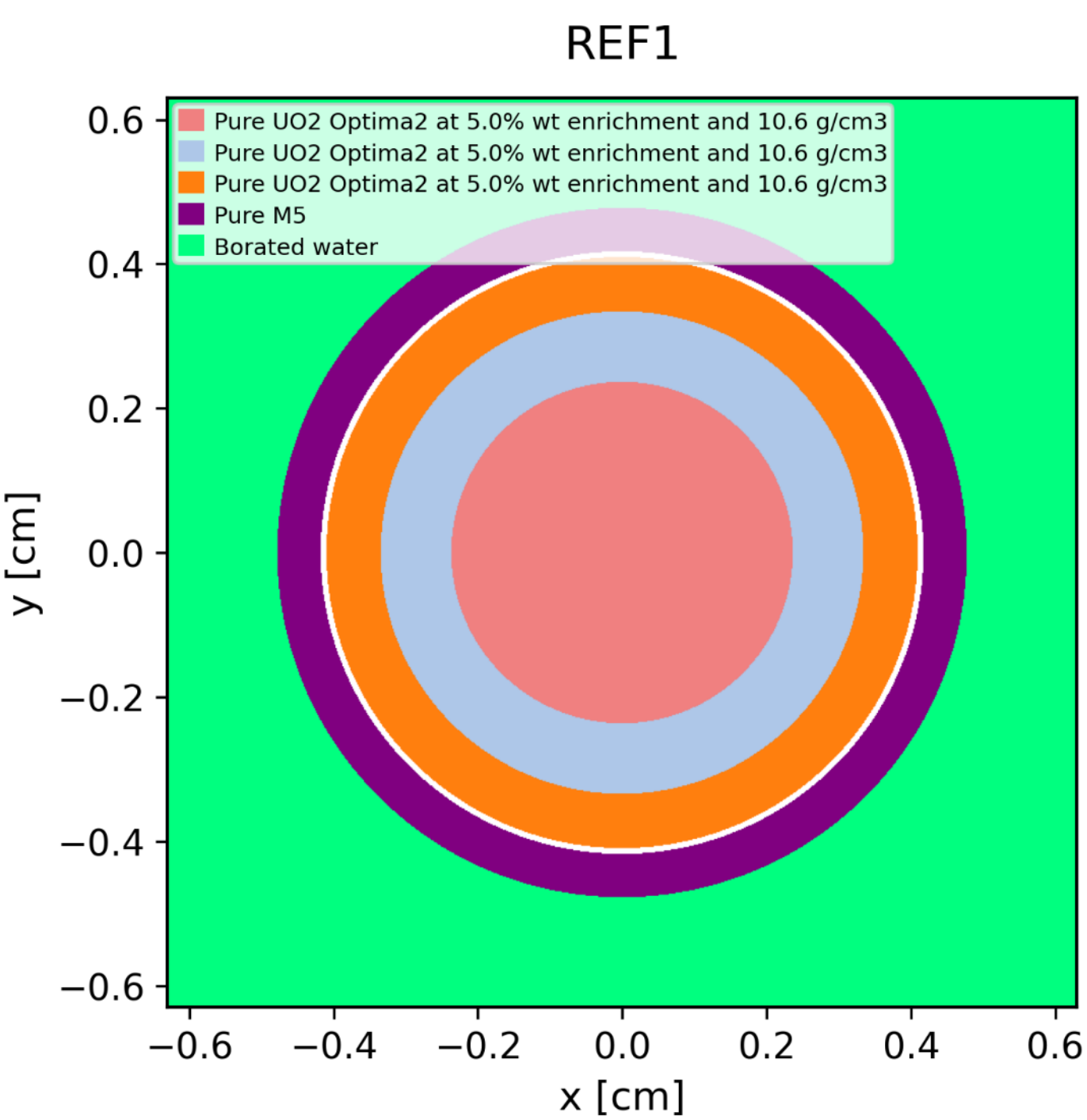

Infinite 2-D pin-cell depletion

Fuel pin at the core center with constant power over 3 cycles (each 18 months).

- 45.7 W/gU_i for 1642.5 days to 75 MWd/kgU_i
- Pitch = 1.26 cm[2],[9]
- 3 fuel depletion zones
- Constant gap = 0.08 mm
- 5.0 wt% at 10.6 g/cm^3
- Cladding 600 K
- Fuel 900 K
- Moderator 583 K and 15 MPa
- 650 ppm of boron (by weight)[10] = constant

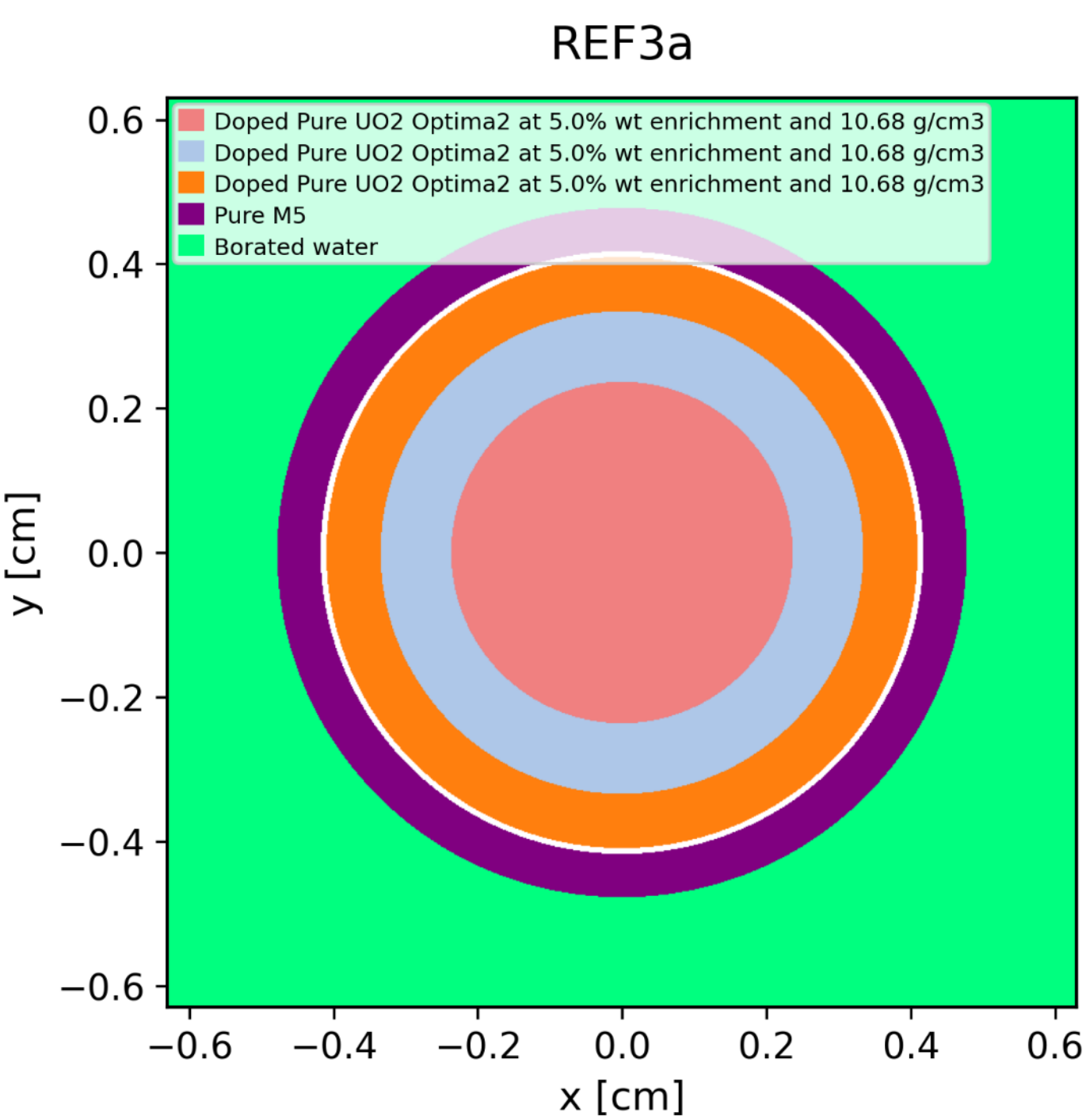

- M5 cladding [3]
- Density increase compared to REF1
- HM +0.65%, ρ +0.75%[1]
- Dopants Cr, Al, O as (n,gamma) absorbers (in 200 ppm Al_2O_3 and 800 ppm Cr_2O_3)[2]

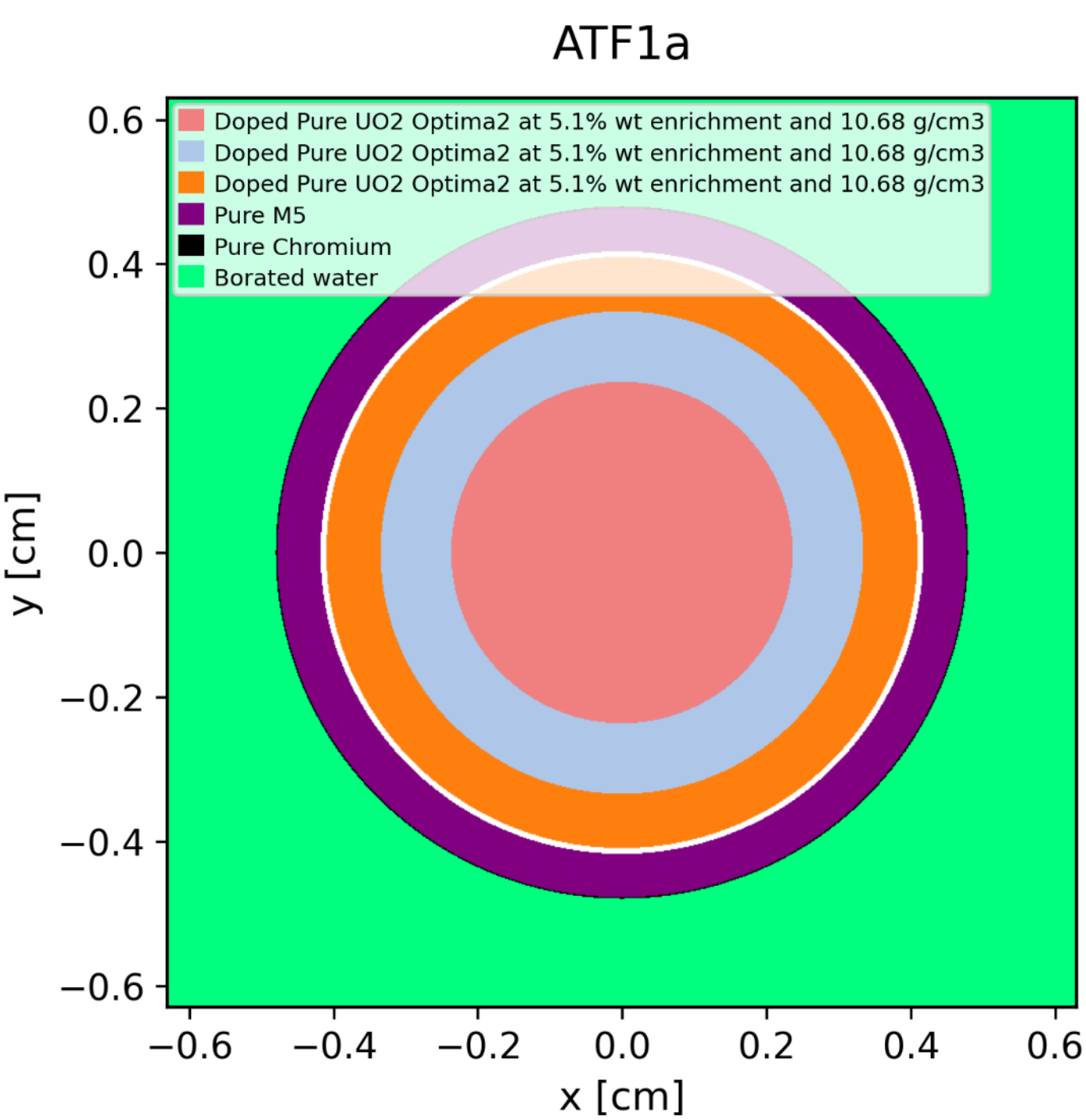

- +20 µm chromium layer [2]
- +0.1 wt% enrichment offset [2]

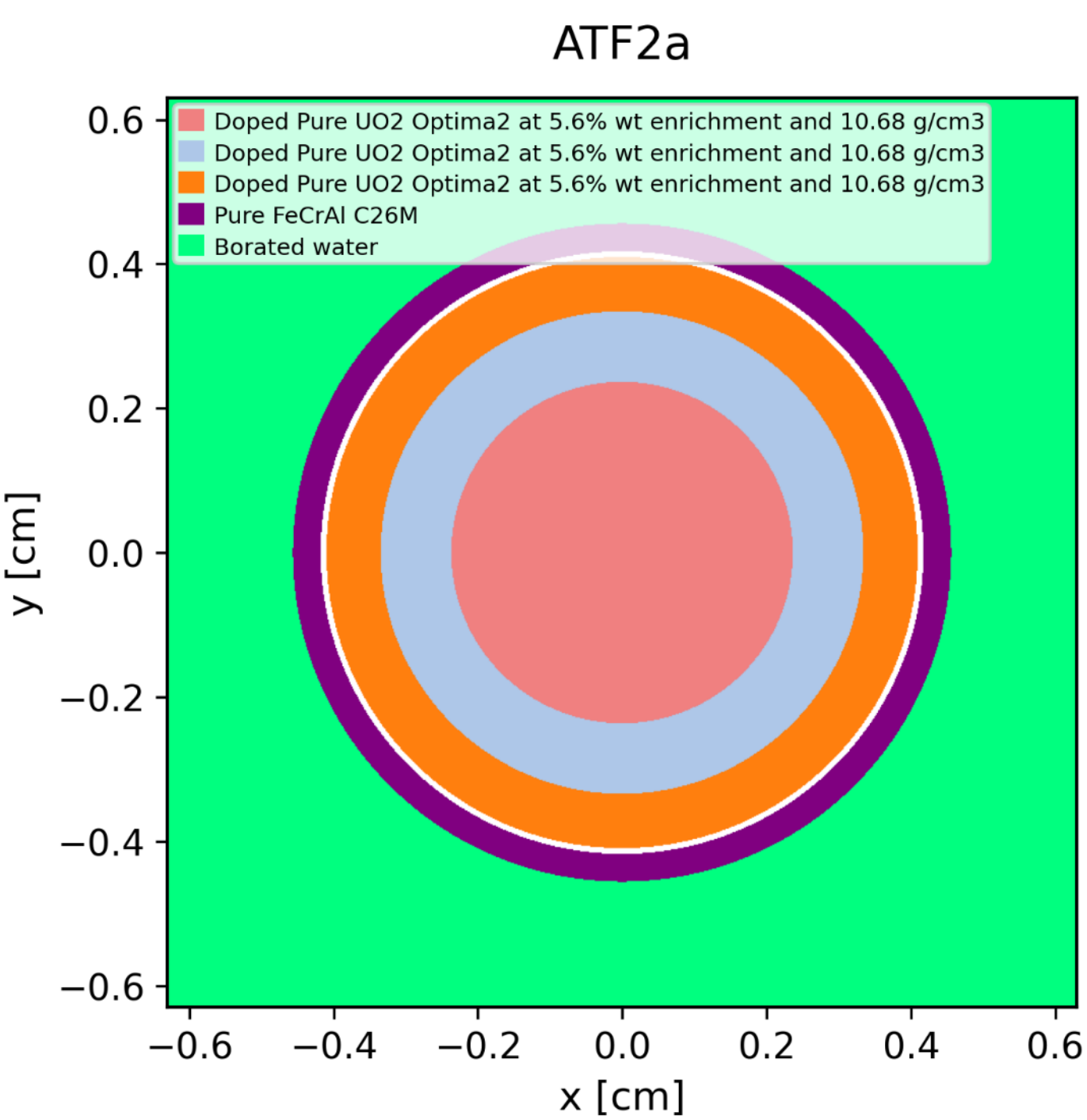

- Significant amount of (n,γ) absorbers through FeCrAlC26M [2]
- +0.6 wt% enrichment offset [2]
- Constant pellet + thinner cladding

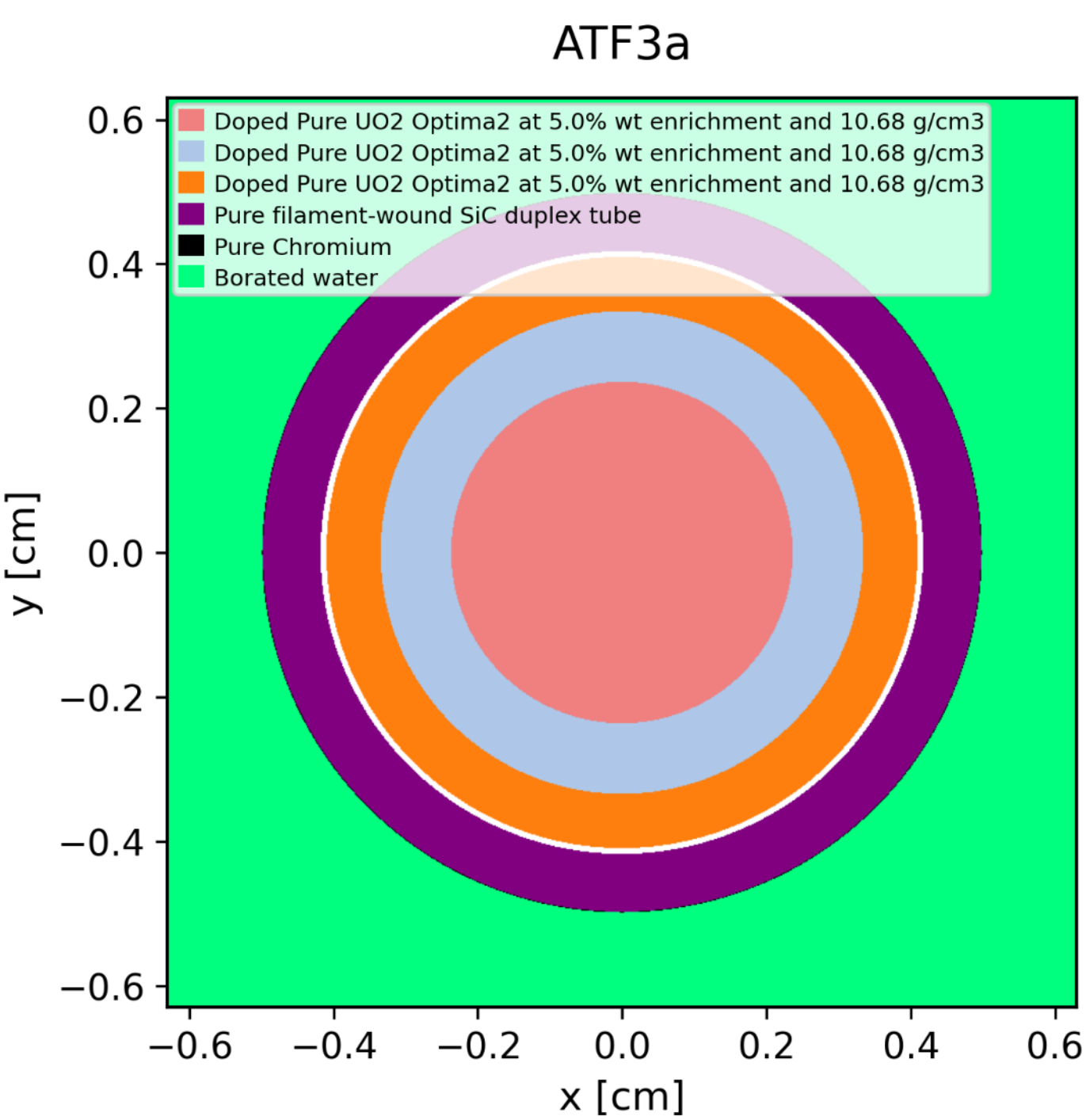

- SiC/SiC[6]+10 µm chromium layer [7],[8]
- No enrichment offset
- Constant pellet + thicker cladding
- Additional case (ATF3c) with 700 K[11] and 1100 K[12] for cladding and fuel respectively (lower λ, open gap)[13]

Case comparisons of accident-tolerant fuel pin-cells

ATF net impact on k_{inf} and Δρ

Reference cell: REF3a doped UO_2 with 5.0% and M5 (0.601 mm)

vs.

1. **ATF1a** doped UO_2 with 5.1% and **M5+20 µm Cr**
2. **ATF2a** doped UO_2 with 5.6 % and **thinner FeCrAl (0.385 mm)**
3. **ATF3a** doped UO_2 with 5.0 % and **thicker SiC (0.8 mm) +10 µm Cr**

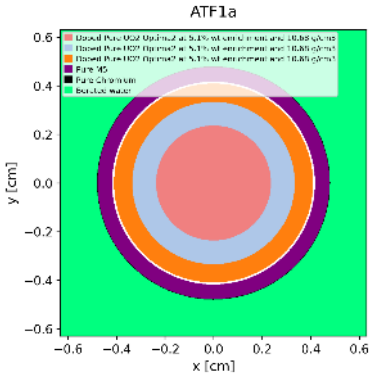

0.601 mm M5
20 µm Cr
5.1%
600 wppm boron

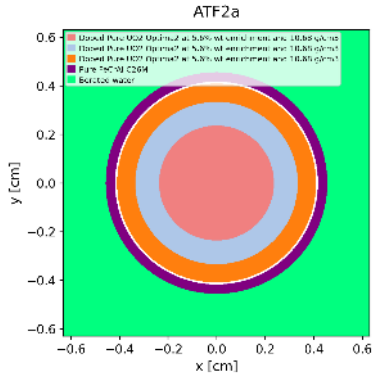

0.385 mm FeCrAl
5.6%
600 wppm boron

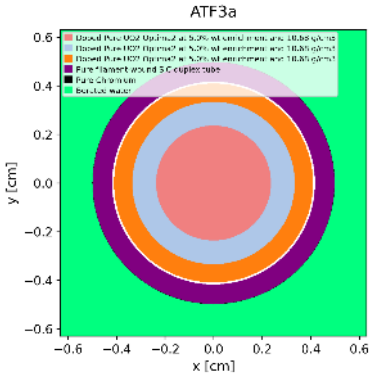

0.8 mm SiC
10 µm Cr
5.0%
600 wppm boron

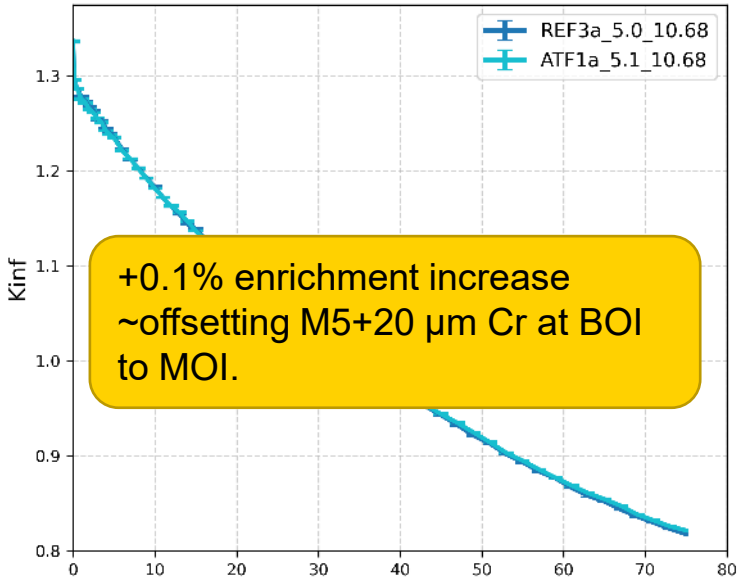

+0.1% enrichment increase ~offsetting M5+20 µm Cr at BOI to MOI.

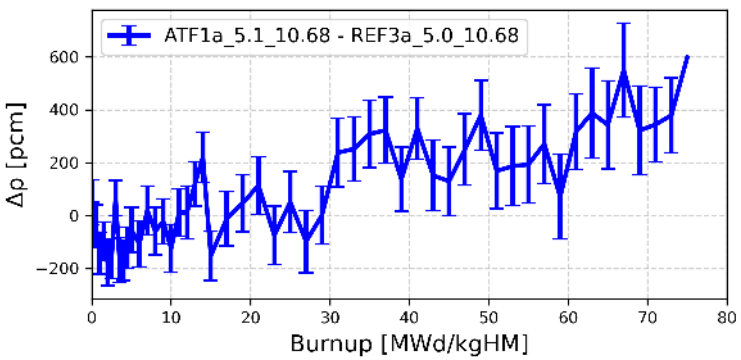

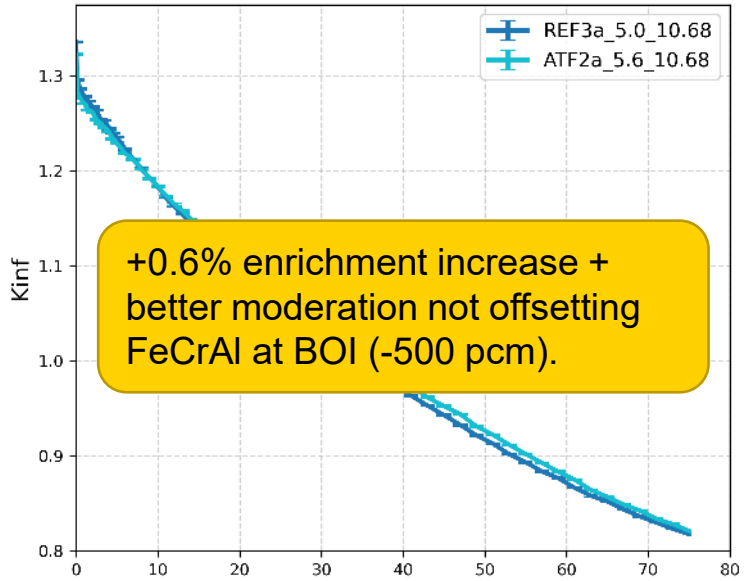

+0.6% enrichment increase + better moderation not offsetting FeCrAl at BOI (-500 pcm).

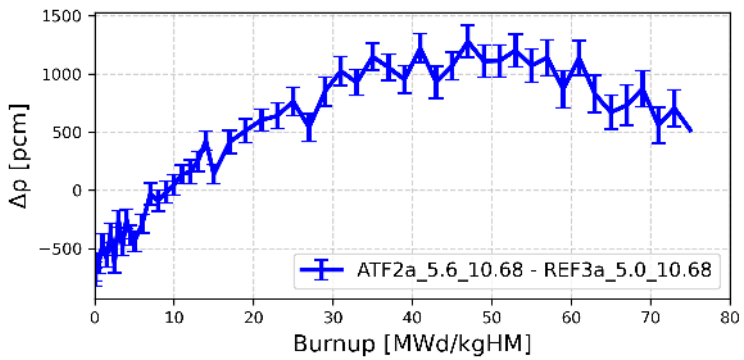

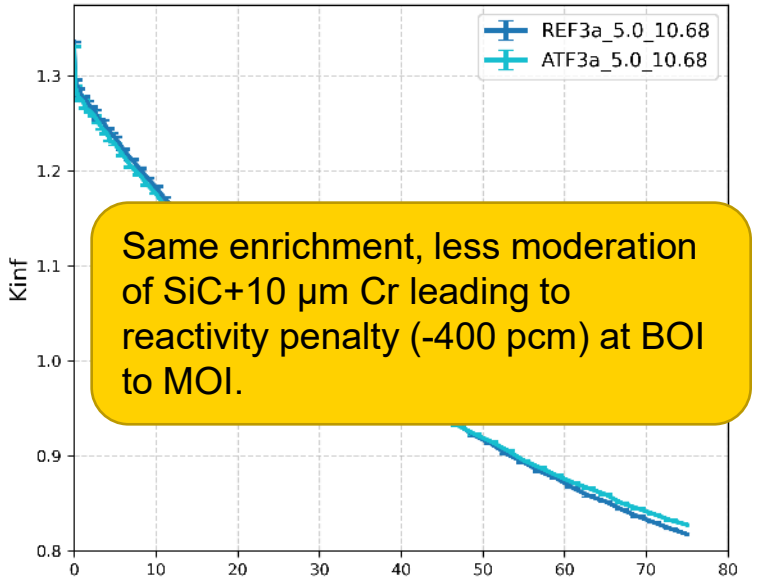

Same enrichment, less moderation of SiC+10 µm Cr leading to reactivity penalty (-400 pcm) at BOI to MOI.

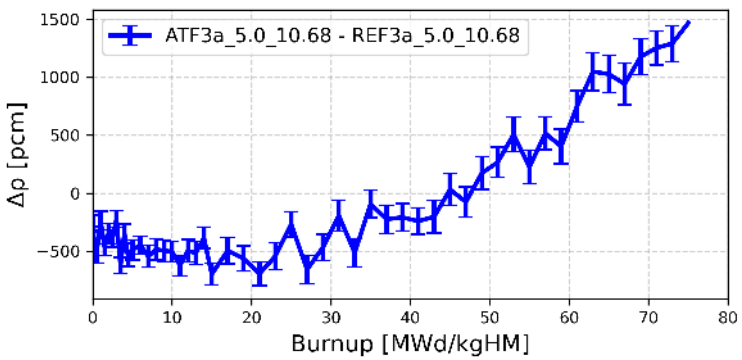

Clad capture rate ratio comparison

ATF1a/REF3a

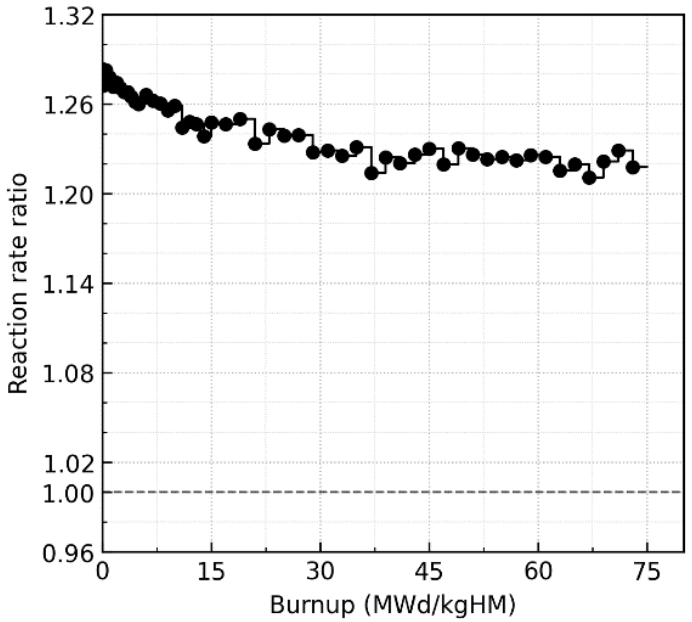

20 µm Cr → ~22% cladding activation rate increase (even at ~same flux level)

ATF2a/REF3a

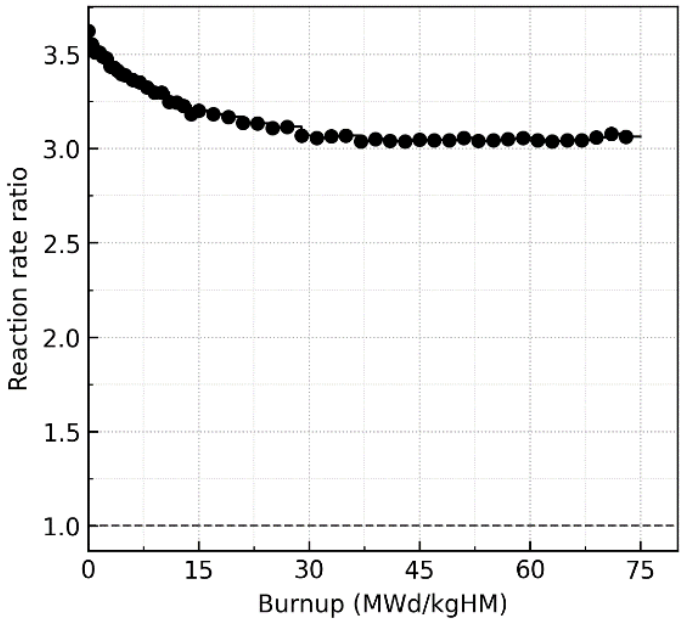

Activation > 3 times higher in thinner FeCrAl (even at lower flux level, minus ~6%).

ATF3a/REF3a

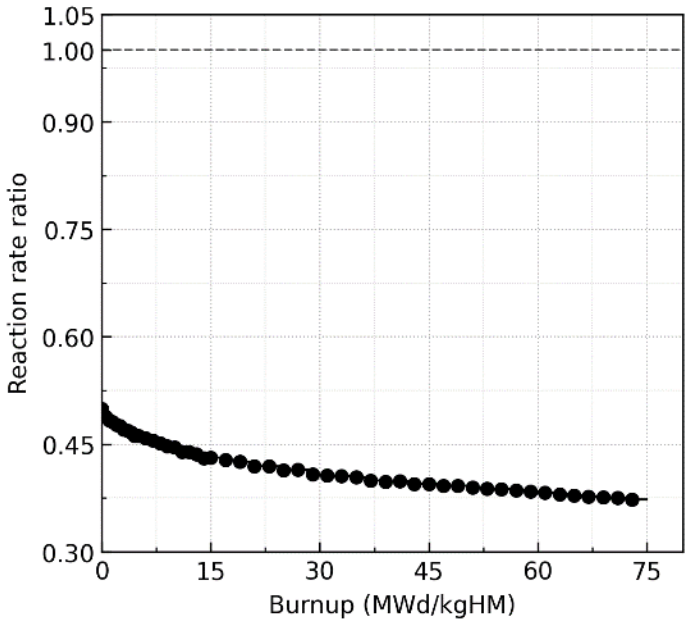

Thicker SiC + 10 µm Cr less than half of M5 activation rate (even at higher flux plus ~+5%)

Further analysis of Δρ and k_{inf} evolution

Analysis of neutron flux shape and neutron flux intensity

Effects of spectral hardening and softening vs. BU different for cases

Four factor formula evolution with burn-up

- Reproduction η
- Thermal utilization f
- Resonance escape probability p
- Fast fission ε

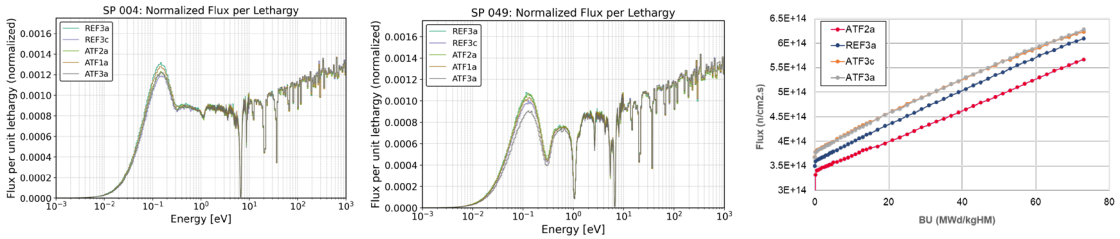

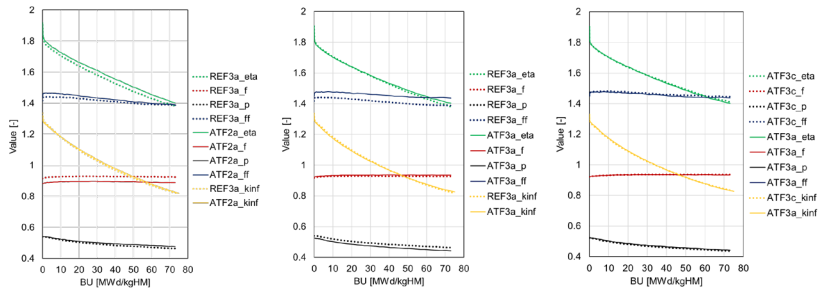

Deep dive out of scope for this workshop (check my analysis in the annex and discuss with me)!

Burn-up conclusions (constant pellet/gap/pitch)

Enrichment offset is necessary for M5+20µmCr as well as FeCrAlC26m

→ Safety improvement coming with clad material leads to extra effort for fuel enrichment

FeCrAlC26M would likely require an adapted boron mngmnt per cycle wrt standard cladding tube

- Enrichment offset not sufficient at BOI + Reactivity rise-and-fall trend with BU
- Improved moderation (p▲) for thinner neutron capturing cladding (f▼) vs enrichment increase (η ▲)
- Thicker FeCrAl cladding would impact neutron economy even more significantly.

Burn-up conclusions (constant pellet/gap/pitch)

For SiC/SiC (0.8 mm) +10µmCr

- Negative reactivity impact due to moderation reduction (thicker clad at constant pitch)
- Worse moderation (p▼ ε▲) for thicker neutron-transparent cladding (f▲).
- Evolution of k_{inf} very different compared to reference cell ($\Delta\rho_{BOI}$ -400 pcm, then ever-increasing).
- Additional penalty of ~400 pcm for (more realistic) higher temperature 700K/1100K case at BOI (see ATF3c in annex)
- Need to increase pitch to get back a good H/U ratio, then evaluate enrichment offset necessity (higher pitch ▲→ HM ▼ in core volume) → smaller power at same size

Clad activation comparison: OpenMC vs. FISPACT-II

- JEFF-3.3 library[21] for OpenMC[18],[19] and FISPACT-II (FP)[20]
- Cladding in both codes at 294 K (FP-II ND availability)

Code benchmark: cladding activation

Comparing the clad inventory (Bq/cm) in the decay space

- Two type of plots

1) **Total activity vs decay time** with dominant nuclides from FP-II as points {half life, activity at t_0}

2) **Isotopic ratios** of OpenMC/FP vs decay time (nuc > 1% contribution)

For OpenMC and FISPACT-II users:

Check analysis and conclusions in the annex and get in touch!

Decay time	Description
5min	End of LOCA
10min	LOCA cooling 1
20min	LOCA cooling 2
30min	LOCA cooling 3 (ORNL)
40min	Quench H2 start
115min	Quench H2 end
5d	Core loading (ORNL)
25d	End of outage (ORNL)
100d	Midpoint 1 (ORNL)
500d	Midpoint 2 (ORNL)
5y	Early wet storage end
10y	Late wet storage end
40y	Intermediate storage 1 (ORNL)
100y	Intermediate storage 2

Accident-tolerant fuel cladding metrics with FP-II

Clad activity at equal 75 MWd/kgHM$_i$ (jeff-3.3)

M5 + 20 µm Cr (6.95e+22 n/cm²)

Activity increase up to 100 d (Cr51) ~20% at 5d

FeCrAlC26m (6.50e+22 n/cm²)

0→1.15d < **M5**

- Nb97m, Nb94m, Nb97, Zr97

1.15d→16y > **M5**

- Cr51, Fe55, Mn54, Co60 vs. Zr95, Nb95

16y→100y < **M5**

- Mo93 vs. Nb93m, Nb94

SiC+10 µm Cr (7.25e+22 n/cm²)

Al28, Si31, V49, H3, C14 + Cr51 < **M5**

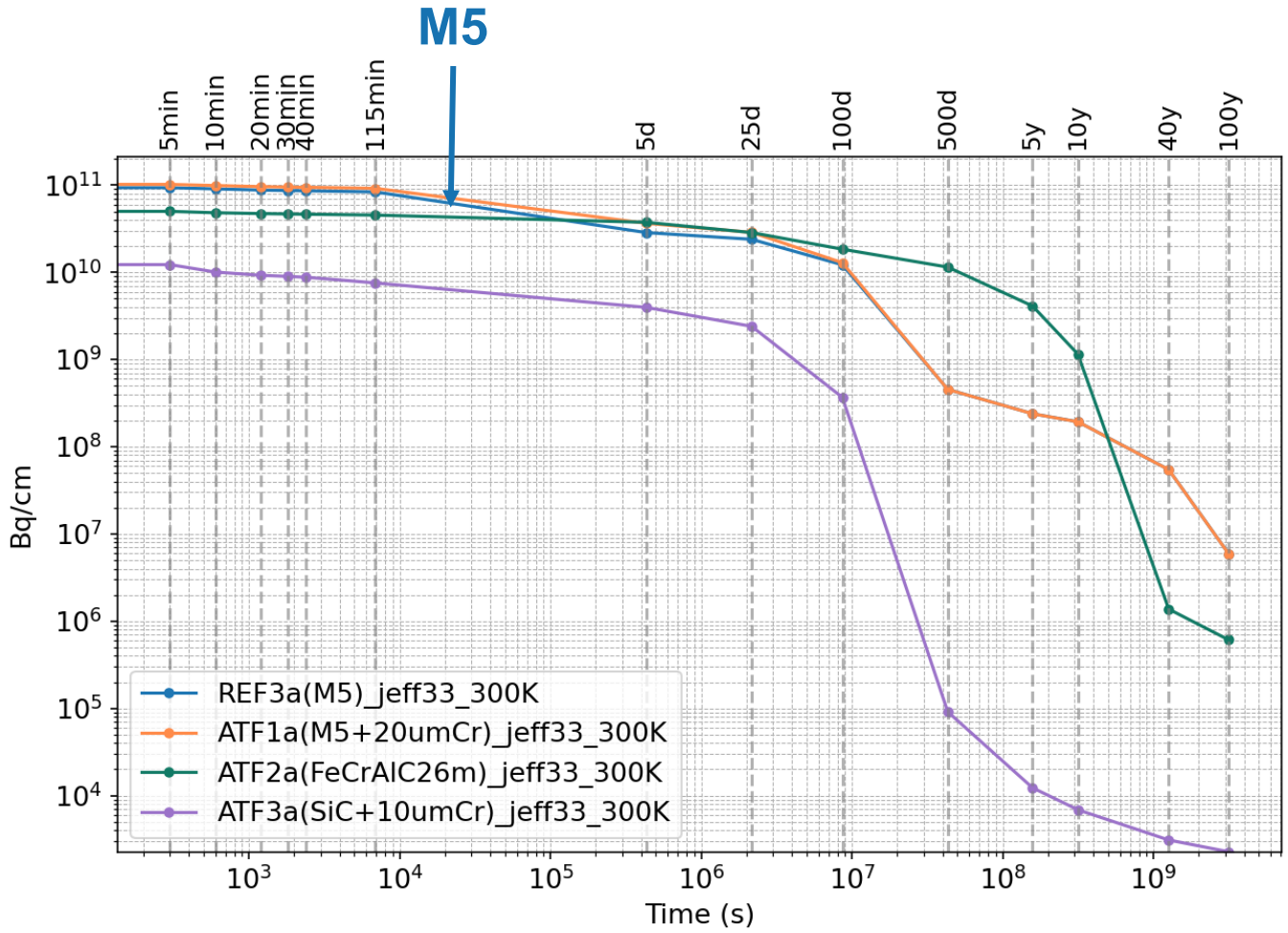

Activity vector (nuc %) vs decay time

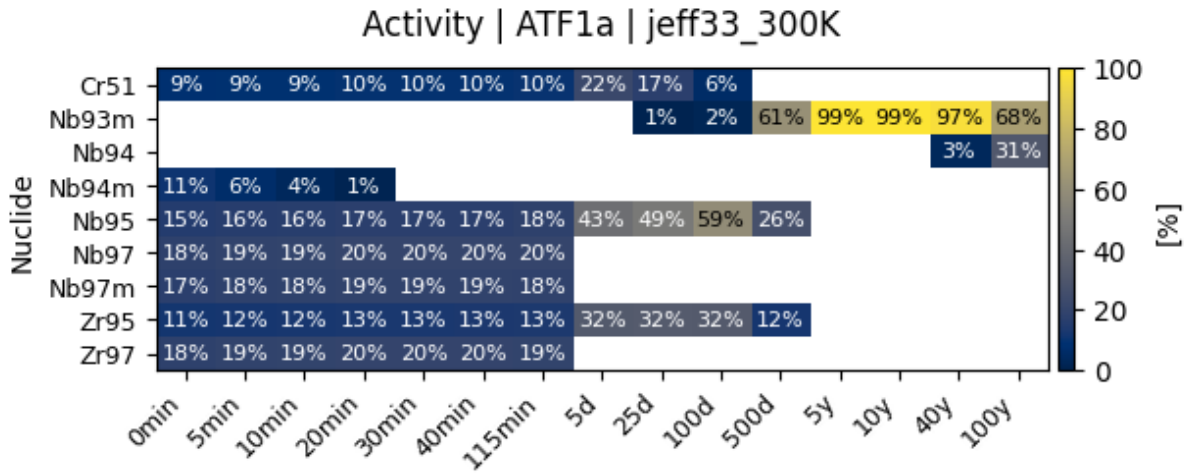

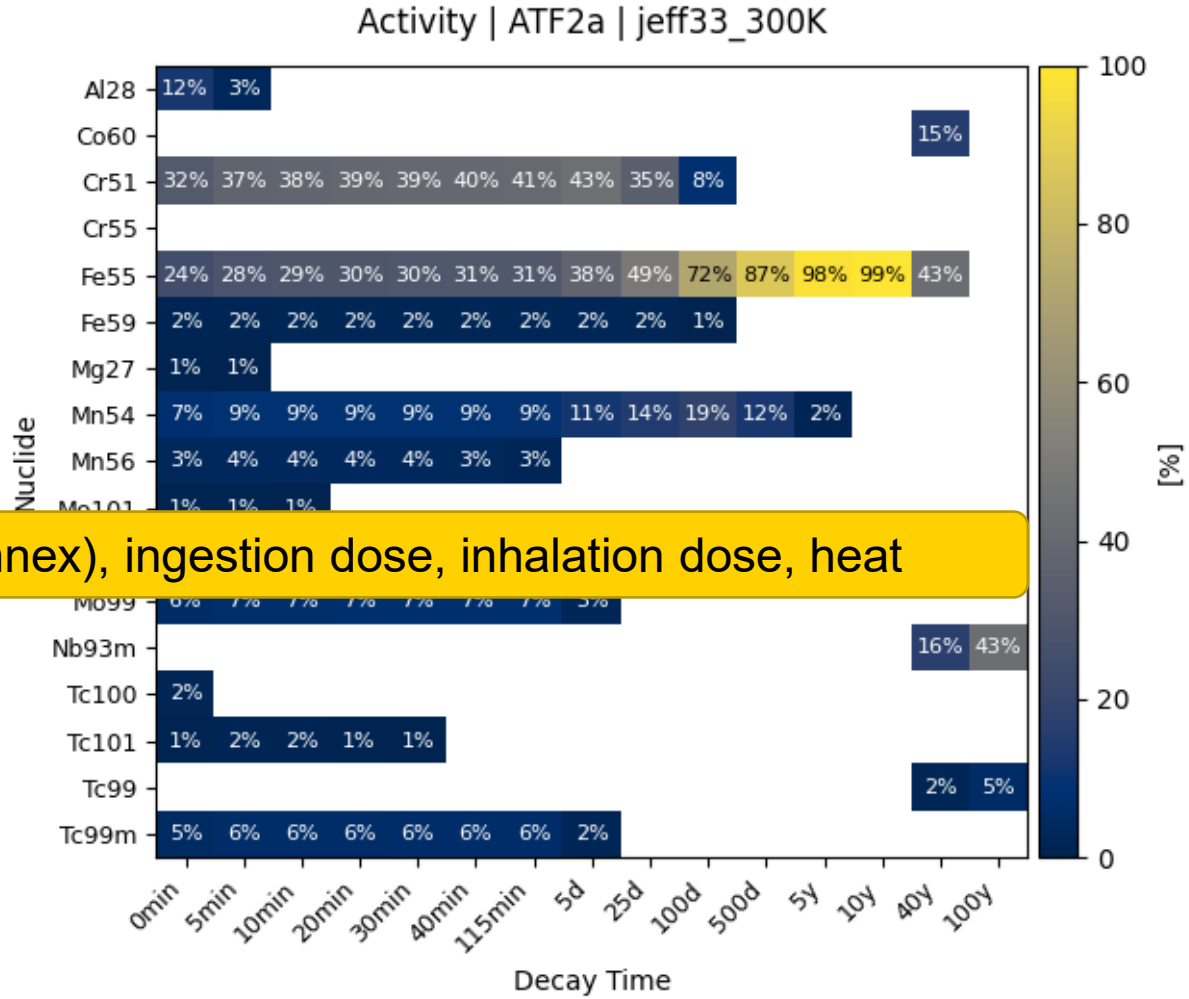

Other possible metrics: contact dose rate (see annex), ingestion dose, inhalation dose, heat

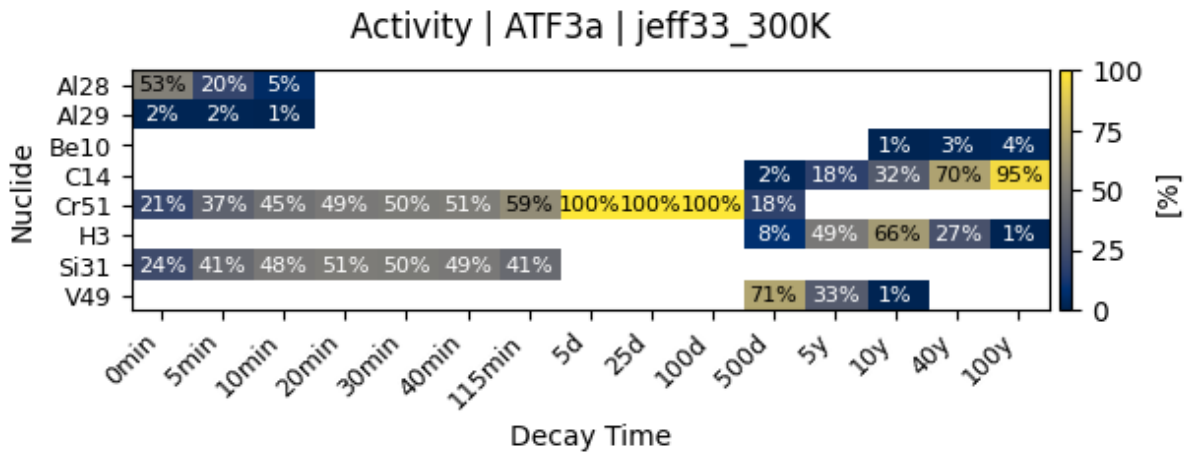

ATF1a with impurities = ATF1b

Element	wppm
Fe	500
Cr	150
Si	120
C	100
Hf	100
Sn	100
Ta	100
W	100
N	80
Al	75
Ni	70
Cu	50
Mo	50
Ti	50
V	50
Ca	30
Pb	30
H	25
Mg	20
Mn	20
Co	10
U	3.5
B	0.5
Cd	0.5

Impact of impurities on cladding activity

- M5 at maximum impurities [27]
- Cr powder at maximum impurities [28],[29]

Additional nuclides (>1%): Co60, Fe55, C14, Ni63, Ta182, Ta183

…

Total activity also increased by ~15% at 5y (Co60) → RP impact

…

100 ppm of Ta (Ta-181)

10 ppm Co (Co-59)

70 ppm Ni (Ni-62)

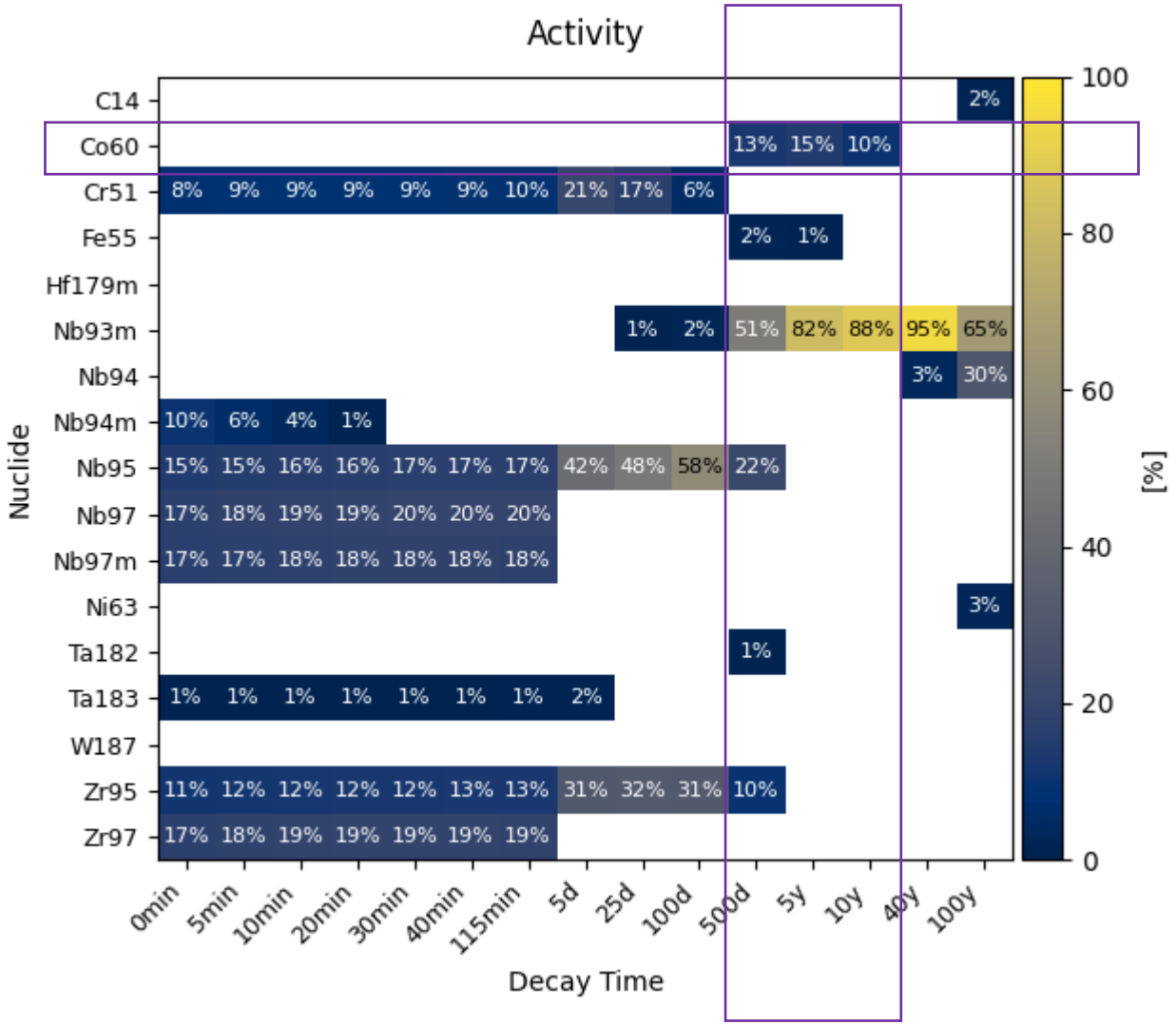

M5+Cr: Evolution of elemental appm (>1appm)

	ATF1a	ATF1b	
Mo	5e+02	5e+02	
H	6e+00	2e+03	
He	3e+00	5e+00	
Y	2e+00	2e+00	
C	1e+00	7e+02	
V	1e+02	2e+02	
Mn	3e+00	3e+01	
Os		3e+00	Tungsten
Re		5e+00	Tungsten
Sr		1e+00	Uranium

Higher order of magnitude nearly entirely due to T_0 elemental wppm impurities (see previous slide)

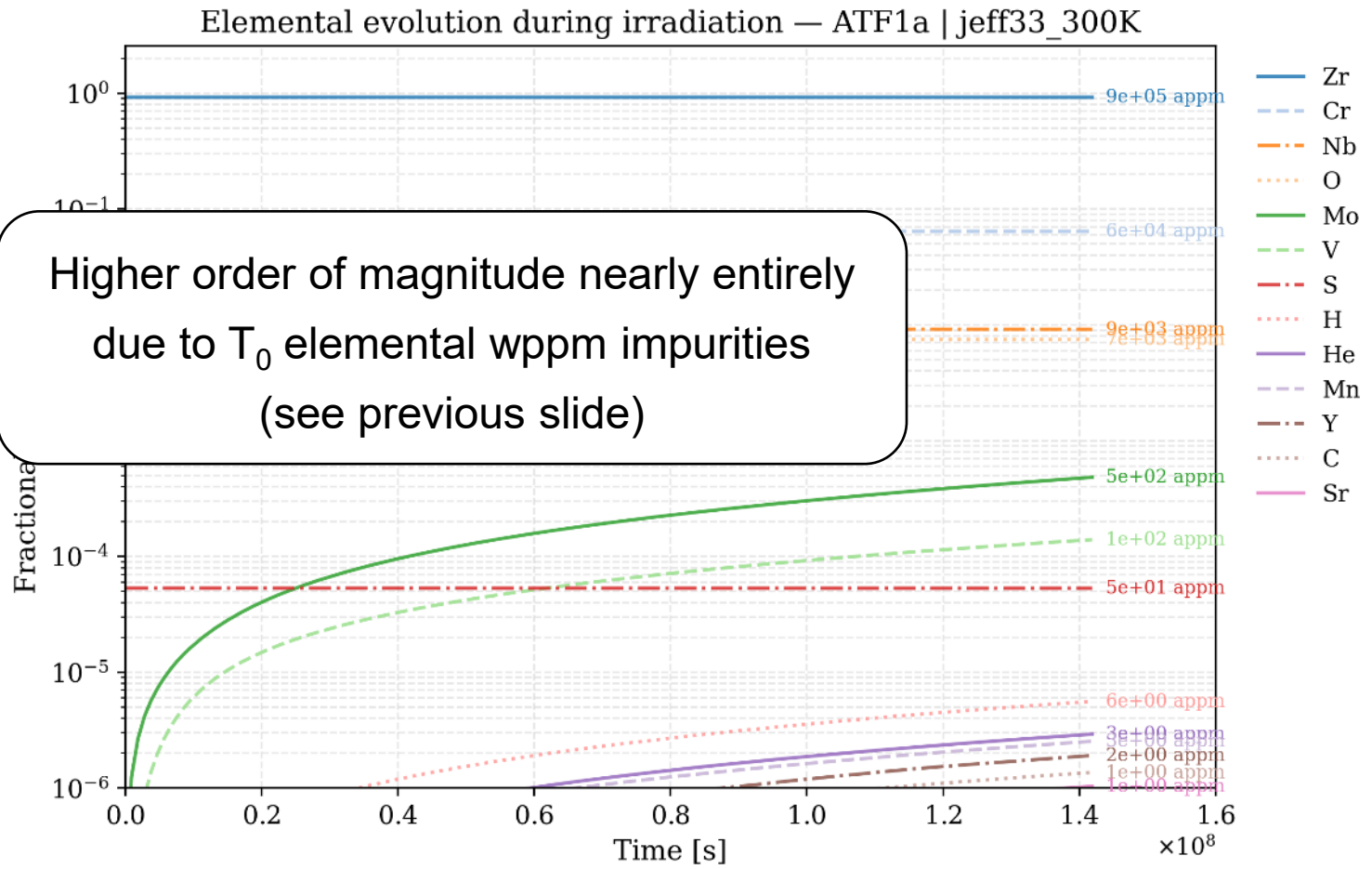

Outlook and conclusions

Outlook and conclusions

- More in depth comparison with ORNL report [2] and other publications.
- Simulation of FeCrAl and SiC+Cr with impurities.
- New material developments and fuel (pin cell) designs (impurity levels, nuclear data) can be analyzed with the complementary use of OpenMC and FISPACT-II.
- BASE-F4 is open to support related research projects with the presented simulation tools.

Thank you very much for your attention — it is greatly appreciated!

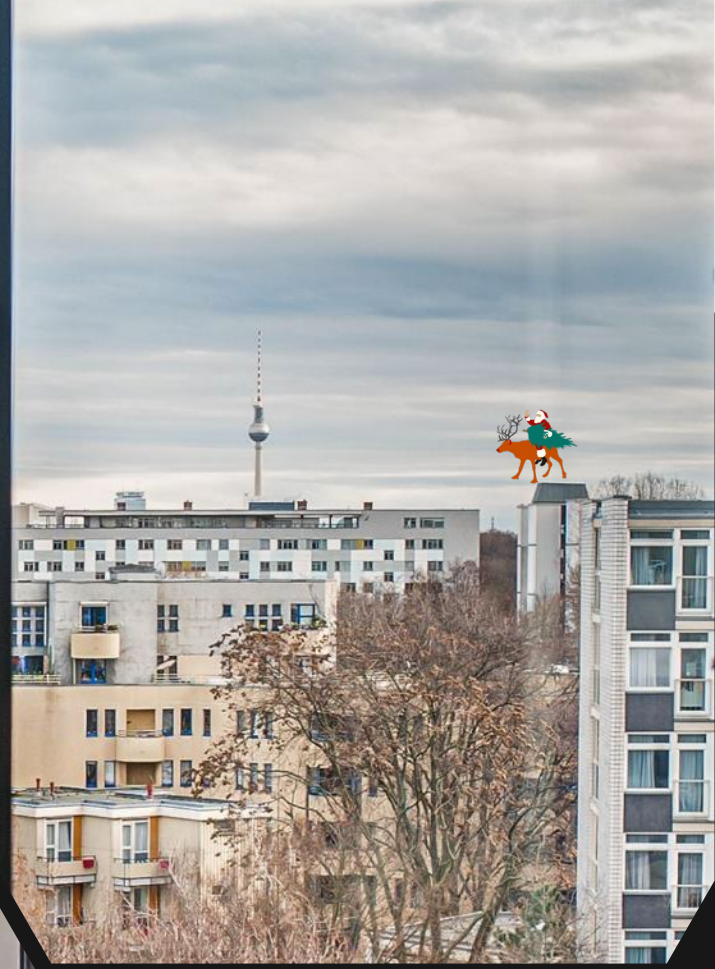

peter.bochtler@base.bund.de

References (1)

1 Arborelius, Jakob; Backman, Karin; Hallstadius, Lars; Limbäck, Magnus; Nilsson, Jimmy; Rebensdorff, Björn et al. (2006): Advanced Doped UO2 Pellets in LWR Applications. In: Journal of Nuclear Science and Technology 43 (9), S. 967–976. DOI: 10.1080/18811248.2006.9711184.

2 Hall, Robert; Sweet, Ryan; Belles, Randy; Wieselquist, William A. (2021): Extended Enrichment Accident Tolerant LWR Fuel Isotopic and Lattice Parameter Trends. Oak Ridge National Laboratory (ORNL) (ORNL/TM-2021/1961).

3 M5 composition
Reaktor-Sicherheitskommission (RSK) (2020): Ergebnisse und Empfehlungen der 514. Sitzung. Online verfügbar unter http://www.rskonline.de/sites/default/files/reports/epanlagersk514hp_0.pdf, zuletzt geprüft am 05.01.2024.

3 M5 density
Kecek, Adam; Tuček, Kamil; Holmström, Stefan; van Uffelen, Paul (2016): Development of M5 Cladding Material Correlations in the TRANSURANUS Code: Publications Office of the European Union.

4 Mitchell, D.; Dunn, B.: Evaluation of Advanced Cladding and Structural Material (M5) in PWR Reactor Fuel. Non Propriertary Version. Framatome Cogema Fuels. 3315 Old Forest Road, Lynchburg, Virginia 24506-0935 (Topical Report BAW-10227-A).

5 Haynes, T. A.; Shepherd, D.; Wenman, M. R. (2020): Preliminary modelling of crack nucleation and propagation in SiC/SiC accident-tolerant fuel during routine operational transients using peridynamics. In: J. Nucl. Mater. 540, S. 152369. DOI: 10.1016/j.jnucmat.2020.152369.

6 SiC/SiC duplex tube architecture (60 v% SiC composite + 40 v% CVD SiC)
SiC composite architecture (20 v% Hi-Nicalon Type S fiber + 80 v% CVI SiC)
Density of duplex tube, monolithic CVD and CVI SiC
Koyanagi, Takaaki; Hu, Xunxiang; Petrie, Christian M.; Singh, Gyanender; Ang, Caen; Deck, Christian P. et al. (2024): Hermeticity of SiC/SiC composite and monolithic SiC tubes irradiated under radial high-heat flux. In: J. Nucl. Mater. 588, S. 154784.

6 Density of Hi-Nicalon Type S fiber
Noda, Tetsuji; Fujita, Mitsutane; Araki, Hiroshi; Kohyama, Akira (2002): Effect of nuclear data and impurities on the evaluation of induced activity of CVI SiCf/SiC composites. In: Fusion Engineering and Design 61, S. 711–716.

7 Quillin, Kyle; Yeom, Hwasung; Dabney, Tyler; Willing, Evan; Sridharan, Kumar (2022): Microstructural and nanomechanical studies of PVD Cr coatings on SiC for LWR fuel cladding applications. In: Surface and Coatings Technology 441, S. 128577.

8 Mouche, Peter A.; Koyanagi, Takaaki; Patel, Deep; Katoh, Yutai (2021): Adhesion, structure, and mechanical properties of Cr HiPIMS and cathodic arc deposited coatings on SiC. In: Surface and Coatings Technology 410, S. 126939.

9 McCarthy, Kathryn A.; Dixon, B.; Choi, Yong-Joon; Boucher, L.; Ono, Kiyoshi; Alvarez-Velarde, Francisco et al. (2012): Benchmark Study on Nuclear Fuel Cycle Transition Scenarios - Analysis Codes. Organisation for Economic Co-Operation and Development, Nuclear Energy Agency - OECD/NEA. Le Seine Saint-Germain, 12 boulevard des Iles, F-92130 Issy-les-Moulineaux (France) (NEA/NSC/WPFC/DOC(2012)16). Online verfügbar unter https://inis.iaea.org/records/0txzt-4km86/files/44089401.pdf?download=1, zuletzt geprüft am 06.10.2025.

10 Papukchiev, Angel (2008): Methoden zur Optimierung der Kernauslegung von Druckwasserreaktoren mit reduziertem Borsäureeinsatz. Dissertation. Technische Universität München. Fakultät für Elektrotechnik und Informationstechnik. Online verfügbar unter https://mediatum.ub.tum.de/625419, zuletzt geprüft am 06.10.2025.

References (2)

11 Increased by 100 K in comparison to M5 for 225 W/cm and conductivities of 15 and 5 W/m.K for M5 and SiC respectively assuming that SiC conductivity range in [6] for 155 W/cm is applicable. M5 conductivity
Geelhood, K.; Luscher, W.; Porter, I.; Kyriazidis, L.; Goodson, C.; Torres, E. (2020): MatLib-1.0: Nuclear Material Properties Library. In: PNNL-29728.

12 George, Nathan Michael; Terrani, Kurt; Powers, Jeff; Worrall, Andrew; Maldonado, Ivan (2015): Neutronic analysis of candidate accident-tolerant cladding concepts in pressurized water reactors. In: Annals of Nuclear Energy 75, S. 703–712.

13 Ben-Belgacem, M.; Richet, Victor; Terrani, Kurt A.; Katoh, Yutai; Snead, Lance Lewis (2014): Thermo-mechanical analysis of LWR SiC/SiC composite cladding. In: J. Nucl. Mater. 447 (1-3), S. 125–142.

14 Sublet, Jean-Christophe; Fleming, Michael; Gilbert, Mark R. (2017): From cutting-edge pointwise cross-section to groupwise reaction rate: A primer. In: EPJ Web Conf 146, S. 2003. DOI: 10.1051/epjconf/201714602003.
UKAEA-1102: https://fispact.ukaea.uk/wiki/UKAEA-1102_group_structure
CCFE-709: https://fispact.ukaea.uk/wiki/CCFE-709_group_structure

15 Žerovnik, Gašper (2024): Characterisation of spent LWR fuel with SMR-relevant initial compositions and operational conditions. Federal Office for the Safety of Nuclear Waste Management (BASE). IAEA. Vienna, 21.10.2024. Online verfügbar unter https://conferences.iaea.org/event/374/contributions/31353/, zuletzt geprüft am 07.10.2025.

16 Häkkinen, Silja (2020): Impurities in LWR fuel and structural materials. VTT Technical Research Centre of Finland (VTT Research Report No. VTT-R-00184-20). Online verfügbar unter https://cris.vtt.fi/en/publications/impurities-in-lwr-fuel-and-structural-materials, zuletzt geprüft am 06.10.2025.

17 Terrani, Kurt A. (2018): Accident tolerant fuel cladding development: Promise, status, and challenges. In: J. Nucl. Mater. 501, S. 13–30.

18 Romano, Paul K.; Horelik, Nicholas E.; Herman, Bryan R.; Nelson, Adam G.; Forget, Benoit; Smith, Kord (2015): OpenMC: A state-of-the-art Monte Carlo code for research and development. In: Annals of Nuclear Energy 82, S. 90–97.

19 Romano, Paul K.; Josey, Colin J.; Johnson, Andrew E.; Liang, Jingang (2021): Depletion capabilities in the OpenMC Monte Carlo particle transport code. In: Annals of Nuclear Energy 152, S. 107989.

20 Sublet, J-Ch; Eastwood, J. W.; Morgan, J. G.; Gilbert; Fleming, M.; Arter, W. (2017): FISPACT-II: an advanced simulation system for activation, transmutation and material modelling. In: Nuclear Data Sheets 139, S. 77–137.

21 Plompen, Arjan J. M.; Cabellos, O.; Saint Jean, Cyrille de; Fleming, Michael; Algora, A.; Angelone, Maurizio et al. (2020): The joint evaluated fission and fusion nuclear data library, JEFF-3.3. In: The European Physical Journal A 56 (7), S. 181.

22 Koning, A. J.; Rochman, D.; Sublet, J-Ch; Dzysiuk, N.; Fleming, M.; van der Marck, S. (2019): TENDL: complete nuclear data library for innovative nuclear science and technology. In: Nuclear Data Sheets 155, S. 1–55.

23 Mickus, Ignas (2021): Towards Efficient Monte Carlo Calculations in Reactor Physics: Criticality, Kinetics and Burnup Problems. KTH Royal Institute of Technology.

24 Radhakrishnan, Krishnan; Hindmarsh, Alan C. (1993): Description and use of LSODE, the Livermore solver for ordinary differential equations.

25 Kluyver, Thomas; Ragan-Kelley, Benjamin; Pérez, Fernando; Granger, Brian E.; Bussonnier, Matthias; Frederic, Jonathan et al. (2016): Jupyter Notebooks-a publishing format for reproducible computational workflows. In: Elpub 2016, S. 87–90.

26 Thomas, Fred; Fleming, Michael (2018): Optimised energy group structures for fusion activation calculations. In: Fusion Engineering and Design 136, S. 1479–1483.

References (3)

27 Parga, Clemente J. (2018): M5 Alloy Specification for TREAT Conceptual Fuel Cladding Selection. Idaho National Lab.(INL), Idaho Falls, ID (United States). Online verfügbar unter https://www.osti.gov/biblio/1484704, zuletzt geprüft am 15.10.2025.

28 99.8 % powder purity reported
Yeom, Hwasung; Dabney, Tyler; Johnson, Greg; Maier, Benjamin; Lenling, Mia; Sridharan, Kumar (2019): Improving deposition efficiency in cold spraying chromium coatings by powder annealing. In: The International Journal of Advanced Manufacturing Technology 100, S. 1373–1382.

29 Atlantic Equipment Engineers (2025): Datasheet CR-102-105, Chromium Powder, Electrolytic. Online verfügbar unter https://docs.google.com/document/d/1nOtHzZLs93N8a96WYtCCJGTKnPxhrXcD/edit, zuletzt geprüft am 17.01.2025.

30 J. Lieberoth, “A Monte Carlo Technique to Solve the Static Eigenvalue Problem of the Boltzmann Transport Equation,” Nukleonik, 11, 213-219 (1968).

31 Pusa, M., & Leppänen, J. (2010). Computing the Matrix Exponential in Burnup Calculations. Nuclear Science and Engineering, 164(2), 140–150. https://doi.org/10.13182/NSE09-14

32 Pusa, M. (2011). Rational Approximations to the Matrix Exponential in Burnup Calculations. Nuclear Science and Engineering, 169(2), 155–167. https://doi.org/10.13182/NSE10-81

33 Maria, P. (2016). Higher-Order Chebyshev Rational Approximation Method and Application to Burnup Equations. Nuclear Science and Engineering, 182(3), 297–318. https://doi.org/10.13182/NSE15-26

34 Thalhammer, M. (2006). A fourth-order commutator-free exponential integrator for nonautonomous differential equations. SIAM journal on numerical analysis, 44(2), 851-864.

Annex

Federal Office
for the Safety of
Nuclear Waste Management

BASE missions and tasks

BASE – Mission and Tasks

- **Regulation:** Disposal, storage and transport of HLW.

- **Supervision:** Deep geological disposals for LAW and MAW.

- **Site selection:** Repository site process and public participation.

- **Expertise:** Advisory role to the federal ministry.

- **Research:** Conducting and financing task-related research

Research at BASE

BASE initiates in-house research projects and awards research contracts to companies and institutes also in the field of nuclear safety (SMR, P&T, ATF)…

Funding of BASE research

- Own research budget (~3.2 M€/a)
- Personnel expenses (desk/scientific officers)
- PhD program (1 finished, 2 ongoing)
- Departmental research plan of the Federal Ministry for the Environment, Climate Action, Nature Conservation and Nuclear Safety (BMUKN)

Federal Office
for the Safety of
Nuclear Waste Management

Research regarding accident-tolerant fuels

Recently finished research project conducted by GRS

- Up-to-date summary of developments
- Simulation of accident scenarios (TMI-2 und Fukushima Daiichi) with FeCrAl cladding with AC2
- *https://www.base.bund.de/de/forschung/themenfelder/nukleare-sicherheit/_documents/atf_sicherheitsanalyse.html*

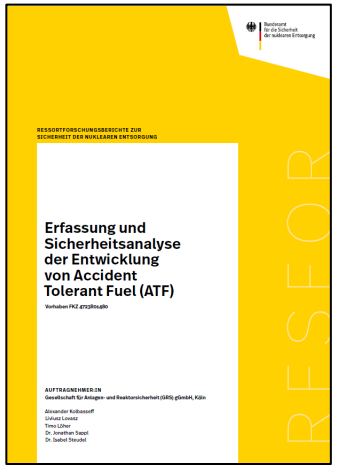

Ongoing in-house research project “ReUnFis”

- Period: July 24 to December 26
- Burn-up simulation of pin-cells with M5+20µmCr, FeCrAlC26M, SiC/SiC+10µmCr in OpenMC
- ATF cladding metrics (opt. impurities) with FP-II

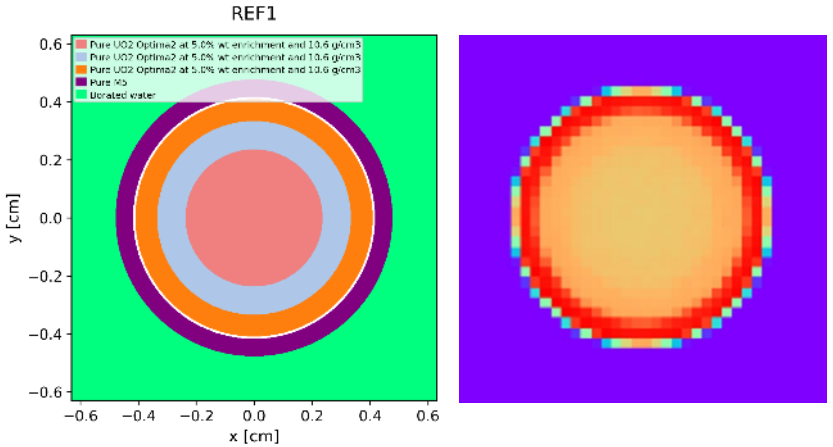

Constant pellet/gap and pitch impacts

Constant pellet impact

Modelling choice

Constant pellet and gap dimensions & change of cladding outer diameter (at constant pitch)

→ HM_i ≈ constant

→ Fair comparison on BU scale (MWd per $kgHM_i$)

Main impacts in ATF cells

1. Reactivity change due to change in cladding thickness (H/U atom ratio change)
2. Reactivity penalty due to cladding neutron capture (FeCrAl, Cr)
3. Reactivity change due to necessary enrichment offset (counterbalance Nr. 2)
4. Differently evolving reactivity impact due to fuel neutron capture (FPs, trans-U, NT-coupled inventory change)

Federal Office
for the Safety of
Nuclear Waste Management

OpenMC k_{inf}

Definition of k_{inf} (in OpenMC)

K_{inf} = A / (B-C)

A: Fission neutrons produced per src

B: Neutrons absorbed per src

C: Neutrons prod. by (n,xn) per src

A = Fission rate [fiss/s] * v [neutrons/fiss]

All models with same power and energy deposition (heating-local tally)

→ Flux level adjustment to total nuclear heating (eV from reactions)

→ Thermal flux level main driver of heating (fission)

→ Fission rate driven by flux level

→ BU leads to shift in flux level (FPs) and v (U35→Pu39)

B = Neutron absorption in model (fuel +moderator +clad)

Main source of evolving neutron poison: neutron capture rate in fuel

+ neutron capture in the cladding

→ For interpreation of k_{inf} difference

C: (skipped)

Federal Office
for the Safety of
Nuclear Waste Management

OpenMC: Effect of pure dopants

Homogenous dilution

Impact of doping with Cr_2O_3 and Al_2O_3

800 ppm of pure Cr_2O_3 and pure 200 ppm Al_2O_3
HM +0.65%, density increase +0.75%

Reactivity difference around 0.

Negligible impact on reactivity for pure dopants.

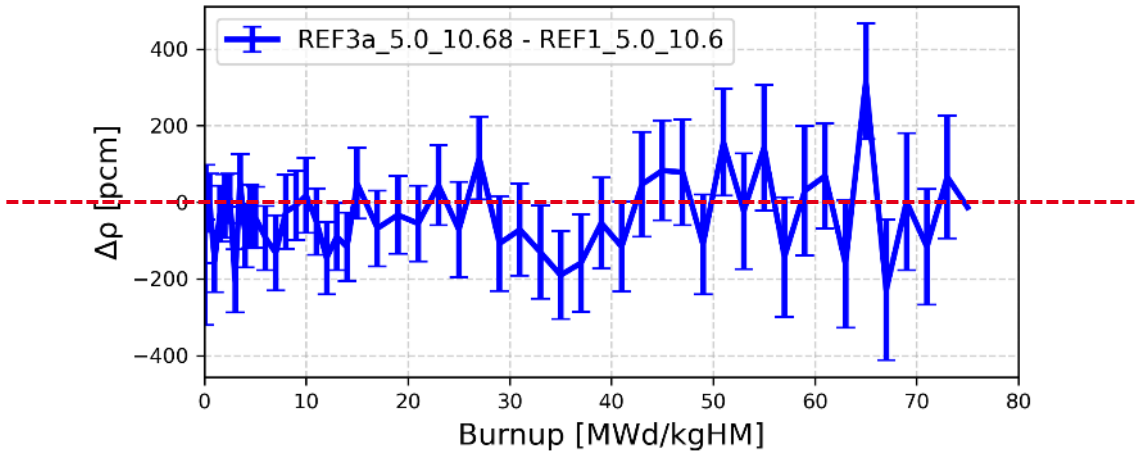

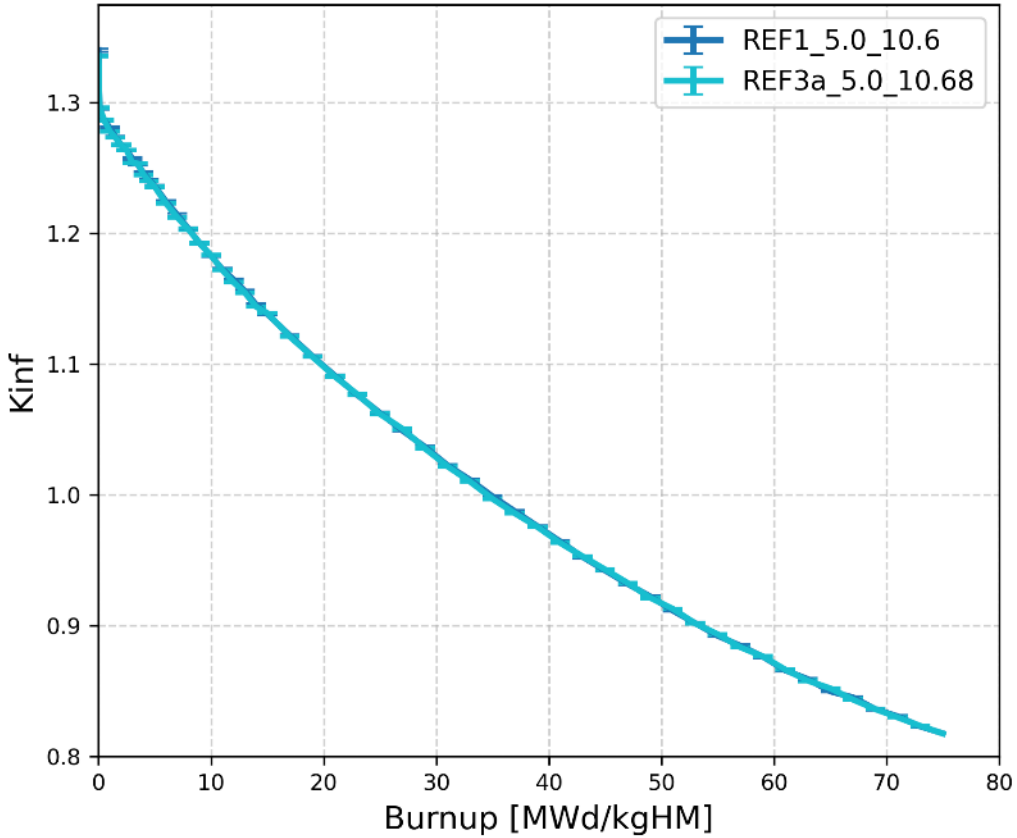

Federal Office
for the Safety of
Nuclear Waste Management

Fuel fission and capture rate ratio vs. BU

ATF1a, ATF2a, ATF3a vs REF3a

Fuel fission and fuel capture rate case ratios

ATF1a/REF3a

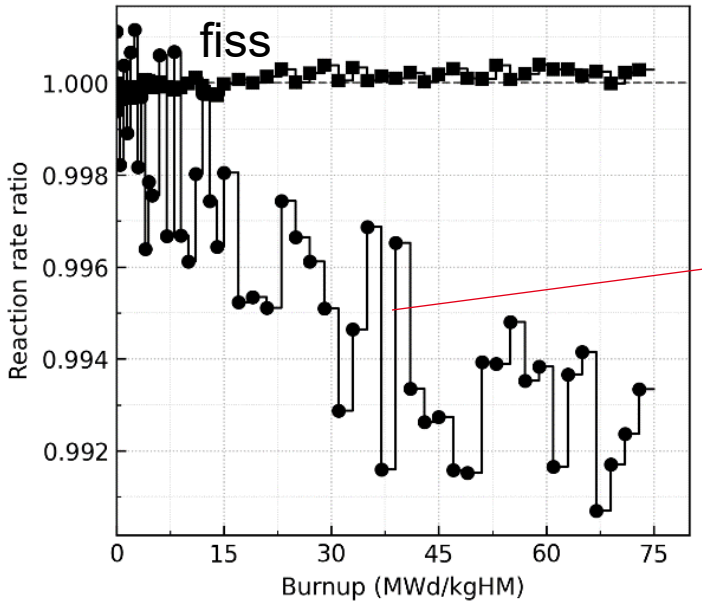

- Decreasing fuel capture rate in ATF1a (wrt REF3a)
- Higher reactivity of ATF1a at later BU

ATF2a/REF3a

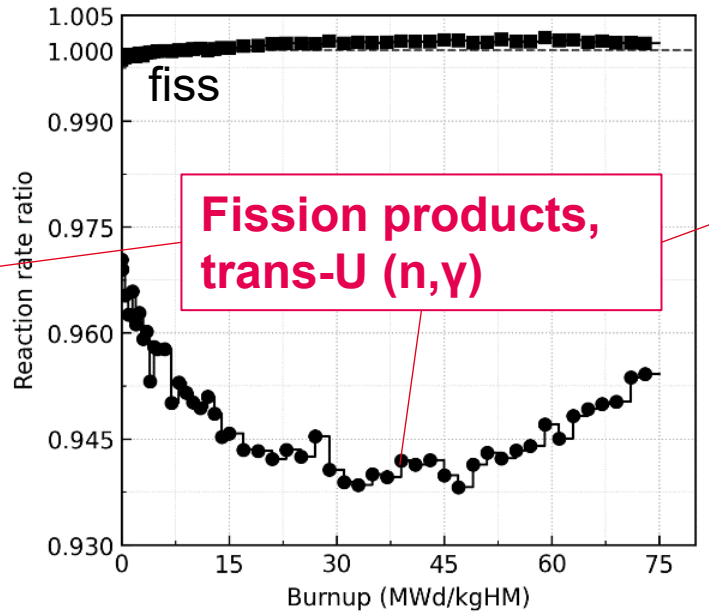

- Lower fuel capture in ATF2a (wrt REF3a).
- Higher clad capture outweighs lower fuel capture at BOI (net reactivity penalty).
- Capture evolution consistent with Δρ evolution

Enrichment▲→ Flux level▼ + Flux hardening▲ (but also hardening▼ due to Moderation▲)

ATF3a/REF3a

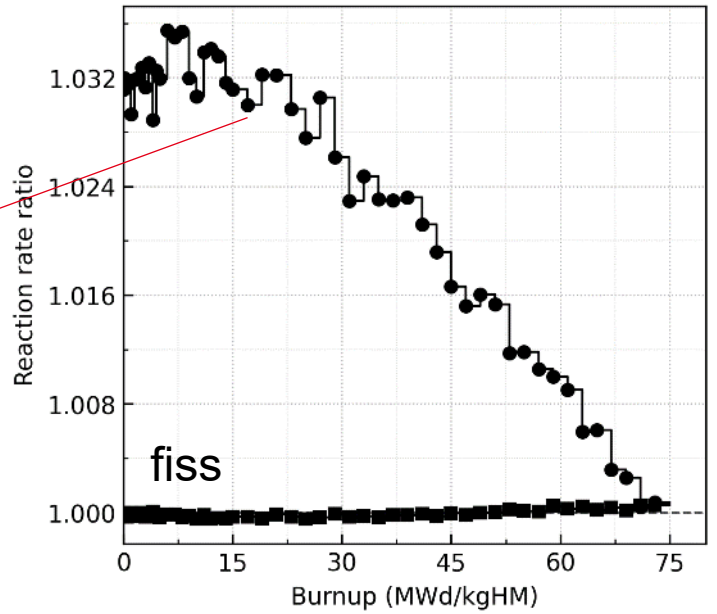

- Higher fuel capture in ATF3a (wrt REF3a).
- Decreasing fuel capture ratio partly explains increasing reactivity difference.

Moderation▼ → Flux level▲ (impacting capture rates)

Federal Office
for the Safety of
Nuclear Waste Management

4 factor formula vs BU

ATF2a vs REF3a, ATF3a vs REF3a

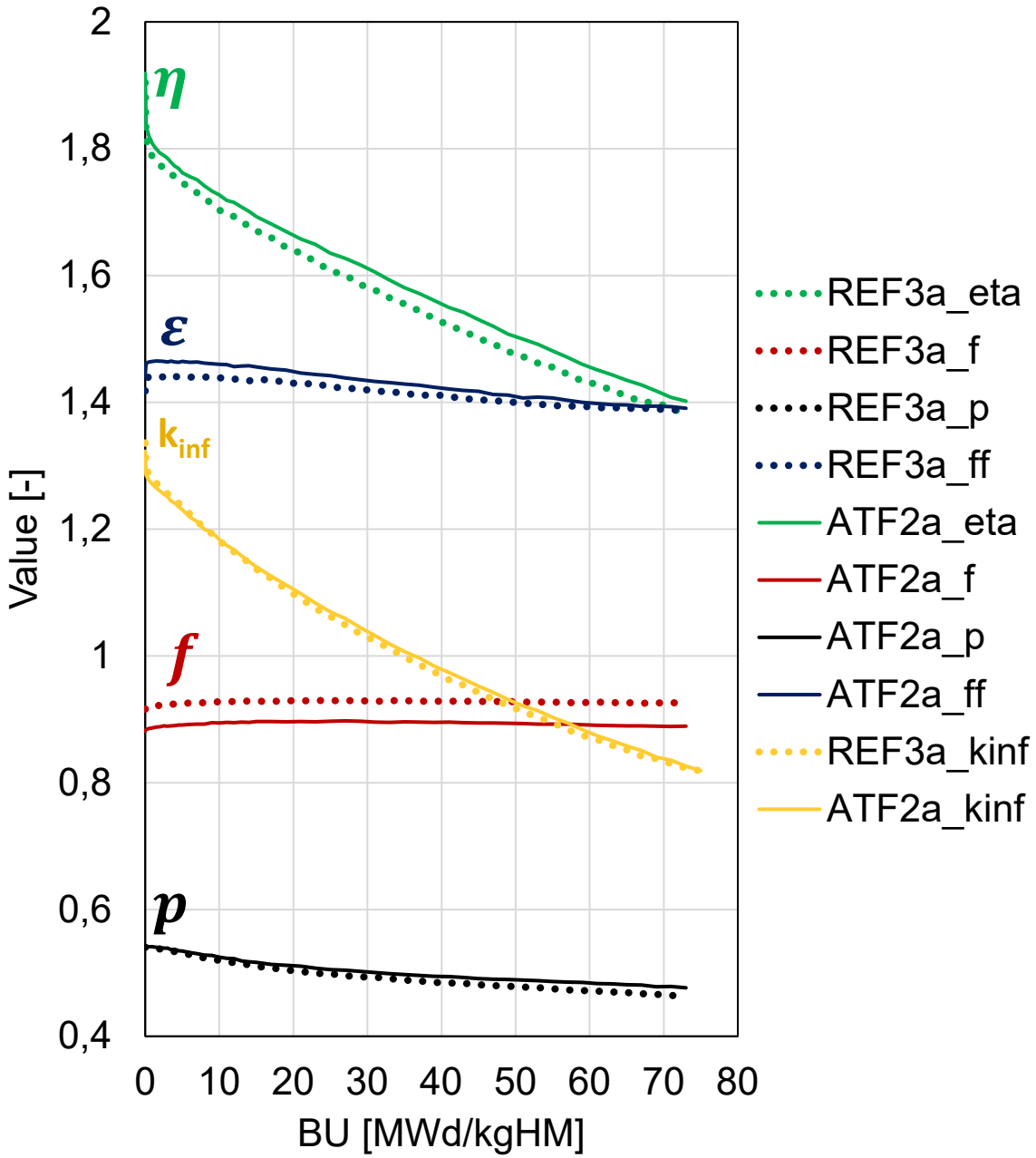
2
1,8
1,6
1,4
1,2
1
0,8
0,6
0,4
Value [-]
η
ε
k_inf
f
p
0
10
20
30
40
50
60
70
80
BU [MWd/kgHM]
REF3a_eta
REF3a_f
REF3a_p
REF3a_ff
ATF2a_eta
ATF2a_f
ATF2a_p
ATF2a_ff
REF3a_kinf
ATF2a_kinf

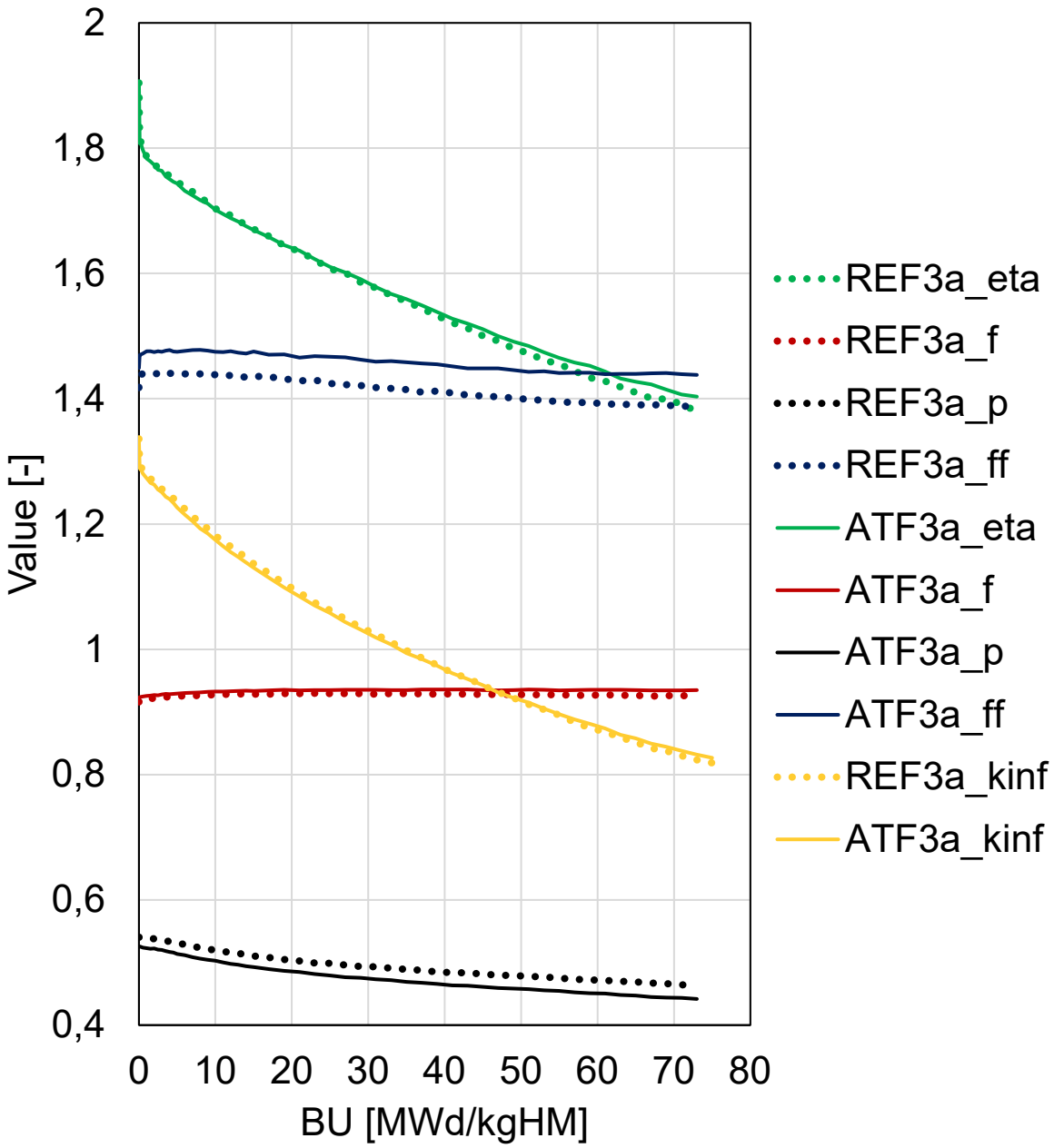
2
1,8
1,6
1,4
1,2
1
0,8
0,6
0,4
Value [-]
0
10
20
30
40
50
60
70
80
BU [MWd/kgHM]
REF3a_eta
REF3a_f
REF3a_p
REF3a_ff
ATF3a_eta
ATF3a_f
ATF3a_p
ATF3a_ff
REF3a_kinf
ATF3a_kinf

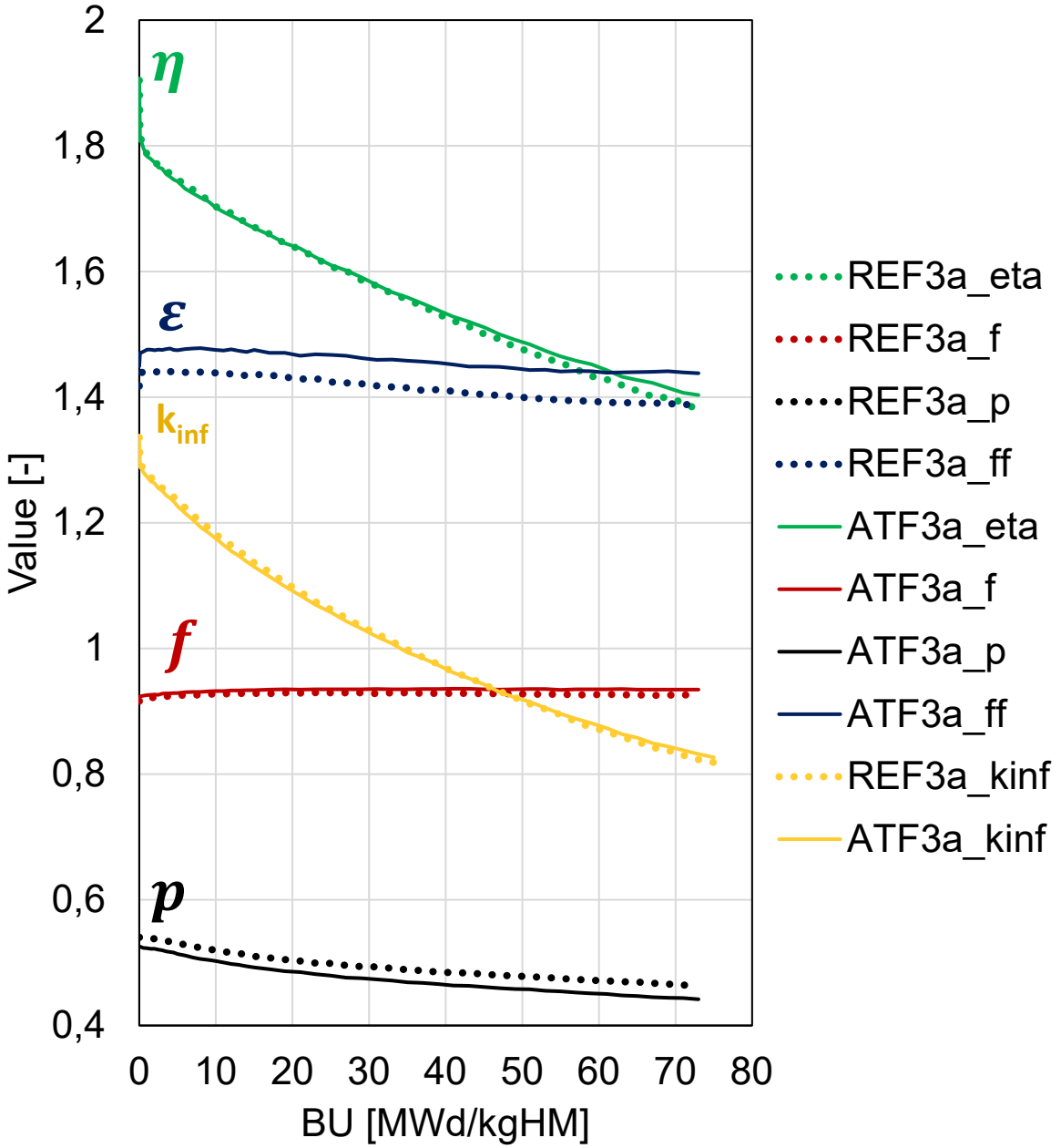
η
ε
k_inf
f
p
Value [-]
BU [MWd/kgHM]
REF3a_eta
REF3a_f
REF3a_p
REF3a_ff
ATF3a_eta
ATF3a_f
ATF3a_p
ATF3a_ff
REF3a_kinf
ATF3a_kinf

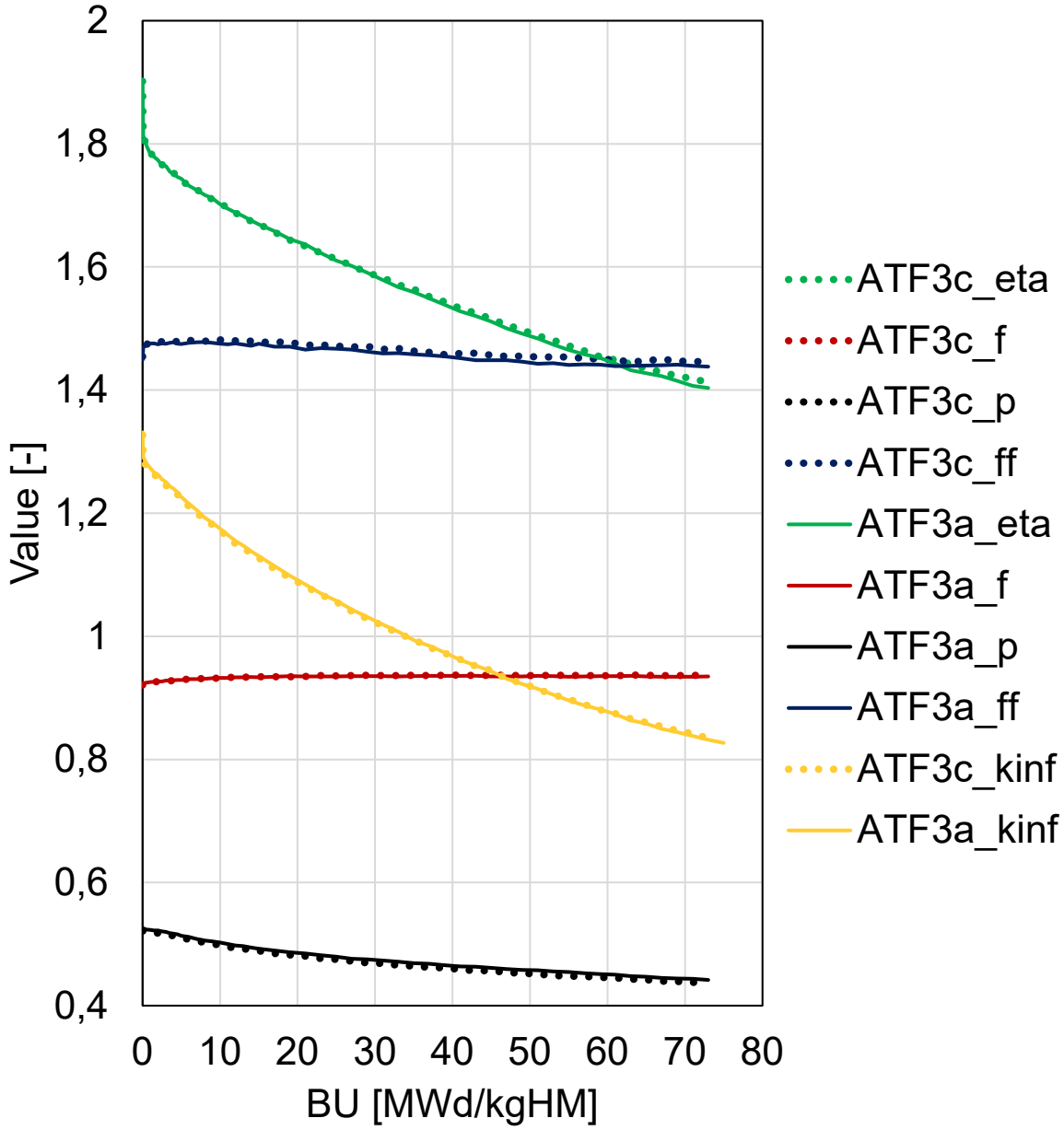
Value [-]
BU [MWd/kgHM]
ATF3c_eta
ATF3c_f
ATF3c_p
ATF3c_ff
ATF3a_eta
ATF3a_f
ATF3a_p
ATF3a_ff
ATF3c_kinf
ATF3a_kinf

Flux change with BU

Flux change with BU (45.7 W/gU$_i$, 4.95 gU$_i$/cm)

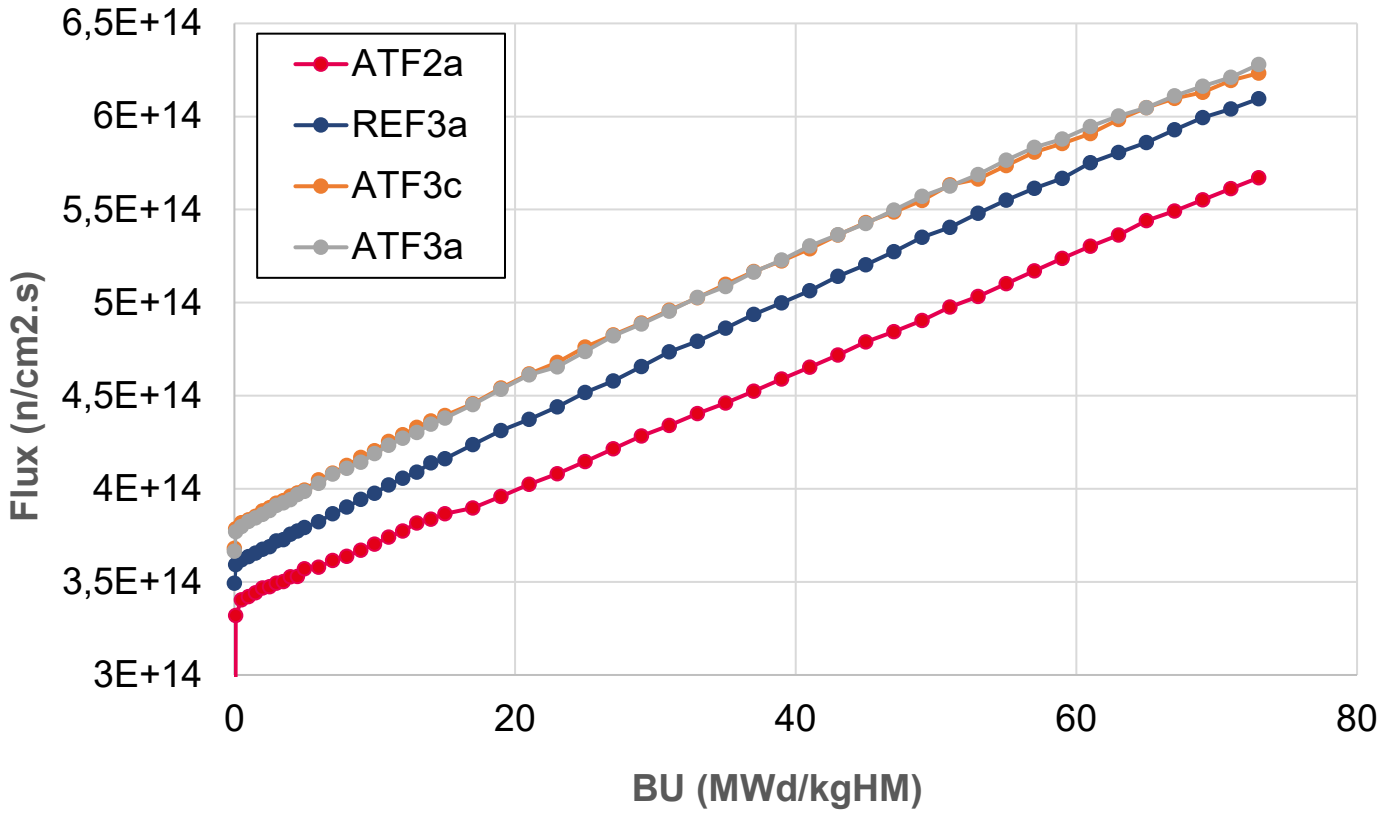

Spectral shifts

Flux ratio to REF3a for ATF1a, ATF2a and ATF3a

ATF1a flux level ~= REF3a flux level

Flux level lowest for **ATF2a** to achieve constant specific power → 5.6 wt% and thinnest cladding (better moderation)

ATF3a needs highest neutron population (thickest cladding at 5.0 wt%), decreasing flux ratio

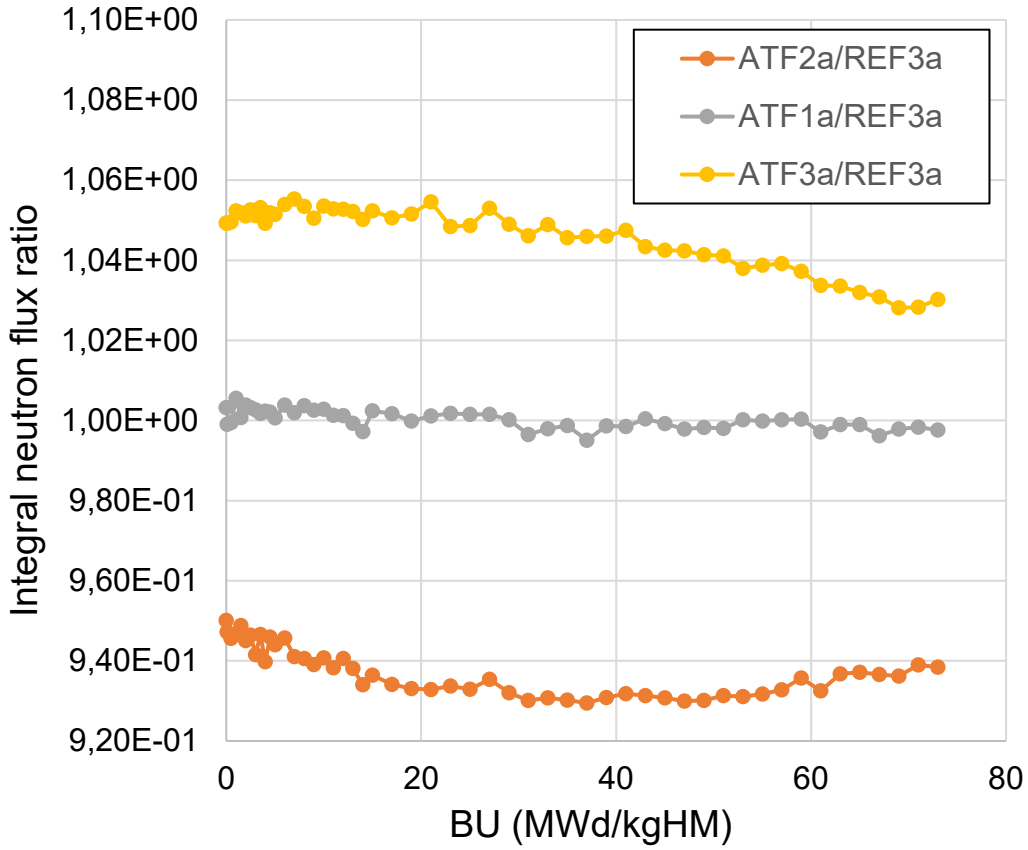

Describing neutron spectrum energy shifts

Thermal indices

How much fission from P39 and U35 compared to neutrons capture in U38?

- $P39_{fiss}/U38_{cap}$
- $U35_{fiss}/U38_{cap}$

Fast index

How much U38 threshold fission >1MeV compared to neutron capture in U38?

- $U38_{fiss}/U38_{cap}$

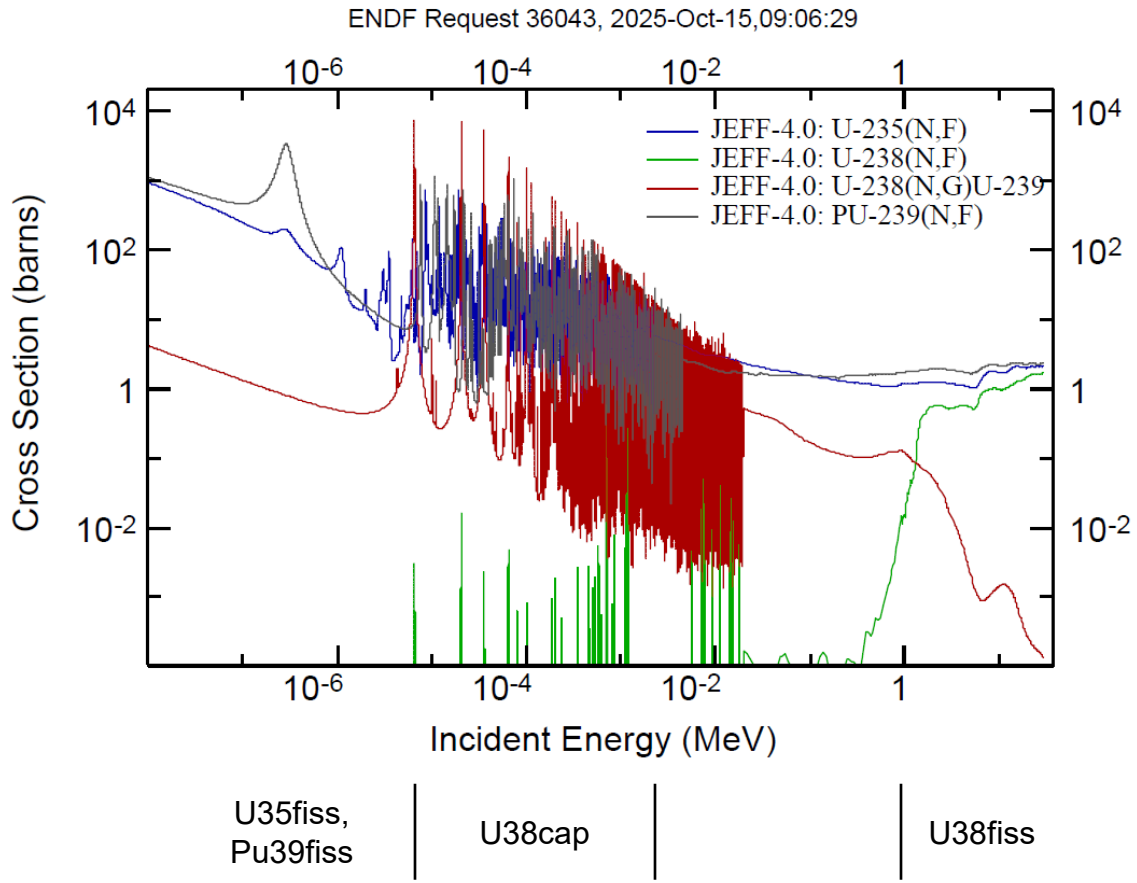

ATF1a/REF3a

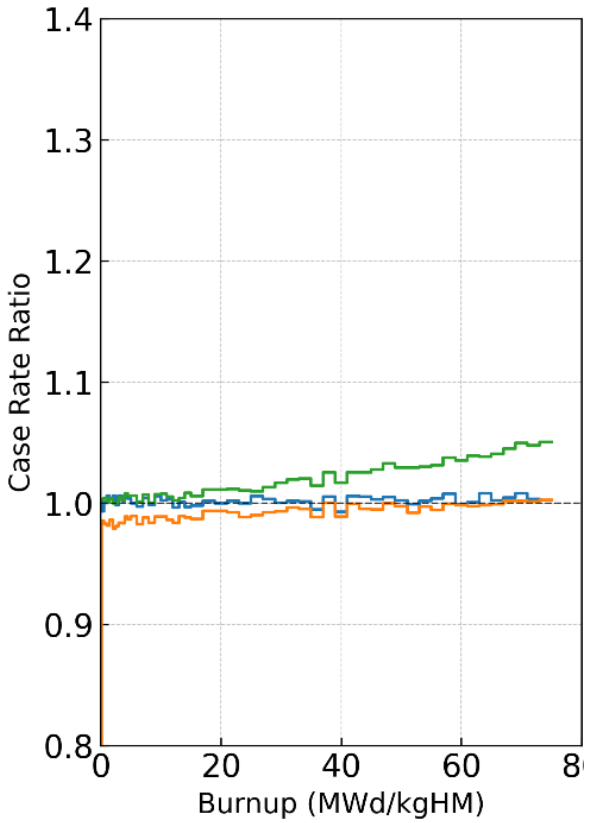

ATF2a/REF3a

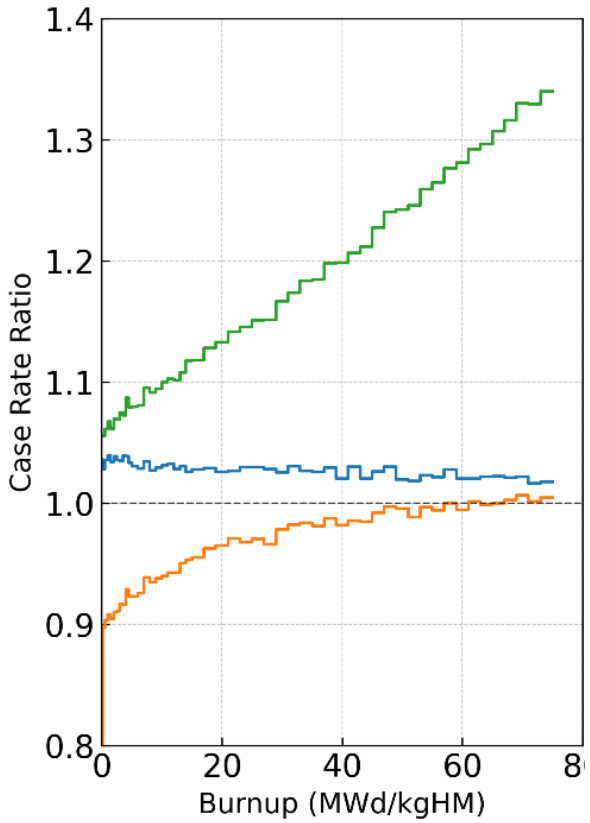

ATF3a/REF3a

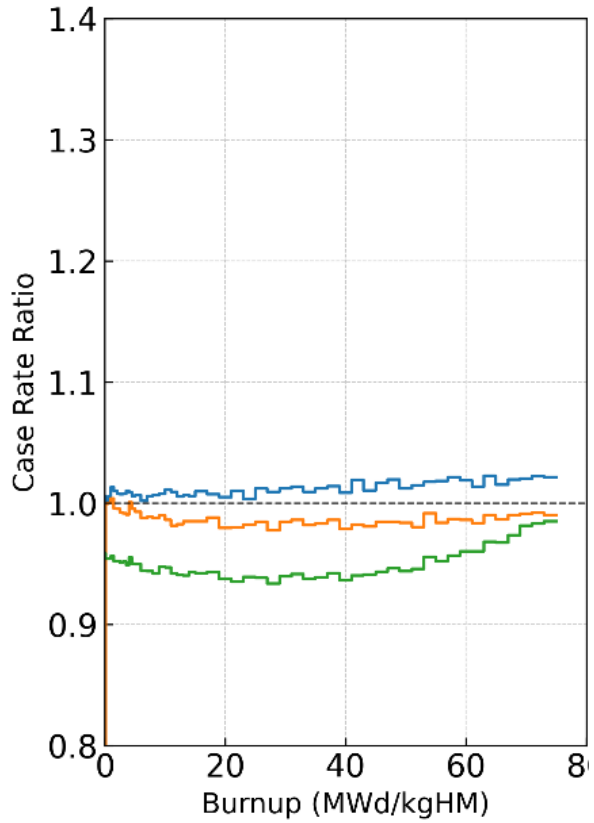

P39fiss/U38cap
U35fiss/U38cap
$U38_{fis}/U38_{cap}$

Small differences in SIs.
U35fiss/U38cap increasing (indicates stronger spectrum softening of ATF1a).

ATF2a with higher fast spectrum component (U238fiss/U238cap).
Increasing thermal SI ratios indicate stronger thermal softening with BU for ATF2a.

Lower thermal spectrum component of ATF3a (worse moderation higher U38cap).
Spectrum hardening (U38fis/U38cap)

BOI fuel neutron spectra shape (UKAEA-1102[14])

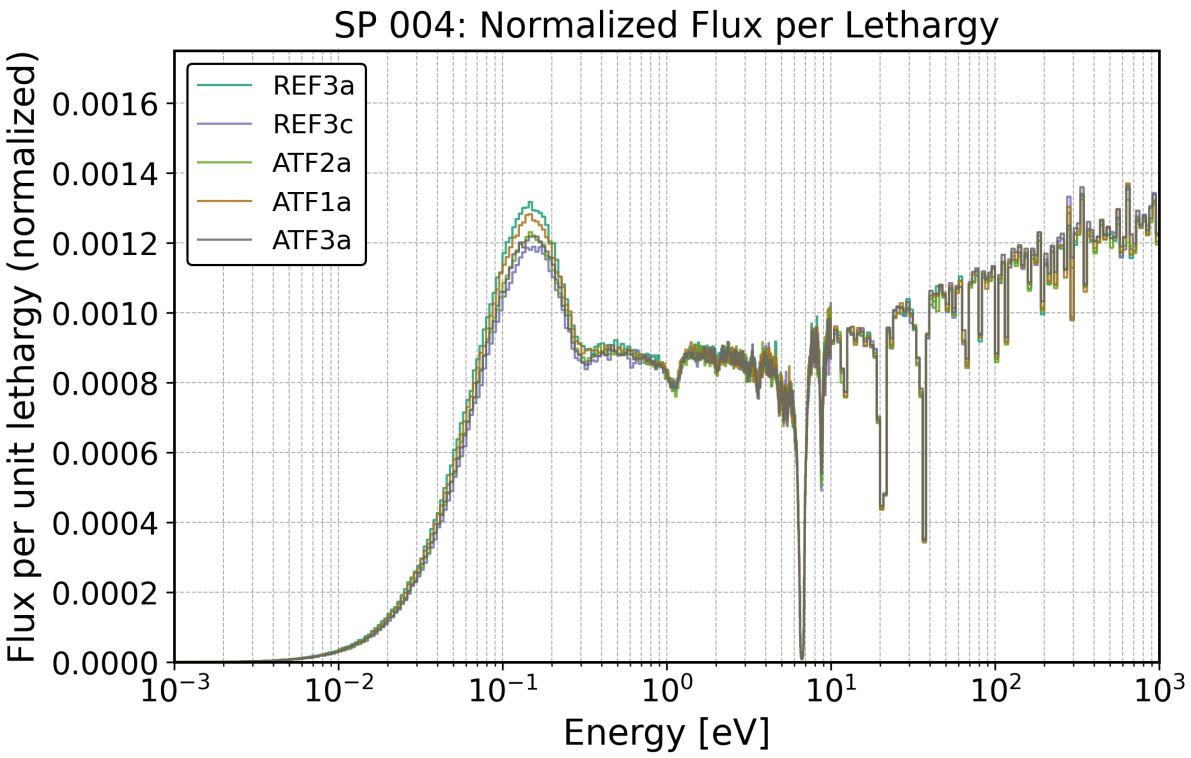

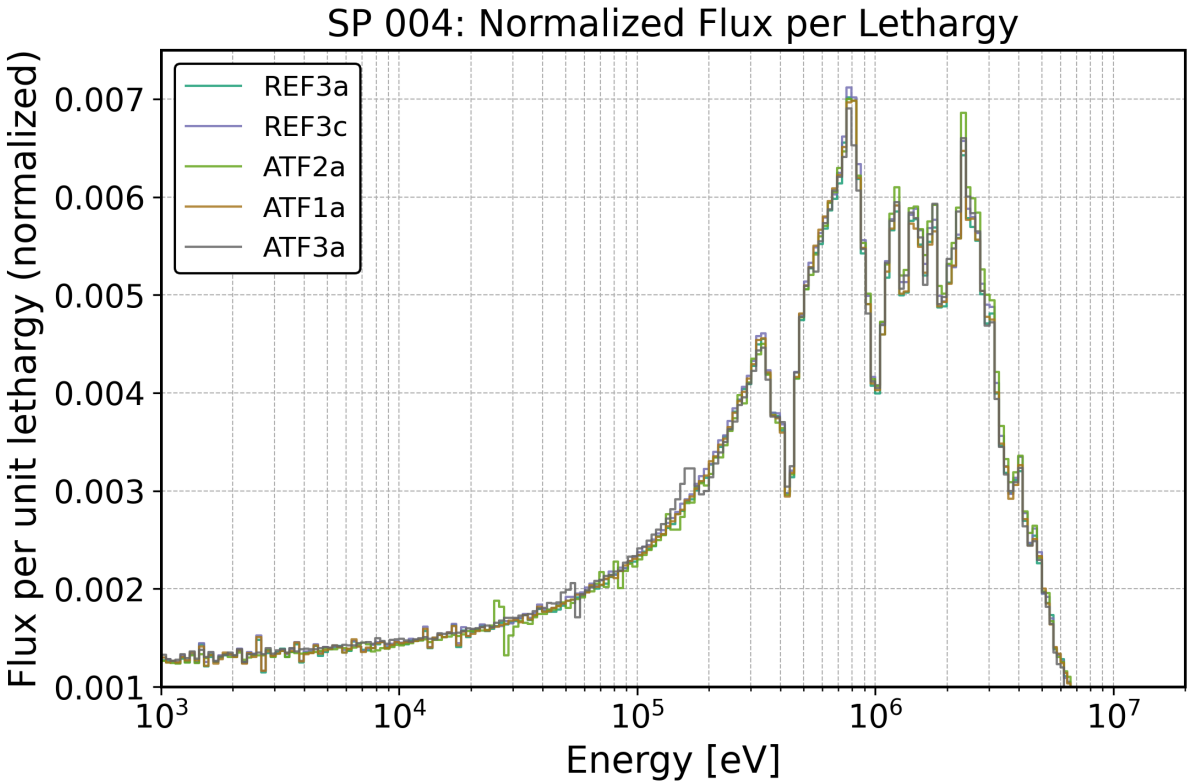

Thermal peak ranking	Case	Enrichment	Moderation
1	REF3a	5.0	0
2	ATF1a	5.1	0
3	ATF3a / ATF2a	5.0 / 5.6	- / +
4	REF3c	5.6	0

EOI fuel neutron spectra shape (UKAEA-1102[14])

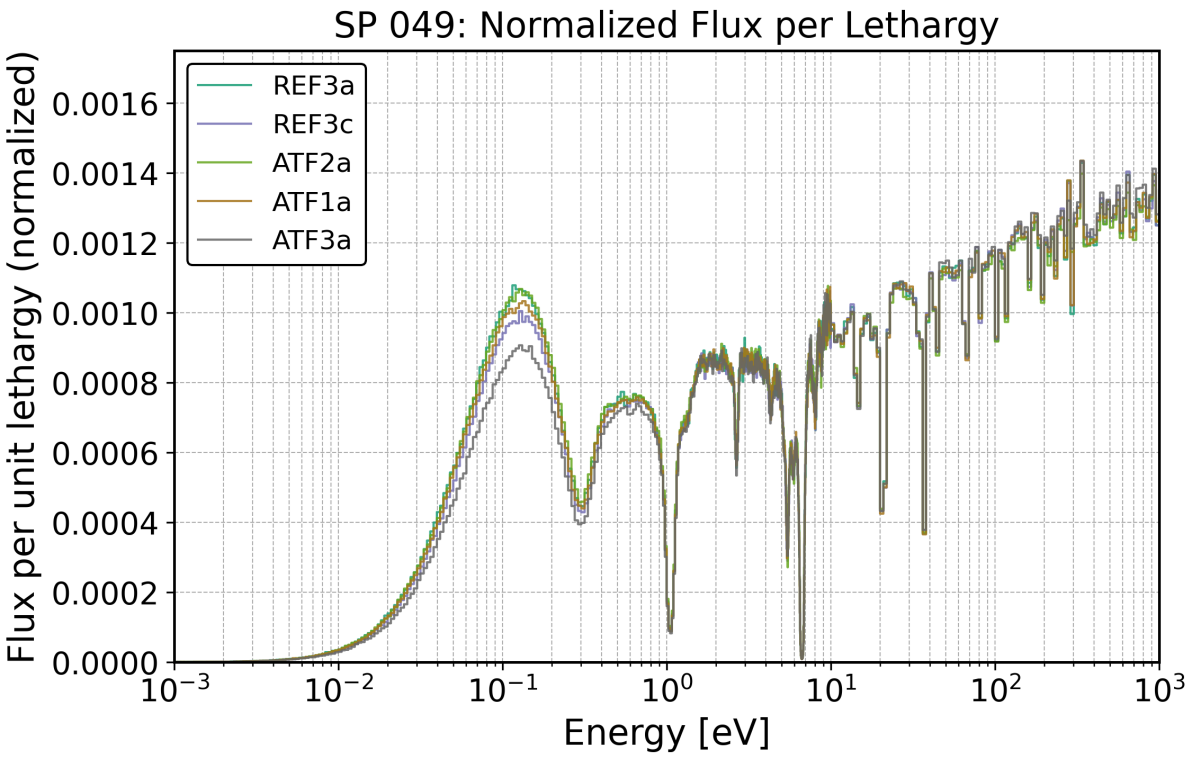

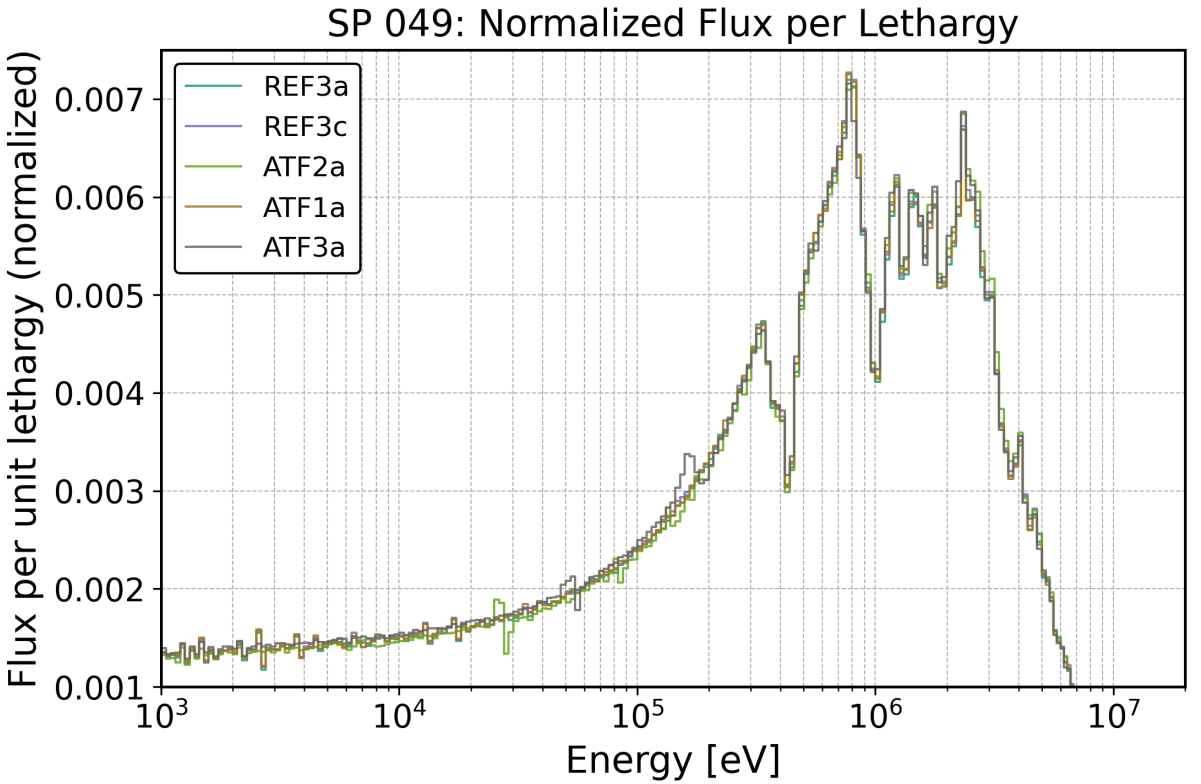

Thermal peak ranking	Case	Enrichment	Moderation
1	REF3a / ATF2a	5.0 / 5.6	0 / +
2	ATF1a	5.1	0
3	REF3c	5.6	0
4	ATF3a	5.0	-

Spectrum conclusions

Increasing enrichment decreases thermal peak and reduces flux level for defined specific power.

Reducing cladding thickness at 5.6% increases thermal peak (BOI REF3c vs ATF2a) due to improved moderation (also necessitates lower flux level to maintain power)

Thermal peak lowest for 5.0% ATF3a with thickest cladding (BOI/EOI REF3a vs ATF3a): indicates impact of lower moderation.

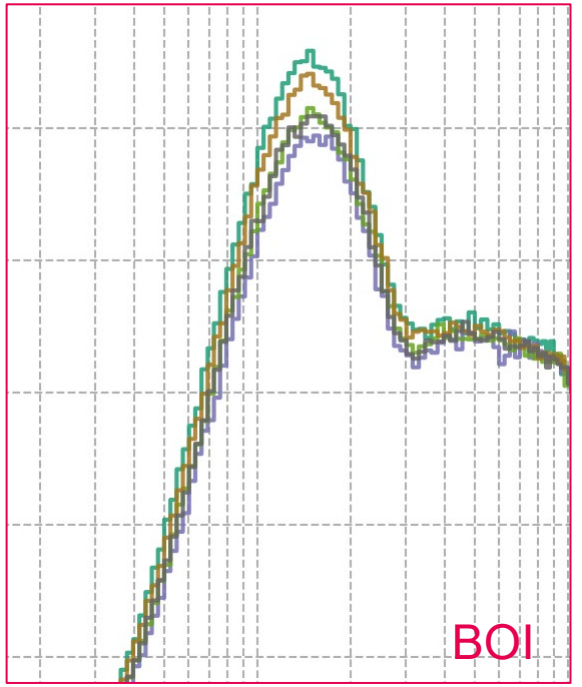

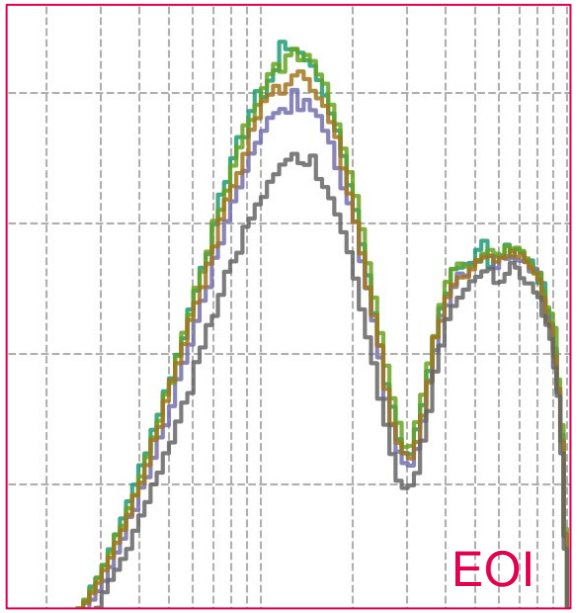

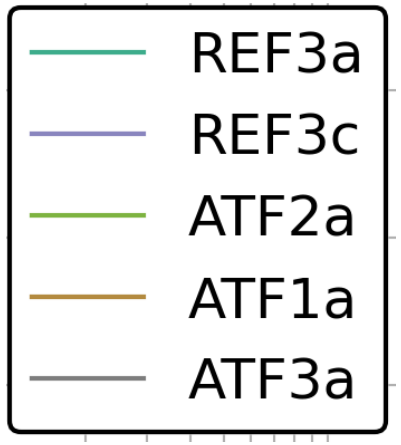

Federal Office
for the Safety of
Nuclear Waste Management

ATF3a vs ATF3c

600K/900K vs 700K/1100K
(clad/fuel)

ATF3a (600, 900 K) vs ATF3c (700, 1100K)

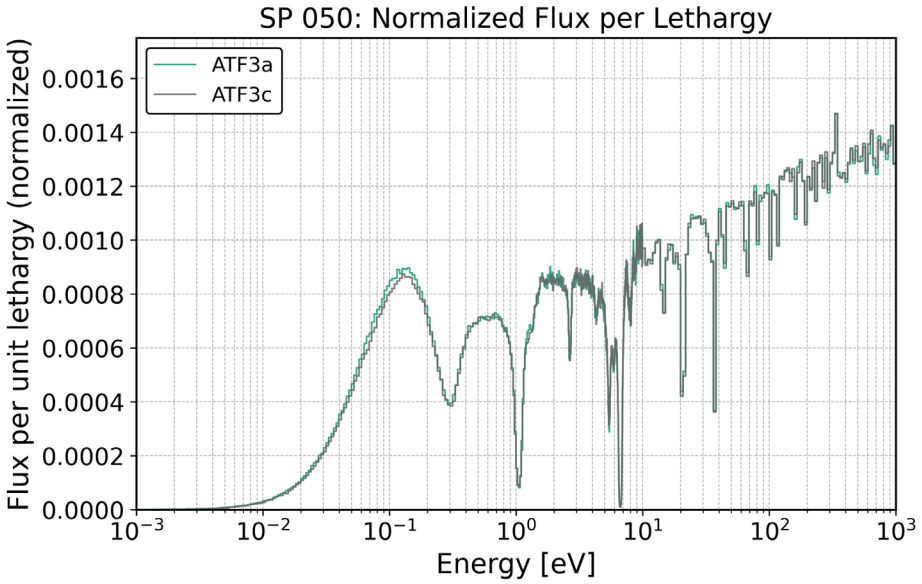

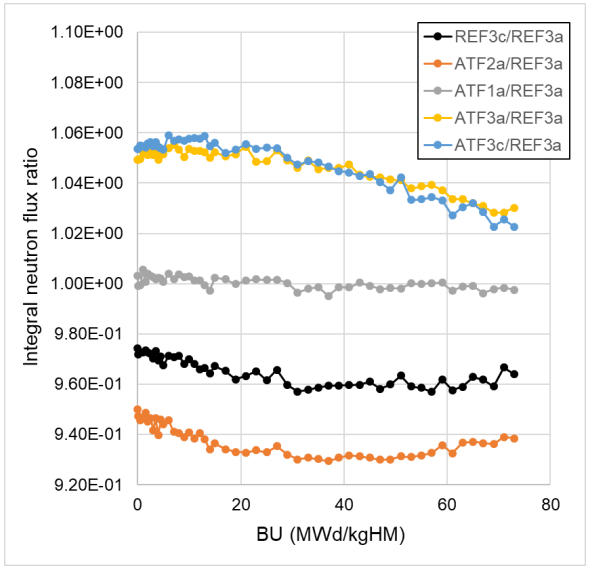

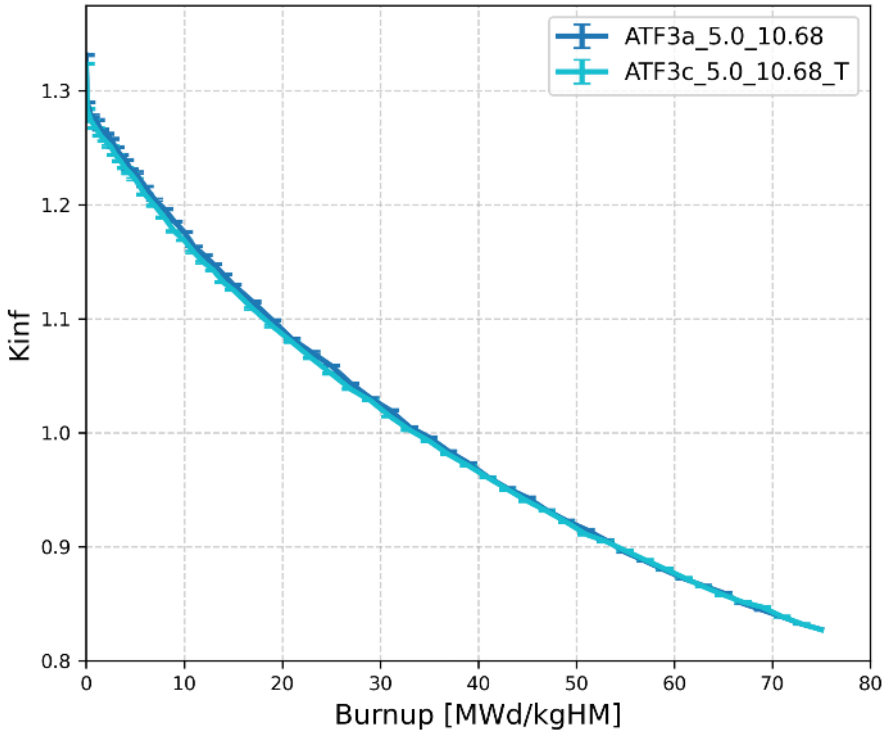

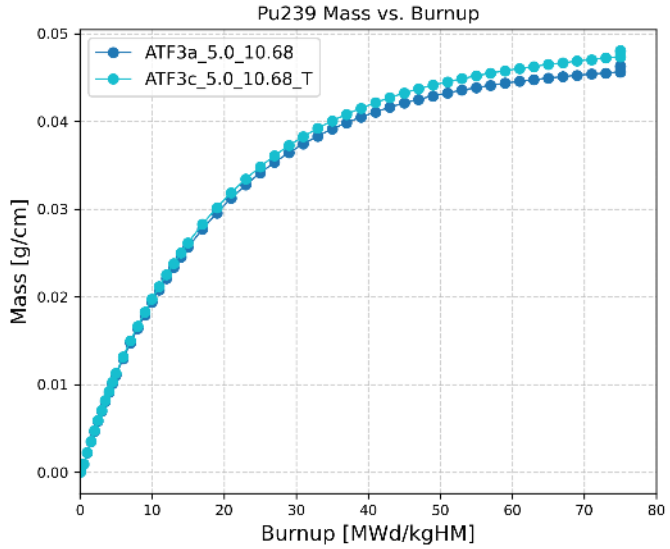

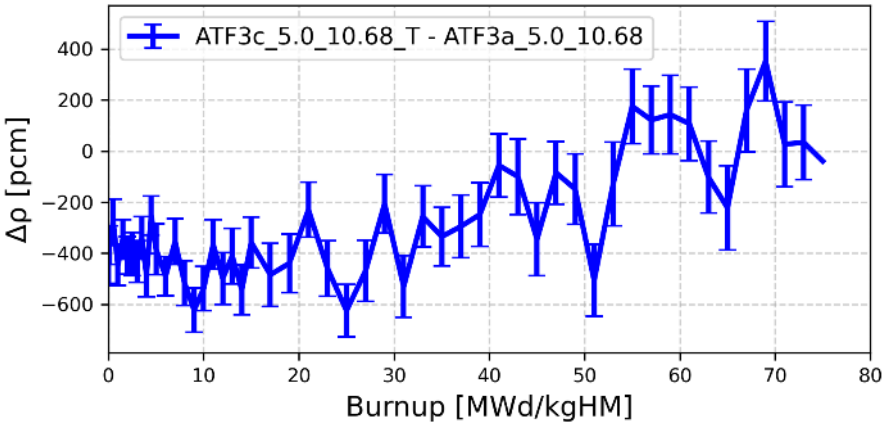

Federal Office
for the Safety of
Nuclear Waste Management

JEFF4 cross-sections

Silicon and Carbon

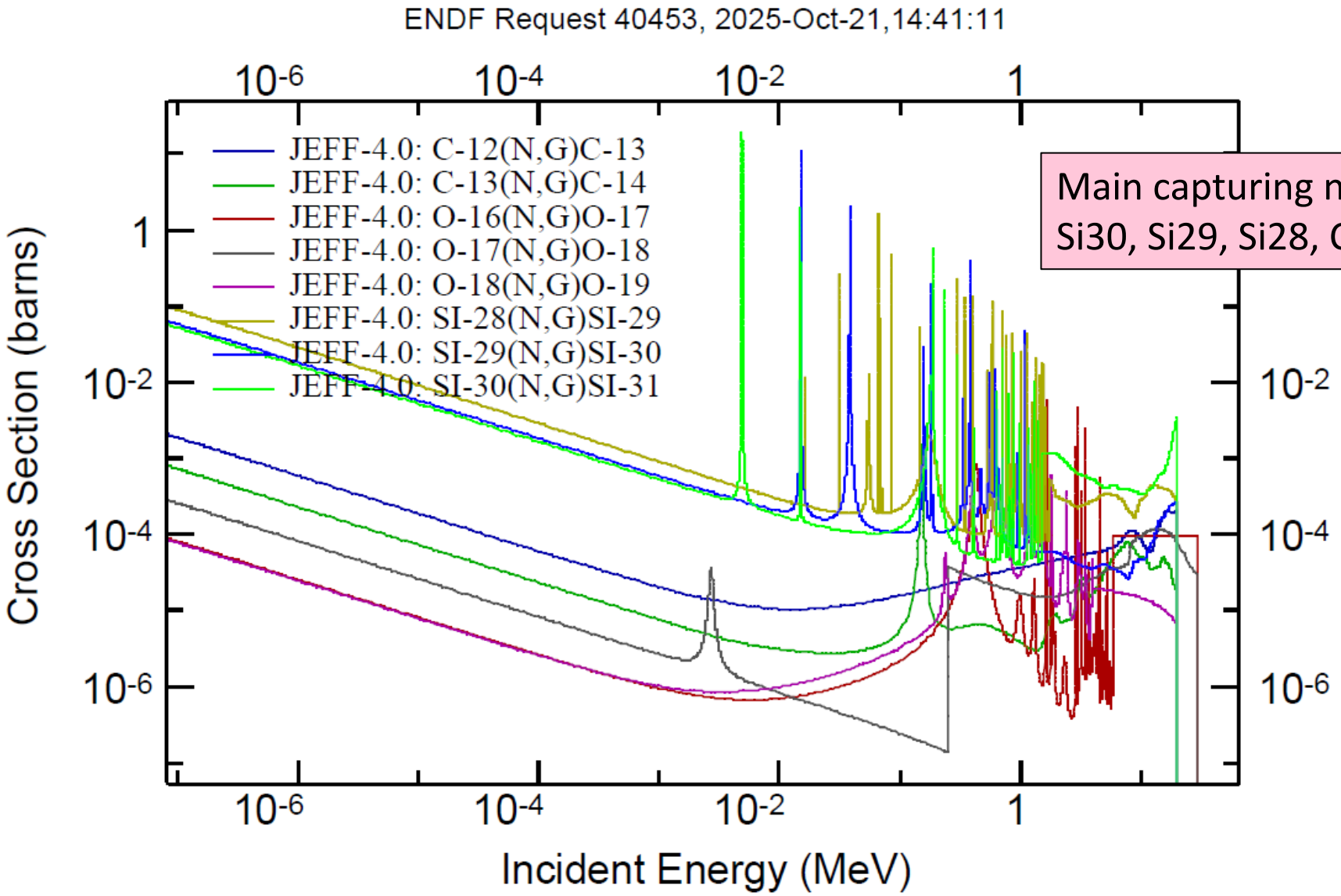

Main capturing nuclides in SiC/SiC:
Si30, Si29, Si28, C13, O18

https://www-nds.iaea.org/exfor/endf.htm

Federal Office
for the Safety of
Nuclear Waste Management

JEFF4 vs. JEFF3.3

M5 + 20 µm Cr (pure) ATF1a
M5 + 20 µm Cr (with impurities) ATF1b

Nuclear data impact: JEFF-3.3 vs JEFF-4

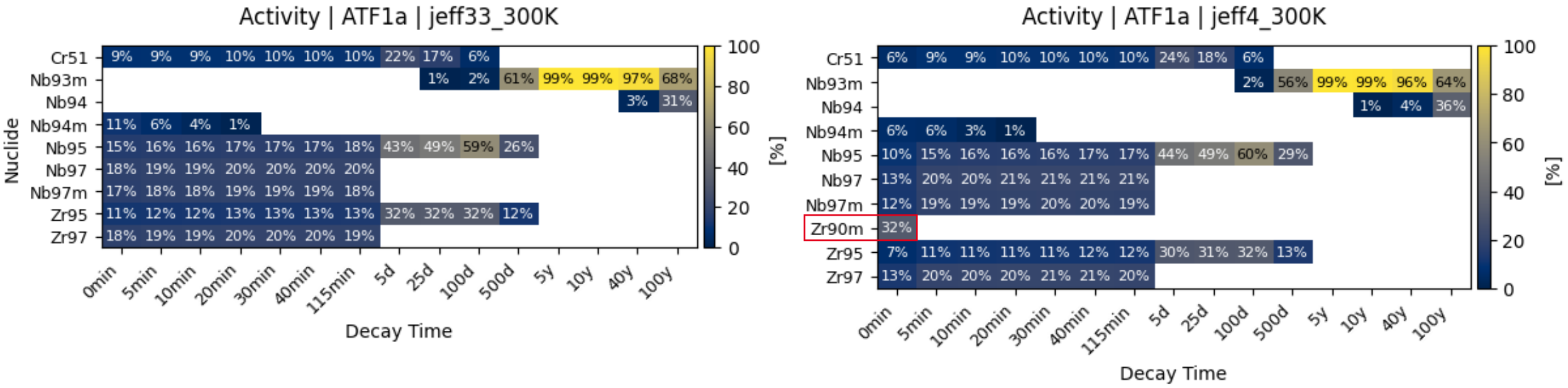

Relative nuclide contributions to activity vector very similar for JEFF-3.3 vs JEFF-4.

(except for Zr90m at EOI for JEFF-4)

JEFF-3.3 vs JEFF-4 on total Bq/cm for ATF1a clad

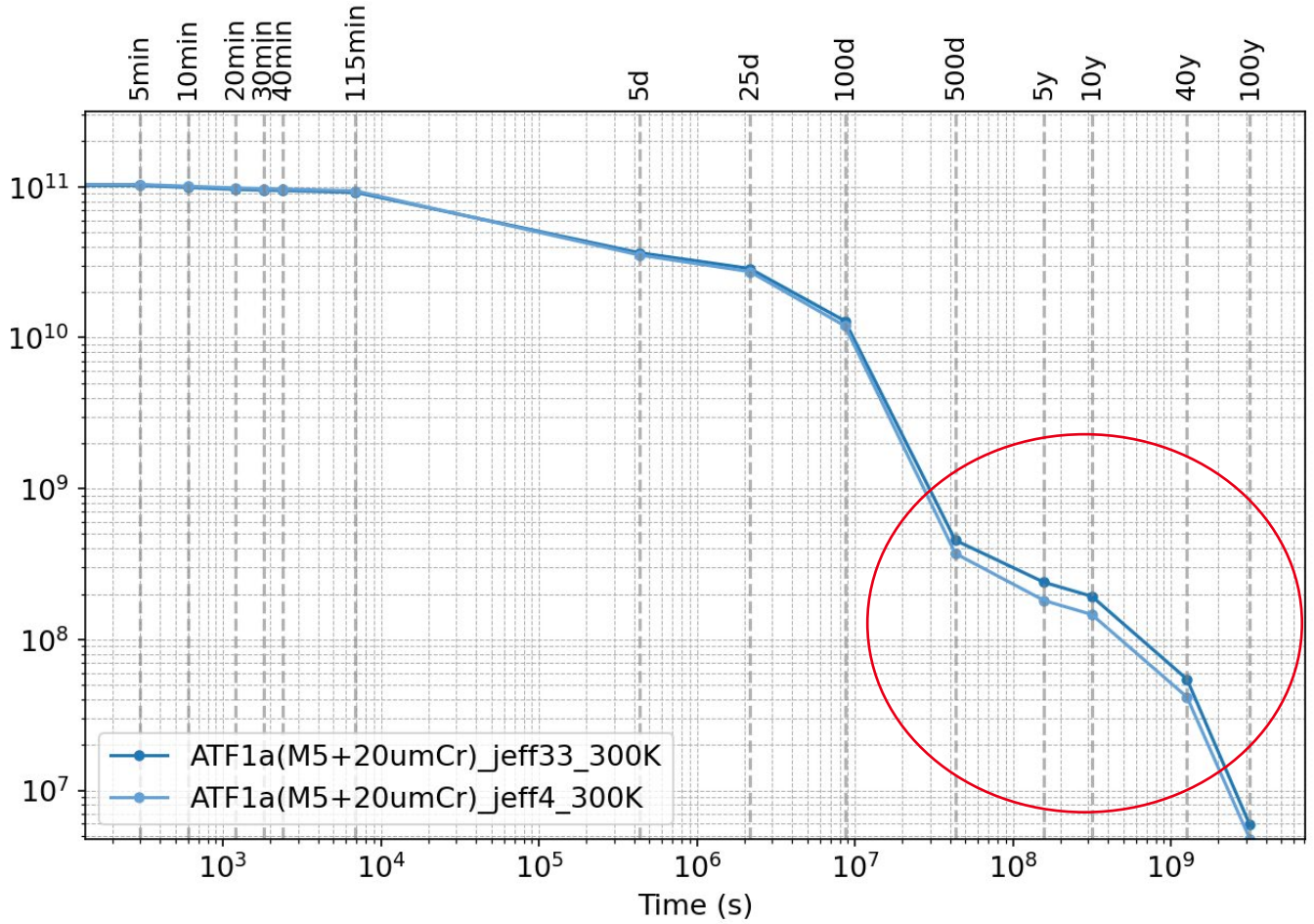

Library impact up to 30 % on total activity (here mainly due to Nb93m).

Higher estimation in JEFF-3.3 due to σ(E) difference (TENDL15 vs TENDL23)

Nb93m activity uncertainty (FP-II) with MOI spectrum:

- JEFF-3.3 → ~6.6 %
- JEFF-4 → ~12.5 %

Impurity impact: JEFF4

ATF1a

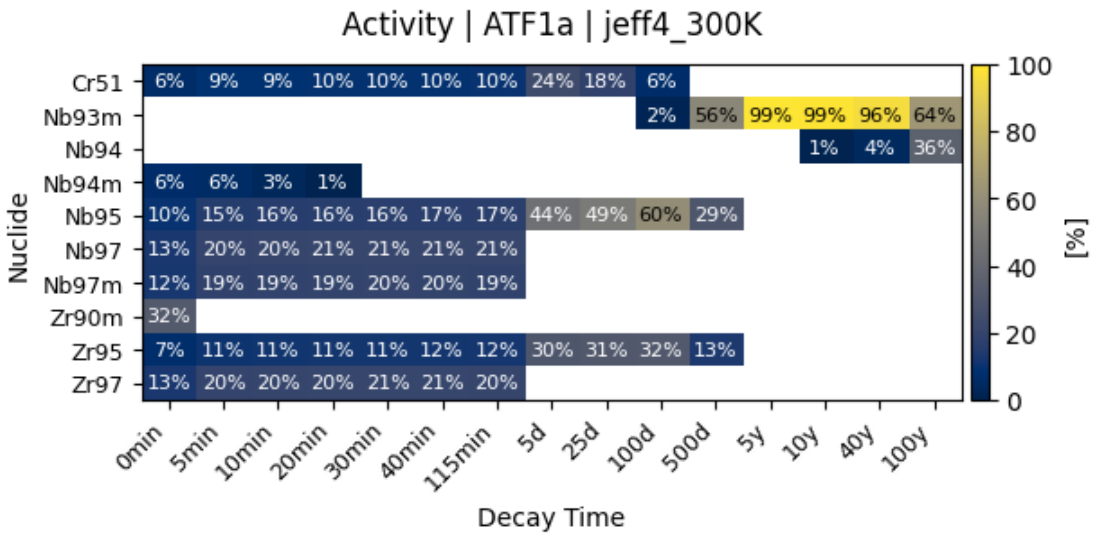

ATF1b

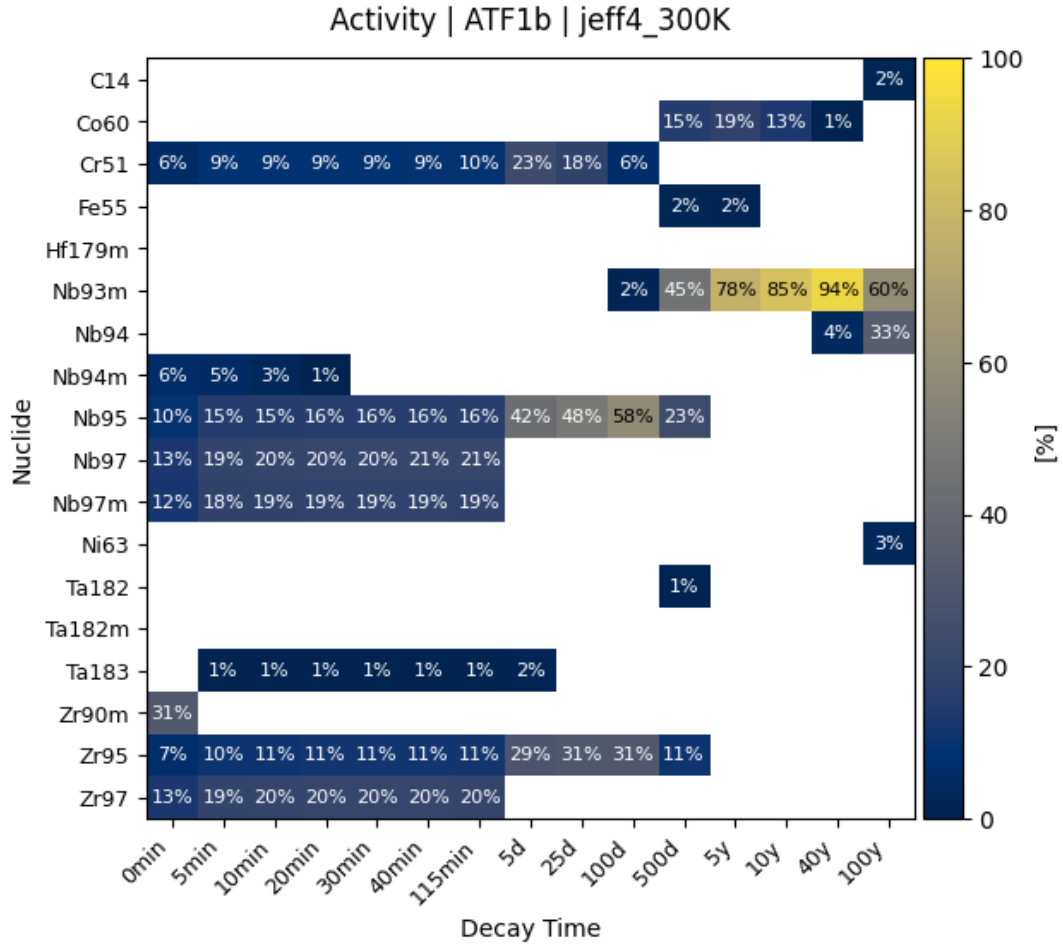

Nuclear data library impact: $\frac{\text{Activity(JEFF3.3)}}{\text{Activity(JEFF4)}}$

ATF1a

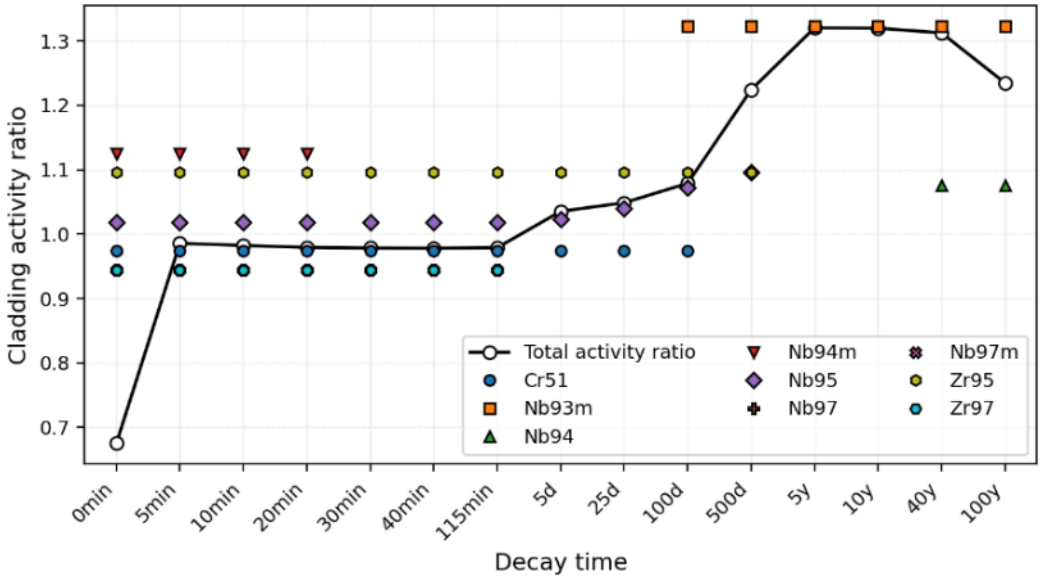

ATF1b (with impurities)

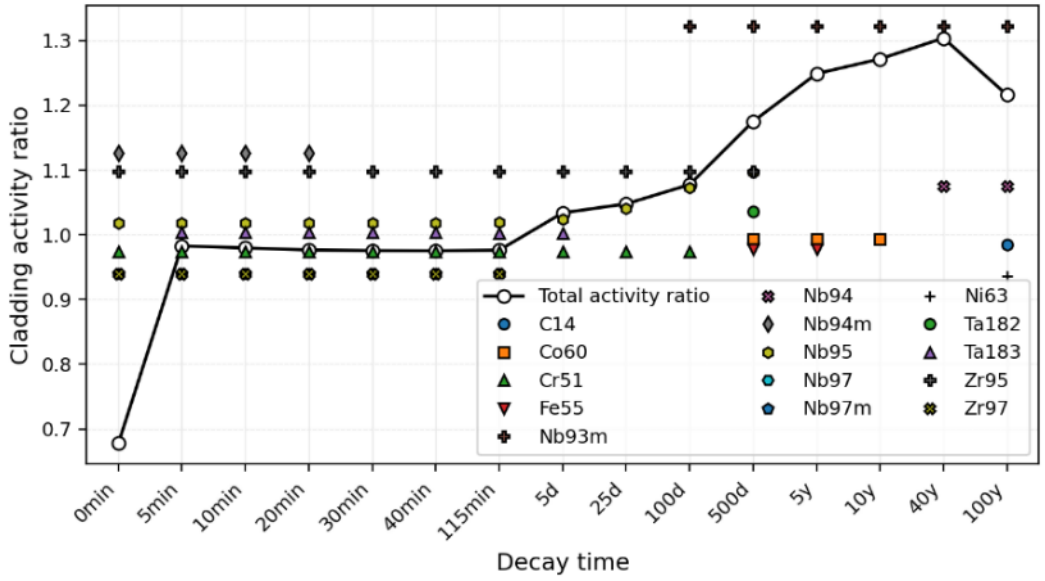

Library impact on nuclide activity is significant (here at 300K)

Federal Office
for the Safety of
Nuclear Waste Management

OpenMC vs. FP-II Cladding benchmark

Isotopic ratios

REF3a_300K

- Nb93m as a candidate for investigation
- Zr95 and Nb95 at lower decay times

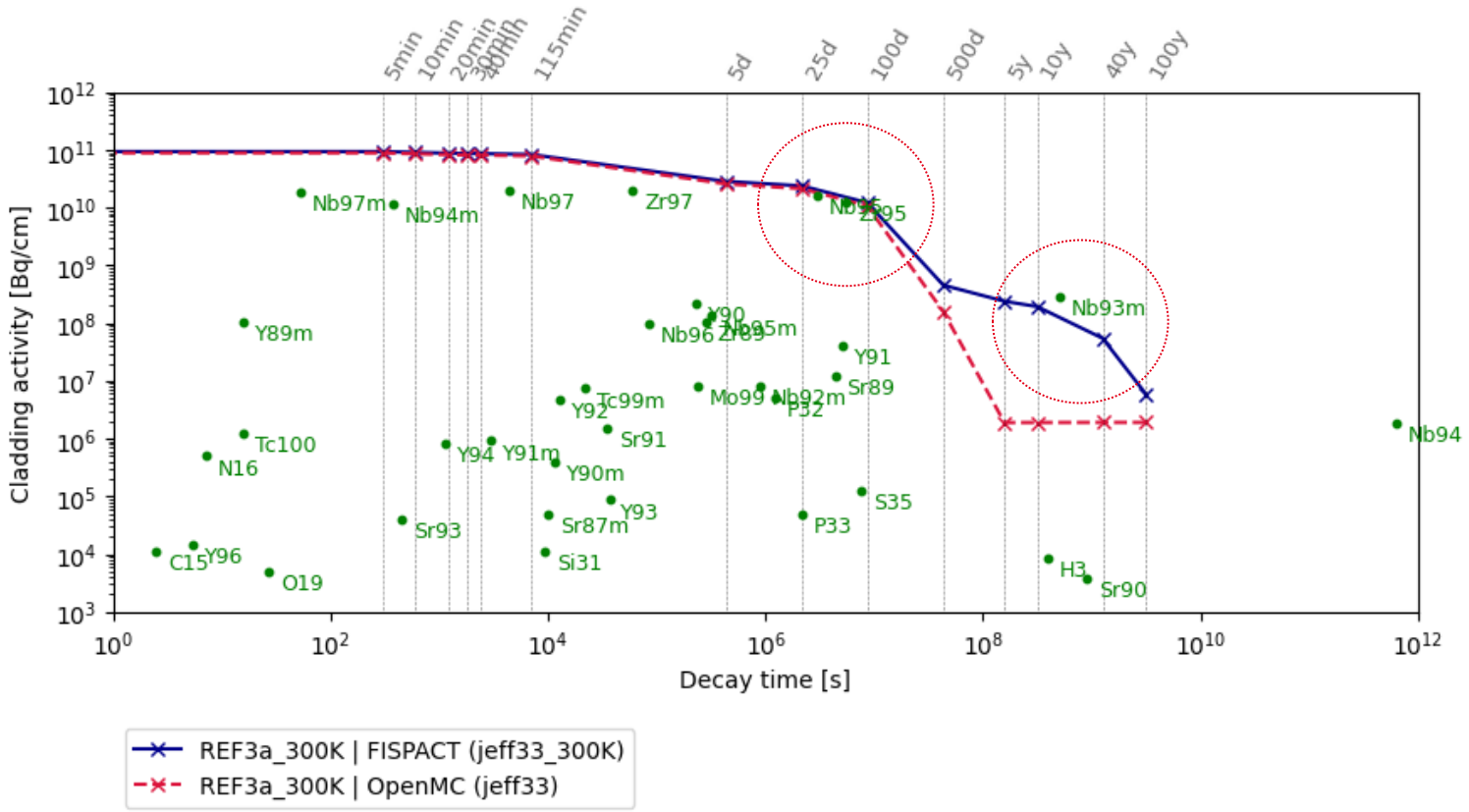

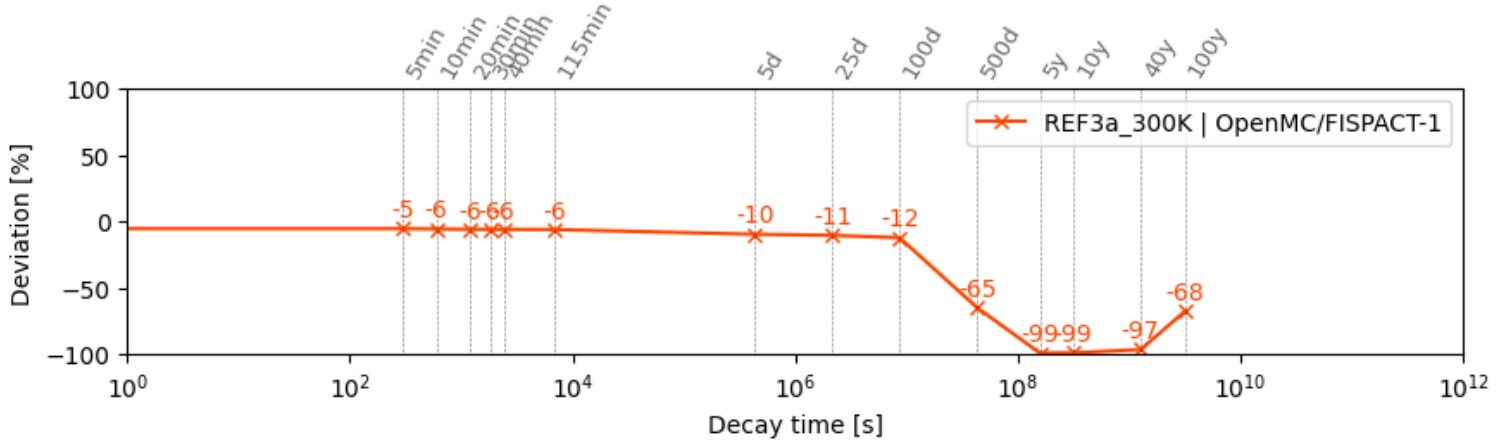

ATF1a_300K

- Nb93m as a candidate for investigation
- FP overprediction ~10% Zr95 and Nb95 (see analysis in the following slides)
- Very good agreement for Cr51 (see coming slides)

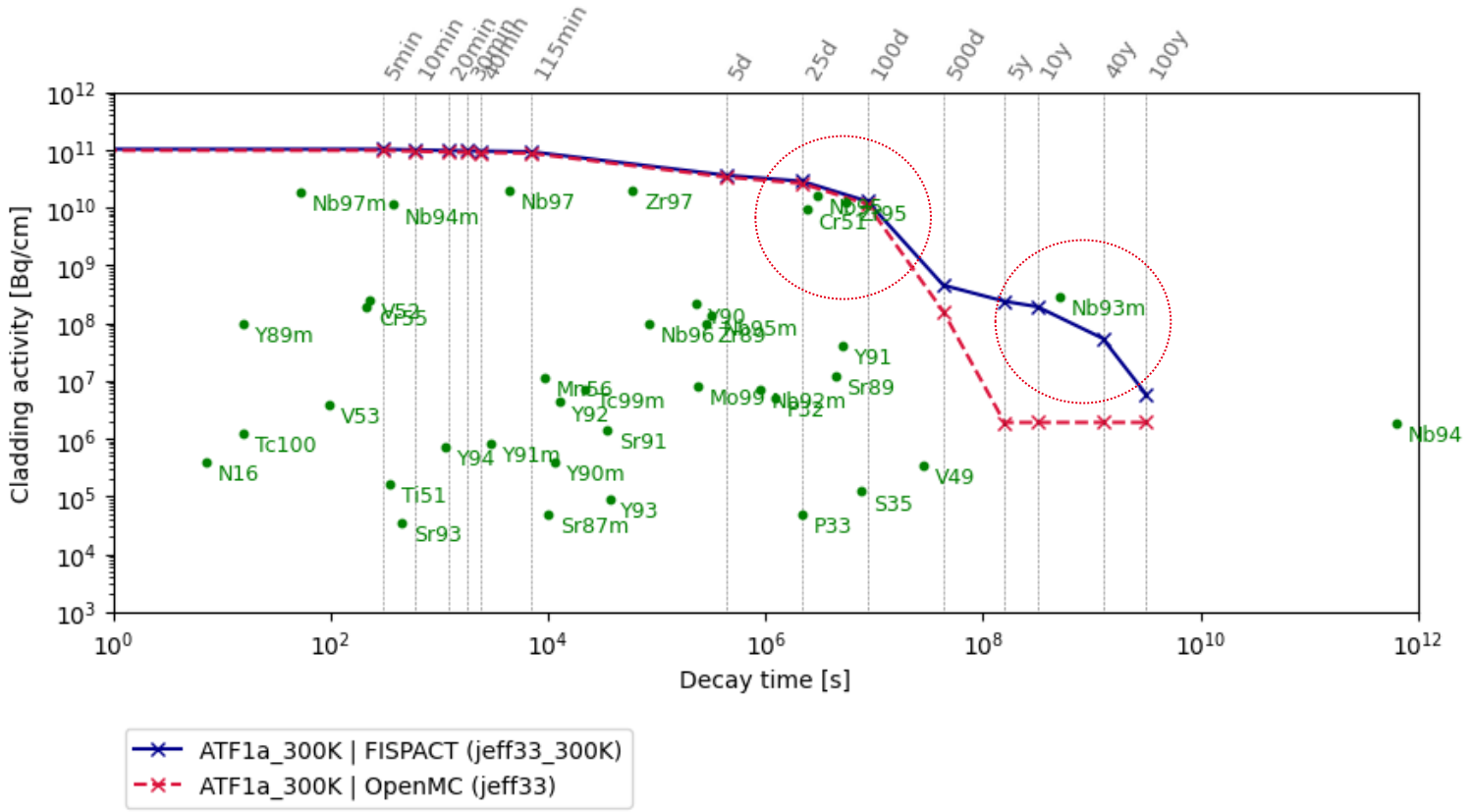

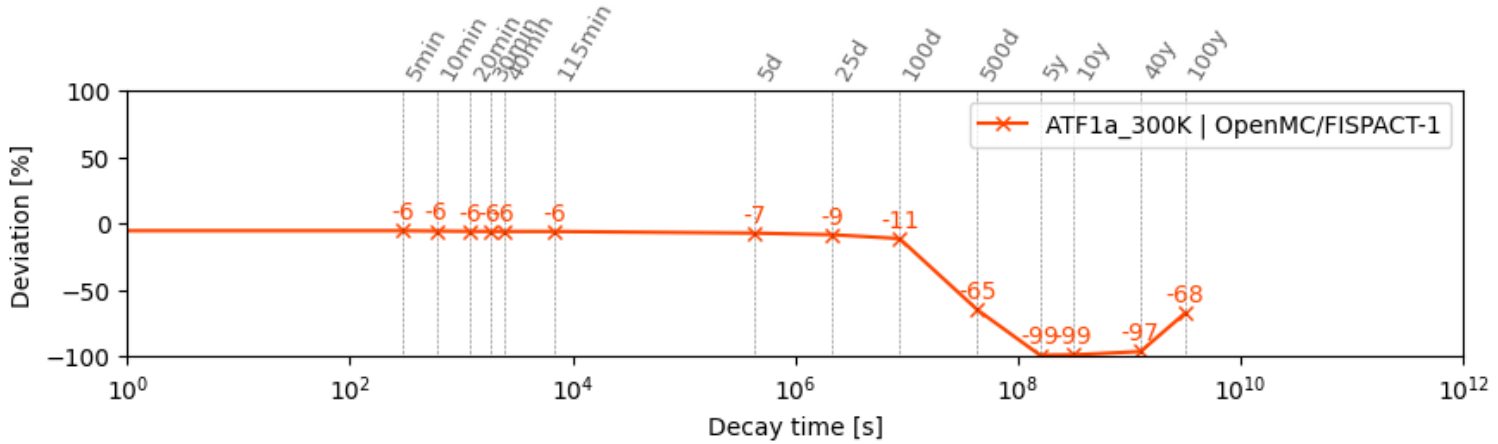

ATF3a_300K

- V49 → candidate for investigation

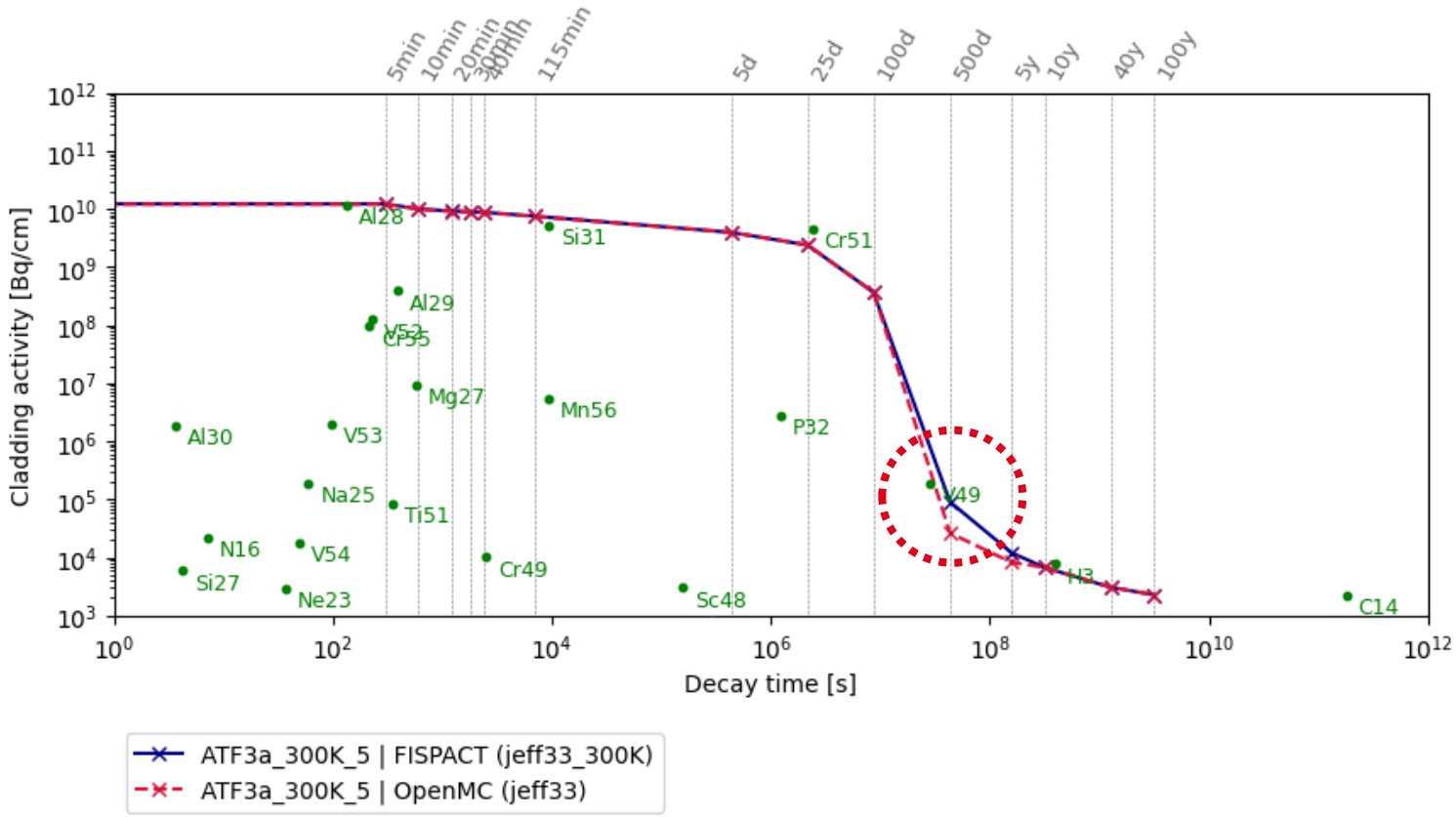

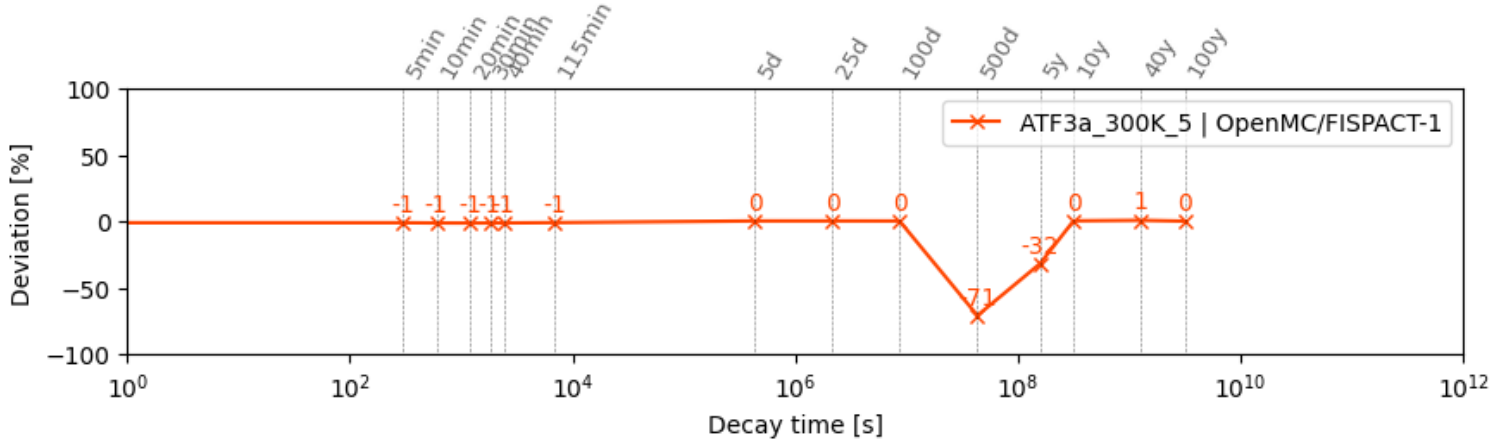

ATF2a_300K

- Very good agreement (also on nuclide level, see annex)
- No self-shielding correction in FP
- FP (σ+λ) uncertainty estimate on total activity ∈ [0, 5d] < 2.8%

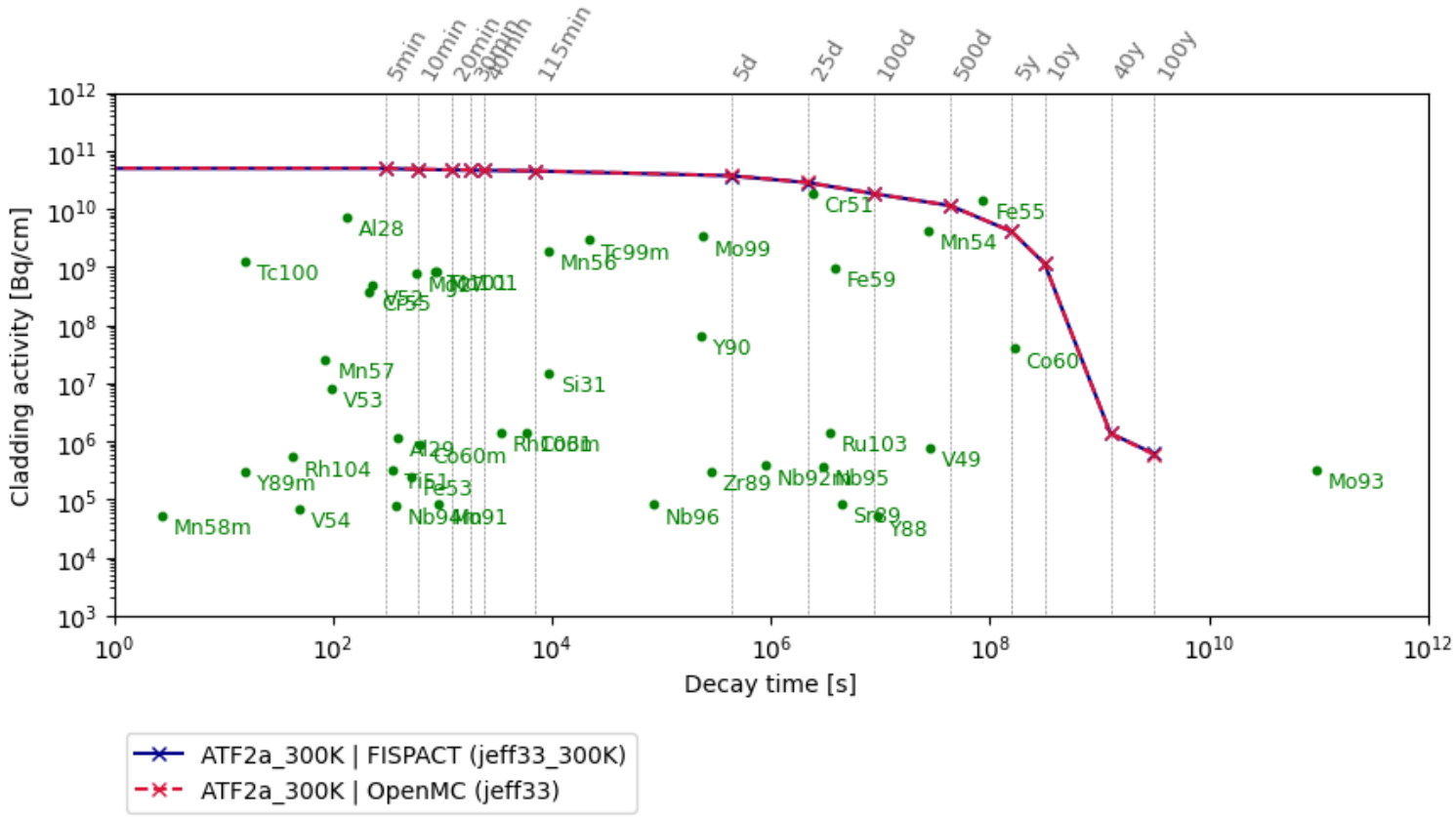

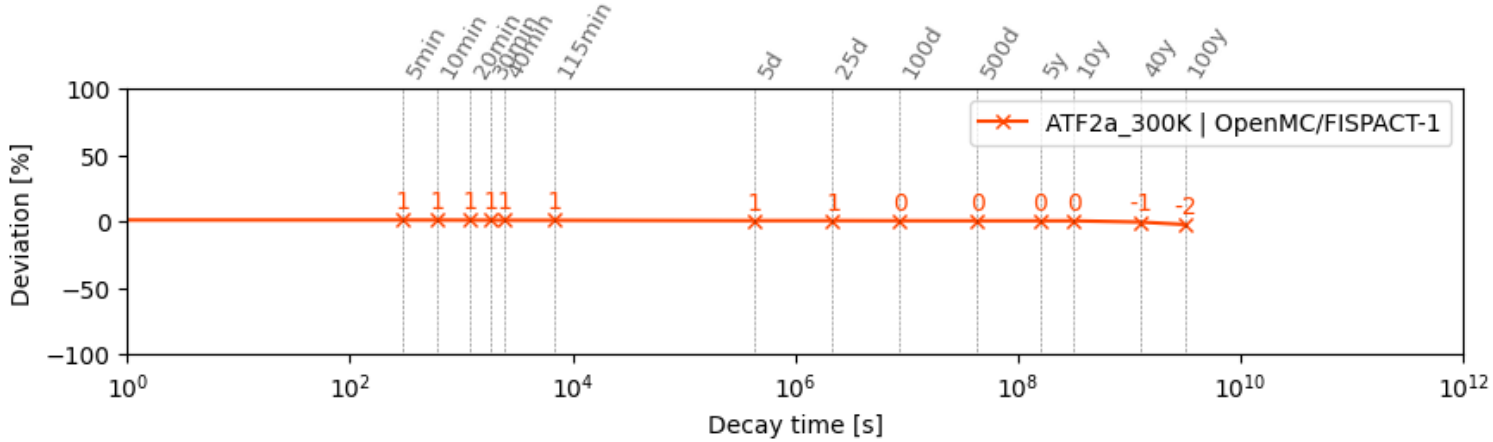

ATF3a_300K: OMC/FP-1 (activity)

- Very good agreement except for V49 (only in FP >1%)
- JEFF33 Cr50(n,anything)V49 in FP-II (MT=5) not implemented in OpenMC depletion chain file
- In TENDL2019[22] this is Cr50(n,np)V49

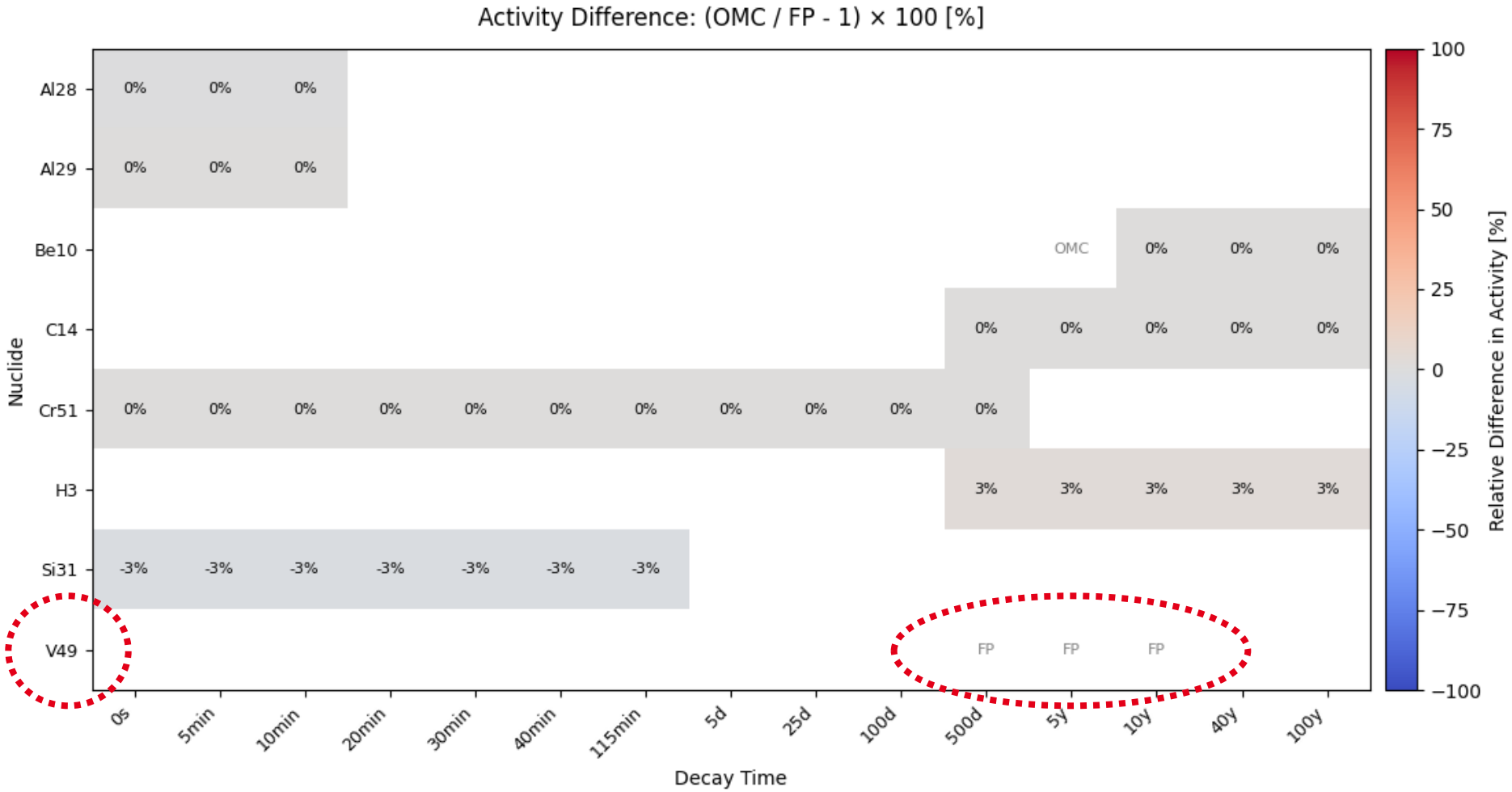

ATF2a_300K: OMC/FP-1 (activity)

- No self-shielding
- Very good agreement

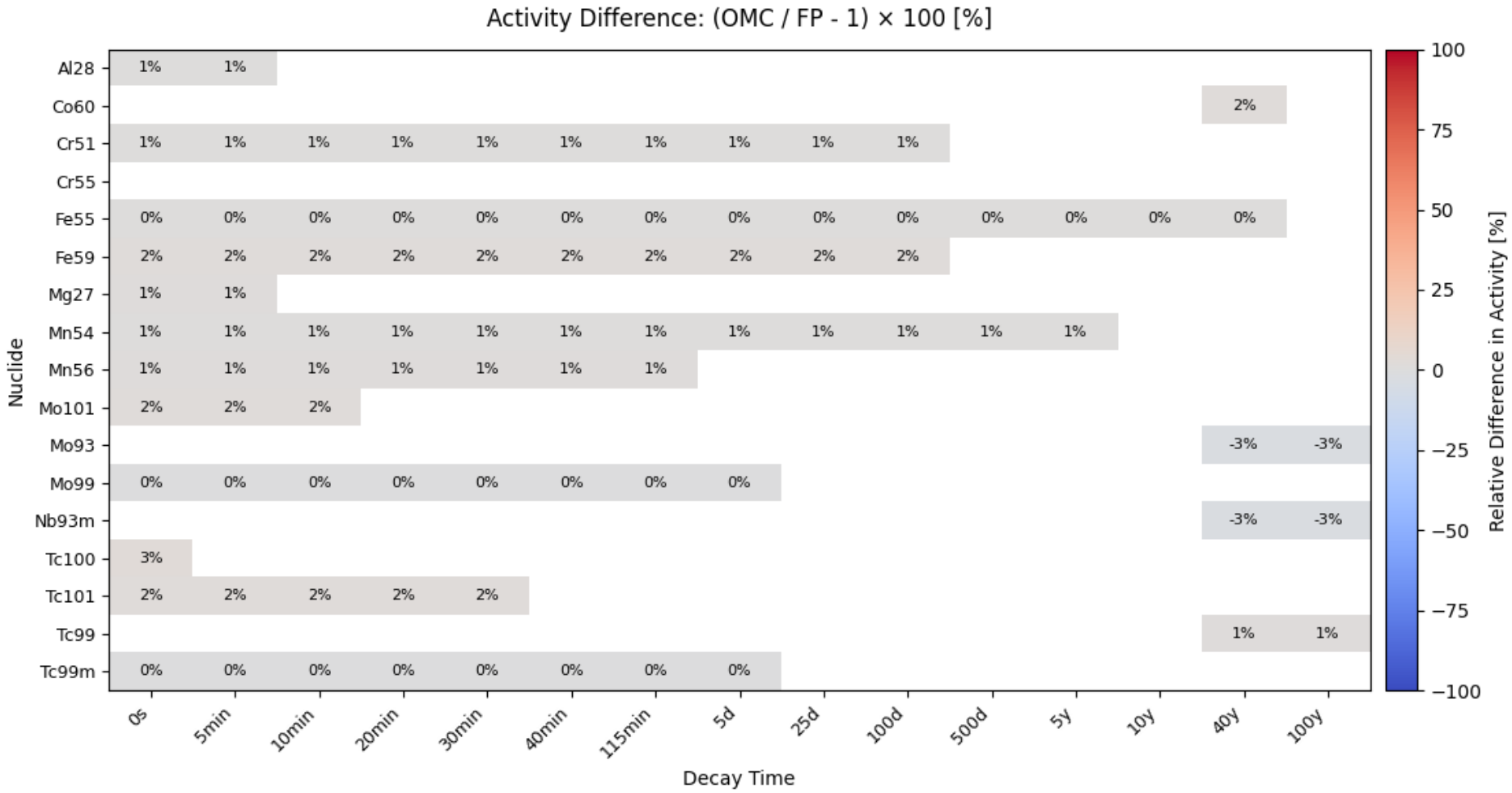

REF3a_300K: OMC/FP-1 (activity)

- Nb93(n,n1)Nb93m in FP-II (MT=3) not in OpenMC (inelastic n-scattering into metastable)
- FP overprediction of Zr95 and Nb95

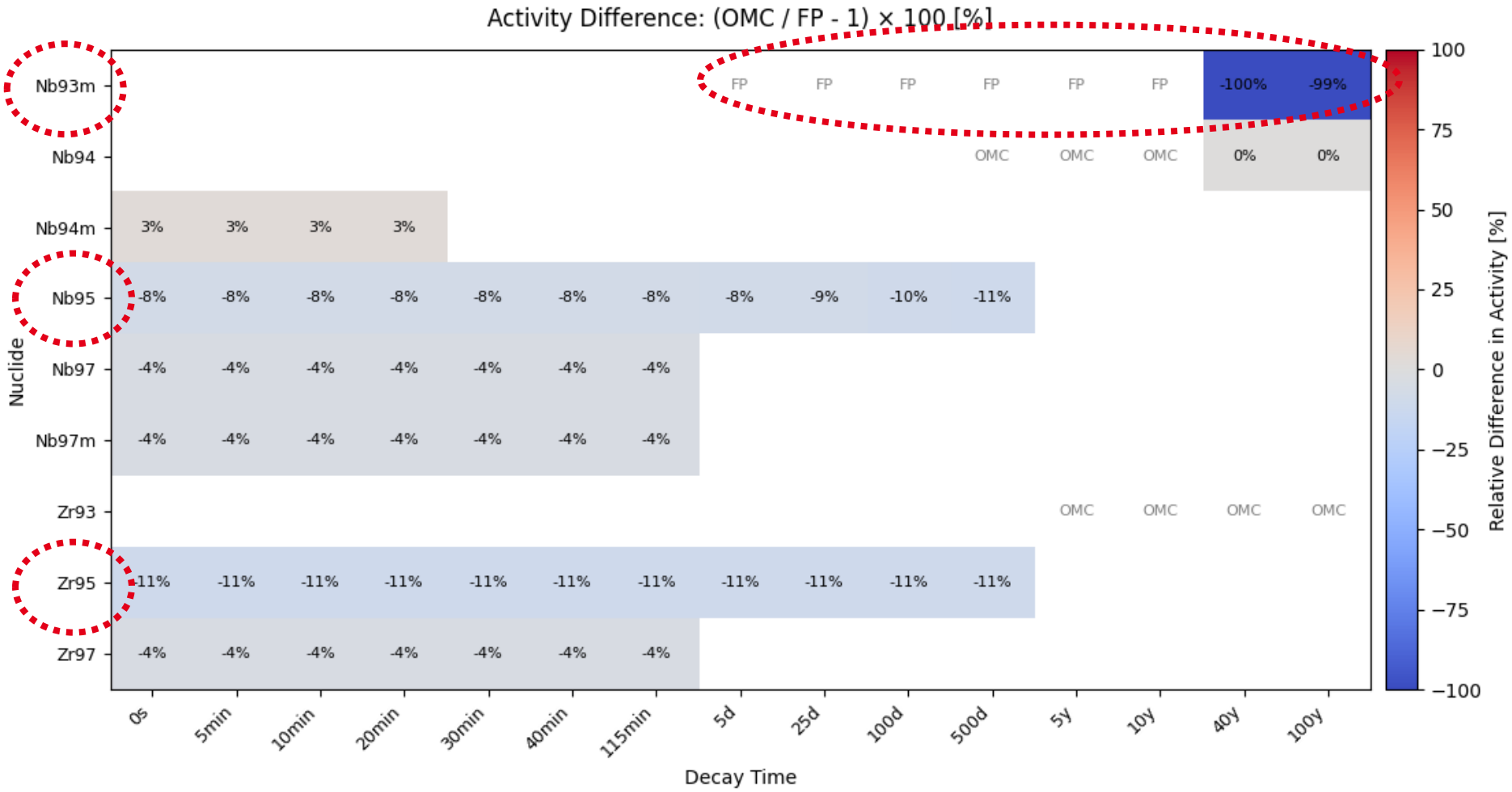

Federal Office
for the Safety of
Nuclear Waste Management

Zr95 analysis

for REF3a

REF3a_300K: OMC/FP-1 (activity)

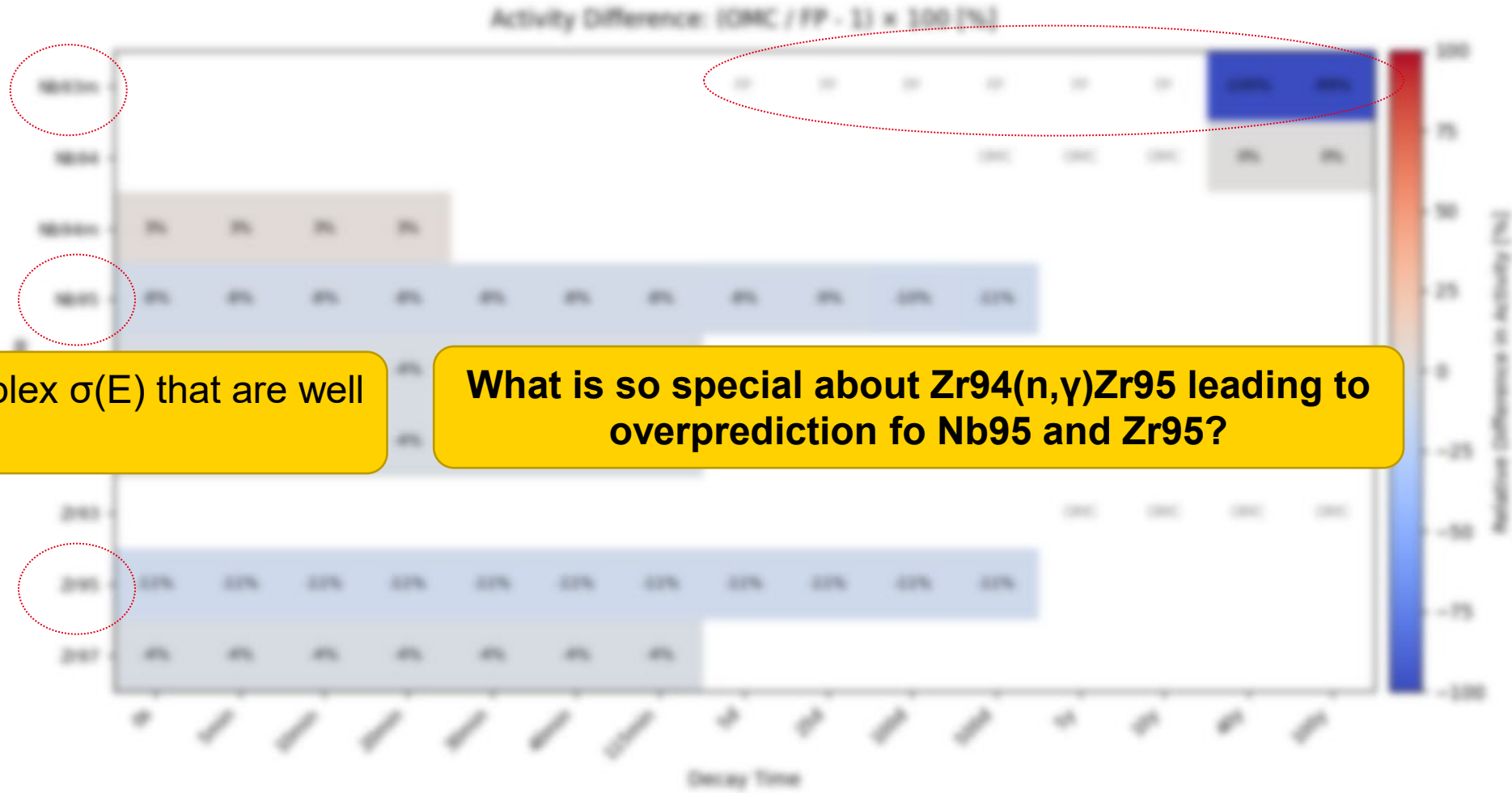

Many nuclides with complex σ(E) that are well within 5 % in FP…

What is so special about Zr94(n,γ)Zr95 leading to overprediction fo Nb95 and Zr95?

REF3a_300K: OMC/FP-1 (activity)

Federal Office
for the Safety of
Nuclear Waste Management

Possible impacts on nuclear reactions: here → Zr94(n,γ)Zr95

1. CCFE-709 and UKAEA-1102 **group structure vs. continous σ (E)?**
2. Particular **resonance structure vs. cumulative reaction rate?**
3. Does a **self-shielding** correction in FP help?

Spoilers:
It is preferred to let FP overestimate the reactions rates (conservatism) and identify such „problematic“ nuclides in the comparison with the continuous energy OpenMC solution.

The particularity of Zr-94 neutron capture and its stronger overprediction in FP remains to be revealed …

Self-shielding (SSFGeometry) vs. no self-shielding

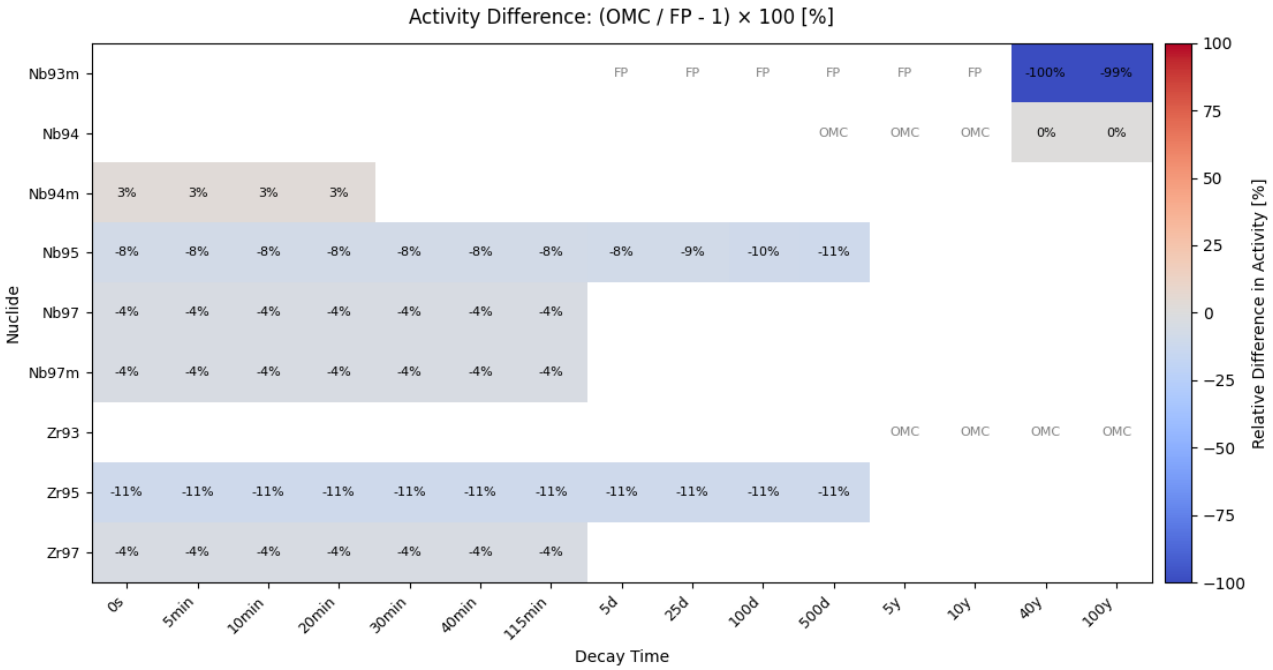

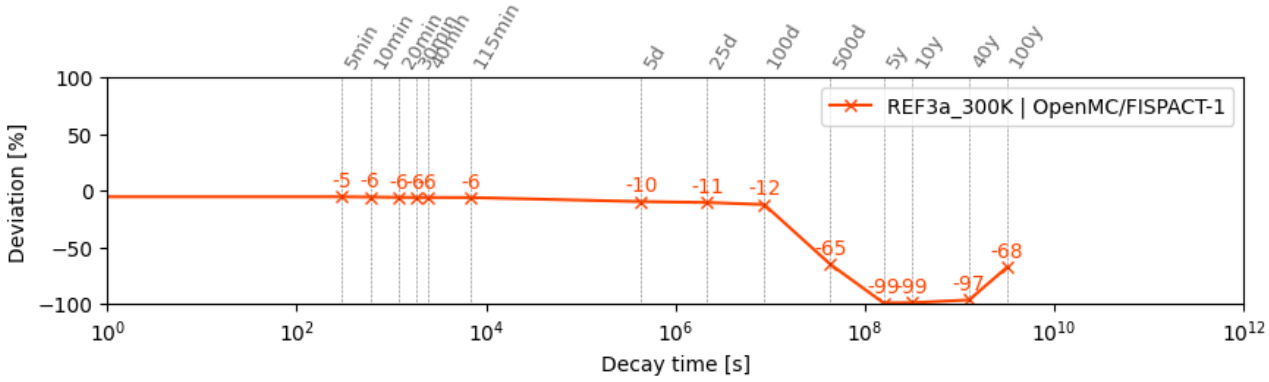

Self-shielding (SSFGeometry) vs. no self-shielding

Federal Office
for the Safety of
Nuclear Waste Management

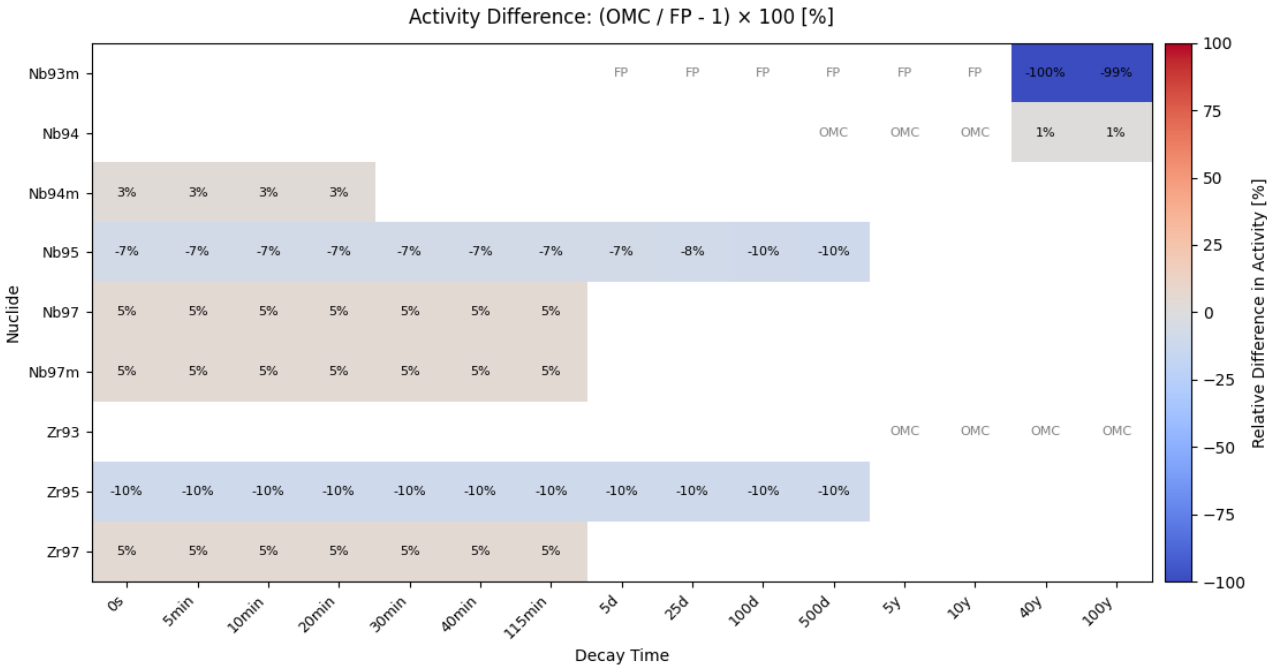

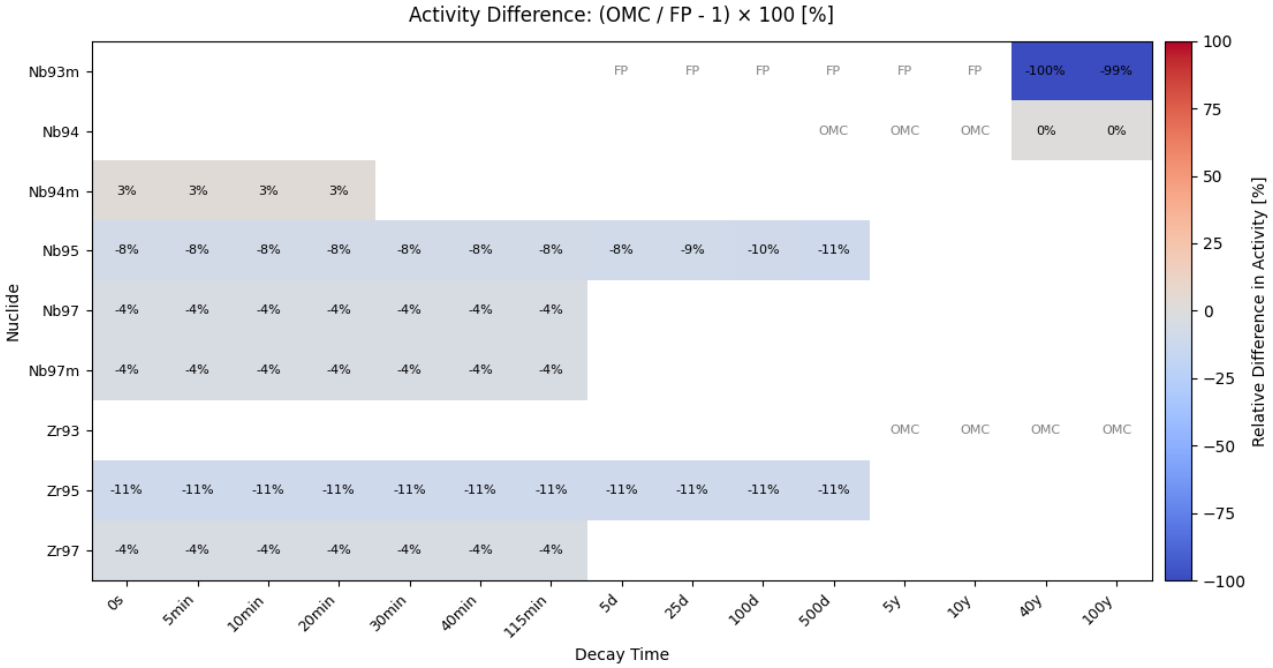

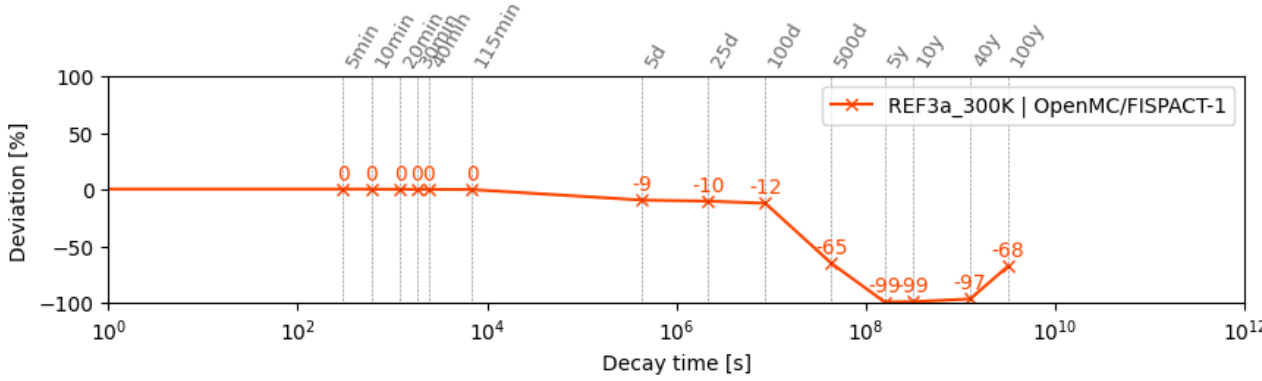

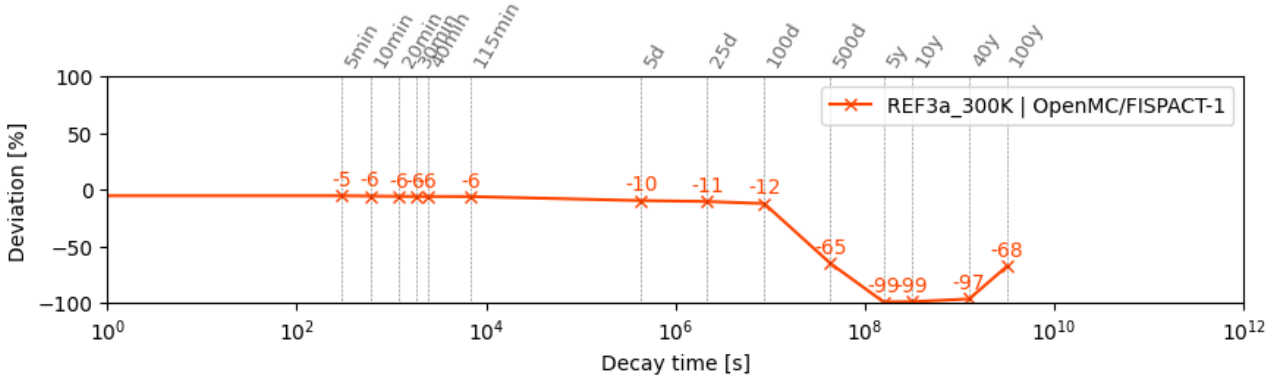

Self-shielding (SSFGeometry) vs. no self-shielding

- Impact of SSFGeometry self-shielding model in FP-II visible on some nuclides (correction for resolved resonances without significant overlap)

- Zr94(n,g)Zr95 reaction rate not changed much (do tricky resonances overlap?)

- Self-shielding model (extended, calibrated correlation by irradiation experiments for simple geometries) is supposed to grasp *„geometry effect“* of self-shielding

- *„Geometry effect“*: cannot be fully separated from energy self-shielding effect, but generally describes how the activation of a material lump is not homogenous through the body (e.g. Pu-239 build-up in pellet rim)

- Here: thin cladding and OpenMC track length cell-averaged neutron spectrum corresponds to average neutron spectrum in the cladding cell → geometry effect should already be covered in average

Self-shielding (ProbTable) vs. no self-shielding

- Other self-shielding model in FP (ProbTable, see below) leads to very strong over-shielding (also reported in literature[26])

- Possibility to use SSFDILUTION to artificially adapt the dilution cross-section in specific energy groups is cumbersome…

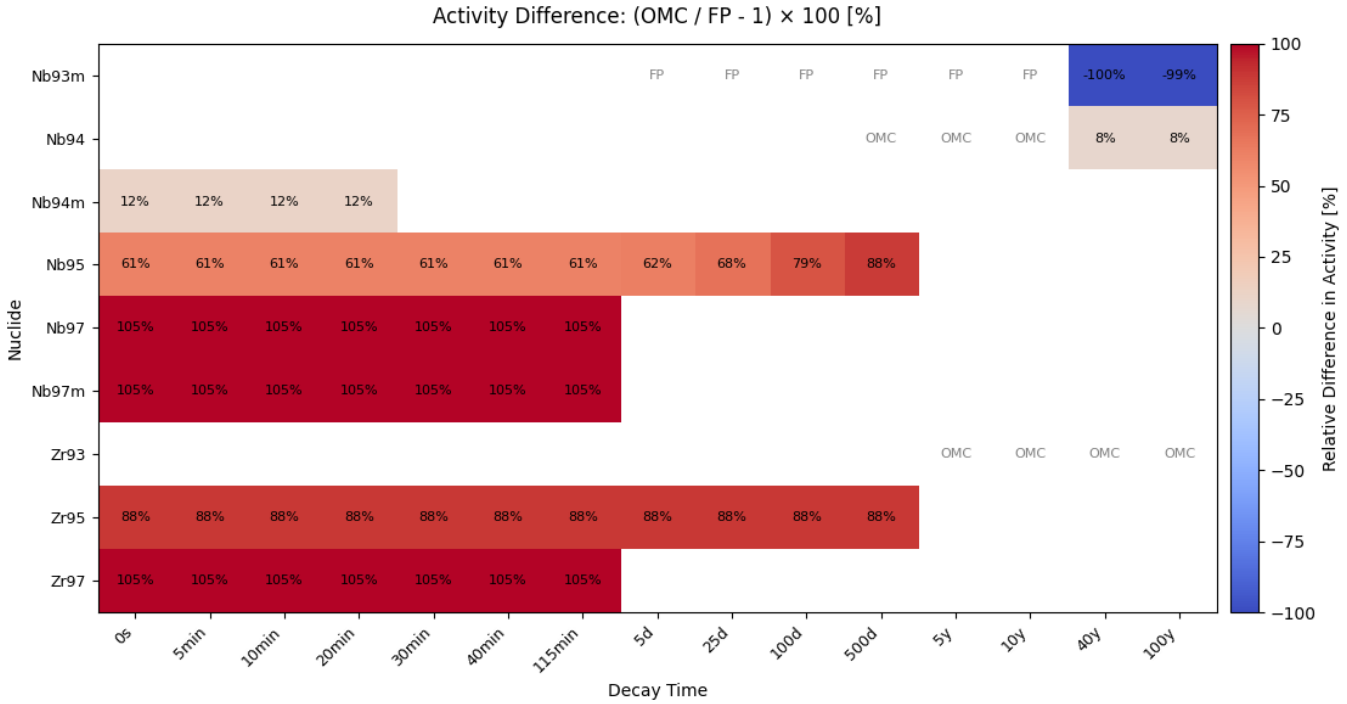

Strong over-shielding in FP with ProbTable SF when using accurately tallied spectra from OpenMC

Self-shielding (ProbTable) vs. no self-shielding

- Other self-shielding model in FP (ProbTable, see below) leads to very strong over-shielding (also reported in literature[26])

- Possibility to use SSFDILUTION to artificially adapt the dilution cross-section in specific energy groups is cumbersome…

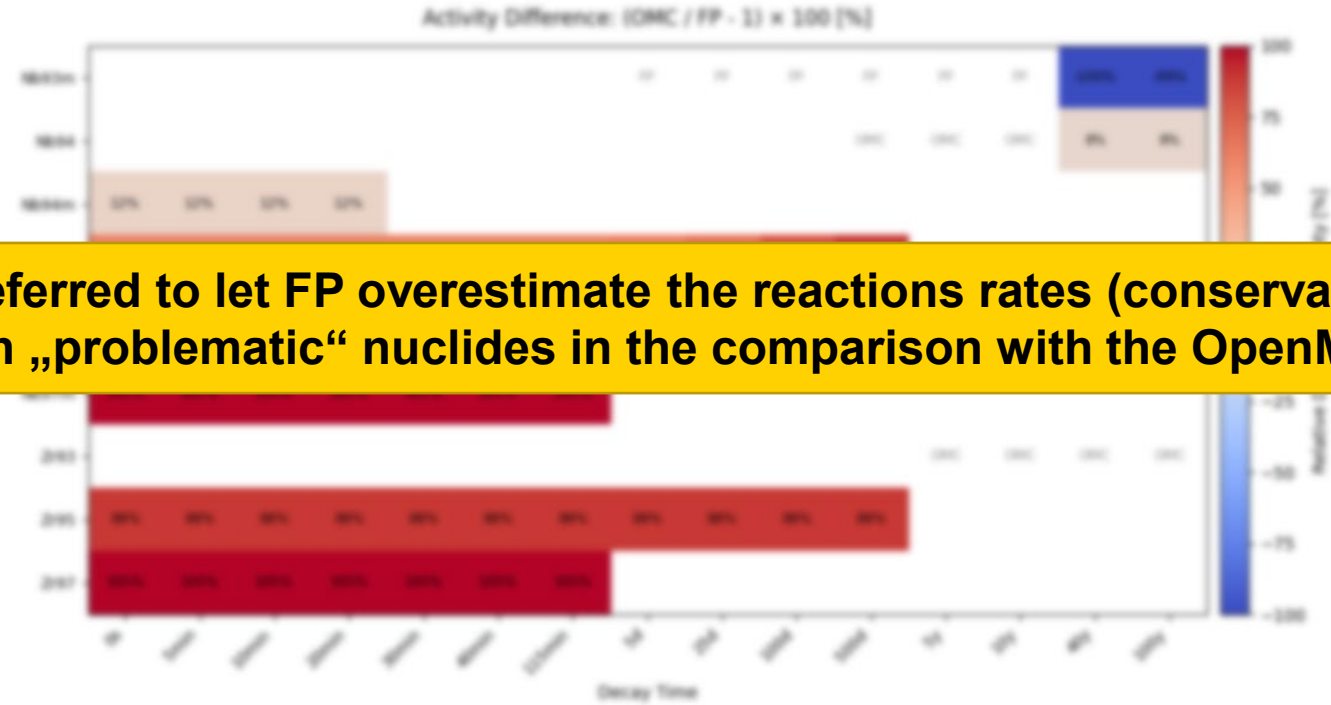

→ It is preferred to let FP overestimate the reactions rates (conservatism) and identify such „problematic“ nuclides in the comparison with the OpenMC solution.

Nuclide resonance structure vs. reaction rate

Having a look at

- nuclear resonance structure and its energy discretization in the group structure and cumulative reaction rate

First, looking at nuclides that are well predicted by FP (compared to OpenMC)

Nb93(n,g)Nb94m:	Δ ~ 3%
Zr96(n,g)Zr97:	Δ ~ 4%
Si30(n,g)Si31:	Δ ~ 3%
C13(n,t)B11:	Δ ~ 3% on ^{3}H
Zr94(n,g)Zr95:	Δ ~ 11%

Zr96(n,g)Zr97: Δ ~ 4% on Zr97

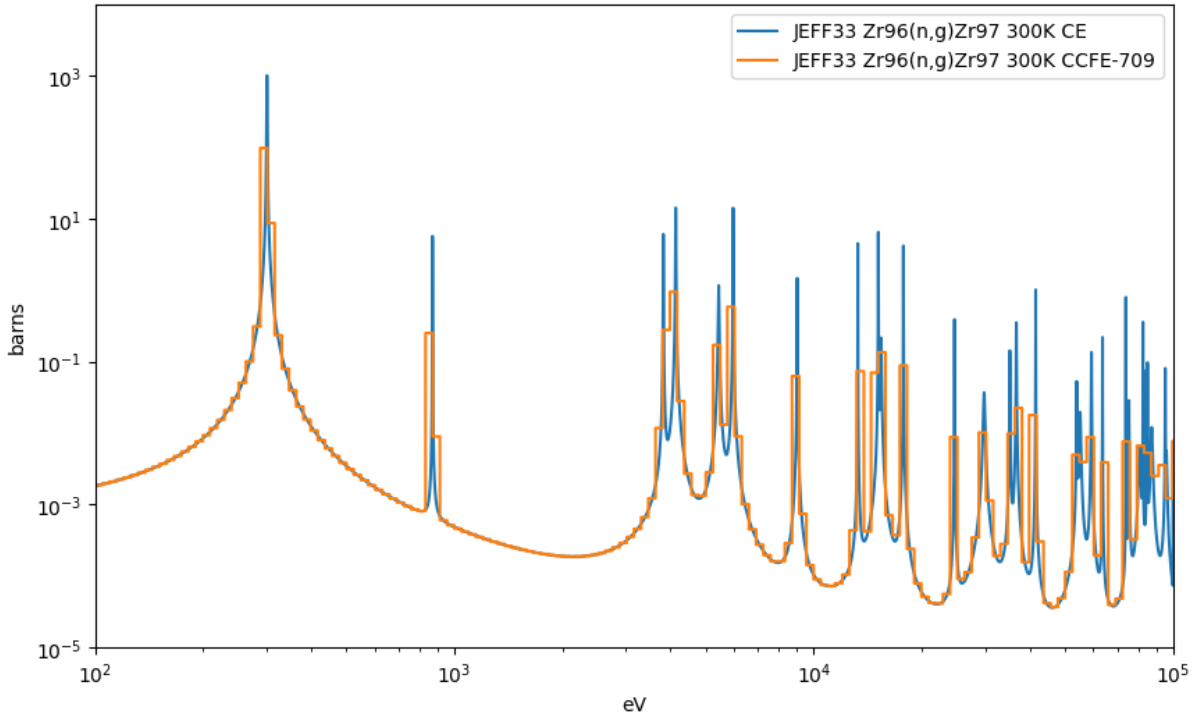

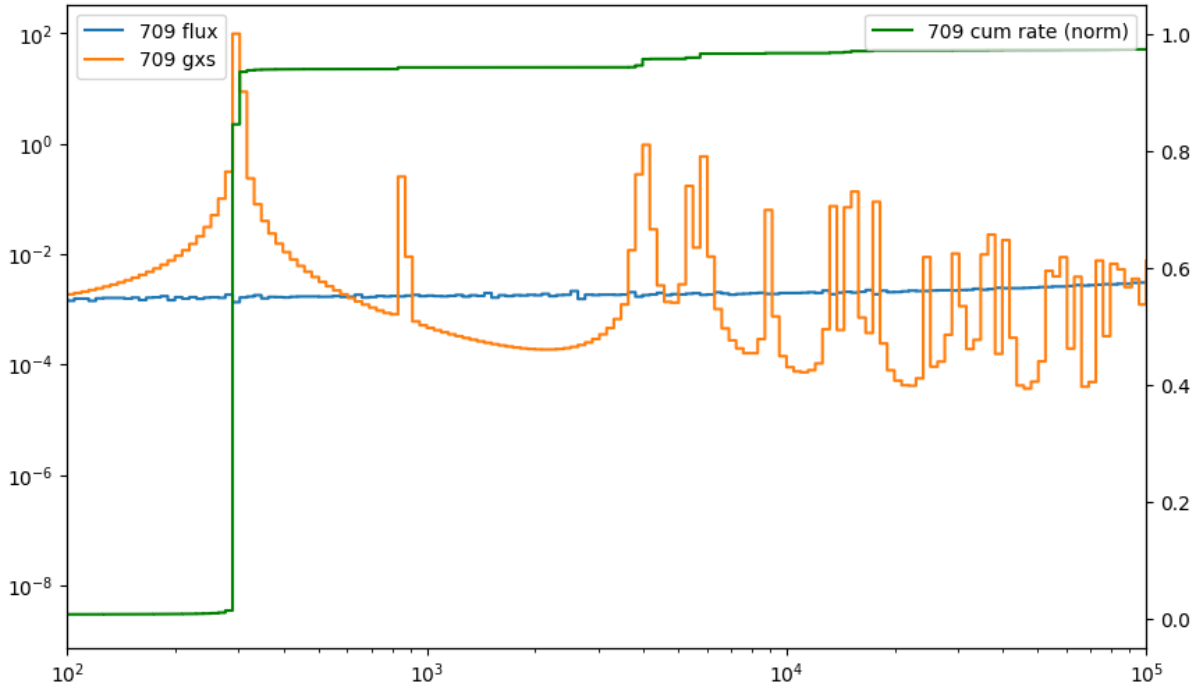

One major resonance ~200-300 eV > 95% of cumul. rate

Si30(n,g)Si31: Δ ~ 3% on Si31

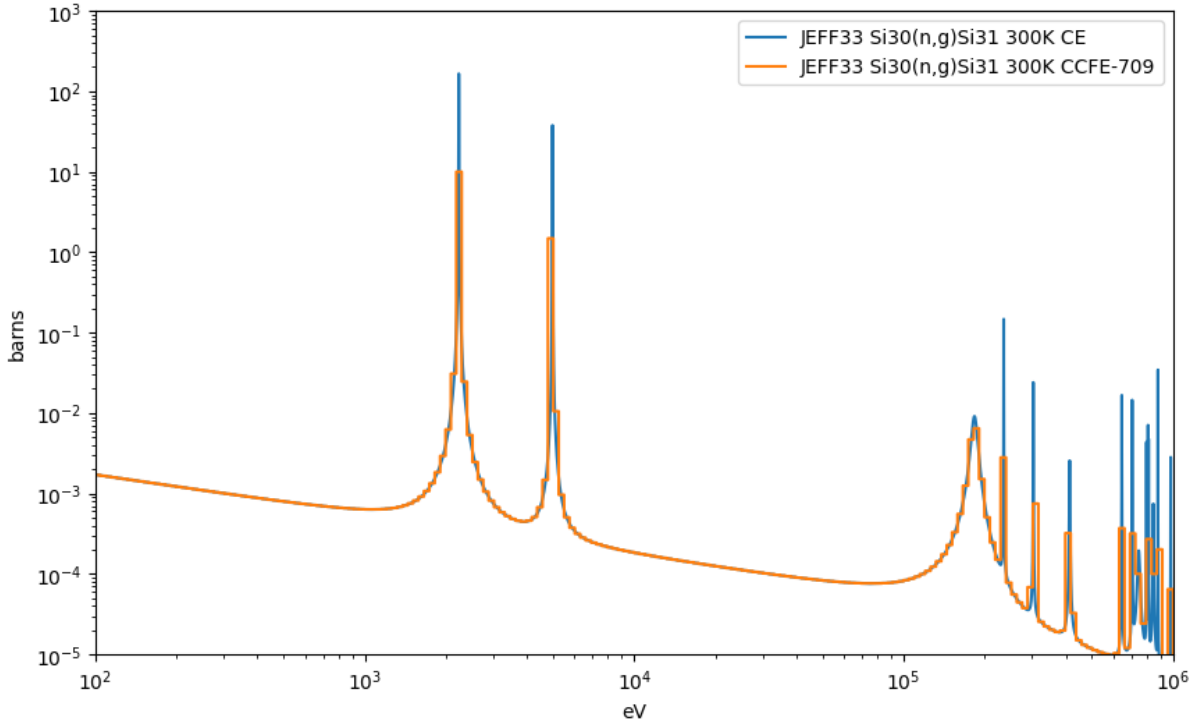

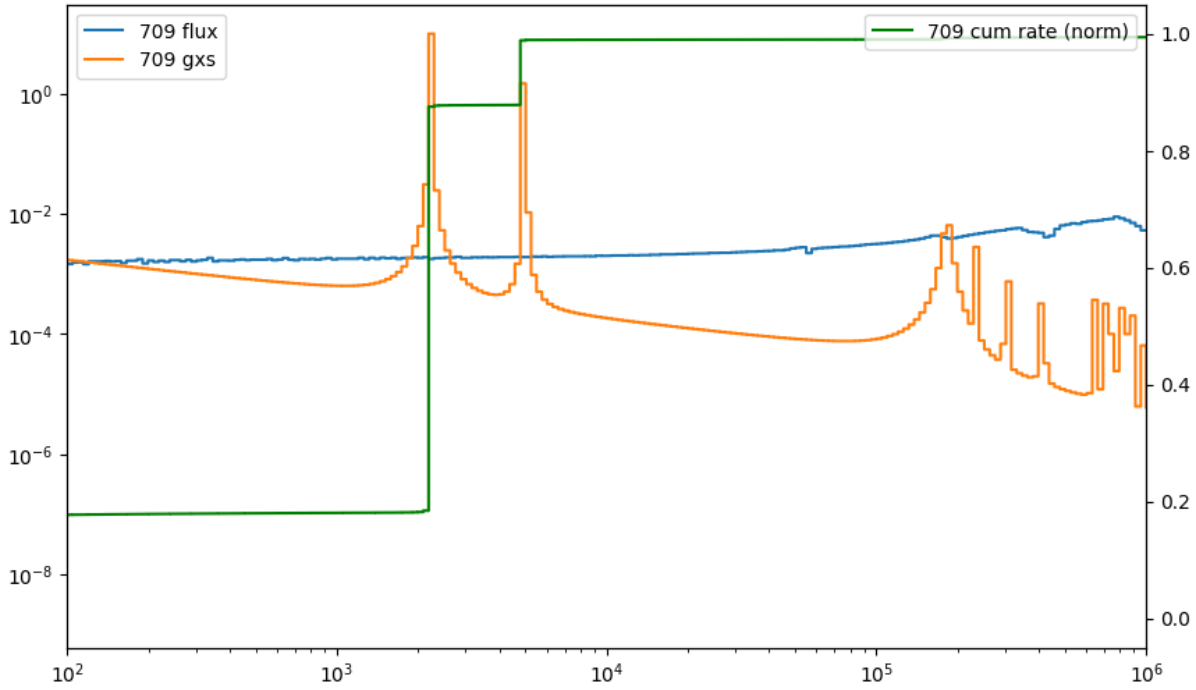

Two major resonances (~2 and ~5 keV) > 99% of cumul. rate

C13(n,t)B11: Δ ~ 3% on H3

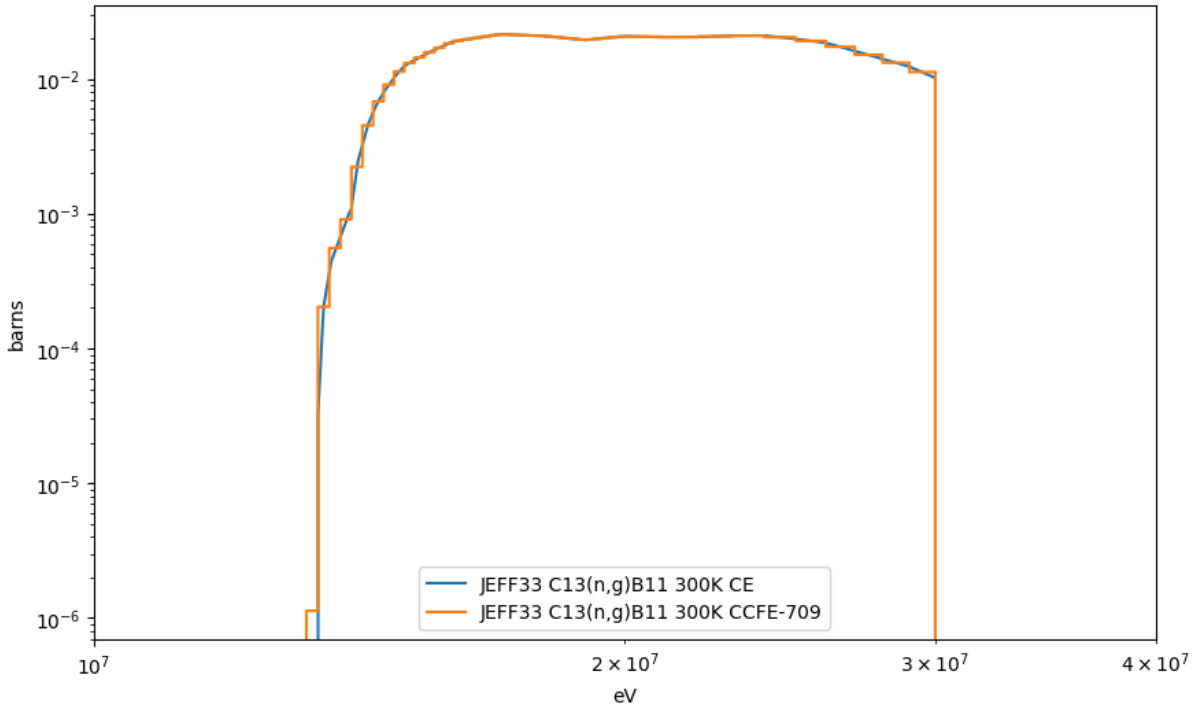

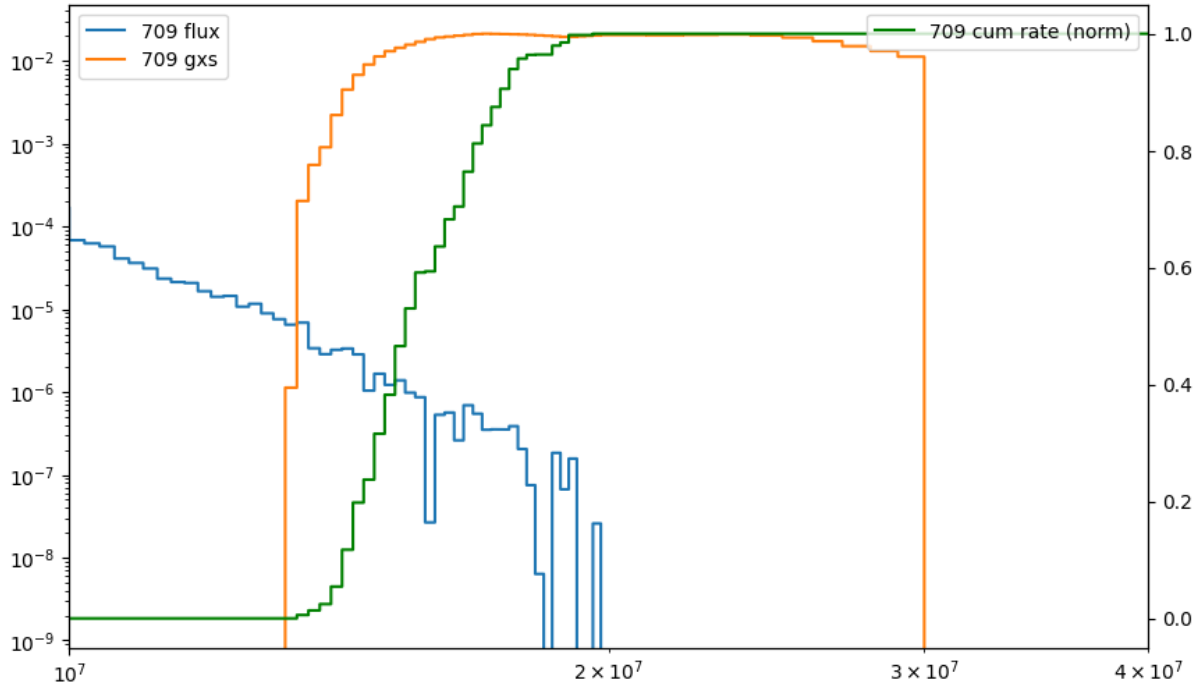

Threshold reaction well predicted even though neutron tail with low statistics.

Nb93(n,g)Nb94m: Δ ~ 3% on Nb94m

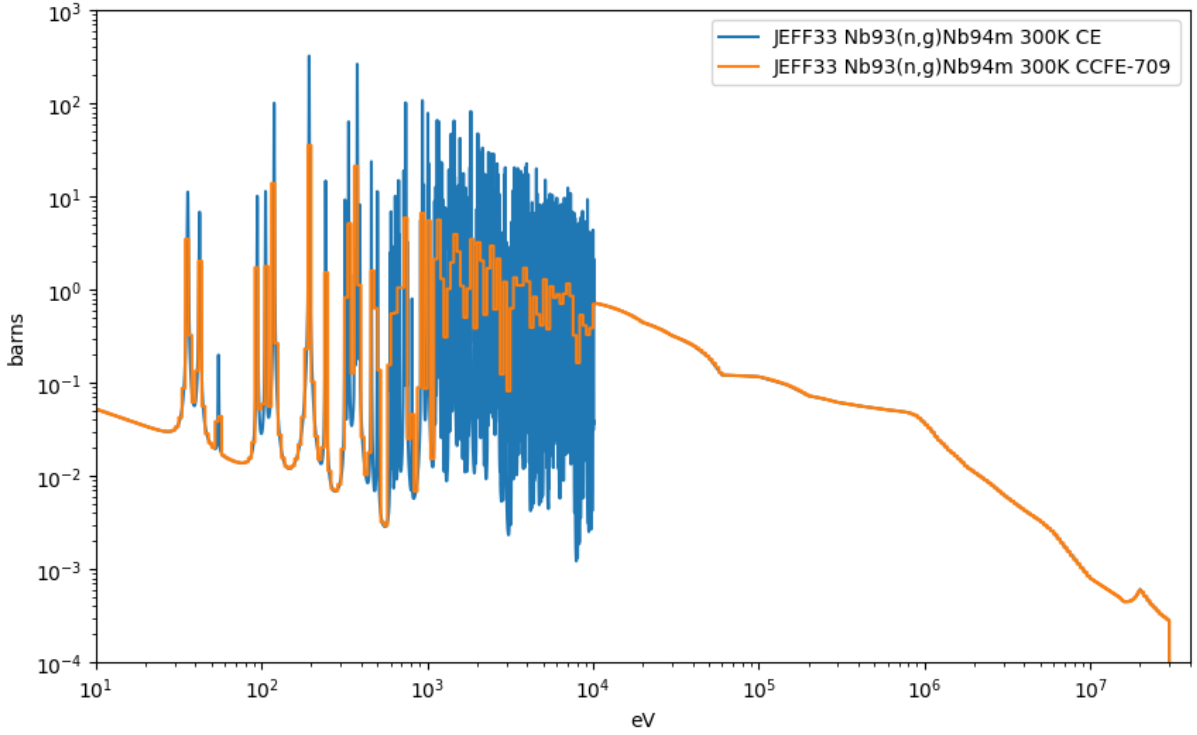

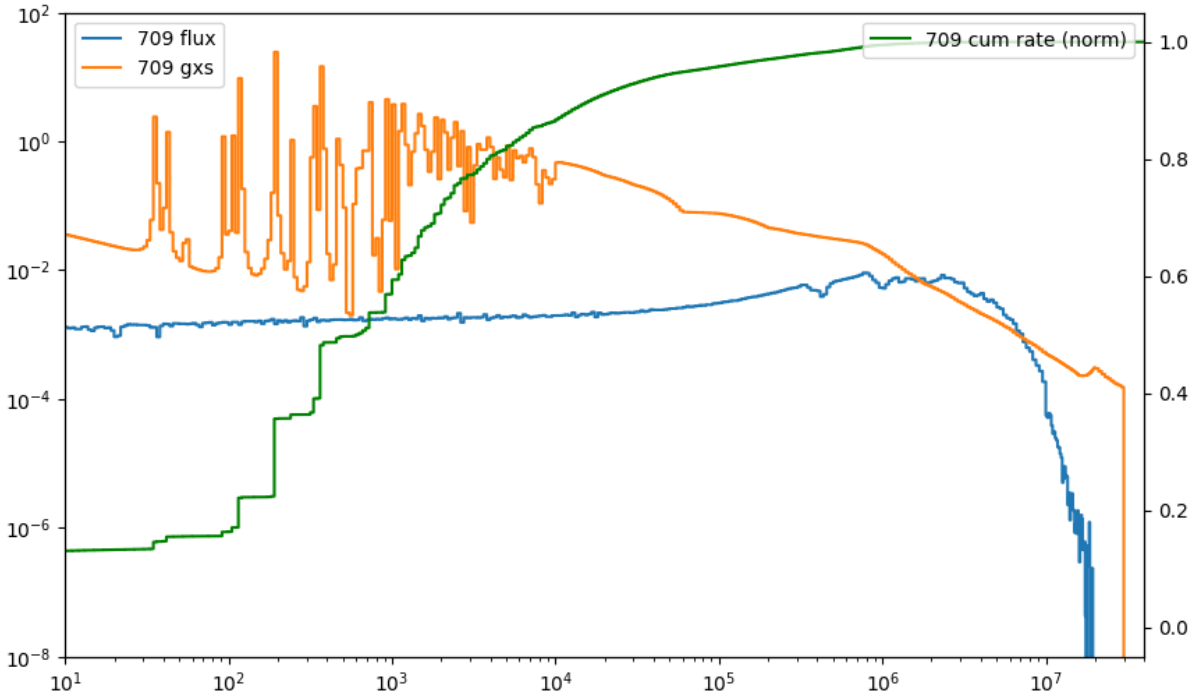

RRR: >50 % of reaction rate with several resonances form 20 to 1000 eV

URR: remaining part from 1000 eV to 10 MeV

Zr94(n,g)Zr95: Δ ~ 11% on Zr95

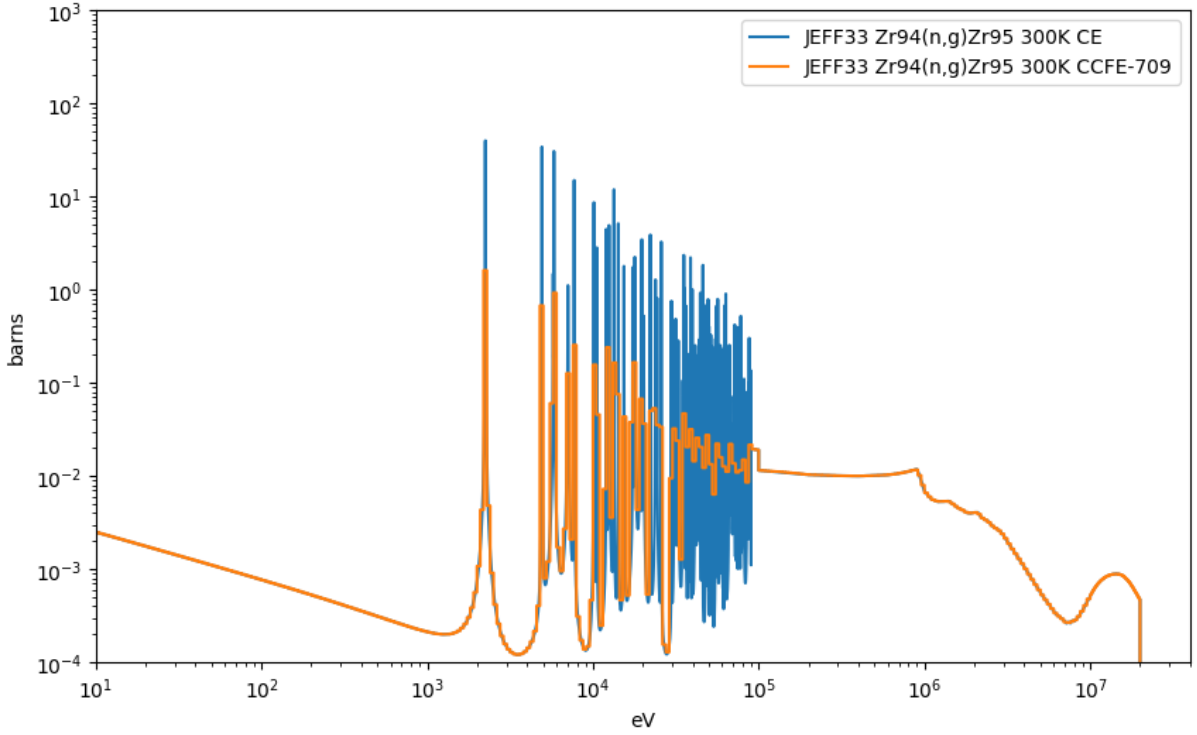

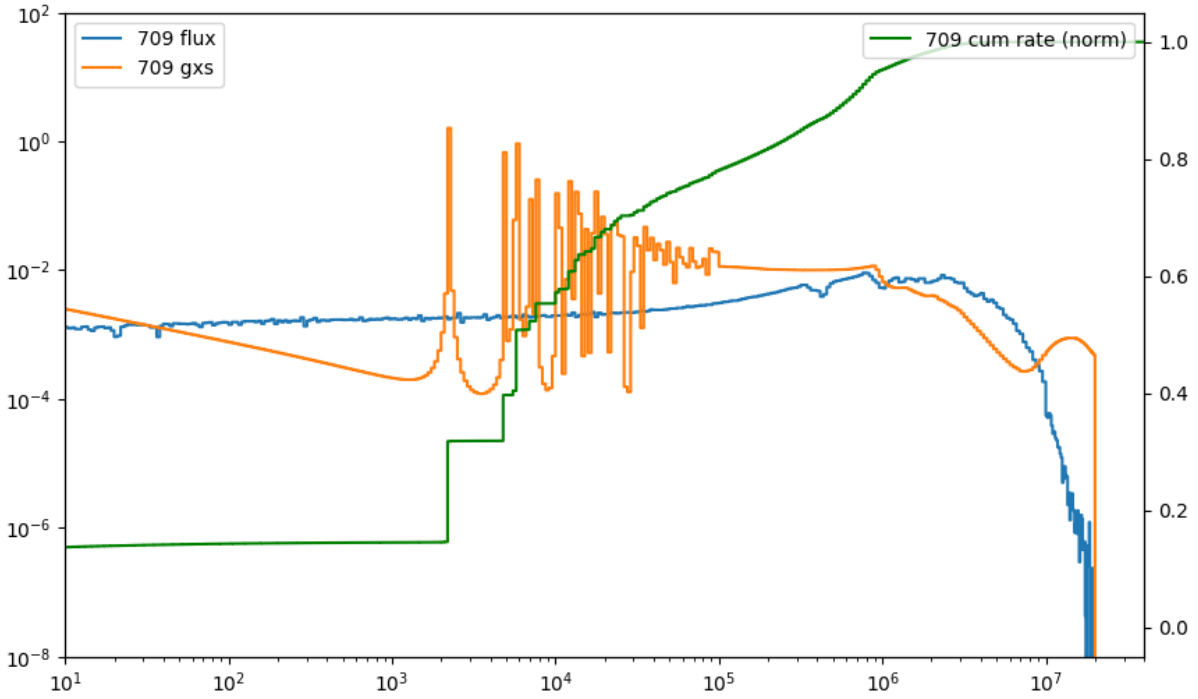

RRR: >50 % of reaction rate with several resonances from 2 to 10 keV

URR: remaining part from 10 keV to 30 MeV

Energy bin width vs group structure

- No difference for 709 and 1102 group structure in RRR of Zr94(n,g)Zr95 from 2 to 10 keV
- No difference for 709 and 1102 group structure in URR of Zr94(n,g)Zr95 up to 40 MeV

→ 1102 group would very likely not perform “better”

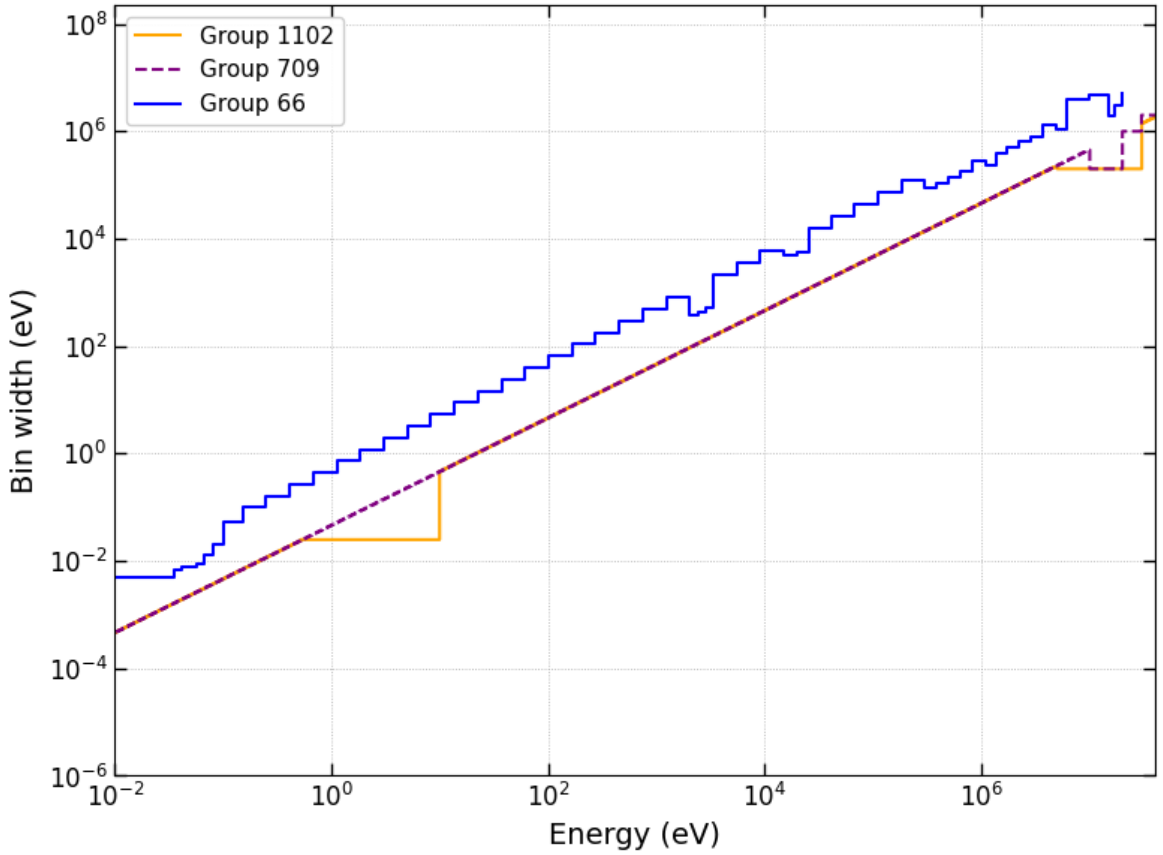

Uncertainty (FP pathway analysis)

- REF3a example (MOI spectra, jeff-3.3 300 K)
- Estimated uncertainty at the end of irradiation (FP path analysis)

Total activity:	**1.61 %**
Nb97:	3.641%
Nb95:	3.910 %
Zr97:	3.826 %
Nb97m:	3.826 %
Zr95:	5.195 % (less than 11% diff to OpenMC)
Nb94m:	3.093 %

Zr94(n,g)Zr95: Δ ~ 11% on Zr95

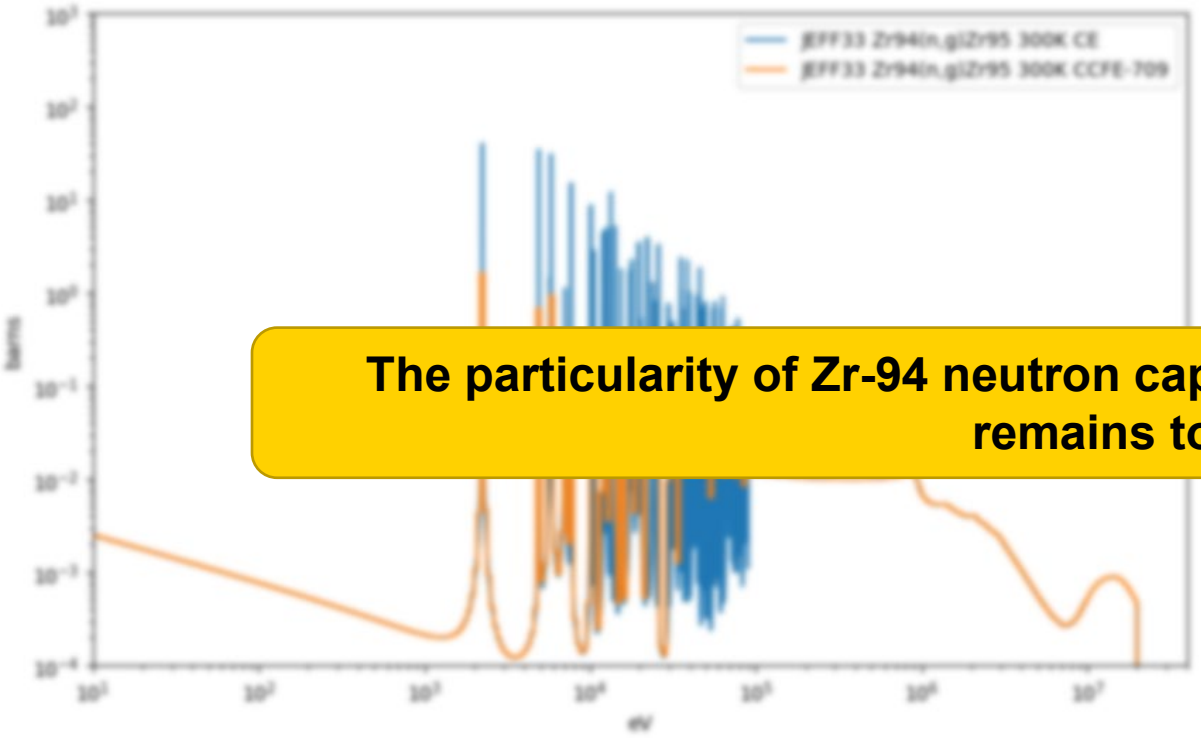

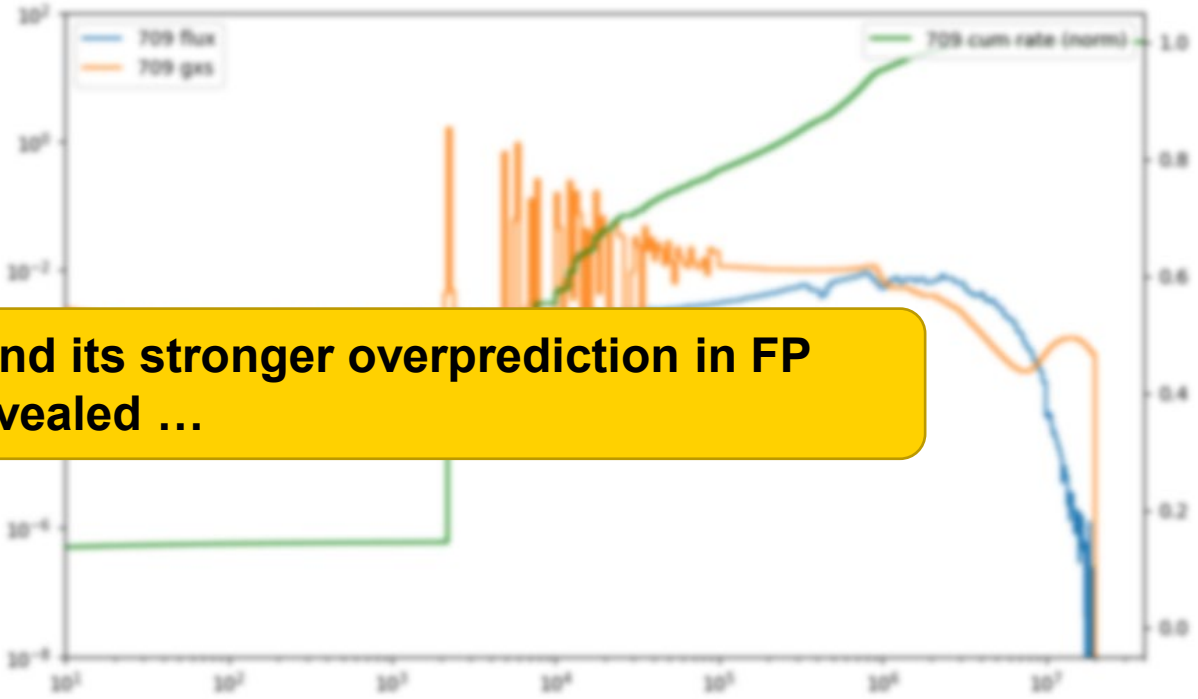

The particularity of Zr-94 neutron capture and its stronger overprediction in FP remains to be revealed …

Conclusions OpenMC vs Fispact-II

- **CE OpenMC solution as reference** except for reactions that cannot be yet included in the depletion chain file for describing the inventory change (Nb93m, V49) *…72 hours per sim*

  → Knowledge about such nuclides through FP-II

- **FP path analysis**: Identification of all relevant paths to dominant nuclides, adding reactions of interest on the nuclide-specific level to the OpenMC depletion chain file → e.g. (n,np) for Cr50 only.

  → Complementary modelling also to estimate inventory uncertainties

- **FP includes all available reactions from ND library**, but library (+SSF) not readily available at temperature of interest *("[…] scripts and processes defined by the UK Atomic Energy Authority […]"* → 3 more ND codes: NJOY, PREPO and CALENDF*)* *…minutes per sim*

- **OpenMC→FP-II workflow**: Using OpenMC tallied spectra with BU in FP evades "constant branching ratios" through collapse of the BU-specific spectrum with nuclear cross-sections

Federal Office
for the Safety of
Nuclear Waste Management

More ATF cladding metrics from FP-II

Tallied clad spectra in OpenMC for use in FP (here: MOI)

FeCrAl

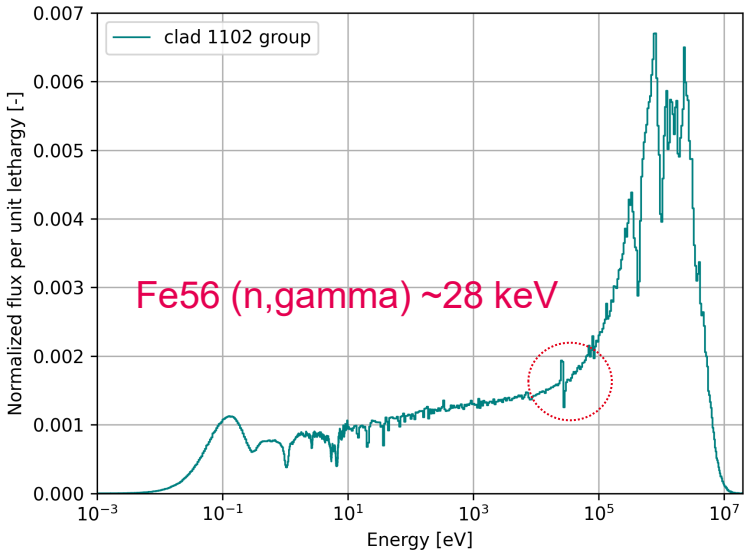

M5+20µmCr

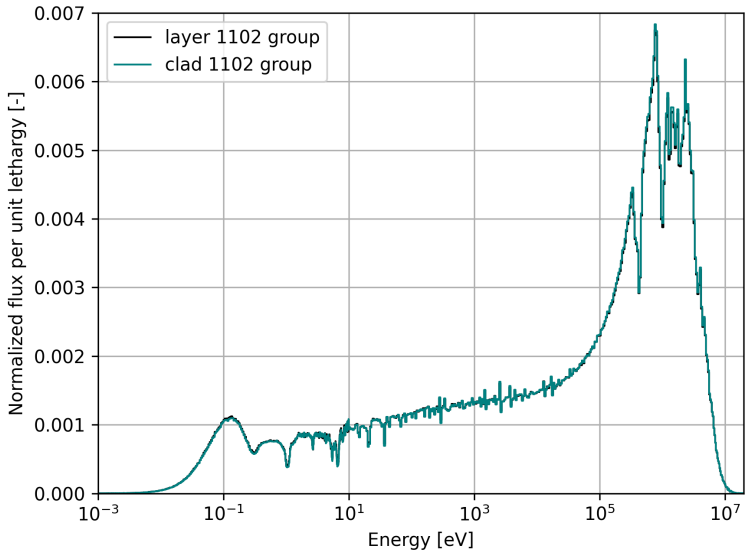

SiC+10µmCr

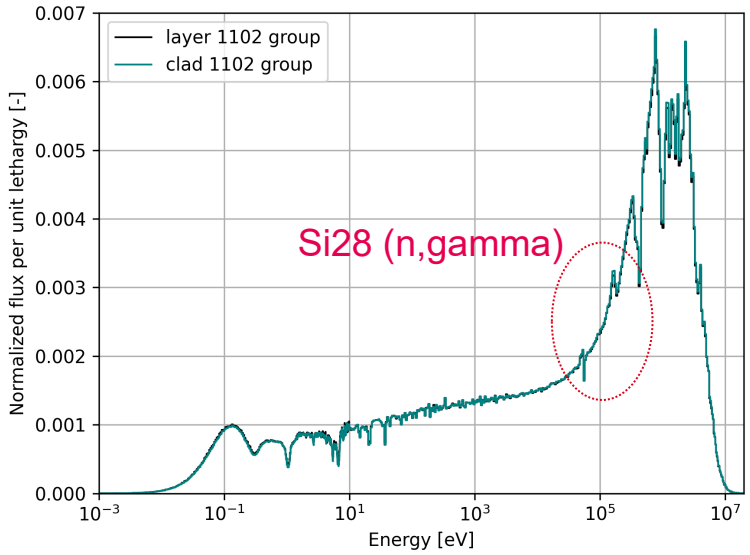

M5+20µmCr (here: MOI)

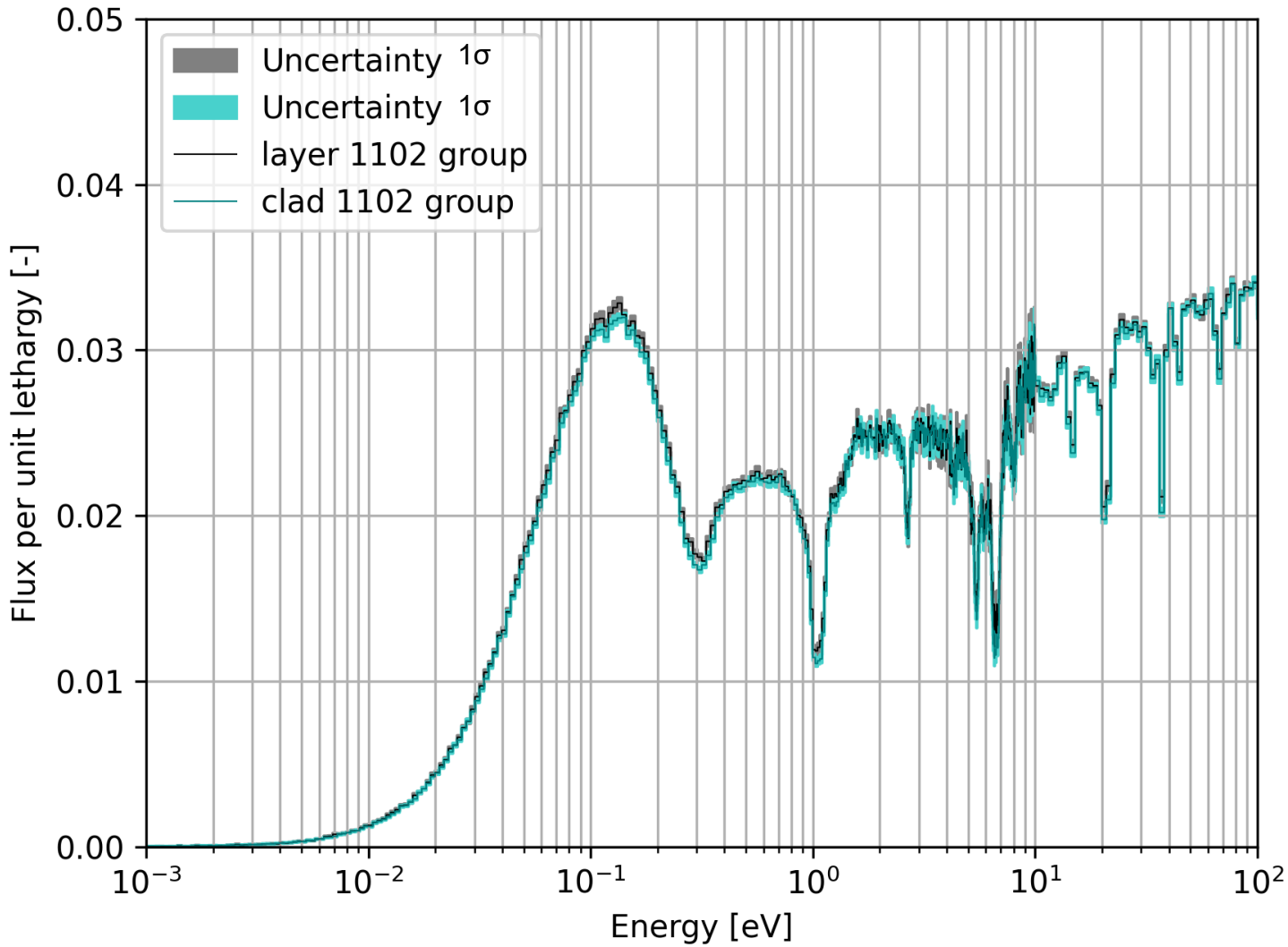

Contact dose rate vector vs decay time

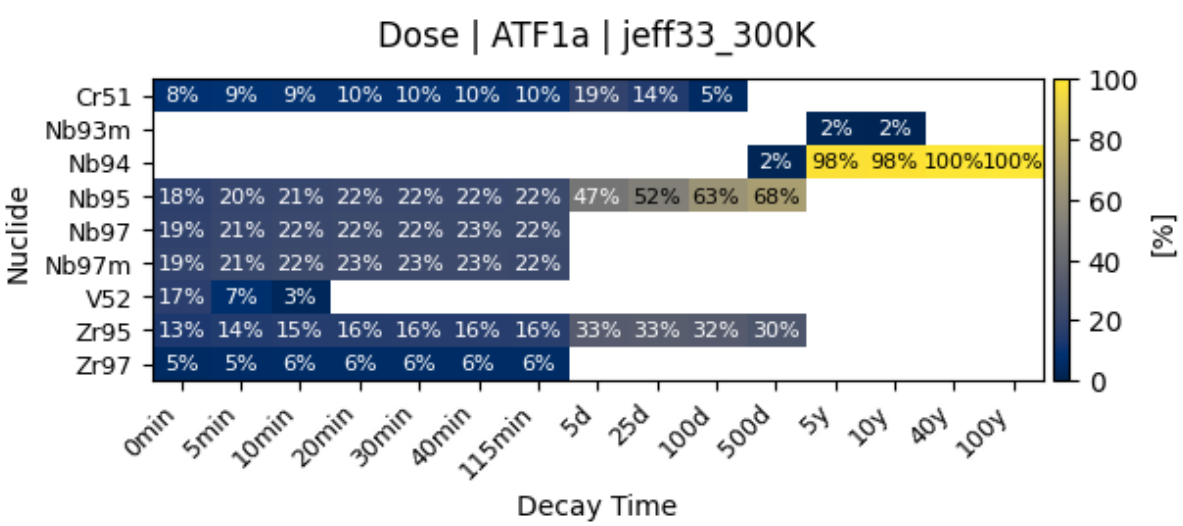

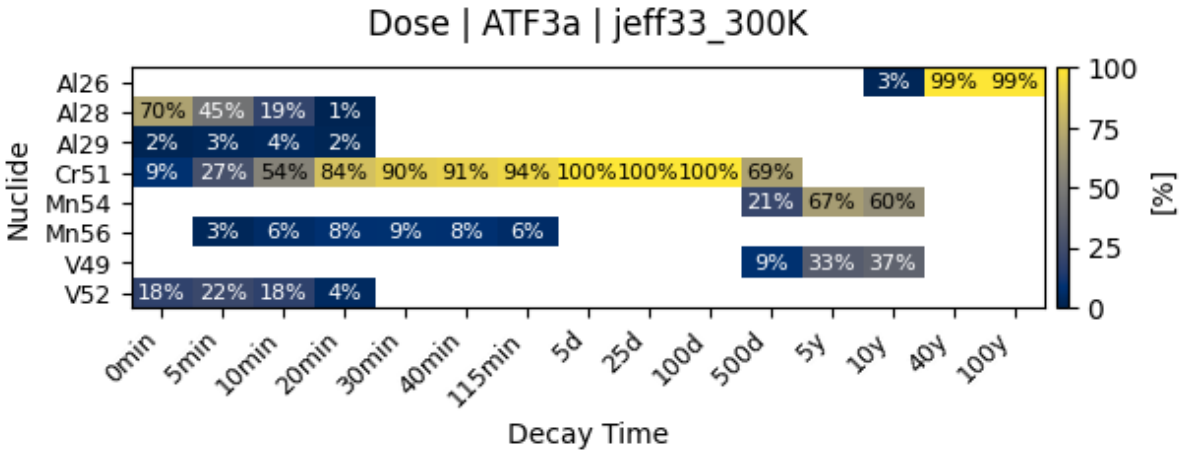

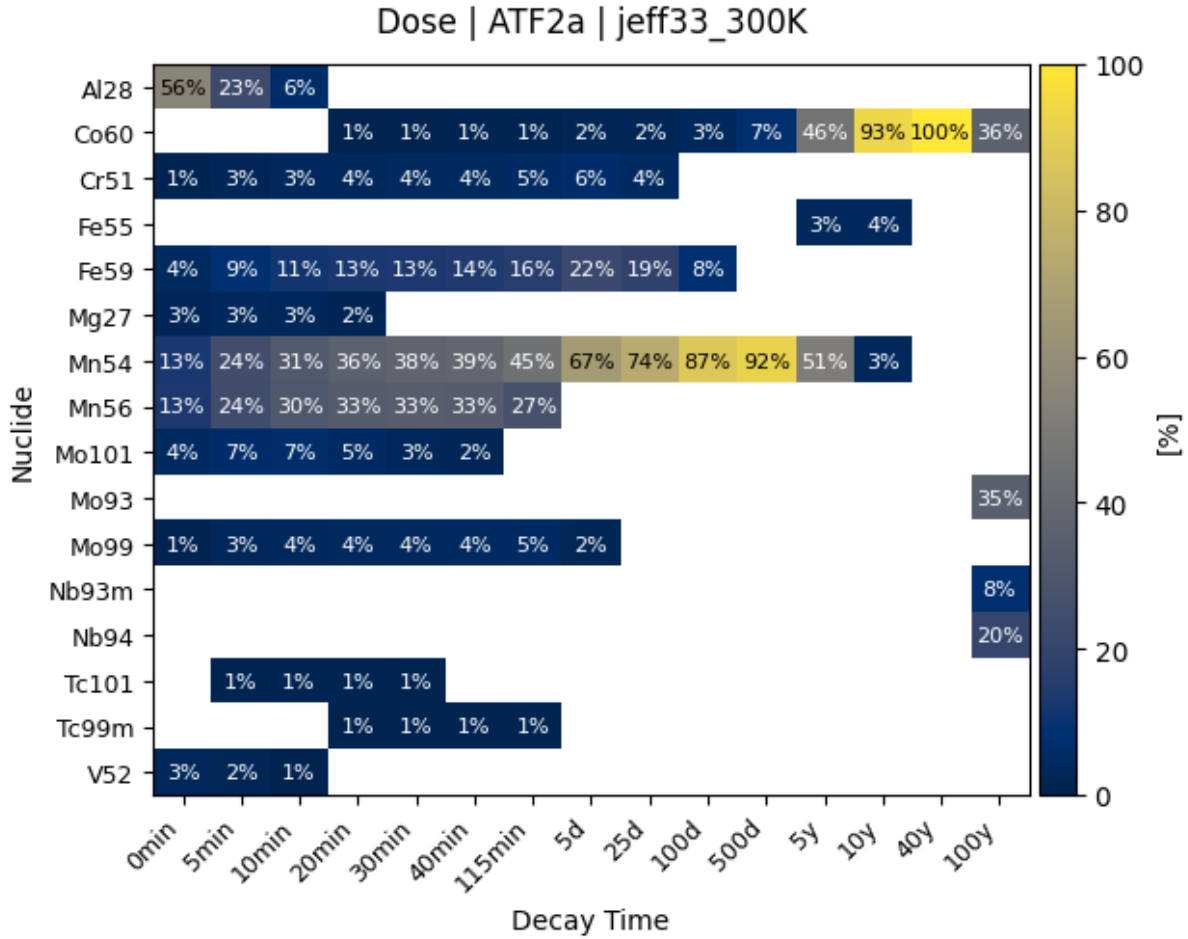

SiC+Cr: Evolution of elemental appm (>1appm)

	ATF3a
H	6e+01
V	3e+01
He	3e+01
P	3e+01
Mg	3e+01

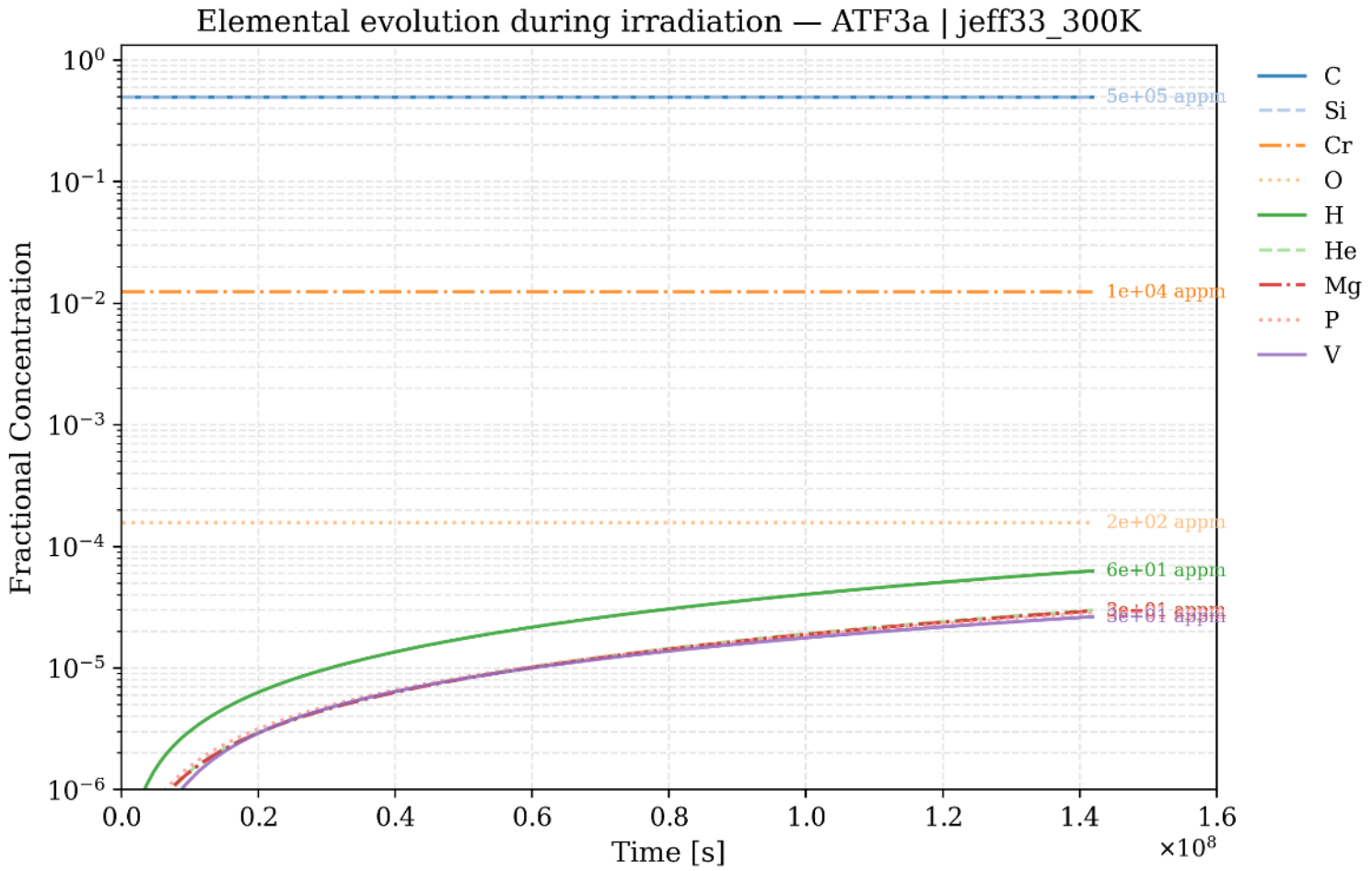

FeCrAl: Evolution of elemental appm (>1appm)

	ATF2a
V	2e+02
Mn	1e+02
H	1e+02
Tc	3e+01
Ru	2e+01
Co	1e+01
He	7e+00

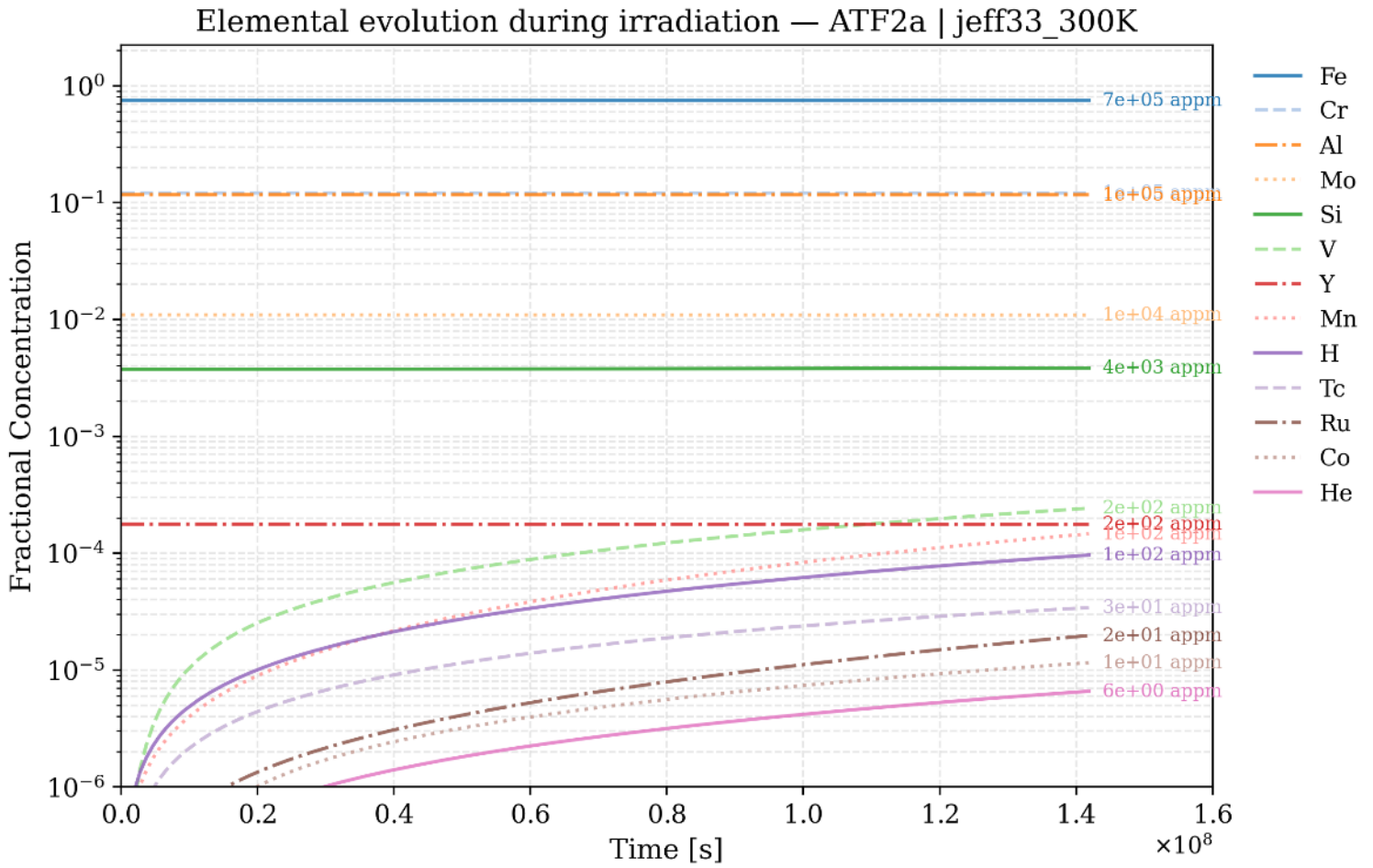

Contact dose rate semi-infinite slab (jeff-3.3)

- Similar order and evolution as for activity
- M5 shifted upwards (higher MeV/second) compared to FeCrAl
- SiC shifted upwards (Cr51 gamma lines)

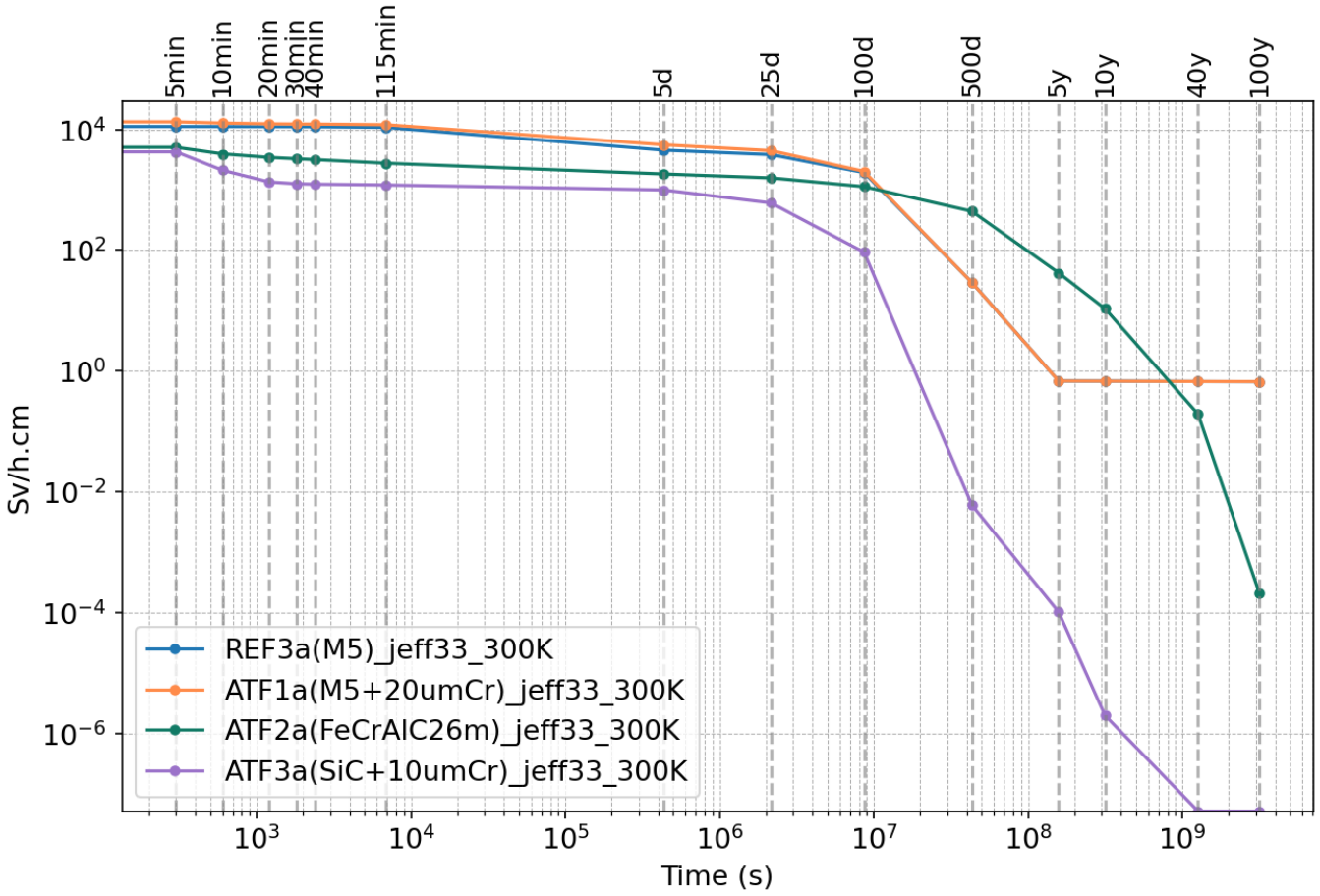

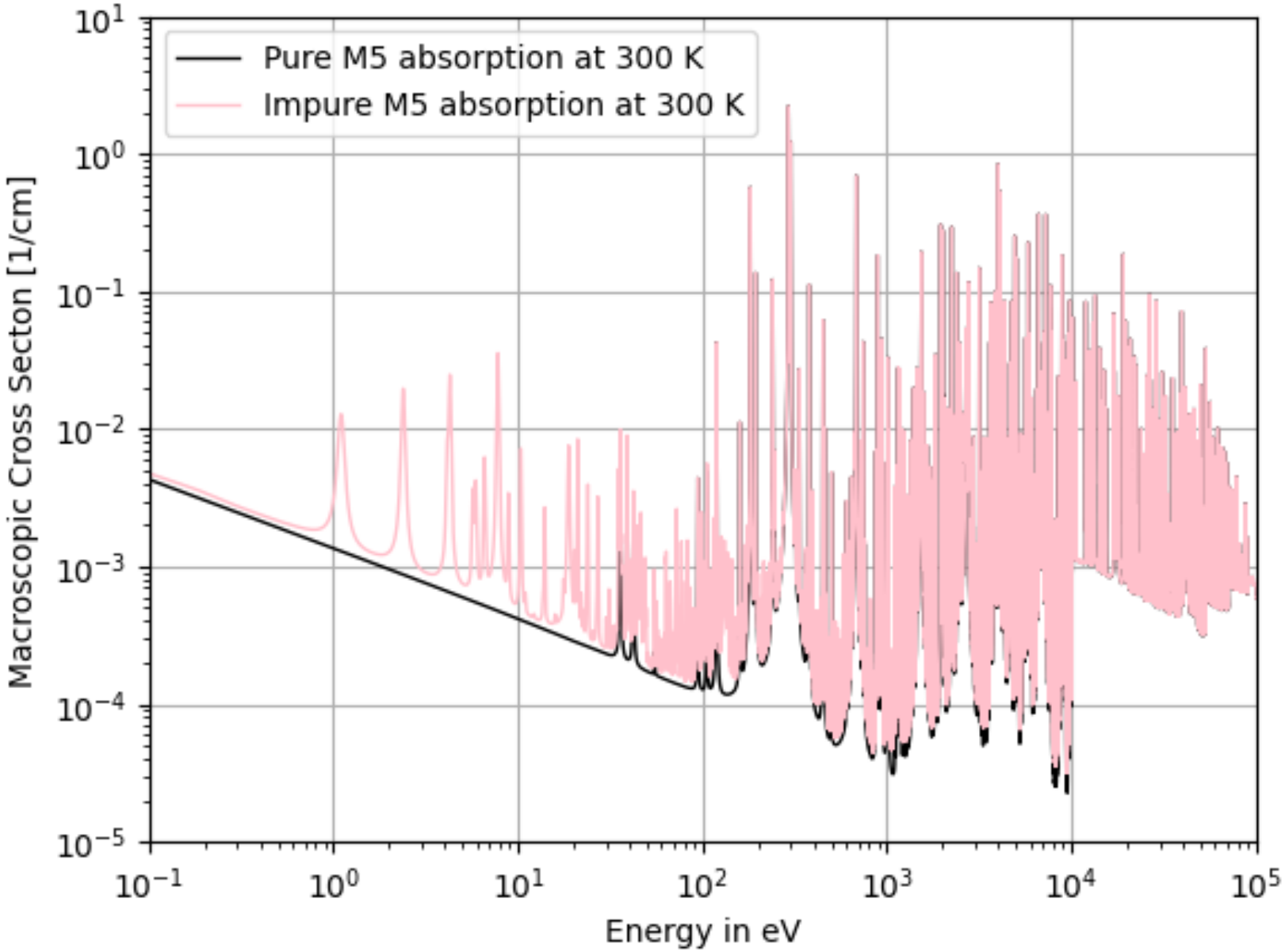
Pure M5 absorption at 300 K
Impure M5 absorption at 300 K
Macroscopic Cross Secton [1/cm]
Energy in eV
10^{1}
10^{0}
10^{-1}
10^{-2}
10^{-3}
10^{-4}
10^{-5}
10^{-1}
10^{0}
10^{1}
10^{2}
10^{3}
10^{4}
10^{5}

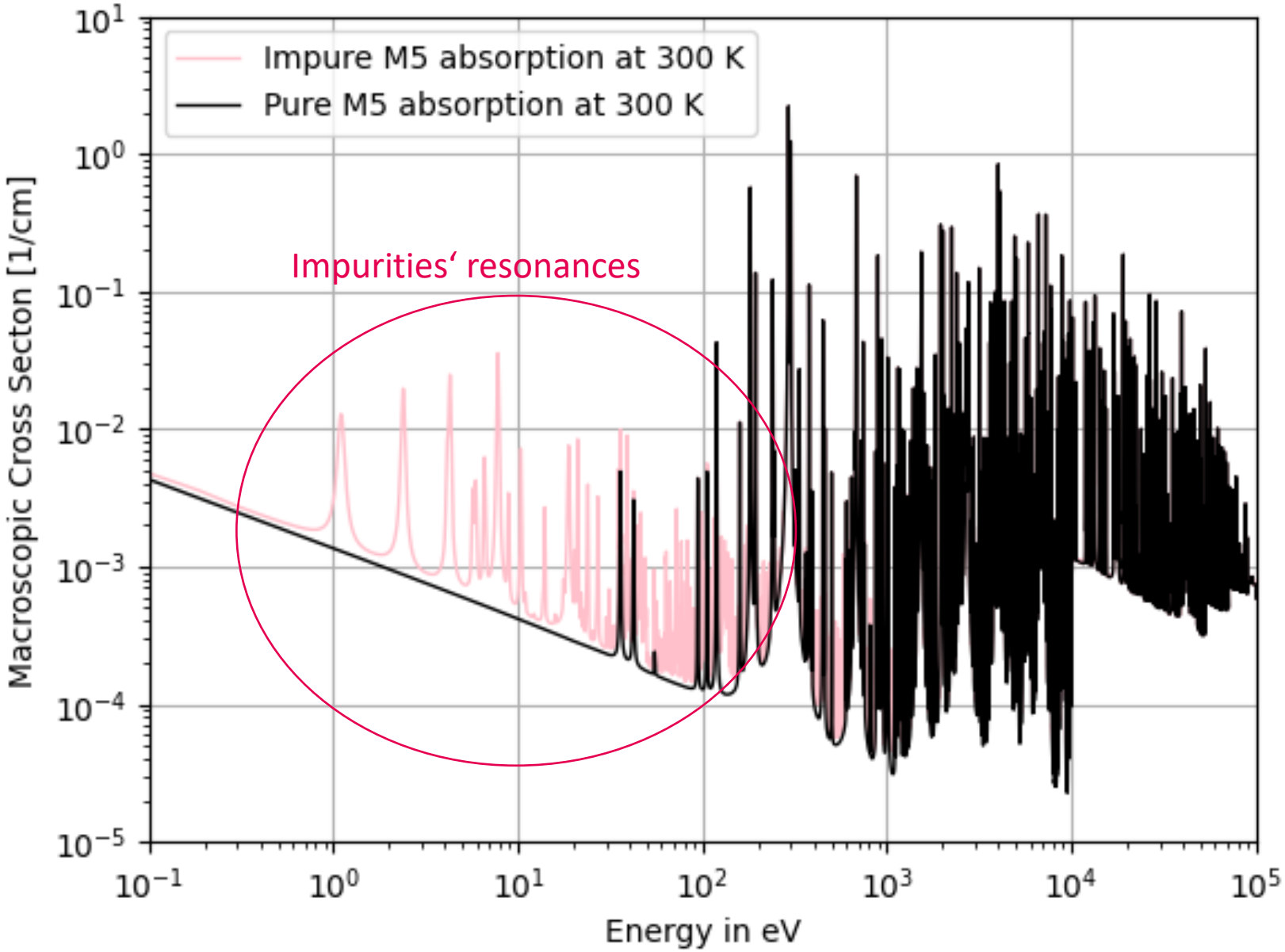
Impure M5 absorption at 300 K
Pure M5 absorption at 300 K
Impurities‘ resonances
Macroscopic Cross Secton [1/cm]
Energy in eV
10^{1}
10^{0}
10^{-1}
10^{-2}
10^{-3}
10^{-4}
10^{-5}
10^{-1}
10^{0}
10^{1}
10^{2}
10^{3}
10^{4}
10^{5}

Bq/cm (activity): Library > +300K > +SSFGeometry

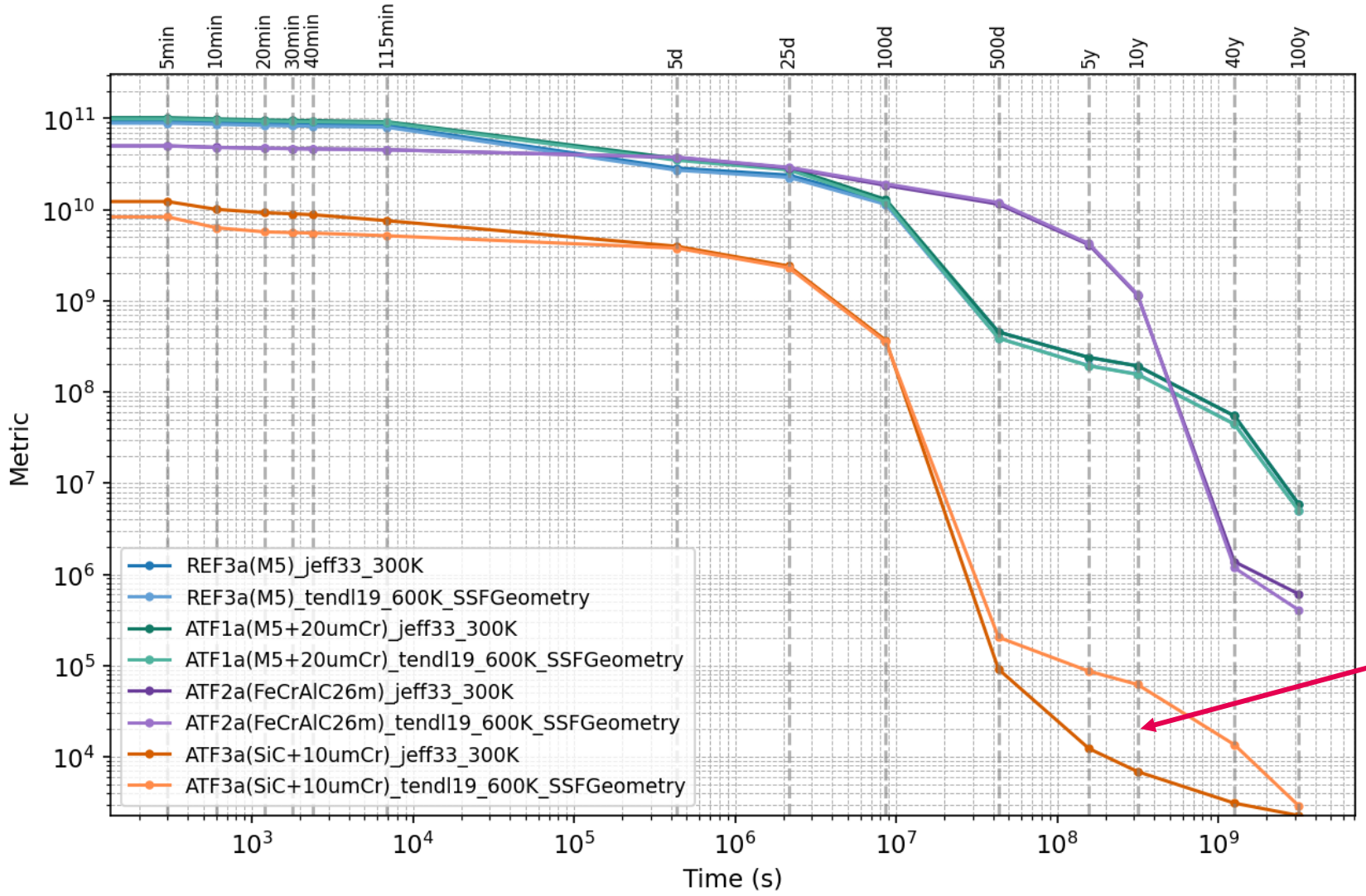

mainly H3

Sv/h.cm (contact dose rate semi-infinite slab)

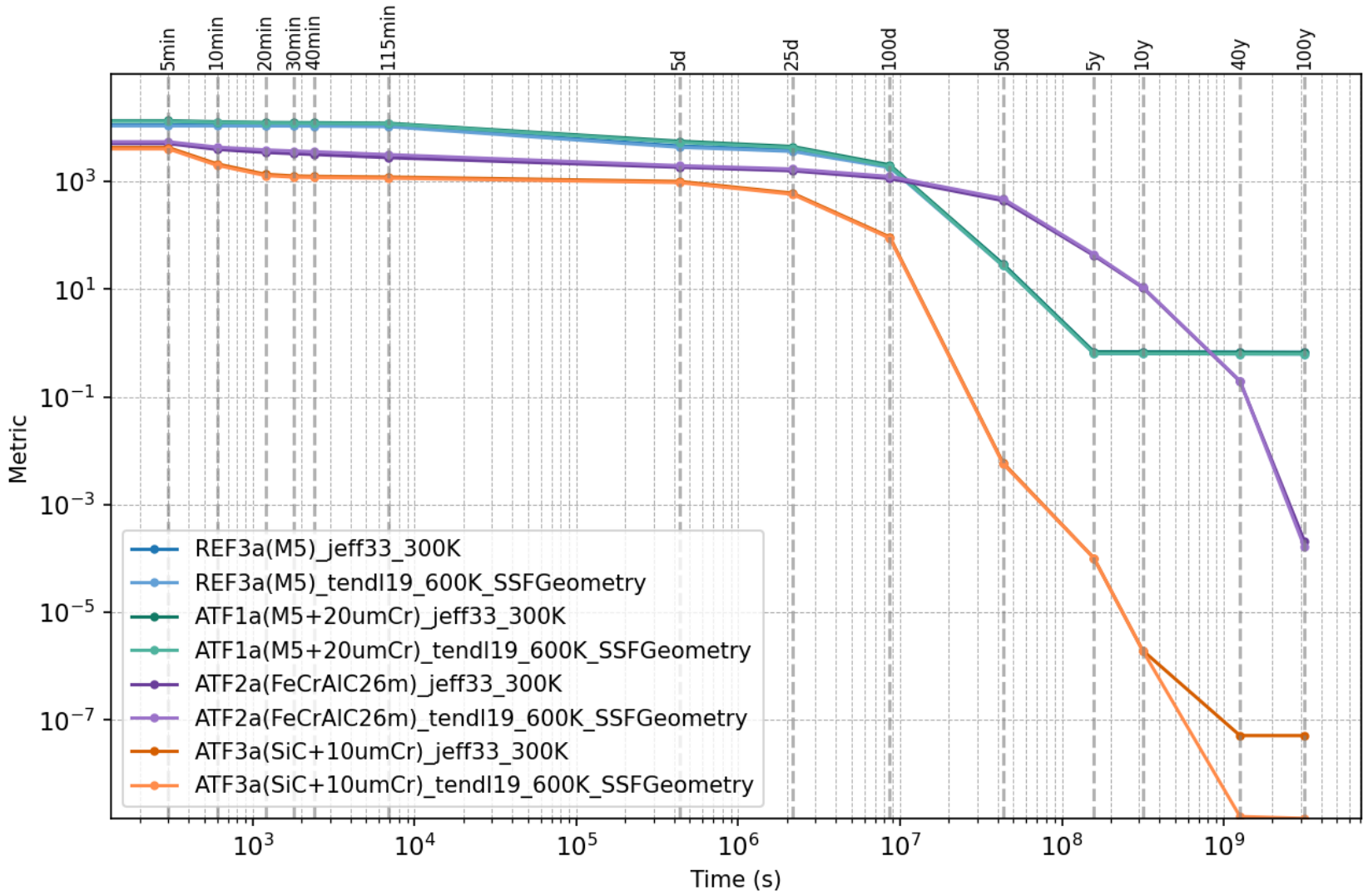

Sv/kg.cm (ingestion)

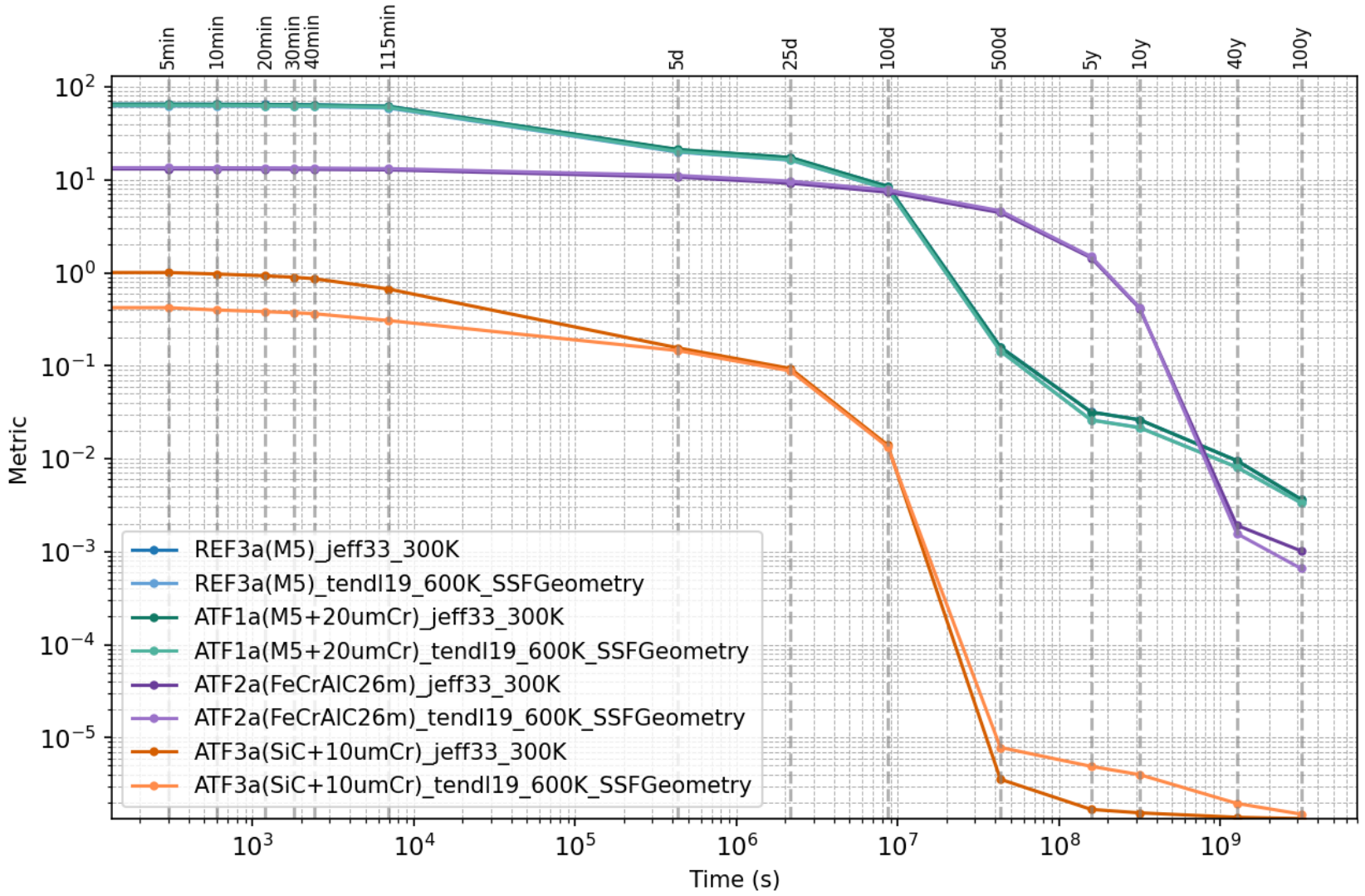

Dong-Hwa Lee

KAERI

Simulation of Cr-coated Zry-4 cladding tube ballooning and burst behavior using MERCURY

Nuclear fuel is inserted into the reactor core to generate thermal energy and transfer the resulting heat to the coolant. Throughout operation, the fuel must remain free from mechanical failure under normal operating conditions, and its thermo-mechanical behavior must stay within regulatory safety limits during accident scenarios.

To support the assessment of nuclear fuel performance under both normal and accident conditions, a variety of finite difference method (FDM) based analysis codes - such as FRAPCON [1], FRAPTRAN [2], and ROPER [3] - have been developed. More recently, to enable higher-fidelity simulations, finite element method (FEM) based performance analysis codes capable of modeling mesh deformation and heterogeneous material behavior have been introduced. Representative FEM-based codes include BISON [4], developed at the Idaho National Laboratory (INL), and MERCURY [5–7], developed by the Korea Atomic Energy Research Institute (KAERI).

MERCURY (Multi-dimensional Entire fuel Rod Code for Understanding Reaction Yield behaviors) V1.0 was developed in accordance with KAERI's software quality assurance (SQA) procedures, and its verification was completed through a series of numerical benchmarks [8]. As part of the validation effort - intended to evaluate the code's ability to reproduce relevant physical phenomena - the MERCURY code was applied to the Zry-4 DIMAT experiment. The DIMAT (Deformation In-situ Measurement Apparatus by image-analysis Technique) experiment reproduces the high-temperature expansion and rupture behavior of nuclear fuel cladding under Loss-of-Coolant Accident (LOCA) conditions, which represent a one of the key reactor Design-Basis-Accidents (DBAs). The deformation response of Zry-4 cladding, including ballooning and burst behavior, was characterized using in-situ imaging techniques [9–10].

In this study, the MERCURY code was used to simulate the DIMAT experiment, and the resulting predictions were compared with experimental measurements to assess the code's predictive capability. Additionally, the MERCURY code was employed to simulate the ballooning and burst behavior of Cr-coated Zry-4 cladding tubes, providing further insight into its applicability to advanced cladding concepts.

References

[1] Geelhood, K. J., et al. FRAPCON-4.0: A Computer Code for the Calculation of Steady-State, Thermal-Mechanical Behavior of Oxide Fuel Rods for High Burnup, PNNL-19418, Vol.1 Rev.2, 2015.
[2] Geelhood, K. J., et al. FRAPTRAN-2.0: A Computer Code for the Transient Analysis of Oxide Fuel Rods, PNNL-19400, Vol.1 Rev2, 2016.

[3] Choi, J. M., et al. A Fuel Rod Performance Analysis and Design Code–ROPER. In: Korean Nuclear Society Spring Meeting. 2009.
[4] J. D. Hales et al. BISON Theory Manual The Equations Behind Nuclear Fuel Analysis. Idaho National Laboratory. Idaho Falls, Idaho, Oct. 2014.
[5] Kim, Hyochan, et al. Development of MERCURY for simulation of multidimensional fuel behavior for LOCA condition. Nuclear Engineering and Design, 2020, 369: 110853.
[6] Lee, Sung-Uk, et al. Validation of MERCURY code under LOCA condition with Out-of-pile and In-pile tests. Nuclear Engineering and Design, 2022, 392: 111775.
[7] Kim, Hyochan, et al., MERCURY V1.0 Theory Manual, KAERI/TR-10442/2024, 2024.
[8] Lee, DongHwa, et al. Verification of FEM based thermo-mechanical solving system for fuel performance code and its results, KAERI/TR-9835, 2023.
[9] Choi, K.H. et al. Development of Strain Measurement Method by Image Analysis for Cladding Deformation, KAERI/TR-7930, 2019.
[10] Choi, K.H. et al. Measurement and Evaluation of High-temperature Deformation of Fuel Cladding using image analysis technique, KAERI/TR-8338, 2020.

2025 30th International QUENCH Workshop
Karlsruhe, Germany

KOREA ATOMIC ENERGY RESEARCH INSTITUTE

Simulation of Cr-coated Zry-4 cladding tube ballooning and burst behavior using MERCURY

December 17, 2025
Dong-Hwa Lee
LWR fuel technology research division, KAERI

KAERI Korea Atomic Energy Research Institute

A nuclear research institute
reshaping the future based on
peoples trust

KAERI

Korea Atomic Energy Research Institute

CONTENTS

Introduction of DIMAT experiment

DIMAT (Deformation In-situ Measurement Apparatus by Image-analysis Technique)

- KAERI's real-time measurement system for high-temperature cladding deformation
- Consists of an IR furnace for heating rate control, an internal pressure controller, and a camera for imaging
- Ar gas injection via the top to create internal rod pressure
- Ar gas injection via the furnace bottom for specimen inerting
- 6 IR lamps arranged outside the quartz tube for heating

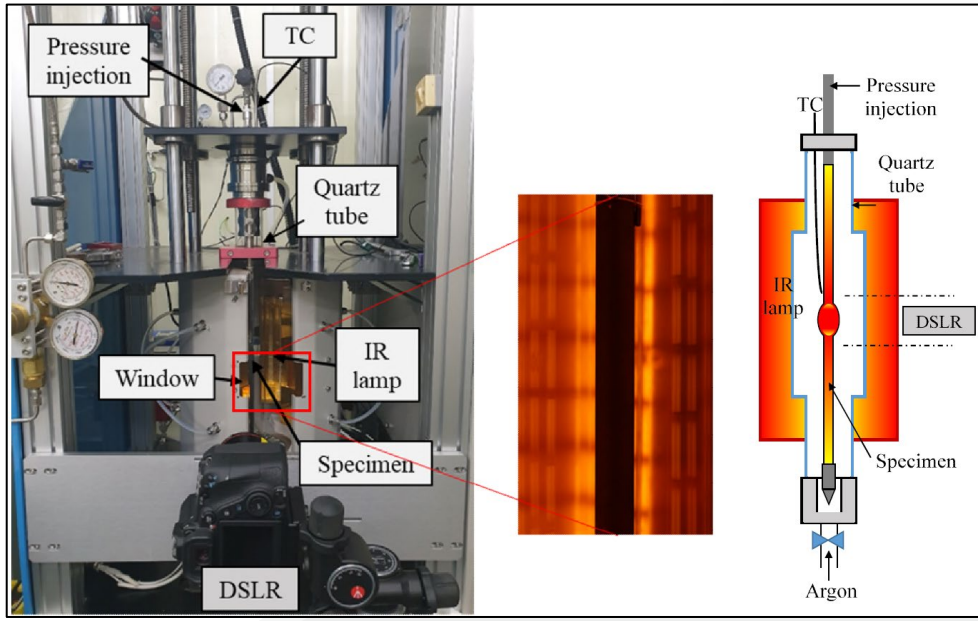

Choi et. Aa., Development of a strain measurement method using image analysis of high-temperature deformation of cladding pipes, KAERI/TR-7930, 2019.

Introduction of DIMAT experiment

Axial temperature gradient

- Due to IR furnace structure, 1% axial temperature gradient exist in +50cm ~ -50cm

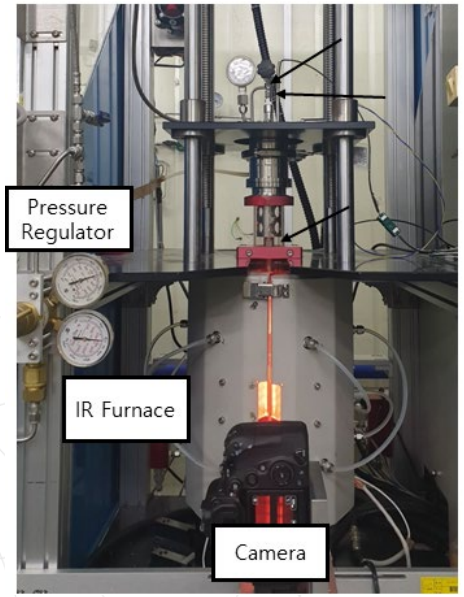

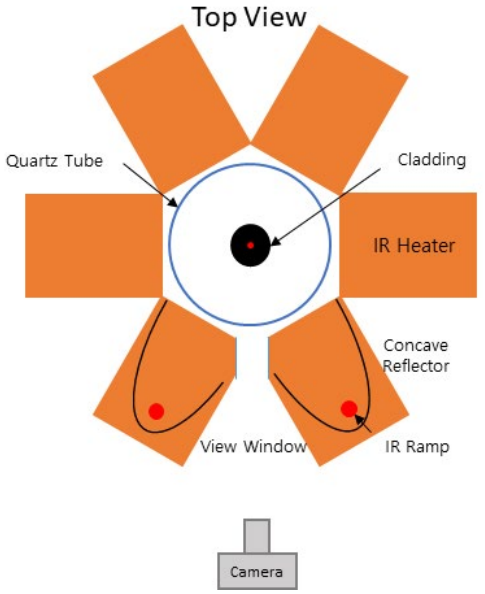

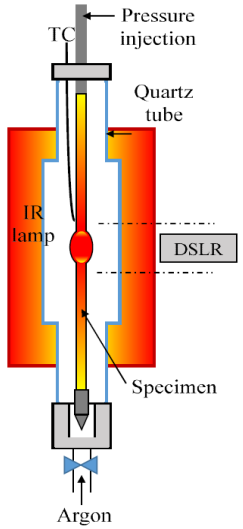

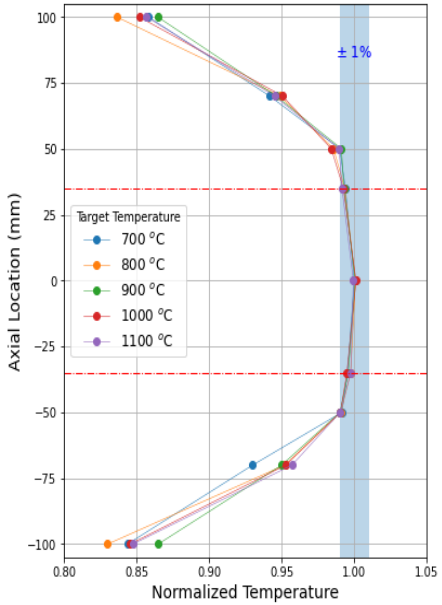

Zircaloy-4 cladding tube

- Outer radius and its thickness are 9.5mm, 0.57mm
- Residual stress has been removed at 753K for 3.5 hour

Shin et. al., Evaluation of a Reference Code High-Temperature Deformation Model Using Nuclear Fuel Cladding High-Temperature Deformation Verification Experimental Technology, KAERI/TR-9213, 2022.

Introduction of DIMAT experiment

Measurement of deformation behavior through image processing

Painted cladding tubes are used to eliminate reflections

- 1 pixel = 21~22μm, uncertainty : 5 pixel

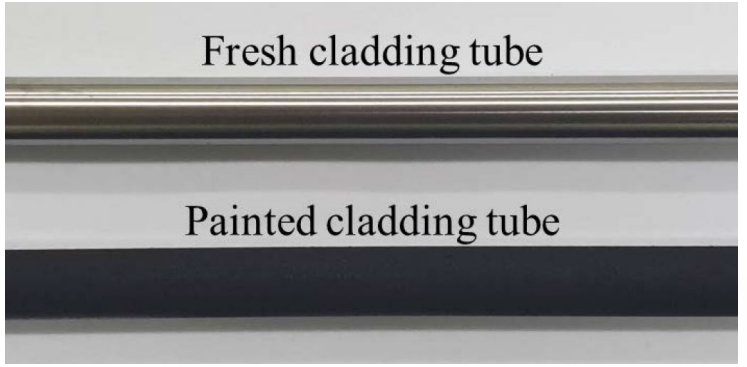

Post processing of images taken by camera

- Canon EOS 90D camera with EF 100mm F2.8L Macro IS USM with a close-up lens

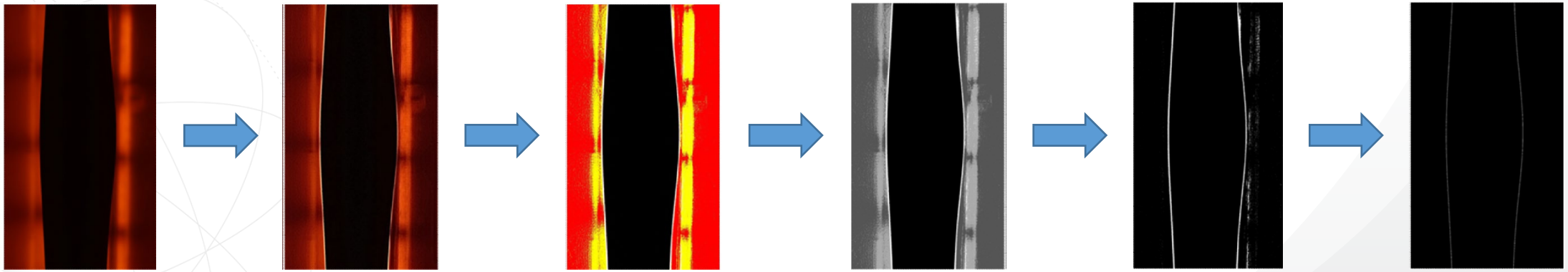

Choi et. al., Measurement and Evaluation of High-Temperature Deformation of Cladding Pipes Using Image Analysis Techniques, KAERI/TR-8338, 2020.

Introduction of DIMAT experiment

High temperature deformation experiment

Tube burst experiment in transient condition

- Step 1. Heating from room temperature to 300℃
- Step 2. Iso-thermal condition for 300s for stabilization
- Step 3. Inject Ar gas to create internal gas pressure
- Step 4. 60s later, increase temperature at constant speed until burst

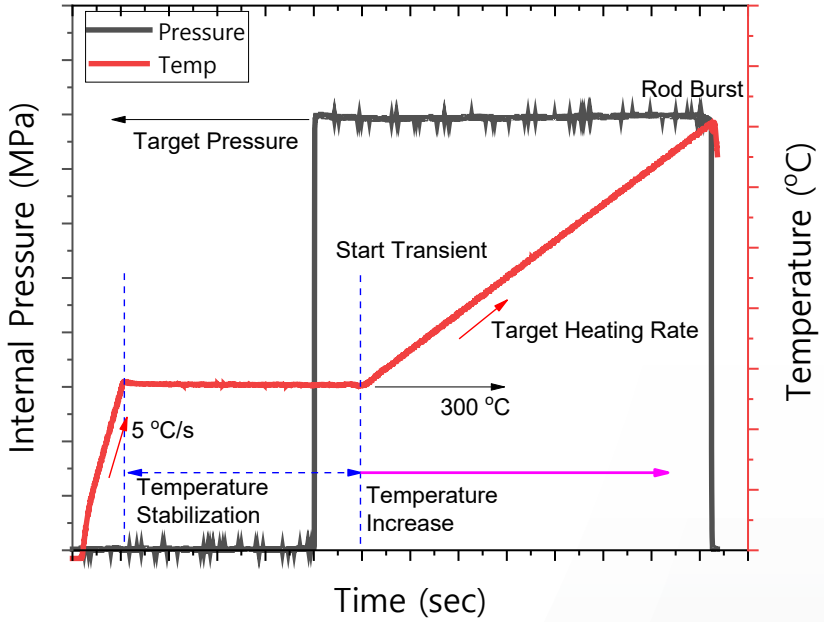

Experiment matrix

- 3 kinds of heating rates (1 K/s, 14 K/s, 28 K/s), 3 kinds ot internal pressure (40 bar, 60 bar, 80 bar)
- 9 experiment conditions in total

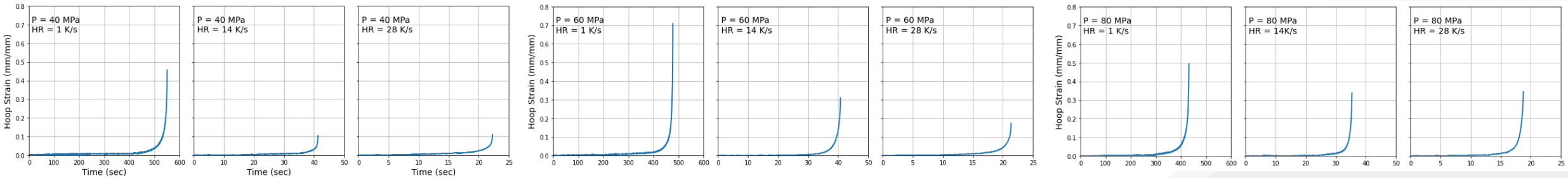

Choi et. al., Measurement and Evaluation of High-Temperature Deformation of Cladding Pipes Using Image Analysis Techniques, KAERI/TR-8338, 2020.

Introduction of MERCURY code

MERCURY (Multi-dimensional Entire fuel Rod Code for Understanding Reaction Yield behavior)

FEM based nuclear fuel performance code

- Thermal/Mechanical coupling analysis of multi-material
- Including large deformation, creeping, etc…

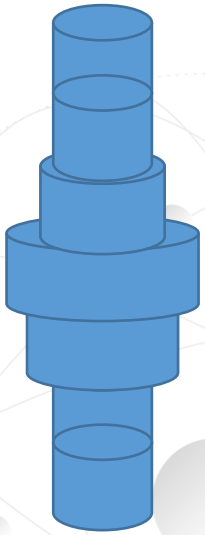

Ballooning analysis using FDM

Ballooning/ Burst experiment

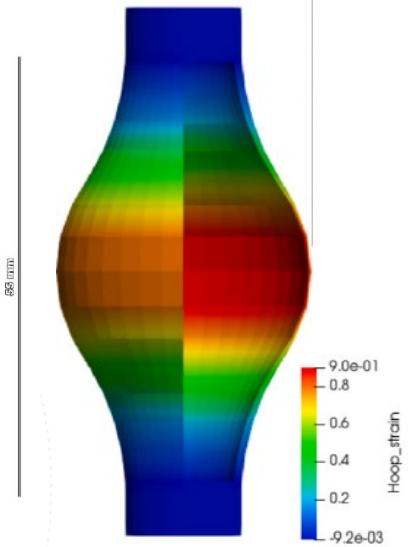

Ballooning analysis using FEM

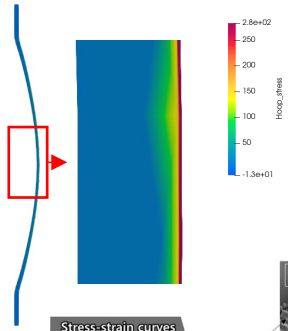

Stress distribution of ATF

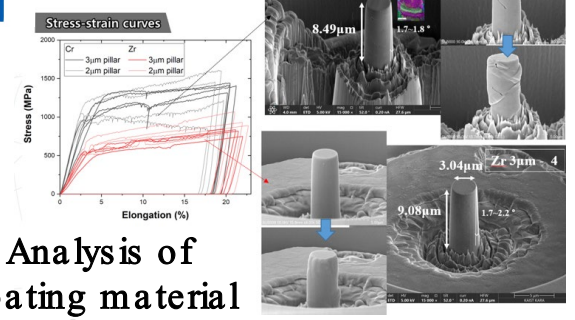

Analysis of coating material

Specimen image

HRP IFA650.9 analysis result

Double ballooning

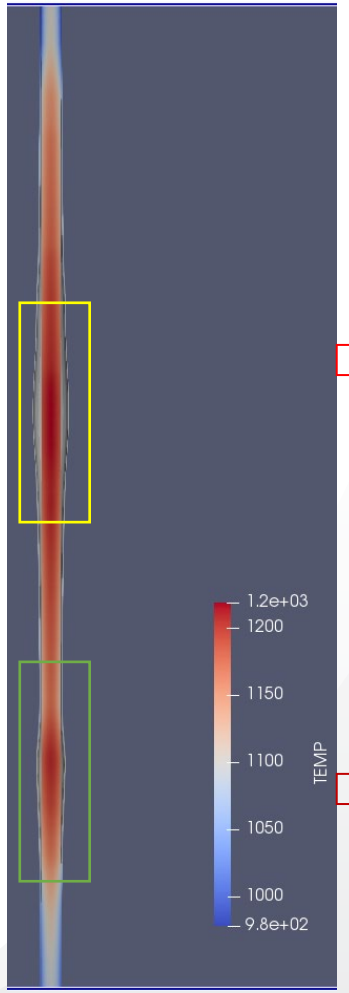

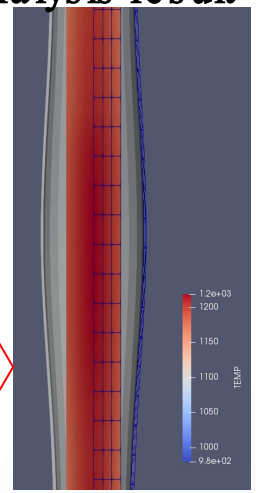

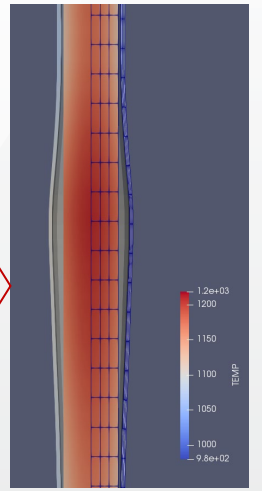

J. Hong et al., Measurement of local mechanical properties for Cr-coated accident tolerant fuel cladding, Journal of Nuclear Materials 579 (2023) 154407.

Introduction of MERCURY code

Korea Atomic Energy Research Institute

Code Verification of MERCURY

- For code Verification, we used Method of Manufactured Solutions (MMS) and checked the simulation results converges to analytic result

	Reference	Transient		Coordinate System			Dimension			Properties and External Sources						Boundary Conditions		
		Transient	Steady State	Cartesian	Cylindrical	Spherical	x_1	x_2	x_3	k_c	$k(T)$	q'''	$q'''(\vec{x})$	α_c	$\alpha(T)$	Dirichlet	Neumann	Convective
Method of Exact Solutions																		
3.1	[26]		✓	✓			✓			✓		✓				✓		
3.2	[26]		✓	✓			✓				✓					✓		
3.3	[27]		✓	✓			✓				✓	✓				✓	✓	
3.4	[28]		✓	✓			✓	✓		✓						✓		
3.5	[26]		✓		✓		✓			✓						✓		
3.6	[26]		✓		✓		✓				✓					✓		
3.7	[28]		✓		✓		✓				✓	✓				✓		
3.8	[29]		✓		✓		✓			✓		✓					✓	✓
3.9	[29]		✓		✓		✓			✓		✓					✓	✓
3.10	[28]		✓		✓		✓		✓	✓						✓		
3.11	[29, 30]		✓			✓	✓			✓		✓				✓		
3.12	[26]		✓			✓	✓			✓						✓		
3.13	[26]		✓			✓	✓				✓					✓		
3.14	[29, 31]		✓			✓	✓			✓			✓			✓		
3.15	[29, 32]		✓			✓	✓			✓		✓						✓
3.16	[29]		✓			✓	✓			✓		✓				✓	✓	
Method of Manufactured Solutions																		
3.17			✓	✓			✓			✓						✓	✓	
3.18			✓	✓			✓	✓		✓						✓		
3.19	[1]	✓		✓			✓			✓				✓		✓		

Verification of BISON using analytic and manufactured solutions, CASL-U-2020-1939-000

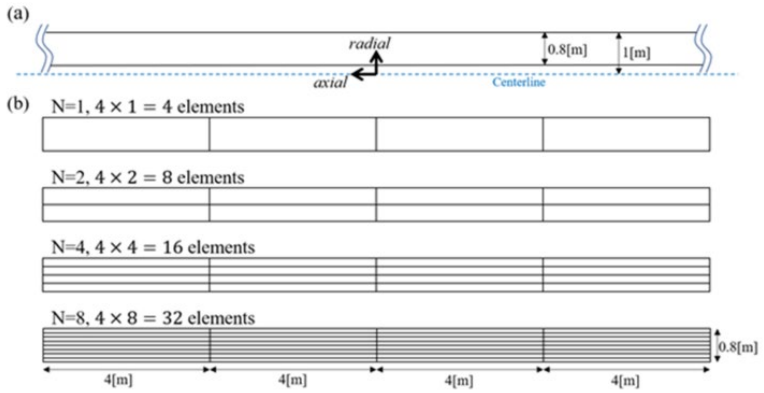

N	온도 오차
1	7.64374E+00
2	1.42421E+00
4	2.14758E-01
8	2.85282E-02
16	3.62220E-03
32	4.54508E-04
64	5.68671E-05
128	7.11006E-06
256	8.88810E-07

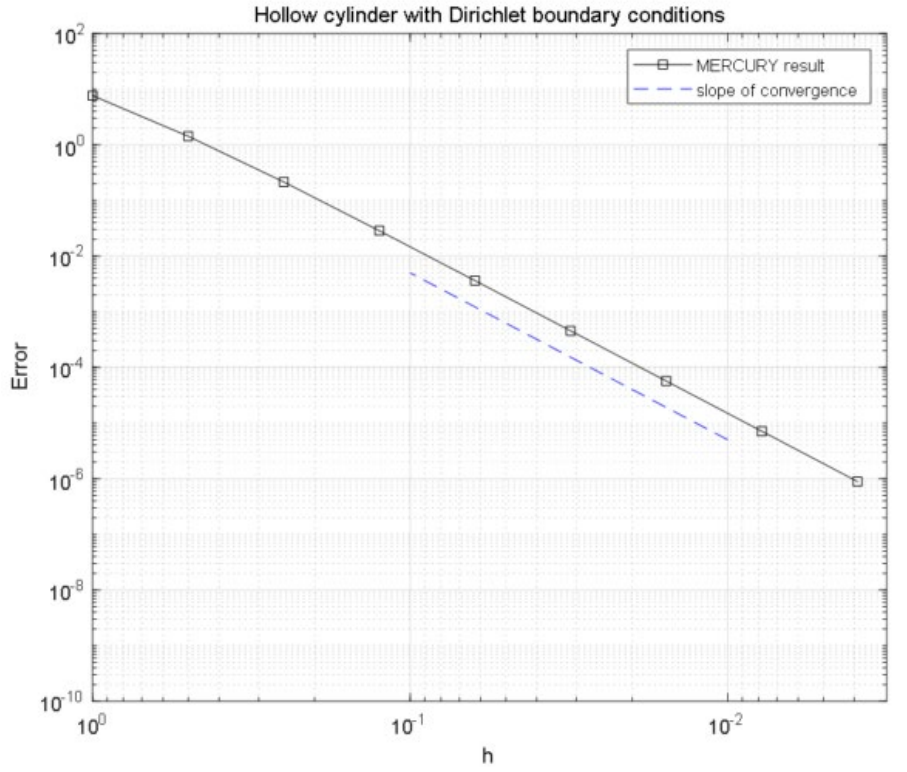

$$u(r) = \frac{u_o \ln(r_i) - u_i \ln(r_o)}{\ln(r_i/r_o)} + \frac{u_i - u_o}{\ln(r_i/r_o)} \ln(r)$$

D.H. Lee et. al. MRC_1.0-STR-24-01; R0 (Software Quality Assurance), 2024

Introduction of MERCURY code

MERCURY code input

Axial temperature gradient input

- The +100mm ~ -100mm section is divided into 10mm units
- Using temperature gradient correlation measured experimentally
- 573K, 1573K, 14573K, 28593K are chosen as peak temperature

HEIGHT[MM]	573K	1573K	14573K	28593K
-100	484.4577	1329.934	12321.12	24157.79
-90	510.7665	1402.157	12990.23	25469.69
-80	530.822	1457.213	13500.29	26469.77
-70	545.7613	1498.224	13880.24	27214.73
-60	556.5917	1527.956	14155.69	27754.79
-50	564.1902	1548.815	14348.94	28133.69
-40	569.3037	1562.853	14478.99	28388.68
-30	572.549	1571.762	14561.53	28550.51
-20	574.4128	1576.879	14608.93	28643.45
-10	575.2517	1579.181	14630.27	28685.28
0	575.292	1579.292	14631.29	28687.29
10	574.6301	1577.475	14614.46	28654.29
20	573.2321	1573.637	14578.9	28584.58
30	570.9342	1567.329	14520.46	28469.99
40	567.4423	1557.743	14431.65	28295.86
50	562.3321	1543.714	14301.69	28041.04
60	555.0494	1523.722	14116.47	27677.88
70	544.9099	1495.887	13858.59	27172.27
80	531.0988	1457.973	13507.34	26483.57
90	512.6716	1407.387	13038.68	25564.69
100	488.5536	1341.178	12425.29	24362.03

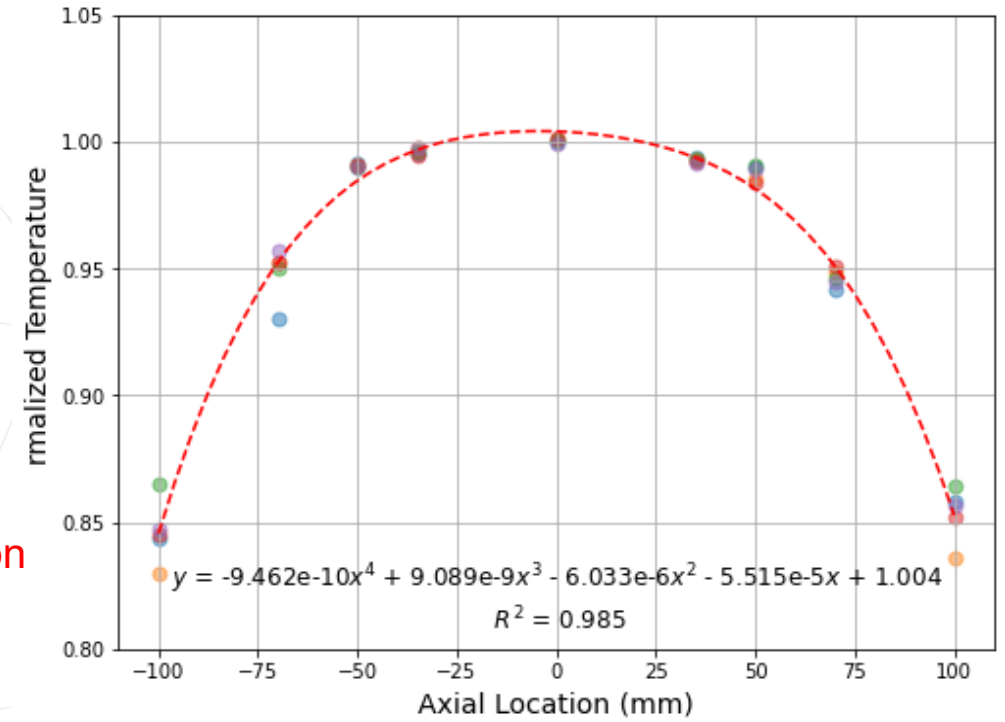

Temperature gradient correlation measured from experiment

Simulation of DIMAT experiment

Mesh inputs

Investigation on Mesh Dependency

- Cladding tube has 200mm in its length, 8.36mm in its inner diameter, 0.57mm on its thickness
- Mesh Dependency is investigated using 4 and 50/100/200 number of 8-node elements

4-by-50

4-by-100

4-by-200

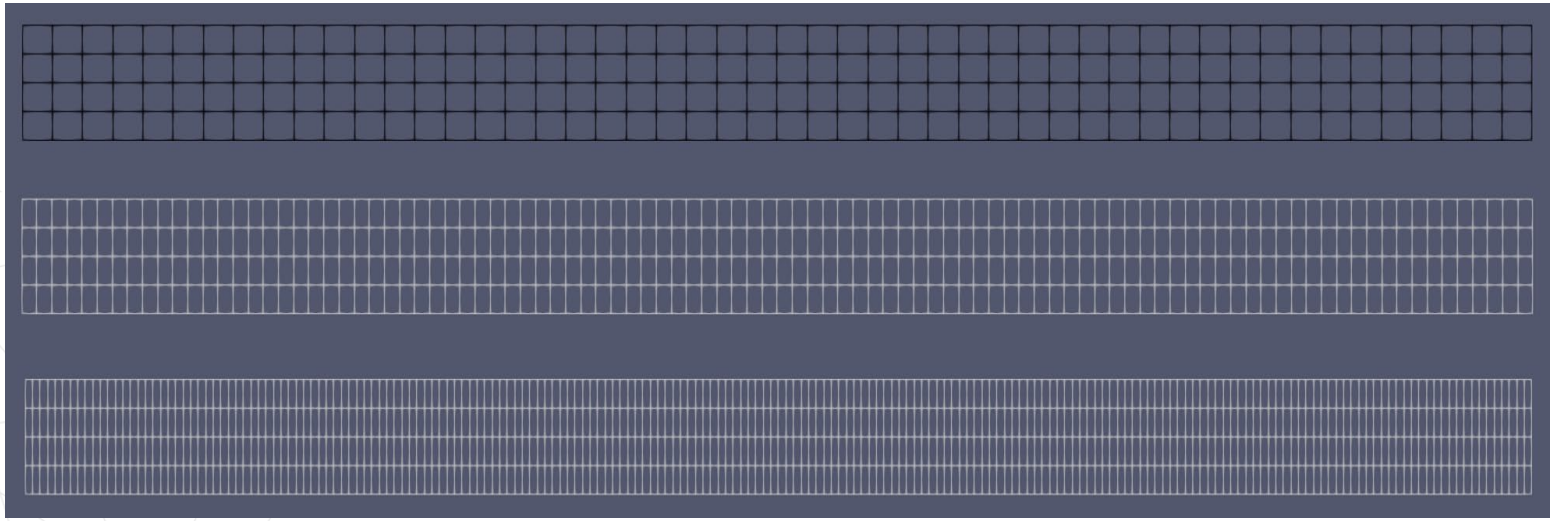

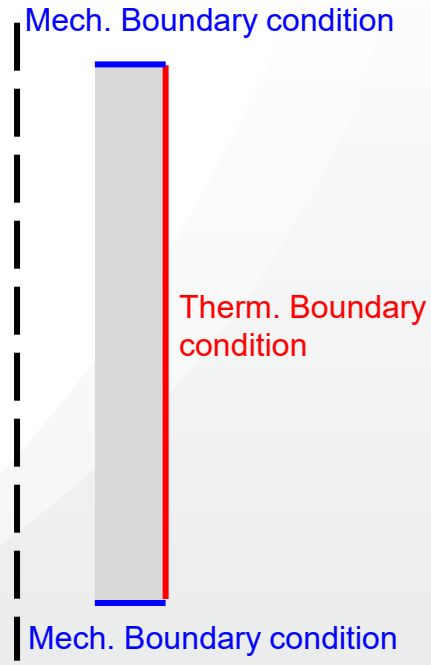

Boundary conditions

- Themal boundary conditions on outer surface of cladding tube
- Mehcanical boundary conditions on upper and lower cladding tube

Simulation of DIMAT experiment

Results of 40 bar internal gas pressure

- Ballooning and burst occurred at the center of cladding tube
- No effect on Mesh Dependency
- Sudden change observed at 1085.1K, where creep coefficient of Zry-4 change from α phase to $\alpha + \beta$ phase

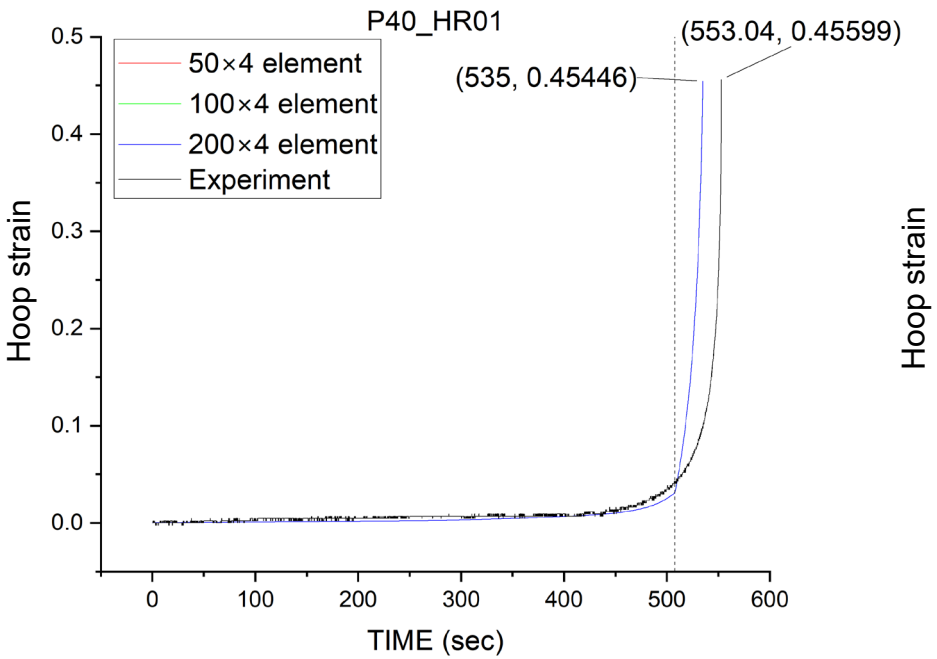

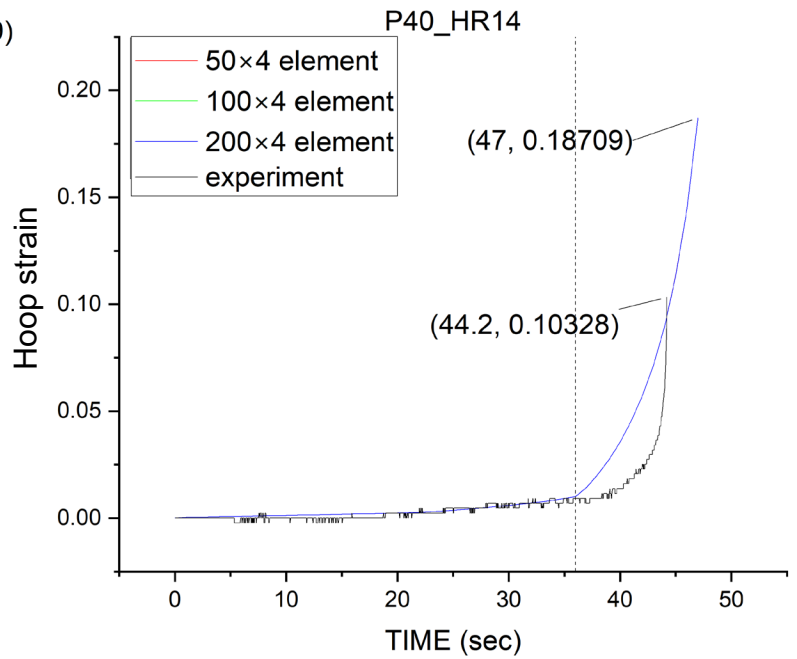

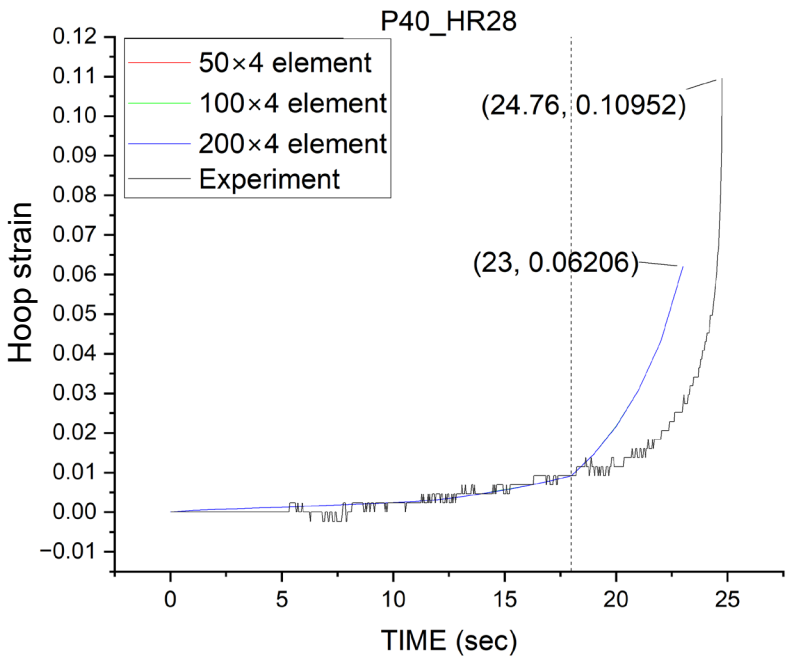

Choi, Gyeong-Ha, et al. "Circumferential steady-state creep test and analysis of Zircaloy-4 fuel cladding." *Nuclear Engineering and Technology* 53.7 (2021): 2312-2322.

Simulation of DIMAT experiment

Results of 60 bar internal gas pressure

- Ballooning and burst occurred at the center of cladding tube
- No effect on Mesh Dependency
- Sudden change observed at 1085.1K, where creep coefficient of Zry-4 change from α phase to $\alpha + \beta$ phase

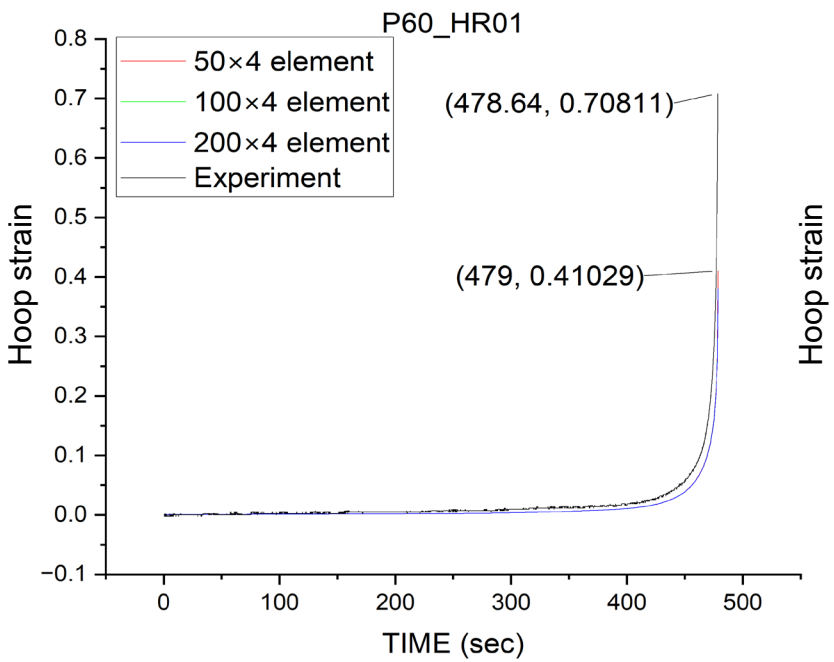

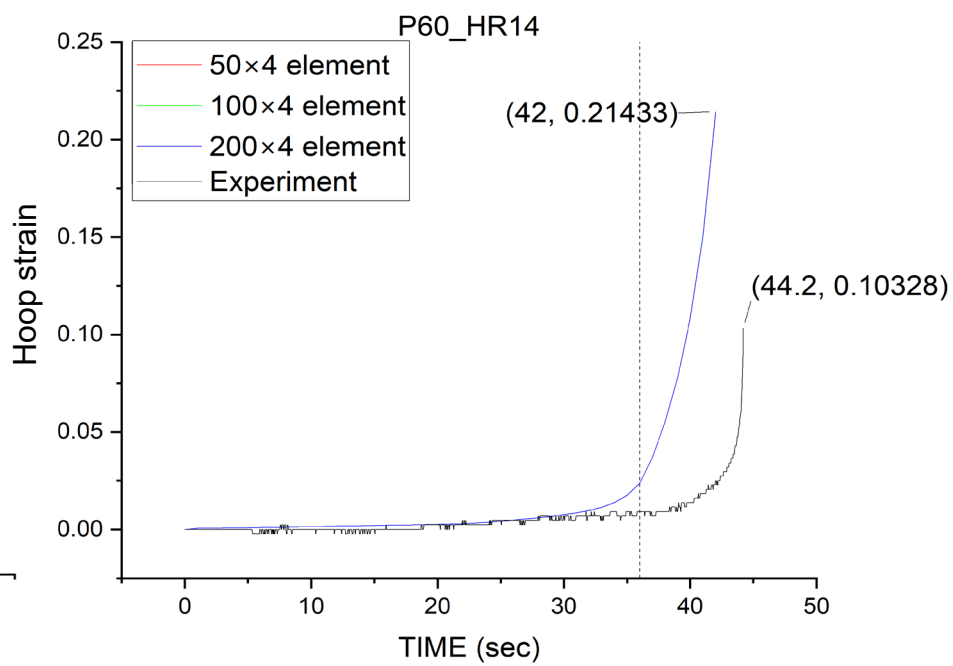

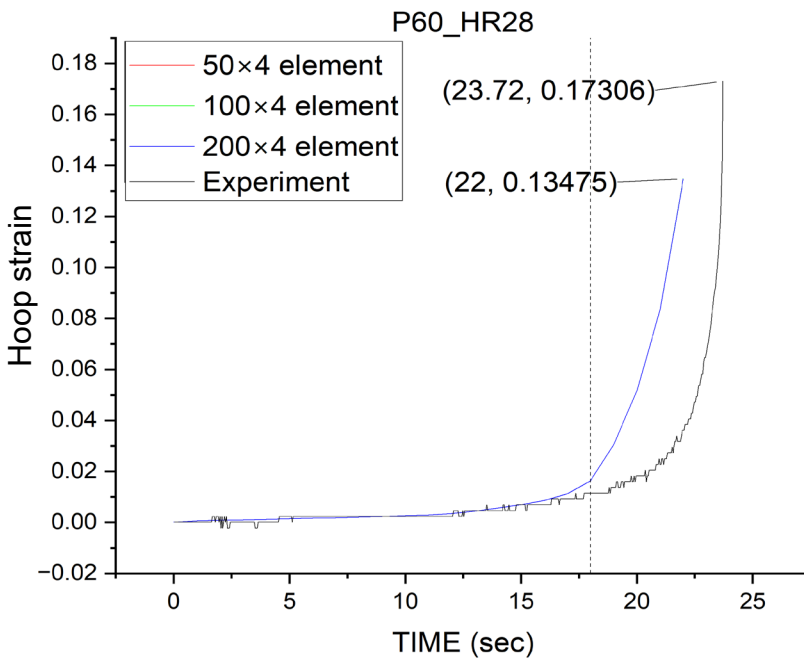

Choi, Gyeong-Ha, et al. "Circumferential steady-state creep test and analysis of Zircaloy-4 fuel cladding." *Nuclear Engineering and Technology* 53.7 (2021): 2312-2322.

Simulation of DIMAT experiment

Results of 80 bar internal gas pressure

- Ballooning and burst occurred at the center of cladding tube
- No effect on Mesh Dependency
- Sudden change observed at 1085.1K, where creep coefficient of Zry-4 change from α phase to $\alpha + \beta$ phase

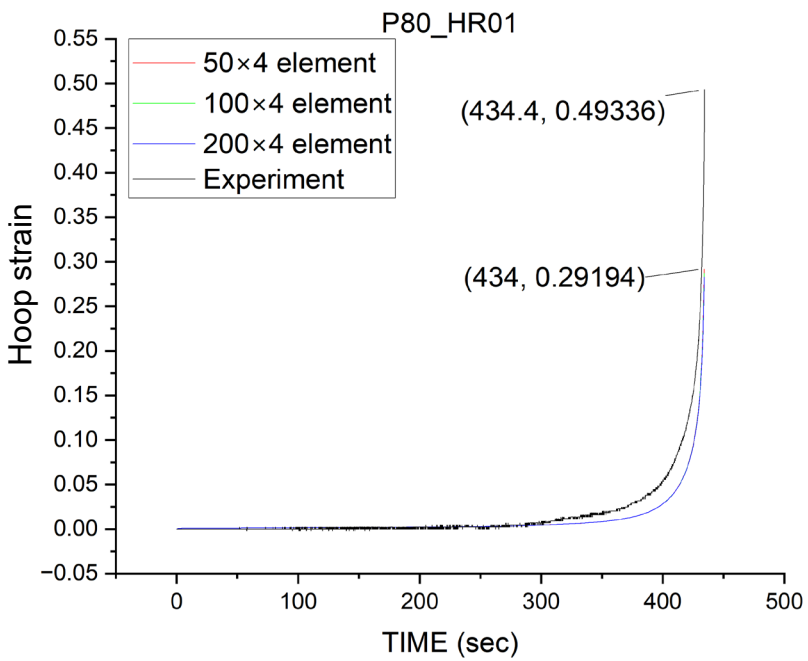

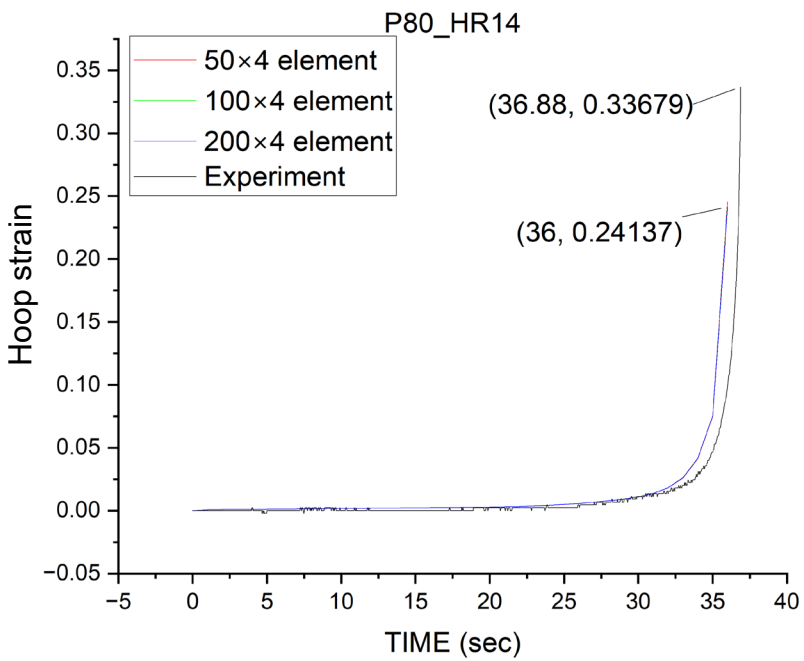

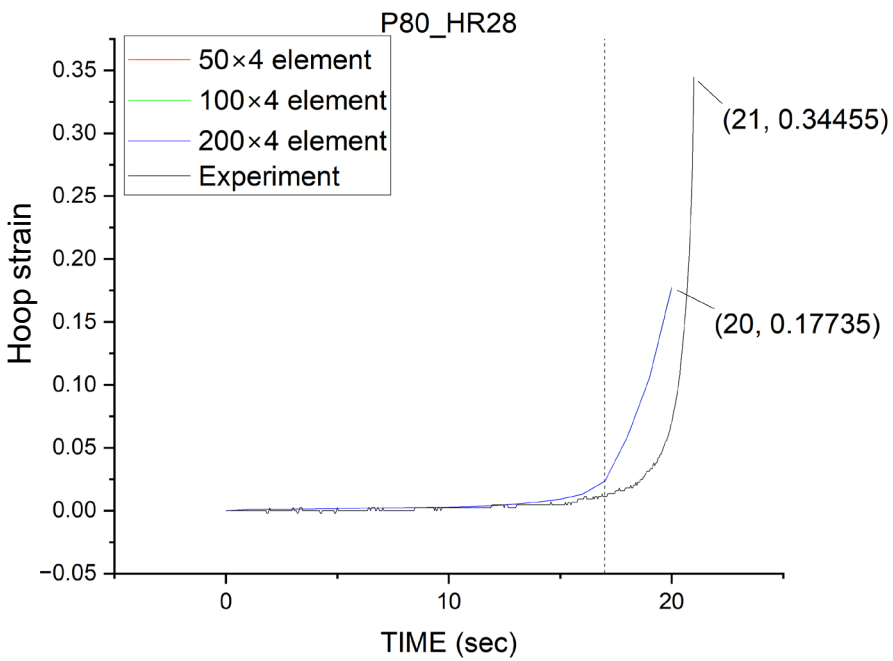

Choi, Gyeong-Ha, et al. "Circumferential steady-state creep test and analysis of Zircaloy-4 fuel cladding." *Nuclear Engineering and Technology* 53.7 (2021): 2312-2322.

Simulation of Cr-coated Zr-4 cladding tube

Mesh inputs

Cr-coated Zr-4 cladding tube

- Cladding tube has 200mm in its length, 8.36mm in its inner diameter, 0.55mm on its thickness, 0.02mm of Cr coating layer
- Same creep coefficients used for both Zry-4 and Cr coating

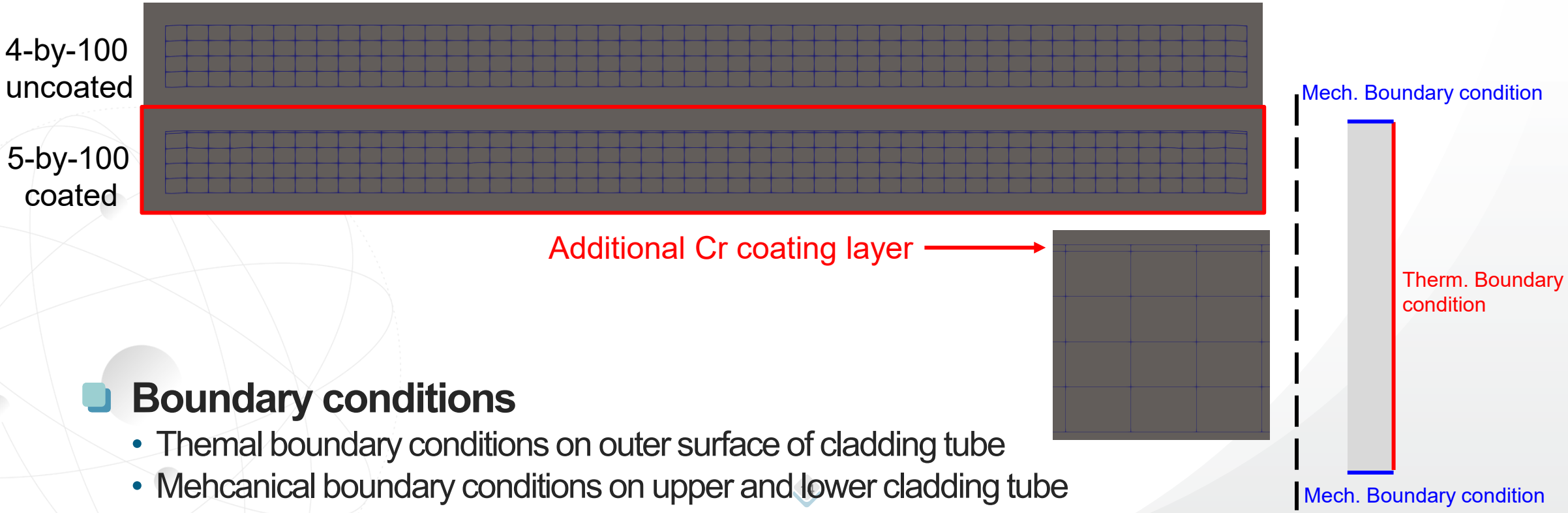

Boundary conditions

- Themal boundary conditions on outer surface of cladding tube
- Mehcanical boundary conditions on upper and lower cladding tube

Simulation of Cr-coated Zr-4 cladding tube

Hoop stress distribution along radial direction

Hoop stress distribution change after deformation

Additional Cr coating layer

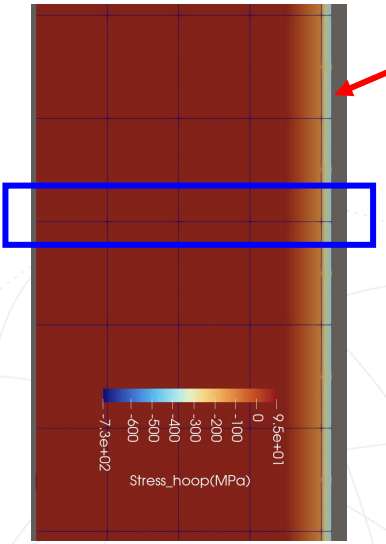

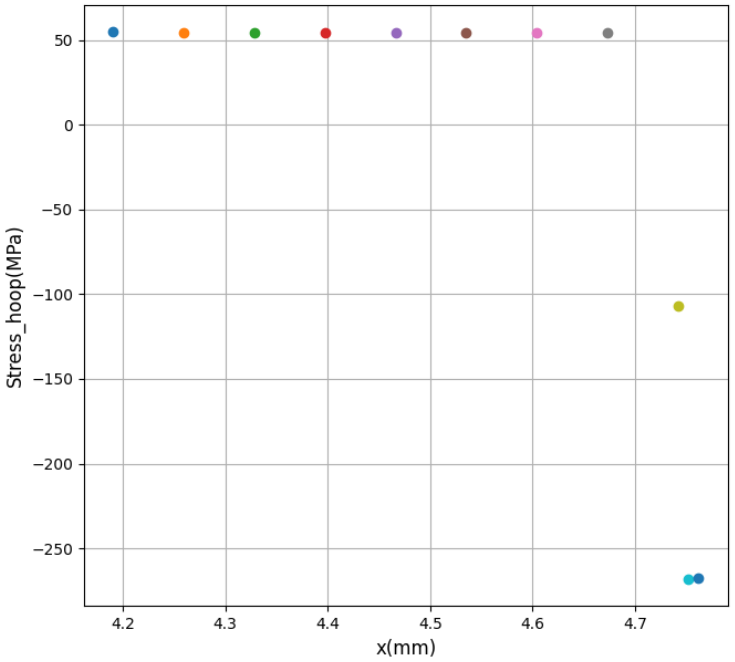

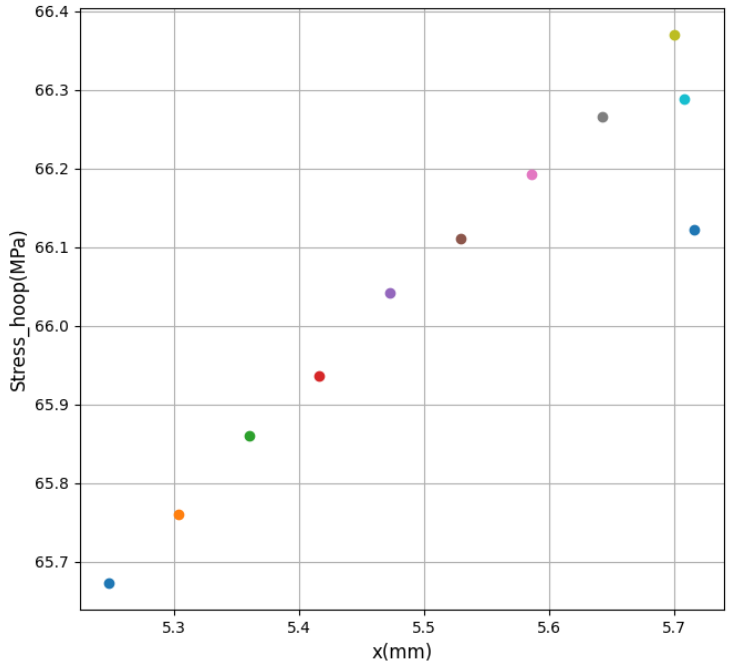

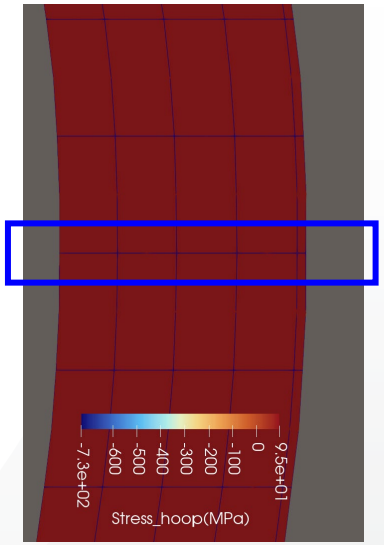

Simulation of Cr-coated Zr-4 cladding tube

Hoop stress distribution along radial direction

Hoop stress dist

Additiona

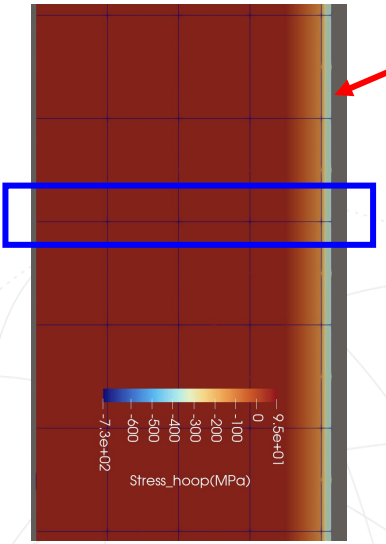

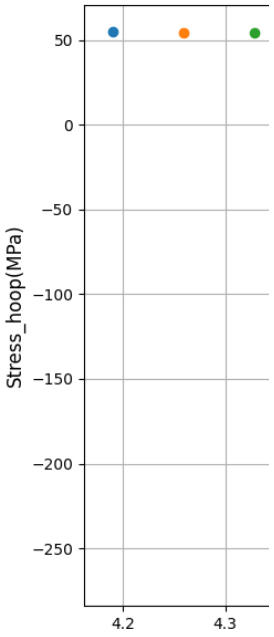

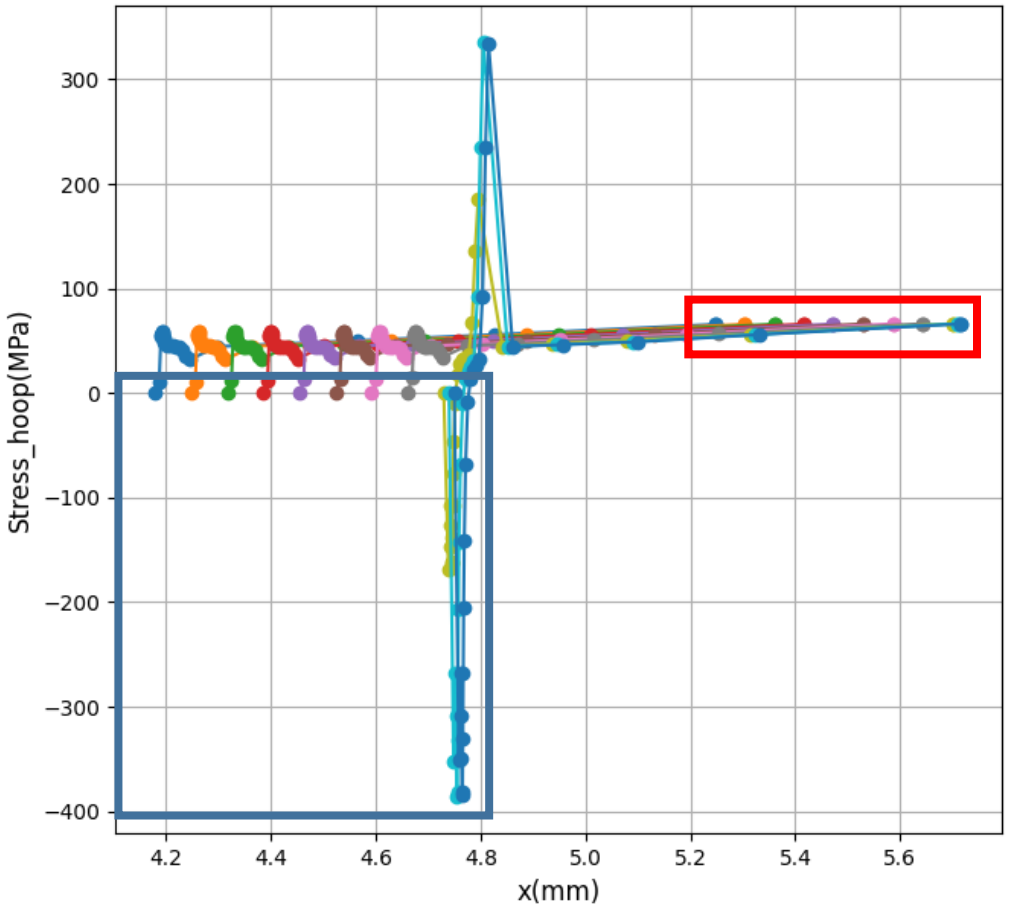

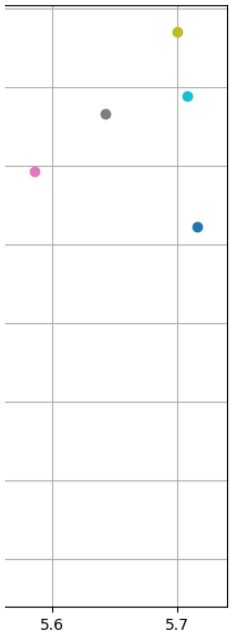

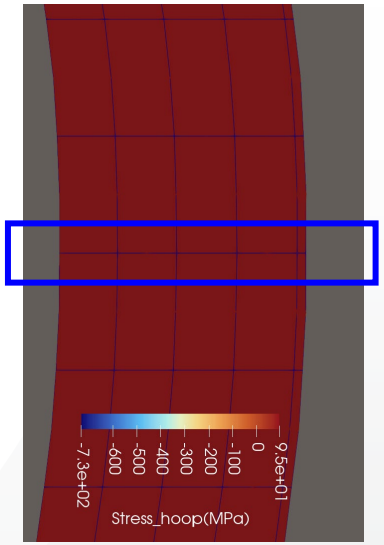

04

Simulation of Cr-coated Zr-4 cladding tube

Korea Atomic Energy Research Institute

Results of 40 bar internal gas pressure

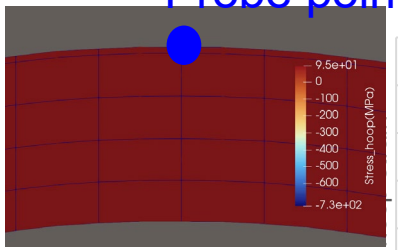

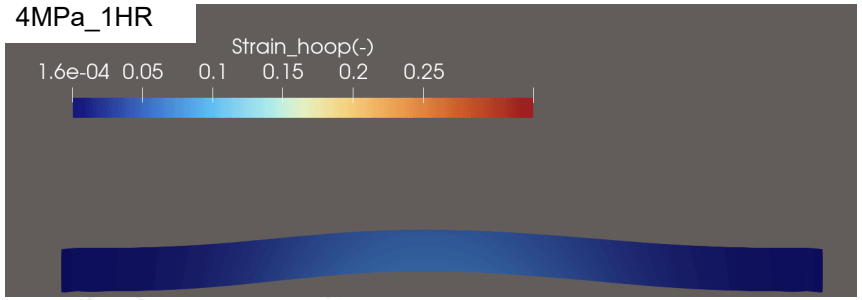

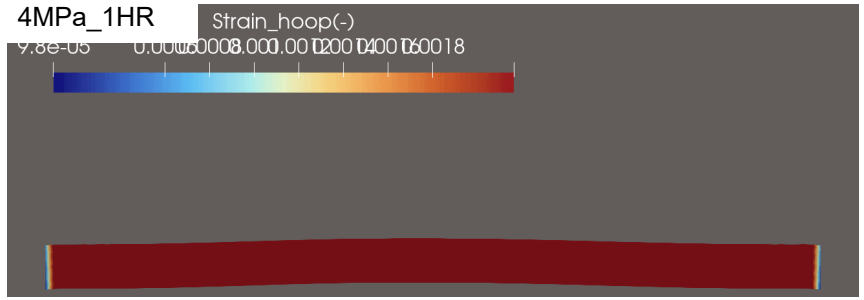

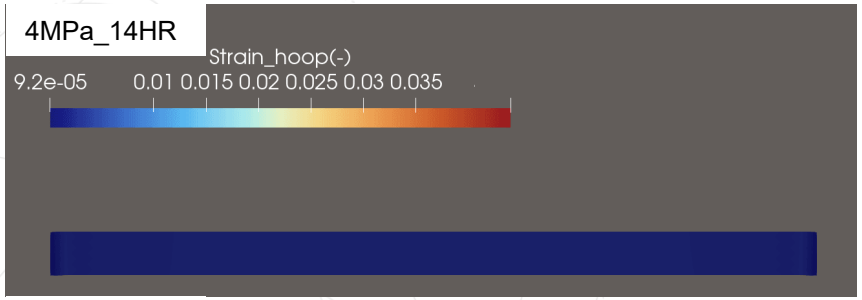

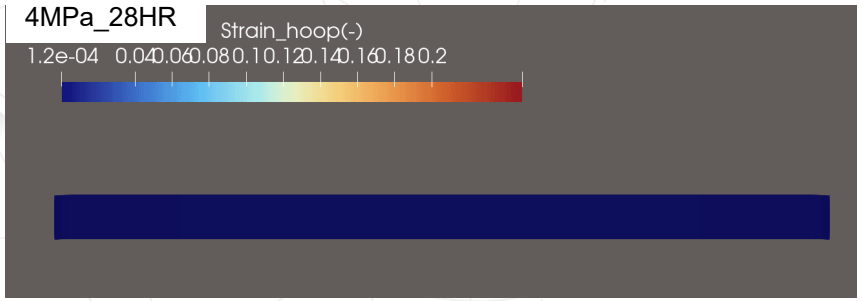

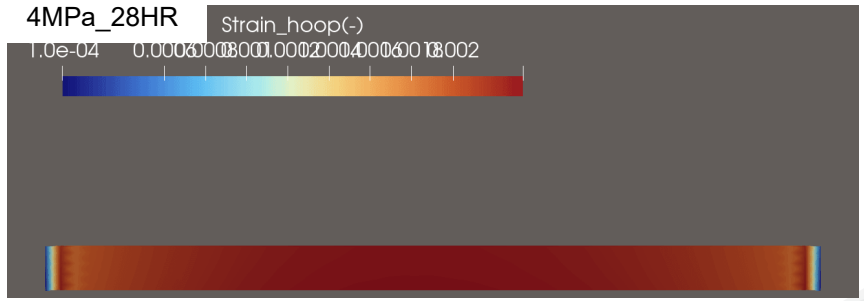

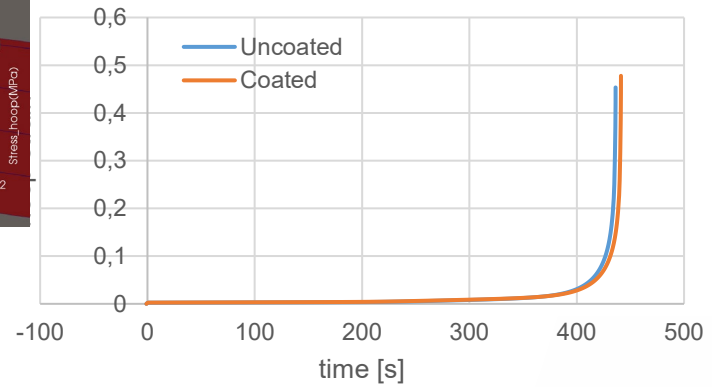

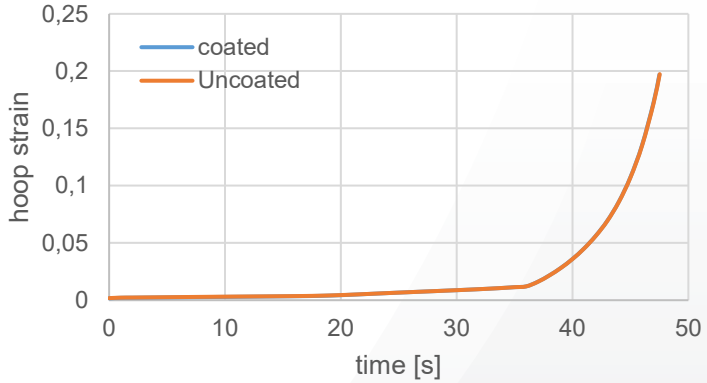

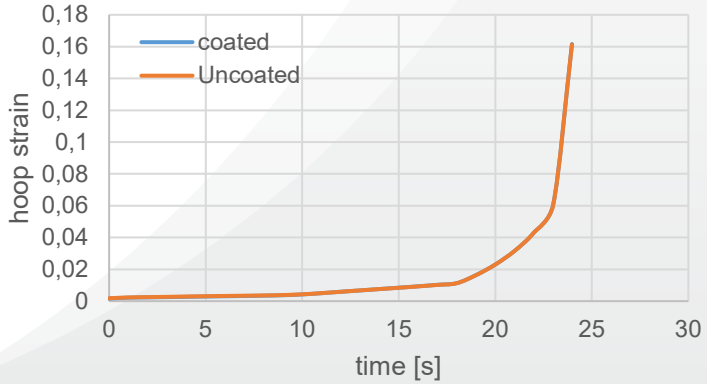

04

Simulation of Cr-coated Zr-4 cladding tube

Korea Atomic Energy Research Institute

Results of 60 bar internal gas pressure

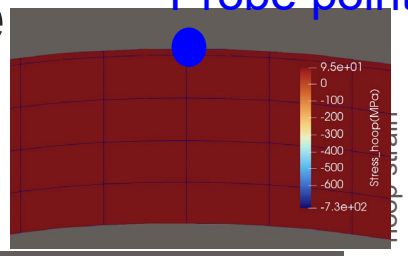

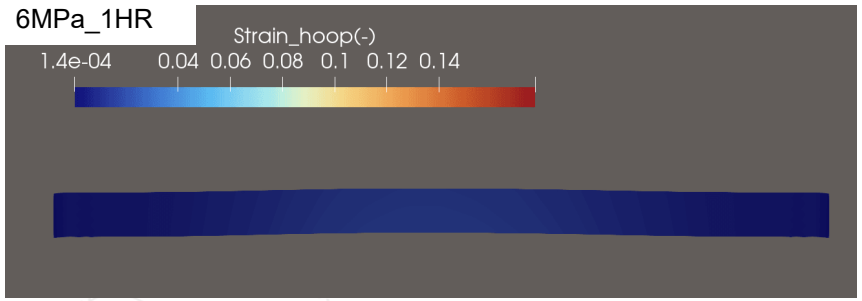

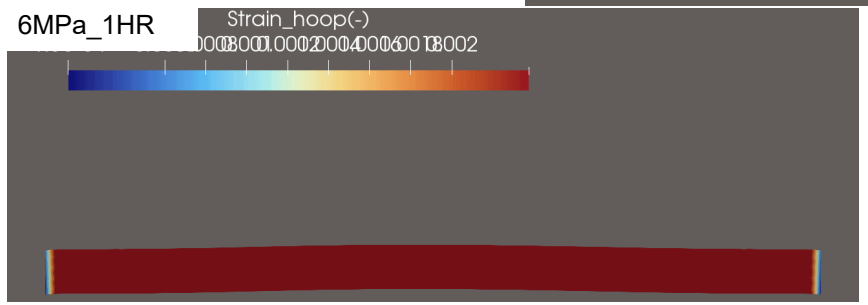

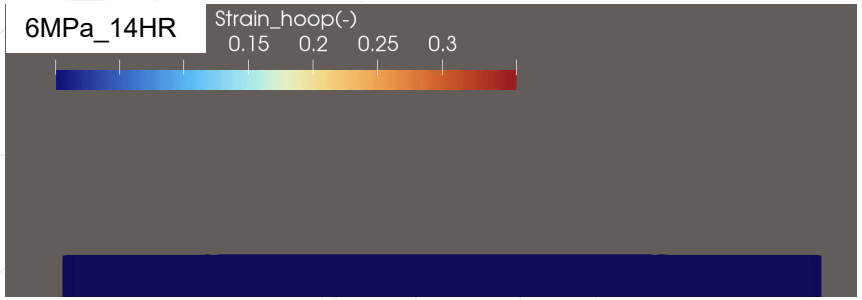

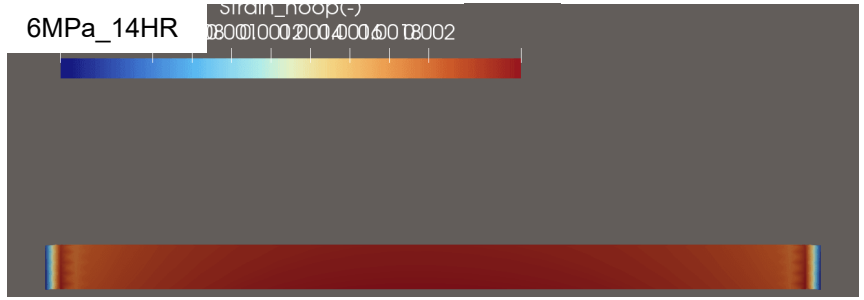

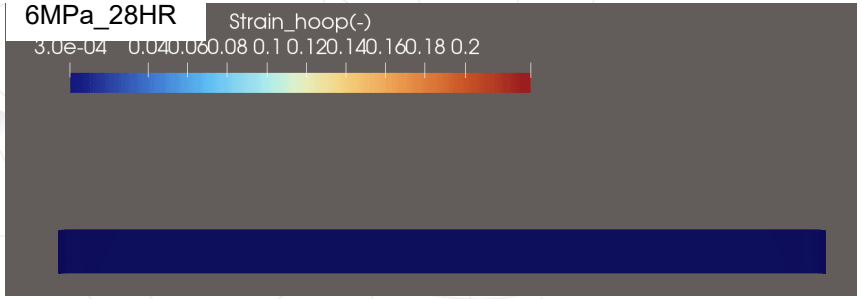

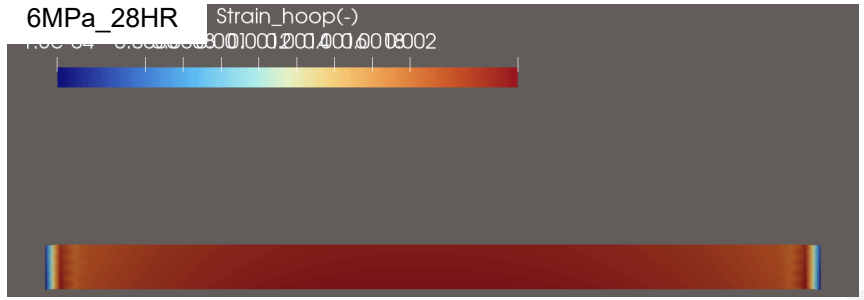

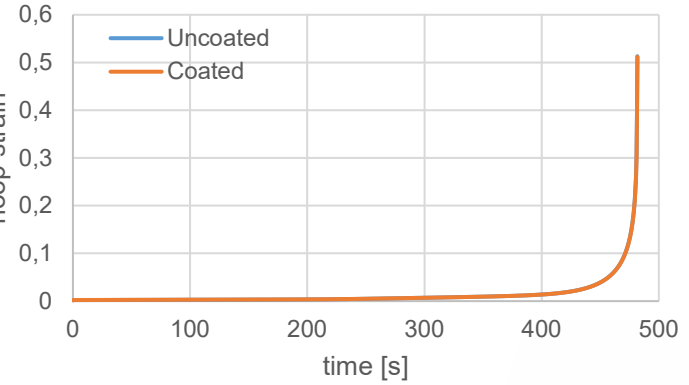

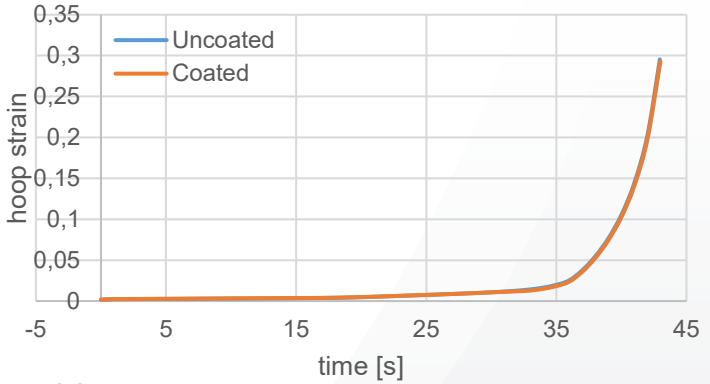

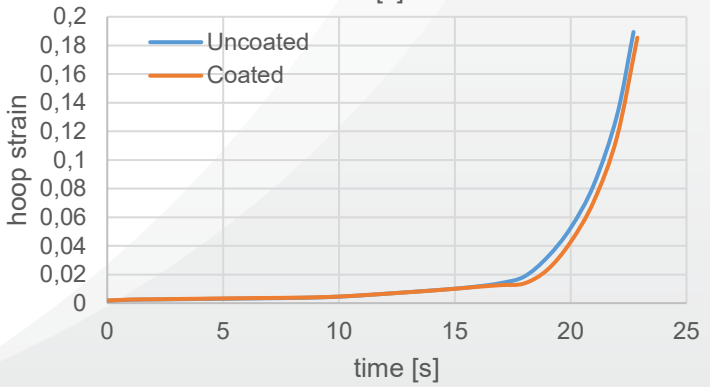

Simulation of Cr-coated Zr-4 cladding tube

Results of 80 bar internal gas pressure

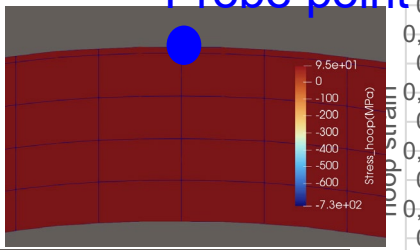

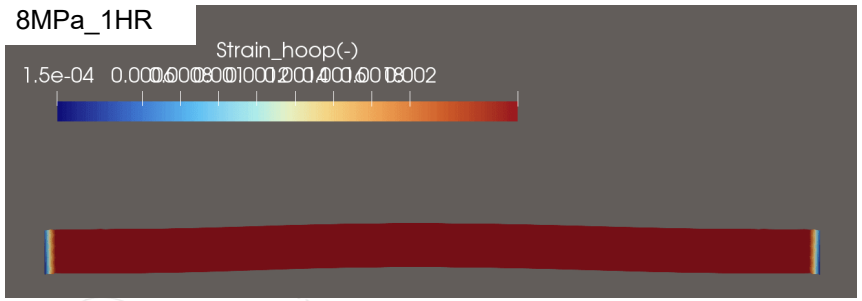

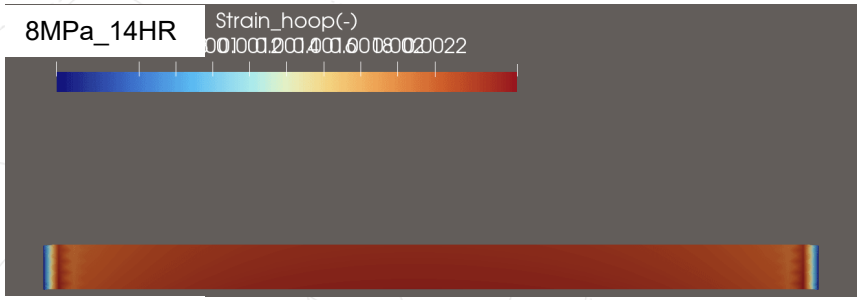

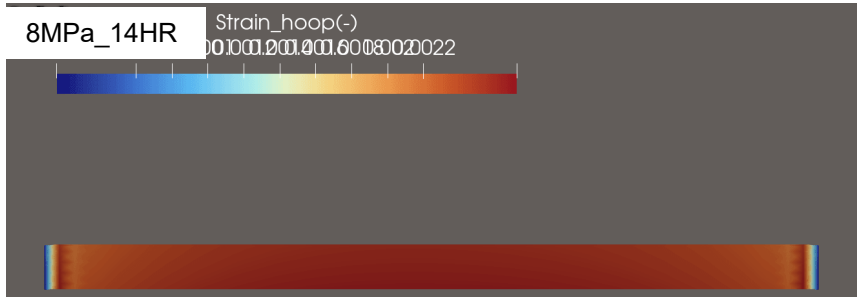

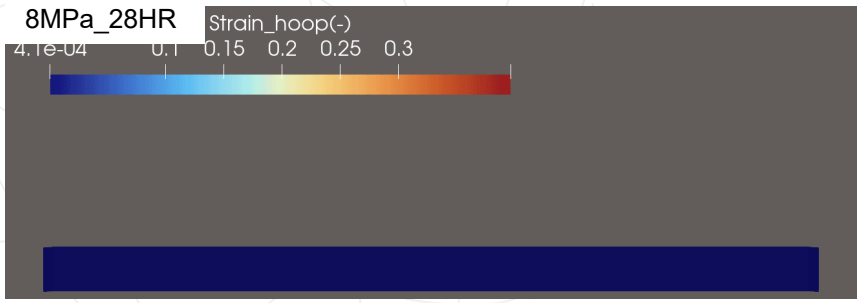

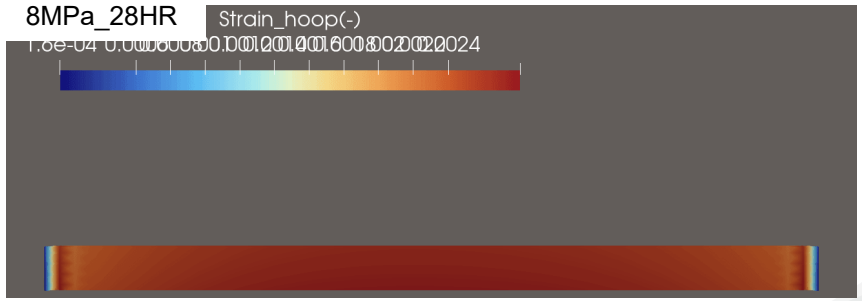

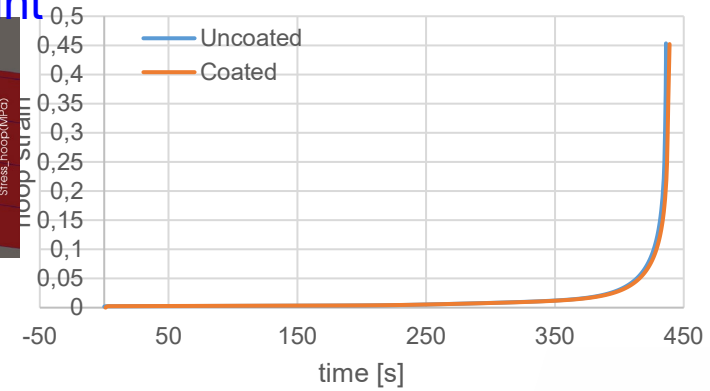

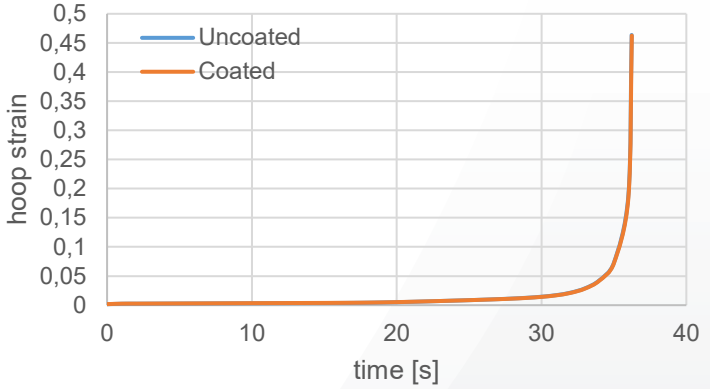

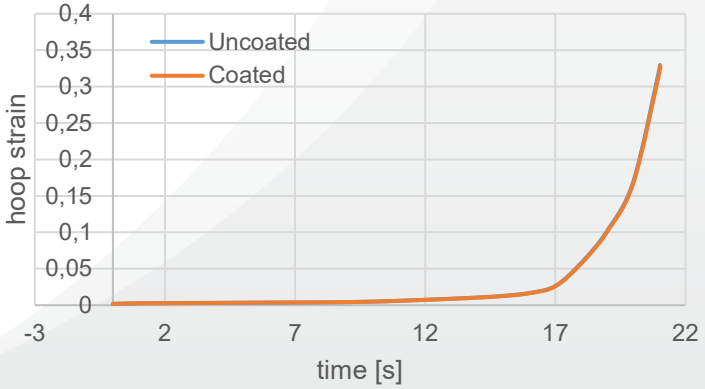

05

Conclusion and future work

Korea Atomic Energy Research Institute

Conclusion

- A real-time measurement system, DIMAT, was established to monitor high-temperature cladding deformation during experiments
- A FEM-based nuclear fuel performance code, MERCURY, was developed and employed to analyze the DIMAT experiment
- The grid size had only a minimal effect on the rupture time and strain change.
- A sudden change was observed due to the input of the discontinuous creep property coefficient of Zry-4.
- The lower the heating rate and the higher the internal pressure, the more consistent the experimental and analytical results were.

	40 bar	60 bar	80 bar
1K/s	o	o	o
14K/s	x	x	o
28K/s	x	x	x

- Burst simulation was conducted using Cr coated Zry-4 cladding tube
- Hoop stress gradient was observed along axial direction
- We aim to develop a continuous phase transition model by applying a temperature-dependent function to the creep coefficients of Zry-4 and Cr-coating

A nuclear research institute
reshaping the future based
on **peoples trust**

THANK YOU
FOR YOUR ATTENTION

Dr. DongHwa Lee
donghwalee@kaeri.re.kr

KAERI Korea Atomic Energy Research Institute

Gregor T. Stahlberg

RUB

Simulating Cr-Coating Behavior with AC²: From QUENCH Analysis towards Integral Plant Application

The integration of Advanced Technology Fuel (ATF) concepts, particularly Chromium (Cr) coated claddings, into safety analyses requires advanced simulation capabilities that go beyond standard Zircaloy models. The primary objective of this work is to present a dedicated modeling approach for the oxidation behavior of Cr-coated core components under severe accident conditions.

This model has been developed and implemented exclusively within an internal development branch (PSS v2025) at Plant Simulation and Safety Group (PSS) at Ruhr-Universitaet Bochum (RUB). While built upon the AC² code package provided by GRS gGmbH, the specific Cr-oxidation logic (Option 27) is an in-house extension and not yet part of the official code distribution. The model logic accounts for the delayed oxidation onset and the critical transition phase once the protective coating fails.

The assessment strategy presented in this work is twofold. The model development and basic validation are grounded in the analysis of the QUENCH-ATF experimental series. However, as the detailed results are subject to data restrictions, this work focuses on an exemplary application by re-investigating the large-scale bundle experiment QUENCH-15. Although the original experiment utilized uncoated claddings, it serves as a thermal-hydraulic reference case to analyze the sensitivity of the new model under hypothetical, beyond-design-basis conditions. Special attention is paid to the delayed hydrogen escalation and the steep increase in oxidation rates following the postulated coating failure at elevated temperatures.

Scaling up to integral plant behavior, the second phase of the analysis applies the model to a generic integral Pressurized Water Reactor (iPWR) type SMR. This application investigates the behavior and potential safety margins gained through the coating. The results highlight the non-linear dependency of safety gains on the assumed failure criteria and identify key areas for future code development regarding the transition from protective Cr-oxidation to rapid Zirconium degradation.

Acknowledgement

Supported by:

Federal Ministry
for the Environment, Climate Action,
Nature Conservation and Nuclear Safety

based on a decision of
the German Bundestag

This work is funded by the German Federal Ministry for the Environment, Climate Action, Nature Conservation and Nuclear Safety (BMUKN) under grant number 1501682A based on a decision by the German Bundestag.

Responsibility for the content lies with the authors.

The results were obtained using in-house versions of the GRS software package AC² 2023 and AC² 2025.

Simulating Cr-Coating Behavior with AC²

From QUENCH Analysis towards Integral Plant Application

Gregor T. Stahlberg, Marco K. Koch

30th International QUENCH-Workshop | Karlsruhe, Germany | December, 2025

PSS Plant Simulation and Safety
Prof. Dr.-Ing. Marco K. Koch

📖 *Stahlberg, G. T., Koch, M. K.: AC² User Meeting. Köln, 2025.*

Agenda

- Introduction
  - Motivation, Current Status
- Modeling
  - Oxidation Correlation
- Results
  - QUENCH-Facility, Plant Application
- Conclusion

Motivation and Objective

- An unmitigated accident can lead to exposure of fuel elements, heat release due to oxidation and fuel damage
  - Evaluation of simulation model(s) of iPWR (and full-scale PWR)
  - Investigations into the progression of the accident, the safety features and the influence of advanced fuel concepts
  - Analyzing possible increased time margins due to improved accident behavior → **ATF**

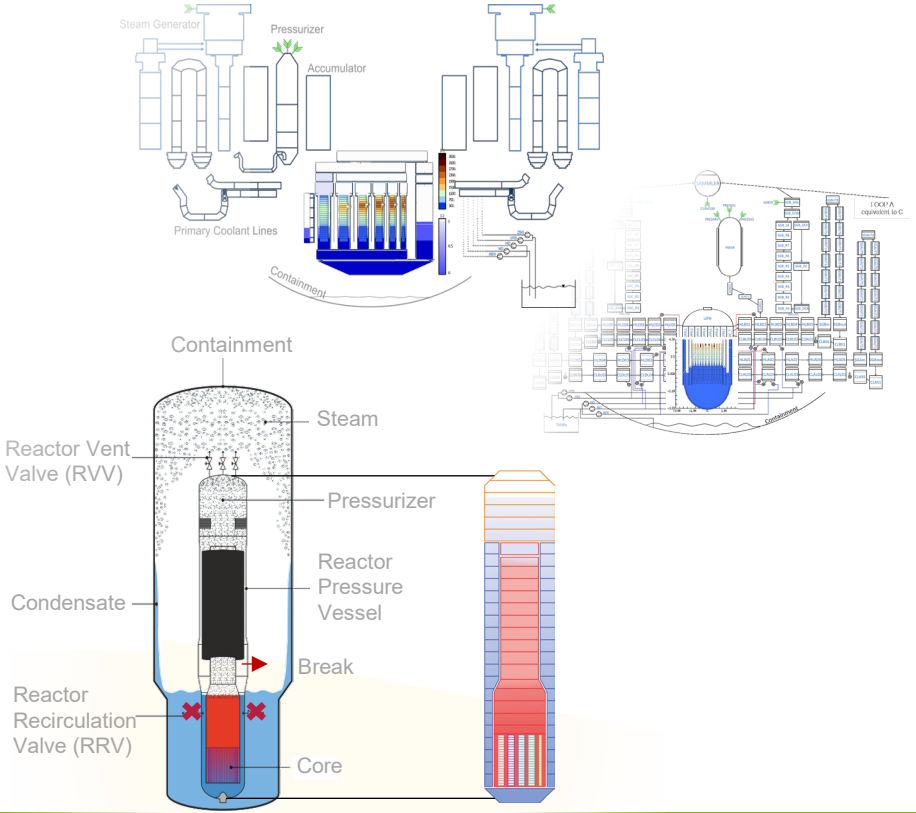

Motivation and Objective
Current Options within AC²

AC² 2023.4 Release

- Opt. 1-3
  - Different correlations for Zircaloy
- Opt. 20-22
  - Different approaches for FeCrAl oxidation (user defined)
- Opt. 23-26
  - Different correlations for Steel

AC² PSS Development (v2025 branch)

- **Opt. 27 -** New Model for Cr-Oxidation
  - Validation: QUENCH-ATF-1 & -ATF-2, prospectively ATF-3 & CODEX
- *Opt. 28*
  - *Testing of new correlations for FeCrAl (EU-Project SASPAM-SA) based on publications by KIT*

- This work utilizes the PSS v2025 development branch, which extends the capabilities of AC² by a dedicated option for oxidation of Cr-coated claddings – a feature currently unique to this in-house version.

Motivation and Objective
ATF Concepts

- **Analysis of technologies that specifically target improved accident behavior and/or favor higher burnup for longer operation**
- Reduce potential hydrogen and heat release, that must be removed by cooling systems (i.e. ECCS) in the event of incidents or accidents → coping time?
  - Development of preliminary model for oxidation of **Cr-coated claddings** available as new option for AC² at RUB PSS (ongoing development)

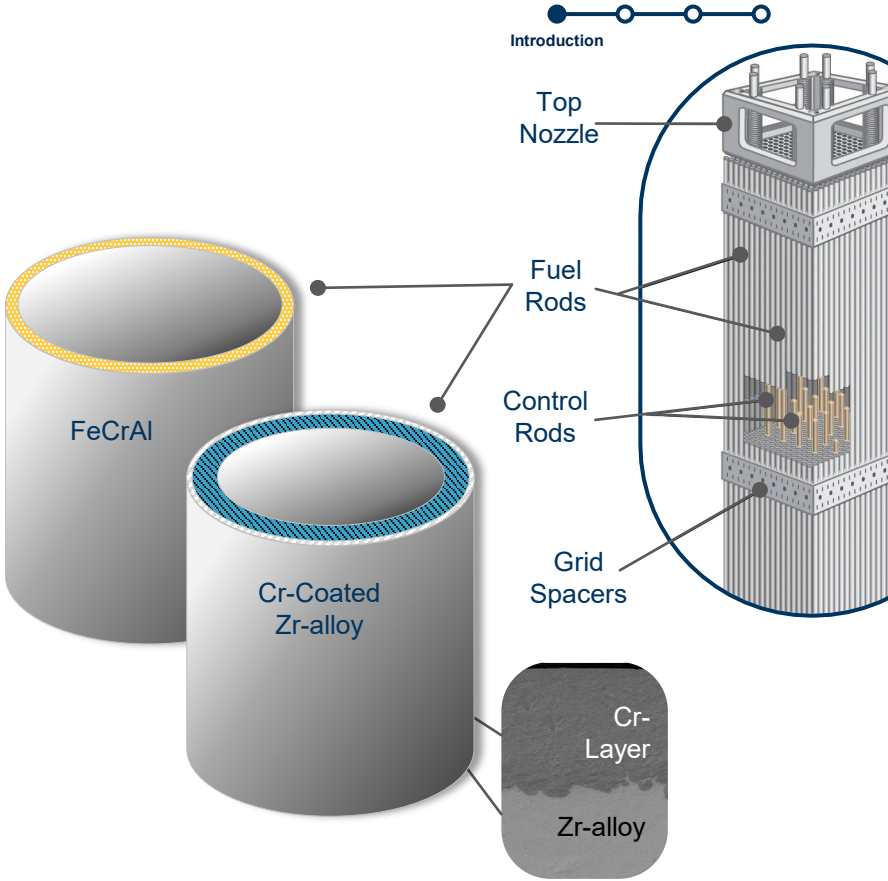

How to model ATF behavior?

ADVANCED TECHNOLOGY FUEL
Cr-Coated Zr-alloy

- Coating as diffusion barrier, protecting substrate material (e.g. Zr-alloy)
- Protective Cr_2O_3 scale prevents rapid oxidation; low weight gain
- Corrosion resistance influenced by several parameters
  - Microstructure (deposition technology)
  - Applied uniform layer thickness
  - Degradation mechanisms
  - **Transient Boundary Conditions**

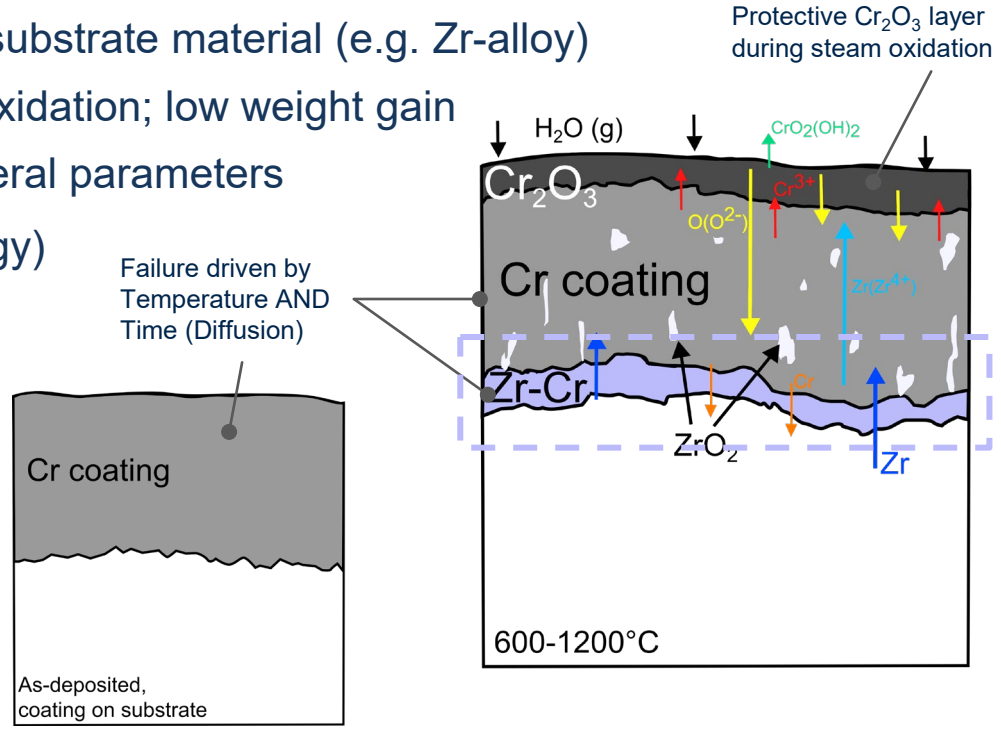

adapted from J. Liu et al. 2021

MODELING
Current correlation under development

- Implemented correlation based on Brachet et al. (2020), representing the current state-of-the-art for Cr-coating behavior
  - Adapted for code-specific Weight Gain
  - Parametric thermal threshold (T_{fail}) to investigate sensitivity of coping time; Transition from Cr → Zr
  - Explicit switch of reaction enthalpy from Cr-oxidation to Zr-oxidation upon failure
  - Inner oxidation currently assumed negligible to focus on primary outer coating failure mechanisms

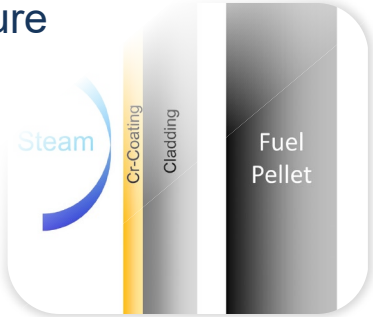

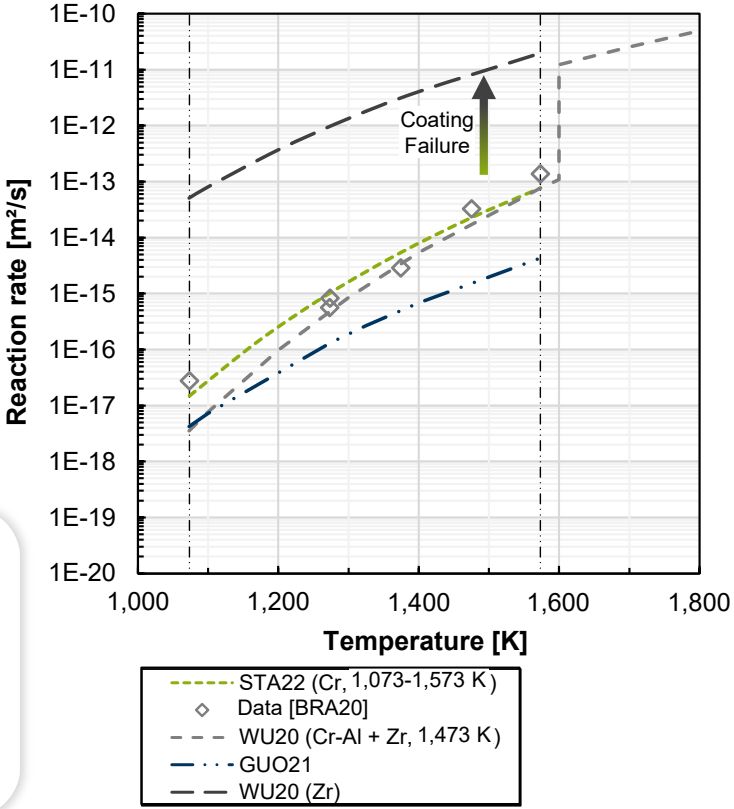

VERIFICATION
Weight Gain at 1,200°C

- Calculated mass gain curve shows good agreement at 1,200°C
  - Calculated mass gain tends to be slightly overestimated; most data are captured adequately (few outliers)
  - Coating failure seems to occur for some isothermal tests around ~5,000 s, despite lower than eutectic temperature
  - *Different experimental settings and different deposition technologies may lead to different failure behavior*

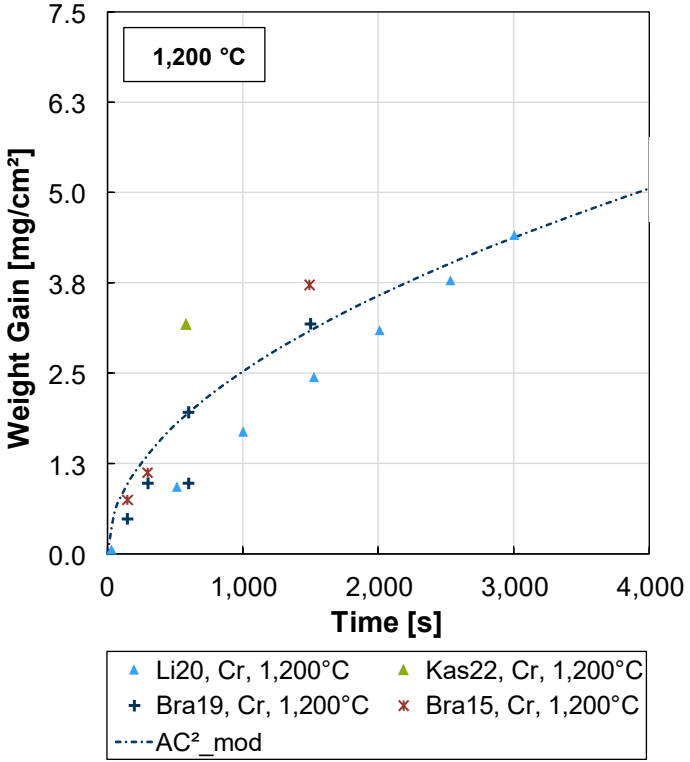

Application to QUENCH-Facility

MODELING
Cr-Oxidation applied to QUENCH-15 simulation model

- QUENCH-15 investigates ZIRLO™ cladding oxidation and reflood behavior under severe accident conditions (up to 2,150 K) using originally Zry claddings
- Adapted as **hypothetical scenario with Chromium oxidation**, as a reference case to analyze the sensitivity of the new model
- For spacer grids and above threshold (T_{fail}) the Zry oxidation for all components is active

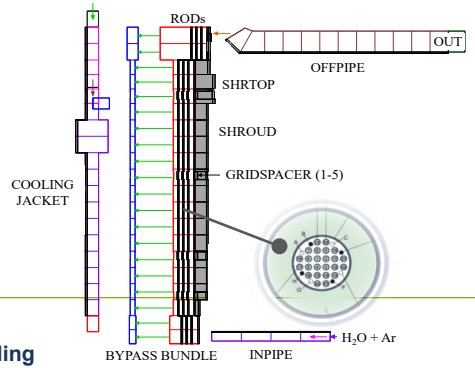

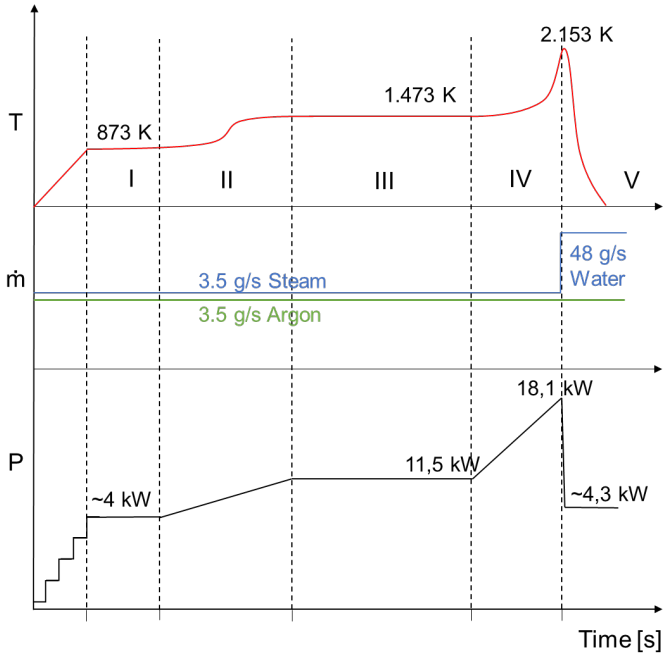

MODELING
Cr-Oxidation applied to QUENCH-15 simulation model

- QUENCH-15 investigates ZIRLO™ cladding ballooning and reflood behavior under severe accident conditions (up to 2,150 K) using originally Zry cladding
- Adapted as **hypothetical scenario with Cr-coated oxidation**, as a reference case to assess the sensitivity of the new model
- For spacer grids and above threshold temperature oxidation for all components is activated

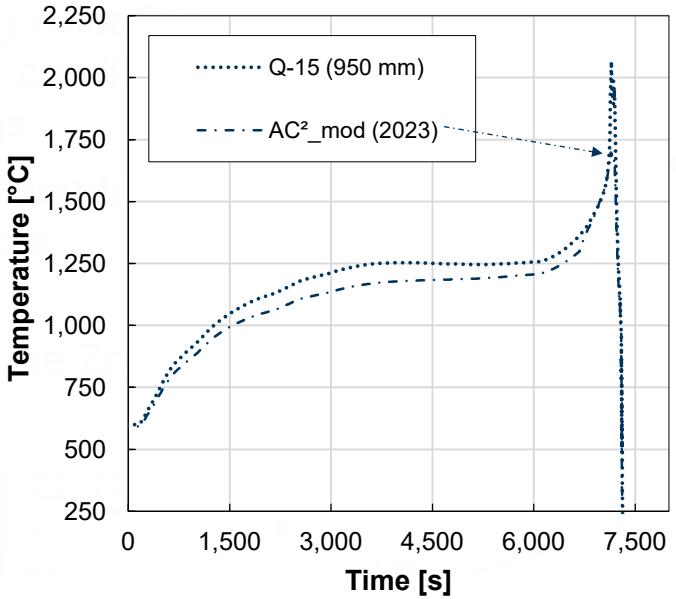

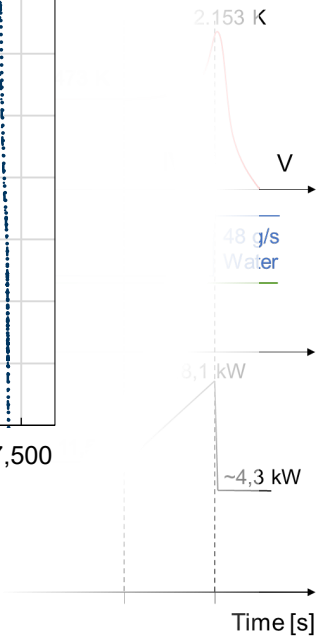

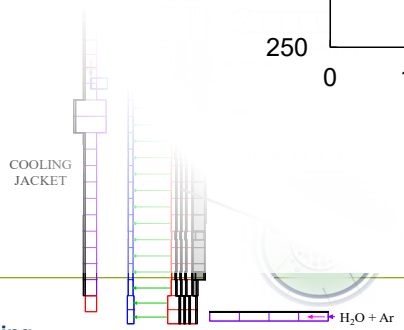

RESULTS

Preliminary: in-house AC² development branch (v2025)

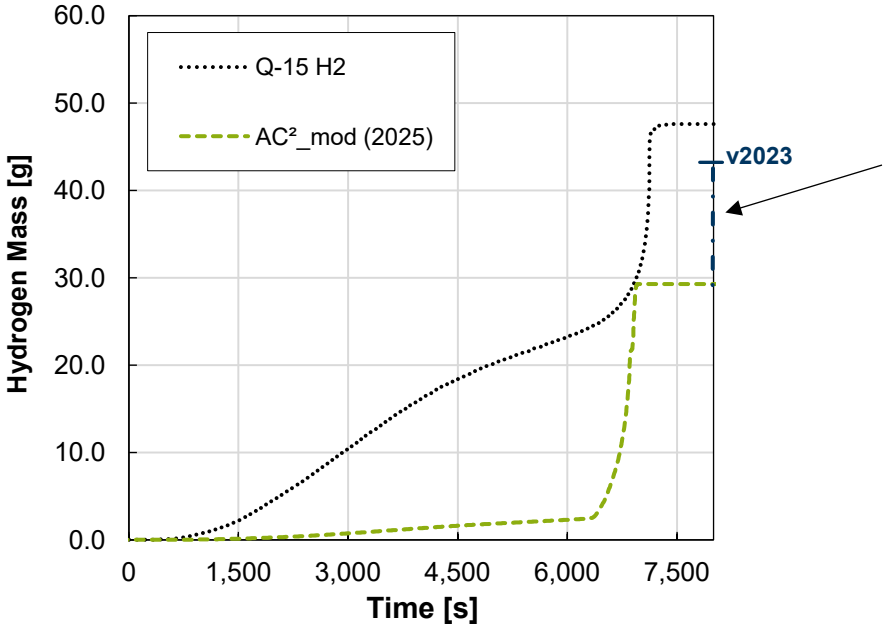

- The update to current AC² code branch (2025) resulted in some deviations (H_2) compared to previous in-house version
- This is likely due to changes in underlying code but also changes to the model itself
- *Current analyses focus on understanding the changes of the transient progression*

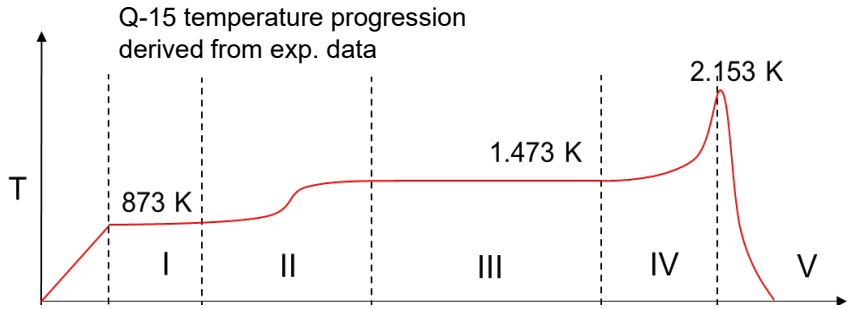

RESULTS

Preliminary: in-house AC² development branch (v2025)

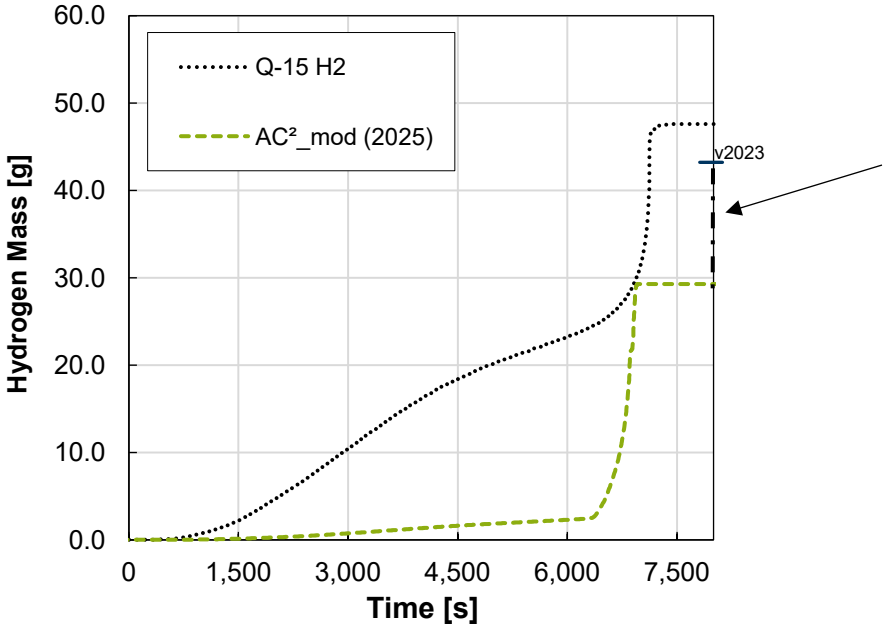

- The Cr-coated simulation [---] effectively delays onset of H_2 generation compared to the uncoated Q-15 experiment [····]
- Post Cr-coating failure (~6,500s): significant H_2 generation with steep slope as underlying Zry is oxidized

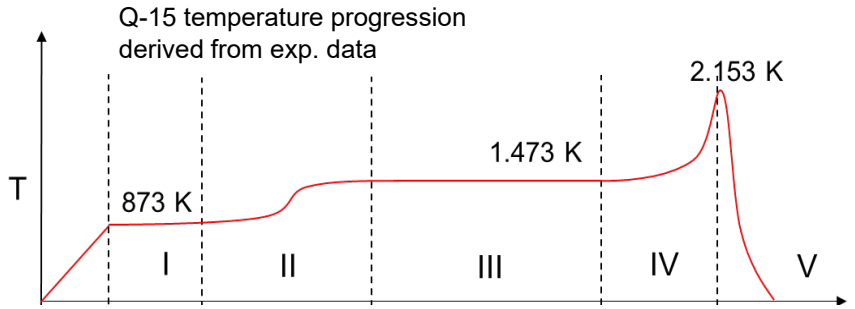

Plant Application - Outlook

MODELING
Plant Modeling using AC² TFD module

- Simulation model of a generic integral PWR modelled with AC² based on public information

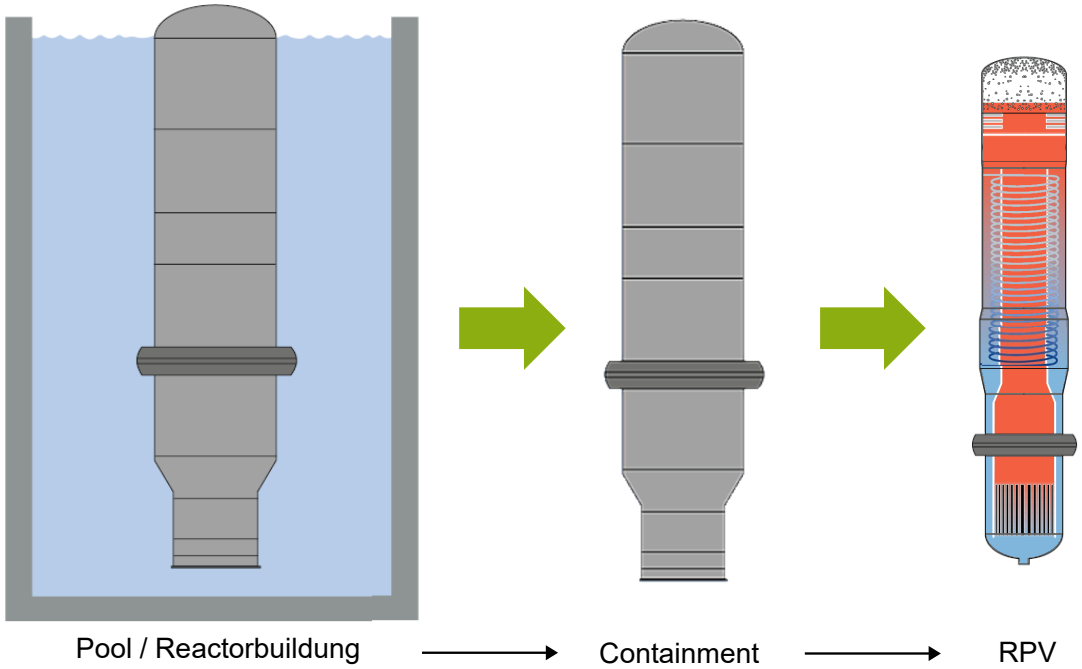

During postulated SA (e.g.)
→ Steam release in containment
→ **No** recirculation (blocked RRV)
→ **Break ~ 3.5 m** above top of active fuel

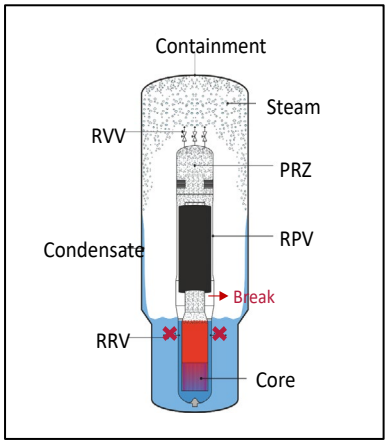

MODELING
Plant Modeling using AC² TFD module

- Simulation model of a generic integral PWR modelled with AC² based on public information

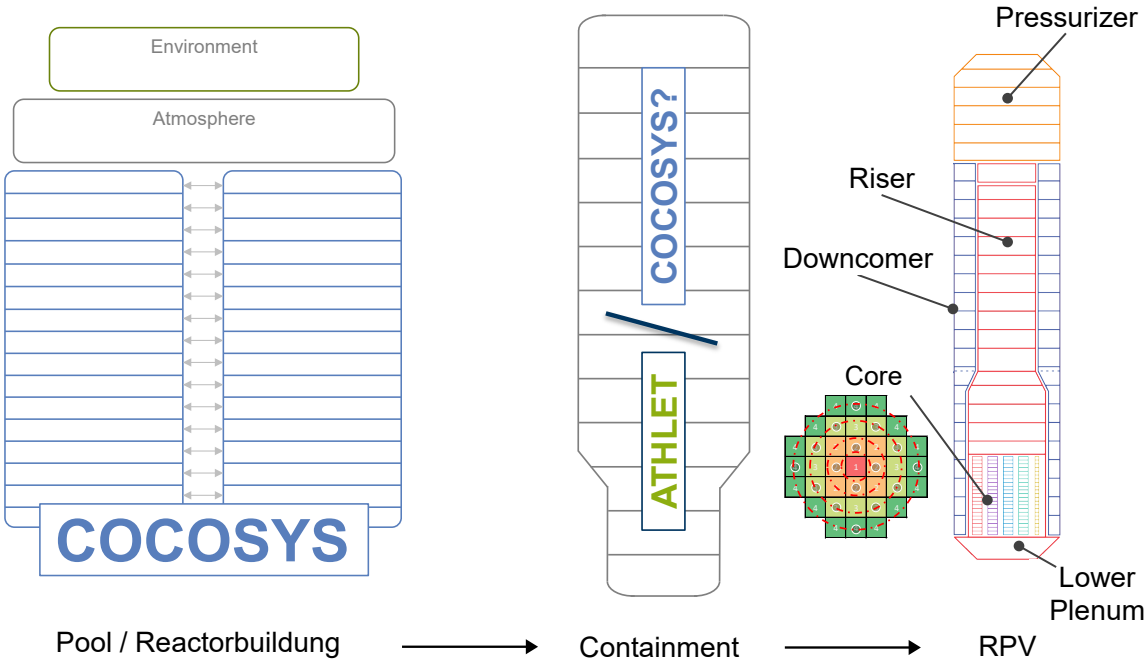

AC² modules

- ECOREMOD – Core
- OREST/FIPISO – Inventory
- AIDA – Late Phase
- FIPREM – FP release
- SAFT – FP behavior

RESULTS

Plant Calculation: Investigating impact of Cr-coating on H_2 release

- Preliminary results with new option for Cr-coating

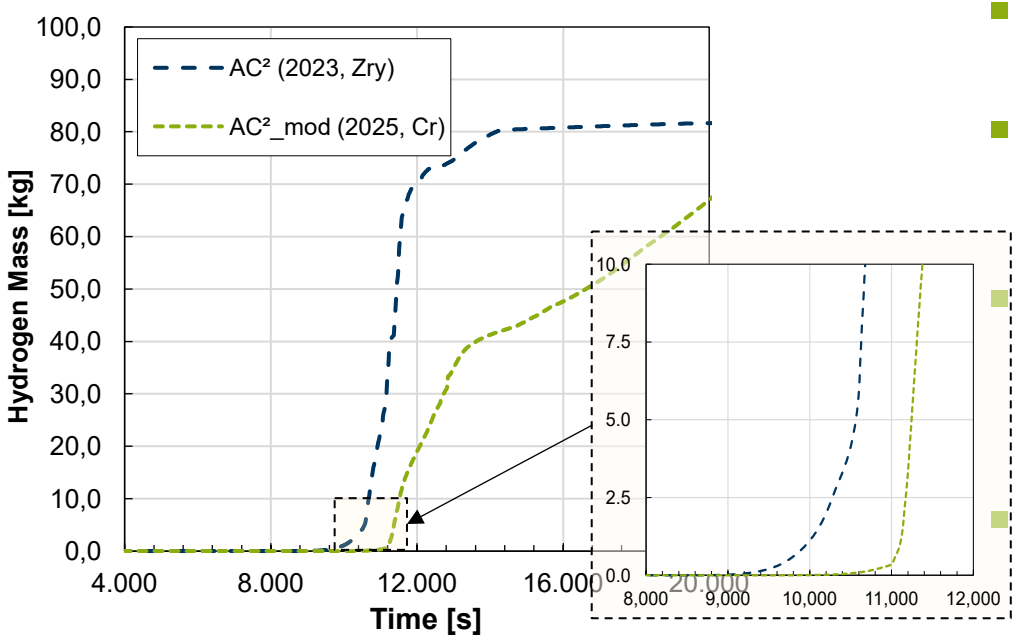

- The Cr-coating model successfully delays onset of the early Zry escalation
- The post-failure rate (green) is observed to be even steeper than the Zry-oxidation (blue)
- This aligns with the hypothesis that failure at these temperatures leads to a more intense oxidation, which the model successfully captures
- This highlights a key modeling challenge: ensuring correct transition from Cr- to Zry-oxidation logic

MODELING PERSPECTIVES
Robustness and Limitations

- **Impact of Failure Temperature (T_{fail}):**
  - Current model utilizes a parametric thermal threshold to trigger loss of protective effect
  - The timing of this loss dictates the onset of the H_2 escalation
  - Sensitivity Check: A variation in T_{fail} results in a notable shift of the escalation onset
  - Determination of failure limits is relevant to reduce uncertainties in predicting hydrogen source term

- **Physical Limitations**
  - Current approach approximates transition using interpolation to capture gradual degradation
  - Interdiffusion; formation of intermetallic layers reduces the effective protective scale (time-at-temperature)
  - Potential for failure below eutectic temperature if exposure time is sufficiently long
  - Investigation of diffusion-based degradation models to be assessed

CONCLUSION

- **Application to QUENCH facility and preliminary plant application**
  - → Model demonstration based on public reference data (QUENCH-15)
  - → Model confirmation based on proprietary data (QUENCH-ATF-1/-2, under NDA)
  - → Plant application shows plausible behavior, indicates hypothetically slight gain in coping time

- **High-Temperature Modeling Challenges**
  - → Numerically smooth transition to Zircaloy oxidation required (approx. 1,300°C)
  - → Highly sensitive to kind of interpolation function and interval size
  - → Potential of diffusion-based approaches for time-dependent failure limits to be assessed in future investigations

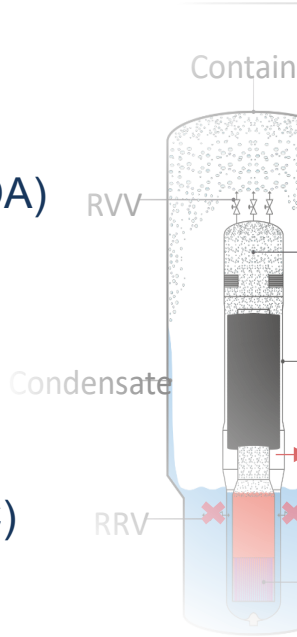

Thank you for your attention!

Gregor Stahlberg

Gregor.Stahlberg@pss.rub.de

Marco K. Koch

Marco.Koch@pss.rub.de

RUHR-UNIVERSITÄT BOCHUM

PSS Plant Simulation and Safety

Prof. Dr.-Ing. Marco K. Koch

Building: IC | Floor 2

Universitätsstr. 150

D-44801 Bochum

pss.rub.de

ACKNOWLEDGEMENT

This work is funded by the German Federal Ministry for the Environment, Climate Action, Nature Conservation and Nuclear Safety (BMUKN) under grant number 1501682A based on a decision by the German Bundestag.

Responsibility for the content lies with the authors.

The results were obtained using in-house versions of the GRS software package AC² 2023 and AC² 2025.

Supported by:

Federal Ministry
for the Environment, Climate Action,
Nature Conservation and Nuclear Safety

based on a decision of
the German Bundestag

References

[Bou19] Bourdon, Gauthier; Ševecek, Martin; Krejčí, Jakub; Cvrček, Ladislav: HIGH-TEMPERATURE STEAM AND AIR OXIDATION OF CHROMIUM-COATED OPTIMIZED ZIRLO™. Acta Polytechnica CTU Proceedings, 24, 2019. DOI: 10.14311/APP.2019.24.0001.

[Bra15] Brachet, Jean-Christophe; Le Saux, Matthieu; Le Flem, Marion; Urvoy, Stephane; Rouesne, Elodie; Guilbert, Thomas; Cobac, C.; Lahogue, F.; Rousselot, J. L.; Tupin, Marc; Billaud, Pierre; Hossepied, Charles; Monsifrot, Eric: On-going studies at CEA on chromium coated zirconium based nuclear fuel claddings for enhanced accident tolerant LWRS fuel, cea-02492582, Top Fuel 2015 - Reactor Fuel Performance Meeting, Zurich, Switzerland, 2015.

[Bra18] Brachet, Jean-Christophe; Guilbert, T.; Le Saux, Matthieu; Rousselot, J.; Nony, G.; Toffolon-Masclet, C.; Michau, Alexandre; Schuster, Frederic; Palancher, Herve; Bischoff, Jeremy; Augereau, J.; Pouillier, Edouard: BEHAVIOR OF Cr-COATED M5 CLADDINGS DURING AND AFTER HIGH TEMPERATURE STEAM OXIDATION FROM 800°C UP TO 1500°C - LOSS-OF-COOLANT ACCIDENT & DESIGN EXTENSION CONDITIONS, Top Fuel 2018 - Reactor Fuel Performance, Prague, Czech Republic, 2018.

[Bra19] Brachet, Jean-Christophe; Idarraga-Trujillo, Isabel; Le Flem, Marion; Le Saux, Matthieu; Vandenberghe, Valérie; Urvoy, Stephane; Rouesne, Elodie; Guilbert, Thomas; Toffolon-Masclet, Caroline; Tupin, Marc; Phalippou, Christian; Lomello, Fernando; Schuster, Frédéric; Billard, Alain; Velisa, Gihan; Ducros, Cédric; Sanchette, Frédéric: Early studies on Cr-Coated Zircaloy-4 as enhanced accident tolerant nuclear fuel claddings for light water reactors. Journal of Nuclear Materials, 517, S. 268–285, 2019. DOI: 10.1016/j.jnucmat.2019.02.018.

[Bra20] Brachet, Jean-Christophe; Rouesne, Elodie; Ribis, Joël; Guilbert, Thomas; Urvoy, Stéphane; Nony, Guillaume; Toffolon-Masclet, Caroline; Le Saux, Matthieu; Chaabane, Nihed; Palancher, Hervé; David, Amandine; Bischoff, Jérémy; Augereau, Julien; Pouillier, Edouard: High temperature steam oxidation of chromium-coated zirconium-based alloys: Kinetics and process. Corrosion Science, 167, 2020. DOI: 10.1016/j.corsci.2020.108537.

[Gre19] Gremme, Florian: Analyse des Einflusses anlageninterner Notfallmaßnahmen auf die Kernkühlbarkeit bei auslegungsüberschreitenden Störfällen in Druckwasserreaktoren. PhD thesis. Ruhr-University Bochum. Plant Simulation and Safety (PSS). Shaker-Verlag. Bochum. Germany. 2019. ISBN 978-3-8440-6516-9.

[Kas22] Kashkarov, E. B.; Sidelev, D. V.; Pushilina, N. S.; Yang, J.; Tang, C.; Steinbrueck, M.: Influence of coating parameters on oxidation behavior of Cr-coated zirconium alloy for accident tolerant fuel claddings. Corrosion Science, 203, S. 110359, 2022. DOI: 10.1016/j.corsci.2022.110359.

[Kim15] Kim, Hyun-Gil; Kim, Il-Hyun; Jung, Yang-Il; Park, Dong-Jun; Park, Jeong-Yong; Koo, Yang-Hyun: Adhesion property and high-temperature oxidation behavior of Cr-coated Zircaloy-4 cladding tube prepared by 3D laser coating. Journal of Nuclear Materials, 465, S. 531–539, 2015. DOI: 10.1016/j.jnucmat.2015.06.030.

References

[Li20] Li, Guangbin; Liu, Yanhong; Zhang, Yingchun; Li, Huailin; Wang, Xiaojing; Zheng, Mingmin; Li, Yusha: High Temperature Anti-Oxidation Behavior and Mechanical Property of Radio Frequency Magnetron Sputtered Cr Coating. Metals, 10, S. 1509, 2020. DOI: 10.3390/met10111509.

[Liu21] Liu, Junkai; Tang, Chongchong; Steinbrück, Martin; Yang, Jianqiao; Stegmaier, Ulrike; Große, Mirco; Di Yun; Seifert, Hans Jürgen: Transient experiments on oxidation and degradation of Cr-coated Zircaloy in steam up to 1600 ℃. Corrosion Science, 192, 2021. DOI: 10.1016/j.corsci.2021.109805.

[Ma21] Ma, Hai-Bin; Yan, Jun; Zhao, Ya-Huan; Liu, Tong; Ren, Qi-Sen; Liao, Ye-Hong; Zuo, Jia-Dong; Liu, Gang; Yao, Mei-Yi: Oxidation behavior of Cr-coated zirconium alloy cladding in high-temperature steam above 1200 °C. npj Materials Degradation, 5, 2021. DOI: 10.1038/s41529-021-00155-8.

[Sha18] Shah, Hemant; Romero, Javier; Xu, Peng; Oelrich, Robert; Walters, Jorie; Wright, Jonathan, Gassmann, William: Westinghouse-Exelon EnCore® Fuel Lead Test Rod (LTR) Program including Coated cladding Development and Advanced Pellets, WAAP-10756, Top Fuel 2018 - Reactor Fuel Performance, Prague, Czech Republic, 2018.

[Wu20] Wu, Xu; Shirvan, Koroush: System code evaluation of near-term accident tolerant claddings during boiling water reactor short-term and long-term station blackout accidents. Nuclear engineering and design, 2020. DOI: 10.1016/j.nucengdes.2019.110362.

REFERENCES (RUB PSS)

[Sta22] Stahlberg, Gregor, T., et al.: Preliminary Simulation Results of the Experiments QUENCH-L3HT and QUENCH-ATF-1 Regarding High-Temperature Oxidation Mechanisms Using the System Code AC^2. 27th International QUENCH Workshop, KIT, Karlsruhe, 2022. https://doi.org/10.5445/ir/1000152245

[Sta23] Stahlberg, Gregor T., et al.: Comparative analyses of the QUENCH experiments L3HT and ATF-1 on high temperature oxidation mechanisms using AC^2, in Proceedings of NURETH-20 - International Topical Meeting on Nuclear Reactor Thermal Hydraulics, pp. 5450–5461, 2023. https://doi.org/10.13182/nureth20-39989

[Sta23] Stahlberg, Gregor, T., Koch, M. K.: *Development of a preliminary model for Cr-coated Claddings for the System Code Package AC^2*. 28th International QUENCH Workshop, KIT, Karlsruhe, 2023.

[Kri24] Krieger, J., Koch, Marco K., Stahlberg, G. T.: *Analyses of a PostulatedSevere Accident in a Generic Small Modular Reactor Using AC2*. Kerntechnik 2024, Leipzig, 11. Juni 2024.

[Sta24a] Stahlberg, Gregor T., Koch, M. K.: *Modeling of Oxidation Behavior of Accident Tolerant Fuel by using AC²*. 11th European Review Meeting on Severe Accidents Research (ERMSAR 2024, edited by F. Gabrielli, L.E. Herranz, and S. Paci). Stockholm, Sweden, 2024.

[Sta24b] Stahlberg, Gregor T., Krieger, J., Koch, M. K.: *Analyses of an integral PressurizedWater Reactor during postulated Accident Conditions using the System CodePackage AC2*. Proceedings of the 14th International Topical Meeting on Nuclear Reactor Thermal-Hydraulics, Operation, and Safety, NUTHOS 2024, S. 1658-1668, 2024. DOI: 10.13182/nuthos14-138 [https://doi.org/10.13182/nuthos14-138].

[Hol24] Hollands, T.M.J., Stahlberg, G., Gabrielli, F., et al.: *Application of AC^2/Athlet-CD and ASTEC for ATF experiments in the frame of ongoing international projects*. 11th European Review Meeting on Severe Accidents Research (ERMSAR 2024, edited by F. Gabrielli, L.E. Herranz, and S. Paci). Stockholm, Sweden, 2024.

[Gab24] F. Gabrielli et al.: *Analysis of Postulated Severe Accidents in Generic IntegralPWR Small Modular Reactors in the frame of the Horizon Euratom SASPAM-SA Project*. 11th European Review Meeting on Severe Accidents Research (ERMSAR 2024, edited by F. Gabrielli, L.E. Herranz, and S. Paci). Stockholm, Sweden, 2024.

Stephan Gabriel

KIT

First experiments at the new thermohydraulic facility

The COSMOS-H facility at KIT is a high-pressure water/steam thermohydraulic test loop capable of up to 17 MPa and 360 °C, reproducing 1:1 conditions of most LWR concepts. It operates with an installed thermal power of 1.8 MW (including 600 kW electrical power for the test section) and uses de-ionised water with precise instrumentation for pressure, temperature and mass-flow control.

Its modular test section features an 80 mm inner-diameter tube up to 3.5 m long, equipped with numerous feedthroughs for heaters, thermocouples (up to 38, 20 currently used) and fiber-optic probes. High-pressure sight glasses and a robotic arm enable optical measurements even when the safety housing is locked, and a trace-heating system with thermal-oil cooling ensures stable two-phase operation.

The first experiment, part of the EU-project OFFERR/COATED, investigated the critical heat flux of a directly heated Zircaloy-4 cladding tube (81 cm heated length) in an annular gap. High-speed recordings identified flow regimes and the onset of nucleate boiling at approximately 12 kW. The state-of-the-art control system rapidly detects boiling crises and reduces power to protect the cladding, allowing repeatable experiments; the dense thermocouple array provides detailed temperature distributions.

Initial results are promising, and future work will extend to chrome-coated cladding tubes and higher pressures while expanding the test track and modular capabilities.

COSMOS-H

Critical heat flux On Smooth and MOdified Surfaces – High pressure

First experiments at the new thermohydraulic facility

Stephan Gabriel, Wilson Heiler, Nicolas Wefers

Institute for Thermal Energy Technologies and Safety (ITES)

Dept. Multiphase Flows (MPF)

12/2025

KIT

ITES Institute for Thermal Energy Technology and Safety

Content

1. Facility overview
2. Test section system
3. First experiments

Facility overview

- COSMOS-H is a thermohydraulic test facility for water/steam experiments under high pressure conditions up to **17 MPa and 360°C**. **Permits 1:1 conditions to most LWR Concepts**
- The experimental loop has an installed **thermal power of 1.8 MW**. This includes 600 kW of electrical power for the test section.
- The COSMOS-H test loop is operated with **deionized water**. All important experimental boundary conditions - e.g. extensively instrument with pressure, temperature, mass flow - can be precisely measured and controlled.
- COSMOS-H can operate with single tubes and small bundles (3x3 up to 3,5 m length) made of **zirconium alloys**, but also other **ATF materials**.

Facility overview

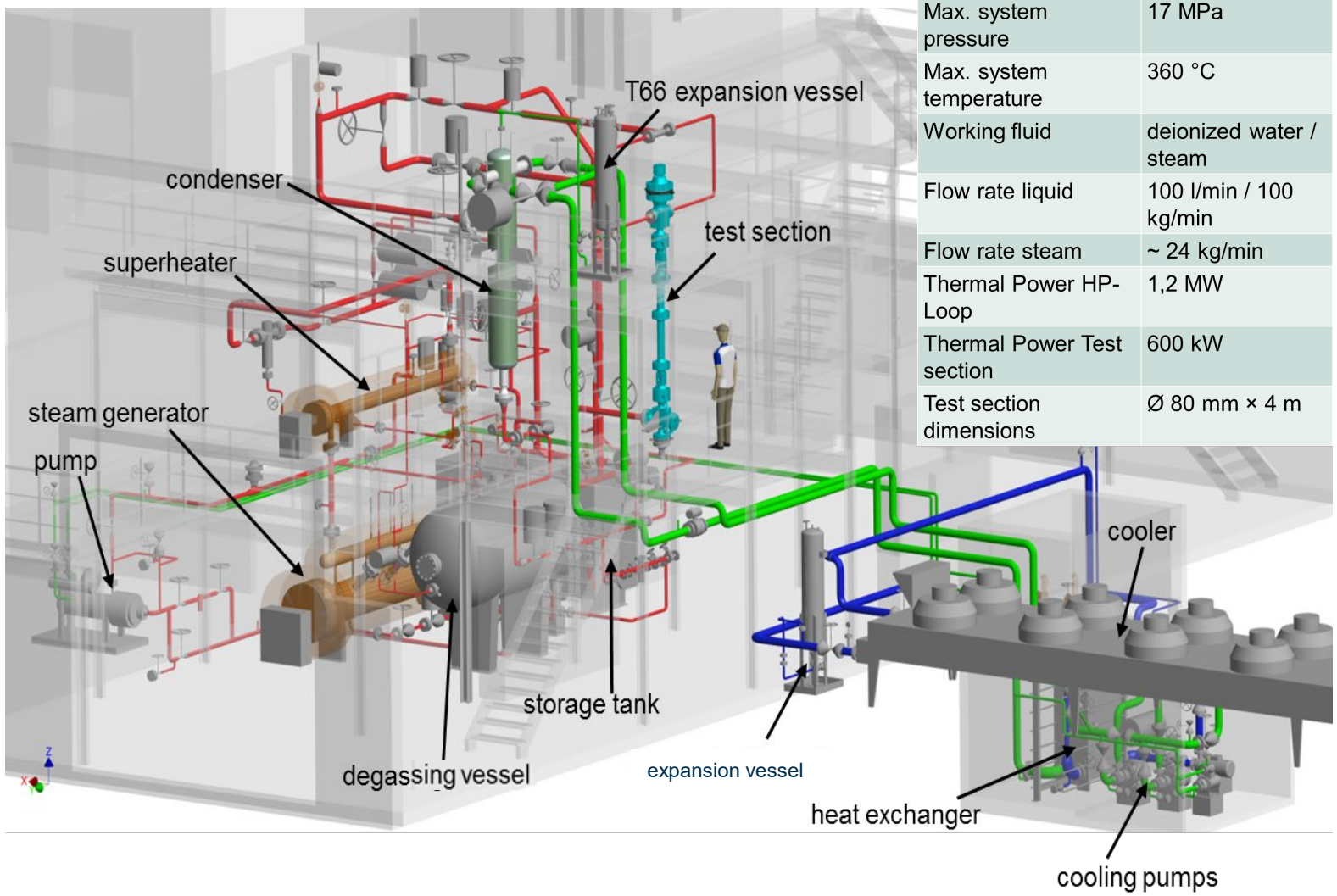

Parameter	Value
Max. system pressure	17 MPa
Max. system temperature	360 °C
Working fluid	deionized water / steam
Flow rate liquid	100 l/min / 100 kg/min
Flow rate steam	~ 24 kg/min
Thermal Power HP-Loop	1,2 MW
Thermal Power Test section	600 kW
Test section dimensions	Ø 80 mm × 4 m

- In addition to the steam generator and steam superheater, COSMOS-H has an extensive trace heating system that allows the thermal boundary conditions to be precisely controlled even for two-phase flows in and around the test section.
- Thermal oil is used as the working medium in the cooling system to ensure constant availability of cooling power for the entire performance spectrum, especially for small cooling loads.
- A comprehensive safety system enables the use of customized measurement equipment such as sight glasses.

Test section system

- The modular test section was built for the detailed investigation of boiling flows up to and including the boiling crisis. It has an inner diameter of 80 mm and a length of up to 3,5 m.
- It consists of a modular pressure hull with numerous feedthroughs for the electrical power supply to the heater and for **instrumentation for pressure, thermocouples and fiber probes**.
- The modules can be arranged as required.
- The high-pressure sight glasses developed in-house can also be used for optical measurements. Using a robotic arm, cameras can be moved to the sight glasses even when the safety housing is locked.

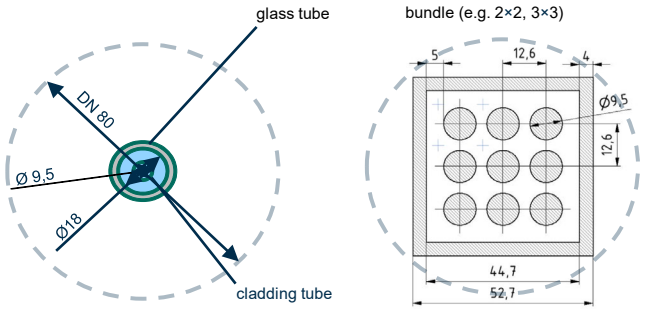

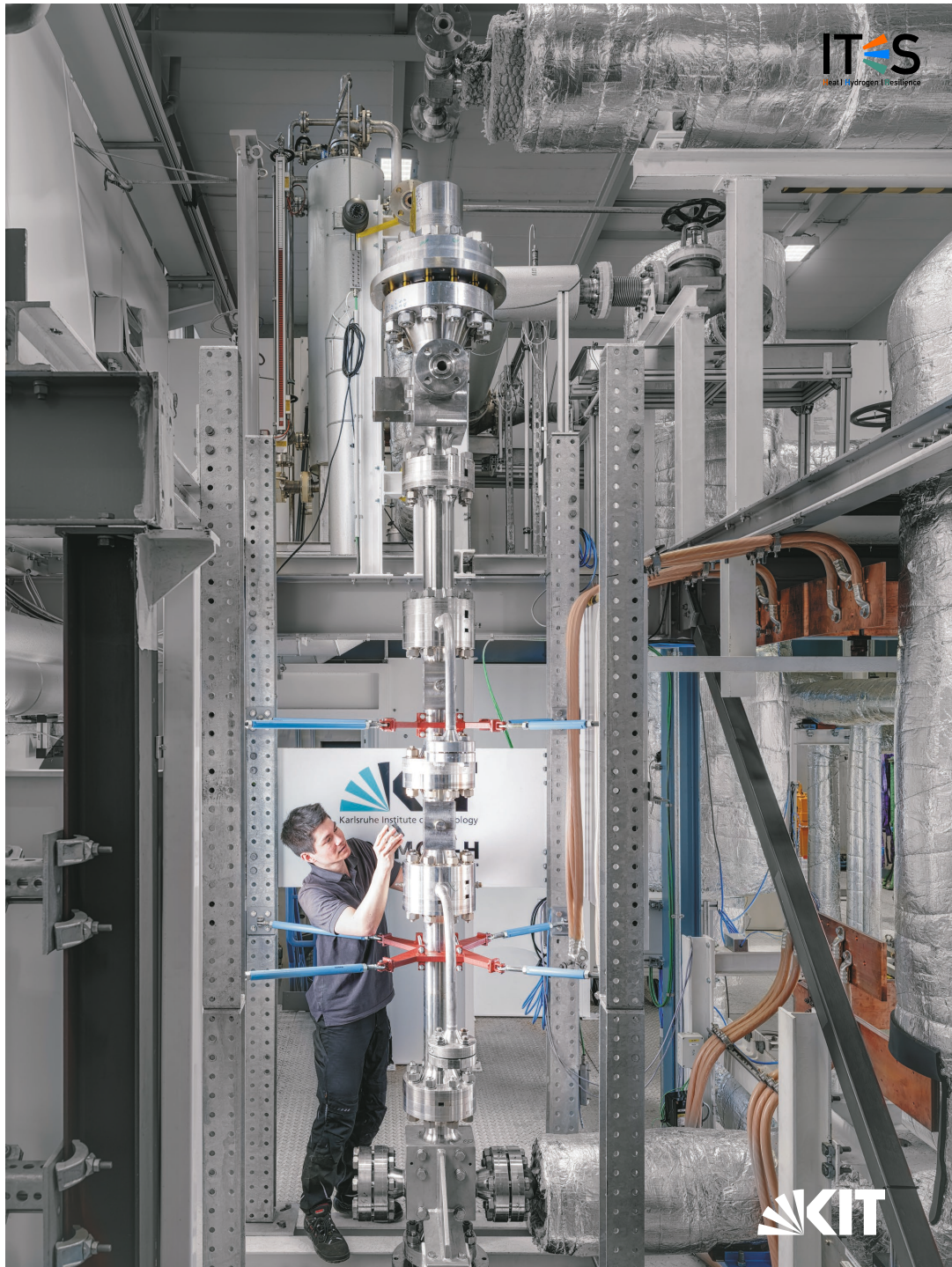

Test section system

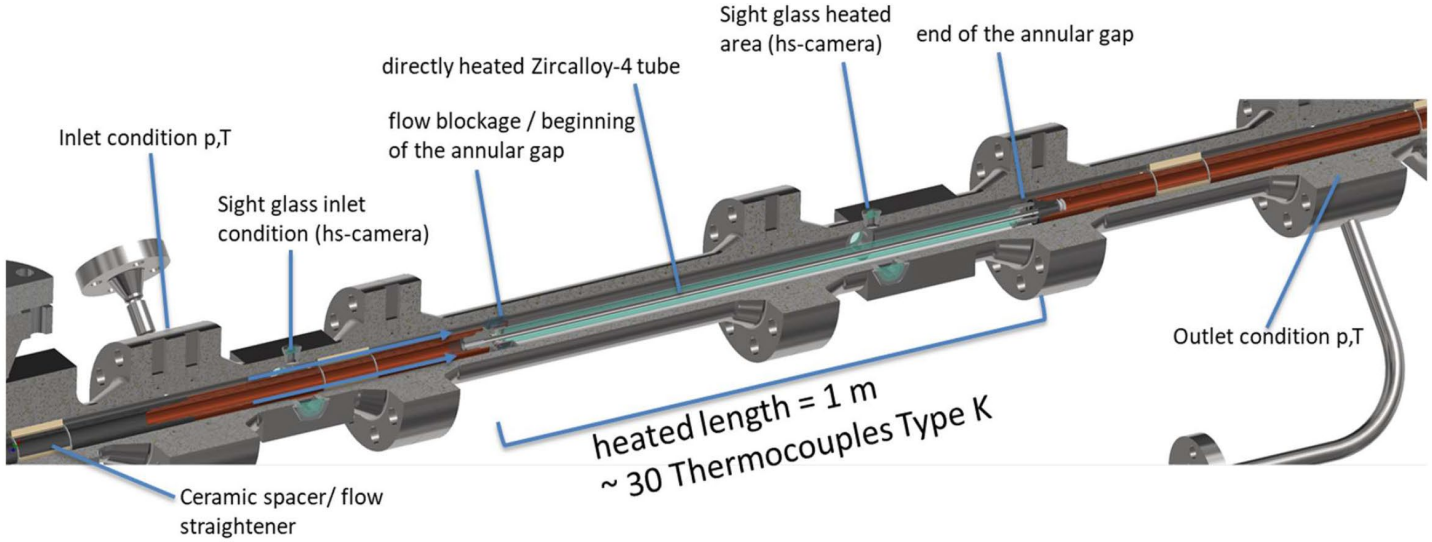

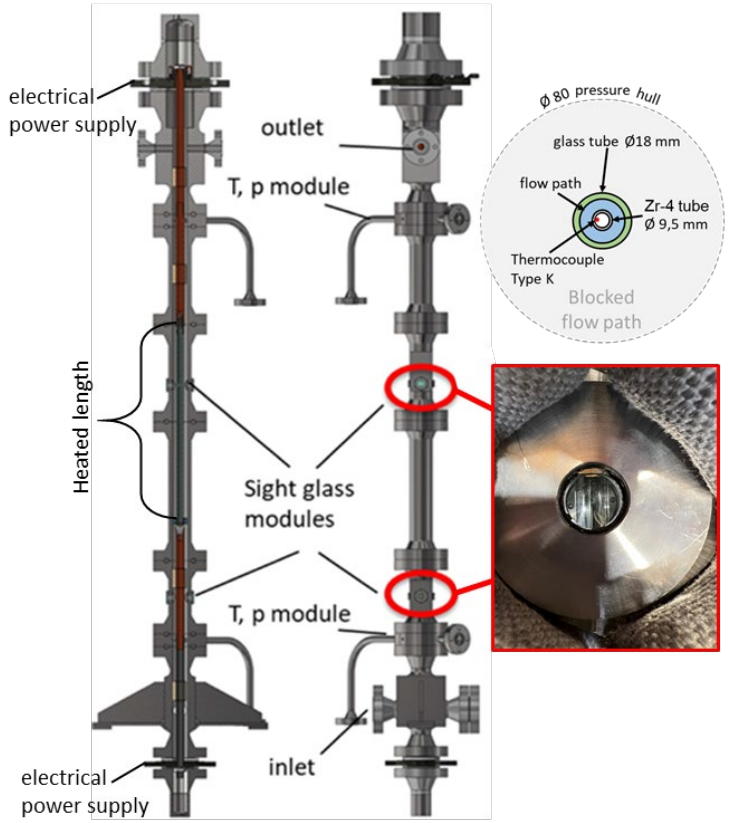

- Directly heated Zircaloy-4 cladding tube, instrumented internally with up to 38 thermocouples. Currently 20 are in use. Heated length 81 cm.
- Pressure sensors before and after the test section, as well as special feedthroughs for glass fibers for void and temperature measurement.
- With the current test section concept, heated lengths of up to 3.5 m and up to 5 tubes in a bundle can be realized. Larger test arrangements are possible, but require a new pressure sleeve for the test section.

EU-Project OFFERR/COATED

Parameter	COSMOS-H BWR_01
Pressure	7,2 MPa
Temperature	271 °C
Subcooling	16 K
Mass flow rate	4000 kg/m²s
Heated length	0,81 m
Heater Material	Zircaloy-4

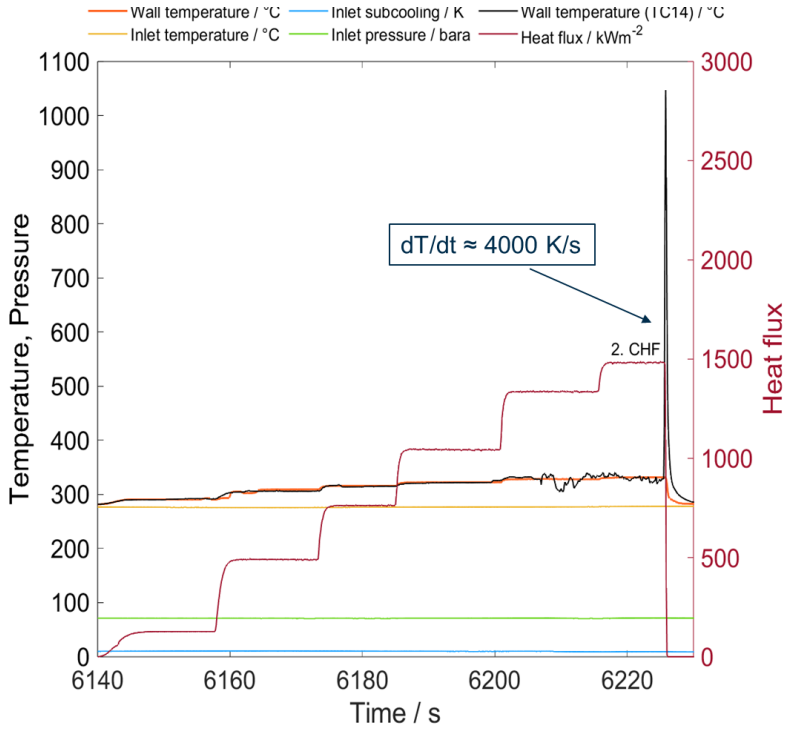

- Detail

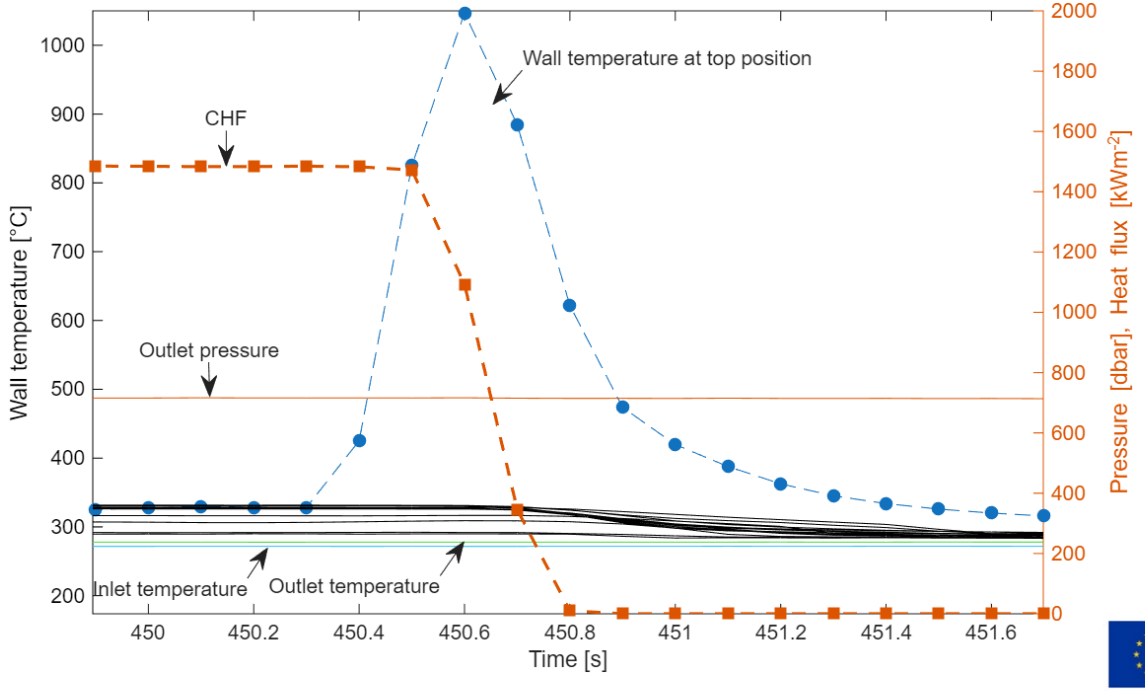

OFFERR

Funded by the European Union

- The main objective of the experiment was to determine the critical heat flux for the Zr-4 cladding tube in the annular gap. This result serves as a reference for later comparison with ATF materials, which will be examined in subsequent experiments.
- Additional data was recorded. Boundary conditions such as temperature, pressure, mass flow, inlet subcooling and temperature distribution at the heater were measured.

EU-Project OFFERR/COATED

Parameter	COSMOS-H BWR_01
Pressure	7,2 MPa
Temperature	271 °C
Subcooling	16 K
Mass flow rate	4000 kg/m²s
Heated length	0,81 m
Heater Material	Zircaloy-4

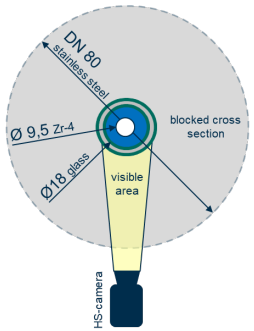

Onset of Nucleate Boiling @ ~12 kW

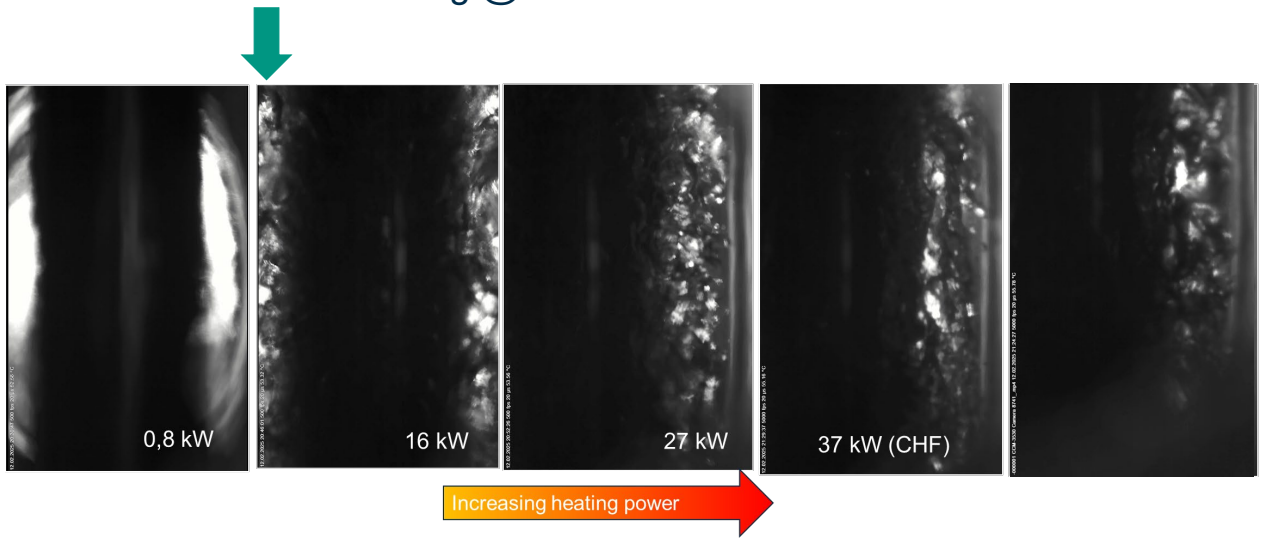

Sequence @ COS-L

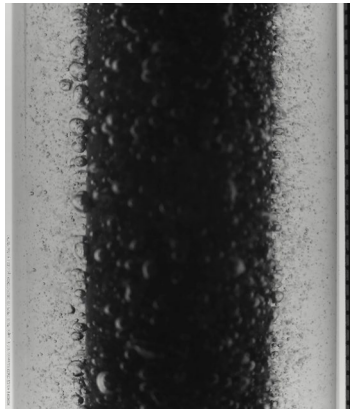

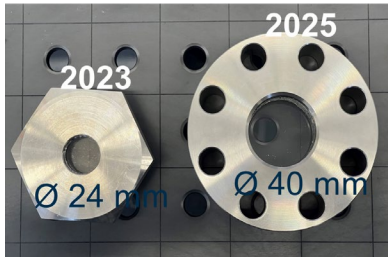

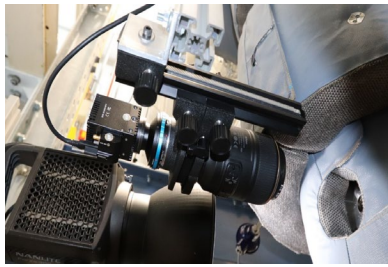

OFFERR
Funded by the European Union

- High-speed recordings were used to determine flow regimes and characteristic values such as bubble size or the onset of nucleate boiling.
- Due to the small sight glass of 28 mm, the illumination is not sufficient for high quality images. Therefore the next generation of sight glasses was developed and the imaging technique was improved.

EU-Project OFFERR/COATED

Parameter	COSMOS-H BWR_01
Pressure	7,2 MPa
Temperature	271 °C
Subcooling	16 K
Mass flow rate	4000 kg/m²s
Heated length	0,81 m
Heater Material	Zircaloy-4

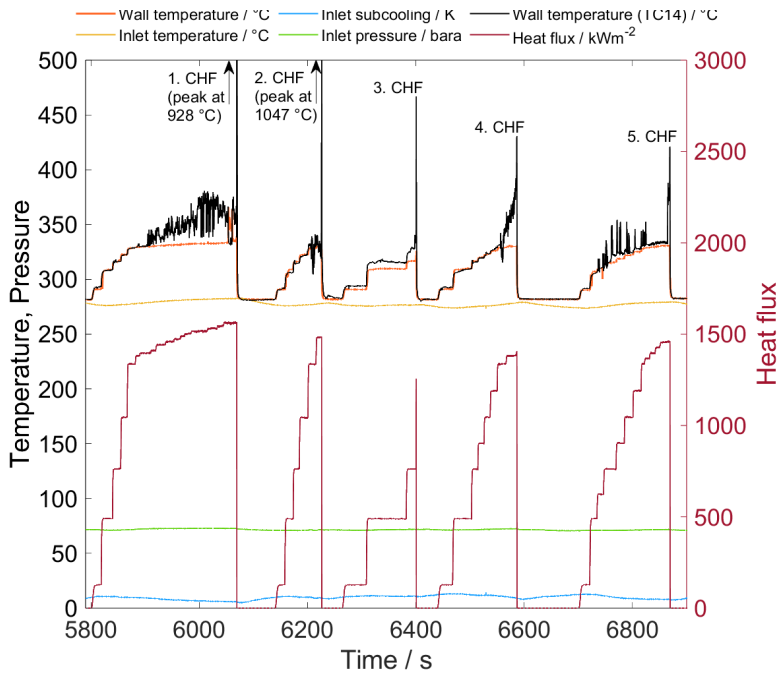

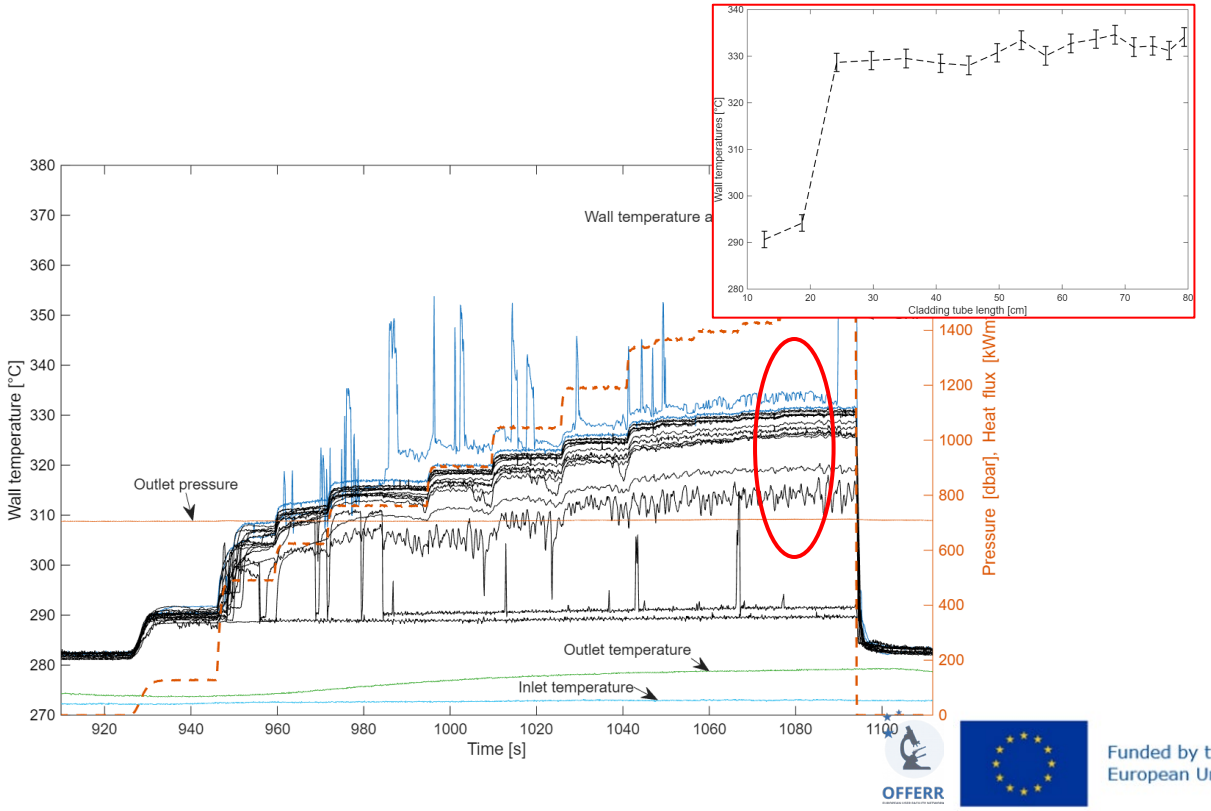

OFFERR

Funded by the European Union

- The State-of-the-art control system allows to detect the boiling crises very quickly and power to be reduced. The cladding tube remains undamaged. This enables to repeated the experiment.
- The high spacial density of thermocouples makes it possible to narrow down the location of the boiling crisis for each event and to create temperature distributions.

Summary

- COSMOS-H a new water/steam thermohydraulic facility for experiments on thermohydraulics and materials under high-pressure conditions is now operational.
- Initial experiments are being conducted, and the experimental facility and test track are being expanded and optimized.
- The first experiment with Zircaloy-4 has already yielded useful results, and further experiments with chrome-coated cladding tubes will follow, including at higher pressures.

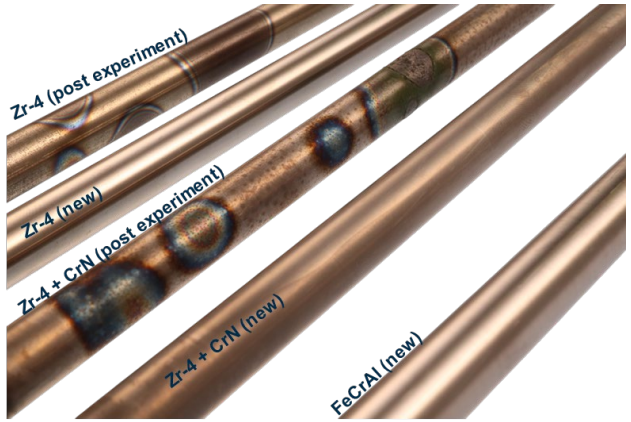

We look forward to get in contact with you!

stephan.gabriel@kit.edu & wilson.heiler@kit.edu

Tapan K. Sawarn

BARC

Synergistic influence of oxygen, hydrogen and microstructure on thermal shock behavior of PHWR fuel cladding subjected to integral LOCA test

During a hypothetical loss of coolant accident (LOCA) in a pressurised heavy water reactor (PHWR), fuel cladding temperature may rise up to 1500°C due to coolant positive void coefficient of reactivity. At such a high temperature, β-Zr phase absorbs significant amount of oxygen and hydrogen causing its embrittlement. A novel approach was attempted to study the synergistic effects of oxygen, hydrogen and prior β-Zr layer thickness on the crack initiation and propagation during the thermal shock.

A series of integral LOCA tests were performed on the PHWR cladding. The tests were carried out according to a temperature-time scenario typical for a large break LOCA in PHWRs. The heating cycle simulates the typical power pulse type of transients, which are unique characteristics of the PHWRs. Clad tubes filled with alumina pellets were internally pressurised (7 & 20 bar) and subjected to induction heating in steam environment. It was heated to various oxidation temperatures in the range 1000 - 1500°C (at interval of 100°C), soaked for 12-20s, cooled down to 800°C & then water quenched. The results showed the presence of non-uniform distribution of oxygen, hydrogen and prior β-Zr phase across the clad thickness along the circumference and axial direction of cladding. The presentation discusses the insights generated from the study.

Synergistic influence of oxygen, hydrogen and microstructure on thermal shock behavior of PHWR fuel cladding subjected to integral LOCA test

Tapan K. Sawarn*, Shefali Shukla, Suparna Banerjee, P. Nanekar

Bhabha Atomic Research Centre, India

***sawarn@barc.gov.in**

30th International QUENCH Workshop
Karlsruhe Institute of Technology (Karlsruhe, Germany),
Campus North, 16 to 18 December 2025.

LOCA transient in PHWRs and LWRs

Parameters	PHWRs	LWRs
Coolant void coefficient of reactivity	Positive	Negative
Transient cycle	▪ Higher and faster rise in cladding temperature during a critical large break LOCA. ▪ Temperature ramp can be in the range of 53°C/s - 120°C/s for very short duration.	▪ Temperature rise slowly due to the simultaneous loss of moderation. ▪ SEH dominate during the first few seconds of the blowdown stage, ramp rate (~100°C/s), followed by a nearly isothermal ramp (~5°C/s) with a DEH.
Peak cladding temperature	1400 -1500°C under critical break condition momentarily with ECCS available	Remain below the regulatory limit of 1204°C, with ECCS available

LOCA transient in PHWRs and LWRs

	PHWRs	LWRs
Quenching rate	A higher quenching rate during reflooding, due to horizontal configuration of the fuel channels.	Reflooding involves a relatively low rate of water injection due to vertical core configuration—usually a few cm/s— until the core is completely flooded and quenched.
Accident progression	▪ Large heat sink capacity that is inherently available (Moderator, End shield & Calandria vault water). ▪ Cause slow progression of accident in case of severe accident.	▪ No such availability of heat sink in case of LWR. ▪ Cause fast progression of accident during severe accident.

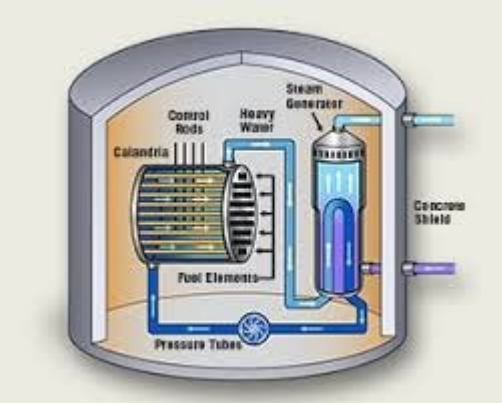

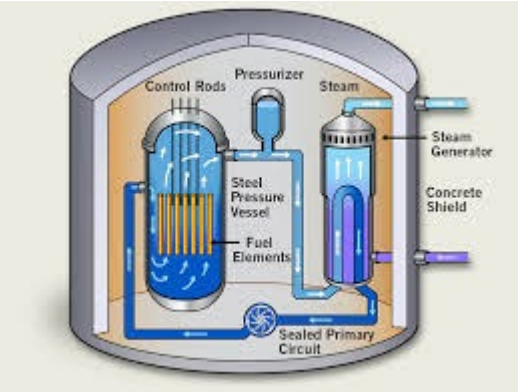

LOCA Integral Tests

Test specimen:
245 mm long, alumina pellets filled PHWR cladding

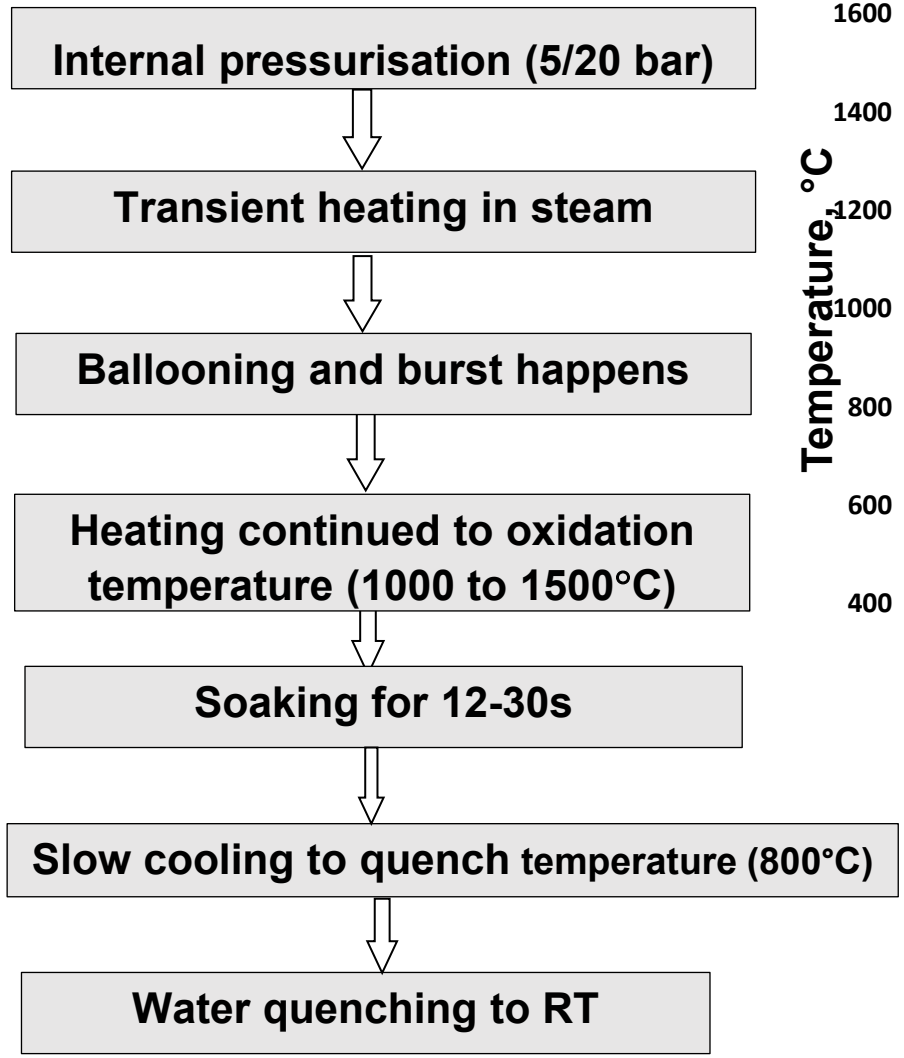

Steps of LOCA Integral Tests

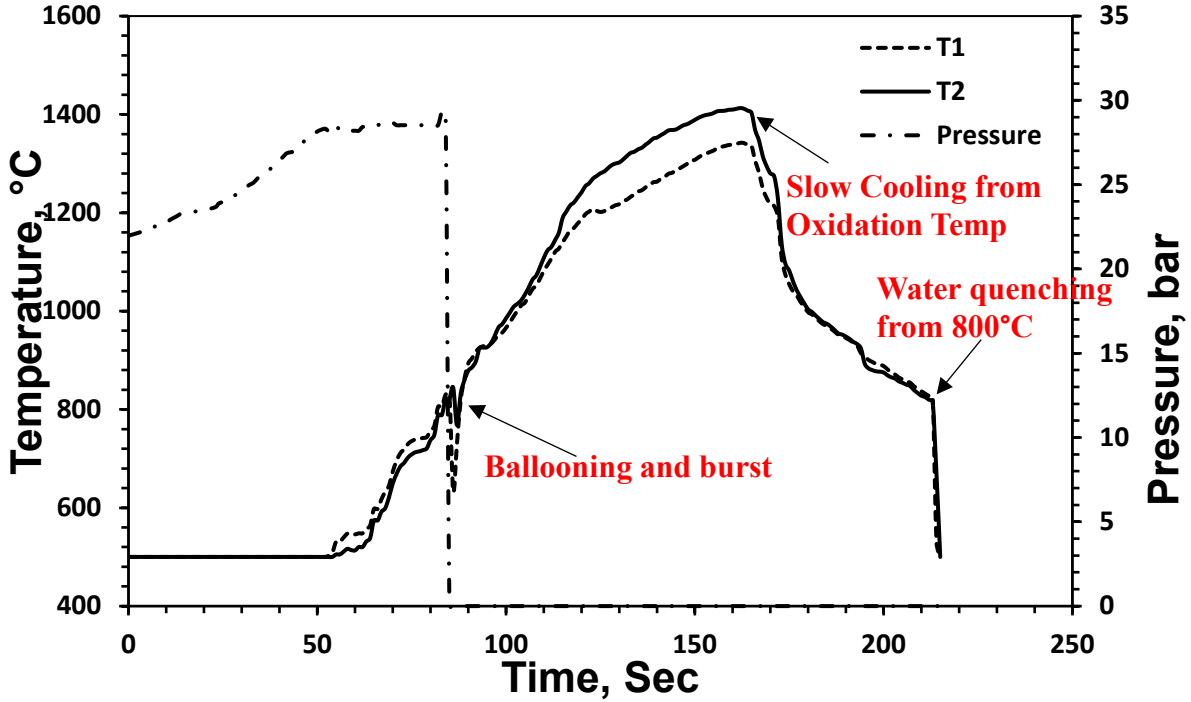

A typical T-P-t plot

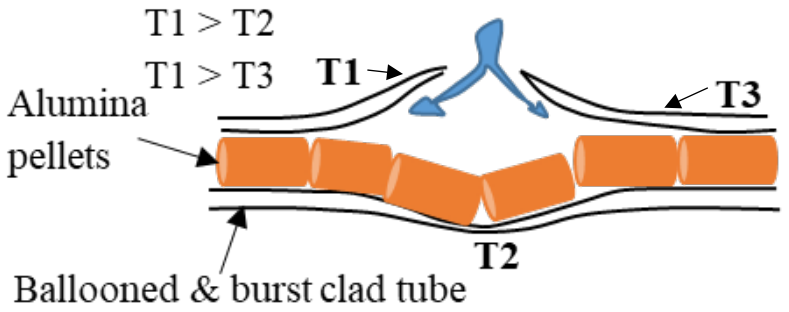

Establishment of temperature gradient

Post-test visual appearance

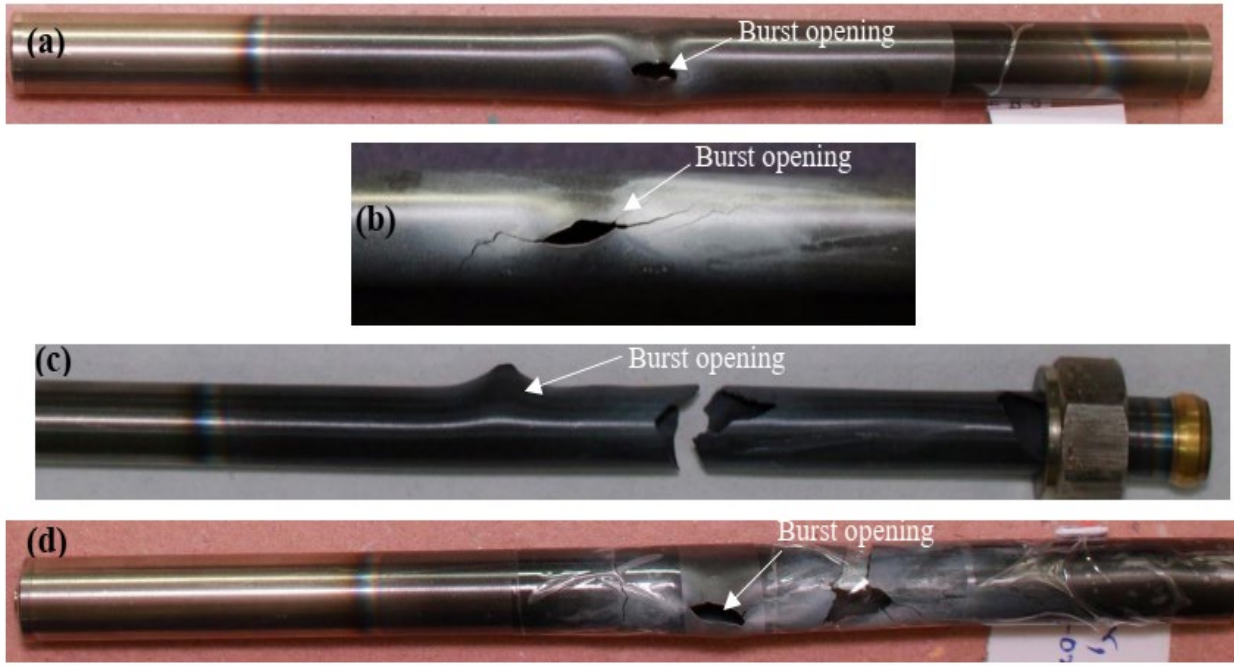

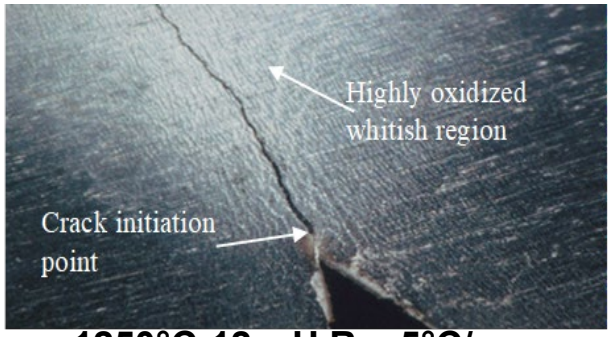

1250°C-12s, H.R. - 5°C/s

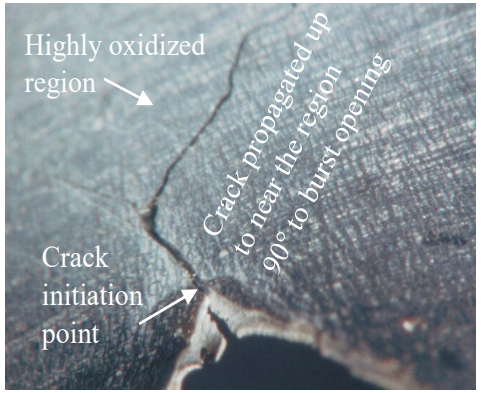

1400°C-12s, H.R. - 10°C/s

Response to thermal shock of the ballooned-burst and oxidized cladding:

i. **Survived,**

ii. **Cracked ahead of the burst opening tip,**

iii. **Disintegrate into two parts during thermal shock or handling away from burst opening, and**

iv. **Fragmented into multiple pieces due to severe oxidation at 1500°C.**

Axial Hydrogen distribution

n-radiography & tomography parameters

Scintillator	^{6}LiF-ZnS
Spatial Resolution	100 µm
Radiography	30 images of 30s exposure
Tomography	30s images 900 angles

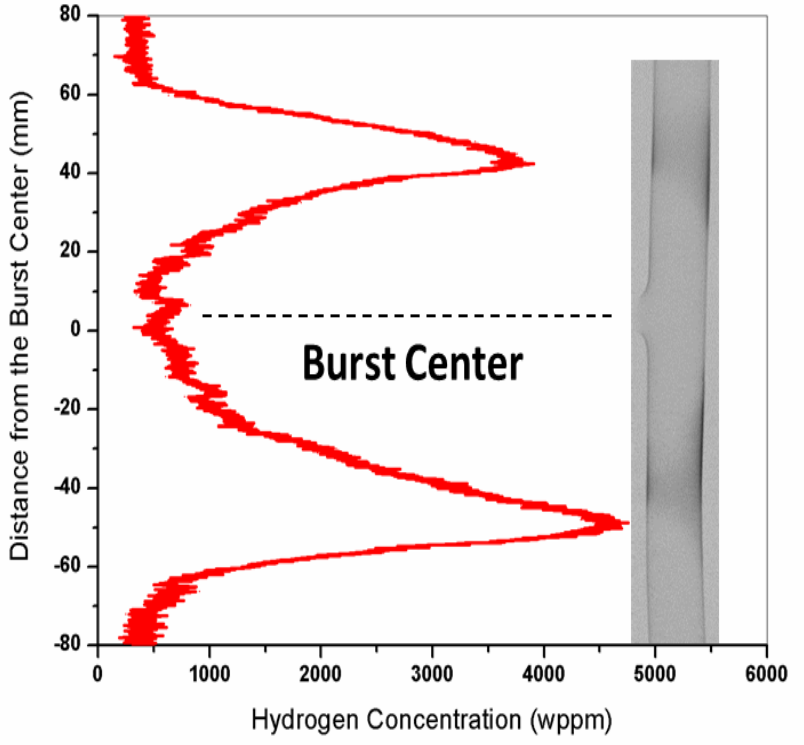

1300°C for 12s

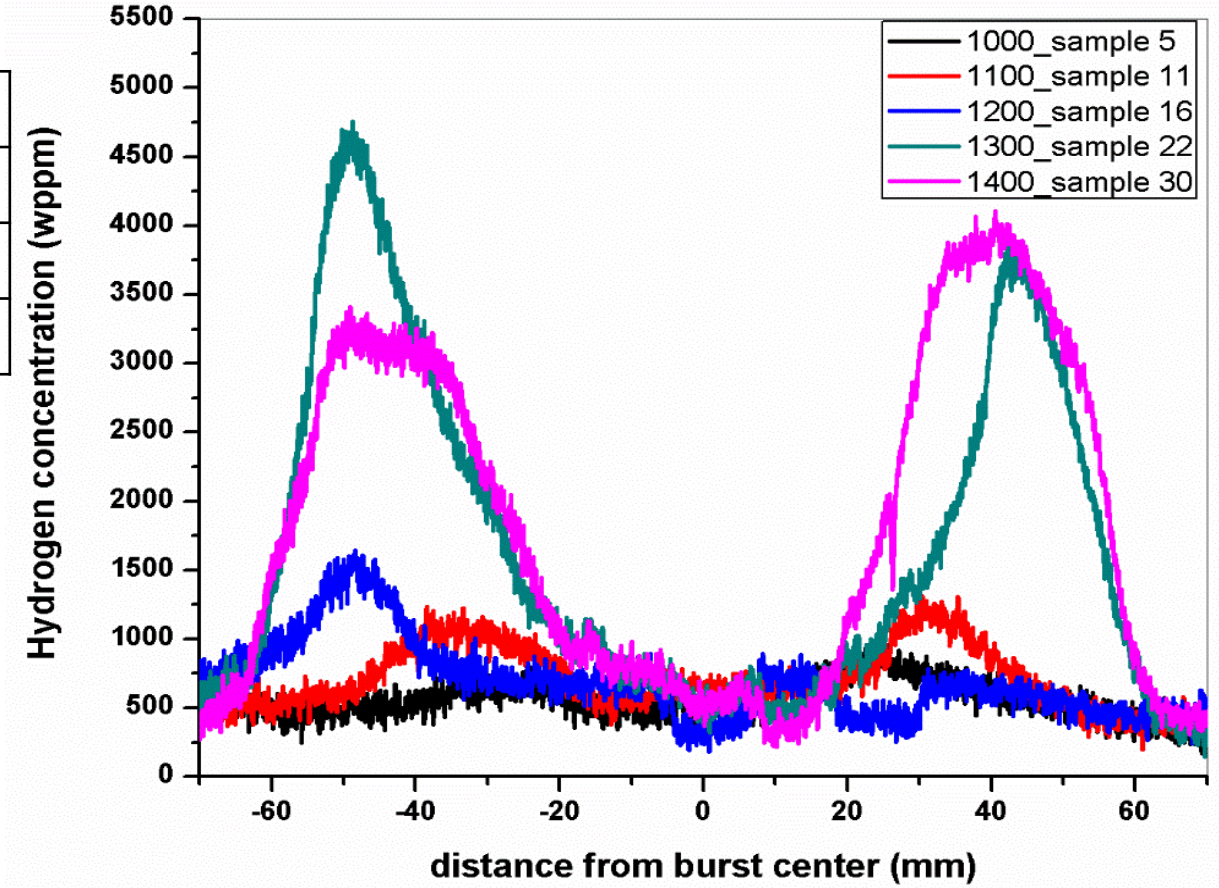

Significantly high hydrogen pick up occurred in the secondary hydriding region (1200 – 4700 wppm), 30 – 50 mm away from the burst opening.

Circumferential and radial hydrogen distribution

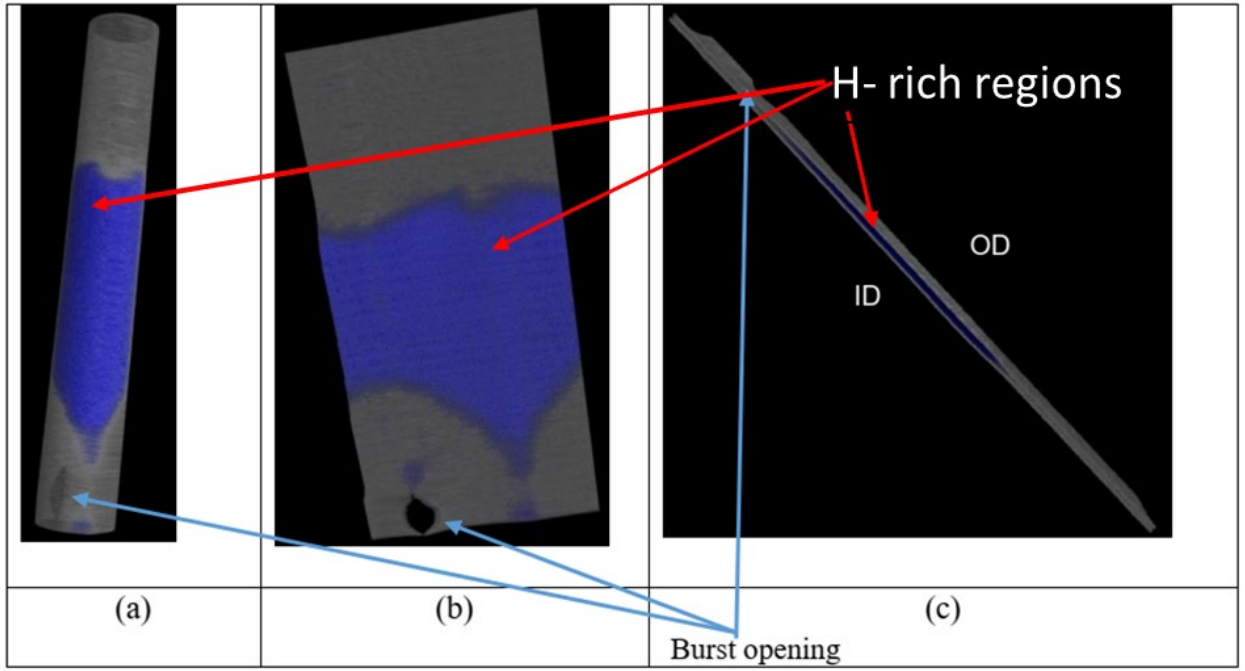

Oxidised at 1250°C for 12s

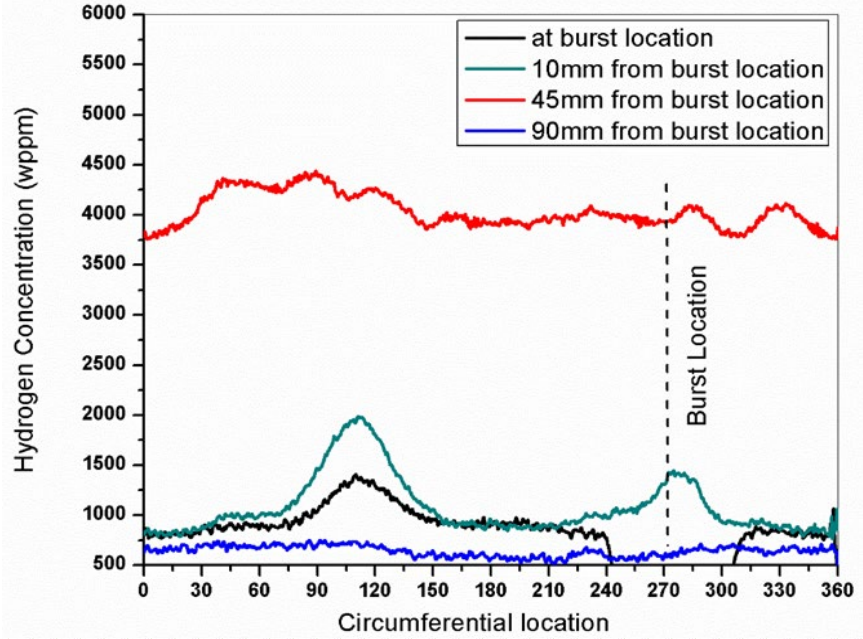

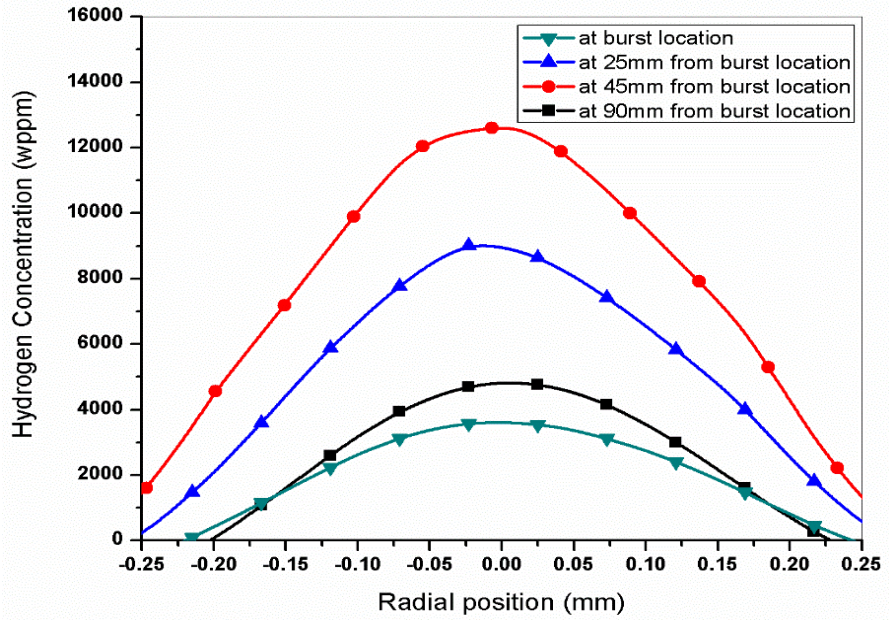

- **Maximum hydrogen was picked up in the region opposite to burst opening.**
- **Radially maximum hydrogen present in the prior β layer.**

Oxygen distribution along the circumference

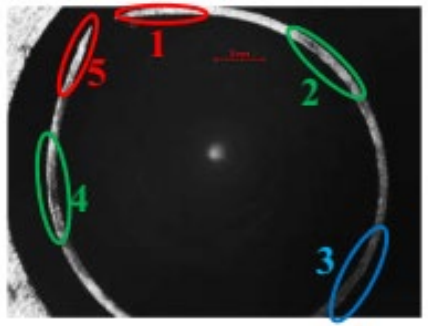

Oxygen in the prior β layer of region

Burst tip	**:**	**Average of locations 1 & 5**	**……..(i)**
90° to burst tip	**:**	**Average of locations 2 & 4**	**……..(ii)**
180° to burst tip:		**location 3**	**……..(iii)**

Average oxygen in the burst region's prior β layer = Average of i, ii & iii

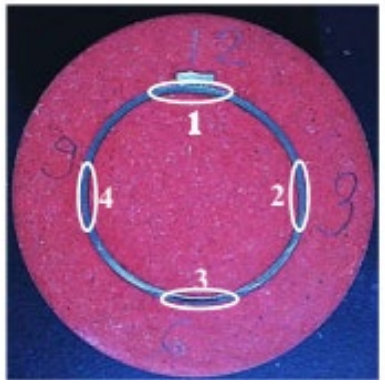

Average oxygen in the region away from the burst opening = Average of locations 1, 2, 3 & 4

Each location spanning over 900μm

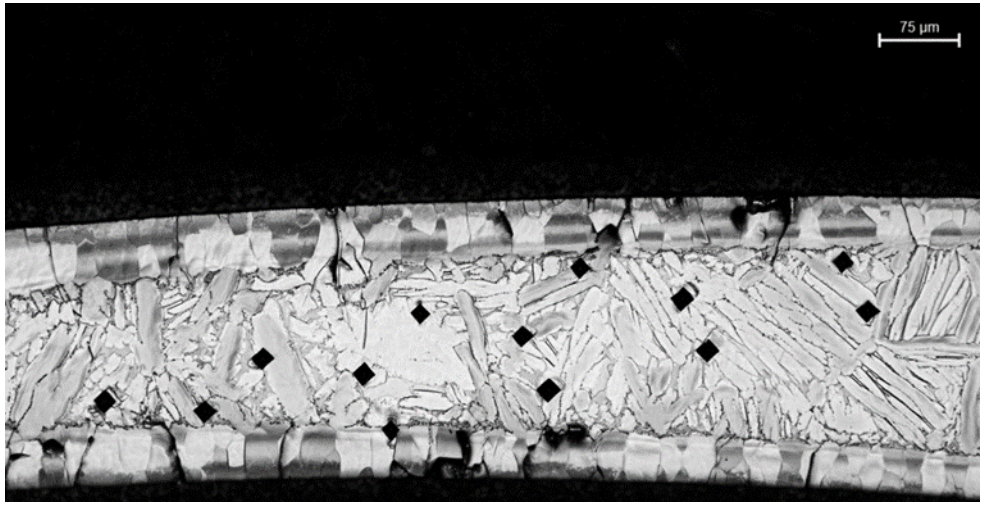

Leistikow correlation used to determine oxygen concentration from Vickers micro-hardness.

Maximum calculated standard error: ±0.05 wt.%

Oxygen distribution along the circumference

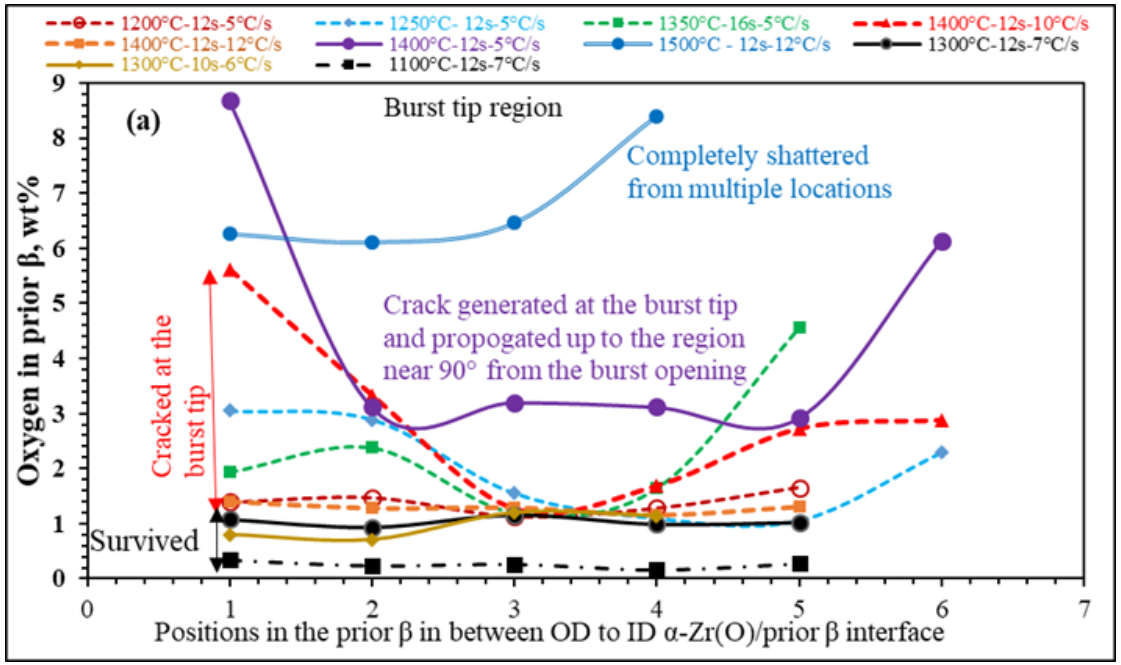

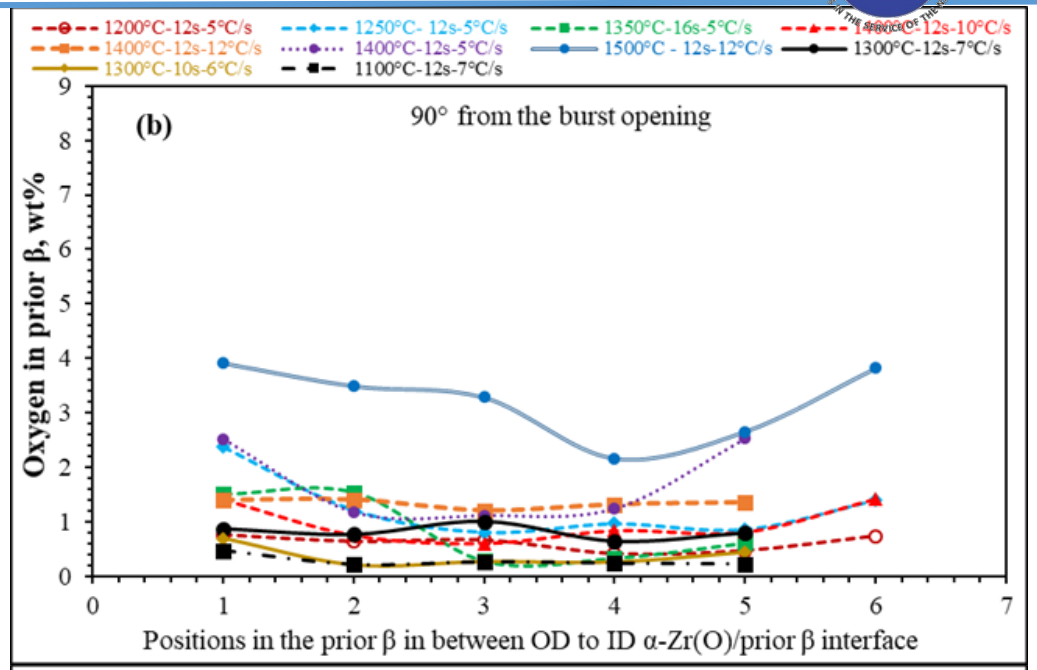

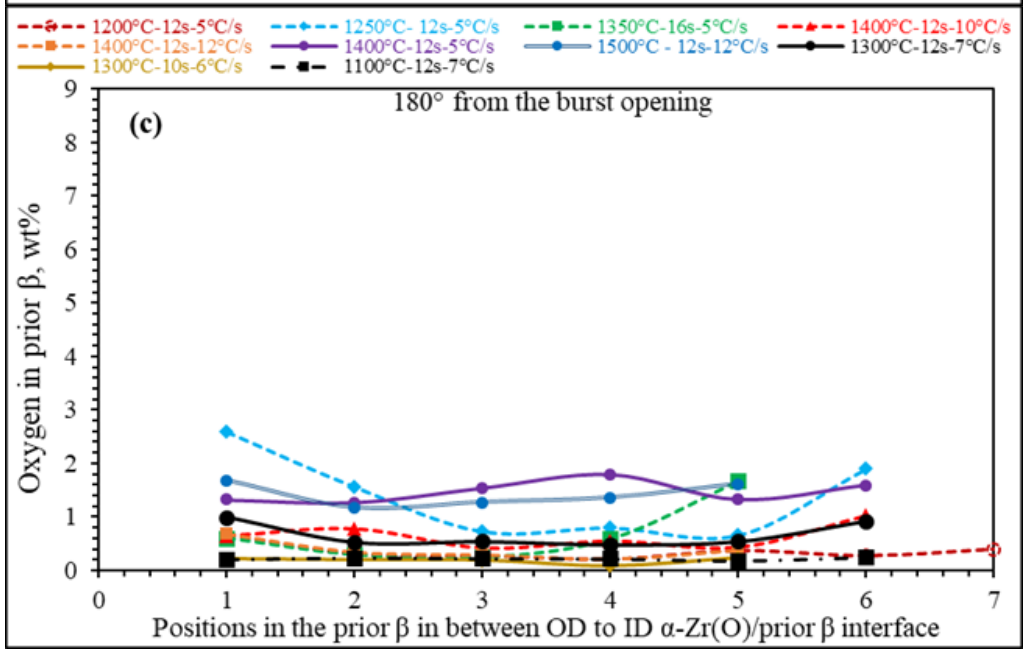

- **Oxygen distribution in the prior β layer was non-uniform.**
- **Maximum non-uniformity & steep concentration gradient was observed in the burst tip region, and**
- **Non-uniformity progressively decreased in the region circumferentially away from burst tip.**

Microstructure near burst region

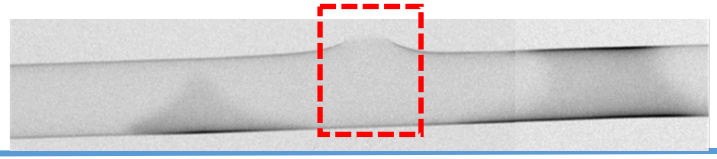

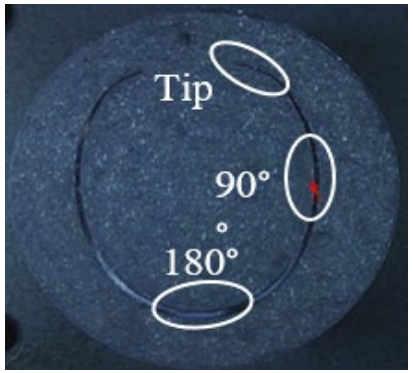

9°C/s-1300°C-35s

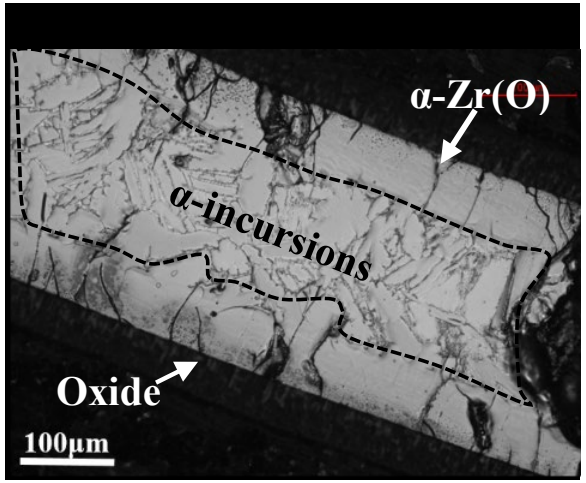

Tip

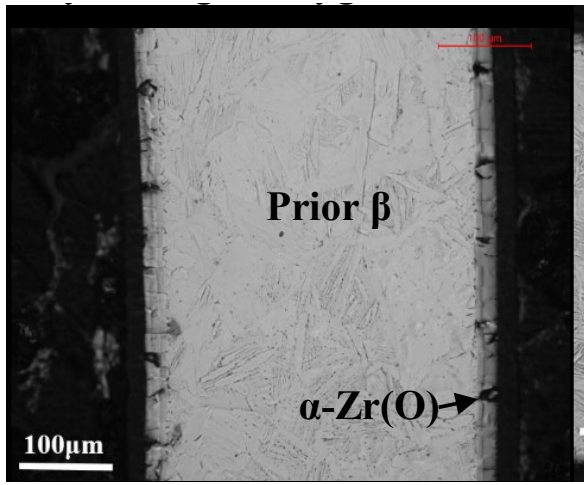

90°

180°

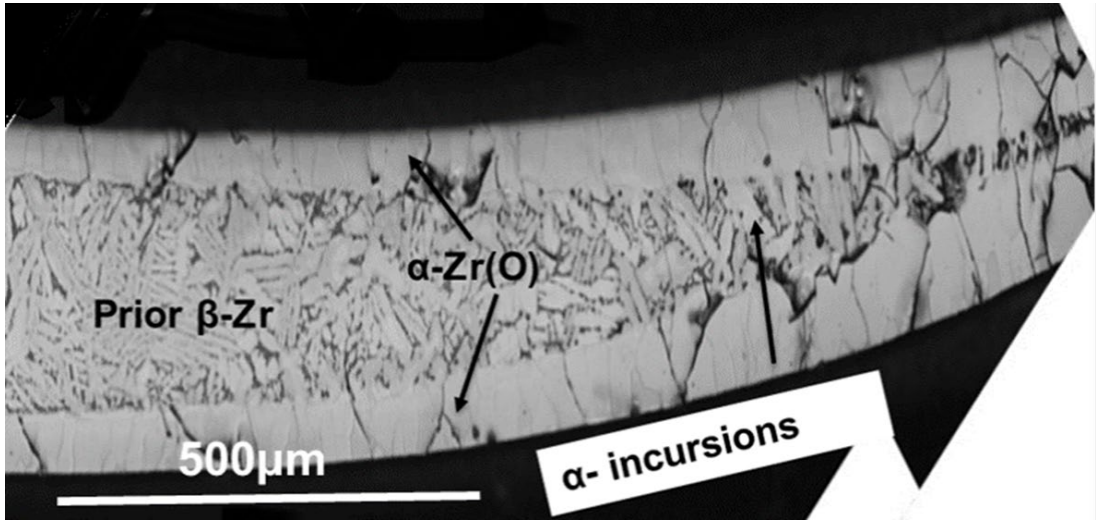

8°C/s-1200°C-12s

- Heterogeneous microstructure developed around the circumference as a result of azimuthal temperature gradient and localized ballooning deformation.
- α-Zr(O) layer thickness reduced progressively from the burst tip to region opposite to it.
- Maximum oxidation occurred close to the burst tip and minimum opposite to it.

Microstructure in the secondary hydriding region

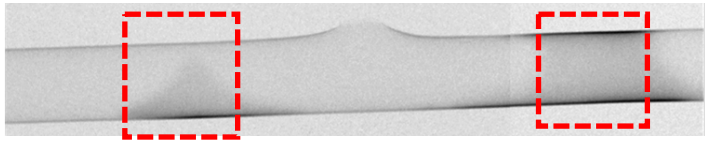

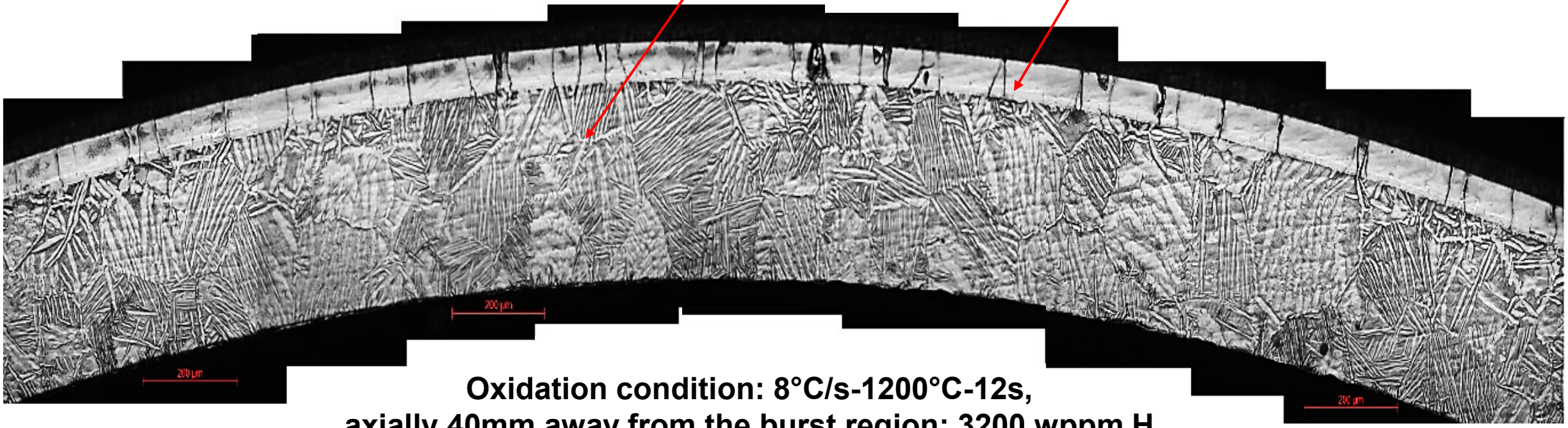

Oxidation condition: 8°C/s-1200°C-12s,
axially 40mm away from the burst region: 3200 wppm H

- **Single sided oxidation occurred.**
- **No α-Zr(O) incursions, smooth and regular α-Zr(O)/prior β interface.**
- **High hydrogen concentration resulted in relatively thicker prior β-Zr layer.**

Hydrides in the burst region

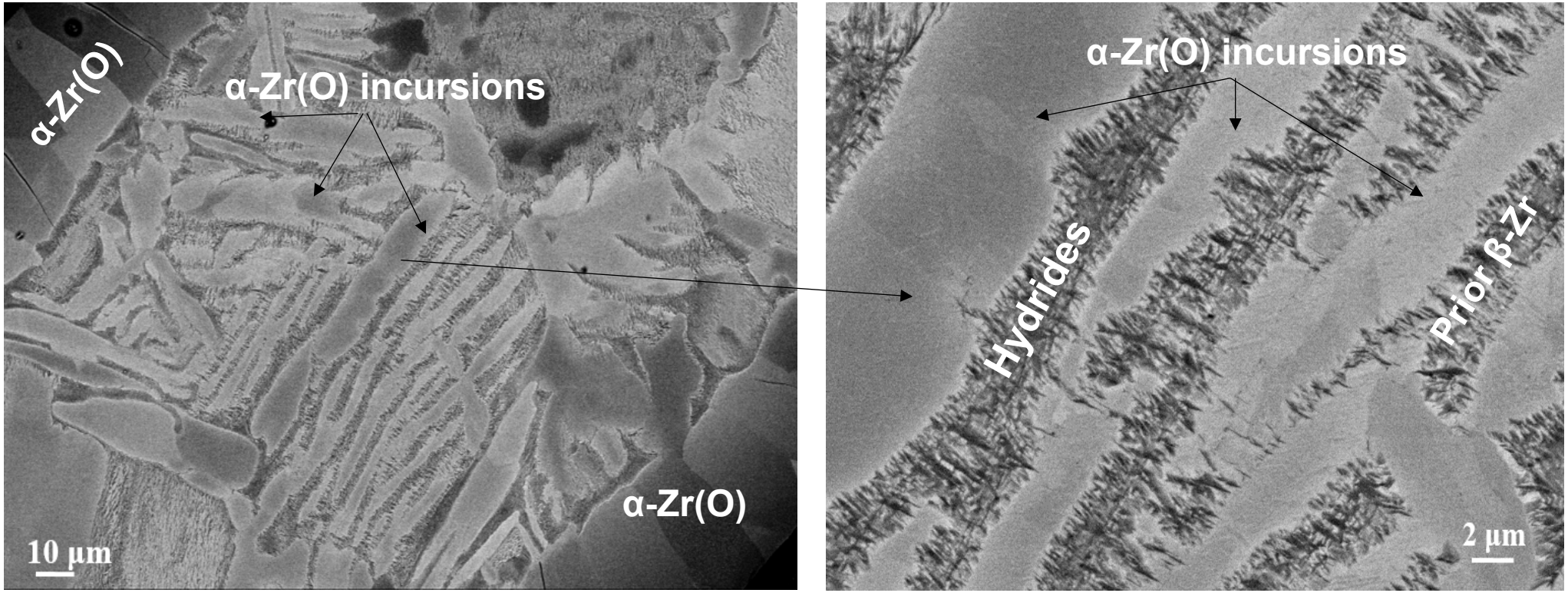

9°C/s-1300°C-35s, O & H in the burst tip region: 1.14 wt.% & 700 wppm respectively

In b/w the α-Zr(O) intrusions, there were densely packed fine hydrides (<2 μm) that took up most of the prior β layer near the burst tip region.

Hydrides in the burst region

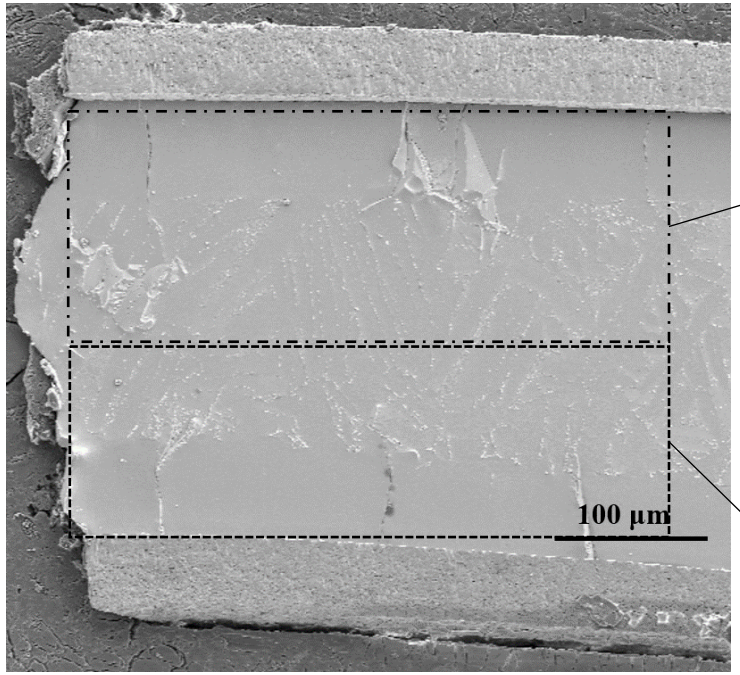

9°C/s-1200°C-12s, O & H in the burst tip region: 1.4 wt.% & 900 wppm respectively

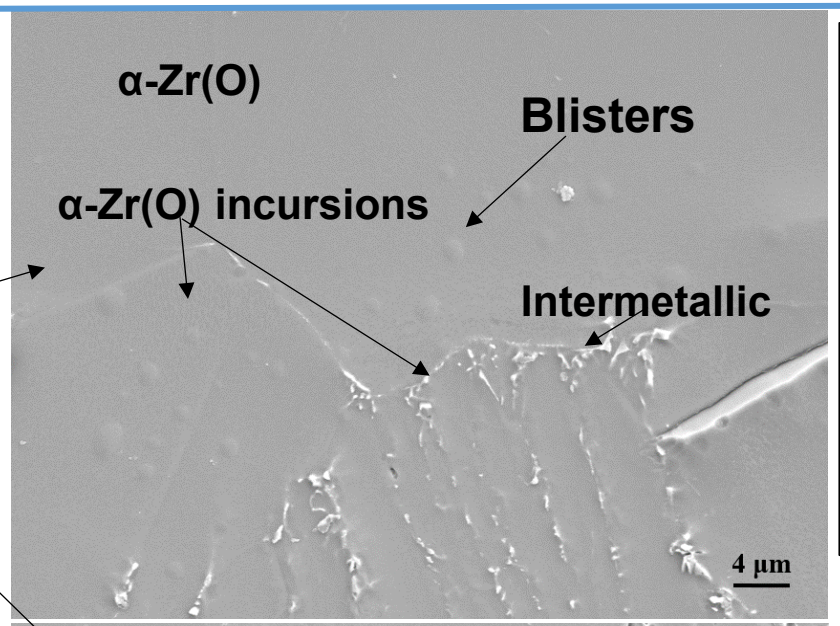

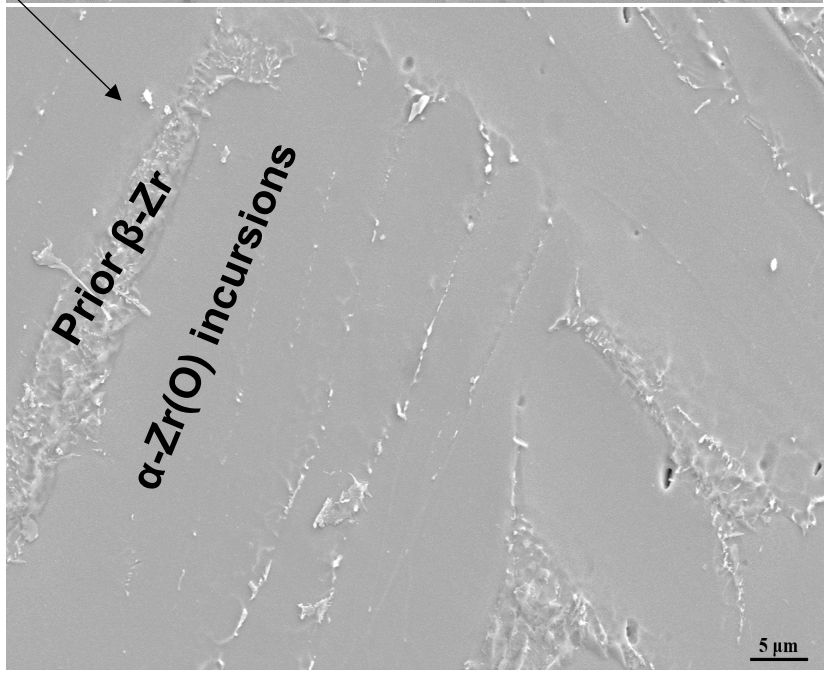

Under the influence of high localised stresses and T gradient, significant amount of hydrogen migrated towards the cladding outer surface and precipitated as hydride blisters.

As O and H concentration increased, hydriding events shift from hydride platelets to hydride blisters.

Hydrides in the secondary hydriding region

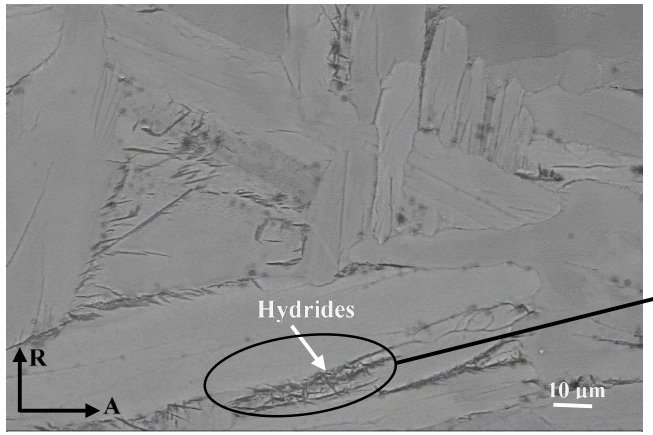

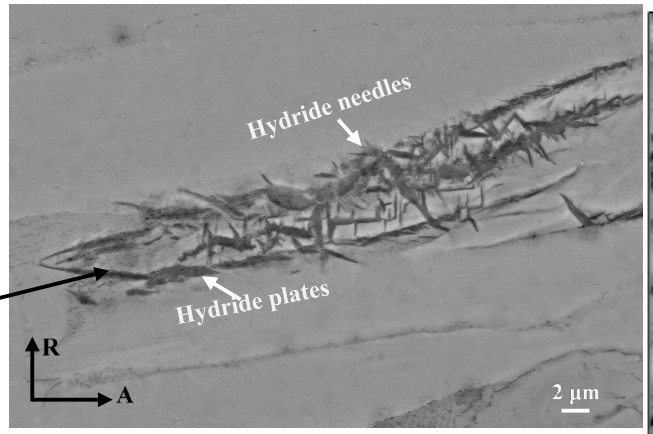

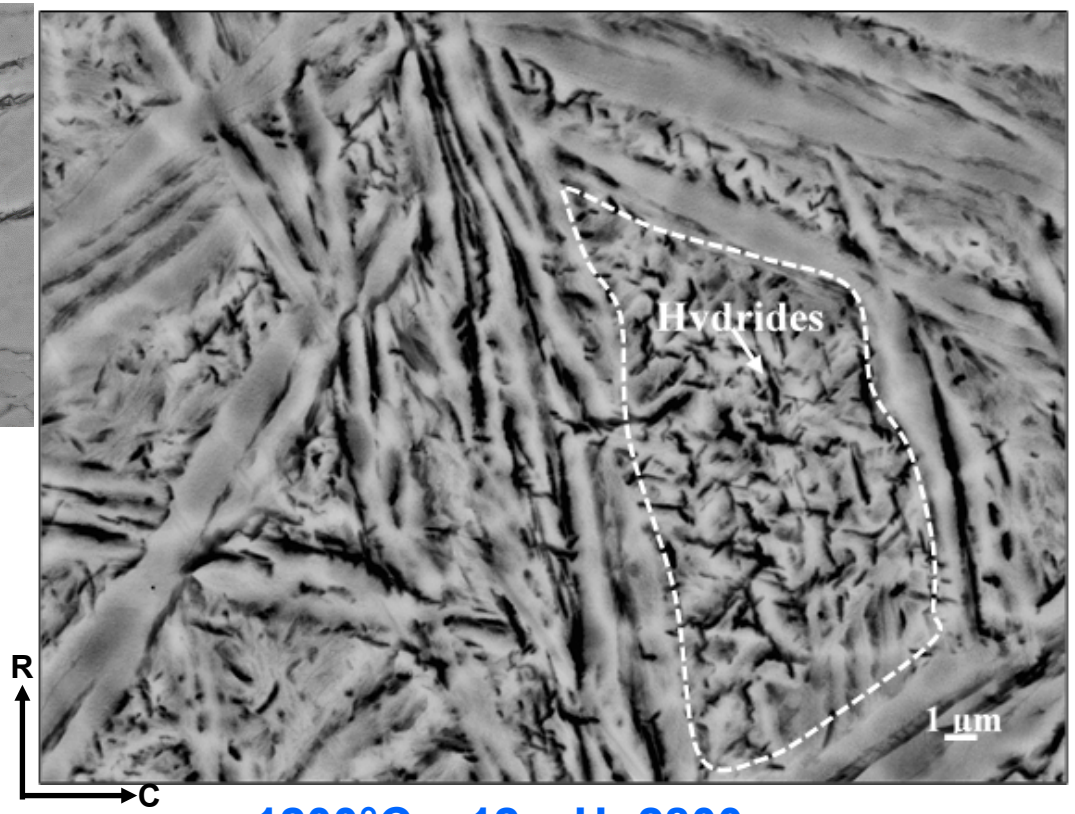

1200°C – 12s, H: 2800 wppm

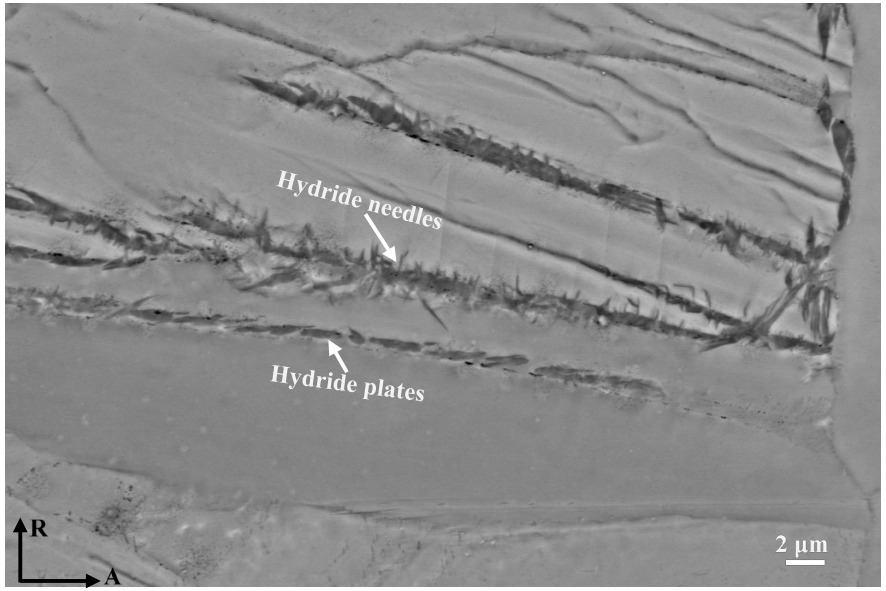

1300°C – 20s, H: 2100 wppm

- Very fine (sub-micron size) hydrides were precipitated.
- Clustering of hydrides also observed.

Elemental Partitioning

O & Sn-enriched zone

Fe & Cr-enriched zone

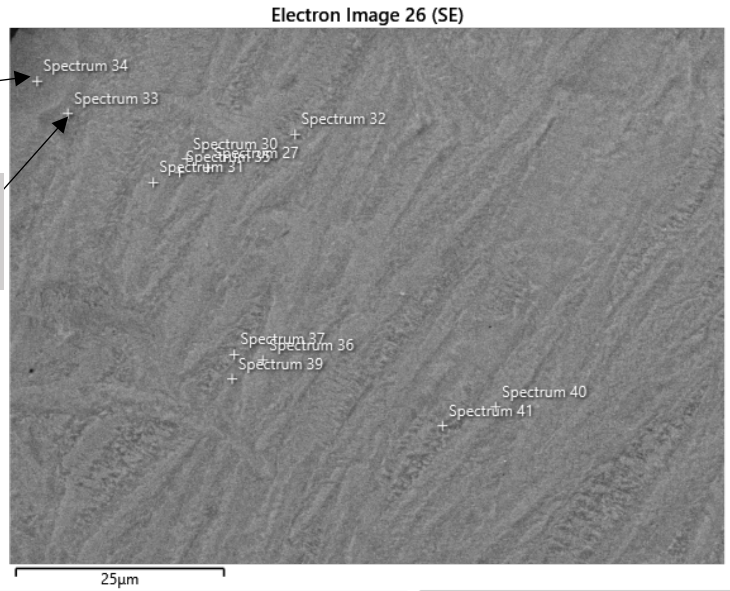

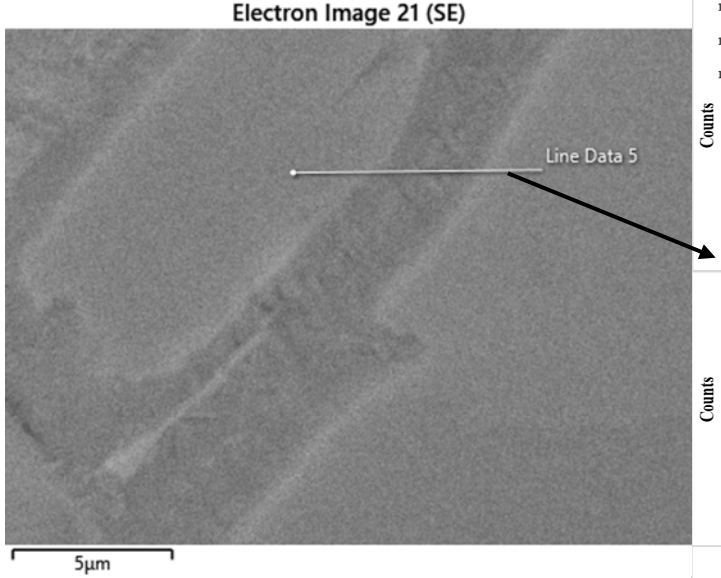

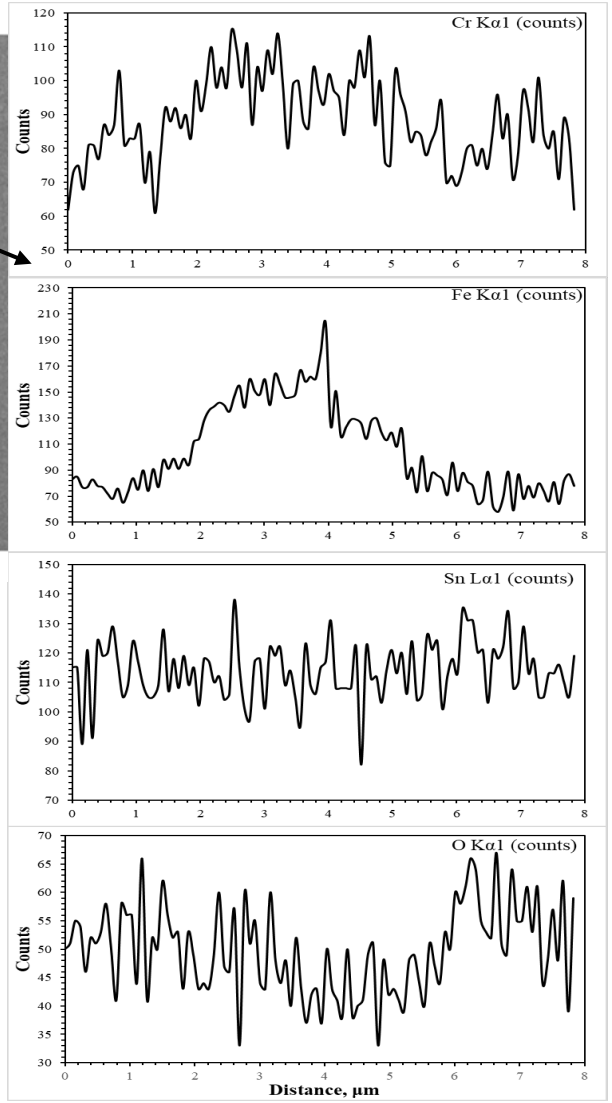

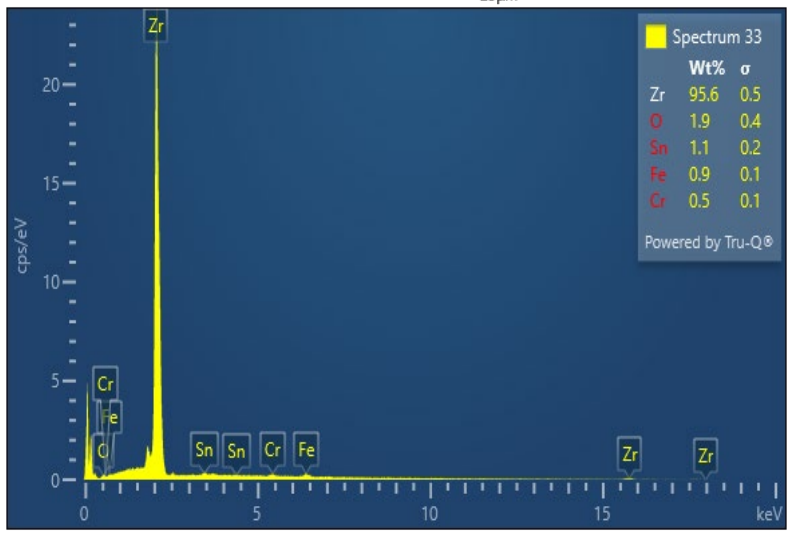

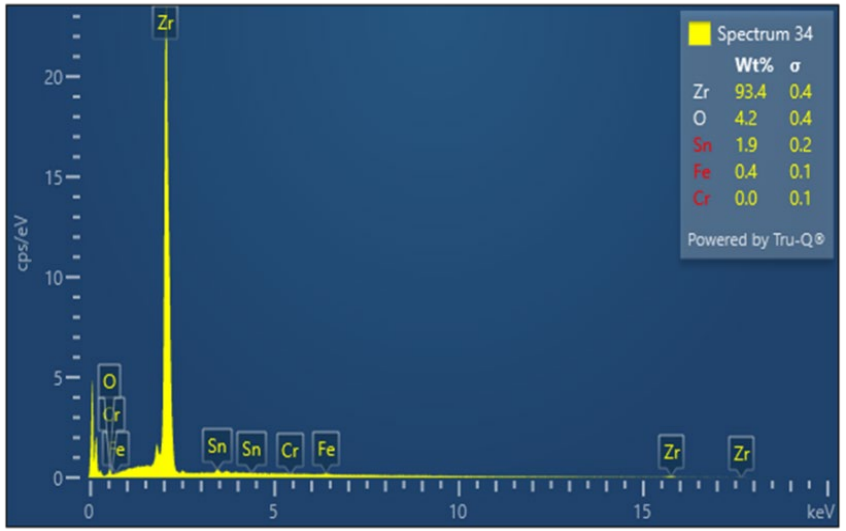

24°C/s-1100°C-12s, O in the burst tip region: 0.25 wt.%

8°C/s-1200°C-12s, O in the burst tip region: 0.7 wt. %

Elemental Partitioning

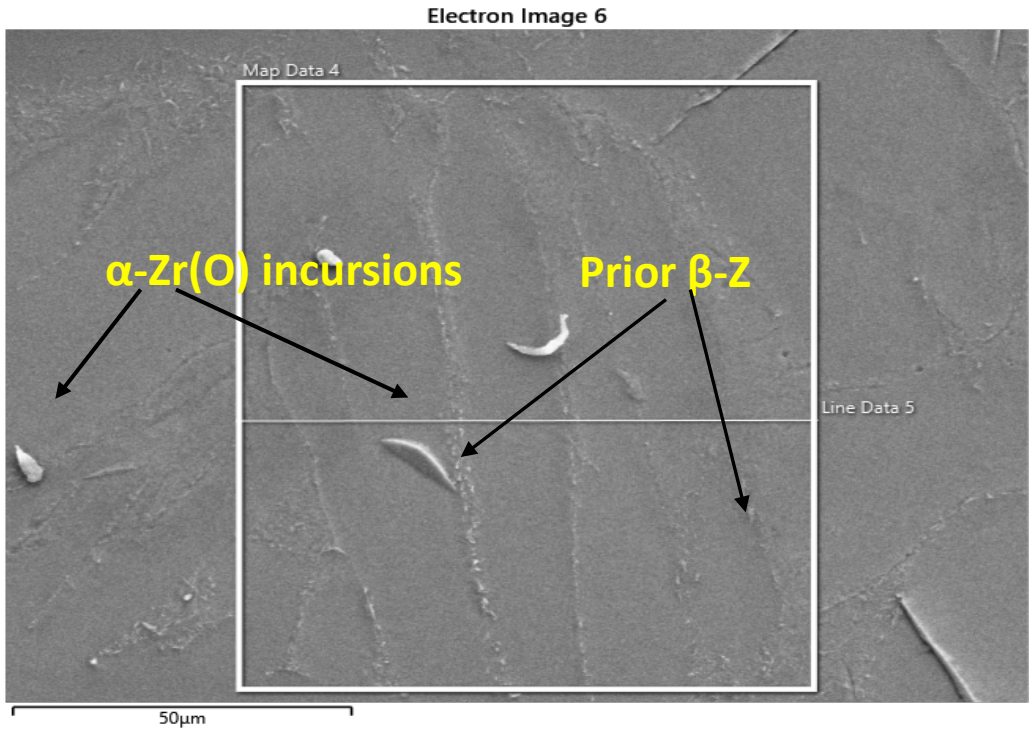

9°C/s-1300°C–12s,O in burst tip region– 1.3 wt.%

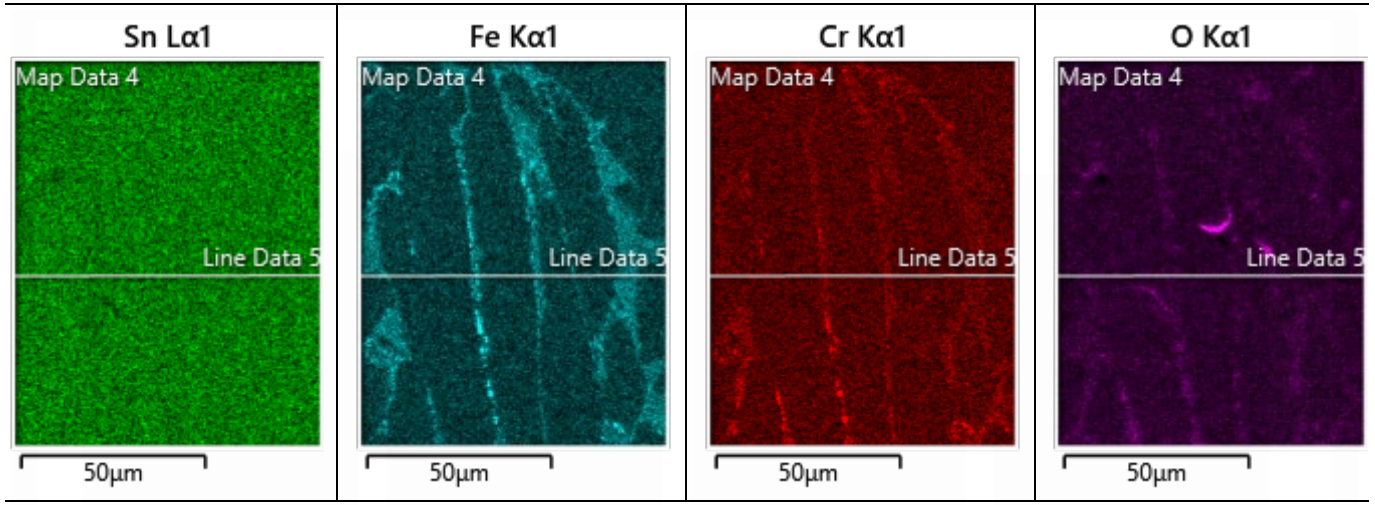

- O, a potent α-stabilizing element, concentrates into the first α platelets to form and encourages the development of "α-Zr(O)-incursions".
- Un-transformed β phase, enriched with β-stabilizing elements like H, Cr, and Fe.
- Sn does not exhibit any discernible partitioning for mean O, 0.7wt.% and beyond.

Influence of hydrogen on oxygen concentration & distribution

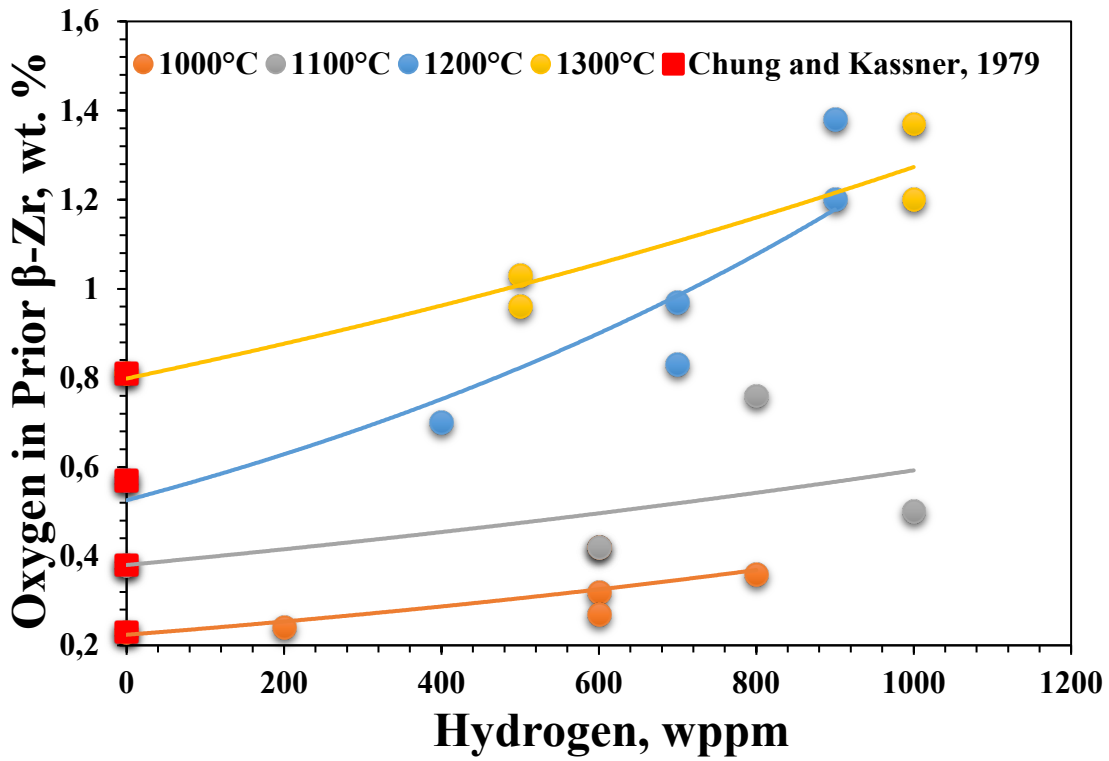

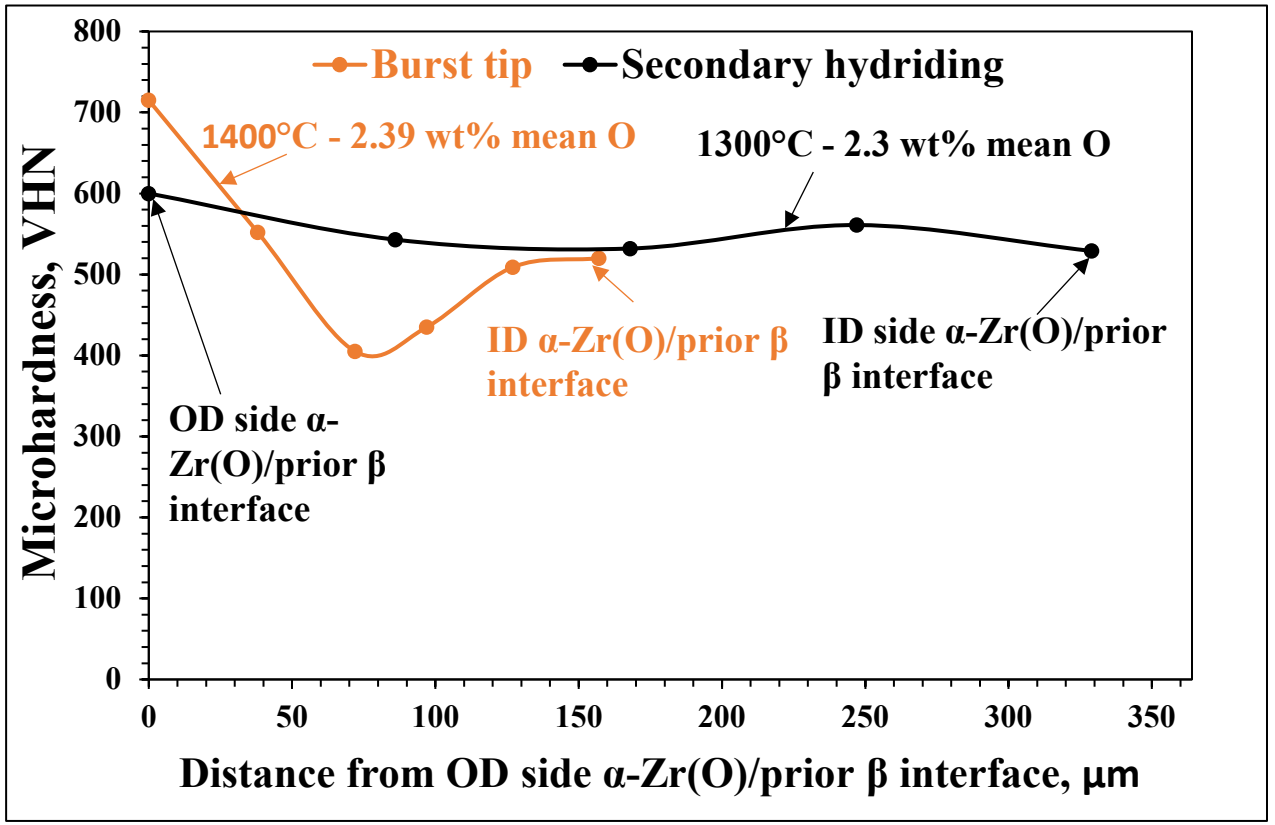

- Oxygen content in prior β increased with increased H for a constant oxidation temperature.
- High dissolved hydrogen in the β-Zr increased oxygen diffusivity and solubility in the secondary hydriding zone and delayed oxygen accumulation at the α-Zr(O)/β-Zr interface, making the entire prior β thickness brittle.

Crack initiation threshold at the burst tip due to thermal shock

Crack initiation site

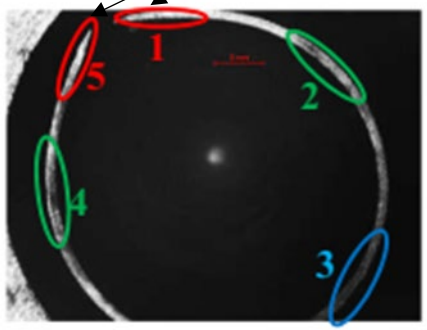

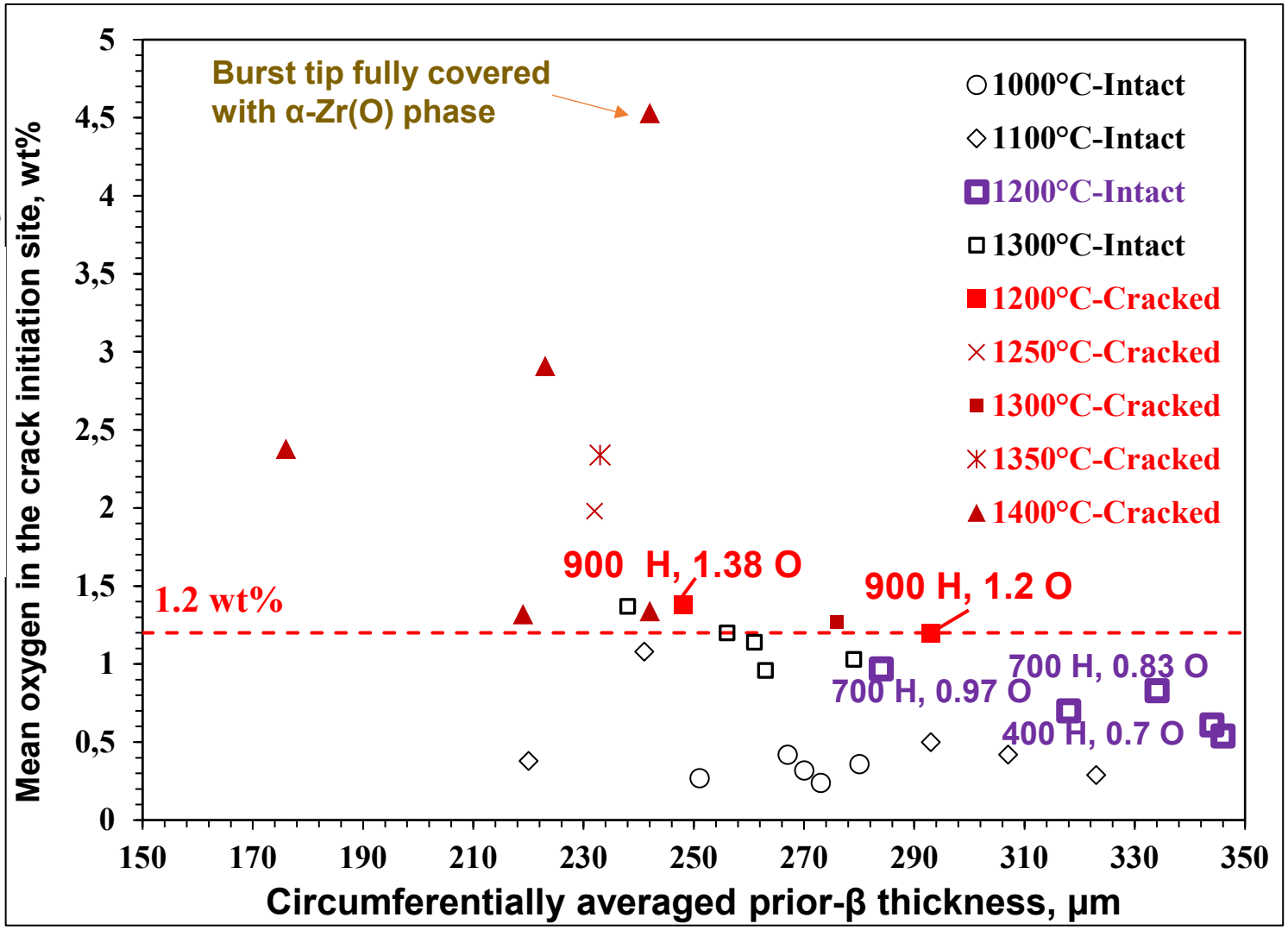

- Crack initiation threshold: Oxygen in prior β near the burst tip region 1.2 wt.% .
- There is no effect of hydrogen on thermal shock below 900 wppm.

Crack propagation during thermal shock

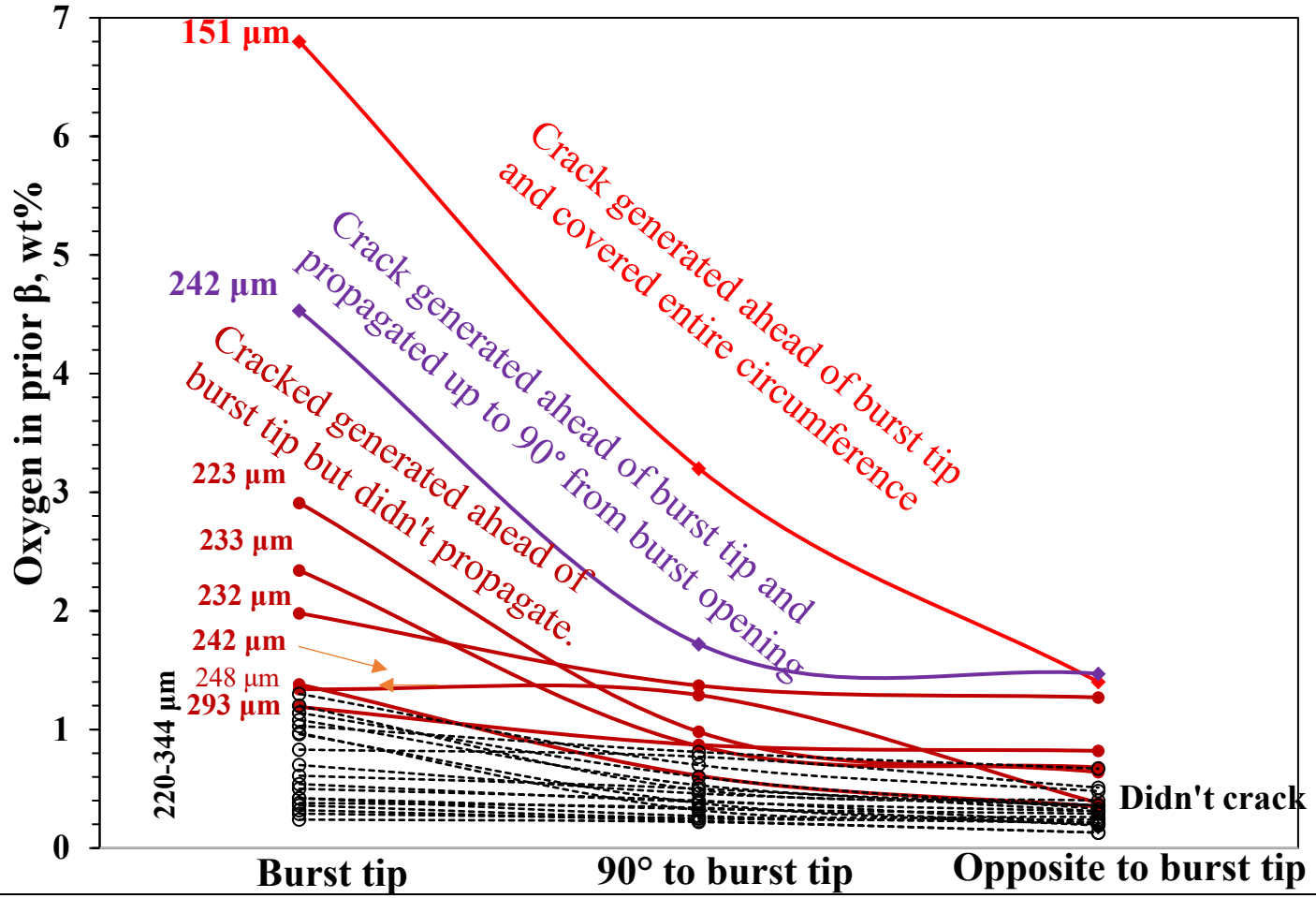

- Circumferential gradient of oxygen concentration existed; highest at the burst tip and lowest at 180°.
- Thermal shock failure initiates at 1.2 wt% oxygen locally in the burst tip region.
- Crack initiated at burst tip could not propagate along the circumference if av. prior β thickness >200 µm

Summary

- Burst tip location was a highly embrittled region on account of synergistic effect of
  a. Thinning of prior β layer due to deformation and formation of thick oxide & α-Zr(O) layer;
  b. Critical oxygen concentration and
  c. Sharp burst tip acting as a stress raiser.
- For ballooned and ruptured clad, the threshold for thermal shock failure (crack initiation) 1.2 wt.% O and 900 wppm H.
- Crack propagation along the circumference stops if av. prior β thickness >200 μm.
- Two types of hydride morphologies were observed, viz. hydride blisters near the burst tip and fine hydride platelets near and away from it.

Summary

- **Higher concentration of hydrogen increased the oxygen solubility and diffusivity in the β-Zr at higher temperature, causing**

  a. **Extensive oxygen partitioning during the cooling from β-Zr to α-Zr leading to formation of highly embrittled α-Zr(O) incursions in the burst region.**

  b. **Oxygen partitioning resulted in segregation of intermetallics along the α-Zr incursions interfaces.**

  c. **In the secondary hydriding region high concentration of hydrogen prevented the oxygen built-up near the α-Zr(O)/prior β interface and flattened the oxygen distribution profile across the prior β-layer, causing brittleness to entire layer.**

Future Outlook

Study of embrittlement mechanism and assessment of fracture strength of integral LOCA tested PHWR cladding using the four-point bend test (4-PBT)

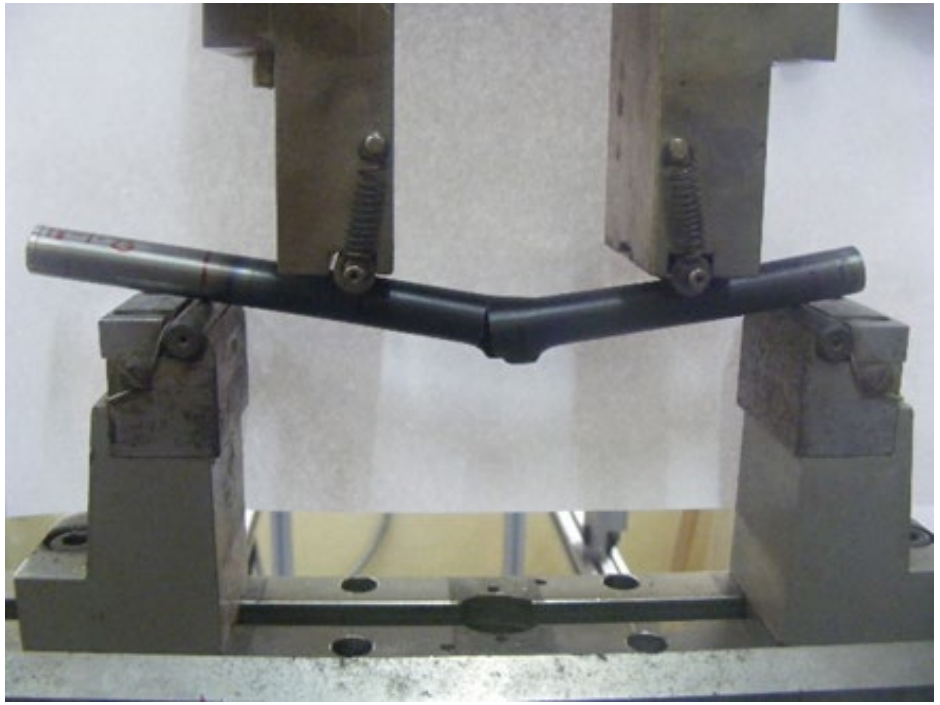

Thank you for your attention

Anzhelika Khaperskaia

IAEA

Results of the IAEA Coordinated Research Project (CRP) on 'Testing and Simulation of Advanced Technology and Accident Tolerant Fuels (ATF-TS)' (2020–2024) and Plans for the Next CRP

The IAEA Coordinated Research Project on Testing and Simulations for Accident Tolerant and Advanced Technology Fuels (CRP ATF-TS), concluded in 2024, supported Member States in developing and accessing advanced nuclear fuels. Motivated by the Fukushima Daiichi accident, the project focused on near-term ATF solutions, including Cr-coated Zircaloy and FeCrAl claddings and doped fuel pellets, offering safety and operational benefits under normal, design-basis accident (DBA), and design extension conditions (DEC).

CRP ATF-TS encompassed four work tasks: experimental testing of ATF claddings and fuels, benchmarking of fuel performance codes, development of a LOCA fuel safety evaluation methodology, and establishment of an open-source ATF material properties database.

Nine organizations conducted tests on 15 types of ATF cladding materials, including chromium-coated Zr-based alloys, Zr alloys with alternative coatings, FeCrAl alloys, and uncoated Zr alloys (as a reference). Experiments across multiple laboratories generated extensive datasets on ballooning and burst tests, high-temperature oxidation, long-term corrosion, mechanical performance, and bundle tests under extended LOCA and BDBA scenarios. Results showed small benefits in time-to-burst, ballooning size, and burst opening, but improvements in oxidation resistance and post-quench ductility, reducing chemical heat and hydrogen release during hypothetical accidents.

Fuel rod modelling and simulation benchmarks involved 19 organizations from 16 member states, while 9 organizations from 8 member states conducted bundle test simulations for selected ATF concepts, including chromia-doped fuel, FeCrAl claddings, and Cr-coated Zr-alloy claddings. These exercises highlighted the need for modifications to oxidation models for FeCrAl and Cr-coated Zr.

The LOCA evaluation methodology confirmed ATF benefits but also emphasized the need for further improvements in mechanical deformation models and input uncertainties to enhance safety evaluations.

The project also established an open-access material database to support future ATF research and licensing.

The presentation will also summarize outcomes from the proposed new CRP on ATF fuels.

30th International QUENCH Workshop
Karlsruhe Institute of Technology, Germany
16-18 December 2025

Results of the IAEA CRP on 'Testing and Simulation of Advanced Technology and Accident Tolerant Fuels (ATF-TS)' (2020–2024) and Plans for the Next CRP

Anzhelika Khaperskaia, Technical Lead
NFCMS /NEFW, IAEA

OUTLINE

- Introduction (IAEA NE structure and activities)
- Completed CRP on 'Testing and Simulation of Advanced Technology and Accident Tolerant Fuels (ATF-TS)' (2020–2024)
- Plans for the Next CRP on ATF Testing and Simulation

Nuclear Fuel Cycle and Materials Section (NFCMS)

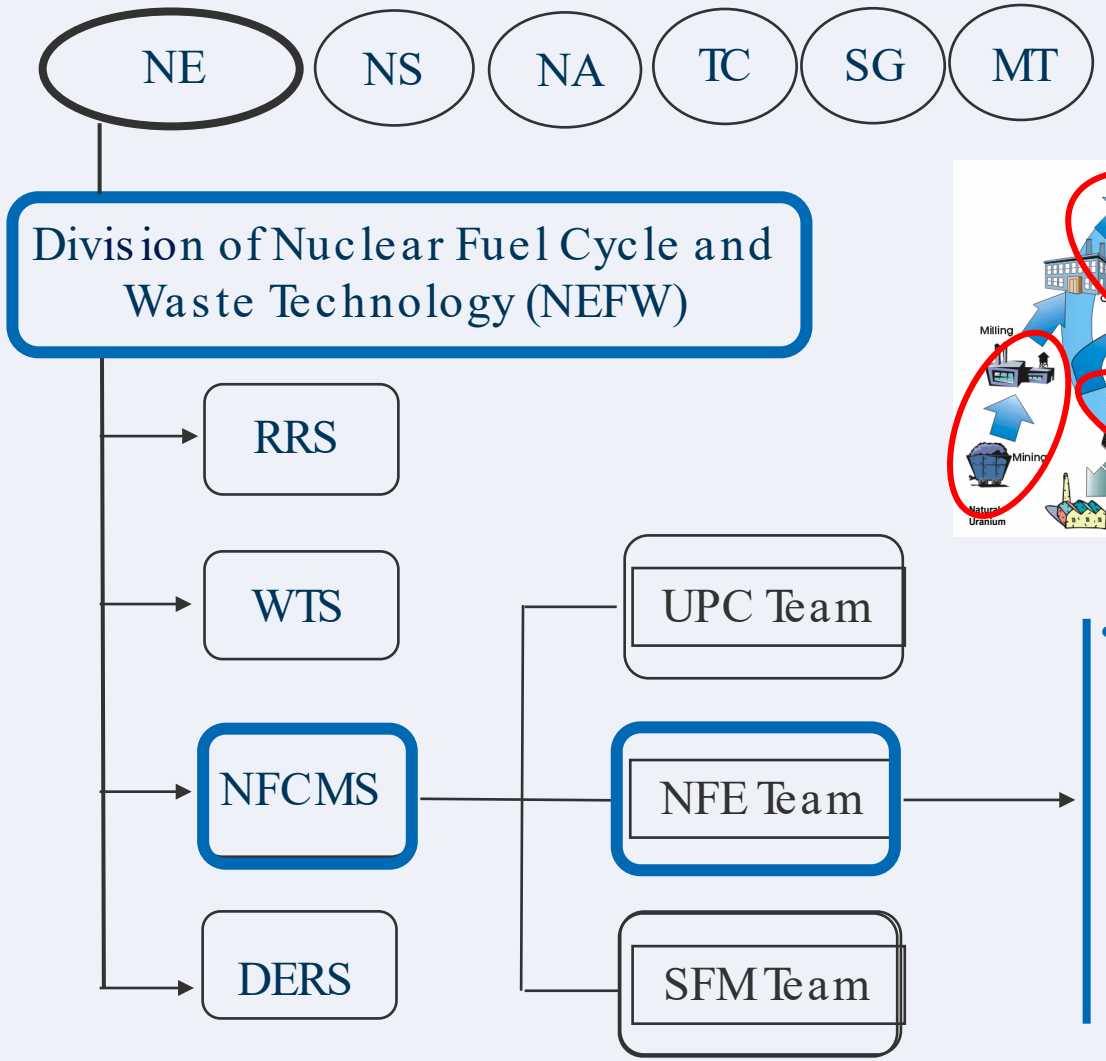

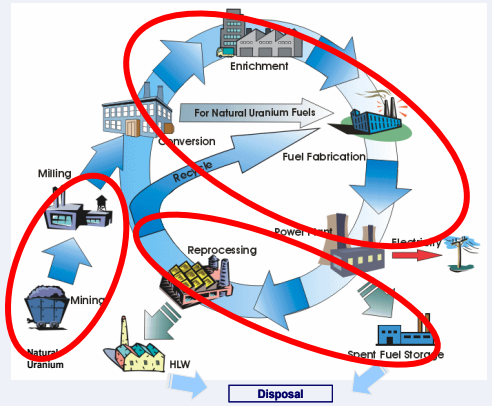

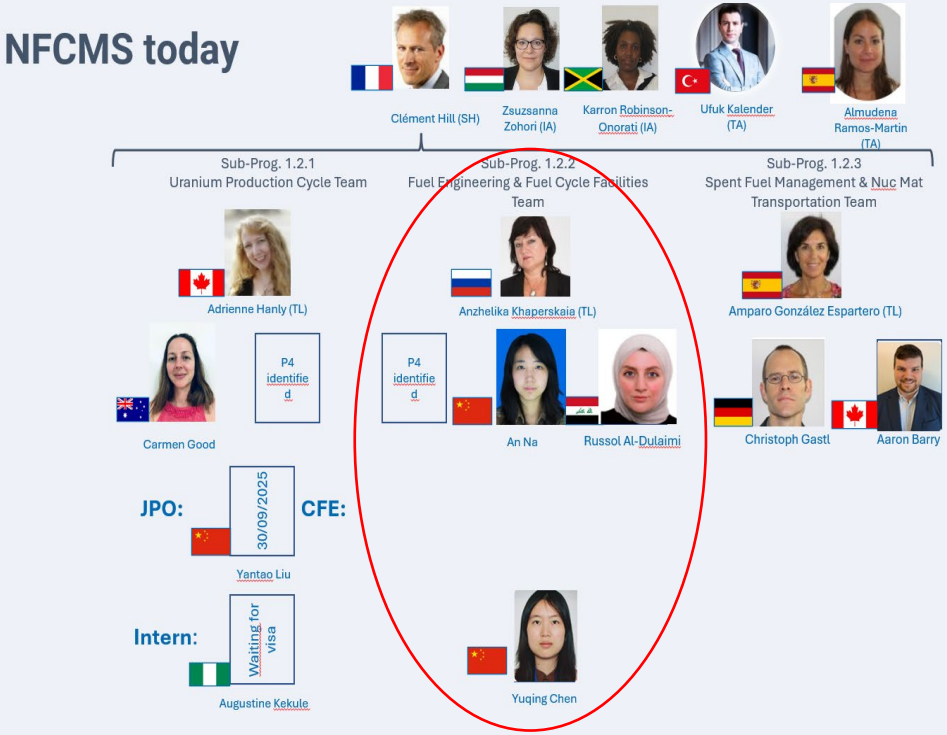

- Project 1.2.2.001 Nuclear Power Reactor Fuel Engineering and Operation: Support Member States (MSs) to understand and address factors affecting the design, fabrication and in-pile behaviour of currently operating and innovative nuclear fuels and materials for power reactors.

- Project 1.2.2.002 Fuel Cycle Facilities Operation and Life Management : Support MSs to technically implement IAEA Safety Standards when operating or upgrading nuclear fuel cycle facilities, and to understand and address factors affecting the ageing of these facilities

IAEA Sub-Programme 1.2.2:
Nuclear Power Reactor Fuel and Fuel Cycle Facilities

- Organizing IAEA meetings and developing IAEA publications
- Coordinating research activities (CRPs)
- Maintaining databases (NFCFs, PIE: Integrated Nuclear Fuel Cycle Information System - IAEA INFCIS), IAEA Fuel and material database (The IAEA Fuel and Material Database - IAEA Data Platform) and NFC simulation tools (NFCSS: Nuclear Fuel Cycle Simulation System (NFCSS))
- Developing e-Learning Materials on nuclear fuel and PIE: OPEN-LMS: All courses
- Building up Networks among experts (NFE-Net): Pages - NFE Net
- Supporting the IAEA Technical Cooperation Programme

To foster collaboration and information exchange, provide reference data, preserve knowledge, and capacity building

- Consultancy Meetings (Expert Reviews)
- Technical Meetings
- Coordinated Research Projects (CRP)

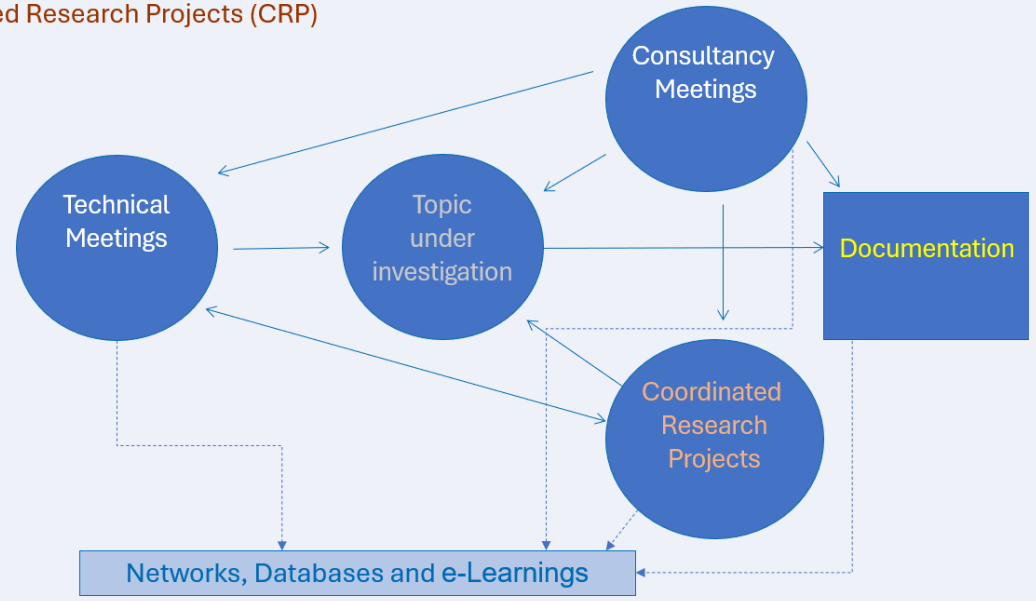

Technical Working Group on Fuel Performance and Technology (TWG-FPT)

TWG FPT is a group of recognized experts from MSs providing advice to DDG-NE and supporting programme implementation, reflecting a global network of excellence and expertise in nuclear power reactor fuel engineering

20 Member States (Argentina , Belgium, Brazil, Canada, China, Finland, France, Hungary, India, Japan, Pakistan , RoK, Romania, Russia, South Africa , Spain, Sweden, UK, Ukraine, USA).

TWG-FPT focuses on nuclear fuel and materials technologies with an emphasis on:
- Status and trends in nuclear power reactor fuel technology and performance
- Nuclear core materials research and development, including fuel design, manufacturing, and quality assurance issues, fuel utilization, coolant chemistry, and fuel performance analysis

with consideration for: Safety, Economy, Management systems, Nuclear science, Nuclear power plant operations

TWG-FPT Meeting, 15–17 April 2025

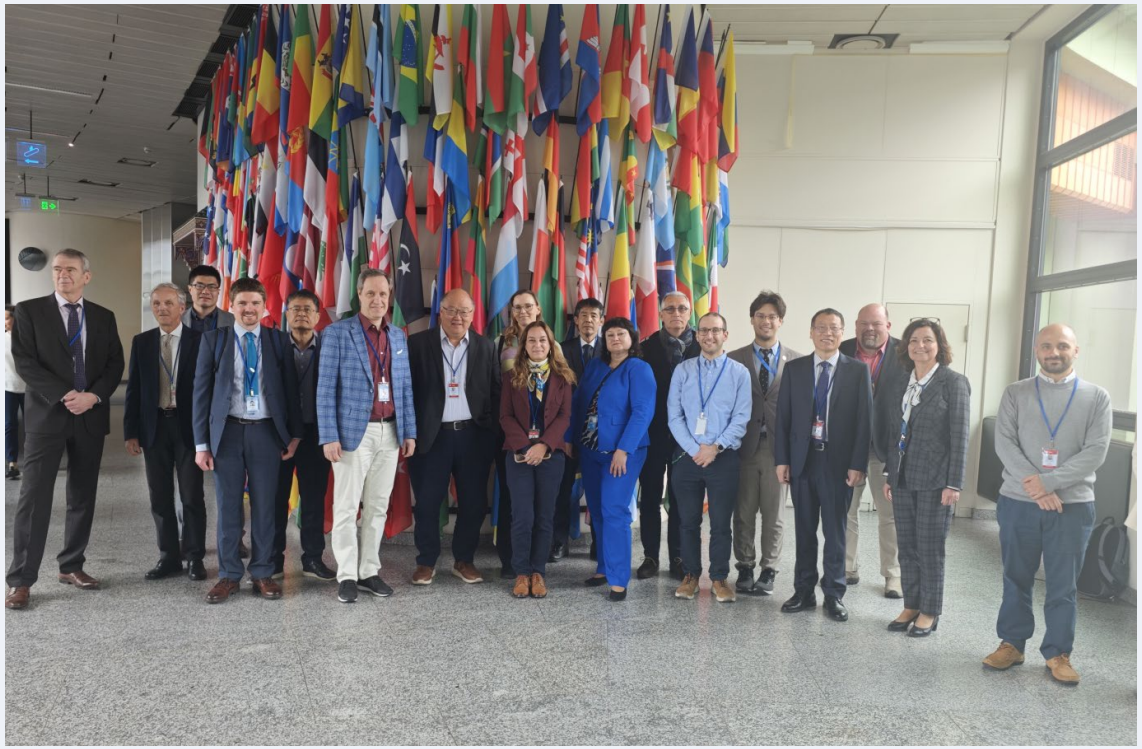

Technical Working Group on Fuel Cycle Facilities (TWG-FCF)

TWG FCF is a group of recognized experts from MSs providing advice to DDG-NE and DDG-NS and supporting programme implementation, reflecting a global network of excellence and expertise in NFCFs operation areas

20 Member States (Argentina , Belgium, Brazil, Canada, Egypt , France, Germany , India, Japan, Kazakhstan, Netherlands, RoK, Russia, South Africa , Spain, Sweden, UK, Ukraine, USA).

TWG-FCFs focuses on:

- status and trends in nuclear fuel cycle facilities (NFCFs) operation areas, including operating experience, optimization, ageing management, long term operation, refurbishment, modernization, and use for capacity building.
- covers fuel cycle facilities from milling to fuel fabrication, through conversion, enrichment, and re-conversion, as well as nuclear research and development (R&D) related fuel cycle facilities (such as research laboratories, Post Irradiation Examination facilities, etc.).

- with consideration for: Safety, Economy, Management systems

TWG-FCF Meeting, 17-20 June 2025

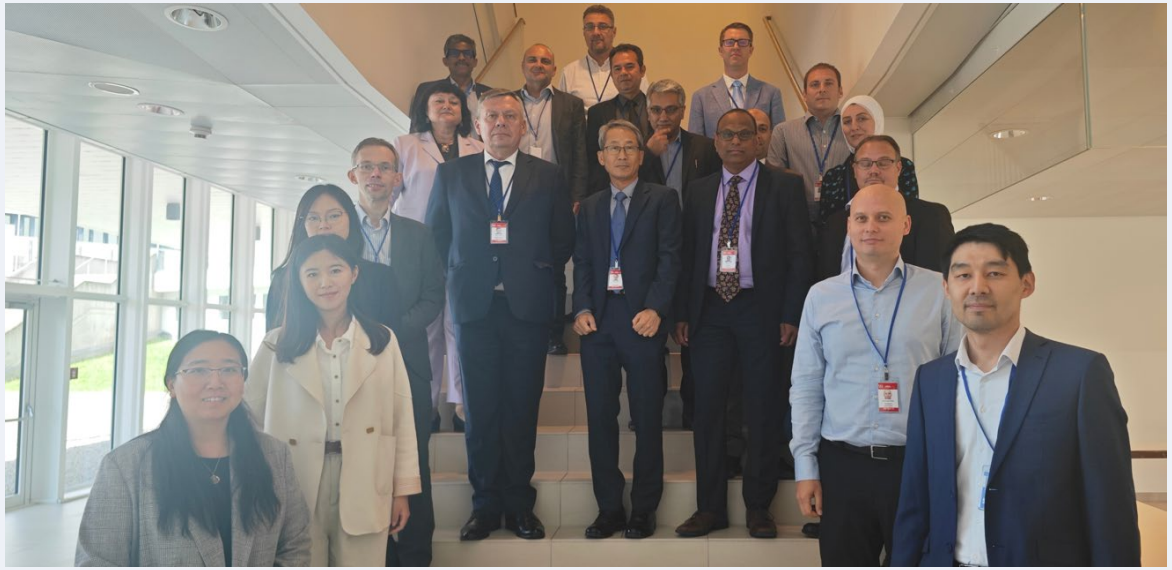

Publications on Fuel Engineering &FCF (2020-2025)

IAEA Book on the Metallurgy of Zirconium (3 Volumes)

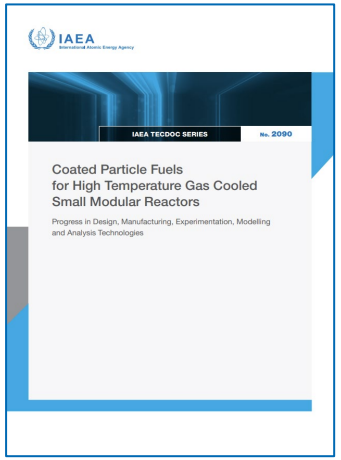

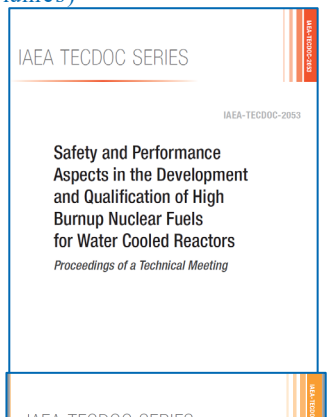

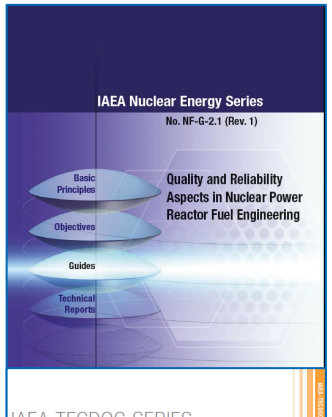

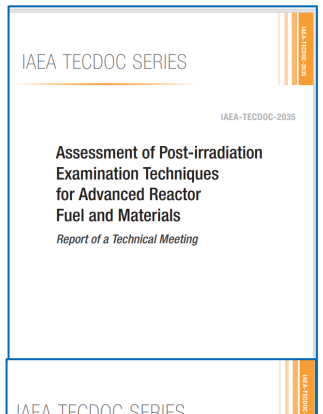

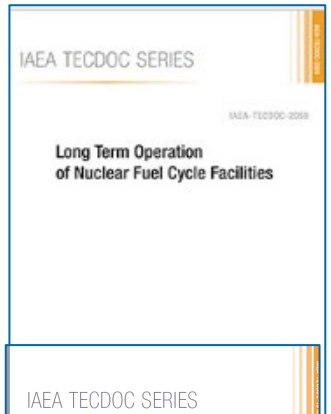

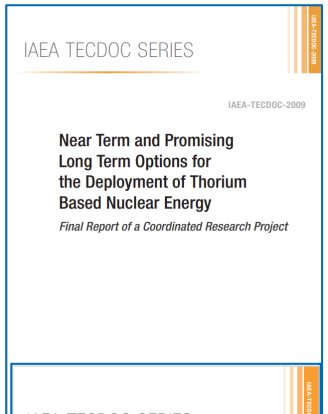

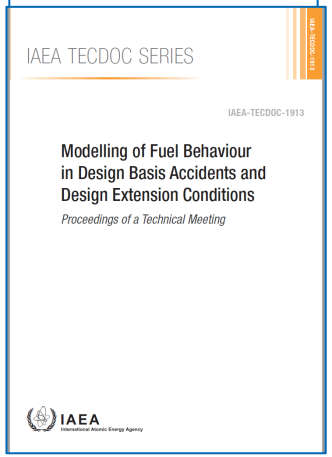

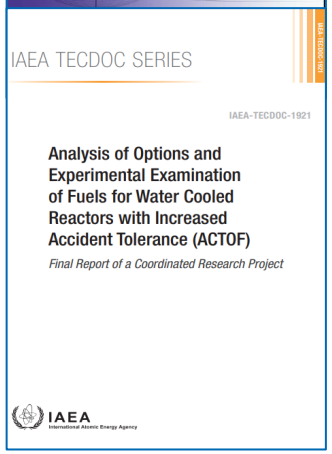

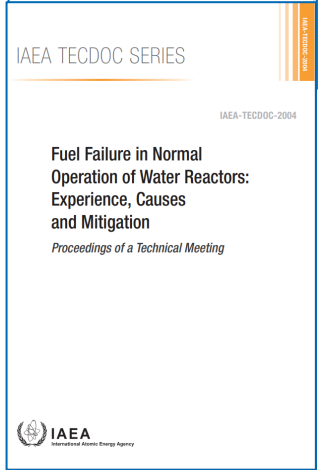

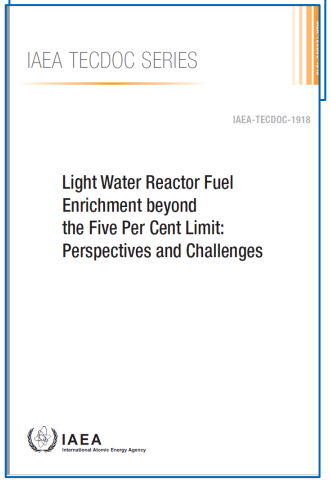

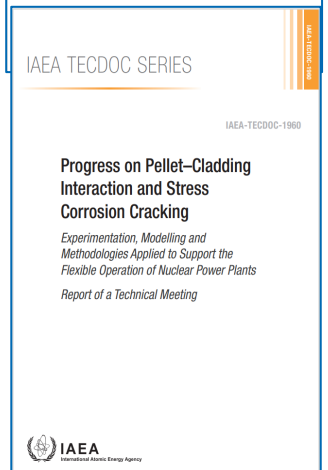

- IAEA-TECDOC-2106 Structural Behaviour of Fuel Assemblies in Light Water Reactors (2025)
- IAEA-TECDOC-2097 Advances in Fabrication Technologies for Power Reactor Fuels: Proceedings of Technical Meetings held in 2021 and 2023 (2025)
- IAEA-TECDOC-2090 Coated Particle Fuels for High Temperature Gas Cooled Small Modular Reactors (2025)
- IAEA-TECDOC-2059 Long Term Operation of nuclear fuel cycle facilities (2024)
- IAEA-TECDOC-2053 : Safety and Performance Aspects in the Development and Qualification of High Burnup Nuclear Fuels for Water Cooled Reactors (2024)
- IAEA NES No NF-G-2.1: Quality and Reliability Aspects in Nuclear Power Reactor Fuel Engineering (2024)
- IAEA-TECDOC-2035: Assessment of Post-irradiation Examination Techniques for Advanced Reactor Fuel and Materials
- IAEA-TECDOC-2009: Near Term and Promising Long-Term Options for the Deployment of Thorium Based Nuclear Energy - Final Report of a Coordinated Research Project
- IAEA Book on the Metallurgy of Zirconium
- NES NF-T-2.5: Review of Fuel Failures in Water Cooled Reactors in 2006-2015
- IAEA-TECDOC-1889: Fuel Modelling in Accident Conditions - Final Report of a Coordinated Research Project on Fuel Modelling in Accident Conditions – FUMAC, 2014–2018
- IAEA-TECDOC-1918: Light Water Reactor Fuel Enrichment beyond the 5% Limit: Perspectives and Challenges
- IAEA-TECDOC-1942: Coolant Chemistry Control and Effects on Fuel Reliability in Pressurized Heavy Water Reactors
- IAEA-TECDOC-1960: Progress on Pellet–Cladding Interaction and Stress Corrosion Cracking: Experimentation, Modelling and Methodologies Applied to Support the Flexible Operation of Nuclear Power Plants
- IAEA-TECDOC-2004: Fuel Failure in Normal Operation of Water Reactors: Experience, Causes and Mitigation. Proceedings of a Technical meeting

IAEA ongoing activity to support current generation of nuclear power reactors fuels

Fuel engineering and operation for current generation of nuclear power reactors

- Accident Tolerant Fuels
- 1. CRP T12032 on "Testing and Simulation of Advanced Technology and Accident Tolerant Fuels (ATF-TS)" (2020-2024)

  2. TM on "Advanced Technology Fuels: Progress on their Design, Manufacturing, Experimentation, Irradiation, and Case Studies for their Industrialization, Safety Evaluation, and Future Prospects" (28-31 October 2025)

  3. Proposed new CRP on "Testing and performance simulation of Advanced Technology Fuels (ATF- HBU) (2026 -?)

  Fuels for recycling/multi-recycling

  1. TECDOC on "Mixed Oxide Fuels Design, Operation and Management" (in preparation to publishing)

  2. IAEA publications on "Challenges and Opportunities in Reprocessed Uranium Fuels" (TECDOC in progress)

  Conventional Water-Cooled Reactor fuels
- 1. NES on "Review of Fuel Failures in Water Cooled Reactors (2016–2020) Rev.1" (preparation for publication)

  2.TM on "Advances in Fuel Design, Manufacturing and Examinations for Pressurized Heavy Water Reactors" (November 2024, Argentina)

  3.TM on "Digitalization and the Use of Artificial Intelligence in Advanced Nuclear Fuel Manufacturing and Quality Control", June 2026

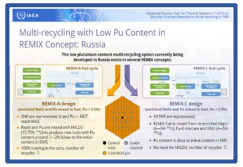

IAEA ongoing activities to support advanced reactors fuels development

Fuel engineering and operation for SMRs and future generations of nuclear power reactors

- Water-cooled SMR fuels
  1. TECDOC on "Core and Plant Simulation with an Emphasis on Fuel Behaviour in Light Water Reactor Based Small Modular Reactors" (based on Workshop 27-29 February 2024, TECDOC in progress)
- Fast reactor fuels
  1. CRP T12031 on "Fuel Materials for Fast Reactors (FMFR)" (2019-2023: Final Report in preparation to publishing)
  2. NES Technical Report on "Nuclear Fuel Technologies for Liquid Metal Cooled Fast Reactors (LMFRs)" (in preparation to publishing)
  3. Workshop on the "Behaviour of Liquid Metal Cooled Fast Reactors Fuels" (30 June – 04 July 2025)
  4. Proposed new CRP on "Benchmark Exercises on Testing and Performance Simulation of Advanced Fuels for Liquid Metal-Cooled Fast Reactors" (2026-..)
- HTRs SMR fuels
  1. CRP T12034 on "Fuel Modelling Exercises for Coated Particle Fuel for advanced reactors including SMR" (2024-2029)

Molten salt SMR fuels

1. New Simulation tool module development for MSR with relevant fuel cycle
2. Workshop on "Molten Salt Reactor Fuel: Recent Development and Future Challenges" (21-25 July 2025)
3. Workshop on "Current Status of Structural Material Development for Molten Salt Reactors and Related Challenges" (July 2026)

HALEU fuel

1. Workshop on "Operational Aspects of Manufacturing High Assay Low Enriched Uranium Advanced Fuels" (August 2026)

PIE for SMR fuels

1. CRP T12033 on "Standardization of Subsized Specimens for Post-Irradiation Examination and Advanced Characterization of Fuel and Structural Materials for Small Modular Reactor and Advanced Reactor Applications (PIE for SMR)" (2024-2028)

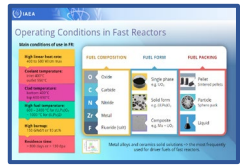

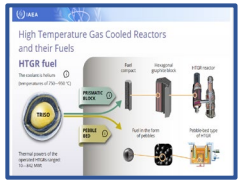

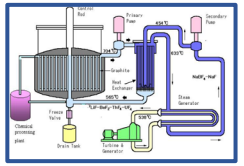

2026 IAEA Meetings on Nuclear Fuel Engineering

Workshop on the Current Status of Structural Material Development for Molten Salt Reactors and Related Challenges 20–24 July 2026 (Vienna, and virtual participation via Cisco Webex)

Status of MSR technology development with a focus on structural material requirements, Corrosion mechanisms in molten fluoride and chloride salts for MSRs and related fuel cycle applications, Experimental methods and loop testing for structural materials in contact with molten salts , Multi-physics modelling to capture the complex interactions among neutronics, thermal-hydraulics, fuel salt chemistry and materials corrosion phenomena, Advanced manufacturing techniques and robotics. Methods and plans to monitor the integrity of structural materials chosen for MSRs, Lessons learned from pilot-scale MSR projects and industry experience

Technical Meeting on Digitalization and the Use of Artificial Intelligence in Advanced Nuclear Fuel Manufacturing and Quality Control, 27-31 July 2026 (Vienna, and virtual participation via Cisco Webex)

AI-based optimisation of fuel and core design; Application of AI/ML in nuclear fuel fabrication and quality control; Application of AI/ML in fuel performance simulation including use of surrogates, and in the material discovering; data management and knowledge retention; Computer and information security, Cross-sectoral insights and best practices from other then nuclear industries experienced in digital and AI technologies

Workshop on Operational Aspects of Manufacturing High Assay Low Enriched Uranium Advanced Fuels, 17–21 August 2026 (Vienna, and virtual participation via Cisco Webex)

National and International Trends Impacting HALEU Deployment, Challenges and Best Practices from Member States, Fabrication Technologies and Process Optimization: Integration of Advanced and Digital Technologies, Criticality Safety and Radiation Protection, Regulatory, Safety, and Security Considerations

International Conference on Fuel Supply Chain for Sustainable Nuclear Power Development, Vienna, from 13 to 15 October 2026

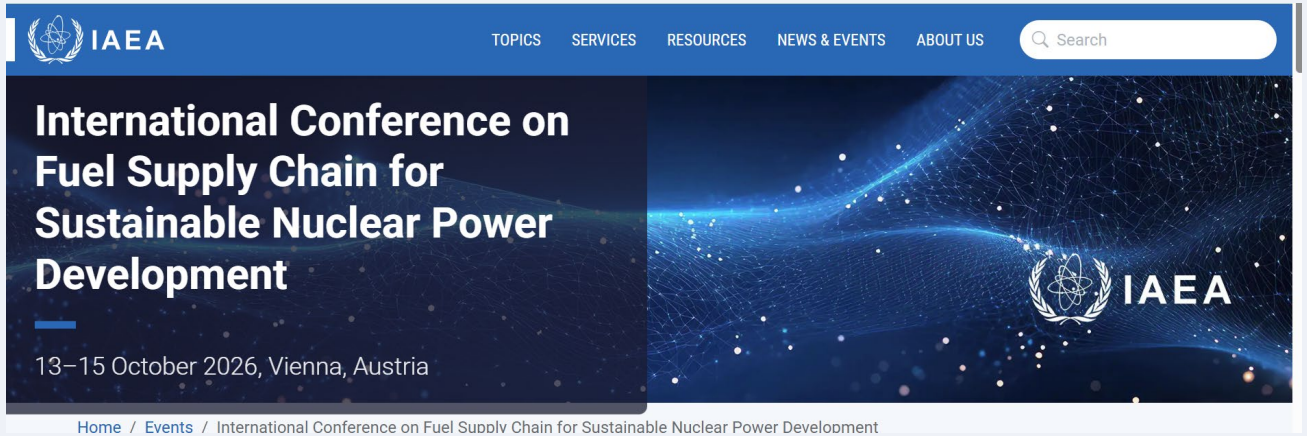

Key Deadlines and Dates

1 February 2026

- Submission of abstracts through IAEA-INDICO
- Submission of Form B (together with Form A) through the InTouch+ platform

31 March 2026

- Notification of acceptance of abstracts for oral or poster presentation

10 April 2026

- Submission of Form C (together with Form A) through the InTouch+ platform

[International Conference on Fuel Supply Chain for Sustainable Nuclear Power Development | IAEA]

Topic 1. Industry Prospects and Challenges Facing Raising Fuel Supply Demand:

Challenges in supply and front-end services to meet the increasing infrastructure requirements for conversion, enrichment and fuel fabrication

Topic 2. Supply and demand for raw materials for nuclear fuel supply:

Innovations in the front end of the nuclear fuel cycle, from exploration to mining: (new uranium exploration and mining projects, Innovative advancements in uranium exploration and mining, Uranium and thorium resources, processing and mining and the circular economy

Topic 3. Advanced nuclear fuels for innovative reactor technologies:

Advanced technology fuels and fuels for advanced reactors: design, qualification and operation of ATFs, LEU+ and HALEU fuels, TRISO fuels, fuels for Fast Reactors, MSRs and multiple recycling in all types of reactors, advances in nuclear fuel fabrication processes and quality control (automation, additive manufacturing and use of artificial intelligence)

Topic 4. Industrial and Innovative technologies for recycling nuclear materials

Industrial operating experience and lessons learned in reprocessing for recycling

CRP T12032 “Testing and Simulation of Accident Tolerant and Advanced Technology Fuels (ATF-TS)” (2020-2024)

Objectives of the CRP

To support Member States to understand and address factors affecting the design, fabrication and in-pile behaviour of currently operating and innovative nuclear fuels and materials for power reactors, to increase technology readiness for candidate ATF materials

- To perform experimental tests including single rod and bundle tests on ATFs' performance under normal, DB and DE conditions
- To benchmark fuel codes against new test data either obtained during the CRP or from existing data relevant to advanced fuel and cladding concepts from Member States' experimental Programmes
- To develop LOCA evaluation methodology for ATF performance with a view for NPP applications

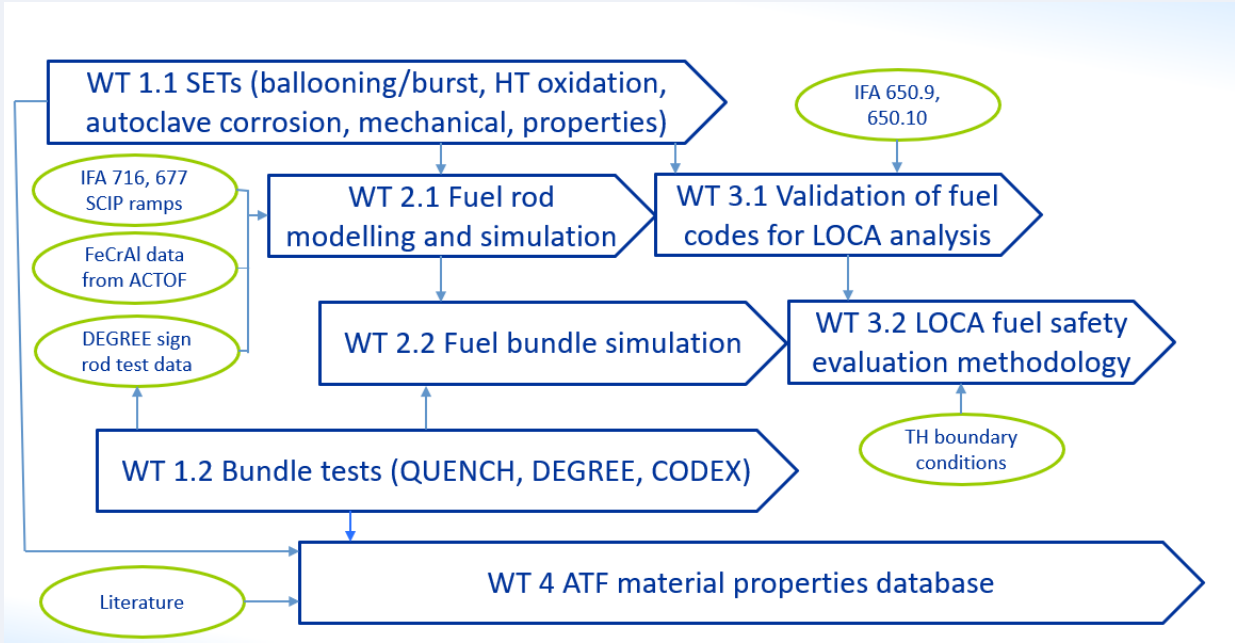

Participants: 29 organizations from 22 Member States

Argentina (CNEA), Belgium (Tractebel), Belarus (BSU), Brazil (IPEN/CNEN), Bulgaria (INRNE), Canada (CNL), China (CNPRI, CNPE, NPIC), Czech Republic (CTU), France (CEA), Germany (KIT, GRS), EC (JRC), Hungary (EK), Iran (AEOI), Italy (NINE), Japan (CRIEPI), Korea (KAERI), Poland (IChTj), Russia (IBRAE RAS), Spain (UPM, CIEMAT, Slovakia (B&J NUCLEAR ltd.), UK (NNL), USA (ISSS, UTK)

CRP T12032 “ATF-TS” structure

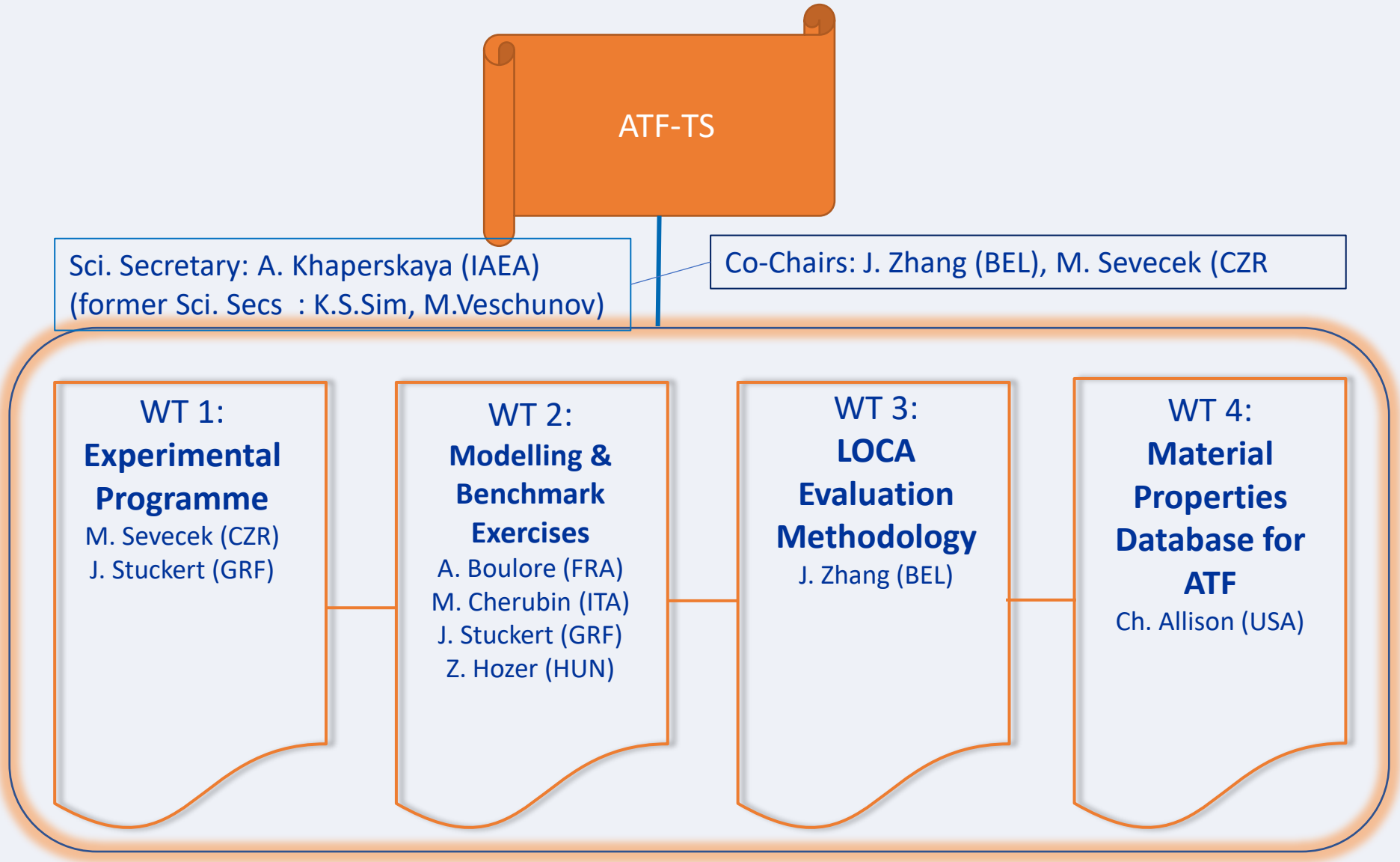

CRP T12032 "Testing and Simulation of Accident Tolerant and Advanced Technology Fuels (ATF-TS) (2020-2024)

Results achieved

Various ATF options were analyzed resulting in improved understanding of ATFs' behaviors and developments of ATF technologies in MSs.

Several coated cladding materials (coated Zircaloy claddings, FeCrAl) were manufactured, tested, characterized and analyzed.

Fuel performance codes and severe accident codes from participating organizations were extended to the analysis of several ATF concepts.

The qualified fuel rod codes to develop a hot rod LOCA fuel safety evaluation methodology were applied to assess the performance of ATFs.

The open-source ATF material properties and experimental datasets have been prepared and uploaded the IAEA fuel database

The TECDOC "Testing and Simulation for Advanced Technology and Accident Tolerant Fuels (ATF-TS). Final Report of a Coordinated Research Project" with 3 volumes:

- Vol. 1; Experimental Programme of Accident Tolerant and Advanced Technology Fuels (ATFs);
- Vol. 2: Fuel Modelling and Computer Codes' Benchmark Exercise for Accident Tolerant and Advanced Technology Fuels (ATFs);
- Vol. 3: LOCA Fuel Safety Evaluation for Accident Tolerant and Advanced Technology Fuels (ATFs).

Under preparation to publication

CRP ATF-TS: Work Task 1 - experimental programme

9 organizations tested 15 types of ATF cladding materials, including chromium-coated Zr-based alloys, Zr-based alloys with alternative coatings, and FeCrAl alloys. Reference uncoated Zr-based alloys were also tested to establish a baseline for comparison.

ATF CLADDING MATERIALS TESTED WITHIN THE CRP ATF-TS

Institute	Country	Coated Zr-based Cladding	Alternative materials
Czech Technical University in Prague	Czech Republic	Cr and CrN-Cr coated Opt. ZIRLO™	
Karlsruhe Institute of Technology (KIT)	Germany	Cr-coated ZIRLO, M5 and Zircaloy-4	FeCrAl B136Y3 – 13Cr-6.2Al-0.03Y (wt.%)
Institute of Nuclear Chemistry and Technology (INCT)	Poland	SiC/YAG coated Zr1Nb	
Canadian Nuclear Laboratories	Canada	TiAl-coated Zircaloy-4	
Nuclear Power Institute of China	China	Cr-coated Zircaloy-4	FeCrAl 13Cr-4.5Al-2Mo-1Nb-0.4Ta-0.05Y (wt%)
China Nuclear Power Engineering	China	Cr-coated Zircaloy-4	
Belarusian State University	Belarus	Cr-coated and plasma-treated E110	
Atomic Energy Organization of Iran	Iran, Islamic Republic of	Cr and CrN/Cr coated Zr1Nb	

ATF CLADDING TESTS WITHIN THE CRP ATF-TS

Organization	Country	Experiments Performed
CTU/UJP Praha	Czech Republic	Ballooning/burst tests; high-temperature (HT) steam oxidation; long-term VVER corrosion
JRC Karlsruhe	European Commission	Thermophysical properties
JRC Petten	European Commission	Mechanical tests in the LWR environment
CRIEPI	Japan	Single rod and bundle tests at DEGREE
KIT	Germany	Single rod and bundle tests at QUENCH
INCT	Poland	Neutron activation analysis; long-term corrosion; HT annealing
CNPE	China	Long-term corrosion (PWR); HT oxidation; ballooning/burst
AEOI	Iran	HT oxidation
China Nuclear Power Technology Research Institute (CNPRI)	China	Axial tensile tests; internal burst tests; internal climb tests; autoclave corrosion tests; HT steam oxidation
EK, Centre for Energy Research	Hungary	Ballooning/burst tests; mandrel tests; HT steam oxidation; bundle tests at CODEX-ATF
Universidad Politécnica de Madrid (UPM)	Spain	Cathodic charge; hydriding; ring compression tests; HT creep
Korea Atomic Energy Research Institute (KAERI)	Korea	Microstructural investigations
Seoul National University (SNU)	Korea	LOCA tests; DSC; post-quench ductility evaluation

CRP ATF-TS: experimental programme: key findings

- Cr-based Coatings: Provided small benefits in time-to-burst, ballooning size, and burst opening, highly dependent on coating quality and methodology used for evaluation
- HT Oxidation Resistance: Both Cr-coated Zr and FeCrAl cladding materials significantly improved oxidation resistance and post-quench ductility, reducing chemical heat and hydrogen release in hypothetical accidents (DBA-A and DEC-A)
- Long-Term Corrosion: Negligible corrosion rates for Cr-based coatings and FeCrAl in all environments
- Mechanical Tests: Showed general agreement across laboratories, with coated Zr claddings performing well in various states. Coated Zr claddings generally exhibited higher strength and lower elongation. Highlighted different coating fracture limits due to microstructure variations. Effects of coating defects and cracks on coated Zr need further investigation
- Supplementary Tests: Demonstrated good resistance of coatings in thermal shock tests. Provided new data on Cr coating mechanical properties and degradation. Indicated that hydrogen uptake mechanisms for coated Zr cladding are not well understood
- Bundle Tests: Proved benefits of Cr-coated claddings in extended LOCA conditions. Revealed significant challenges in DEC after protective coatings fail. Suggested potential benefits of diffusion barriers to limit degradation mechanisms

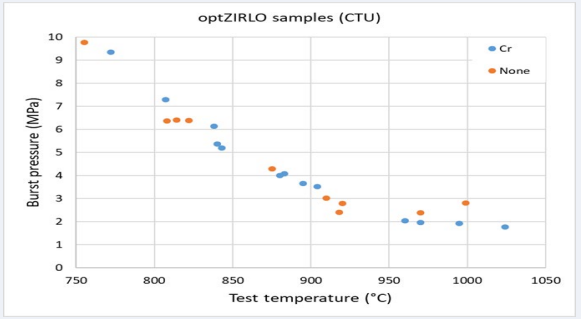

Item	S1'	S2	S3	S4	S5	S6
Coating thickness and materials	-	10 µm Cr	20 µm Cr	16/10 µm Cr/CrN	10 µm Cr	20 µm Cr
Max. Temp. (°C)	1350				1600	
Steam flow rate (g/s)	0.41	0.41	0.46	0.46	0.50	0.46
Heating rate (K/s)*	3.5-1.5	1.5	2.4-1.8	2.5-2.2	3.0-1.6	3.0-1.8
RIP at RT (MPa, He)	6.0					
Gas plenum volume (ml)	10	15	10			
Balloon & burst region						

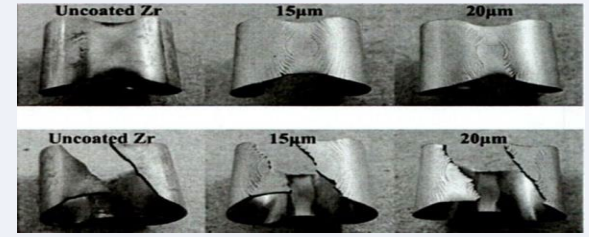

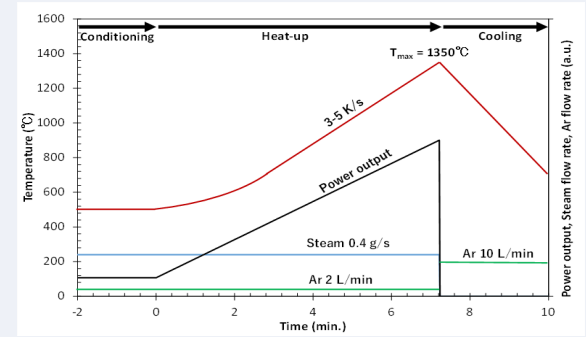

CRP ATF-TS : Work Task 2 - Fuel modelling and Benchmark Exercise

19 organizations from 16 MSs participated in fuel rod modelling and simulation benchmarks, and 9 organizations from 8 MSs participated in bundle tests simulation, focusing on selected ATF concepts (Chromia doped fuel, FeCrAl, and Cr-coated claddings)

Benchmark of codes for simulation of selected separate effect tests (WT2.1)

Organization	Country	Code	UO2 Cr- doped			FeCrAl	Coated Zr claddings	Coated Zr claddings
			IFA716	IFA677	SCIP II power ramps	ACTOF cases + ATF-TS SET	ATF-TS SET	DEGREE Single rod test
CNEA	Argentina	DIONISIO	x	x	x	x	x	x
Tractebel	Belgium	FRAPCON/ FRAPTRAN					x	
IPEN	Brazil	TRANSURANUS				x		
INRNE-BAS	Bulgaria	TRANSURANUS				x		
CNPRI	China	JASMINE	x	x		x	x	
CNPE	China	FRAPCON/ FRAPTRAN				x		
NPIC	China	FUPAC	x	x		x	x	
CTU	Czech Republic	FRAPCON/ FRAPTRAN TRANSURANUS	x		x		x	
CEA	France	ALCYONE	x	x	x			
GRS	Germany	TESPA-ROD				x		
ANCC	Iran	PARS/PART	x	x	x		x	
NINE	Italy	TRANSURANUS	x	x	x	x		
CRIEPI	Japan	FRAPCON						x
KAERI	Korea	FRAPCON/ MERCURY	x			x	x	x
IBRAE	Russia	SOCRAT					x	x
B&J	Slovakia	FEMAXI	x	x	x			
UPM	Spain	TRANSURANUS				x		
CIEMAT	Spain	FRAPCON/ FRAPTRAN	x	x	x	x		
UTK	USA	BISON	x	x	x	x		

Benchmark of codes for simulation of bundle tests (WT2.2)

Organization	Country	Code	QUENCH-19 with FeCrAl	DEGREE Bundle test B3 with Cr coated Opt. ZIRLO	CODEX-ATF with Cr coated Opt. ZIRLO (pre-test calculations)
CNEA	Argentina	DIONISIO	x		
CTU	Czech Republic	MELCOR	x		
GRS	Germany	ATHLET-CD	x		
KIT	Germany	ASTEC	x	x	x
NUBIKI	Hungary	ASTEC			x
NINE	Italy	MELCOR	x		
CRIEPI	Japan	FRAPTRAN		x	
IBRAE	Russia	SOCRAT	x	x	x
UPM	Spain	MELCOR	x		

CRP ATF-TS : Work Task 2 - Fuel modelling and Benchmark Exercise: key findings

- Chromia Doped Fuel:
  - Benchmark results aligned well with experimental data, highlighting the importance of uncertainty analysis in fuel performance code validation
- ATF Claddings:
  - Burst pressure predictions were accurate with available data, though hoop strain predictions varied.
  - Improvements suggested in code predictions and the need for further work on material properties
- Bundle Tests:
  - Showed potential for adapting codes for new materials, with modifications to oxidation models for FeCrAl and Cr-coated Zr
  - Thermal-hydraulic parameters were calculated using existing algorithms, while oxidation models were modified for FeCrAl and Cr oxidation
  - FeCrAl oxidation covered the entire temperature range, and Cr coating behavior was modeled up to the Cr/Zr eutectic melt point: further enhancements are needed for processes above this eutectic point and after coating failure

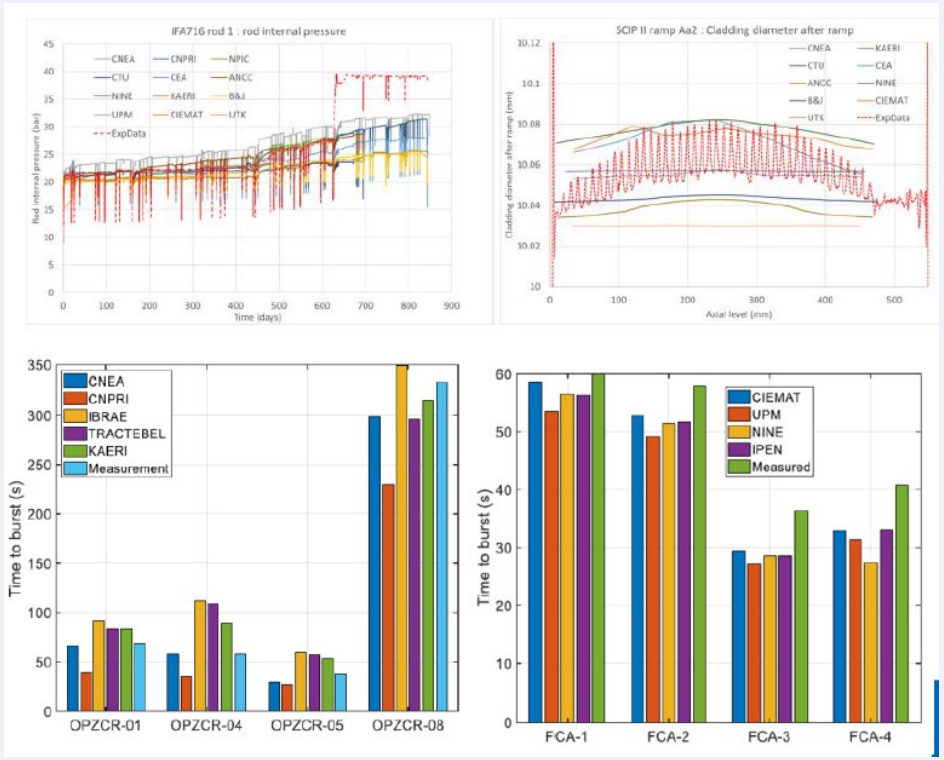

CRP ATF-TS: Work Task 3 - LOCA fuel safety evaluation methodology

11 organizations from 10 MSs used 9 fuel rod codes and 1 system thermal hydraulic code to simulate and predict the fuel behaviours for reference fuel and ATFs (Cr-coated cladding, FeCrAl cladding, doped pellet, and micro-cell pellet)

LOCA cases:

Halden LOCA tests IFA-650.9 and IFA-650.10

DBA large-break LOCA (LBLOCA) of a real NPP

DEC small-break LOCA (SBLOCA) of a real NPP

Organization	Country	Fuel Rod Code	UA/SA Code	ATF concept	WT3.1. Code validation & prediction for ATF		WT3.2. LOCA FSEM for NPP & prediction for ATF	
					IFA-650.9	IFA-650.10	LBLOCA	DEC SBLOCA
CNEA	Argentina	DIONISIO	DAKOTA	FeCrAl, Doped pellet	x	x		
Tractebel	Belgium	FRAPCON/ FRAPTRAN-TE-1.5	DAKOTA	Coated Zr cladding	x	x	x	
IPEN/USP	Brazil	TRANSURANUS	SUNSET	FeCrAl	x	x	x	x
CNPE	China	FRAPCON/ FRAPTRAN-2.0P1	DAKOTA	FeCrAl	x	x	x	x
CEA	France	ALCYONE	URANIE	Doped pellet		x		
AEOI	Iran	PARS/PART	SUAP	Coated Zr cladding, Doped pellet	x	x		
NINE	Italy	TRANSURANUS	MC built-in	FeCrAl	x	x		
KAERI	Korea	MERCURY	OpenTURNS	Coated Zr cladding, doped pellet, micro-cell pellet	x	x	x	x
UPM/Nfq	Spain	TRACE	DAKOTA	FeCrAl		x	x	x
		TRANSURANUS	DAKOTA	FeCrAl		x		
CIEMAT	Spain	FRAPCON/ FRAPTRAN-2.0P1	DAKOTA	FeCrAl	x	x	x	x
NNL	UK	ENIGMA	CASINO	Coated Zr cladding		x		

List of participants, used codes and simulated tests in WT3

CRP ATF-TS: Work Task 3 - LOCA fuel safety evaluation methodology: results

- Reasonable agreement for reference fuel, with some dispersions and large uncertainty bands
- Limited benefits with ATF concepts and large uncertainty bands
- Further improvements are needed in modelling and simulation, particularly in mechanical deformation models and input uncertainties

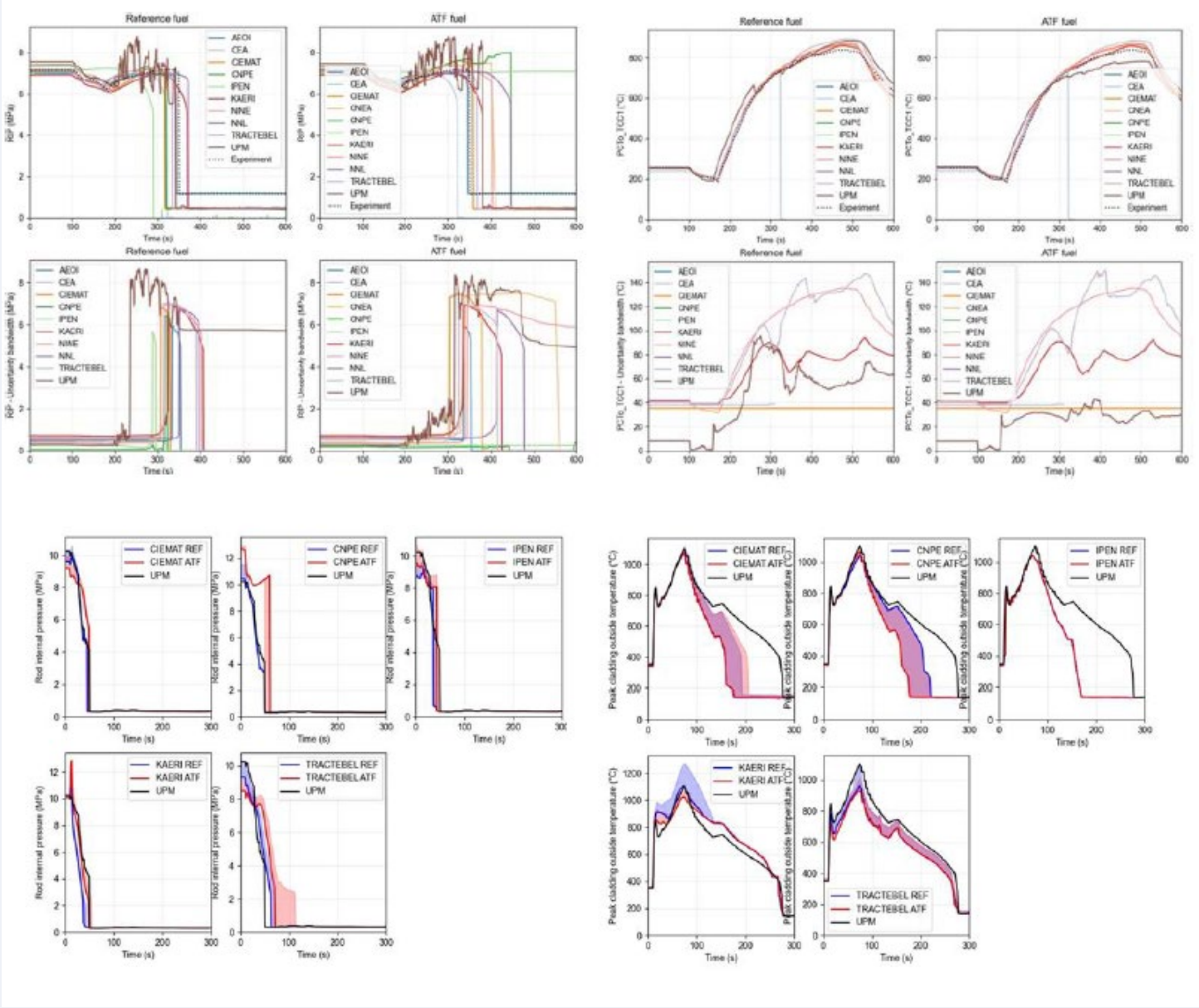

IAEA fuel experimental database

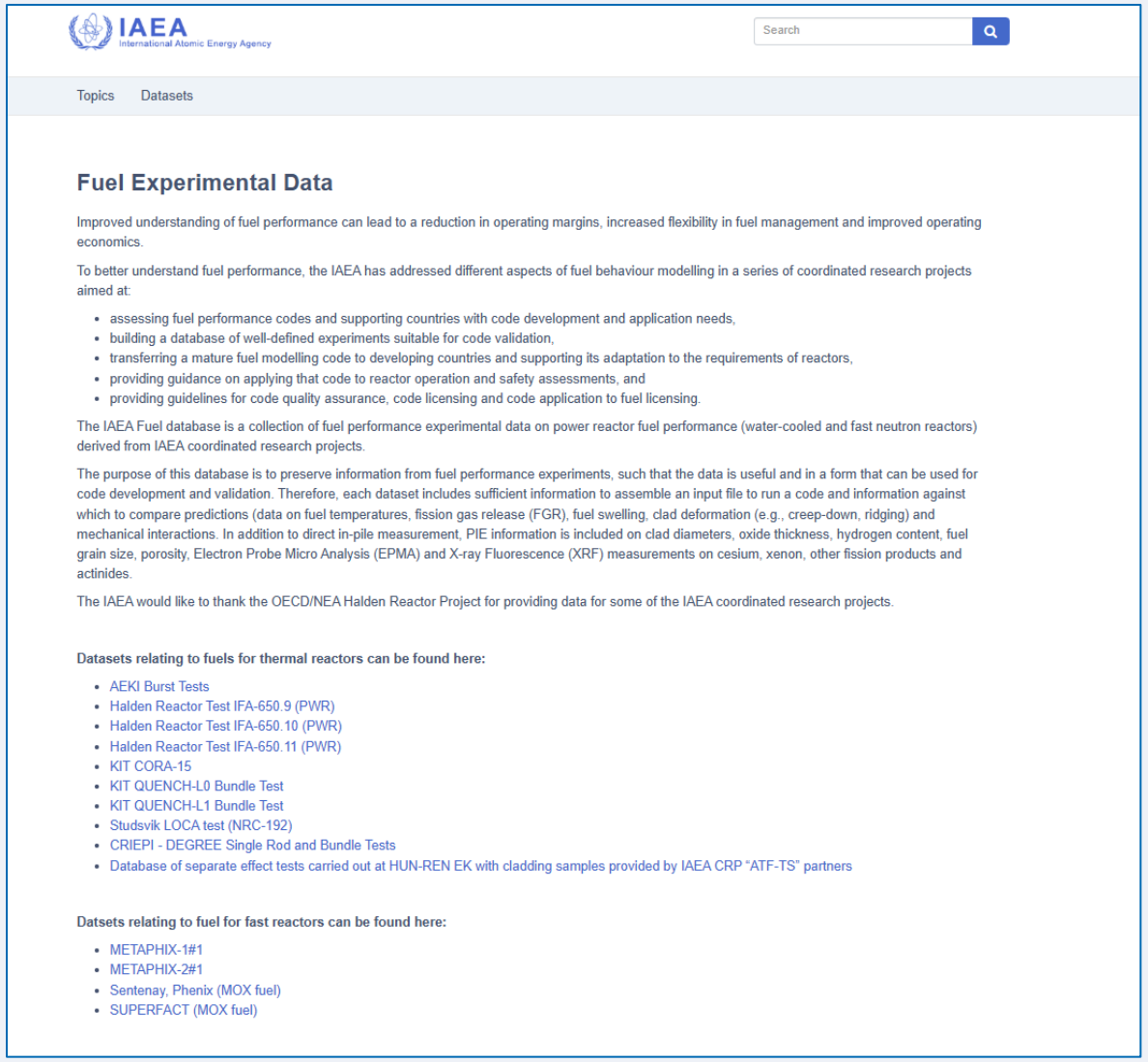

IAEA International Atomic Energy Agency

Search

Topics Datasets

Fuel Experimental Data

Improved understanding of fuel performance can lead to a reduction in operating margins, increased flexibility in fuel management and improved operating economics.

To better understand fuel performance, the IAEA has addressed different aspects of fuel behaviour modelling in a series of coordinated research projects aimed at:

- assessing fuel performance codes and supporting countries with code development and application needs,
- building a database of well-defined experiments suitable for code validation,
- transferring a mature fuel modelling code to developing countries and supporting its adaptation to the requirements of reactors,
- providing guidance on applying that code to reactor operation and safety assessments, and
- providing guidelines for code quality assurance, code licensing and code application to fuel licensing.

The IAEA Fuel database is a collection of fuel performance experimental data on power reactor fuel performance (water-cooled and fast neutron reactors) derived from IAEA coordinated research projects.

The purpose of this database is to preserve information from fuel performance experiments, such that the data is useful and in a form that can be used for code development and validation. Therefore, each dataset includes sufficient information to assemble an input file to run a code and information against which to compare predictions (data on fuel temperatures, fission gas release (FGR), fuel swelling, clad deformation (e.g., creep-down, ridging) and mechanical interactions. In addition to direct in-pile measurement, PIE information is included on clad diameters, oxide thickness, hydrogen content, fuel grain size, porosity, Electron Probe Micro Analysis (EPMA) and X-ray Fluorescence (XRF) measurements on cesium, xenon, other fission products and actinides.

The IAEA would like to thank the OECD/NEA Halden Reactor Project for providing data for some of the IAEA coordinated research projects.

Datasets relating to fuels for thermal reactors can be found here:

- AEKI Burst Tests
- Halden Reactor Test IFA-650.9 (PWR)
- Halden Reactor Test IFA-650.10 (PWR)
- Halden Reactor Test IFA-650.11 (PWR)
- KIT CORA-15
- KIT QUENCH-L0 Bundle Test
- KIT QUENCH-L1 Bundle Test
- Studsvik LOCA test (NRC-192)
- CRIEPI - DEGREE Single Rod and Bundle Tests
- Database of separate effect tests carried out at HUN-REN EK with cladding samples provided by IAEA CRP "ATF-TS" partners

Datsets relating to fuel for fast reactors can be found here:

- METAPHIX-1#1
- METAPHIX-2#1
- Sentenay, Phenix (MOX fuel)
- SUPERFACT (MOX fuel)

[Fuel Experimental Data - IAEA Data Platform]

Datasets relating to fuels for thermal reactors can be found here:

- AEKI Burst Tests
- Halden Reactor Test IFA-650.9 (PWR)
- Halden Reactor Test IFA-650.10 (PWR)
- Halden Reactor Test IFA-650.11 (PWR)
- KIT CORA-15
- KIT QUENCH-L0 Bundle Test
- KIT QUENCH-L1 Bundle Test
- Studsvik LOCA test (NRC-192)
- CRIEPI - DEGREE Single Rod and Bundle Tests
- Database of separate effect tests

Datsets relating to fuel for fast reactors can be found here:

- METAPHIX-1#1
- METAPHIX-2#1
- Sentenay, Phenix (MOX fuel)
- SUPERFACT (MOX fuel)
- FBTR MOX
- The JOYO B5D-2 test

ATF-TS experimental datasets. ATF Database of SET , HUN-REN_EK

At HUN-REN EK, extensive work has been carried out to characterize the behaviour of candidate materials for ATFs and to compare newly measured data with the parameters of traditional cladding alloys
The database includes the main characteristics and results of the separate effect tests: ballooning and burst tests, oxidation tests in high-temperature steam, tensile testing using ring samples, ring compression tests, mandrel tests, scanning Electron Microscopy (SEM) examinations

13 cladding types were tested:
Reference Claddings: Zircaloy-4, ZIRLO™, Optimized ZIRLO™ (optZIRLO™), Zr-1%Nb alloy

Coated Claddings (Zr alloy base): Cr coating, CrN coating, CrN/Cr multilayer coating, TiAl coating

Alternative Alloy: FeCrAl alloy

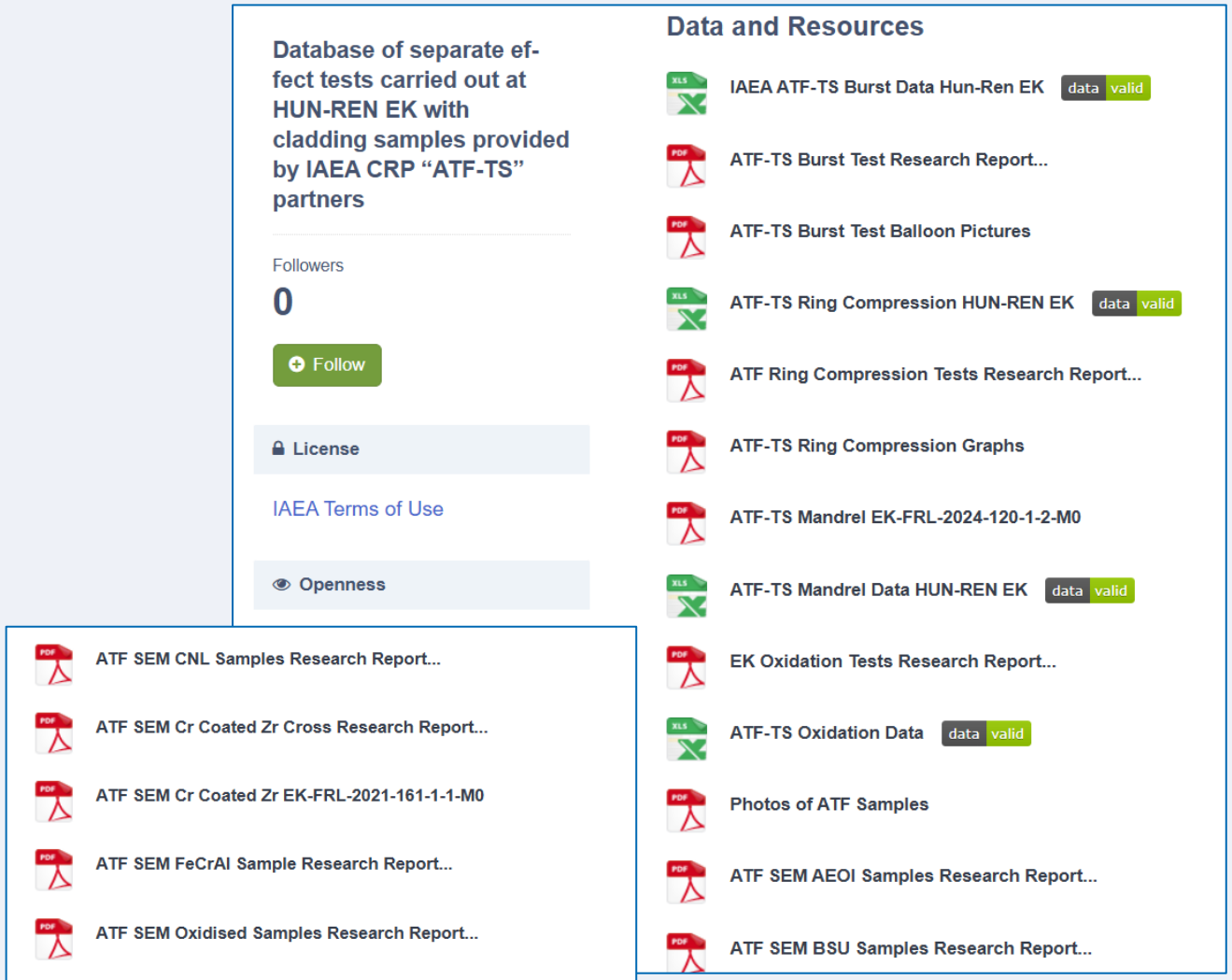

Database of separate effect tests carried out at HUN-REN EK with cladding samples provided by IAEA CRP "ATF-TS" partners - Database of separate effect tests carried out at HUN-REN EK with cladding samples provided by IAEA CRP "ATF-TS" partners - Datasets - IAEA Data Platform

ATF-TS experimental datasets.
CRIEPI - DEGREE Single Rod and Bundle Tests

Series of single rod tests (S1–S13) and 3x3 bundle tests (B1–B7) were performed at the DEGREE facility, CRIEPI (Japan) for simulation Design Extension Conditions (DEC) LOCA scenarios using an induction heating furnace.
Cladding types tested: Zircaloy-4, Optimized ZIRLO, E110 , all coated with either chromium (Cr) or Cr/CrN.
Heating conditions: Peak temperatures: 1350°C, 1500°C, 1600°C; heating rate: 3–5 K/s, atmosphere: Steam/Ar mixture
Test phases: Pre-heating to 500°C, conditioning at 500°C; heat-up to target temperature, cool-down in Ar atmosphere

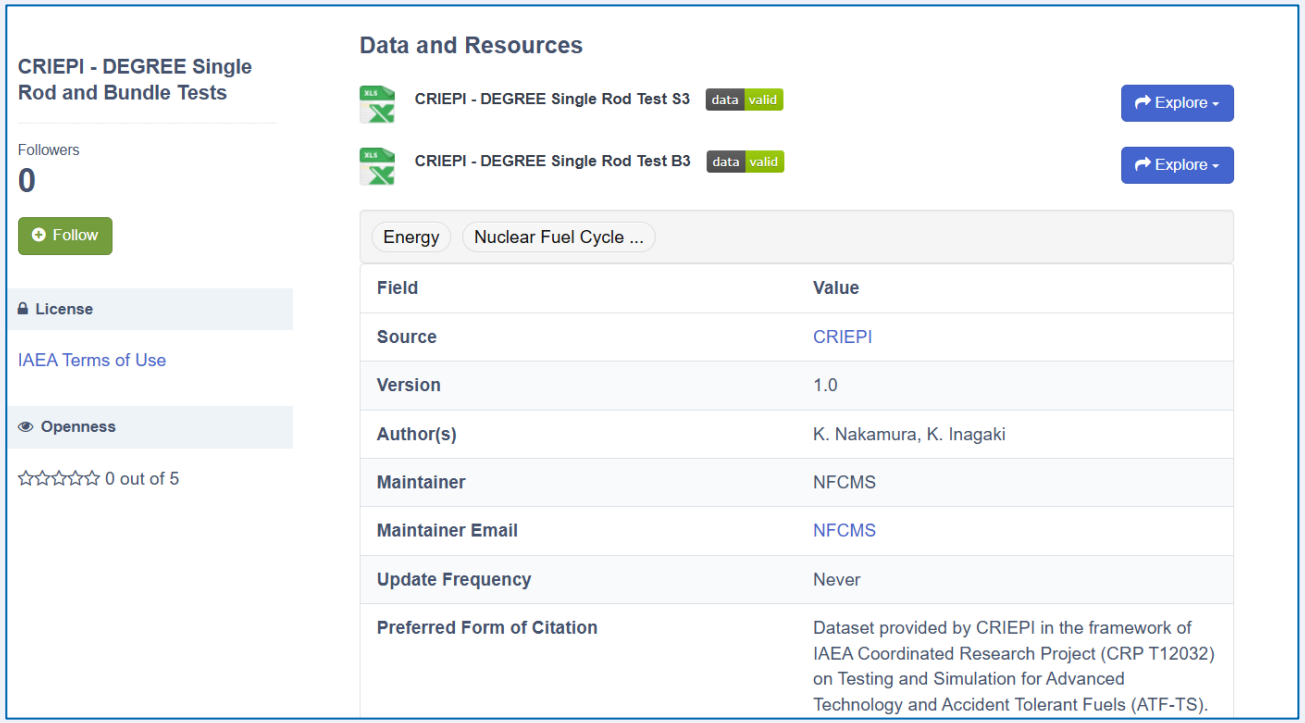

CRIEPI - DEGREE Single Rod and Bundle Tests - CRIEPI - DEGREE Single Rod and Bundle Tests - Datasets - IAEA Data Platform

Thermohydraulic Boundary Conditions for Simulation

Thermohydraulic Boundary Conditions for Simulation were developed in the framework of IAEA CRP "Fuel Modelling in Accident Conditions" (FUMAC, IAEA-TECDOC-1889) project partner for three Halden LOCA tests:

- IFA-650.9 (PWR fuel)
- IFA-650.10 (PWR fuel)
- IFA-650.11 (VVER fuel)

and calculated by the integral code SOCRAT/V3

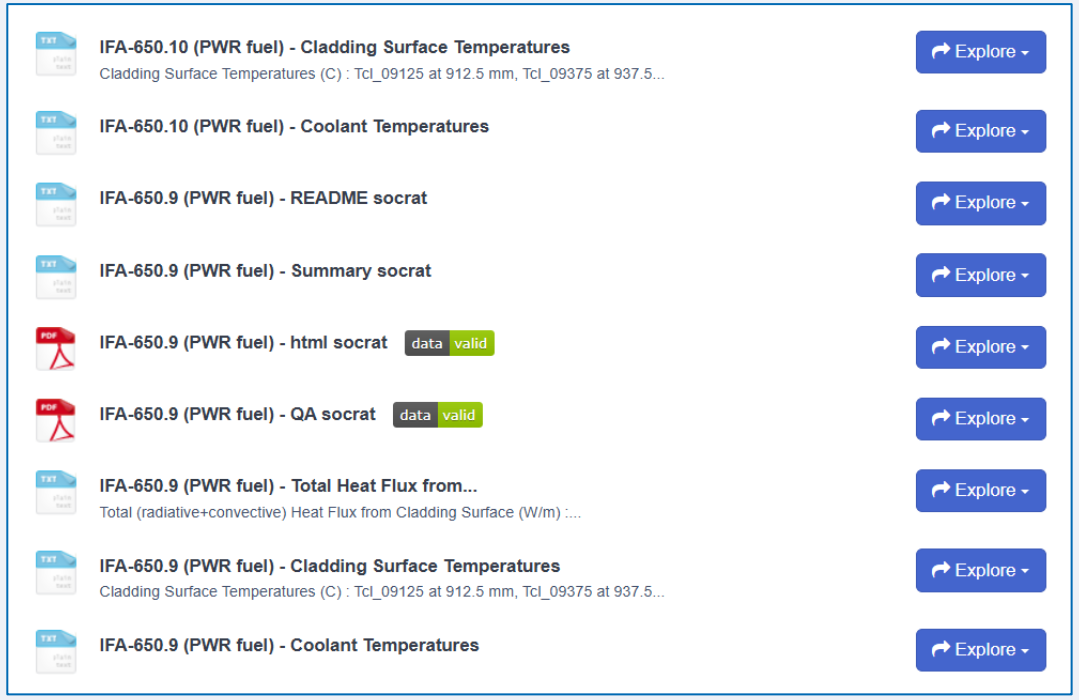

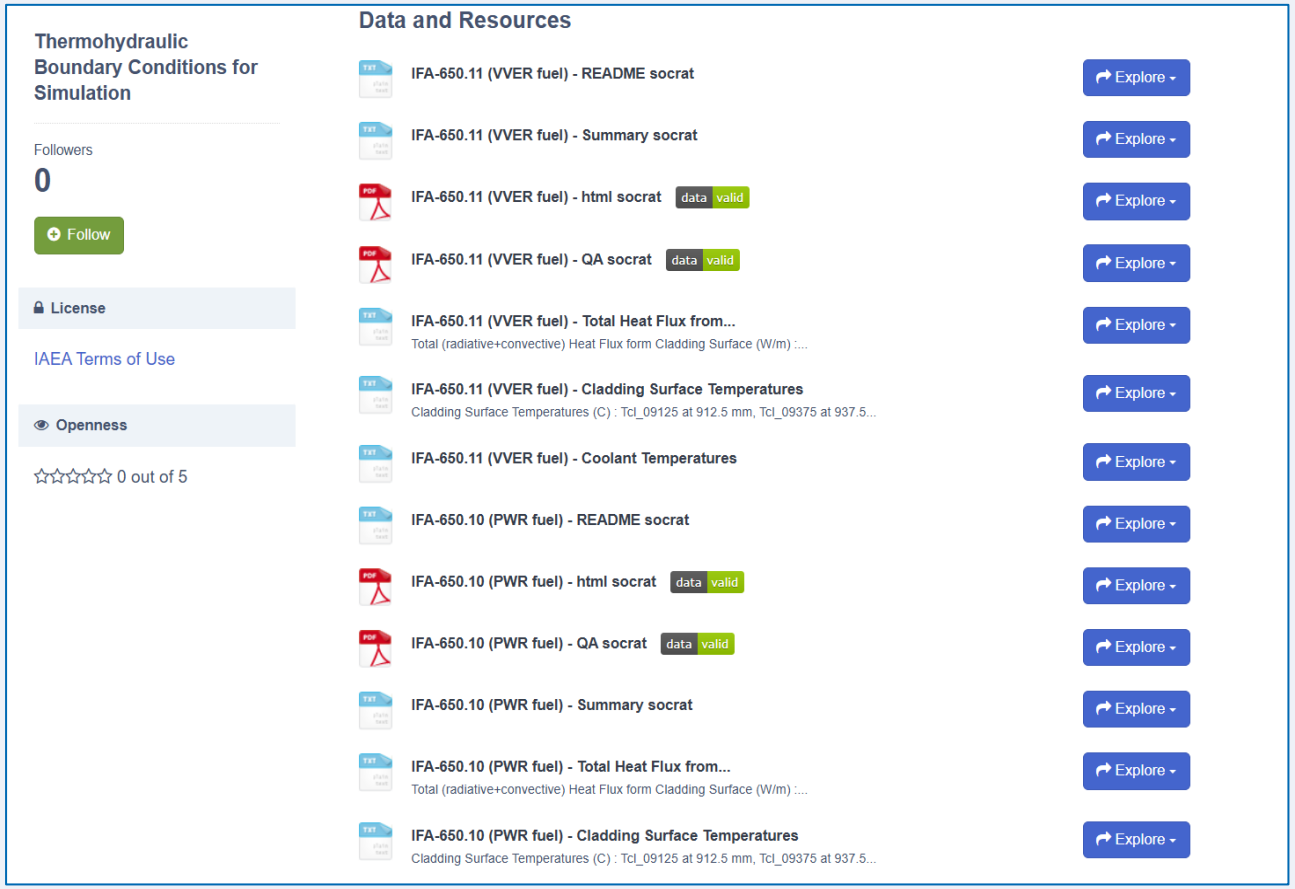

Thermohydraulic Boundary Conditions for Simulation - Thermohydraulic Boundary Conditions for Simulation - Datasets - IAEA Data Platform

Open-source ATF material properties database

Advanced Material Database

IAEA Material database covers thermodynamic, electro-chemical, phase-diagram, and physical properties of advance materials for nuclear fuels for the current and future nuclear fleet.

Datasets relating to fuels for the advanced materials databse can be found here:

- Minor Actinide Property Database (MADB) - Datasets - IAEA Data Platform
- ATF open sources material properties database

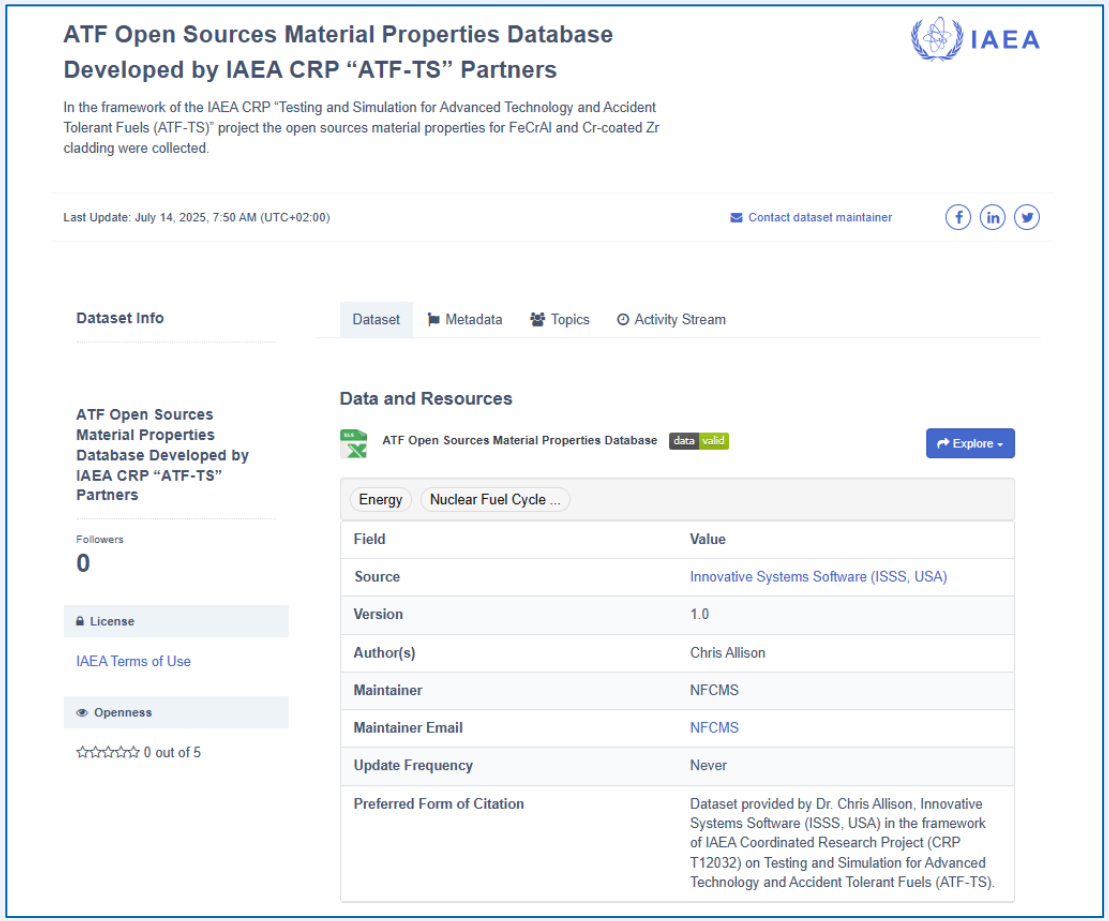

ATF Open Sources Material Properties Database Developed by IAEA CRP "ATF-TS" Partners

IAEA

In the framework of the IAEA CRP "Testing and Simulation for Advanced Technology and Accident Tolerant Fuels (ATF-TS)" project the open sources material properties for FeCrAl and Cr-coated Zr cladding were collected.

Last Update: July 14, 2025, 7:50 AM (UTC+02:00)

Contact dataset maintainer

Dataset Info

Dataset | Metadata | Topics | Activity Stream

ATF Open Sources Material Properties Database Developed by IAEA CRP "ATF-TS" Partners

Followers 0

License

IAEA Terms of Use

Openness

☆☆☆☆☆ 0 out of 5

Data and Resources

ATF Open Sources Material Properties Database data valid

Explore

Energy | Nuclear Fuel Cycle ...

Field	Value
Source	Innovative Systems Software (ISSS, USA)
Version	1.0
Author(s)	Chris Allison
Maintainer	NFCMS
Maintainer Email	NFCMS
Update Frequency	Never
Preferred Form of Citation	Dataset provided by Dr. Chris Allison, Innovative Systems Software (ISSS, USA) in the framework of IAEA Coordinated Research Project (CRP T12032) on Testing and Simulation for Advanced Technology and Accident Tolerant Fuels (ATF-TS).

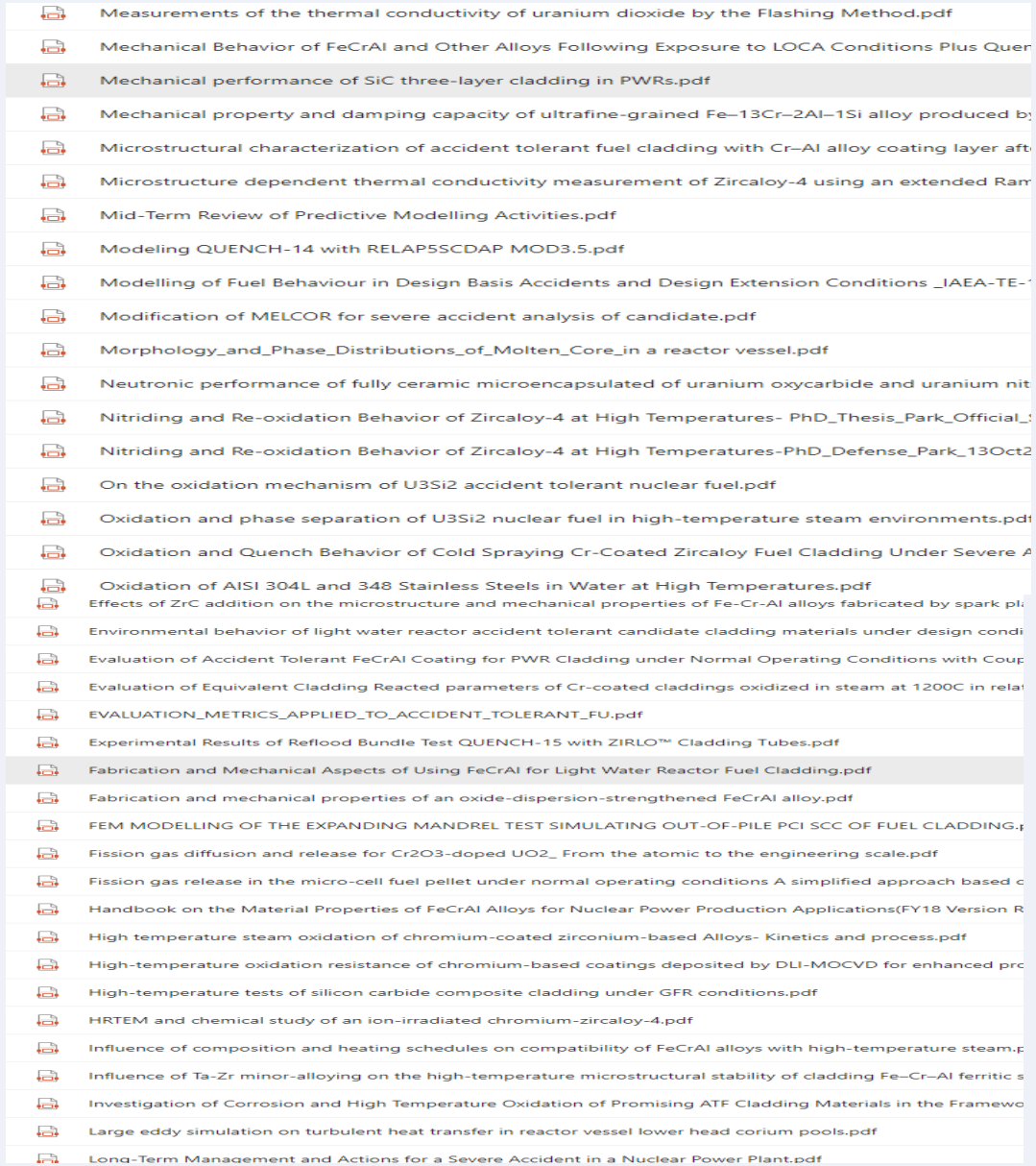

Measurements of the thermal conductivity of uranium dioxide by the Flashing Method.pdf
Mechanical Behavior of FeCrAl and Other Alloys Following Exposure to LOCA Conditions Plus Quen
Mechanical performance of SiC three-layer cladding in PWRs.pdf
Mechanical property and damping capacity of ultrafine-grained Fe–13Cr–2Al–1Si alloy produced by
Microstructural characterization of accident tolerant fuel cladding with Cr–Al alloy coating layer aft
Microstructure dependent thermal conductivity measurement of Zircaloy-4 using an extended Ram
Mid-Term Review of Predictive Modelling Activities.pdf
Modeling QUENCH-14 with RELAP5SCDAP MOD3.5.pdf
Modelling of Fuel Behaviour in Design Basis Accidents and Design Extension Conditions _IAEA-TE-
Modification of MELCOR for severe accident analysis of candidate.pdf
Morphology_and_Phase_Distributions_of_Molten_Core_in a reactor vessel.pdf
Neutronic performance of fully ceramic microencapsulated of uranium oxycarbide and uranium nit
Nitriding and Re-oxidation Behavior of Zircaloy-4 at High Temperatures- PhD_Thesis_Park_Official_
Nitriding and Re-oxidation Behavior of Zircaloy-4 at High Temperatures-PhD_Defense_Park_13Oct2
On the oxidation mechanism of U3Si2 accident tolerant nuclear fuel.pdf
Oxidation and phase separation of U3Si2 nuclear fuel in high-temperature steam environments.pdf
Oxidation and Quench Behavior of Cold Spraying Cr-Coated Zircaloy Fuel Cladding Under Severe A
Oxidation of AISI 304L and 348 Stainless Steels in Water at High Temperatures.pdf
Effects of ZrC addition on the microstructure and mechanical properties of Fe-Cr-Al alloys fabricated by spark pl
Environmental behavior of light water reactor accident tolerant candidate cladding materials under design condi
Evaluation of Accident Tolerant FeCrAl Coating for PWR Cladding under Normal Operating Conditions with Coup
Evaluation of Equivalent Cladding Reacted parameters of Cr-coated claddings oxidized in steam at 1200C in rela
EVALUATION_METRICS_APPLIED_TO_ACCIDENT_TOLERANT_FU.pdf
Experimental Results of Reflood Bundle Test QUENCH-15 with ZIRLO™ Cladding Tubes.pdf
Fabrication and Mechanical Aspects of Using FeCrAl for Light Water Reactor Fuel Cladding.pdf
Fabrication and mechanical properties of an oxide-dispersion-strengthened FeCrAl alloy.pdf
FEM MODELLING OF THE EXPANDING MANDREL TEST SIMULATING OUT-OF-PILE PCI SCC OF FUEL CLADDING.
Fission gas diffusion and release for Cr2O3-doped UO2_ From the atomic to the engineering scale.pdf
Fission gas release in the micro-cell fuel pellet under normal operating conditions A simplified approach based c
Handbook on the Material Properties of FeCrAl Alloys for Nuclear Power Production Applications(FY18 Version R
High temperature steam oxidation of chromium-coated zirconium-based Alloys- Kinetics and process.pdf
High-temperature oxidation resistance of chromium-based coatings deposited by DLI-MOCVD for enhanced pro
High-temperature tests of silicon carbide composite cladding under GFR conditions.pdf
HRTEM and chemical study of an ion-irradiated chromium-zircaloy-4.pdf
Influence of composition and heating schedules on compatibility of FeCrAl alloys with high-temperature steam.p
Influence of Ta-Zr minor-alloying on the high-temperature microstructural stability of cladding Fe–Cr–Al ferritic s
Investigation of Corrosion and High Temperature Oxidation of Promising ATF Cladding Materials in the Framewo
Large eddy simulation on turbulent heat transfer in reactor vessel lower head corium pools.pdf
Long-Term Management and Actions for a Severe Accident in a Nuclear Power Plant.pdf

ATF Open Sources Material Properties Database Developed by IAEA CRP "ATF-TS" Partners - ATF Open Sources Material Properties Database Developed by IAEA CRP "ATF-TS" Partners - Datasets - IAEA Data Platform

Technical Meeting on Advanced Technology Fuels: Progress on their Design, Manufacturing, Experimentation, Irradiation, and Case Studies for their Industrialization, Safety Evaluation, and Future Prospects, 28 - 31 October 2025

89 experts from 33 MSs and 2 IOs (NEA OECD +EC) participated in the Workshop.

A total of 39 presentations were provided during its sessions.

Participants represented research organizations, nuclear fuel design institutions, nuclear power plant operators and engineering companies, regulatory bodies and technical support organizations, universities, and other entities engaged in near- and mid-term ATF fuel development, design, manufacturing, licensing, and operation for both large and small water-cooled reactors.

The meeting was highly successful, featuring high-quality presentations and extensive technical discussions. Valuable recommendations were provided to guide future IAEA activities related to ATF testing, modelling and simulation, and safety analysis.

Technical Meeting on Advanced Technology Fuels Sessions

1. Advances in ATF Materials and Manufacturing (ATF cladding and fuel fabrication; Coating designs and optimization; Industrialization of ATFs and associated challenges) (N.Doncel (Spain) and Mr K. Sakamoto (Japan),

2. Experimental Testing of ATF Materials and Validation Database (Bundle Tests – Bundle tests with ATFs simulating DBA, DEC-A and DEC-B conditions including tests with air ingress; Separate Effect Tests (SETs) – SETs focused on nominal operating conditions and anticipated occupational occurrences (long-term corrosion testing, mechanical tests, coating defects), accidental scenarios (HT steam/air oxidation, LOCA- and RIA-related SETs) ; In-pile Testing– Irradiation testing of candidate ATF materials (LTRs, LTAs) (R. Hansen (USA) and Mr Z. Hózer (Hungary)

3. ATF Modelling (Verification, Validation, and Uncertainty Quantification of fuel performance codes ; Multi-physics and Multi-scale Modelling; Benchmarking of fuel performance codes for ATF materials in operational and accident conditions; Data-driven and artificial intelligence (AI) applications) (P. Van Uffelen (JRC) and A. Bouloré (CEA, France),

4. ATF Safety Analysis and Licensing Practices (New Safety Criteria for ATFs, Innovative Qualification & Licensing Approaches for DBA and DEC scenarios; Risk-Informed Approaches; Margin Quantification and Management (J. Zhang (Belgium),

5. Future prospects of ATF (Effect of ATFs on occurrence and consequences of Fuel Fragmentation, Relocation, and Dispersal (FFRD), Definition of Post- Critical Heat Flux (CHF) Time at Temperature Limits; Improved ATF designs; Use of LEU+ with ATFs for High Burnup (HBU); Deployment of ATFs in Small Modular Reactors (SMRs) (Yongjun Jiao (China) and Mr Zoltan Hozer (Hungary)

Panel - “What is the future for ATFs?” (Martin Ševeček)

Proposed scope of new CRP on ATF testing and simulation including for SMRs

General objective: to complements the completed CRP ATF-TS by

Addressing high-burnup applications for existing LWRs.

Advancing testing and simulation frameworks for innovative fuels and SMRs

Specific Objective 1: Experimental Program and Test Data

- Investigate behaviour of advanced claddings: Cr-coated, FeCrAl, SiC —focusing on improved integrity and oxidation resistance beyond LOCA. Activities will include microscale, temperature-dependent testing for coating creep and integrity characterization, assessment of pre-corroded coatings, and development of coating-specific creep laws.
- Published FeCrAl data (e.g. from ORNL) and open literature on coating technologies will be compiled and include into the IAEA ATF materials database.
- Harmonize ATF testing procedures to ensure reproducibility and comparability.
- Expand ATF datasets under representative thermal–hydraulic conditions for design-basis (DB) and beyond-design-basis (BDB) scenarios.
- Support bundle-scale Integral Effect Tests (IETs) (QUENCH, CODEX, DEGREE) engaging at least three institutions.
- Strengthen cooperation with OECD for quench and transient test data exchange

Proposed scope of new CRP on ATF testing and simulation including for SMRs:

Specific Objective 2: Simulation and Modelling

- Develop cross-scale models for:
  Fission gas behaviour, creep, swelling in large-grain pellets.

- Improve modelling of:
  Cladding ballooning, burst, oxidation, and FFRD at high burnup.

- Apply multi-physics coupled codes (fuel performance + thermal-hydraulics) for steady-state and transients.

- Conduct comparative assessments of simulation vs experimental data to quantify ATF benefits.

- Expand benchmarking:
  Include semi-integral and integral irradiation tests.
  Harmonize user-input effects;
  Use system-code-derived boundary conditions when LOCA data unavailable.

Proposed scope of new CRP on ATF testing and simulation including for SMRs

Specific Objective 3: PCMI, LOCA & RIA Safety Evaluation

- Address gap in fuelled ATF LOCA and RIA experiments; aim for experimental validation
- Improve hot rod LOCA safety evaluation for ATF and SMRs,

    Provide detailed thermal–hydraulic boundary conditions (THBCs) for nominal and upper-bound cases.

    Verify THBC applicability;

    Refine uncertainty quantification.
- Incorporate PCMI, multiple LOCA and RIA scenarios in benchmarks
- Consider RIA scenarios for high-burnup fuels (e.g., JAEA data with doped pellets).
- Integrate ATF models into coupled fuel performance–safety analysis codes for operational and accident conditions.
- Emphasize:

    Uncertainty analysis and material property verification.

    Improved methodologies for quantifying ATF safety and economic benefits, especially for near-term and SMR applications.

Planned Timeline for the New CRP on ATF

- March 2026 – Convening of a Consultancy Meeting to shape the new CRP, including:
  - Detailed discussions on available experimental datasets, experimental and code benchmark, and margin quantification activities within CRP
  - Defining the scope of the CRP and specific tasks
  - Drafting the CRP Proposal

- Mid 2026 – Finalization of the CRP Proposal

- Q3 2026 – Submission of the CRP Proposal for review and approval by the Committee for Coordinated Research Activities (CCRA)

- Q4 2026 – Official launch of the CRP on ATF

Conclusion

- The completed IAEA CRP on ATF-TS (2020–2024) has supported IAEA MSs to understand and analyse ATF behaviours in normal and accident conditions by sharing experimental data and best practices in fuel modelling, increasing technology readiness for candidate ATF materials
- Building on this foundation, the new CRP will further advance testing and simulation of ATF concepts through coordinated experiments, expanded material datasets, and harmonized methodologies. It will enhance high-burnup fuel modelling, incorporate PCMI and multiple LOCA and RIA scenarios in benchmarks with improved boundary-condition and refined uncertainty quantification, and apply multi-physics coupled codes (fuel performance + thermal-hydraulics) to support advanced fuel development.

IAEA

Thank you

A.Khaperskaia@iaea.org

Martin Ševeček

CTU

Separate effects tests with ATF cladding materials within the IAEA ATF-TS CRP

The presentation by Martin Ševeček reviewed the outcomes of the IAEA Coordinated Research Project on Advanced-Fuel-Cladding-Technologies (ATF-TS) and highlighted key experimental findings on a broad portfolio of coated-zirconium and alternative cladding concepts. Ten institutes supplied nine zirconium-based reference alloys (Zircaloy-4, Opt. Zirlo, Zr1Nb, HANA6, M5, E110) together with various chromium-based, CrN/Cr, TiAl, SiC and FeCrAl coatings. Over a dozen laboratories performed high-temperature steam oxidation, balloon-/burst, autoclave corrosion and mechanical tests, generating extensive datasets for model validation.

Chromium-coated Zr showed modest benefits for ballooning and burst resistance, but the gain depends strongly on test conditions, coating thickness and substrate alloy. New failure criteria and creep correlations for coated claddings were derived and supplied to the WT2 fuel-performance model. FeCrAl alloys exhibited markedly different behavior compared with Zr, with a strengthening effect that is partially offset by thinner wall limitations; their high-temperature oxidation kinetics were investigated at 1350–1375 °C under various dwell times. TiAl coatings on Zr-4 were targeted to 10 µm thickness for CANDU applications. Overall, the ATF-TS project delivered more than 100 open datasets, numerous publications, and validated correlations for HT oxidation, ballooning, burst and corrosion, establishing a solid experimental basis for the upcoming ATF-HBU program.

Separate effects tests with ATF cladding materials within the IAEA ATF-TS CRP

Martin Ševeček

30th International QUENCH Workshop
18th of December, 2025
KIT, Karlsruhe, Germany

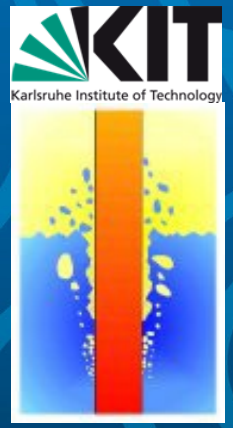

ATF-TS Experimental Programme - SETs

Participants proposed to provide ATF cladding materials for testing

- ✓ Quantity and geometry limitations – e.g. tubes vs. coupons
- ✓ Limited volume of materials – e.g. FeCrAl B136Y
- ✓ Priorities of sample suppliers

Other participants proposed testing campaigns using their facilities

- ✓ Different testing capacities, geometry, test parameters, methodologies, manpower, and resources

Low TRL concepts were investigated in the previous CRP. In ATF-TS, suppliers were asked to provide optimized high TRL products. The optimization was not part of the project, and the fabrication parameters were selected solely by material providers.

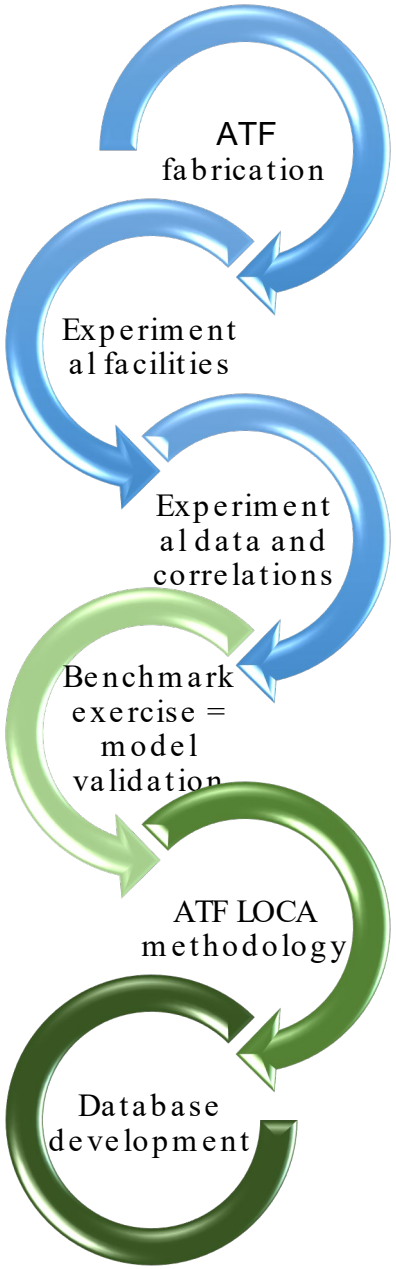

CTU
CZECH TECHNICAL UNIVERSITY IN PRAGUE

ATF Cladding Materials

ATF concepts fabricated within ATF-TS

- 6 institutes fabricated ATF **cladding** materials for testing
- [illegible]ted Zr-based alloys to be used as a reference [illegible]NA6, M5, E110)
- [illegible]
  - [illegible]
  - TiAl – CNL
  - SiC/ YAG– INCT (Zr1Nb plates [illegible]
- FeCrAl, SiC
  - KIT FeCrAl B136Y (ORNL)
  - NPIC FeCrAl, SiC/ SiC

In total, more than 160 meters of reference and ATF tubes and several m² of reference and ATF plates were shared and tested.

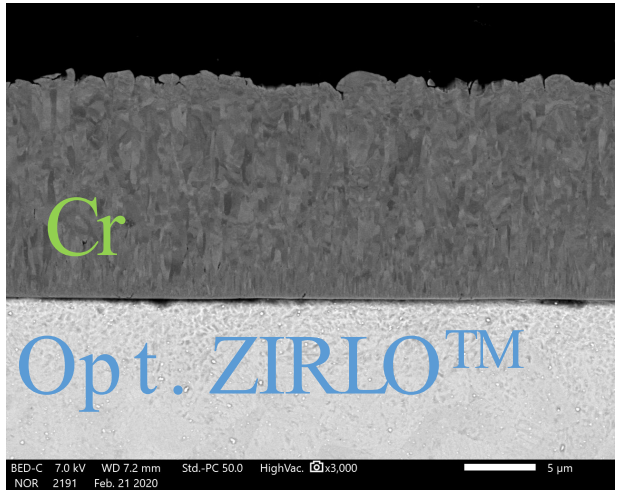

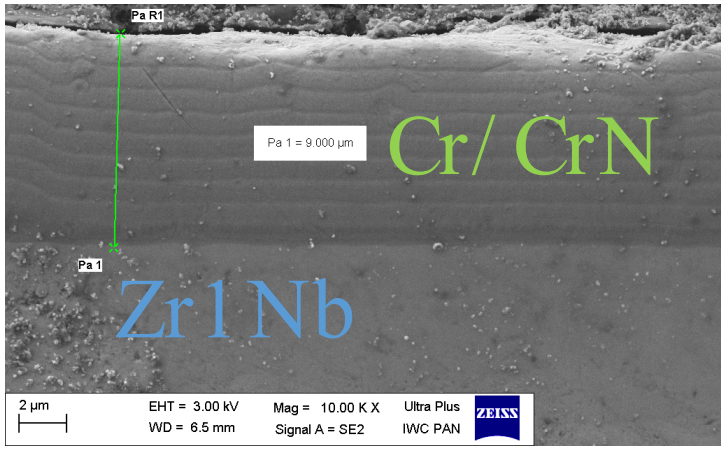

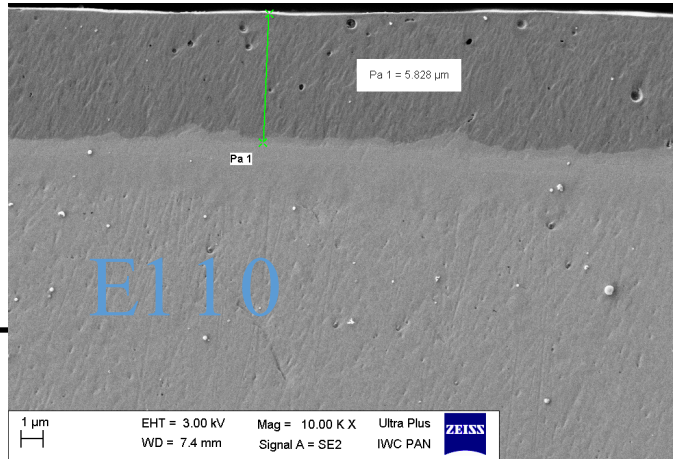

CTU– Cr and Cr/ CrN coated Opt. ZIRLO ™


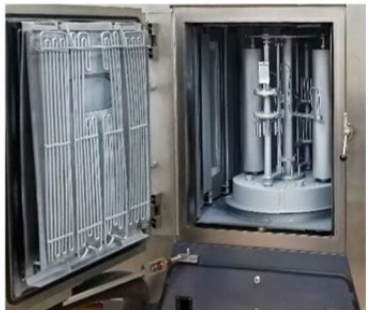


Opt. ZIRLO (OD=9.144mm), kindly provided by Westinghouse Electric Company for the ATF -TS CRP project

Two coating machines/chambers, optimized power sources and deposition parameters:

- Semi-industrial - Hauzer Flexicoat 850
- Industrial – Hauzer Flexicoat 1500


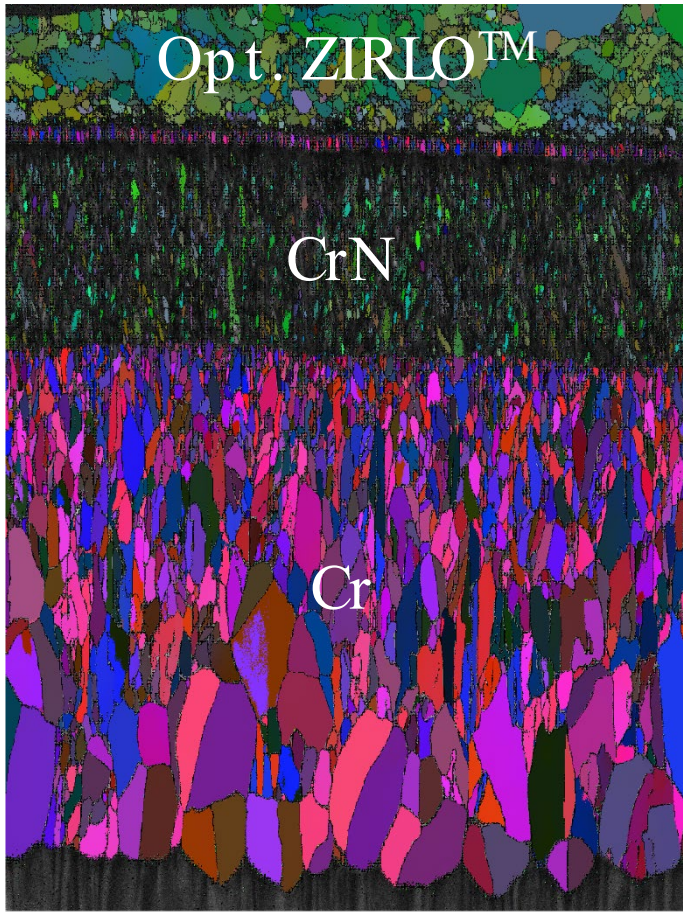
Opt. ZIRLO™
CrN
Cr
6 µm

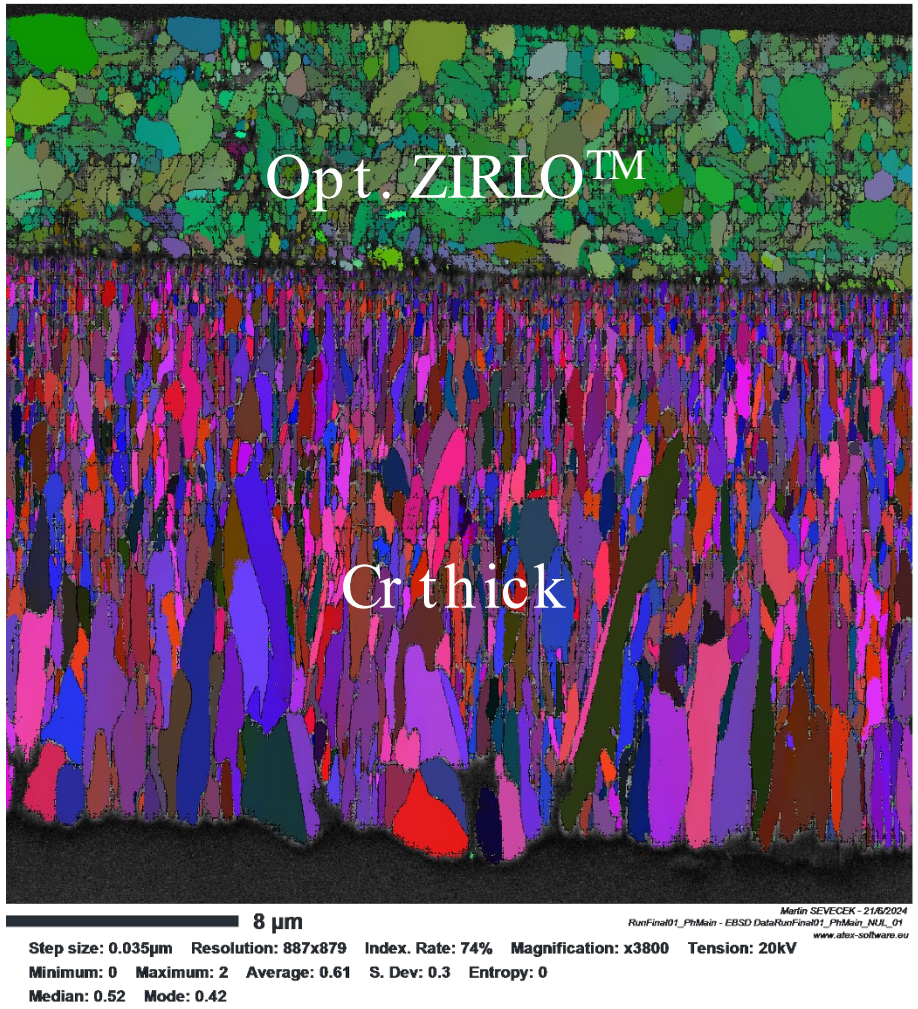
Opt. ZIRLO™
Cr thick
8 µm
Martin SEVECEK - 21/6/2024
RunFinal01_PhMain - EBSD DataRunFinal01_PhMain_NUL_01
www.alex-software.eu
Step size: 0.035µm Resolution: 887x879 Index. Rate: 74% Magnification: x3800 Tension: 20kV
Minimum: 0 Maximum: 2 Average: 0.61 S. Dev: 0.3 Entropy: 0
Median: 0.52 Mode: 0.42


Opt. ZIRLO™
Cr thin
8 µm
Martin SEVECEK - 21/6/2024
RunFinal01 PhMain - EBSD DataRunFinal01 PhMain
www.alex-software.eu
Step size: 0.03µm Resolution: 1001x592 Index. Rate: 81% Magnification: x4000 Tension: 20kV
Minimum: 0 Maximum: 2 Average: 0.65 S. Dev: 0.33 Entropy: 0
Median: 0.57 Mode: 0.37

KIT - Cr-coated Zr

Oerlikon Balzers coating company GmbH

- Variety of Zr -based t ubes provided by KIT, proprietary deposition parameters (deposition temperature ~270 °C)
- Coating thicknesses – 7.5 and 10.5 microns

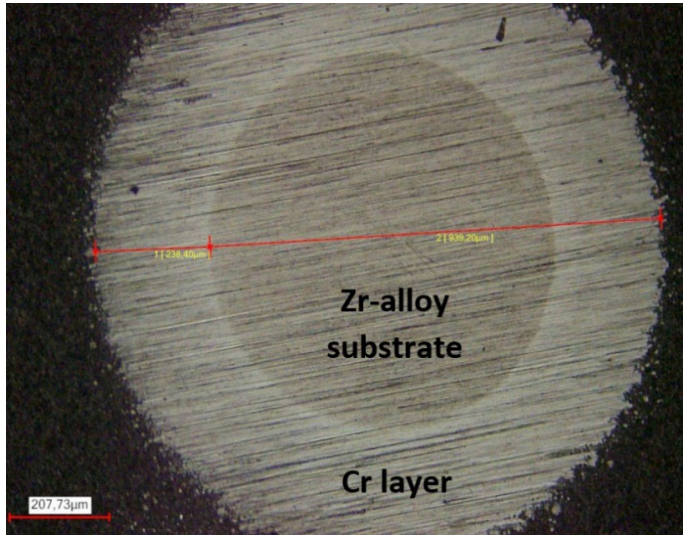

BSU – Cr coated plasma treated Zr

Zr1Nb (E110) – 20mm used as a substrate

- 1st step – Cr deposition
- 2nd step - compression plasma flow treatment

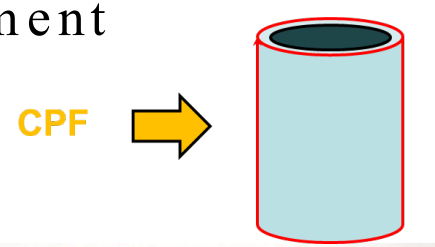

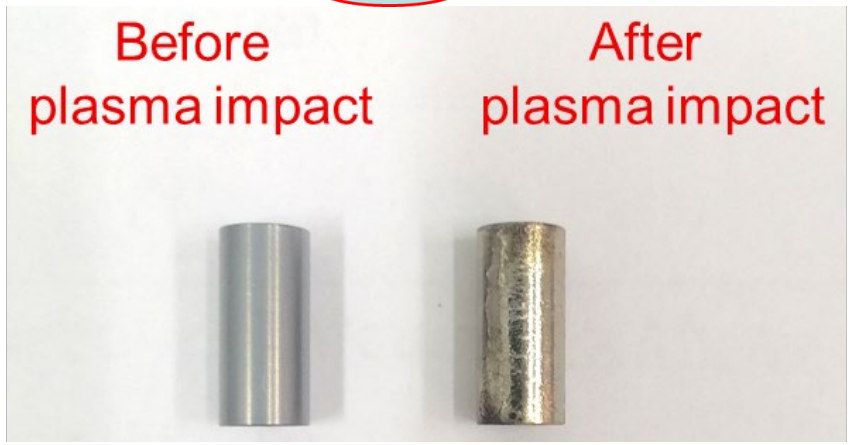

CNPE – Cr coated Zr

- Type 1 – Zr-Sn-Nb alloy – MS Cr
- Type 2 – Zircaloy -4 – arc ion plated Cr

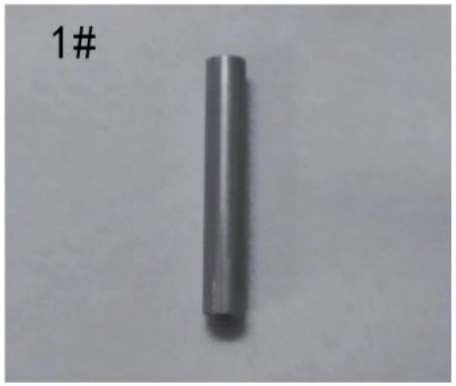

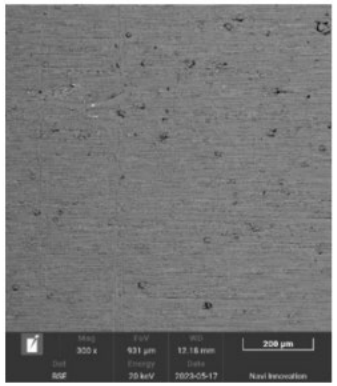

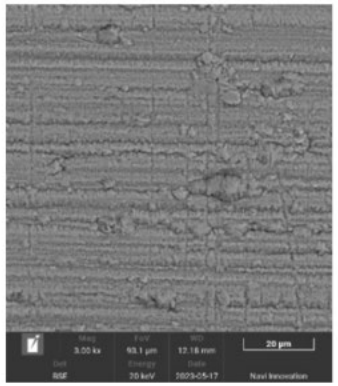

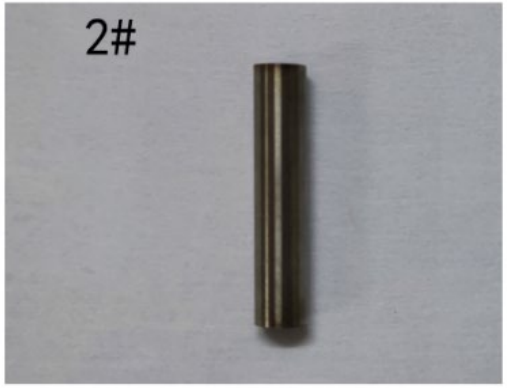

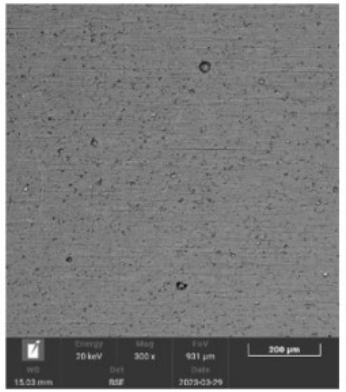

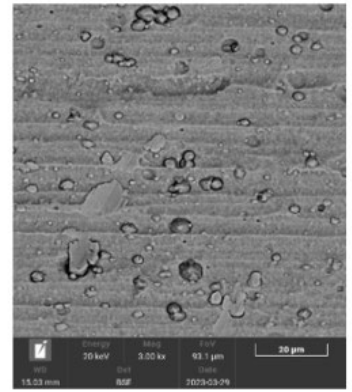

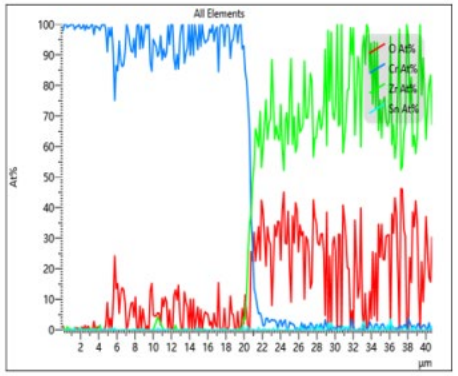

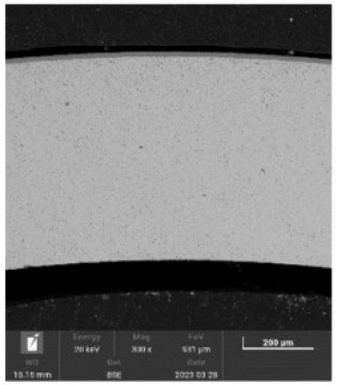

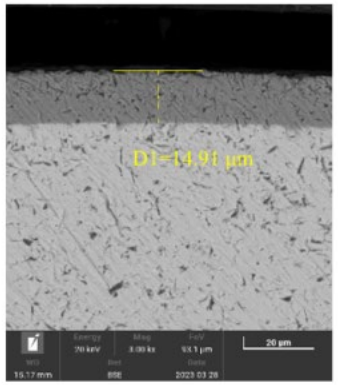

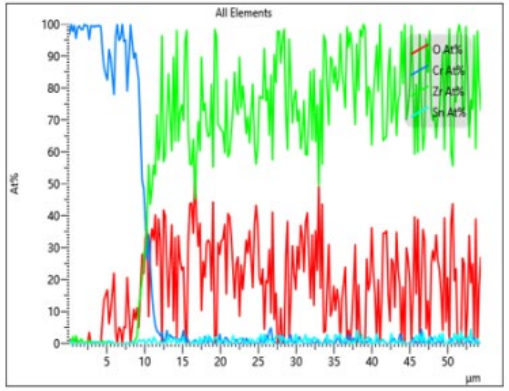

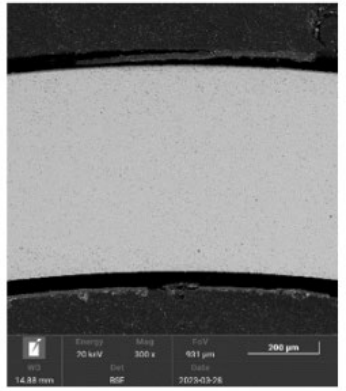

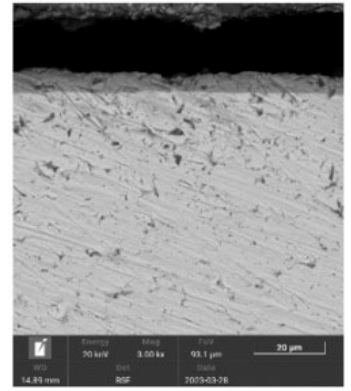

NPIC – Cr coated Zircaloy-4

Zircaloy -4 (Zr-1.5Sn-0.2Fe-0.1Cr), outer diameter 9.5 mm, wall thickness 0.57 mm

- Multi-arc ion plating technology (15–17 μm)

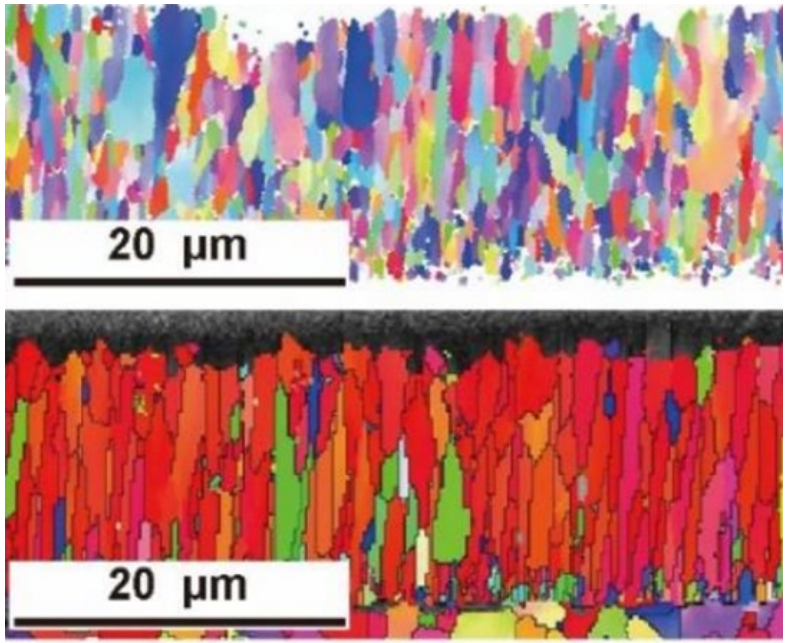

KNF – Cr coated HANA6

HANA-6 manufactured by KNF used as a substrate

- Arc Ion Plating – 9 and 19 microns
- LTRs inserted in Korea in spring 2025

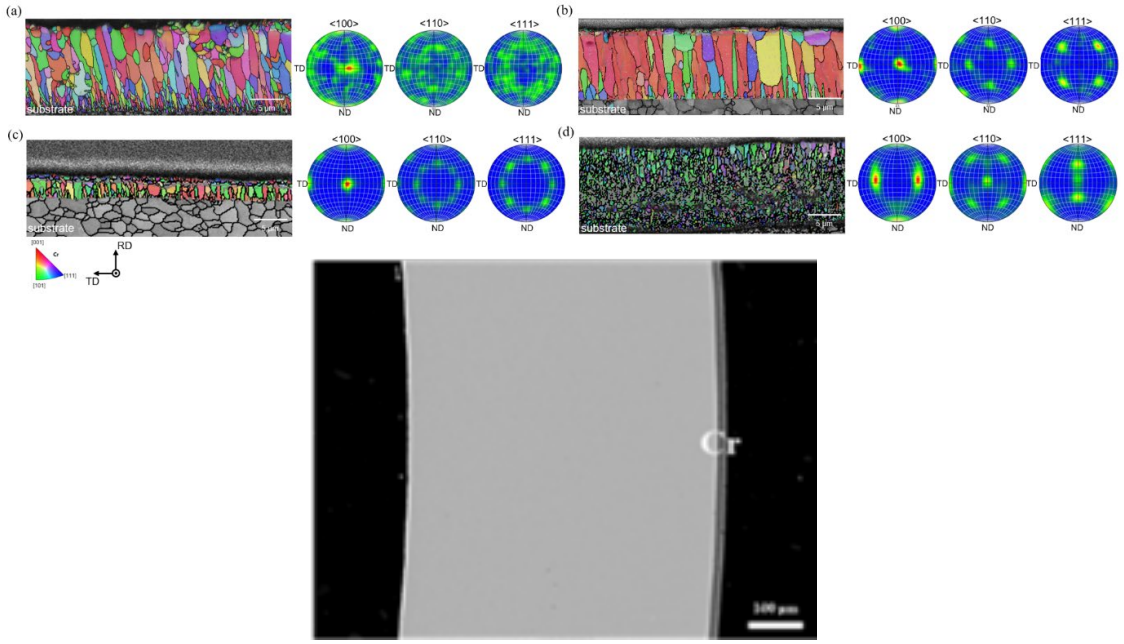

AEOI – CrN and CrN/Cr

CrN, and Cr/CrN multilayer coatings deposited on AEOI's Zr-1%Nb by AIP

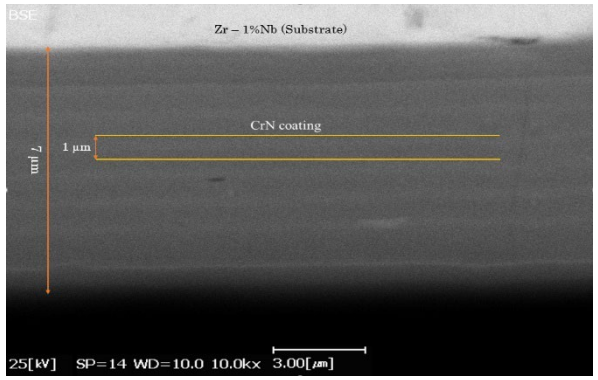

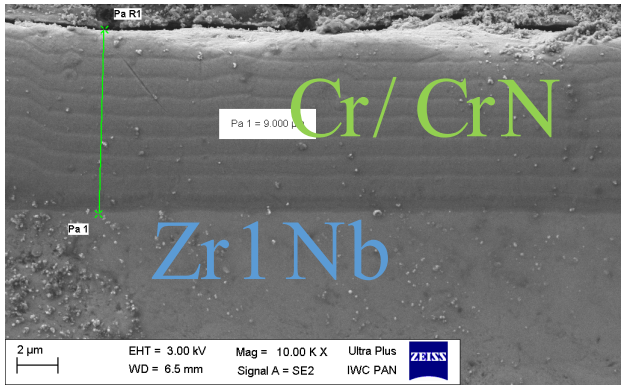

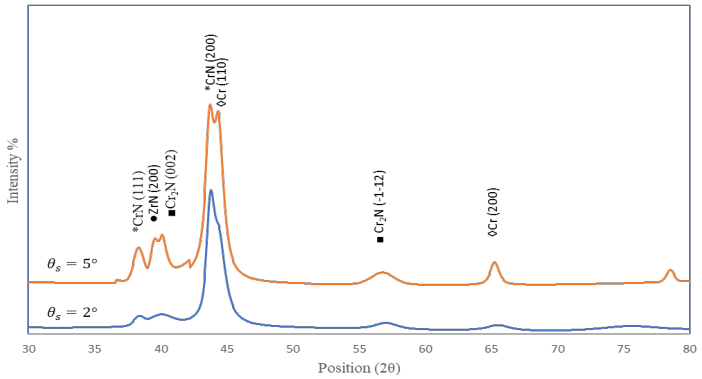

CNL – TiAl coated Zry-4

Focus on CANDU – two dimensions – OD= 5.3 and 13.08 mm

- TiAl MS, target thickness of 10 µm and a composition of 45–50 at.% Ti to 55–50 at.% Al on the tubes
- Unbalanced closed field UMS-PVD coater (Teer 650) using two Ti and two Al targets, with argon as the working gas.

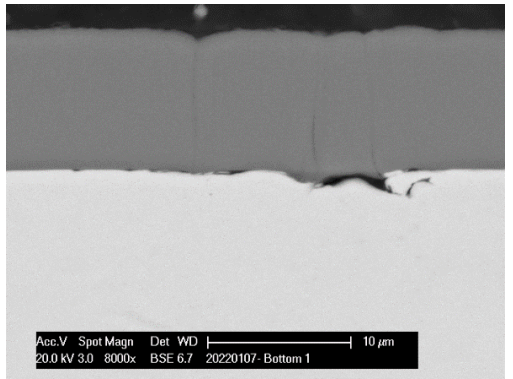

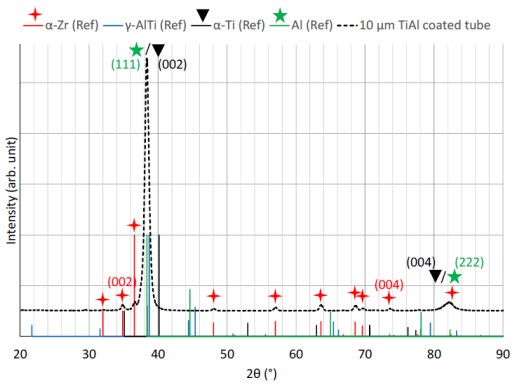

FeCrAl NPIC

- 13Cr-4.5Al-2Mo-1Nb-0.4Ta-0.05Y (wt.%)
- Vacuum induction melting → homogenization → red feeding forging → extrusion → warm rolling (three passes) → cold rolling (seven passes) → recrystallization annealing
- The final geometry of the cold pilgered thin-wall tube are 9.5*0.38 mm

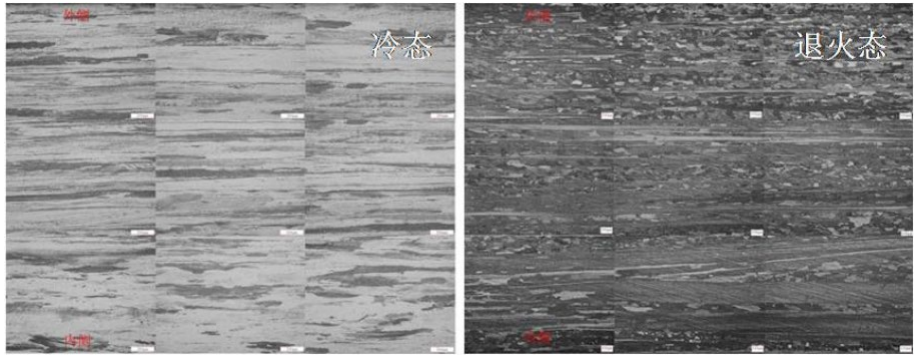

FeCrAl B136Y3 (KIT/ORNL)

- 13Cr-6.2Al-0.03Y-0.01C (wt.%)
- Produced by ORNL– B-type alloy
- Used in the QUENCH-19 bundle test = link to Q19 benchmark exercise + support with SETs

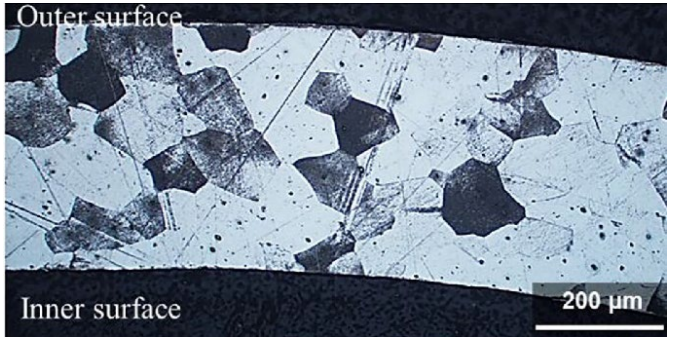

Experiments – DBA/ DEC

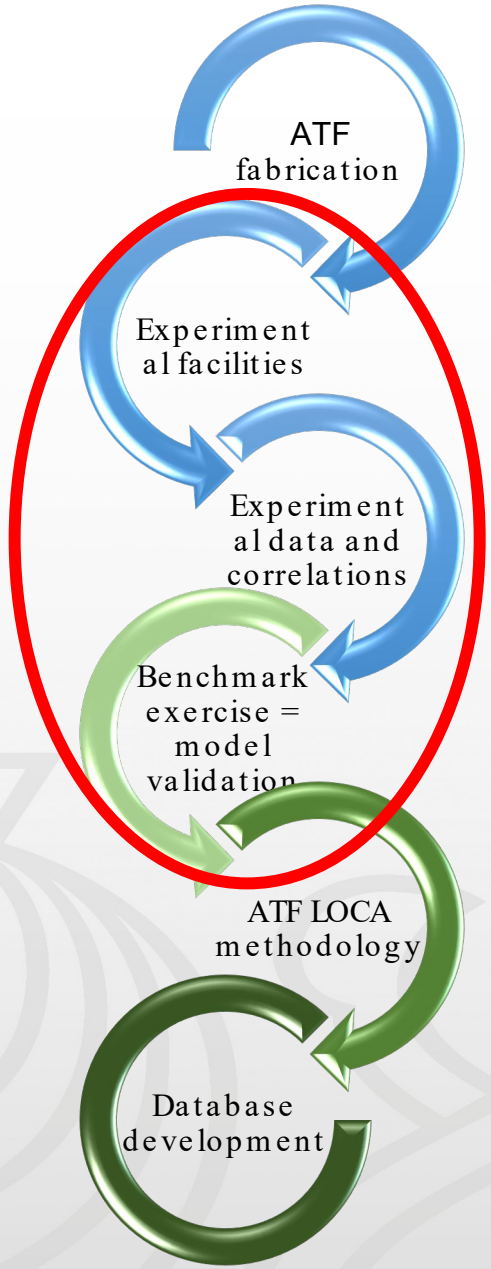

+VTT, BSU, INL that left during the project

Experimental facilities

- 12 laboratories/institutes proposing various testing campaigns
  - CNPE – HT oxidation; Ballooning/burst
  - CNPRI – axial tensile tests; internal burst tests; internal creep tests; autoclave corrosion tests; HT steam oxidation
  - CRIEPI – bundle/single rod tests
  - CTU/UJP – ballooning/burst tests; HT steam oxidation; Autoclave corrosion
  - EK – HT oxidation; ballooning/burst tests; Mechanical tests; CODEX bundle test
  - INCT – autoclave corrosion tests; HT air oxidation; NAA
  - JRC – thermal characterization; mechanical tests
  - KAERI/SNU – LOCA testing; PQD evaluation; DSC-eutectic study; Micro -mechanics
  - KIT – HT oxidation tests; single rod tests
  - NPIC – FeCrAl-thermomechanical tests; SiC – thermal shock tests; irradiation tests
  - UPM – Autoclave corrosion; Ring compression tests; Cathodic charge; Burst tests

CTU
CZECH TECHNICAL UNIVERSITY IN PRAGUE

Ballooning/burst tests

TASK 2: HT creep/ballooning/burst

Originally defined for a round robin exercise. But due to different limitations, the tests are not standard RRTs but rather complementary tests of several cladding candidates. However, RRTs was possible in several instances.

HT creep/ballooning/burst

- CTU/UJP
  - Constant pressure-temperature ramp (0.7K/sec and 7K/sec)
  - Isothermal isobaric creep tests (constant moles of gas vs. infinite volume) at 750 and 950 °C
- EK
  - Constant temperature (750, 850 and 950 °C; 800, 900 and 1000 °C) – pressure ramps (5; 100 kPa/s)
  - As-received and pre-oxidized samples
- UPM
  - Isothermal pressure ramps (1 bar/s) – 100mm; 600 °C
  - Autoclave pre-oxidized and as-received
- CNPE
  - Isothermal (800, 840, 900 °C) pressure ramps (6 and 100 kPa/s)
- CNPRI
  - Lower temperature (350 °C) pressure ramps (13.8 MPa/s)
- SNU
  - Single rod LOCA tests with surrogate pellets/fragments; (closed volume, 60–80 °C/s using IR heating)

HT creep/ballooning/burst – Main Findings

Coated Zr cladding

- Limited benefit of coatings in time-to-burst (within the uncertainty range)
- Ballooning and opening size – coated Zr provides some benefits but the magnitude depends on the specific test conditions and methodology.
- New creep correlation and burst criteria derived (both stress- and strain-based for coated cladding) and provided to WT2 for model implementation and validation. Correction coefficients proposed for fuel performance models.

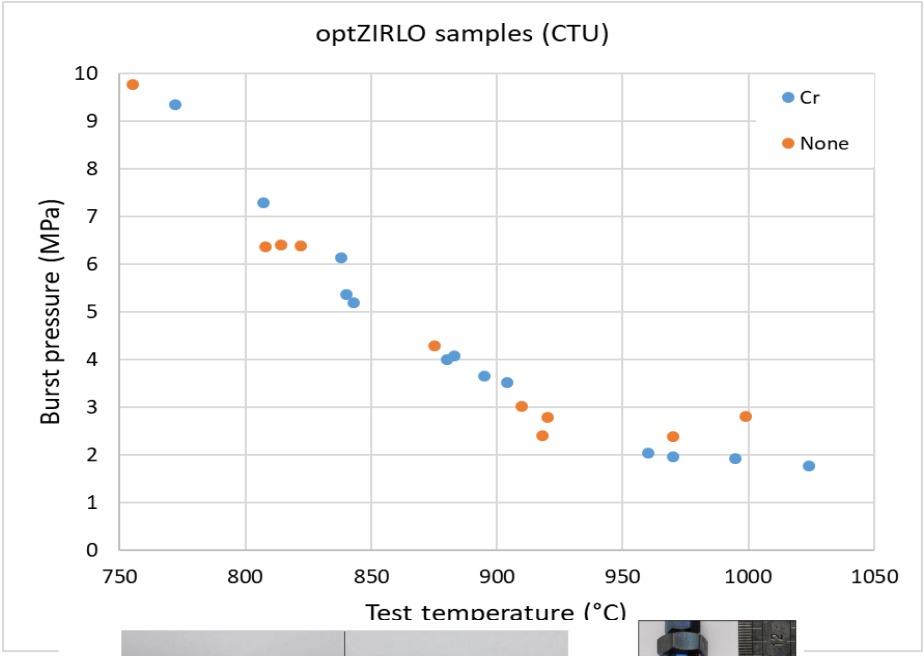

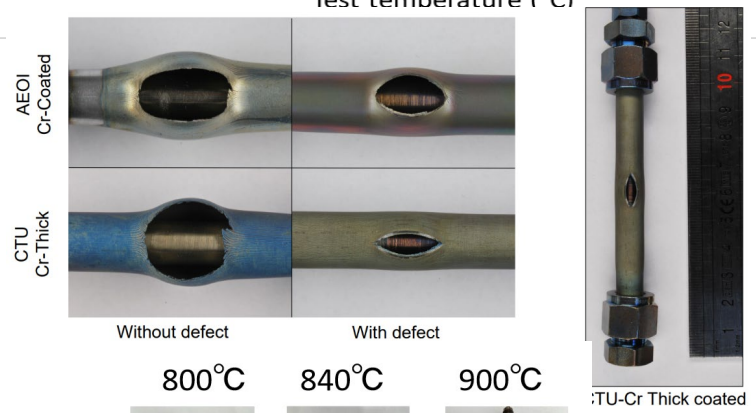

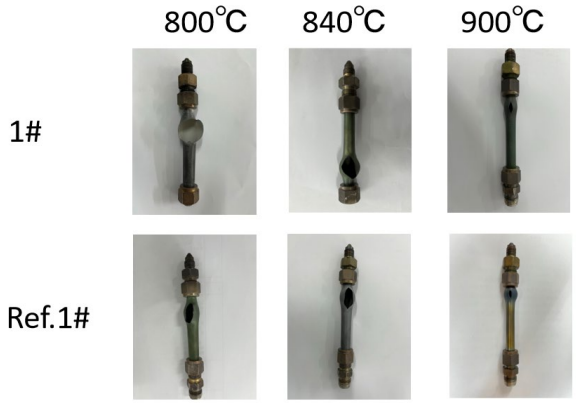

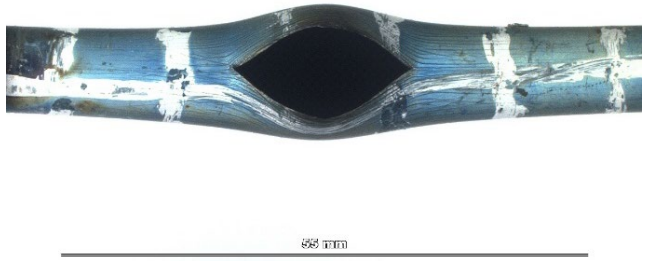

Coating cracking - different patterns and consequences for each type

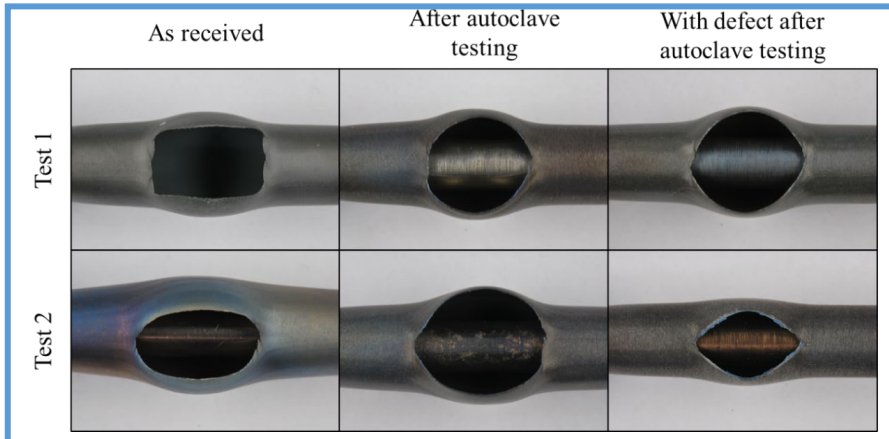

Ballooning size reduction – closely linked to chosen Zr alloy (more beneficial for softer Zr/Nb alloys)

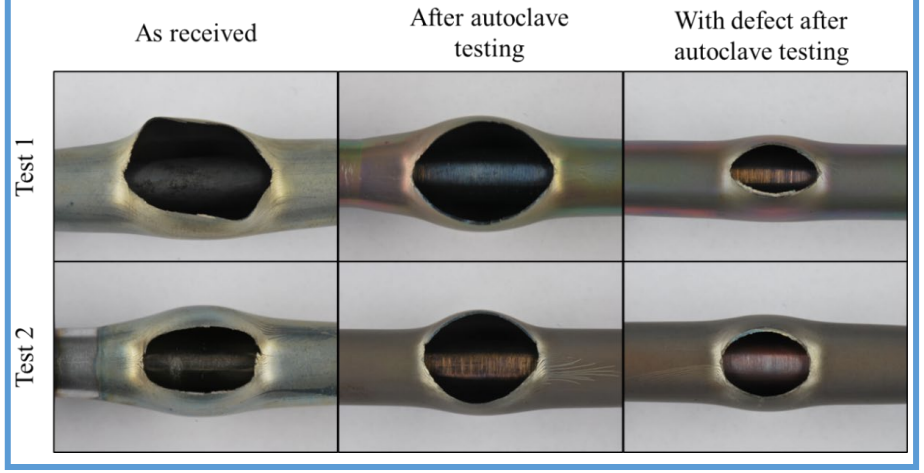

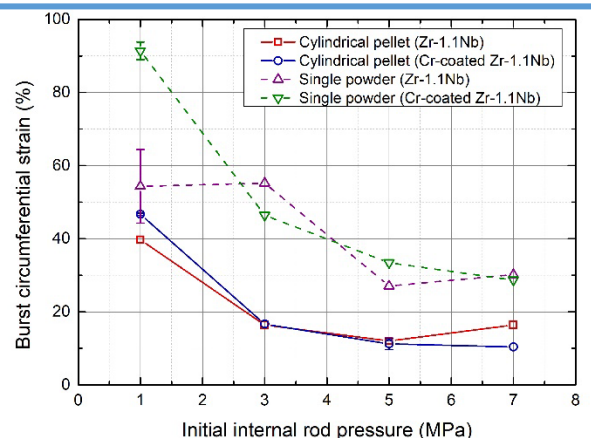

Strong effect of methodologies – pre-oxidation, geometry of fuel matrix, closed/infinite volume…

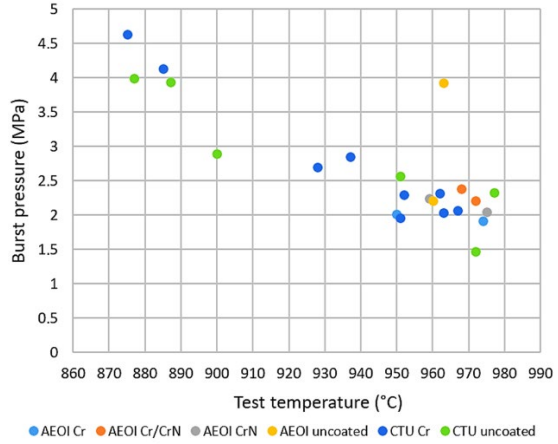

HT creep/ballooning/burst – Main Findings

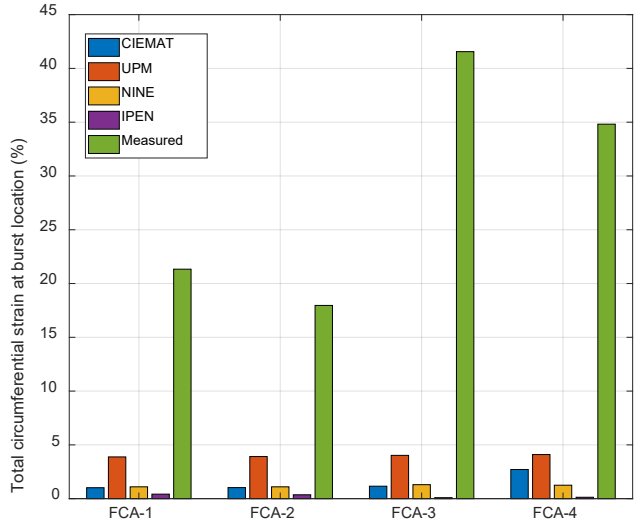

FeCrAl

- Very different performance of FeCrAl compared to Zr.
- Strengthening effect confirmed but partially eliminated by thinner wall.
- Fuel performance codes were not able to predict this behavior because the models were historically developed and tuned for Zr-based materials.

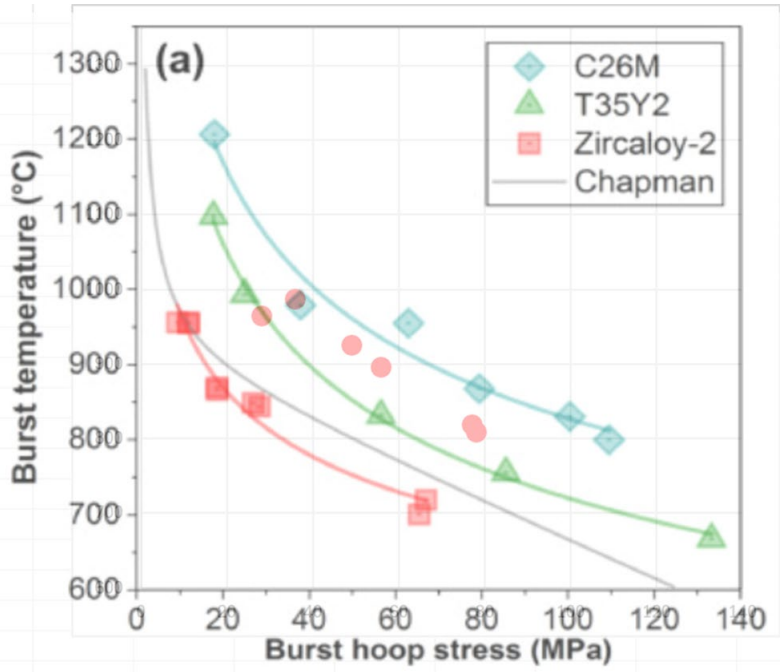

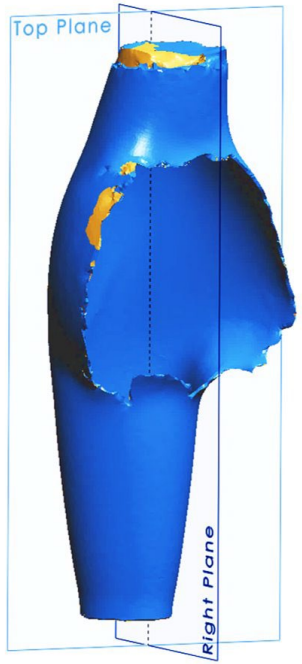

CTU
CZECH TECHNICAL UNIVERSITY IN PRAGUE

High-temperature oxidation

TASK 3: HT oxidation

High-temperature oxidation tests

- Small scale SETs (test parameters according to internal methodologies):
  - CNPRI – HT double-sided steam oxidation up to 1400 °C
  - CTU/ UJP – double and single-sided steam oxidation + PQD evaluation
  - EK – steam oxidation tests + RCTs
  - KAERI/ SNU – LOCA testing; PQD evaluation
  - INCT – Ar annealing test
  - CNPE – steam oxidation test

- KIT, CRIEPI, KAERI/ SNU - single rod tests – ramp/ isothermal

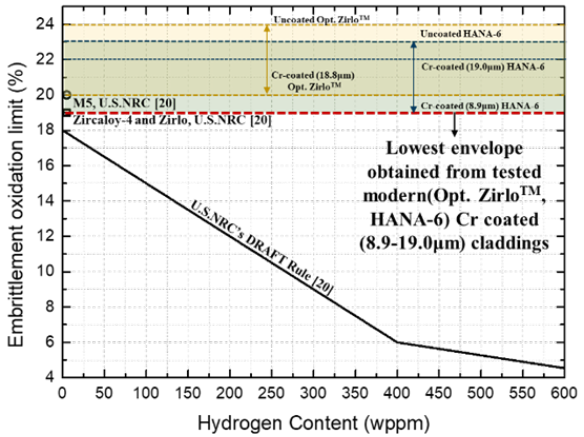

Current ECR a PCT criteria are conservative and can be used for Cr/Zr evaluation. But the degradation mechanisms change significantly.

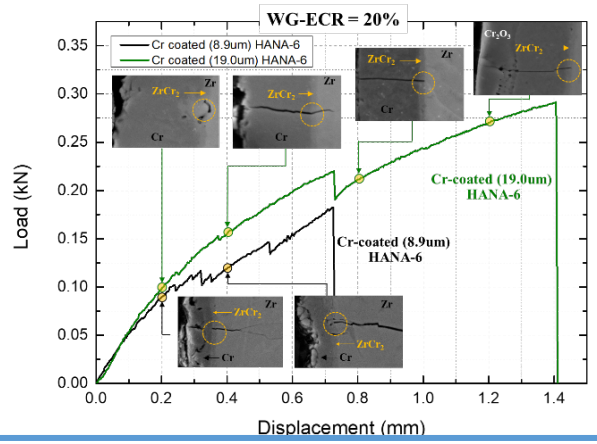

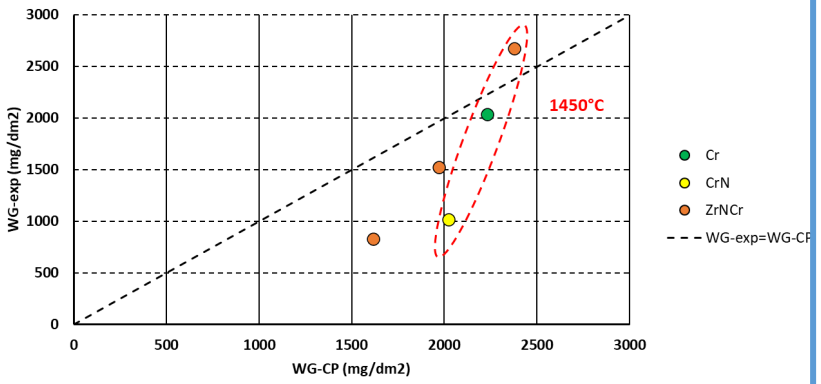

There are alternative materials/interlayers that can delay degradation observed for Cr/Zr.

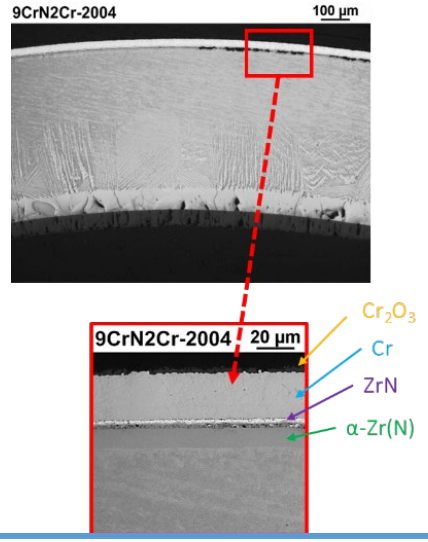

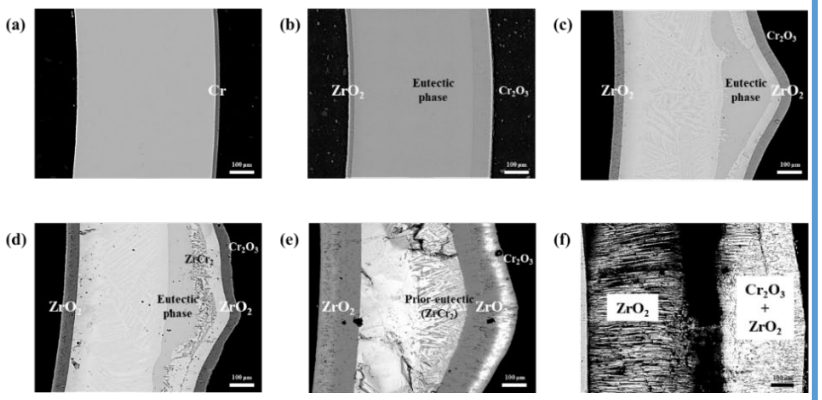

Coating quality and defects are very important for evaluation. There's no generic Cr/Zr cladding.

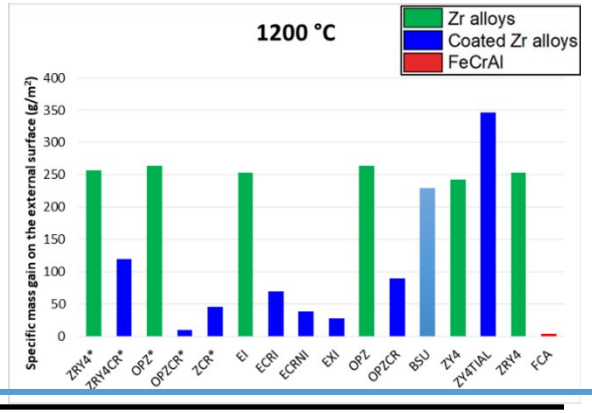

Item	S1'	S2	S3	S4	S5	S6
Coating thickness and materials	-	10 µm Cr	20 µm Cr	16/10 µm Cr/CrN	10 µm Cr	20 µm Cr
Max. Temp. (°C)	1350				1600	
Steam flow rate (g/s)	0.41	0.41	0.46	0.46	0.50	0.46
Heating rate (K/s)*	3.5-1.5	1.5	2.4-1.8	2.5-2.2	3.0-1.6	3.0-1.8
RIP at RT (MPa, He)	6.0					
Gas plenum volume (ml)	10	15	10			
Balloon & burst region	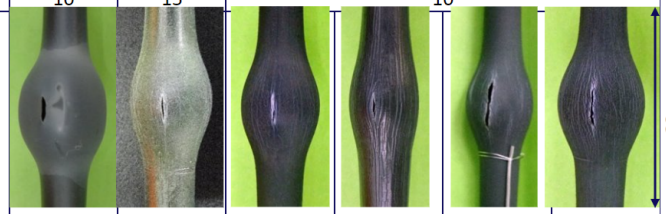					

HT oxidation – Main findings

Coated Zr:

- Eutectic Cr/Zr – another degradation mechanism (e.g. secondary hydriding, oxygen embrittlement), not hard limit (melting point). Effect of coating thickness observed.
- ECR criteria for coated Zr – does not have physical meaning and should be replaced. But it's conservative and can be used by industry if needed.
- CrN/Cr – benefits in BDBA conditions confirmed by CRIEPI, KIT. Open questions remain but it seems like a feasible way to further improve pure Cr coatings.

FeCrAl:

- Focus on FeCrAl HT oxidation kinetics:

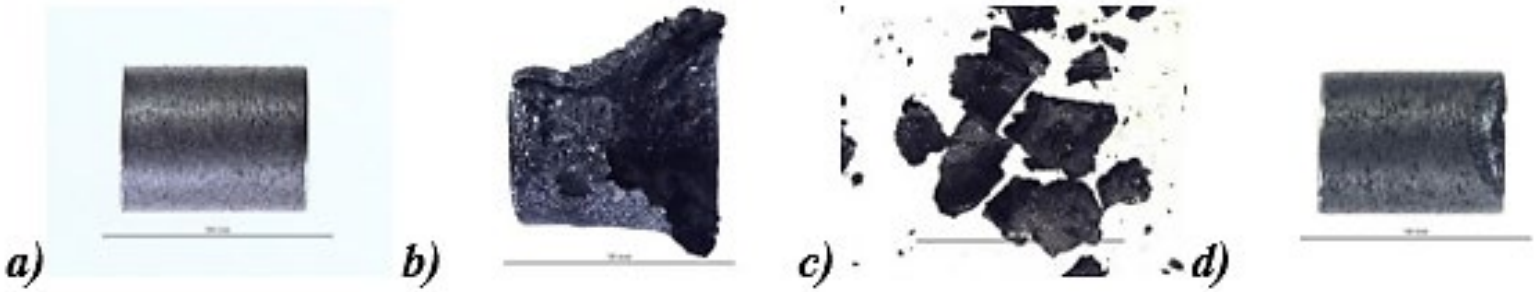

a) 1350 °C/30 min; b) 1360 °C/5 min; c) 1375 °C/30 min d) 1375 °C/RAMP 900.

Conclusions and Summary

- Coordinated Research Project ATF -TS– organized by IAEA between 2019 and 2024.
- ATF-TS was divided into several work packages with strong interlinks – WPs 2, 3 and 4 relied on experimental results from WP1.
- Ten organizations fabricated and shared their ATF cladding materials, and 12 laboratories performed various experimental investigations. Variations in quantities, geometries and preferred partnerships.
- Optimization of fabrication parameters was out of the scope of the project – it was done previously by CRP participants = focus on higher TRLs. Material providers shared the materials based on their preferences and needs.
- Focus mostly on Cr coated Zr – but many different variations produced (substrates, deposition technologies, coating thicknesses, pre - and post -treatment).
- Alternative coating materials proposed and provided to eliminate the drawbacks of Cr/Zr ATF concept. Two types of FeCrAl and one type of SiC were also investigated.
- Detailed fabrication parameters are presented in the TECDOC. The material fabrication parameters should be linked to their performance.

Conclusions and Summary

- 14 laboratories performed various experimental investigations
  - Ballooning and burst – new failure criteria and creep correlations
  - HT steam oxidation – independent evaluation of all degradation mechanisms for all concepts
  - Autoclave corrosion – good performance confirmed even with low coating thicknesses and lower quality.
  - Mechanical performance – complex fracture mechanisms of different coating based on their microstructure (deposition parameters) which will further change with irradiation.
  - + many more tests documented in the TECDOC not covered here (hydrogen uptake, microstructure, thermal shock tests, thermophysical properties…)
- Despite many challenges, ATF -TS was the most successful and productive CRP in the Fuels&Materials area, especially in the experimental field.
- Hundreds of new open datasets, dozens of journal and conference publications, new material correlations and models, validation cases from both, separate effect and integral bundle tests… which provide a good foundation for the new CRP ATF -HBU.

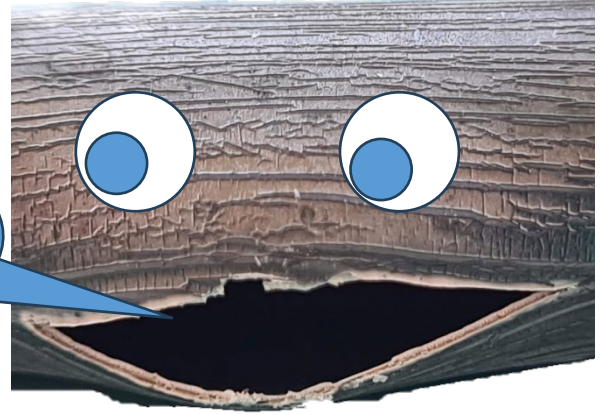

Special thanks to all participants and partners within ATF -TS CRP.

We dedicate the CRP outcomes to the memory of Dr. Giovanni Pastore, who has made a significant contribution to this IAEA CRP and the fuel performance community in general.

Kinya Nakamura

CRIEPI

Development Status of Accident-Tolerant Control Rods in Light Water Reactors at CRIEPI

It is well known that during accident progression in current PWRs and BWRs, degradation of core structural materials such as control rod (CR), grid spacer (GS), and channel box (CB), precedes fuel rod failure (ex. P. Hofmann, 1999). The CR, in particular, is believed to trigger early core damage, as demonstrated by the CORA and QUENCH test series at KIT, the PHEBUS-FP test series at IRSN (now ASNR), and the LEISAN tests at JAEA. Fukushima Daiichi NPP accident enhanced efforts to improve the safety of light water reactors worldwide, and one of the activities is the development and deployment of Advanced Technology or Accident Tolerant Fuels (ATFs). In the near-term, it is envisaged that an ATF concept employing Cr-coated Zr alloy cladding will be practically used with the same core structural materials as currently in use.

PWR CRs using Ag-In-Cd alloys as a neutron absorber are susceptible to overpressure failure of the stainless steel (SS) cladding or damage caused by eutectic between the SS cladding and the Zr alloy guide tube during an accident, causing molten Ag-In-Cd alloy to chemically destroy the Zr alloy guide tube and neighboring fuel rods. BWR CRs using B_4C or Hf as neutron absorbers are susceptible to B_4C/SS eutectic damage to the SS blades and adjacent Zr alloy channel boxes. It has been suggested that the introduction of ATF technology with current CRs may not reduce the risk of early core damage. As one solution to this issue, CRIEPI has been proposing a concept of replacing the neutron absorbers in current PWR and BWR CRs with rare-earth sesqui-oxide-stabilized zirconia or hafnia, which is believed to simultaneously achieve longer life and improved accident tolerance. This concept of Accident Tolerant Control Rod (ATCR) involves replacing only the neutron absorbers while maintaining the current CR design and operating procedures.

This paper summarizes an overview of the current status of the ATCR in terms of neutronic reactivity worth, dimensional stability under thermal neutron irradiation, compatibility with primary coolant under PWR conditions, compatibility with steam and core structural materials at high temperatures, and coexistence with molten fuel at high temperatures leading to significantly reducing the re-criticality risk during accident progression, fuel debris retrieval, and mid- to long-term storage.

Development Status of Accident-Tolerant Control Rods in Light Water Reactors at CRIEPI

Kinya Nakamura, Hirokazu Ohta, Naoki Tarumi

Central Research Institute of Electric Power Industry (CRIEPI)

30th International QUENCH Workshop

Karlsruhe Institute of Technology, Germany

16-18 December, 2025

CRIEPI
Central Research Institute of Electric Power Industry

Outline

1. Current Knowledge on Early Stage of Core Degradation
2. Accident Tolerant Control Rods
   - Concept
   - Roadmap
   - Current Status
3. Conclusion

1. Current Knowledge on Early Stage of Core Degradation

During a SA in LWRs, not only the fuel rods but also core component materials are degraded by high-temperature (HT) chemical reactions and decrease in mechanical strength, accelerating the progression of reactor core degradation.

Control Rod (CR)

- At temperatures above 1200°C, CR cladding (SS) and neutron absorbers (Ag-In-Cd or B_4C) may melt and fail before the fuel rods.
- The molten absorbers may relocate and damage neighboring fuel rods, increasing the risk of early FP release, reactor core degradation, and re-criticality.

Grid Spacer (GS)

- Deformation and damage of GS, made of Zircaloy or Inconel, due to HT oxidation and liquefaction leads to a loss of its function of holding the fuel assemblies in place, accelerating core degradation.

- It has been suggested that the introduction of ATF technology with current core component materials may not reduce the risk of early core degradation.
- Along with the deployment of ATF claddings, it is also crucial to improve the accident tolerance of core component materials.

*1: Z. Hozer, et al., IAEA TM on ATF, IAEA HQ, Oct. 28-31, 2025.

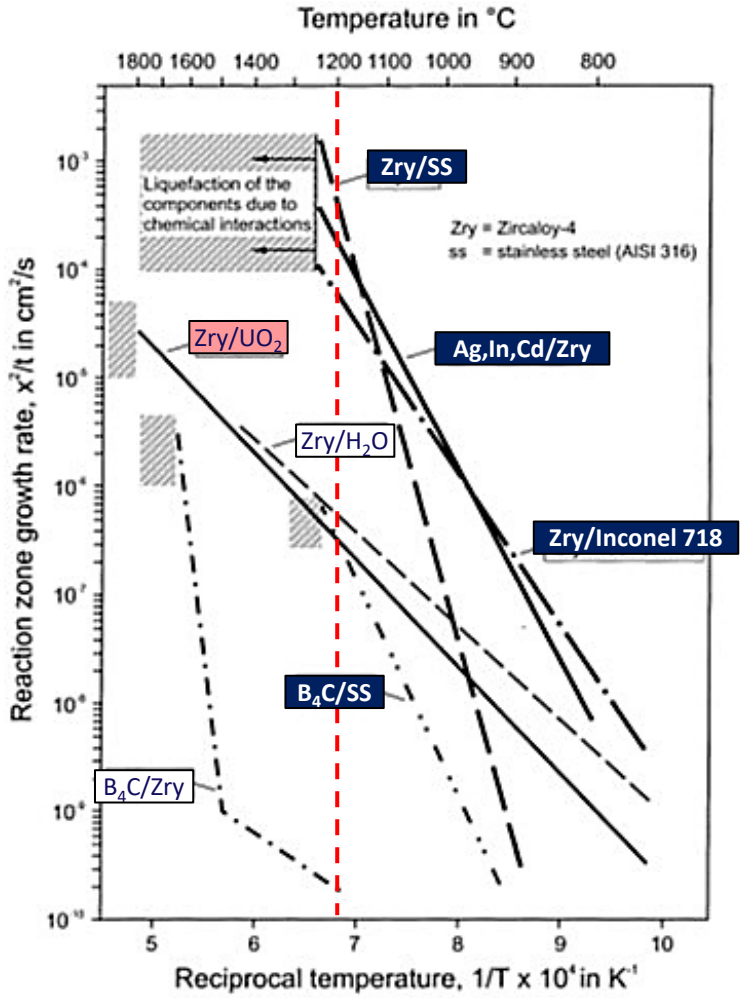

Fig. 10. Total reaction zone growth rates of various reaction couples of fuel element components. In most cases liquefaction of the materials occurs below their melting points.

P. Hofmann, JNM, 1999.

Zry: Zr alloy

1. Current Knowledge on Early Stage of Core Degradation *Control Rods*

PWR

- Degradation of CR, Ag-In-Cd/SS system, at **1200-1400℃**
  - Overpressure failure due to Cd vaporization
  - Eutectic of SS cladding/Zircaloy guide tube
- Molten alloy including Ag may chemically destroy the local fuel rods.

BWR

- Degradation of CR, B_4C/SS system, at **1200-1400℃**
  - Eutectic of B_4C/SS cladding and/or blades, leading to interaction with Zircaloy channel box and local fuel rods

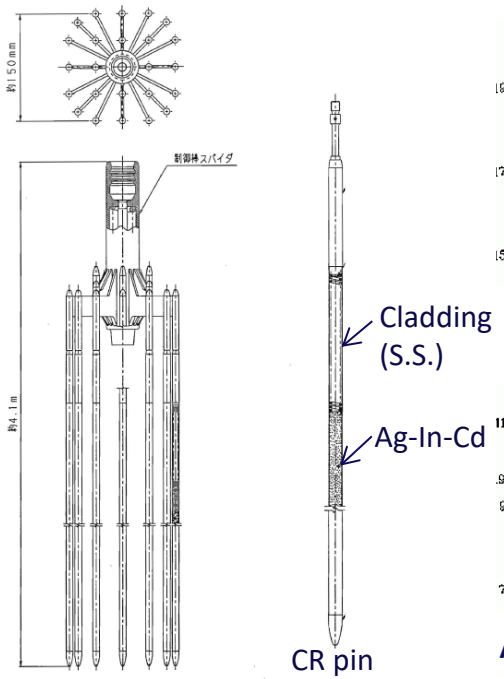

Rod control cluster

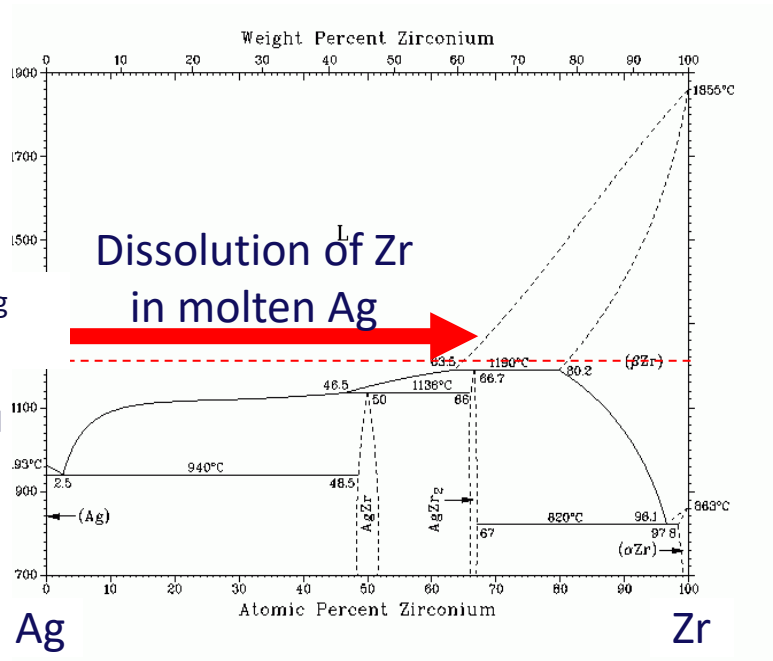

Phase diagram of Ag-Zr binary system

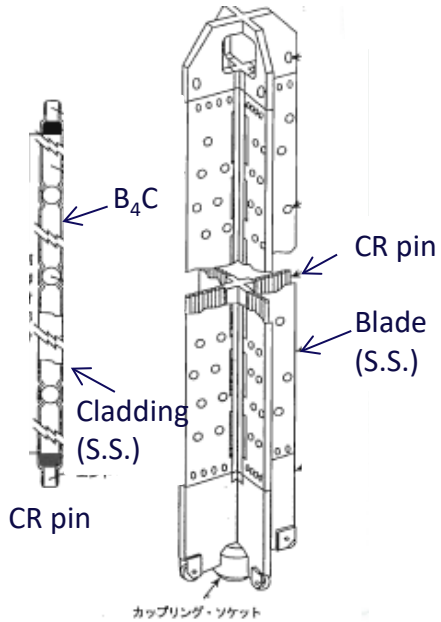

Control blade

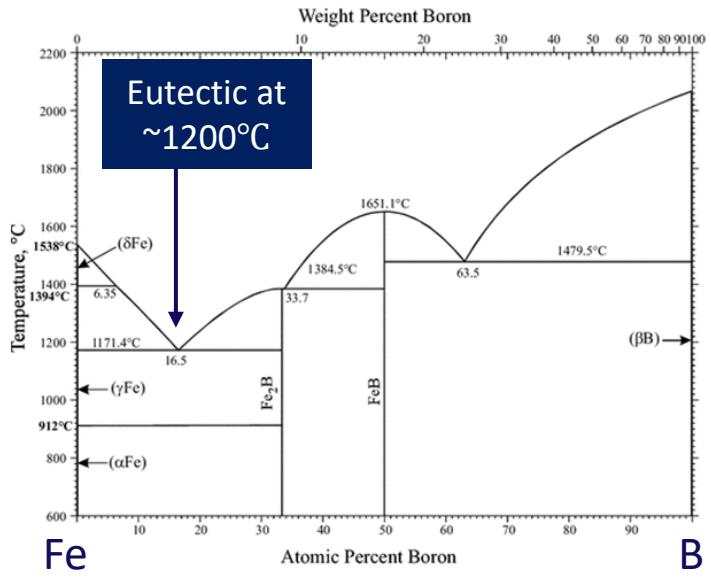

Phase diagram of Fe-B binary system

1. Current Knowledge on Early Stage of Core Degradation *Control Rods*

To investigate the impact of CR failure on early stage of core degradation, series of integral tests have been carried out by CORA, Phebus-FP, CODEX, QUENCH, and LEISAN etc.

Common knowledge

- CR failure before the fuel rods
- HT reactions between CR and core component materials:
  Ex. SS/Zr, Ag/Zr, and B_4C/SS
- Acceleration of local core degradation due to melt relocation
- Increase of the risk of early FP release (such as I and Cs) and re-criticality

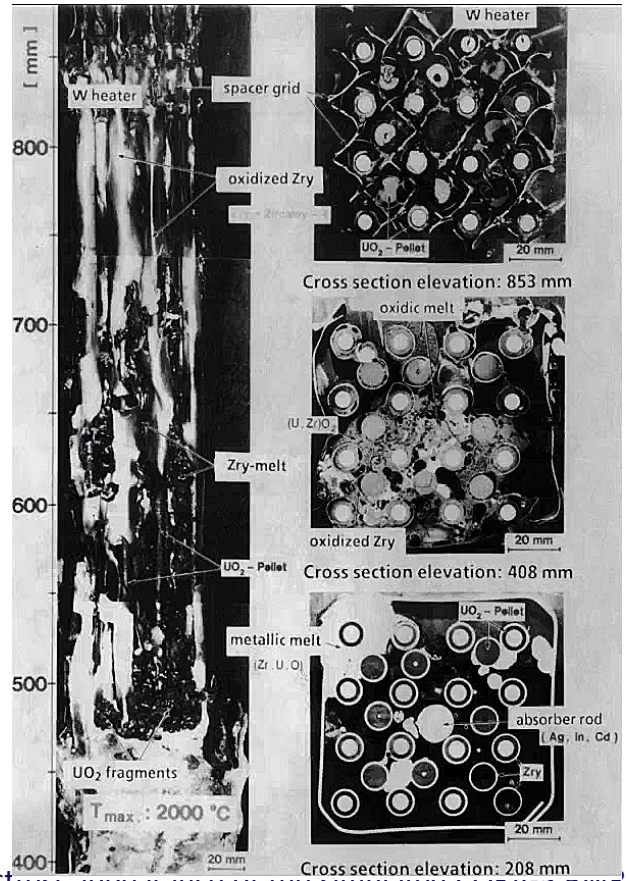

Posttest appearance of the simulated CORA-5 PWR bundle with one Ag-In-Cd absorber rod and Zircaloy guide tube. T_{max}. in the bundle was ~2300 K.

P. Hofmann, NT, 1997.

These knowledge have deepened understanding of core degradation processes and provided an essential foundation for the improvement of SA analysis codes and current ATCR development.

2. ATCR: Concept

Requirements

ATCR should have

- Sufficient neutron absorption effect equivalent to or higher than conventional CRs,
- Higher failure temperature than that of conventional CRs (~ 1200 - 1400 ˚**C**),
- Favorable compatibility with core component materials (SS, Zircaloy or ATF),
- High melting points comparable to fuel failure temperatures (~2300˚**C**), and
- Favorable miscibility with molten corium and fuel debris.

Candidate Materials

For both PWR & BWR,

- Absorber: RE_2O_3 stabilized ZrO_2 or HfO_2, RE (Rare Earth) =Eu or Sm
- Cladding and/or blade: SS, Cr-coated Zircaloy or SiC_f-SiC

BWR

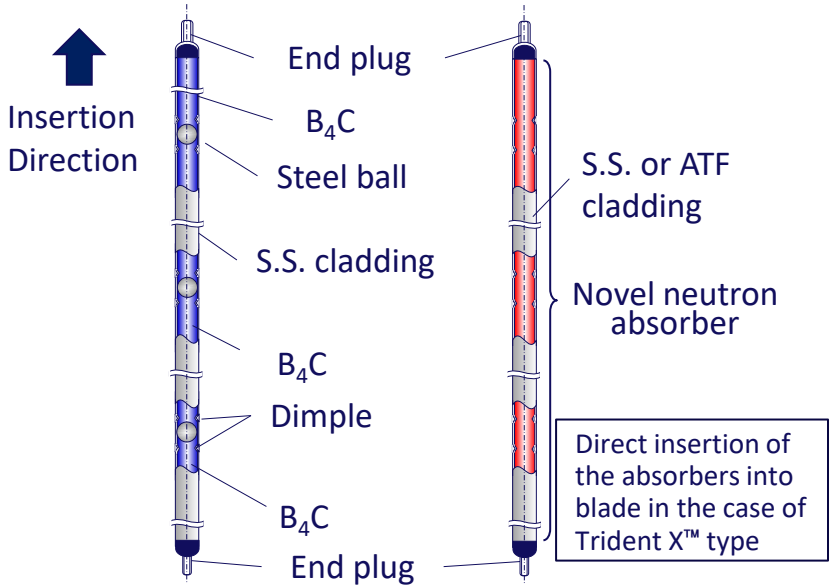

Conventional CR | ATCR

PWR

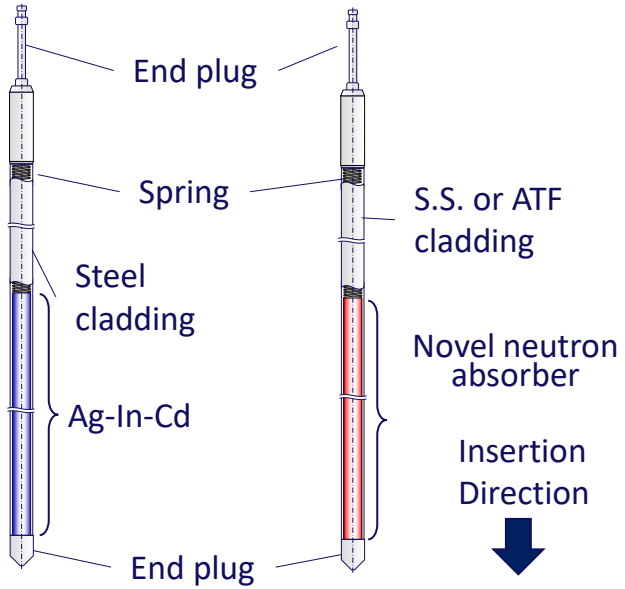

Conventional CR | ATCR

Composition range

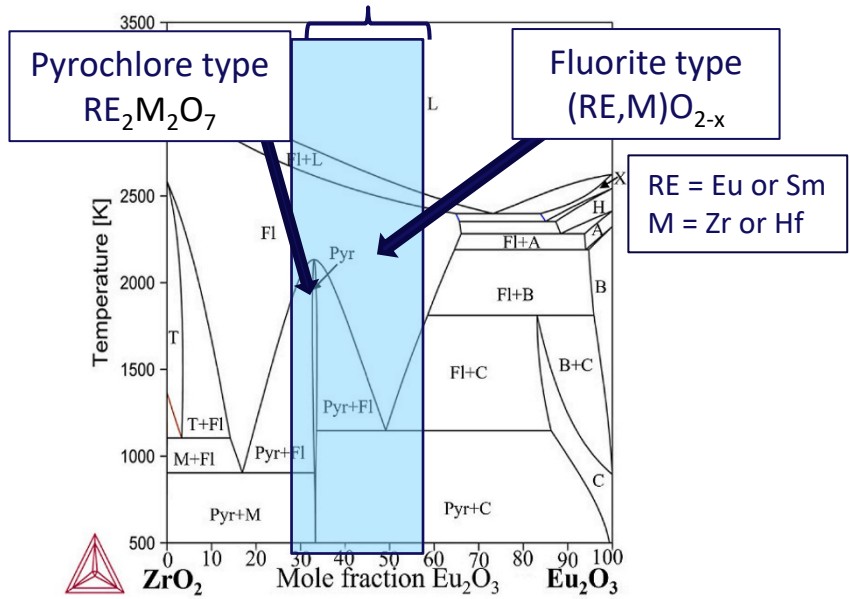

Phase diagram of ZrO_2-Eu_2O_3 system

Qu, Gang, et al., Ceramics International 50.14 (2024): 24948-24959.

2. ATCR: Roadmap

Technology Readiness Levels

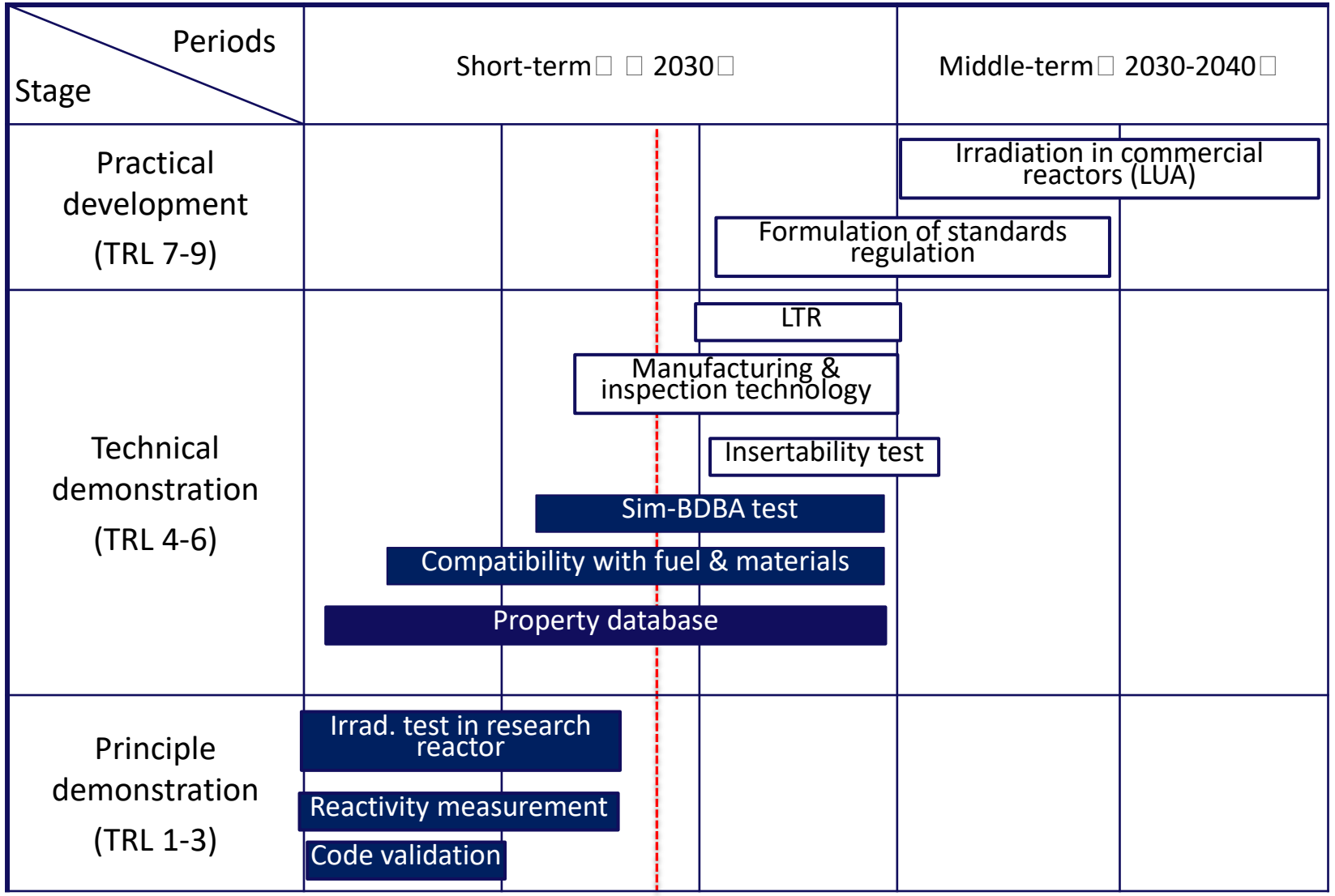

2. Current Status: Neutronic Properties

- Enough neutronic reactivity worth comparable to or higher than the conventional absorbers
- Applicable to conventional CR assemblies without significant change in design and reactor operation
- Extended neutronic lifetime by 2 - 5 times, resulting in reduction of the storage space of used CRs

CR reactivity worth in LWRs (Continuous-energy Monte Carlo code: MVP)

Materials	Reactivity Worth [%Δk/kk']	
	BWR	PWR
Sm_2O_3-HfO_2	-15.9	-5.4
Sm_2O_3-ZrO_2	*(-14.5 ~ -14.7)**	-4.9
Eu_2O_3-HfO_2	-19.2	-6.4
Eu_2O_3-ZrO_2	-18.5	-6.2
B_4C	-18.6	
Ag-In-Cd		-5.2
Composition equivalent worth to B_4C or AIC	Eu_2O_3-50 at% ZrO_2	Eu_2O_3-87 at% ZrO_2

* *Estim$_a$ted value*

Change in neutronic reactivity worth under neutron irradiation

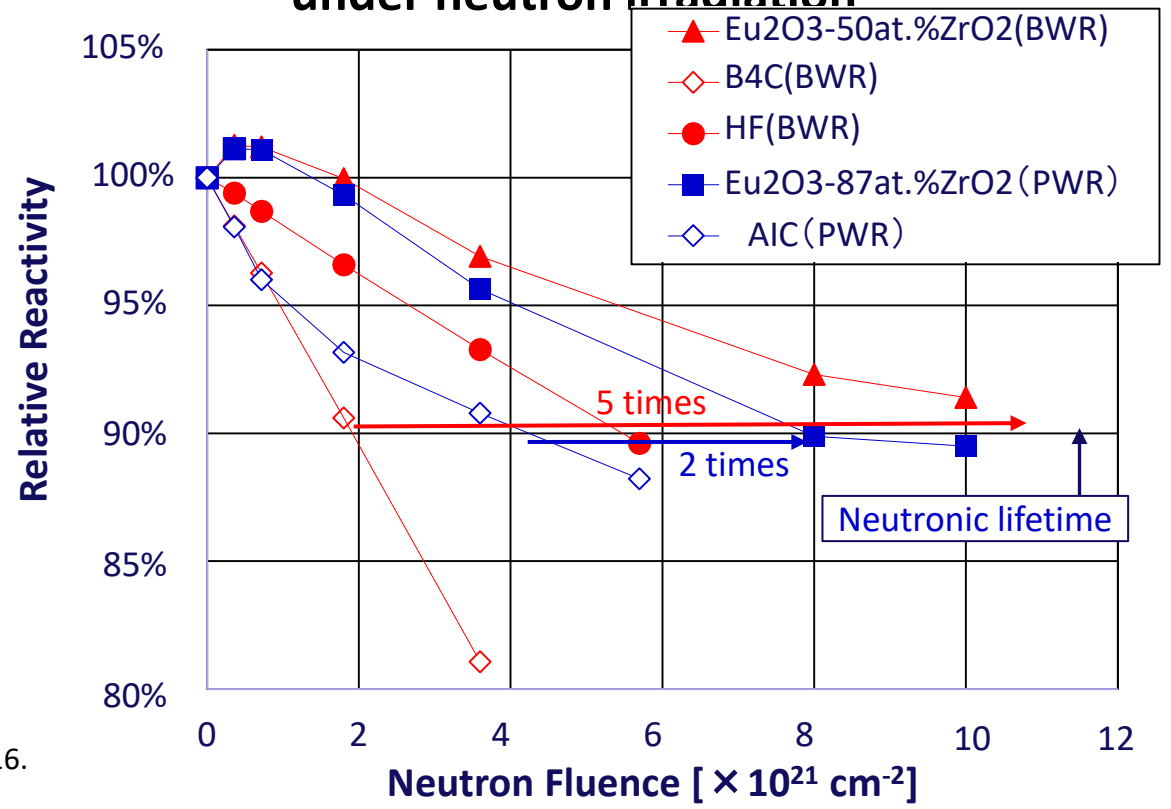

H. Ohta, et al., *Top Fuel 2016*, Boise, Idaho, USA, 11-15 Sep. 2016.
H. Ohta, et al., *AESJ Annual Meeting*, 8 Sep. 2016.

2. Current Status: Neutron Irradiation Stability

- RE isotopes do not generate gases by neutron absorption due to (n,γ) reaction.
- Neutron capture product with the same element and higher mass numbers without change in composition
- Expected lower irradiation swelling than conventional absorbers
- Neutron irradiation test results in research reactor KUR indicated negligible change in weight and dimension under low neutron fluence condition.
- The feasibility of LTR or LUA irradiation tests in a commercial LWR is being investigated.

Weight change of Sm_2O_3-50 mol% ZrO_2 sintered samples after irradiation in Kyoto University Reactor (KUR)

Sample No.	Neutron fluences (n/cm^2)	(1)	(2)	(3)
Pre-irrad.		1.95 mg	6.21 mg	5.15 mg
1st post-irrad.	2.39×10^{19}	1.97 mg	6.15 mg	5.11 mg
2nd post-irrad.	2.13×10^{19}	1.91 mg	6.24 mg	5.16 mg

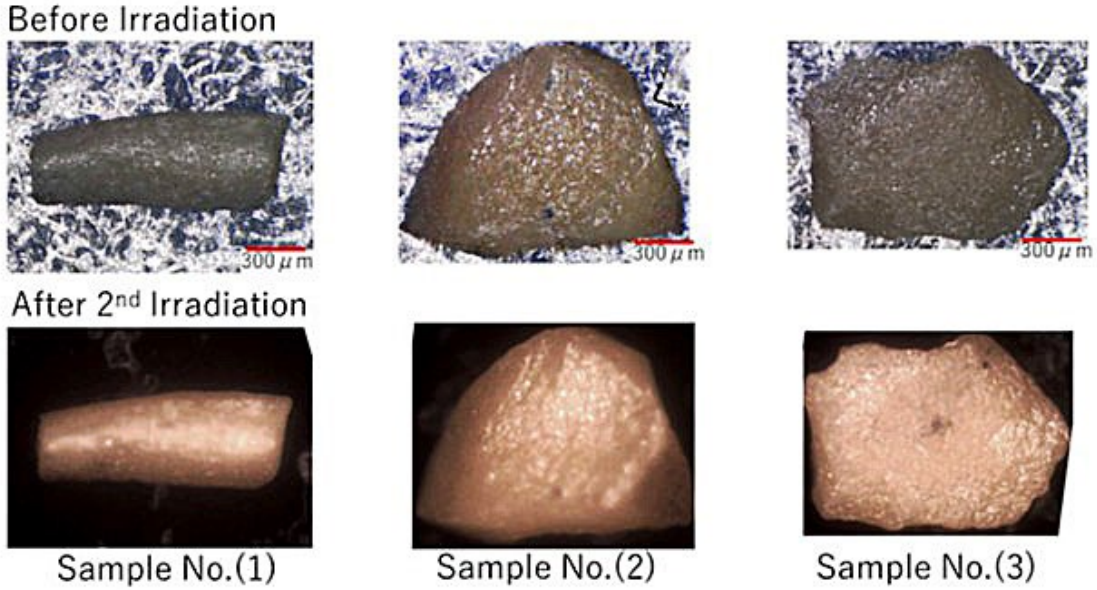

Neutron capture products have also high neutron capture cross-sections.

- $^{151}Eu \rightarrow {}^{152}Eu \rightarrow \underline{^{153}Eu} \rightarrow {}^{154}Eu \rightarrow {}^{155}Eu \rightarrow {}^{156}Eu \rightarrow \cdots$
- $^{146}Sm \rightarrow {}^{147}Sm \rightarrow {}^{148}Sm \rightarrow {}^{149}Sm \rightarrow {}^{150}Sm \rightarrow {}^{151}Sm \rightarrow \underline{^{152}Sm} \rightarrow {}^{153}Sm \rightarrow {}^{154}Sm \rightarrow \cdots$

Red: Natural isotopes, underline: most abundance

H. Ohta, et al., *NuMat 2022*, Ghent, Belgium, October 24-28, 2022.

2. Current Status: Compatibility with core component materials

- Favorable compatibility with core component materials, such as SS, Zircaloy, B_4C, Ag-In alloy, and a mixture of two of these materials, in the temperature range of 1600-2000˚C
- Limited corrosion rate with Cr-coated Zircaloy, FeCrAl, and SiC up to 2000 ˚C
- Good coexistence with $(U,Zr)O_2$ as corium or fuel debris simulant at 2200-2600 ˚C

Experimental Set-up

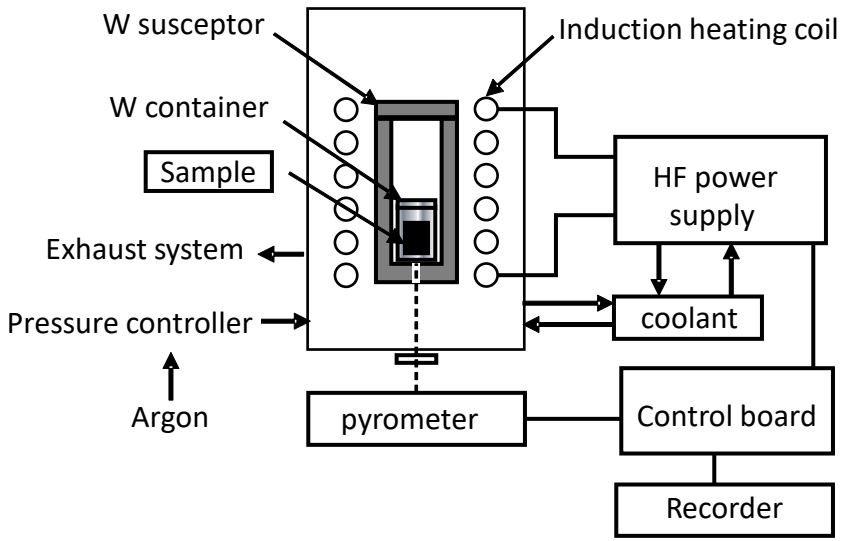

Sample

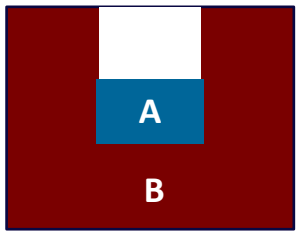

- Temperature: 1600-2000 ˚C
- Holding time: 10-60 min.
- Atmosphere: Argon

Test grid

Concept	**A: core component materials** 5mm in diameter, 3mm height	**B: Neutron absorbers** ID 5.5 mm, IH 7 mm, 5 mm height
SS clad ATCR	➢ Fe ➢ SS ➢ SS+Zircaloy-4 ➢ B_4C ➢ SS+B_4C ➢ Ag-In alloy	➢ fluorite $(Eu,Hf)O_{2-x}$ ➢ fluorite $(Eu,Zr)O_{2-x}$ ➢ pyrochlore $Eu_2Hf_2O_7$
ATF clad ATCR	➢ Zircaloy-4[*1] ➢ FeCrAl[*1,2] ➢ SiC[*1]	➢ fluorite $(Eu,Zr)O_{2-x}$ ➢ fluorite $(Sm,Zr)O_{2-x}$
Molten fuel	➢ $(U,Zr)O_2$	➢ fluorite $(Eu,Hf)O_{2-x}$

[*1] Assumption that unpressurized ATCR cladding tubes will not burst up to 2000°C

[*2] $Fe_{0.777}Cr_{0.13}Al_{0.07}Mo_{0.02}Si_{0.002}Y_{0.0005}$ in wt. fraction

K. Nakamura, et al, 11th EPRI/DOE/INL Joint Workshop on Accident Tolerant Fuel, 28–29 Mar 2022.
K. Nakamura, et al, 27th International QUENCH Workshop 27 - 29 Sep. 2022

2. Current Status: Compatibility with core component materials

SS clad ATCR

* Simulating of ATCR with SS cladding

SS / Eu_2O_3-ZrO_2 at 1600˚C held for 60 min.

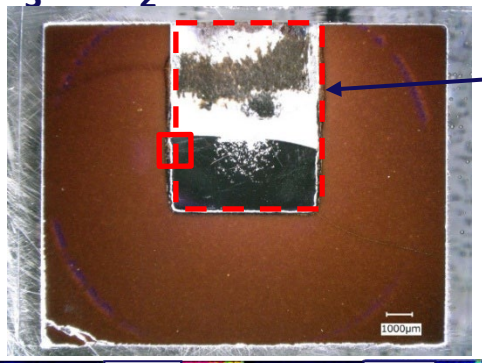

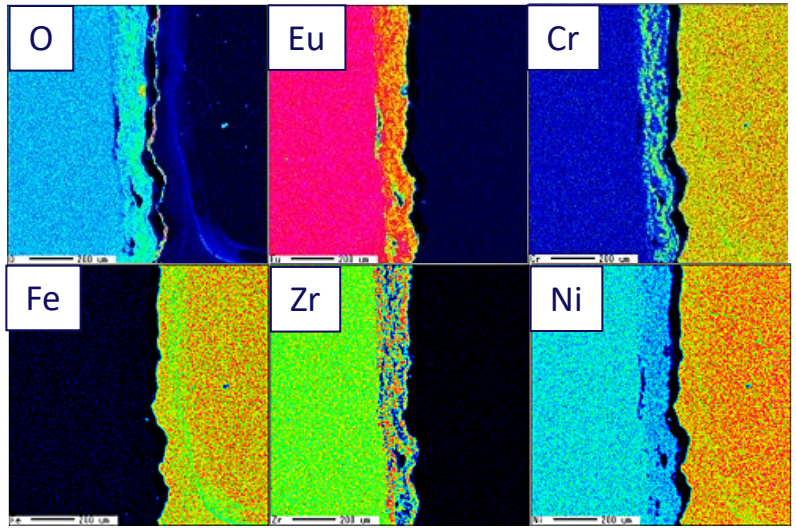

SS / Eu_2O_3-ZrO_2 at 2000˚C held for 10 min.

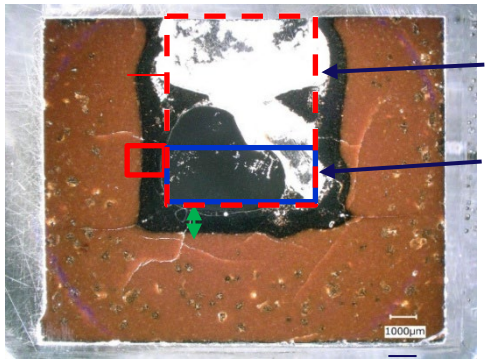

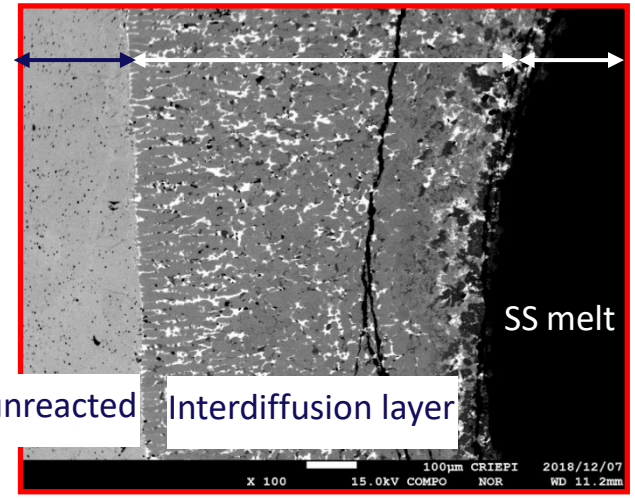

SEI: Secondary electron image,
BEI: Backscattered electron image

- Interdiffusion layer thickness: 140 μm at 1600℃ for 60 min, and 1500 μm at 2000℃ for 10 min

2. Current Status: Compatibility with core component materials

ATF* clad ATCR

* Simulating of Cr coated Zircaloy cladding

	1800℃ for 30 min	2000℃ for 10 min
Zircaloy-4 / Fluorite $(Eu,Zr)O_{2-x}$	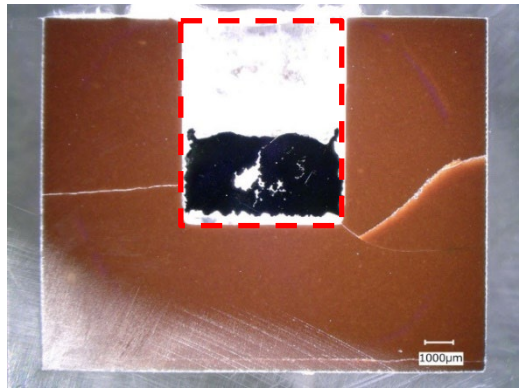	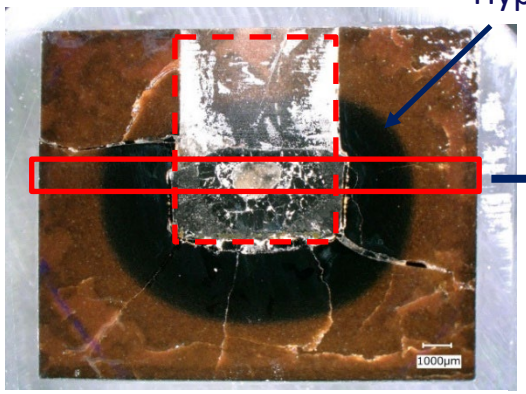
Zircaloy-4 / Fluorite $(Sm,Zr)O_{2-x}$	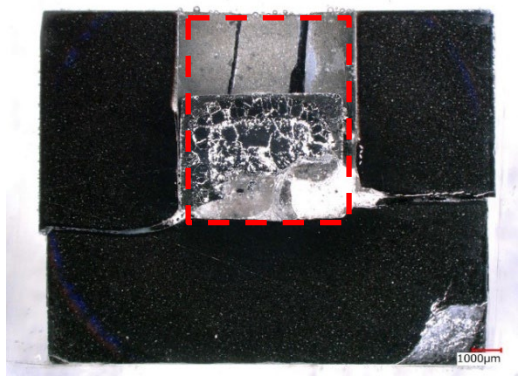	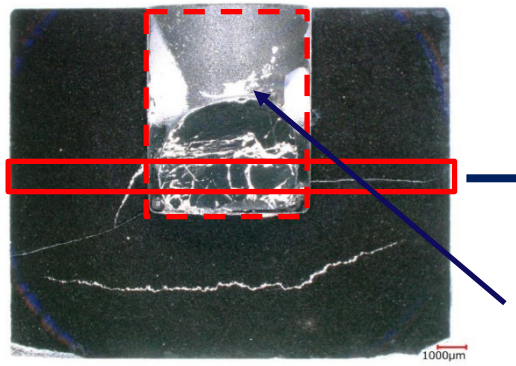

Hypo-stoichiometric composition region

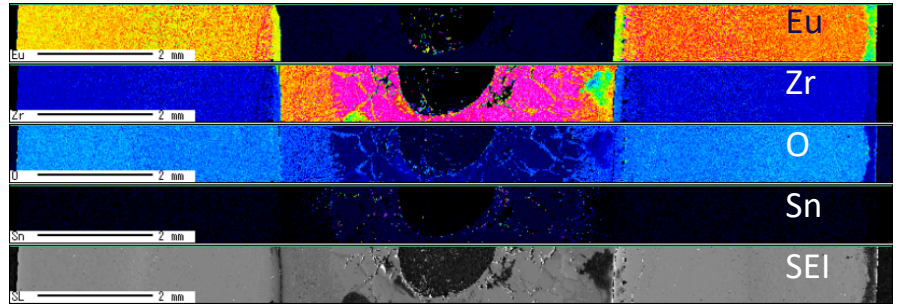

Interdiffusion layer thickness 230μm

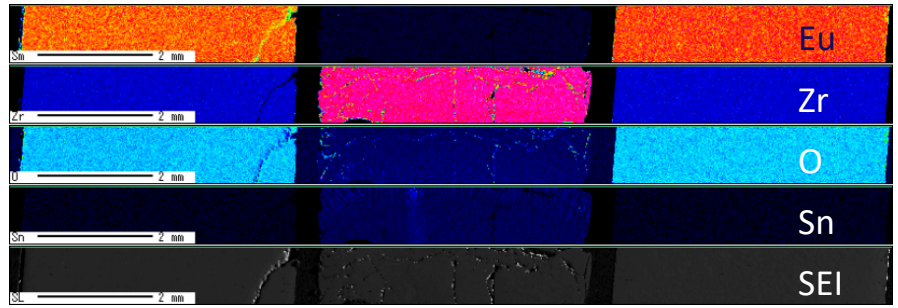

Oxygen stabilized α-Zr as solid

Interdiffusion layer thickness 30μm

- Limited interdiffusion layer formation with oxygen dissolved Zircaloy at both 1800 ℃ and 2000 ℃.
- Diffusion of oxygen in the absorber into the Zircaloy-4 resulted in the formation of hypo-stoichiometric regions in the absorber and the formation of solid α-Zr (O) in Zircaloy-4.

2. Current Status: Late phase severe accident phenomena

Miscibility of $(Eu,Hf)O_2$ and Corium $(U,Zr)O_2$ at 2600℃ for 3 min.

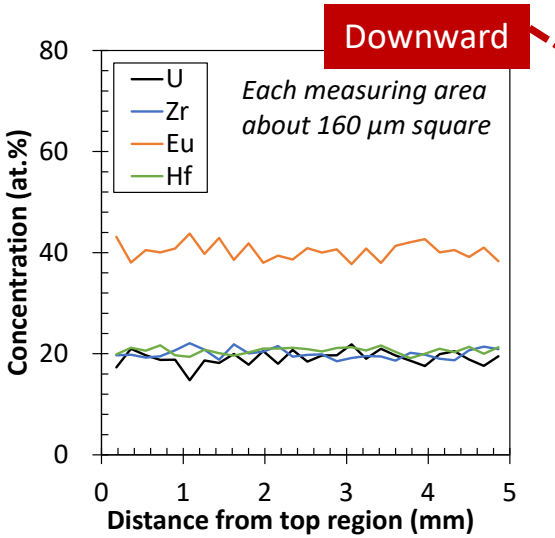

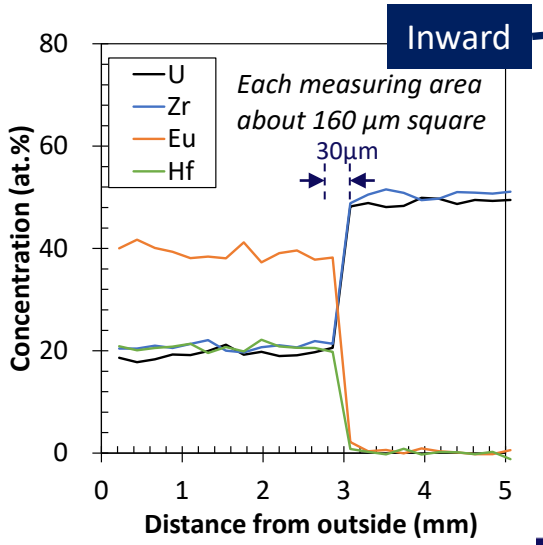

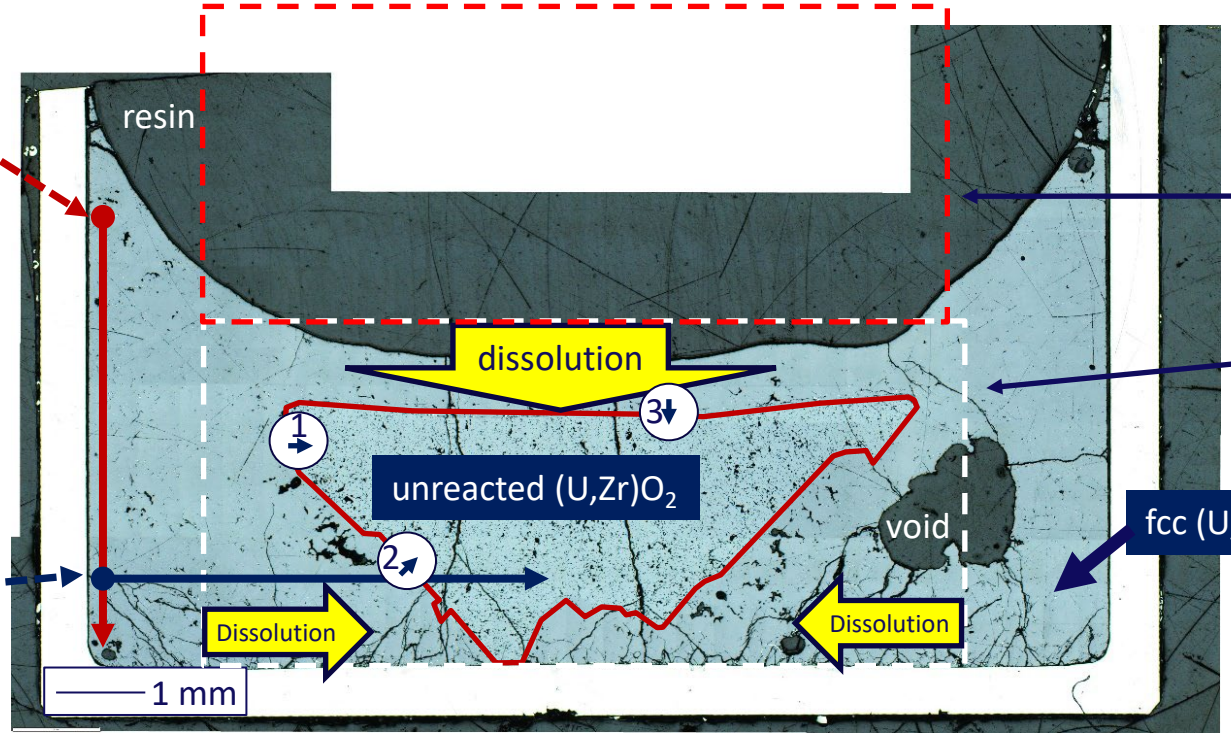

- The molten $(Eu,Hf)O_x$ enveloped the entire $(U,Zr)O_2$ pellet and partially dissolved it to form a **homogeneous fcc-$(Eu,Hf,U,Zr)O_2$ solid solution**.
- Suggesting spreading evenly once dissolved
- A limited solid-liquid interaction layer, ca. 30 μm
- Very high affinity of $(Eu,Hf)O_x$ for molten and resolidified fuel materials

2. Current Status: Stability in Primary Coolant

- RE_2O_3 has a high melting point but is highly hygroscopic when in contact with water or moisture even at room temperature, producing powdered $RE(OH)_3$.
- Mixing with ZrO_2 or HfO_2 as a stabilizer significantly reduce the hygroscopicity.
- Long-term stability of RE_2O_3 - MO_2 sintered pellets in PWR primary coolant water condition was confirmed.

Autoclave tests in PWR primary loop system

- Water volume: 350 L
- Temperature : ~300 ˚C
- Pressure : ~16 MPa
- Water chemistry:
  - B 1248 – 1310 wt ppm
  - Li 6.8 - 7.0 wt ppm
  - H_2 ≤ 2.7 wt ppm
  - O_2 ≤ 0.5 wt ppb
- Period : ~63 days (15, 16, and 32 days)

Samples	Weight change ratio
Sm_2O_3-HfO_2	No data*
Sm_2O_3-ZrO_2	-0.0822%～-0.0075%
Eu_2O_3-HfO_2	-0.0246%～+0.0339%
Eu_2O_3-ZrO_2	+0.0253%～+0.0798%

* Complete powderization due to non-uniform mixing during the manufacturing process

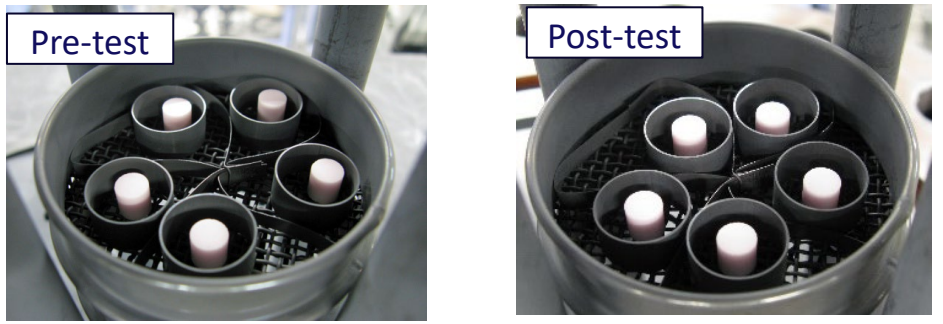

Eu_2O_3-50 mol% ZrO_2 sintered pellets

H. Ohta, et al., *NuMat 2022*, Ghent, Belgium, October 24-28, 2022.

2. Current Status: Manufacturability

- Depending on the CR design, it may be possible to manufacture high-density neutron absorbers such as solid or annular pellets, rods, plates, or granules using conventional manufacturing techniques, such as
  - Powder compaction,
  - Slip casting, and
  - Hot Isostatic Press.

Solid pellets

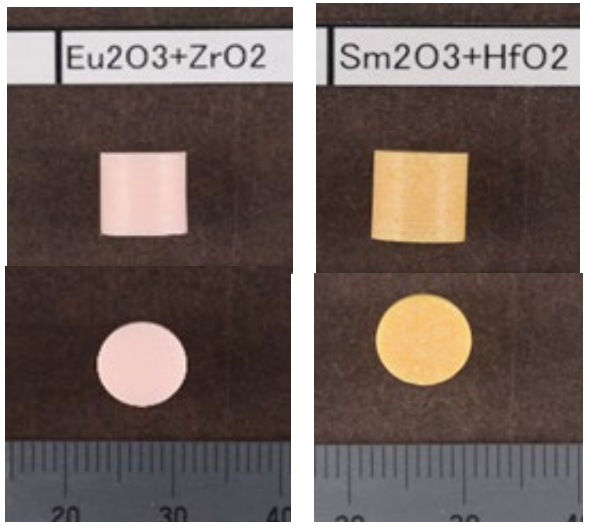

Annular pellets

items	Preliminary specifications	No. 1	No. 2
Chemical composition	Eu_2O_3-50mol% ZrO_2		
Crystal structure	Fluorite-$(Eu,Zr)O_2$		
Outer diameter (mm)	8.0±0.05	7.998	7.983
Inner diameter (mm)	5.0±0.05	5.016	5.020
Height (mm)	8.0±0.05	8.033	8.035
Chamfering	-		
Purity of oxide raw materials	ZrO_2 >99.9%, Eu_2O_3 >99.9%		

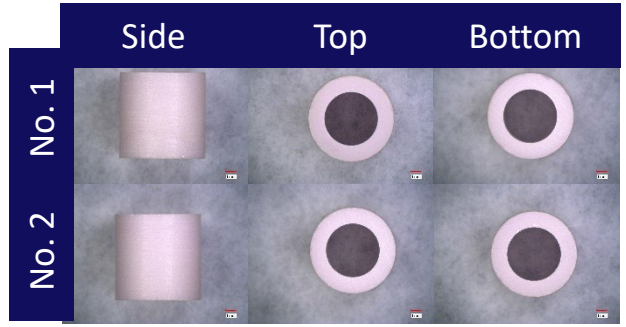

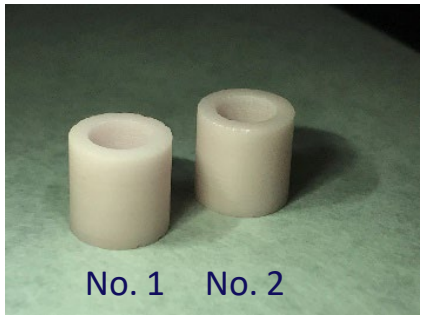

3. Conclusion

- To improve nuclear safety in LWRs, CRIEPI has been developing a concept of ATCR, which replace the neutron absorbers in current PWR and BWR with rare-earth sesqui-oxide-stabilized zirconia or hafnia, which is believed to simultaneously achieve extension of lifetime and improved accident tolerance.
- Overview of the current developments of the ATCR was summarized:
  - Neutronic Properties
  - Neutron Irradiation Stability
  - Compatibility with core component materials
  - Late phase severe accident phenomena
  - Stability in Primary Coolant
  - Manufacturability
- ATCRs with extended neutronic lifetime, will not be damaged before fuel failure in accidents, which is expected to reduce the risk of early core damage, early release of FPs, and re-criticality.

Why not add these to your wish list in 2026?

FDR2026

NUTHOS-15
Kashiwa-no-ha, JAPAN

September 28 - October 1, 2026.

Kashiwa-no-ha, Chiba, JAPAN

1 hour by train or bus from Narita Airport

Abstract Deadline: Dec. 31, 2025 Extended

Topics:

- General Thermal-Hydraulics
- Advanced Thermal-Hydraulics
- Plant Operations
- Regulation, Accident Analysis and Source Term
- Thermal Hydraulics and Safety of Advanced Reactors
- Machine Learning and Artificial Intelligence
- Big Data Applications
- Advanced-Technology Fuels

Technical Tour: Fukushima-Daiichi NPP

TopFuel 2026 TOKYO

October 02-05, 2026

J-Village, Naraha, Fukushima, JAPAN

4+ hours by train from Haneda Airport

Abstract Deadline: April 30, 2026

Tracks:

- Accident Analysis, Fuel Debris Retrieval
- Robot Technology, Remote Control System
- Radiation Measurement and Analysis
- Waste Management

Technical Tour: Fukushima-Daiichi NPP

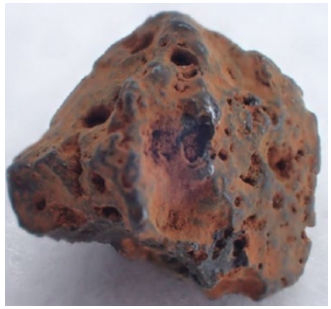

October 12 - 15, 2026

Shinagawa, Tokyo, JAPAN

30 min by train from Hanada Airport

Abstract Deadline: Jan 16, 2026

Tracks:

- Operation and Experience
- Advances in Designs, Materials, and Manufacturing
- Evolutionary and Innovative Advanced Technology Fuels (ATF)
- Modeling, Analysis, and Methods
- Transient Fuel Behavior and Safety Related Issues
- Used Fuel Storage, Transportation, and Re-Use
- Advanced Reactor Fuel Designs and Performance

CRIEPI
Central Research Institute of Electric Power Industry

Thank you for your attention!

Robert Farkas

HUN-REN EK

Post-test examination of the integral air ingress experiment CODEX-ATF-AIT

The CODEX-ATF-AIT integral air ingress test was successfully performed at the HUN-REN Centre for Energy Research (EK), Budapest. The test section included an electrically heated seven-rod bundle composed of Cr coated optZIRLO^{TM} cladding tubes provided by the Czech Technical University in Prague (CTU). The design of the test section was similar to the previous CODEX tests [1][2][3].The fuel rods were filled with zirconia pellets. The rods were pressurized by krypton. The bundle was fixed by Cr coated Zr spacer grids. Electrical heating with two tungsten heaters in each rod was used. External heating was also applied to the test section. The bundle was covered by a Cr-coated Zr shroud and several thermal insulation layers. The proposed scenario focused on covering several phenomena of fuel behavior during accidents (burst, oxidation, nitriding, eutectic formation).

In the preparatory phase the facility was heated up to 600 °C in steam – argon flow using both external heaters and fuel rod heaters. The pre-oxidation phase continued with the same flow rates and with stepwise increased heating power on the rods. During the heat-up phase the rods were pressurized and cladding burst took place between 750-800 °C on most of the rods. The opening allowed the coolant to enter the rods and start chemical reactions on both sides of the cladding. In the intermediate cool-down phase the temperatures were reduced below 750 °C. In the steam-air phase the temperature increase was very smooth compared to the reference experiment CODEX-AIT-3 [2]. The reason of the slower temperature increase was the protective effect of the Cr coating. The duration of air ingress phase in the reference experiment was 1 hour with 1600 °C maximum cladding temperature, and it was 1.5 hour in the CODEX-ATF-AIT with 1545 °C maximum cladding temperature. The temperature profile significantly changed during the air ingress phase similar to the reference experiment: the maximum temperature moved from the upper section of the bundle to lower elevations due to the intense chemical interactions in the less oxidized and/or melted lower part. The maximum shroud temperature was similarly around 1470 °C at 300, 500 and 700 mm elevations.

The outlet gas composition showed that during the air ingress phase steam and oxygen starvation conditions were established. The partial consumption of nitrogen indicated the formation of nitrides as well. The total of 1.4 g hydrogen was produced during the pre-oxidation phase and 3.3 g of hydrogen during the air ingress phase. Slow cool-down of the bundle was performed in argon flow in order to avoid interactions that might take place during water quench.

Post-test examinations (endoscopy, LOM, SEM, EDX) focused on the identification of cladding degradation mechanisms. At the lower half of the bundle (between about 200 and 500 mm) the rods did not suffer any ballooning and the Cr coating remained intact and could prevent the zirconium oxidation in the pre-oxidation phase. The main degradation mechanism of rods at these elevations was the Cr-Zr eutectic melt formation (Cr diffused into the Zr cladding wall to a large extent) and its fast oxidation/nitriding in the last phase of the experiment. From 600 mm upwards, all the pressurized rods were ballooned and the Cr coating became cracked on their surfaces. The zirconium oxidation started locally through the cracks of the Cr layer in the pre-oxidation phase and continued in the air ingress phase. These rods were strongly oxidized and nitrided. The oxygen penetrated into the zirconium metal prohibited the Cr diffusion into the cladding wall. The cladding tube walls often cracked through where the local oxidation started. In the case of the non-pressurized rod, the Cr coating remained intact and could prevent the zirconium oxidation both in the pre-oxidation phase and air ingress phase because of the not too high (lower than the Cr-Zr eutectic formation) temperatures at these elevations of the bundle.

The CODEX-ATF-AIT test showed that under high-temperature air ingress accident conditions, the bundle with Cr-coated components exhibited a longer coping time compared to bundles with conventional fuel materials. The observed fuel degradation phenomena were similar in both cases; however, the presence of the Cr coating led to eutectic formation and localized melting.

[1] Farkas, R., Hózer, Z., Nagy, I., Vér, N., Szabó, P., Horváth, M., Kostka, P., Lajtha, G. (2023). Experimental simulation of selected design extension condition scenarios without core meltdown in the CODEX facility. *Progress in Nuclear Energy*, 161, 104720.

[2] Farkas, R., Hozer, Z., Nagy, I., Ver, N., Horvath, M., Steinbrück, M., Stuckert, J., Grosse, M. (2022). Effect of steam and oxygen starvation on severe accident progression with air ingress. *Nuclear Engineering and Design*, 396, 111884.

[3] Hózer, Z., Windberg, P., Nagy, I., Maróti, L., Matus, L., Horváth, M., Csordás, A., P., Balaskó, M., Jani, P. (2003). Interaction of failed fuel rods under air ingress conditions. *Nuclear Technology*, 141(3), 244-256.

HUN REN | Centre for Energy Research

HUN-REN Hungarian Research Network

Post-test examination of the integral air ingress experiment CODEX-ATF-AIT

Róbert Farkas, Nóra Vér, Berta Bürger, Zoltán Hózer, Anna Pintér-Csordás

30th International QUENCH Workshop
Karlsruhe Institute of Technology, Campus North, H.-von-Helmholtz-Platz 1, 76344 Egg.-Leopoldshafen, Germany
16-18 December 2025

Objectives

Integral testing of accident tolerant fuel design under air ingress conditions (CODEX-ATF-AIT)

- The CODEX-ATF-AIT experiment was performed in the framework of the EU OFFERR project.
- The main objective of the proposed test was to check if Cr coating would have a protective role in case of NPP accidents with air ingress.
- The proposed scenario was focused on covering several phenomena of fuel behavior during accidents
  - burst,
  - oxidation,
  - nitriding,
  - eutectic formation.
- CODEX-AIT-3 experiment was chosen for reference test which was an air ingress test conducted with traditional Zr materials.

Test facility

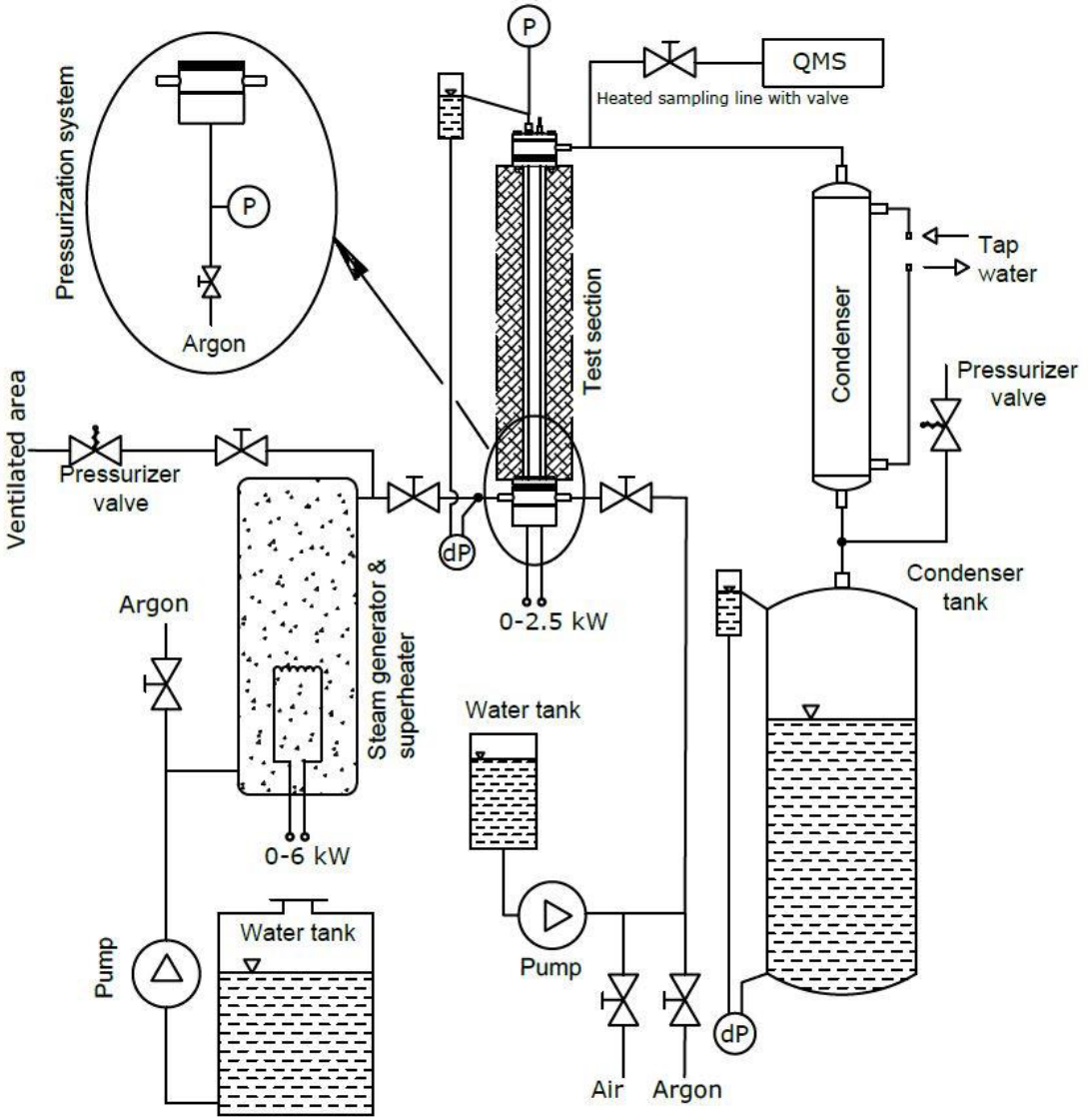

Schematic view of the CODEX facility

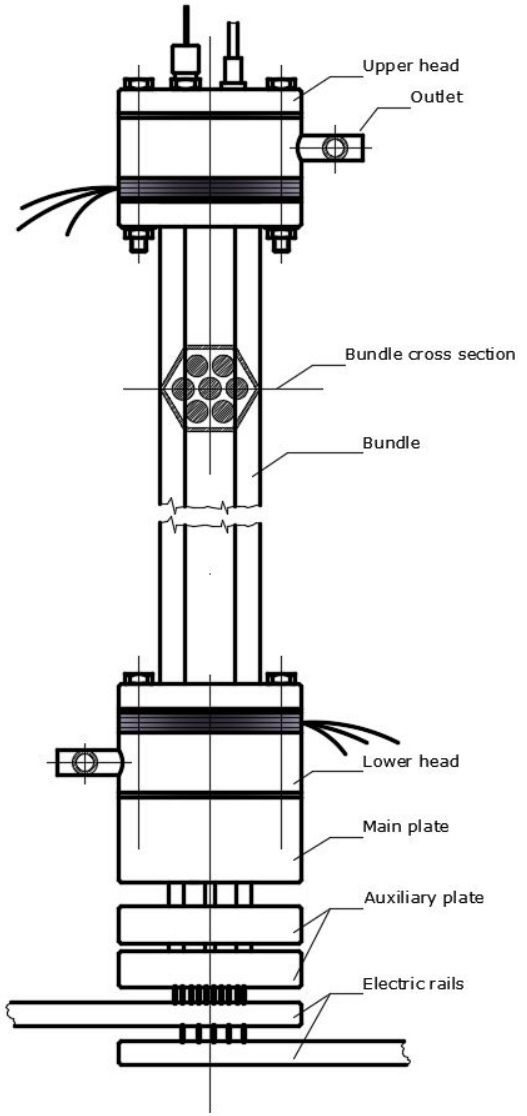

View of the test section with seven-rod bundle

Test section and bundle design

- VVER bundle type:
  hexagonal arrangement of 7 rods

- 6 rods electrically heated with tungsten heaters
  1 rod unheated
  - CODEX-AIT-3: rod No. 1. (in the center)
  - CODEX-ATF-AIT: rod No. 7. (periphery)

- Rods pressurized
  - CODEX-AIT-3: rod No. 1. (in the center) pressurized with Ar
  - CODEX-ATF-AIT: all rods pressurized with Kr except rod No. 6.

- ZrO_2 ceramic pellets

- 3 spacer grids

- Hexagonal shroud

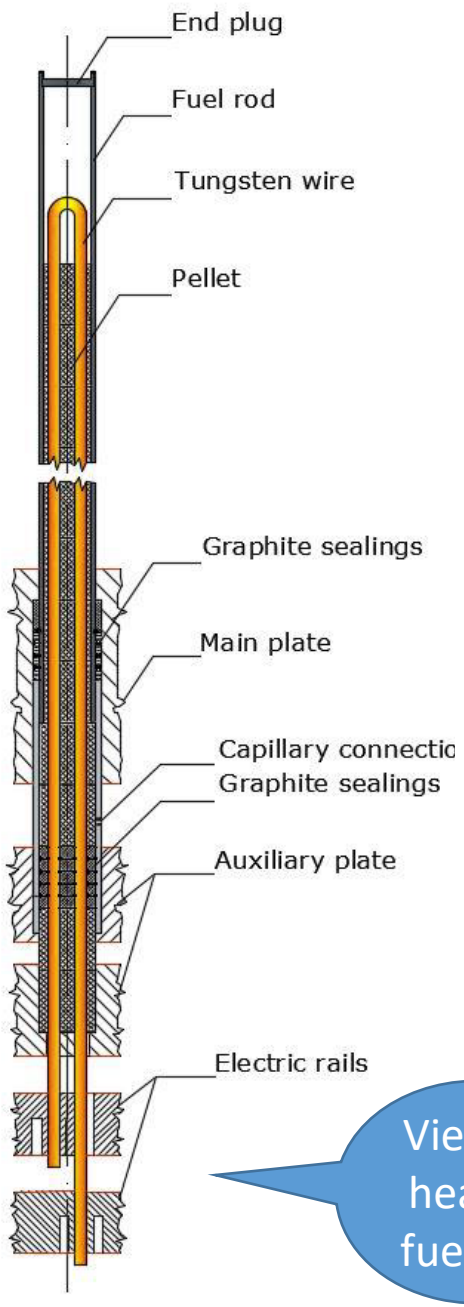

View of heated fuel rod

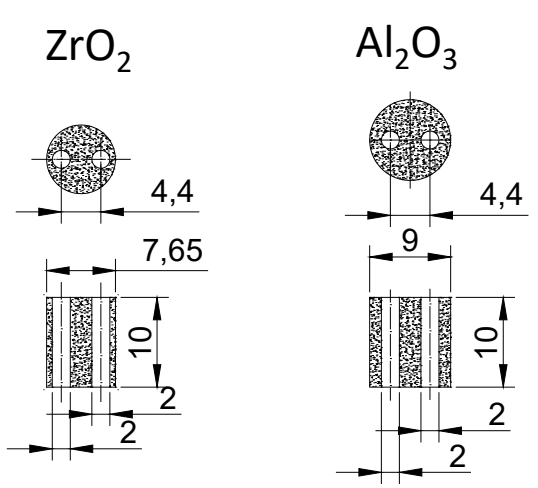

View of ceramic pellets

Cross section of the test section

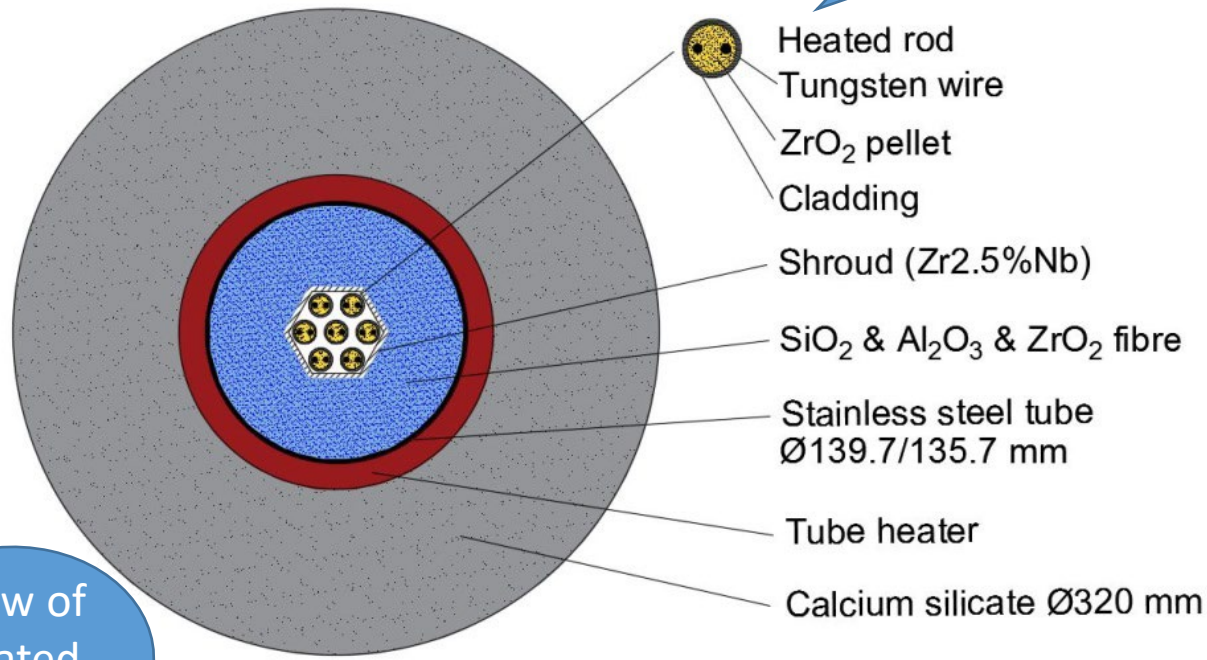

Assembly of the CODEX facility

Main characteristics of the test section

CODEX-AIT-3
Reference test

Number of fuel rods	7
Cladding of fuel rods	**E110G**
Length of fuel rods	**1000 mm**
External diameter of fuel rods	9.1 mm
Cladding wall thickness	0.69 mm
Pellet material	ZrO_2
Pellet material in the bottom of the rods	Al_2O_3
Height of pellet	10 mm
Diameter of pellet	7.65 mm
Hole diameter in the pellet	2 mm
Spacer grid material	**Zr1%Nb**
Height of spacer grid	10 mm
Thickness of spacer grid	0.4 mm
Number of spacer grids	3
Shroud material	**Zr2.5%Nb**
Shroud thickness	2 mm
Length of shroud	1000 mm

CODEX-ATF-AIT

Number of fuel rods	7
Cladding of fuel rods	**Cr-coated optZIRLO™**
Length of fuel rods	**900 mm**
External diameter of fuel rods	9.1 mm
Cladding wall thickness	0.57 mm
Pellet material	ZrO_2
Pellet material in the bottom of the rods	Al_2O_3
Height of pellet	10 mm
Diameter of pellet	7.65 mm
Hole diameter in the pellet	2 mm
Spacer grid material	**Cr-coated Zr1%Nb**
Height of spacer grid	10 mm
Thickness of spacer grid	0.4 mm
Number of spacer grids	3
Shroud material	**Cr-coated Zr2.5%Nb**
Shroud thickness	2 mm
Length of shroud	1000 mm

Cr coating: Czech Technical University in Prague, PVD technique

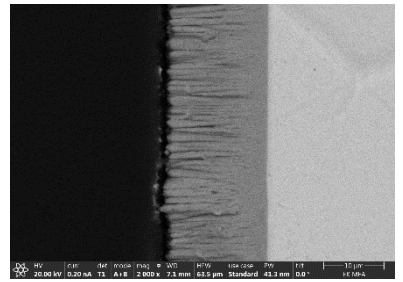

Uniform Cr coating layer around the circumference of the cladding ~**15.5 µm**

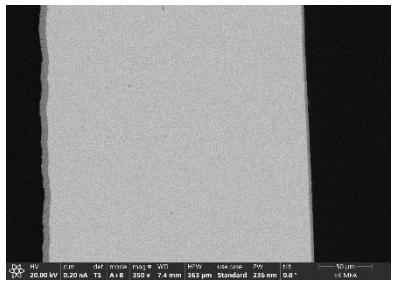

Thickness of the Cr layer on spacer grid

- at the straight sections almost uniform ~**10 – 12 µm**
- at the curved parts ~**2 – 3 µm**

Measurements

On-line measurements and data acquisition:

- **temperatures** (rod surfaces, others: shroud, stainless steel tube, coolant , off-gas, …)
- **pressures** (system and rods),
- **flowrates** (argon, air),
- **power**,
- **outlet gas composition**.

Thermocouple positions

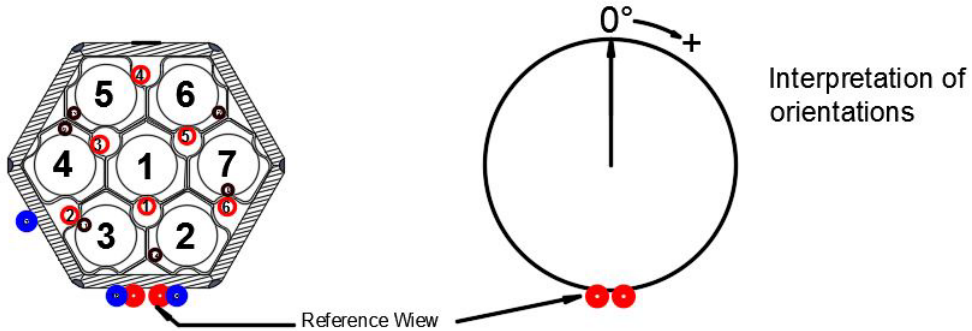

① W5Re/W26Re at elevation 850 mm with orientation of 180°
② W5Re/W26Re at elevation 650 mm with orientation of 300°
③ W5Re/W26Re at elevation 750 mm with orientation of 60°
④ W5Re/W26Re at elevation 650 mm with orientation of 60°
⑤ W5Re/W26Re at elevation 750 mm with orientation of 180°
⑥ W5Re/W26Re at elevation 500 mm with orientation of 180°

High temperature thermocouples (6 pieces)

⑦ "K" type at elevation 50 mm with orientation of 0°
⑩ "K" type at elevation 50 mm with orientation of 180°
⑪ "K" type at elevation 150 mm with orientation of 300°
⑫ "K" type at elevation 150 mm with orientation of 120°
⑬ "K" type at elevation 500 mm with orientation of 240°
⑭ "K" type at elevation 200 mm with orientation of 240°
"K" type at elevation 750 mm
"K" type at elevation 650 mm
"K" type at elevation 500 mm

K-type thermocouples (26 pieces)

Power

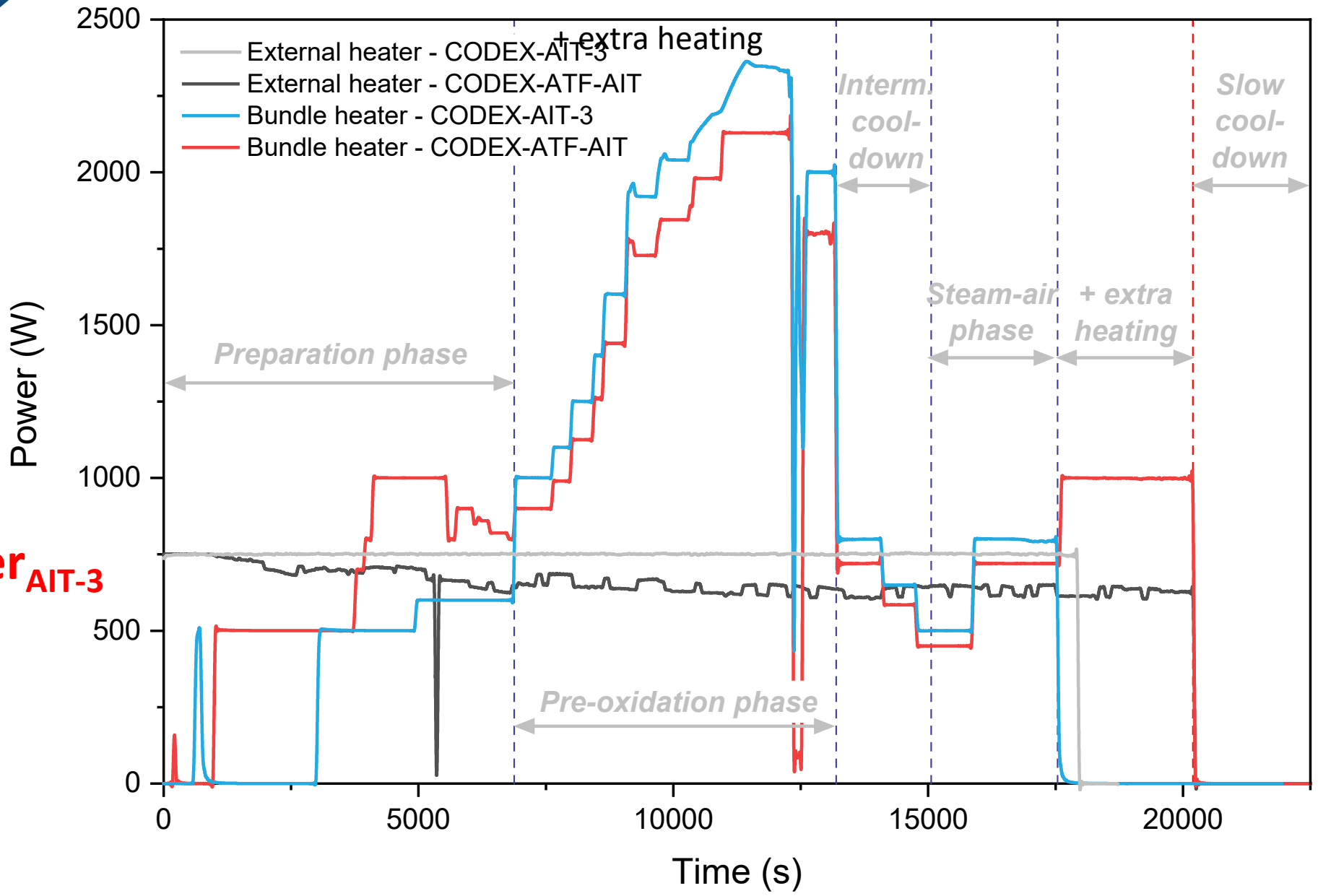

0.9 x Power$_{AIT-3}$

Rod pressures

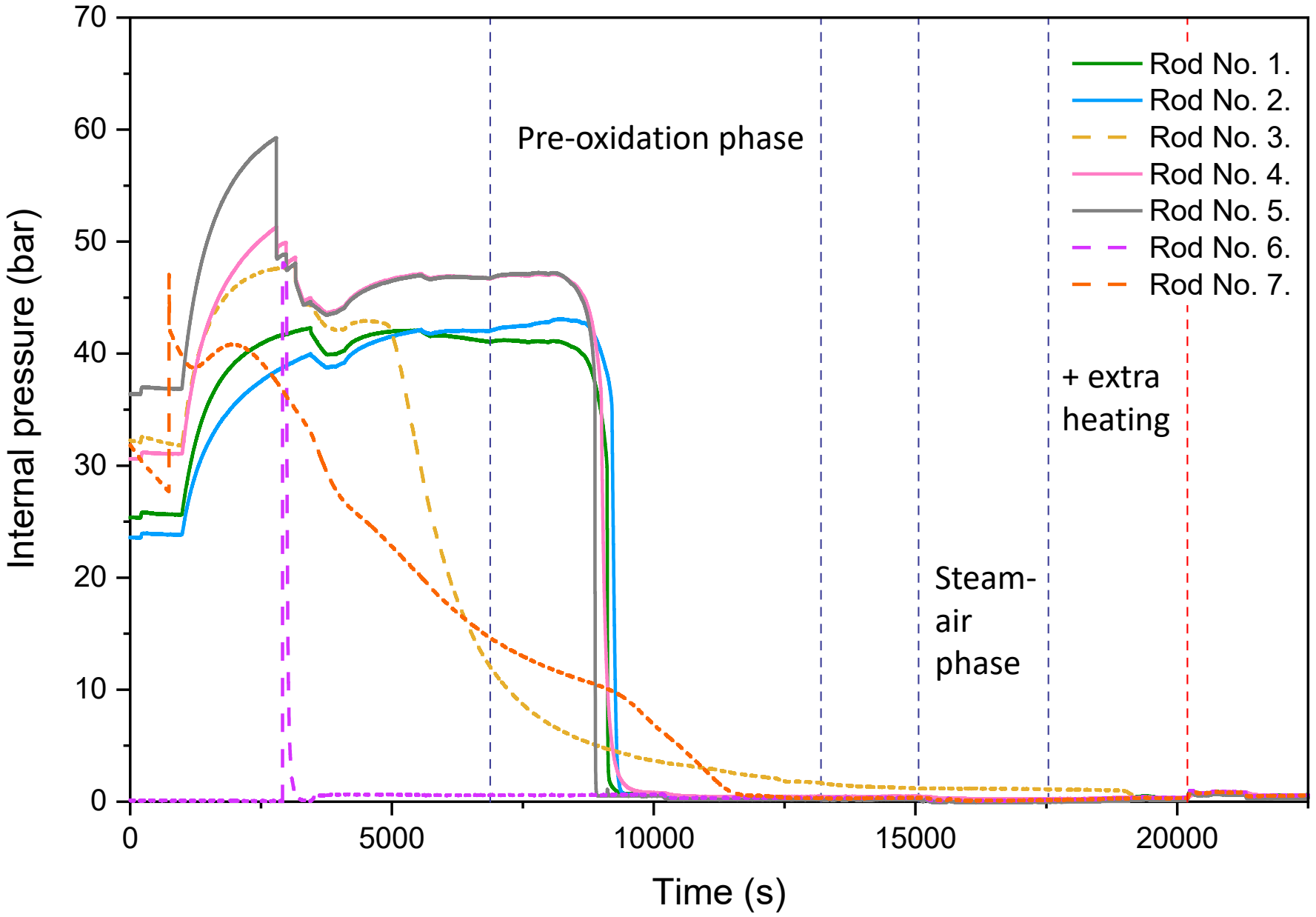

Rod temperatures

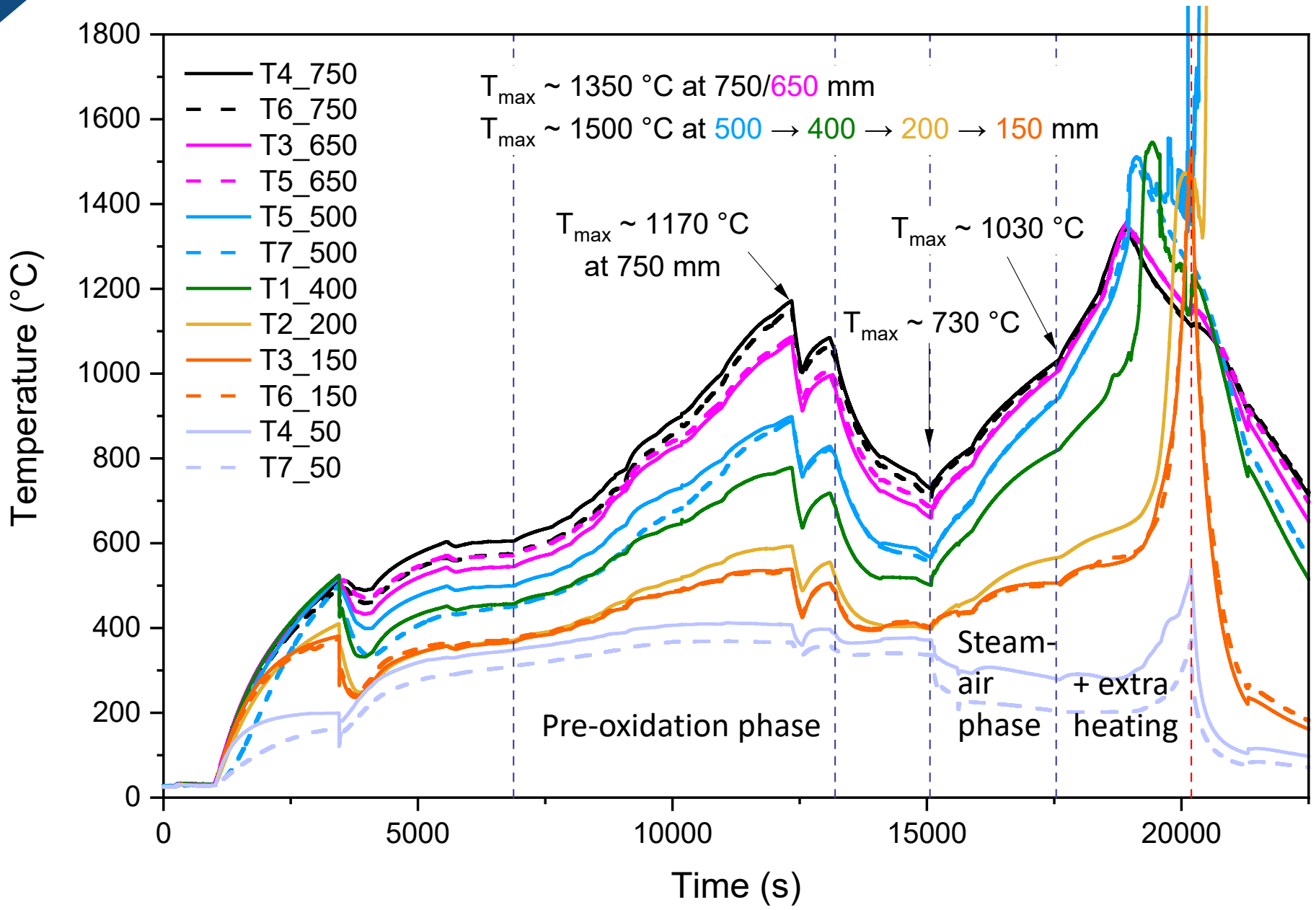

CODEX-ATF-AIT results – Temperatures

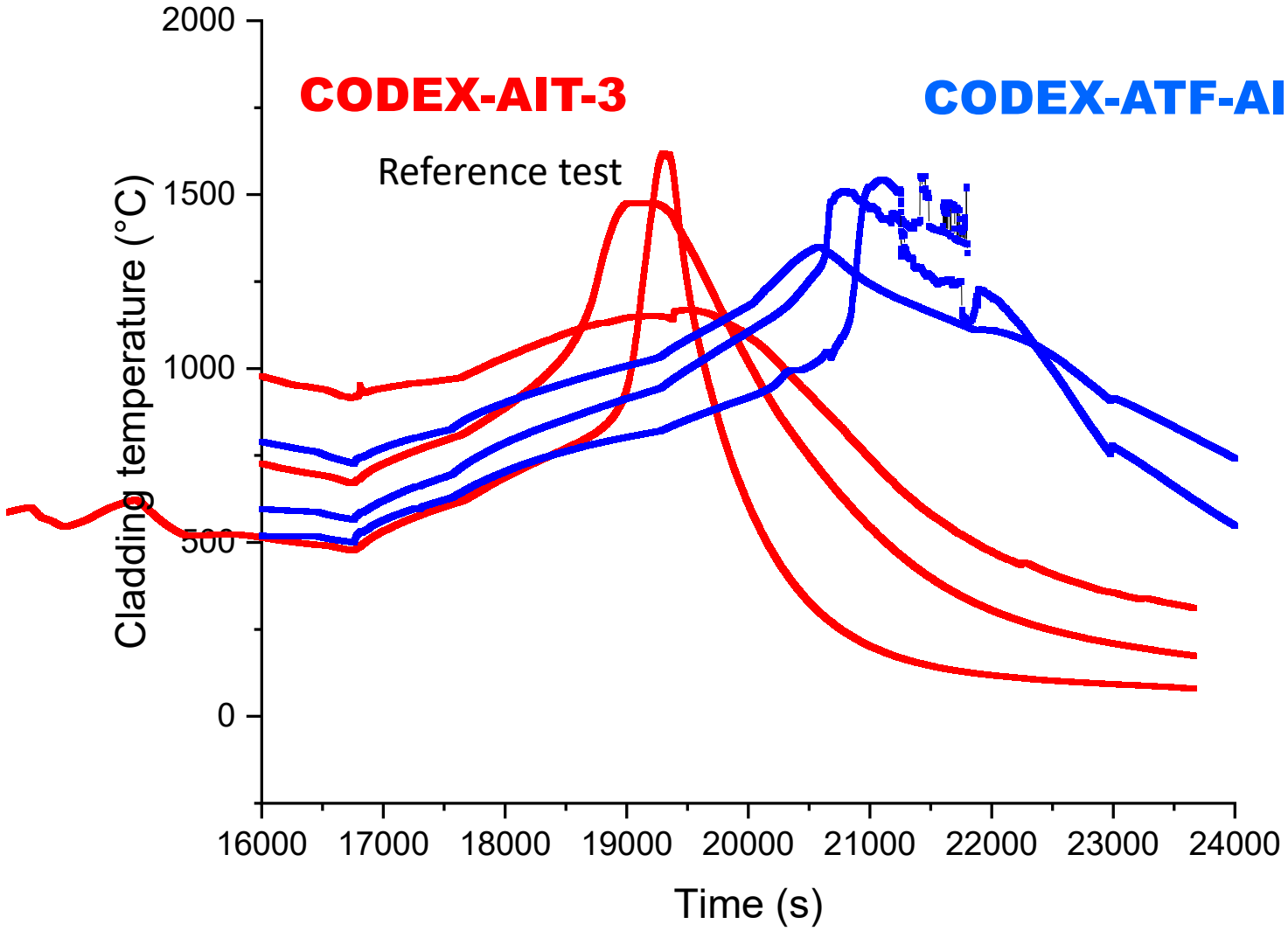

- Extra power was needed with Cr coating to accelerate temperature increase, thanks to the protection of the Cr coating
- Half hour delay in escalation

CODEX-ATF-AIT results – Outlet gas composition

CODEX-AIT-3

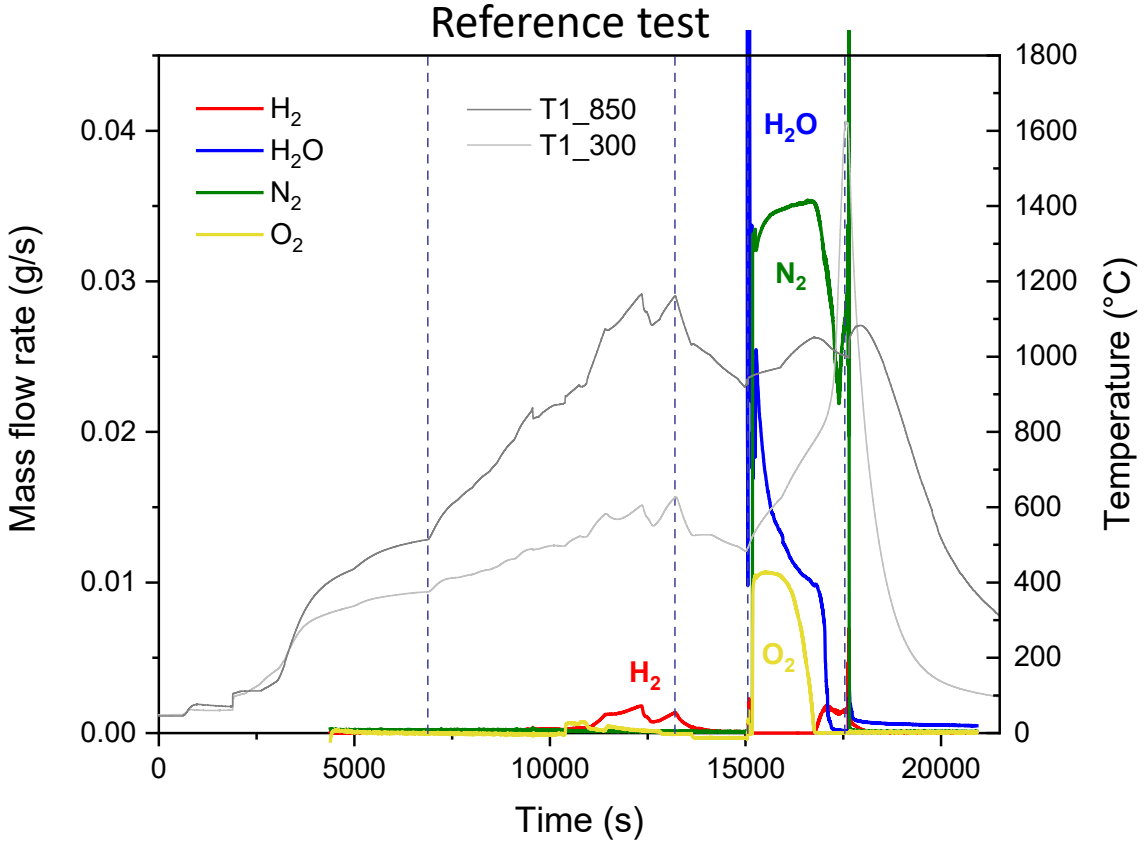

CODEX-AIT-3		
Total	Pre-oxidation phase	Air-ingress phase
H_2 release (g)	3,8	1,4
O_2 uptake (g)		12
N_2 uptake (g)		3

CODEX-ATF-AIT

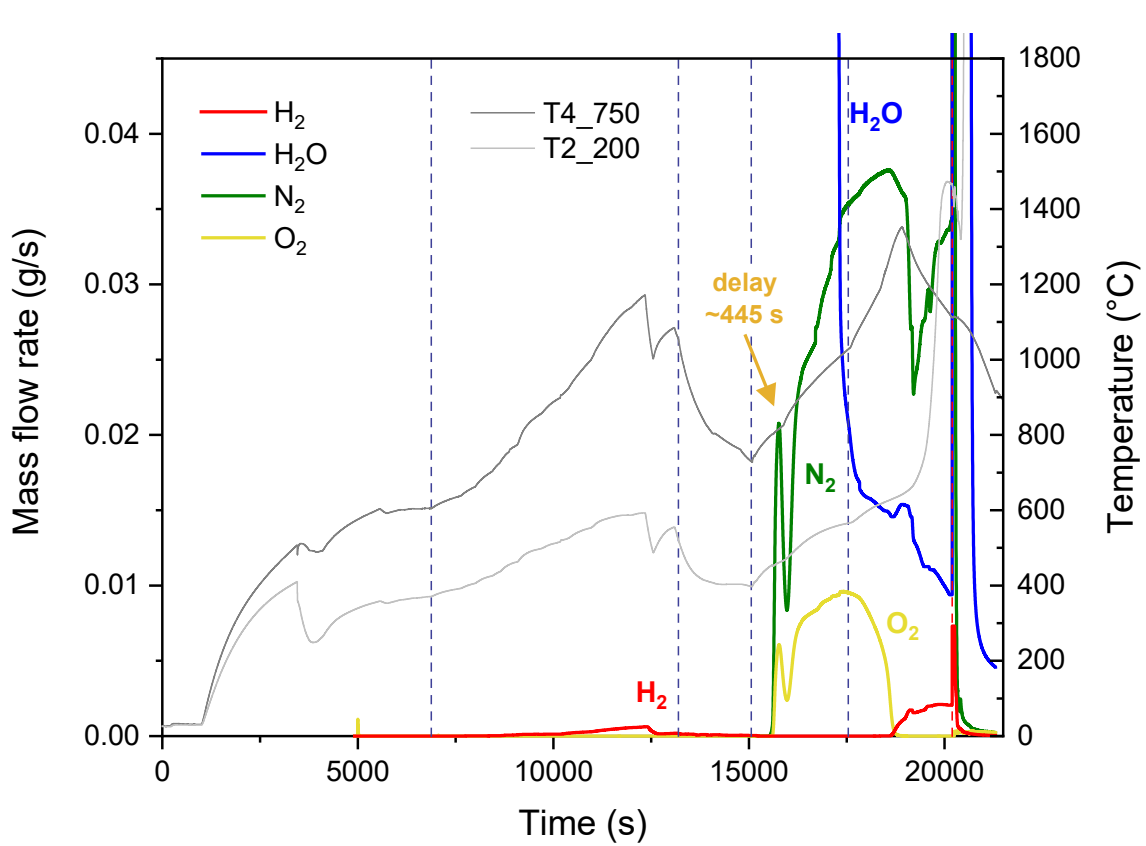

CODEX-ATF-AIT			
Total	Pre-oxidation phase	Air-ingress phase	Extra air-ingress phase
H_2 release (g)	1,4	-	3,3
O_2 uptake (g)		-	17
N_2 uptake (g)		-	9

Cross sections of the CODEX-ATF-AIT bundle

PRE-OXIDATION PHASE: NO BALLONING, NO OXIDATION → **EXTENDED AIR INGRESS PHASE**: EUTECTIC MELT FORMATION

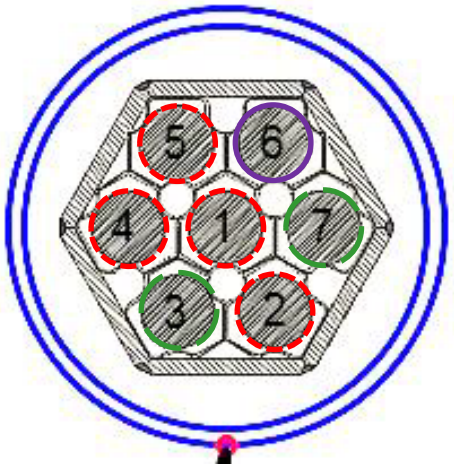

non-ballooned

ballooned and non-burst

ballooned and burst

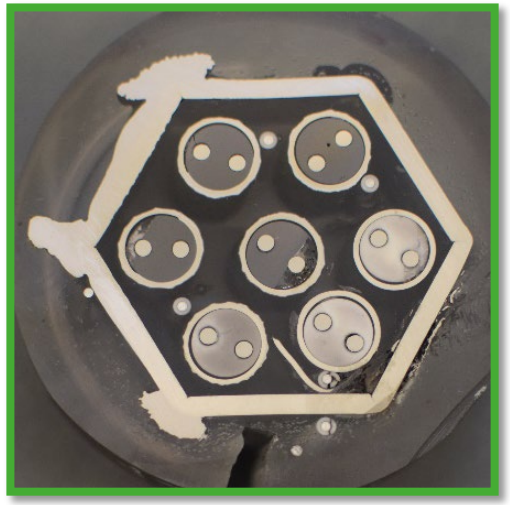

125 mm

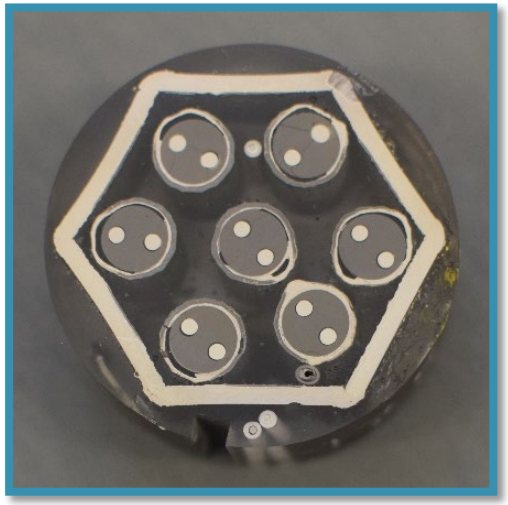

200 mm

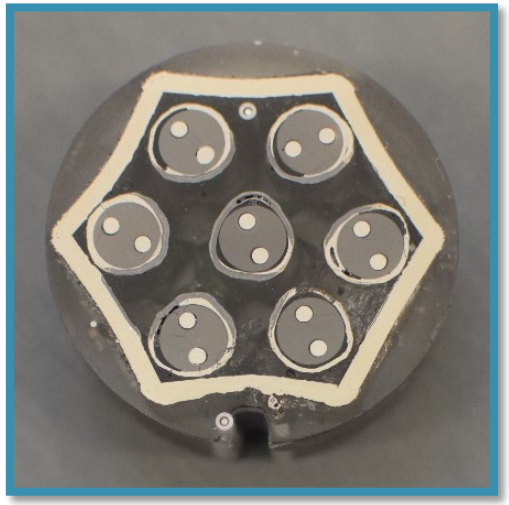

300 mm

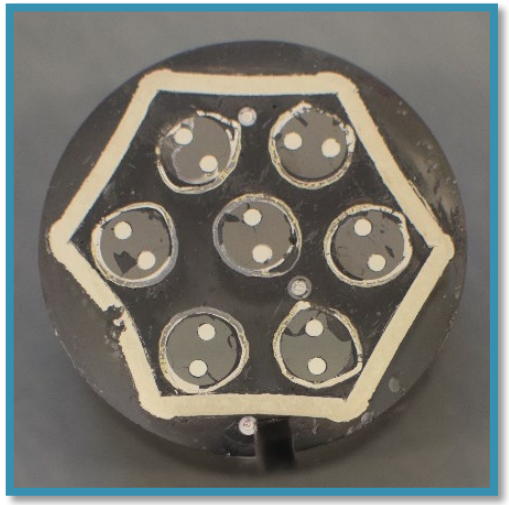

400 mm

PRE-OXIDATION PHASE: BALLONING, OXIDATION → **EXTENDED AIR INGRESS PHASE**: (NO) EUTECTIC MELT FORMATION

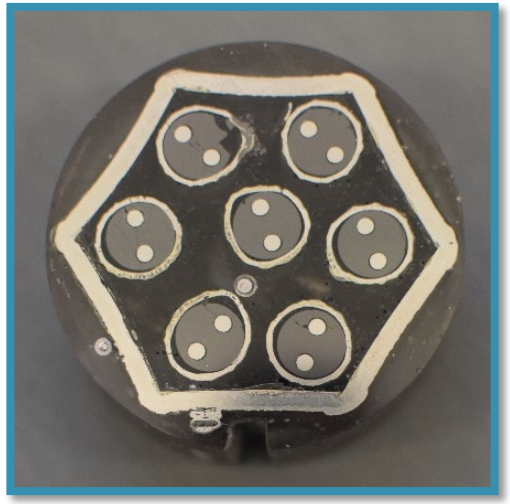

500 mm

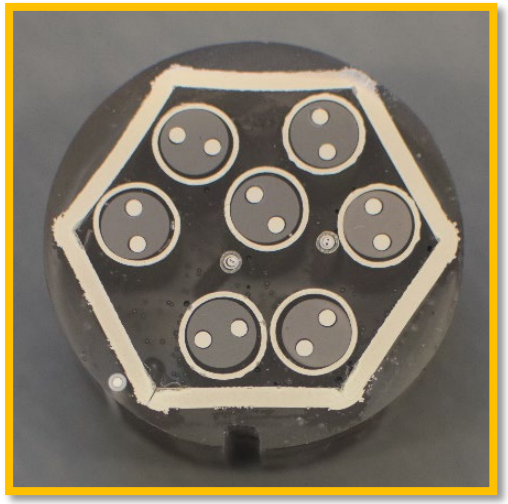

600 mm

700 mm

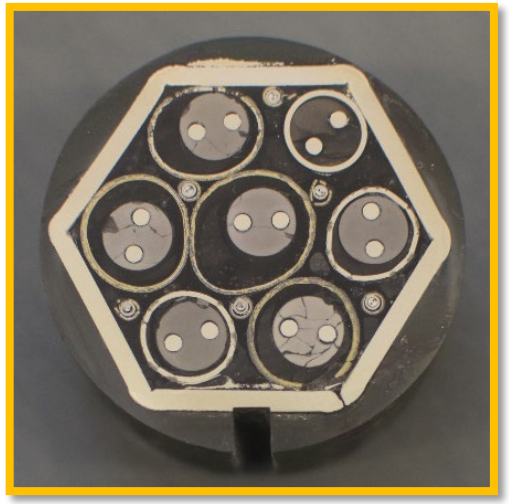

800 mm

Cross section of rods at 125 mm

PRE-OXIDATION PHASE: no balloning, no oxidation (T < 600 °C)

EXTENDED AIR INGRESS PHASE: eutectic melt formation (T_{max} ≈ 1400 °C)

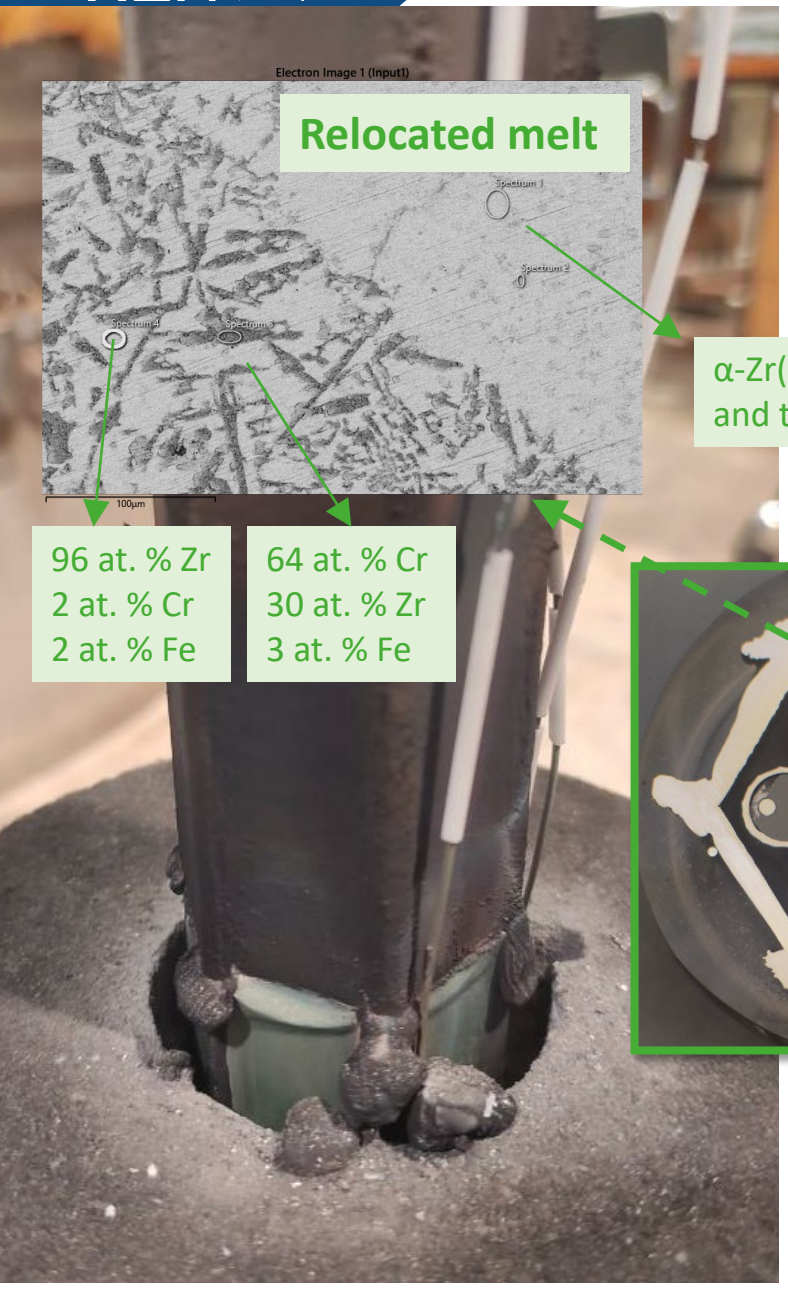

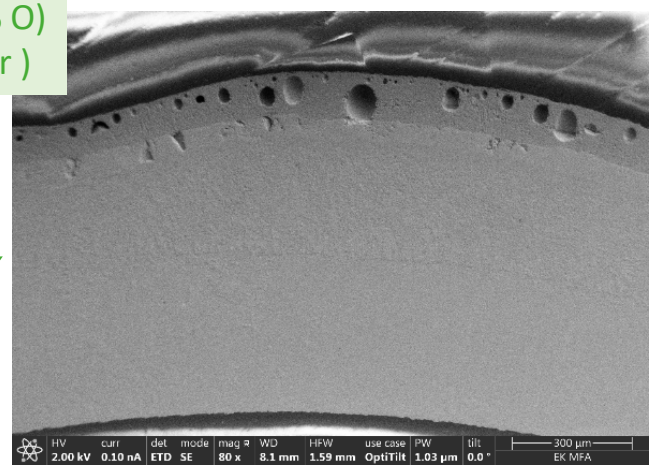

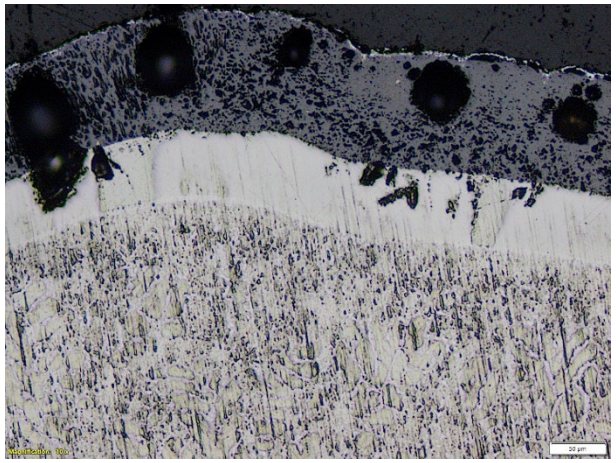

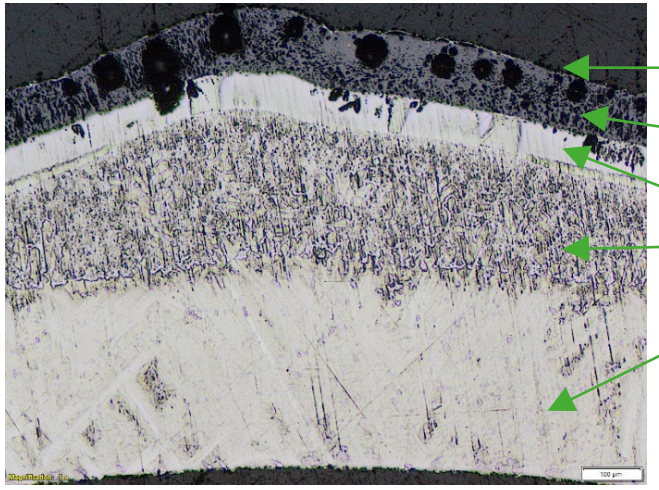

1. Cr coating
2. ≈100 µm ZrO_2 layer
3. 50-60 µm α-Zr(O) layer
4. 150-250 µm eutectic region
5. ≈350 µm β-Zr layer

Cross sections of rods at 200 - 500 mm

PRE-OXIDATION PHASE: no balloning, no oxidation (T < 900 °C)
EXTENDED AIR INGRESS PHASE: eutectic melt formation (T_{max} ≈ 1400 °C)

Rods were strongly degraded- main degradation mechanism was the Cr-Zr eutectic melt formation and its fast oxidation/nitriding in the last phase.

200 mm

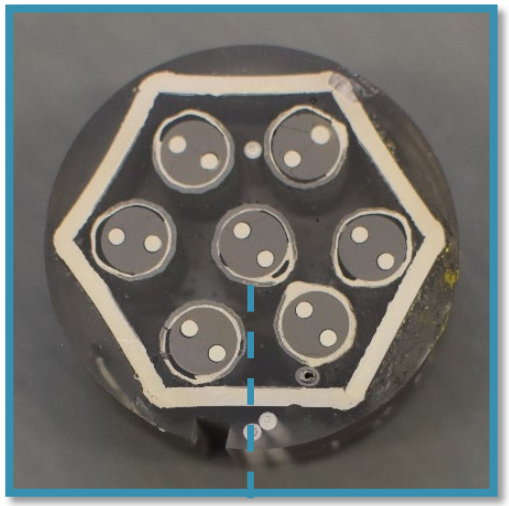

Rod No. 1.

300 mm

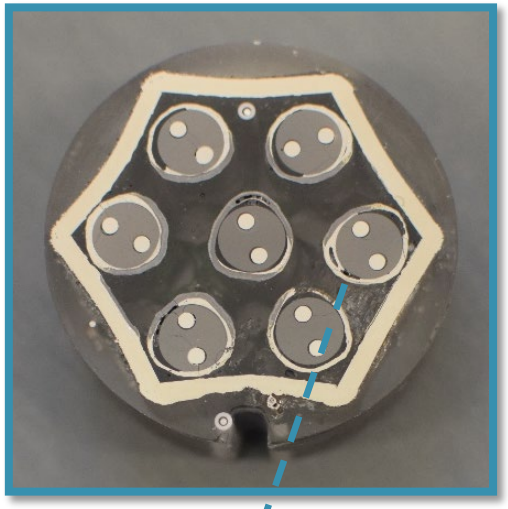

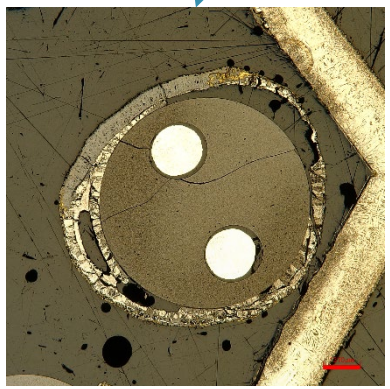

Rod No. 7 .

400 mm

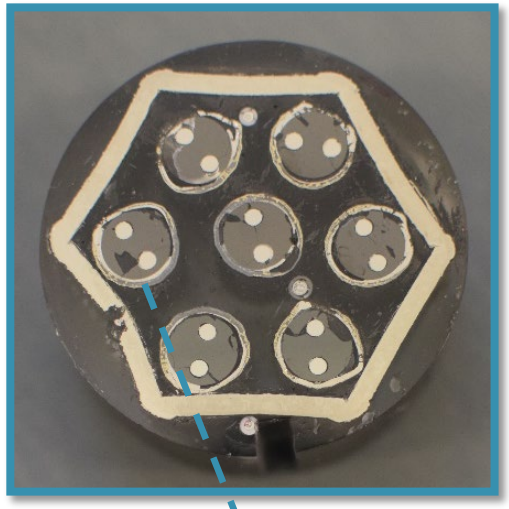

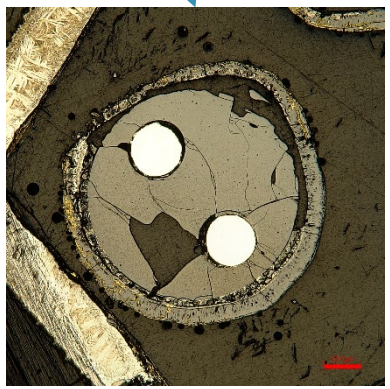

Rod No. 4 .

500 mm

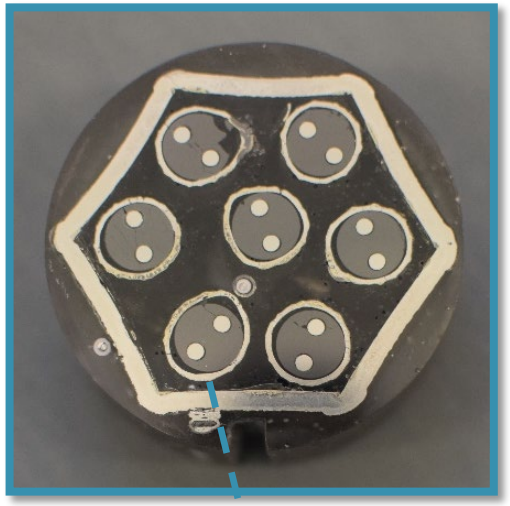

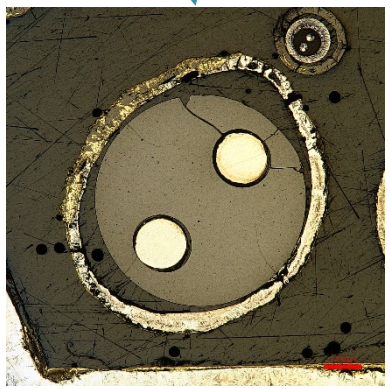

Rod No. 3.

Rod No. 6 at 400 mm

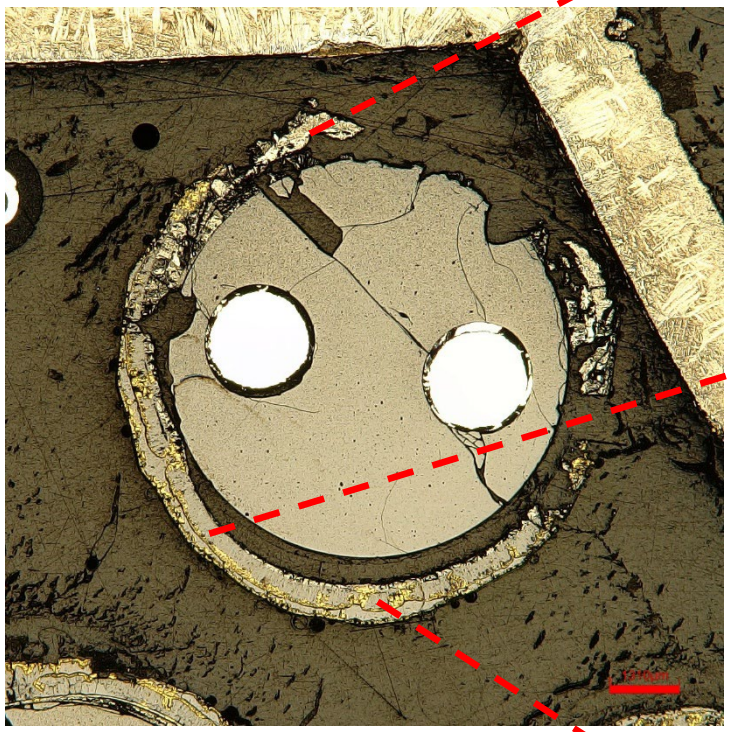

No Cr layer- Cr diffused into the Zr cladding wall-extensive Cr-Zr eutectic region

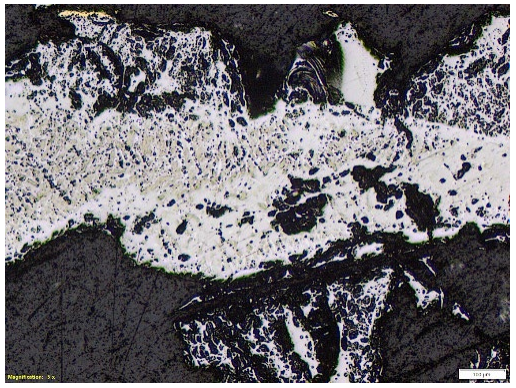

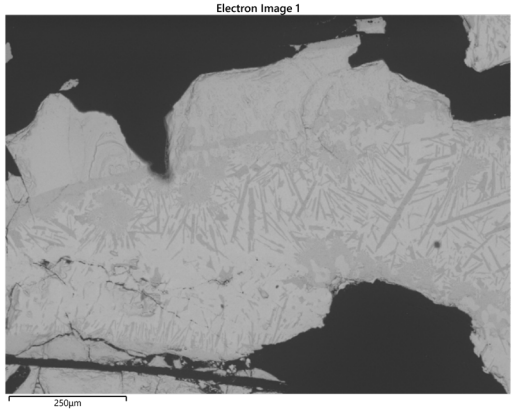

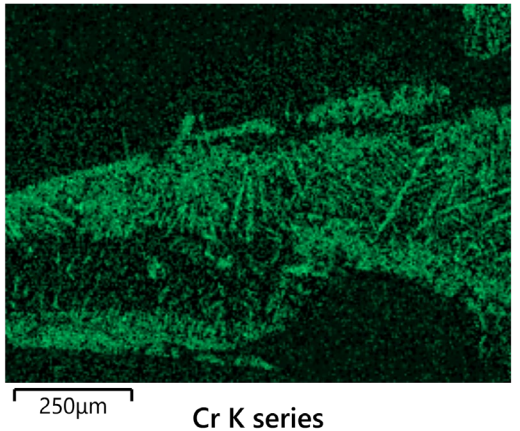

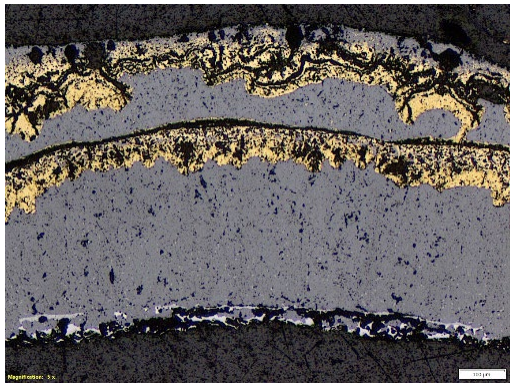

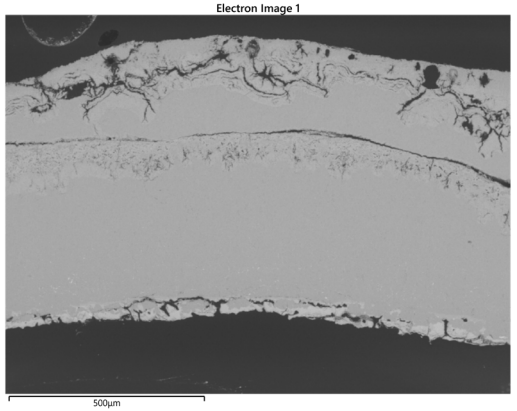

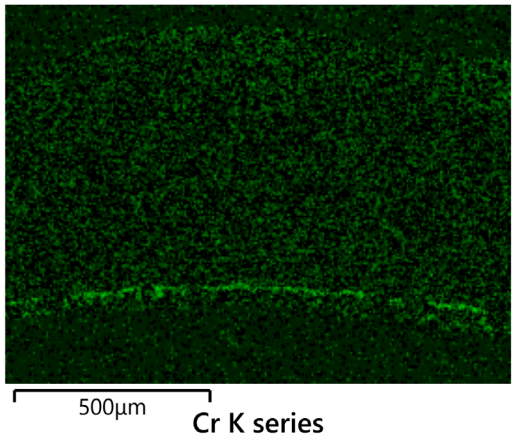

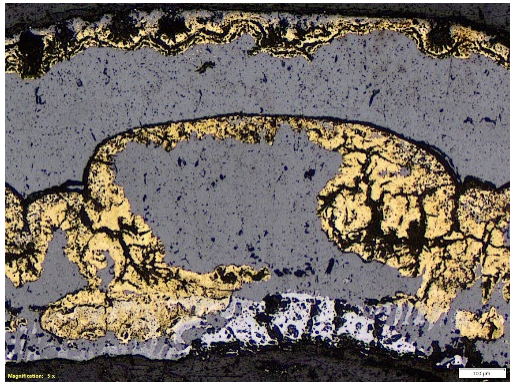

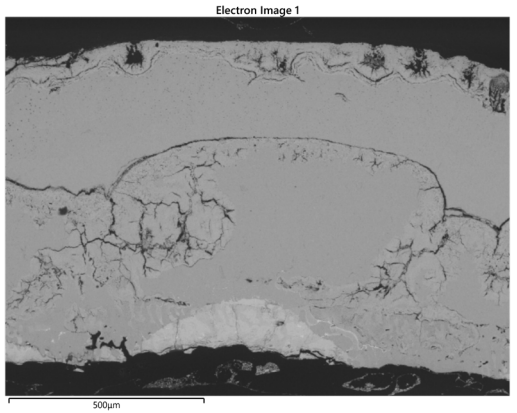

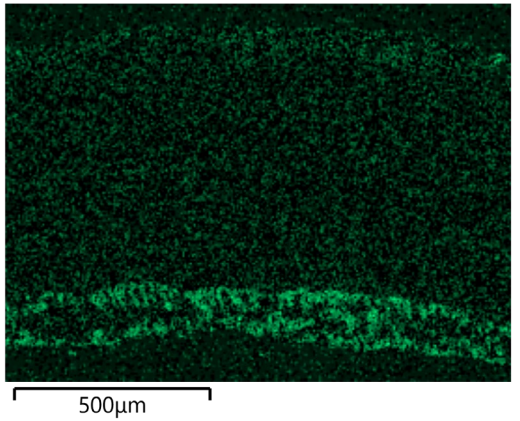

Cross sections of rods at 600 - 800 mm

PRE-OXIDATION PHASE: ballooning, oxidation (T_{max} < 1000 - 1150 °C)

EXTENDED AIR INGRESS PHASE: eutectic melt formation at 600 and 700 mm,
no eutectic melt formation at 800 mm

600 mm

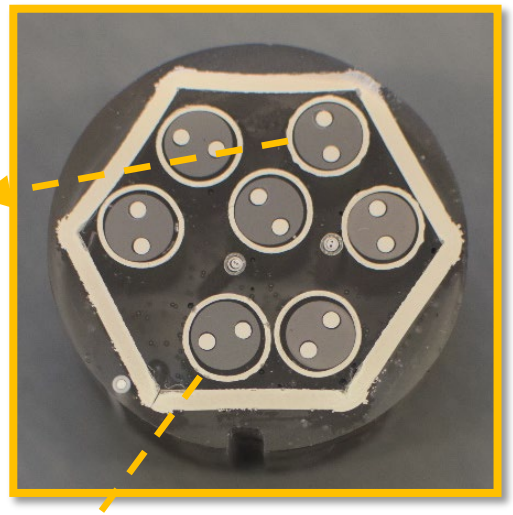

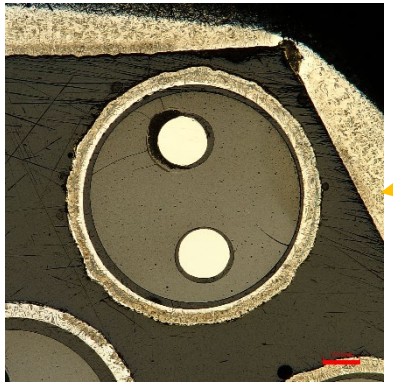

Rod No. 6.

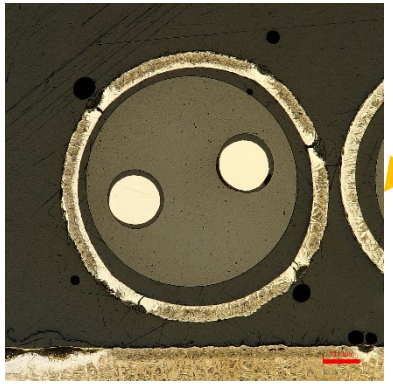

Rod No. 3.

700 mm

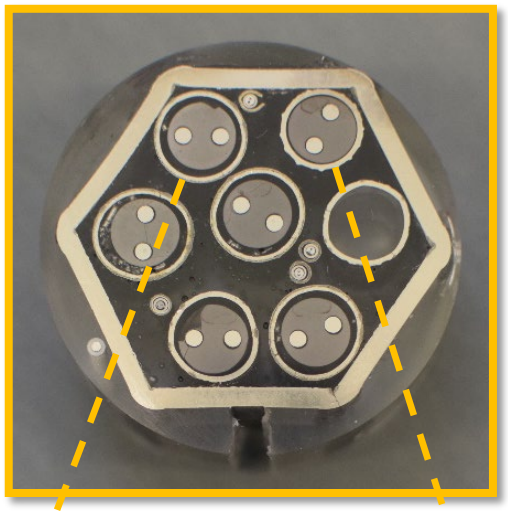

Rod No. 5.

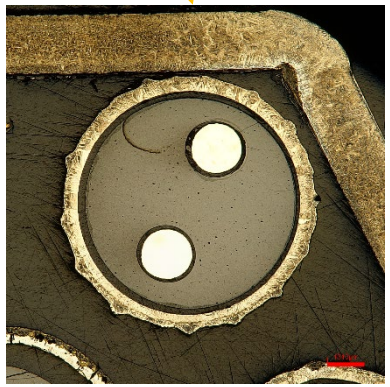

Rod No. 6.

800 mm

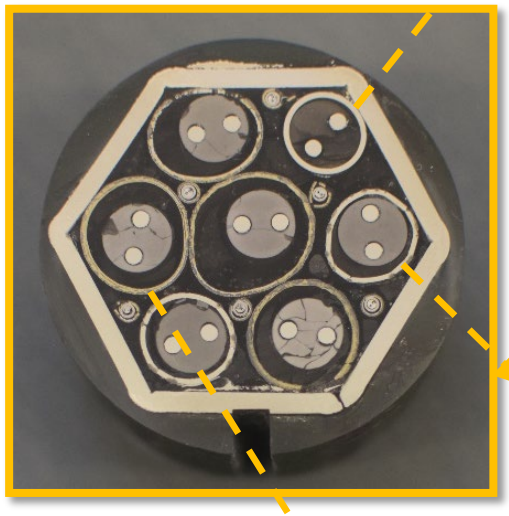

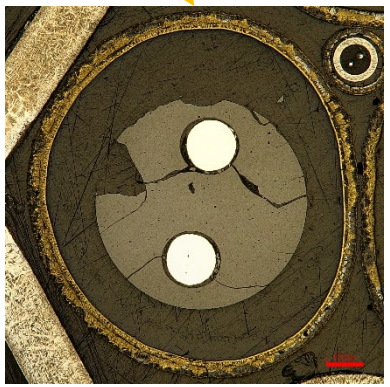

Rod No. 4.

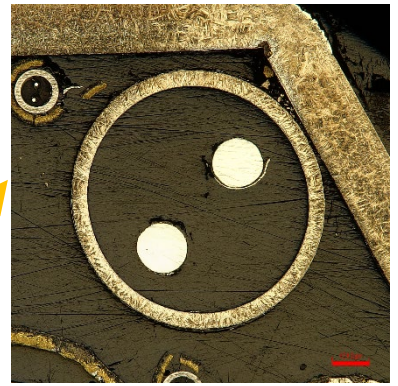

Rod No. 6.

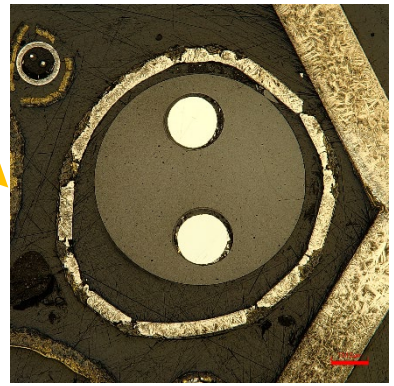

Rod No. 7.

Cracked Cr-layer

Cross sections of rods at 600 mm

Zr oxidation locally through the cracks of the Cr-layer in the pre-oxidation phase

O penetrated through the cracks of the Cr-layer into the zirconium metal and prohibited the Cr diffusion into the cladding wall

No. 4.
ballooned
and burst

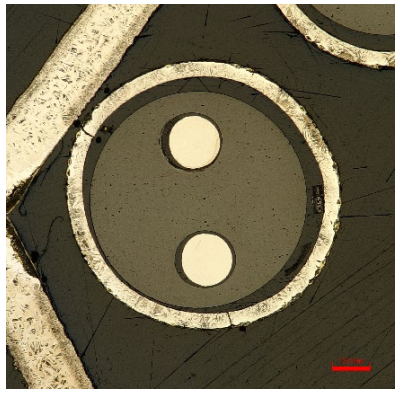
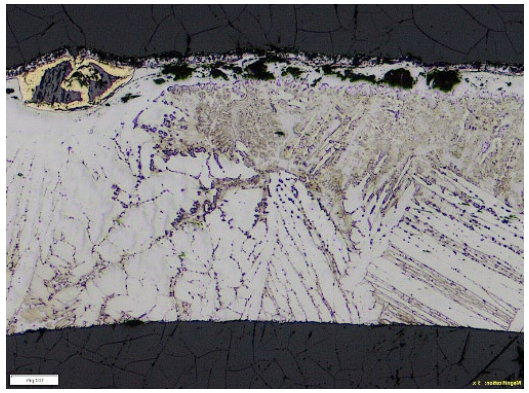
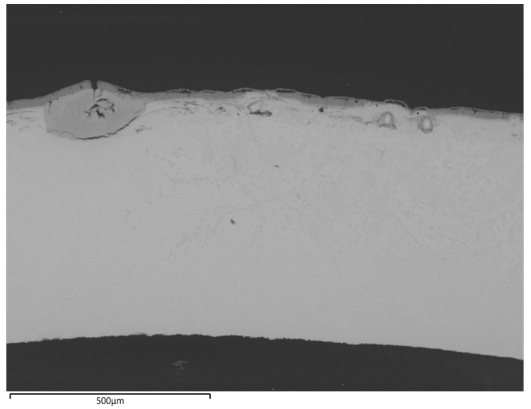

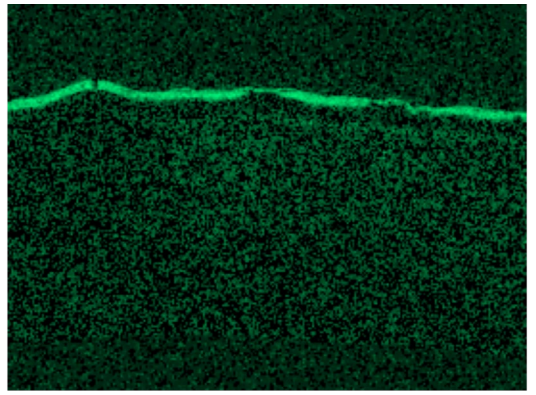

No. 7.
ballooned and
non-burst

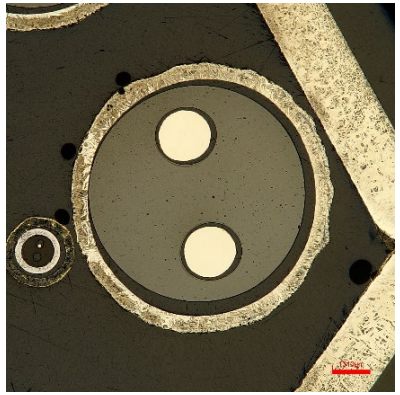
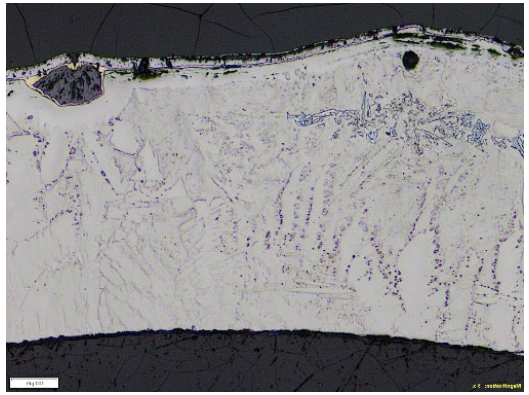
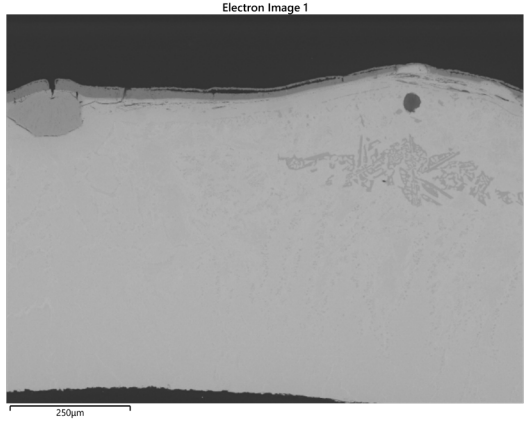

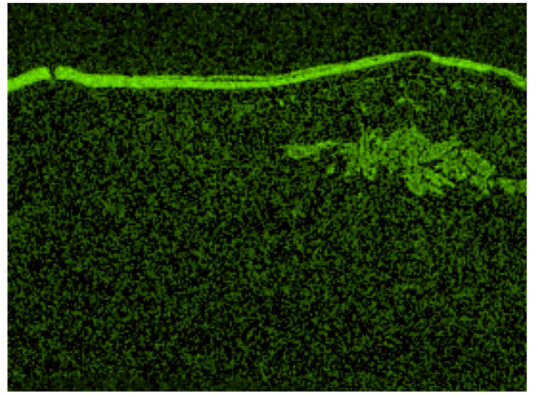

No. 6.
non-ballooned

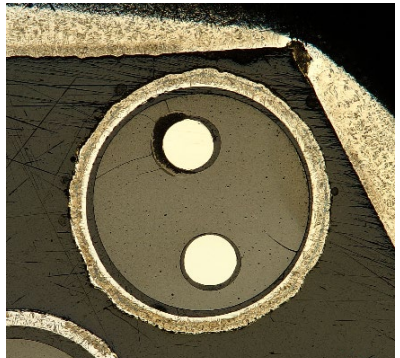
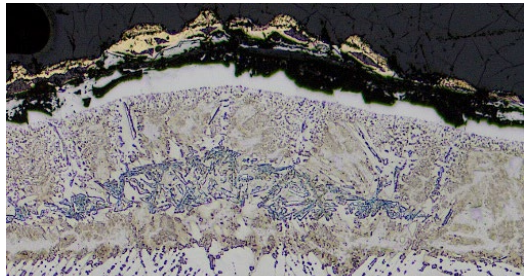
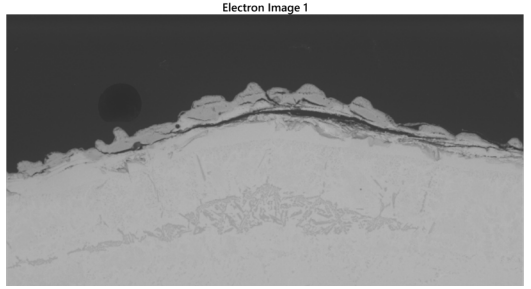

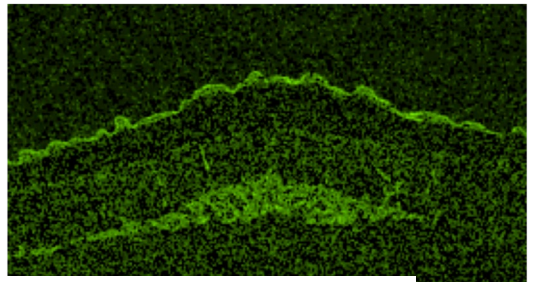

Cr coating diffused the most into the cladding wall amongst the rods at 600 mm

Cross sections of rods at 700 mm

Ballooning- Cr coating became cracked. The Cr layer lost its protective role and these rods oxidised and nitrided the most

No. 5.
ballooned
and burst


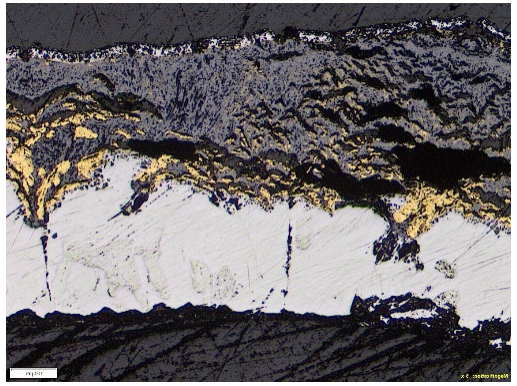
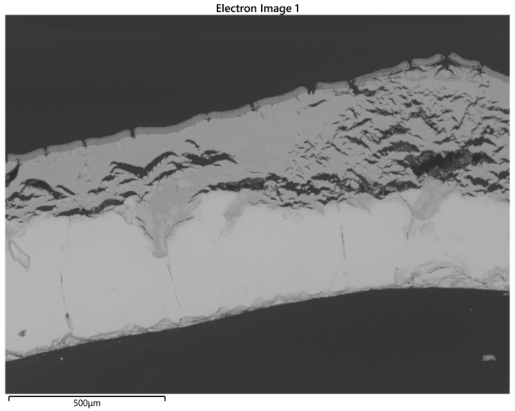

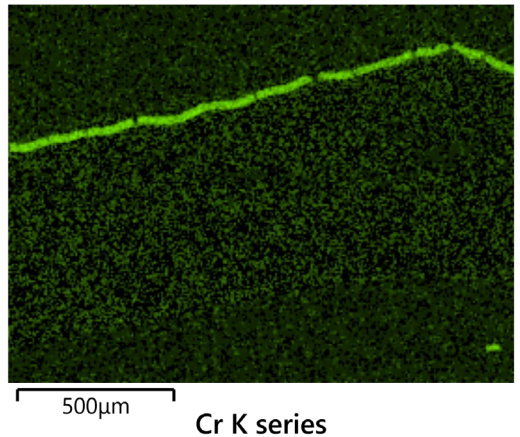

No. 7.
ballooned
and non-burst

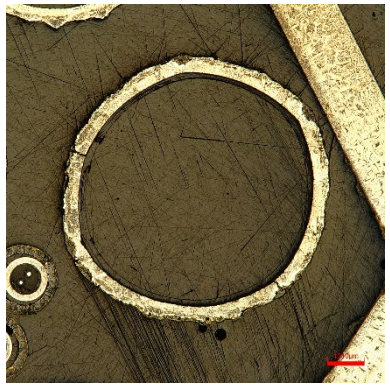
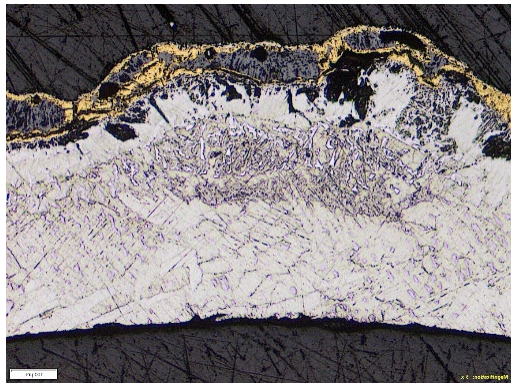
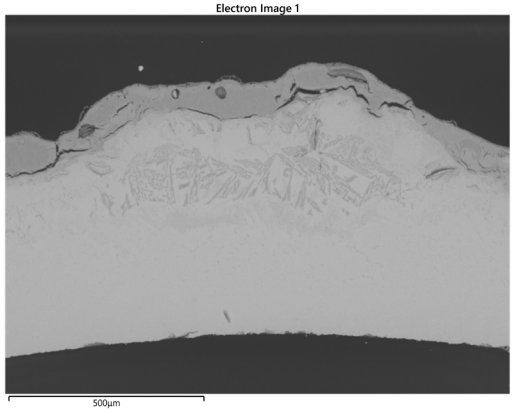

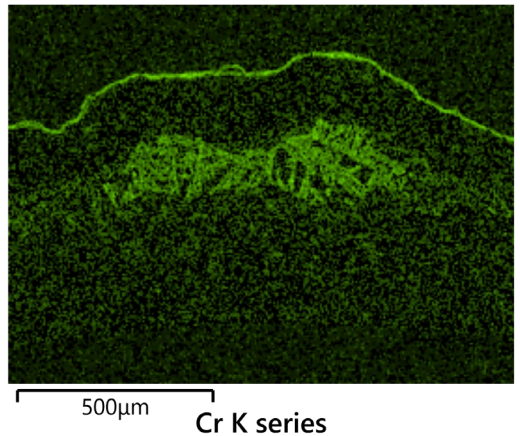

No. 6.
non-ballooned

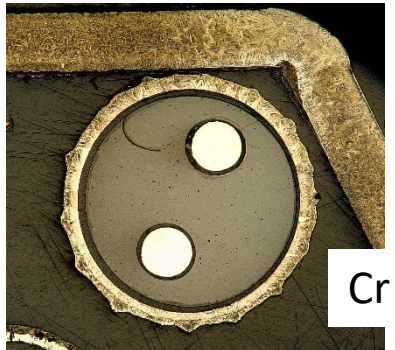
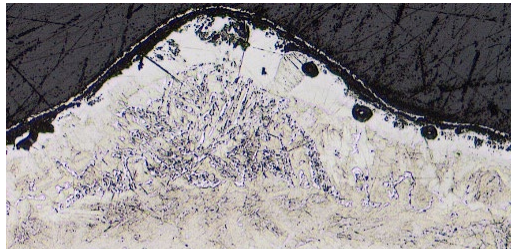
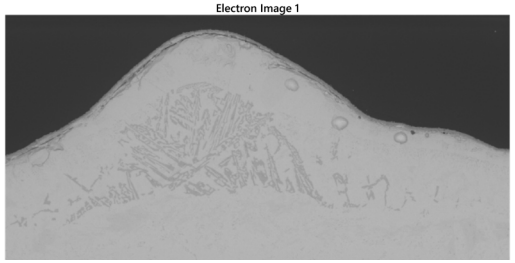

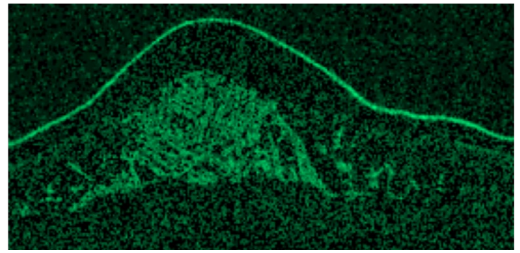

Cr layer remained intact: rod was not oxidised. But strong Cr-Zr eutectic formation occured

Cross sections of rods at 800 mm

Strong ballooning, burst: oxidised and nitrided the most.
Burst location were near to this position: inner oxidation/nitriding

No. 2.
ballooned
and burst

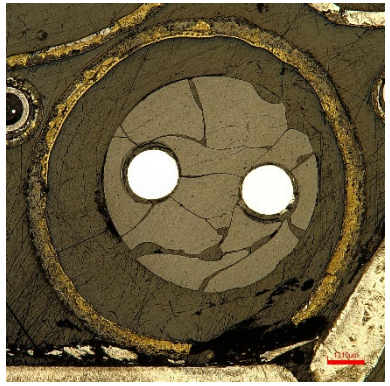
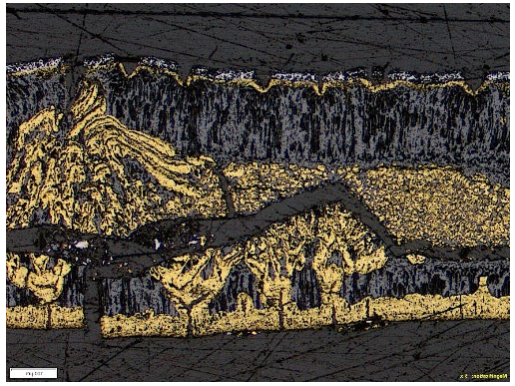

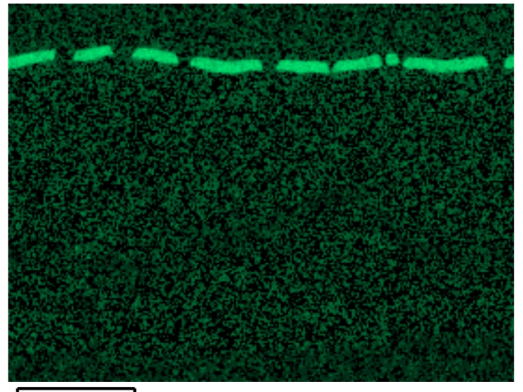

No. 3.
ballooned
and non-burst

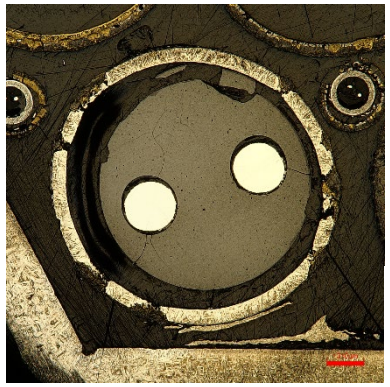
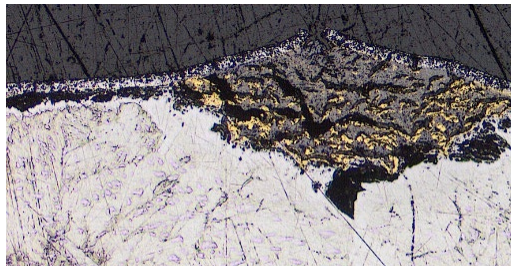
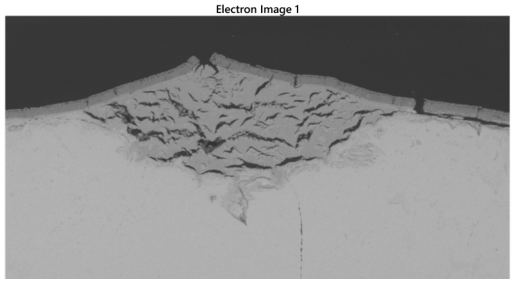

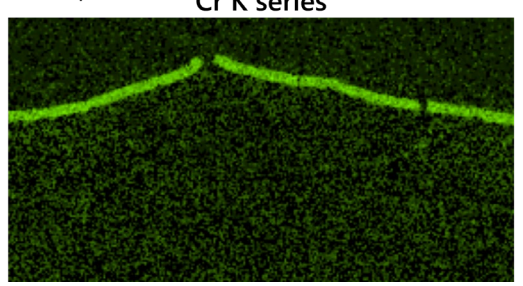

Oxidation occurred locally and the tube wall often cracked through where the local oxidation started.

No. 6.
non-ballooned


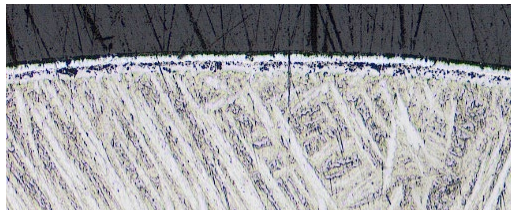
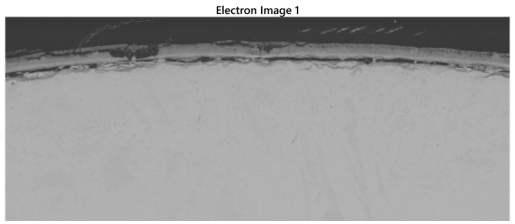

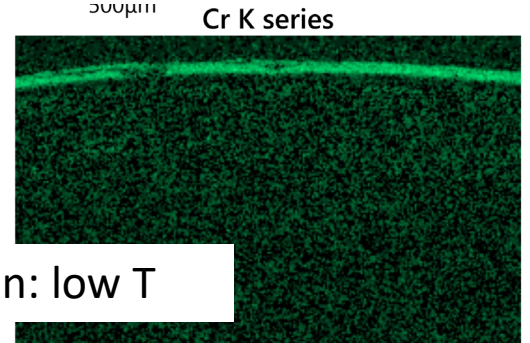

Cr layer remained intact: no oxidation. No eutectic formation: low T

Conclusions

- The comparison of results from the CODEX-AIT-3 and CODEX-ATF-AIT tests suggests that ATF materials can increase the coping time in the event of air ingress type reactor accidents.

- The ATF cladding reacted significantly less with high-temperature steam below 1200 °C than traditional Zr cladding material.

- In the reference test, air ingress led to a temperature excursion, with cladding temperatures reaching 1625 °C within 40 minutes. Under the same conditions in the CODEX-ATF-AIT test, the cladding temperature increased only to 1030 °C over the same period.

Conclusions

- The Cr coating provided significant protection against oxidation in both steam and air atmospheres as long as the coating remained intact.
  - Effect of ballooning: after cracking of the Cr layer, local oxidation of Zr began. The local oxidation spots could facilitate full cross-sectional fracture of the cladding tube wall.
  - Cr-Zr eutectic melt formation: can take place if Cr diffuses into the Zr cladding wall to a large extent and the temperature reach the Cr-Zr eutectic melt formation temperature. Fast oxidation/nitriding of the metallic Cr-Zr eutectic melt could start.
- The degradation of the ATF fuel occurred more slowly in the integral tests compared to traditional fuel.

HUN REN Centre for Energy Research

OFFERR EUROPEAN USER FACILITY NETWORK

Many thanks to Martin Steinbrück, Juri Stuckert, Mirco Grosse (KIT), Tadas Kaliatka (LEI), Martin Ševeček (CTU), Liviusz Lovász (GRS)

Thank you for your attention!

The CODEX-ATF-AIT experiment was supported by OFFERR.

Katerina Frederick

WEC LLC

Accident Tolerant Fuel: Cr Coated Cladding Development at Westinghouse

In response to the nuclear industry's desire for improved fuel performance in accident conditions following the Fukushima accident in Japan in 2011, Westinghouse's **EnCore®** accident tolerant fuel (ATF) program is developing and commercializing advanced fuel cladding and fuel pellet products with the main goals of improving safety and economic performance through power uprates and increased burnups. The program includes a near-term high energy **EnCore** ATF product, comprised of chromium-coated zirconium-alloy fuel cladding and doped fuel pellets with potential enrichments greater than 5% 235U. The chromium-coated cladding has undergone testing in various environments and facilities to provide valuable results to validate the design and specification of the chrome coating. Lead test rod (LTR) and lead test assembly (LTA) campaigns with utility partners provide real-world data on the irradiation performance of the coated cladding. LTR post-irradiation examination (PIE) data will be presented and discussed. Additionally, out-of-pile testing highlighting coating differences from development will be presented.

Accident Tolerant Fuel: Cr Coated Cladding Development at Westinghouse

Katerina Frederick

30th International QUENCH Workshop

December 16-18, 2025

The following material is based upon work supported by the United Stated Department of Energy under Award Number DE-NE0009033

Outline

- Westinghouse **EnCore®** High Energy Fuel Program
  - LTA and LTR Status
  - Operating Experience
- Hydrogen Absorption Testing
- SiC Update

EnCore® High Energy Fuel Program

Utilities are striving for maximum electricity generation and reduced operating costs while enhancing safety with Accident Tolerant Fuel (ATF) technologies

The EnCore High Energy Fuel (HEF) Program combines near-term and future advancements to support these critical nuclear industry drivers

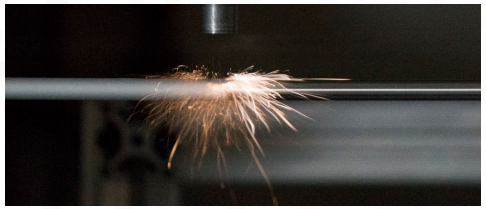

Chromium Coated Cladding

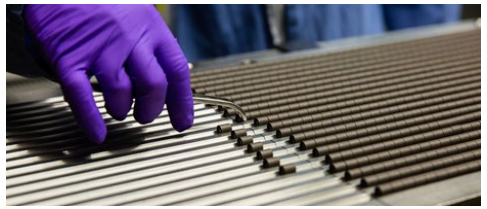

ADOPT™

Fuel Pellets

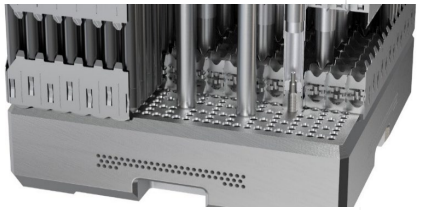

PRIME™

Fuel Features

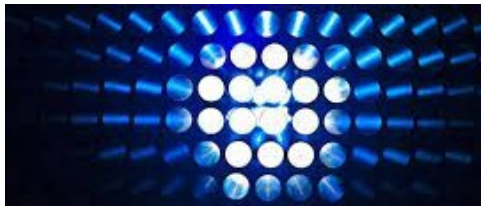

AXIOM®

High Performance Cladding

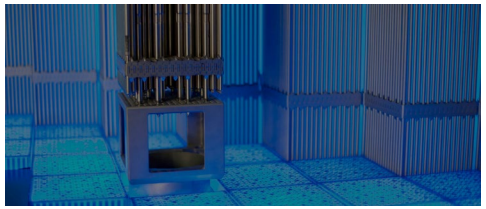

LEU+ and Higher Burnup

(>5 w/o & >62 GWd/MTU)

Applications

- Enhanced Safety
- Optimization of Fuel Cycle Costs
- 24-Month Cycle Operations
- Power Uprating

EnCore® HEF Irradiation Campaigns

- Lead Test Rod (LTR) campaigns with Utility Partners provide data for fuel qualification
- Campaigns 1 and 2 complete
  - Poolside PIE throughout irradiation to 54-month high burnup complete. Hot cell PIE underway.
- Campaign 3 started Spring 2025 (contains LEU+)
- Additional programs in planning stages

	Cr Coated Cladding	ADOPT Pellets	LEU+ Pellets
Campaign 1 (2019)	✓	✓	
Campaign 2 (2020)	✓		
Campaign 3 (2025)	✓	✓	✓

Campaign 1 LTRs

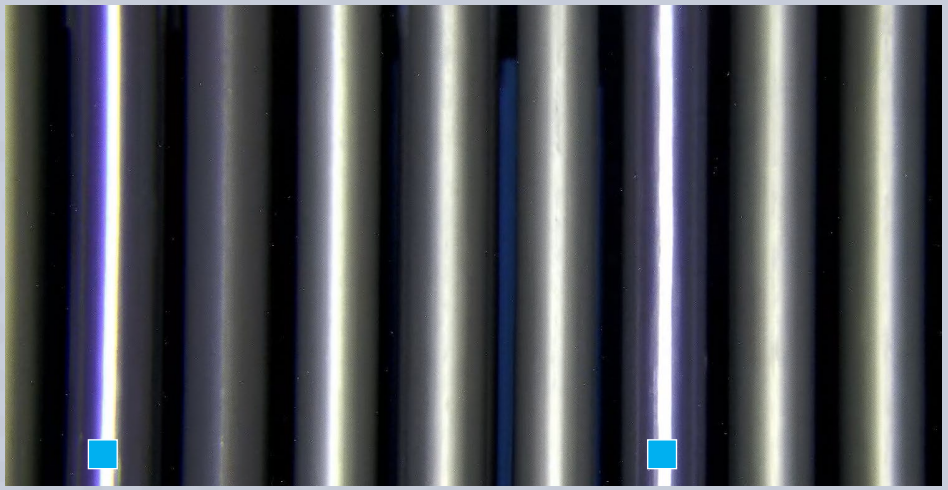

Poolside PIE after 3 Cycles, BNGS (≈75 MWd/kgU)

Campaign 2 LTRs

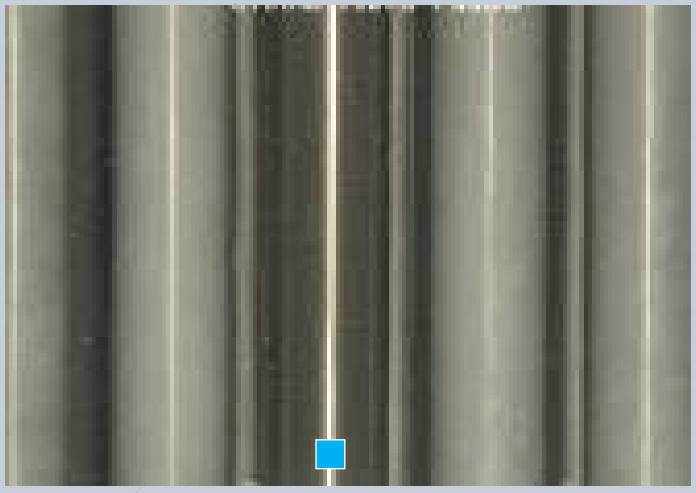

Poolside PIE after 2 Cycles

■ Cr Coated Rods

Cr coated cladding appears "pristine" with excellent adherence and little indication of crud

ATF and HEF: Ongoing Operating Experience

Reduced Normal Operation Corrosion

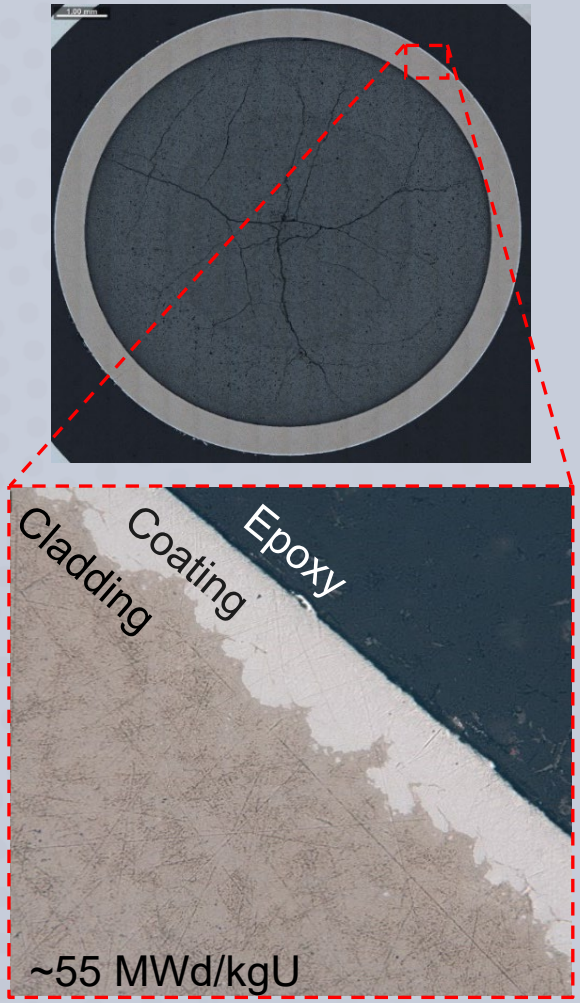

Reduced Hydrogen Pickup

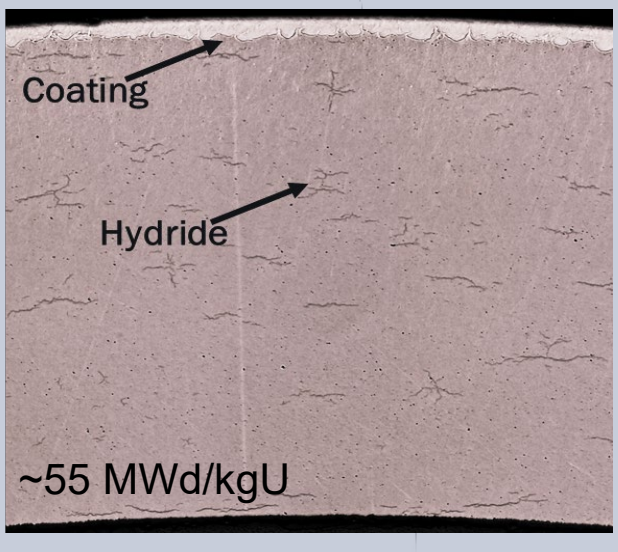

Burnup (MWd/kgU)	Average H-Content (ppm)
~31	< 50
~55	
~75	**Coming soon!**

Improved Accident Performance

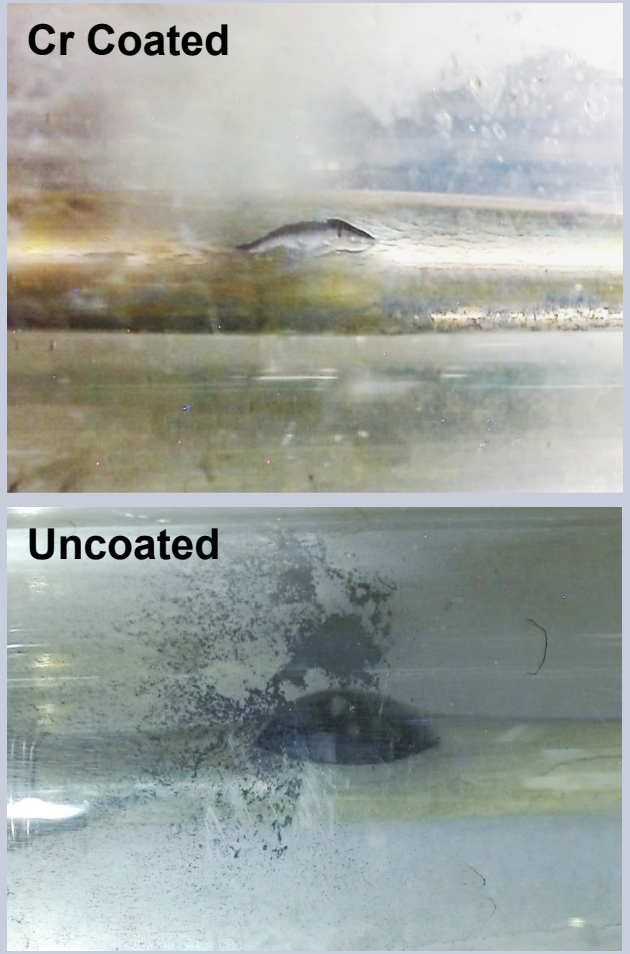

LOCA Burst Test Results (Irradiated)

EnCore® High Energy Fuel Program

Integrated Timeline for LEU+ Fuel Deployment

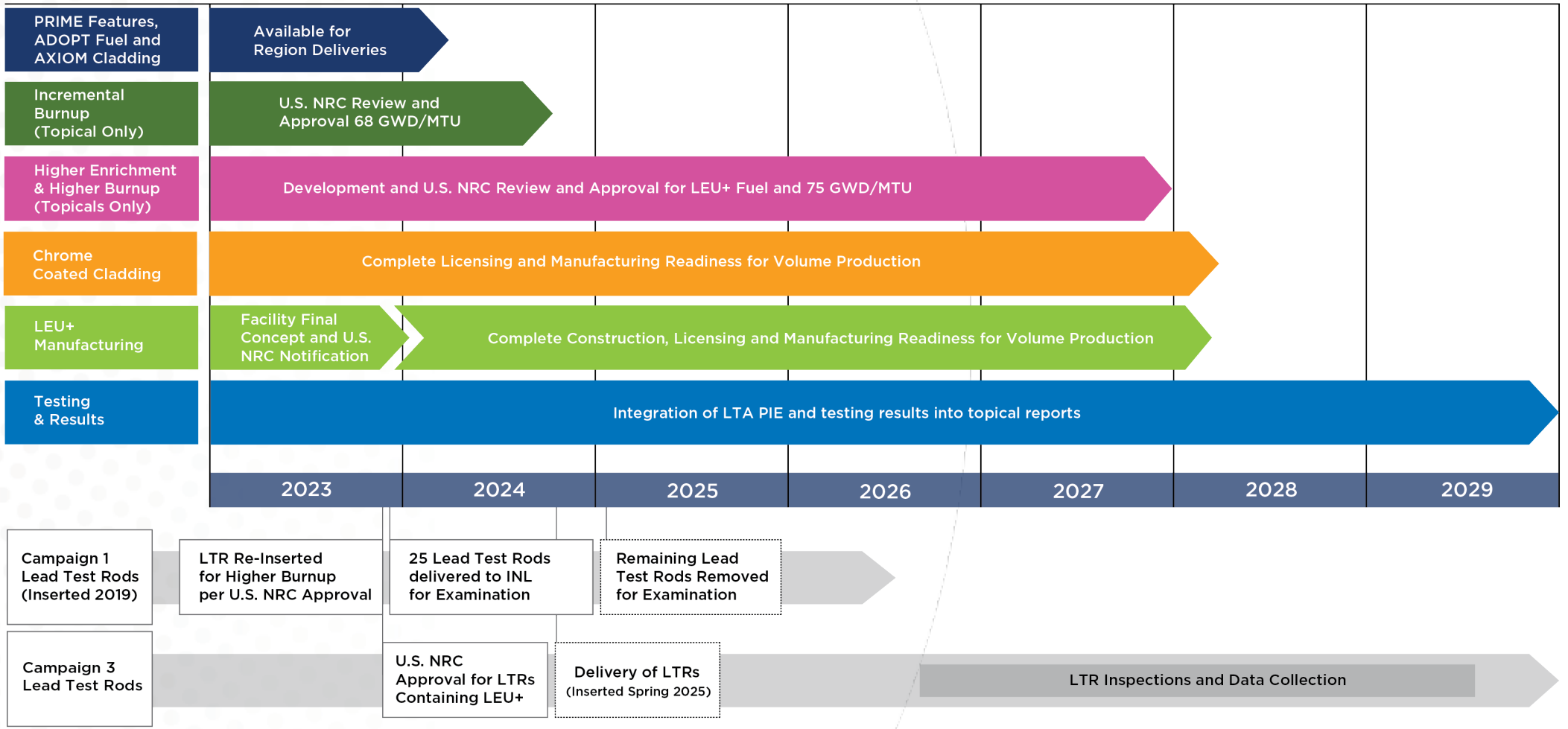

Engaging U.S. NRC early for multiple licensing actions to support 2028 reloads

Westinghouse

Hydrogen Absorption as Coating Quality Indicator

Test Conditions

$$P_{RT}V_{net} = nRT_{RT}$$

V_{net} = net quartz tube volume

n = moles H_2 gas to increase H concentration by C_H (ppm)

M_s = mass of cladding exposed to H_2

R = gas constant

T_{RT} = room temperature (293 K)

$$P_{RT} = \frac{0.0091 C_H M_s}{V_{net}}$$

Parameter	Value
V_{net} (L)	0.45
M_s (g)	7.6
C_H (ppm)	*2186*
P_{293K} (torr)	*336*
$T_{charging}$ (°C)	*430*
P_{703K} (torr)	*504*

Final Test Parameters

Duration: Maximum 48 hours or a pressure drop of 100 torr

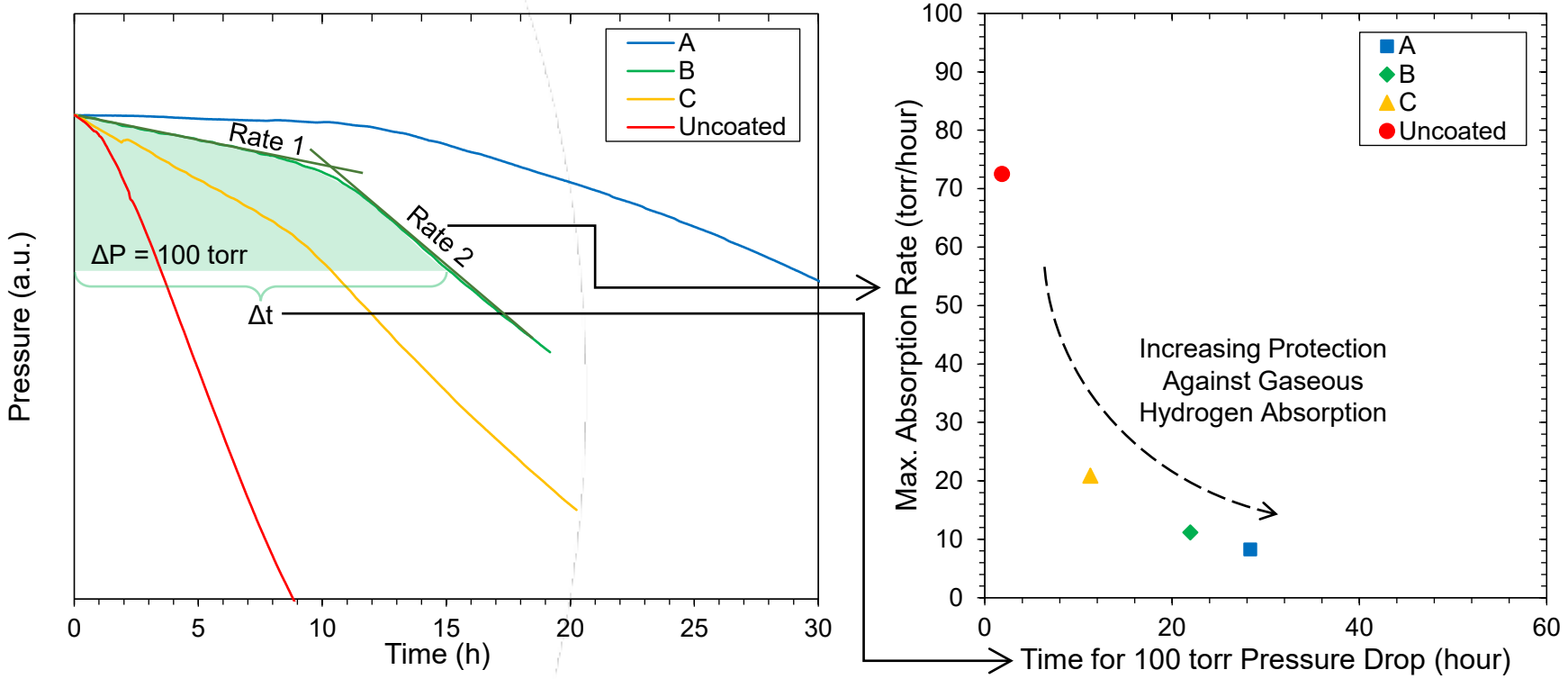

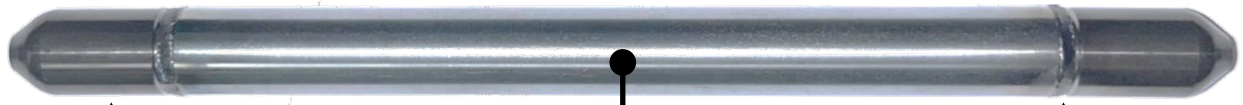

Welded Pre-Oxidized End Plugs

Purge ID with Argon

No Cr Machining at Weld

Westinghouse

Effect of Oxidation on Hydrogen Absorption

Simulating Materials In-Reactor

- Normal operation is in an oxidizing environment
- Assumption: 1 μm ZrO_2 is impermeable to H_2
- Open tube samples oxidized in steam autoclave environment
- Pre-oxidized samples were tested for better comparison of coating protection after initial oxidation occurs

Note: Gaseous hydrogen is not representative of real-world H pickup mechanisms, therefore data is *only* used to assess coating integrity

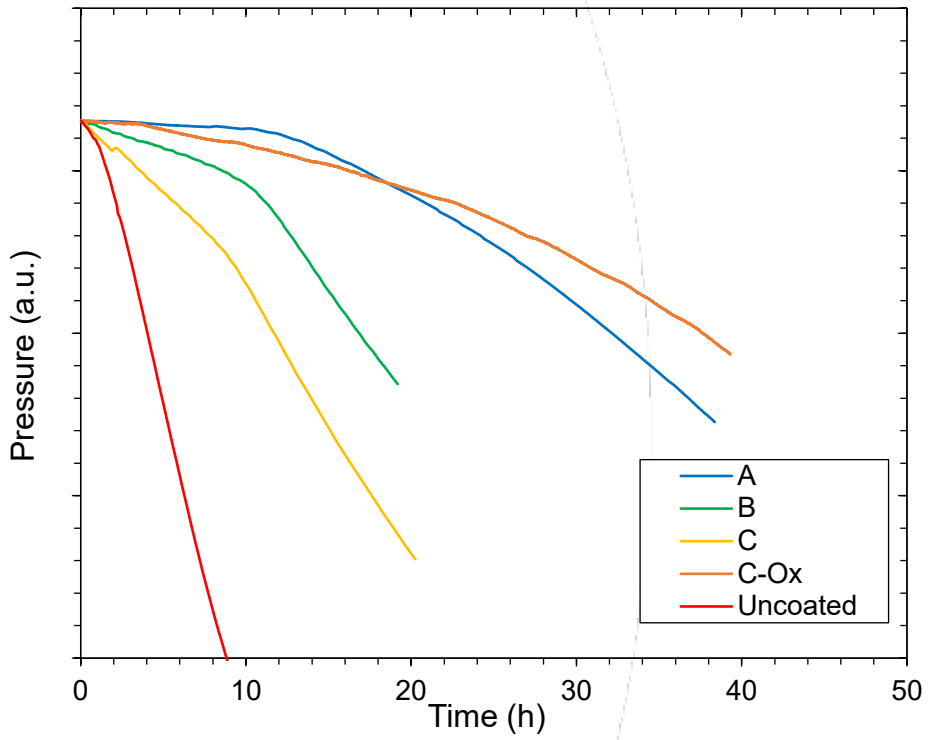

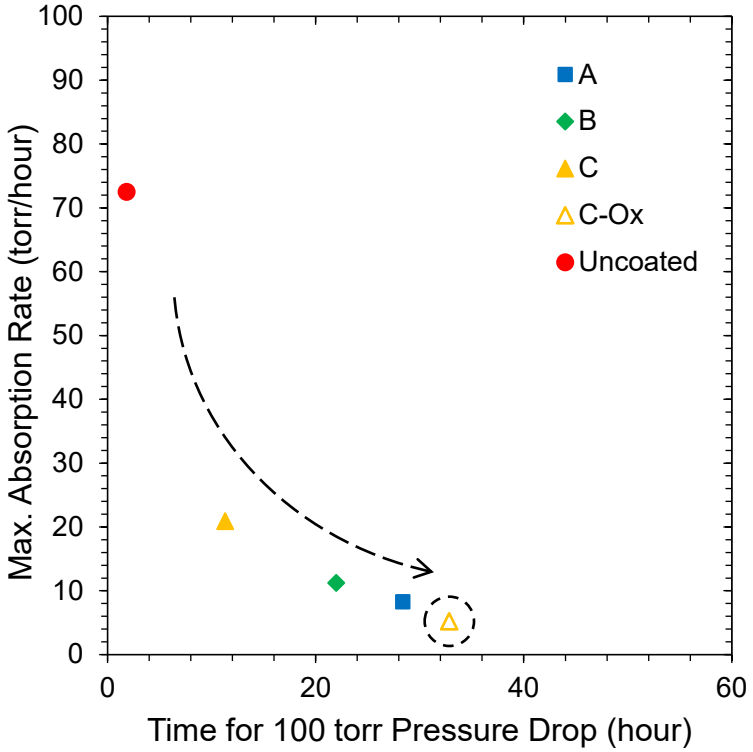

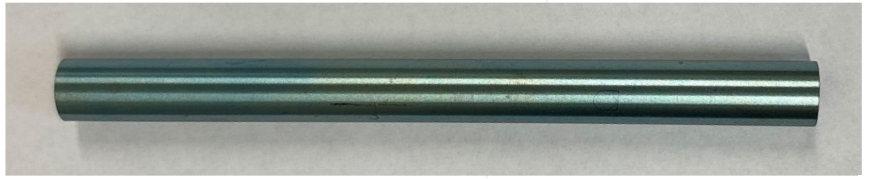

Pre-Oxidized Open Tube

Oxidation occurring on coatings in-reactor provides added protection

Next Generation Fuels: SiC and SiC Reinforced Cladding

- Continued autoclave and high temperature testing of General Atomics SiGA® and Ceramic Tubular Products fully ceramic SiC cladding
- Potential additional operating margin (fuel temperatures) and safety margin (response time)
- Next steps in 2026
  - Fabricate cladding test samples with fiber holding mechanism
  - High temperature burst testing and hermeticity testing

SiC Reinforced Zr Alloy Cladding

- Exploratory work with the University of Wisconsin and Free Form Fibers
- Minimal increase in cost over Zr only cladding due to short manufacturing time and minimal SiC fiber use
- Hybrid SiC/Zr Cladding Shows Significant Performance Gains (Ramp Rate: 833 °C/min)

Sample	Burst Temperature (°C)
Control Zr-Alloy	750
Thin Layer (0.25 mm)	975
Thick Layer (0.50 mm)	1100

Courtesy of University of Wisconsin

Thank You

Westinghouse Electric Company

@WECNuclear

Westinghouse Electric Company

wecchinanuclear

westinghousenuclear.com

Westinghouse

Martin Steinbrück

KIT

Oxidation and degradation of Cr-coated zirconium alloy: Effect of Cr thickness

This presentation examines the influence of chromium (Cr) coating thickness on the oxidation and degradation behavior of zirconium alloys under high-temperature conditions relevant to severe nuclear accidents. Using magnetron-sputtered Cr coatings of 5–25 µm on Zry-4 substrates, isothermal tests (1000–1400°C in steam) and transient tests up to 1500°C were performed. Results show that all coatings provide effective protection at 1000°C, while at 1200°C only coatings ≥15 µm maintain integrity for one hour; thinner coatings fail due to rapid consumption by oxidation and diffusion. Above the Zr-Cr eutectic temperature (1330°C), protective effects vanish regardless of thickness, and eutectic melt formation accelerates degradation. Post-test analyses revealed a four-layer structure (Cr_2O_3/Cr/$ZrCr_2$/Zry) and edge effects influencing oxidation kinetics. Optimal coating thickness was identified as 15–20 µm, balancing durability and thermomechanical stability, whereas excessive thickness may induce cracking. These findings provide critical input for Accident Tolerant Fuel (ATF) design and modeling, highlighting the limitations of Cr coatings under extreme conditions and their role in improving severe accident management strategies.

Karlsruhe Institute of Technology

Oxidation and degradation of Cr-coated zirconium alloy: Effect of Cr thickness

M. Steinbrueck, I. Lee, U. Stegmaier, C. Tang

30th International QUENCH Workshop, Karlsruhe, Germany, 16-18 Dez 2025

Oxidation and degradation of Cr/Zry at high temperatures

- $2\ Cr + 3\ H_2O \rightarrow Cr_2O_3 + 3\ H_2$
  - Adherent and well protective oxide scale
  - Consumption of Cr layer
- $Zr + 2\ Cr \rightarrow ZrCr_2$
  - Consumption of Cr coating by formation of an intermetallic layer
- Solubility of Cr in Zry bulk (and vice versa)
  - Consumption of Cr coating by diffusion into Zry bulk
- Zr-Cr eutectic melt formation at 1332°C
  - Ultimate upper limit of application

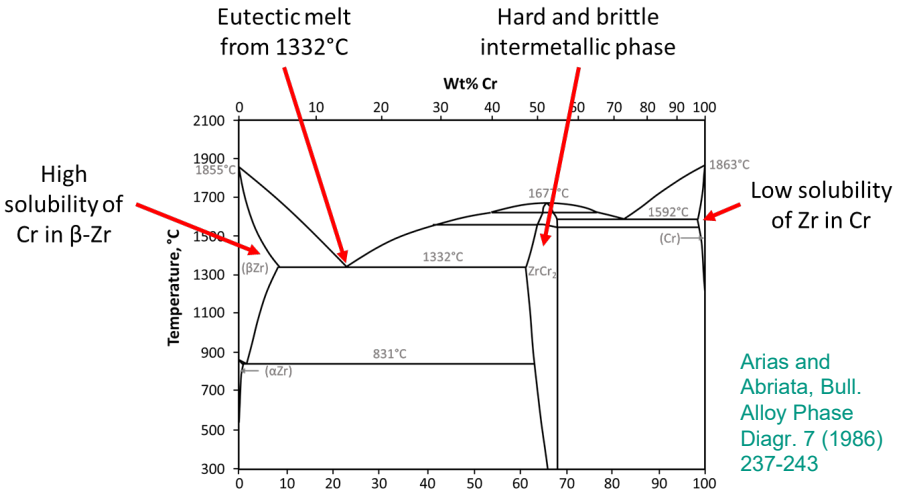

Zr-Cr phase diagram

Brachet et al., JNM 517 (2019) 268-285

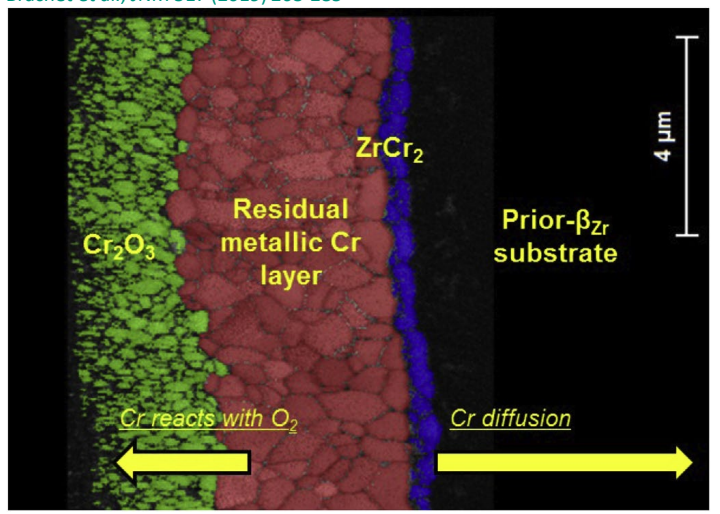

4-layer structure of protective coating

Test facilities

Thermal balance Netzsch STA449

- Max. temperature in dry atmosphere 1600°C
- Max. temperature in steam 1250°C
- Coupled with steam supply system (inlet) and mass spectrometer (outlet)
- Applied for isothermal tests at 1000 and 1200°C in steam, and for transient test in O_2

BOX tube furnace

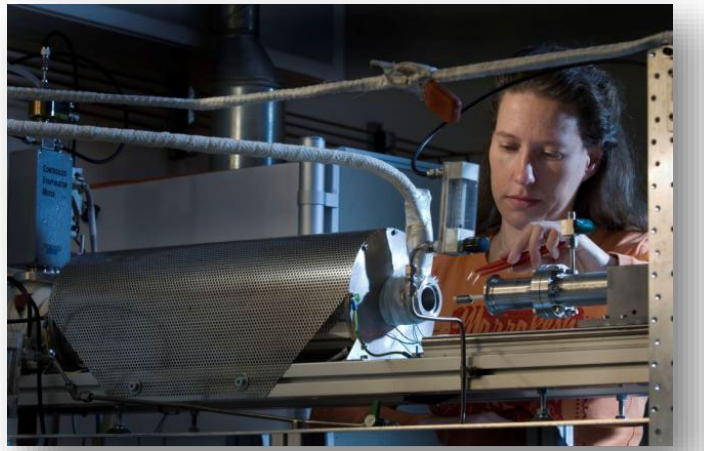

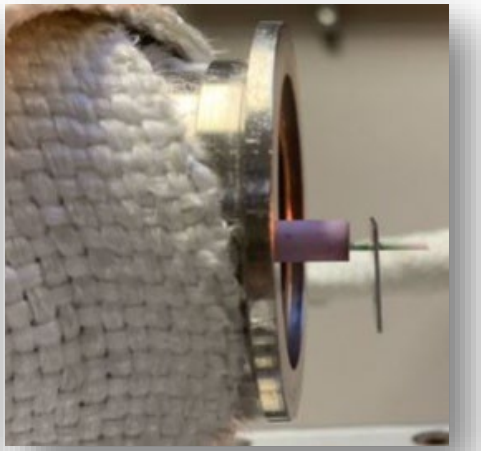

- Max. temperature in steam 1600°C
- Coupled with sample lock, steam supply system (inlet) and mass spectrometer (outlet)
- Applied for isothermal tests at 1400°C and transient tests up to 1500°C

Samples and test conduct

Samples

- Zry-4 plates 15 x 10 x 0.65 mm^3
- PVD Cr coating produced in-house by magnetron sputtering

Test series

- 2 hours at 1000°C in steam
- 1 hour at 1200°C in steam
- 10 min at 1400°C in steam

} **5-25 µm Cr**

- Transient tests with 17-µm samples in oxygen from 500 to 1380°C with **2-50 K/min** heating rate

As-coated sample

Edge effect

- ZrO_2 formation at the poorly coated edges of the samples
- Correction methods:
  - Subtraction of the mass gain by Zr oxidation at the edges ✓
  - Calculation of the mass gain based on Cr_2O_3, ZrO_2 and α-Zr(O) ✓
    - Shown in this presentation by colored dots
  - Subtraction of the mass gain by Zr oxidation using C/P correlation

Isothermal tests

Mass gain in dependence on temperature and Cr thickness

1000°C

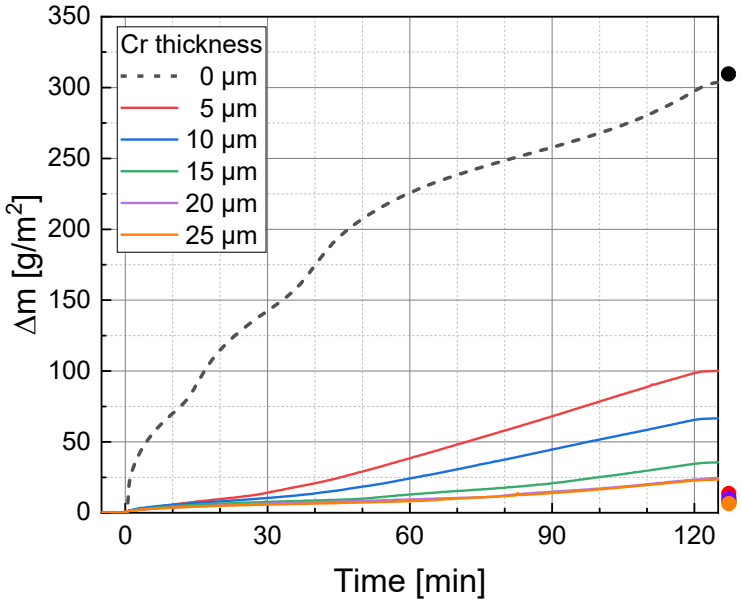

1200°C

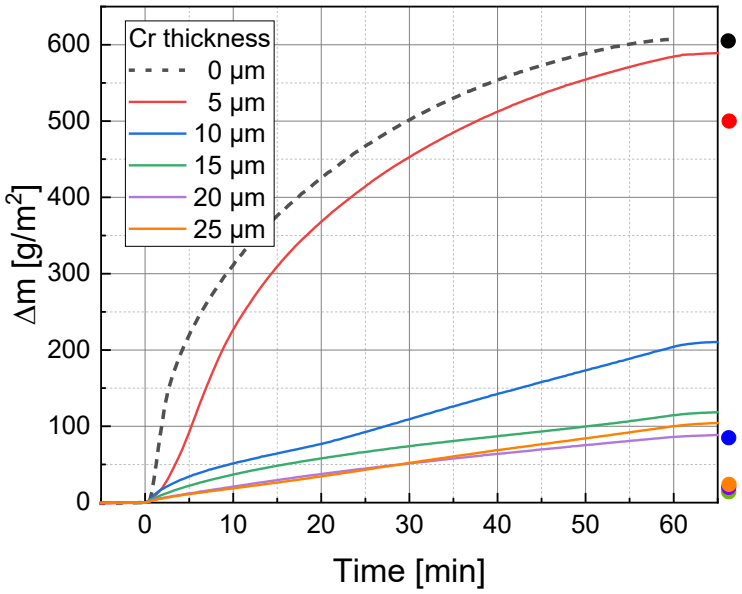

1400°C

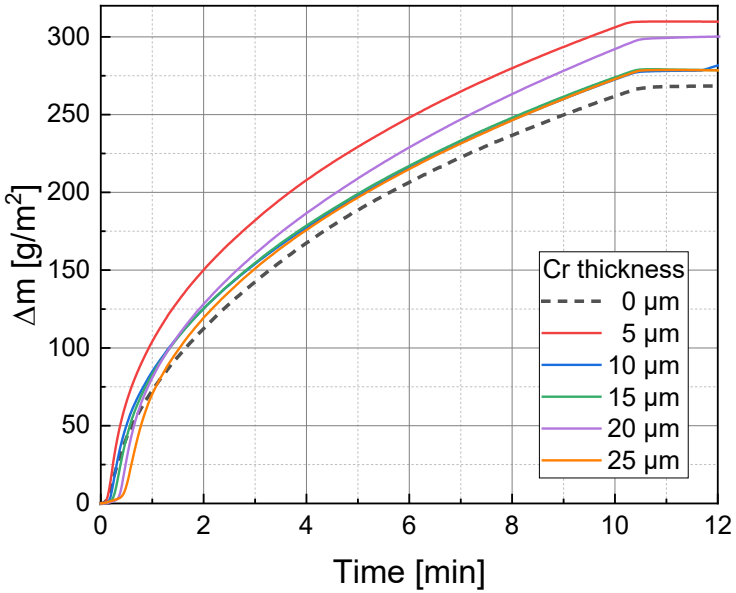

- 1000°C: All coatings provide protection for two hours
- 1200°C: Almost no protective effect of 5-µm Cr coating, slow degradation of the 10-µm coating, and protection for one hours from 15 to 25 µm Cr thickness
- 1400°C: No protective effect independent on Cr thickness → comparable oxidation kinetics of coated and uncoated samples

Mass gain rates and integral values

1000°C

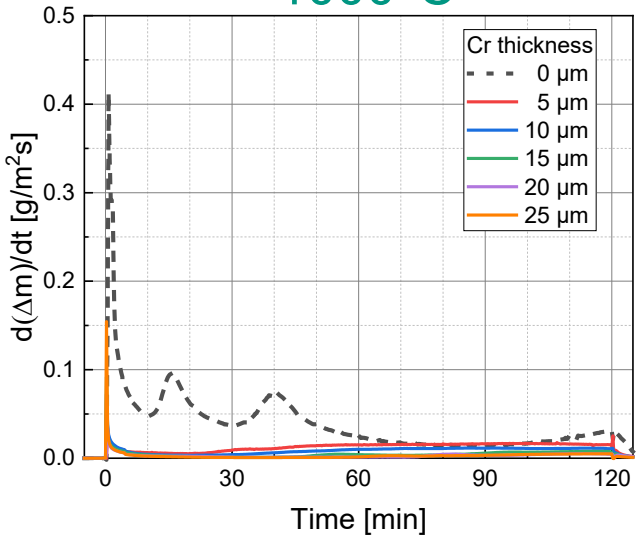

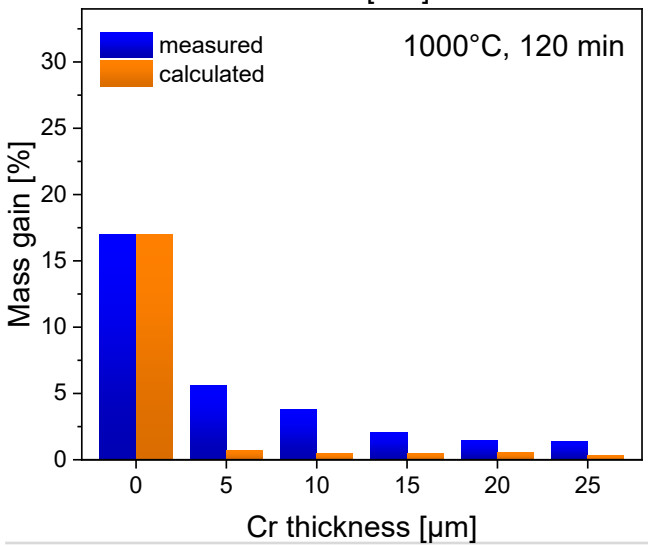

1200°C

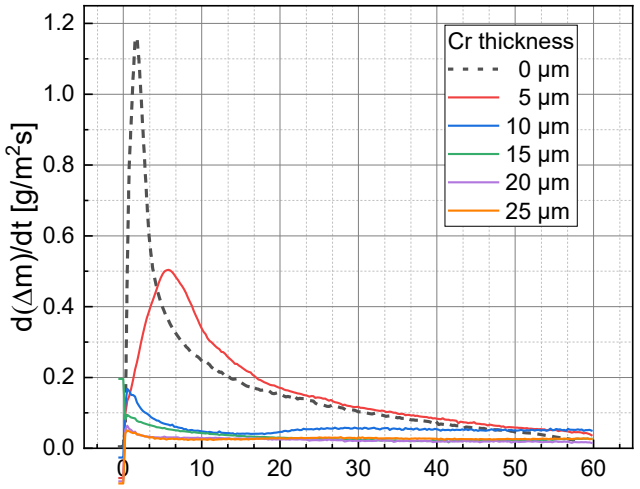

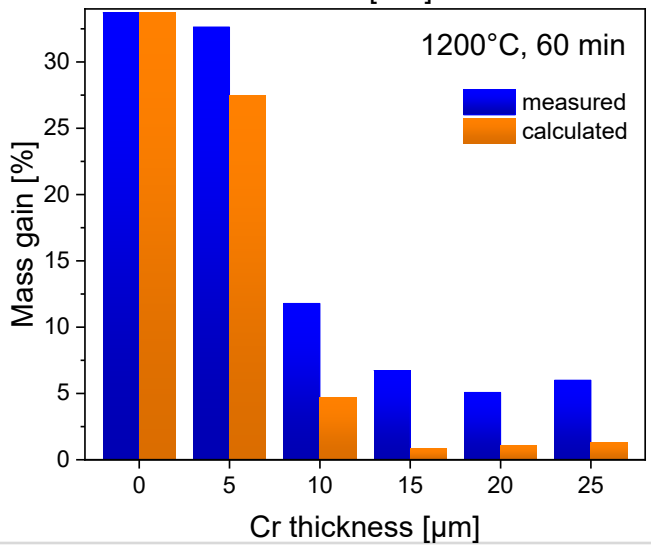

1400°C

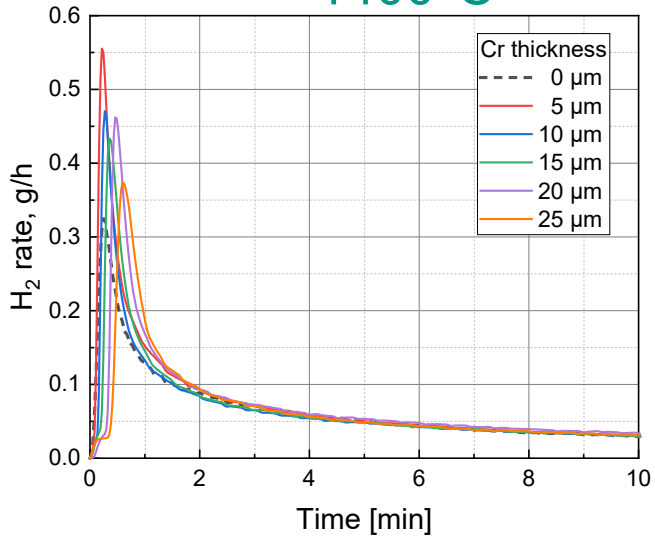

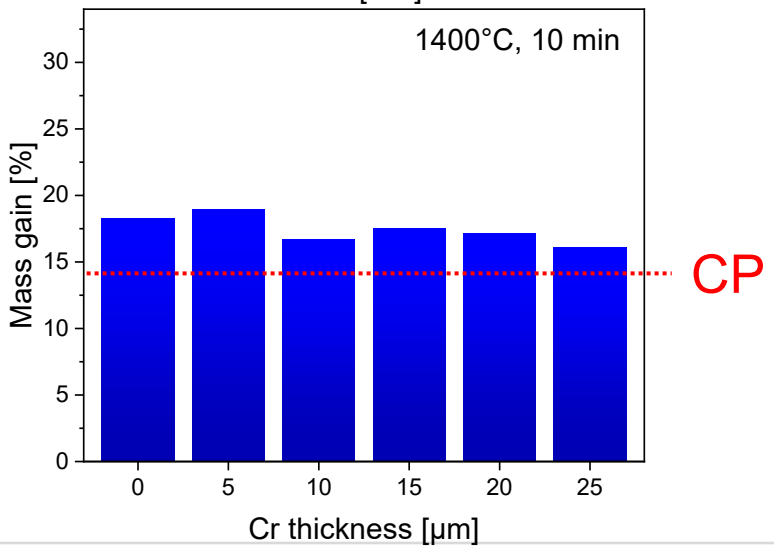

Post-test examination of 1000°C samples

- Enhanced oxidation at poorly coated edges (edge effect)
- Four-layer structure for all samples: Cr_2O_3/Cr/$ZrCr_2$/Zry
- 2-5 µm Cr_2O_3 layer
- ~1 µm $ZrCr_2$ interface layer
- ➡ Protective effect for all samples
- <u>5 µm Cr</u>: rough interface, ZrO_2 diffusion paths along Cr GBs

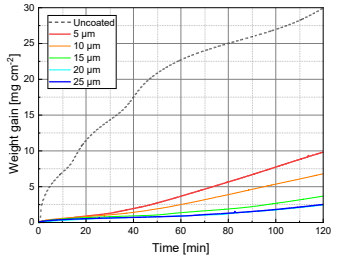

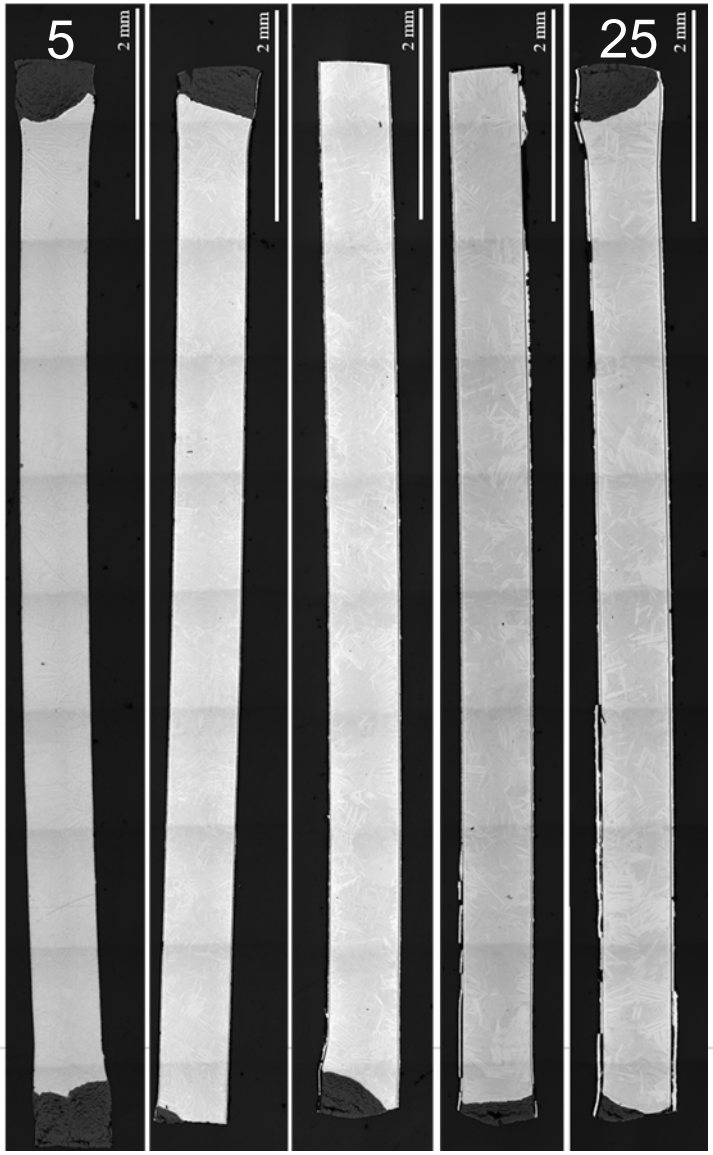

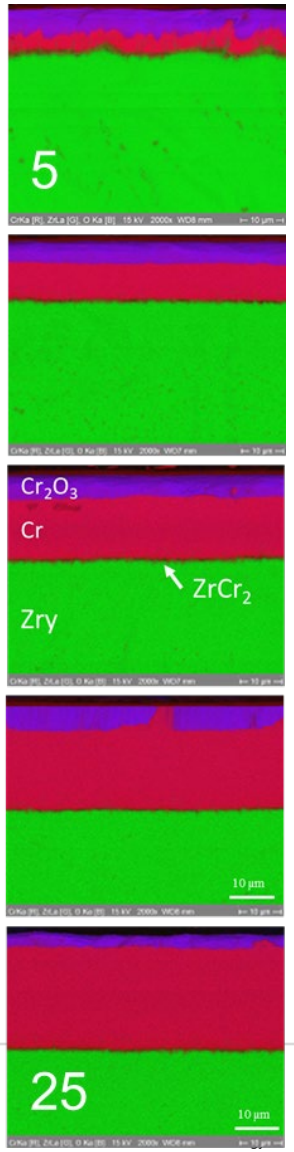

Post-test examination of 1200°C samples

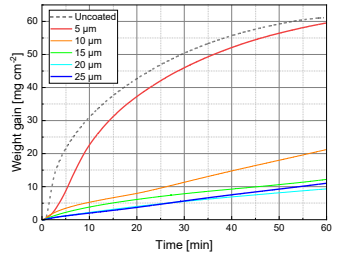

- Strong edge effects
- 5 µm Cr: Almost complete oxidation of sample
- 10 µm Cr: Degraded coating and significant α-Zr(O) formation
- 15-25 µm Cr: 4-layer structure with ZrO_2 paths along Cr GBs
- 25 µm Cr: local defects in coating

➡ Best protection for 15-20 µm Cr thickness

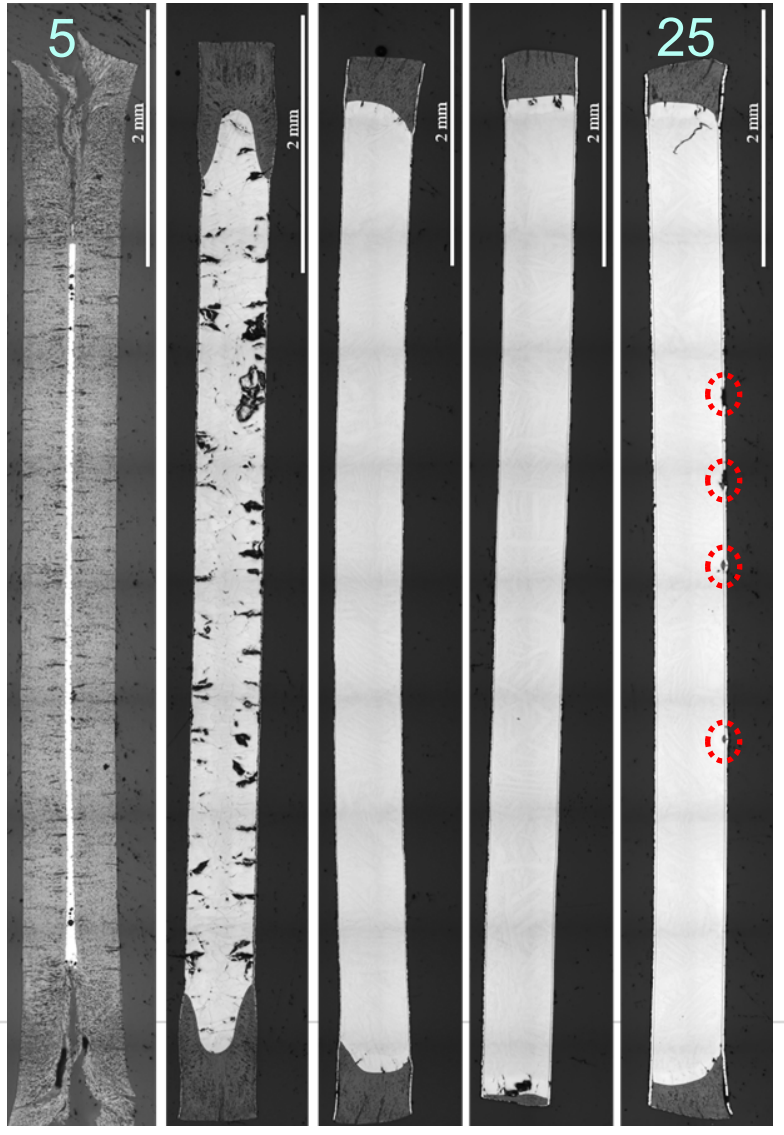

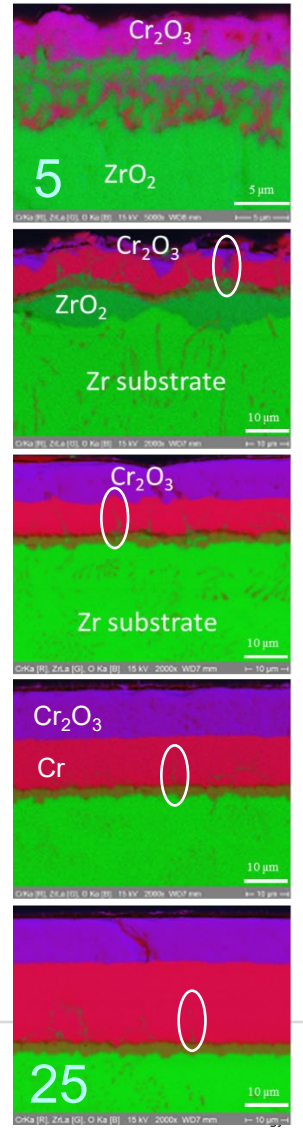

Special feature only for 25-µm sample at 1200°C

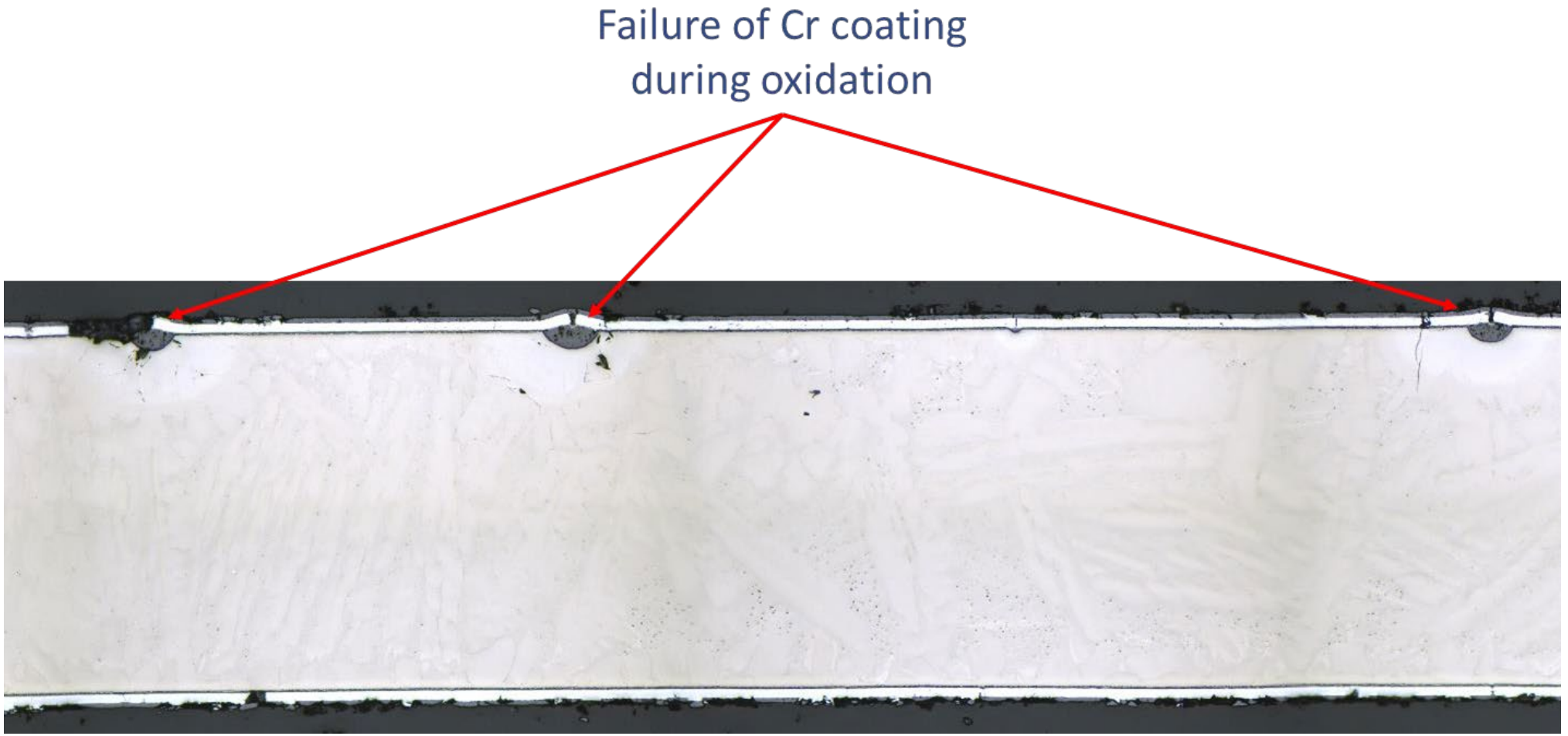

- Indication for too thick Cr coating resulting in thermo-mechanical mismatch?

ZrO_2 diffusion paths along Cr grain boundaries

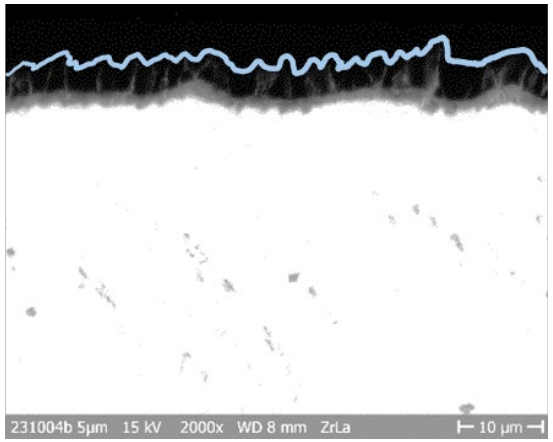

1000°C, 5 µm Cr

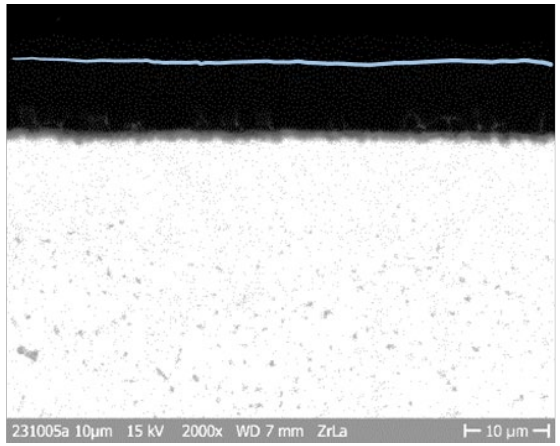

1000°C, 10 µm Cr

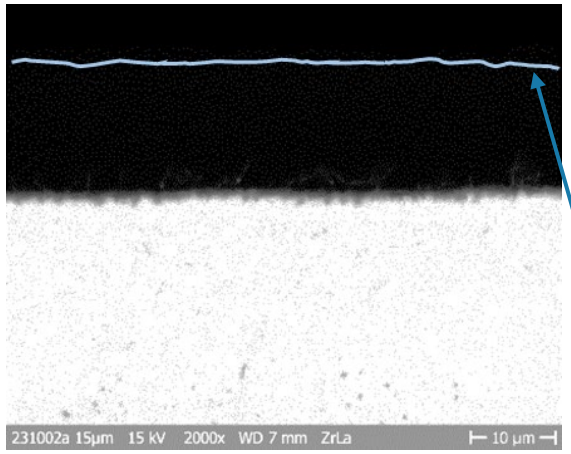

1000°C, 15 µm Cr

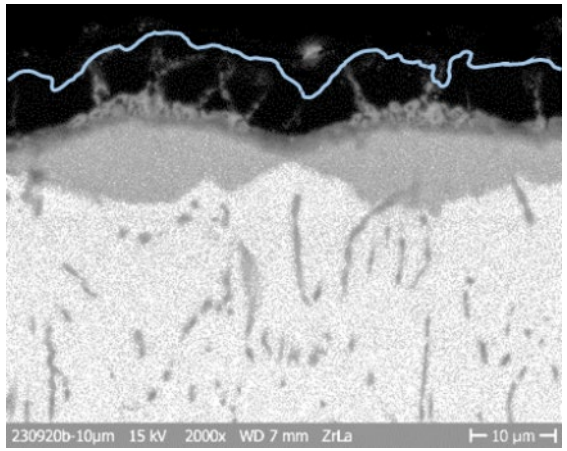

1200°C, 10 µm Cr

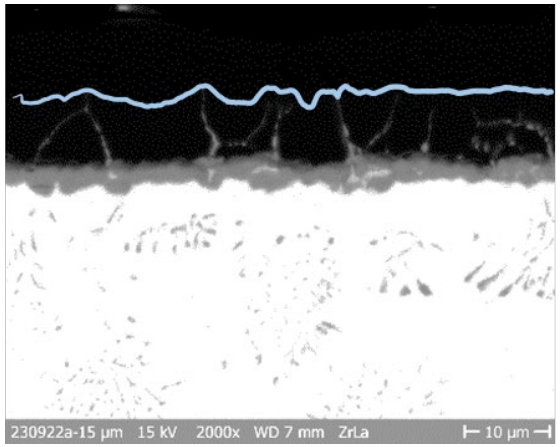

1200°C, 15 µm Cr

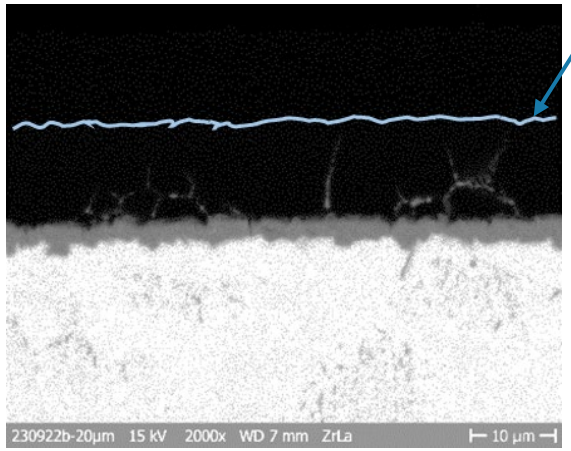

1200°C, 20 µm Cr

Cr/Cr_2O_3 interface

Post-test examination of 1400°C samples

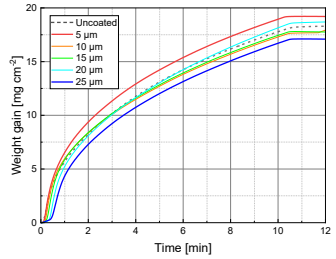

- Significant oxidation of all samples, almost independent on Cr thickness
- Increasing eutectic melt formation with thicker Cr coating
- $ZrCr_2$ precipitates in frozen melt
- Cr_2O_3 layer on surface
- ➡ No protective effect of Cr coating above eutectic temperature (1330°C)

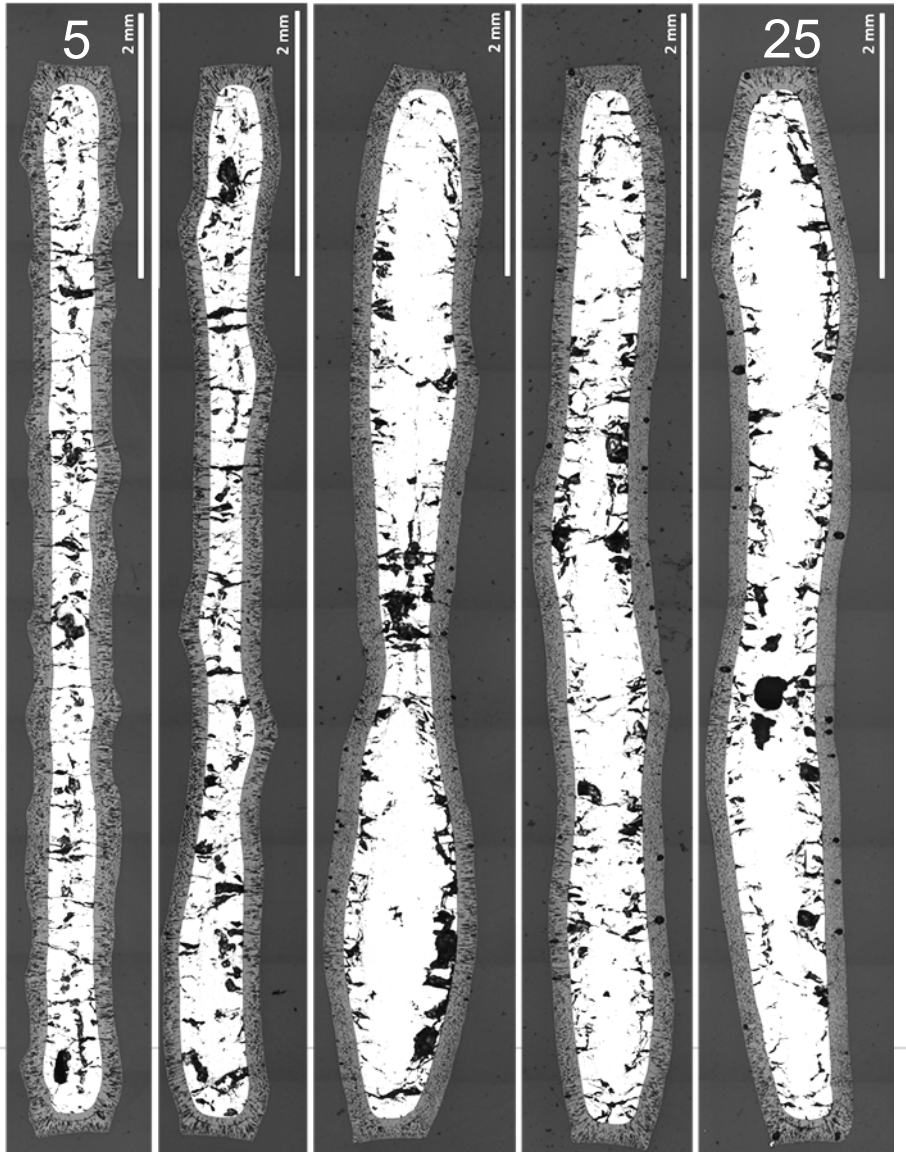

XRD below and above eutectic temperature

- 1200°C: Strong (110) texture of the epitaxially grown Cr_2O_3
- 1400°C: Evenly distributed Cr_2O_3 grains
  - Initially formed Cr_2O_3 reduced by Zr-Cr eutectic melt and reformed on top of the ZrO_2 layer

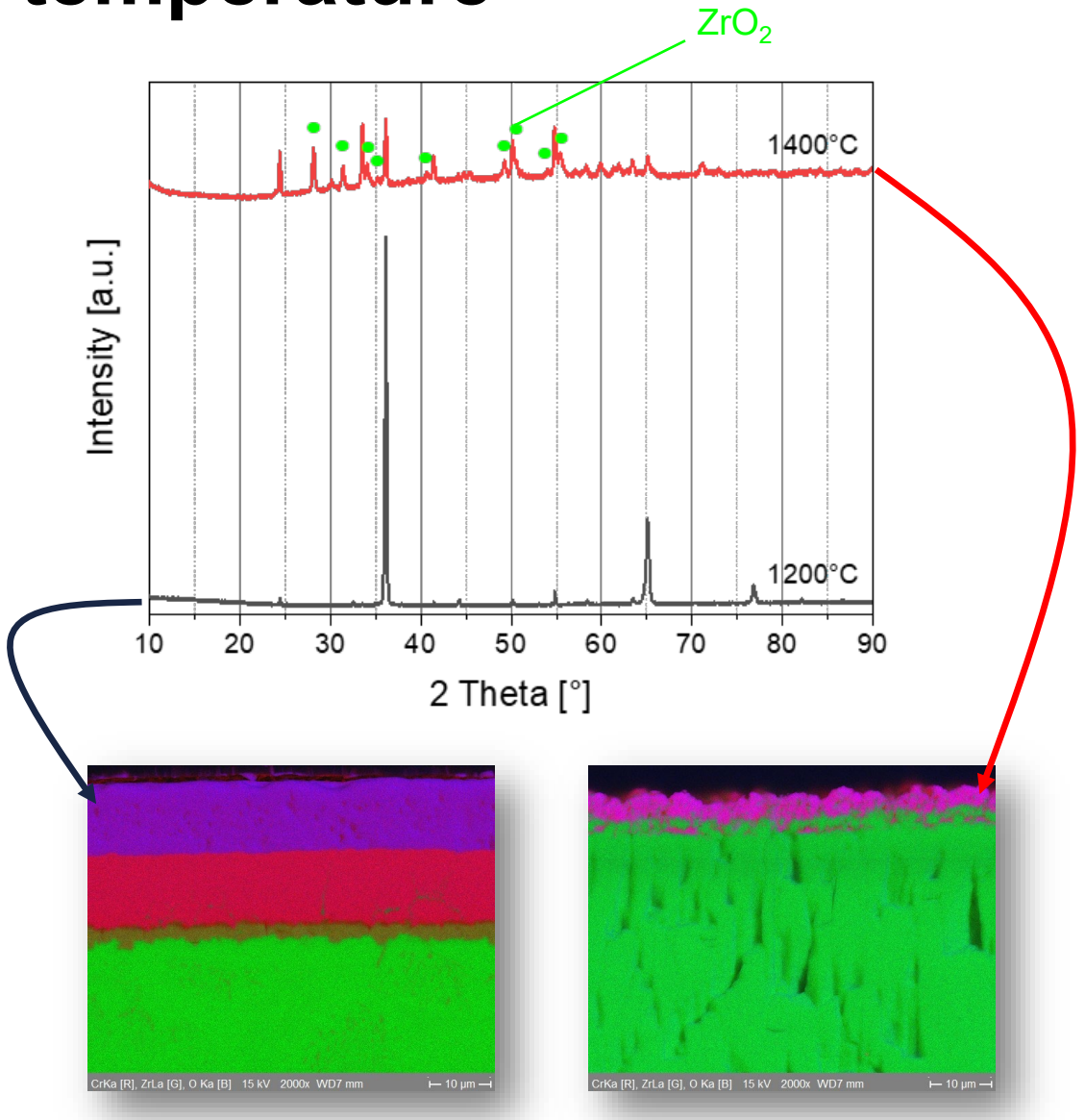

Transient tests

Oxidation rates vs. temperature

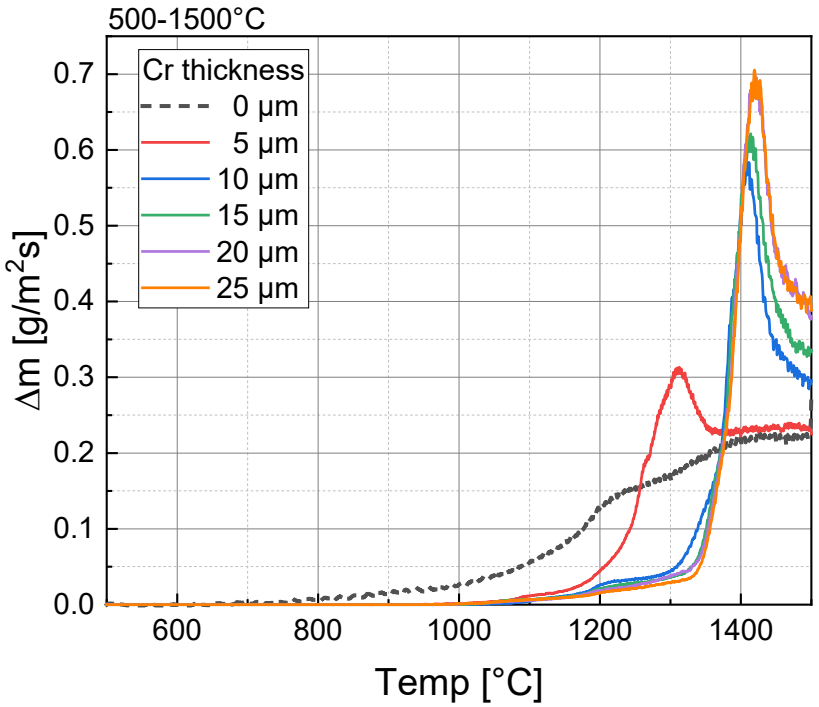

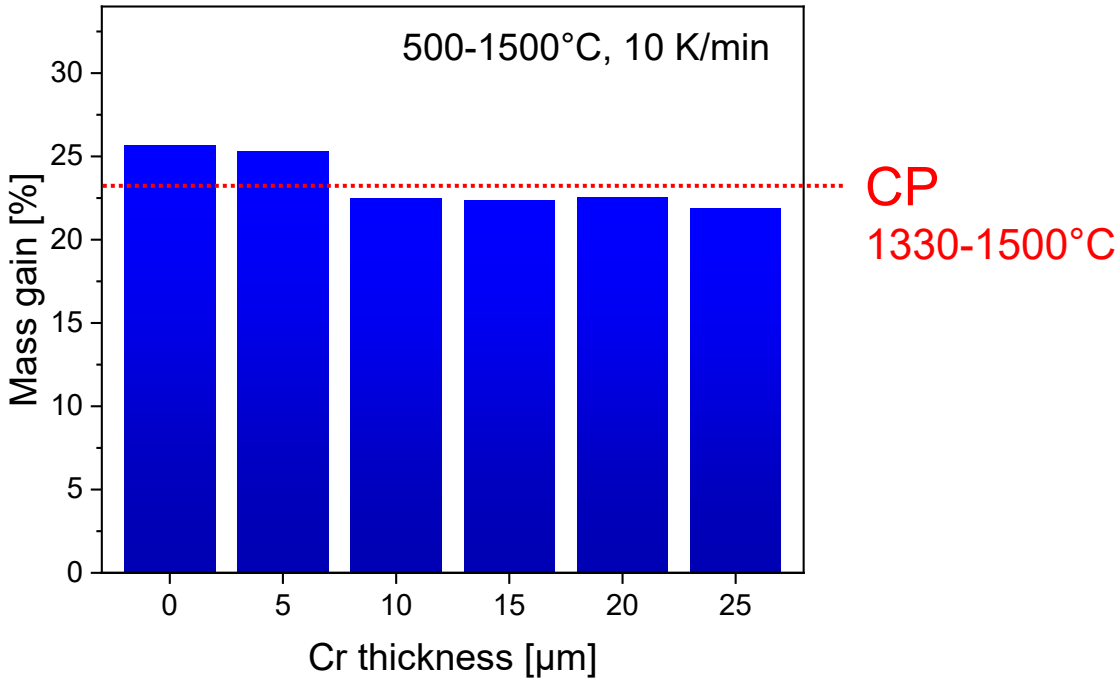

- Protective effect of all coatings up to 1200°C
- Early failure of 5-µm sample above 1200°C due to oxidation and mutual diffusion
- 10-25-µm samples: Rapid increase of oxidation rates above eutectic temperature of 1330°C
- Comparable integral oxidation for all samples

Post-test examination samples after transient tests

Examples: 5 µm and 25 µm Cr

5 µm

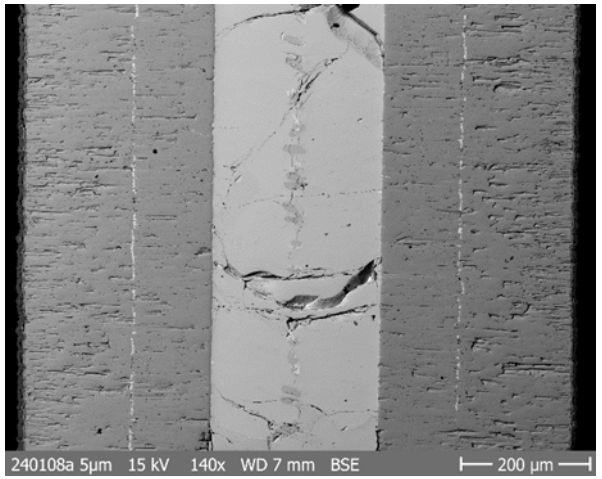

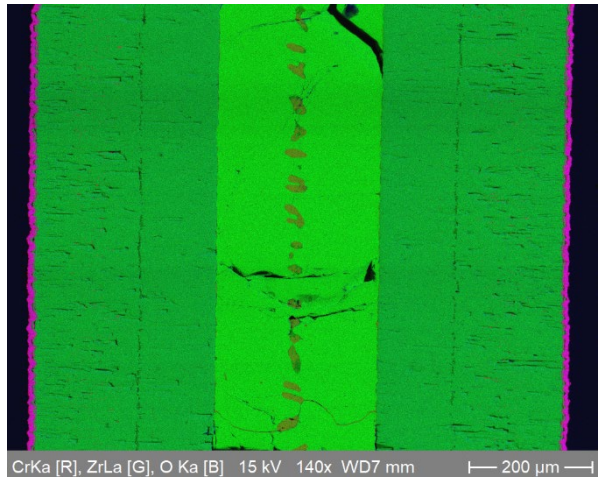

25 µm

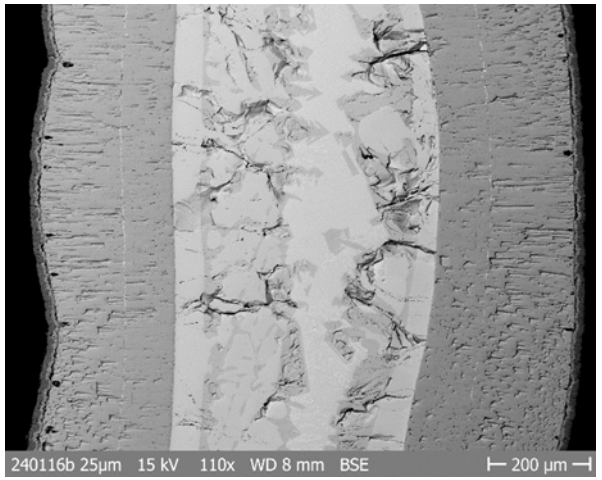

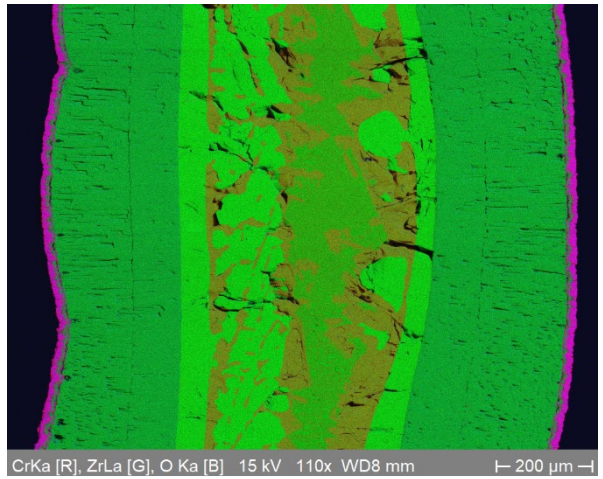

Optical micrographs

EDS mappings

- Inverse “crocodile skin” of samples with ≥ 10 µm Cr
- Thin superficial (re-formed) Cr_2O_3 layer
- Thick ZrO_2 layer with tin line
- Increasing eutectic melt formation with thicker Cr coating in the center of the sample

Estimation of Cr consumption

Based on Brachet, Proceedings TOPFUEL2024, Grenoble, France
(considering Cr oxidation and diffusion of Cr into Zry)

Cr consumption during isothermal tests

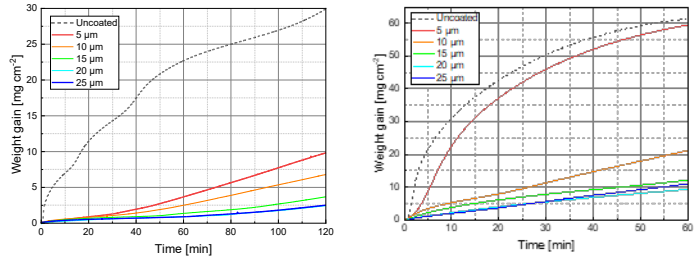

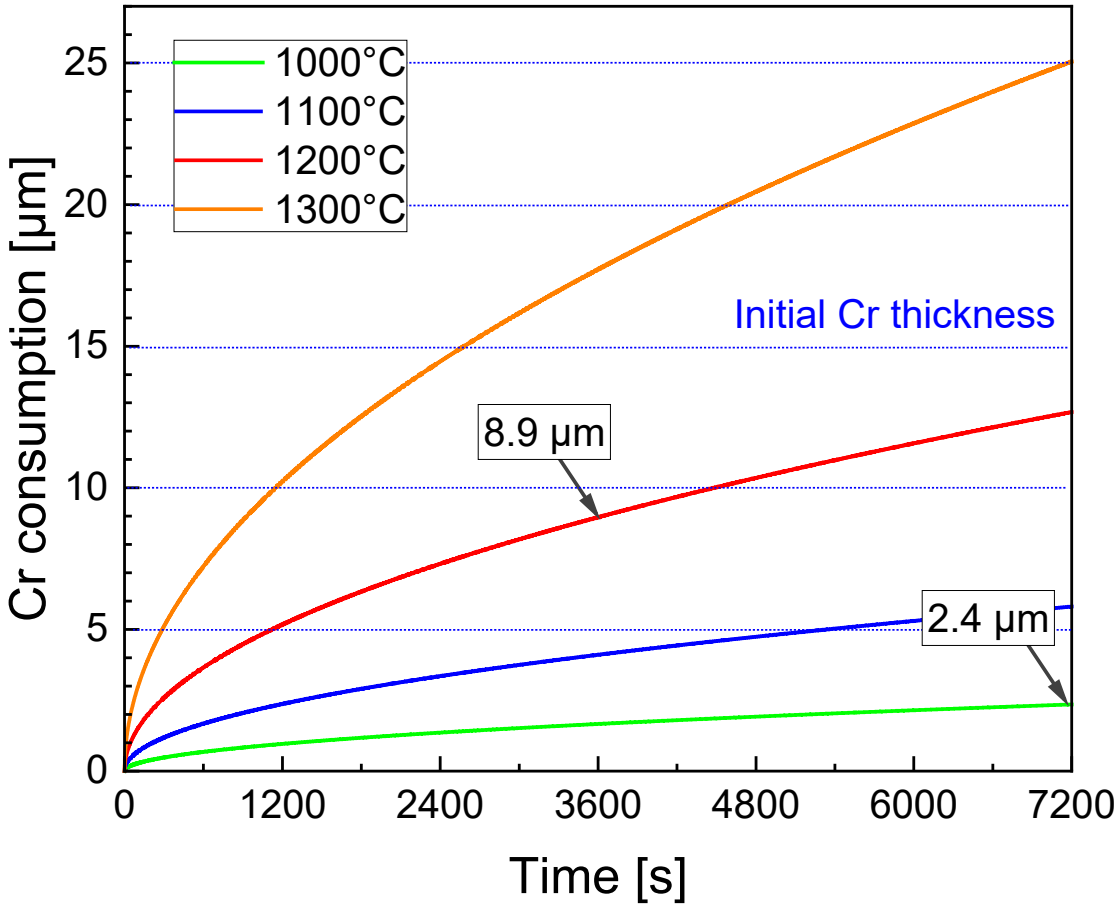

Cr consumption due to oxidation and diffusion

- 1000°C: only partial consumption of Cr coating for all samples for 2 hours
- 1200°C: full consumption of 5-µm Cr, partial consumption of thicker coatings
- Good correspondence with experimental results

Cr consumption during transient tests

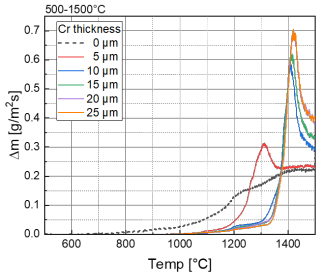

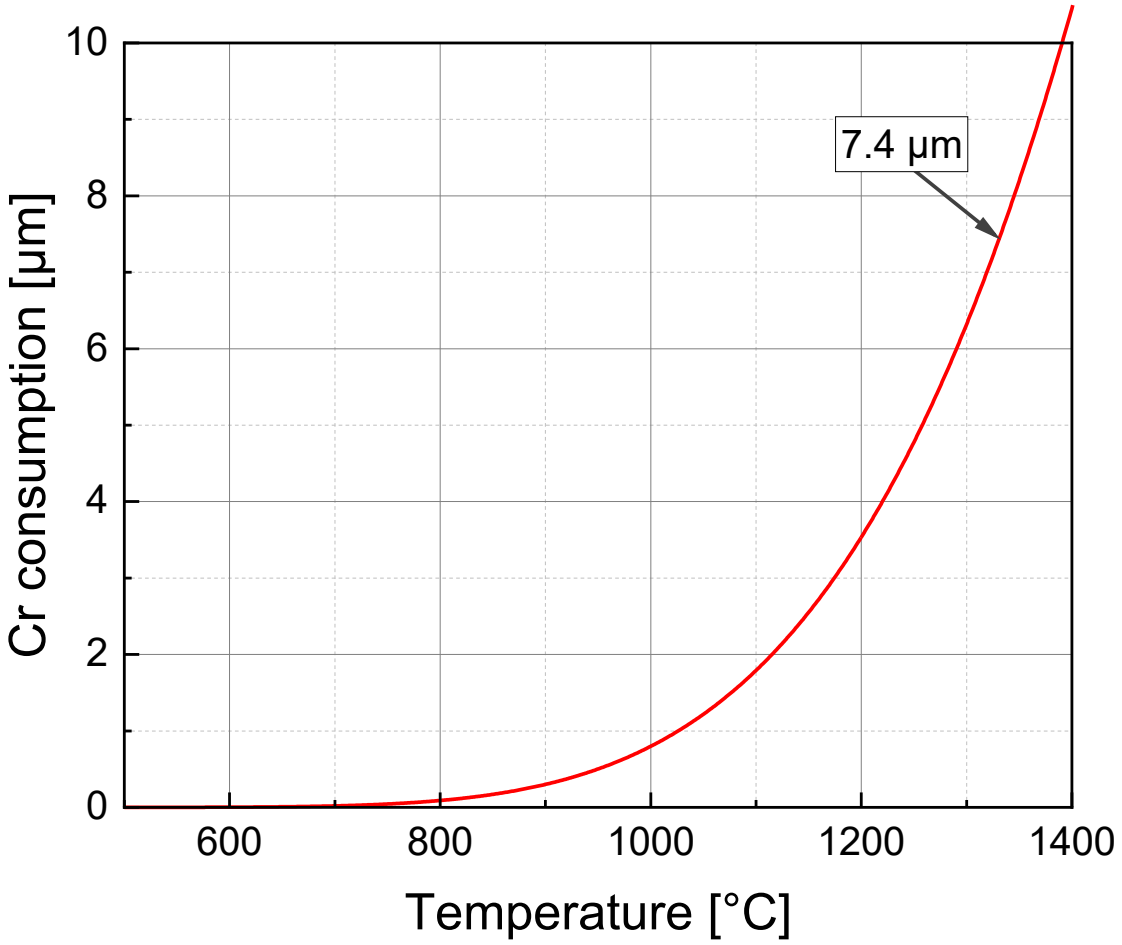

Cr consumption due to oxidation and diffusion

- 7.4 µm Cr consumed when eutectic temperature is reached
- Complete consumption of Cr coating at this point for 5-µm coating
- Partial consumption of thicker coatings
- Good correspondence with experimental results

Conclusion

- Increasing protective effect with increasing Cr thickness up to 1300°C
  - Oxidation and degradation are determined by diffusion processes
- Optimal (PVD) Cr thickness is between 15 and 20 µm
  - Thinner coating: early consumption and loss of protective effect
  - Too thick coating: Thermomechanical stresses may cause cracks in Cr coating
- Rapid failure of Cr coating at 1330°C with complete loss of protective effect caused by Cr-Zr eutectic interaction
- The more metallic Cr is present when the eutectic temperature is reached, the more eutectic melt is formed
- Oxidation kinetics above 1330°C determined by Zry oxidation

➡ Cr_2O_3 kinetics → transition → ZrO_2 kinetics

➡ Slow transition for T<1330°C, fast transition for T>1330°C

Graphical summary

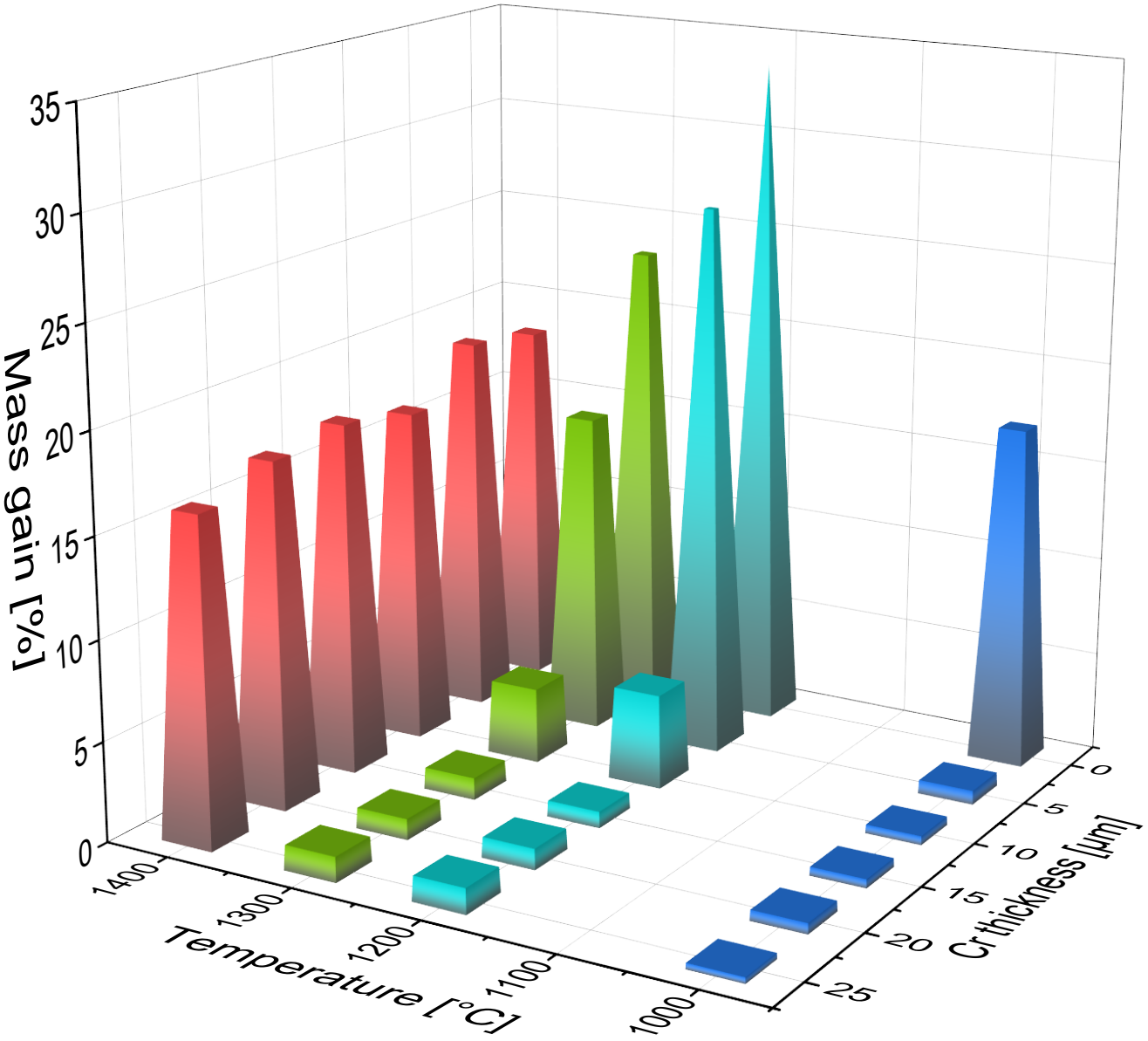

Calculated mass gain based on layer thicknesses vs. temperature and Cr thickness

Acknowledgment

- Injae Lee's internship at KIT was supported by the Korean KONICOF program
- HGF program NUSAFE for funding
- Jean-Christophe Brachet for fruitful discussions during post-test analyses

- Thank YOU for your patience

Jean-Christophe Brachet

CEA

Effect of initial Cr-coating thickness on the high-temperature steam oxidation behavior of Cr-coated Zr-based alloys: Comparison between TGA experiments conducted at several institutes using "Equivalent Chromium Reacted" (ECrR) parameter

Karlsruhe Institute of Technology (KIT) has recently carried out several Thermo-Gravimetric Analysis (TGA) oxidation tests at High-Temperature (HT) in steam environment on Zircaloy-4 sheets coated by Cr using Physical Vapor Deposition (PVD), with initial Cr coating thicknesses ranging from 5 to 25 µm. Along with observations made at CEA and in other research institutes, these recent TGA data from KIT confirm that increasing the initial Cr coating thickness reduces the oxidation kinetics at HT of Cr-coated Zr-based alloys. To take this effect into account, CEA has recently derived a new "Equivalent Cladding Reacted" parameter, called: "Equivalent Chromium Reacted" (ECrR) [1] [2], expressed as a function of HT oxidation conditions (temperature and time) and the initial Cr coating thickness:

ECrR (%) = 6.73 x 105 exp(-15784/T) x (t)1/2 / X0

(T in Kelvin, t in seconds, X0 being the initial Cr-coating thickness in µm)

This simple parameter appears efficient to predict the overall "consumption kinetics" of Cr coating upon HT oxidation. Moreover, this new metric has been successfully used to account for the initial Cr coating thickness effect on the Post-Quenching (PQ) residual cladding strength and ductility, following one-sided HT steam oxidation. Regardless of the initial Cr thickness, ranging from ~5 µm to ~25 µm, it was demonstrated that the PQ Ductile-to-Brittle Transition (DBT) of the failure mode in the Cr-coated cladding occurs at an apparent "critical" value of the ECrR parameter of nearly 70% [1]. Indeed, for Cr-coated claddings steam oxidized at 1100-1300°C and when the Cr-coating loses its protectiveness, it has been shown that this ECrR value corresponds to an averaged oxygen content that has diffused into the prior-βZr reaching a value higher than ~0.4wt.% [2] which is known to be a "critical" value inducing DBT of the water quenched prior-βZr value at room temperature [3].

Furthermore, as will be shown in this presentation and illustrated in Figs 1 & 2, the use of this new "ECrR" allows rationalizing and capturing the effect of the initial Cr coating on the Weight Gain (WG) evolution during HT oxidation for various initial Cr coating thicknesses, oxidation temperatures, and durations, and under both isothermal and anisothermal conditions. Fig. 2 also highlights an acceleration of the WG increase beyond an ECrR of about 70-100%, consistent with the expected loss of HT oxidation protectiveness of the Cr coating beyond this "critical" ECrR range.

References:

[1] Brachet, J.-C., Guilbert, T., Hamon, D., Nony, G., & Gokelaere, P. (2024). "*A new « ECR » parameter to support high-temperature (one-sided) steam oxidation behavior of Cr-coated Zr-based E-ATF claddings, in relation with their post-quenching (PQ) mechanical strength and ductility (for LOCA and slightly beyond conditions)*", Proceedings of the Topfuel / Reactor Fuel Performance International Symposium, 29 September – 3 October 2024, Grenoble, France.

[2] Brachet, J.-C., Guilbert, T., Urvoy, S., Rouesne, E., Peyret, M., Vandenberghe, T., Prou, C., Le Hong, T., Hamon, D., *"Some practical methodologies to assess the overall high temperature (one-sided) steam oxidation protectiveness of chromium-based coatings on a zirconium-based substrate, as Enhanced - Accident Tolerant (Nuclear) Fuels (E-ATF) claddings"*, Journal of Nuclear Materials (2025), doi: https://doi.org/10.1016/j.jnucmat.2025.155620

[3] Brachet, J.-C, Maillot, V., Portier, L., Gilbon, D., Lesbros, A., Waeckel, N., Mardon, J.-P., "*Hydrogen Content, Pre Oxidation and Cooling Scenario Influences on Post-Quench Mechanical Properties of Zy-4 and M5TM Alloys in LOCA Conditions - Relationship with the Post-Quench Microstructure*", ASTM 15th International Symposium on Zirconium in the Nuclear Industry, June 24-28, 2007, Sunriver, Oregon, USA, Journal of ASTM International, Vol. 5, No. 4, Paper ID JAI101116, (2008)

Effect of initial Cr-coating thickness on the HT steam oxidation behavior of Cr-coated Zr-based alloys: Comparison between TGA experiments conducted at several institutes using “Equivalent Chromium Reacted” (ECrR) parameter

J.-C. Brachet

Paris-Saclay University, CEA, Service de Recherche en Matériaux et procédés Avancés, 91191, Gif-sur-Yvette, France

Main references:

[1] J.-C. Brachet, et al., “High Temperature Steam Oxidation of Chromium-Coated Zirconium-Based Alloys: Kinetics and Process”, Corrosion Science 167 (2020) 108537, doi: https://doi.org/10.1016/j.corsci.2020.108537

[2] J.-C. Brachet,, et al., “Evaluation of Equivalent Cladding Reacted parameters of Cr-coated claddings oxidized in steam at 1200°C in relation with oxygen diffusion/partitioning and post-quench ductility”, JNM 533 (2020) 152106, https://doi.org/10.1016/j.jnucmat.2020.152106

[3] J.-C. Brachet et al., "A new « ECR » parameter to support high-temperature (one-sided) steam oxidation behavior of Cr-coated Zr-based E-ATF claddings, in relation with their post-quenching mechanical strength and ductility…", Proceedings of Topfuel-2024, Grenoble, France, (Sept. 29th - Oct. 03rd 2024);

[4] J.-C. Brachet, et al., "Some practical methodologies to assess the overall high temperature (one-sided) steam oxidation protectiveness of Cr-based coatings on a zirconium-based substrate…", Journal of Nuclear Materials (2025), doi: https://doi.org/10.1016/j.jnucmat.2025.155620

30th Int. QUENCH Workshop, KIT (Karlsruhe, Germany), 16-18th Dec. 2025

jean-christophe.brachet@cea.fr

Recall - Consumption kinetics of Cr coatings on Zr-based substrate upon HT steam oxidation (*1000-1300°C, LOCA and slightly beyond conditions*) by two main mechanisms:

(1) Outer Cr_2O_3 scale thickening

$$\Delta Cr(consumed\ by\ Cr_2O_3) = Kp_1'\sqrt{oxidation\ time}$$

(3) Cr volatilization and Cr consumption due to the interlayer $ZrCr_2$ thickening are neglected (i.e., less than ~2µm Cr consumed by these mechanisms…)

JC, Brachet et al.,JNM 2019

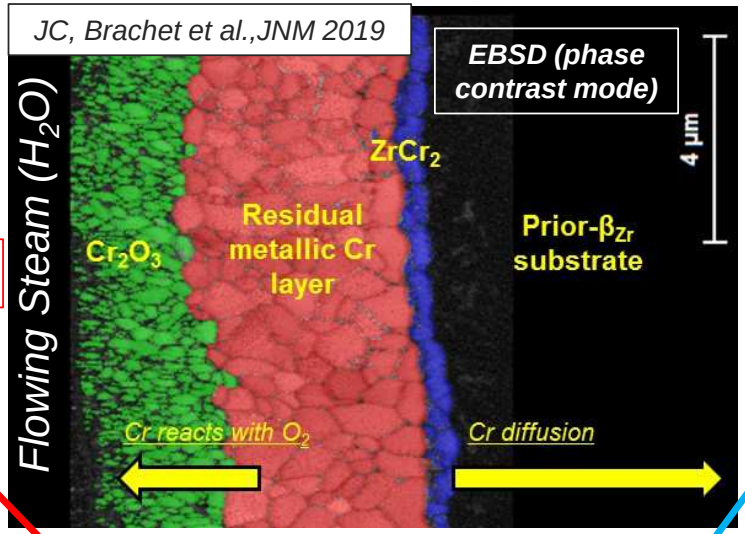

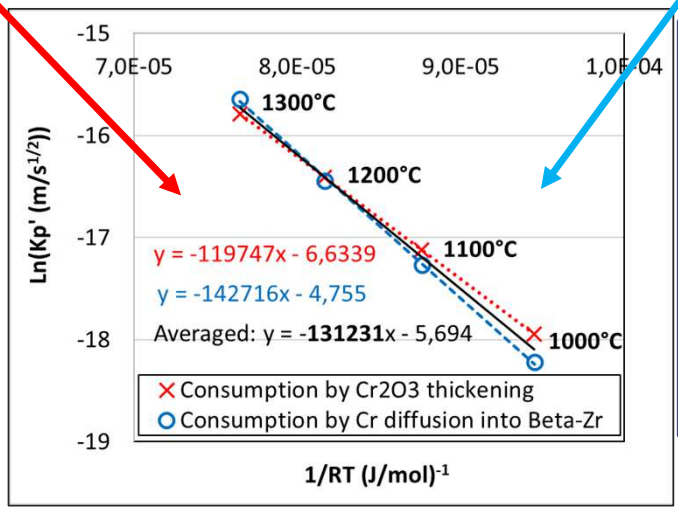

(2) Cr diffusion into the β_{Zr} substrate

$$\Delta Cr(Cr\ diffusion\ into\ \beta_{Zr}) = Kp_2'\sqrt{oxidation\ time}$$

Due to similar parabolic rate constant (Kp') values, one can identify an **"averaged" Kp' describing the overall contributions of both Cr-coating consumption mechanisms**

$$\Delta Cr_{(Cr2O3\ +\ Cr\ diffusion\ into\ \beta\text{-}Zr)} = 2 \times Kp'_{Averaged}\sqrt{oxidation\ time}$$

$$= 6{,}73.10^3.\exp(-15784/T).\sqrt{oxidation\ time}$$

*With: **ΔCr in µm**, T in Kelvin and t in seconds*

JC, Brachet et al., Topfuel, 2024

New ECR parameter, *i.e.*, « *Equivalent Chromium Reacted* » proposed, taking into account the initial Cr-coating thickness (X_0):

$ECrR\ (\%) = 6{,}73.10^5.\exp(-15784/T).(t)^{1/2} / X_0$ *(X_0 in µm)*

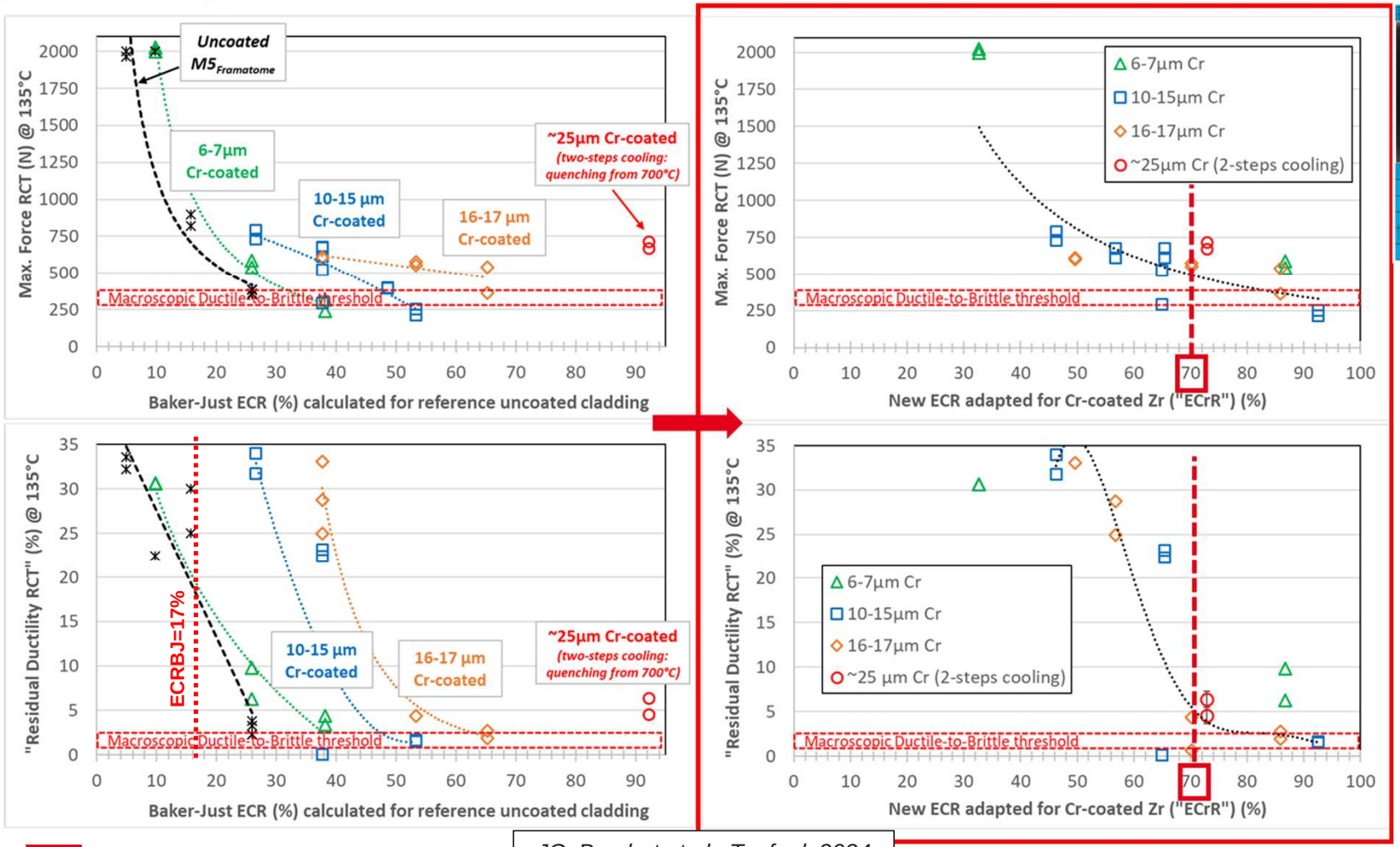

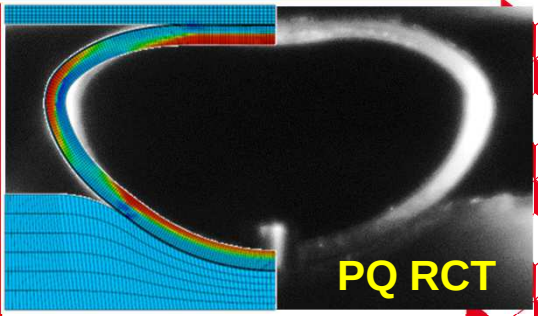

Partial Conclusion (1):

- **New "ECrR"** parameter helps to "rationnalise" the PQ clad mechanical properties of Cr-coated materials derived from RCT, by **taking into account the initial Cr-coating thickness influence**

Partial Conclusion (2):

- After **1sided** steam oxidation & water quenching, determination of an apparent **"critical ECrR" ~ 70%** which *corresponds to Ductile-to-Brittle-Transition derived from RCT* @ 20 & 135°C

JC, Brachet et al., Topfuel, 2024

jean-christophe.brachet@cea.fr

Relationship between the apparent critical « ECrR» ~ 70% inducing Ductile-to-Brittle transition of the failure mode of HT (one-sided) oxidized Cr-coated claddings following water quenching down to RT vs. the prior-β_{Zr} oxygen content

(neglecting the additional influence of Cr diffusion and/or of potential H uptake…)

Cross-section fractograph of an uncoated Zr-based cladding after HT oxidation and PQ Impact testing at RT:

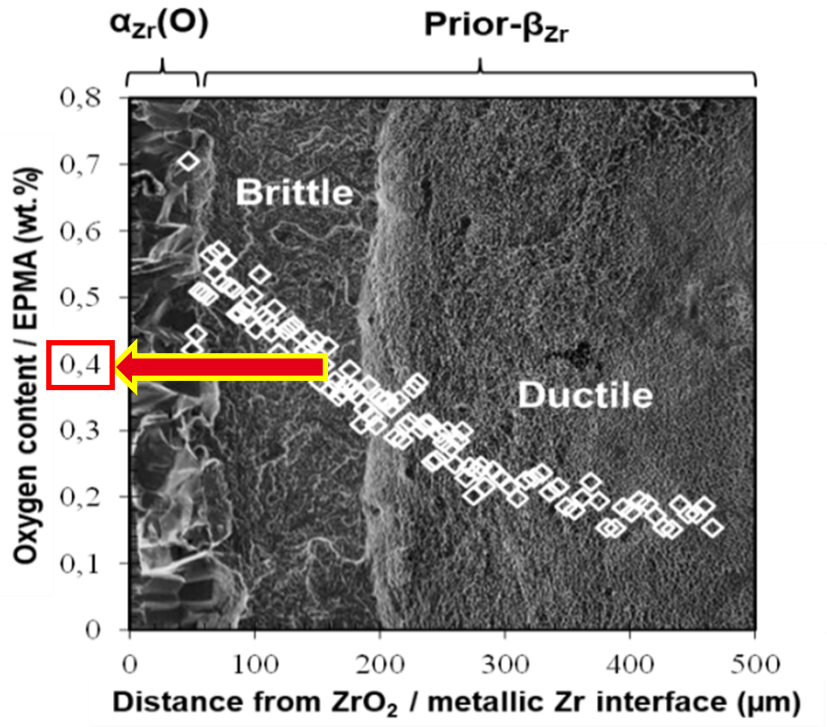

JC. Brachet, V. Maillot et *al.*,
J. of ASTM International (2008)

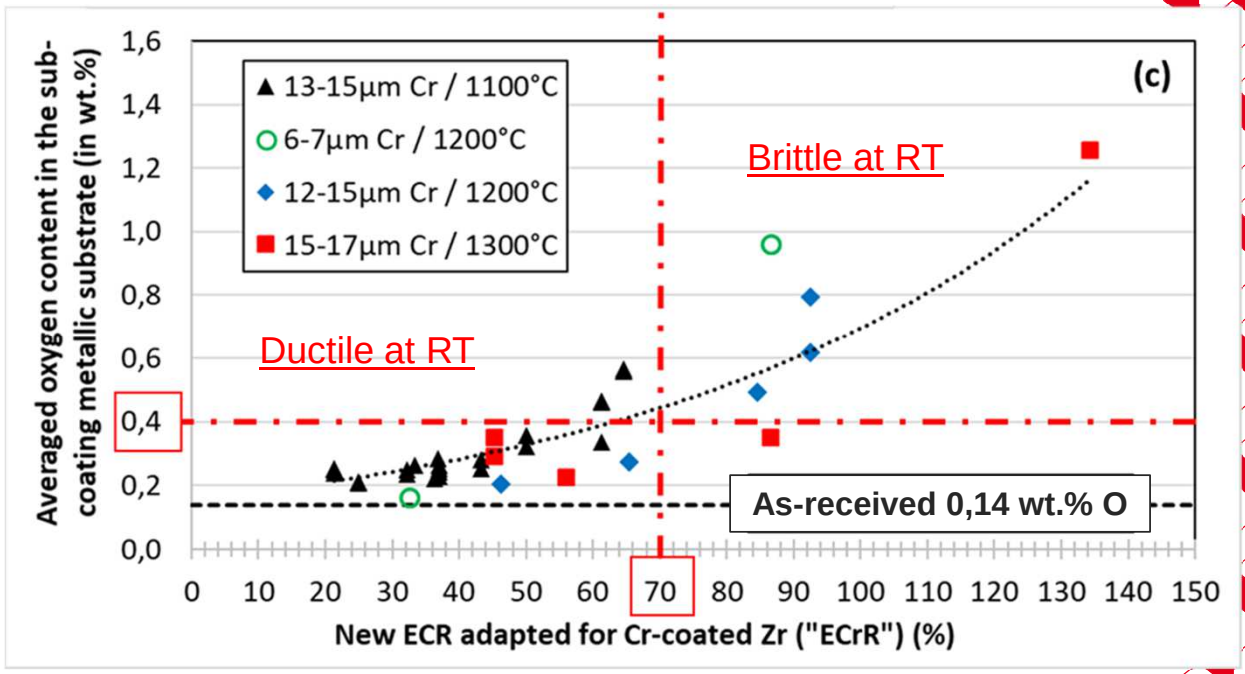

JC, Brachet et al., JNM, 2025

jean-christophe.brachet@cea.fr

Partial conclusions:

New "ECrR" parameter helps to "rationnalise" the PQ clad mechanical properties of Cr-coated materials derived from RCT, by taking into account :

- **the initial Cr-coating thickness influence : within the 5-30µm thicknesses range**
- **oxidation duration : from a few minutes to several hours**
- **oxidation temperature : within the 1100-1300°C temperature range**

⇒ ***Apparent "critical ECrR" ~ 70% which corresponds to:***

- ***Achievement of ~0,4 wt. % of oxygen having diffused within the residual prior-β_{Zr} layer substrate***
- ***PQ Ductile-to-Brittle transition of the macroscopic failure mode (derived from PQ RCT and/or from PQ impact testing at RT…)***

Aim of the present study/analysis:

Extend and apply these new "ECrR" metrics to Cr-coated materials developed and studied at different institutes and for different initial thicknesses, in relation with their continuous Weigh-Gain (WG) evolution, as measured by Thermo-Gravimetric Analysis (TGA) upon one-sided steam oxidation at HT, for both isothermal and anisothermal (transient) conditions

Ex. 1 (1/2): KIT TGA data obtained on Cr-coated Zirc-4 with Cr thicknesses ranging from 5 to 25µm - $T_{oxidation}$ = 1300°C (*see previous Martin S. presentation, submitted to JNM…*)

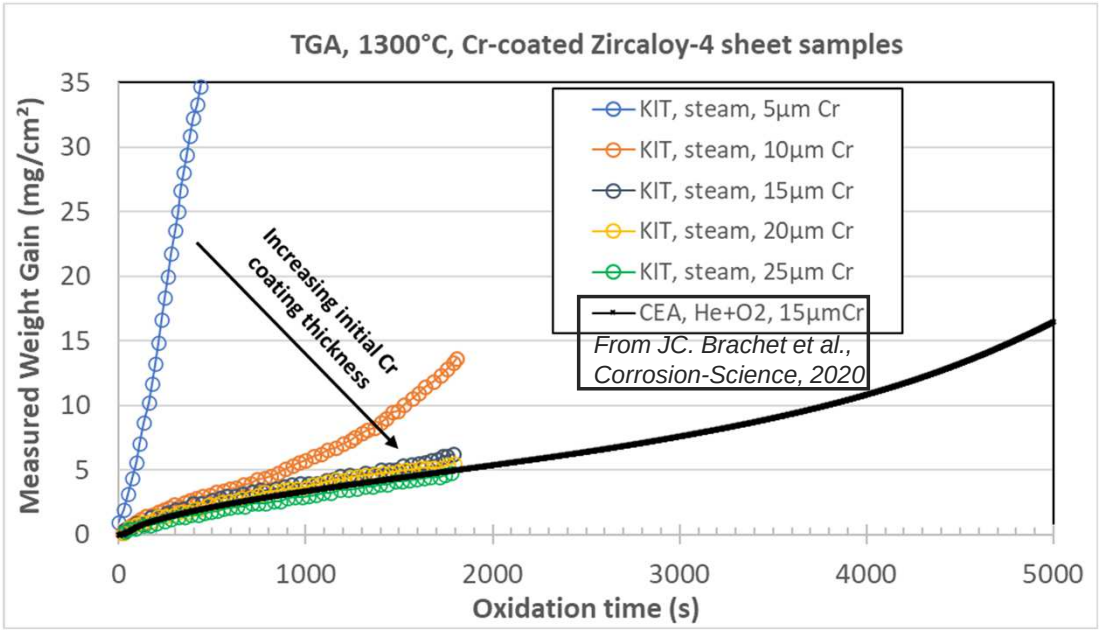

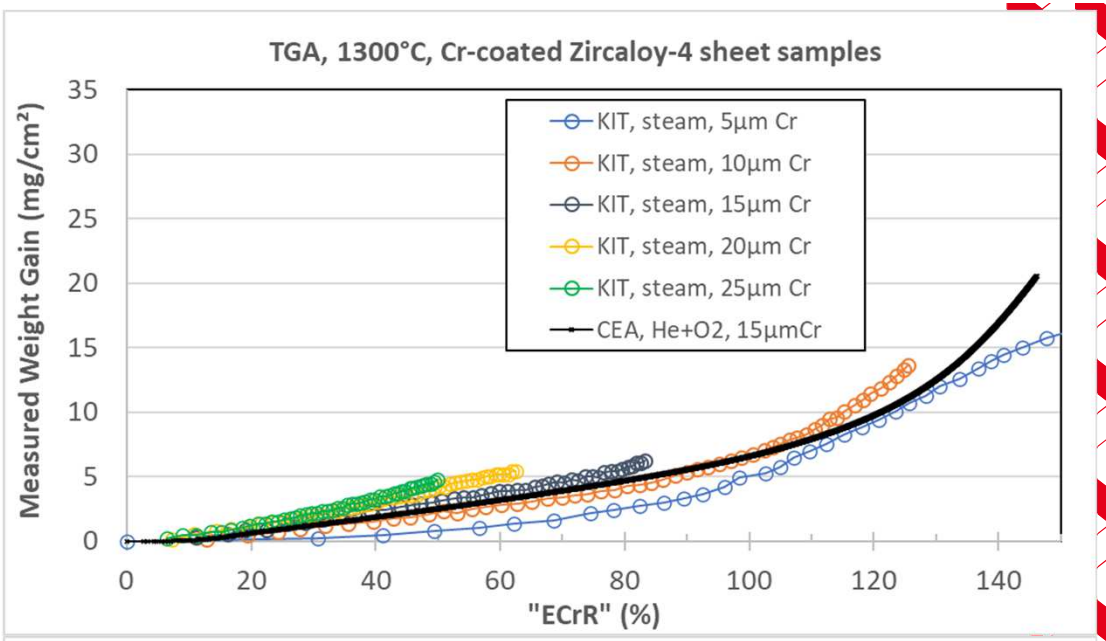

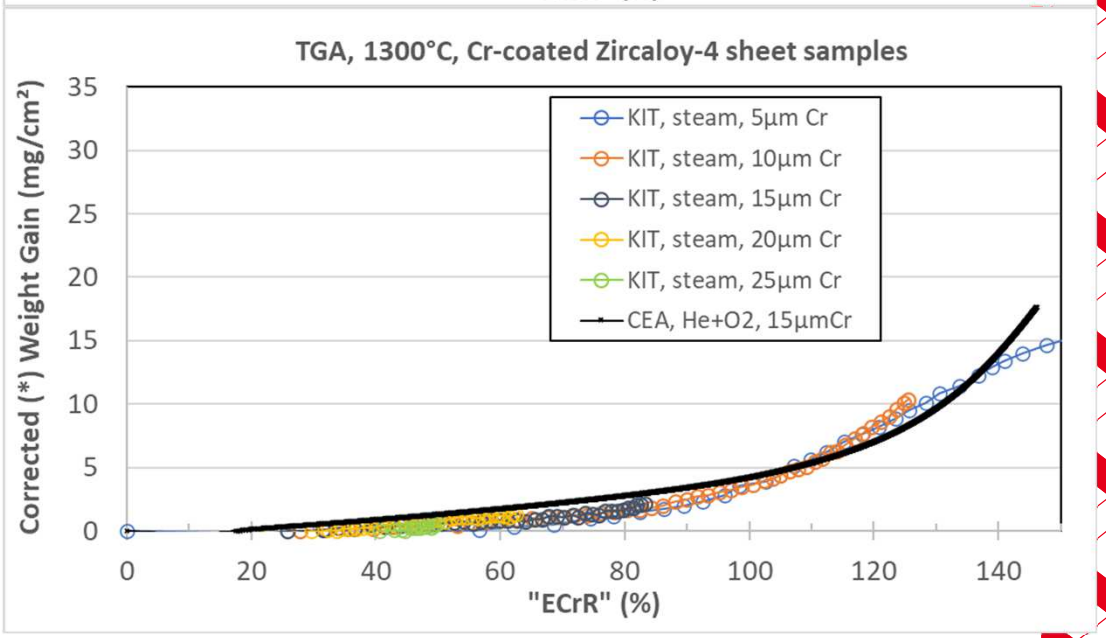

(*) Attempts have been done to correct the « extra-WG » measured due to uncoated or poorly coated samples areas with a quite conservative assumption that 10% of the total surface is uncoated…

jean-christophe.brachet@cea.fr

Ex. 1 (2/2): KIT TGA data Cr = 5 - 25µm; $T_{oxidation}$ = 1300°C

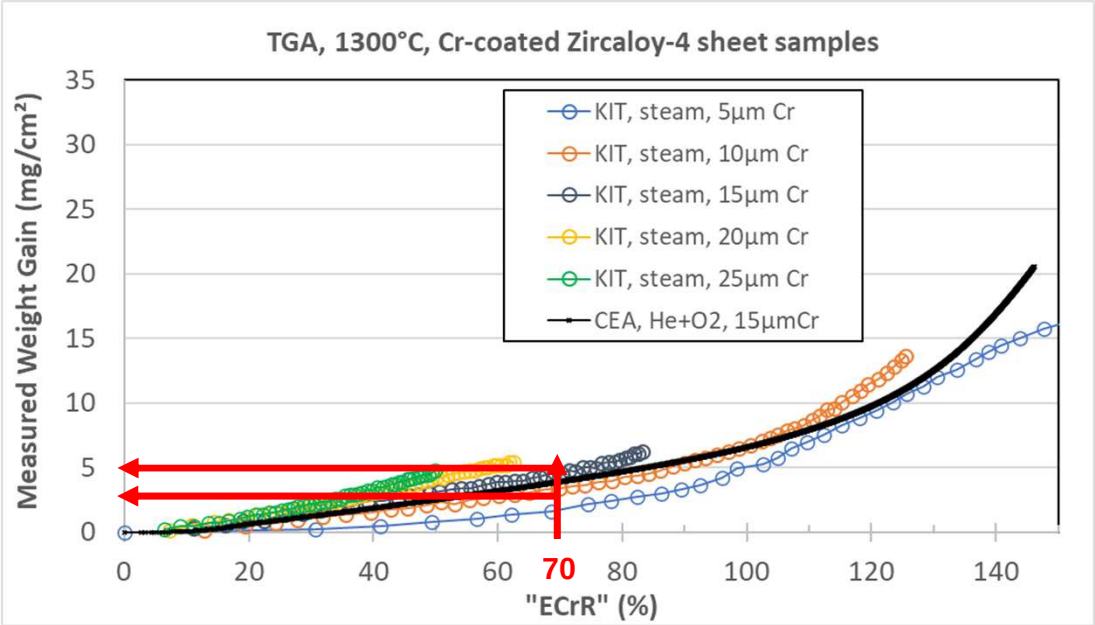

Apparent **« critical ECrR = 70% »**
(*corresponding to HT oxidation kinetics acceleration, i.e., loss of Cr coating protectiveness threshold)*
⇔ Apparent **« critical WG » ~3-5 mg/cm²**

Ex. 2: KIT TGA data Cr = 5 - 25µm, Transient (anisothermal) conditions, **10°C/min up to 1500°C**;

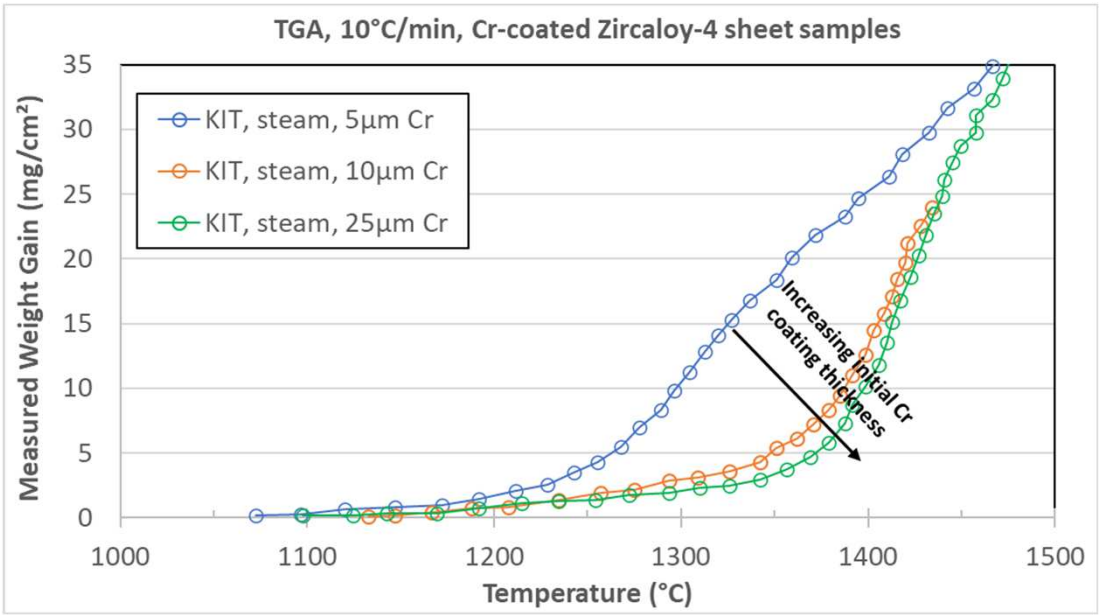

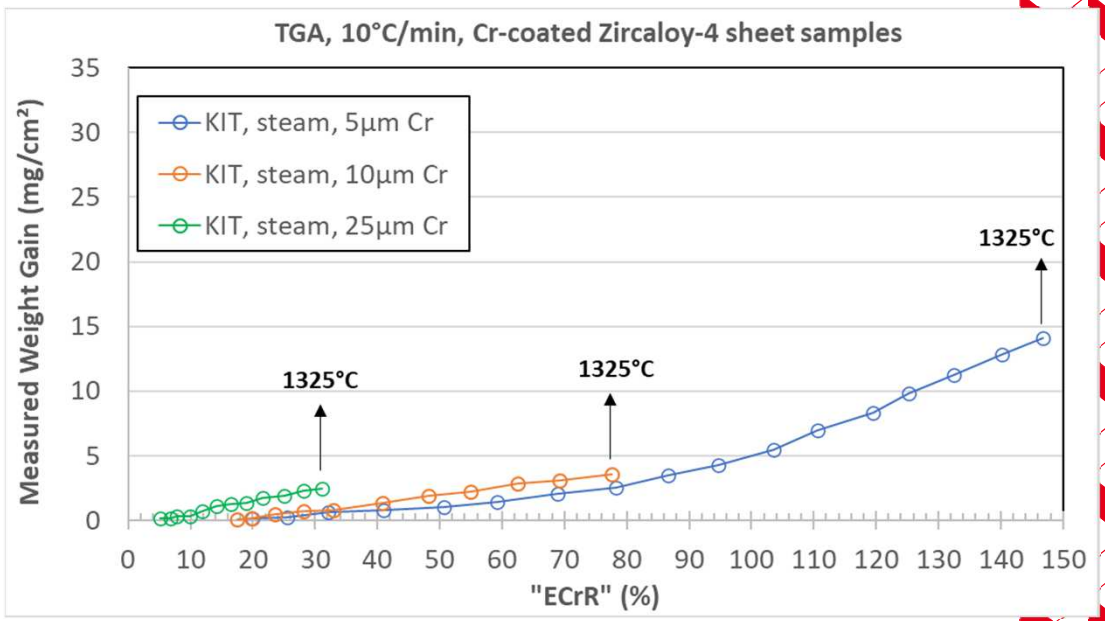

No correction of the uncoated or poorly coated sufaces influence on the measured WG

Rem.: data obtained above 1325°C not considered here, because of the « Zr-Cr eutectic » reaction inducing fast loss of the coating's protectiveness…

Ex. 3 (1/2): Previous KIT TGA data obtained on 1st generation Cr-coated E110, **isothermal conditions, 1200°C**
Kashkarov et al., Corrosion Science, 2020

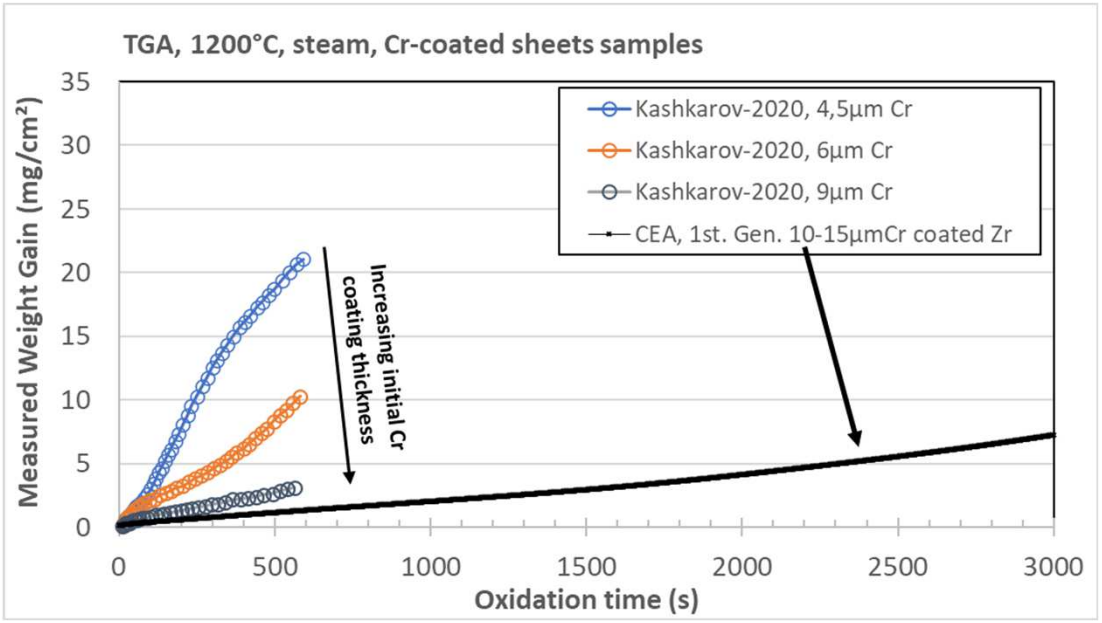

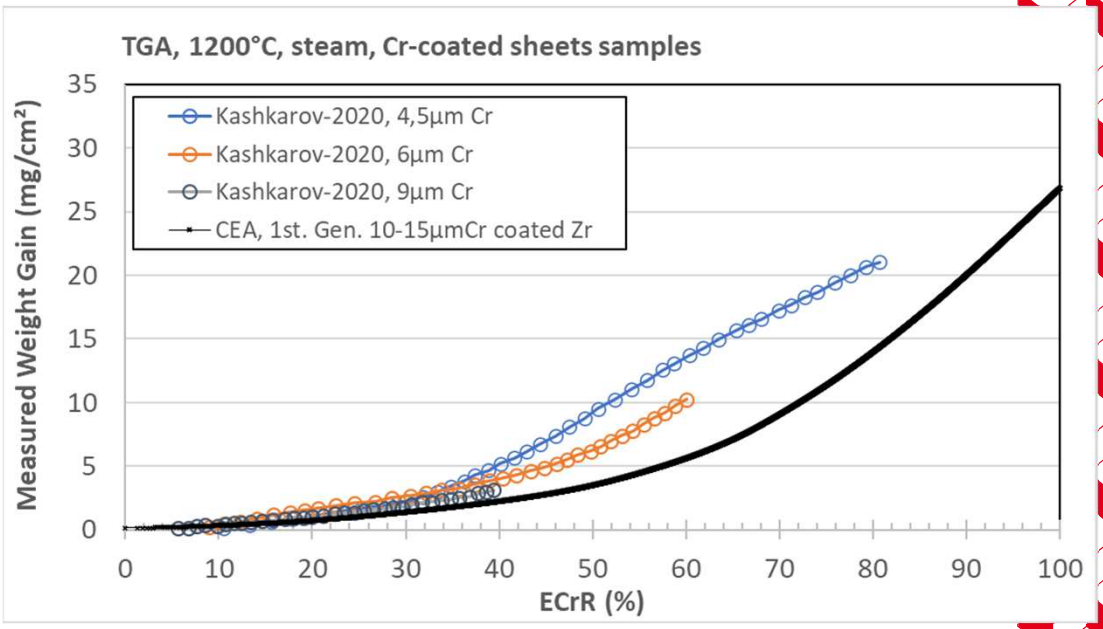

No correction of the uncoated or poorly coated sufaces influence on the measured WG

Apparent loss of Cr protectiveness (*i.e., oxidation kinetics acceleration*) seems to occur earlier, for an **ECrR~40%.** Could be due to not fullly optimized Cr-coating of these first generation coated E110 materials, having quite low Cr thicknesses…

Ex. 3 (2/2): Previous KIT TGA data obtained on 1st generation Cr-coated E110, **transient (20°C/min) conditions => 1200°C**
Kashkarov et al., Corrosion Science, 2020

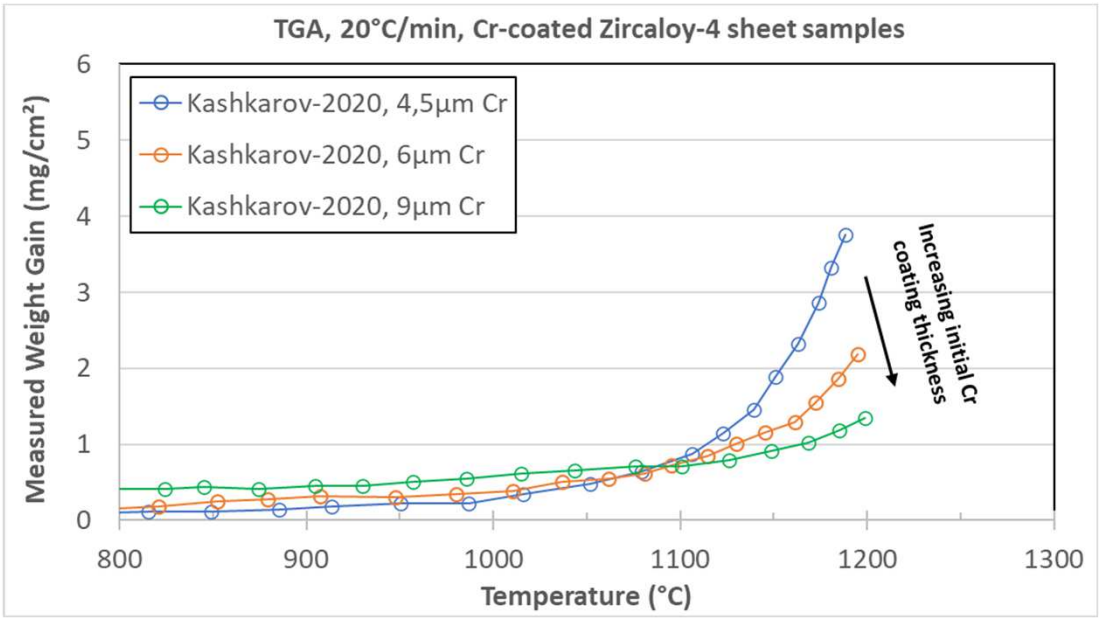

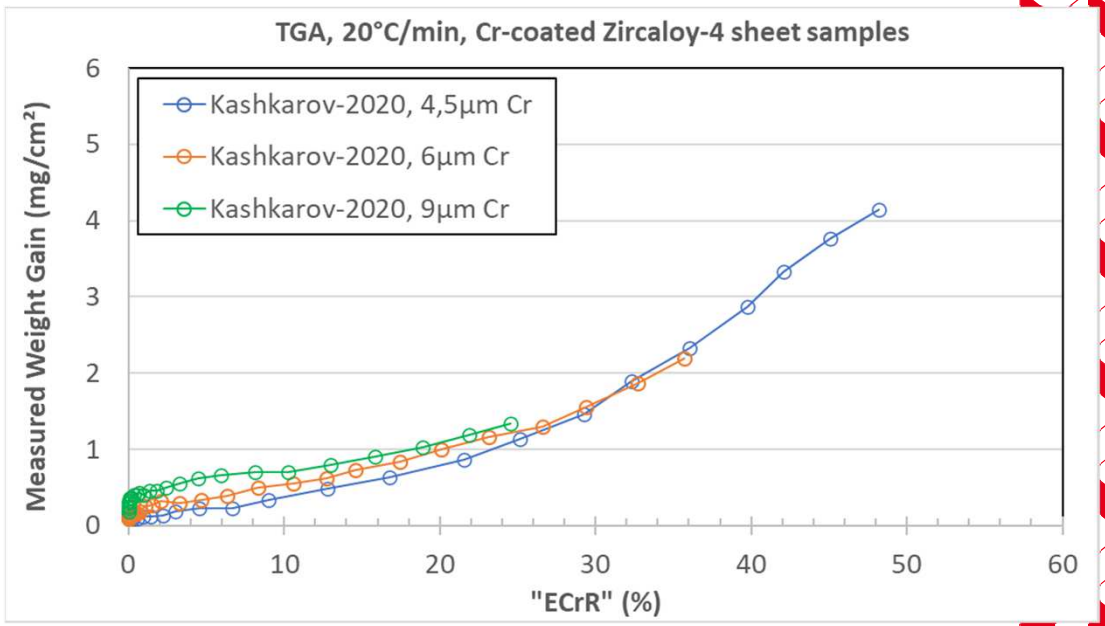

No correction of the uncoated or poorly coated sufaces influence on the measured WG

Confirmation of the capacity of the ECrR metrics to account for the effect of the initial Cr thickness not only in isothermal conditions but also for transient conditions which are more LOCA-prototypical…

Extending the approach to some other TGA and discrete PQ weigthing data from several institutes (*including CEA*) (1/2)

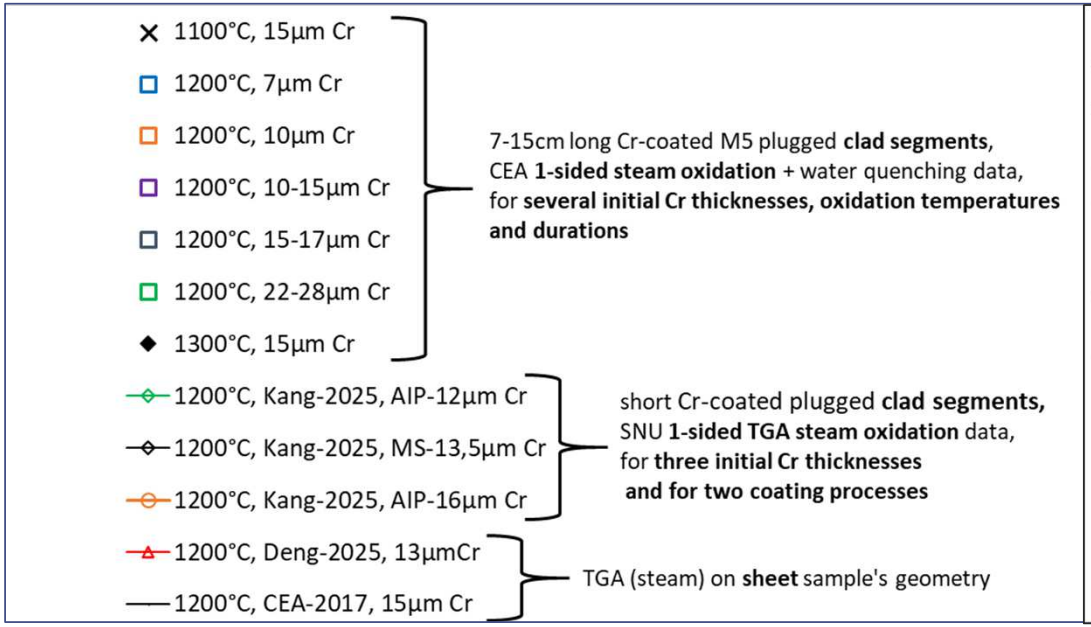

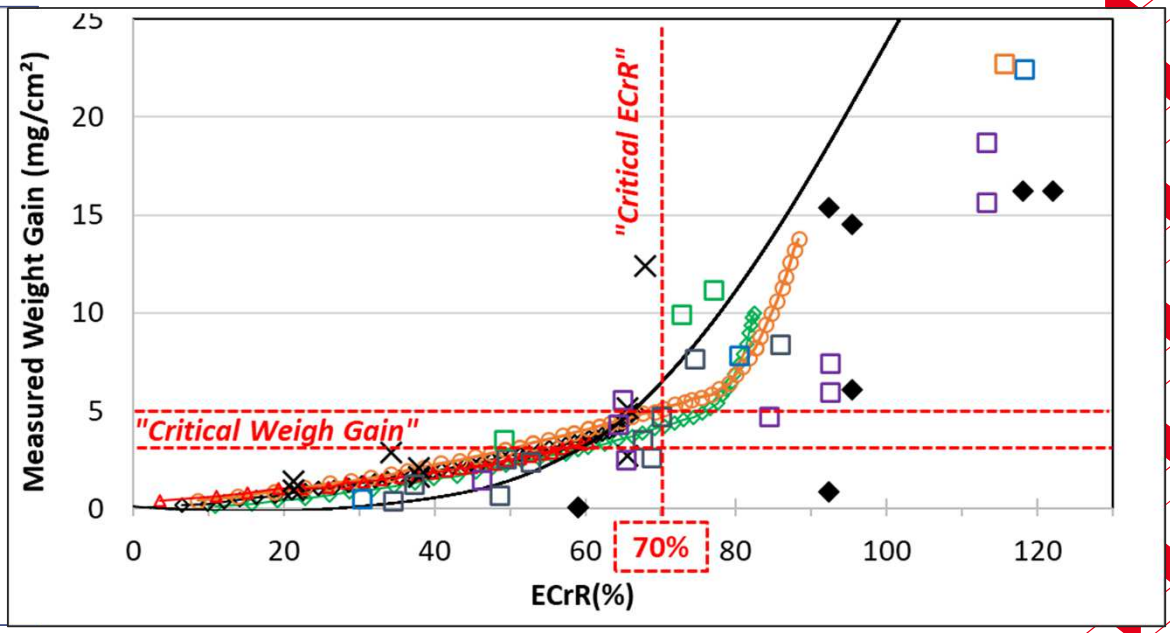

PQ weigthing – CEA data – Cr ~ 5 - 25µm / different oxidation durations and temperatures (1100-1300°C)

+ one TGA – CEA data for Cr = 15µm carried out at 1200°C (steam environment)…

+ TGA - 1200°C from Kang *et al.* – Cr = 12-16µm, JNM-2025

+ TGA - 1200°C from Deng *et al.* – Cr = 13µm, JMR&T-2024

Extending the approach to some other TGA and discrete PQ weigthing data from several institutes (*including CEA*) (2/2)

- ✕ 1100°C, 15µm Cr
- □ 1200°C, 7µm Cr
- □ 1200°C, 10µm Cr
- □ 1200°C, 10-15µm Cr
- □ 1200°C, 15-17µm Cr
- □ 1200°C, 22-28µm Cr
- ◆ 1300°C, 15µm Cr

7-15cm long Cr-coated M5 plugged **clad segments**, CEA **1-sided steam oxidation** + water quenching data, for **several initial Cr thicknesses, oxidation temperatures and durations**

- ○ 1300°C, Steinbrueck-2025, 5µm Cr (*)
- ○ 1300°C, Steinbrueck-2025, 10µm Cr (*)
- ○ 1300°C, Steinbrueck-2025, 15µm Cr (*)
- ○ 1300°C, Steinbrueck-2025, 20µm Cr (*)
- ○ 1300°C, Steinbrueck-2025, 25µm Cr (*)
- × 1300°C, Brachet-2020, 15µm Cr, He+O2 (*)
- ● 1300°C, Li-2024, Post-oxidation weigthing, 17µmCr

TGA (*steam, except CEA data with He+O_2 environment*) - **sheet** sample's gometry

(*) 5% uncoated surface correction

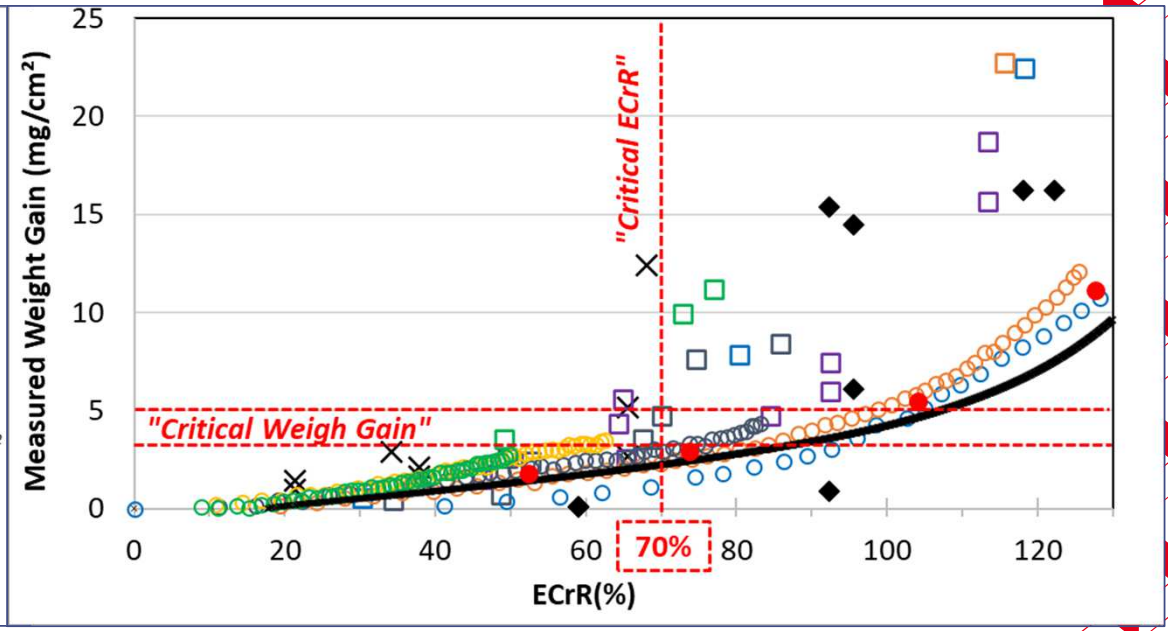

PQ weigthing – CEA data – Cr ~ 5 - 25µm / different oxidation durations and temperatures (1100-1300°C)

+ one TGA – CEA data for Cr = 15µm carried out at 1300°C (He+O_2)…

+ TGA - 1300°C from Steinbrueck *et al.* – Cr = 5 – 25µm, this workshop, to be published in JNM

+ PQ weighting data - 1300°C – Cr = 17µm from Li *et al.* JMR&T-2024

Some conclusions , on-going and further work

Beyond its practical use in relationship with PQ clad mechanical properties of Cr-coated materials having experienced one-sided HT steam oxidation (1100-1300°C) and quenching, new "ECrR" metrics appear to be useful to rationnalise the continuous WG evolutions derived from TGA experiments, taking into account the initial Cr-coating thickness influence + oxidation temperature and duration.

Thus, the ECrR parameter should be a practical metrics to compare Cr-coating's relative performances upon HT oxidation even with different initial Cr thicknesses and/or different oxidation temperatures.

Additionnally, this approach can be used in transient (*more LOCA-prototypical*) conditions…

On-going and further work:

- **account for the effect of pre-damaged / pre-cracked coatings**

⇒ **"Connect-NM / Crocodox" project**

- **account for two-sided oxidation conditions and the associated 2^{dary} hydriding resulting from clad ballooning and burst**

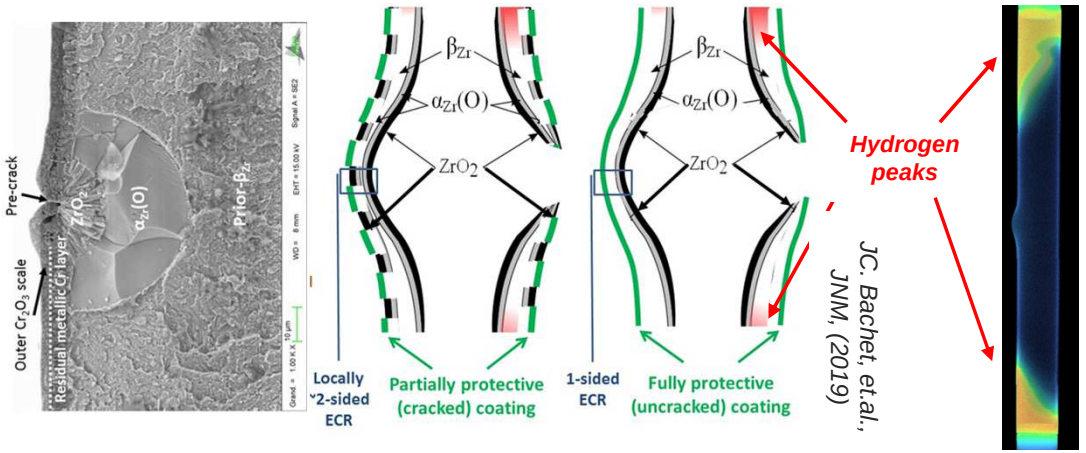

Thank you for your attention

This work has been funded by the French Nuclear Institute (I3P). Many thanks to the numerous colleagues and students at CEA who have contributed to the developement and evaluation of E-ATF Cr-coated Zr-based claddings over past twelve years, and to our industrial partners for partial funding and fruitful discussions (and Framatome for providing the $M5_{Framatome}$ substrate)

jean-christophe.brachet@cea,fr

Back slides...

New « ECrR » / Introduction (1/2)

⇒ Following HT steam oxidation *(for LOCA and beyond conditions)*, **both experimental (based on measured Weight Gain) and calculated "$ECR_{BJ/CP}$"** (*used since the 70ties for the uncoated Zr-based claddings*) **are not adapted "metrics" to rely on the PQ mechanical properties of Cr-coated claddings**;

⇒ **Fundamentally due to the different underlying HT oxidation mechanisms** (*between uncoated & coated materials*) and the **different induced oxygen diffusion profiles and partitioning into the Zr-base (β_{Zr})** substrate

Materials	Oxidation time at 1200 °C (s)	WG (mg/cm²)	ECR_{WG} (%)	Fraction of ECR corresponding to oxygen which has diffused into the metallic substrate
Uncoated $M5_{Framatome}$	60 - 1420s	4 - 24	3 - 20	20-30 %
12-15µm Cr-coated $M5_{Framatome}$	9000	15 - 16	12 - 13	85 %

Brachet et al., JNM 2020

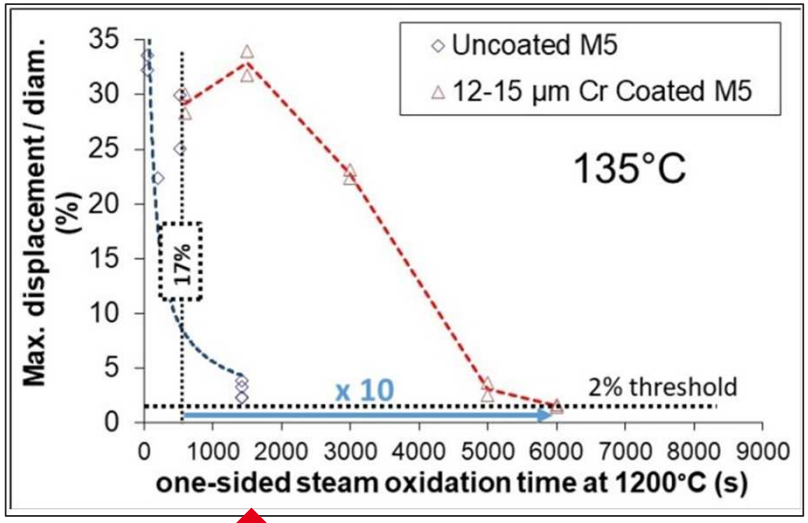

Seems to be contradictory?

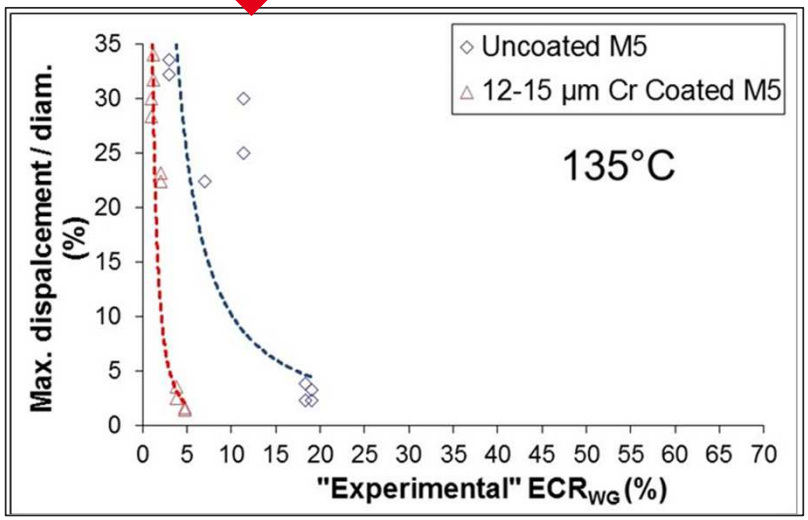

jean-christophe.brachet@cea.fr

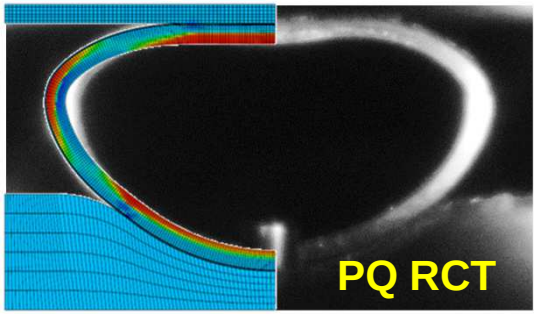

New « ECrR » / Introduction (2/2)

=> Additional limitation by using **conventional approaches** (*i.e., calculated Baker-Just or Cathcart-Pawel ECR correlations that have been derived for the uncoated reference claddings and/or experimental / WG ECR)* is that such parameters **are <u>not able to account for the influence of the initial Cr-coating thickness</u>**

Offset strain (~ « Residual ductility »)

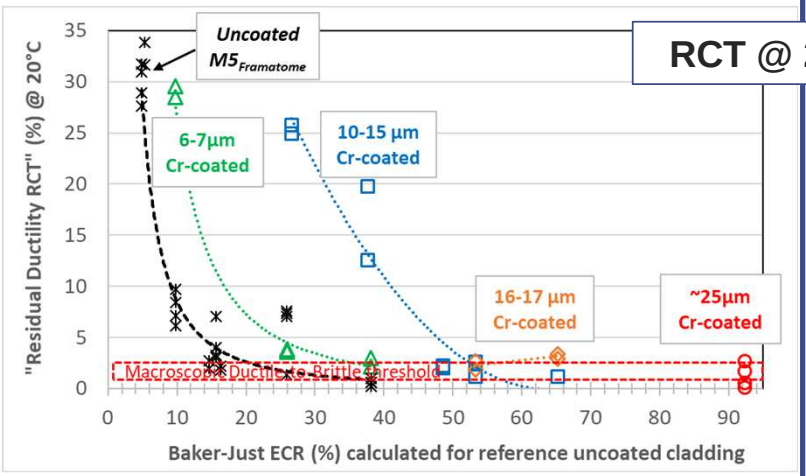

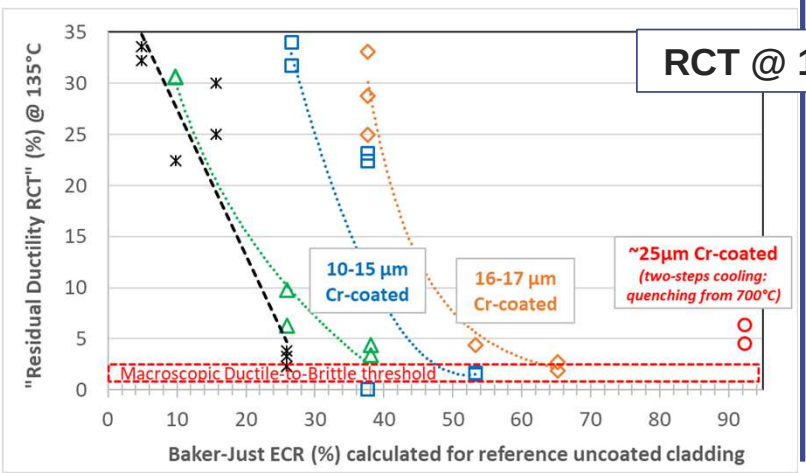

Max. Force (~ « Residual strength »)

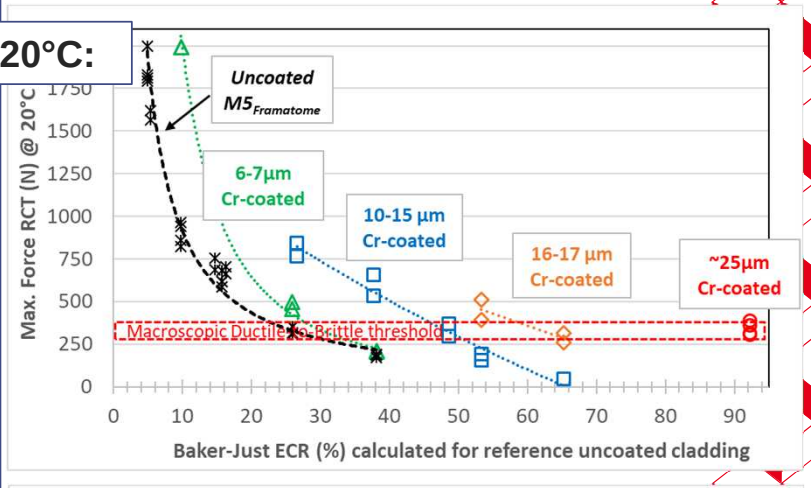

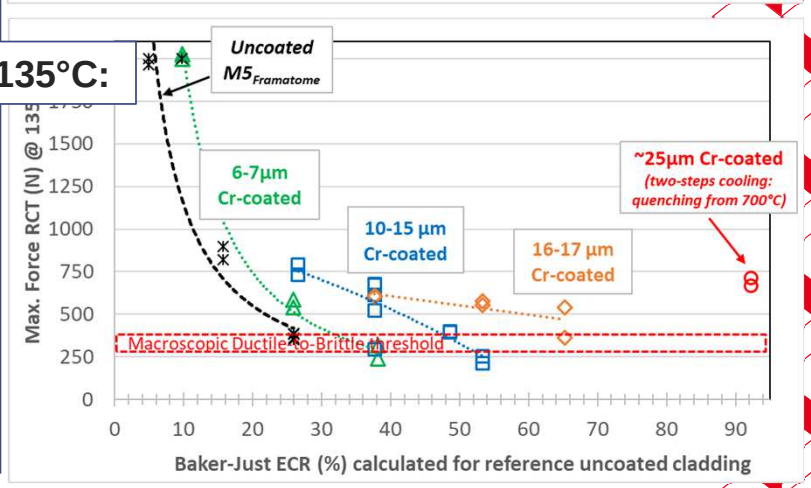

jean-christophe.brachet@cea.fr

Using the “critical” ECrR=70% threshold value, one can calculate typical “grace time” of Cr-coated Zr based claddings before reaching PQ Ductile-to-Brittle transition vs. initial Cr thickness
(*for <u>one-sided</u> steam oxidation and ~0.6 mm thick claddings*):

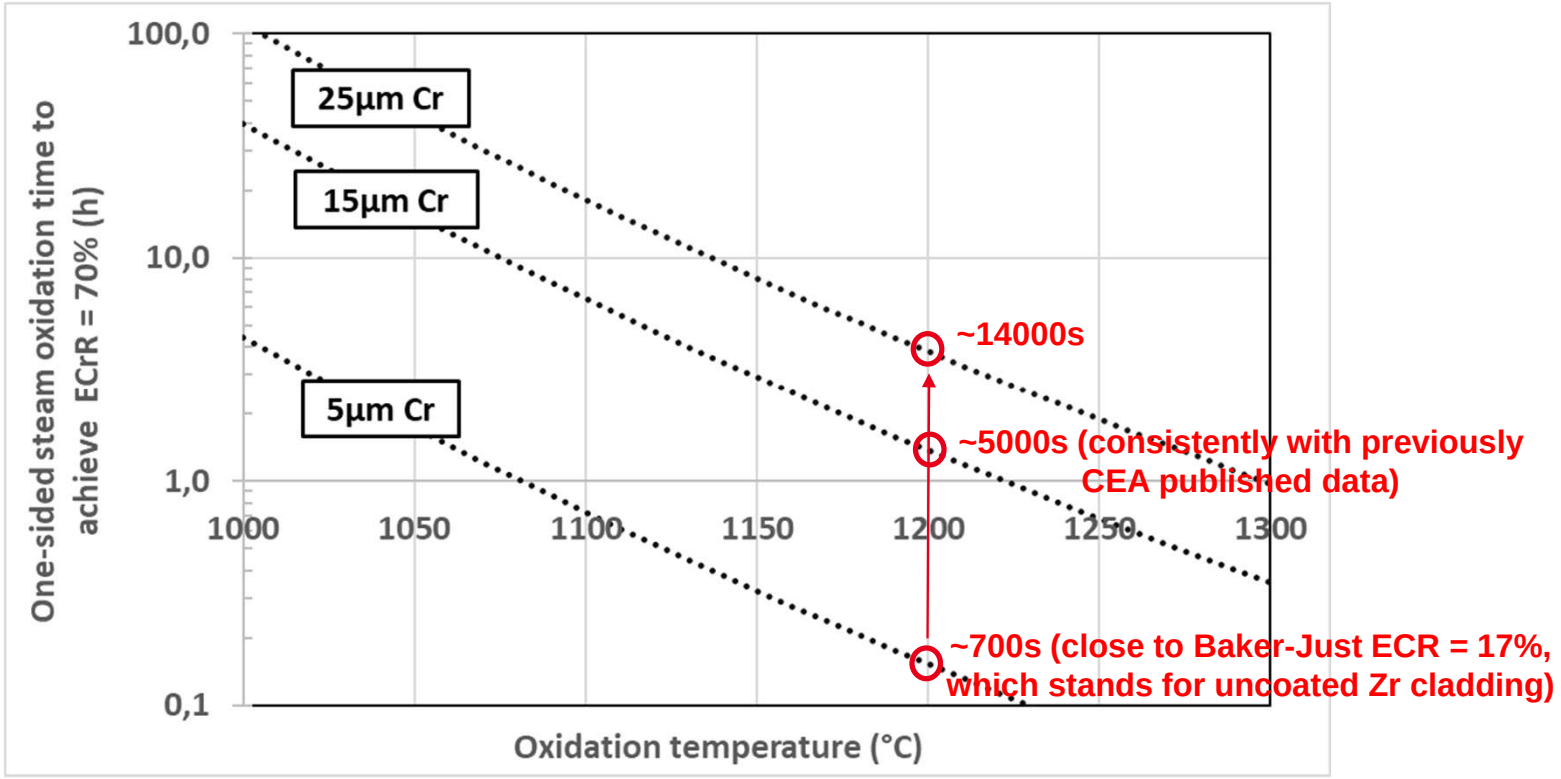

⇒ Among other results, such predictions confirm that **Cr-thickness lower than 10µm brings limited “grace time”**…

Uncoated:

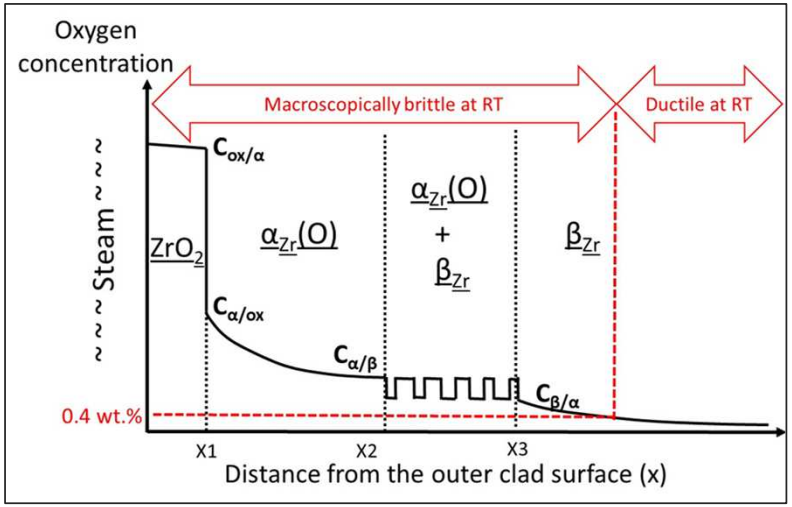

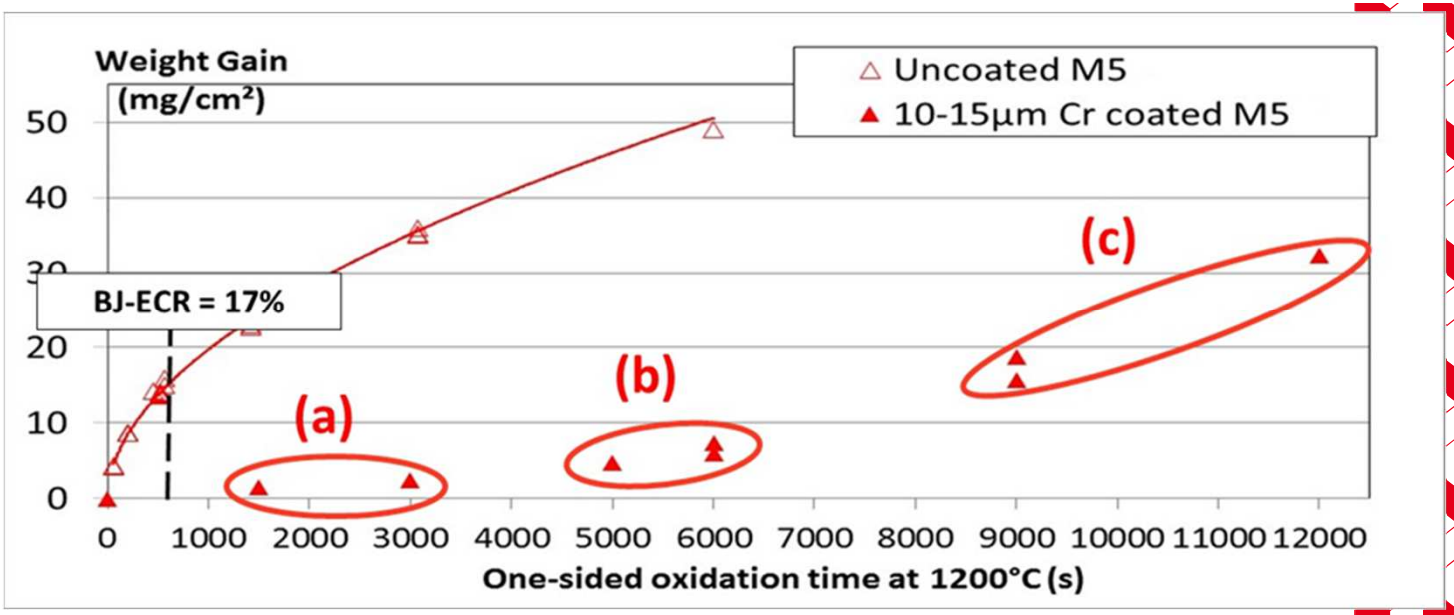

Cr-coated:

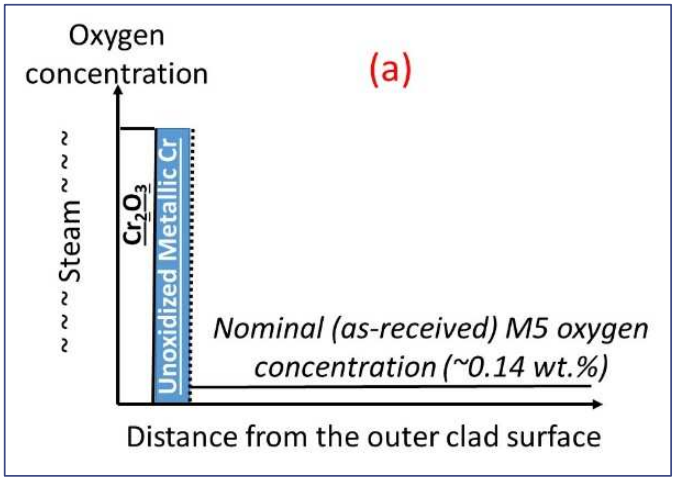

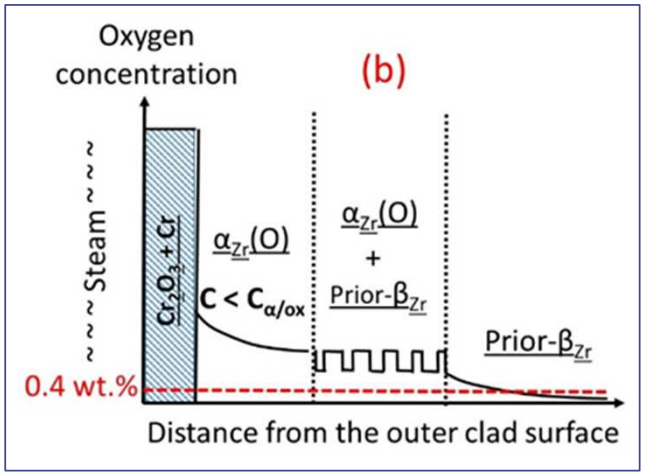

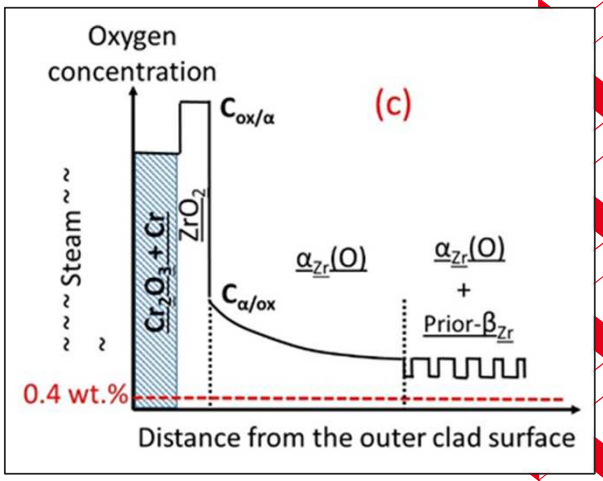

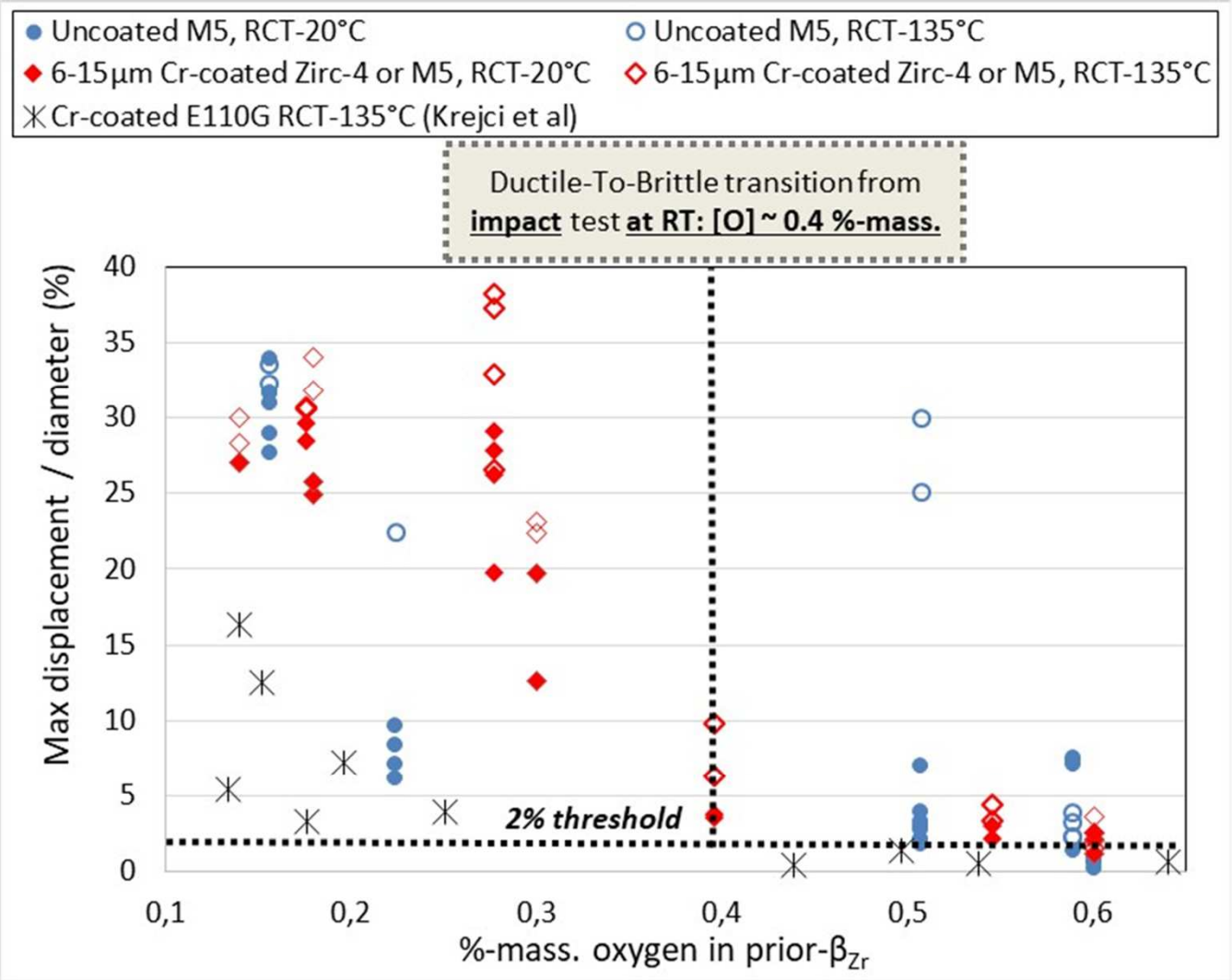

Figure 1 - Post-Quenching "residual ductility" derived from RCTs performed at 20 and 135 °C on uncoated and 6 to 15 µm thick Cr-coated zircaloy-4 or M5$_{Framatome}$, and from Krejci et al. on Cr-coated E110G substrate ***Erreur ! Source du renvoi introuvable.****, as a function of the mean oxygen content of the residual prior-β$_{Zr}$ layer*

jean-christophe.brachet@cea.fr

Diana Bachurina

KIT

Steam Oxidation of Cr-Coated Zircaloy-4 Rods Across a Wide Range of Heating Rates

Although Cr-coated zirconium tubes have been extensively investigated in recent years, many open questions remain, particularly regarding their behavior above 1330 °C – the eutectic temperature in the Cr-Zr system. Once this reaction occurs, the protective properties of the coating are lost, and oxidation proceeds more severely than in uncoated Zr alloys. In this study, we examined the effect of heating rate on high-temperature steam oxidation and degradation of Cr-coated Zry-4 rods above the eutectic temperature.

Zircaloy fuel cladding coated with a 15 µm Cr layer using the PVD method (Oerlikon) was tested (12.5 cm length, ⌀10.75 mm outer, ⌀9.3 mm inner). Experiments were conducted in the QUENCH-Single Rod facility under steam conditions. Heating rates of 5, 10, 30, 50, 100, and 300 K/min were applied. Steam was introduced at 800 °C, and the temperature increased up to 1500 °C. After testing, samples were examined using optical and electron microscopy. A source of uncertainty arose during internal temperature measurements: samples at lower heating rates experienced overheating, while those at higher rates were slightly underheated. This should be considered when interpreting the results.

Macro- and microscopic analysis revealed that at 5 K/min, no “crocodile skin” structure formed; instead, a brittle oxide scale appeared. At 10 K/min and above, “crocodile skin” ridges developed, while eutectic microstructure was first observed at 30 K/min. The area covered by eutectic structure showed no clear dependence on heating rate.

Oxide scale thicknesses (ZrO_2 and Cr_2O_3) decreased with increasing heating rate. ZrO_2 thickness matched theoretical predictions for uncoated Zr alloys at higher heating rates, but measured thicknesses at ≤30 K/min were higher, likely due to temperature overshoot during testing.

Hydrogen release was also monitored. The H_2 release rate increased with heating rate, reaching ≈6 L/h at 5 K/min and about ten times higher at 100 K/min. Maximum release rates not only increased with heating rate but also shifted to higher temperatures. Total H_2 release decreased with heating rate and was already lower than that of uncoated samples at 100 K/min.

Steam Oxidation of Cr-Coated Zircaloy-4 Rods Across a Wide Range of Heating Rates

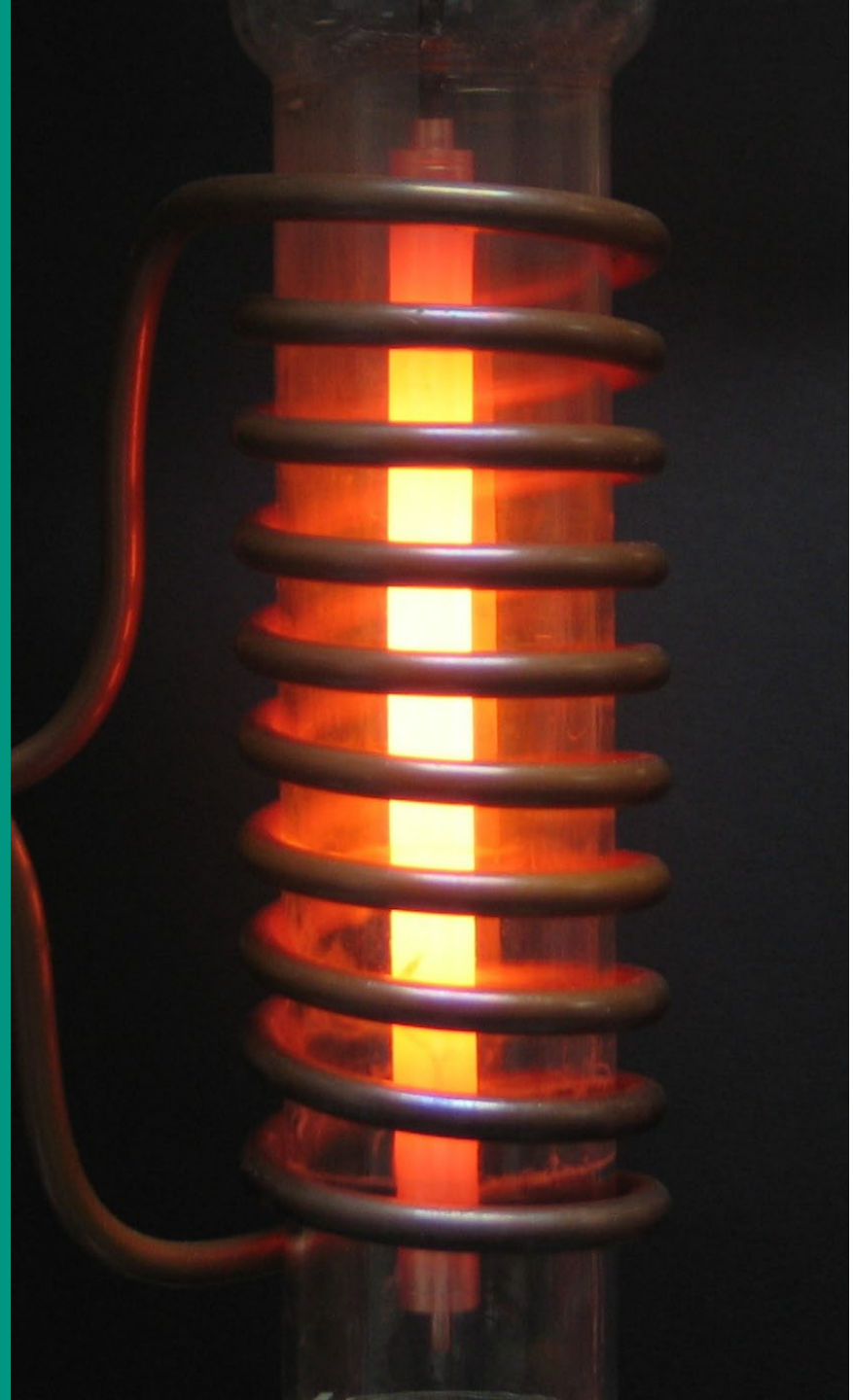

Diana Bachurina, Ulrike Stegmaier, Jaeyoon Bae,
Martin Steinbrück

QUENCH Workshop, 16-18 December 2025

Background

- Aim: examine the effect of heating rates on high-temperature steam oxidation and degradation of Cr-coated Zry-4 rods above eutectic temperature

- Previous data on oxidation in O_2 limited to **50 K/min**

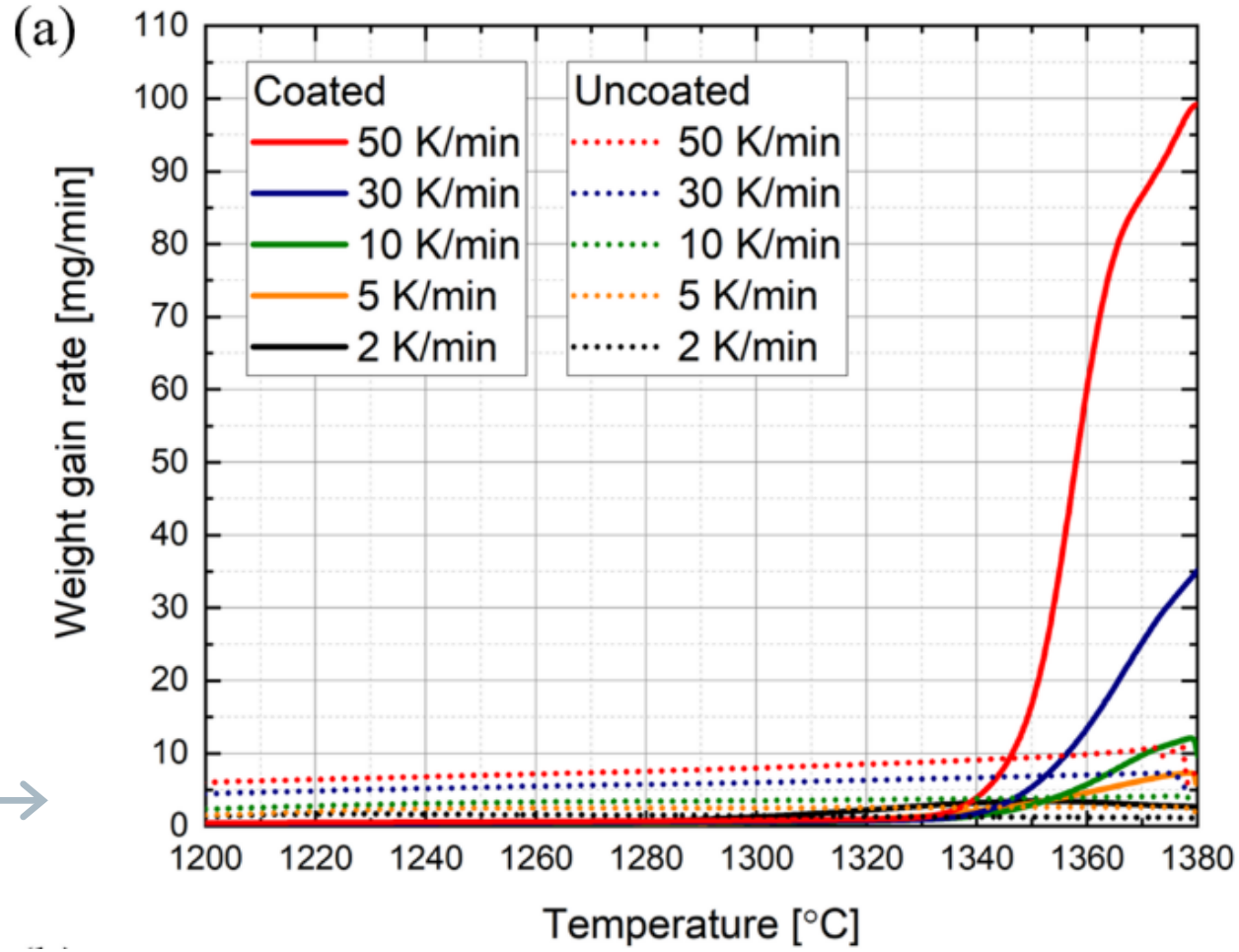

Kim d. et al, DOI:10.1016/J.JNUCMAT.2023.154538

Materials and methods

Zry-4

Cr-coating (Oerlikon), PVD,

15 µm thick

12 cm long, ⌀10.75 mm outer, ⌀9.3 mm inner

+ uncoated plugs

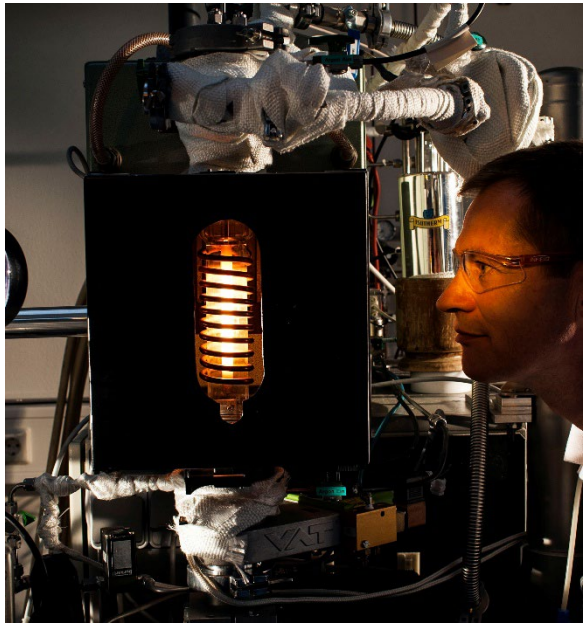

QUENCH-SR

Atmosphere – steam starting 800°C

Argon flow <800°C and >1500°C 40l/h

Coupled with mass spectrometry

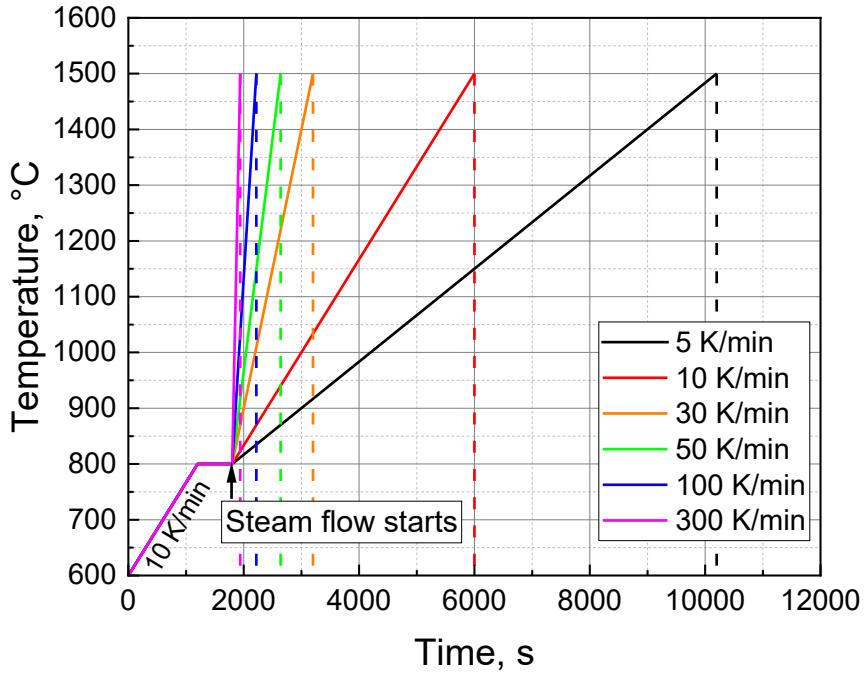

Post-test examination

OM, SEM

Source of Uncertainty

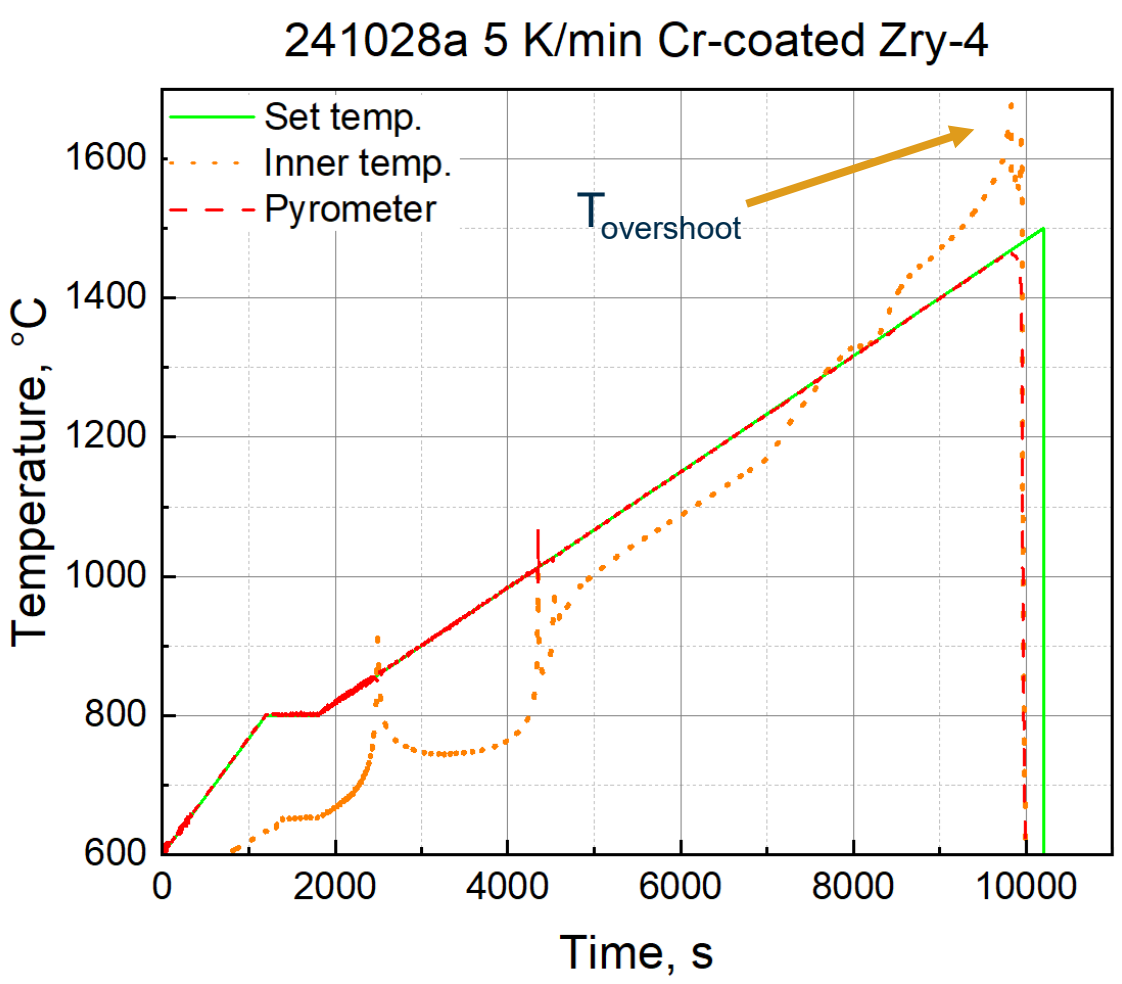

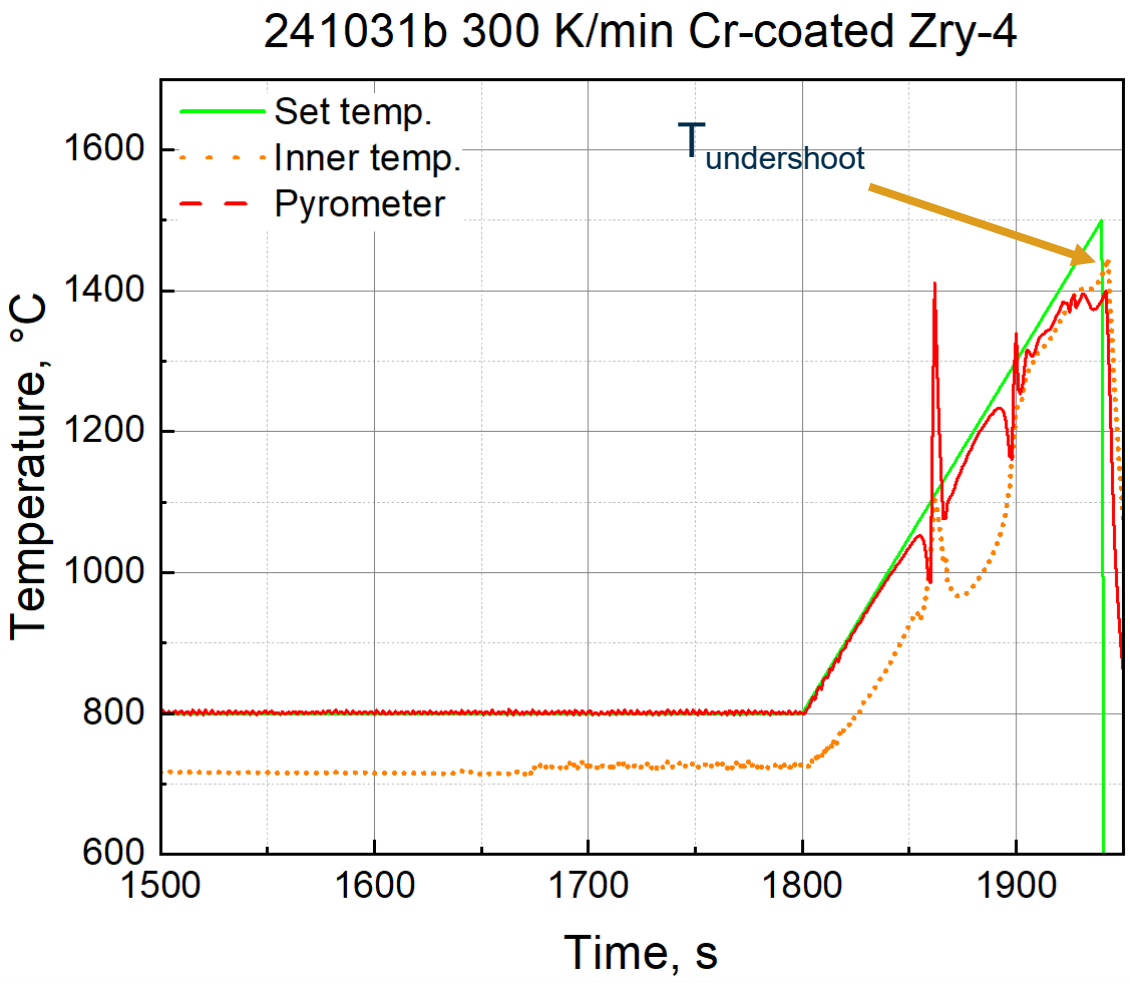

Results

Macroscopic examination

As-received 5K/min 10K/min 30K/min 50K/min 100K/min 300K/min

Cr-Coated Zry-4 (PVD)

As-received 5K/min 30K/min 100K/min

Uncoated Zry-4

Macroscopic examination

Cr-Coated Zry-4 (PVD)

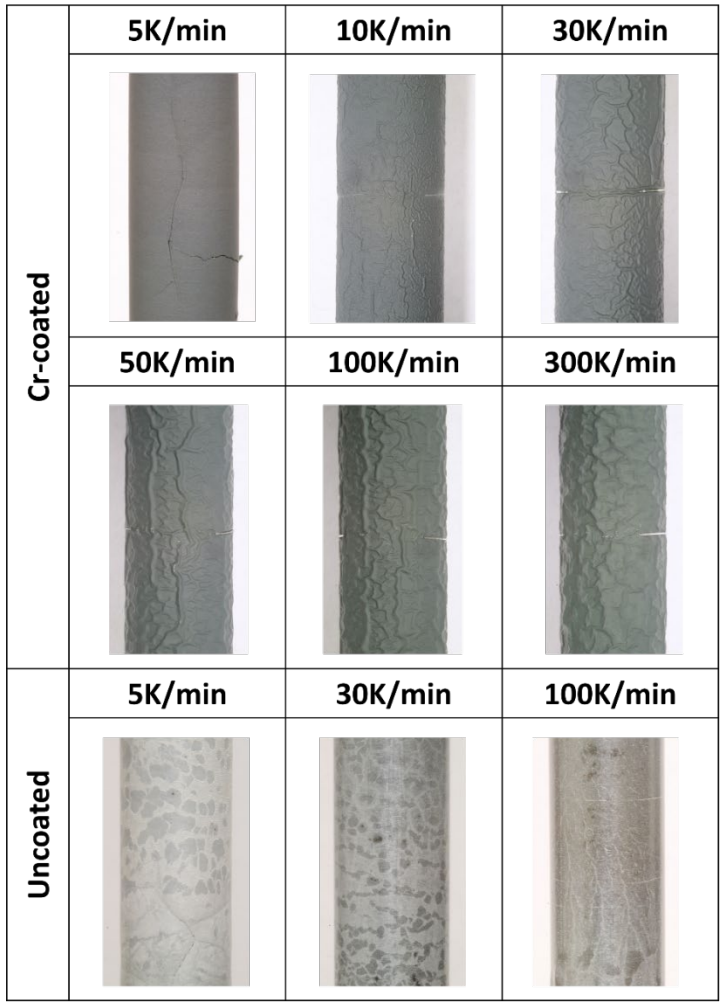

Magnified

Microscopic examination

Cr-coated	5K/min	10K/min	30K/min
			
	50K/min	100K/min	300K/min
			
Uncoated	5K/min	30K/min	100K/min
			

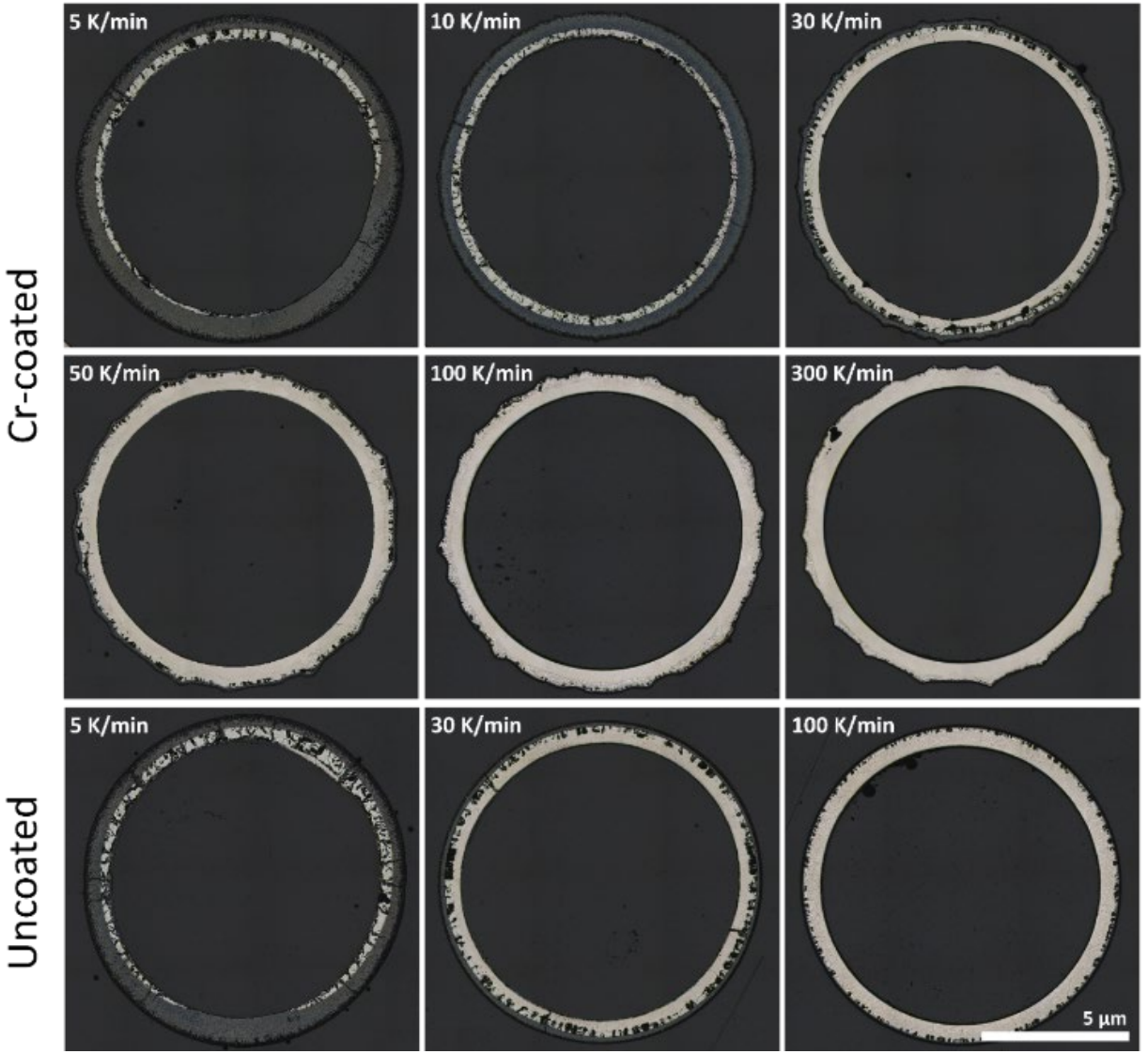

Microscopic examinations

Microscopic examination

Cr_2O_3 ZrO_2 αZr(O) prior β eutectic

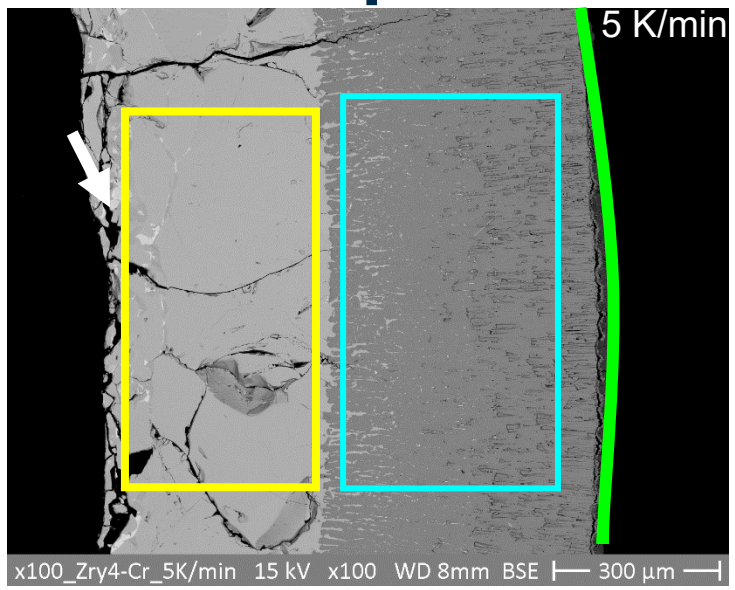

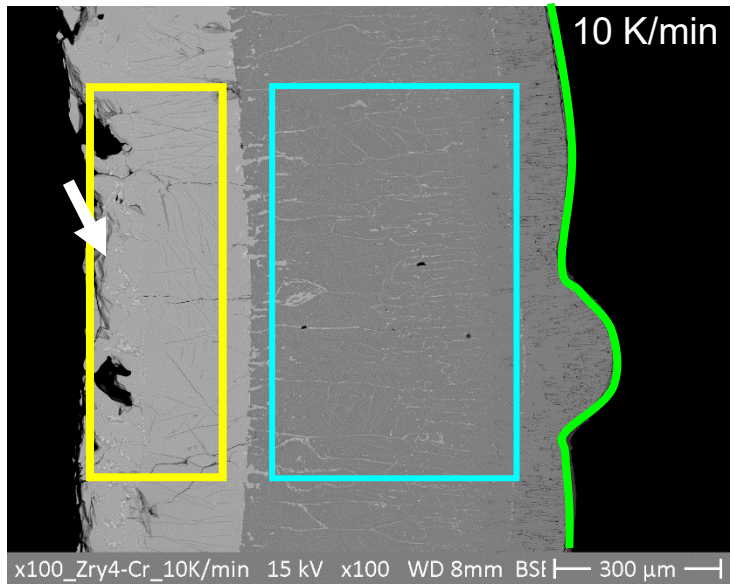

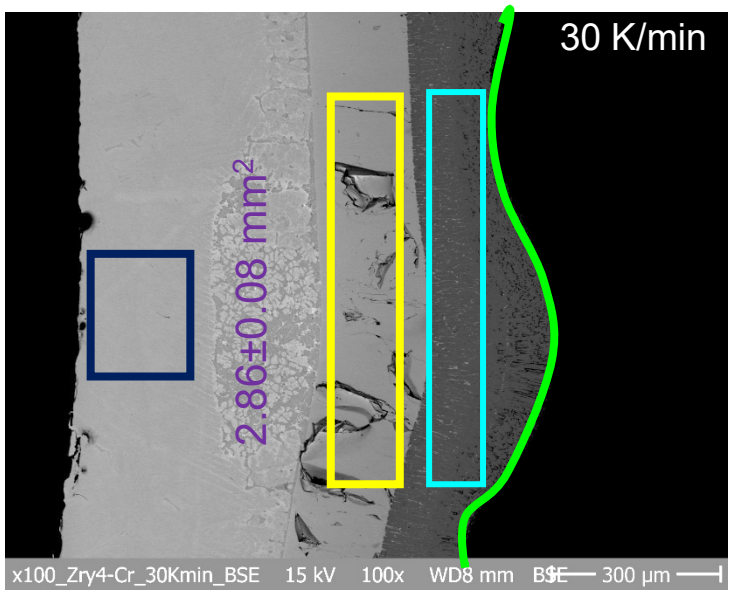

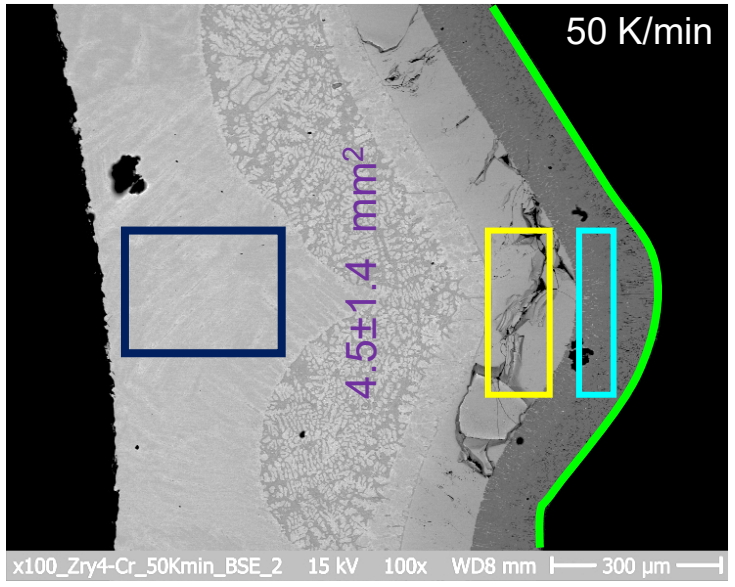

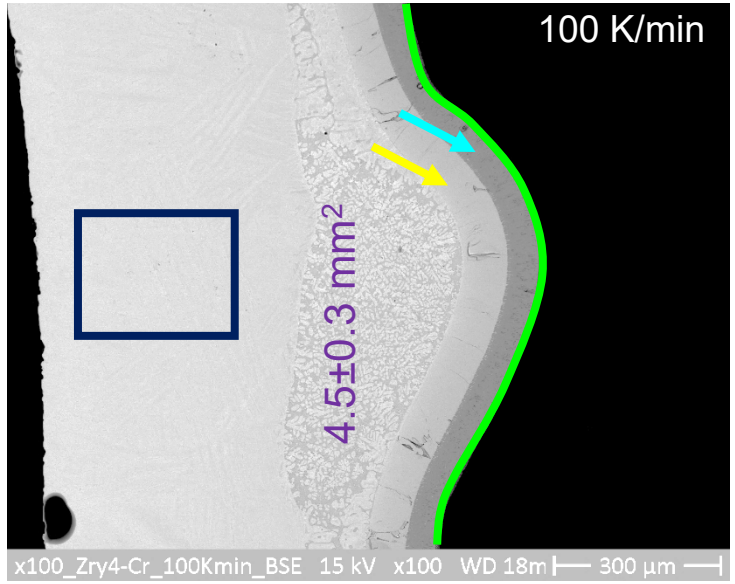

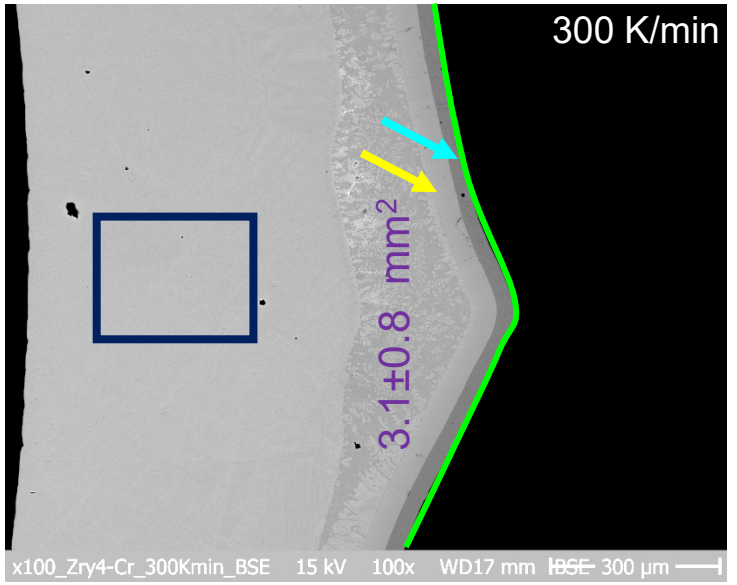

$x \pm \Delta x$ mm² – area covered by eutectic

Magnified view of eutectic microstructure

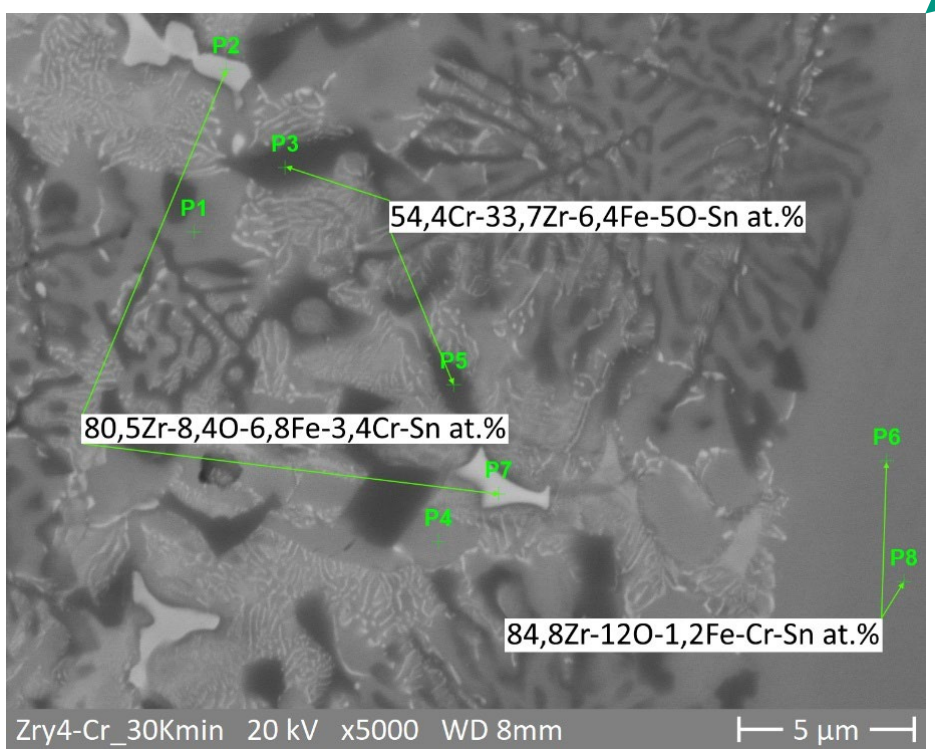

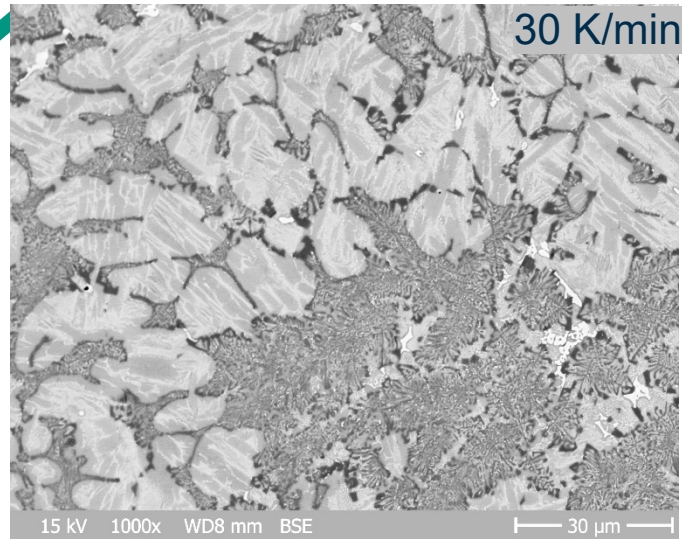

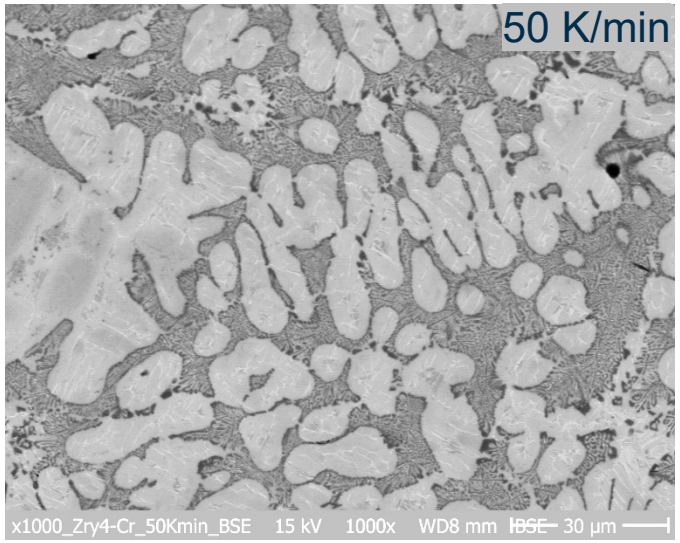

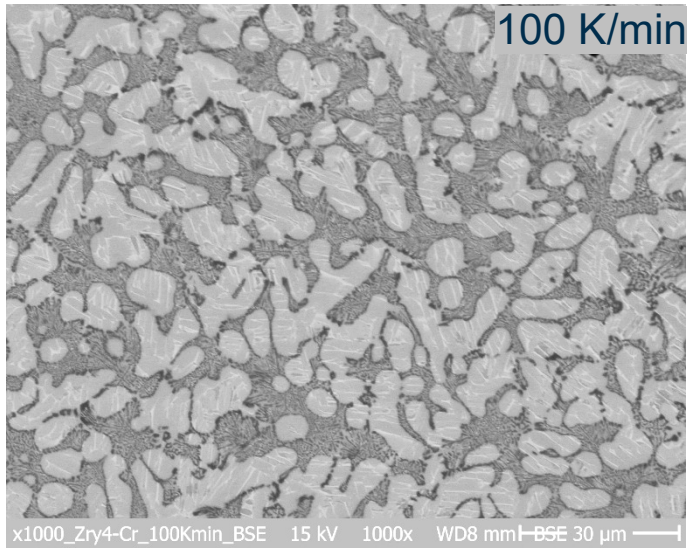

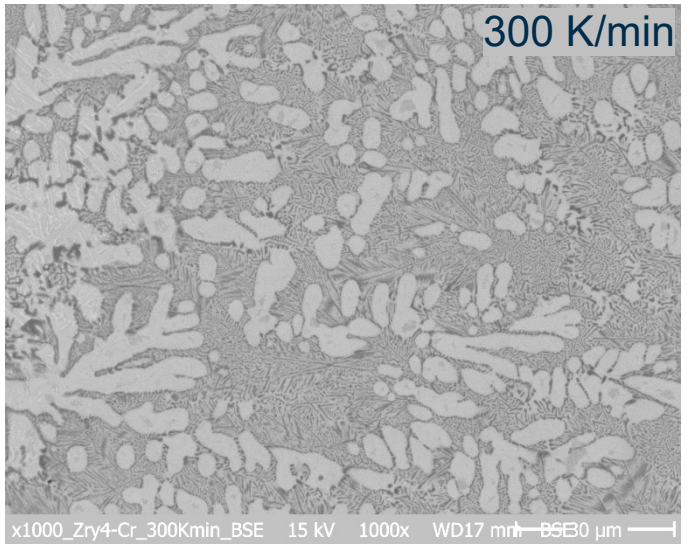

Oxide layers

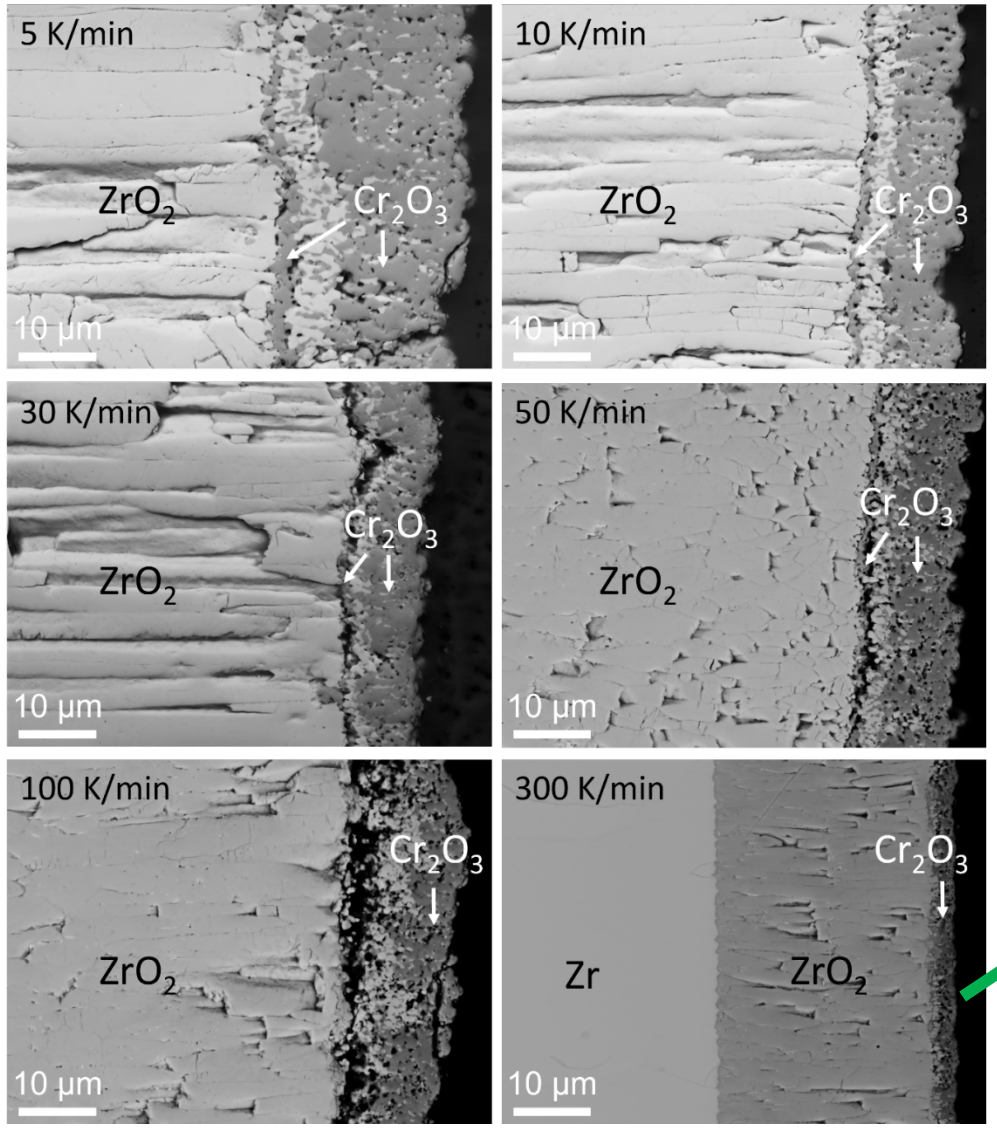

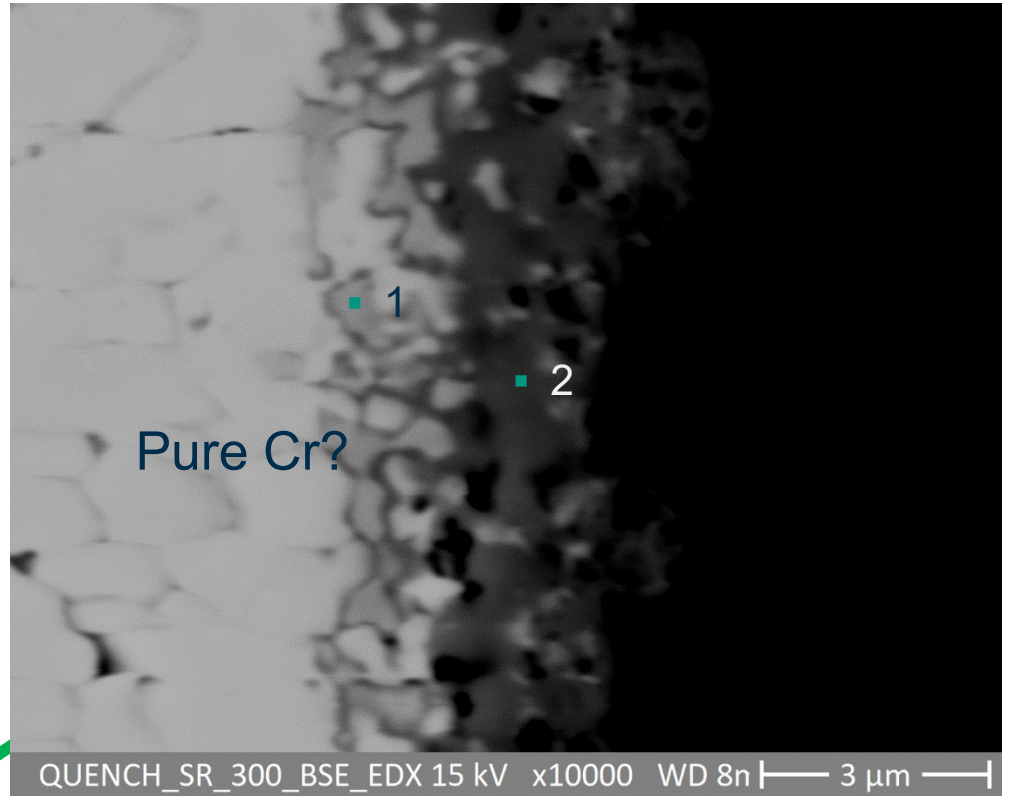

EDX

- 1. 61Cr – 32O – 7Zr at.%
- 2. 54O – 43Cr – 2Zr at.%

Thickness of oxide layers

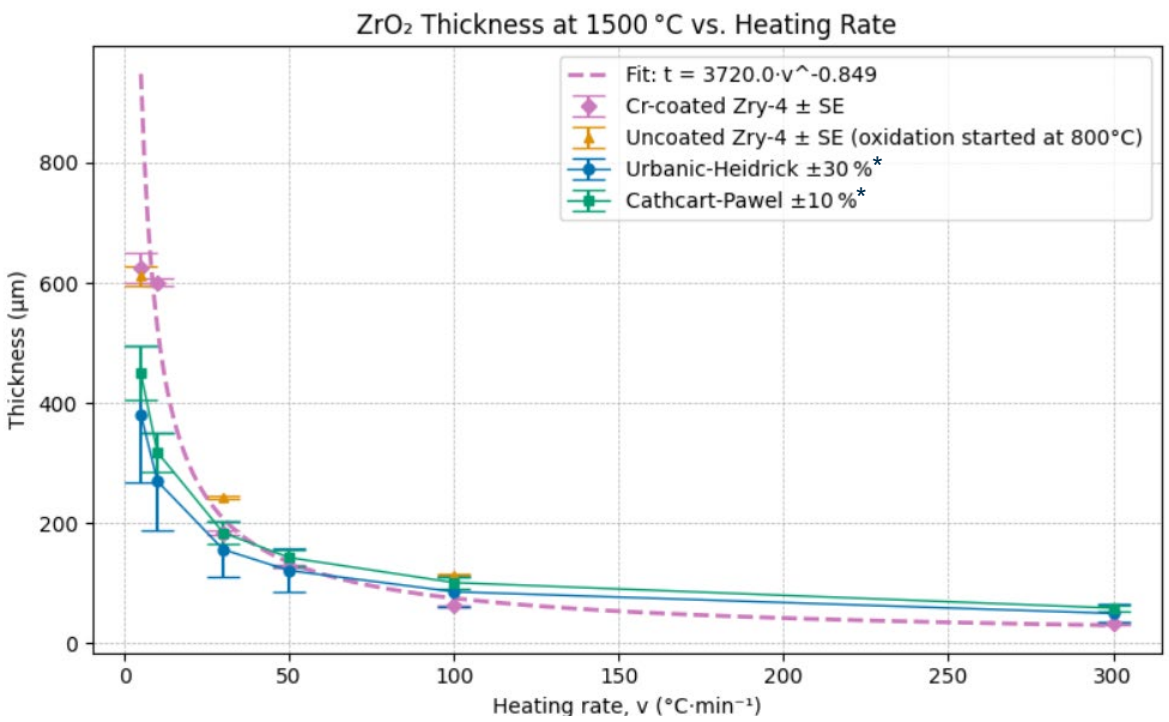

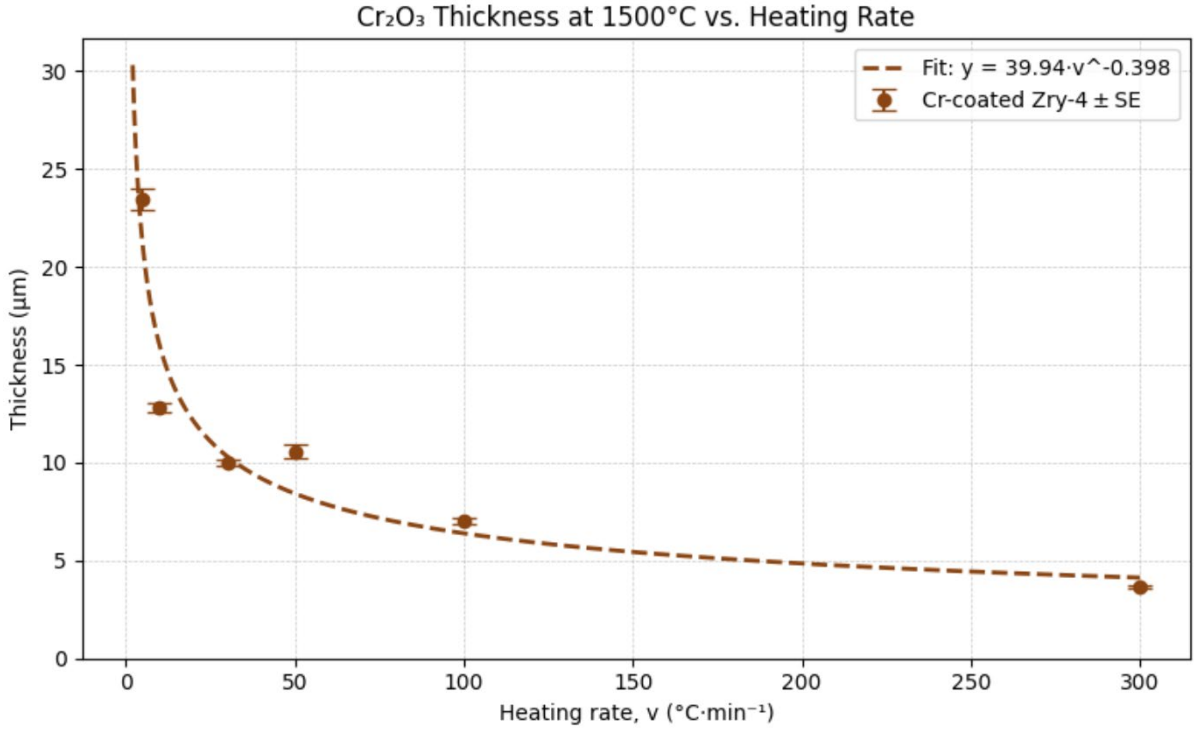

*Schanz. G., et al. 10.1016/j.nucengdes.2004.02.013

H_2 release

H_2 release

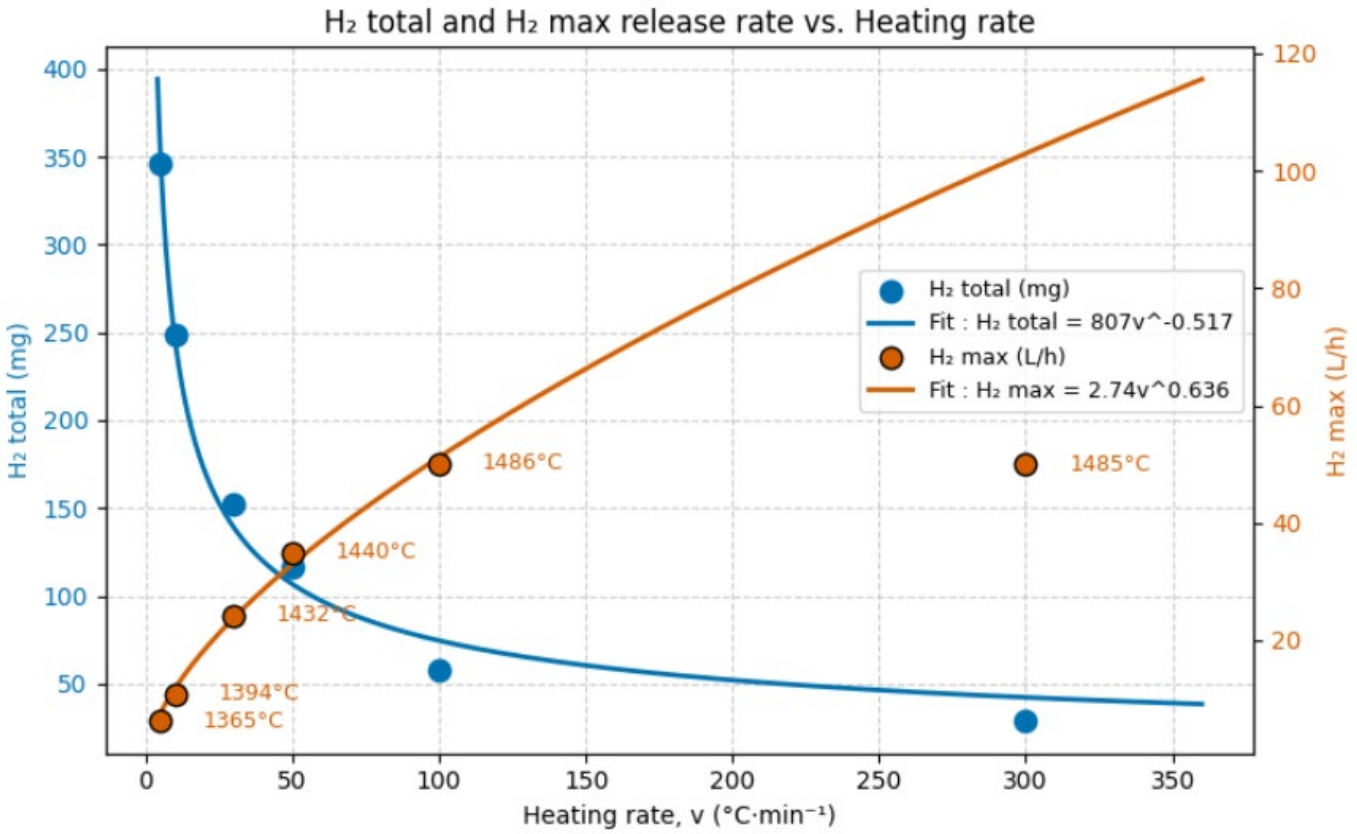
H₂ total and H₂ max release rate vs. Heating rate
H₂ total (mg)
Fit : H₂ total = 807v^-0.517
H₂ max (L/h)
Fit : H₂ max = 2.74v^0.636
1486°C
1485°C
1440°C
1432°C
1394°C
1365°C
H₂ total (mg)
H₂ max (L/h)
Heating rate, v (°C·min⁻¹)

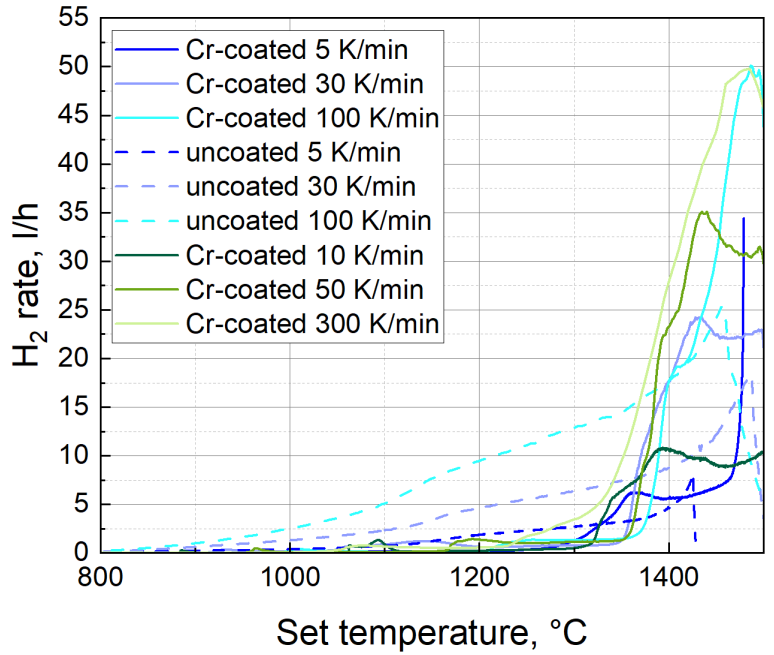
Cr-coated 5 K/min
Cr-coated 30 K/min
Cr-coated 100 K/min
uncoated 5 K/min
uncoated 30 K/min
uncoated 100 K/min
Cr-coated 10 K/min
Cr-coated 50 K/min
Cr-coated 300 K/min
H2 rate, l/h
Set temperature, °C

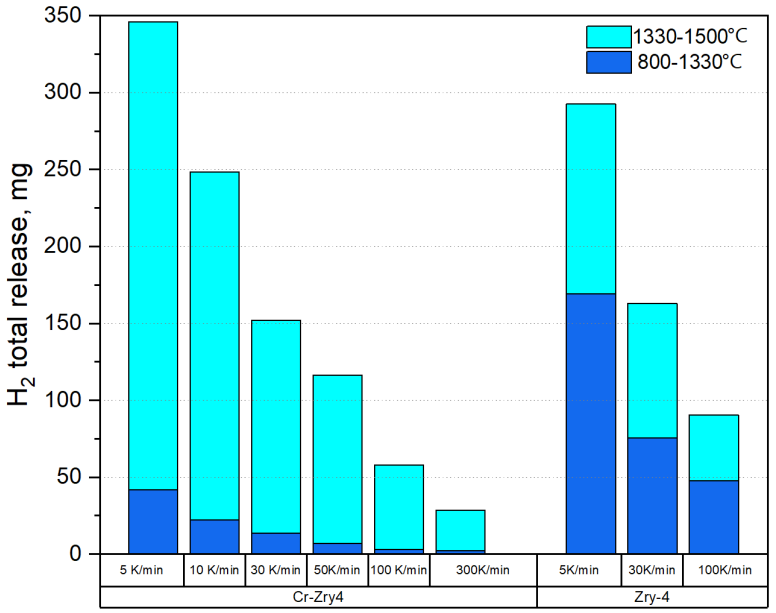
1330-1500°C
800-1330°C
H2 total release, mg
5 K/min
10 K/min
30 K/min
50K/min
100 K/min
300K/min
5K/min
30K/min
100K/min
Cr-Zry4
Zry-4

H_2 release rate

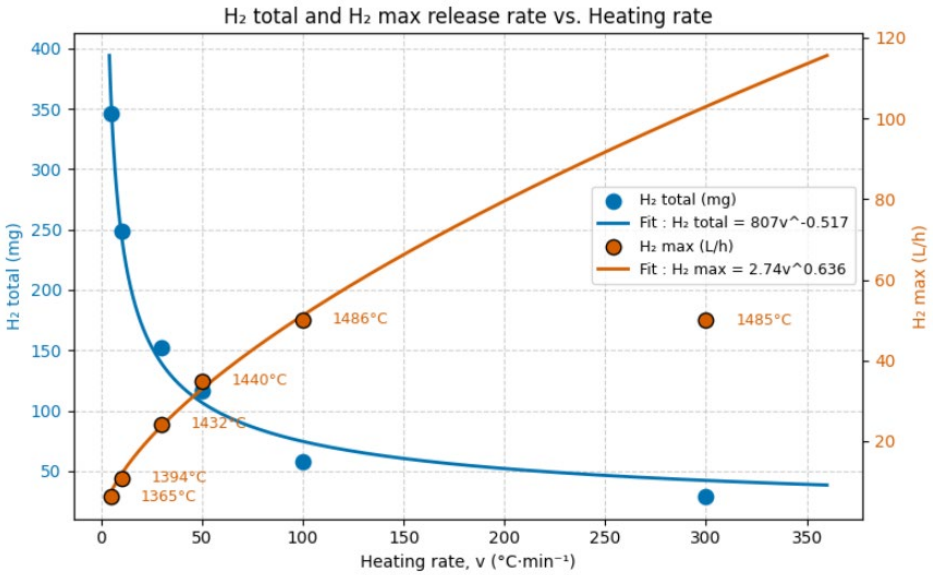

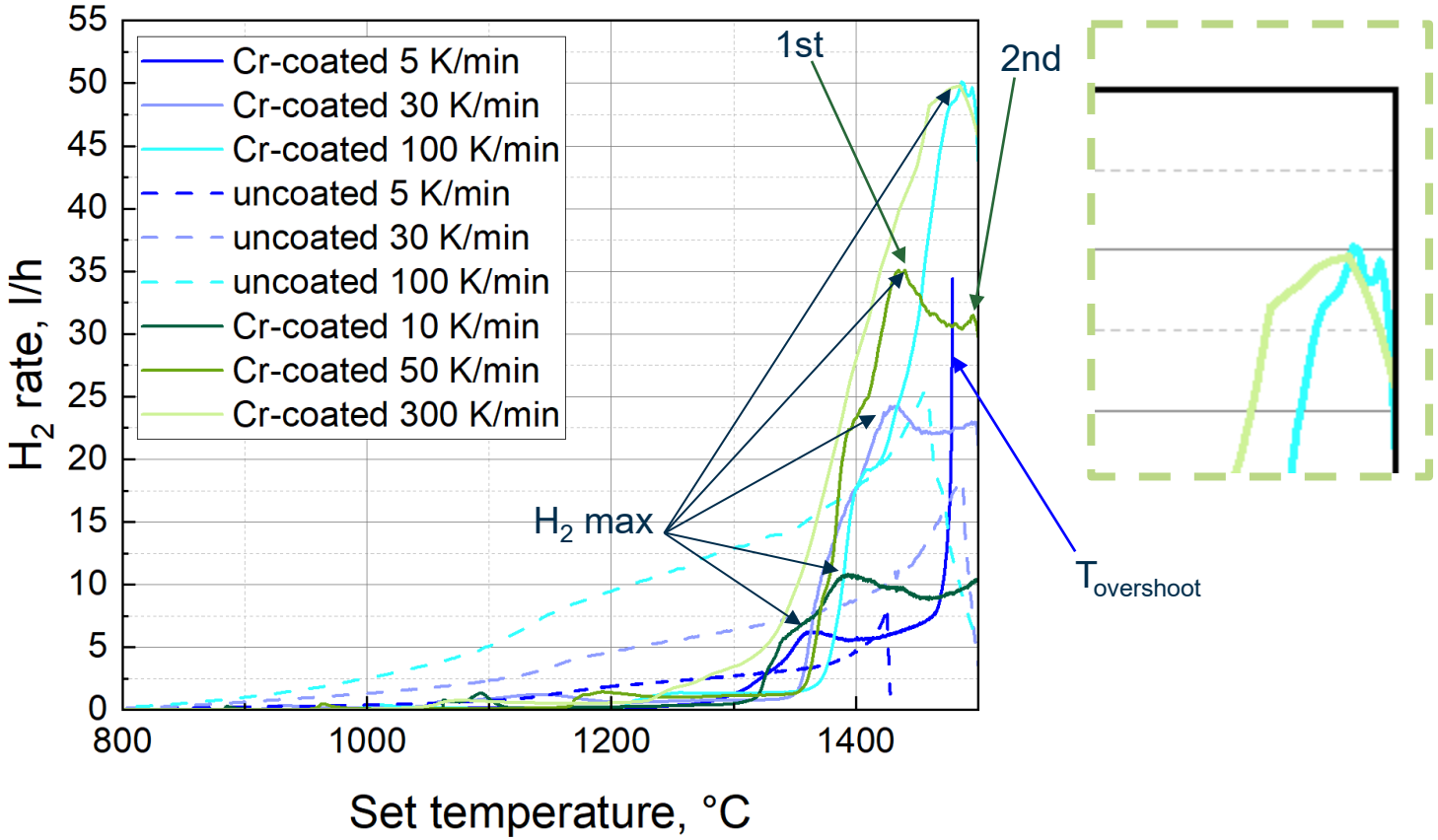

- Two peaks, similar to those observed in tests on plate samples at 10 K/min[1].
- 2nd Second peak corresponds to tetr→cub ZrO_2 transition[2].
- At 5 K/min 2nd peak – $T_{overshoot}$.
- At 300 K/min 2nd peak is not visible → max H_2 rate may not have been achieved.
- Max H_2 release rate increases with heating rate.
- All peaks shift to higher temperature as the heating rate increases.

1. https://doi.org/10.1016/j.corsci.2021.109805
2. https://doi.org/10.1007/s11085-008-9124-z

H_2 total

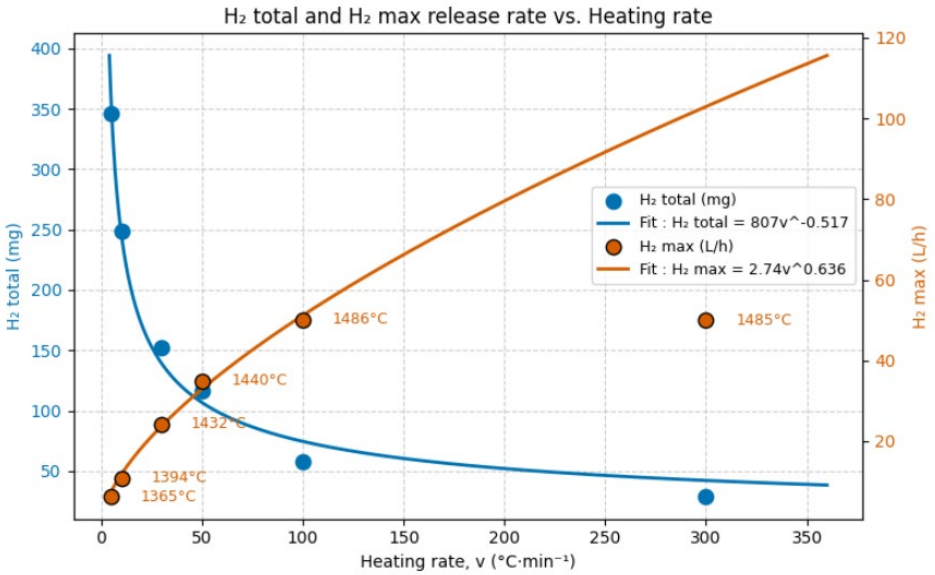

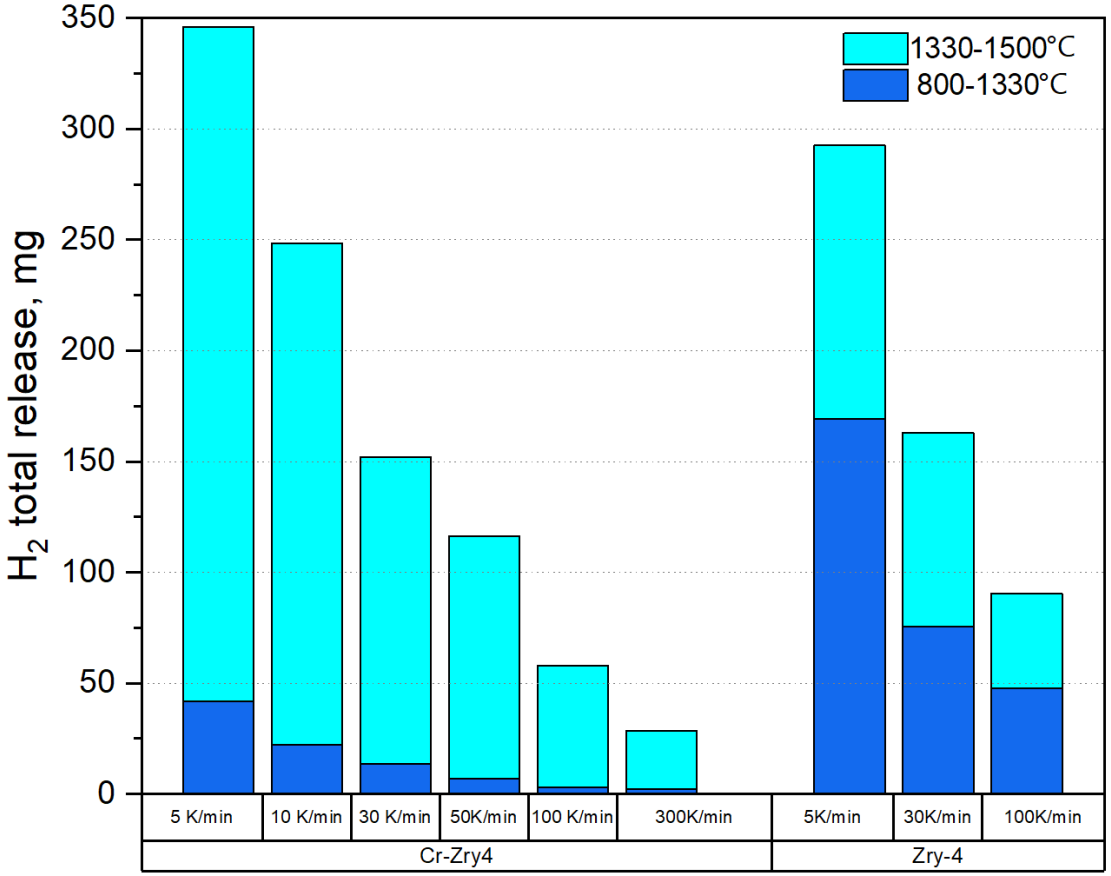

- Most H_2 is generated after the eutectic reaction.
- Total H_2 release decreases as the heating rate increases.
- At 100 K/min, total H_2 release is already lower than for uncoated Zry-4.

1. https://doi.org/10.1016/j.corsci.2021.109805
2. https://doi.org/10.1007/s11085-008-9124-z

Highlights

Highlights

QUENCH-SR tests of Cr-coated Zry-4 were conducted in steam up to 1500 °C at heating rates of 5, 10, 30, 50, 100, and 300 K/min.

Microstructure

- “Crocodile skin” morphology appeared at heating rates ≥ 10 K/min.
- A clear eutectic microstructure was first observed at 30 K/min. No correlation between eutectic area and heating rate was observed.
- ZrO_2 and Cr_2O_3 oxide thicknesses decreased with heating rate following an inverse power law.

Hydrogen release

- Total hydrogen release decreased with heating rate, approximately following an inverse square-root trend.
- Cr-coated tubes released less hydrogen than uncoated tubes at 100 K/min.
- Hydrogen release rates increased with heating rate, showing near square-root scaling and peaks shifted to higher temperatures.

Thank you for your attention!

Diana Bachurina
diana.bachurina@kit.edu

Tong Liu

SJTU

Multiscale Insights into Embrittling Mechanisms of Cr Coated Zircaloy Cladding under Ultra High Temperature Conditions

The talk by Tong Liu presented multiscale experimental insights into embrittling mechanisms of Cr-coated Zircaloy cladding under ultra-high-temperature LOCA-like conditions. Using an instrumented visual LOCA furnace with in-situ high-speed imaging and DIC strain mapping, the team tracked surface morphology, eutectic onset and real-time strain evolution during high-temperature steam oxidation and quench. Cr-coated tubes (15 µm magnetron sputtered Cr on 9.5 mm × 0.57 mm Zircaloy) showed strongly reduced oxide growth (oxide thickness reduced by factors ~20–43 versus uncoated at 1200–1350 °C) but developed a Cr–Zr eutectic layer with characteristic “crocodile-skin” morphology at higher temperatures. Ring compression tests (RCT) combined with DIC revealed that after 1200 °C HTO+quench Cr-coated cladding tended to fail in a brittle through-thickness mode (offset strain <2%), whereas uncoated material failed by ductile fracture; at 1350 °C the coated cladding exhibited better piecewise integrity (fewer fragments) and a much higher maximum load in some cases. Microstructural analyses linked embrittlement to formation of hard, brittle eutectic and intermetallic phases (Cr_2O_3, $ZrCr_2$, eutectic layer) and identified the inner wall as the preferred crack-initiation site. The authors concluded that standard RCT methods may not fully capture degradation of Cr-coated cladding and advocated for new mechanical assessment methods and integrated experiment-simulation approaches, as well as exploration of multilayer or alternative coatings to suppress eutectic formation and improve accident tolerance.

Multiscale Insights into Embrittling Mechanisms of Cr-Coated Zircaloy Cladding under Ultra-High Temperature Conditions

TONG LIU, SHIJIE WANG

SHANGHAI JIAO TONG UNIVERSITY, CHINA

Content

UNITED NATIONS

IAEA
International Atomic Energy Agency

IAEA Prediction:
561 GW~992 GW

COP30 Declaration:
33 countries have issued a declaration to **triple nuclear energy** capacity by 2050

Data of Global Nuclear Power:
376GW operational
64 GW under construction

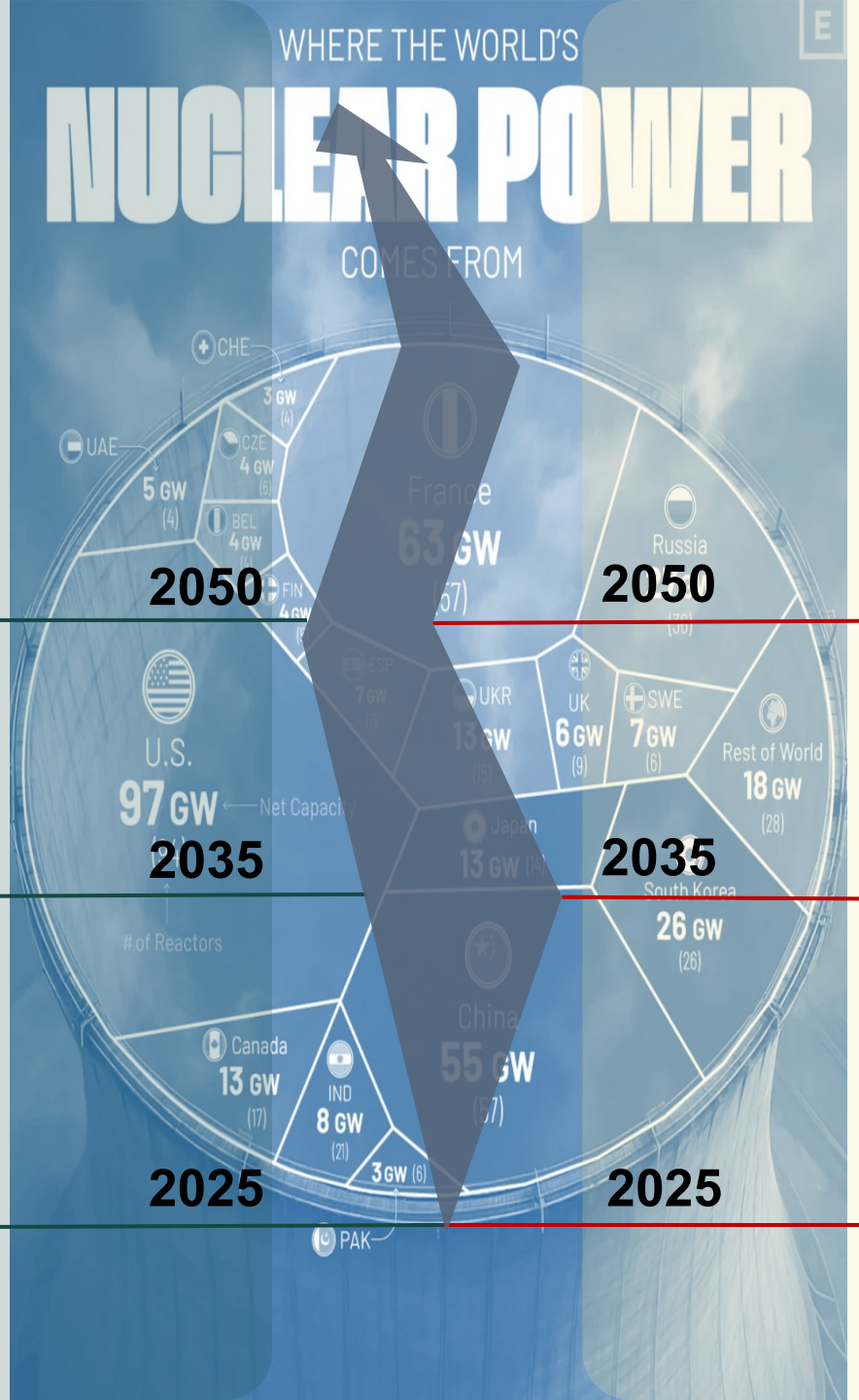

BP Energy Outlook:
China's nuclear energy production accounts for approximately **40%** of the global total

China NSSA Prediction:
China's nuclear power capacity in operation and under construction is projected to reach **113 GW**

Data of Chinese Nuclear Power:
56.3 GW operational
28.6 GW under construction

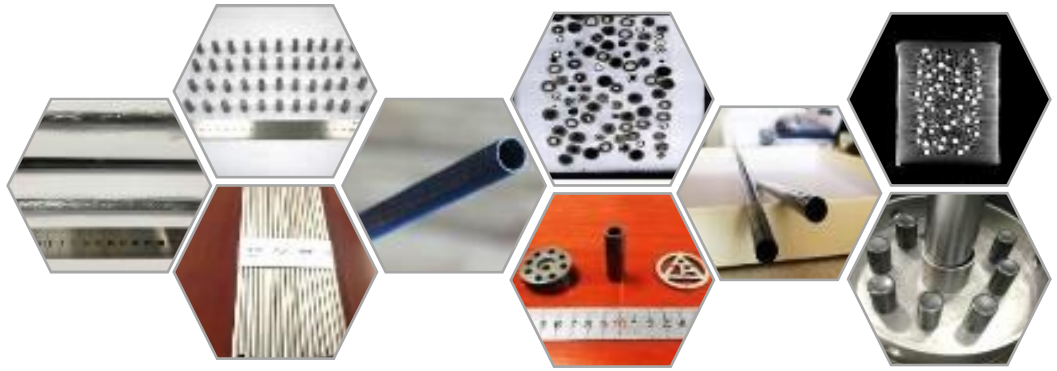

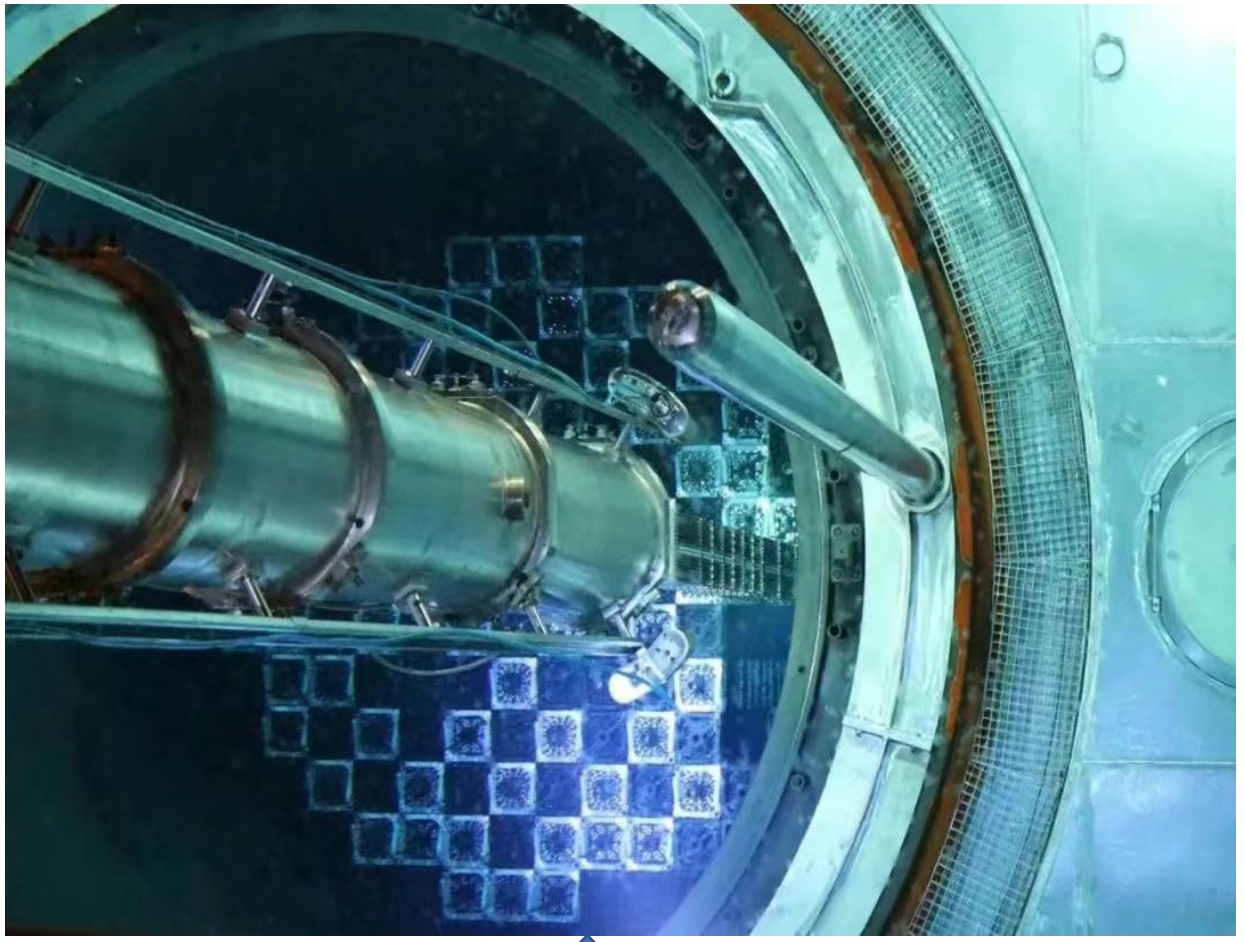

Chromium-Coated Zircaloy: A Leading ATF Cladding

- Lead Test Assemblies (LTAs) deployed in commercial reactors

Cladding Performance Analysis-Numerical Simulations

- **Despite providing real-time, in-situ data on the cladding's thermo-mechanical response, the accuracy of numerical simulations must be validated.**
- **——Absence of experimental validation**

Limited data

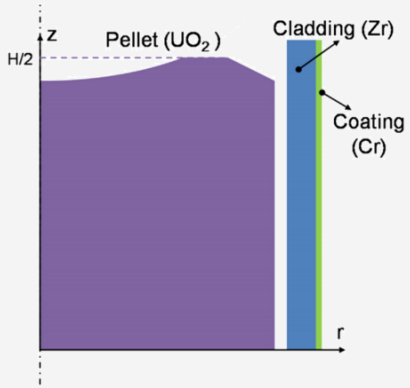

Geometric model

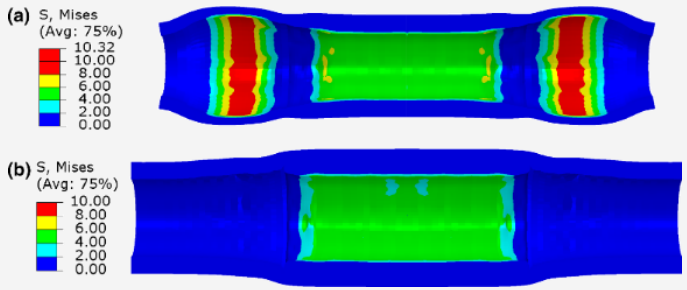

Stress distribution contour

Conventional Zircaloy tube	Normal Operation	Lack of Cr-Coated Zircaloy under Accident

Indirect assessment approach

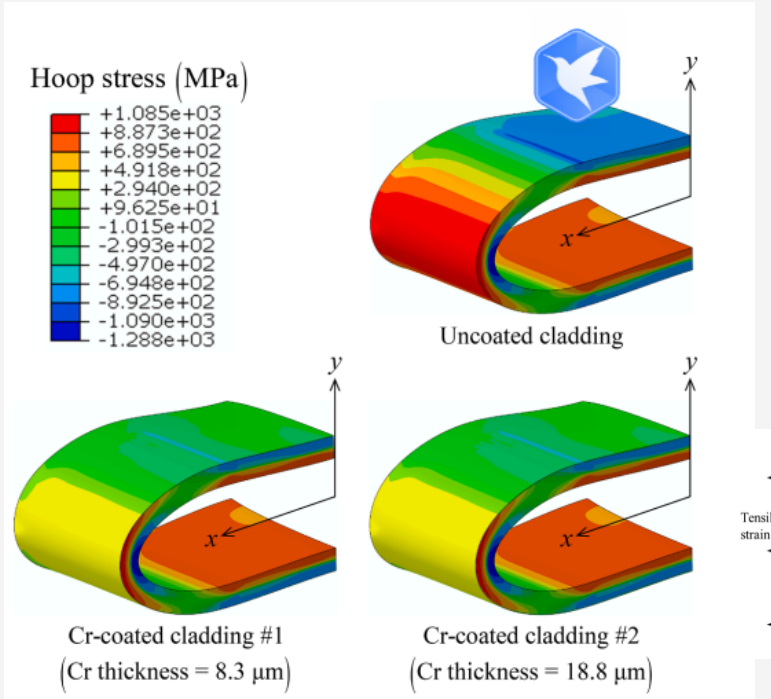

Stress-strain Constitutive model

Crack initiation and propagation

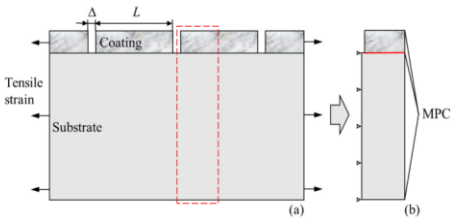

Nucl. Eng. Des. 367 (2020) 110792 J. Nucl. Mater. 585 (2023) 154603 Surf. Coat. Technol. 394 (2020) 125747

Cladding Performance Analysis-Traditional Experimental Approach

- **The intrusive nature of contact-based sensors distorts the intrinsic thermo-mechanical fields of the cladding and fails to capture critical local strain peaks**
- **—— Compromising the accuracy and reliability of the experimental data**

Invisible in Closed System

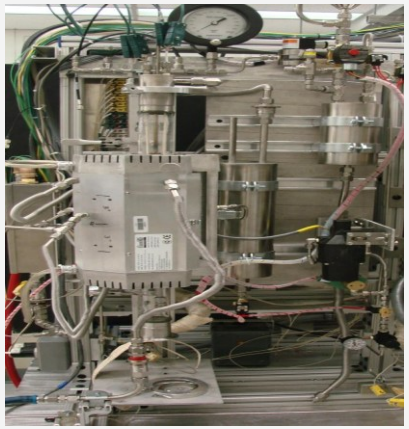

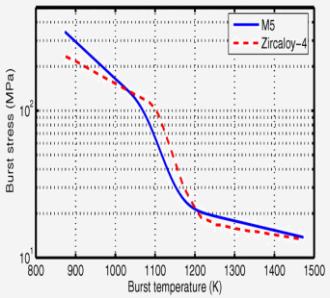

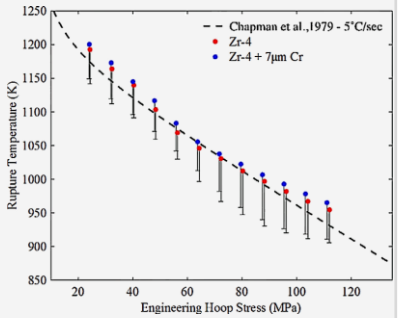

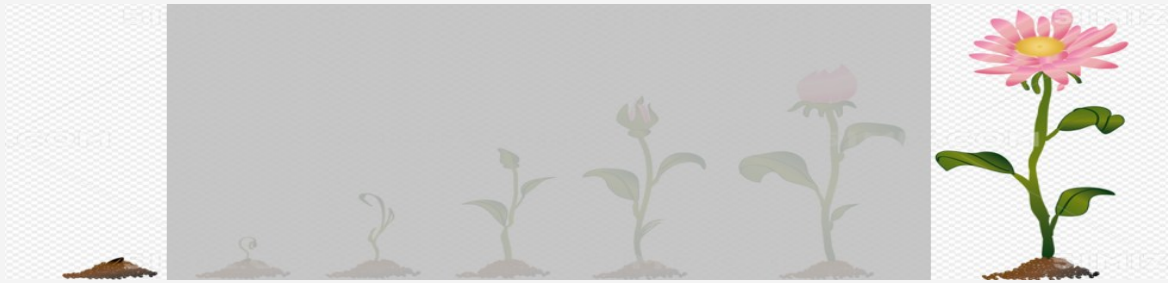

Interference/ Insufficiency/Undetection

The maxmum local strain data is missing due to limited SGs deployment

10^4 ~10^6 data

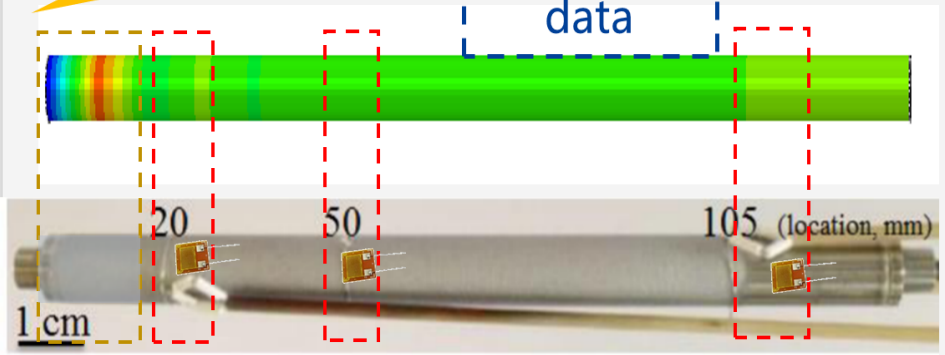

Numerical simulation

Experimental

3data

Temperature,stress,strain and corrosion of cladding samples are interfered by SGs and TCs

Content

Visual Experimental Platform

Ultra-high temperature LOCA device with visual system

Online Projection Image Measuring Instrument

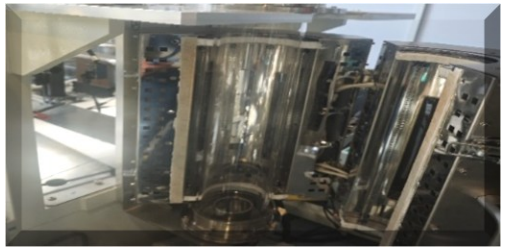

Furnace

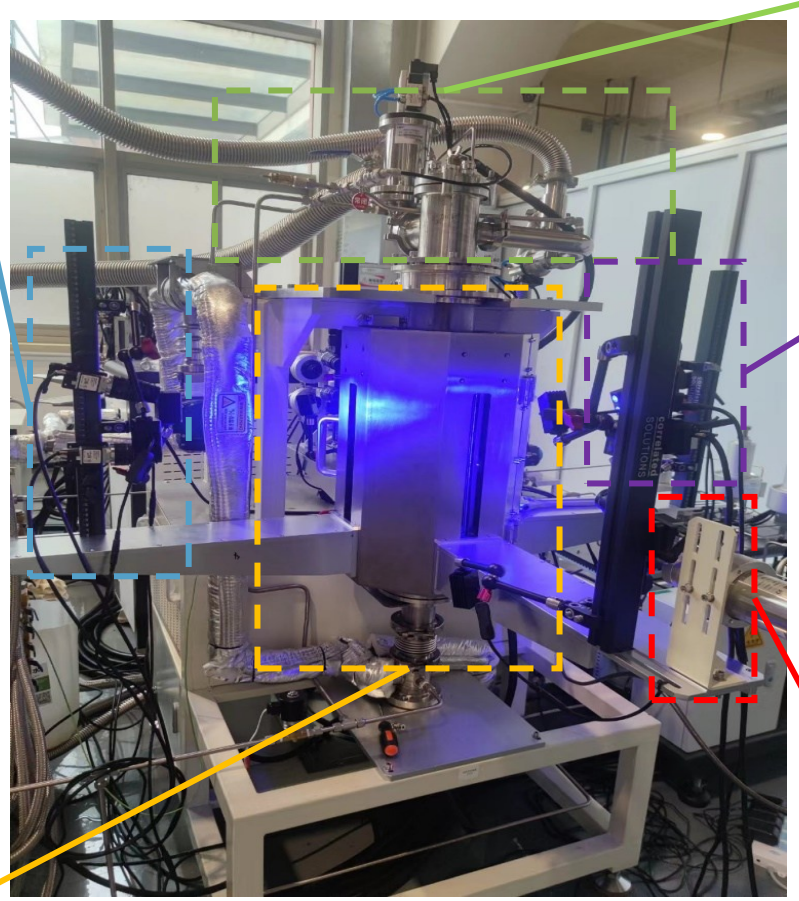

Pressure control system

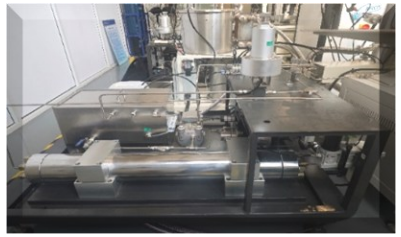

DIC system

Temperature measurement and control system

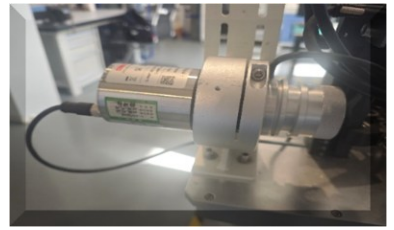

- ✓ **Maximum heating temperature** **2300 ℃**
- ✓ **Maximum heating rate** **300 ℃/s**

Experimental Facilities

Determining Post Quench Ducitility

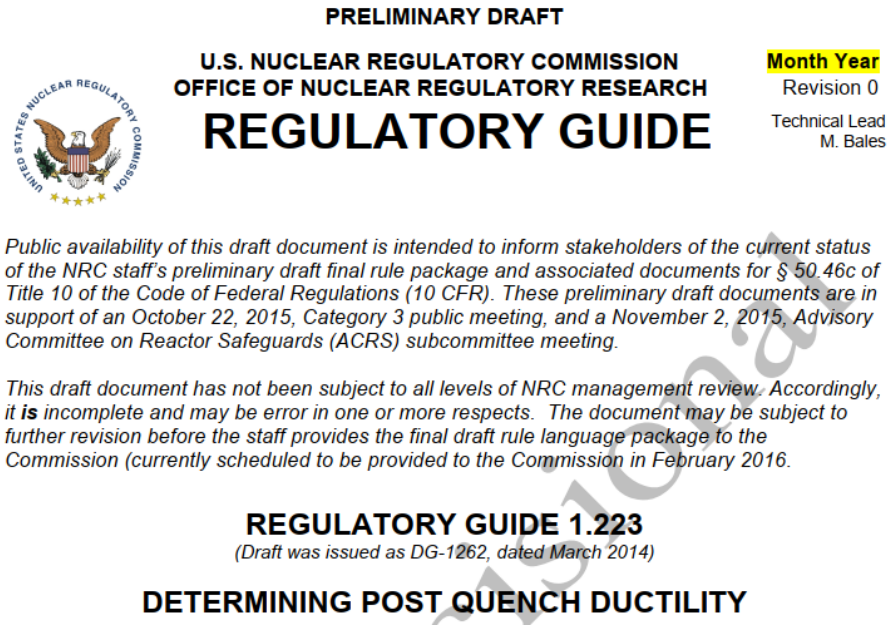

PRELIMINARY DRAFT

U.S. NUCLEAR REGULATORY COMMISSION
OFFICE OF NUCLEAR REGULATORY RESEARCH

Month Year
Revision 0

Technical Lead
M. Bales

REGULATORY GUIDE

Public availability of this draft document is intended to inform stakeholders of the current status of the NRC staff's preliminary draft final rule package and associated documents for § 50.46c of Title 10 of the Code of Federal Regulations (10 CFR). These preliminary draft documents are in support of an October 22, 2015, Category 3 public meeting, and a November 2, 2015, Advisory Committee on Reactor Safeguards (ACRS) subcommittee meeting.

*This draft document has not been subject to all levels of NRC management review. Accordingly, it **is** incomplete and may be error in one or more respects. The document may be subject to further revision before the staff provides the final draft rule language package to the Commission (currently scheduled to be provided to the Commission in February 2016.*

REGULATORY GUIDE 1.223
(Draft was issued as DG-1262, dated March 2014)

DETERMINING POST QUENCH DUCTILITY

NRC Regulatory Guide 1.223 Determining Post Quench Ductility (PQD)

Mechanical Test System (MTS)

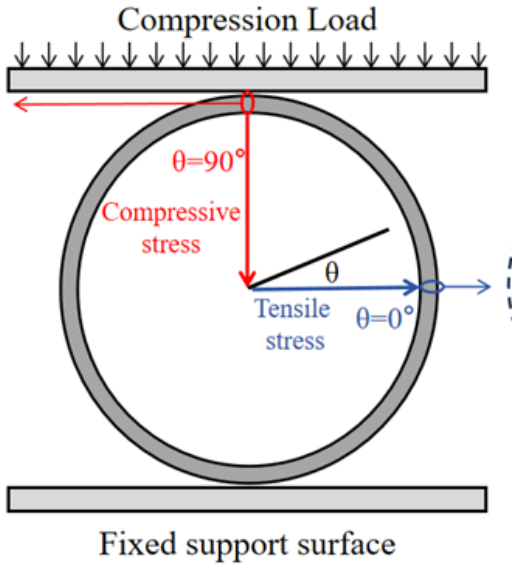

Schematic of simulated Ring Compression Test (RCT)

Content

Experimental materials and conditions

☐ Experimental materials

zircaloy cladding

- Diameter
  9.5 mm
- thickness
  0.57 mm

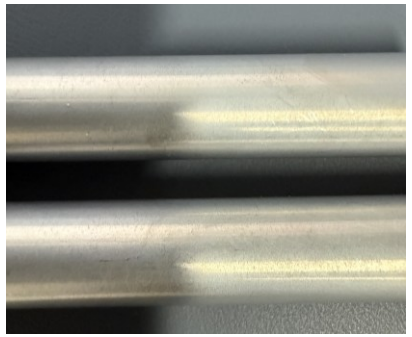

Cr-coated cladding

- Magnetron sputtering process
- Coating thickness
  15 μm

☐ Experimental conditions

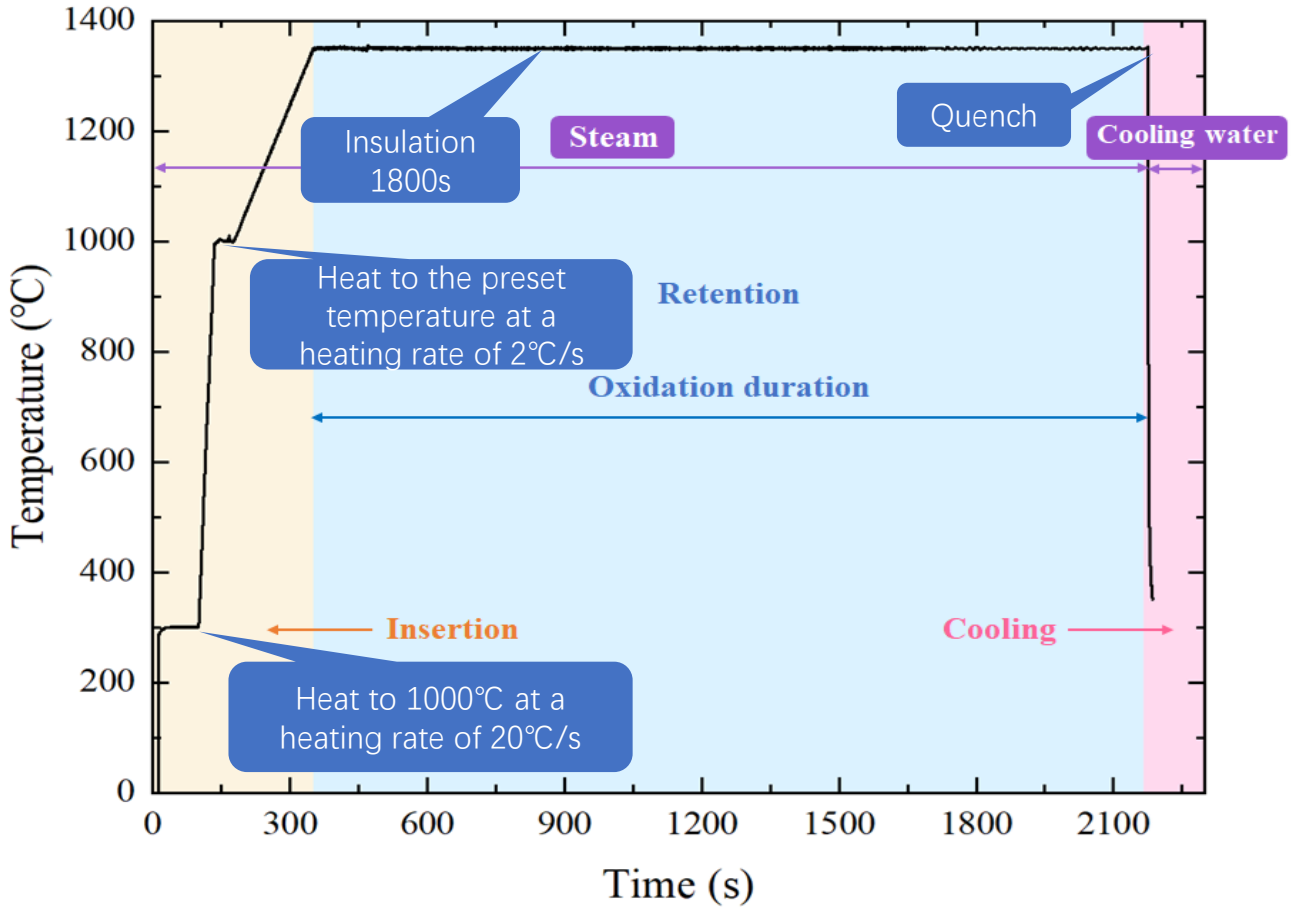

In-situ Visualization during HTO and Quench

HT Steam Oxidation &Quench

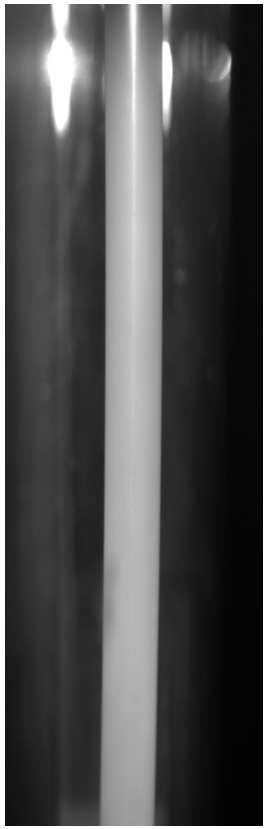

Start

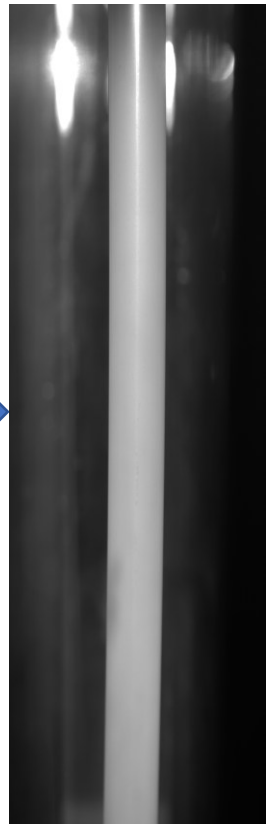

Oxidation

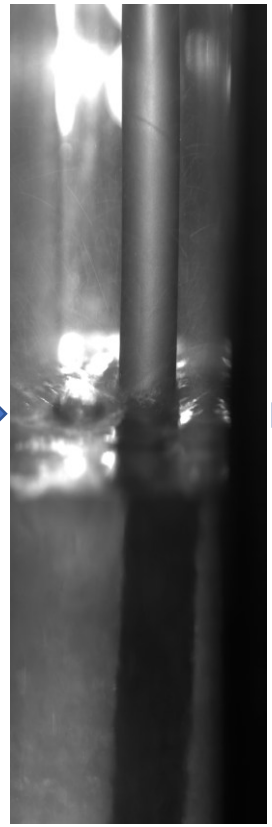

Quench

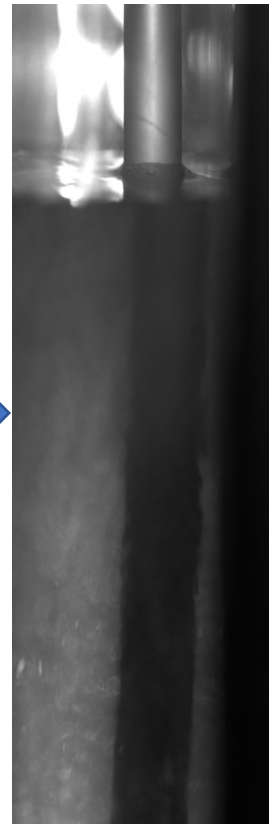

Finish

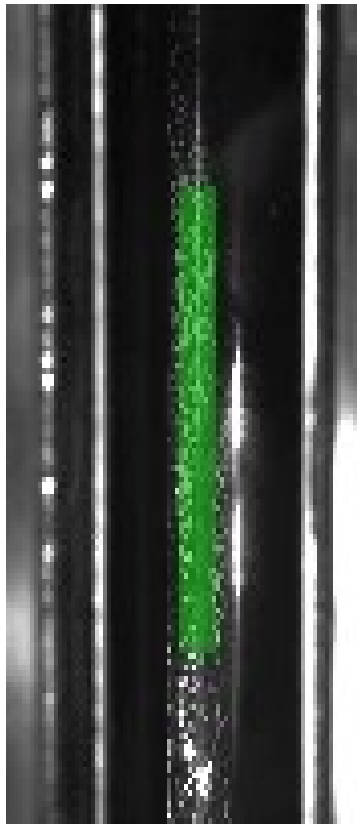

Real-time and in-situ strain distribution

- **In-situ high speed camera tracks surface morphology during HTO+Q**

Pre-/Post-HT Oxidation Cladding Morphology

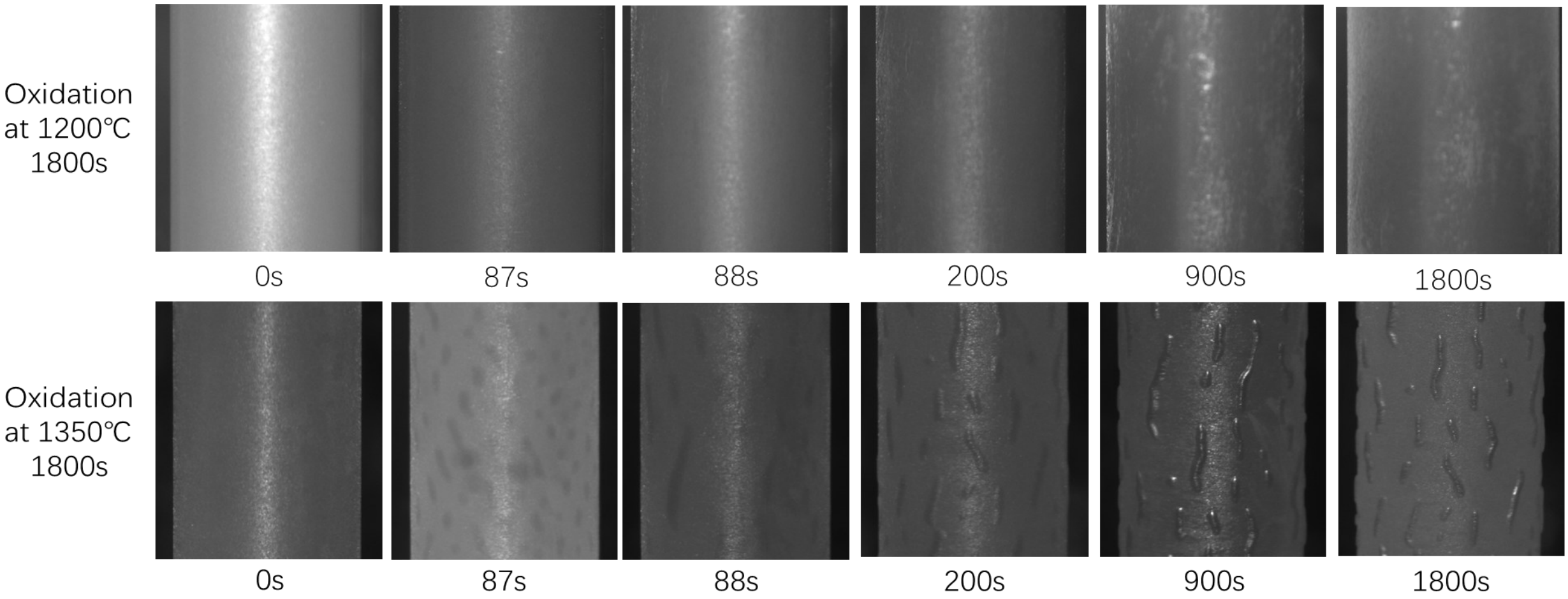

The onset of the chromium-zirconium eutectic reaction and the subsequent evolution of its surface morphology were precisely captured using in-situ high-speed photography.

Nuclear Engineering and Design, 2025, 443, 114337.

Pre-/Post-HTO+Q Cladding Morphology

Type	As-received	Oxidation at 1200℃ 1800s	Oxidation at 1350℃ （Trant.） 1800s
Uncoated Zr cladding			
Cr-coated Zr cladding			

- **Uncoated Zr: metallic luster → rough black/brown**
- **Cr-coated Zr: silvery white → dark green; 1350 °C shows eutectic “crocodile-skin” morphology.**

Pre-/Post-HTO Cladding Microstructure

Type	As-received	Oxidation at 1200 ° C 1800s	Oxidation at 1350 ° C 1800s
Uncoated Zr cladding	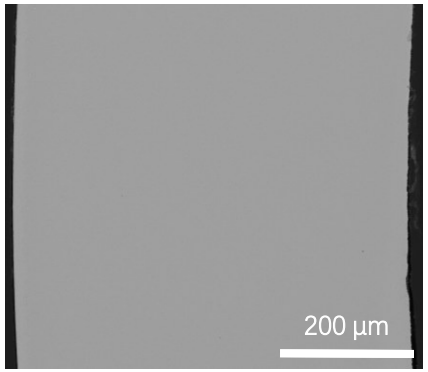	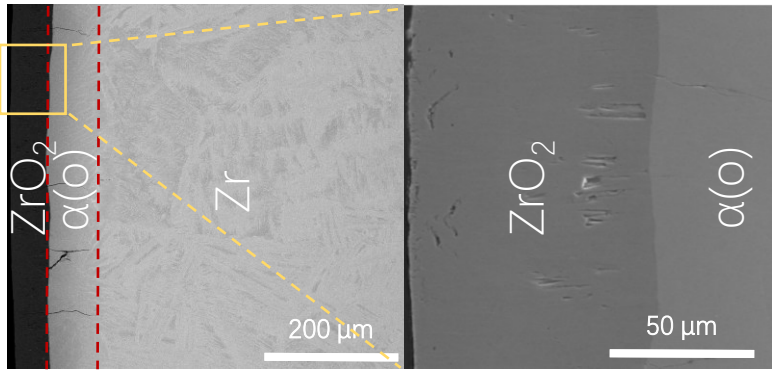	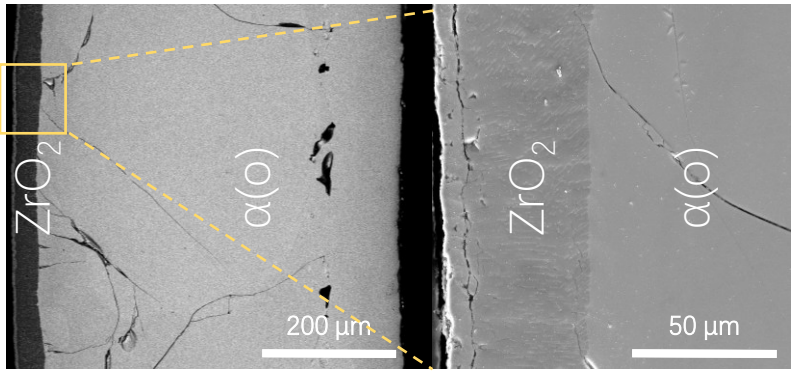
Cr-coated Zr cladding	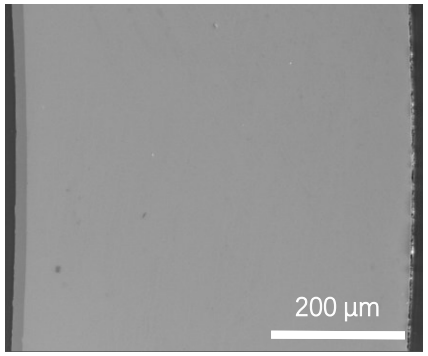	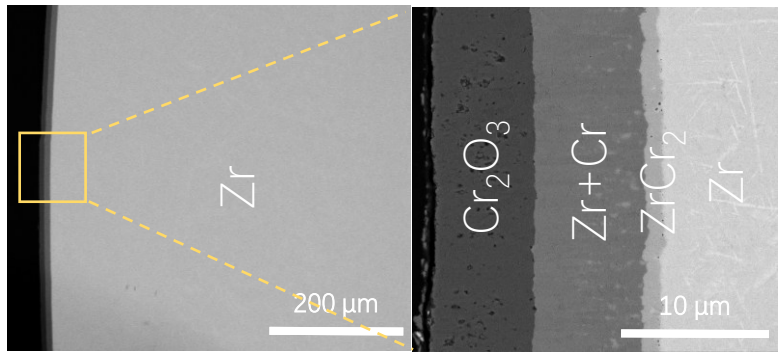	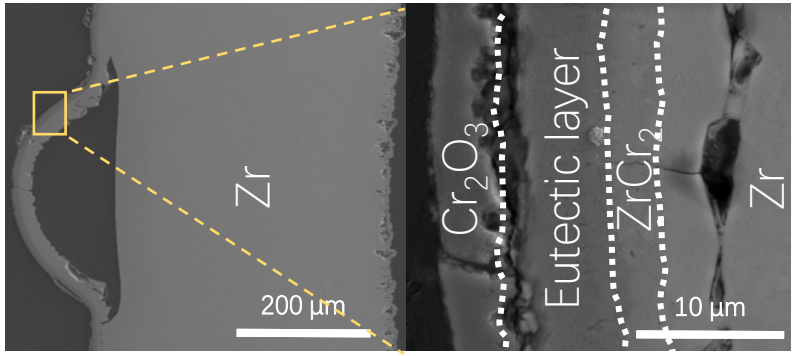

➢ **The coated cladding exhibited a reduction in oxide layer thickness by factors of ~20 and ~43 at 1200°C and 1350°C as compared to uncoated.**

Pre-/Post-HTO Cladding Composition

Type	As-received	Oxidation at 1200 ° C 1800s	Oxidation at 1350 ° C Tran 1800s
Uncoated Zr cladding	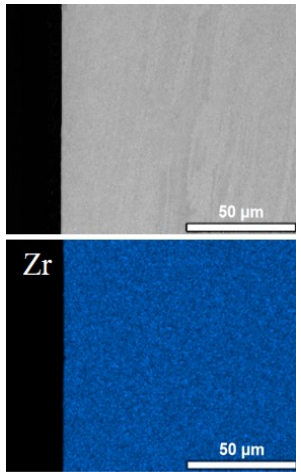	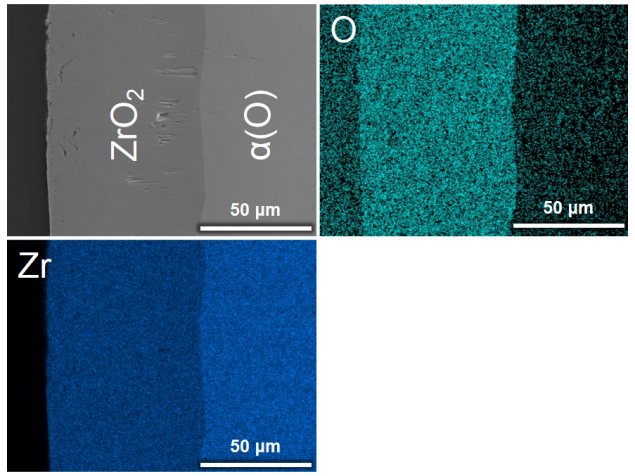	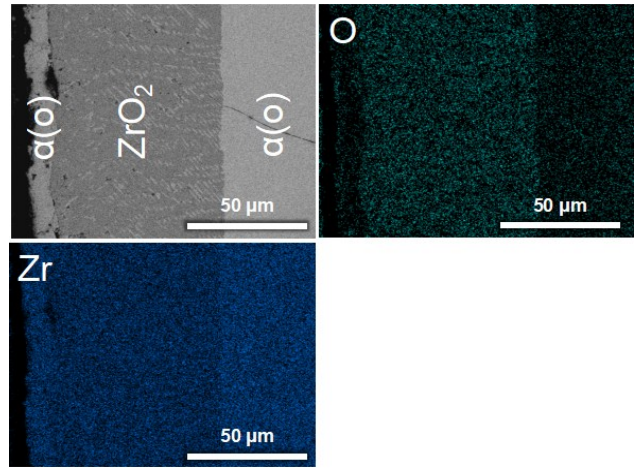
Cr-coated Zr cladding	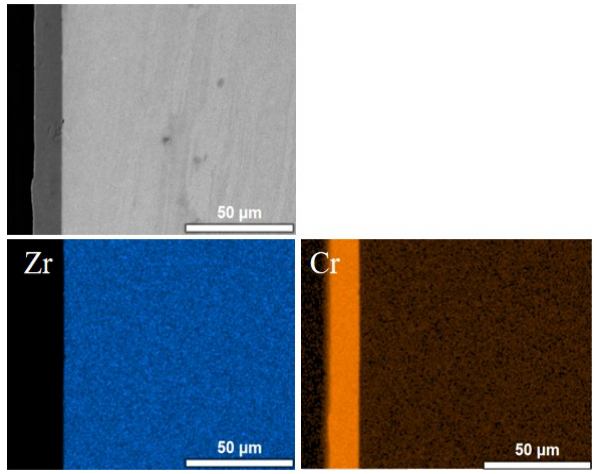	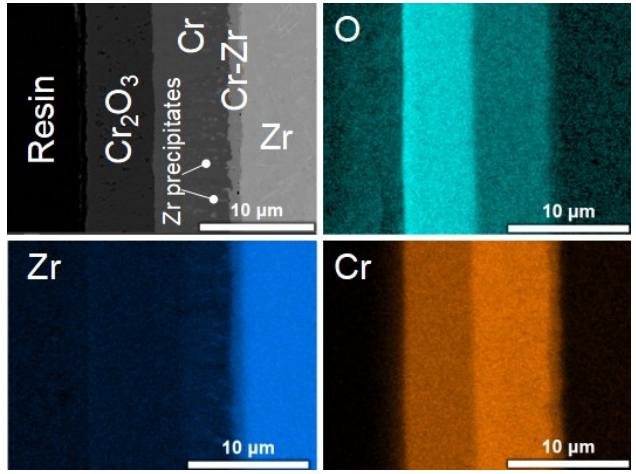	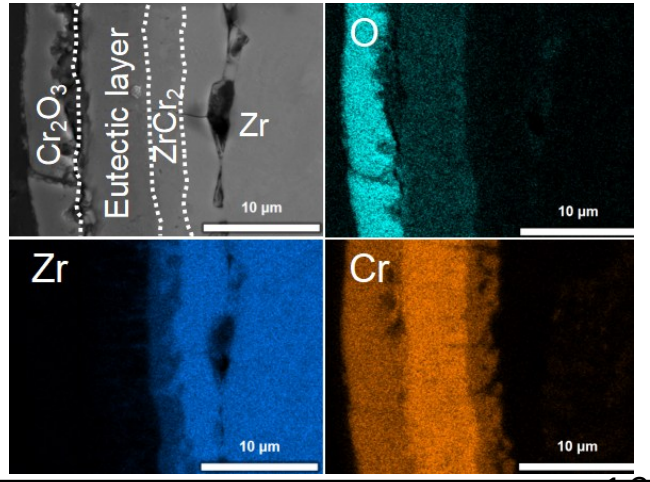

Pre-/Post-HTO Coated Cladding Grain Structure

Type	As-received	Oxidation at 1200℃ 1800s	Oxidation at 1350℃ 1800s
Cr-coated Zr cladding	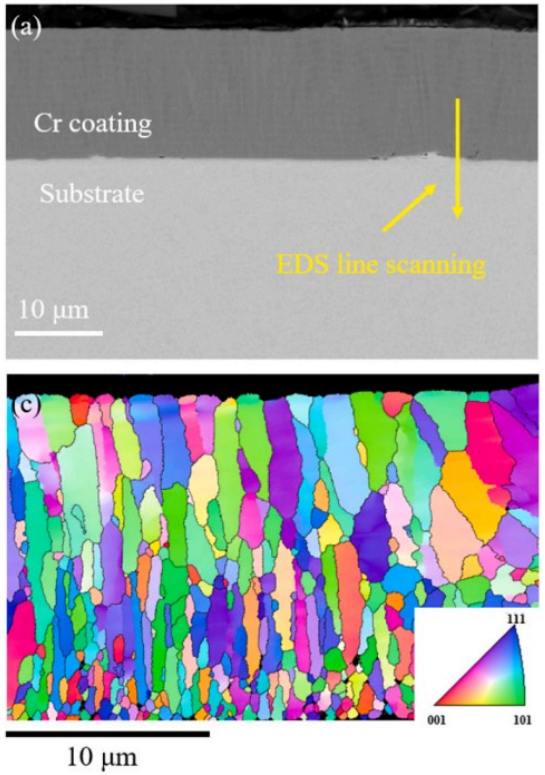	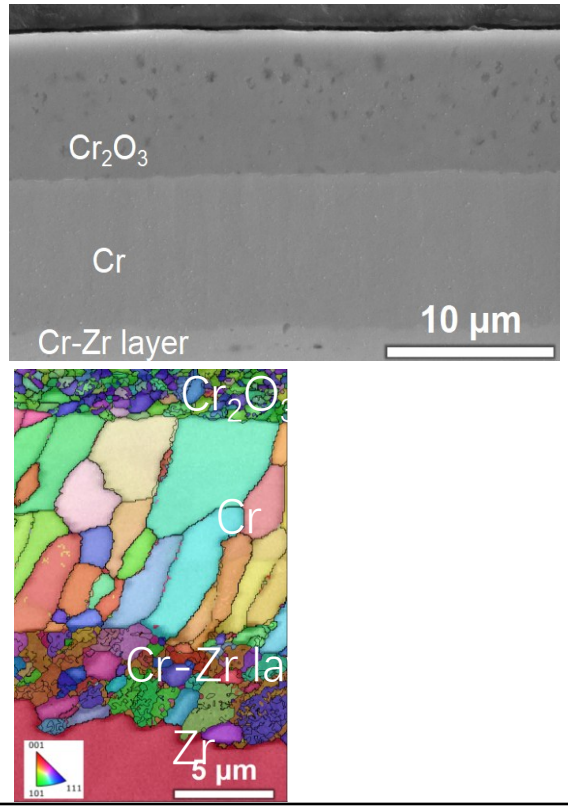	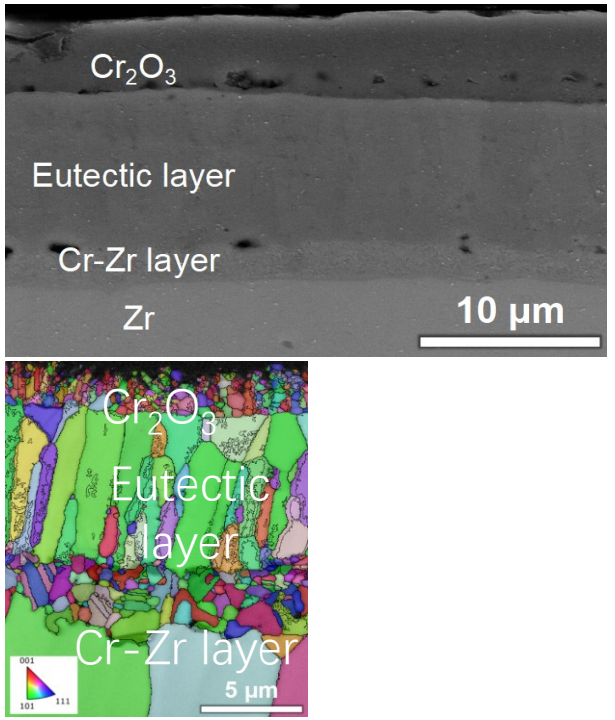
	➢ Cr layer:Columnar crystal	➢ Cr_2O_3 layer:Equiaxed crystal ➢ Cr layer:Columnar crystal ➢ Zr-Cr layer:Equiaxed crystal	➢ Cr_2O_3 layer:Equiaxed crystal ➢ Eutectic layer:Columnar crystal ➢ Zr-Cr layer:Equiaxed crystal

1200℃ 30min

1350℃ 30min

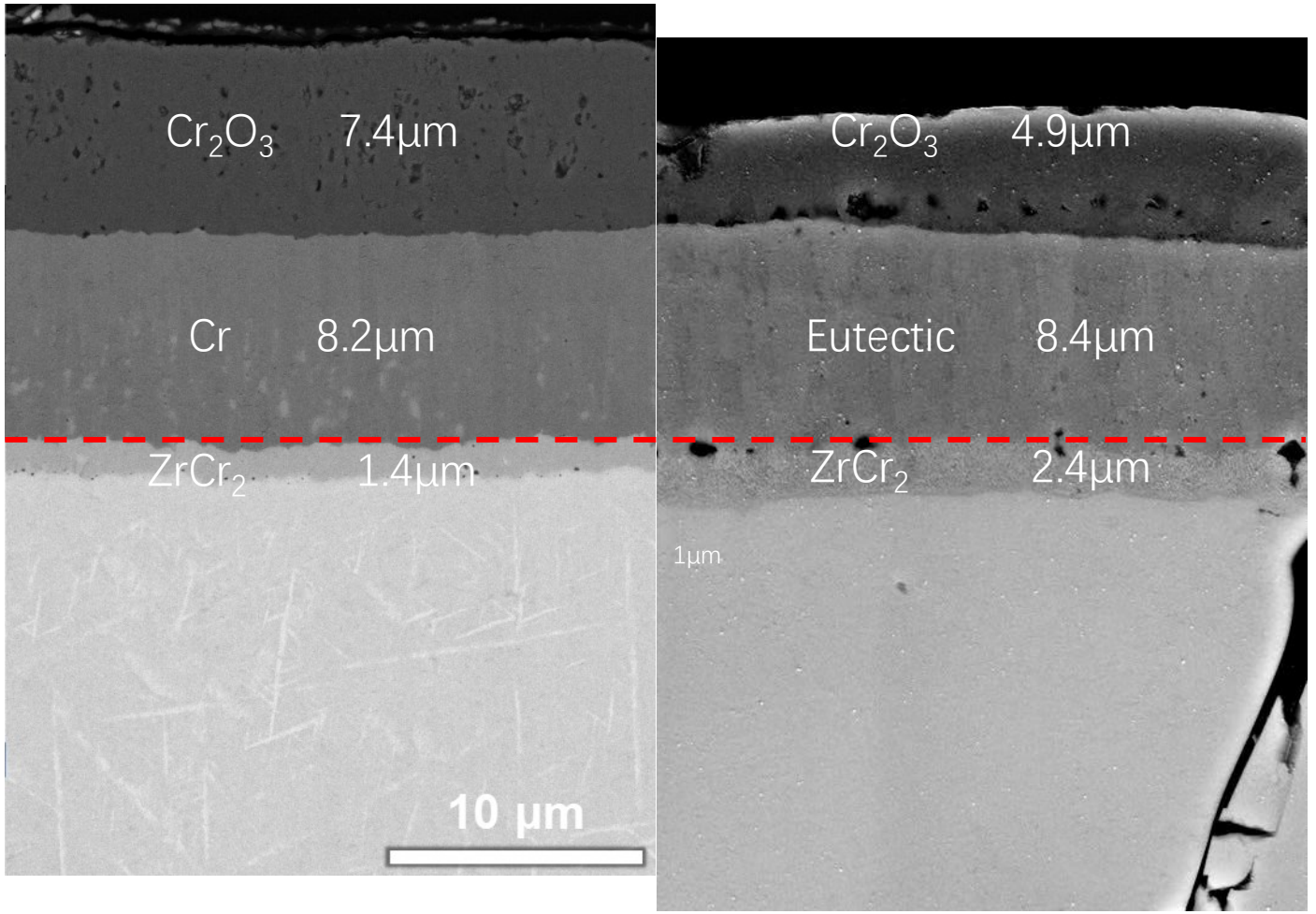

Ring Compression Test

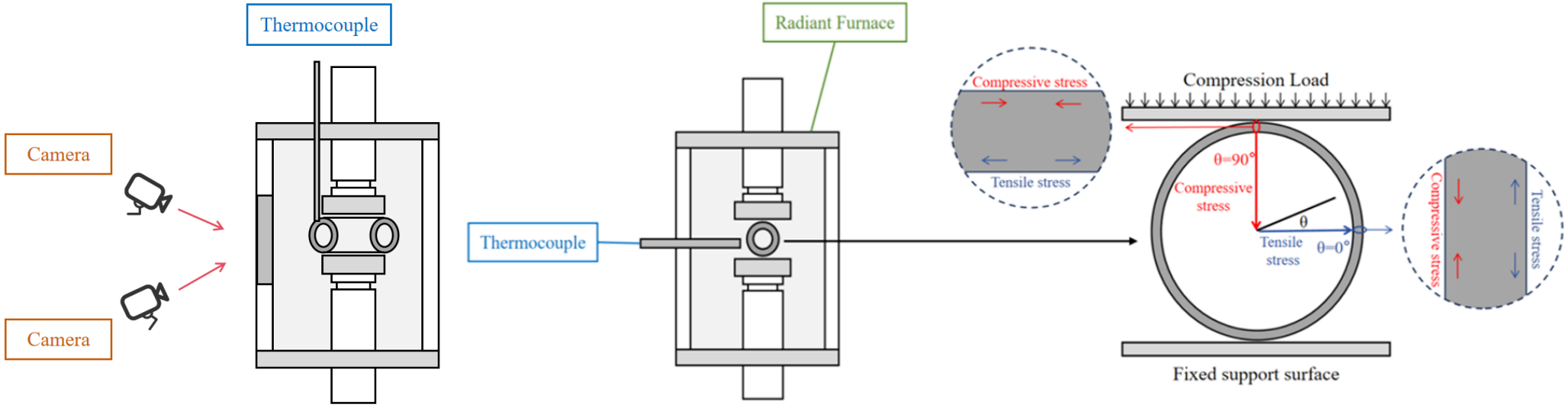

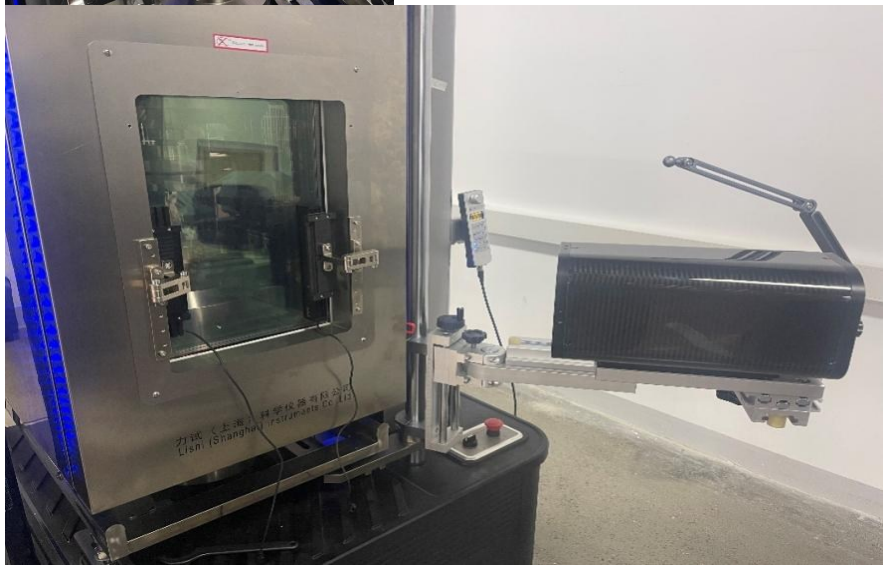

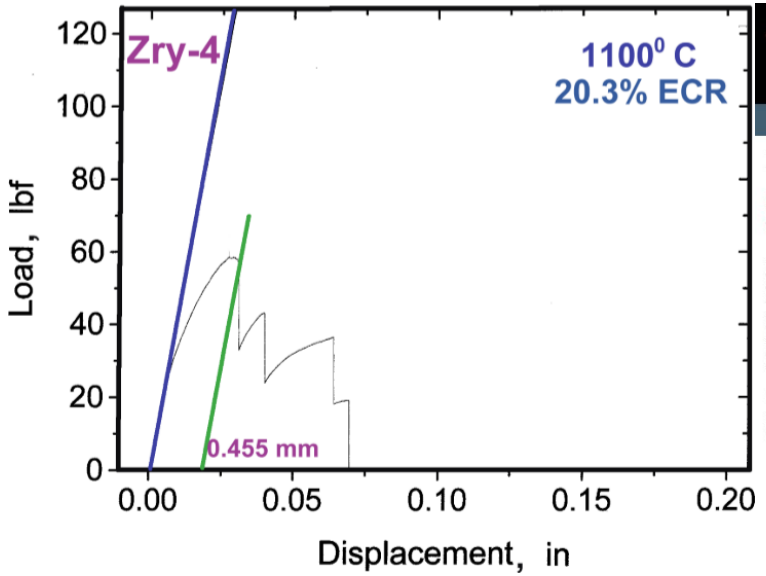

Typical load-displacement curve[1]

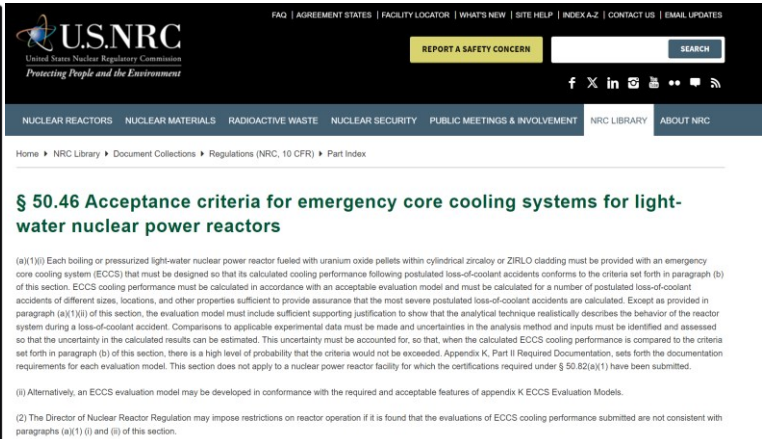

NRC Fuel safety criteria during LOCA [2]

offset strain

<2% Brittle failure

>2% Ductile failure

1] No. NUREG/CR-696. Argonne National Lab.(ANL), Argonne, IL (United States), 2008.; [2] NRC, 10CFR50.46 [3]REGULATORY GUIDE 1.223

Pre-/Post-RCT Cladding Morphology

- **Specimen 8.00 ± 0.05 mm (axial length); crosshead rate 0.033 mm/s.**

Type	As-received	Oxidation at 1200 ° C 1800s	Oxidation at 1350 ° C 1800s
Uncoated Zr cladding			
Cr-coated Zr cladding	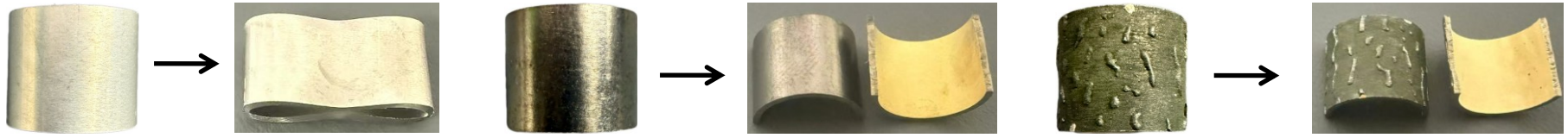		
	Pre-RCT	Post-RCT	Pre-RCT	Post-RCT	Pre-RCT	Post-RCT

The oxide layer spalls off.

- **1200 °C: Uncoated—local/non-penetrating; Cr-coated—through-thickness → weaker fracture resistance.**
- **1350 °C: Uncoated—4 pieces; Cr-coated—2 pieces → superior fracture resistance for Cr-coated.**

DIC mapping during RCT after 1200℃ HTO+Quench

Type	Tangential strain	Typical location	Moment of load drop	**Load-displacement curve**
Uncoated Zr cladding	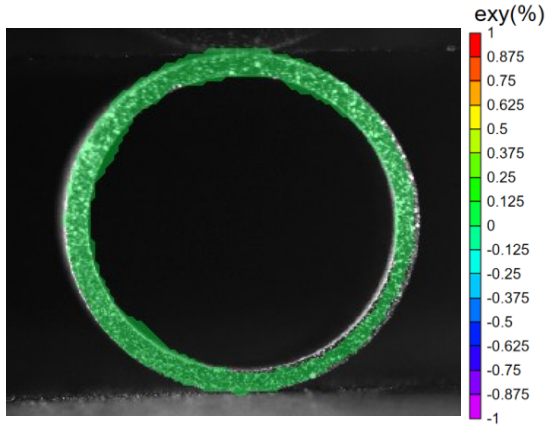	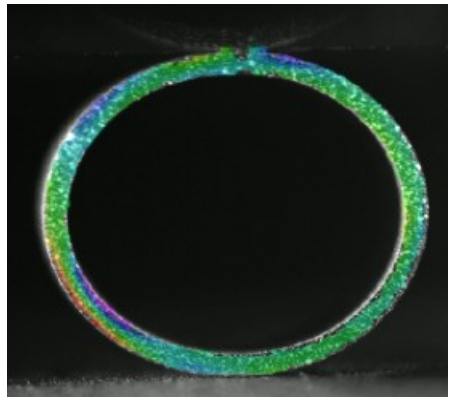	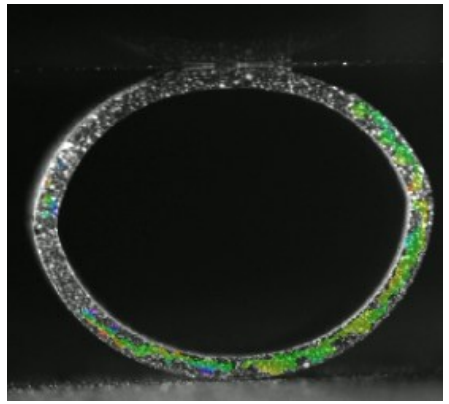	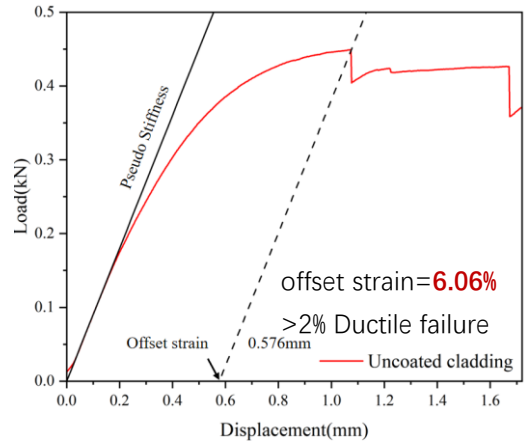
Cr-coated Zr cladding	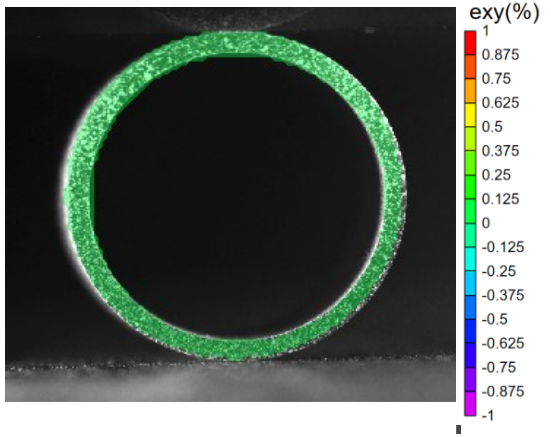	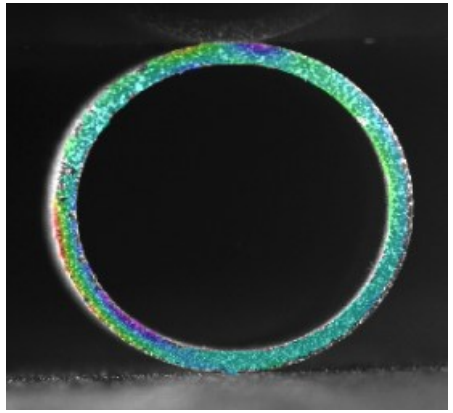	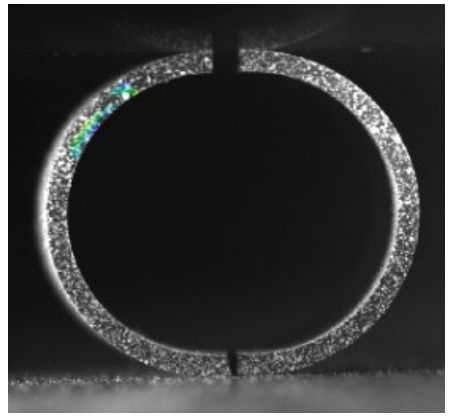	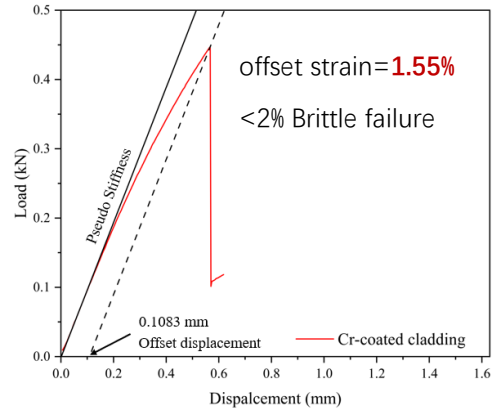

- **After HTO at 1200 °C, the uncoated cladding fails by ductile fracture, whereas the Cr-coated cladding fails by brittle fracture, with similar maximum load-bearing capacity**

DIC mapping during RCT after 1350℃ HTO+Quench

Type	Tangential strain	Typical location	Moment of load drop	Load-displacement curve
Uncoated Zr cladding	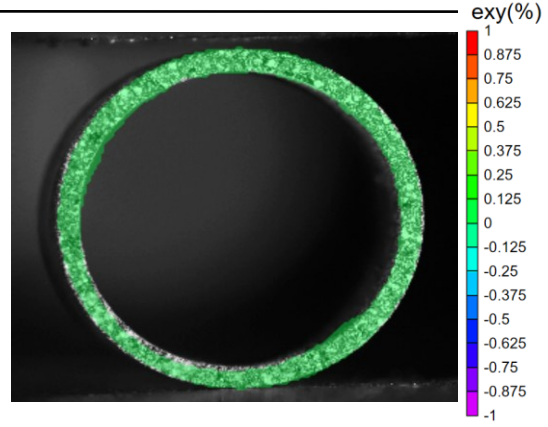	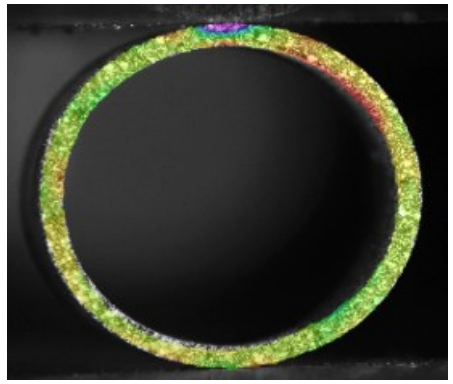	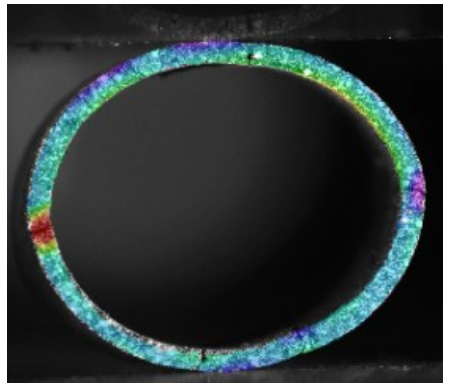	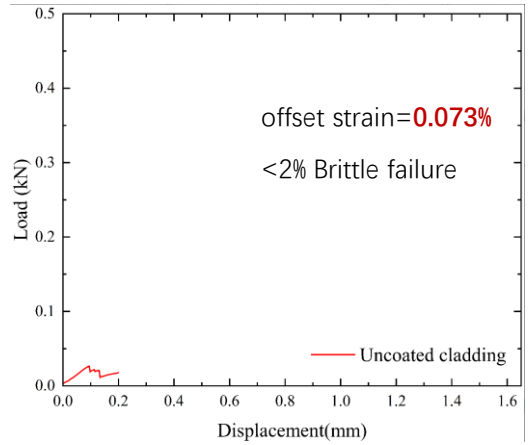
Cr-coated Zr cladding	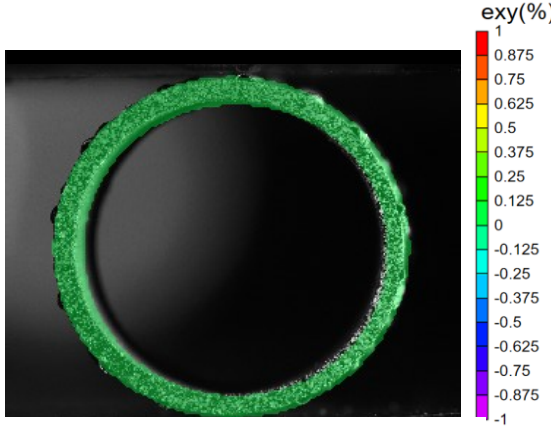	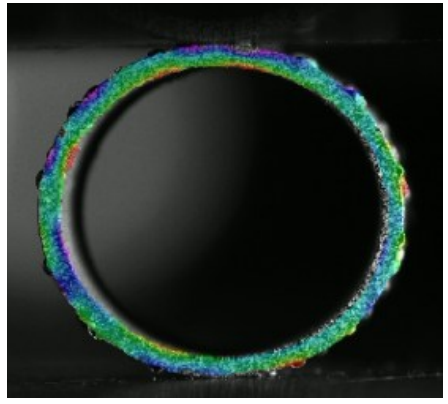	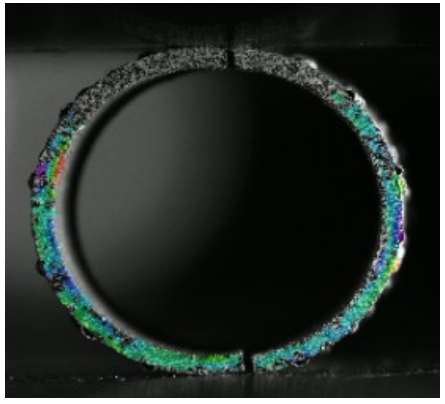	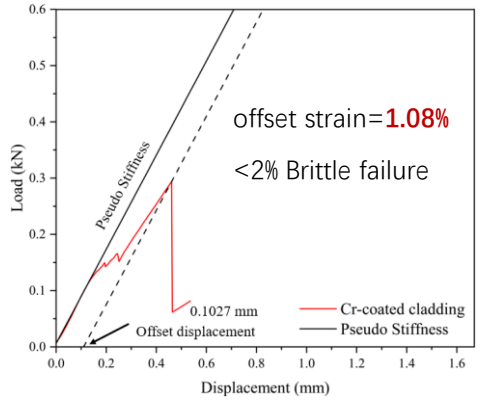

The Cr-coated cladding exhibited an approximately 16.7-times increase in maximum load-bearing capacity.

Content

Summary

- A combined in-situ/ex-situ approach correlated mechanical embrittlement of Cr-coaed Zircaloy cladding with its microstructure.
- Dynamic monitoring identified the Cr-Zr eutectic onset and associated "crocodile-skin" morphology
- The eutectic reaction degrades mechanical properties by creating hard-brittle phases and initiating crack nucleation and growth.
- RCT+DIC on single-sided oxidized specimens shows peak tensile stress on the inner wall, identifying it as the preferred crack-initiation site.
- RCT following exposure to 1200°C HTO reveal that the chromium coating significantly reduces oxidation; nevertheless, it induces premature brittle fracture of the cladding.
- The standard ring compression test may not be suitable for evaluating the mechanical degradation of Cr-coated cladding.

Outlook

- **Mechanical Assessment Methodology**

New mechanical assessment methods in experimental and numerical modeling must be developed to accurately characterize its performance degradation.

- **Integration of Experiment and Simulation**

The experimental phenomenology for visualizing extreme-scenario responses provides a critical foundation. Subsequent research will focus on quantitatively correlating these findings with numerical simulations to validate and refine predictive models.

- **Advanced Coating Systems**

Exploring multi-layer or alternative coating materials could provide pathways to suppress eutectic formation and achieve superior accident tolerance.

Ballooning and Burst Test

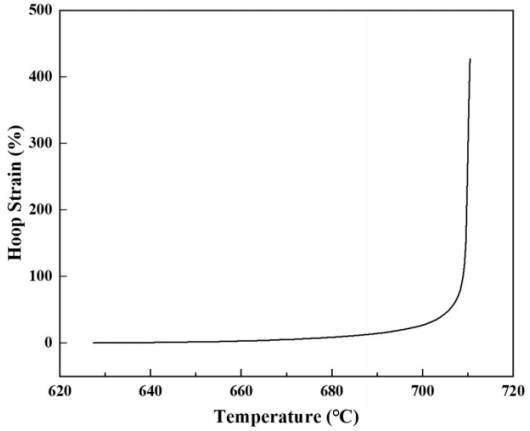

Hoop Strain vs Temperature

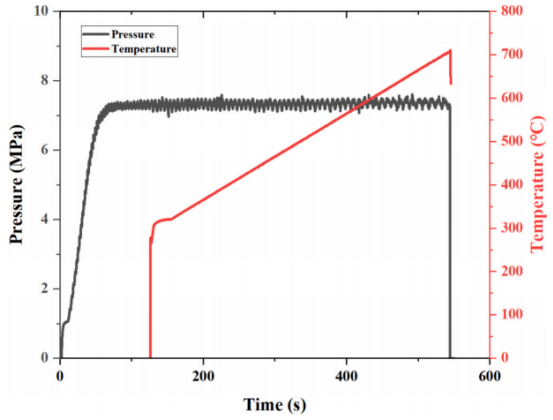

Pressure/Temperature vs Time

Optical image	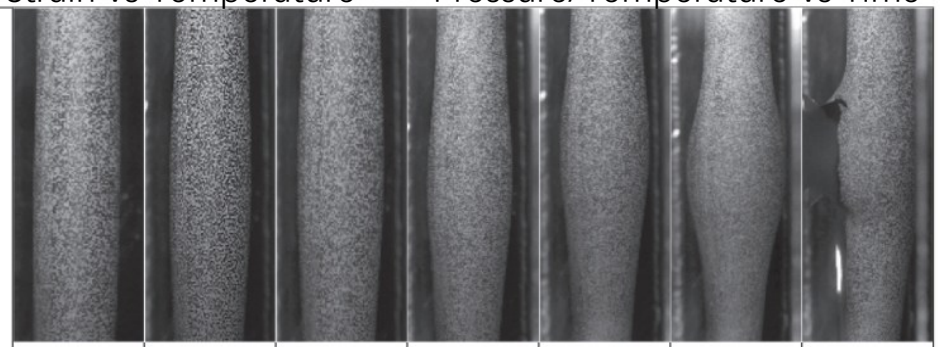						
	(a)	(b)	(c)	(d)	(e)	(f)	(g)
Temperat-ure	683.1°C	708.9°C	709.3°C	709.7°C	709.9°C	710.2°C	710.5°C
Strain variations	0	0.007	0.082	0.104	0.149	0.223	0.611

Optical image sequence during the onset of the eutectic reaction

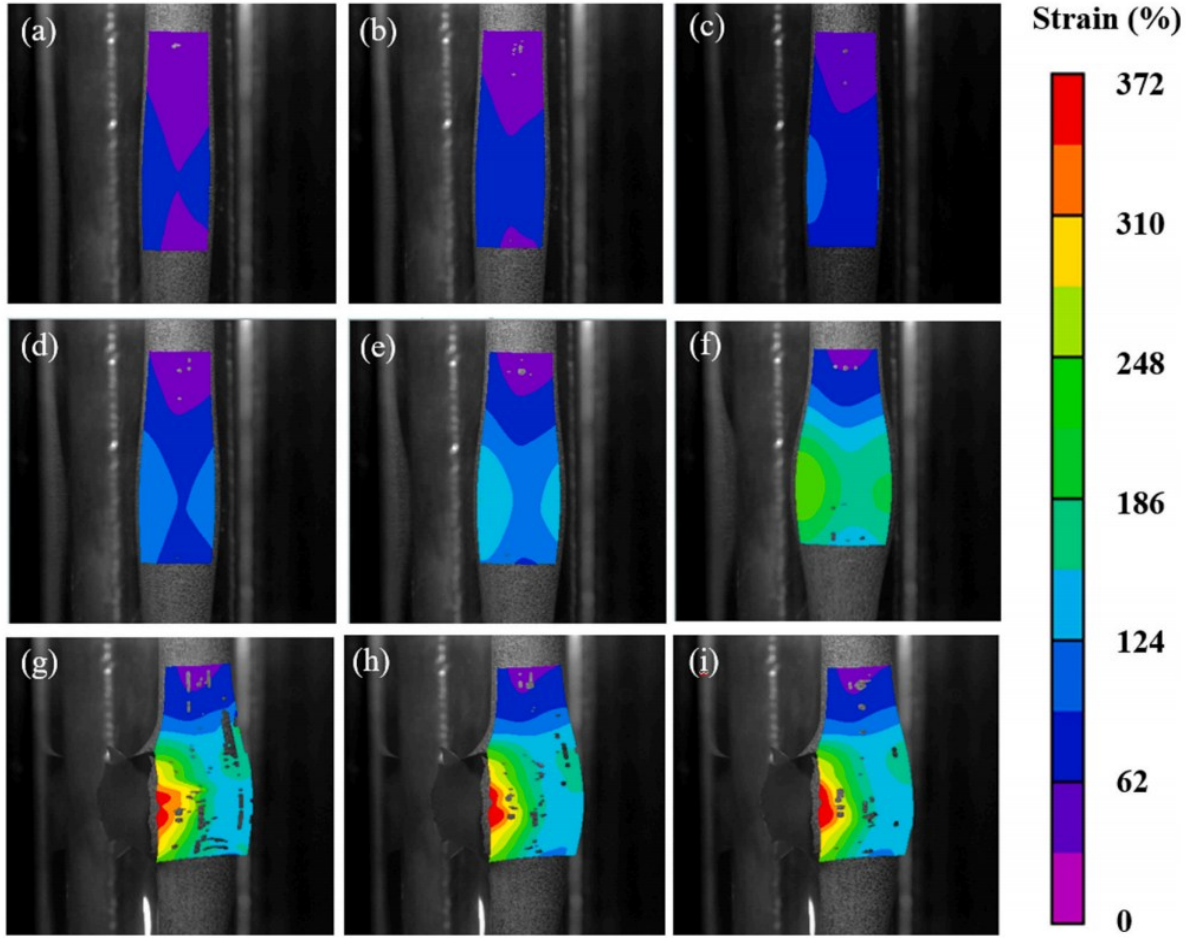

Strain distribution mapping on Zry-4 cladding tube during the B&B test

Ballooning burst experimental curves and strain calculation results[1]

Nuclear Engineering and Design, 2025, 443, 114337.

Acknowledgments

Prof. Jun Sun
Prof. Zhongxiao Song
Dr. Martin Steinbruck
Prof. Xiaoqin Zeng
Dr. Yehong Liao
Mr. Shijie Wang
Mr.Yi Li
Ms.Beiqi Wang

supported by NNFC(Grant No.12575296) HNKF202314(48) CNNC-LCKY-202242

Welcome to Shanghai and SJTU!

Thank for your attention

tongliu@sjtu.edu.cn

Václav Bouček

UJP

Behavior of Fuel Cladding with Cr Coating during LOCA and Study of Oxygen Diffusion into Zr-alloy using Different methods

The advancement of Accident Tolerant Fuel (ATF) technologies is critical for enhancing the safety of nuclear reactors under accident conditions. Chromium (Cr) coatings on conventional zirconium alloys have been identified as the most promising near-term ATF concept due to their high-temperature resistance to oxidation. However, the presence of Cr influences the solubility of oxygen in the zirconium alloy, which can influence the mechanical properties and potentially lead to fuel cladding failure at unanticipated temperatures.

The presentation deals with the oxidation behavior of damaged Cr-coated claddings under Loss-of-Coolant Accident (LOCA) scenarios, with particular emphasis on the effects of oxygen diffusion into the zirconium substrate. The protective Cr layer was locally removed to simulate coating defects, and the subsequent oxidation behavior of the exposed zirconium substrate was analyzed.

Particular attention was paid to the diffusion of oxygen into the Zr-substrate. The oxygen concentration profiles were determined using various microanalytical and spectroscopic techniques, including Electron Probe Microanalysis (EPMA), Wavelength Dispersive Spectroscopy (WDS), and Inert Gas Fusion (IGF). The results indicate that oxygen diffusion has a complex effect on the cladding microstructure and mechanical integrity.

Behaviour of Fuel Cladding with Cr Coating during LOCA and Study of Oxygen Diffusion into Zr-alloy using Different methods

A. Endrychová, V. Bouček

UJP PRAHA a.s., Czech Technical University in Prague

30th International QUENCH Workshop

18. 12. 2025

1. ATF cladding concepts

- Development and testing of different concepts of **A**ccident **T**olerant **F**uels (**ATFs**) - 2 concepts:

1. Protective coatings on zirconium-based alloys (Near Term ATF)

- Cr, CrN, CrNCr, ZrNCr
- CrNb, CrAl

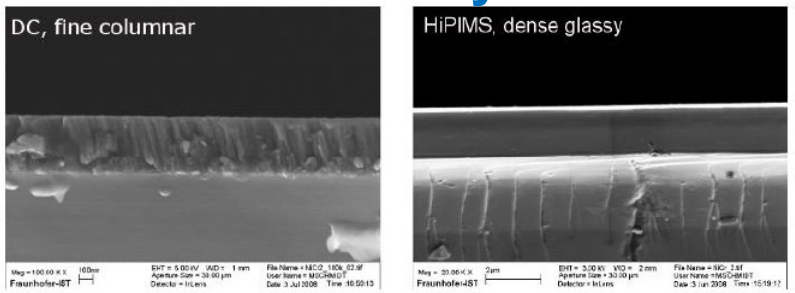

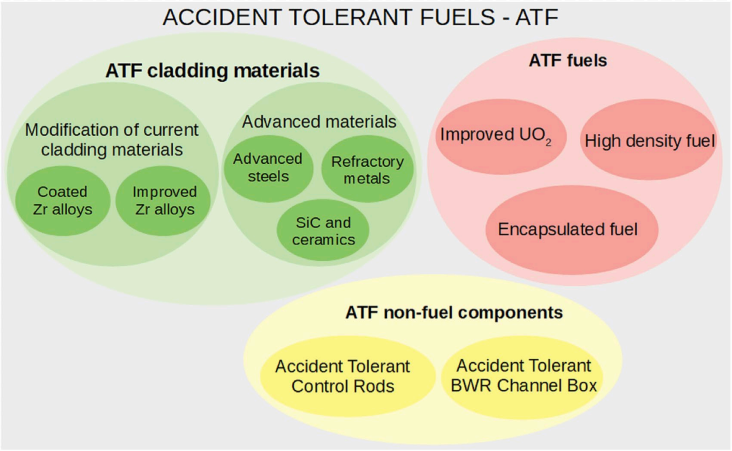

ATF concepts[1]

2. „New“ materials (Longer Term ATF)

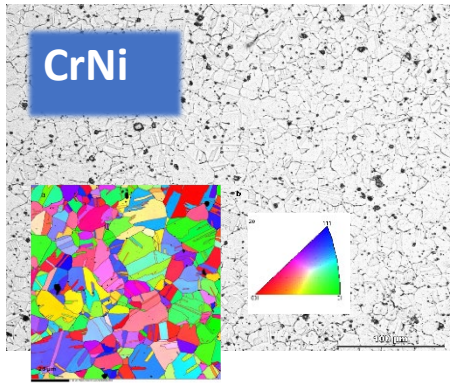

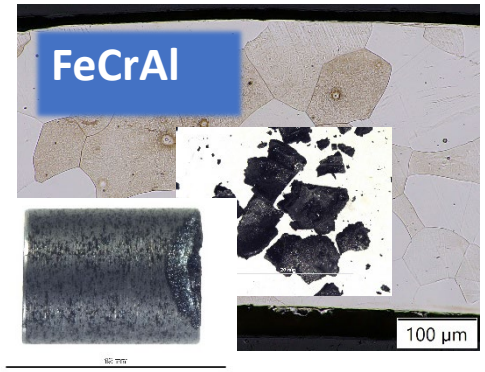

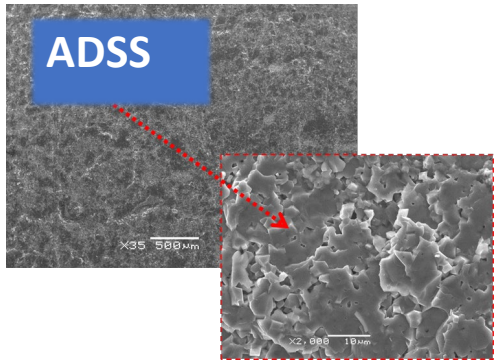

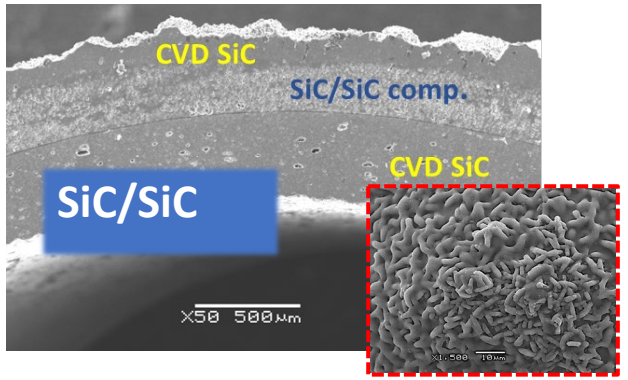

2. Zr-alloy with Cr coating: Diffusion

- Cr coating as **the most promising near-term concept**:
  - Already being tested in commercial reactors in Europe and the USA (Framatome – Gösgen in Switzerland, Westinghouse – Doel 4 in Belgium and Byron 2 in the United States).
- During oxidation at high temperatures (1000–1300 °C),typical for a LOCA accident, **the protective coating is "consumed"** mainly in two ways:
  1. **Formation of Cr_2O_3 oxide on the outer side of the cladding**

$$\Delta Cr_2O_3 = \sqrt{K_{p(Cr_2O_3)}.t}$$

  2. **Diffusion of Cr into Zr-alloy**

$$\Delta \boldsymbol{Cr}_{(\boldsymbol{Cr\rightarrow\beta-Zr})} = 8{,}61 \cdot 10^3 \cdot \exp\left(\frac{-17166}{T}\right) \cdot t^{1/2}$$

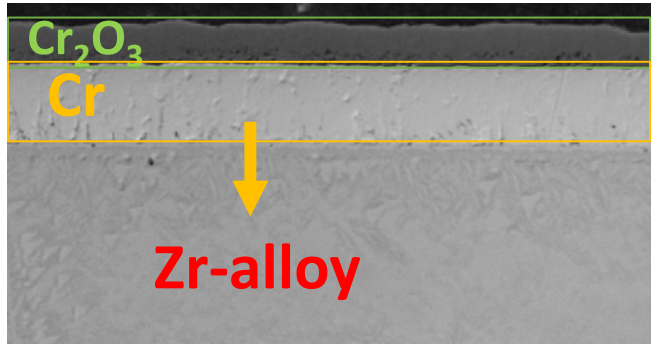

Zr-alloy with protective coating - 1200°C/30 min

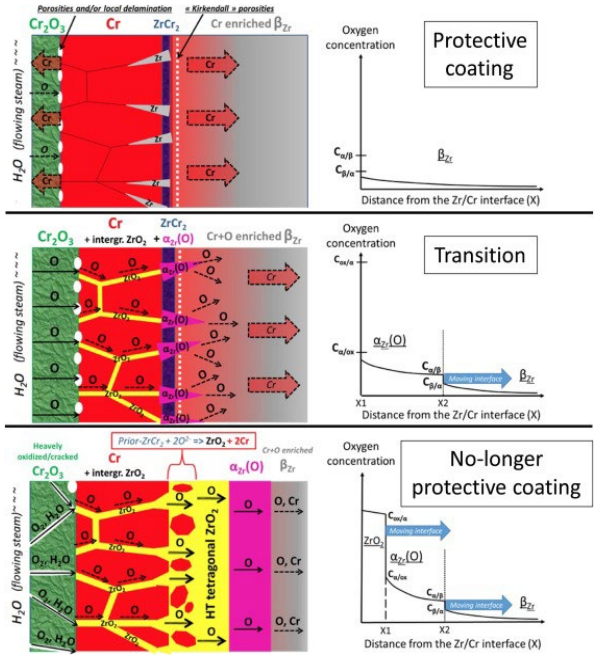

Diffusion of Cr [4]

2. Zr-alloy with Cr coating: Diffusion

- Assumption: Cr is a β-stabilizer, and oxygen diffusion in β-Zr proceeds significantly faster -> The presence of Cr increases the oxygen solubility limit in β-Zr, which can **negatively impact the ductility and brittleness of the material**
- **Criterion "O_{β}" based on the critical oxygen concentration** in the original β-phase, which is crucial for determining the ductility of the samples. (The limit value - 0.38 wt.%)
- Most studies focus on a compact Cr layer, but regarding a **damaged coating:**
  - A new testing methodology for „damaged coating“ will be developed -> monitoring of O and Cr diffusion
  - Pseudobinary phase diagram (Cr-Zr1Nb)-O

Dependence of oxygen content on ECR[47]

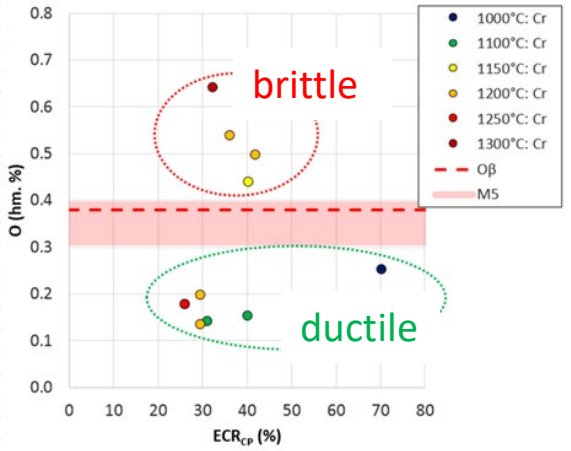

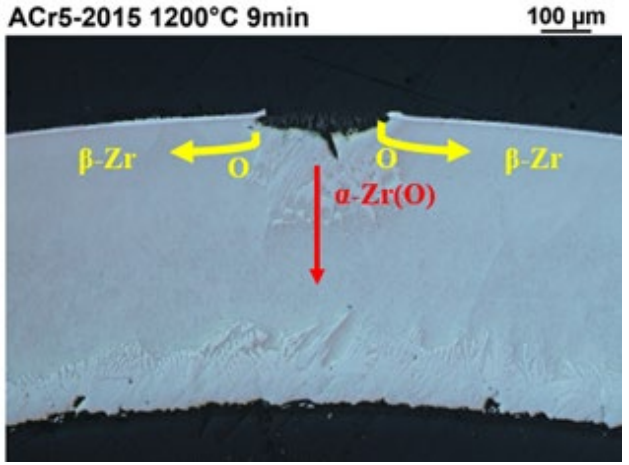

3. Construction of diagram (Cr-Zr1Nb)-O: Method

1. **<u>Introduce a controlled defect into the Cr-coated sample</u>**
2. Partially dissolve the Cr layer into the substrate
3. Perform the high-temperature oxidation test
4. Measure oxygen equilibrium concentrations using WDS (EPMA)
5. Optionally analyze oxygen concentration using SIMS or IGF (TEA)
6. Use the obtained concentrations to estimate phase boundaries
7. Construction of (Cr+Zr1Nb)-O diagram

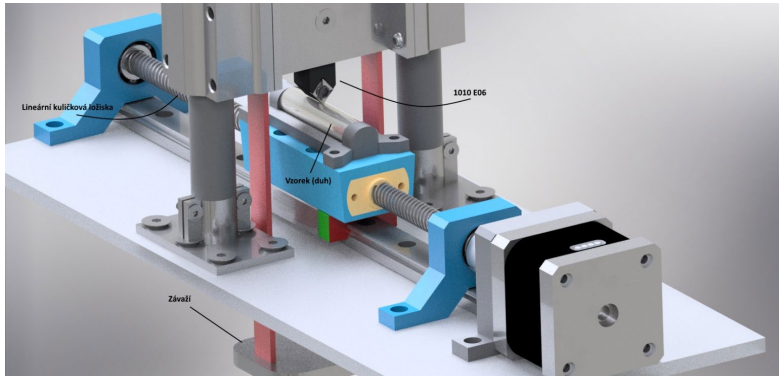

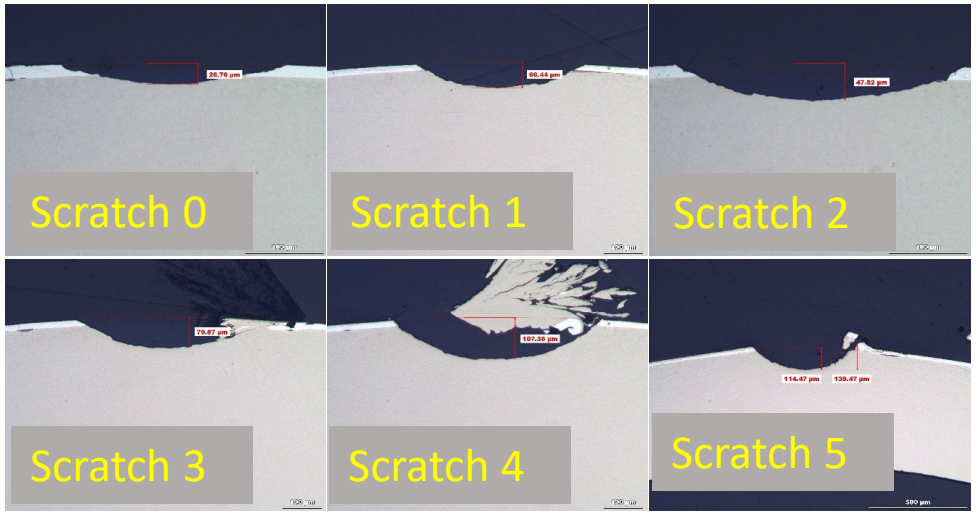

3. Construction of diagram (Cr-Zr1Nb)-O: Method

1. Introduce a controlled defect into the Cr-coated sample
2. **<u>Partially dissolve the Cr layer into the substrate (1200 °C/4,5 min, Ar)</u>**
3. **<u>Perform the high-temperature oxidation test (1000, 1100, 1200 °C Ar + steam)</u>**
4. Measure oxygen equilibrium concentrations using WDS (EPMA)
5. Measurement of oxygen concentration using IGF (TEA)
6. Use the obtained concentrations to estimate phase boundaries
7. Construction of (Cr+Zr1Nb)-O diagram

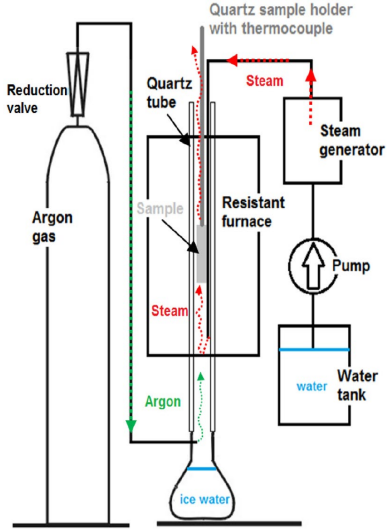

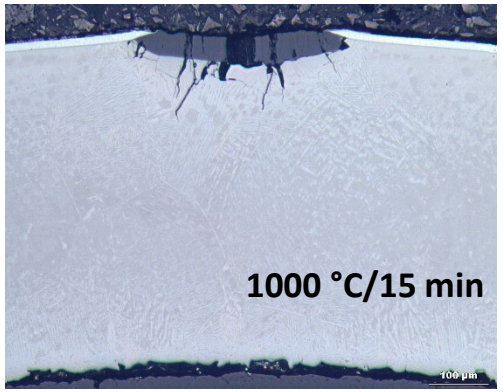

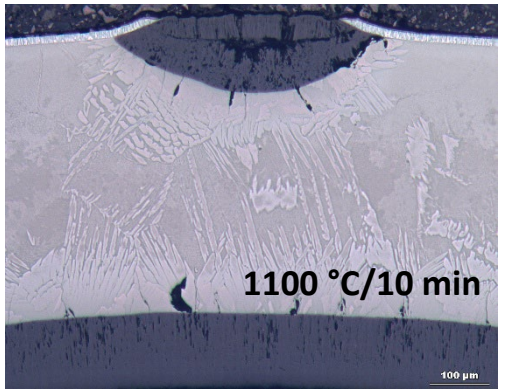

3. Construction of diagram (Cr-Zr1Nb)-O: Method

1. Introduce a controlled defect into the Cr-coated sample
2. Partially dissolve the Cr layer into the substrate
3. Perform the high-temperature oxidation test
4. **Measure oxygen equilibrium concentrations using WDS (EPMA, SEM-WDS)**
5. Measurement of oxygen concentration using IGF (TEA)
6. Use the obtained concentrations to estimate phase boundaries
7. Construction of (Cr+Zr1Nb)-O diagram

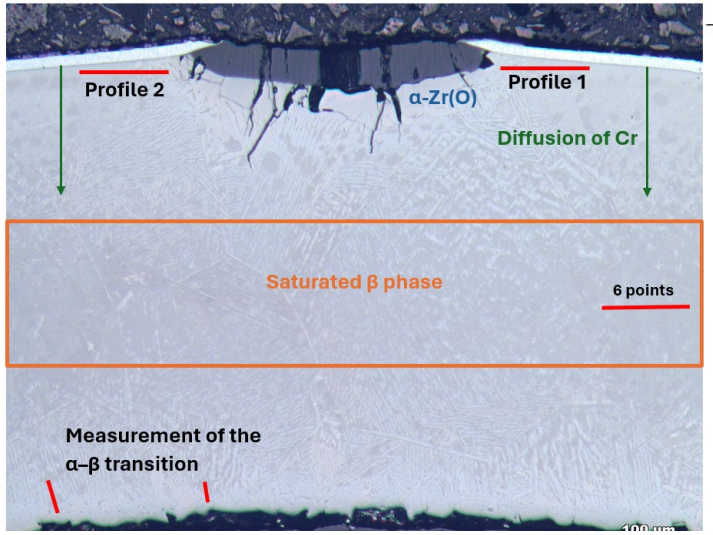

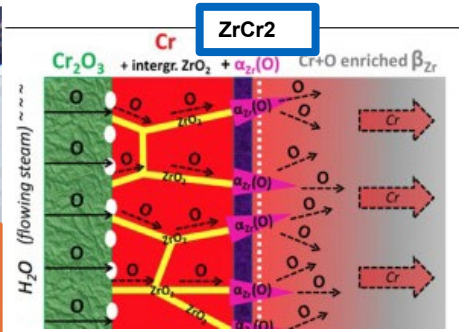

$$\frac{C(x,t)-C_0}{C_s-C_0} = 1 - \mathrm{erf}\left(\frac{x}{2\sqrt{Dt}}\right) \quad [3]$$

$$D = D_0 \cdot \left(-\exp\left(\frac{Q}{RT}\right)\right)$$

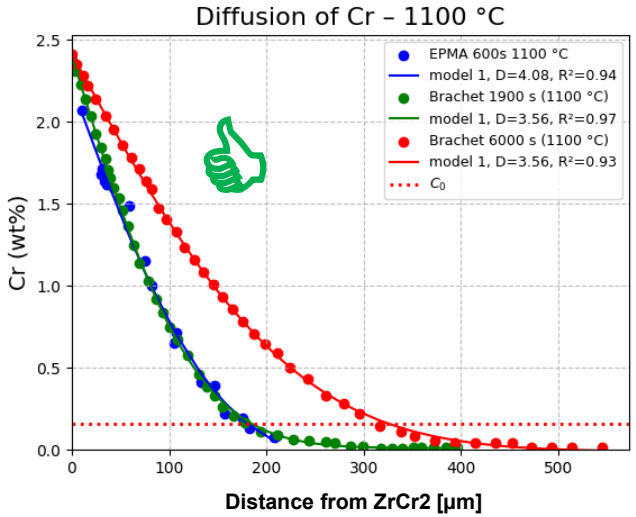

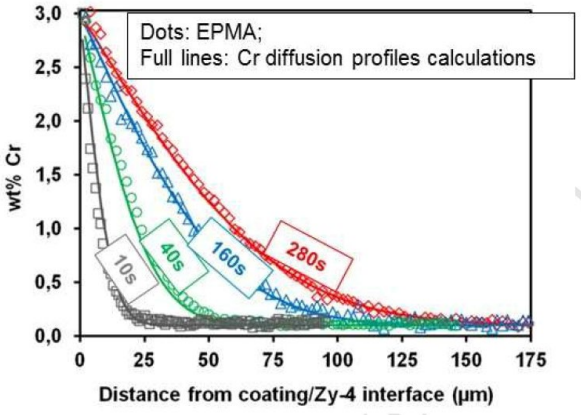

3. Construction of diagram (Cr-Zr1Nb)-O: Method

1. Introduce a controlled defect into the Cr-coated sample
2. Partially dissolve the Cr layer into the substrate
3. Perform the high-temperature oxidation test
4. **<u>Measure oxygen equilibrium concentrations using WDS (EPMA, SEM-WDS)</u>**
5. Measurement of oxygen concentration using IGF (TEA)
6. Use the obtained concentrations to estimate phase boundaries
7. Construction of (Cr+Zr1Nb)-O diagram

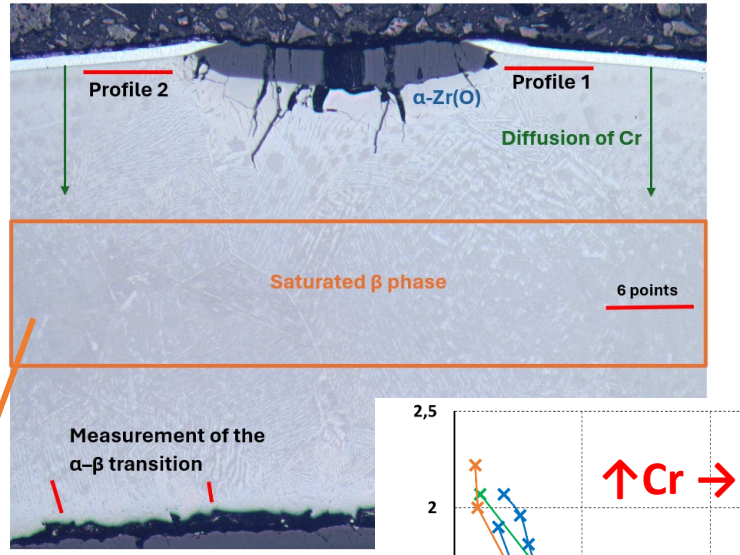

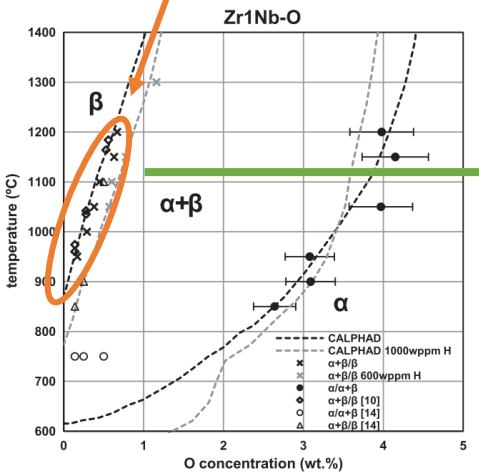

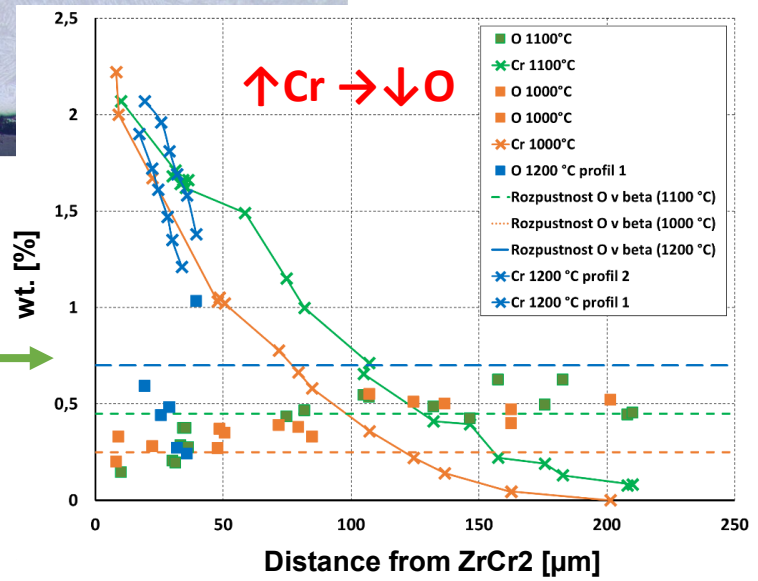

3. Construction of diagram (Cr-Zr1Nb)-O: Method

1. Introduce a controlled defect into the Cr-coated sample
2. Partially dissolve the Cr layer into the substrate
3. Perform the high-temperature oxidation test
4. **<u>Measure oxygen equilibrium concentrations using WDS (EPMA, SEM-WDS)</u>**
5. Measurement of oxygen concentration using IGF (TEA)
6. Use the obtained concentrations to estimate phase boundaries
7. Construction of (Cr+Zr1Nb)-O diagram

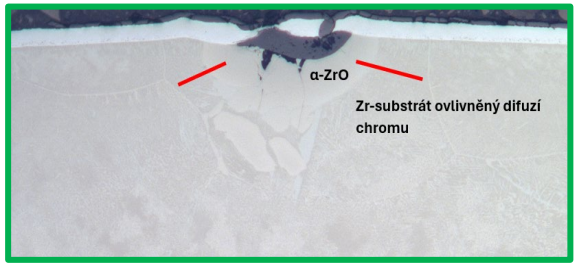

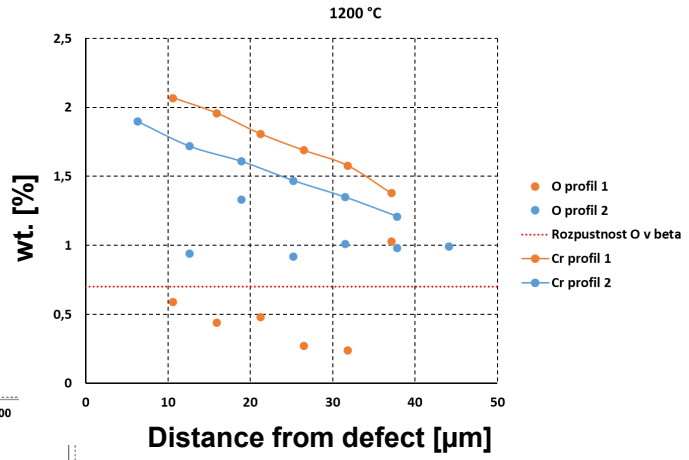

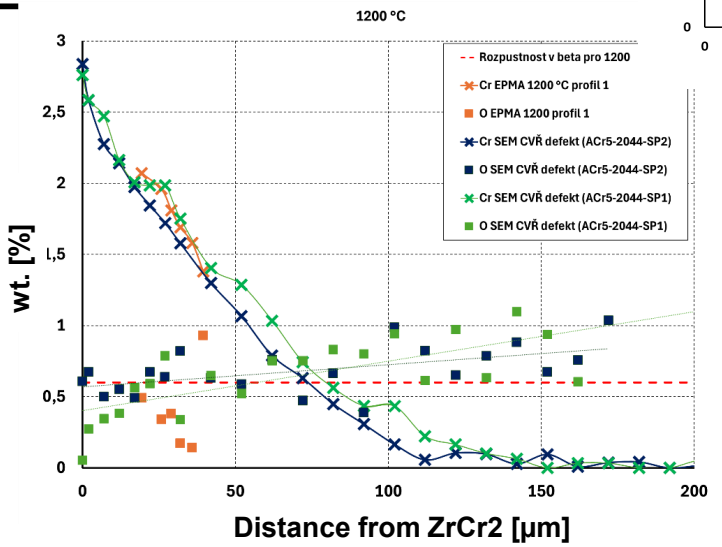

↑Cr →↓O

Reduced mobility of interstitial oxygen in the presence of diffused chromium, which inhibits diffusion and increases the activation energy of the diffusion process.

3. Construction of diagram (Cr-Zr1Nb)-O: Method

1. Introduce a controlled defect into the Cr-coated sample
2. Partially dissolve the Cr layer into the substrate
3. Perform the high-temperature oxidation test
4. Measure oxygen equilibrium concentrations using WDS (EPMA, SEM-WDS)
5. **<u>Measurement of oxygen concentration using IGF (TEA)</u>**
6. Use the obtained concentrations to estimate phase boundaries
7. Construction of (Cr+Zr1Nb)-O diagram

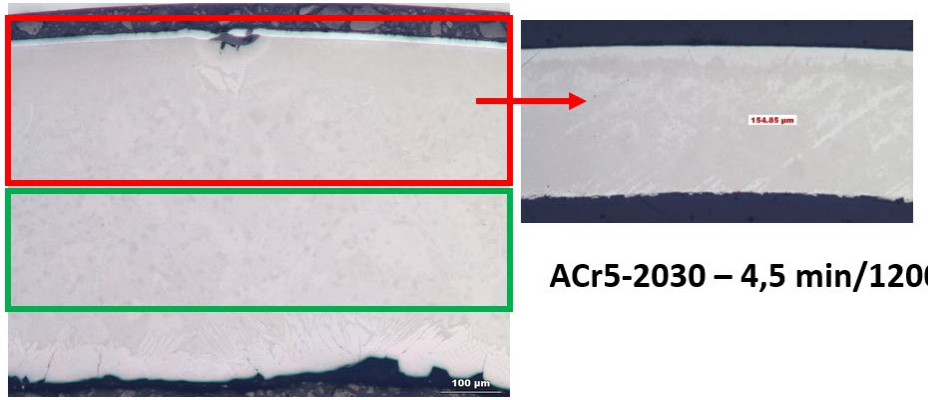

ACr5-2030 – 4,5 min/1200°C

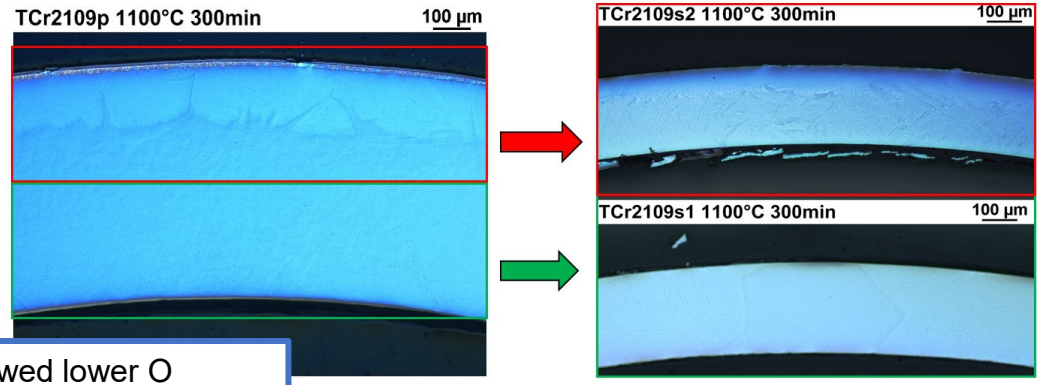

IGF results showed lower O concentrations and higher variability than EPMA, strongly dependent on **machining quality** and removal of oxide/α-Zr(O)

3. Construction of diagram (Cr-Zr1Nb)-O: Method

1. Introduce a controlled defect into the Cr-coated sample
2. Partially dissolve the Cr layer into the substrate
3. Perform the high-temperature oxidation test
4. Measure oxygen equilibrium concentrations using WDS (EPMA, SEM-WDS)
5. **<u>Measurement of oxygen concentration using IGF (TEA)</u>**
6. Use the obtained concentrations to estimate phase boundaries
7. Construction of (Cr+Zr1Nb)-O diagram

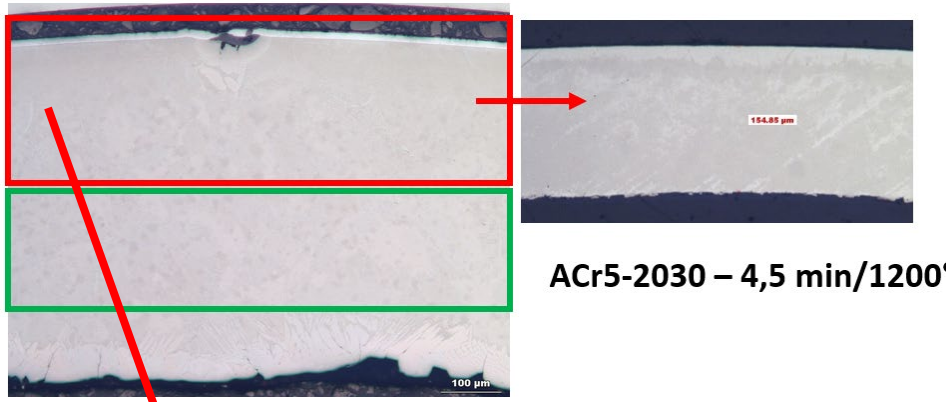

ACr5-2030 – 4,5 min/1200°C

Temp [°C]	IGF [wt. %]	IGF STD	EPMA [wt. %]	EPMA STD	Diff	Eq. Conc. [wt. %]
1000	0,156	0,010	0,322	0,058	-0,166	0,25
1000	0,159	0,006	0,322	0,058	-0,163	0,25
1200	0,299	0,024	0,406	0,132	-0,107	0,70
1200	0,277	0,038	0,406	0,132	-0,128	0,70
1200	0,156	0,003	–	–	–	0,70
1200	0,338	0,012	–	–	–	0,70

IGF results showed lower O concentrations and higher variability than EPMA, strongly dependent on **machining quality** and removal of oxide/α-Zr(O)

3. Construction of diagram (Cr-Zr1Nb)-O: Method

1. Introduce a controlled defect into the Cr-coated sample
2. Partially dissolve the Cr layer into the substrate
3. Perform the high-temperature oxidation test
4. Measure oxygen equilibrium concentrations using WDS (EPMA, SEM-WDS)
5. Measurement of oxygen concentration using IGF (TEA)
6. **Use the obtained concentrations to estimate phase boundaries**
7. Construction of (Cr+Zr1Nb)-O diagram

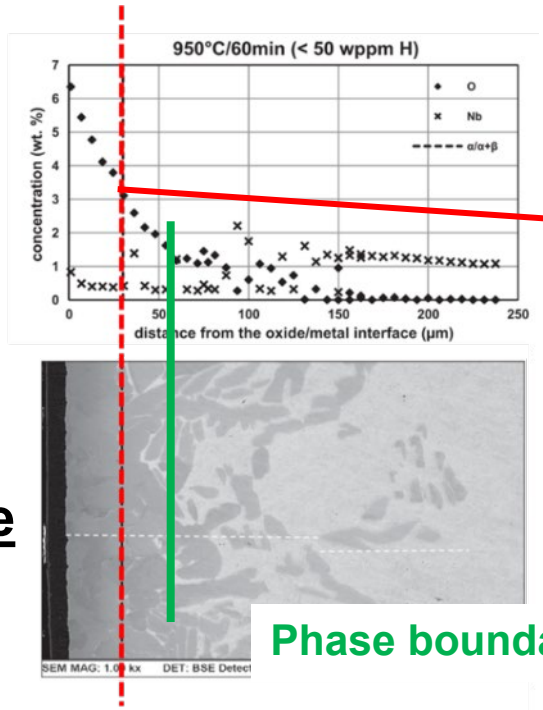

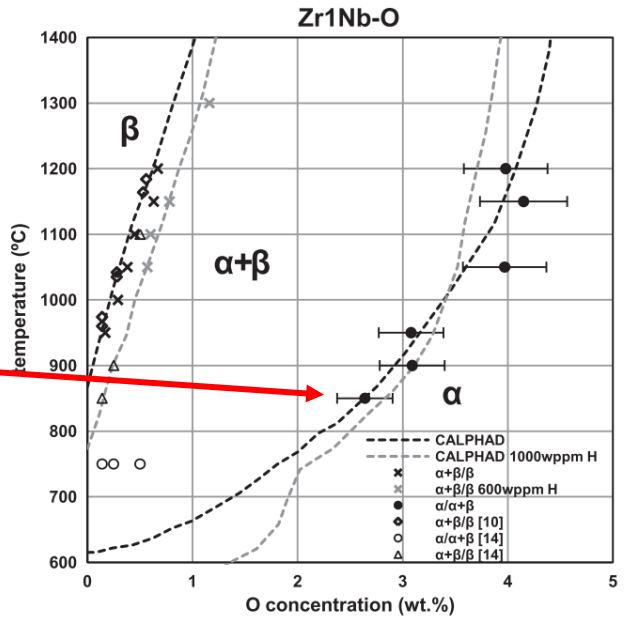

Pseudobinary Zr1Nb-Oxygen phase diagram [6].

Phase boundary of α-Zr(O)/β-Zr

Phase boundary of α-Zr(O)/(α +β)-Zr

3. Construction of diagram (Cr-Zr1Nb)-O: Method

1. Introduce a controlled defect into the Cr-coated sample
2. Partially dissolve the Cr layer into the substrate
3. Perform the high-temperature oxidation test
4. Measure oxygen equilibrium concentrations using WDS (EPMA, SEM-WDS)
5. Measurement of oxygen concentration using IGF (TEA)
6. Use the obtained concentrations to estimate phase boundaries
7. **Construction of (Cr+Zr1Nb)-O diagram**

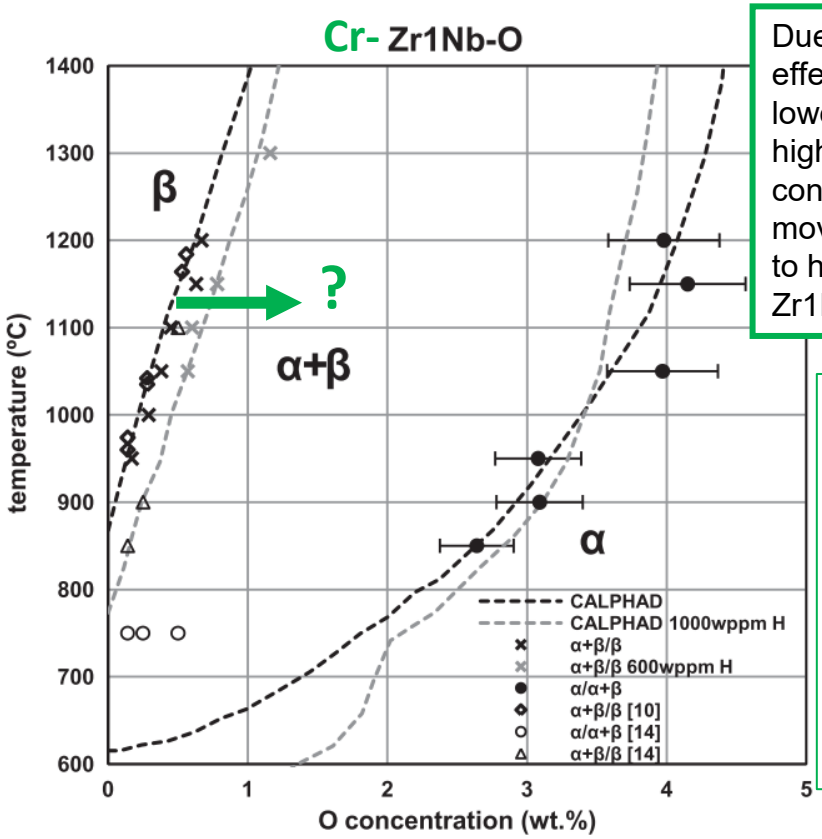

Pseudobinary Zr1Nb-Oxygen phase diagram [6].

Due to the diffusion barrier effect of Cr, regions with lower Cr content exhibit higher oxygen concentrations, effectively moving the local composition to higher O levels in the Zr1Nb–O phase diagram.

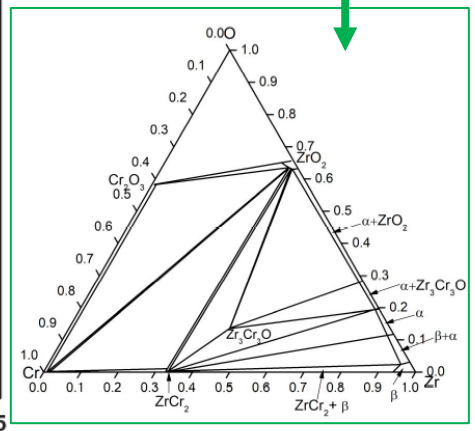

4. Future work

- Study of **the influence of multiple defects** (varying the distance between them) and potential effect of **grain orientation** on oxygen concentration (EBSD analysis) + microhardness measurement

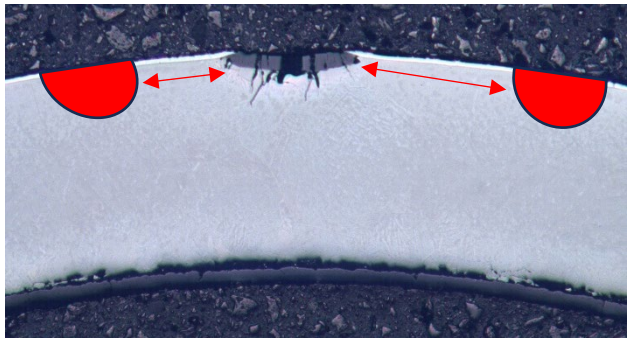

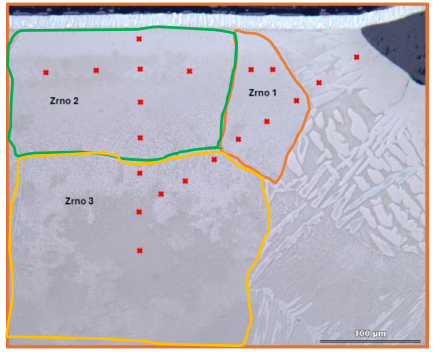

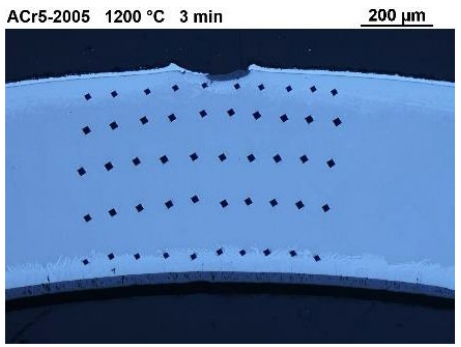

- Refinement of the IGF methodology and machining of rings with various diameters to obtain oxygen-concentration data at different depths corresponding to different Cr-concentration levels + **perform one-side high-temperature oxidation**

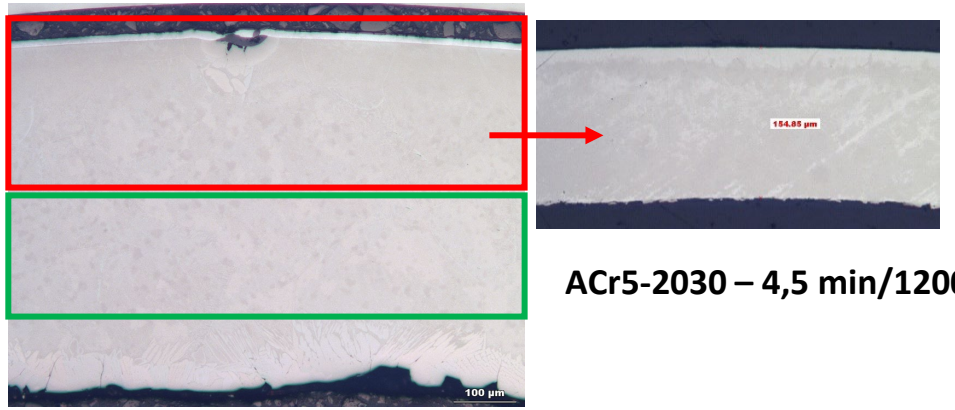

ACr5-2030 – 4,5 min/1200°C

5. Conclusion

- **WDS measurements** showed that **decreasing Cr content leads to locally increased O concentration**, indicating reduced O mobility and higher diffusion activation energy in the presence of diffused Cr.
- According to α–β phase-transformation theory in Zr-alloys, O strongly stabilizes the α phase, while Cr stabilizes β → Observed **local O enrichment in low-Cr regions may shift the effective α/β transformation conditions**, potentially promoting earlier α formation inside the cladding wall during high-temperature transients.
- **IGF results** showed lower O concentrations and higher variability than EPMA, strongly dependent on **machining quality** and removal of oxide/α-Zr(O) - the method is suitable mainly for comparative use.
- **For IGF**, **improved and standardized mechanical sample preparation** is essential—particularly control of removed-layer thickness and elimination of oxide and α-Zr(O) - measurements should be conducted on samples with **varying Cr/O diffusion depths**.
- Given the strong influence of Cr on O diffusion, this effect should be incorporated into oxygen-transport models near defects and phase boundaries
- **Additional tests across a broader range of temperatures are required to fully evaluate the coupled Cr–O influence on diffusion and phase stability.**

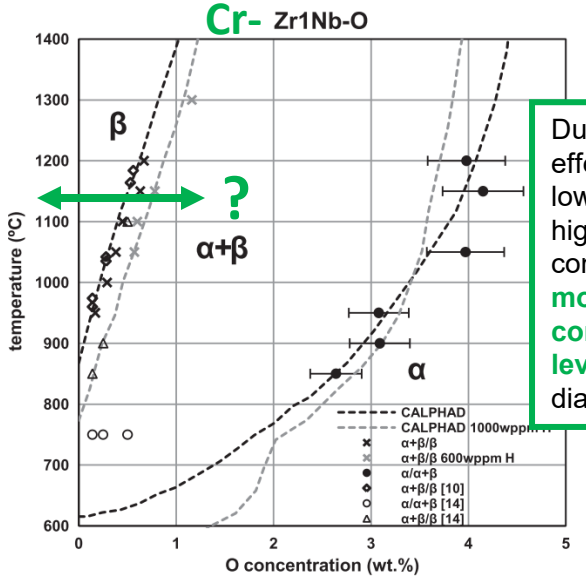

Due to the diffusion barrier effect of Cr, regions with lower Cr content exhibit higher oxygen concentrations, effectively **moving the local composition to higher O levels** in the Zr1Nb–O phase diagram.

Pseudobinary Zr1Nb-Oxygen phase diagram [6].

ČVUT
ČESKÉ VYSOKÉ UČENÍ TECHNICKÉ V PRAZE

ujp praha

Thank you for your attention

Sources

[1] ŠEVEČEK, Martin, Anil GURGEN, Arunkumar SESHADRI, Yifeng CHE, Malik WAGIH, Bren PHILLIPS, Victor CHAMPAGNE a Koroush SHIRVAN. Development of Cr cold spray–coated fuel cladding with enhanced accident tolerance. Nuclear Engineering and Technology [online]. 2018, 50(2), 229–236. ISSN 17385733. Dostupné z: doi:10.1016/j.net.2017.12.011

[2] TERRANI, Kurt A. Accident tolerant fuel cladding development: Promise, status, and challenges. Journal of Nuclear Materials [online]. 2018, 501, 13–30. ISSN 00223115. Dostupné z: doi:10.1016/j.jnucmat.2017.12.043

[3] BRACHET, Jean-Christophe, Isabel IDARRAGA-TRUJILLO, Marion Le FLEM, Matthieu Le SAUX, Valérie VANDENBERGHE, Stephane URVOY, Elodie ROUESNE, Thomas GUILBERT, Caroline TOFFOLON-MASCLET, Marc TUPIN, Christian PHALIPPOU, Fernando LOMELLO, Frédéric SCHUSTER, Alain BILLARD, Gihan VELISA, Cédric DUCROS a Frédéric SANCHETTE. Early studies on Cr-Coated Zircaloy-4 as enhanced accident tolerant nuclear fuel claddings for light water reactors.

[4] BRACHET, Jean-Christophe, Thomas GUILBERT, Stéphane URVOY, Elodie ROUESNE, Marion PEYRET, Thierry VANDENBERGHE, Cédric PROU, Thai LE HONG a Didier HAMON. Some practical methodologies to assess the overall high temperature (one-sided) steam oxidation protectiveness of chromium-based coatings on a zirconium-based substrate, as Enhanced – Accident tolerant (Nuclear) fuels (E-ATF) claddings. Journal of Nuclear Materials [online]. 2025, 606, 155620. ISSN 00223115. Dostupné z: doi:10.1016/j.jnucmat.2025.155620

[5] ČERVENKA, Petr, KREJČÍ, Jakub, CVRČEK, Ladislav, ROZKOŠNÝ, Vojtěch, MANOCH, František, RADA, David and KABÁTOVÁ, Jitka. EXPERIMENTAL STUDY OF DAMAGED CR-COATED FUEL CLADDING IN POST-ACCIDENT CONDITIONS. *Acta Polytechnica CTU Proceedings*. Online. 1 December 2020. Vol. 28, p. 1–7. [Accessed 8 August 2023]. DOI 10.14311/APP.2020.28.0001.

[6] NÉGYESI, M., J. BURDA, V. KLOUČEK, J. LORINČÍK, J. SOPOUŠEK, J. KABÁTOVÁ, L. NOVOTNÝ, S. LINHART, T. CHMELA, J. SIEGL a V. VRTÍLKOVÁ. Contribution to the study of the pseudobinary Zr1Nb-Oxygen phase diagram by local oxygen measurements of Zr1Nb fuel cladding after high temperature oxidation. Journal of Nuclear Materials [online]. 2012, 420(1–3), 314–319. ISSN 00223115. Dostupné z: doi:10.1016/j.jnucmat.2011.10.022

[7] BRACHET, Jean-Christophe, ROUESNE, Elodie, RIBIS, Joël, GUILBERT, Thomas, URVOY, Stéphane, NONY, Guillaume, TOFFOLON-MASCLET, Caroline, LE SAUX, Matthieu, CHAABANE, Nihed, PALANCHER, Hervé, DAVID, Amandine, BISCHOFF, Jérémy, AUGEREAU, Julien and POUILLIER, Edouard. High temperature steam oxidation of chromium-coated zirconium-based alloys: Kinetics and process. Corrosion Science. Online. May 2020. Vol. 167, p. 108537. [Accessed 21 August 2023]. DOI 10.1016/j.corsci.2020.108537.

[8] GOLDNER, FRANK J., MCCAUGHEY, W, WACHS, DANIEL M., KAMERMAN, D, JENSEN, COLBY, HAYES, STEVE L., NELSON, ANDREW, HARP, JASON, CAPPS, NATHAN, LINTON, KORY, PETRIE, CHRISTIAN, SALEH, TARIK A., and WHITE, JOSHUA T. Accident Tolerant Fuels Program — Update on a National Initiative. In : *TopFuel*. Online. United States, 2021. Available from: https://www.osti.gov/servlets/purl/1873835.

[9] CHUNG, H. M. a T. F. KASSNER. PSEUDOBINARY ZIRCALOY-OXYGEN PHASE DIAGRAM. Journal of Nuclear Materials. 1979, 84, 327–339.

Acknowledgements

- This project is supported by Technology Agency of the Czech Republic
- Project No. TN02000012, TS01020133

Brock Nowak

Queen's University

High-Temperature Oxidation of Cr Coated Claddings with Interdiffusion Barrier & Solute (Al, Si) Additions

Accident Tolerant Fuels (ATFs) are a proposed advanced reactor technology that aims to increase safety margins during anticipated operational occurrences (AOOs), and severe loss-of-coolant accidents (LOCA). Coated zirconium alloy claddings (CZACs) are one class of ATF that aim to enhance oxidation performance while minimizing the neutronic penalty (reduced keff). Two parameters are of interest: (i) coating thickness (5 to 20 μm), and (ii) coating composition (Cr, MoCr, MoCrAl, MoCrSi) with or without a 150 nm Mo diffusion barrier. Coatings were deposited on Zircaloy-4 tube sections (h = 400-450 µm) using magnetron sputtering. Transient and isothermal tests were performed in steam at temperatures up to 1400 °C to observe coating performance under design-basis (DBA) and beyond design-basis accident (BDBA) conditions. Oxidation rates were tracked using mass gain (microbalance, TG) up to 1250 °C or using mass spectrometry (MS) to measure hydrogen gas evolution. Results indicate reduced protection for coatings less than 10 μm and those containing Al, and improved protection in Cr coatings doped with Si until coating breakdown occurs at 1200 °C.

High-Temperature Oxidation of Cr Coated Claddings with Interdiffusion Barrier & Solute (Al, Si) Additions

Brock Nowak

Ph.D. Candidate
Queen's University

E: brock.nowak@queensu.ca

Supervision:
Suraj Y. Persaud & Zhongwen Yao

REACTOR MATERIALS TESTING LAB
Smith Engineering at Queen's University

Our Group:

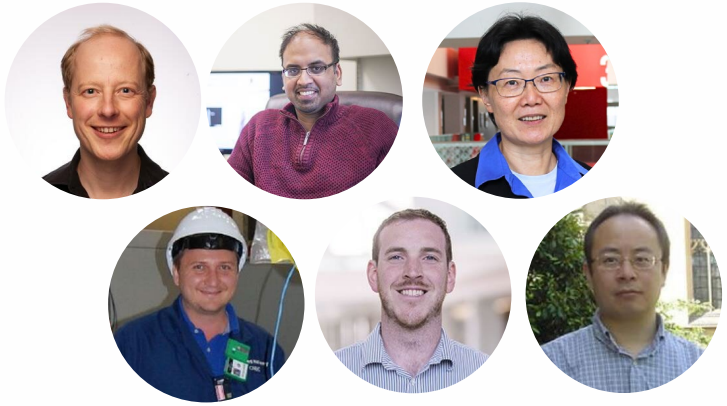

Mark Daymond | Suraj Y. Persaud | **Yanwen Zhang**

Levente Balogh | Laurent Beland | Zhongwen Yao

Research Areas:

- Mechanics of Materials
- Corrosion Control
- Simulation & Modelling
- Irradiation Effects
- Focus on CANDU Support
- + SMR/GenIV (MSR, HTGR)

The CANDU®Reactor

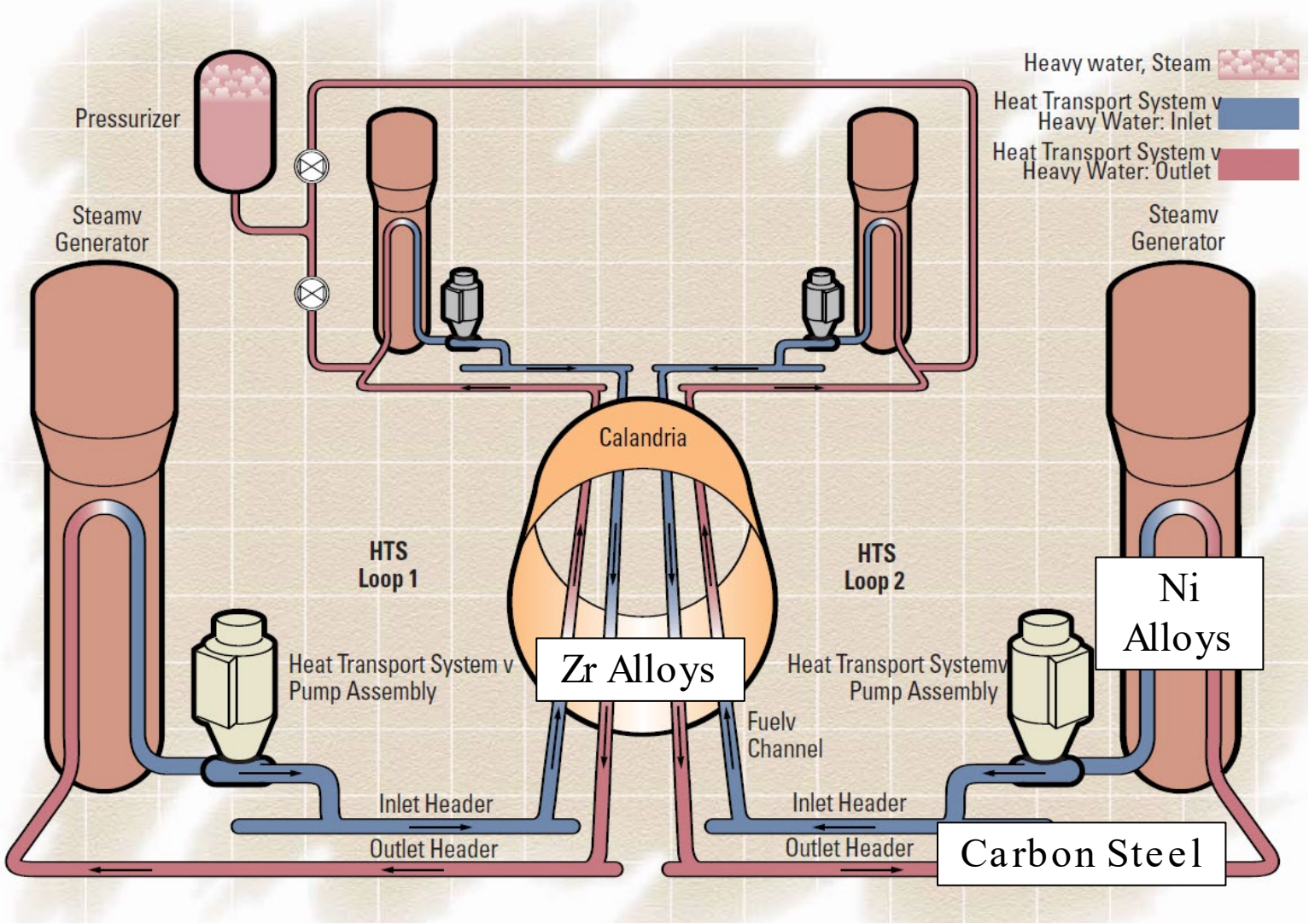

CANDU®primary heat transfer system, from the CANDU®6 Technical Summary

CANDU® (PHWR) Properties

Primary Coolant: D_2O (280-310 °C), 10 MPa

Chemistry: pH = ~10.2 (LiOH)

Moderator: D_2O (~70 °C)

Fuel: UO_2 (0.71% U-235, NU)**

Cladding: Zry-4 (0.4 mm) - Bundles

Pressure Tube: Zr-2.5Nb

Calandria Tube: Zry-2

Power Output: 500 – 900 MWe

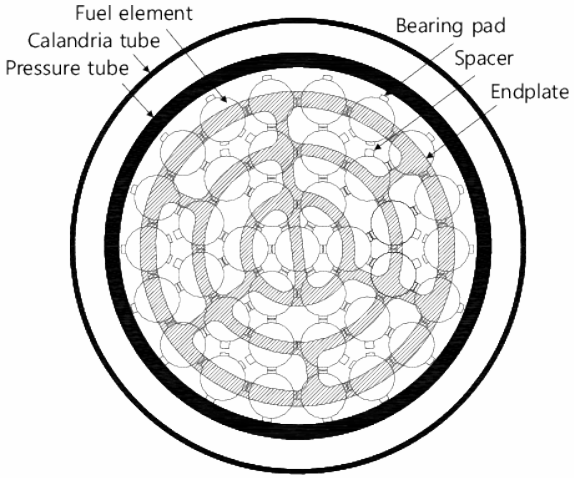

** Designed with CANFlex fuel cycle flexibility

Research Question

Can we optimize coating protectiveness vs. neutronics penalty?

Why?

- CANDU® reactors operate on natural uranium (NU) but were designed with other fuel cycles in mind
- CANDU® fuel sheaths are 0.4 mm thick, and therefore have less cladding volume to react before failure
- Reducing the neutronic impact increases the viability for use in future CANDU® iterations

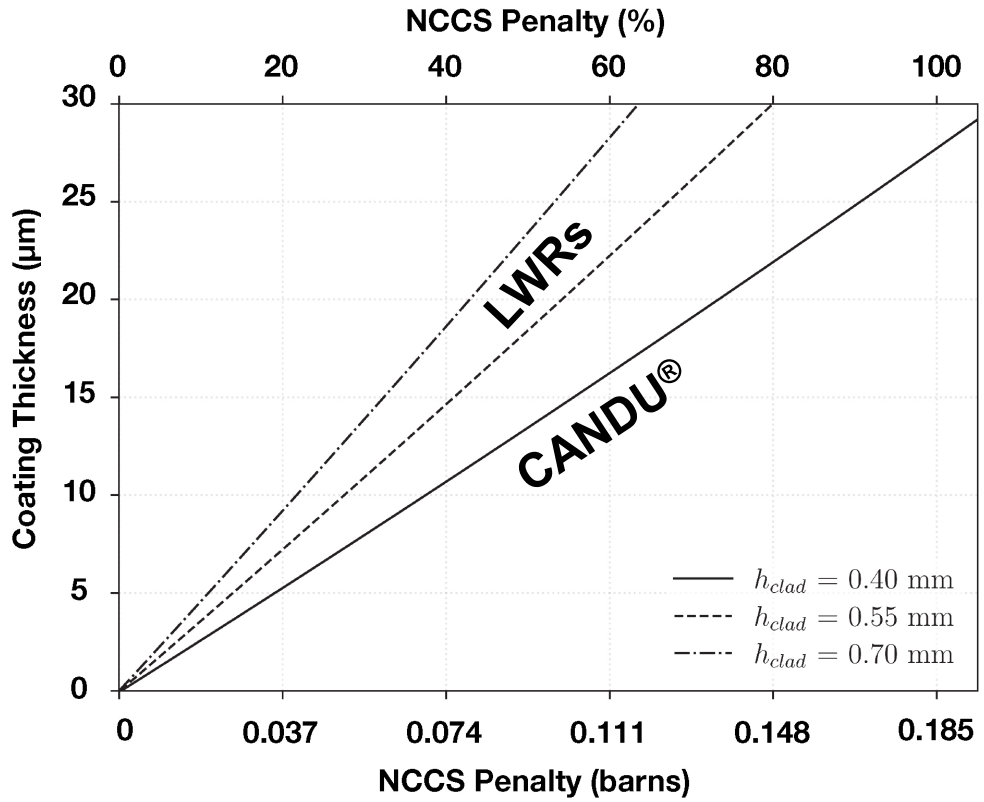

Weighted neutron capture penalty for Cr coating thickness.

Prior study - minimum effective coating thickness

Tube Furnace 2 – TF2
Steam flow: 75 g/h (air/steam mixture)

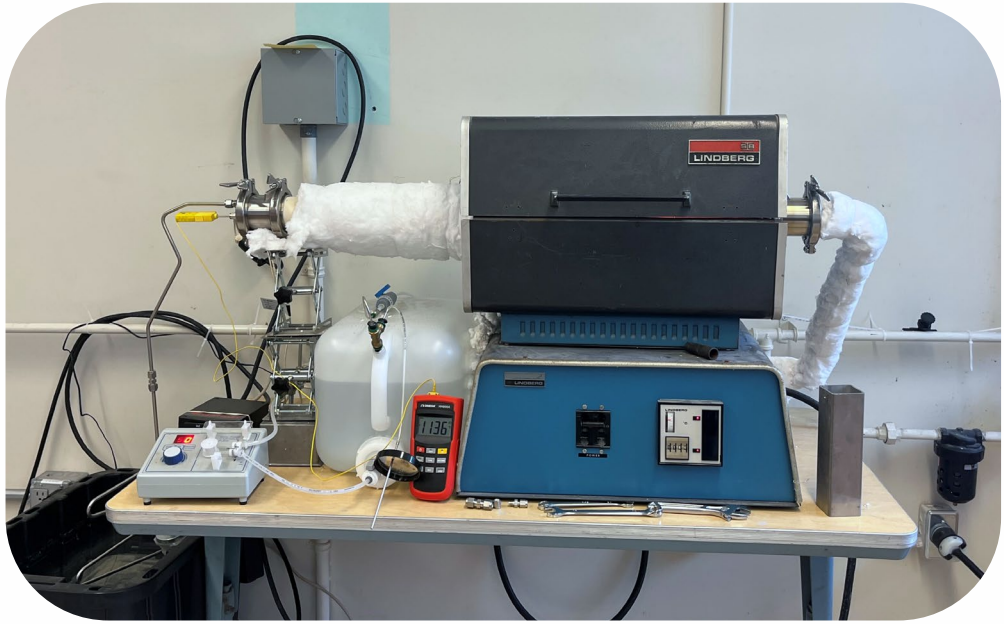

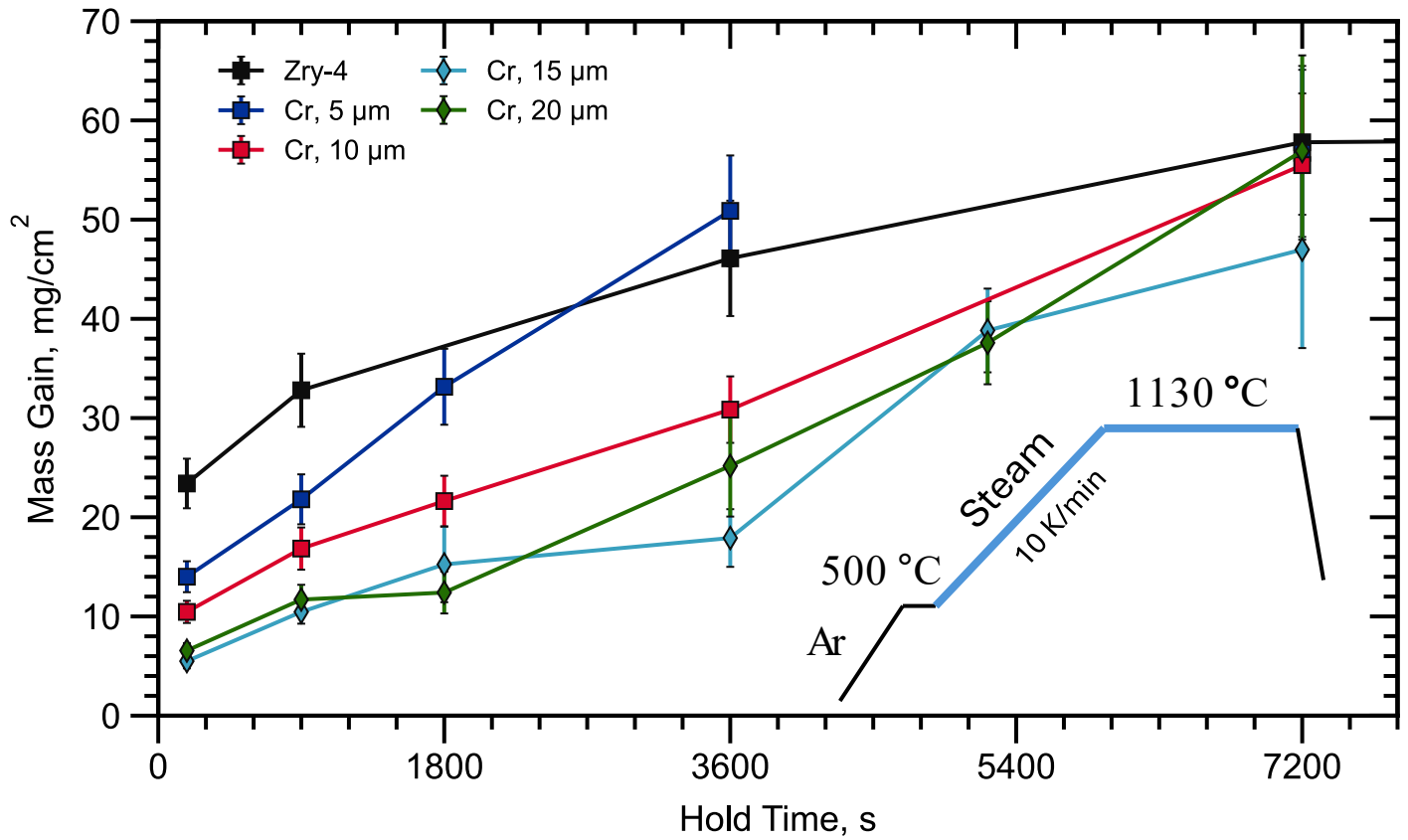

Minimum Effective Thickness =~10 µm

Sample Fabrication

CSA N285.6, ASTM B350/B350M, UNS R60804

Zr	Sn	Fe	Cr	O	V
Bal.	1.2-1.7	0.18-0.24	0.07-0.13	0.09-0.16	<0.005

1. Materials

Zry-4 tube (15 mm OD) from Canadian Nuclear Laboratories (CNL).

2. Sectioning

Tubing sectioned into quadrants. Mounting hole installed.

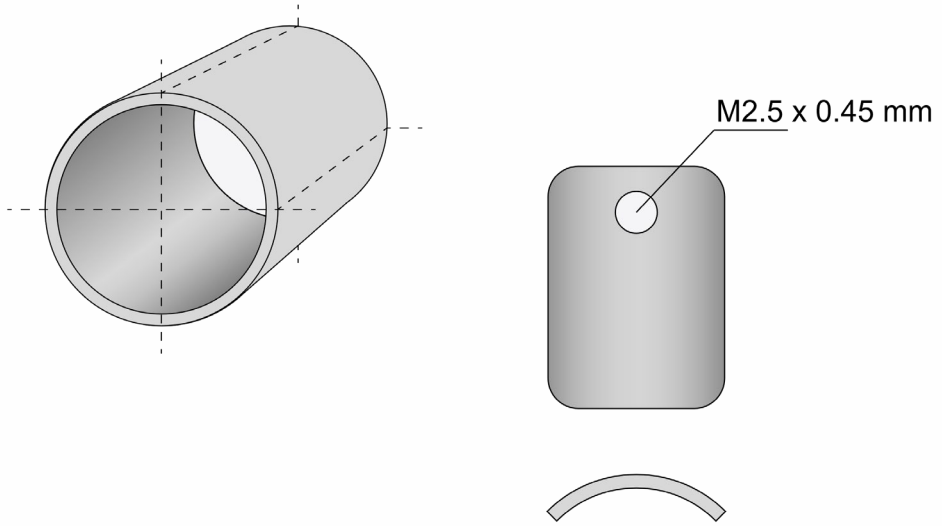

3. Surface Refinement

Two-stage surface refinement in vibratory tumbler:

1) 400 grit SiC + 600 grit Al_2O_3, 18 hours
2) 40 mesh walnut shells + diamond polish, 24 hours

4. Coating Process

Four coating architectures, 10 µm thick:

1) Cr (Type 1)
2) Mo/Cr/Cr (Type 2)
3) Mo/Cr/CrAl (Type 2)
4) Mo/Cr/CrSi (Type 2)

Type 1

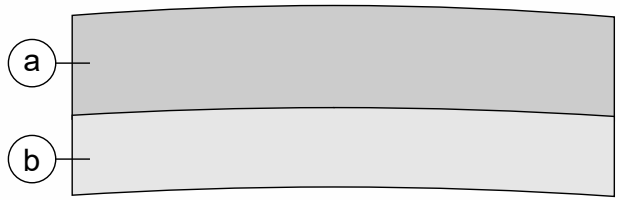

Type 2

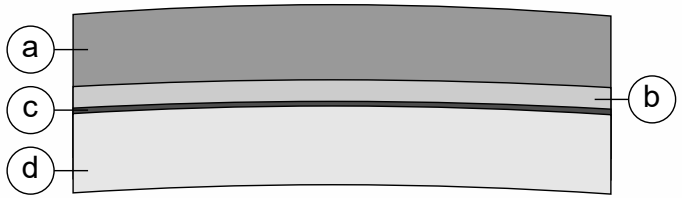

Sample Fabrication

Dual cathode (DC, RF) magnetron sputtering
381 °C, 5 mTorr, -60 V stage bias
Base pressure = 10^{-6} Torr

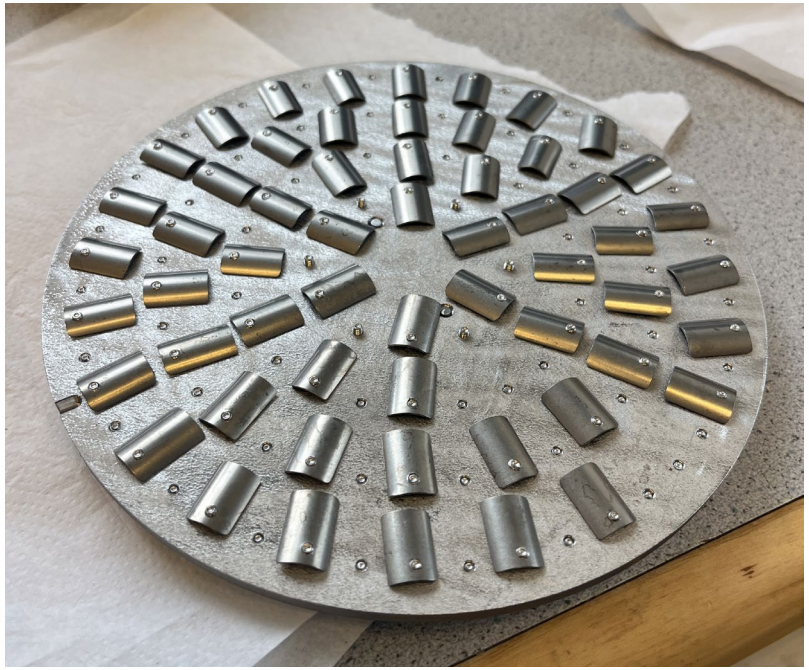

Custom Substrate Holder Plate

Angstrom Engineering NexDep, MS-PVD Chamber

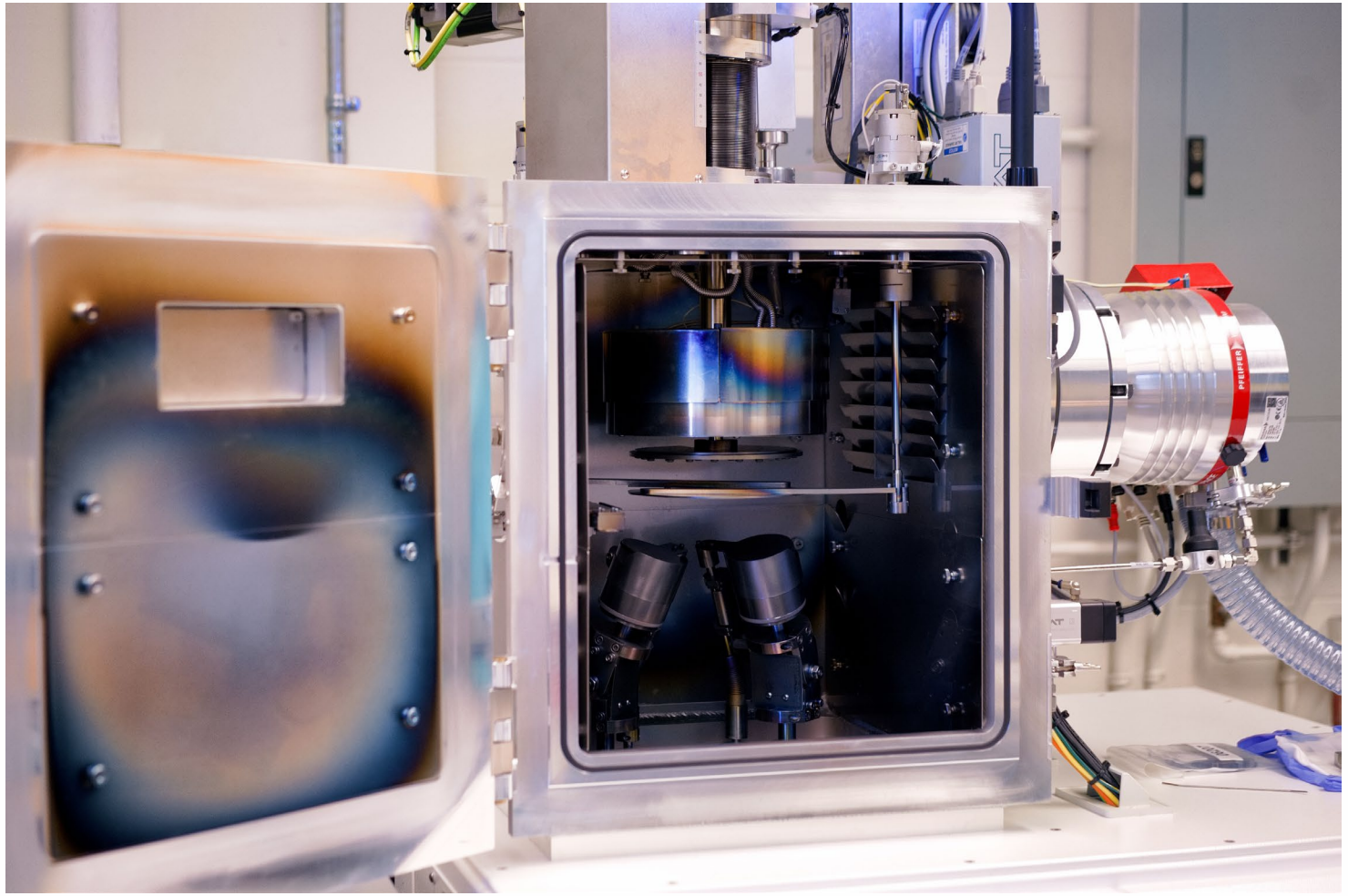

Effect of Solute Additions and Interdiffusion Barrier

Al additions, left shift (stretched lattice) – Si additions, right shift (compressed lattice)

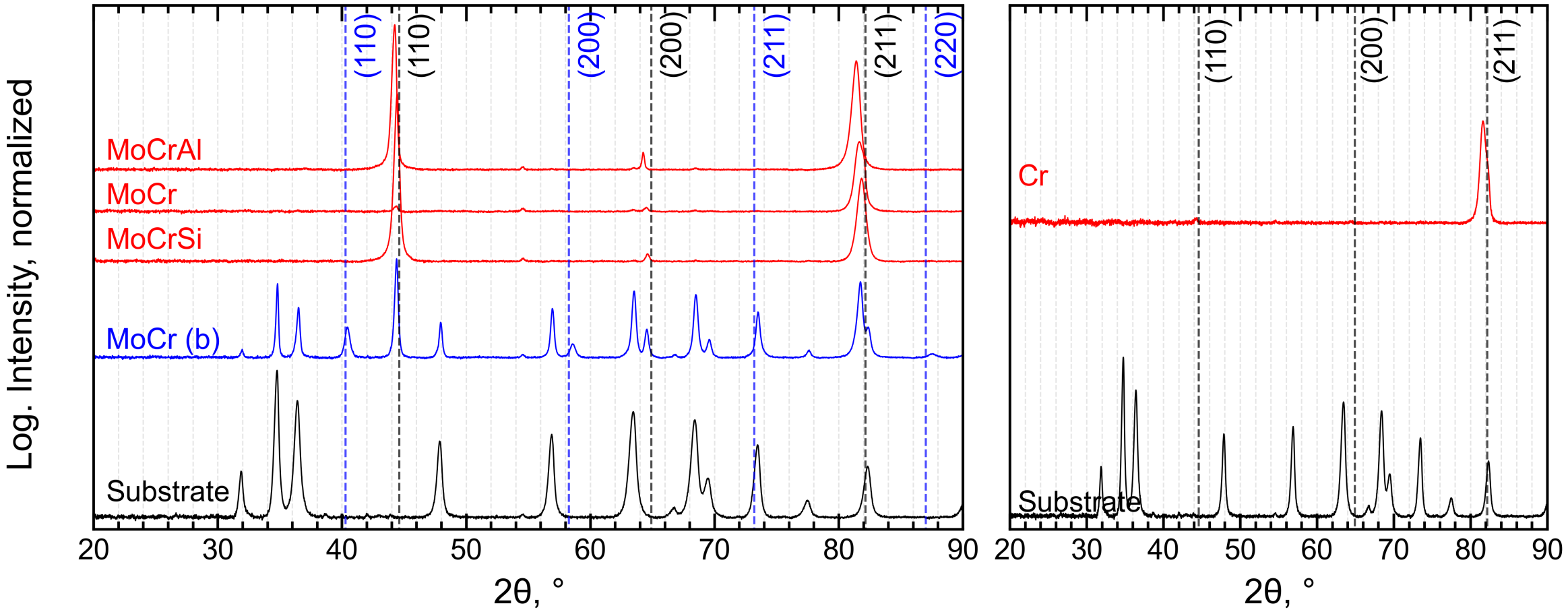

XRD, Rigaku SmartLab 9 kW, CuKα$_1$ = 0.1506 nm, parallel beam, 20° incidence

Testing Matrix

- CAT1 – Isothermal Steam Oxidation (STA)
- CAT2 – Transient Steam Oxidation (STA/BOX)
- CAT3 – Transient + Hold Steam Oxidation (STA)


STA

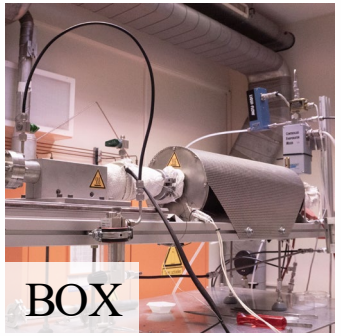
BOX

Karlsruher Institut für Technologie

	Test	Zry-4	Cr	MoCr	MoCrAl	MoCrSi
CAT 1	1000 °C, 90 min	27	2.7	2.4	8.2	1.3
	1100 °C, 60 min	43	7.1	6.8	14	3.1
	1200 °C, 60 min	45	42	45	50	27
CAT 2	500-1175 °C	18	2.4	2.1	5.1	1
	500-1200 °C	21	**2.2**	2.5	6	**1.2**
	500-1225°C	24	2.2	9	11	1.9
	500-1250 °C	25	6.9	10	16	7.2
	800-1300 °C	30	5.6	7.1	9.9	5.3
	800-1325 °C	30	7.2	9.1	15.7	12
	800-1350 °C	30	14	15	20	17
	800-1400 °C	37	26	25	30	29
CAT 3	500-1150 °C, 60 min	31	15	11	20	11
	500-1200 °C, 10 min	25	**6.9**	7.3	12	**1.8**

Mass gain – mg/cm^2

CAT1 – Isothermal Steam Oxidation (STA)

Effect of Solute Additions and Interdiffusion Barrier

CAT1 – Isothermal Steam Oxidation (STA)

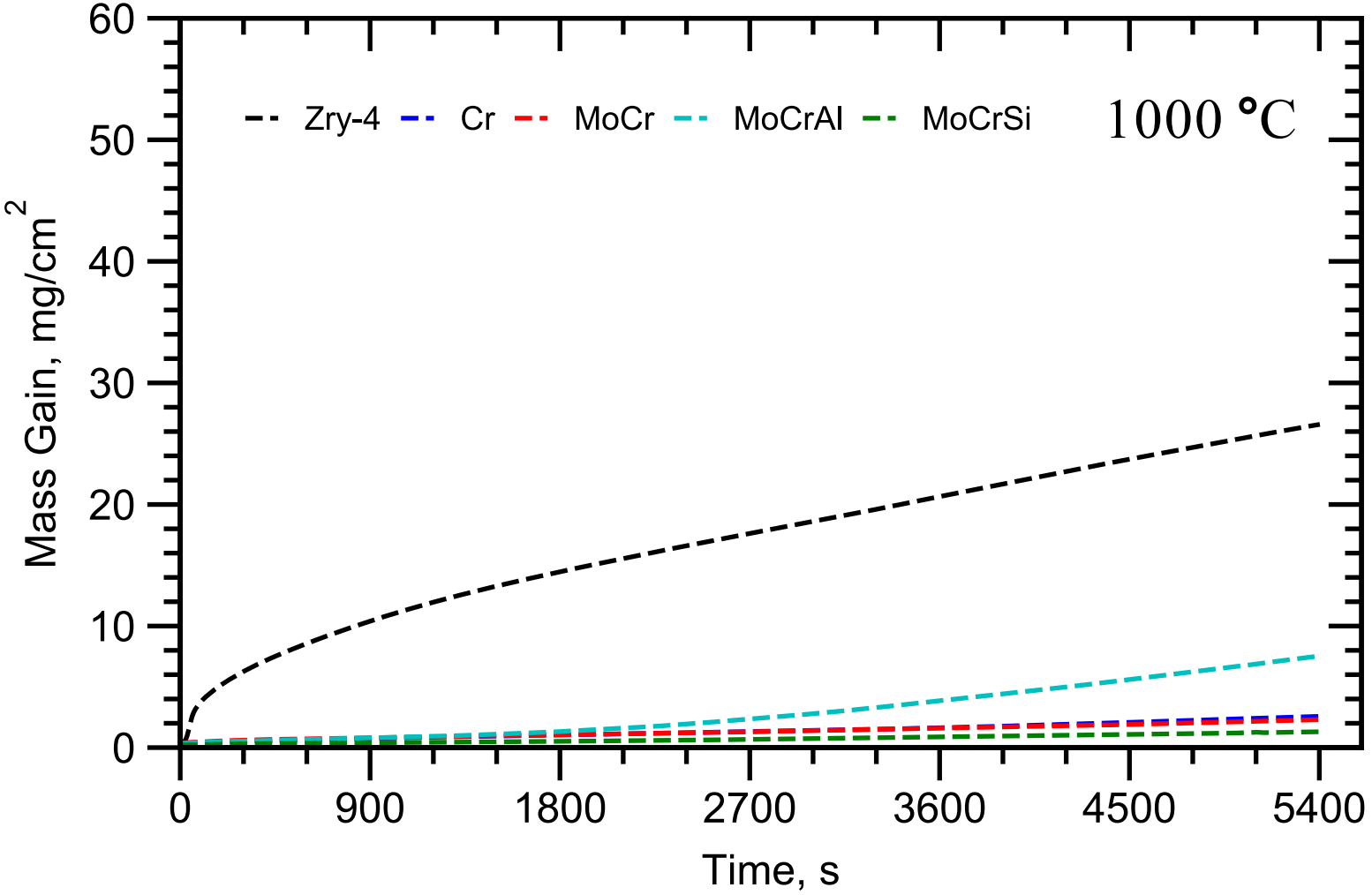

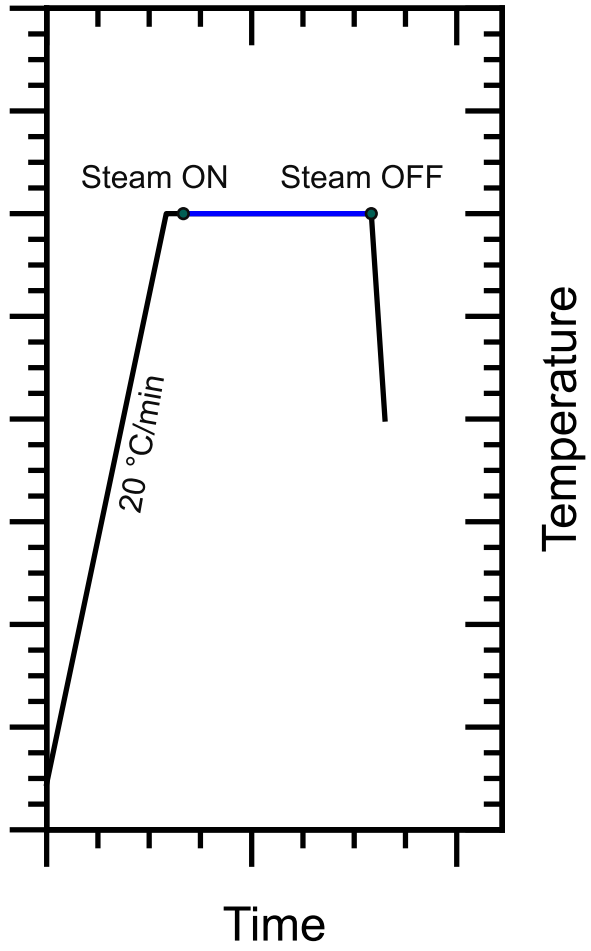

Effect of Solute Additions and Interdiffusion Barrier

CAT1 – Isothermal Steam Oxidation (STA)

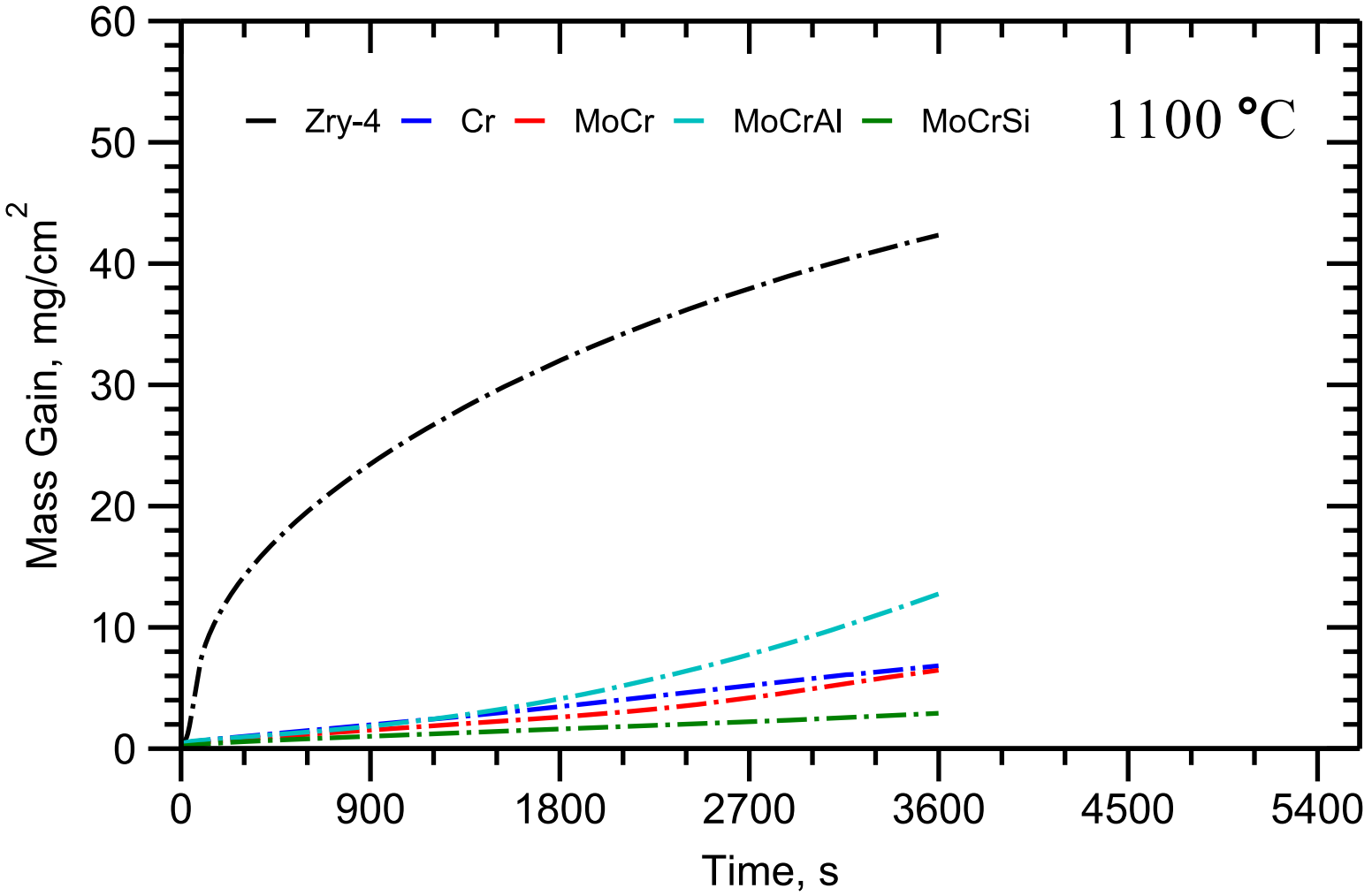

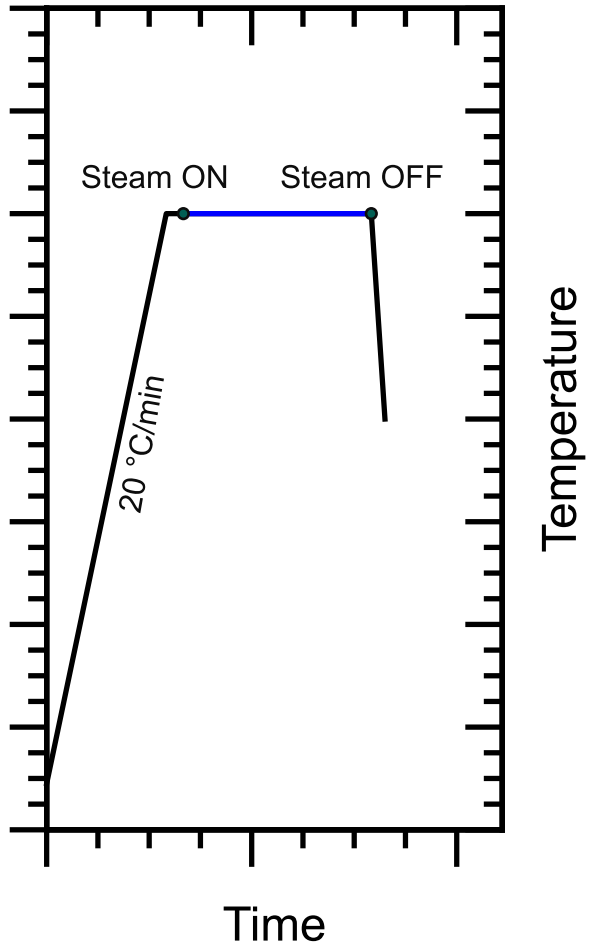

Effect of Solute Additions and Interdiffusion Barrier

CAT1 – Isothermal Steam Oxidation (STA)

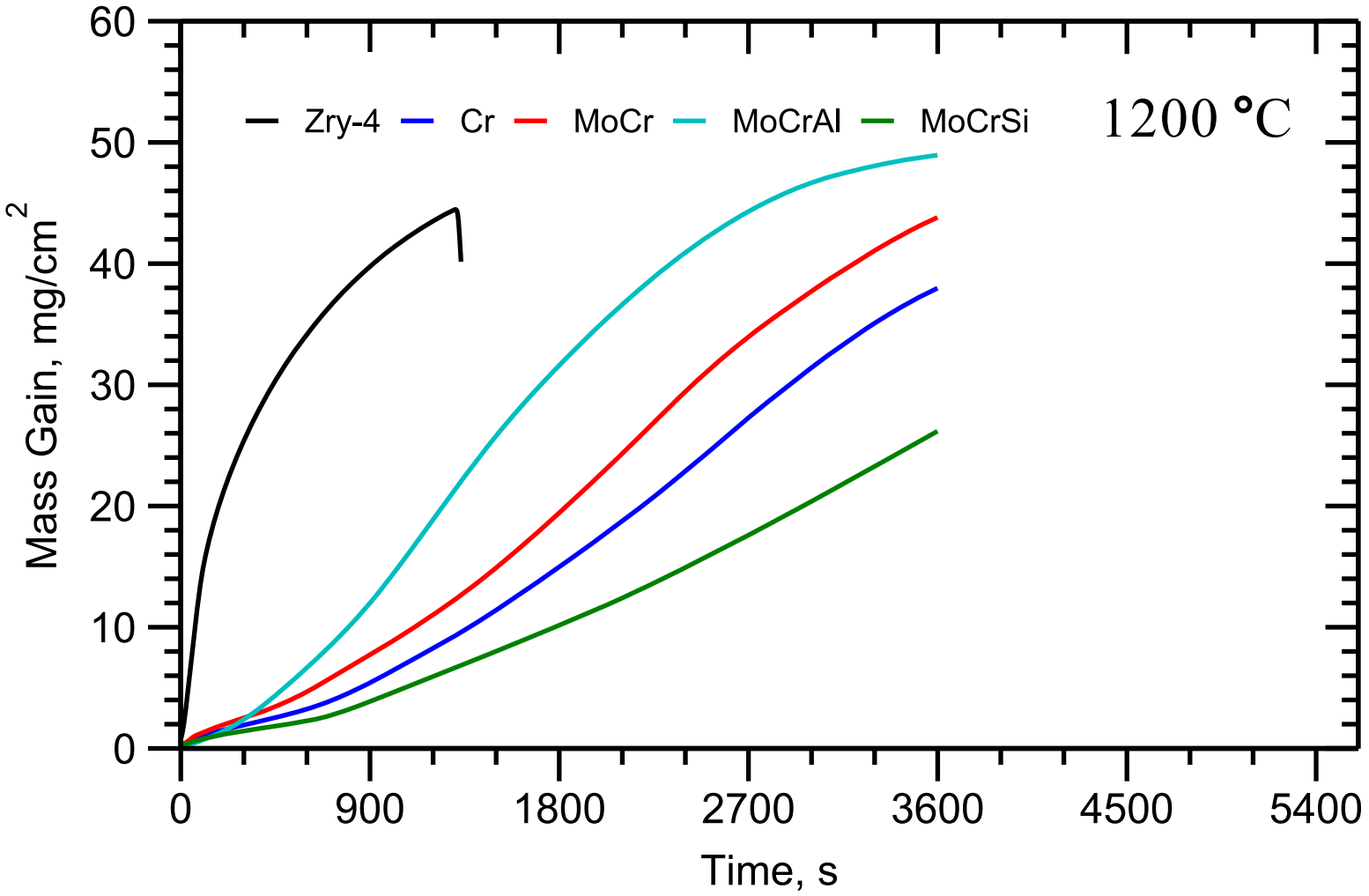

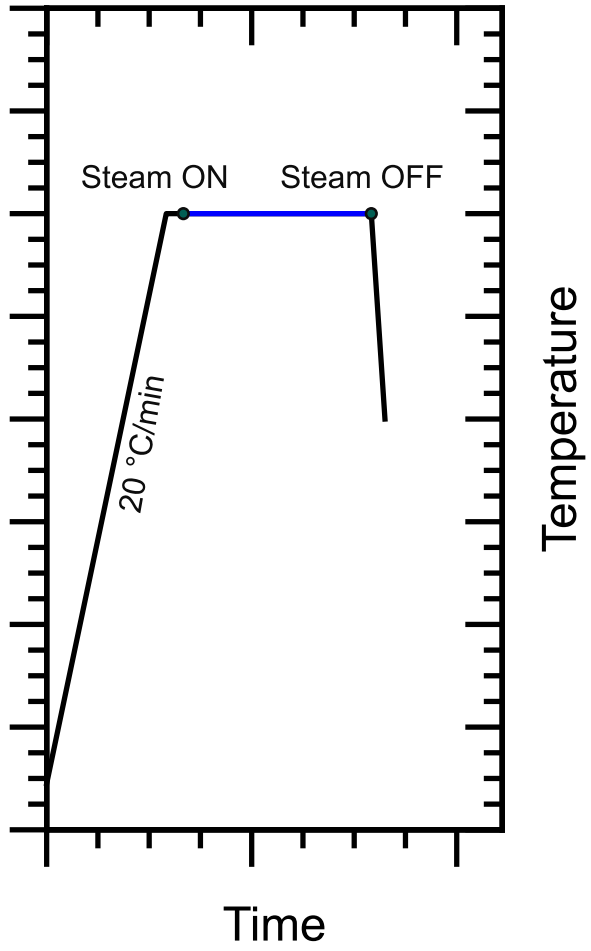

Effect of Solute Additions and Interdiffusion Barrier

CAT1 – Isothermal Steam Oxidation (STA)

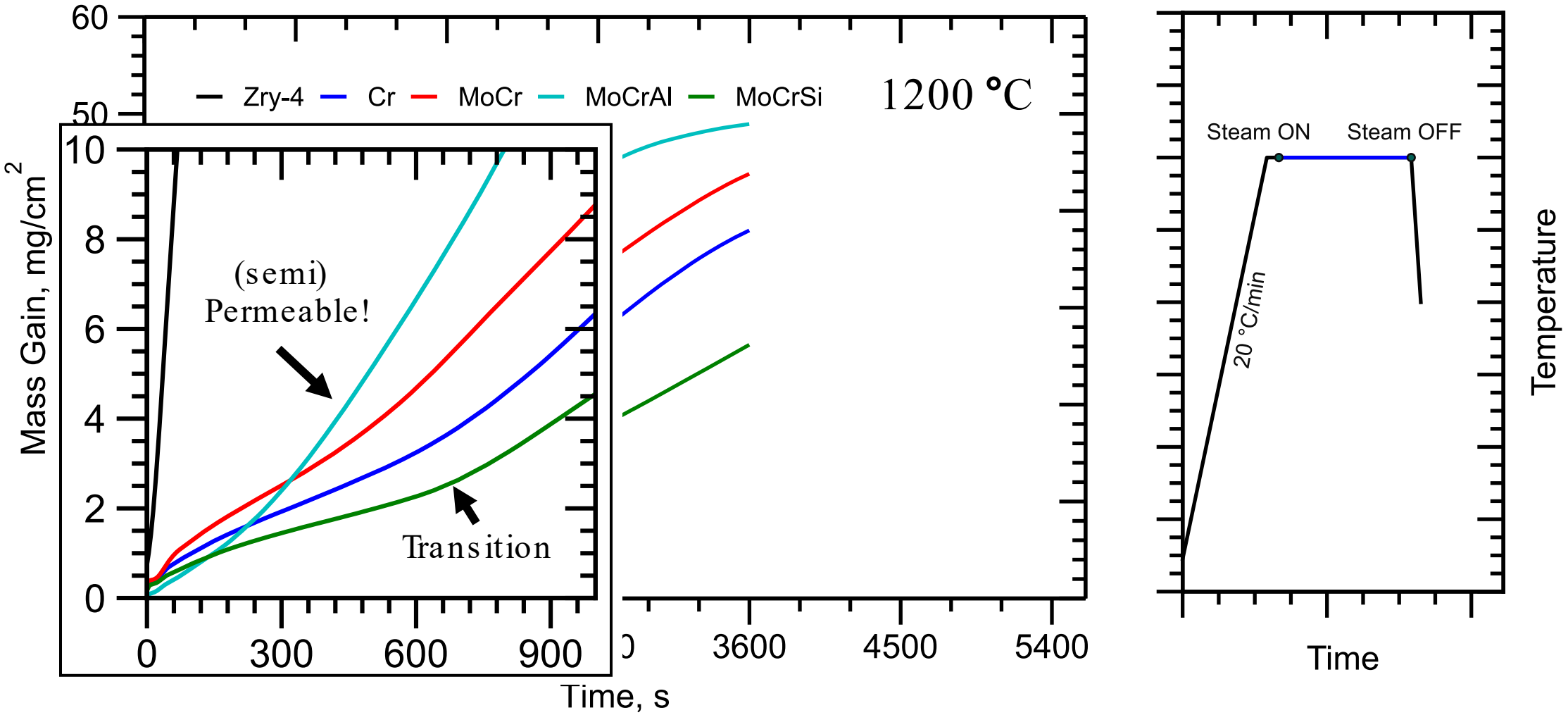

Effect of Solute Additions and Interdiffusion Barrier

CAT1 – Isothermal Steam Oxidation (STA)

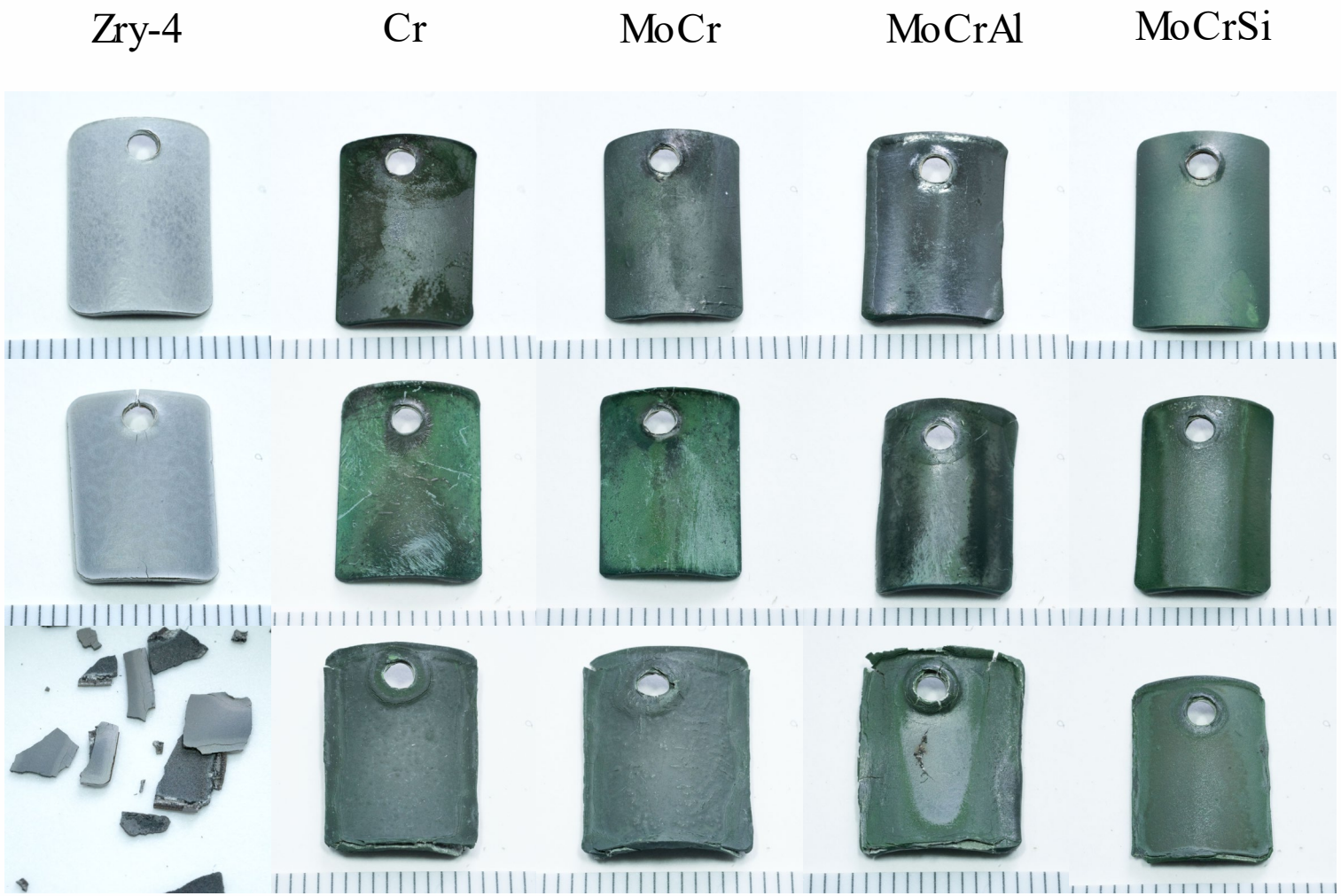

Effect of Solute Additions and Interdiffusion Barrier

CAT1 – Isothermal Steam Oxidation (STA)

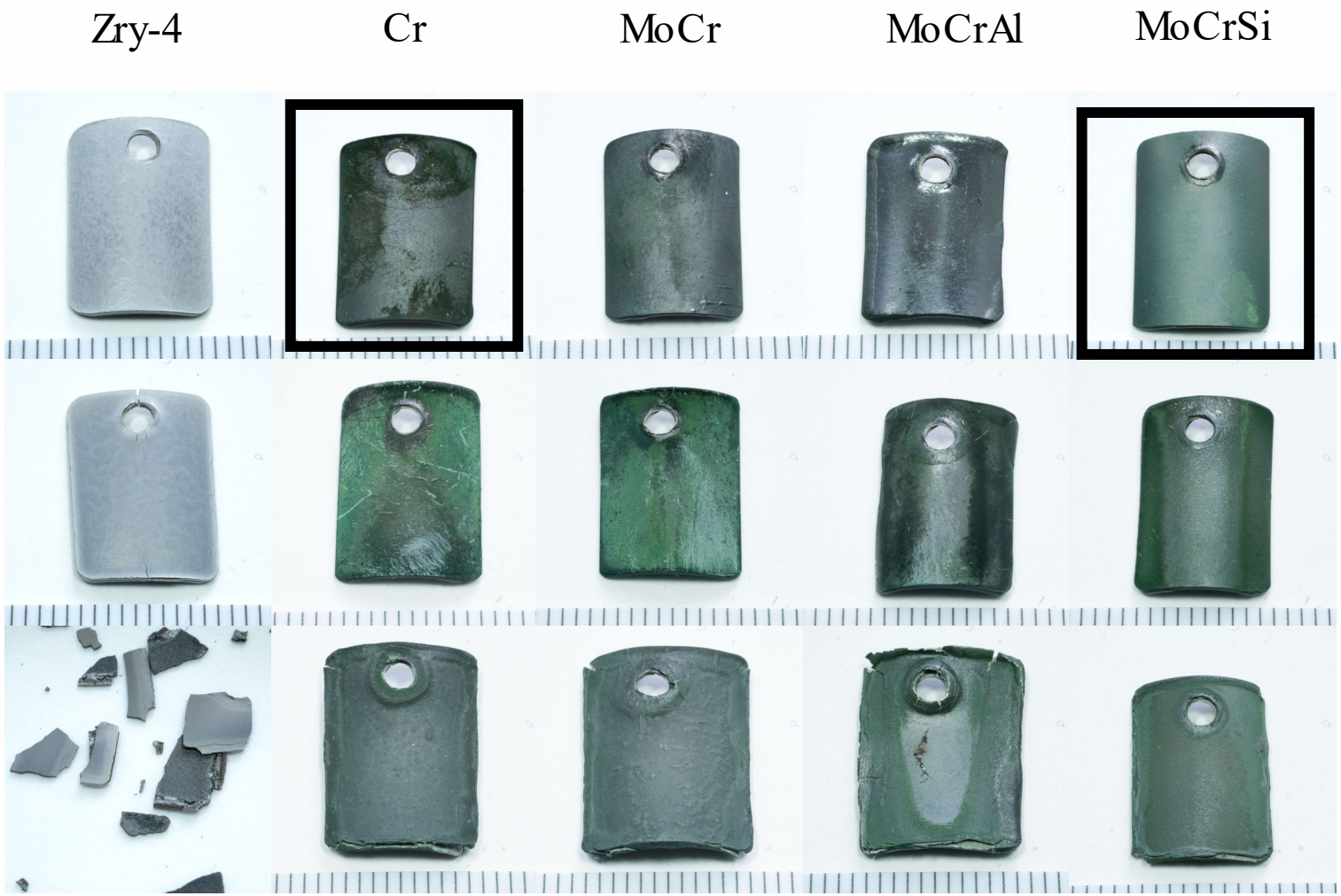

Cr, 1000 °C, 90 min

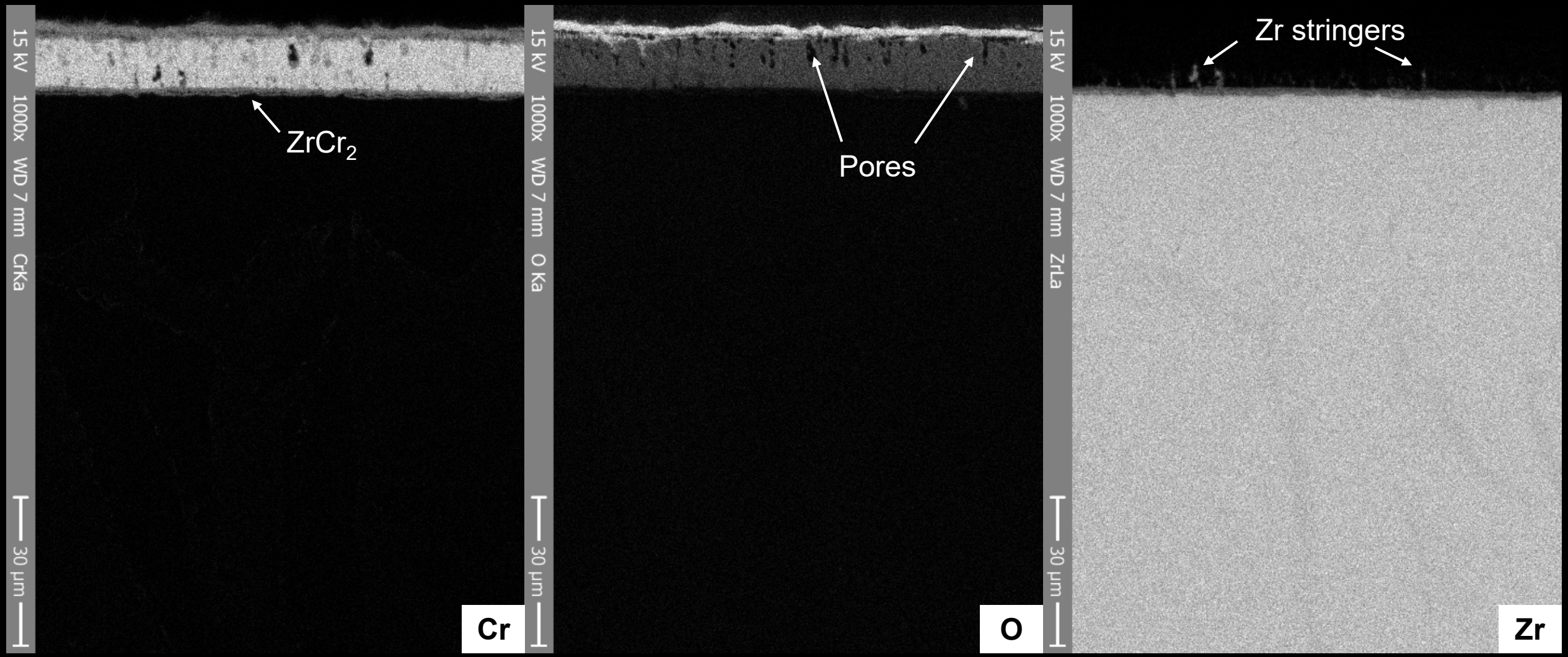

MoCrSi, 1000 °C, 90 min

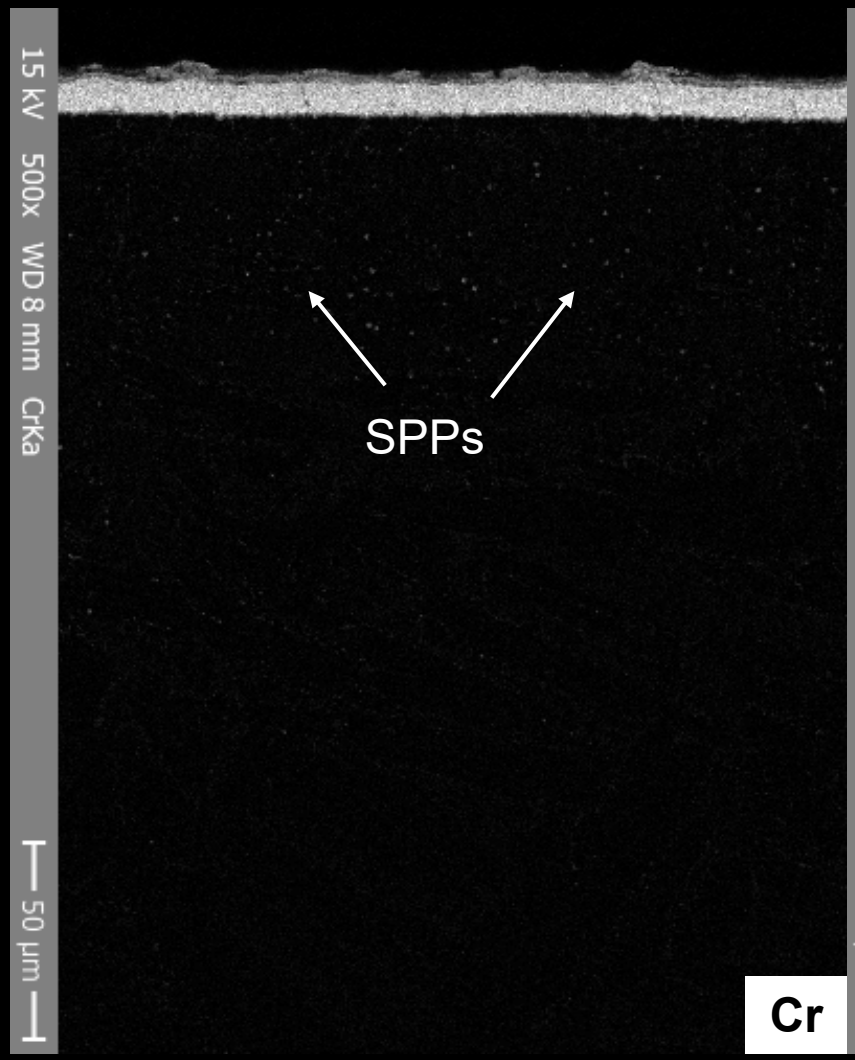

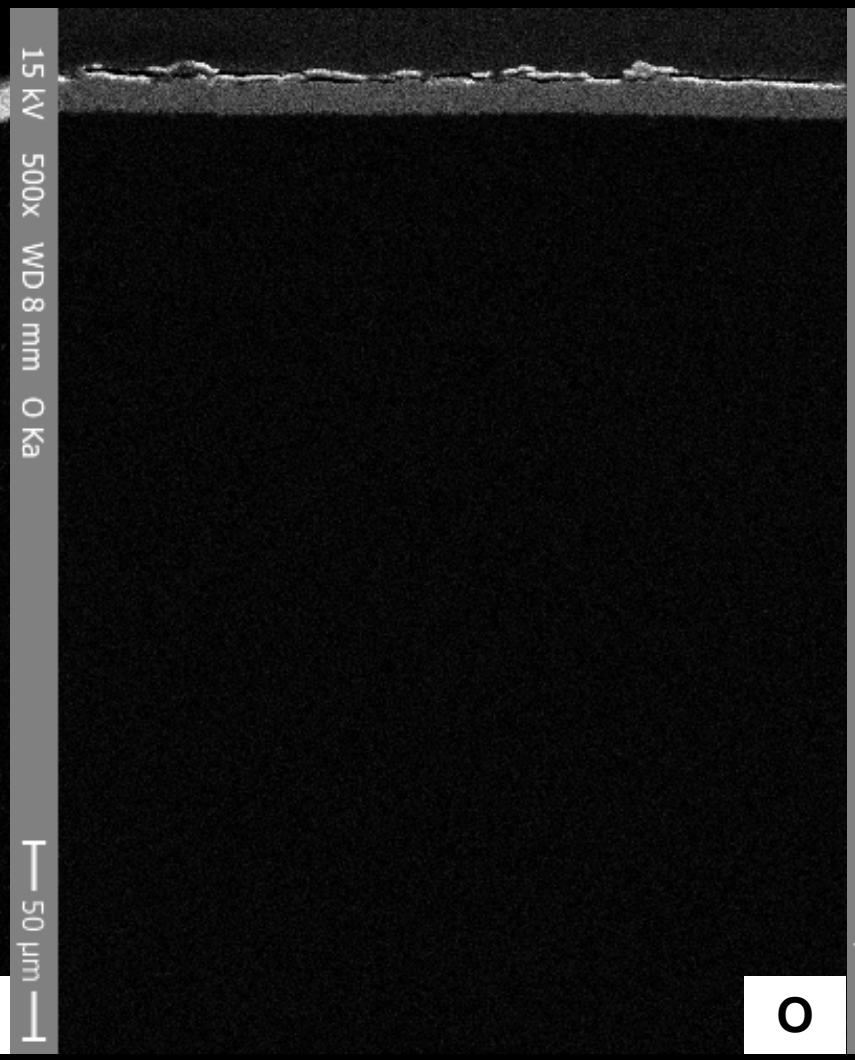

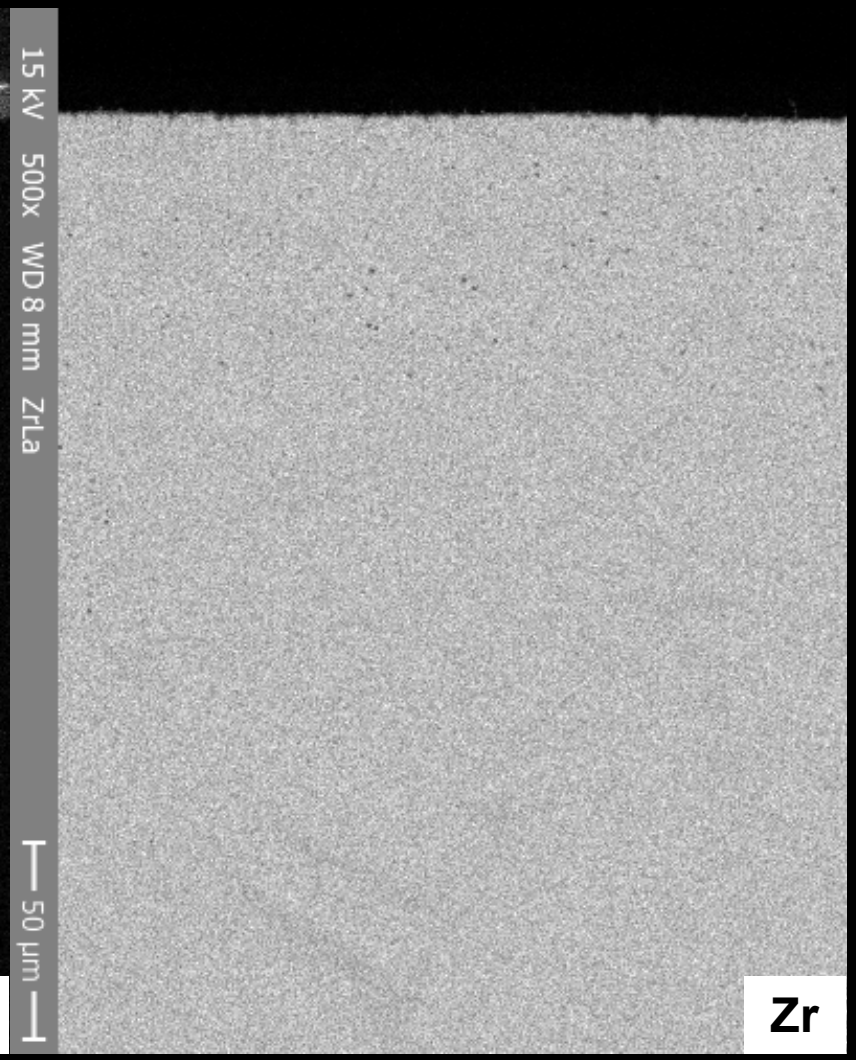

MoCrSi, 1000 °C, 90 min

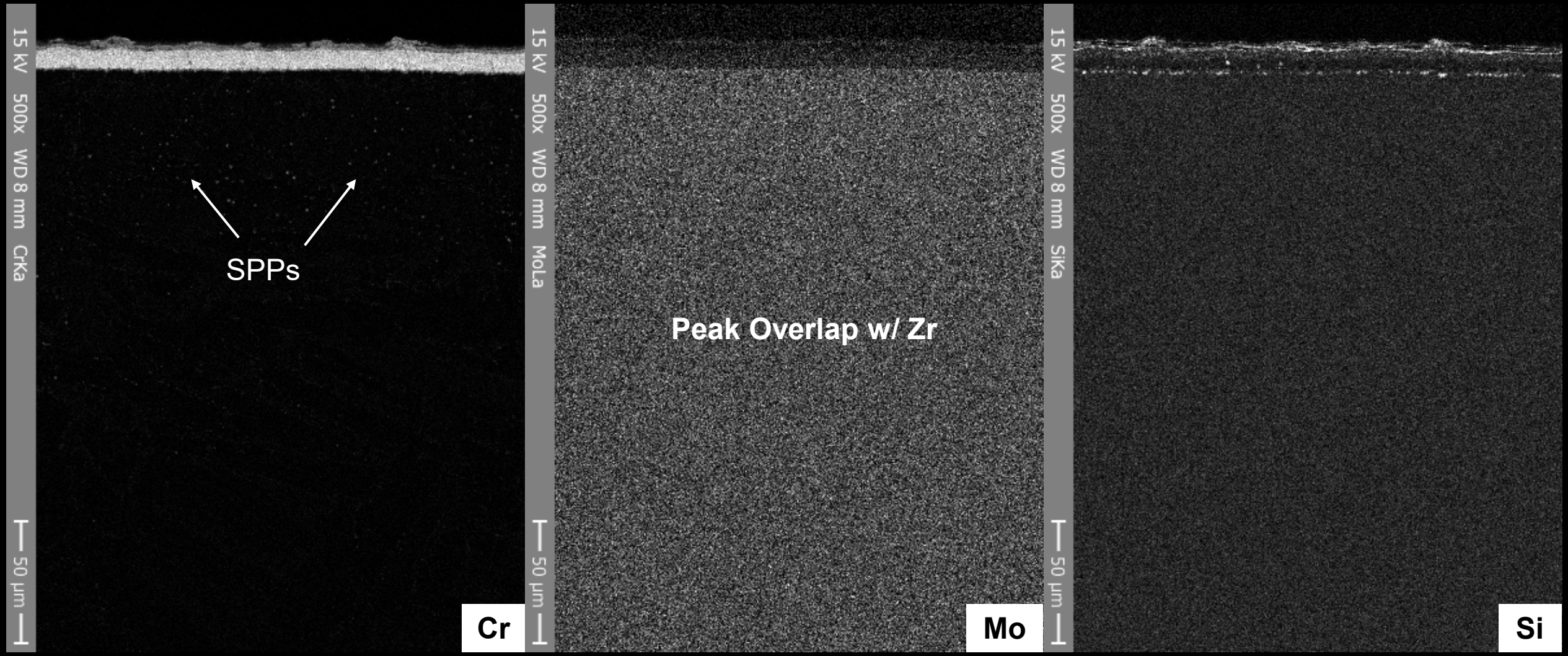

Cr, 1000 °C, 90 min

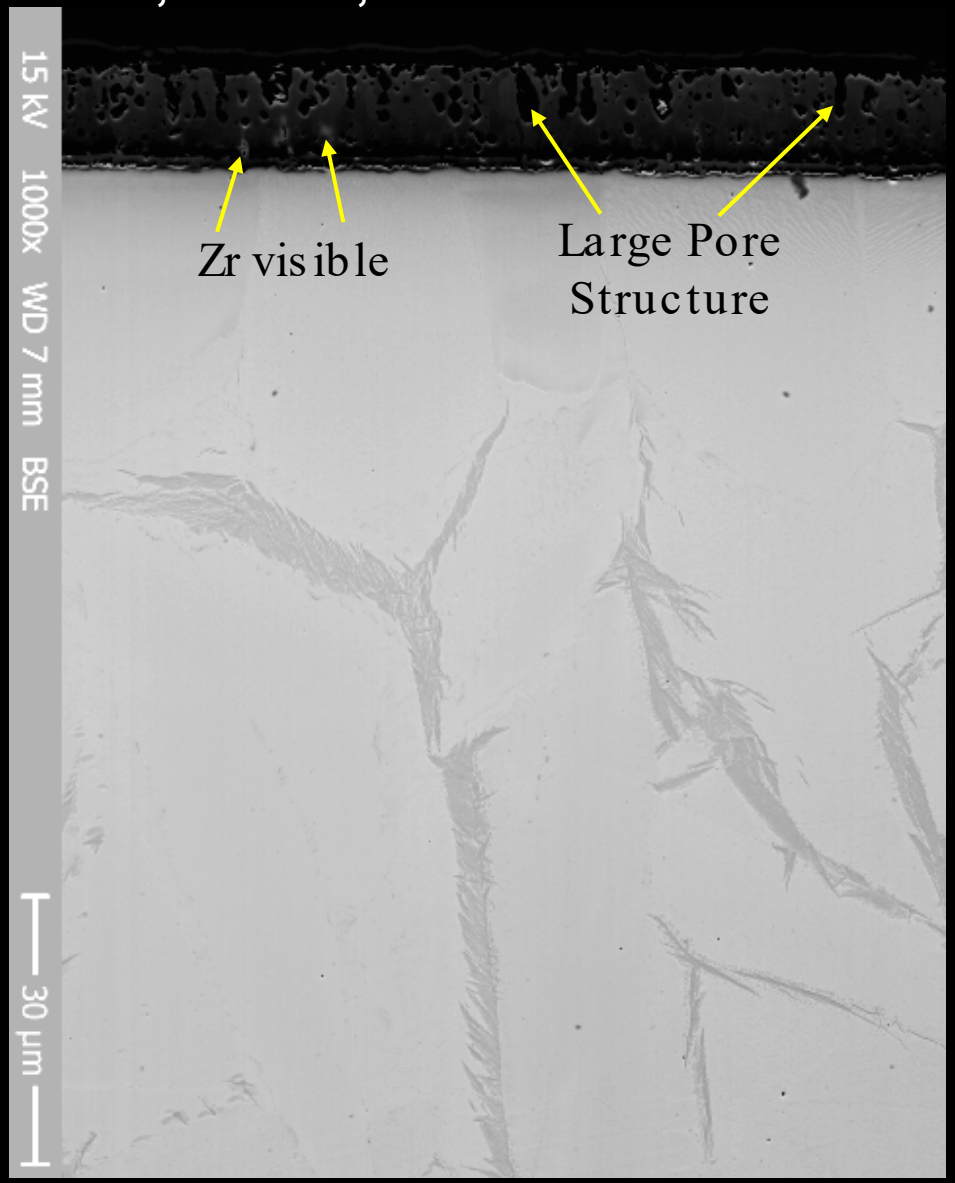

MoCrSi, 1000 °C, 90 min

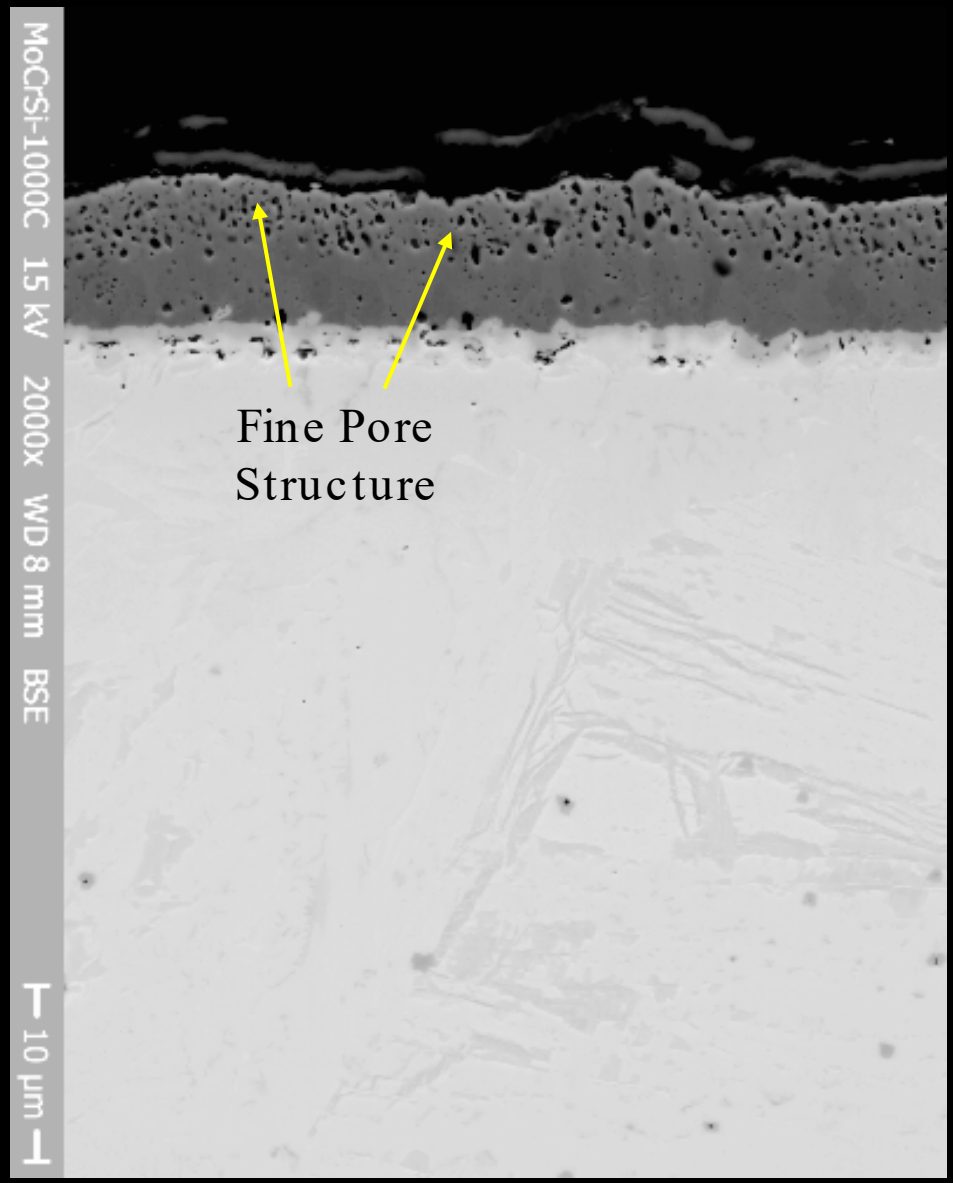

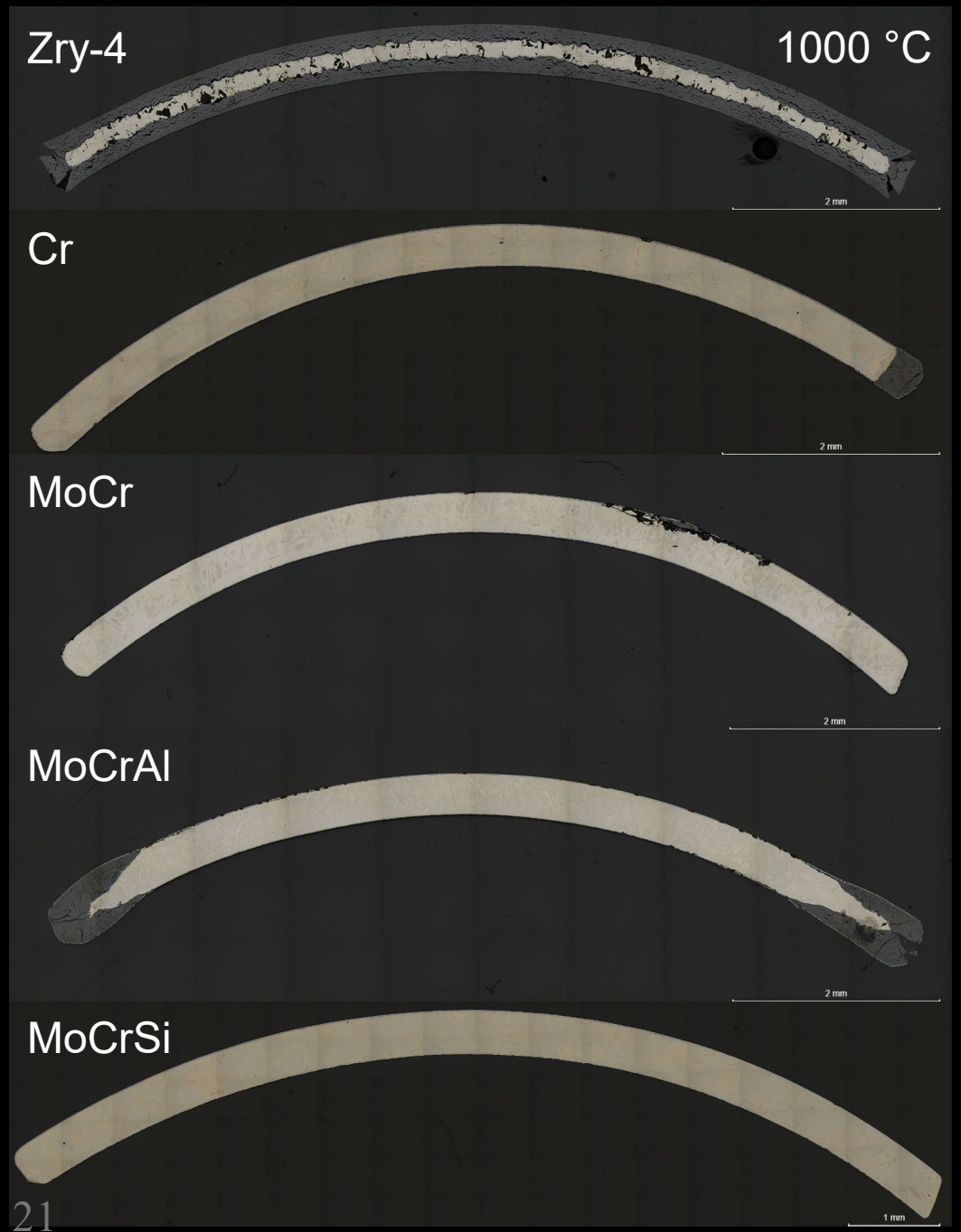
Zry-4
1000 °C
2 mm
Cr
2 mm
MoCr
2 mm
MoCrAl
2 mm
MoCrSi
1 mm

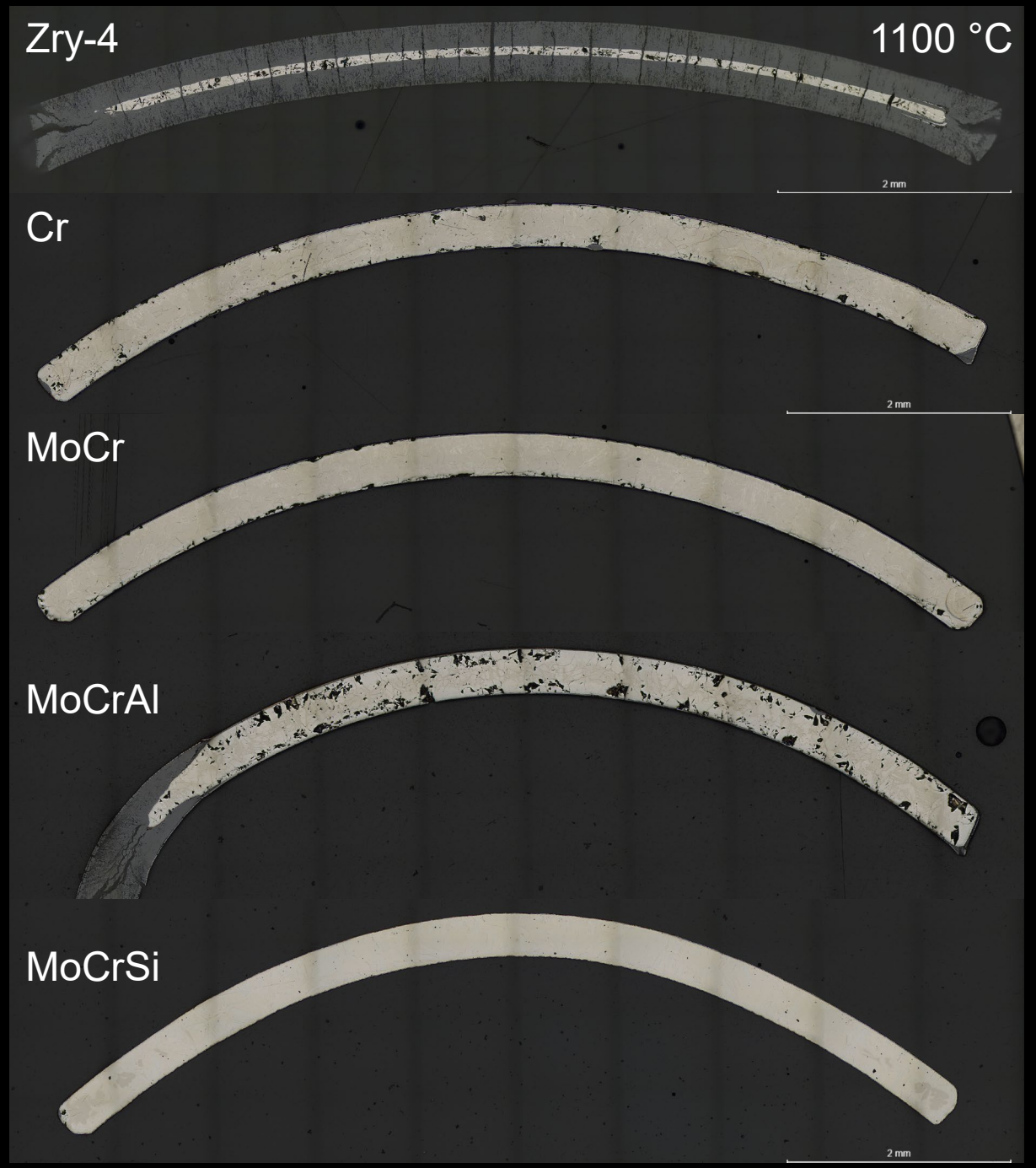
Zry-4
1100 °C
2 mm
Cr
2 mm
MoCr
MoCrAl
MoCrSi
2 mm

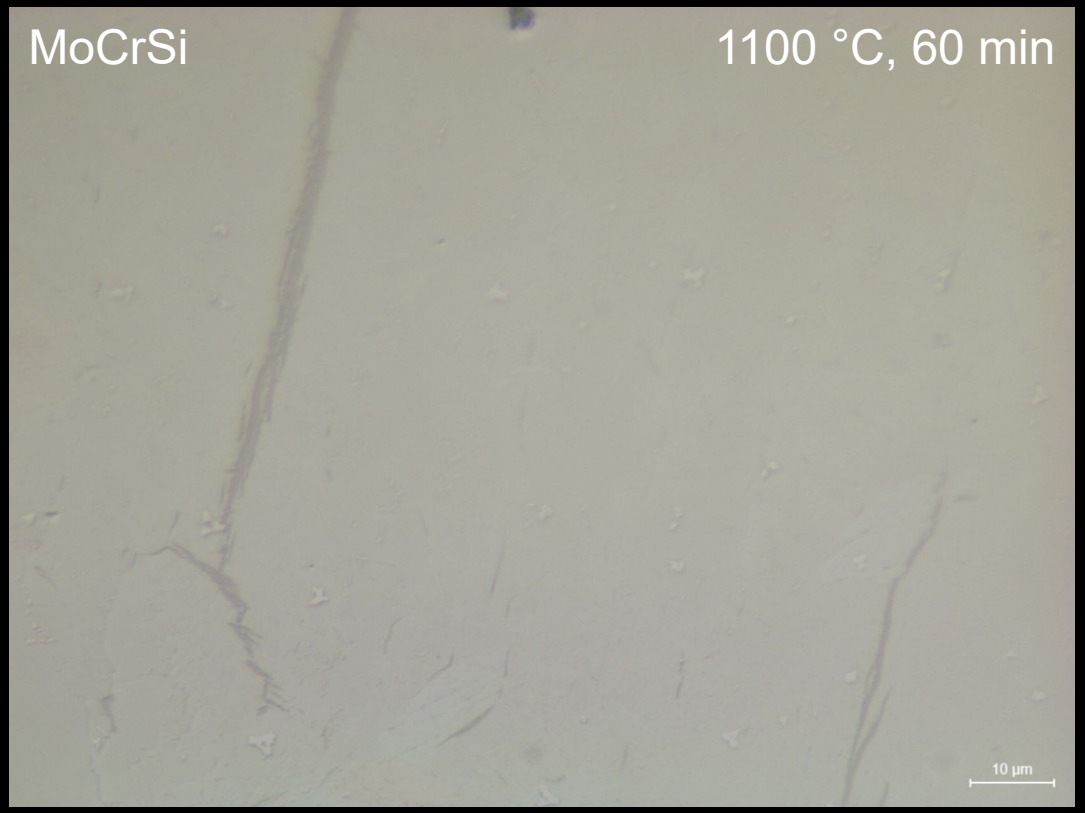
MoCrSi
1100 °C, 60 min
10 µm


Cr
1000 °C, 90 min
25 µm

CAT2 – Transient Steam Oxidation (STA/BOX)

Effect of Solute Additions and Interdiffusion Barrier

CAT2 – Transient Steam Oxidation (STA/BOX)

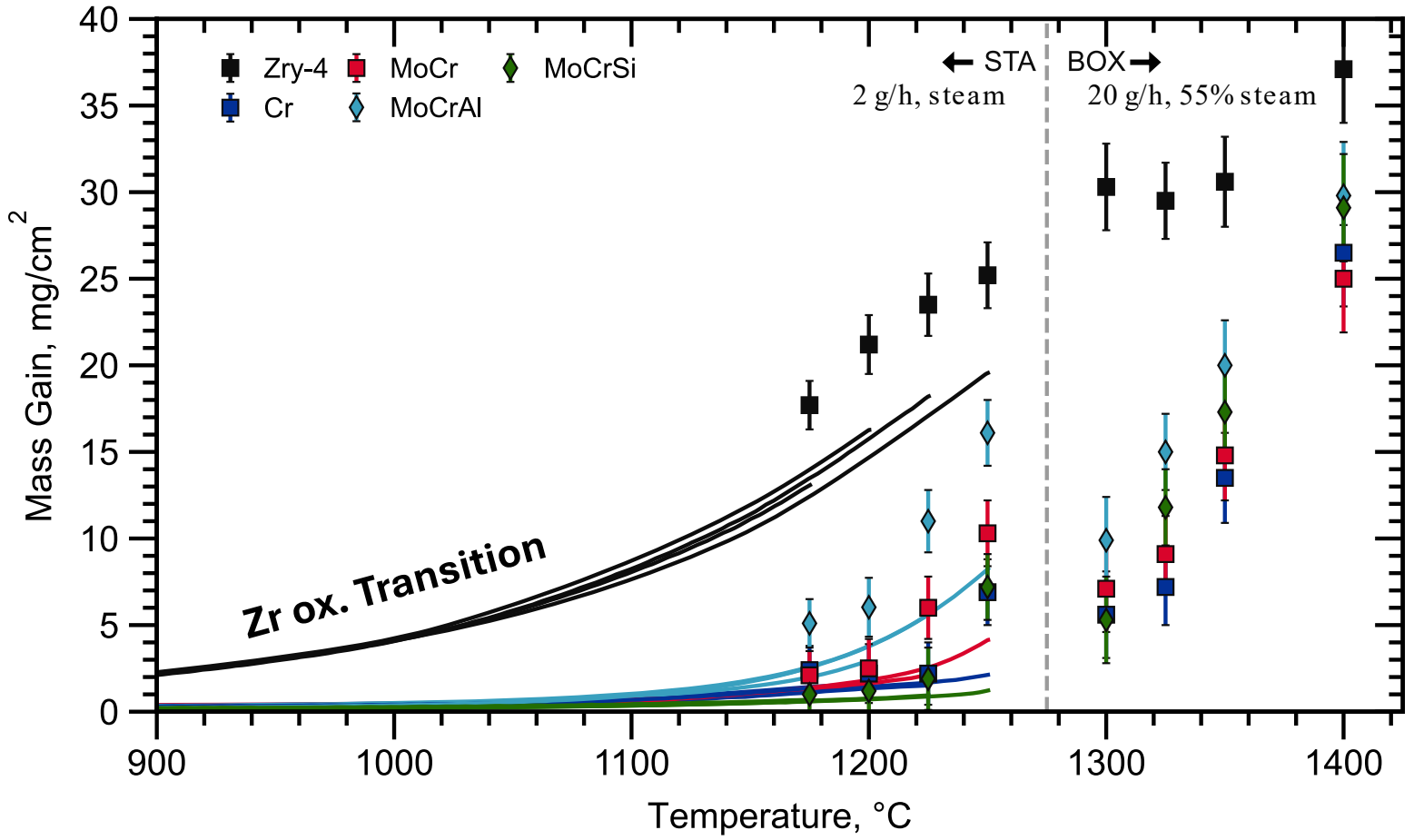

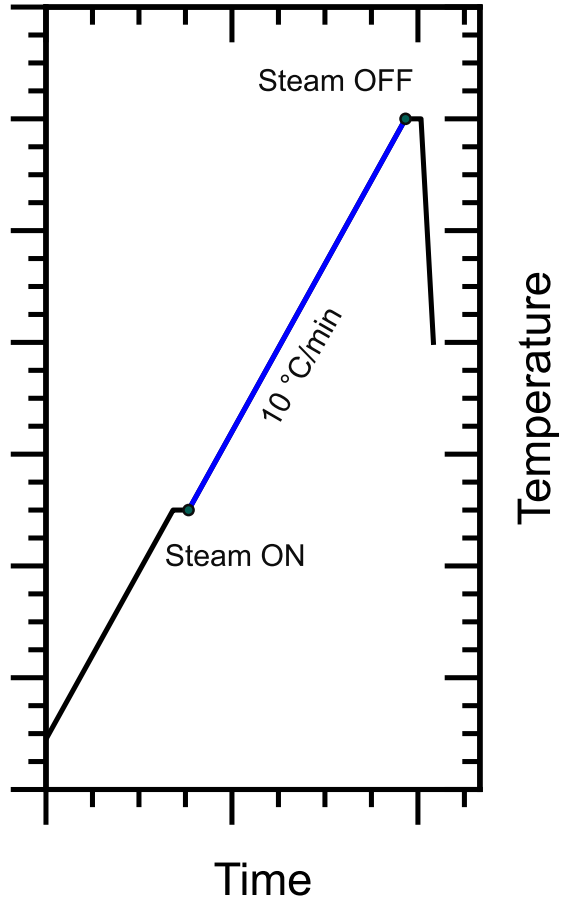

Effect of Solute Additions and Interdiffusion Barrier

CAT2 – Transient Steam Oxidation (STA/BOX)

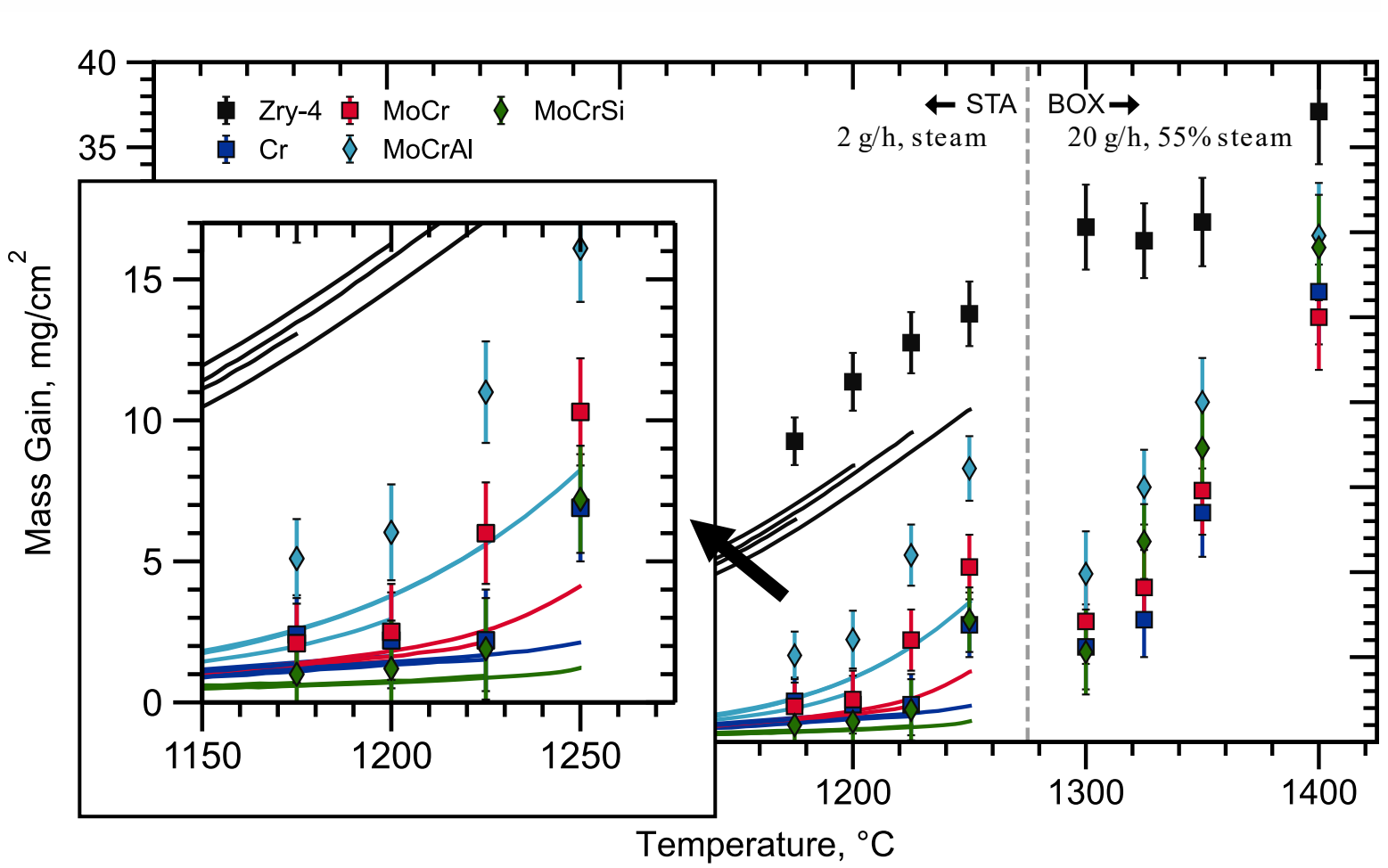

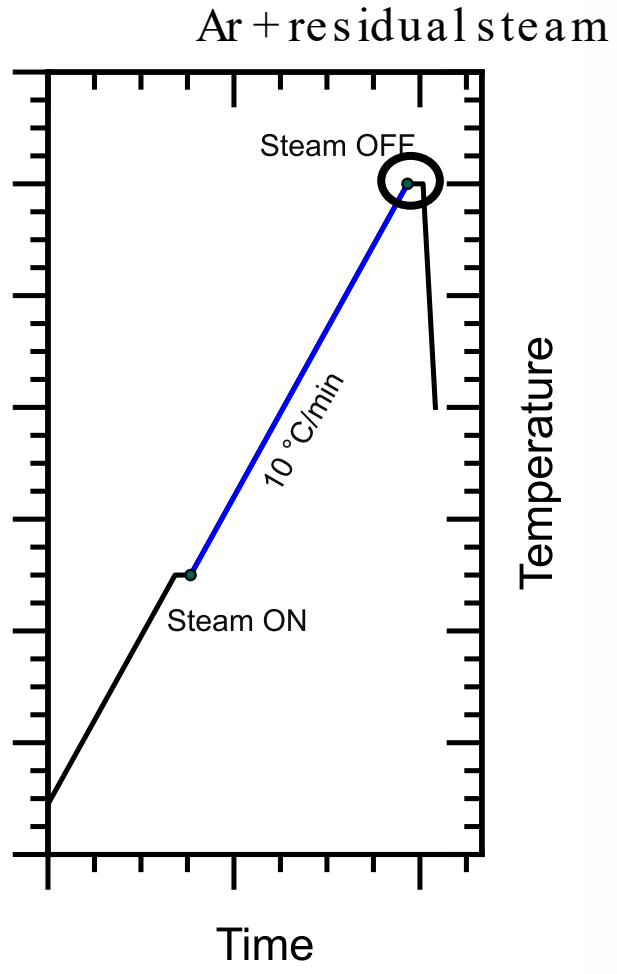

Effect of Solute Additions and Interdiffusion Barrier

CAT2 – Transient Steam Oxidation (STA/BOX)

…further characterization at QU

XRD, EDS/EBSD

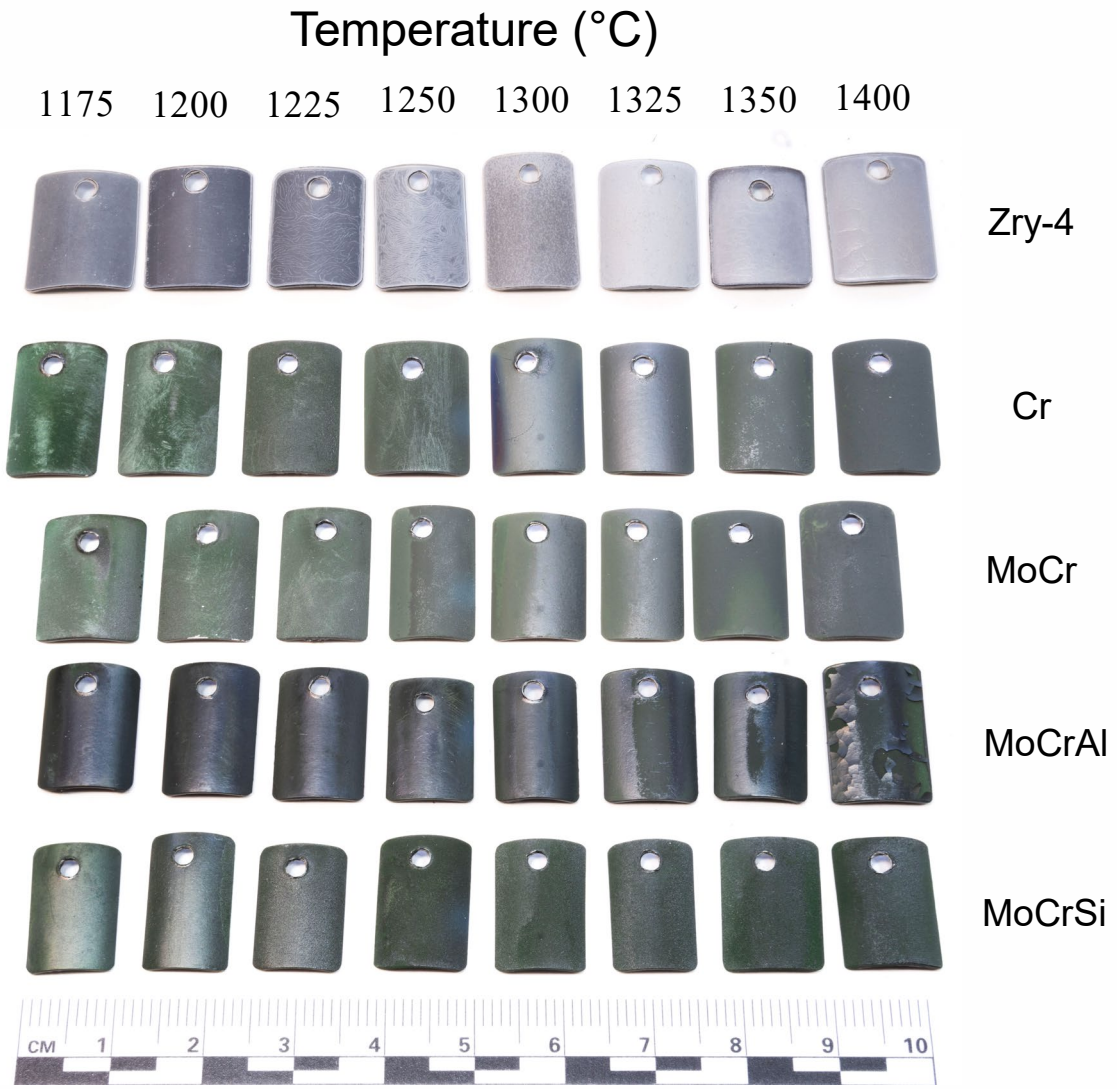

Early Takeaways

1. Cr, MoCrSi coatings significantly reduce steam oxidation until 1225 °C – rapid transition
2. Al inclusions accelerate oxidation – faster permeation of oxygen into Zr
3. Cr and MoCrSi were compared following SEM-EDS after 1000 °C, 90 min:
   - Cr coating exhibits large pore structure & interfacial $ZrCr_2$ intermetallic
   - MoCrSi has a fine pore structure & coarsened SPPs ($ZrCr_2$) in Zr matrix

Future Work

- TGA steam exposures of thickness variant Cr coatings (previous study)
- TGA O_2 eutectic temperature ramps on chemistry variant coatings (current study)
- TGA steam oxidation of coated Zr-2.5Nb (future study) – CANDU® PT application
  - Markus Piro (McMaster University)
  - Supported by the NSERC CREATE-CORRECT Program

Additional work:

- Autoclave exposure in CANDU® chemistry – Si dissolution
- Gaseous hydriding of coated Zry – heat treatment, c-ring tests
- Neutronics assessment of Cr coated CANDU bundles (DRAGON5/DONJON5)

Acknowledgements

- OECD-NEA NEST TCOFF-II Fellowship for sponsorship of the work during this exchange
  - Daniel Shephard (administrative support)
- KIT High Temperature Materials Group
  - Martin Steinbrück, Diana Bachurina, Ulrike Stegmeier, and Mirco Große
  - And the rest of the QUENCH group for being pleasant hosts!

Thank You!

Brock Nowak

Ph.D. Candidate
Queen's University

E: brock.nowak@queensu.ca

LinkedIn

Hope to reconnect at NuMat2026 Halifax!

Supplementary

The CANDU® History

NPD - 1962, 1 sLOCA

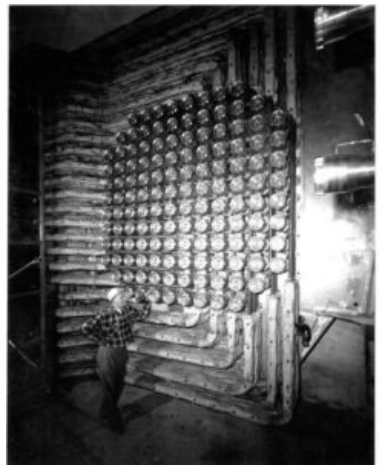

22 MW_e

Coolant leak during first ever attempt of online fueling…

2 sLOCA

1986, PTbreak

1994, FTbreak

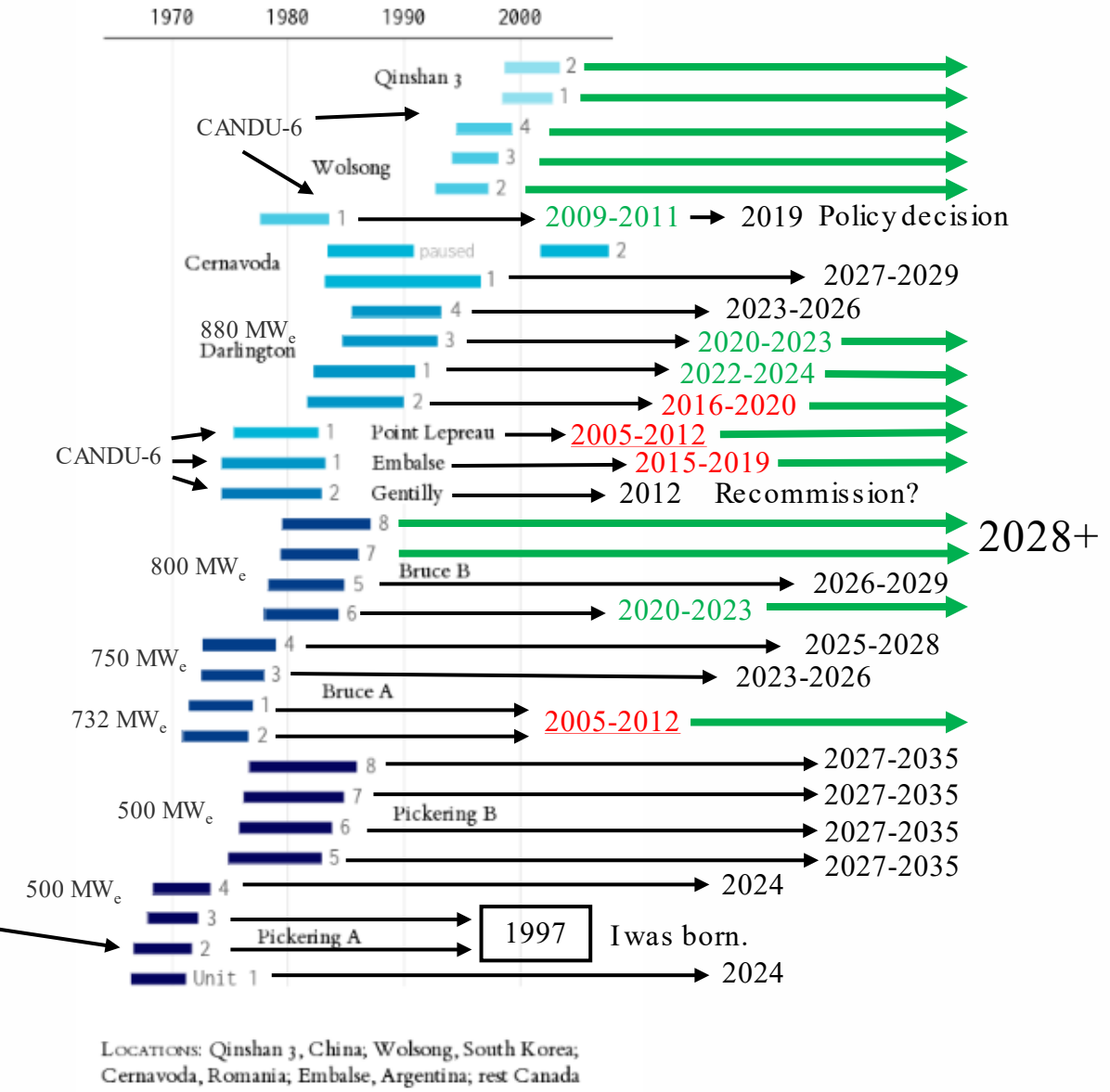

The CANDU®Future?

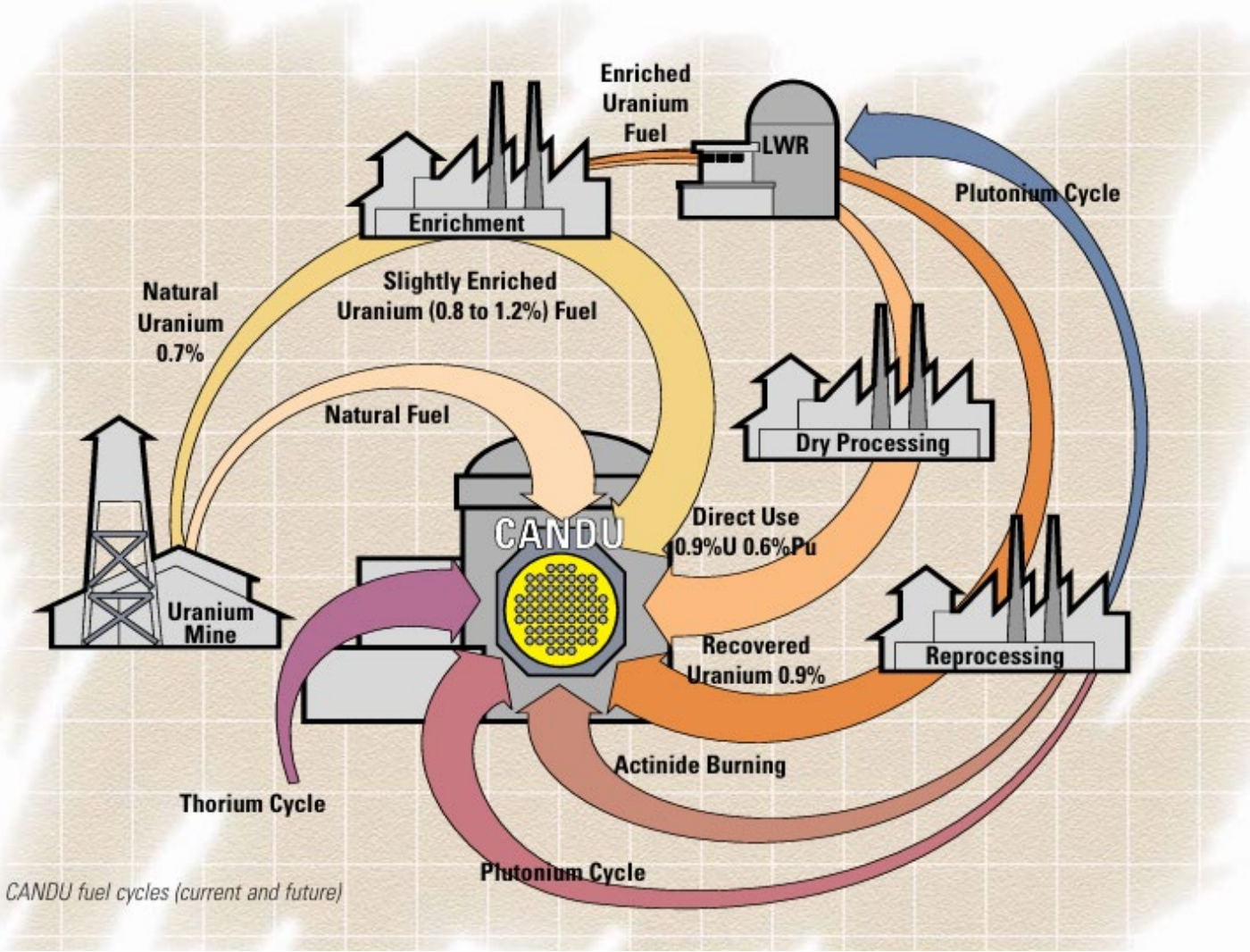

CANDU® CANFlex fuel cycles, from the CANDU® 6 Technical Summary

CANDU®Fuel Cycles

1. Natural Uranium (NU)
2. Slightly-Enriched Uranium (SEU)
3. Direct Use PWR in CANDU (DUPIC)
4. Recovered Uranium (RU)
5. Thorium (Th)
6. Plutonium (Pu)
7. Actinides (reducing waste)
8. …SMR fuels, CANDU ACR

CANDU®Refurbishment (Retubing)

- Currently bringing several units back online after refurbishment
- Extends service life out to 60 years, further iterations out to 90+ years

Research Question

Can we optimize coating protectiveness vs. neutronics penalty?

Methodology

- Prior work:
  - Minimum effective coating thickness (Cr, 5-20 μm)
- Ongoing study:
  - Solute additions (Al, Si)
  - Mo interdiffusion barrier at Cr/Zry-4 interface

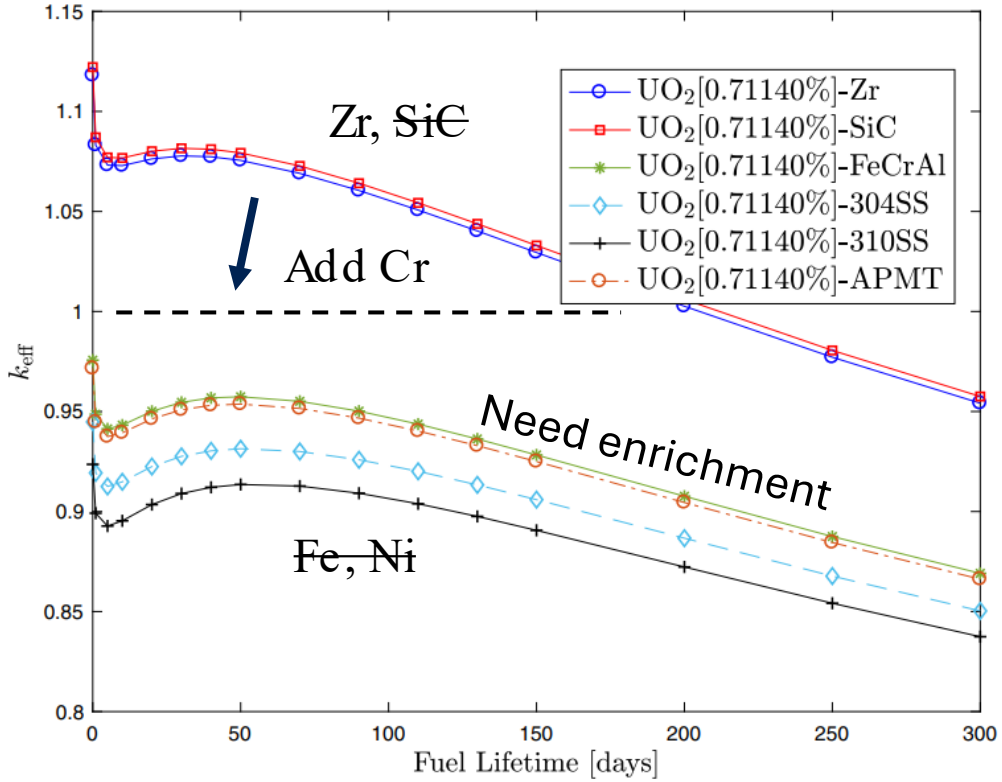

Effective multiplication factor vs. fuel residence time in a standard CANDU-6 natural cell lattice.

Naceur, A. & Marleau, G. Neutronic analysis for accident tolerant cladding candidates in CANDU-6 reactors. Annals of Nuclear Energy 113, 147–161 (2018).

Nicolas Wefers

KIT

Experimental Observations on the CHF Performance of Cr/ CrN-Coated Zircaloy-4 in Low-Pressure Flow Boiling

Accident Tolerant Fuel (ATF) concepts based on chromium coatings are investigated with respect to their influence on critical heat flux (CHF) and boiling heat transfer behavior. The presented work builds on two preceding projects focusing on the onset of boiling crisis in Cr-based ATF claddings and extends the investigation towards post-CHF phenomena and their relevance for cladding integrity.

Experiments were conducted in both annular gap and small rod bundle geometries under pressurized water conditions. CHF was identified using a standardized procedure based on inlet enthalpy variation, while post-CHF tests employed an active power cut-off at a cladding temperature of 1000 °C. Test samples included Zr-4 reference cladding, Zr-4 coated with 8 µm CrN (with Ti interlayer), and Zr-4 coated with 16 µm Cr. Surface roughness remained comparable across samples, enabling a direct assessment of material effects.

Across all investigated flow conditions, CHF exhibits a robust linear dependence on inlet enthalpy (or boiling number), with correlation coefficients up to $R \approx 0.99$. The observed CHF differences between coated and uncoated samples are moderate, in the range of 8-9% with an accuracy of 3.5% and largely independent of mass flux, pressure and inlet subcooling. This indicates that CHF is primarily governed by flow conditions rather than by smooth Cr-based surface modifications below ~20 µm thickness.

To gain mechanistic insight, high-speed visualizations were used to quantify nucleation site density (NSD) and bubble departure frequency (BDF). The results show that Cr-based coatings primarily affect NSD, while BDF remains comparatively unchanged. The tested pure Cr coatings delay NSD activation, whereas CrN coatings promote earlier bubble coalescence and transition to churn flow. Existing NSD correlations reproduce global trends but fail to distinguish material-specific effects.

Overall, the findings suggest limited CHF sensitivity to Cr-based ATF coatings, while subcooled boiling characteristics and post-CHF behavior remain key performance-limiting phenomena for future investigation.

Experimental Observations on the CHF Performance of Cr/ CrN-Coated Zircaloy-4 in Low-Pressure Flow Boiling

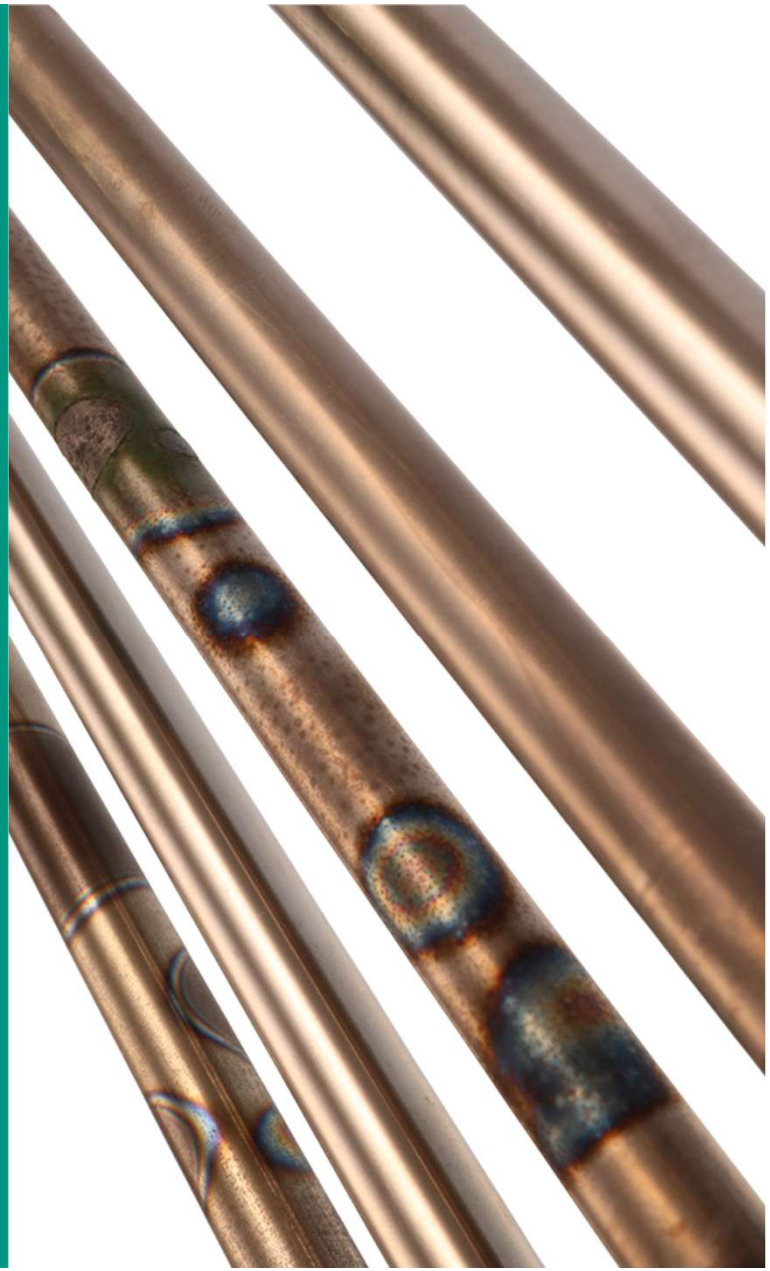

Nicolas Wefers[1], Daniel Vlček[2], Tereza Kinkorova[2], Taron Petrosyan[3], Stephan Gabriel[1]

[1]Karlsruhe Institute of Technology

[2]Czech Technical University in Prague

[3]Brno University of Technology

18. December 2025

1. Outline & Motivation
2. Experimental Set-Up
3. CHF-Results
4. Boiling Parameter
5. Outlook & Future Work

Outline of ATF-Cladding Tube Activities

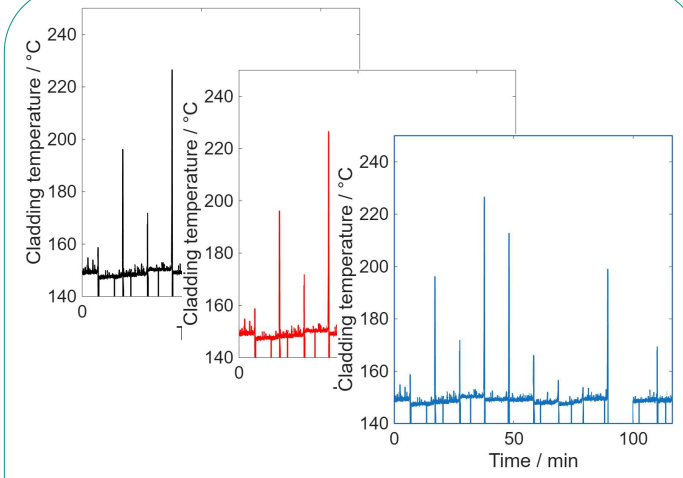

GRS: KEK-MESA/ OFFEER: COATED

CHF-Benchmark of Cr-based ATF‘s at COSMOS lap

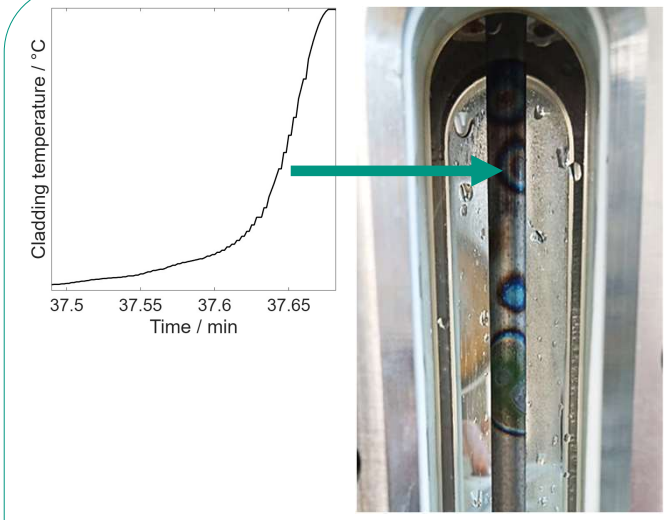

OFFEERR: ChroTemp

Post-CHF behavior of Cr-based ATF‘s at COSMOS lap and post tests/ simulation at CTU

Further activities based on ChroTemp

Post-CHF impact on strength and fracture mechanics of cladding tubes

Motivation & Background

- Critical Heat Flux (CHF): upper limit for safe heat removal in nuclear fuel—exceeding it triggers a boiling crisis, rapid temperature rise, and possible cladding damage
- Nucleation Site Density (NSD): quantifies the number of active bubble nucleation sites per unit area during boiling. Higher NSD usually enhances heat transfer, delaying CHF (good for safety)
- NSD is influenced by cladding material, surface roughness, wettability, and coatings
- Computational Fluid Dynamics (CFD): Predictive CFD models need accurate input data for boiling and CHF, including reliable NSD trends
- New ATF materials/coatings (like CrN, Cr) may shift NSD and CHF, boosting performance and safety
- Need to understand how these innovations impact boiling at the micro-scale and reactor-scale

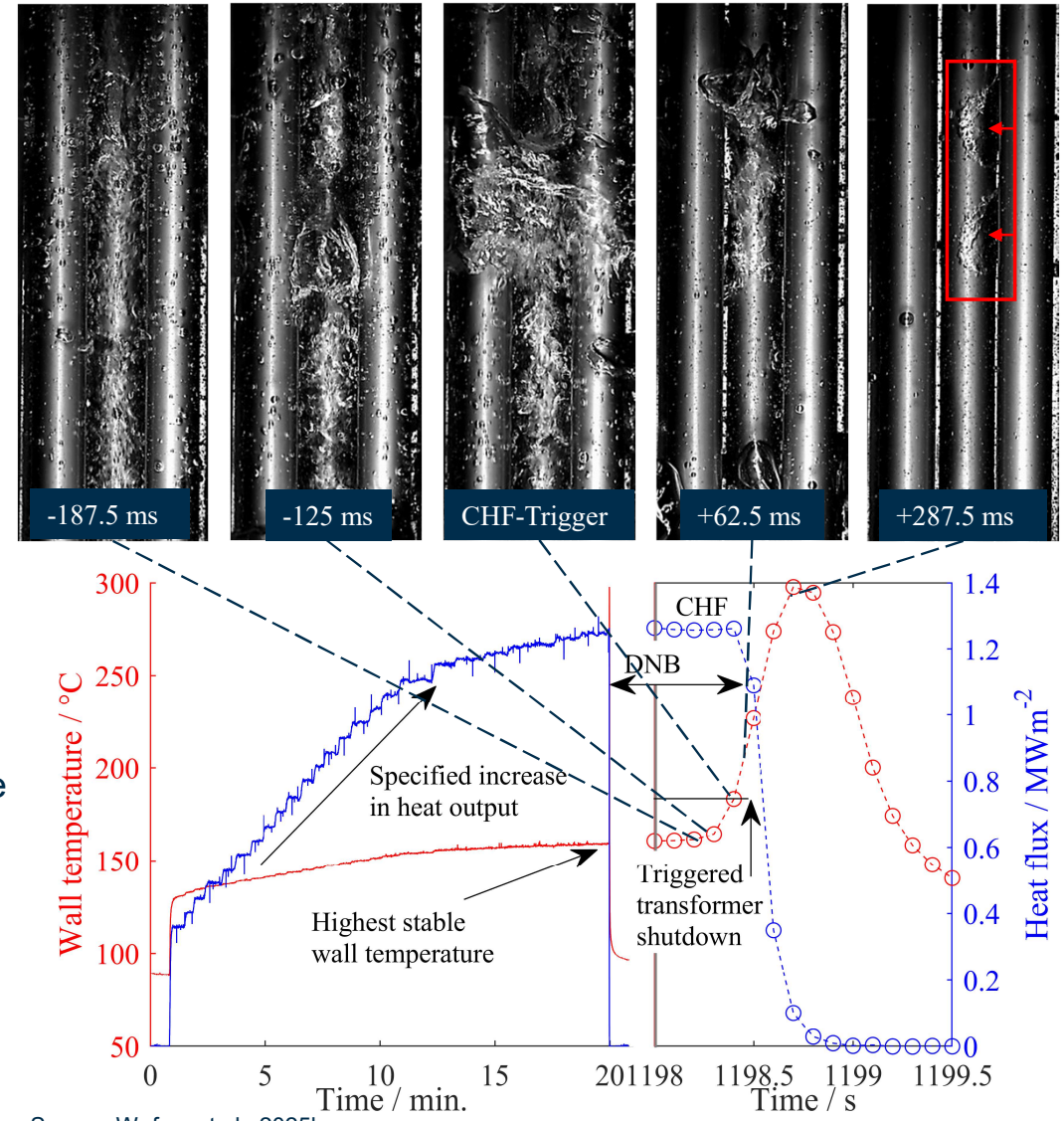

Source: Wefers et al., 2025b

Experimental Set-Up

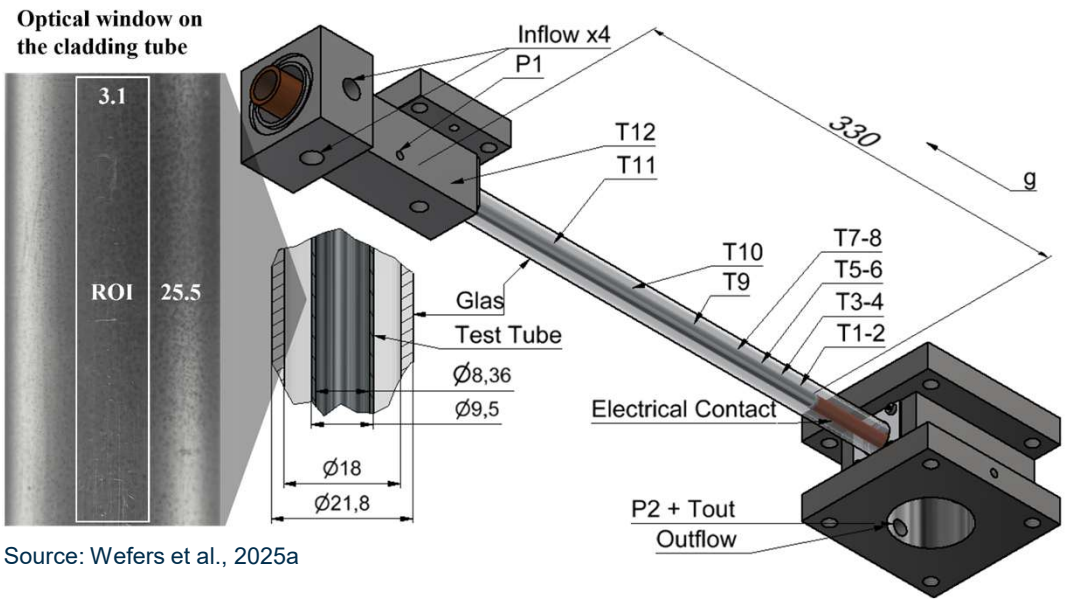

Source: Wefers et al., 2025a

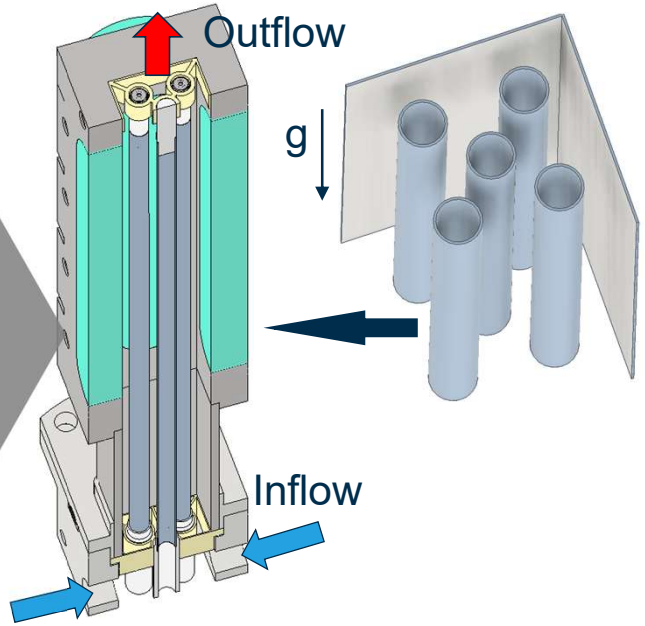

Adapted from Wefers et al., 2025b

COSMOS-L: low-pressure flow boiling loop at KIT

- Annular gap and assembly test section simulates rod bundle conditions
- Direct electrically heated (AC) claddings (heated length up to 400 mm)
- Glass outer tube/ sight glasses for optical access
- High-speed camera on a robot hand. Tracks bubbles, nucleation sites and DNB

Cladding Samples

Bare Zircaloy-4

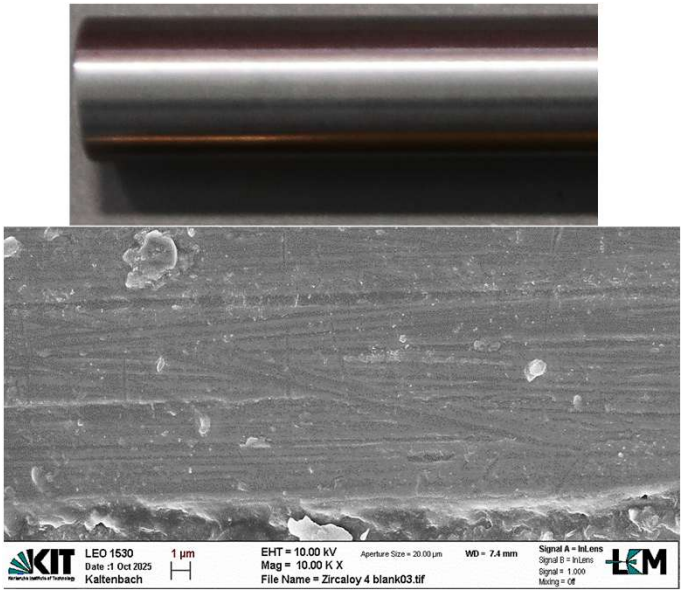

CrN coated Zircaloy-4 (8 µm)

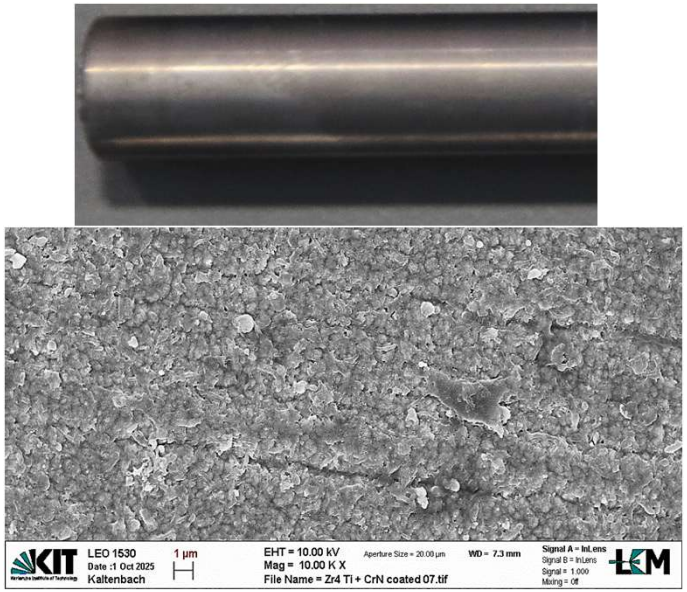

Cr coated Zircaloy-4 (16 µm)

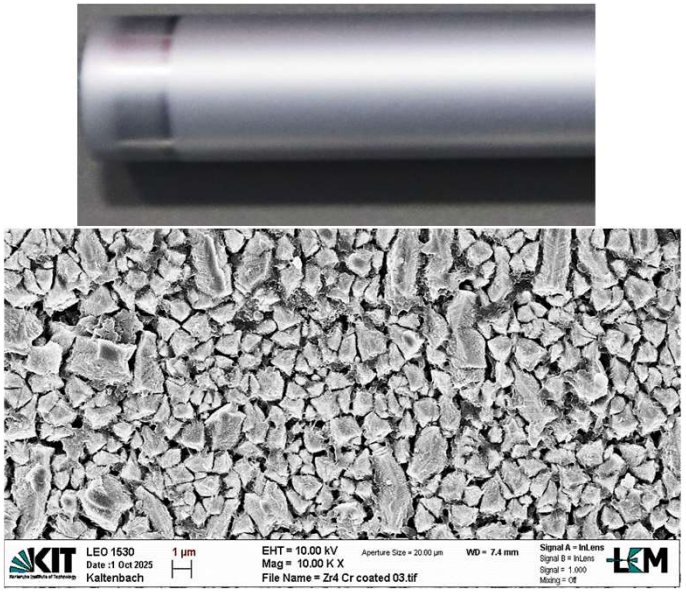

Adapted from Wefers et al., 2025a

Mean Wetting Angle (°)	84.5	73	78
Specific Heat (J/kg·K) (300/400 K)	281 / 302	460 / 480	449 / 500
Thermal Cond. (W/m·K) (300/400 K)	13.4 / 14.2	2.0 / 1.8	93.7 / 80

Surface Characterization and Area of Interest

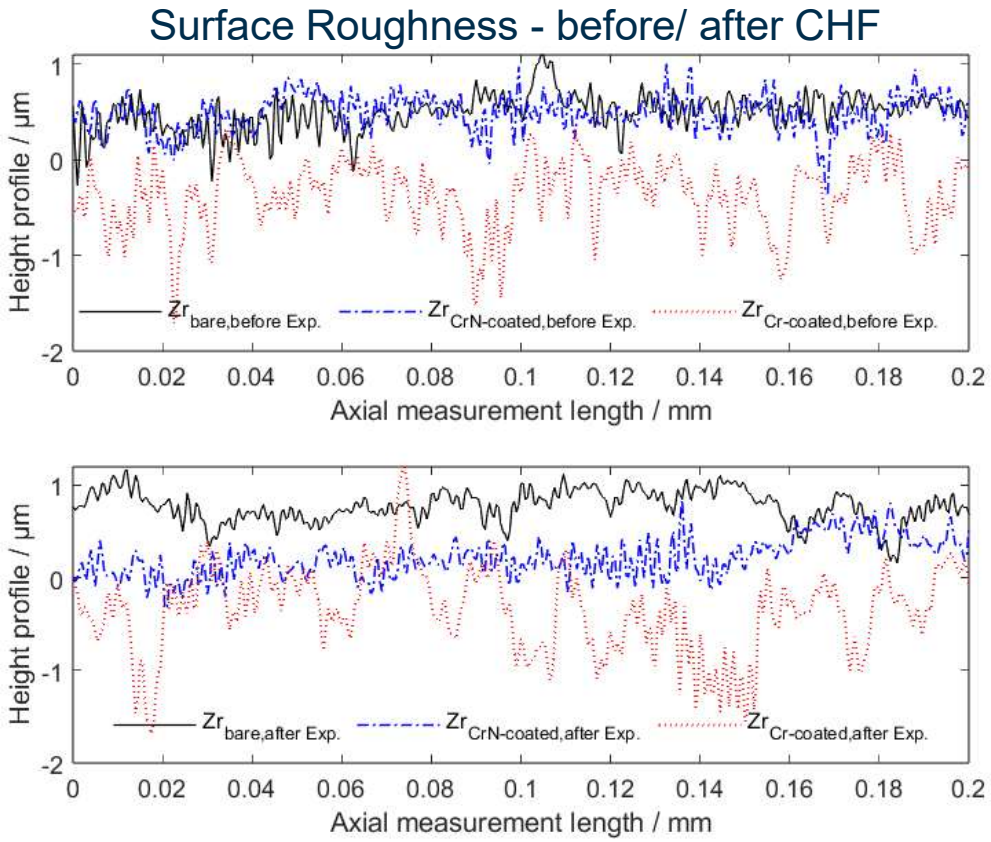

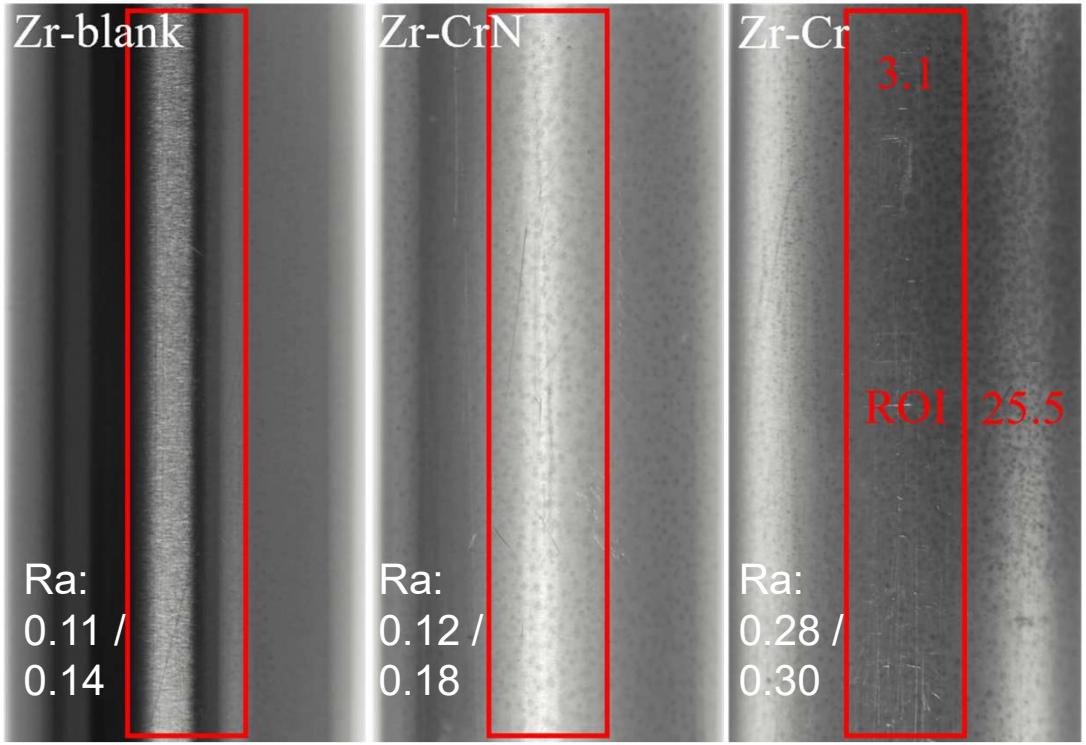

Source: Wefers et al., 2025a

Key Observations

- All claddings: CHF increases linearly with boiling number or inlet enthalpy flow
- High correlation for all materials (R^2 from 0.92 up to 0.99): trend is robust
- No significant difference in CHF trend between Zr-4, Cr, or CrN surfaces
- Offset between fits: only minor, coatings do not improve CHF significantly under these conditions (~8%)
- CHF also shows clear (inverse) correlation with excess enthalpy
- Again, surface coating effect is minimal: dominant parameters remain mass flux, pressure, subcooling

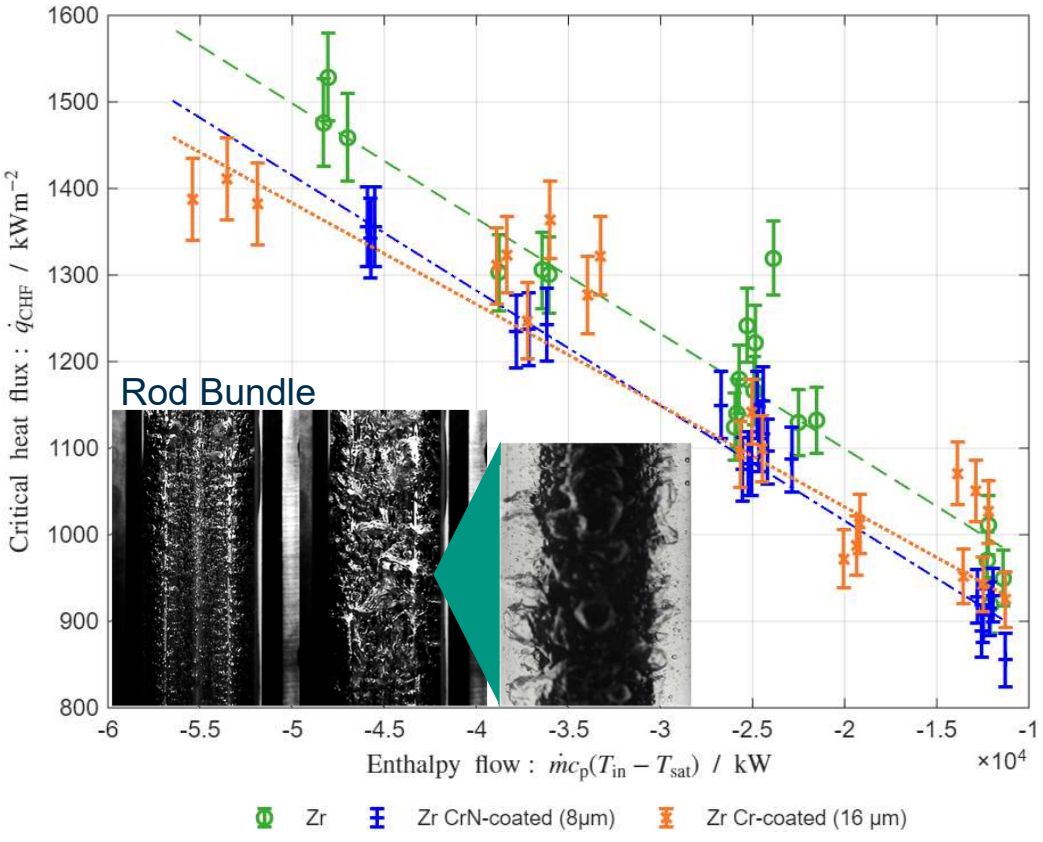

Adapted from Wefers et al., 2025b

Measurement & Image Analysis Method

- High-speed imaging: 5000 fps, region of interest near outlet
- Video: tracks bubble nucleation, growth, and departure
- Detection: custom code, tracks brightness changes (bubble flashes)
- Signal processing: adaptive filter (proper orthogonal decomposition, UNET) removes glare/noise
- Nucleation sites: counted by connected-pixel algorithm
- Frequency portraits: map bubble activity, visualize NSD and BDF
- All measurements synchronized with thermal-hydraulic data

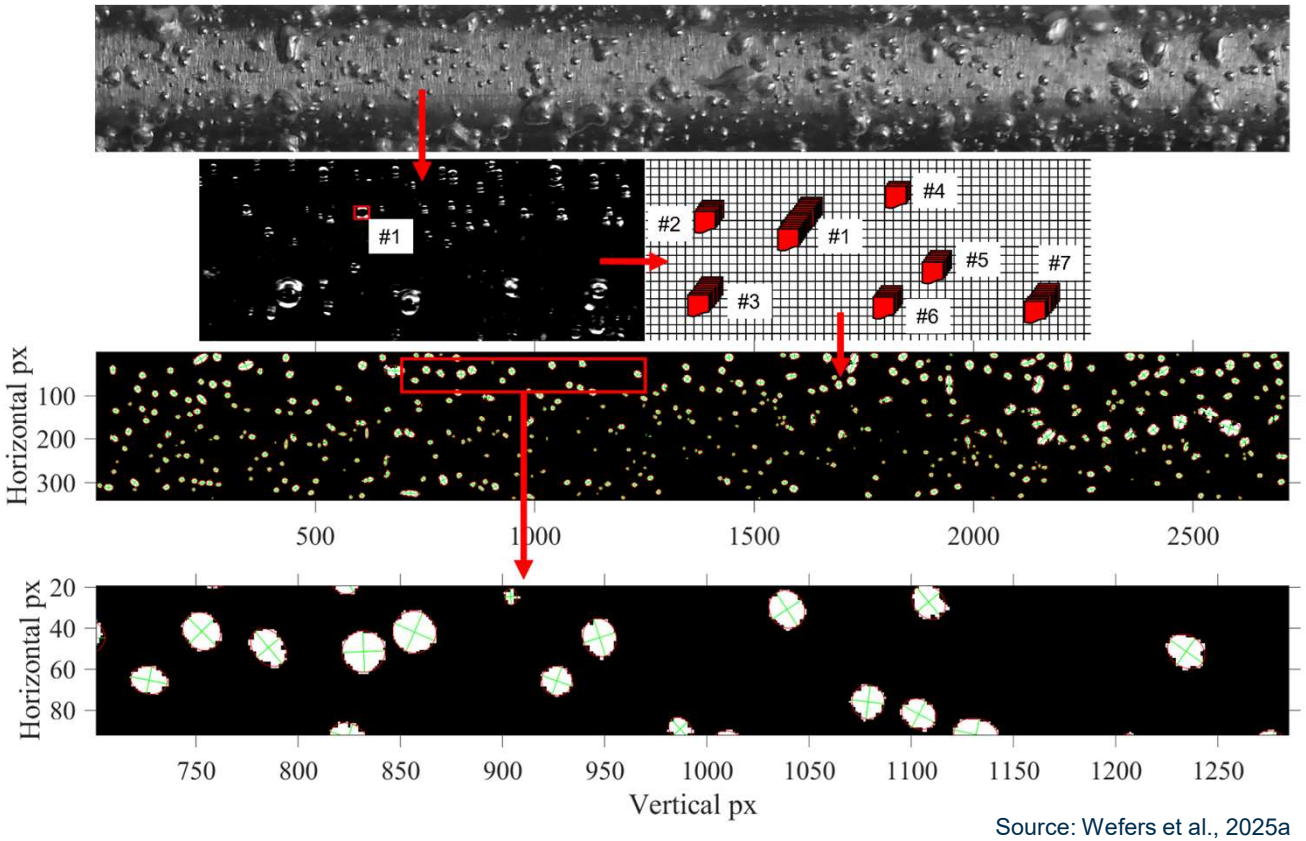

Source: Wefers et al., 2025a

Results NSD Images

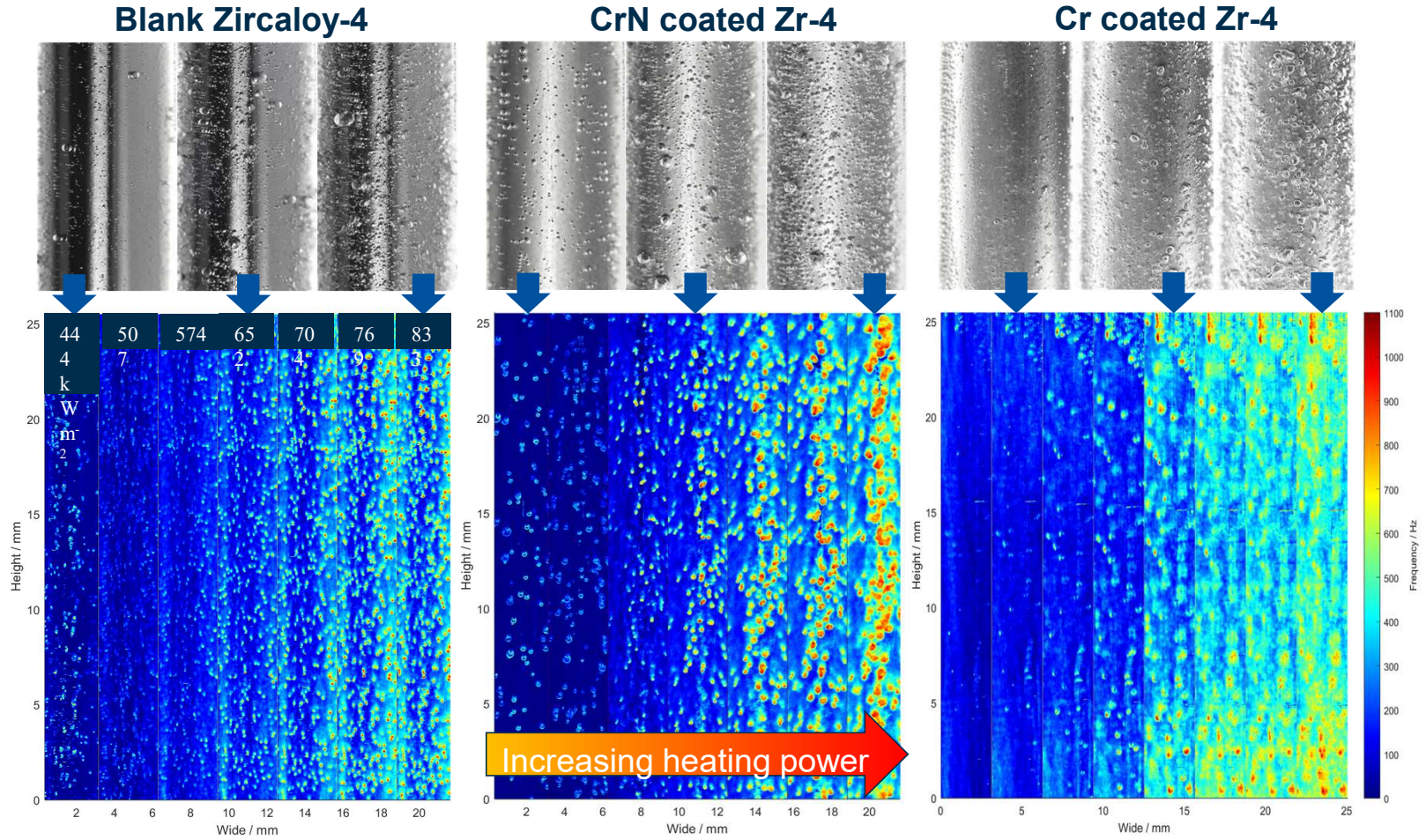

Series of 2D histograms of boiling activity (Glaire point scores) at different heating rates

Adapted from Wefers et al., 2025a

Key Observations

NSD:

- Zr-4: highest NSD overall
- Cr-coated: delayed NSD activation with heat flux
- CrN-coated: suppressed NSD at high flux (bubble merging)
- Lemmert & Chawla (1977) and Li et al. (2018) correlations capture overall trends but fail to separate material effects – issues with capturing the exact wall temperature

BDF:

- Similar across materials
- Frequency distribution of the Cr-coating is smaller than in the smoother cases
- Cole's (1967) correlation with Tolubinski & Kostanchuk (1970) departure diameter matches average values but misses frequency increase at higher flux

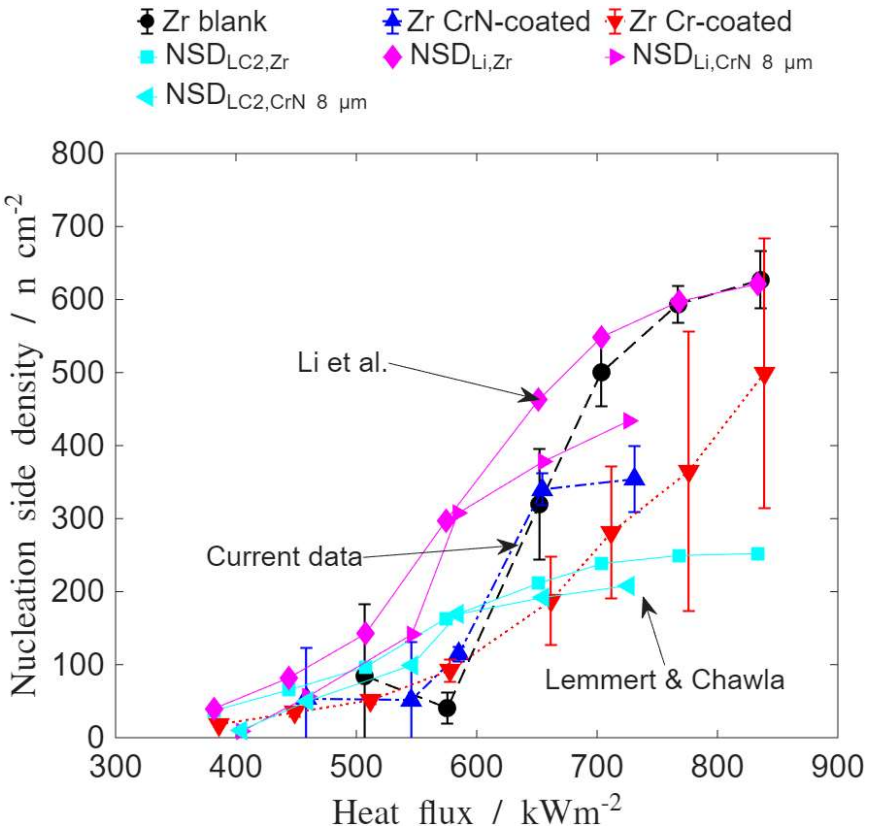

Adapted from Wefers et al., 2025a

Conclusion

Coating/roughness effects:

- Clear influence on NSD, less on BDF
- Models capture general trends but miss coating- and defect-driven effects
- Small effect on CHF trend: CHF scaling governed by flow conditions

Future & current work:

- Analyze bubble size and departure in more detail
- Advanced surface analysis (AFM, wettability vs. temperature)
- Wider range: pressure, mass flux, inlet temp, more coatings
- Integrate findings into CFD for better CHF prediction
- More materials and broader range for CHF experiments as well
- **ChroTemp – Post CHF Experiments**: oxidation and mechanical tests of the cladding tubes

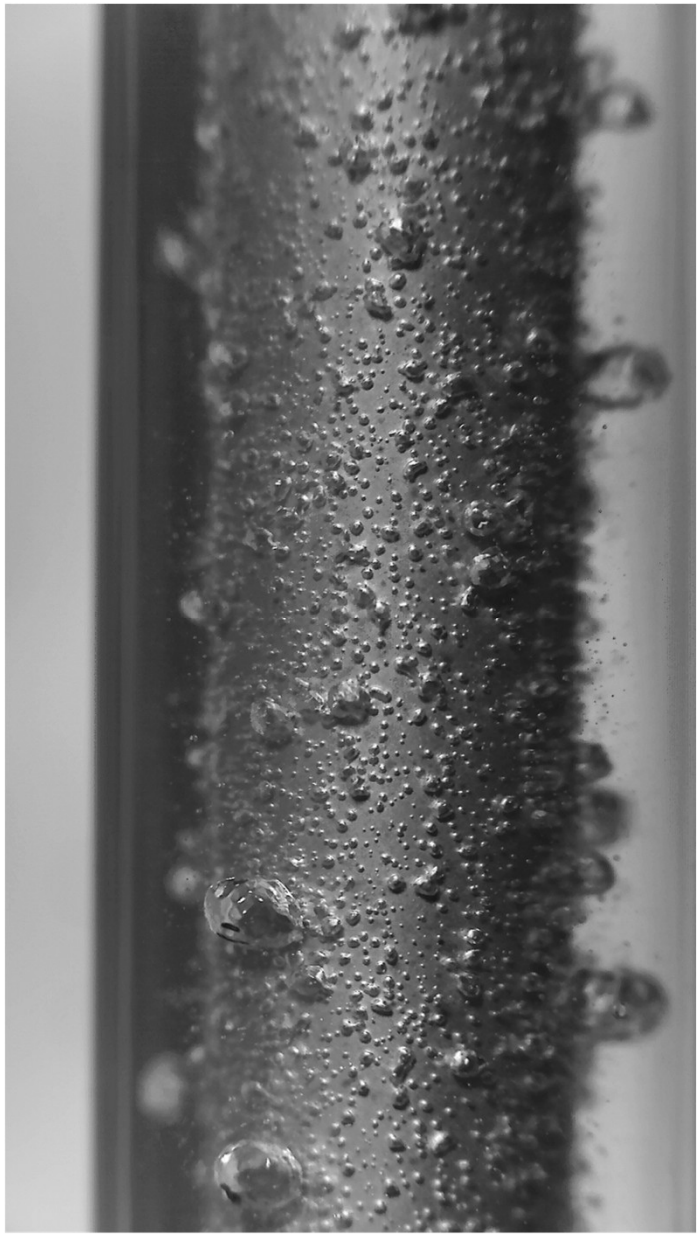

Acknowledgement

This work was supported by the OFFERR ChroTemp project as well as by the GRS as part of the KEK program (1501646).

The author gratefully acknowledge the experimental and technical support provided by staff at the Karlsruhe Institute of Technology and the Czech Technical University in Prague and Brno.

Supported by:

Federal Ministry
for the Environment, Climate Action,
Nature Conservation and Nuclear Safety

based on a decision of
the German Bundestag

Thank you for your attention!

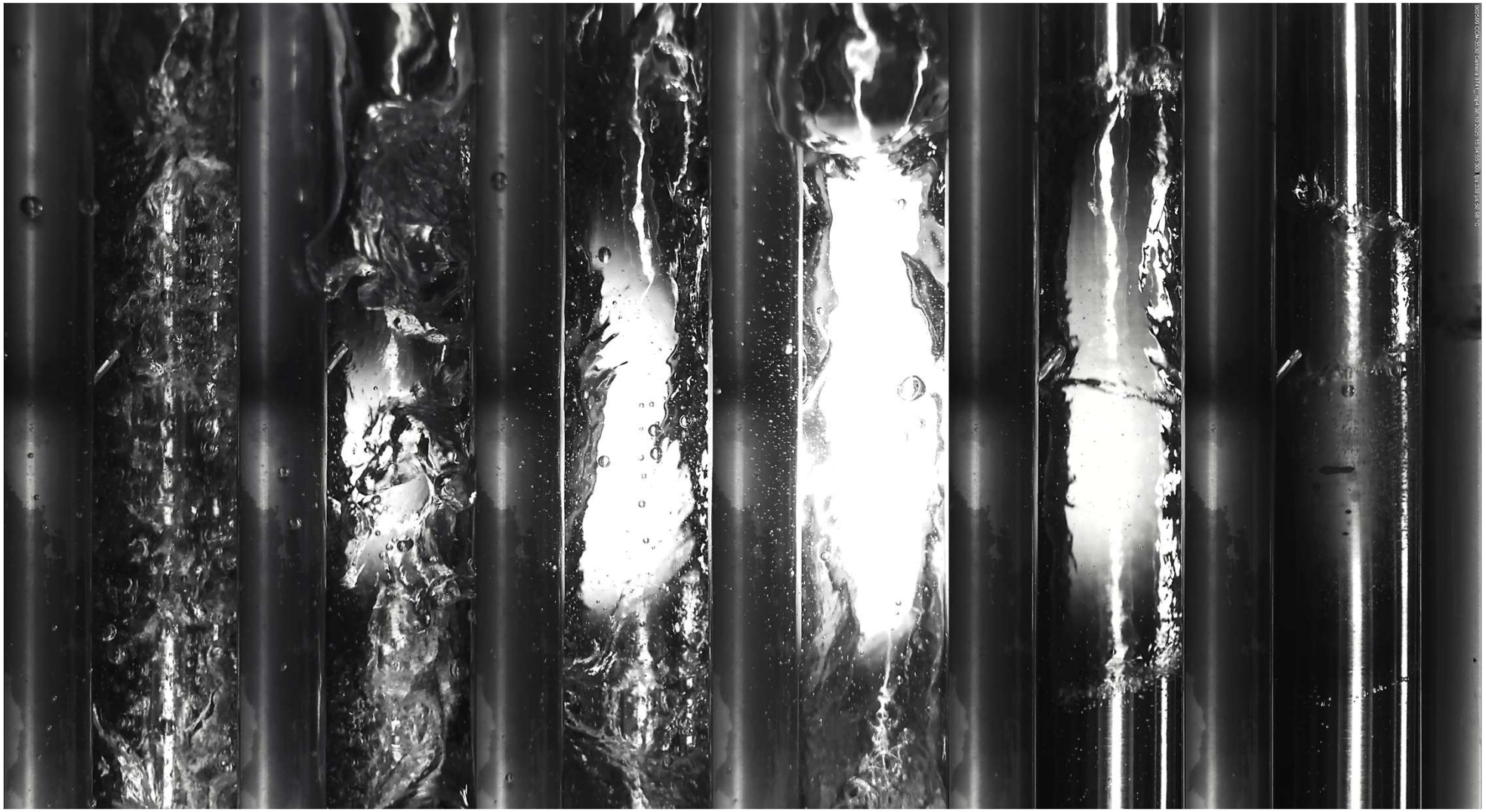

Image Sources

1. Wefers, N., Vlček, D., Heiler, W., & Gabriel, S. (2025). High-speed imaging and analysis of nucleation site density on nuclear fuel claddings. In Proceedings of NURETH-21 (Busan, South Korea, August 31–September 5).

2. Wefers, N., Vlček, D., Heiler, W., Gabriel, S., & Class, C. (2025). Influence of ATF cladding tube candidates on the critical heat flux in a vertical rod bundle during flow boiling of water at low pressure. Nuclear Technology, 1–18.

Mirco Große
KIT

Update of the KIT contributions to the SCORPION project

A certain porosity is needed in the fiber range of SiC_f/SiC ceramic matrix compounds to ensure the pseudo-plastic deformation behavior. On the other hand, porosity increases the reacting surface and enhances chemical reactions. The formation of protective SiO_2 scales at SiC can close open porosity and with it neglect the negative effect on the chemical reaction kinetics.

High temperature oxidation tests (1600°C for 1 h) in different atmospheres were performed comparing compact and porous SiC. The tests were performed in steam, hydrogen + steam, oxygen and air atmospheres. The porous and compact samples had 37% and 97%, respectively, of the theoretical density of SiC. The pores had sizes between 0.5 and 5 µm.

The mass gain differs between the compact and the porous sample by up to three orders of magnitude. Hints for closing open porosity were only found for the reaction in oxygen. Surprising were the differences between the reaction in oxygen and in air. The reaction in air is stronger than the one in oxygen for both compact and the porous samples. Reasons for this effect can be a local reduction of the oxygen partial pressure in the pores and with it a change from passive to active oxidation and/or a chemical reaction of SiO_2 with nitrogen forming Si_2N_2O and consuming the protective SiO_2 scale.

It can be concluded from these results that no closing of pores with sizes in the order of magnitude of few micrometres would occur during severe nuclear accidents. Open porosity must be prevented for cladding tubes made of SiC_f/SiC ceramic matrix compounds.

Update of the KIT contributions to the SCORPION project

Mirco Grosse, Martin Steinbrück, Tobias Fey, Konstantina Lambrinou

30. Intern. QUENCH Workshop,
KIT Campus North, 2025/12/18

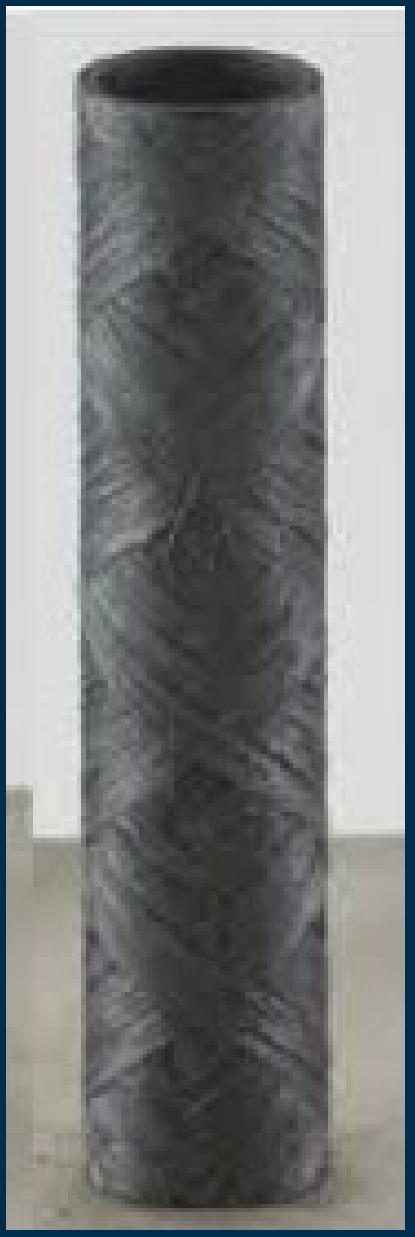

Introduction

Porosity in the fiber range is needed for the quasi ductility.

Open porosity results in an increase of the reacting surface.

Does the formation of SiO_2 close the open porosity?

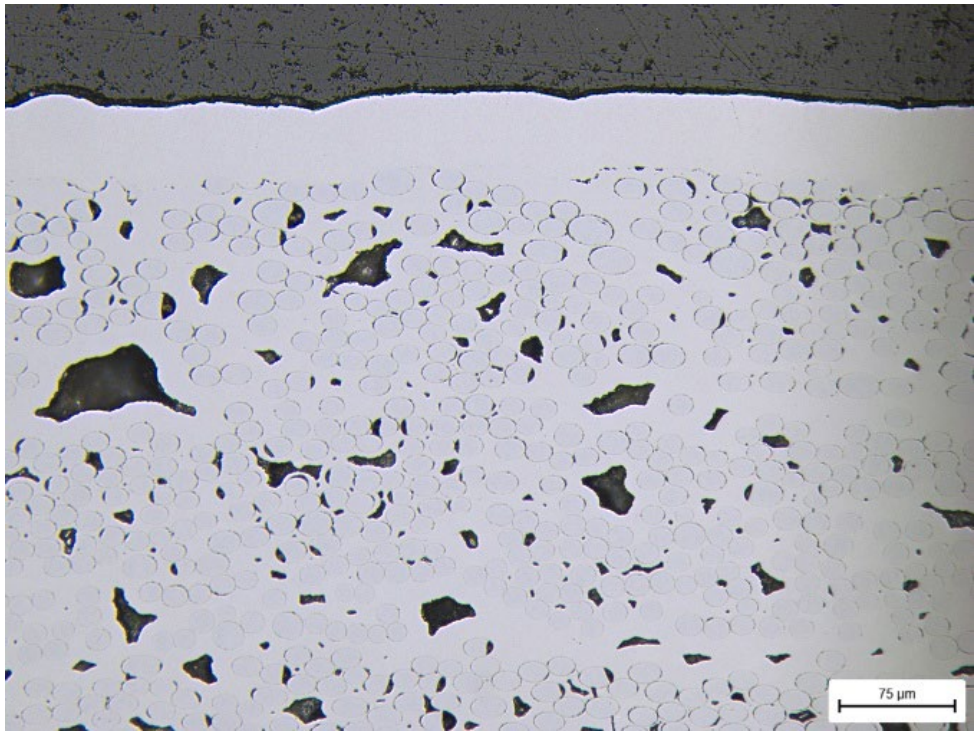

Introduction

- $SiC(s) + 2H_2O(aq,g) = SiO_2(s) + CH_4(g)$
- $SiC(s) + 2H_2O(aq,g) = SiO_2(s) + 2H_2(g) + C(s)$
- $SiC(s) + 3H_2O(aq,g) = SiO_2(s) + 3H_2(g) + CO(g)$ **passive oxidation**
- **$SiC(s) + 4H_2O(aq,g) = SiO_2(s) + 4H_2(g) + CO_2(g)$**
- **$SiO_2(s) + 2H_2O(aq) = Si(OH)_4(aq)$**
- $SiC(s) + H_2O(g) = SiO(g) + CO(g)$ (for low p_{O2}) **active oxidation**
- **$2SiO_2(s,l) + SiC(s) = 3SiO(g) + CO(g)$** (at VHT)

Introduction

$3Si(s) + 2N_2(g) = Si_3N_4(s)$

$SiO_2(s) + Si_3N_4(s) = 2Si_2N_2O(s)$ consumption of the protective

$2SiO_2(s) + N_2(g) = 2Si_2N_2O(s) + 3/2O_2$ SiO_2 scale

$3Si_2N_2O(s) + N_2(g) = 2Si_eN_4(s) + 3/2O_2$

$3Si_2N_2O(s) = 3SiO(g) + N2 + Si_3N_4(s)$ relevant at T > 1700°C

Materials and test conditions

	compact SiC	Porous SiC
Origin	EKasic®	FAU Erlangen
Density [g/cm^3]	3.17 ± 0.050	1.19 ± 0.055
Percentage of theoretical density	98.6 ± 1.6 %	37.1 ± 1.7 %

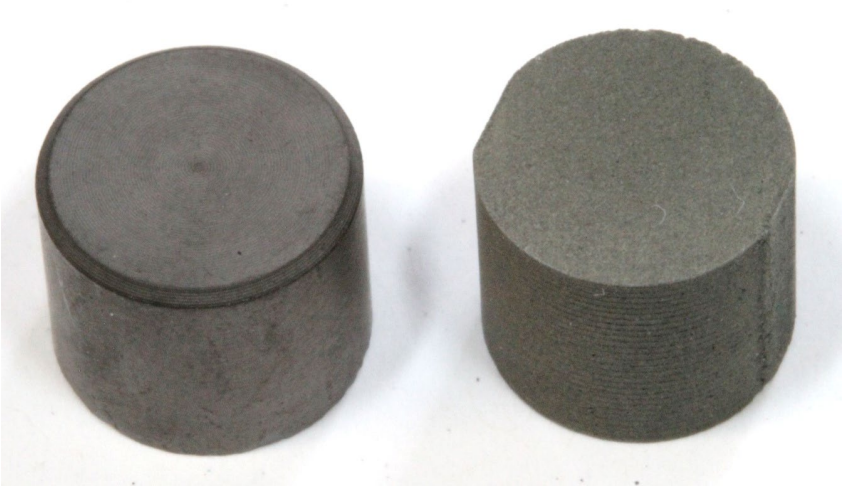

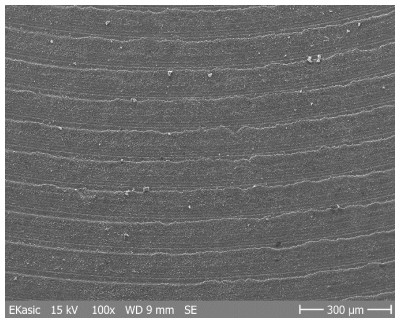

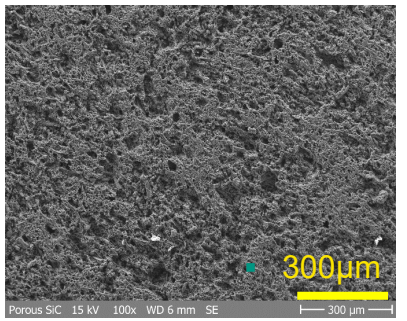

Atmospheres:

- Steam (passive oxidation)
- H_2 + steam (active oxidation)
- Air (passive oxidation?)
- Oxygen (passive oxidation)

Materials and test conditions

Transition of passive to active oxidation in the range of the molar flux ratio H_2/H_2O of 1 .. 5.

High hydrogen concentrations can occur locally in cracks or pores.

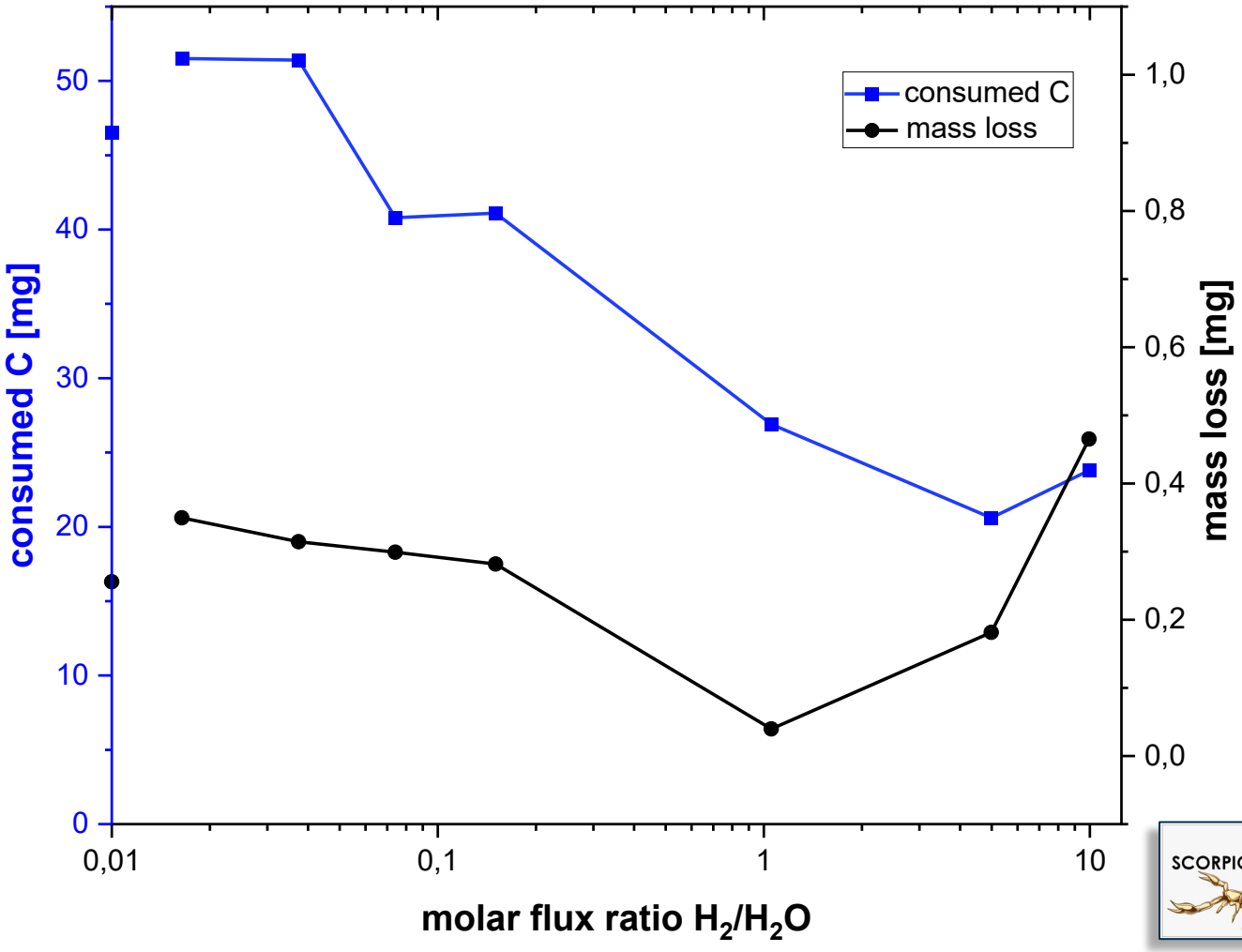

Materials and test conditions

Total gas flows were kept constant (65 l/h)

- 20 l/h Ar + 36 g/h (~45 l/h) steam
- 20 l/h Ar + 38 g/h H_2 + 6 g/h (~7 l/h) steam
- 20 l/h Ar + 45 l/h air
- 20 l/h Ar + 45 l/h O_2

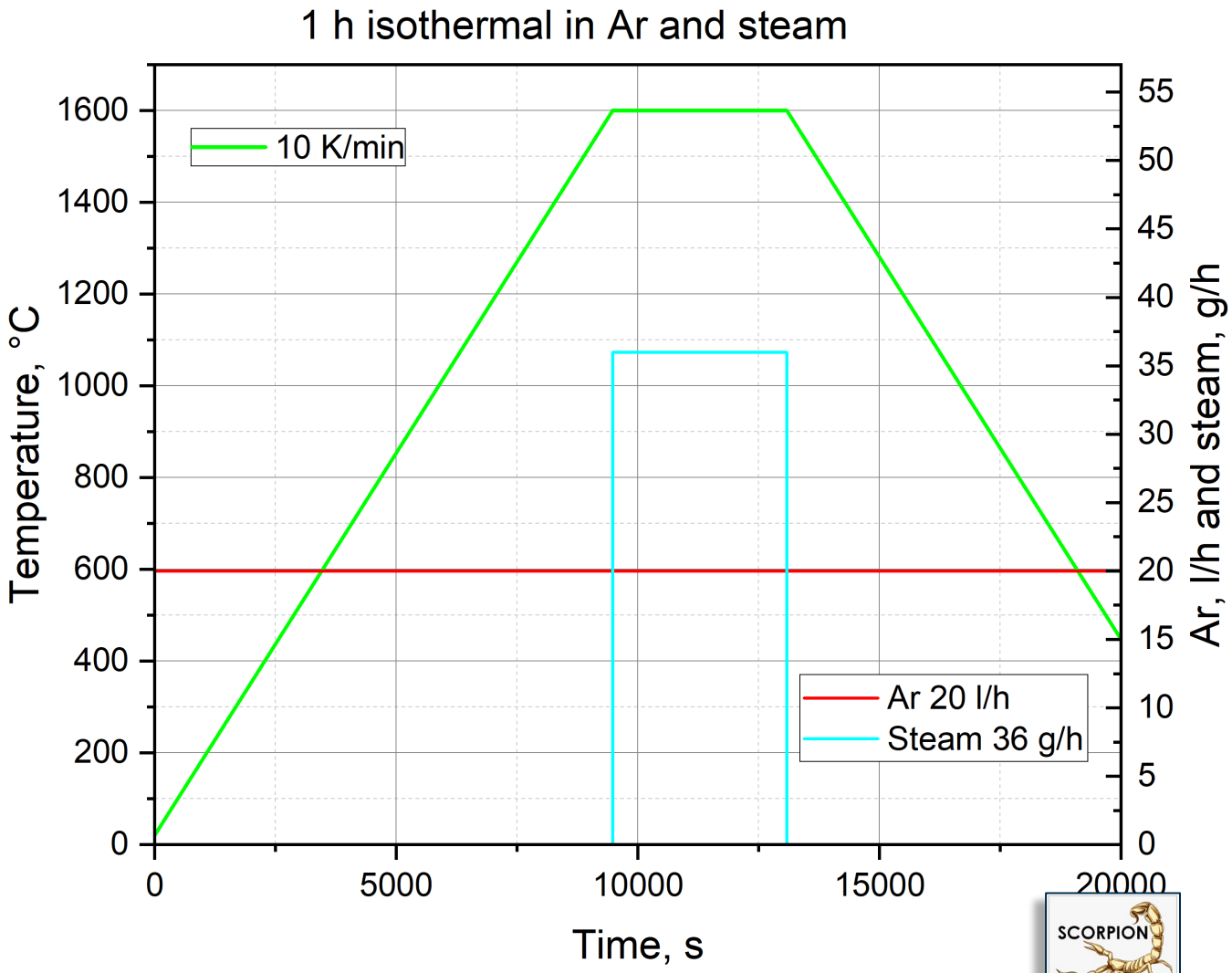

Results

Sample	steam	H_2 + steam	air	oxygen
compact			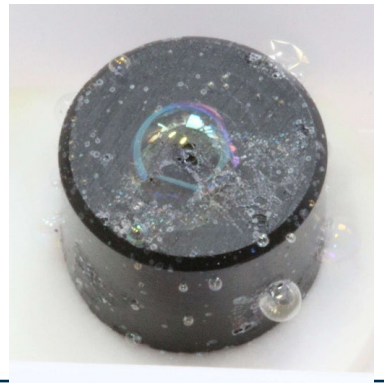	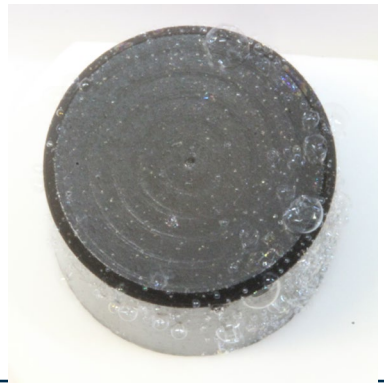
porous			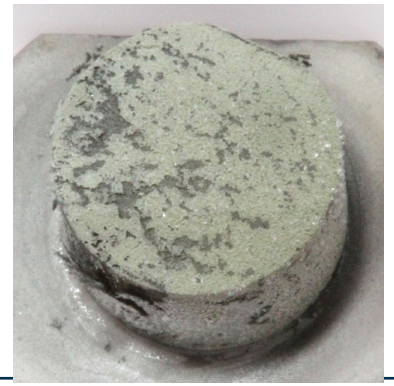	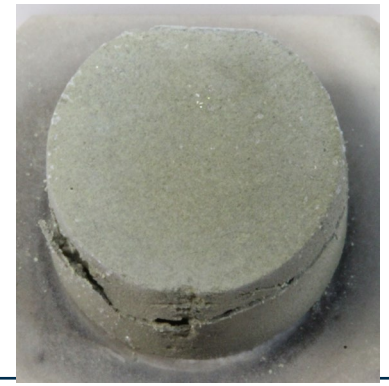

Results

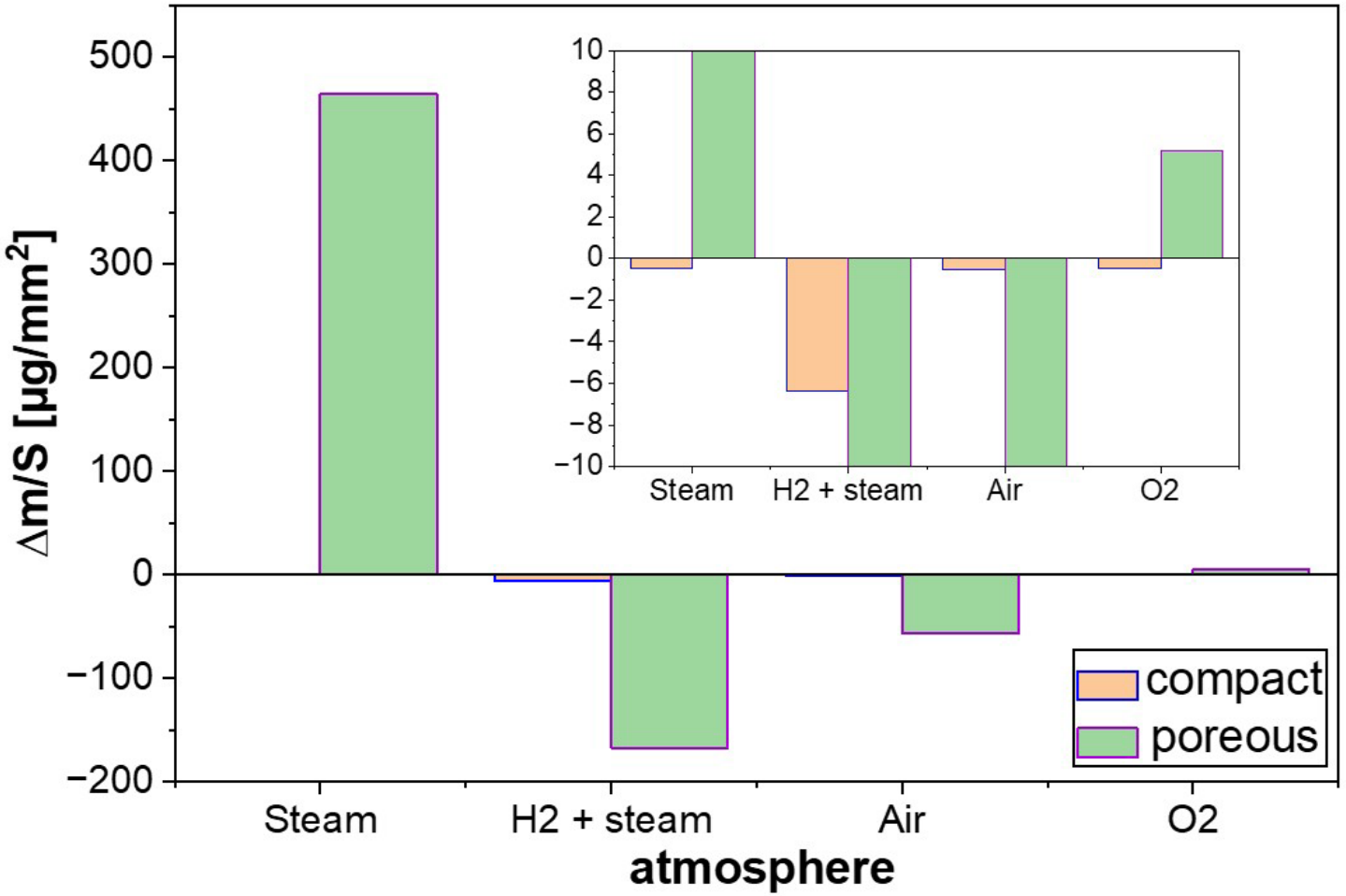

Orders of magnitude higher mass changes in the porous material

Only mass lost of the compact material

Mass gain of the porous material in steam and oxygen

Mass change is higher in steam than in hydrogen steam for the compact material

Effect of nitrogen:

- chemical reaction
- blockage of the oxygen transport into the pores

Results

	Compact SiC	Porous SiC
steam	-0.49 g/m^2	464.3 g/m^2
H_2 + steam	-6.36 g/m^2	-157.3 g/m^2
air	-0.54 g/m^2	-57.2 g/m^2
oxygen	-0.49 g/m^2	6.2 g/m^2

- Nearly the same mass change of the compact samples but strong differences in the mass changes of the porous samples in steam, air and oxygen.
- Higher mass loss in air than in steam or oxygen
  - Reduction of the oxygen partial pressure by the nitrogen resulting in active oxidation?
  - Chemical interactions with nitrogen? Formation of Si_3N_4 or Si_2N_2O?
- Closing of open porosity in oxygen but not in steam.

Results

Gas release during reaction in steam

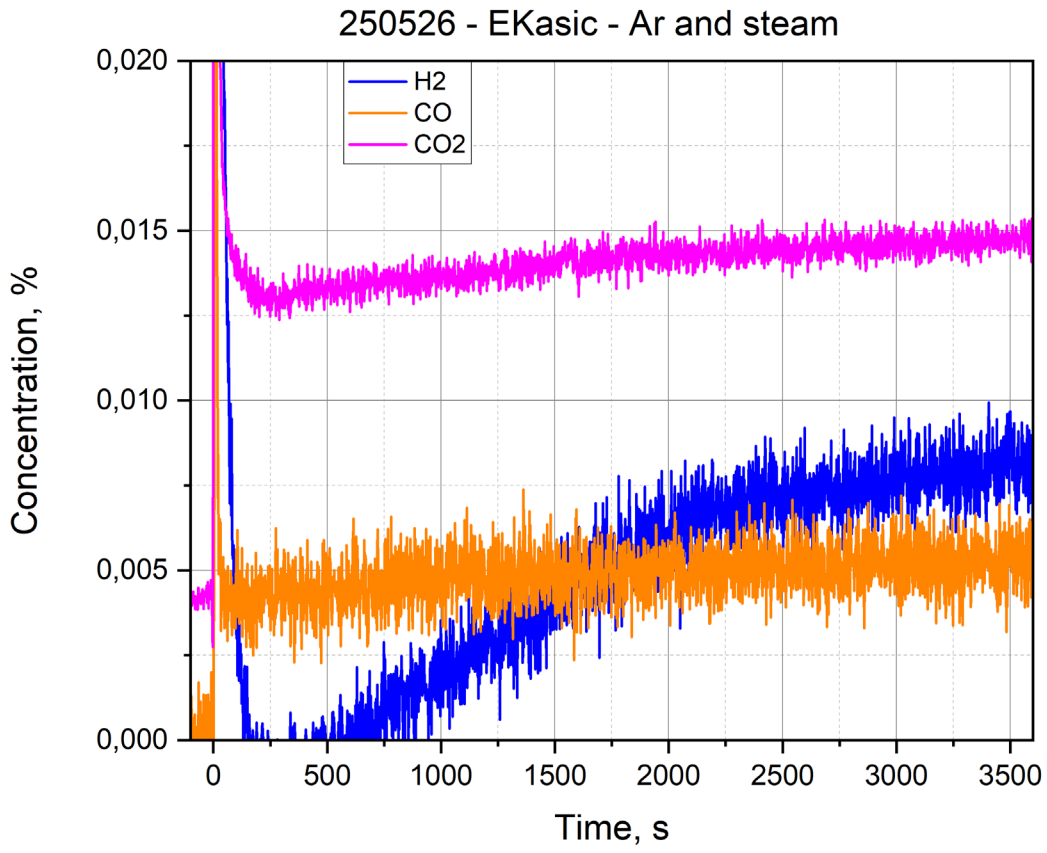

Compact material

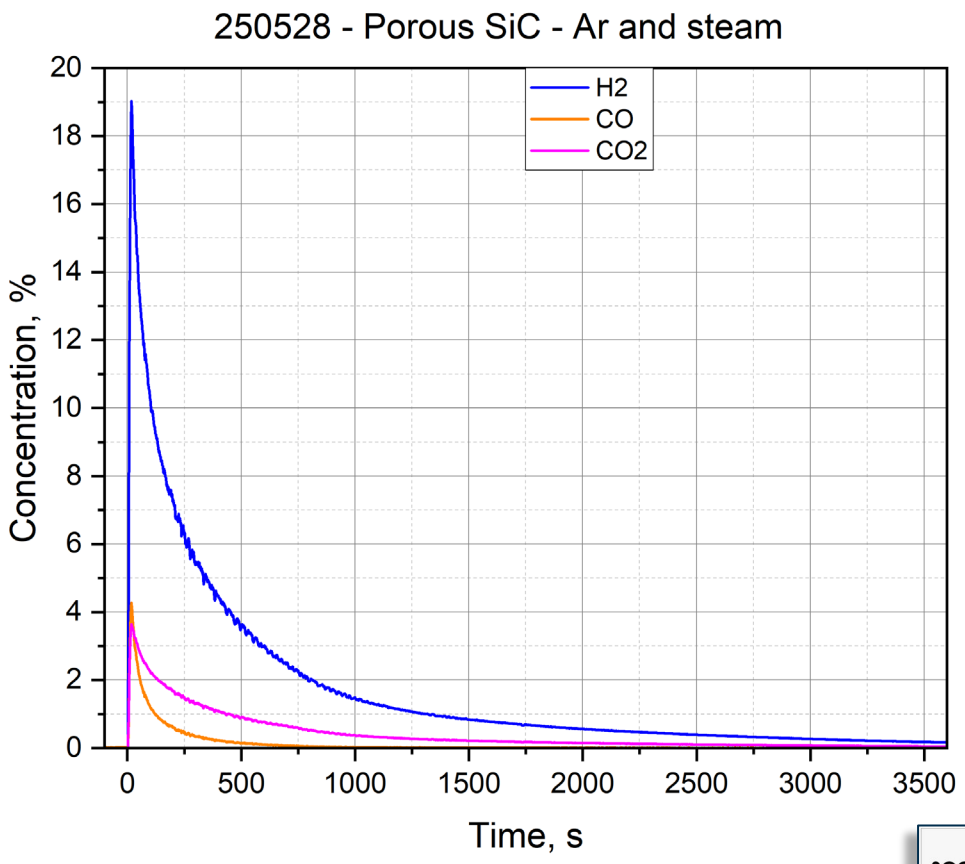

porous material

Results

Gas release during reaction in hydrogen + steam

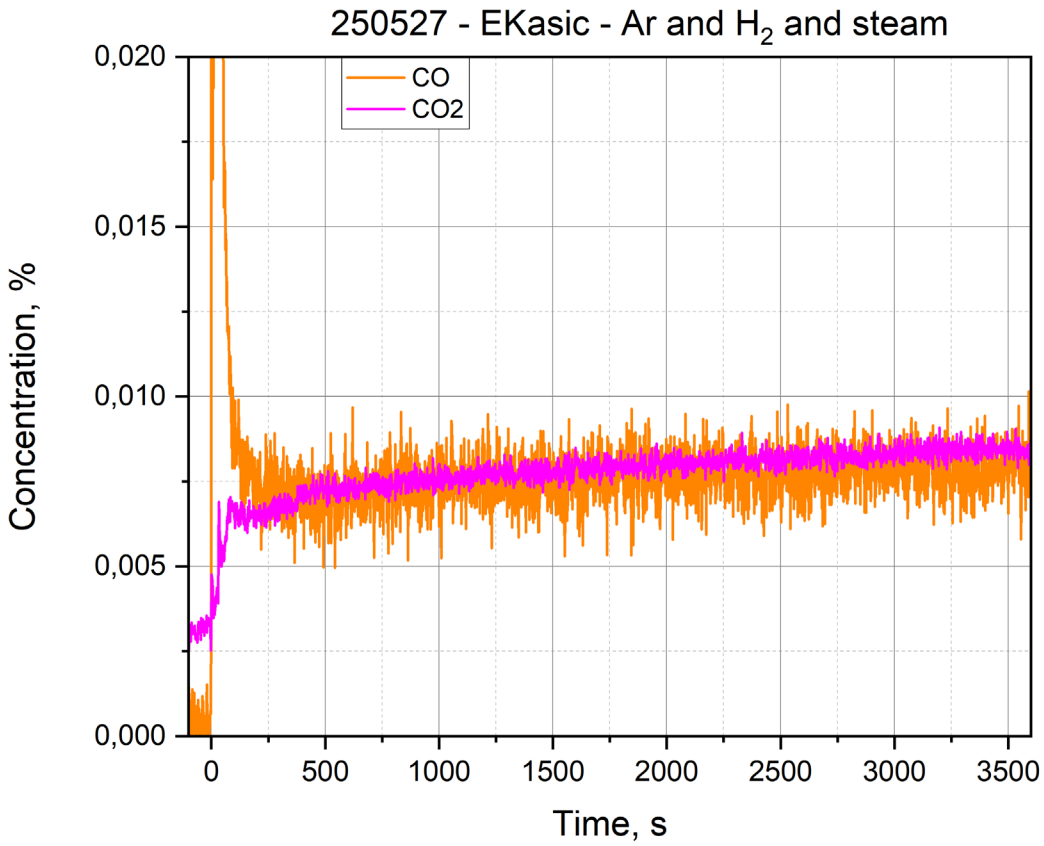

Compact material

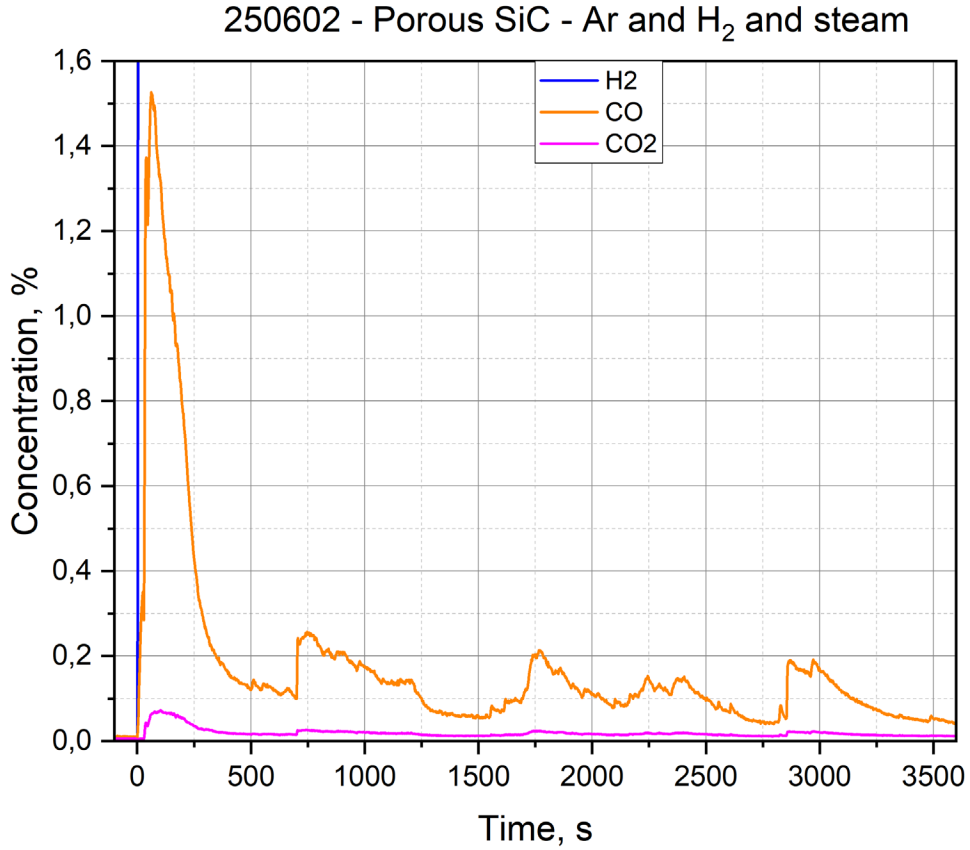

porous material

Results

Gas release during reaction in air

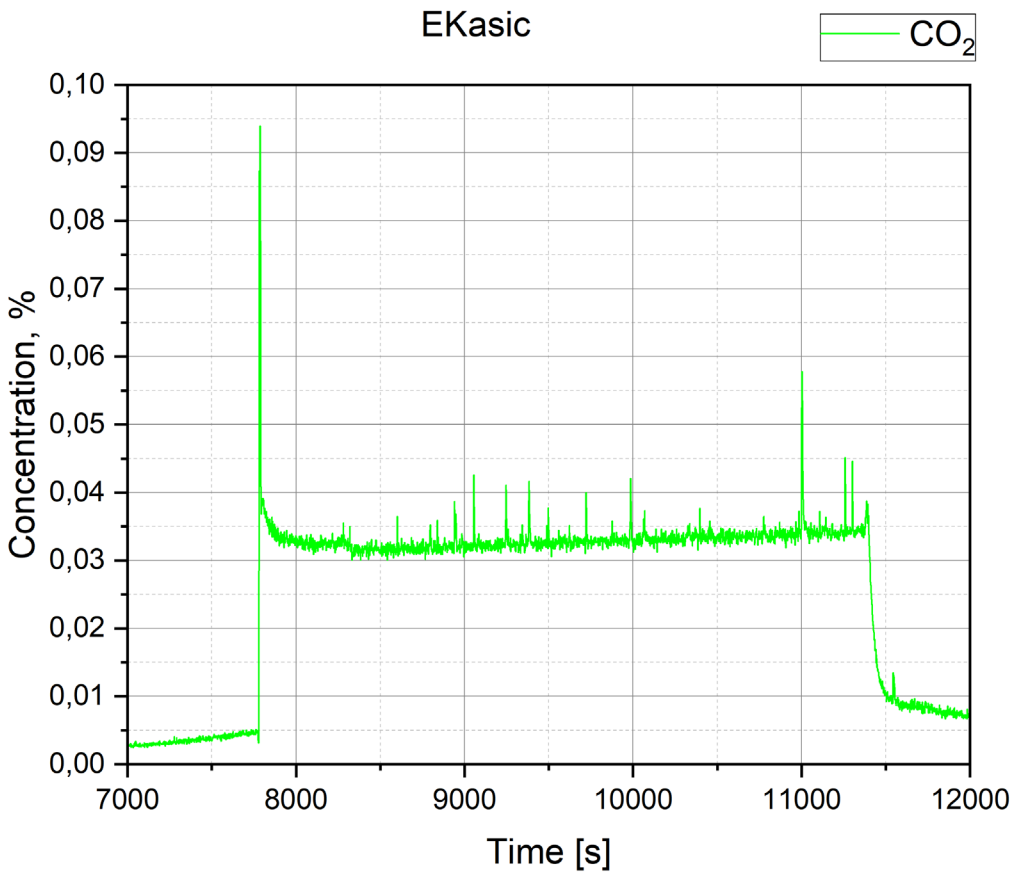

Compact material

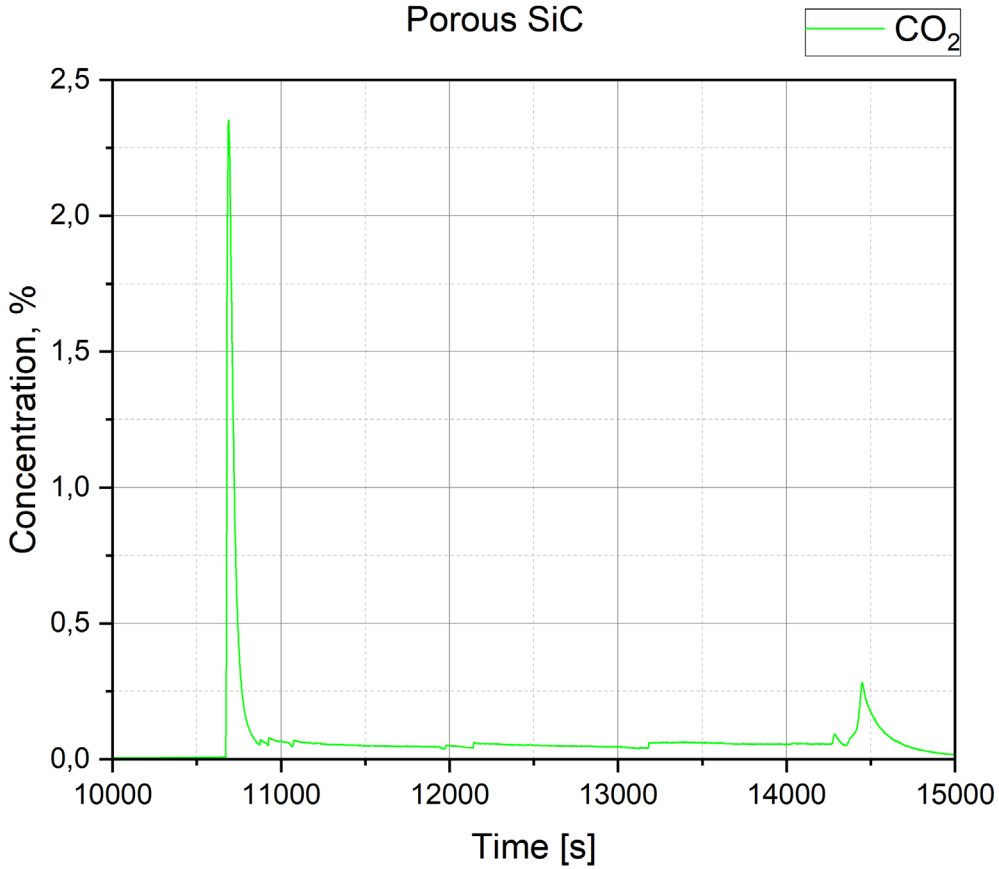

porous material

Results

Gas release during reaction in air

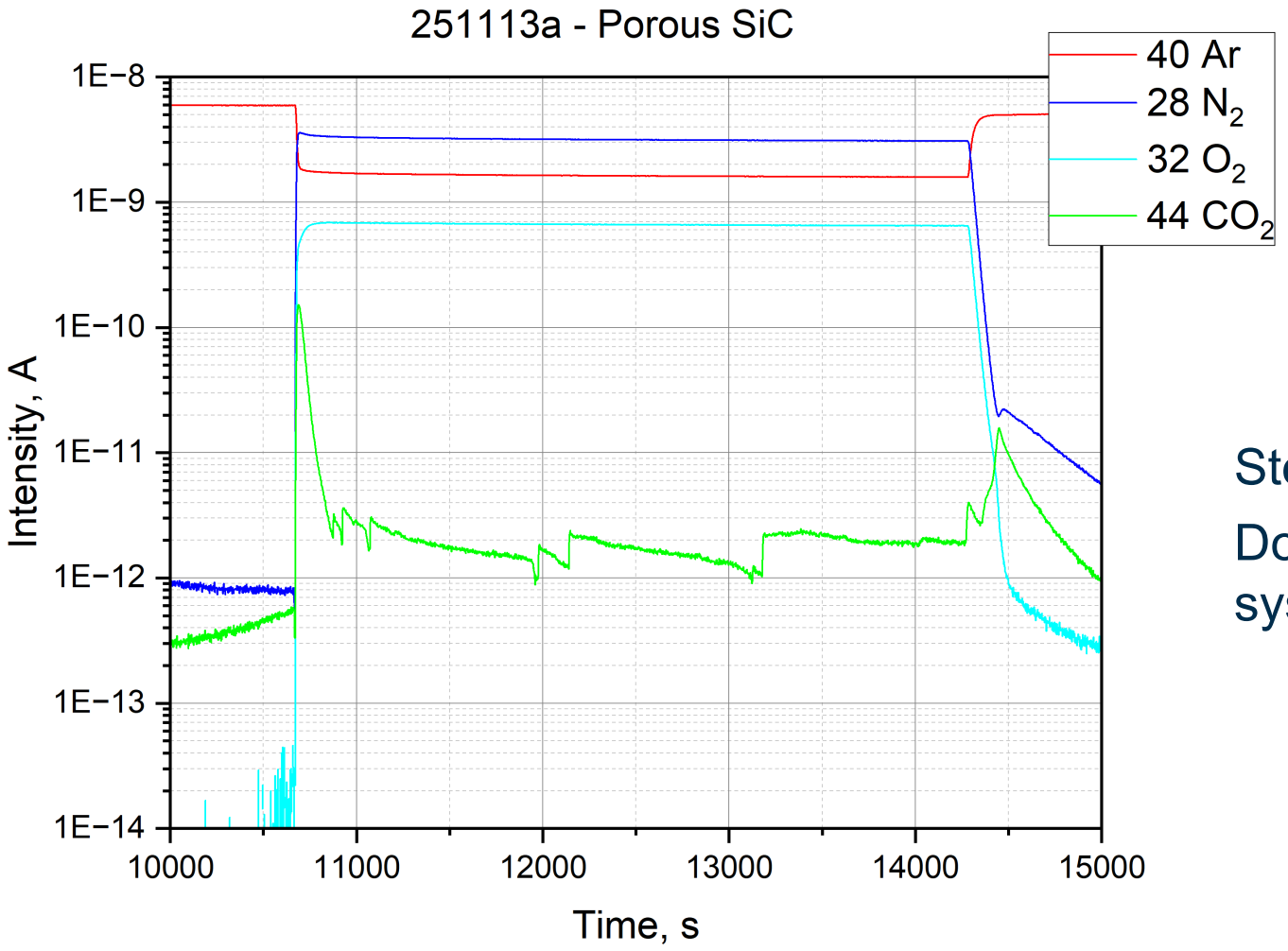

Steps in the CO_2 release

Does the oxidation opens new pore systems below the surface?

Results

Gas release during reaction in oxygen

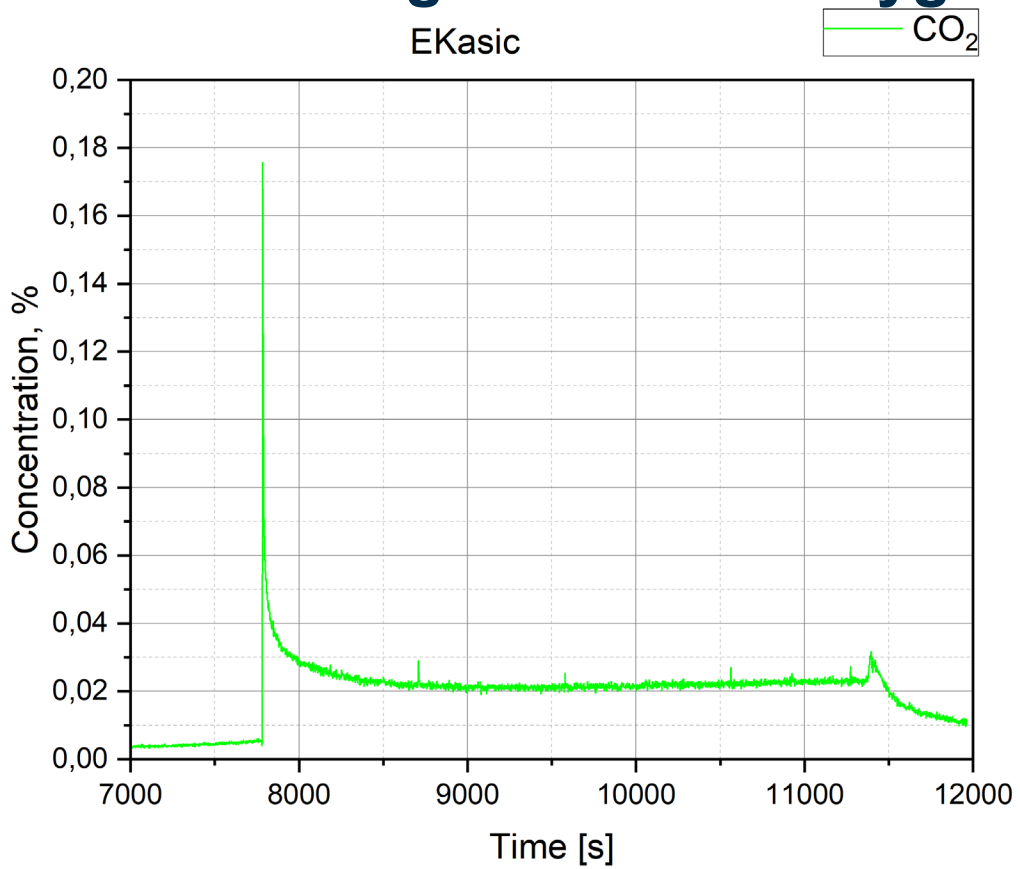

Compact material

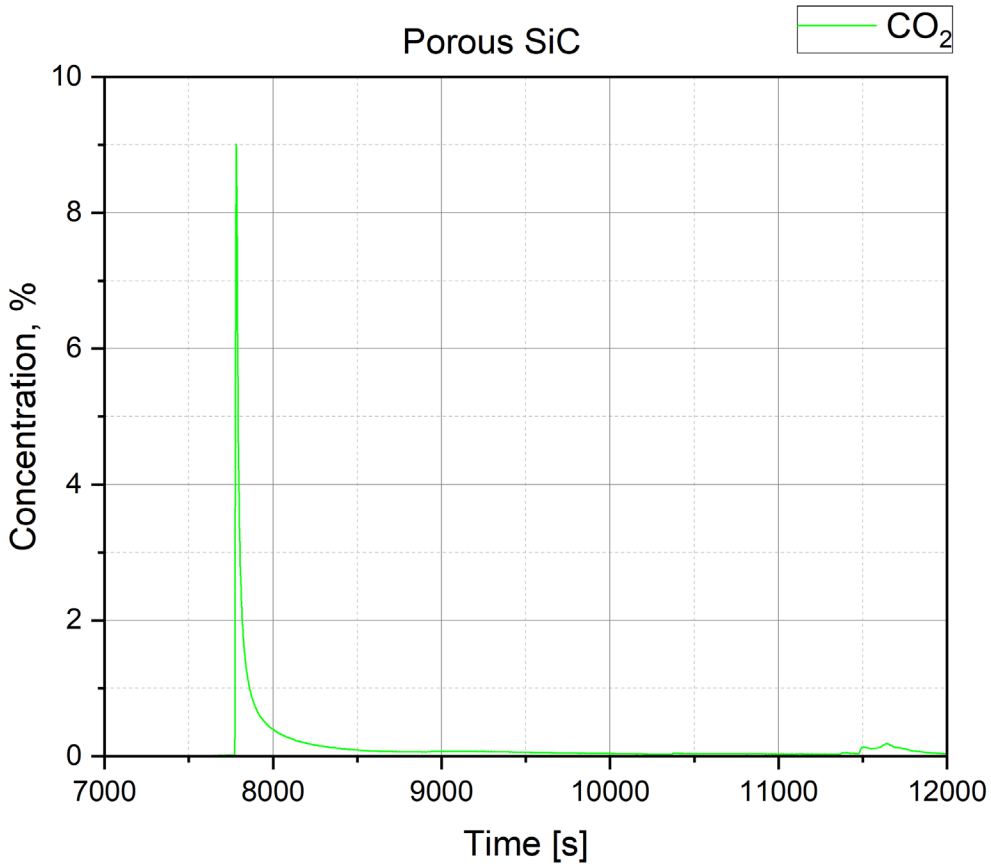

porous material

Conclusions and Next Steps

- Open porosity results in a much higher reaction rate because of the larger reacting surface.
- The open porosity is not closed in steam but in oxygen. The reason is the formation of volatile $Si(OH)_4$ in steam.
- The mass loss is in air higher than in steam and oxygen. Reasons can be the reduction of the oxygen partial pressure in air and/or the formation of Si_3N_4 or Si_2N_2O.

Prevent contact of porous part of the CMC with steam, oxygen or air!

Next step: Corrosion and high temperature oxidation tests with coated SiC CMC tube segments.

Acknowledgement

Many thanks to Ulrike Stegmaier for performing the tests and the post-test analysises.

The SCORPION project has received funding from the Euratom Research and Training Program 2021-2025 under Grant Agreement No 101059511.

The authors thank all project partners for their contributions and fruitful discussions.

Thank you for your attention!

Update of the KIT contributions to the SCORPION project

Ulrike Stegmaier, Mirco Grosse, Martin Steinbrück, Tobias Fey, Konstentza Lambrinou

30. Intern. QUENCH Workshop,
KIT Campus North, 2025/12/18

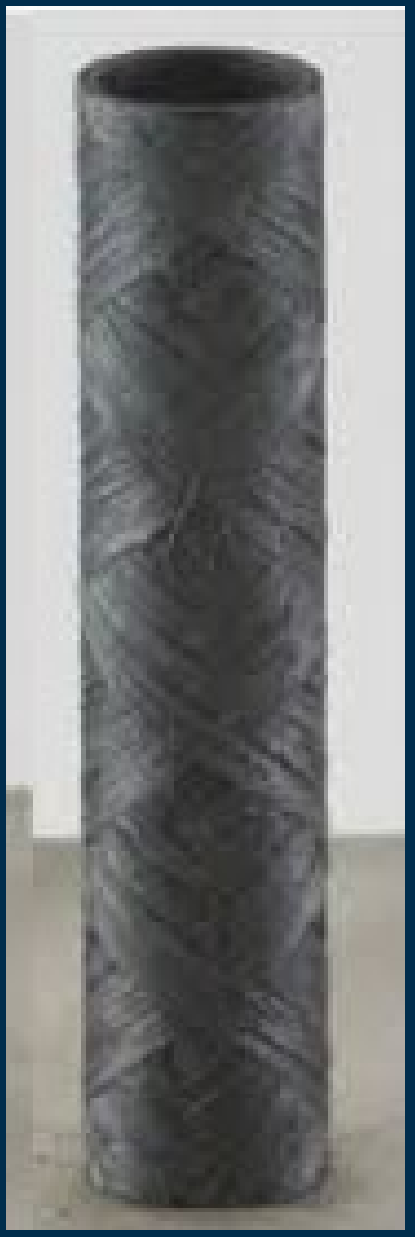

Participants of the 30th International QUENCH Workshop
16 - 18 December 2025, KIT, Germany

Family Name	First Name	Institution	Country	e-mail
Aragón	Pau	EC - JRC	Germany	pau.aragon-grabiel@ec.europa.eu
Bachurina	Diana	KIT	Germany	diana.bachurina@kit.edu
Bertsch	Johannes	PSI	Switzerland	johannes.bertsch@psi.ch
Bochtler	Peter Ulrich	Federal Office for the Safety of Nuclear Waste Management (BASE)	Germany	peter.bochtler@base.bund.de
Bottomley	David	ex-JRC-Karlsruhe	Germany	dboksb3@email.com
Boucek	Vaclav	UJP Praha a.s.	Czech Republic	boucek@ujp.cz
Bourret	Victor	CEA	France	victor.bourret@cea.fr
Brachet	Jean-Christophe	CEA	France	jean-christophe.brachet@cea.fr
Campbell	Shawn	US NRC	USA	shawn.campbell@nrc.gov
Cazado	Mauricio Exequiel	KIT	Germany	mauricio.cazado@kit.edu
Charbal	Ali	CEA	France	ali.charbal@cea.fr
Choi	Yong-Seok	Korea Atomic Energy Research Institute	Korea	cys@kaeri.re.kr
Dunbar	Cole	University of Wisconsin-Madison	USA	cjdunbar@wisc.edu
Fargette	Andre	Framatome	France	andre.fargette@framatome.com
Farkas	Róbert	HUN-REN Centre for Energy Research	Hungary	robert.farkas@ek.hun-ren.hu
Frederick	Katerina	Westinghouse Electric Company	United States	katerina.frederick@westinghouse.com
Gabriel	Stephan	KIT	Germany	stephan.gabriel@kit.edu
Gabrielli	Fabrizio	KIT	Germany	fabrizio.gabrielli@kit.edu
Gerža	Jakub	UJP PRAHA a.s.	Czech Republic	jakub.gerza@centrum.cz
Goto	Shota	Nagoya University	Japan	goto.shota.e8@s.mail.nagoya-u.ac.jp
Grosse	Mirco	KIT	Germany	mirco.grosse@kit.edu
Hollands	Thorsten	GRS	Germany	thorsten.hollands@grs.de

Participants of the 30th International QUENCH Workshop
16 - 18 December 2025, KIT, Germany

Family Name	First Name	Institution	Country	e-mail
Howell	Jutta	KIT	Germany	jutta.howell@kit.edu
Hózer	Zoltán	HUN-REN Centre for Energy Research	Hungary	hozer.zoltan@ek.hun-ren.hu
Jaramillo	Diego	EC - JRC	Germany	diego.jaramillo-sierra@ec.europa.eu
Kaliatka	Tadas	Lithuanian Energy Institute	Lithuania	tadas.kaliatka@lei.lt
Khalil	Sarah	Alexandria University Egypt	Egypt	SY.KHALIL@gmail.com
Khaperskaia	Anzhelika	International Atomic Energy Agency	Austria	A.Khaperskaia@iaea.org
Kim	Hyochan	Korea Atomic Energy Research Institute	South Korea	hyochankim@kaeri.re.kr
Kim	Dong-Joo	Korea Atomic Energy Research Institute	Republic of Korea	djkim@kaeri.re.kr
Kim	Chaerin	KEPCO Nuclear Fuel	Korea	chaerin@knfc.co.kr
Kolesnik	Mikhail	KIT	Germany	mikhail.kolesnik@kit.edu
Kpemou	Apou Martial	ASNR	France	apou-martial.kpemou@asnr.fr
Krejci	Jakub	UJP PRAHA a.s.	Czech Republic	krejci@ujp.cz
Lee	Chungyong	KEPCO NF	Rep. of Korea	cylee@knfc.co.kr
Lee	Sungyong	KEPCO Nuclear Fuel	Korea	leesy@knfc.co.kr
Lee	Dong-Hwa	Korea Atomic Energy Research Institute	Republic of Korea	donghwalee@kaeri.re.kr
Liu	Tong	Shanghai Jiao Tong University	China	tongliu@sjtu.edu.cn
Lovasz	Liviusz	GRS	Germany	liviusz.lovasz@grs.de
Moch	Jürgen	KIT	Germany	juergen.moch@kit.edu
Moon	Sang Ki	Korea Atomic Energy Research Institute	Republic of Korea	skmoon@kaeri.re.kr
Nakamura	Kinya	CRIEPI	Japan	kinya@criepi.denken.or.jp
Nowak	Brock	Queen's University	Canada	brock.nowak@queensu.ca
Nyman	Johan	Westinghouse Electric Sweden AB	Sweden	johan.nyman@westinghouse.com

Participants of the 30th International QUENCH Workshop
16 - 18 December 2025, KIT, Germany

Family Name	First Name	Institution	Country	e-mail
Pericas	Raimon	Innovative System Sofware	USA	raipercas@yahoo.es
Peters	Ursula	KIT	Germany	Ursula.Peters@kit.edu
Popp	Manfred		Germany	
Probert	Allison	University of Florida	USA	robertsallison@ufl.edu
Rezchikova	Aleksandra	GRS	Germany	aleksandra.rezchikova@grs.de
Rössger	Conrado	KIT	Germany	conrado.roessger@kit.edu
Sanchez Espinoza	Victor Hugo	KIT	Germany	victor.sanchez@kit.edu
Sappl	Jonathan	GRS	Germany	jonathan.sappl@grs.de
Sawarn	Tapan Kumar	Bhabha Atomic Research Centre	India	sawarn@barc.gov.in
Schaefer	Daniel Auri	KIT	Germany	daniel.schaefer2@kit.edu
Schubert	Arndt	EC - JRC	Germany	Arndt.Schubert@ec.europa.eu
Ševeček	Martin	Czech Technical University in Prague	Czech Republic	martin.sevecek@fjfi.cvut.cz
Shepherd	Daniel	NEA	France	daniel.shepherd@oecd-nea.org
Stahlberg	Gregor T.	Ruhr-Universitaet Bochum	Germany	stahlberg@pss.rub.de
Stegmaier	Ulrike	KIT	Germany	ulrike.stegmaier@kit.edu
Steinbock	Lothar	private	Germany	lothar@sibex.de
Steinbrück	Martin	KIT	Germany	martin.steinbrueck@kit.edu
Stuckert	Juri	KIT	Germany	juri.stuckert@kit.edu
Tang	Chongchong	KIT	Germany	chongchong.tang@kit.edu
Tromm	Walter	KIT	Germany	walter.tromm@kit.edu
Ver	Nora	HUN-REN Centre for Energy Research	Hungary	ver.nora@ek.hun-ren.hu
Wang	Shijie	Shanghai Jiao Tong University	China	pengpeng520@sjtu.edu.cn

Participants of the 30th International QUENCH Workshop
16 - 18 December 2025, KIT, Germany

Family Name	First Name	Institution	Country	e-mail
Wefers	Nicolas	KIT	Germany	nicolas.wefers@kit.edu


KIT
FORSCHUNG
LEHRE
INNOVATION


FORSCHUNG
LEHRE
INNOVATION
KIT
Air ingress experiments / QUENCH-16 (2011)
• EU LACOMECO project
• AEKI proposal
• Slow oxidation and nitriding of Zr in air
• Final quench close to melting point
• Participation of Hungarian experts at the test












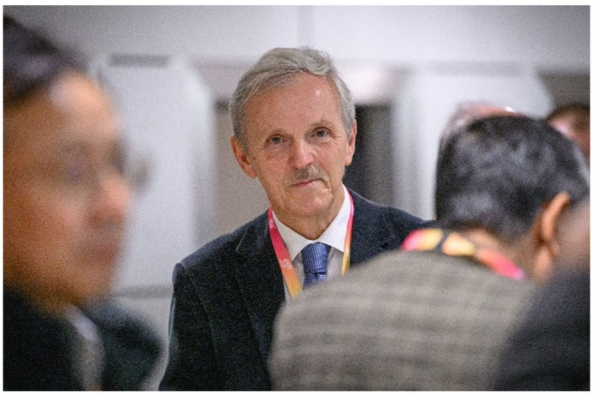


D,0
Reaktor

Any comments, corrections, complaints?

Please contact
martin. steinbrueck@kit.edu